GLIA IN HEALTH AND DISEASE

EDITED BY: Margaret S. Ho, Alexei Verkhratsky, Shumin Duan and Vladimir Parpura

PUBLISHED IN: Frontiers in Molecular Neuroscience, Frontiers in Cellular Neuroscience, Frontiers in Neuroscience and Frontiers in Aging Neuroscience

frontiers Research Topics

frontiers

ISSN 1664-8714
ISBN 978-2-88945-850-9
DOI 10.3389/978-2-88945-850-9

About Frontiers

Frontiers is more than just an open-access publisher of scholarly articles: it is a pioneering approach to the world of academia, radically improving the way scholarly research is managed. The grand vision of Frontiers is a world where all people have an equal opportunity to seek, share and generate knowledge. Frontiers provides immediate and permanent online open access to all its publications, but this alone is not enough to realize our grand goals.

Frontiers Journal Series

The Frontiers Journal Series is a multi-tier and interdisciplinary set of open-access, online journals, promising a paradigm shift from the current review, selection and dissemination processes in academic publishing. All Frontiers journals are driven by researchers for researchers; therefore, they constitute a service to the scholarly community. At the same time, the Frontiers Journal Series operates on a revolutionary invention, the tiered publishing system, initially addressing specific communities of scholars, and gradually climbing up to broader public understanding, thus serving the interests of the lay society, too.

Dedication to Quality

Each Frontiers article is a landmark of the highest quality, thanks to genuinely collaborative interactions between authors and review editors, who include some of the world's best academicians. Research must be certified by peers before entering a stream of knowledge that may eventually reach the public - and shape society; therefore, Frontiers only applies the most rigorous and unbiased reviews.
Frontiers revolutionizes research publishing by freely delivering the most outstanding research, evaluated with no bias from both the academic and social point of view. By applying the most advanced information technologies, Frontiers is catapulting scholarly publishing into a new generation.

What are Frontiers Research Topics?

Frontiers Research Topics are very popular trademarks of the Frontiers Journals Series: they are collections of at least ten articles, all centered on a particular subject. With their unique mix of varied contributions from Original Research to Review Articles, Frontiers Research Topics unify the most influential researchers, the latest key findings and historical advances in a hot research area! Find out more on how to host your own Frontiers Research Topic or contribute to one as an author by contacting the Frontiers Editorial Office: researchtopics@frontiersin.org

GLIA IN HEALTH AND DISEASE

Topic Editors:
Margaret S. Ho, ShanghaiTech University, China
Alexei Verkhratsky, The University of Manchester, United Kingdom; University of Copenhagen, Denmark; IKERBASQUE, Basque Foundation for Science, Spain
Shumin Duan, Zhejiang University, China
Vladimir Parpura, The University of Alabama at Birmingham, United States

Citation: Ho, M. S., Verkhratsky, A., Duan, S., Parpura, V., eds. (2019). Glia in Health and Disease. Lausanne: Frontiers Media. doi: 10.3389/978-2-88945-850-9

Table of Contents

frontiers in Molecular Neuroscience

EDITORIAL
published: 19 March 2019
doi: 10.3389/fnmol.2019.00063

Editorial: Glia in Health and Disease

Margaret S. Ho[1]*, *Alexei Verkhratsky*[2,3,4]*, *Shumin Duan*[5]* and *Vladimir Parpura*[6]*

[1] School of Life Science and Technology, ShanghaiTech University, Shanghai, China, [2] Faculty of Biology, Medicine and Health, The University of Manchester, Manchester, United Kingdom, [3] Center for Basic and Translational Neuroscience, Faculty of Health and Medical Sciences, University of Copenhagen, Copenhagen, Denmark, [4] Achucarro Center for Neuroscience, IKERBASQUE, Basque Foundation for Science, Bilbao, Spain, [5] Department of Neurobiology, School of Medicine, Zhejiang University, Hangzhou, China, [6] Department of Neurobiology, The University of Alabama at Birmingham, Birmingham, AL, United States

Keywords: glia, astrocytes, ALS, OPC, microglia

Editorial on the Research Topic

Glia in Health and Disease

Half a billion of years of evolution of the central nervous system (CNS) resulted in emergence of two highly integrated and interconnected cellular networks (Verkhratsky and Nedergaard, 2016) of neurones (executive arm of the CNS) and neuroglia (CNS homoeostatic and defensive division). Concerted activity of these networks underlies CNS function and output including behavior, intelligence, emotions and consciousness. Evolutionary specialization produced division of function in which neurones provide for information processing and creation of circuit-mediated behavior, whereas neuroglia assume full responsibility for homeostatic support of the nervous system. In addition, neuroglia provide (through conserved programmes of activation) for the defense of the nervous tissue. These distinct functions are reflected by distinct physiology of these two types of cells. Neuronal signaling relies on electrical excitability mediated by voltage-gated ionic channels and fast (millisecond range) synaptic transmission. Glia employ controlled fluctuations in intracellular ions and messengers; intercellular fluxes of these molecules underlie long-range signaling in glial syncytia that occur (within seconds) in the form of propagated ionic or metabolic (slow) waves (Verkhratsky and Nedergaard, 2018). Intercellular communications between the two networks are mediated by chemical transmission and a complement of receptors; neuroglial cells are capable to perceive neuronal activity and to secrete ions and signaling molecules [although secretion mechanisms/tool sets differ from that in synaptic terminals—(Verkhratsky et al., 2016)].

The homeostatic and defensive capacity of neuroglia stipulates their fundamental role in neuropathology. Conceptually, the glial component is present in every type of neurological disease, with glial contribution being either primary and/or secondary. Astrocytes undergo several types of pathological transformation from pathological remodeling and atrophy/degeneration with a loss of function to astrogliotic transformation (Verkhratsky et al., 2013; Sofroniew, 2014b; Pekny et al., 2016; Verkhratsky and Parpura, 2016); the latter producing numerous reactive phenotypes with neuroprotective or neurotoxic features (Pekny and Pekna, 2014; Sofroniew, 2014a; Liddelow et al., 2017). Microglial cells, that constantly scan brain parenchyma for damage or pathogen-associated molecular patterns, respond to lesions by highly complex activation that produces multiple neuroprotective or neurotoxic phenotypes (Kettenmann et al., 2011; Salter and Stevens, 2017). Finally, oligodendroglia and their precursors (also known as NG2 glia) respond to pathology with Wallerian degeneration, proliferation, and remyelination (Sun et al., 2010; Catenaccio et al., 2017).

Edited and reviewed by:
Jochen C. Meier, Technische Universitat Braunschweig, Germany

***Correspondence:**
Margaret S. Ho
margareth@shanghaitech.edu.cn
Alexei Verkhratsky
alexej.verkhratsky@manchester.ac.uk
Shumin Duan
duanshumin@zju.edu.cn
Vladimir Parpura
vlad@uab.edu

Received: *08 February 2019*
Accepted: *25 February 2019*
Published: *19 March 2019*

Citation:
Ho MS, Verkhratsky A, Duan S and Parpura V (2019) Editorial: Glia in Health and Disease. Front. Mol. Neurosci. 12:63. doi: 10.3389/fnmol.2019.00063

This Research Topic aims to address the role of neuroglia in healthy and diseased nervous tissue through a collection of 28 articles that include 2 mini-reviews, 4 reviews, 1 opinion, 19 original research article, 1 Perspective, and 1 Protocol. These articles provide a comprehensive overview on a broad spectrum of molecular and cellular basis of glial function in normal and pathological CNS.

The Research Topic discusses some of the physiological functions of neuroglia. The opinion on Ca^{2+}-dependent and Ca^{2+}-independent release of ATP from murine astrocytes is discussed by Xiong et al. while several articles discuss the regulation and molecular mechanisms of glial plasticity (Boerboom et al.; Lalo et al.; Wang and Parpura). Glial metabolism and other aspects of murine glial function were also included. A new signaling pathway associated with extracellular lactate, lactate receptor, and subsequent increase in cyclic-AMP was found to modulate astroglial metabolism by enhancing aerobic glycolysis (Vardjan et al.). In Zebrafish (Zhang et al.), microglial cells were shown to mediate clearance of apoptotic endothelial cells associated with vessel pruning. A novel method to study micropinocytosis in fly, *Drosophila,* hemocytes, phagocytic cells similar to microglia in mammals has been also described (Chen et al.).

Both astrocytes and microglia contribute to acute pathology such as ischemic stroke and epilepsy. Astrocytic $K_{ir}4.1$, an inwardly rectifying K^+ channel, is central to regulation of K^+ buffering to rebalance the blast of increased extracellular K^+ concentration during ischemic conditions (Milton and Smith). In ischaemic conditions, microglia get activated by microRNA miR-145-5p/ Nuclear receptor related 1 protein (Nurr1)/Tumor necrosis Factor-α cascade which can be used to define a novel therapeutic strategy to relieve neuronal damage as a consequence of microglial activation (Xuemei et al.). In the rat lithium-pilocarpine model of status epilepticus (SE), a significant reduction in the number of distal astrocytic branches were detected upon SE induction, suggesting that astrocytic atrophy correlates with SE-induced epileptic pathological conditions (Plata et al.). During central post-stroke pain, the Stromal cell-derived factor (SDF)-1 (CXC chemokine ligand-12)—(CXC chemokine receptor CXCR4) signaling is up-regulated and provide positive feedback to regulate glial-glial and glial-neuronal interactions (Fei et al.). Astrocytes are also involved in chronic pathologies; in particular they can mediate noradrenergic pathways responsible for neurodegeneration and cognitive decline in Alzheimer's disease (Leanza et al.).

Microglia-mediated response of the CNS significantly contributes to various chronic pathologies, including neurodegeneration. Articles assembled in this Research Topic indicate that microglial activation (induced by exposure to lipopolysaccharide, LPS) can be ameliorated by the natural plant compounds polyphenols and the glucagon like peptide-1 receptor (GLP-1R) agonist exendin-4 (EX-4) upon LPS exposure (Gullo et al.). Similar effects were exerted by caffeine/modafinil in a rat model of sleep deprivation; the treatment led to a significant improvement of the anxious behavior (Wadhwa et al.). As for the identification of molecular components involved in microglia-mediated pathological processes, the Dendritic cell-derived factor 1 (Dcf1), a factor in neural stem cell differentiation, glioma apoptosis, and dendritic spine formation, microglial lectins including galectins, siglecs, mannose-binding lectins (MBLs) as well as other glycan binding proteins, all play pivotal role in regulating microglia contribution to pathology (Siew and Chern; Wang et al.).

Glia contribute to many diseases. For instance, methyl CpG binding protein 2 (MeCP2) deficiency in various types of glia causes various defects and anomalies that contribute to Rett syndrome (Xu-Rui et al.). Activation of $P2X_7$ purinoreceptor triggers microglial response through autophagy and mammalian target of rapamycin (mTOR) pathway in amyotrophic lateral sclerosis (ALS) mouse model with mutated (G93A) superoxide dismutase; this signaling cascade could represent a potential target for modulating ALS progression (Fabbrizio et al.). Microglial expression of lipoprotein lipase is required for supporting remyelination and repair through the clearance of lipid debris, a feature crucial for demyelinating disorders, including multiple sclerosis (Bruce et al.). An overview on the proteomic and metabolic profiling of vanishing white matter mouse astrocytes has been provided by Wisse et al.

The cell adhesion molecule with homology *to* L1 (CHL1) promotes cell proliferation, metastasis and migration in human glioma cells both *in vitro* and *in vivo* (Yang et al.). The origin of glioblastomas can be potentially associated wit adult neural stem cells (NSCs) and oligodendrocyte precursor cells (OPCs) serving as cells of origin for glioblastoma, as reviewed by Shao and Lui. In this aspect, another important finding demonstrates that ryanodine receptors (RyR3) mediate Ca^{2+} release from the endoplasmic reticulum in order to regulate OPC differentiation (Li et al.). Several other factors affect glial transformations. B-cell chronic lymphocytic leukemia (CLL)/lymphoma 11B f(Bcl11b) protein, a C2H2-type zinc finger transcriptional factor, negatively regulates glial progenitor cell differentiation through the repression of oligodendrocyte differentiation-associated genes (Wang et al.), whereas epithelial growth factor (EGF) enhances oligodendrocyte differentiation from glial progenitor cells (Yang et al.). Finally, Cloarec and colleagues show that administration of clodronate liposomes or maternal feeding with doxycyline, both result in alternation of microglial activity and abundance, improved survival in a rate model of cytomegalovirus infection (Cloarec et al.).

Glial cells were long thought to serve merely as the supporting cast and scenery behind the neuronal stars of the show. Relatively recent evidence, however, indicates that the glial cells are intimately involved in many of the brain's functions in health and disease. The intent of this Research Topic was to provide an update on recent developments in glial biology be that in health and disease.

AUTHOR CONTRIBUTIONS

All four authors contribute in writing the editorial and organizing the research topic.

REFERENCES

Catenaccio, A., Llavero Hurtado, M., Diaz, P., Lamont, D. J., Wishart, T. M., and Court, F. A. (2017). Molecular analysis of axonal-intrinsic and glial-associated co-regulation of axon degeneration. *Cell Death Dis*. 8:e3166. doi: 10.1038/cddis.2017.489

Kettenmann, H., Hanisch, U. K., Noda, M., and Verkhratsky, A. (2011). Physiology of microglia. *Physiol. Rev*. 91, 461–553. doi: 10.1152/physrev.00011.2010

Liddelow, S. A., Guttenplan, K. A., Clarke, L. E., Bennett, F. C., Bohlen, C. J., Schirmer, L., et al. (2017). Neurotoxic reactive astrocytes are induced by activated microglia. *Nature* 541, 481–487. doi: 10.1038/nature21029

Pekny, M., and Pekna, M. (2014). Astrocyte reactivity and reactive astrogliosis: costs and benefits. *Physiol. Rev*. 94, 1077–1098. doi: 10.1152/physrev.00041.2013

Pekny, M., Pekna, M., Messing, A., Steinhäuser, C., Lee, J. M., Parpura, V., et al. (2016). Astrocytes: a central element in neurological diseases. *Acta Neuropathol*. 131, 323–345. doi: 10.1007/s00401-015-1513-1

Salter, M. W., and Stevens, B. (2017). Microglia emerge as central players in brain disease. *Nat. Med*. 23, 1018–1027. doi: 10.1038/nm.4397

Sofroniew, M. V. (2014a). Astrogliosis. *Cold Spring Harb Perspect Biol*. 7:a020420. doi: 10.1101/cshperspect.a020420

Sofroniew, M. V. (2014b). Multiple roles for astrocytes as effectors of cytokines and inflammatory mediators. *Neuroscientist* 20, 160–172. doi: 10.1177/1073858413504466

Sun, F., Lin, C. L., McTigue, D., Shan, X., Tovar, C. A., Bresnahan, J. C., et al. (2010). Effects of axon degeneration on oligodendrocyte lineage cells: dorsal rhizotomy evokes a repair response while axon degeneration rostral to spinal contusion induces both repair and apoptosis. *Glia* 58, 1304–1319. doi: 10.1002/glia.21009

Verkhratsky, A., Matteoli, M., Parpura, V., Mothet, J. P., and Zorec, R. (2016). Astrocytes as secretory cells of the central nervous system: idiosyncrasies of vesicular secretion. *EMBO J*. 35, 239–257. doi: 10.15252/embj.201592705

Verkhratsky, A., and Nedergaard, M. (2016). The homeostatic astroglia emerges from evolutionary specialization of neural cells. *Philos. Trans. R Soc. Lond. B Biol. Sci*. 371:20150428. doi: 10.1098/rstb.2015.0428

Verkhratsky, A., and Nedergaard, M. (2018). Physiology of Astroglia. *Physiol. Rev*. 98, 239–389. doi: 10.1152/physrev.00042.2016

Verkhratsky, A., and Parpura, V. (2016). Astrogliopathology in neurological, neurodevelopmental and psychiatric disorders. *Neurobiol. Dis*. 85, 254–261. doi: 10.1016/j.nbd.2015.03.025

Verkhratsky, A., Rodríguez, J. J., and Parpura, V. (2013). Astroglia in neurological diseases. *Future Neurol*. 8, 149–158. doi: 10.2217/fnl.12.90

Conflict of Interest Statement: The authors declare that the research was conducted in the absence of any commercial or financial relationships that could be construed as a potential conflict of interest.

frontiers in Cellular Neuroscience

SYSTEMATIC REVIEW
published: 17 December 2018
doi: 10.3389/fncel.2018.00491

Astrocyte-Mediated Neuromodulatory Regulation in Preclinical ALS: A Metadata Analysis

Kathleen Jordan[1], *Joseph Murphy*[1], *Anjanya Singh*[1,2] *and Cassie S. Mitchell*[1]*

[1] *Laboratory for Pathology Dynamics, Department of Biomedical Engineering, Georgia Institute of Technology, Emory University School of Medicine, Atlanta, GA, United States,* [2] *School of Medicine, University of Texas Southwestern Medical Center, Dallas, TX, United States*

Amyotrophic Lateral Sclerosis (ALS) is a neurodegenerative disease characterized by progressive degradation of motoneurons in the central nervous system (CNS). Astrocytes are key regulators for inflammation and neuromodulatory signaling, both of which contribute to ALS. The study goal was to ascertain potential temporal changes in astrocyte-mediated neuromodulatory regulation with transgenic ALS model progression: glutamate, GTL-1, GluR1, GluR2, GABA, ChAT activity, VGF, TNFα, aspartate, and IGF-1. We examine neuromodulatory changes in data aggregates from 42 peer-reviewed studies derived from transgenic ALS mixed cell cultures (neurons + astrocytes). For each corresponding experimental time point, the ratio of transgenic to wild type (WT) was found for each compound. ANOVA and a student's *t*-test were performed to compare disease stages (early, post-onset, and end stage). Glutamate in transgenic SOD1-G93A mixed cell cultures does not change over time ($p > 0.05$). GLT-1 levels were found to be decreased 23% over WT but only at end-stage ($p < 0.05$). Glutamate receptors (GluR1, GluR2) in SOD1-G93A were not substantially different from WT, although SOD1-G93A GluR1 decreased by 21% from post-onset to end-stage ($p < 0.05$). ChAT activity was insignificantly decreased. VGF is decreased throughout ALS ($p < 0.05$). Aspartate is elevated by 25% in SOD1-G93A but only during end-stage ($p < 0.05$). TNFα is increased by a dramatic 362% ($p < 0.05$). Furthermore, principal component analysis identified TNFα as contributing to 55% of the data variance in the first component. Thus, TNFα, which modulates astrocyte regulation via multiple pathways, could be a strategic treatment target. Overall results suggest changes in neuromodulator levels are subtle in SOD1-G93A ALS mixed cell cultures. If excitotoxicity is present as is often presumed, it could be due to ALS cells being more sensitive to small changes in neuromodulation. Hence, seemingly unsubstantial or oscillatory changes in neuromodulators could wreak havoc in ALS cells, resulting in failed microenvironment homeostasis whereby both hyperexcitability and hypoexcitability can coexist. Future work is needed to examine local, spatiotemporal neuromodulatory homeostasis and assess its functional impact in ALS.

Keywords: glutamate, GABA, GLT-1, ChAT, VGF, TNFα, aspartate

OPEN ACCESS

Edited by:
Margaret Su-chun Ho,
ShanghaiTech University, China

Reviewed by:
Yu-Feng Wang,
Harbin Medical University, China
Erik B. Malarkey,
Vertex Pharmaceuticals, United States
Manoj K. Gottipati,
Rensselaer Polytechnic Institute, United States

***Correspondence:**
Cassie S. Mitchell
cassie.mitchell@bme.gatech.edu

Received: *15 January 2018*
Accepted: *29 November 2018*
Published: *17 December 2018*

Citation:
Jordan K, Murphy J, Singh A and Mitchell CS (2018) Astrocyte-Mediated Neuromodulatory Regulation in Preclinical ALS: A Metadata Analysis. Front. Cell. Neurosci. 12:491. doi: 10.3389/fncel.2018.00491

INTRODUCTION

Amyotrophic Lateral Sclerosis (ALS) is a neurodegenerative disease characterized by the progressive degradation of motoneurons, which results in muscle paralysis, respiratory failure, and ultimately death. Its multifactorial nature, population heterogeneity, and inherent complexity has made both clinical survival prediction (Pfohl et al., 2018) and intervention optimization (Khamankar et al., 2018) extremely difficult.

Because the multi-factorial nature of ALS is difficult to study in humans, experimental mouse models are critical for etiological and treatment elucidation. The superoxide dismutase 1 glycine 93 to alanine (SOD1-G93A) transgenic mouse is currently the predominant means of investigating the preclinical pathophysiology of ALS (Pfohl et al., 2015) because it of its rich publication history and reproducibility. ALS pathophysiology has multi-scalar disturbances that impact numerous processes, including inflammation, apoptosis, energetics, excitability, genetic transcription, cellular chemistry, oxidative stress, proteomics, and systemic function (Irvin et al., 2015; Kim et al., 2016). While ALS is a motoneuron disease, non-neuronal tissues are also affected, including astrocytes, glia, and muscle. In fact, inflammation, a process that is predominantly driven by non-neural tissue, is the most published etiology examined in SOD1-G93A ALS mice (Kim et al., 2016).

Evidence suggests that non-neuromuscular cells, such as astrocytes, play one of the earliest roles in ALS and are being considered as therapeutic targets (Vargas and Johnson, 2010; Pehar et al., 2017). Astrocytes are the most abundant subtype of glial cells found in the central nervous system (CNS), comprising 20–50% of the brain volume (Rossi and Volterra, 2009). One function of astrocytes is to stabilize the neural microenvironment after an injury through the release of cytokines (Rossi and Volterra, 2009). Ideally, the inflammatory regulators of astrocytes stimulate the healing process and lay down a protective glial scar (Sofroniew and Vinters, 2010). However, inflammation is also negatively implicated across neuropathology, where its consequences can expand the lesion volume (Mitchell and Lee, 2008) or perpetuate local dysregulation. For example, in SOD1-G93A ALS, there is a dynamic imbalance of cytokines that inappropriately amplifies inflammation (Jeyachandran et al., 2015). Glial fibrillary acid protein (GFAP) levels in SOD1-G93A mice are almost double those of wild type (WT) mice prior to onset and continue to significantly increase with disease progression. Furthermore, ITPR2 gene expression is significantly upregulated before and after the induction of inflammation (Staats et al., 2016).

Another key function of astrocytes is to assist in reuptake of neuromodulatory agents. It has been proposed that the hyperexcitability of motoneurons is caused by overstimulation by the main excitatory neurotransmitter, glutamate, which leads to a large influx of calcium ($Ca2+$) and sodium ($Na+$) into the cell through glutamate transporter 1 (GLT-1) (Van Den Bosch et al., 2006; Do-Ha et al., 2017). Intracellular $Ca2+$ levels are further increased as $Na+$ is passed out through the $Na+$-$Ca2+$ exchanger (Van Den Bosch et al., 2006). Motoneurons possess little ability to counteract the effects of $Ca2+$ influx, so overstimulation can easily lead to excitotoxicity and cell death (Do-Ha et al., 2017). Glutamate excitotoxicity and impaired intracellular calcium signaling in astrocytes is theorized to significantly impact disease progression in ALS and other types of neuropathology (Staat and Van Den Bosch, 2009; Kawamata et al., 2014). Yet, such neuromodulatory regulation mediated by astrocytes is much lesser-studied than inflammation.

Astrocyte neuromodulatory dysregulation, resulting in failed neuromodulatory homeostasis, is thought to contribute significantly to neuronal depolarization, hyperexcitability, excitotoxicity, and subsequent neuronal death in ALS (Lin et al., 2013). Increased levels of glutamate and reduced levels of excitatory amino acid transporter 2 (EAAT2) have been found in the CNS of ALS patients, suggesting EAAT2 dysfunction and glutamate excitotoxicity is involved in the disease progression (Rothstein et al., 1990, 1995). It is still unknown as to what causes the glutamate to initially collect within the CNS. One possible explanation is that, prior to functional onset of the disease, the astrocytes fail to reuptake the extracellular glutamate at the proper homeostatic rate, resulting in a slow accumulation. Another explanation is that the motoneurons, or another nearby cell, releases glutamate at a significantly higher rate than normal. As part of the latter explanation, astrocytes do not compensate for the increased glutamate release and, rather, simply continue to reabsorb at a normal rate, resulting in glutamate accumulation over time. Many studies (Li et al., 2015) have sought to increase GLT-1 levels in astrocytes to increase astrocyte reuptake, albeit unsuccessfully.

The inhibitory neurotransmitter gamma-Aminobutyric acid (GABA) also has therapeutic potential. Mildly reduced expression of GABAergic markers and interneurons have been found in some SOD1 mice and ALS patients (Nihei et al., 1993; Hossaini et al., 2011). GABA transmission can decrease levels of glutamate and protect against excessive neuronal damage (Brockington et al., 2013). However, clinical trials of gabapentin, a pharmaceutical anti-epileptic drug that modulates GABA, did not extend life span or slow the rate of muscle decline or respiratory function (Diana et al., 2017). Elucidation of temporal relationships among glutamate levels, transporter proteins, such as GLT-1 and glutamate receptors (GluR), and GABA is needed to determine therapeutic timing and efficacy. For example, if glutamate-related treatment must occur well before ALS symptom onset to have a functional impact, its clinical treatment value is greatly diminished.

The adjunctive regulation of intracellular $Ca2+$ by astrocytes is vital for cell signaling. Astrocytes are able to signal neurons by $Ca2+$ dependent release of glutamate (Appel et al., 2001; Rossi and Volterra, 2009). Intracellular concentrations of $Ca2+$ are characteristically elevated in response to pathological signaling (Rossi and Volterra, 2009; Guerra-Gomes et al., 2018). The glutamate-mediated excitotoxicity of astrocytes relies on intracellular concentrations of $Ca2+$ but has also been found to be accompanied by the cytokine TNFα (Rossi and Volterra, 2009). The blockage of the formation of TNFα and endoplasmic reticulum (ER) $Ca2+$ overload have a significant negative effect on astrocyte glutamate release (Rossi and Volterra, 2009;

Kawamata and Manfredi, 2010). Other cytokines, such as VGF nerve growth factor (VGF), insulin-like growth factor 1 (IGF-1), aspartate, and choline acetyltransferase (ChAT) can also be linked to intracellular calcium levels (Palmieri et al., 2001; Fernández et al., 2004; Kandinov et al., 2013).

An examination of dynamic, temporal interactions among key players in astrocyte-mediated neuromodulatory regulation is necessary to better evaluate ALS etiology and therapy. Of course, pathological extracellular increases of glutamate, calcium, and other co-factors does lead, or minimally contribute, to co-existing pathology, like oxidative stress, inflammation, and excitotoxicity. Such pathological overlap makes detangling the multi-factorial ALS etiology all the more difficult (Kim et al., 2016). Due to the large number of variables, a single all-encompassing *in vivo* experiment is not feasible. The goal of this study is to determine temporal trends of intrinsic astrocyte-mediated compounds that contribute to neuromodulatory regulation over the disease progression of preclinical ALS, with the primary focus on regulation of glutamate, GABA, and related compounds. Specifically, this metadata analysis is comprised of temporal neuromodulatory data compiled from 42 peer-reviewed studies that utilized mixed cultures of astrocytes and neurons predominantly derived from *in vivo* SOD1-G93A ALS mice and normal WT mice.

METHODS

A metadata analysis was performed to construct a macroscopic view of astrocyte-mediated neuromodulatory regulation over the course of transgenic ALS mouse model disease progression. The general method involved (1) mining, selecting and recapturing published data from preclinical ALS experiments examining astrocytes; (2) normalizing recaptured data to enable aggregation across studies; (3) analyzing aggregate data using appropriate statistical methods.

Data Source Identification and Inclusion Criteria

Keywords were used to identify potential data sources in PubMed/Medline. All potential data sources were initially searched using key words "Amyotrophic Lateral Sclerosis" OR "ALS" AND "transgenic mouse." Searches were limited to articles published in English and with publication dates through June 2018. Primary search articles were downloaded into a Filemaker Pro relational database (Mitchell et al., 2015a; Kim et al., 2016) and had relevant data recaptured using our lab's highly accurate biocuration process (Mitchell et al., 2015a). Secondary searches on relevant sub-topics were performed within the Filemaker Pro database including all synonyms (see **Table 1**). We specifically utilized the "high-copy" transgenic SOD1-G93A mouse model, which is not only more common but also has less implicit outcome heterogeneity (Pfohl et al., 2015). Recaptured data included measures of glutamate, GTL-1, GluR1, GluR2, GABA, ChAT activity, VGF, TNFα, aspartate, and IGF-1, which were identified using searches of figure axis labels and figure/table captions. As astrocytic compensation can only be studied in the presence of neurons, most data was taken from mixed cultures. Only studies that presented quantified data for both transgenic and age-matched WT control mice were included. A total of 42 articles with quantifiable experimental data had data extracted for analysis. A diagram of the literature review structure is shown in the **Supplementary Figure 1**.

TABLE 1 | Keywords for "*Astrocytes*" and terms associated with each subtopic.

Category	Keywords
Glutamate	Nitric oxide, NO* conc*, synth*, glutamate, glutamate* conc*, GLT1, GLT1* transporter*, GluRA, GluR1, GluR2, GluR3, GluR4, GluR*, excitotoxicity, excito*
Calcium	Membrane potential, cyto* cal* conc*, cal* buffer* capacity, mito* cal* conc*, cal* uptake, cal* conc*, cal* transient, permeability transition pore, acetylcholine, voltage-gated, calcium channel*, calcium pump*, GABA, ER([Ca]), endoplasmic reticulum, AMPA receptor*, VDAC, CypD, FCCP, IGF-1, VGF, TNF-alpha, TNF*, aspartate, ChAT*

*The subtopics were broad topics that were used to categorize articles discussing ALS studies. The keywords were used in searches in the database to determine article numbers and potential data points for each subtopic. The searches were performed on figure axis labels and captions. *indicates that pieces of the word/phrase or synonyms were included in the search.*

Data Normalization and Aggregation

Recaptured quantified data was used to construct ratios of ALS-representative mouse models to WT (such as, SOD1-G93A/WT) for each included metric at each temporal disease stage. The genetic background, onset, survival, tissue origin/measurement procedure of each included study is detailed in **Supplementary Table 1**. Temporal data points were aggregated into three disease stages; pre-onset (0–96 days), post-onset (97–116 days), and end stage (117+ days). Disease stages were determined by finding the average age of onset (97 days) and survival duration (117+ days) for the included mice in the present study. Non-aggregated raw data can be found in **Supplementary Figure 2**. Six of the post-onset glutamate data points were empirically extrapolated using standard statistical regression to obtain the necessary sample size determined by a standard power analysis. **Table 2** illustrates the breakdown of the 264 data points (e.g., ratios of transgenic to WT for each included factor for each temporal disease stage). Aggregation is an inherent limitation to meta-analysis, and this is further discussed in the context of this study in the Limitations.

Not every included journal article expressed the mouse sample size corresponding to each of their data points. Thus, each data point (e.g., ratio of transgenic to WT for the included factor measured at a specific temporal disease stage) in the present metadata analysis is weighted equally on a per-article basis rather than the corresponding mouse sample size comprising the data point.

To determine the ALS disease stages, the average onset (97 days) and time of death (117 days) was calculated using all included onset and time of death data from the original experimental studies (see **Supplementary Data Sheet**). Note that these averages are within what is expected for high copy SOD1-G93A ALS mice (Pfohl et al., 2015).

TABLE 2 | Number of data points used in each sub-category.

Sub-Category	Time bin	Sample size	References
Glutamate	Pre-onset Post-onset End-Stage	22 12* 15	Alexander et al., 2000; Guo et al., 2000, 2003; Bendotti et al., 2001; Raiteri et al., 2004; Niessen et al., 2007; Choi et al., 2009; Gu et al., 2010; Milanese et al., 2011; Albano et al., 2013; Valbuena et al., 2016; Tefera and Borges, 2018
GLT-1	Pre-onset Post-onset End-Stage	22 10 16	Alexander et al., 2000; Bendotti et al., 2001; Deitch et al., 2002; Chen et al., 2004; Rothstein et al., 2005; Boston-Howes et al., 2006; Pardo et al., 2006; Yang et al., 2009; Gu et al., 2010; Benkler et al., 2013; Morel et al., 2013
GluR1	Pre-onset End-Stage	24 7	Petri et al., 2005; Spalloni et al., 2006; Martinez et al., 2008; Zhao P. et al., 2008 Caioli et al., 2011
GluR2	Pre-onset End-Stage	17 5	Petri et al., 2005; Spalloni et al., 2006; Tortarolo et al., 2006; Zhao P. et al., 2008
GABA	Pre-onset End-Stage	4 11	Raiteri et al., 2004; Tsai et al., 2010; Caioli et al., 2013; Tefera and Borges, 2018
ChAT Activity	Pre-onset Post-onset End-Stage	24 12 23	Crochemore et al., 2005, 2009; Kalmar et al., 2012
VGF	Pre-onset End-Stage	12 6	Zhao Z. et al., 2008
TNFα	Pre-onset End-Stage	8 3	Fang et al., 2010; Yang and Cheng, 2010; Song et al., 2013; Cai et al., 2015; Jeyachandran et al., 2015; Lee et al., 2015
Aspartate	Pre-onset	7	Alexander et al., 2000; Niessen et al., 2007; Choi et al., 2009; Tefera and Borges, 2018
IGF-1	Pre-onset	4	Kaspar et al., 2005; Wu et al., 2006; Messi et al., 2007; Fergani et al., 2011

** To reach the desired sample size, 6 of the 12 data points were linearly extrapolated for this time bin.*

Statistical Analysis

The distributions of all data sets were tested with Shapiro-Wilks tests to assure sufficient distribution normality for the corresponding statistical tests. To determine statistical significance of differences between disease stages, an ANOVA was performed using the Bonferroni correction. To compare protein levels, a Student's *t*-test with a Bonferroni correction was performed for each disease stage. Error bars on figures correspond to the standard deviation. All statistical tests were performed with built-in functions in MATLAB (version R2016a). Correlation matrices were constructed to visualize the relationships between the analyzed measures. A principal component analysis (PCA) was used to evaluate contributions to data variance and visualized reduced data structure. The correlation matrices and PCA were generated in MATLAB (version R2016a).

RESULTS

A total of nine astrocyte-mediated neuromodulatory regulators were examined from 42 peer-reviewed articles. As stated in the Introduction, nearly all of these factors still have secondary ties to inflammation. However, the focus of the present study was not on the inflammatory roles of astrocytes but rather neuromodulatory regulation of GABA, glutamate and calcium related co-factors. **Table 2** lists the measures along with the included sample size (number of data points). The glutamate excitotoxicity sub-categories included glutamate, GLT-1, GluR1, GluR2, and GABA concentrations. The calcium homeostasis sub-categories included ChAT activity, VGF, TNFα, aspartate, and IGF-1 levels.

Glutamate and Glutamate Transporter Proteins

Glutamate and glutamate transporter levels from mixed cell cultures from SOD1-G93A ALS mice are compared to WT. There was no significant difference in glutamate concentrations over disease progression (**Figure 1A**). Glutamate concentrations were also not significantly increased from WT concentrations at any disease stage. GLT-1 and GluR1 levels decrease over disease progression. At end-stage, GLT-1 levels were 23% lower than end-stage WT values ($p = 0.008$) (**Figure 1B**). GluR1 concentrations at end-stage were 21% decreased from pre-onset levels ($p = 0.035$) (**Figure 1C**). There was no significant difference in GluR2 concentrations over disease progression (**Figure 1C**).

GABA

Next, GABA levels were compared in ALS mice and WT mice (**Figure 2**). GABA concentrations showed no significant difference between WT and ALS transgenic values. Moreover, there was no significant change in GABA over the course of ALS disease stage or progression.

Other Neuromodulatory Factors

Other calcium-related cytokines and neuromodulatory factors were examined over temporal SOD1-G93A disease progression (**Figure 3**). Choline acetyltransferase (ChAT), a transferase enzyme, is responsible for producing the neurotransmitter, acetylcholine (ACH). ChAT activity did not significantly vary over disease progression (**Figure 3A**). The lack of a significant trend in ChAT, which otherwise qualitatively appears to be depressed in SOD1-G93A compared to WT, is confounded by the large variance in experimental sample population. Nerve growth factor (VGF) is a secreted protein and neuropeptide precursor that may play a role in regulating energy homeostasis, metabolism and synaptic plasticity. VGF levels are depressed in SOD1-G93A ALS mixed cultures. VGF levels are significantly decreased from WT levels at both pre-onset ($p = 0.0036$) and end-stage ($p < 0.0001$), with end-stage being further significantly decreased from pre-onset ($p = 0.0002$; **Figure 3B**). Tumor necrosis factor alpha (TNFα) is a cytokine involved in inflammation, apoptosis, and synaptic function. TNFα expression in ALS mixed cultures significantly increased 362%

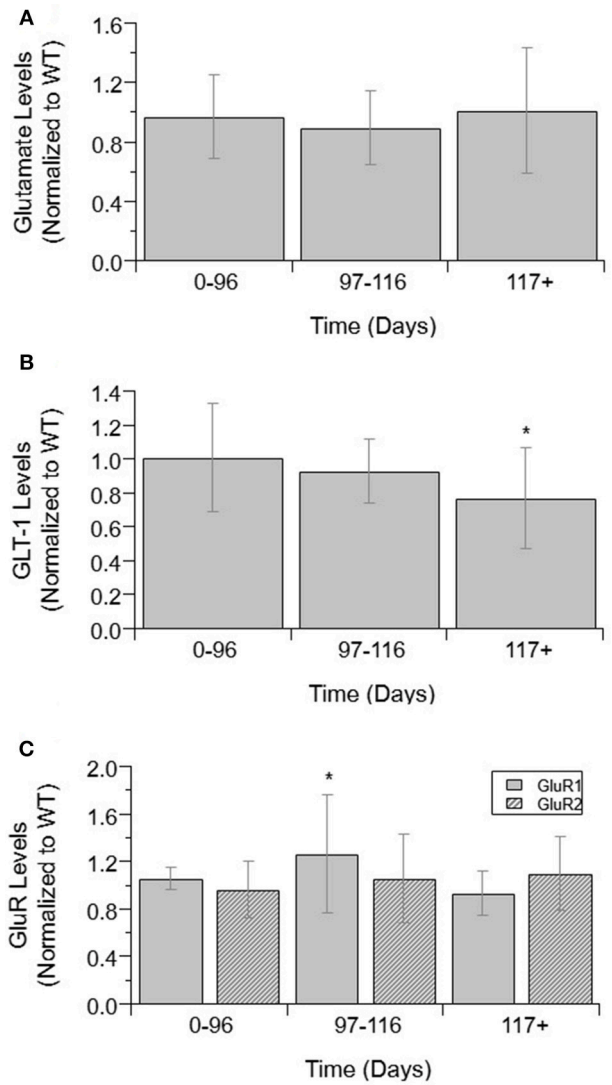

FIGURE 1 | Glutamate, GLT-1, and GluR complex levels in mixed cultures over ALS disease progression**. (A)** Glutamate level average in SOD1-G93A mice normalized to wild-type (ratio presented as SOD1-G93A/WT) in three temporal stages: 0–96 days, 97–116 days, and 117+ days. There was no significant change in glutamate levels between any of the temporal stages. **(B)** GLT-1 average in SOD1-G93A normalized to wild-type (ratio presented as SOD1-G93A/WT) in three temporal stages: 0–96 days, 97–116 days, and 117+ days. GLT-1 is significantly decreased from WT (*$p = 0.0075$) at 117 + days. **(C)** GluR1 (solid bars) and GluR2 (stripped bars) average in SOD1-G93A normalized to wild-type (ratio presented as SOD1-G93A/WT) in three temporal stages: 0–96 days, 97–116 days, and 117+ days. There was no significant change in GluR2 levels between temporal stages. GluR1 at 117+ days was significantly decreased from 0–96 (*$p = 0.0346$). Error bars represent SD.

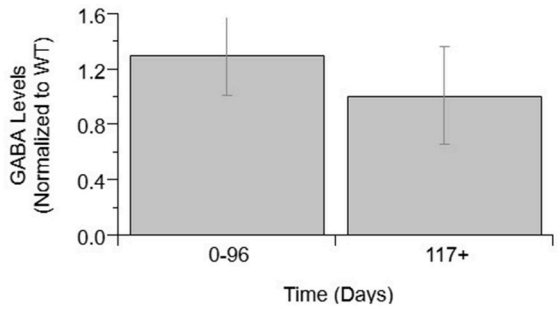

FIGURE 2 | GABA levels over ALS disease progression. GABA level average normalized to wild-type (ratio presented as transgenic/WT) in two temporal stages: 0–96 days and 117+ days. Error bars represent SD.

from WT at end-stage (**Figure 3C**). Aspartate concentrations also significantly increased 25% from WT (**Figure 3D**).

Glutamate, GABA, and Cytokine Relationships

A series of cross-correlation matrices were used to examine the correlations between various neuromodulatory regulators examined in this study (**Figure 4**). A cross-correlation matrix with correlations was constructed for each disease stage: 0–96 days (pre-onset); 97–116 days (post-onset); and 117+ days (end-stage). Highly negatively correlated factors are closer to −1, uncorrelated factors are closer to 0, and highly positively correlated factors are closer to 1; the illustrated gray scale represents the degree and sign of corresponding correlation. Only factors with a sample size calculated as having sufficient statistical power were included in each disease stage matrix. Thus, not every matrix included all factors. The pre-onset matrix included the most factors. The notable result from this analysis is that ChAT and VGF levels are high positively correlated at pre-onset ($p = 0.0003$; **Figure 5**).

A principal component analysis (PCA) was used to determine the individual components, which contribute the most to variance in the data (**Figure 5**). PCA is a type of exploratory and dimensionality reduction analysis. It is mathematically defined as an orthogonal linear transformation that transforms the data to a new coordinate system such that the greatest variance by some projection of the data comes to lie on the first coordinate (called the first principal component), the second greatest variance on the second coordinate, etc. The biplot displays how much the variables contribute to the variance of the first two principal components while also identifying reduced variable clusters (**Figure 5A**). The length of each factor's vector corresponds to the variance explained. Component 1 accounted for 55% of the variance and was almost completely comprised of TNFα (**Figure 5B**). Component 2 accounted for 17% of the variance and was mostly comprised of GABA and aspartate (**Figure 5C**). Interestingly, TNFα was nearly orthogonal to GluR1, indicating a lack of relationship.

Finally, an analysis was performed to determine which normalized cytokine co-factor levels were significantly different than either glutamate or GABA in mixed cultures across each temporal disease stage (**Figure 6**). VGF levels were significantly decreased from glutamate at pre-onset and end-stage ($p = 0.0331$ and $p = 0.0028$; **Figure 6A**). TNFα was significantly increased from glutamate levels at pre-onset ($p = 0.0018$; **Figure 6B**). GABA levels were not significantly increased from glutamate at any ALS disease stage (**Figure 6C**). ChAT activity

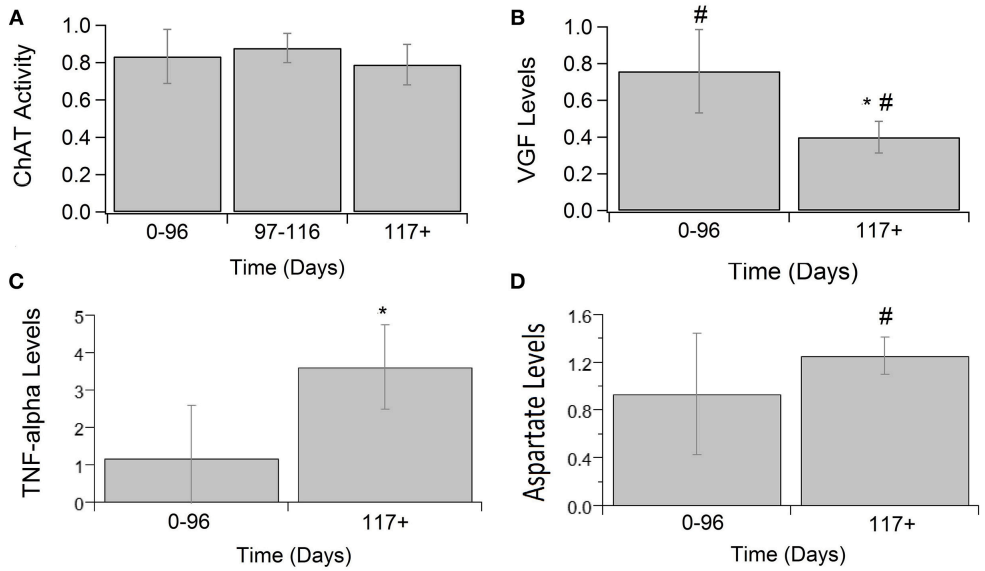

FIGURE 3 | Calcium-related cytokine levels over ALS disease progression. ChAT activity **(A)**, VGF **(B)**, TNFα **(C)**, and aspartate **(D)** averages in SOD1-G93A normalized to wild type (ratio presented as SOD1-G93A/WT) in three stages: 0–96 days, 97–116 days, and 117 + days. SOD1-G93A VGF levels were significantly decreased compared to WT at 0–96 days (#$p = 0.0036$) and 117+ days (#$p < 0.0001$). SOD1-G93A VGF levels at end-stage are also significantly lower than early-stage (*$p = 0.0002$). TNFα (*$p = 0.0488$) and aspartate (#$p = 0.0350$) levels were significantly increased at end-stage compared to WT. Error bars represent SD.

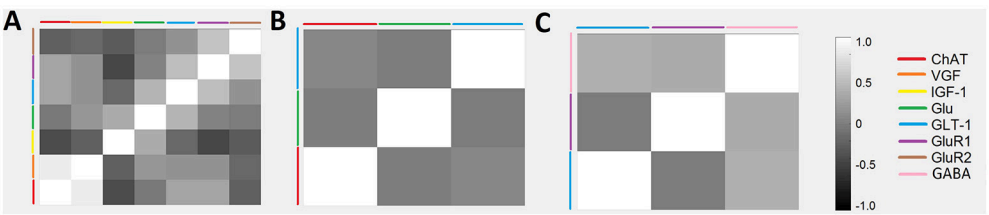

FIGURE 4 | Temporal relationships between non-inflammatory regulators of astrocytes visualized as a cross-correlation matrix. Average concentrations of glutamate, GABA, and related cytokines for ALS mice were normalized to wild-type mice with data aggregated across three temporal stages: **(A)** 0–96 days, **(B)** 97–116 days, and **(C)** 117+ days. Highly positive correlations were found between VGF and ChAT at 0–96 days. Note that only factors with sufficient sample sizes (calculated using standard statistical power analysis) were included.

was significantly lower than GABA at pre-onset ($p = 0.0033$) and end-stage ($p = 0.009$; **Figure 6D**). Aspartate concentrations were not significantly lower than GABA at any disease stage (**Figure 6E**).

DISCUSSION

The metadata analysis results do not paint a picture of widespread, overt glutamate-mediated excitotoxicity in preclinical ALS as measured in mixed cell cultures. The key neuromodulators, namely glutamate, glutamate receptors, and transports, GABA, and ChAT, showed no so significant changes in ALS compared to WT or significant changes over the course of ALS disease progression. GLT-1 and GluR1 were significantly decreased at end stage, whereas aspartate was significantly increased at end stage. TNFα was significantly and drastically increased throughout ALS disease duration, whereas VGF was significantly decreased throughout the ALS disease course. Other than TNFα, directly measured changes in neuromodulators are modest at best. Below we discuss what these results suggest about the role of astrocyte-mediated neuromodulatory regulation in ALS etiology and potential treatments.

Evaluating the Case for and Against ALS Excitotoxicity

Astrocytes play a critical role in reabsorbing excess extracellular glutamate and maintaining homeostasis for the motoneurons, which normally prevents excitotoxicity. There has been ongoing debate as to the presence or source of possible excitotoxicity (e.g., Leroy and Zytnicki, 2015; Rosenblum and Trotti, 2017; Martínez-Silva et al., 2018), especially given some animal model experiments suggest ALS motoneurons are hyperexcitable (Jiang et al., 2017) whereas other work suggests they are hypoexcitable (Martínez-Silva et al., 2018).

Previous clinical work illustrated evidence of increased glutamate levels in the CNS of ALS patients (Rothstein et al., 1990). Lack of resorption results in glutamate being left in the extracellular fluid resulting in continuous over-stimulation of the postsynaptic neurons (Rosenblum and Trotti, 2017). However, there was no identified increase in the excitatory transmitter, glutamate, in the preclinical ALS model mixed cell cultures examined in this study. As improved technology enables further examination, future experimental studies should focus on the specific localization of neurotransmitters to determine if key neurotransmitter changes are a function of spatial resolution, specific cell type, or a function of the type of ALS model.

Astrocytes use the enzyme glutamine synthetase (GS) to convert glutamate to glutamine as part of the glutamate/GABA-glutamine cycle (Norenberg and Martinez-hernandez, 1979; Bak et al., 2006). It is possible the constant levels of glutamate indicate SOD1-G93A astrocytes are reuptaking glutamate at higher rates and immediately converting it to maintain homeostasis. However, if glutamate was being taken in at higher rates it would require significant increases in GLT-1 and GluR to transport it into the cells. No such increases were found in this analysis. Rather, GLT-1 and GluR1 levels actually decreased compared to WT near end stage.

There are a few possible explanations for the decrease in GLT-1 and/or GluR1 levels. First, GLT-1 decreases could possibly be attributed to the difference in metabolic needs of astrocytes and neurons. Since GLT-1 activity in astrocytes leads to an influx of *Ca2+* through the energy powered Na+-*Ca2+* exchanger (Bazargani and Attwell, 2016), metabolic impairment in astrocytes would also lead to decreased GLT-1 activity. A second explanation for the decrease of GLT-1 and GluR1 over ALS disease progression could simply be due to the lower number of living or fully functioning cells in later stages of ALS. Finally, *if* there are potential cell-specific or spatially localized increases in excitation [spatial differences were not able to be examined in the present work], decreases in GLT-1 could suggest failed regulation or an inadequate compensatory response.

Beyond glutamate-related findings, there were several other neuromodulatory findings in the present study that provide further insight. For example, GABA, an inhibitory neurotransmitter, is not upregulated over the course of ALS in mixed cell cultures. If glutamate and other excitatory transmitters were in excess (either due to over-production or do to impaired re-uptake), it would be expected that GABA follow a similar trend due to innate compensatory mechanisms to balance excitation and inhibition. In the present study, neither GABA nor glutamate were significantly different in preclinical ALS compared to WT. Notably, aspartate, another excitatory neurotransmitter similar to glutamate, did show a slight increase in end stage preclinical ALS. However, ChAT, which is used to make the neurotransmitter acetylcholine, showed no significant difference.

In summary, there were no major changes in key neuromodulators that would point to very obvious glutamate-related excitotoxicity. Rather, the evidence presented here for mixed ALS cell cultures would suggest that direct neuromodulatory changes are subtle to modest, at least in

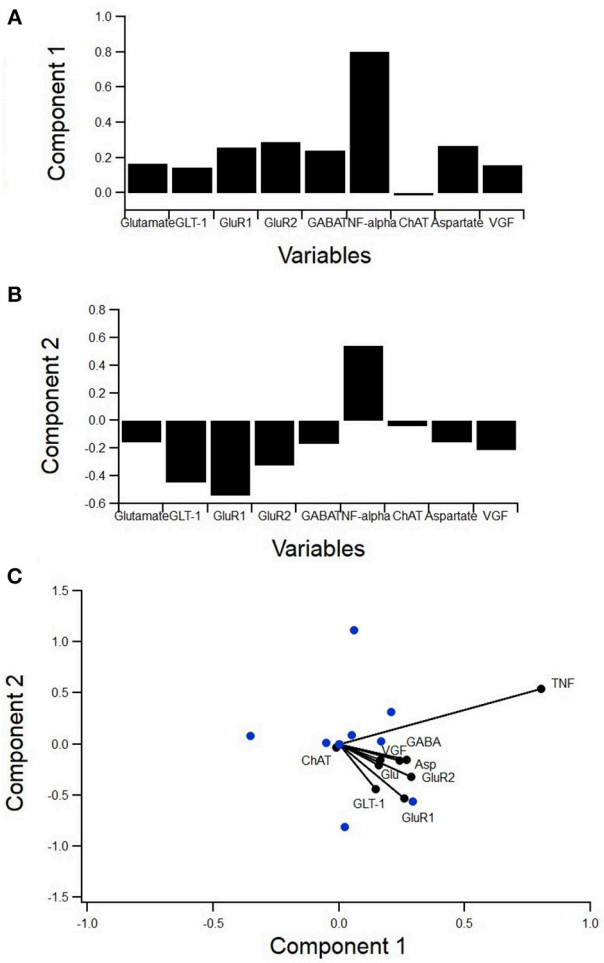

FIGURE 5 | PCA to determine variance contribution of non-inflammatory regulators of astrocytes. Biplot showing variable contributions to the first two PCA-determined components **(A)** broken down to the first two components and the comprising variables **(B,C)**. Component 1 accounted for 55% of the variance and was almost completely comprised of TNFα **(B)**. Component 2 accounted for 17% of the variance and was mostly comprised of GABA and aspartate **(C)**.

SOD1 G93A ALS mixed cell cultures. This would suggest that, if excitotoxicity is present, it could be due to the fact that ALS neurons and astrocytes have properties that make them simply more susceptible or sensitive to even small changes in neuromodulation. Thus, even small or seemingly insignificant oscillatory increases or decreases in neuromodulators, which could easily be rectified with compensatory regulation in normal cells, could potentially wreak havoc in ALS cells. In fact, as discussed in more detail in the Section Astrocyte GluR as a Potential Pre-onset ALS Treatment Target, motoneurons are mathematically and functionally more susceptible to such instability (Mitchell and Lee, 2012; Irvin et al., 2015). Other recent work has also illustrated that motoneuron microcircuits are more prone to homeostatic dysregulation (Brownstone and Lancelin, 2018). Given the large variance in experimental data, small changes that were statistically insignificant may actually

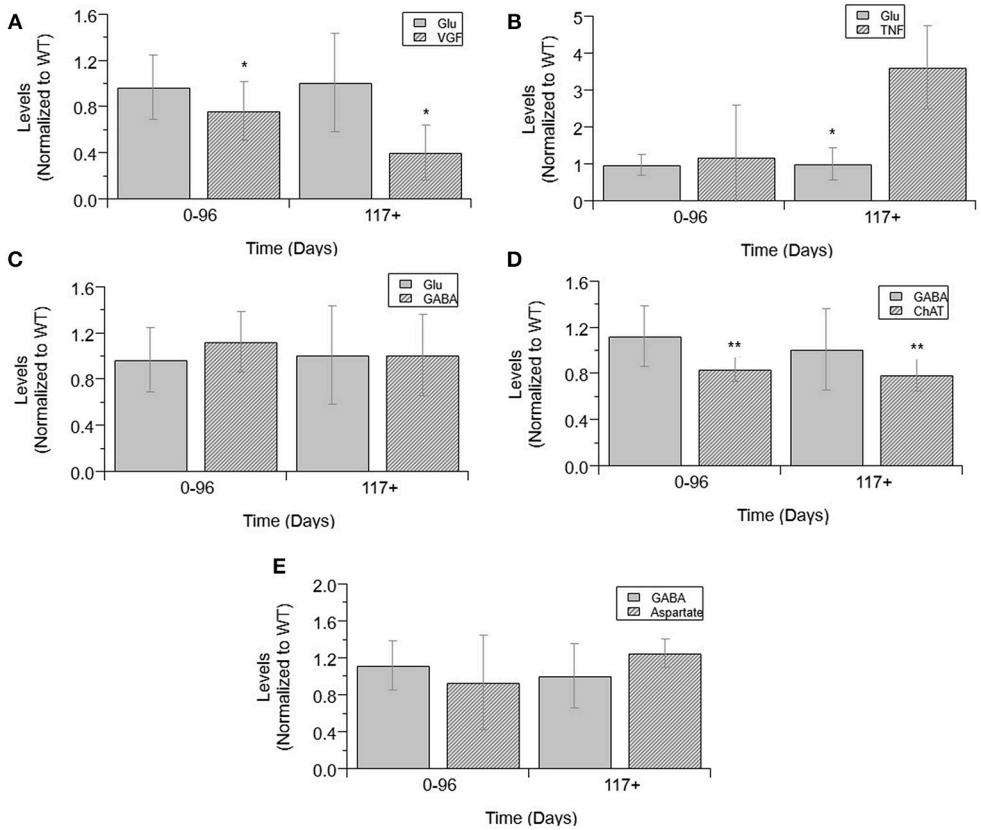

FIGURE 6 | Cytokine levels compared to glutamate and GABA levels in mixed cultures over ALS disease progression**.** VGF **(A)**, TNFα **(B)**, GABA **(C)**, and glutamate **(D)** averages normalized to wild-type (ratio presented as transgenic/WT) in three temporal stages: 0-96 days, 97-116 days, and 117+ days. ChAT activity **(D)**, aspartate **(E)**, and GABA average normalized to wild-type (ratio presented as transgenic/WT) in two temporal stages: 0–96 days and 117+ days, as insufficient data was available for 97–116 days. VGF levels were significantly decreased from glutamate levels at both stages (*$p < 0.05$). TNFα levels were significantly increased from glutamate levels at 117+ days (*$p = 0.0018$). GABA levels were significantly decreased from ChAT levels at 0–96 days (**$p = 0.0033$) and at 117+ days (**$p = 0.009$). Error bars represent SD.

be physiologically significant to ALS cells. If ALS cells are not able to sufficiently control their microenvironment, there could be spatial "pockets" or temporal phases of both hyperexcitability and hypoexcitability. This could mean that both hyperexcitability and hypoexcitability could co-exist in ALS, which could explain the discrepancies seen in previous literature.

Astrocyte GLT-1 as a Potential Post-onset ALS Treatment Target

Due to the modest success of Riluzole, a drug used to treat ALS that is thought to increase glutamate reuptake, there has been significant focus on finding ways to increase the reuptake of glutamate by astrocytes (Do-Ha et al., 2017). Additionally, post-mortem studies of ALS tissue and mice have found reduced levels of EAAT2 and GLT-1, respectively (Rothstein et al., 1995; Pardo et al., 2006). It is believed that decreased GLT-1 levels are contributing to the accumulation of extracellular glutamate and increasing the levels could help prevent the hyperexcitability of the motoneurons. Few experiments have had any notable success, however, due to the complex interaction and timing of the pathophysiology (Li et al., 2015). The present study found that GLT-1 levels only decrease significantly from post-onset to end-stage (**Figure 1B**). This finding suggests that increasing GLT-1 levels before ALS end-stage may increase glutamate reuptake, thereby prolonging survival or minimally prolonging muscle function after ALS onset.

If cell-specific or spatially localized excitation is present, extrinsically increasing GLT-1 levels before ALS end-stage may increase glutamate reuptake, thereby prolonging survival or minimally prolonging muscle function after ALS onset. Recent analysis has illustrated the potential impact of treatments that can increase patient quality of life by preserving muscle function for as long as possible even if corresponding survival increases are not dramatic. For example, similar metadata analysis of oxidative stress treatments in high copy SOD1-G93A ALS mice prolong limb muscle function by 59.6% but only prolong survival by 11.2% (Bond et al., 2018).

Astrocyte GluR as a Potential Pre-onset ALS Treatment Target

The influx of *Ca2+* caused by the overstimulation of motoneurons leads to cell death as *Ca2+* is involved in

many apoptotic pathways. The permeability of glutamate receptors is determined by GluR subunits. Glutamate receptors with GluR1 subunits are highly permeable to *Ca2+* and causes the mobilization of intracellular *Ca2+* when activated (D'antoni et al., 2011). GluR2 lacking glutamate receptors are highly permeable to *Ca2+* (Grosskreutz et al., 2010). Studies have shown that a lack of GluR2 increased motoneuron degeneration (Van Damme et al., 2005) in mice and increasing GluR2 levels in motoneurons prolonged survival of mice (Tateno et al., 2004). While decreased GluR2 levels were not observed in ALS mixed cultures in this study, there was a decrease in GluR1 levels at end-stage when compared to post-onset (**Figure 1C**), possibly from the high levels of cell death that have occurred by that point. Additionally, GluR1 is elevated from WT at post-onset, though this difference was not found to be significant, likely owing to small sample size. These findings suggest that reducing GluR1 levels in astrocytes at pre-onset, prior to their elevation post-onset, could reduce intracellular *Ca2+* levels and *Ca2+* dysregulation effects. Due to the limited number of data points available for intracellular *Ca2+* measured, the relationships of *Ca2+* and the GluR subunits were unable to be examined.

Of course, treatment at "pre-onset" in clinical terms would mean treatment in familial or genetic cases of ALS, referred to as FALS, where disease predisposition or the presence or pre-symptomatic ALS could be identified well before symptoms. Such a treatment is not realistic at this point because precise, reliable tests for explicit ALS identification [prior to symptom onset] are not yet available, even for FALS. The ability to identify more reliable biomarkers, genetic or otherwise, that predict future onset of ALS would open up the possibility of prophylactic treatment pre-onset. Such an approach would be similar to the familial amyloid-β treatments being tested prophylactically in a known Colombian family where genetic tests can predict with certainty who will get a very specific form of familial Alzheimer's Disease well before cognitive symptoms appear (Reardon, 2018). Early preclinical evidence illustrates that infamous amyloid-β treatments, when used alone, may require prophylactic treatment to be successful (Huber et al., 2018). While many FALS markers have been identified, albeit SOD1, C9orf72, or the even more rare mutations like FUS/TLS, VAPB, etc. (Ajroud-Driss and Siddique, 2015), no such marker has yet been identified that definitively, with great sensitivity and specificity, can pre-determine a future FALS onset.

Elucidating Etiology of *Ca2+* Increase in ALS

Measuring intracellular calcium can be very complicated. *Ca2+* transients are spatially localized within the astrocyte (Bazargani and Attwell, 2016). Due to methodological constraints, the full intracellular *Ca2+* store may not be found by simply looking at the soma, which complicates experimental *Ca2+* examination in astrocytes at the present time. Given the complications of local, spatial, and temporal *Ca2+* experimental examination, it is difficult to determine what mechanism is most directly related to the increases in *Ca2+* that have been previously identified in ALS (Irvin et al., 2015).

In healthy astrocytes, glutamate transporter activity leads to an increased entry of *Na+* as GLT-1 couples glutamate and *Na+* (Bazargani and Attwell, 2016). In addition to the *Na+*-*K+* ATPase pump, the *Na+*-*Ca2+* exchange provides a way for this *Na+* to exit while *Ca2+* enters. Therefore, an increase in glutamate uptake through GLT-1 activity can lead to increase in intracellular *Ca2+*. ALS astrocytes do not appear to increase glutamate uptake over disease progression and, consequently, do not increase intracellular *Ca2+* concentrations. Neurons, however, can become increasingly more susceptible to glutamate excitotoxicity over time and, thus, see a rise in intracellular *Ca2+*.

Interestingly, early pre-onset elevation of intracellular *Ca2+* in SOD1-G93A mixed cell cultures occurs without a concurrent increase in intracellular glutamate. Thus, the mechanisms causing failed astrocytic *Ca2+* regulation is not explicitly tied to glutamate. Exocytosis of GABA is, in part, dependent on the influx of *Ca2+* through voltage-gated calcium channels (VGCCs) (Sitges and Chiu, 1995). However, we found no increase in GABA in ALS preclinical model mixed cell cultures. Thus, unless there are localized changes in excitatory neurotransmitters that have not yet been experimentally measured, the increase in *Ca2+* appears to not be directly tied to changes in excitatory neurotransmitter balance—at least not in preclinical ALS mixed cell cultures analyzed in the present study. Interestingly, a recent study showed that clinical patients with the C9ORF72 mutation had motoneurons that were more vulnerable to *Ca2+* permeable AMPA receptors (Selvaraj et al., 2018).

Ca2+ increases could come from a variety of mechanisms beyond direct or significant changes in neuromodulatory transmission. As proposed in prior work (Mitchell and Lee, 2012; Mitchell et al., 2015b; Hollinger et al., 2016; Kim et al., 2016), failed homeostasis in nearly ten different major pathways could explain how a variety of different perturbations that result in ALS and identified homeostatic regulatory instability. *Ca2+* regulation is also greatly impacted by changes in energetic pathways (namely mitochondria and endoplasmic reticulum *Ca2+* stores) and oxidative stress (Bond et al., 2018), and to a lesser degree, by apoptotic signaling (Irvin et al., 2015).

Motoneurons are more prone to instability due to their long length (Mitchell and Lee, 2012), which requires transport and signaling over very long distances in the axon. Any delays or offset in signaling within cells or even between cells, such as between neurons and astrocytes, could contribute to oscillatory instability. The oscillations seen in CNS experimental data, and especially *Ca2+*, support the homeostatic instability theory (Irvin et al., 2015) of ALS. Given the very small margin of error for homeostatic regulation in motoneurons (Mitchell and Lee, 2012), localized examination of *Ca2+* with sufficient spatio-temporal resolution in the future could provide key evidence for experimentally confirming the contributions, or lack thereof, of neuromodulatory regulation mechanisms in neurons and astrocytes.

Puzzling Non-correlation Between Calcium-Permeable GluR1 and TNFα

In general, TNFα production and secretion is believed to be highly dependent upon calcium levels (Watanabe et al., 1996). One mechanism proposed for TNFα-induced neuron death is through the rapid TNFα-induced surface expression changes of AMPA-type glutamate receptors, such as GluR1 (Ferguson

et al., 2008). Dysregulation of glutamate receptor trafficking can alter neuronal calcium permeability and contribute to excitotoxic vulnerability (Olmos and Llado, 2014; Kia et al., 2018).

Therefore, the lack of a statistically significant relationship between TNFα and GluR1 levels in SOD1-G93A mixed cultures was unexpected (**Figure 6**). Moreover, the PCA (**Figure 5A**) showed TNFα and GluR1 levels to be practically decoupled given TNFα is almost orthogonal to GluR1 on the biplot (**Figure 5A**), which also indicates a lack of relationship.

Of course, TNFα has a complex relationship with many cellular processes. It could be that the data variance identified and imparted by TNFα in the PCA is more related to its other roles, including inflammation, synaptic function, and especially caspase-8 initiated apoptosis (Kia et al., 2018). On a more detailed level, TNFα and NF-κB have been shown to participate in oscillatory positive feedback loops wherein NF-κB can regulate TNFα transcription. This process plays a key role in regulating inflammatory responses across a variety of cell types, and has been found to be central in the FUS mutation of ALS (Pekalski et al., 2013) as well as other neurodegenerative diseases. Another possible role of TNFα could be its relationship with glial derived neurotrophic factor, GDNF. Recent work has shown that TNFα contributes to rises in astrocytic GDNF that have a protective effect on neuron damage (Brambilla et al., 2016); in fact, the TNFα –GDNF mechanism is currently being sought as a potential therapeutic target. Most recently, astrocytes in the ALS FUS model were shown to induce motoneuron death directly via the release of TNFα (Kia et al., 2018).

Thus, while more research is necessary to examine the puzzling lack of relationship seen between TNFα and GluR1 levels, it appears both GluR1 and TNFα are each having an impact on ALS pathology, but the direct relationship between TNFα and GluR1 is simply not substantial in SOD1-G93A ALS mixed cell cultures.

Aspartate Increases Near End-Stage

Aspartate is another excitatory neurotransmitter, similar to glutamate, that is found in the brain. In the present metadata analysis of preclinical ALS mixed cell cultures, the aspartate increase is not seen until end-stage. This supports the finding of normal or slightly decreased aspartate levels in cerebral spinal fluid serum of ALS patients with a mild disease course (Niebroj-Dobosz and Janik, 1999). In severely progressing patients, aspartate levels were increased, and GABA levels were normal or increased. When the imbalance of these amino acids favors the excitatory over the inhibitory, it appears to contribute to a more rapid decline in survival.

Failed Regulation Could Contribute to Spatial Spread of ALS

An important characteristic of ALS is the spread of motoneuron degeneration and corresponding cell death. Recent research has found that transplanting familial ALS astrocytes into healthy mice causes ALS-like degeneration in non-specific healthy neurons (Qian et al., 2017). The spread has been partially attributed to a prion-like mechanism (Grad et al., 2015). More research is needed to better understand the mechanistic etiology of the spread of ALS. Nonetheless, one of the most prominent theories has been related to excitotoxic spillover. For example, gliotransmitters, such as increased glutamate or decreased GABA, can propagate the rise of intracellular calcium levels in astrocytes and adjacent neurons. Glutamate can be released from astrocytes through *Ca2*+-activated bestrophin-1 anion channels. Changes in intracellular calcium levels in astrocytes can also affect the activity of membrane transporters, such as GluRs (Bazargani and Attwell, 2016). Yet, in the present metadata analysis in preclinical ALS mixed cell cultures, we did not see glaring evidence of severe excitotoxic spillover in preclinical ALS mixed cell cultures, as key excitatory (glutamate) and inhibitory transmitters (GABA) were not elevated. However, the identified decrease in inhibitory GLT-1 and increase of excitatory aspartate that occurs with disease progression does suggest there is at least a mild form of neuromodulatory regulation, or lack thereof, that is contributing to ALS etiology. Additionally, the presented analysis does illustrate potential evidence of upregulation, spillover or spread of other chemokines, especially TNFα. Dysregulated or delayed neuromodulator regulatory signaling between neurons and astrocytes should be further explored in future experimental work; evidence of dysregulation could be subtler than what is typically seen with primary excitotoxicity but could nonetheless help to explain the underlying "spread" mechanism(s) of ALS.

Other Non-inflammatory Functions of Astrocytes

ALS-causing genes are also linked to lipid homeostasis, glucose homeostasis, mitochondrial formation, ATP production, and other metabolic functions (Ngo and Steyn, 2015). Extracellular concentrations of ATP in the CNS regulate activation and migration of immune and glial cells and increase in response to trauma and inflammation (Gandelman et al., 2010). In astrocytes, it can cause pro-inflammatory signaling which causes an increased production of nitric oxide and various chemokines (Gandelman et al., 2010). It has been found that G93A astrocytes degrade ATP at a faster rate than non-transgenic astrocytes and display ATP-dependent proliferation. It has also been shown that high extracellular concentrations of ATP can cause non-transgenic astrocytes to induce motoneuron death (Gandelman et al., 2010). Evidence shows that a complicated cycle of bioenergetic deficits may worsen disease progression over time (Ngo and Steyn, 2015). An analysis of extracellular ATP was not completed as part of this study due to lack of data meeting inclusion criteria. However, a similar analysis of ATP in the CNS shows deficiency throughout the SOD1-G93A ALS life span (Irvin et al., 2015). Like glutamate, the temporal trends of metabolic homeostasis need to be determined to identify the most effective time for potential therapeutic intervention.

LIMITATIONS

The biggest limitations to any metadata analysis is the ability to aggregate data sources in a way that sufficiently increases sample size but not so aggregated that group definitions are too diverse to provide meaningful insight. The adage of "apples to

apples" and "apples to oranges" is a good analogy for metadata analysis. To carry this analogy into an easy to understand example, a specific metadata analysis group defined as "apples" must literally include all apples, although different individual apples in the group may look slightly different (red, green, yellow, etc.). Transitioning to the present work, "glutamate," for example, include metrics that are slightly different: acutely released glutamate (Milanese et al., 2011; Albano et al., 2013; etc.), steady state extracellular measurements of glutamate (Alexander et al., 2000), whole brain MRI levels of glutamate (Niessen et al., 2007; Choi et al., 2009, etc.), among many other slight variations of direct or indirect glutamate measurement, which are contained within the "glutamate" data aggregate as shown in **Table 2** and the **Supplementary Data Sheet**. It would be preferable to have more specifically defined groups based on different glutamate locations, functions, and/or experimental methodology. However, the number of available studies and their corresponding heterogeneity does not allow more specifically defined sub-groups at the time of this writing; there simply would not be enough statistical power. Thus, the present work utilized more generalized groupings and aggregation schemes (see Methods) that met the standardized criteria and statistical power required by metadata analysis. Nonetheless, this study's presented results still provide new high-level insights as to which of the different biomedical concepts are impacting astrocyte-mediated ALS neuromodulatory regulation over the course of ALS disease progression. Such high-level insight helps researchers to better synthesize complex interactions as well as assess and prioritize biomedical concept research aimed at improving diagnostics, prognostics, and therapeutics. It is an acknowledged limitation that many more data sources are needed to construct narrow aggregate definitions that enable very specific mechanistic hypotheses to be confirmed.

AUTHOR CONTRIBUTIONS

KJ: data collection, statistical analysis, results interpretation, drafting of initial manuscript, critical review of content; JM: data collection, results interpretation, critical review of content; AS: data collection, statistical analysis, critical review of content; CM: framing of study, project oversight, results interpretation, drafting of final manuscript, critical review of content.

FUNDING

Financial support provided by National Institute of Health grant NS069616, NS081426, and NS098228 to CM.

SUPPLEMENTARY MATERIAL

The Supplementary Material for this article can be found online at: https://www.frontiersin.org/articles/10.3389/fncel.2018.00491/full#supplementary-material

REFERENCES

Ajroud-Driss, S., and Siddique, T. (2015). Sporadic and hereditary amyotrophic lateral sclerosis (ALS). *Biochim Biophys Acta* 1852, 679–684. doi: 10.1016/j.bbadis.2014.08.010

Albano, R., Liu, X., and Lobner, D. (2013). Regulation of system x(c)- in the SOD1-G93A mouse model of ALS. *Exp. Neurol.* 250, 69–73. doi: 10.1016/j.expneurol.2013.09.008

Alexander, G. M., Deitch, J. S., Seeburger, J. L., Valle, L. D., and Heiman-Patterson, T. D. (2000). Elevated cortical extracellular fluid glutamate in transgenic mice expressing human mutant (G93A) Cu/Zn superoxide dismutase. *J. Neurochem.* 74, 1666–1673. doi: 10.1046/j.1471-4159.2000.0741666.x

Appel, S. H., Beers, D., Siklos, L., Engelhardt, J. I., and Mosier, D. R. (2001). Calcium: the darth vader of ALS. *Amyotroph. Lateral Scler. Other Motor Neuron Disord.* 2 (Suppl. 1), S47–54. doi: 10.1080/14660820152415744

Bak, L. K., Schousboe, A., and Waagepetersen, H. S. (2006). The glutamate/GABA-glutamine cycle: aspects of transport, neurotransmitter homeostasis, and ammonia transfer. *J. Neurochem.* 98, 641–653. doi: 10.1111/j.1471-4159.2006.03913.x

Bazargani, N., and Attwell, D. (2016). Astrocyte calcium signaling: the third wave. *Nat. Neurosci.* 19, 182–189. doi: 10.1038/nn.4201

Bendotti, C., Tortarolo, M., Suchak, S. K., Calvaresi, N., Carvelli, L., Bastone, A., et al. (2001). Transgenic SOD1 G93A mice develop reduced GLT-1 in spinal cord without alterations in cerebrospinal fluid glutamate levels. *J. Neurochem.* 79, 737–746. doi: 10.1046/j.1471-4159.2001.00572.x

Benkler, C., Ben-Zur, T., Barhum, Y., and Offen, D. (2013). Altered astrocytic response to activation in SOD1(G93A) mice and its implications on amyotrophic lateral sclerosis pathogenesis. *Glia* 61, 312–326. doi: 10.1002/glia.22428

Bond, L., Bernhardt, K., Madria, P., Sorrentino, K., Scelsi, H., and Mitchell, C. S. (2018). A metadata analysis of oxidative stress etiology in preclinical amyotrophic lateral sclerosis: benefits of antioxidant therapy. *Front. Neurosci.* 12:10. doi: 10.3389/fnins.2018.00010

Boston-Howes, W., Gibb, S. L., Williams, E. O., Pasinelli, P., Brown, R. H. Jr., and Trotti, D. (2006). Caspase-3 cleaves and inactivates the glutamate transporter EAAT2. *J. Biol. Chem* 281, 14076–14084. doi: 10.1074/jbc.M600653200

Brambilla, L., Guidotti, G., Martorana, F., Iyer, A. M., Aronica, E., Valori, C. F., et al. (2016). Disruption of the astrocytic TNFR1-GDNF axis accelerates motor neuron degeneration and disease progression in amyotrophic lateral sclerosis. *Hum. Mol. Genet.* 25, 3080–3095. doi: 10.1093/hmg/ddw161

Brockington, A., Ning, K., Heath, P. R., Wood, E., Kirby, J., Fusi, N., et al. (2013). Unravelling the enigma of selective vulnerability in neurodegeneration: motor neurons resistant to degeneration in ALS show distinct gene expression characteristics and decreased susceptibility to excitotoxicity. *Acta Neuropathol.* 125, 95–109. doi: 10.1007/s00401-012-1058-5

Brownstone, R. M., and Lancelin, C. (2018). Escape from homeostasis: spinal microcircuits and progression of amyotrophic lateral sclerosis. *J Neurophysiol.* 119, 1782–1794. doi: 10.1152/jn.00331.2017

Cai, M., Choi, S. M., and Yang, E. J. (2015). The effects of bee venom acupuncture on the central nervous system and muscle in an animal hSOD1G93A mutant. *Toxins* 7, 846–858. doi: 10.3390/toxins7030846

Caioli, S., Curcio, L., Pieri, M., Antonini, A., Marolda, R., Severini, C., et al. (2011). Substance P receptor activation induces downregulation of the AMPA receptor functionality in cortical neurons from a genetic model of amyotrophic lateral sclerosis. *Neurobiol. Dis.* 44, 92–101. doi: 10.1016/j.nbd.2011.06.008

Caioli, S., Pieri, M., Antonini, A., Guglielmotti, A., Severini, C., and Zona, C. (2013). Monocyte Chemoattractant Protein-1 upregulates GABA-induced current: evidence of modified GABAA subunit composition in cortical neurons from the G93A mouse model of Amyotrophic Lateral Sclerosis. *Neuropharm* 73, 247–260. doi: 10.1016/j.neuropharm.2013.05.045

Chen, L. C., Smith, A., Ben, Y., Zukic, B., Ignacio, S., Moore, D., et al. (2004). Temporal gene expression patterns in G93A/SOD1 mouse.

Amyotroph. Lateral. Scler. Other Motor Neuron Disord. 5, 164–171. doi: 10.1080/14660820410017091

Choi, J., Kustermann, E., Dedeoglu, A., and Jenkins, B. G. (2009). Magnetic resonance spectroscopy of regional brain metabolite markers in fals mice and the effects of dietary creatine supplementation. *Eur. J. Neurosci*. 30, 2143–2150. doi: 10.1111/j.1460-9568.2009.07015.x

Crochemore, C., Pena-Altamira, E., Virgili, M., Monti, B., and Contestabile, A. (2005). Disease-related regressive alterations of forebrain cholinergic system in SOD1 mutant transgenic mice. *Neurochem Int*. 46, 357–368. doi: 10.1016/j.neuint.2004.12.004

Crochemore, C., Virgili, M., Bonamassa, B., Canistro, D., Pena-Altamira, E., Paolini, M., et al. (2009). Long-term dietary administration of valproic acid does not affect, while retinoic acid decreases, the lifespan of G93A mice, a model for amyotrophic lateral sclerosis. *Muscle Nerve* 39, 548–552. doi: 10.1002/mus.21260

D'antoni, S., Berretta, A., Seminara, G., Longone, P., Giuffrida-Stella, A. M., Battaglia, G., et al. (2011). A prolonged pharmacological blockade of type-5 metabotropic glutamate receptors protects cultured spinal cord motor neurons against excitotoxic death. *Neurobiol. Dis*. 42, 252–264. doi: 10.1016/j.nbd.2011.01.013

Deitch, J. S., Alexander, G. M., Del Valle, L., and Heiman-Patterson, T. D. (2002). GLT-1 glutamate transporter levels are unchanged in mice expressing G93A human mutant SOD1. *J. Neurol. Sci.* 193, 117–126. doi: 10.1016/S0022-510X(01)00656-6

Diana, A., Pillai, R., Bongioanni, P., O'Keeffe, A. G., Miller, R. G., and Moore, D. H. (2017). Gamma aminobutyric acid (GABA) modulators for amyotrophic lateral sclerosis/motor neuron disease. *Cochrane Database Syst. Rev.* 1:CD006049. doi: 10.1002/14651858.CD006049.pub2

Do-Ha, D., Buskila, Y., and Ooi, L. (2017). Impairments in motor neurons, interneurons and astrocytes contribute to hyperexcitability in als: underlying mechanisms and paths to therapy. *Mol. Neurobiol*. 55, 1410–1418. doi: 10.1007/s12035-017-0392-y

Fang, L., Teuchert, M., Huber-Abel, F., Schattauer, D., Hendrich, C., Dorst, J., et al. (2010). MMP-2 and MMP-9 are elevated in spinal cord and skin in a mouse model of ALS. *J. Neurol. Sci*. 294, 51–56. doi: 10.1016/j.jns.2010.04.005

Fergani, A., Eschbach, J., Oudart, H., Larmet, Y., Schwalenstocker, B., Ludolph, A. C., et al. (2011). A mutation in the dynein heavy chain gene compensates for energy deficit of mutant SOD1 mice and increases potentially neuroprotective IGF-1. *Mol. Neurodegener*. 6:26. doi: 10.1186/1750-1326-6-26

Ferguson, A. R., Christensen, R. N., Gensel, J. C., Miller, B. A., Sun, F., Beattie, E. C., et al. (2008). Cell death after spinal cord injury is exacerbated by rapid TNF alpha-induced trafficking of GluR2-lacking AMPARs to the plasma membrane. *J. Neurosci*. 28, 11391–11400. doi: 10.1523/JNEUROSCI.3708-08.2008

Fernández, M., Sanchez-Franco, F., Palacios, N., Sanchez, I., Fernandez, C., and Cacicedo, L. (2004). IGF-I inhibits apoptosis through the activation of the phosphatidylinositol 3-kinase/Akt pathway in pituitary cells. *J. Mol. Endocrinol*. 33, 155–163. doi: 10.1677/jme.0.0330155

Gandelman, M., Peluffo, H., Beckman, J. S., Cassina, P., and Barbeito, L. (2010). Extracellular ATP and the P2X7 receptor in astrocyte-mediated motor neuron death: implications for amyotrophic lateral sclerosis. *J. Neuroinflam*. 7, 33–33. doi: 10.1186/1742-2094-7-33

Grad, L. I., Fernando, S. M., and Cashman, N. R. (2015). From molecule to molecule and cell to cell: prion-like mechanisms in amyotrophic lateral sclerosis. *Neurobiol. Dis*. 77, 257–265. doi: 10.1016/j.nbd.2015.02.009

Grosskreutz, J., Van Den Bosch, L., and Keller, B. U. (2010). Calcium dysregulation in amyotrophic lateral sclerosis. *Cell Calcium* 47, 165–174. doi: 10.1016/j.ceca.2009.12.002

Gu, R., Hou, X., Pang, R., Li, L., Chen, F., Geng, J., et al. (2010). Human adipose-derived stem cells enhance the glutamate uptake function of GLT1 in SOD1 G93A-bearing astrocytes. *Biochem. Biophys. Res. Commun*. 393, 481–486. doi: 10.1016/j.bbrc.2010.02.029

Guerra-Gomes, S., Sousa, N., Pinto, L., and Oliveira, J. F. (2018). Functional roles of astrocyte calcium elevations: from synapses to behavior. *Front. Cell Neurosci*. 11:427. doi: 10.3389/fncel.2017.00427

Guo, H., Lai, L., Butchbach, M. E., Stockinger, M. P., Shan, X., Bishop, G. A., et al. (2003). Increased expression of the glial glutamate transporter EAAT2 modulates excitotoxicity and delays the onset but not the outcome of ALS in mice. *Hum Mol Genet*. 12, 2519–2532. doi: 10.1093/hmg/ddg267

Guo, Z., Kindy, M. S., Kruman, I., and Mattson, M. P. (2000). ALS-Linked Cu/Zn-SOD Mutation impairs cerebral synaptic glucose and glutamate transport and exacerbates ischemic brain injury. *J. Cereb. Blood. Flow Metab*. 20, 463–468. doi: 10.1097/00004647-200003000-00004

Hollinger, S. K., Okosun, I. S., and Mitchell, C. S. (2016). Antecedent disease and amyotrophic lateral sclerosis: what is protecting whom? *Front. Neurol*. 7:47. doi: 10.3389/fneur.2016.00047

Hossaini, M., Cano, S. C., van Dis, V., Haasdijk, E. D., Hoogenraad, C. C., Holstege, J. C., et al. (2011). Spinal inhibitory interneuron pathology follows motor neuron degeneration independent of glial mutant superoxide dismutase 1 expression in SOD1-ALS mice. *J. Neuropath. Exp. Neurol*. 70, 662–677. doi: 10.1097/NEN.0b013e31822581ac

Huber, C. M., Yee, C., May, T., Dhanala, A., and Mitchell, C. S. (2018). Cognitive decline in preclinical alzheimer's disease: amyloid-beta versus tauopathy. *J. Alz. Dis*. 61, 265–281. doi: 10.3233/JAD-170490

Irvin, C. W., Kim, R. B., and Mitchell, C. S. (2015). Seeking homeostasis: temporal trends in respiration, oxidation, and calcium in SOD1 G93A amyotrophic lateral sclerosis mice. *Front. Cell Neurosci*. 9, 248. doi: 10.3389/fncel.2015.00248

Jeyachandran, A., Mertens, B., Mckissick, E. A., and Mitchell, C. S. (2015). Type I Vs. Type II cytokine levels as a function of SOD1 G93A mouse amyotrophic lateral sclerosis disease progression. *Front. Cell Neurosci*. 9:462. doi: 10.3389/fncel.2015.00462

Jiang, M. C., Adimula, A., Birch, D., and Heckman, C. J. (2017). Hyperexcitability in synaptic and firing activities of spinal motoneurons in an adult mouse model of amyotrophic lateral sclerosis. *Neuroscience* 362:33–46. doi: 10.1016/j.neuroscience.2017.08.041

Kalmar, B., Edet-Amana, E., and Greensmith, L. (2012). Treatment with a coinducer of the heat shock response delays muscle denervation in the SOD1-G93A mouse model of amyotrophic lateral sclerosis. *Amyotroph. Lateral. Sclerosis* 13, 378–392. doi: 10.3109/17482968.2012.660953

Kandinov, B., Grigoriadis, N. C., Touloumi, O., Drory, V. E., Offen, D., and Korczyn, A. D. (2013). Immunohistochemical analysis of sympathetic involvement in the SOD1-G93A transgenic mouse model of amyotrophic lateral sclerosis. *Amyotroph. Lateral. Scler. Frontotemporal. Degener*. 14, 424–433. doi: 10.3109/21678421.2013.780622

Kaspar, B. K., Frost, L. M., Christian, L., Umapathi, P., and Gage, F. H. (2005). Synergy of insulin-like growth factor-1 and exercise in amyotrophic lateral sclerosis. *Ann. Neurol*. 57, 649–655. doi: 10.1002/ana.20451

Kawamata, H., and Manfredi, G. (2010). Mitochondrial dysfunction and intracellular calcium dysregulation in ALS. *Mech. Aging Develop*. 131, 517–526. doi: 10.1016/j.mad.2010.05.003

Kawamata, H., Ng, S. K., Diaz, N., Burstein, S., Morel, L., Osgood, A., et al. (2014). Abnormal intracellular calcium signaling and SNARE-dependent exocytosis contributes to SOD1G93A astrocyte-mediated toxicity in amyotrophic lateral sclerosis. *J. Neurosci*. 34, 2331–2348. doi: 10.1523/JNEUROSCI.2689-13.2014

Khamankar, N., Coan, G., Weaver, B., and Mitchell, C. S. (2018). Associative increases in amyotrophic lateral sclerosis survival duration with non-invasive ventilation initiation and usage protocols. *Front. Neurol*. 9, 578. doi: 10.3389/fneur.2018.00578

Kia, A., Mcavoy, K., Krishnamurthy, K., Trotti, D., and Pasinelli, P. (2018). Astrocytes expressing ALS-linked mutant FUS induce motor neuron death through release of tumor necrosis factor-alpha. *Glia* 66, 1016–1033. doi: 10.1002/glia.23298

Kim, R. B., Irvin, C. W., Tilva, K. R., and Mitchell, C. S. (2016). State of the field: An informatics-based systematic review of the SOD1-G93A amyotrophic lateral sclerosis transgenic mouse model. *Amyotroph. Lateral. Scler. Frontotemporal. Degener*. 17, 1–14. doi: 10.3109/21678421.2015.1047455

Lee, J. K., Shin, J. H., Gwag, B. J., and Choi, E. J. (2015). Iron accumulation promotes TACE-mediated TNF-alpha secretion and neurodegeneration in a mouse model of ALS. *Neurobiol. Dis*. 80, 63–69. doi: 10.1016/j.nbd.2015.05.009

Leroy, F., and Zytnicki, D. (2015). Is hyperexcitability really guilty in amyotrophic lateral sclerosis?. *Neural Regen Res*. 10, 1413–1415 doi: 10.4103/1673-5374.165308

Li, K., Hala, T. J., Seetharam, S., Poulsen, D. J., Wright, M. C., and Lepore, A. C. (2015). GLT1 overexpression in SOD1G93A mouse cervical spinal cord does not preserve diaphragm function or extend disease. *Neurobiol. Dis*. 78, 12–23. doi: 10.1016/j.nbd.2015.03.010

Lin, C.-L. G., Kong, Q., Cuny, G. D., and Glicksman, M. A. (2013). Glutamate transporter EAAT2: a new target for the treatment of neurodegenerative diseases. *Future Med. Chem*. 4, 1689–1700. doi: 10.4155/fmc.12.122

Martinez, J. A., Francis, G. J., Liu, W. Q., Pradzinsky, N., Fine, J., Wilson, M., et al. (2008). Intranasal delivery of insulin and a nitric oxide synthase inhibitor in an experimental model of amyotrophic lateral sclerosis. *Neuroscience* 157, 908–925. doi: 10.1016/j.neuroscience.2008.08.073

Martínez-Silva, M. L., Imhoff-Manuel, R. D., Sharma, A., Heckman, C. J., Shneider, N. A., Roselli, F., et al. (2018). Hypoexcitability precedes denervation in the large fast-contracting motor units in two unrelated mouse models of ALS. *Elife*. 7:e30955. doi: 10.7554/elife.30955

Messi, M. L., Clark, H. M., Prevette, D. M., Oppenheim, R. W., and Delbono, O. (2007). The lack of effect of specific overexpression of IGF-1 in the central nervous system or skeletal muscle on pathophysiology in the G93A SOD-1 mouse model of ALS. *Exper. Neurol*. 207, 52–63. doi: 10.1016/j.expneurol.2007.05.016

Milanese, M., Zappettini, S., Onofri, F., Musazzi, L., Tardito, D., Bonifacino, T., et al. (2011). Abnormal exocytotic release of glutamate in a mouse model of amyotrophic lateral sclerosis. *J. Neurochem*. 116, 1028–1042. doi: 10.1111/j.1471-4159.2010.07155.x

Mitchell, C. S., Cates, A., Kim, R. B., and Hollinger, S. K. (2015a). Undergraduate biocuration: developing tomorrow's researchers while mining today's data. *J. Undergrad. Neurosci. Educ.* 14, A56–A65.

Mitchell, C. S., Hollinger, S. K., Goswami, S. D., Polak, M. A., Lee, R. H., and Glass, J. D. (2015b). Antecedent disease is less prevalent in amyotrophic lateral sclerosis. *Neurodegener. Dis*. 15, 109–113. doi: 10.1159/000369812

Mitchell, C. S., and Lee, R. H. (2008). Pathology dynamics predict spinal cord injury therapeutic success. *J. Neurotrauma*. 25, 1483–1497. doi: 10.1089/neu.2008.0658

Mitchell, C. S., and Lee, R. H. (2012). "Dynamic meta-analysis as a therapeutic prediction tool for amyotrophic lateral sclerosis," *in Amyotrophic Lateral Sclerosis*, ed. M. Maurer (Intech), 59–80. doi: 10.5772/32384

Morel, L., Regan, M., Higashimori, H., Ng, S. K., Esau, C., Vidensky, S., et al. (2013). Neuronal exosomal miRNA-dependent translational regulation of astroglial glutamate transporter GLT1. *J. Biol. Chem*. 8, 7105–7116. doi: 10.1074/jbc.M112.410944

Ngo, S. T., and Steyn, F. J. (2015). The interplay between metabolic homeostasis and neurodegeneration: insights into the neurometabolic nature of amyotrophic lateral sclerosis. *Cell Regen* . 4:5. doi: 10.1186/s13619-015-0019-6

Niebroj-Dobosz, I., and Janik, P. (1999). Amino acids acting as transmitters in amyotrophic lateral sclerosis (ALS). *Acta Neurol. Scand*. 100, 6–11. doi: 10.1111/j.1600-0404.1999.tb00717.x

Niessen, H. G., Debska-Vielhaber, G., Sander, K., Angenstein, F., Ludolph, A. C., Hilfert, L., et al. (2007). Metabolic progression markers of neurodegeneration in the transgenic G93A-SOD1 mouse model of amyotrophic lateral sclerosis. *Eur. J. Neurosci*. 25, 1669–1677. doi: 10.1111/j.1460-9568.2007.05415.x

Nihei, K., McKee, A. C., and Kowall, N. W. (1993). Patterns of neuronal degeneration in the motor cortex of amyotrophic lateral sclerosis patients. *Acta Neuropathologica* 86, 55–64. doi: 10.1007/BF00454899

Norenberg, M. D., and Martinez-hernandez, A. (1979). Fine structural localization of glutamine synthase in astrocytes of rat brains. *Brain Res*. 161, 303–310. doi: 10.1016/0006-8993(79)90071-4

Olmos, G., and Llado, J. (2014). Tumor necrosis factor alpha: a link between neuroinflammation and excitotoxicity. *Mediators Inflamm*. 2014:861231. doi: 10.1155/2014/861231

Palmieri, L., Pardo, B., Lasorsa, F. M., Del Arco, A., Kobayashi, K., Iijima, M., et al. (2001). Citrin and aralar1 are Ca(2+)-stimulated aspartate/glutamate transporters in mitochondria. *EMBO J*. 20, 5060–5069. doi: 10.1093/emboj/20.18.5060

Pardo, A. C., Wong, V., Benson, L. M., Dykes, M., Tanaka, K., Rothstein, J. D., et al. (2006). Loss of the astrocyte glutamate transporter GLT1 modifies disease in SOD1 G93A mice. *Exper. Neurol*. 201, 120–130. doi: 10.1016/j.expneurol.2006.03.028

Pehar, M., Harlan, B. A., Killoy, K. M., and Vargas, M. R. (2017). *Role and Therapeutic Potential of Astrocytes in Amyotrophic Lateral Sclerosis. Curr. Pharm. Des*. 23, 5010–5021. doi: 10.2174/1381612823666170622095802

Pekalski, J., Zuk, P. J., Kochanczyk, M., Junkin, M., Kellogg, R., Tay, S., et al. (2013). Spontaneous NF-kappaB activation by autocrine TNFalpha signaling: a computational analysis. *PLoS ONE* 8:e78887. doi: 10.1371/journal.pone.0078887

Petri, S., Schmalbach, S., Grosskreutz, J., Krampfl, K., Grothe, C., Dengler, R., et al. (2005). The cellular mRNA expression of GABA and glutamate receptors in spinal motor neurons of SOD1 mice. *J. Neurol. Sci*. 238, 25–30. doi: 10.1016/j.jns.2005.06.005

Pfohl, S. R., Halicek, M. T., and Mitchell, C. S. (2015). Characterization of the contribution of genetic background and gender to disease progression in the SOD1 G93A mouse model of amyotrophic lateral sclerosis: a meta-analysis. *J. Neuromuscul. Dis*. 2, 137–150. doi: 10.3233/JND-140068

Pfohl, S. R., Kim, R. B., Coan, G. S., and Mitchell, C. S. (2018). Unraveling the complexity of amyotrophic lateral sclerosis survival prediction. *Front. Neuroinform*. 12:36. doi: 10.3389/fninf.2018.00036

Qian, K., Huang, H., Peterson, A., Hu, B., Maragakis, N. J., Ming, G. L., et al. (2017). Sporadic ALS astrocytes induce neuronal degeneration *in vivo*. *Stem Cell Rep*. 8, 843–855. doi: 10.1016/j.stemcr.2017.03.003

Raiteri, L., Stigliani, S., Zappettini, S., Mercuri, N. B., Raiteri, M., and Bonanno, G. (2004). Excessive and precocious glutamate release in a mouse model of amyotrophic lateral sclerosis. *Neuropharm* 46, 782–792. doi: 10.1016/j.neuropharm.2003.11.025

Reardon, S. (2018). Pioneering Alzheimer's study in Colombia zeroes in on enigmatic protein. *Nature* 555, 567–568. doi: 10.1038/d41586-018-03848-4

Rosenblum, L. T., and Trotti, D. (2017). EAAT2 and the molecular signature of amyotrophic lateral sclerosis. *Adv. Neurobiol*. 16, 117–136. doi: 10.1007/978-3-319-55769-4_6

Rossi, D., and Volterra, A. (2009). Astrocytic dysfunction: insights on the role in neurodegeneration. *Brain Res. Bull*. 80, 224–232. doi: 10.1016/j.brainresbull.2009.07.012

Rothstein, J. D., Patel, S., Regan, M. R., Haenggeli, C., Huang, Y. H., Bergles, D. E., et al. (2005). Beta-lactam antibiotics offer neuroprotection by increasing glutamate transporter expression. *Nature* 433, 73–77. doi: 10.1038/nature03180

Rothstein, J. D., Tsai, G., Kunci, R. W., Clawson, L., Conblath, D. B., Pestronk, A., et al. (1990). Abnormal excitatory amino acid metabolism in amytrophic lateral sclerosis. *Ann. Neruol*. 28, 18–25. doi: 10.1002/ana.410280106

Rothstein, J. D., Van Kammen, M., Levey, A. I., Martin, L. J., and Kuncl, R. W. (1995). Selective loss of glial glutamate transporter GLT-1 in amyotrophic lateral sclerosis. *Ann. Neurol*. 38, 73–84. doi: 10.1002/ana.410380114

Selvaraj, B. T., Livesey, M. R., Zhao, C., Gregory, J. M., James, O., Cleary, E. M., et al. (2018). C9ORF72 repeat expansion causes vulnerability of motor neurons to Ca2+-permeable AMPA receptor-mediated excitotoxicity. *Nat Commun*. 9:347. doi: 10.1038/s41467-017-02729-0

Sitges, M., and Chiu, L. M. (1995). Characterization of the type of calcium channel primarily regulating GABA exocytosis from brain nerve endings. *Neurochem. Res*. 20, 1073–1088. doi: 10.1007/BF00995562

Sofroniew, M. V., and Vinters, H. V. (2010). Astrocytes: biology and pathology. *Acta Neuropathologica*. 119, 7–35. doi: 10.1007/s00401-009-0619-8

Song, L., Gao, Y., Zhang, X., and Le, W. (2013). Galactooligosaccharide improves the animal survival and alleviates motor neuron death in SOD1G93A mouse model of amyotrophic lateral sclerosis. *Neuroscience* 246, 281–290. doi: 10.1016/j.neuroscience.2013.05.002

Spalloni, A., Geracitano, R., Berretta, N., Sgobio, C., Bernardi, G., Mercuri, N. B., et al. (2006). Molecular and synaptic changes in the hippocampus underlying superior spatial abilities in pre-symptomatic G93A+/+ mice overexpressing the human Cu/Zn superoxide dismutase (Gly93 –> ALA) mutation. *Exp. Neurol*. 197, 505–514. doi: 10.1016/j.expneurol.2005.10.014

Staat, K. A., and Van Den Bosch, L. (2009). Astrocytes in amytrophic lateral sclerosis: direct effects on motor neuron survival. *J. Biol. Phys*. 35, 337–346. doi: 10.1007/s10867-009-9141-4

Staats, K. A., Humblet-Baron, S., Bento-Abreu, A., Scheveneels, W., Nikolaou, A., Deckers, K., et al. (2016). Genetic ablation of IP_3 receptor 2 increases cytokines and decreases survival of $SOD1^{G93A}$ mice. *Hum. Mol. Genet*. 25, 3491–3499. doi: 10.1093/hmg/ddw190

Tateno, M., Sadakata, H., Tanaka, M., Itohara, S., Shin, R. M., Miura, M., et al. (2004). Calcium-permeable AMPA receptors promote misfolding of mutant SOD1 protein and development of amyotrophic lateral sclerosis in a transgenic mouse model. *Hum. Mol. Genet*. 13, 2183–2196. doi: 10.1093/hmg/ddh246

Tefera, T. W., and Borges, K. (2018). Neuronal glucose metabolism is impaired while astrocytic TCA cycling is unaffected at symptomatic stages in the

hSOD1(G93A) mouse model of amyotrophic lateral sclerosis. *J. Cereb. Blood. Flow Metab*. doi: 10.1177/0271678X18764775. [Epub ahead of print].

Tortarolo, M., Grignaschi, G., Calvaresi, N., Zennaro, E., Spaltro, G., Colovic, M., et al. (2006). Glutamate AMPA receptors change in motor neurons of SOD1G93A transgenic mice and their inhibition by a noncompetitive antagonist ameliorates the progression of amytrophic lateral sclerosis-like disease. *J. Neurosci. Res*. 83, 134–146. doi: 10.1002/jnr.20715

Tsai, K. J., Yang, C. H., Fang, Y. H., Cho, K. H., Chien, W. L., Wang, W. T., et al. (2010). Elevated expression of TDP-43 in the forebrain of mice is sufficient to cause neurological and pathological phenotypes mimicking FTLD-U. *J. Exp. Med*. 207, 1661–1673. doi: 10.1084/jem.20092164

Valbuena, G. N., Rizzardini, M., Cimini, S., Siskos, A. P., Bendotti, C., Cantoni, L., et al. (2016). Metabolomic analysis reveals increased aerobic glycolysis and amino acid deficit in a cellular model of amyotrophic lateral sclerosis. *Mol. Neurobiol*. 53, 2222–2240. doi: 10.1007/s12035-015-9165-7

Van Damme, P., Dewil, M., Robberecht, W., and Van Den Bosch, L. (2005). Excitotoxicity and amyotrophic lateral sclerosis. *Neurodegener. Dis*. 2, 147–159. doi: 10.1159/000089620

Van Den Bosch, L., Van Damme, P., Bogaert, E., and Robberecht, W. (2006). The role of excitotoxicity in the pathogenesis of amyotrophic lateral sclerosis. *Mol. Basis Dis.* 1762, 1068–1082. doi: 10.1016/j.bbadis.2006.05.002

Vargas, M. R., and Johnson, J. A. (2010). Astrogliosis in amytrophic lateral sclerosis: role and therapeutic potential of astrocytes. *Neurotherapeutics* 7, 471–481. doi: 10.1016/j.nurt.2010.05.012

Watanabe, N., Suzuki, J., and Kobayashi, Y. (1996). Role of calcium in tumor necrosis factor-alpha production by activated macrophages. *J. Biochem*. 120, 1190–1195. doi: 10.1093/oxfordjournals.jbchem.a021540

Wu, D. C., Re, D. B., Nagai, M., Ischiropoulos, H., and Przedborski, S. (2006). The inflammatory NADPH oxidase enzyme modulates motor neuron degeneration in amyotrophic lateral sclerosis mice. *Proc Natl Acad Sci USA*. 103, 12132–12137. doi: 10.1073/pnas.0603670103

Yang, X., and Cheng, B. (2010). Neuroprotective and anti-inflammatory activities of ketogenic diet on MPTP-induced neurotoxicity. *J. Mol. Neurosci*. 42, 145–153. doi: 10.1007/s12031-010-9336-y

Yang, Y., Gozen, O., Watkins, A., Lorenzini, I., Lepore, A., Gao, Y., et al. (2009). Presynaptic regulation of astroglial excitatory neurotransmitter transporter GLT1. *Neuron* 61, 880–894. doi: 10.1016/j.neuron.2009.02.010

Zhao, P., Ignacio, S., Beattie, E. C., and Abood, M. E. (2008). Altered presymptomatic AMPA and cannabinoid receptor trafficking in motor neurons of ALS model mice: implications for excitotoxicity. *Eur. J. Neurosci*. 27, 572–579. doi: 10.1111/j.1460-9568.2008.06041.x

Zhao, Z., Lange, D. J., Ho, L., Bonini, S., Shao, B., Salton, S. R., et al. (2008). Vgf is a novel biomarker associated with muscle weakness in amyotrophic lateral sclerosis (ALS), with a potential role in disease pathogenesis. *Int. J. Med. Sci*. 5, 92–99. doi: 10.7150/ijms.5.92

Conflict of Interest Statement: The authors declare that the research was conducted in the absence of any commercial or financial relationships that could be construed as a potential conflict of interest.

frontiers in Molecular Neuroscience

ORIGINAL RESEARCH
published: 30 July 2018
doi: 10.3389/fnmol.2018.00256

Dcf1 Deficiency Attenuates the Role of Activated Microglia During Neuroinflammation

Jiao Wang[1], Jie Li[1], Qian Wang[1], Yanyan Kong[2], Fangfang Zhou[1], Qian Li[1], Weihao Li[1], Yangyang Sun[1], Yanli Wang[3], Yihui Guan[2], Minghong Wu[4] and Tieqiao Wen[1]**

[1] Laboratory of Molecular Neural Biology, School of Life Sciences, Shanghai University, Shanghai, China, [2] Positron Emission Computed Tomography Center, Huashan Hospital, Fudan University, Shanghai, China, [3] Institute of Nanochemistry and Nanobiology, Shanghai University, Shanghai, China, [4] Shanghai Applied Radiation Institute, School of Environmental and Chemical Engineering, Shanghai University, Shanghai, China

Microglia serve as the principal immune cells and play crucial roles in the central nervous system, responding to neuroinflammation via migration and the execution of phagocytosis. Dendritic cell-derived factor 1 (Dcf1) is known to play an important role in neural stem cell differentiation, glioma apoptosis, dendritic spine formation, and Alzheimer's disease (AD), nevertheless, the involvement of the *Dcf1* gene in the brain immune response has not yet been reported. In the present paper, the RNA-sequencing and function enrichment analysis suggested that the majority of the down-regulated genes in *Dcf1*$^{-/-}$ (*Dcf1*-KO) mice are immune-related. *In vivo* experiments showed that *Dcf1* deletion produced profound effects on microglial function, increased the expression of microglial activation markers, such as ionized calcium binding adaptor molecule 1 (Iba1), Cluster of Differentiation 68 (CD68) and translocator protein (TSPO), as well as certain proinflammatory cytokines (Cxcl1, Ccl7, and IL17D), but decreased the migratory and phagocytic abilities of microglial cells, and reduced the expression levels of some other proinflammatory cytokines (Cox-2, IL-1β, IL-6, TNF-α, and Csf1) in the mouse hippocampus. Furthermore, *in vitro* experiments revealed that in the absence of lipopolysaccharide (LPS), the majority of microglia were ramified and existed in a resting state, with only approximately 10% of cells exhibiting an amoeboid-like morphology, indicative of an activated state. LPS treatment dramatically increased the ratio of activated to resting cells, and *Dcf1* downregulation further increased this ratio. These data indicated that *Dcf1* deletion mediates neuroinflammation and induces dysfunction of activated microglia, preventing migration and the execution of phagocytosis. These findings support further investigation into the biological mechanisms underlying microglia-related neuroinflammatory diseases, and the role of *Dcf1* in the immune response.

Keywords: *Dcf1*, microglia, neuroinflammation, cytokines, migration, phagocytosis

OPEN ACCESS

Edited by:
Margaret Su-chun Ho, ShanghaiTech University, China

Reviewed by:
Zun-Ji Ke, Shanghai University of Traditional Chinese Medicine, China
Juan Pablo De Rivero Vaccari, University of Miami, United States
Munjal M. Acharya, University of California, Irvine, United States

***Correspondence:**
Minghong Wu
mhwu@shu.edu.cn
Tieqiao Wen
wtq@t.shu.edu.cn

Received: *10 November 2017*
Accepted: *06 July 2018*
Published: *30 July 2018*

Citation:
Wang J, Li J, Wang Q, Kong Y, Zhou F, Li Q, Li W, Sun Y, Wang Y, Guan Y, Wu M and Wen T (2018) Dcf1 Deficiency Attenuates the Role of Activated Microglia During Neuroinflammation. Front. Mol. Neurosci. 11:256. doi: 10.3389/fnmol.2018.00256

Abbreviations: *Ccl7*, chemokine (C-C motif) ligand 7; CD68, Cluster of Differentiation 68; *Cox-2*, cyclooxygenase-2; *Csf1*, colony stimulating factor 1; *Cxcl1*, chemokine (C-X-C motif) ligand 1; DAPI, 4′,6-diamidino-2-phenylindole; *Dcf1*, dendritic cell-derived factor 1; *Dcf1*-KO, *Dcf1*$^{-/-}$; ^{18}F-DPA-714, N,N-Diethyl-2-(2-(4-(2-[^{18}F]fluoroethoxy) phenyl)-5,7-dimethylpyrazolo [1,5-a]pyrimidin-3-yl) acetamide; Iba1, ionized calcium-binding adapter molecule 1; *IL-1β*, interleukin-1*β*; *IL-6*, interleukin-6; *IL17D*, interleukin 17D; LPS, lipopolysaccharide; PBS, phosphate-buffered saline; PET, positron emission tomography; qPCR, real-time quantitative PCR; RT, room temperature; *Tnfsf11*, tumor necrosis factor (ligand) superfamily, member 11; *TNF-α*, tumor necrosis factor alpha; TSPO, translocator protein; WT, wile-type.

INTRODUCTION

Neuroinflammation is widely regarded as a chronic innate immune response in the brain and a potentially pathogenic factor in a number of neurodegenerative diseases such as Alzheimer's disease (AD), as well as traumatic brain injury (Panicker et al., 2015; Andreasson et al., 2016; Fernandez-Calle et al., 2017). Recently, due to its key signaling steps in the initiation of immune activation, greater attention has been paid to the potential of neuroinflammation as a therapeutic target (Panicker et al., 2015).

Microglia, which comprise approximately 20% of all glial cells, are the principal immune cells in the central nervous system and play a critical role in host defense against invading microorganisms and neoplastic cells (Rio-Hortega, 1932; Gonzalez-Scarano and Baltuch, 1999; von Bernhardi et al., 2015). In the normal adult brain, microglia display a remarkable branched, ramified morphological phenotype and are dispersed throughout the entire brain (Amor and Woodroofe, 2014). Upon injury, microglia undergo transformation to an amoeboid-like morphology, migrate to the site of injury, and execute phagocytosis (Andreasson et al., 2016). Microglia can also be activated by pathogen-associated molecules. Moreover, microglia also play a role in the regulation of activity-triggered synaptic plasticity and the remodeling of neural circuits, and further contribute to learning and memory (Koeglsperger et al., 2013; Parkhurst et al., 2013; Sofroniew, 2015). In the AD mouse brain, microglia have been shown to be clustered at the sites of Aβ plaques, with an activated, amoeboid-like morphology (Eisenberg and Jucker, 2012). Despite microglia being tightly packed and ubiquitously positioned in the tissue of young mice, coverage is impaired in old mice, and particularly more severely in 9-month-old $APP_{Sw,Ind}$ Tg mice, leaving tissue devoid of microglial processes (Baron et al., 2014). It has been suggested that inflammation may be involved in the pathogenesis of AD (Miklossy, 2008). In the aged brain, microglia extend ramified processes into the surrounding tissue (Mosher and Wysscoray, 2014). A recent study using two-photon microscopy in the living brain of murine models of AD to examine microglial behavior, reported data showing that microglia in the aged brain were less motile and had fewer processes (Meyer-Luehmann et al., 2008), which supports the notion that aging is accompanied by impaired microglial function (Streit et al., 2008). However, despite recent progress, the understanding of the cellular and molecular mechanisms that mediate microglial activation is still far from comprehensive.

Dendritic cell-derived factor 1 (Dcf1) is a membrane protein that plays an important role in neural stem cell differentiation, glioma apoptosis, dendritic spine formation, and social interaction, as well as amyloid precursor protein metabolism (Wen et al., 2002; Wang et al., 2008; Ullrich et al., 2010; Xie et al., 2014; Liu et al., 2017a,b). Downregulation of the *Dcf1* gene facilitates differentiation of neural stem cells into astrocytes (Wang et al., 2008) and deletion of *Dcf1* leads to dendritic spine dysplasia in the mouse hippocampus (Liu et al., 2017a). Therefore, *Dcf1* is an important regulator of neural development.

It is known that certain neural development-regulating molecules also play important roles in the regulation of the immune response in the brain (Garay and McAllister, 2010). To explore the function of *Dcf1* in the neural immune system, we investigated the effect of *Dcf1* deletion on the activation of microglia and expression of proinflammatory cytokines under different conditions *in vitro* and *in vivo*. We found that *Dcf1* deletion produced profound effects on microglial function, increased the expression of microglial activation markers such as TSPO, Iba1, and CD68 as well as some proinflammatory cytokines, but decreased the migration and phagocytosis abilities of microglial cells and the expression levels of other proinflammatory cytokines.

MATERIALS AND METHODS

Positron Emission Tomography (PET)

PET experiments were performed using a Siemens Inveon PET/CT system (Siemens Medical Solutions, Knoxville, United States) and conducted by the Huashan Hospital of China, according to the standard protocols and procedures (Kong et al., 2016). ^{18}F-DPA-714 was given via the catheter system intravenously in a slow bolus. Isoflurane is an inhaled anesthetic that is mobilized through the respiratory tract and into the body of mice under the influence of oxygen. Dynamic PET was performed for 60 min on isoflurane-anesthetized male nude mice after intravenous injection of ^{18}F-DPA-714. The experiments were carried out in compliance with national laws for the conduct of animal experimentation and were approved by the Animal Ethics Committee of Shanghai University.

Immunohistochemical Staining

Brain samples from WT and *Dcf1*-KO mice (C57BL/6 male mice, 2–3 months-old) were cut by frozen sectioning. Slices were rinsed 3 times with PBS and permeabilized with 0.1% Triton X-100 in PBS for 40 min. The slices were subsequently blocked in 5% bovine serum albumin (Invitrogen, United States) in PBS at RT for 2 h, followed by incubation with a goat anti-Iba1 monoclonal primary antibody (1:500, Abcam, United States) at 4°C overnight. The following day, the slices were washed 3 times with PBS, incubated sequentially with a donkey anti-goat IgG secondary antibody Alexa 488 (1:1000, Abcam, United States) at RT for 2 h and the nuclear stain DAPI (Invitrogen, United States) at RT for 10 min, and finally washed 3 times with PBS. Fluorescence intensity was detected using a Zeiss LSM710 fluorescence microscope. All animals were treated in accordance with the guidelines of the Society for Neuroscience Ethics Committee on Animal Research. The study design was approved by the Animal Ethics Committee of Shanghai University.

Cell Culture

BV2 cells, a mouse microglia cell line, were cultured in Dulbecco's Modified Eagle Medium (Invitrogen, United States) supplemented with 10% fetal bovine serum (Invitrogen, United States) and 1% penicillin/streptomycin (Invitrogen, United States), and maintained at 37°C in a 95% humidified

atmosphere with 5% CO_2. At approximately 90% confluence, the cells were detached with 0.1% trypsin-EDTA (Invitrogen, United States), seeded onto appropriate plates with fresh medium, and incubated overnight.

Transfection

BV2 cells were seeded onto 24-well plates at a density of 1×10^5 cells/well and cultured overnight at 37°C in an atmosphere of 5% CO_2. The following day, cells were transfected with the psiRNA-hH1neo plasmid or the psiRNA-*Dcf1* plasmid using *Lipofectamine*™ 2000 (Invitrogen, United States), according to the manufacturer's protocol.

Observation of BV2 Microglia Cell Morphology

BV2 cells were cultured on 24-well plates and transfected as described above. 24 h post-transfection, cells were stimulated with 1000 ng/ml LPS for 12 h, followed by collection of bright-field images using a Nikon microscope. The cells were then rinsed with PBS, fixed in 4% paraformaldehyde in PBS at RT for 10 min, and permeabilized with 0.1% Triton X-100 in PBS for 10 min. The cells were subsequently blocked in 2% bovine serum albumin in PBS at RT for 1 h, followed by incubation with a goat anti-Iba1 monoclonal primary antibody (1:500, Abcam, United States) at 4°C overnight. The following day, the cells were washed 3 times with PBS, and incubated sequentially with a donkey anti-goat IgG secondary antibody Alexa 488 (1:1000, Abcam, United States) at RT for 2 h, the cytoskeleton red fluorescent probe ActinRed (1:50, KeyGEN BioTECH, China) at RT for 20 min, and DAPI at RT for 5 min, and finally washed 3 times with PBS. Fluorescence intensity was detected using a Zeiss LSM710 fluorescence microscope.

Total RNA Extraction, cDNA Synthesis, and Real-Time Quantitative PCR (qPCR)

BV2 cells were cultured on 24-well plates and transfected as described above. 24 h post-transfection, cells were treated with 1000 ng/ml LPS for 12 h. Subsequently, the total RNA was extracted using a total RNA extraction kit (Promega, United States), according to the manufacturer's protocol. The total RNA in the WT and *Dcf1*-KO hippocampal tissue was extracted in the same manner. The concentration of RNA was determined by measuring the absorbance at 260 nm, and 2 μg RNA was used for cDNA synthesis using an RT master mix (TaKaRa, Japan). QPCR amplification was performed in at least triplicate using a mixture of Top Green qPCR super mix (Transgen, China), cDNA samples, and designated primers (**Table 1**). The relative gene expression was calculated by comparing the CT value of the gene of interest with that of *Gapdh*, the internal control.

TABLE 1 | List of primers used for qPCR.

Gene name	Primer sequence (5′–3′)
Dcf1	Upstream: CGCTGCTGCTGTTGACTATG
	Downstream: GTAGGTGTGCAAGGGGTAGG
Ccl7	Upstream: GCTGCTTTCAGCATCCAAGTG
	Downstream: CCAGGGACACCGACTACTG
Cxcl1	Upstream: CTGGGATTCACCTCAAGAACATC
	Downstream: CAGGGTCAAGGCAAGCCTC
Csf1	Upstream: ATGAGCAGGAGTATTGCCAAGG
	Downstream: TCCATTCCCAATCATGTGGCTA
IL17D	Upstream: AGCACACCCGTCTTCTCTC
	Downstream: GCTGGAGTTCGCACTGTCC
Tnfsf11	Upstream: CAGCATCGCTCTGTTCCTGTA
	Downstream: CTGCGTTTTCATGGAGTCTCA
Cox-2	Upstream: CAGTTTATGTTGTCTGTCCAGAGTTTC
	Downstream: CCAGCACTTCACCCATCAGTT
IL-6	Upstream: AACGATGATGCACTTGCAGA
	Downstream: CTCTGAAGGACTCTGGCTTTG
IL-1β	Upstream: CTTCCTTGTGCAAGTGTCTG
	Downstream: CAGGTCATTCTCATCACTGTC
TNF-α	Upstream: AAATTCGAGTGACAAGCCTGTAG
	Downstream: GAGAACCTGGGAGTAGACAAGGT
Gapdh	Upstream: TCACCACCATGGAGAAGGC
	Downstream: GCTAAGCAGTTGGTGGTGCA

Western Blotting

The total protein in the WT and *Dcf1*-KO hippocampal tissue was extracted using cell lysis buffer (Beyotime, China), according to the manufacturer's protocol. For protein extraction from BV2 cells, transfected cells cultured on 24-well plates were stimulated with 1000 ng/ml LPS for 12 h. Following the treatment, cells were washed twice with ice-cold PBS and the total protein was extracted using cell lysis buffer (Beyotime, China), according to the manufacturer's protocol. Protein samples were separated by sodium dodecyl sulfate polyacrylamide gel electrophoresis and electroblotted onto nitrocellulose membranes. The membranes were blocked with 5% bovine serum albumin in PBS at RT for 1 h and then incubated with the following primary antibodies at 4°C overnight: goat anti-Iba1 (1:1000, Abcam, United States), rabbit anti-IL17D (1:500, Abcam, United States), rabbit anti-CD68 (1:500, Abways, China), rabbit anti-Cox-2 (1:500, Wanleibio, China), rabbit anti-IL-6 (1:500, Wanleibio, China), rabbit anti-IL-1β (1:500, Wanleibio, China), and rabbit anti-TNF-α (1:500, Wanleibio, China). The following day, the membranes were incubated with a mouse anti-GAPDH (1:1000, Abcam, United States) at RT for 1 h, followed by an infrared dye 700-conjugated goat anti-mouse IgG (1:10000, Zemed, United States) and either an infrared dye 800-conjugated goat anti-rabbit IgG (1:10000, Zemed, United States) or an infrared dye 700-conjugated donkey anti-goat IgG secondary antibody (1:10000, Zemed, United States) at RT for a further 1 h. Visualization and quantification was carried out using LI-COR Odyssey scanner and software (LI-COR Biosciences). The relative protein expression level was normalized to Gapdh of the same lane, and data were obtained from four independent immunoblots.

Cell Migration Assay

BV2 cells were seeded at a density of 1×10^5 cells per well on a 24-well plate and cultured for 24 h at 37°C with 5% CO_2, followed by

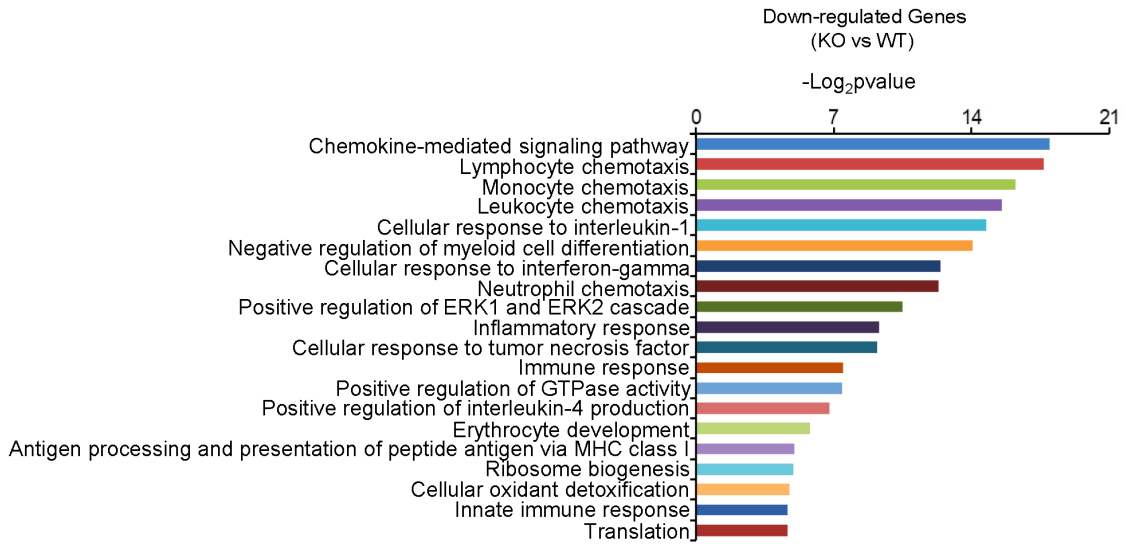

FIGURE 1 | The function enrichment analysis of downregulated genes induced by *Dcf1* knockout using the DAVID platform. The gene function enrichment analysis of downregulated genes from RNA-sequencing results in WT and KO mice. The DAVID platform was used for analysis. The results showed that the majority of the downregulated genes were immune-related.

transfection as described above. 36 h post-transfection, a wound healing assay was used to evaluate alterations in the migration rate. Briefly, lineation was carried out at the central region of cell growth in each well using a P-20 pipette tip, and the cells were observed every 12 h for 48 h using a Nikon Ti-S fluorescence microscope. The results were analyzed using the Image Pro Plus software[1].

Cell Phagocytosis Assay

BV2 cells were seeded at a density of 1×10^5 cells per well on a 24-well plate and cultured for 24 h at 37°C with 5% CO_2, followed by transfection as described above. 36 h post-transfection, fresh culture medium containing 5 μl grapheme quantum dots (2–3 μm) was added to each well and incubated at 37°C for 5 min, followed by a PBS wash, fixation with 4% paraformaldehyde for 30 min and permeabilization with 0.1% Triton X-100 in PBS for 10 min at RT. Cells were subsequently incubated with ActinRed at a dilution of 1:50 for 30 min at RT and washed three times with PBS. The phagocytic activity of the cells was evaluated by confocal microscopy.

Statistical Analysis

All data were analyzed using the Graphpad Prism software and were presented as the mean ± SEM. The mRNA and protein expression levels of WT and *Dcf1*-KO mice were analyzed using a *t*-test. The microscope images were analyzed using the Image Pro Plus software. The changes in cell morphology, mRNA and protein expression levels, and the migratory and phagocytic capacities of BV2 cells were analyzed using a one-way Analysis of Variance. Significance was set to $p < 0.05$.

[1]http://dx.doi.org/10.17504/protocols.io.iascaee

RESULTS

Dcf1 Deletion Downregulates the Expression of Immune-Related Genes in the Hippocampus

In order to gain insight into the molecular activities with which *Dcf1* may be involved in the nervous system, we examined and compared the mRNA levels in the hippocampus of both WT and *Dcf1*-KO mice by RNA sequencing and function enrichment analysis using DAVID (The Database for Annotation, Visualization, and Integrated Discovery). We found that the majority of downregulated genes in *Dcf1*-KO mice were immune-related (**Figure 1**). Since microglia are the major components of the immune system in the brain, we hypothesized that *Dcf1* may regulate microglial function. To test this hypothesis, we assessed the effects of *Dcf1* deletion on microglial activation and the production of cytokines in microglial cells using *Dcf1*-KO mice. In addition, the effects of *Dcf1* downregulation by RNAi on the LPS-induced changes in morphology, migratory and phagocytic capacity, and the expression levels of proinflammatory cytokines, in cultured BV2 cells were evaluated as described below.

Dcf1 Deletion Induces Microglial Activation *in Vivo*

The activation of microglia is characterized by an increase in the expression level of TSPO (translocator protein) and Iba1 (ionized calcium binding adaptor molecule 1). Recently, a technique was developed to monitor the expression level of TSPO by PET imaging of a radiolabeled TSPO-binding tracer, ^{18}F-DPA-714 (Auvity et al., 2017; Rizzo et al., 2017; Saba et al., 2017). Using this PET imaging technique, we found that TSPO expression was significantly increased in certain brain regions of *Dcf1*-KO mice,

including the hippocampus, as compared with that of WT mice (**Figures 2A–C**), indicating that *Dcf1* deletion upregulated the ratio of activated microglia to resting microglia. Consistently, the expression level of Iba1 was also significantly increased in *Dcf1*-KO mice, as reflected by immunostaining and Western blotting analysis, which both show that the mean density in KO mice is 1.5 times that in WT mice (**Figures 2D–F**). Furthermore, Western blotting analysis shows that the expression level of CD68 was significantly increased in *Dcf1*-KO mice (**Figure 2G**).

Dcf1 Deletion Induces Abnormal Expression of Proinflammatory Cytokines *in Vivo*

Cytokines have been reported to promote neuronal differentiation and remodeling in the brain (Jeon and Kim, 2016). Many reports have shown that proinflammatory cytokines were dramatically increased in activated microglial cells (Hwang et al., 2014). In the central nervous system, central cytokines such as IL-6, TNF-α, and IL-1β are secreted from microglia, and are considered to be involved in neuronal development and neuroplasticity (Moynagh, 2005; Jeon and Kim, 2016). Thus, to investigate the molecular differences in proinflammatory cytokines between WT and *Dcf1*-KO mouse hippocampal tissue, we examined both the mRNA and protein expression levels of Cox-2, IL-1β, Tnfsf11, Cxcl1, Ccl7, IL-6, IL17D, TNF-α, and Csf1. As illustrated in **Figure 3A**, the mRNA levels of *Ccl7* and *IL17D* dramatically increased by 2-fold in KO as compared with WT mice, in addition to *Tnfsf11* and *Cxcl1*, although the latter two were not significantly increased. Moreover, the mRNA levels of *Cox-2*, *IL-1β*, *IL-6*, *TNF-α*, and *Csf1* were significantly decreased by approximately 50% in the *Dcf1*-KO mice. Western blotting was used to verify these changes. As can be seen in **Figures 3B,C**, the protein expression levels of Cox-2, IL-1β, IL-6, and TNF-α were consistently significantly reduced in the *Dcf1*-KO mice as compared with the WT mice, and IL17D was significantly increased by approximately 40%.

Downregulation of *Dcf1* Alters the LPS-Induced Morphological Change in Cultured BV2 Microglial Cells

To better understand the role that *Dcf1* plays in the changes in the microglial morphology induced by inflammatory stimulation, we investigated the effect of *Dcf1* downregulation on the morphological changes of cultured BV2 cells caused by LPS treatment. LPS is an outer membrane component of *Gram-negative* bacteria and a strong stimulator of microglial cells (Qin et al., 2004). As shown in Supplementary Figure S1 and Supplementary Table S13, psiRNA-*Dcf1* plasmid was used to knock down the *Dcf1* gene, and qPCR analysis of the *Dcf1* mRNA level revealed a significant decrease in the LPS + psiRNA-*Dcf1* group, with no significant differences seen among the other groups. Cell morphology was examined using immunostaining against ActinRed and Iba1. As shown in **Figure 4**, in the absence of LPS, the vast majority of cells were ramified and existed in a resting state, with approximately 10% of cells exhibiting an amoeboid-like morphology, indicative of the activated state. LPS treatment dramatically increased the ratio of activated to resting cells, with *Dcf1* downregulation further increasing this ratio. This result is consistent with the elevated activation of microglia cells seen in *Dcf1*-KO mice.

Downregulation of *Dcf1* Affects the Expression of Cytokines *in Vitro*

To examine whether the silencing of *Dcf1* affected the inflammatory response at the molecular level, qPCR was performed in order to quantify the mRNA expression of the nine cytokines examined above *in vivo* studies. The relative abundance of each mRNA was expressed relative to *Gapdh*. As illustrated in **Figure 5A**, the mRNA levels of *Cox-2*, *IL-1β*, *Cxcl1*, *Ccl7*, *IL-6*, *TNF-α*, and *Csf1* were significantly increased in the LPS + vehicle group as compared with the group in the absence of LPS (blank). However, downregulation of *Dcf1* in the LPS + psiRNA-*Dcf1* group significantly decreased the levels of *Cox-2*, *IL-1β*, *IL-6*, *TNF-α*, and *Csf1*. In contrast, *Cxcl1* and *Ccl7* were dramatically increased, and IL17D was also elevated, although not significantly, as compared with the LPS + vehicle group. Western blotting was performed to further confirm whether downregulation of *Dcf1* affected the expression of these cytokines. As shown in **Figures 5B,C**, cells treated with LPS had increased expression of proinflammatory cytokines such as Cox-2, IL-1*β*, IL-6, and TNF-*α*, however, these four proinflammatory factors were significantly reduced upon *Dcf1* downregulation as compared with the LPS + vehicle group. These data demonstrated that LPS-stimulated BV2 microglial cells had increased the expression of proinflammatory cytokines, whereas downregulation of the *Dcf1* dramatically decreased the expression of most factors that were detected in LPS-stimulated BV2 cells, with the exception of Cxcl1, Ccl7, and IL17D. These results suggested that downregulation of *Dcf1* suppressed the expression of the majority of proinflammatory factors in activated BV2 microglial cells, supporting the previous results (**Figure 3**) showing differences in the expression of these genes between the hippocampal tissue from WT and *Dcf1*-KO mice.

Downregulation of *Dcf1* Decreases the Migratory Ability of Microglia

Microglial cells respond to neuroinflammation with the processes of migration (Andreasson et al., 2016) and phagocytosis (Dheen et al., 2007). It has been shown that once activated, microglia migrate toward injured areas, and that this process is controlled by the presence of cytokines and chemokines (Noda and Suzumura, 2012). It can be speculated therefore, that *Dcf1* may affect microglial migration; and thus, a wound-healing assay was employed to study the effect of *Dcf1* downregulation on the migratory ability of BV2 cells. The representative images show the scratched areas of BV2 cells in different groups from 0 to 48 h (**Figure 6A**). Upon deletion of *Dcf1*, the migration rate of BV2 cells was increased by approximately 2-fold as compared with the LPS + vehicle group at 48 h. Statistical analysis reveals that *Dcf1* downregulation significantly decreased the migratory ability of BV2 cells (**Figure 6B**), suggesting that *Dcf1* may be involved in LPS-stimulated microglial cell migration.

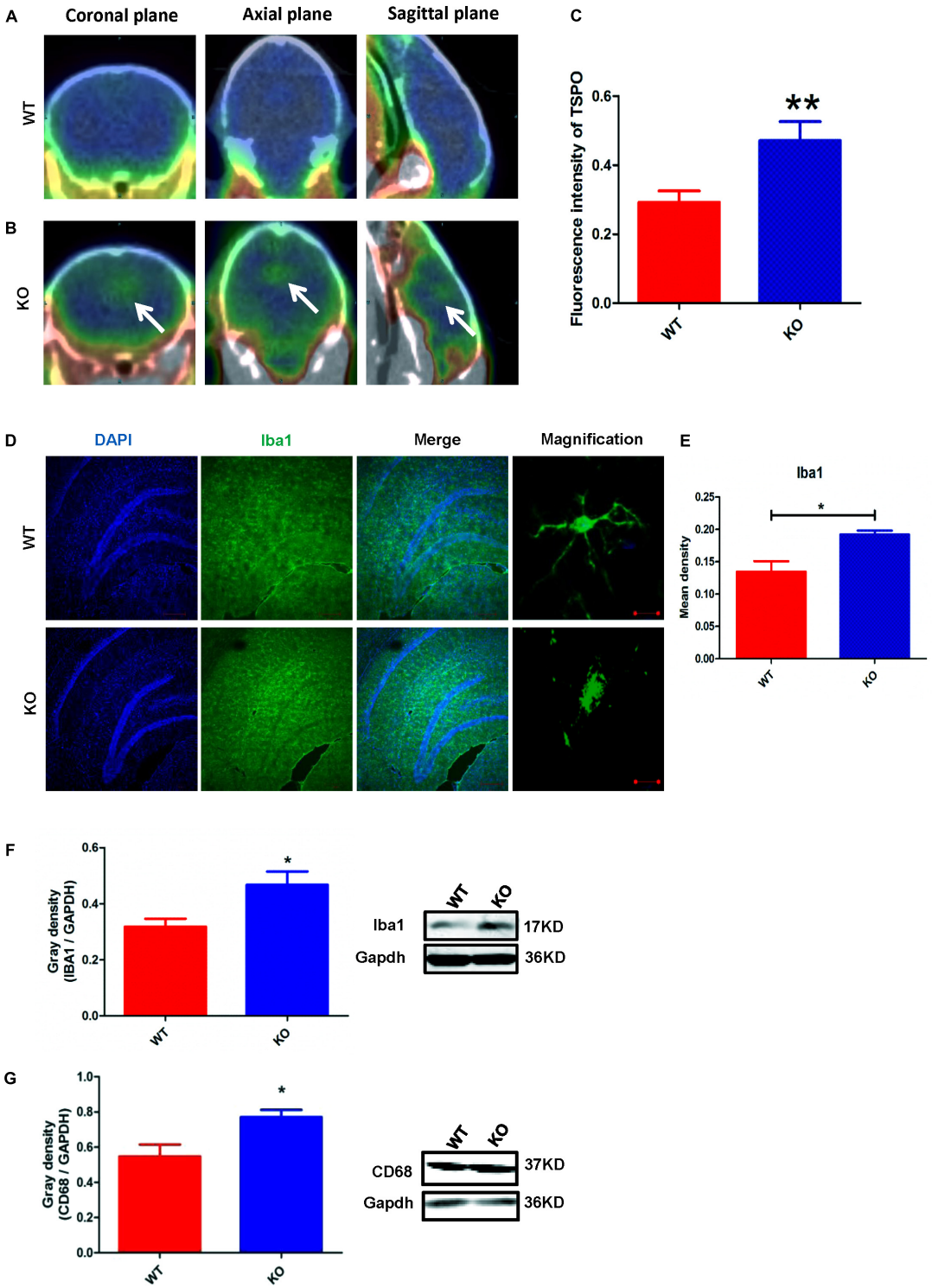

FIGURE 2 | *Dcf1* deletion induces activation of microglial cells *in vivo*. ^{18}F-DPA-714 (green) was used to trace TSPO (a biomarker of microglia) by PET to observe the activity of microglia *in vivo*. **(A,B)** Brain observation by PET in WT **(A)** and *Dcf1*-KO **(B)** mice. White arrowhead denotes activated microglia. **(C)** Quantitation of the TSPO in WT and *Dcf1*-KO mouse brain (Supplementary Table S1). **(D)** Immunohistochemical observation of microglia from WT and *Dcf1*-KO mouse brain sections. Microglial cells were detected by the Iba1 biomarker (green), and the nuclei were counterstained with DAPI (blue). Scale bars represent 200 μm. Higher magnification of confocal images were shown in right panel. Scale bars, 10 μm. **(E)** Quantitation of the mean density of Iba1 staining in WT and *Dcf1*-KO mouse brain sections (Supplementary Table S2) (mean ± SEM). $n = 4$. $^{*}p < 0.05$. Protein expression of Iba1 **(F)** and CD68 **(G)** in WT and *Dcf1*-KO mouse brain tissue (Supplementary Tables S3, S4). Quantification of protein expression levels normalized to Gapdh. Data are expressed as the mean ± SEM. $n = 3$. $^{*}p < 0.05$; $^{**}p < 0.01$.

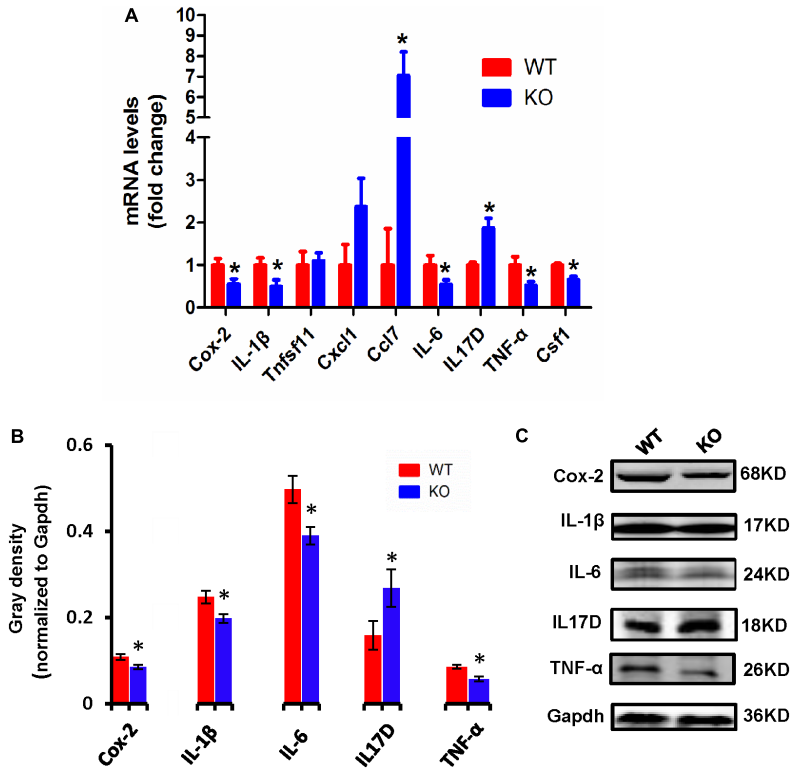

FIGURE 3 | Expression of proinflammatory cytokines in WT and *Dcf1*-KO mice. **(A)** The mRNA levels of *Cox-2*, *IL-1β*, *Tnfsf11*, *Cxcl1*, *Ccl7*, *IL-6*, *IL17D*, *TNF-α*, and *Csf1* were assessed by qPCR in WT and KO mice. The relative abundance of each mRNA was expressed relative to *Gapdh*. Data are expressed as the mean ± SEM. $n = 3$. $^*p < 0.05$ (Supplementary Table S5). **(B)** Protein expression of Cox-2, IL-1*β*, IL-6, IL17D, and TNF-*α* were assessed by Western blotting in WT and KO mice. Quantification of protein expression levels normalized to Gapdh. Datas are expressed as the mean ± SEM. $n = 3$. $^*p < 0.05$ (Supplementary Table S6). **(C)** Sample Western blotting shown for *Cox-2*, *IL-1β*, *IL-6*, *IL17D*, *TNF-α*, *and Gapdh.*

Downregulation of *Dcf1* in LPS-Activated Microglia Results in a Diminished Phagocytic Capacity

To explore the effect of *Dcf1* downregulation on the phagocytic ability of LPS-activated microglia, a cell phagocytosis assay was performed. Following transfection, cells were incubated with medium containing green fluorescent grapheme quantum dots, and subjected to confocal microscopy. The cell skeleton was labeled with ActinRed (red) to form a composite image with which to count phagocytic cells (**Figure 7A**). The ratio of phagocytic cells to total cell number was calculated to evaluate the phagocytic capacity (**Figure 7B**). Image analysis shows that compared with the blank, the phagocytic capacity of BV2 cells following treatment with LPS was increased by approximately 10%. Moreover, downregulation of *Dcf1* led to a significant decrease of approximately 50% in microglial phagocytic ability as compared with the LPS + vehicle group.

DISCUSSION

Here, we provide evidence of neuroinflammatory responses induced by *Dcf1* deficiency (**Figure 8**). The RNA-sequencing and function enrichment analysis show that the majority of the downregulated genes in *Dcf1*-KO mice were immune-related (**Figure 1**), suggesting that *Dcf1* may play a role in brain immunity. Previous work has identified that microglial cells are responsible for surveillance immunity in the CNS and are activated in response to inflammation (Streit, 2002). TSPO is consistently raised in activated microglia of the CNS. In the present study, we found that *Dcf1* deficiency induced brain immunity and activation of microglial cells, as reflected by the upregulation of TSPO, IbaI, and CD68 *in vivo* (**Figure 2** and Supplementary Figure S2). *In vitro*, downregulation of *Dcf1* increased the morphological transformation of BV2 microglial cells to an amoeboid-like structure, which indicated an activated state (**Figure 4**). Following brain injury, microglial cells rapidly respond by activating the proinflammatory process, releasing inflammatory mediators and resolving the inflammatory response (Carniglia et al., 2017). The neuroinflammatory cytokines, Cxcl1, Ccl7, and IL17D were increased in *Dcf1*-KO mice (**Figure 3** and Supplementary Figure S3). Interestingly, a defect in *Dcf1* reduced the expression of other proinflammatory factors including Cox-2, IL-1β, IL-6, TNF-α, and Csf1 (**Figure 3**), implying that *Dcf1* influences multiple inflammatory responses. *In vitro*, downregulation of *Dcf1* decreased the expression of the majority detected cytokines, with the exception of Cxcl1,

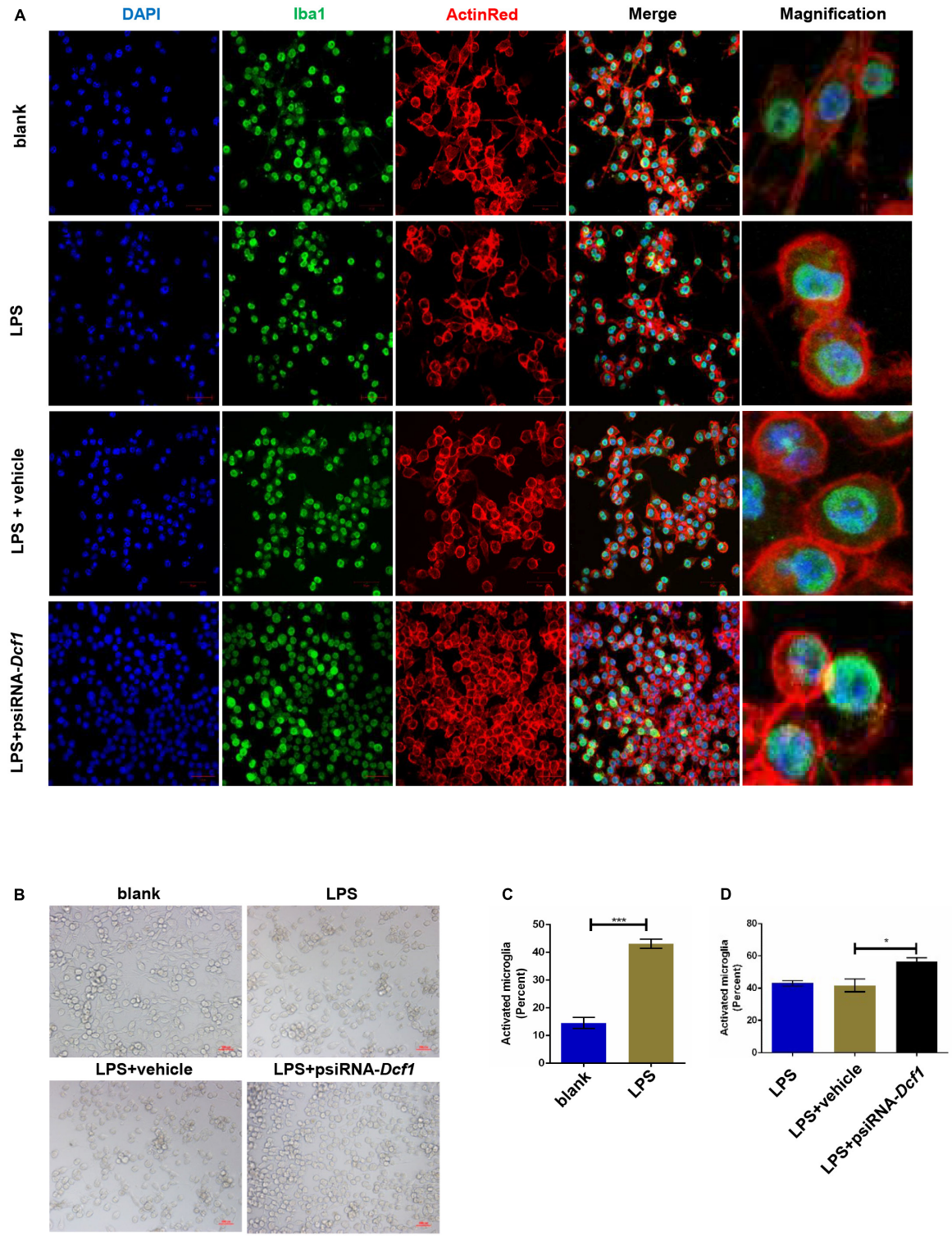

FIGURE 4 | Morphology of LPS-stimulated BV2 microglial cells *in vitro*. BV_2 microglial cells were transfected with the psiRNA-hH1neo plasmid or the psiRNA-*Dcf1* plasmid. 24 h post-transfection, BV2 microglia were stimulated with LPS (1000 ng/ml) and incubated for 12 h. **(A)** Immunofluorescence observation of the morphology in LPS-stimulated BV2 microglia *in vitro*. BV2 microglial cells were detected by the Iba1 marker (green), the cell skeleton by ActinRed (red), and the nuclei by DAPI (blue). Scale bars represent 50 μm. Higher magnification of confocal images were shown in right panel. Scale bars, 10 μm. **(B)** Bright field images of BV2 microglia. Scale bars represent 100 μm. **(C)** Comparison of the percentage of activated BV2 microglia stimulated with LPS (Supplementary Table S7). **(D)** Comparison of the percentage of LPS-activated BV2 microglia transfected with psiRNA-*Dcf1*. Data are expressed as the mean ± SEM. $n = 6$. *$p < 0.05$; ***$p < 0.001$ (Supplementary Table S8).

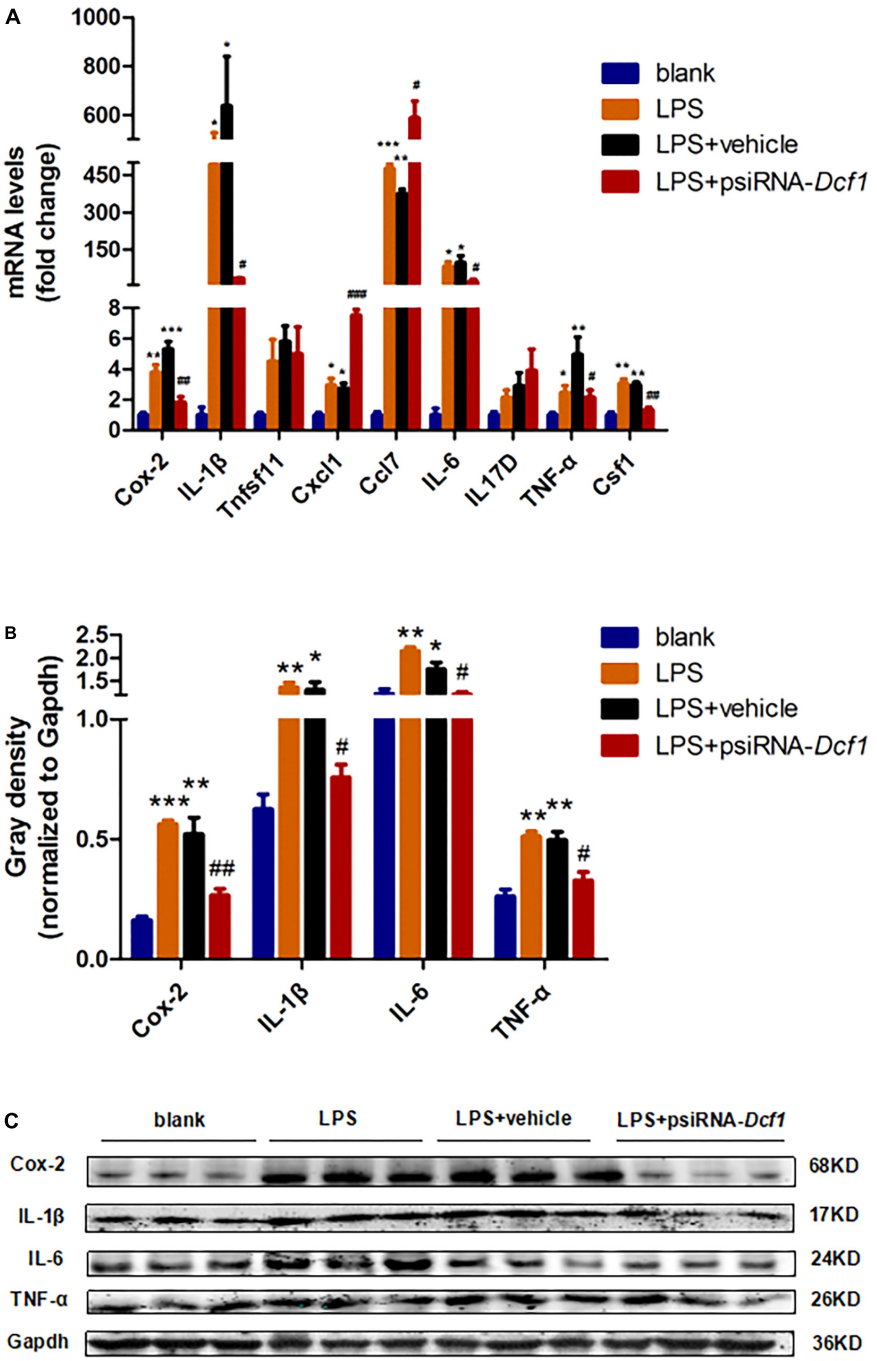

FIGURE 5 | Effects of *Dcf1* downregulation on proinflammatory cytokines expression in LPS-stimulated BV2 microglia. BV_2 microglial cells were transfected with the psiRNA-hH1neo plasmid or the psiRNA-*Dcf1* plasmid. 24 h post-transfection, BV2 microglia were stimulated with LPS (1000 ng/ml) and incubated for 12 h. **(A)** The expression of *Cox-2*, *IL-1β*, *Tnfsf11*, *Cxcl1*, *Ccl7*, *IL-6*, *IL17D*, *TNF-α*, and *Csf1* were assessed by qPCR. The relative abundance of each mRNA was expressed relative to *Gapdh* (Supplementary Table S9). **(B)** Protein expression of Cox-2, IL-1β, IL-6, and TNF-α were assessed by Western blotting. Quantification of protein expression levels normalized to Gapdh. Data are expressed as the mean ± SEM. $n = 3$. $^{*}p < 0.05$; $^{**}p < 0.01$; $^{***}p < 0.001$ vs. blank. $^{\#}p < 0.05$; $^{\#\#}p < 0.01$; $^{\#\#\#}p < 0.001$ vs. LPS + vehicle (Supplementary Table S10). **(C)** Sample Western blots shown for *Cox-2*, *IL-1β*, *IL-6*, *TNF-α*, *and Gapdh.*

Ccl7, and IL17D (**Figure 5** and Supplementary Figure S4). Moreover, *Dcf1* knockdown diminished migratory (**Figure 6**) and phagocytic (**Figure 7**) abilities of BV2 cells, indicating that *Dcf1* deletion induced microglial dysfunction. Therefore, the deficiency of *Dcf1* induced an abnormal activation of microglial cells and disturbed the release of neuroinflammatory cytokines, which may destroy the immune homeostasis in the brain.

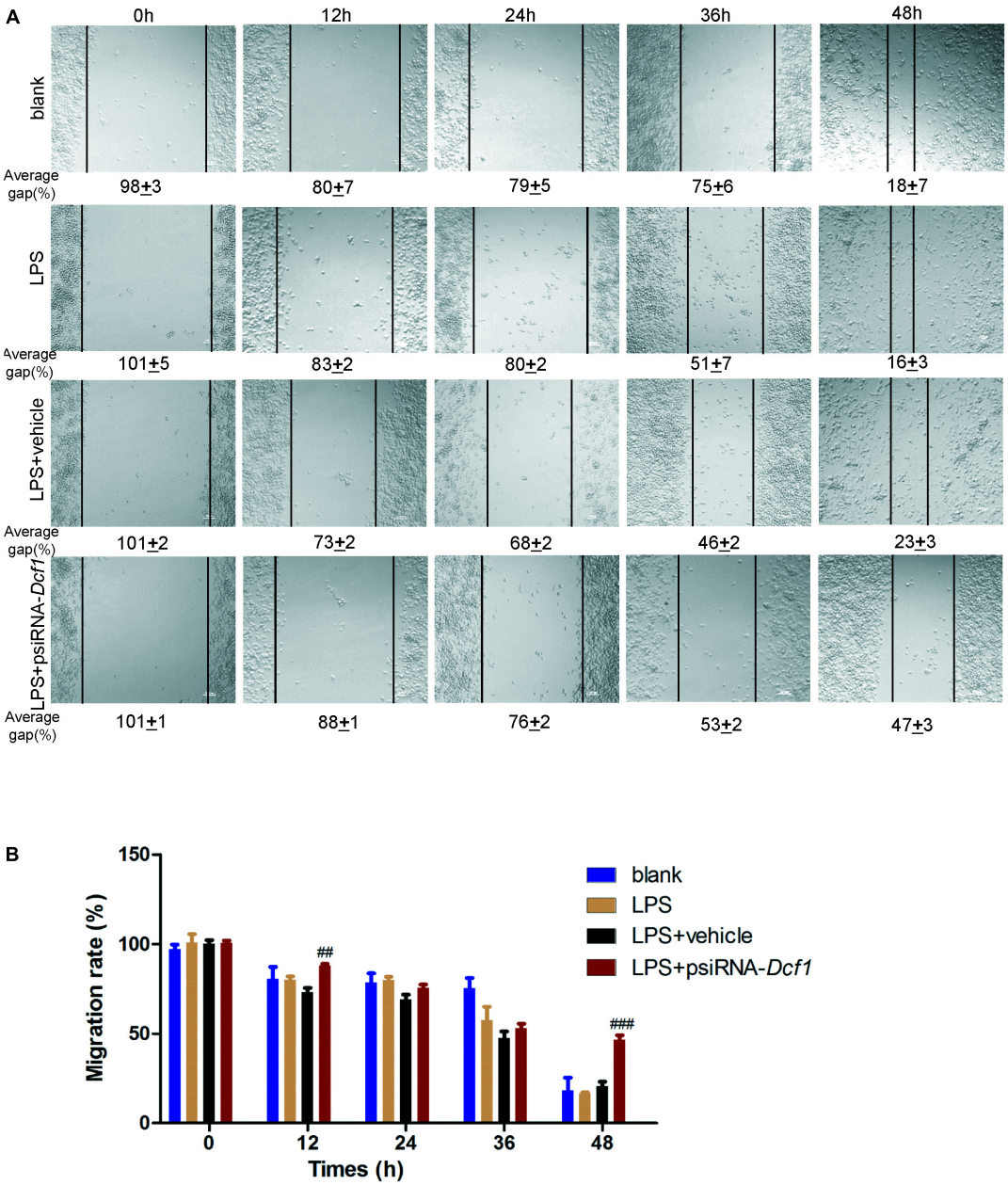

FIGURE 6 | *Dcf1* deletion decreases the migratory capacity of BV2 microglial cells. BV2 microglial cells were transfected with the psiRNA-hH1neo plasmid or the psiRNA-*Dcf1* plasmid. 24 h post-transfection, BV2 microglia were stimulated with LPS (1000 ng/ml) and incubated for 12 h. **(A)** Representative images of the scratched areas in each condition at different time points were photographed. The average gap (AG, %) was used to quantify the relative migration of the cells. Scale bars represent 200 μm. **(B)** Statistical analysis of the BV2 microglial migration rate. Data are expressed as the mean ± SEM. $n = 8$. $^{\#\#}p < 0.01$; $^{\#\#\#}p < 0.001$ vs. LPS + vehicle (Supplementary Table S11).

In order to assess the effects of *Dcf1* on microglia activation, PET technology was used to detect and monitor neuroinflammation *in vivo* (Auvity et al., 2017). TSPO was used as a biomarker for brain inflammation (Kong et al., 2016), since it is poorly expressed in the brain under normal physiological conditions, but is upregulated in activated microglial cells in response to inflammation or brain injury. Moreover, ^{18}F-DPA-714, a novel TSPO radiotracer, has been used to detect and monitor neuroinflammation in various central system diseases (Wang et al., 2014; Lavisse et al., 2015; Kong et al., 2016). An increase in TSPO reflects increased microglial activation, which is a key event in the neuroinflammatory response (Dickens et al., 2014; Kong et al., 2016). **Figure 2** showed a PET image in which the green TSPO radiotracer was significantly increased and aggregated in *Dcf1*-KO mice, indicating activation of microglial cells. Moreover, morphological changes in mitochondria and

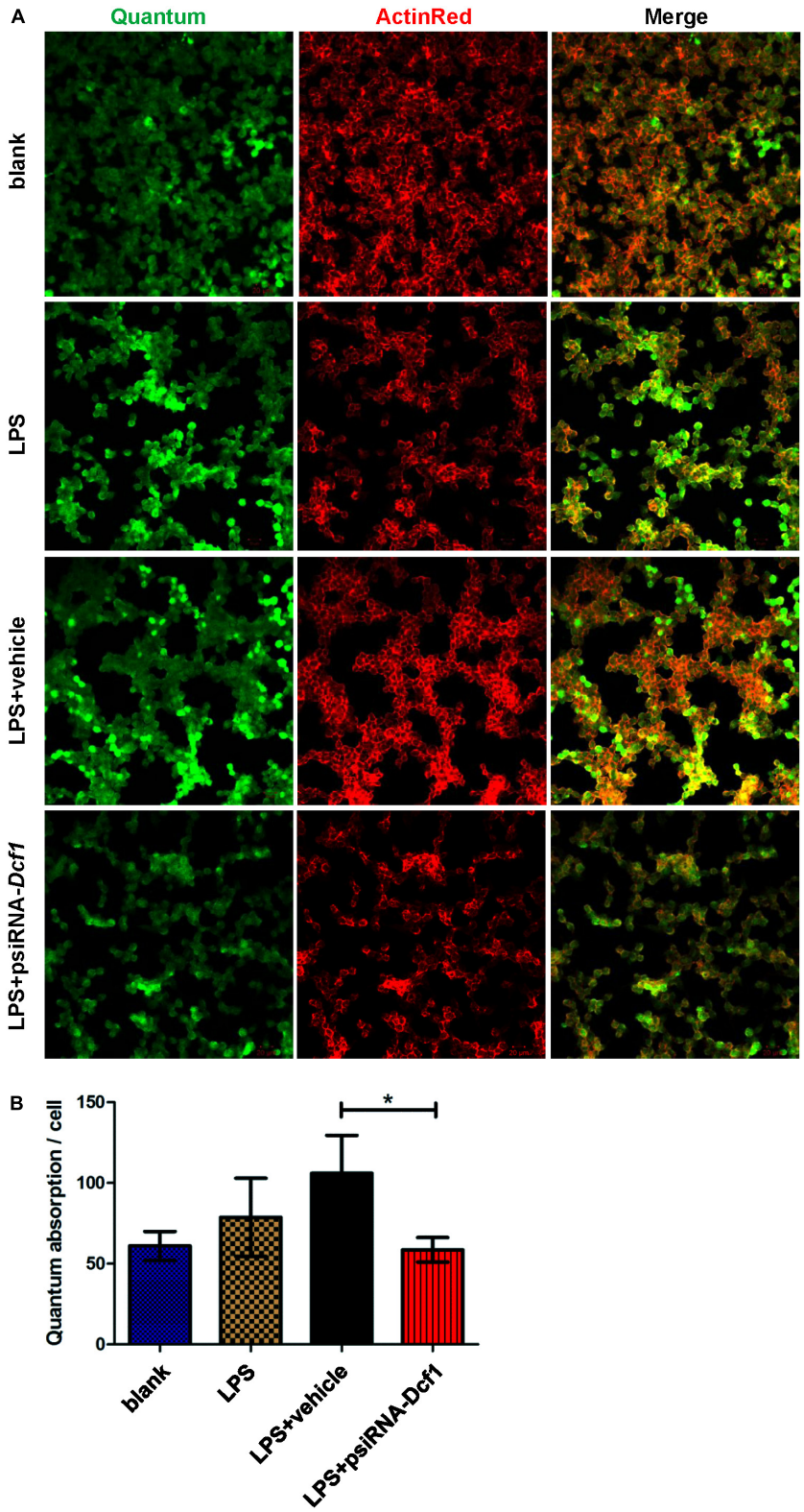

FIGURE 7 | *Dcf1* deletion suppresses the phagocytic ability of BV2 microglia cells. BV2 microglial cells were transfected with the psiRNA-hH1neo plasmid or the psiRNA-*Dcf1* plasmid. 24 h post-transfection, BV2 microglia were stimulated with LPS (1000 ng/ml) and incubated for 12 h. **(A)** Image showing the phagocytic ability of BV2 microglia cells. Quanta were spontaneous green, and the cell skeleton was detected by ActinRed (red). Scale bars represent 20 μm. **(B)** Analysis of the average quantum absorption in each cell to assess the phagocytic activity of BV2 microglia. Data are expressed as the mean ± SEM. $n = 4$. $^*p < 0.05$ (Supplementary Table S12).

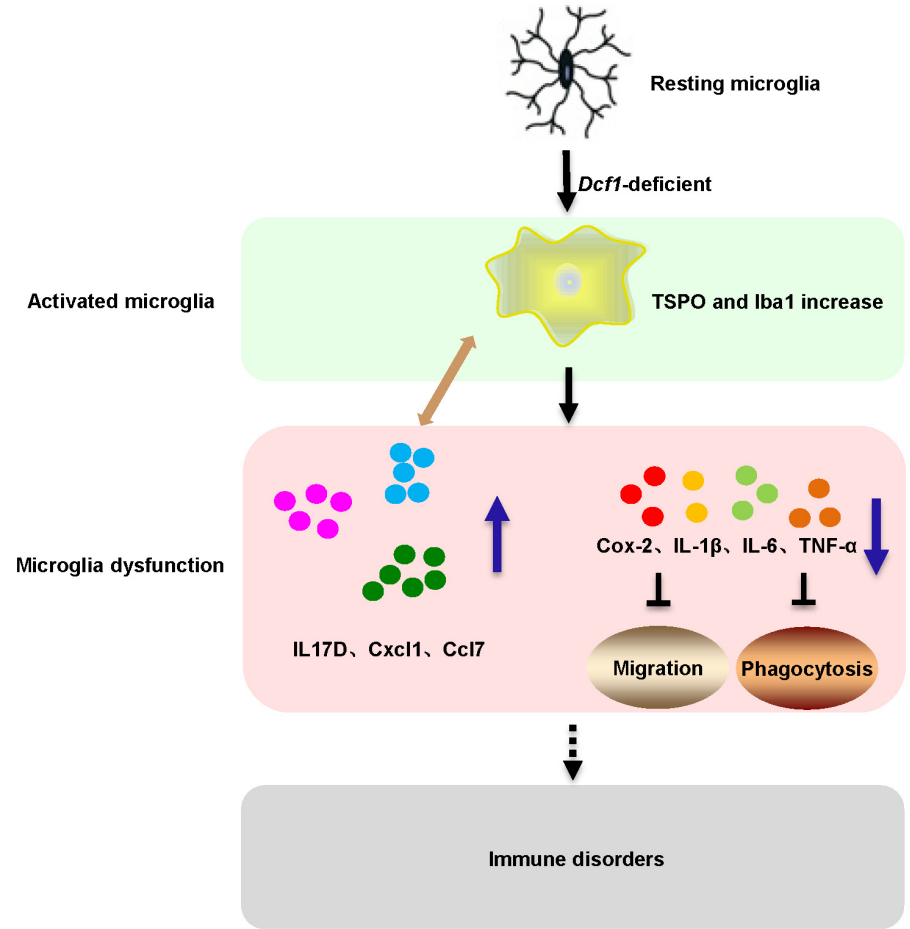

FIGURE 8 | Schematic diagram of microglial activation and dysfunction induced by *Dcf1* deficiency. *Dcf1*-deficient activated microglia, induced subsequent aberrant proinflammatory cytokines release and microglial dysfunction, which blocked the migratory and phagocytic abilities of activated microglia.

the resulting dysfunction is one of the critical steps in neuroinflammation (Xie et al., 2014; Martins et al., 2015). It has been reported that TSPO is primarily located in the outer mitochondrial membrane, and our previous data have shown that *Dcf1* is also localized within mitochondria (Xie et al., 2014), suggesting that *Dcf1* may interact with TSPO in the mitochondria of microglial cells and influence their activation.

The neuroinflammatory cytokines Cxcl1, Ccl7, and IL17D were increased during local inflammatory reaction, which can expand the immune recruitment (Boissiere-Michot et al., 2014). Cxcl1 is a chemokine produced by glial cells that attracts immune cells to the brain (Wohleb et al., 2013; Miller and Raison, 2016), and Ccl7 has been reported to exert potent proinflammatory actions through chemotaxis of monocyte-derived macrophages and other inflammatory leukocytes in the central neural system (Stuart et al., 2015). The nature of these factors and their participation in neuroinflammatory responses (Johnson et al., 2011; Jung et al., 2015) are consistent with our results of increased *Cxcl1* and *Ccl7* (**Figure 3**) accompanied by the activation of microglia (**Figure 2**). This process also included an increase in IL17D (**Figure 3**), implying an important function of IL17D during microglial activation. Moreover, Cox-2, IL-1β, IL-6, TNF-α, and Csf1 are pleiotropic cytokines that are involved in various immune responses (Liew, 2003; Kishimoto, 2006; De et al., 2014; Leppkes et al., 2014), the levels of which were decreased in both *Dcf1*-KO mice (**Figure 3**) and LPS-stimulated BV2 cells (**Figure 5**). The same phenomena were also observed in BV2 microglial cells activated by Prostaglandin E2 (Petrova et al., 1999), where the mRNA levels of *IL-6* and *TNF-α* were modestly decreased. Reduced IL-1β did indeed inhibit the secretion of IL-6, TNF-α, and Cox-2; and high levels of IL-1β have been suggested to potentially induce the production of IL-6, TNF-α, and Cox-2 (Erta et al., 2012; Seibert and Masferrer, 1994). This is consistent with our results showing that lower expression levels of IL-1β may inhibit the secretion of IL-6, TNF-α, and Cox-2. The roles of central cytokines in the brain are not yet fully understood (Jeon and Kim, 2016), resulting in the paradox phenomena seen among different research studies (Felger and Lotrich, 2013; Farooq et al., 2017). Moreover, certain signaling pathways in dendritic cells, and immune cell types, have been shown to prevent the production of cytokines such as IL-6 (Hansen and Caspi, 2010), suggesting

that *Dcf1* may also regulate the secretion of cytokines in the brain.

Microglia were activated *in vivo* detecting by ^{18}F-DPA-714 in the *Dcf1*-KO brain (**Figure 2**), and silencing of *Dcf1* significantly promoted the LPS-induced changes in microglial morphology *in vitro* (**Figure 4**), suggesting that downregulation of *Dcf1* increased the activation of BV2 microglia cells. Iba1 is a microglia-specific protein (Ohsawa et al., 2004), and as such, in order to confirm the expression level of Iba1 in *Dcf1*-KO mice, immunohistochemical staining and Western blotting were performed. We found that the ratio of activated to resting microglial cells were dramatically increased, and the protein expression of Iba1 and CD68 was consistently elevated in *Dcf1*-KO mice (**Figures 2F,G**). It has previously been reported that the expression of Iba1 is regulated by cytokines and interferons (Imai and Kohsaka, 2002), and our data showed that the levels of the cytokines *Cxcl1*, *Ccl7*, and *IL17D*, were increased (**Figure 3A**), which may have induced a higher expression of Iba1. In addition, the levels of *Cox-2*, *IL-6*, *IL-1β*, *TNF-α*, and *Csf1* were all reduced (**Figure 3A**), implying that deletion of *Dcf1* interfered with the production of various inflammatory factors.

When neuronal damage occurs, microglia adopt an activated state and exert diversified functions including migration, phagocytosis, and the production of various cytokines and chemokines (Noda and Suzumura, 2012). We found that in the presence of LPS, downregulation of *Dcf1* decreased the migratory capacity of BV2 microglial cells compared with the LPS + vehicle group (**Figure 6**). Cell migration during the immune response appears to be modulated by two fundamental processes: cell adhesion systems located at the site of inflammation, and chemotactic signals elicited through cytokines and chemokines (Simson and Foster, 2000). It has also been reported that the release of inflammatory cytokines and chemokines initiates the inflammatory response and leads to the migration of microglia toward sites of injury (Zhou et al., 2014). In the present study, the decreased mRNA levels of the majority detected proinflammatory cytokines (**Figure 5**) in conjunction with the RNA sequencing results (**Figure 1**), in which the majority of downregulated genes were related to neuroimmune responses, showed a defect in the first step of microglial migration process. Therefore, the microglial migratory ability was reduced upon downregulation of *Dcf1* (**Figure 6**), which was accompanied by the downregulation of proinflammatory cytokines.

Our results showed that *Dcf1* deletion activated microglial cells in the brain *in vivo* (**Figures 2A,B**), and that downregulation of *Dcf1* led to a significant decrease in the phagocytic capacity of BV2 microglia *in vitro* (**Figure 7**). In contrast, enhanced microglia-activated phagocytosis has been proposed to be required for the removal of injured neurons, axons, and myelin sheaths (Fu et al., 2014). It has also been reported that cytokines was involved in the regulation of phagocytic capacity (Koenigsknecht-Talboo and Landreth, 2005; Tamura et al., 2017), and the activation of microglia induced cytokine secretion (such as IL-6 and TNF-α) and phagocytosis (Heo et al., 2015). However, our results showed that the downregulation of *Dcf1* inhibited the expression of the majority detected proinflammatory cytokines including IL-6 and TNF-α (**Figure 5**). Considering that the production of proinflammatory cytokines is typically accompanied by an increased phagocytic ability, it is reasonable to suggest that the decreased secretion of different proinflammatory cytokines impeded the phagocytic ability of microglia in the present study. Moreover, it has been reported that activated microglia migrate toward injured areas, and subsequently phagocytose foreign substances or unwanted self-debris (Noda and Suzumura, 2012). Furthermore, phagocytes such as microglia follow the cytokine gradient to the infected area (Strohmeyer et al., 2005). Our results indicated that the migratory ability of microglia was impaired by the downregulation of *Dcf1* (**Figure 6**), and that the diminished migratory ability maybe the first inhibitory step in the blockade of phagocytic capacity (**Figure 7**).

Interestingly, we were not the first to notice the paradox phenomena between activated microglia and the reduced secretion of proinflammatory cytokines, since it has been reported that deviations from microglial homeostasis induce diseases (Yirmiya et al., 2015). Our present results showed that *Dcf1* deletion decreased the expression of proinflammatory cytokines such as Cox-2, IL-1β, IL-6, Csf1and TNF-α (**Figure 3**), thus, we suggested that the downregulation of these proinflammatory cytokines (**Figure 3**) impaired the normal function of activated microglia, including the migratory (**Figure 6**) and phagocytic (**Figure 7**) abilities. Moreover, *Dcf1* deletion also increased the expression of other proinflammatory cytokines such as IL17D and Ccl7 (**Figure 3**), which may be secreted by the activated microglia. From these results, we can also speculate that the absence of *Dcf1* may induce the abnormal function of the immune system, causing an aberrant secretion of proinflammatory factors and block the normal immune response involving activated microglia. This demonstrates that the intimate details of abnormal inflammatory responses remain unclear, and that further research is required to determine the biological mechanisms induced by *Dcf1* deletion.

CONCLUSION

In conclusion, our data indicates that *Dcf1*-deficient microglia induced aberrant proinflammatory cytokines release and subsequent microglial dysfunction, which blocked the migratory and phagocytic abilities of activated microglia. Taken together, these observations provide novel insight into the role of *Dcf1* in activated microglial cells during the neuroimmune response, and further lay the foundation for the elucidation of the mechanism underlying neuroinflammatory-related diseases.

AUTHOR CONTRIBUTIONS

JW, JL, and QW designed the experiments. JL, QW, and FZ conducted most of the experiments, with assistance from YK,

QL, WL, YS, YW, and YG. JL, QW, and YK collected data and contributed to the statistical analysis. JW, JL, and QW analyzed the data and wrote the manuscript. JW, MW, and TW obtained funding and revised the manuscript. All authors read and approved the final manuscript.

FUNDING

This work was sponsored by the National Natural Science Foundation of China (Grant Number: 31500827), Young Eastern Scholar (Grant Number: QD2015033), the Natural Science Foundation of Shanghai (Grant Number: 14ZR1414400), the National Natural Science Foundation of China (Grant Numbers: 81471162; 81571345; and 41430644) and the Science and Technology Commission of Shanghai (Grant Number: 14JC1402400), Program for Changjiang Scholars and Innovative Research Team in University (No. IRT_17R71).

ACKNOWLEDGMENTS

We would like to thank Dr. Natalie Ward (Medical College of Wisconsin, Wauwatosa, WI, United States) for editing this manuscript and Dr. Yonghua Ji (Shanghai University, Shanghai, China) for providing the BV2 cells.

SUPPLEMENTARY MATERIAL

The Supplementary Material for this article can be found online at: https://www.frontiersin.org/articles/10.3389/fnmol.2018.00256/full#supplementary-material

REFERENCES

Amor, S., and Woodroofe, M. N. (2014). Innate and adaptive immune responses in neurodegeneration and repair. *Immunology* 141, 287–291. doi: 10.1111/imm.12134

Andreasson, K. I., Bachstetter, A. D., Colonna, M., Ginhoux, F., Holmes, C., Lamb, B., et al. (2016). Targeting innate immunity for neurodegenerative disorders of the central nervous system. *J. Neurochem.* 138, 653–693. doi: 10.1111/jnc.13667

Auvity, S., Goutal, S., Theze, B., Chaves, C., Hosten, B., Kuhnast, B., et al. (2017). Evaluation of TSPO PET imaging, a marker of glial activation, to study the neuroimmune footprints of morphine exposure and withdrawal. *Drug Alcohol Depend.* 170, 43–50. doi: 10.1016/j.drugalcdep.2016.10.037

Baron, R., Babcock, A. A., Nemirovsky, A., Finsen, B., and Monsonego, A. (2014). Accelerated microglial pathology is associated with Abeta plaques in mouse models of Alzheimer's disease. *Aging Cell* 13, 584–595. doi: 10.1111/acel.12210

Boissiere-Michot, F., Lazennec, G., Frugier, H., Jarlier, M., Roca, L., Duffour, J., et al. (2014). Characterization of an adaptive immune response in microsatellite-instable colorectal cancer. *Oncoimmunology* 3:e29256. doi: 10.4161/onci.29256

Carniglia, L., Ramirez, D., Durand, D., Saba, J., Turati, J., Caruso, C., et al. (2017). Neuropeptides and microglial activation in inflammation, pain, and neurodegenerative diseases. *Mediators Inflamm.* 2017:5048616. doi: 10.1155/2017/5048616

De, I., Nikodemova, M., Steffen, M. D., Sokn, E., Maklakova, V. I., Watters, J. J., et al. (2014). CSF1 overexpression has pleiotropic effects on microglia in vivo. *Glia* 62, 1955–1967. doi: 10.1002/glia.22717

Dheen, S. T., Kaur, C., and Ling, E. A. (2007). Microglial activation and its implications in the brain diseases. *Curr. Med. Chem.* 14, 1189–1197. doi: 10.2174/092986707780597961

Dickens, A. M., Vainio, S., Marjamaki, P., Johansson, J., Lehtiniemi, P., Rokka, J., et al. (2014). Detection of microglial activation in an acute model of neuroinflammation using PET and radiotracers 11C-(R)-PK11195 and 18F-GE-180. *J. Nucl. Med.* 55, 466–472. doi: 10.2967/jnumed.113.125625

Eisenberg, D., and Jucker, M. (2012). The amyloid state of proteins in human diseases. *Cell* 148, 1188–1203. doi: 10.1016/j.cell.2012.02.022

Erta, M., Quintana, A., and Hidalgo, J. (2012). Interleukin-6, a major cytokine in the central nervous system. *Int. J. Biol. Sci.* 8, 1254–1266. doi: 10.7150/ijbs.4679

Farooq, R. K., Asghar, K., Kanwal, S., and Zulqernain, A. (2017). Role of inflammatory cytokines in depression: focus on interleukin-1beta. *Biomed. Rep.* 6, 15–20. doi: 10.3892/br.2016.807

Felger, J. C., and Lotrich, F. E. (2013). Inflammatory cytokines in depression: neurobiological mechanisms and therapeutic implications. *Neuroscience* 246, 199–229. doi: 10.1016/j.neuroscience.2013.04.060

Fernandez-Calle, R., Vicente-Rodriguez, M., Gramage, E., Pita, J., Perez-Garcia, C., Ferrer-Alcon, M., et al. (2017). Pleiotrophin regulates microglia-mediated neuroinflammation. *J. Neuroinflammation* 14:46. doi: 10.1186/s12974-017-0823-8

Fu, R., Shen, Q., Xu, P., Luo, J. J., and Tang, Y. (2014). Phagocytosis of microglia in the central nervous system diseases. *Mol. Neurobiol.* 49, 1422–1434. doi: 10.1007/s12035-013-8620-6

Garay, P. A., and McAllister, A. K. (2010). Novel roles for immune molecules in neural development: implications for neurodevelopmental disorders. *Front. Synaptic Neurosci.* 2:136. doi: 10.3389/fnsyn.2010.00136

Gonzalez-Scarano, F., and Baltuch, G. (1999). Microglia as mediators of inflammatory and degenerative diseases. *Annu. Rev. Neurosci.* 22, 219–240. doi: 10.1146/annurev.neuro.22.1.219

Hansen, A. M., and Caspi, R. R. (2010). Glutamate joins the ranks of immunomodulators. *Nat. Med.* 16, 856–858. doi: 10.1038/nm0810-856

Heo, D. K., Lim, H. M., Nam, J. H., Lee, M. G., and Kim, J. Y. (2015). Regulation of phagocytosis and cytokine secretion by store-operated calcium entry in primary isolated murine microglia. *Cell. Signal.* 27, 177–186. doi: 10.1016/j.cellsig.2014.11.003

Hwang, I. K., Choi, J. H., Nam, S. M., Park, O. K., Yoo, D. Y., Kim, W., et al. (2014). Activation of microglia and induction of pro-inflammatory cytokines in the hippocampus of type 2 diabetic rats. *Neurol. Res.* 36, 824–832. doi: 10.1179/1743132814Y.0000000330

Imai, Y., and Kohsaka, S. (2002). Intracellular signaling in M-CSF-induced microglia activation: role of Iba1. *Glia* 40, 164–174. doi: 10.1002/glia.10149

Jeon, S. W., and Kim, Y. K. (2016). Neuroinflammation and cytokine abnormality in major depression: cause or consequence in that illness? *World J. Psychiatry* 6, 283–293. doi: 10.5498/wjp.v6.i3.283

Johnson, E. A., Dao, T. L., Guignet, M. A., Geddes, C. E., Koemeter-Cox, A. I., and Kan, R. K. (2011). Increased expression of the chemokines CXCL1 and MIP-1alpha by resident brain cells precedes neutrophil infiltration in the brain following prolonged soman-induced status epilepticus in rats. *J. Neuroinflammation* 8:41. doi: 10.1186/1742-2094-8-41

Jung, K. H., Das, A., Chai, J. C., Kim, S. H., Morya, N., Park, K. S., et al. (2015). RNA sequencing reveals distinct mechanisms underlying BET inhibitor JQ1-mediated modulation of the LPS-induced activation of BV-2 microglial cells. *J. Neuroinflammation* 12:36. doi: 10.1186/s12974-015-0260-5

Kishimoto, T. (2006). Interleukin-6: discovery of a pleiotropic cytokine. *Arthritis Res. Ther.* 8(Suppl. 2):S2. doi: 10.1186/ar1916

Koeglsperger, T., Li, S., Brenneis, C., Saulnier, J. L., Mayo, L., Carrier, Y., et al. (2013). Impaired glutamate recycling and GluN2B-mediated neuronal calcium overload in mice lacking TGF-beta1 in the CNS. *Glia* 61, 985–1002. doi: 10.1002/glia.22490

Koenigsknecht-Talboo, J., and Landreth, G. E. (2005). Microglial phagocytosis induced by fibrillar beta-amyloid and IgGs are differentially regulated by proinflammatory cytokines. *J. Neurosci.* 25, 8240–8249. doi: 10.1523/JNEUROSCI.1808-05.2005

Kong, X., Luo, S., Wu, J. R., Wu, S., De Cecco, C. N., Schoepf, U. J., et al. (2016). (18)F-DPA-714 PET imaging for detecting neuroinflammation in rats with chronic hepatic encephalopathy. *Theranostics* 6, 1220–1231. doi: 10.7150/thno.15362

Lavisse, S., Inoue, K., Jan, C., Peyronneau, M. A., Petit, F., Goutal, S., et al. (2015). [18F]DPA-714 PET imaging of translocator protein TSPO (18 kDa) in the normal and excitotoxically-lesioned nonhuman primate brain. *Eur. J. Nucl. Med. Mol. Imaging* 42, 478–494. doi: 10.1007/s00259-014-2962-9

Leppkes, M., Roulis, M., Neurath, M. F., Kollias, G., and Becker, C. (2014). Pleiotropic functions of TNF-alpha in the regulation of the intestinal epithelial response to inflammation. *Int. Immunol.* 26, 509–515. doi: 10.1093/intimm/dxu051

Liew, F. Y. (2003). The role of innate cytokines in inflammatory response. *Immunol. Lett.* 85, 131–134. doi: 10.1016/S0165-2478(02)00238-9

Liu, Q., Feng, R., Chen, Y., Luo, G., Yan, H., Chen, L., et al. (2017a). Dcf1 triggers dendritic spine formation and facilitates memory acquisition. *Mol. Neurobiol.* 55, 763–775. doi: 10.1007/s12035-016-0349-6

Liu, Q., Shi, J., Lin, R., and Wen, T. (2017b). Dopamine and dopamine receptor D1 associated with decreased social interaction. *Behav. Brain Res.* 324, 51–57. doi: 10.1016/j.bbr.2017.01.045

Martins, C., Hulkova, H., Dridi, L., Dormoy-Raclet, V., Grigoryeva, L., Choi, Y., et al. (2015). Neuroinflammation, mitochondrial defects and neurodegeneration in mucopolysaccharidosis III type C mouse model. *Brain* 138, 336–355. doi: 10.1093/brain/awu355

Meyer-Luehmann, M., Spires-Jones, T. L., Prada, C., Garcia-Alloza, M., de Calignon, A., Rozkalne, A., et al. (2008). Rapid appearance and local toxicity of amyloid-beta plaques in a mouse model of Alzheimer's disease. *Nature* 451, 720–724. doi: 10.1038/nature06616

Miklossy, J. (2008). Chronic inflammation and amyloidogenesis in Alzheimer's disease – role of spirochetes. *J. Alzheimers Dis.* 13, 381–391. doi: 10.3233/JAD-2008-13404

Miller, A. H., and Raison, C. L. (2016). The role of inflammation in depression: from evolutionary imperative to modern treatment target. *Nat. Rev. Immunol.* 16, 22–34. doi: 10.1038/nri.2015.5

Mosher, K. I., and Wysscoray, T. (2014). Microglial dysfunction in brain aging and Alzheimer's disease. *Biochem. Pharmacol.* 88, 594–604. doi: 10.1016/j.bcp.2014.01.008

Moynagh, P. N. (2005). The interleukin-1 signalling pathway in astrocytes: a key contributor to inflammation in the brain. *J. Anat.* 207, 265–269. doi: 10.1111/j.1469-7580.2005.00445.x

Noda, M., and Suzumura, A. (2012). Sweepers in the CNS: microglial migration and phagocytosis in the Alzheimer disease pathogenesis. *Int. J. Alzheimers Dis.* 2012:891087. doi: 10.1155/2012/891087

Ohsawa, K., Imai, Y., Sasaki, Y., and Kohsaka, S. (2004). Microglia/macrophage-specific protein Iba1 binds to fimbrin and enhances its actin-bundling activity. *J. Neurochem.* 88, 844–856. doi: 10.1046/j.1471-4159.2003.02213.x

Panicker, N., Saminathan, H., Jin, H., Neal, M., Harischandra, D. S., Gordon, R., et al. (2015). Fyn kinase regulates microglial neuroinflammatory responses in cell culture and animal models of Parkinson's disease. *J. Neurosci.* 35, 10058–10077. doi: 10.1523/JNEUROSCI.0302-15.2015

Parkhurst, C. N., Yang, G., Ninan, I., Savas, J. N., Yates, J. R. III, Lafaille, J. J., et al. (2013). Microglia promote learning-dependent synapse formation through brain-derived neurotrophic factor. *Cell* 155, 1596–1609. doi: 10.1016/j.cell.2013.11.030

Petrova, T. V., Akama, K. T., and Van Eldik, L. J. (1999). Selective modulation of BV-2 microglial activation by prostaglandin E(2). Differential effects on endotoxin-stimulated cytokine induction. *J. Biol. Chem.* 274, 28823–28827. doi: 10.1074/jbc.274.40.28823

Qin, L., Liu, Y., Wang, T., Wei, S. J., Block, M. L., Wilson, B., et al. (2004). NADPH oxidase mediates lipopolysaccharide-induced neurotoxicity and proinflammatory gene expression in activated microglia. *J. Biol. Chem.* 279, 1415–1421. doi: 10.1074/jbc.M307657200

Rio-Hortega, P. D. (1932). "Microglia," in *Cytology and Cellular Pathology of the Nervous System*, Vol. 2, ed. W. Penfield (New York, NY Hoeber).

Rizzo, G., Veronese, M., Tonietto, M., Bodini, B., Stankoff, B., Wimberley, C., et al. (2017). Generalization of endothelial modelling of TSPO PET imaging: considerations on tracer affinities. *J. Cereb. Blood Flow Metab.* doi: 10.1177/0271678X17742004 [Epub ahead of print]. doi: 10.1177/0271678X17742004

Saba, W., Goutal, S., Auvity, S., Kuhnast, B., Coulon, C., Kouyoumdjian, V., et al. (2017). Imaging the neuroimmune response to alcohol exposure in adolescent baboons: a TSPO PET study using ^{18} F-DPA-714. *Addict. Biol.* doi: 10.1111/adb.12548 [Epub ahead of print]. doi: 10.1111/adb.12548

Seibert, K., and Masferrer, J. L. (1994). Role of inducible cyclooxygenase (COX-2) in inflammation. *Receptor* 4, 17–23.

Simson, L., and Foster, P. S. (2000). Chemokine and cytokine cooperativity: eosinophil migration in the asthmatic response. *Immunol. Cell Biol.* 78, 415–422. doi: 10.1046/j.1440-1711.2000.00922.x

Sofroniew, M. V. (2015). Astrocyte barriers to neurotoxic inflammation. *Nat. Rev. Neurosci.* 16, 249–263. doi: 10.1038/nrn3898

Streit, W. J. (2002). Microglia as neuroprotective, immunocompetent cells of the CNS. *Glia* 40, 133–139. doi: 10.1002/glia.10154

Streit, W. J., Miller, K. R., Lopes, K. O., and Njie, E. (2008). Microglial degeneration in the aging brain–bad news for neurons? *Front. Biosci.* 13:3423–3438.

Strohmeyer, R., Kovelowski, C. J., Mastroeni, D., Leonard, B., Grover, A., and Rogers, J. (2005). Microglial responses to amyloid beta peptide opsonization and indomethacin treatment. *J. Neuroinflammation* 2:18.

Stuart, M. J., Singhal, G., and Baune, B. T. (2015). Systematic review of the neurobiological relevance of chemokines to psychiatric disorders. *Front. Cell. Neurosci.* 9:357. doi: 10.3389/fncel.2015.00357

Tamura, T., Aoyama, M., Ukai, S., Kakita, H., Sobue, K., and Asai, K. (2017). Neuroprotective erythropoietin attenuates microglial activation, including morphological changes, phagocytosis, and cytokine production. *Brain Res.* 1662, 65–74. doi: 10.1016/j.brainres.2017.02.023

Ullrich, S., Munch, A., Neumann, S., Kremmer, E., Tatzelt, J., and Lichtenthaler, S. F. (2010). The novel membrane protein TMEM59 modulates complex glycosylation, cell surface expression, and secretion of the amyloid precursor protein. *J. Biol. Chem.* 285, 20664–20674. doi: 10.1074/jbc.M109.055608

von Bernhardi, R., Eugenin-von Bernhardi, L., and Eugenin, J. (2015). Microglial cell dysregulation in brain aging and neurodegeneration. *Front. Aging Neurosci.* 7:124. doi: 10.3389/fnagi.2015.00124

Wang, L., Wang, J., Wu, Y., Wu, J., Pang, S., Pan, R., et al. (2008). A novel function of dcf1 during the differentiation of neural stem cells in vitro. *Cell. Mol. Neurobiol.* 28, 887–894. doi: 10.1007/s10571-008-9266-1

Wang, Y., Yue, X., Kiesewetter, D. O., Wang, Z., Lu, J., Niu, G., et al. (2014). [(18)F]DPA-714 PET imaging of AMD3100 treatment in a mouse model of stroke. *Mol. Pharm.* 11, 3463–3470. doi: 10.1021/mp500234d

Wen, T., Gu, P., and Chen, F. (2002). Discovery of two novel functional genes from differentiation of neural stem cells in the striatum of the fetal rat. *Neurosci. Lett.* 329, 101–105. doi: 10.1016/S0304-3940(02)00585-2

Wohleb, E. S., Powell, N. D., Godbout, J. P., and Sheridan, J. F. (2013). Stress-induced recruitment of bone marrow-derived monocytes to the brain promotes anxiety-like behavior. *J. Neurosci.* 33, 13820–13833. doi: 10.1523/JNEUROSCI.1671-13.2013

Xie, Y., Li, Q., Yang, Q., Yang, M., Zhang, Z., Zhu, L., et al. (2014). Overexpression of DCF1 inhibits glioma through destruction of mitochondria and activation of apoptosis pathway. *Sci. Rep.* 4:3702. doi: 10.1038/srep03702

Yirmiya, R., Rimmerman, N., and Reshef, R. (2015). Depression as a microglial disease. *Trends Neurosci.* 38, 637–658. doi: 10.1016/j.tins.2015.08.001

Zhou, X., He, X., and Ren, Y. (2014). Function of microglia and macrophages in secondary damage after spinal cord injury. *Neural Regen. Res.* 9, 1787–1795. doi: 10.4103/1673-5374.143423

Conflict of Interest Statement: The authors declare that the research was conducted in the absence of any commercial or financial relationships that could be construed as a potential conflict of interest.

frontiers in Molecular Neuroscience

MINI REVIEW
published: 27 July 2018
doi: 10.3389/fnmol.2018.00254

Noradrenergic Hypothesis Linking Neurodegeneration-Based Cognitive Decline and Astroglia

Giampiero Leanza[1]*, *Rosario Gulino*[2] and *Robert Zorec*[3,4]*

[1] Department of Drug Sciences, University of Catania, Catania, Italy, [2] Department of Biomedical and Biotechnological Sciences, University of Catania, Catania, Italy, [3] Laboratory of Neuroendocrinology-Molecular Cell Physiology, Faculty of Medicine, Institute of Pathophysiology, University of Ljubljana, Ljubljana, Slovenia, [4] Laboratory of Cell Engineering, Celica Biomedical, Ljubljana, Slovenia

In the past, manipulation of the cholinergic system was seen as the most likely therapeutic for neurodegeneration-based cognitive decline in Alzheimer's disease (AD) (Whitehouse et al., 1982). However, targeting the noradrenergic system also seems a promising strategy, since more recent studies revealed that in post-mortem tissue from patients with AD and other neurodegenerative disorders there is a robust correlation between cognitive decline and loss of neurons from the Locus coeruleus (LC), a system with diffuse noradrenaline (NA) innervation in the central nervous system (CNS). Therefore, the hypothesis has been considered that increasing NA signaling in the CNS will prevent, or at least halt the progression of neurodegeneration and cognitive decline. A hallmark of the age- and neurodegeneration-related cognitive decline is reduced neurogenesis. We here discuss noradrenergic dysfunction in AD-related cognitive decline in humans and its potential involvement in AD pathology and disease progression. We also focus on animal models to allow the validation of the noradrenergic hypothesis of AD, including those based upon the immunotoxin-mediated ablation of LC based on saporin, a protein synthesis interfering agent, which offers selective and graded demise of LC neurons, Finally, we address how astrocytes, an abundant and functionally heterogeneous cell type of neuroglia maintaining homeostasis, may participate in the regulation of neurogenesis, a new strategy for preventing LC neuron loss.

Keywords: noradrenaline (norepinephrine), cognitive decline, Alzheimer's disease, neurodegeneration, neurogenesis, astroglia

OPEN ACCESS

Edited by:
Margaret Su-chun Ho, ShanghaiTech University, China

Reviewed by:
Claudio Liguori, Università degli Studi di Roma Tor Vergata, Italy
Wolfgang Härtig, Leipzig University, Germany

***Correspondence:**
Giampiero Leanza
gleanza@units.it
Robert Zorec
robert.zorec@mf.uni-lj.si

Received: *21 March 2018*
Accepted: *05 July 2018*
Published: *27 July 2018*

Citation:
Leanza G, Gulino R and Zorec R (2018) Noradrenergic Hypothesis Linking Neurodegeneration-Based Cognitive Decline and Astroglia. Front. Mol. Neurosci. 11:254. doi: 10.3389/fnmol.2018.00254

INTRODUCTION

With its widespread efferent projections, the small brainstem nucleus Locus coeruleus (LC) represents the main source of noradrenergic innervation to the entire CNS, and plays a pivotal regulatory role in a variety of physiological processes, including attention, arousal, sleep/wakefulness, consciousness as well as in specific aspects of learning and memory (Amaral and Sinnamon, 1977; Aston-Jones and Cohen, 2005; Benarroch, 2009; Sara, 2009). Notably, increasing clinical and imaging evidences (Peterson and Li, 2018) indicate that LC degeneration constitutes a crucial early event in the pathogenesis of Alzheimer's (AD) and Parkinson's disease and most of the LC-regulated functions have been shown to be severely affected during its progression (Chan-Palay and Asan, 1989; Rub et al., 2001; Wilson et al., 2013; Arendt et al., 2015).

Taken together, these observations have pointed at the noradrenergic system as a viable therapeutic target for the treatment of diseases characterized by memory loss and cognitive decline. However, a feasible animal model recapitulating noradrenergic neuronal and terminal fiber loss and its histopathological and cognitive sequelae has not yet been achieved, mainly due to the objective difficulty to selectively and efficiently target LC neurons. This review seeks to briefly summarize noradrenergic dysfunction in AD-related memory loss and its potential involvement in AD pathology and progression. Also, recent findings emerging from our own studies addressing selective immunotoxic ablation of LC neurons and its effects upon cognitive performance, tissue pathology and hippocampal neurogenesis will be briefly outlined. Then we focus into impaired neurogenesis in neurodegeneration and point to the possible contribution of astroglia to this process. Invariably, much relevant literature on the aforementioned topics will not be mentioned here, and we apologize for this.

LOCUS COERULEUS DYSFUNCTION IN ALZHEIMER'S DISEASE

The existence of an association between noradrenergic depletion and neurodegeneration including AD has long been known (Ishii, 1966; Forno and Alvord, 1971; Mann et al., 1980, 1982; Tomlinson et al., 1981; Iversen et al., 1983), however only in relatively recent years has noradrenergic neuron loss in LC been widely acknowledged as a prominent feature of neurodegeneration and AD, being present often decades prior to the appearance of clinical symptoms, and having been related to neurofibrillary pathology and the severity of cognitive deficits, when overtly present (Haglund et al., 2006; Grudzien et al., 2007; Braak and Del Tredici, 2011a,b; Wilson et al., 2013; Andres-Benito et al., 2017; Peterson and Li, 2018).

There have also been conflicting reports regarding the NA levels in the brain of AD patients. In fact, while some studies have reported marked decline in regional NA brain tissue content, whose magnitude correlated with the severity of cognitive impairments (Martignoni et al., 1992; Nazarali and Reynolds, 1992; Matthews et al., 2002; Chen et al., 2014), others reported no changes (Sparks et al., 1988; Herregodts et al., 1989; Tohgi et al., 1992) or even increased NA levels (Tohgi et al., 1992; Elrod et al., 1997).

Similar conflicting observations in post-mortem brain specimens from AD patients have been reported for adrenergic receptors (Shimohama et al., 1986; Kalaria et al., 1989; Pascual et al., 1992; Leverenz et al., 2001), known to be key mediators of noradrenergic activity, and recently considered relevant candidates as novel therapeutic targets for AD (Chen et al., 2014). These discrepancies, likely reflecting compensatory responses, or their lack, at more advanced stages of the disease (Szot et al., 2006, 2007), have thus driven the need to conclusively dissect the exact role played by the noradrenergic system in the cognitive sequelae and pathogenesis that characterize AD and neurodegeneration in general. During the last decades, numerous animal studies and reviews (Mather and Harley, 2016; Borodovitsyna et al., 2017; Gannon and Wang, 2018) have provided valuable insights into the factors underlying the disease. It has been shown, for example, that - possibly via their direct connections to the prefrontal cortex and hippocampus - LC neurons have a fundamental role in sustaining behavioral responsiveness upon exposure to relevant, reward-predicting, stimuli (Bouret and Sara, 2004; Hagena et al., 2016), including those related to working memory (Milstein et al., 2007; Coradazzi et al., 2016). Furthermore, LC neuron degeneration offers a major contribution to AD pathogenesis and progression (Braak et al., 2011; Iba et al., 2015). In fact, a prevailing hypothesis for noradrenergic neuron and fiber depletion in AD holds that LC neurons are uniquely susceptible to tau toxicity (Chandler et al., 2014) and are especially vulnerable to oxidative stress, possibly owing to their high bioenergetic needs (Sanchez-Padilla et al., 2014). In such scenario, accumulation of abnormally phosphorylated tau in LC neurons and its spreading to most of the brain due to the extremely diffuse efferent projections, would account for the progression of the disease (Braak and Del Tredici, 2015), and the resulting neuronal degeneration and cognitive impairments.

EXPERIMENTAL ANIMAL PARADIGMS TO STUDY NORADRENERGIC DYSFUNCTION

Animal studies have so far been extremely helpful to dissect the importance of NA in cognition and in the pathological events associated to its loss. Experimental manipulation of the noradrenergic system by e.g., pharmacological blockade (Mair et al., 2005; Khakpour-Taleghani et al., 2009), lesioning with N-(2-chloro-ethyl)-N-ethyl-2- bromobenzylamine (DSP4), reportedly an LC-selective neurotoxin (Lapiz et al., 2001; Sontag et al., 2008) or the knockout of the dopamine-β-hydroxylase (DBH) gene (Thomas and Palmiter, 1997; Marino et al., 2005; Hammerschmidt et al., 2013) have all resulted in impaired performance in several learning and memory tasks, demonstrating the existence of an association between NA loss and disturbances in various aspects of cognition. However, in many cases, the impairments observed in these studies have appeared rather inconsistent, both in efficiency and selectivity, thus highlighting the potential limitations inherent to each method (Sontag et al., 2008; Khakpour-Taleghani et al., 2009; Szot et al., 2010; Gannon et al., 2015). In fact, pharmacological agents lack anatomical and neurochemical resolution, acting on most monoaminergic neurons and cells throughout the central and peripheral nervous system. Likewise, DSP4 does not seem to be specific for noradrenergic neurons and has been shown to produce only a modest noradrenergic neuron loss, at best. Finally, although DBH (–/–) knockout mice have provided the unique opportunity to precisely assess the effects of NA loss *per se*, with respect to the various modulators produced and released by the very same LC neurons, they do not seem to offer the possibility to obtain partial or graded neurotransmitter depletions. In light of these limitations, we have chosen an alternative lesioning approach based on the use of the immunotoxin anti-DBH-saporin (Picklo et al., 1994), able

to target noradrenergic neurons in the LC with unprecedented selectivity and efficiency. This immunotoxin results from the conjugation of saporin, a powerful ribosome-inactivating plant lectin extracted from *Saponaria officinalis* (Caryophyllaceae) (Lappi et al., 1985; Barthelemy et al., 1993) to a monoclonal antibody raised against DBH (the enzyme converting dopamine to NA) that, in addition to its main localization in the cytosol, is also expressed at the plasma membrane surface of noradrenergic neurons (Weinshilboum, 1978; Studelska and Brimijoin, 1989). Due to its structure, saporin cannot enter the cell (Contestabile and Stirpe, 1993), but when coupled to a carrier molecule (e.g., an antibody), is able to specifically bind a surface antigen protein (such as DBH, in this case), the toxin gains access to the cytosol and binds to the ribosomal 60S subunit, interfering with protein synthesis, and soon leading to cell death (Wiley and Kline, 2000). In initial anatomical investigations, the immunotoxin, infused into the lateral ventricles of either adults (Wrenn et al., 1996) or developing rats (Coradazzi et al., 2010) has been observed to produce highly specific and dose-dependent depletions of LC neurons, with no effects on other cholinergic, dopaminergic or serotonergic neuronal populations (**Figure 1**). Notably, the possibility to induce a partial or total noradrenergic loss (by varying the injected dose) makes this immunotoxic approach extremely suitable to address compensatory events within the noradrenergic projection system, in addition to providing an excellent tissue environment for the survival and integration of implanted NA-rich progenitors (Coradazzi et al., 2010).

NORADRENALINE AND ADULT HIPPOCAMPAL NEUROGENESIS

The subgranular zone of the hippocampal dentate gyrus is one of the brain regions where generation of neural progenitor cells occurs thoughout life in various species, including humans (Altman and Das, 1965; Cameron et al., 1993; Eriksson et al., 1998; Gould et al., 1998). From here, proliferating newborn cells migrate to the granule cell layer, where they differentiate into neurons and glia and functionally integrate into the local tissue environment (Markakis and Gage, 1999; Carlen et al., 2002; van Praag et al., 2002). Many factors have been observed to affect hippocampal neurogenesis, including environmental or stressful stimuli (Dranovsky and Hen, 2006), various kinds of hormones and drugs (Duman et al., 2001), as well as neurotransmitter activity (Brezun and Daszuta, 1999; Mohapel et al., 2005, 2006; Aztiria et al., 2007; Walker et al., 2008). Notably, the hippocampus is the region where explicit memories are apparently acquired and consolidated (Murchison et al., 2004), and one of the brain areas receiving the densest LC-derived noradrenergic innervation (Swanson and Hartman, 1975). Moreover, hippocampal neurogenesis has been proposed to underlie some of the behavioral effects of antidepressant drugs (Santarelli et al., 2003; Warner-Schmidt and Duman, 2006; Airan et al., 2007), whose actions are mainly exerted by increasing extracellular levels of serotonin and/or noradrenaline (Fuller et al., 1994; Sacchetti et al., 1999). It is therefore not surprising that several studies have begun to investigate the contribution of LC neurons to the regulation of hippocampal neurogenesis, and have generally reported a permissive role for NA upon hippocampal neurogenesis (Kulkarni et al., 2002; Jhaveri et al., 2010, 2014; Masuda et al., 2012). Again, however, none of the lesion or pharmacological manipulations adopted in these investigations proved to be region-or transmitter specific, nor were any of the observed effects analyzed also in terms of impact upon cognitive performance. In our study using selective and discrete immunolesioning of LC neurons, associated with a series of hippocampus-dependent spatial navigation tasks (Coradazzi et al., 2016), we found severe deficits in working memory, which correlated with the magnitude of hippocampal noradrenergic depletion and the lesion-induced reduction in the numbers of proliferating cells within the dentate gyrus. Notably, no changes were detected in reference memory abilities, nor did the lesion affect long-term survival or differentiation of granule cell progenitors (Coradazzi et al., 2016). Thus, the noradrenergic regulation of complex aspects of cognitive function (e.g., those related to working memory) may take place via the proliferation of progenitor cells in the hippocampal dentate gyrus.

NORADRENALINE, ASTROGLIA AND NEUROGENESIS

It appears that noradrenergic receptors are densely present in astroglia (Aoki, 1992), therefore it is likely that NA may affect neuronal circuits via astroglia (Ding et al., 2013; Paukert et al., 2014; Pankratov and Lalo, 2015; Gao et al., 2016; Dong et al., 2017) (**Figure 2**. graphical abstract). Current view holds that neurodegeneration in AD is a consequence of neuron-specific deficits. However, it is more likely that preceding or concomitant changes in neuroglia may also contribute to this process (Heneka et al., 2015; Verkhratsky and Parpura, 2015; De Strooper and Karran, 2016; Rodriguez-Vieitez et al., 2016; Stenovec et al., 2016; Verkhratsky et al., 2016). Astroglia, a type of neuroglia, consisting also of oligodendroglia, microglia and NG2 cells, are functionally and morphologically heterogeneous, and are involved in sustaining brain homeostasis at cellular and whole organ levels, by regulating extracellular levels of ions and neurotransmitters, by controlling vascular and metabolic functions, the integrity of blood-brain barrier (BBB) (Terry, 2000; Giaume et al., 2007; Kano and Hashimoto, 2009; Heneka et al., 2010; Nedergaard et al., 2010; Parpura and Zorec, 2010; Verkhratsky and Nedergaard, 2014, 2018; Zorec et al., 2018). Importantly, astrocytes are essential in orchestrating defense in the CNS as well; pathological states in the CNS lead to reactive astrogliosis, a process that contains and isolates events taking place in the damaged brain regions. Moreover, reactive astrogliosis is also augmenting post-damage regeneration and repair of brain tissue (Parpura et al., 2012; Pekny et al., 2016; Verkhratsky et al., 2016); however, under certain conditions reactive astrogliosis can be neurotoxic (Liddelow et al., 2017). Astrocytes were also termed gliocrine cells (Vardjan and Zorec, 2015), since they secrete gliosignalling molecules into the extracellular space and are then convectively distributed thoroughout the brain by the glymphatic system (at least in

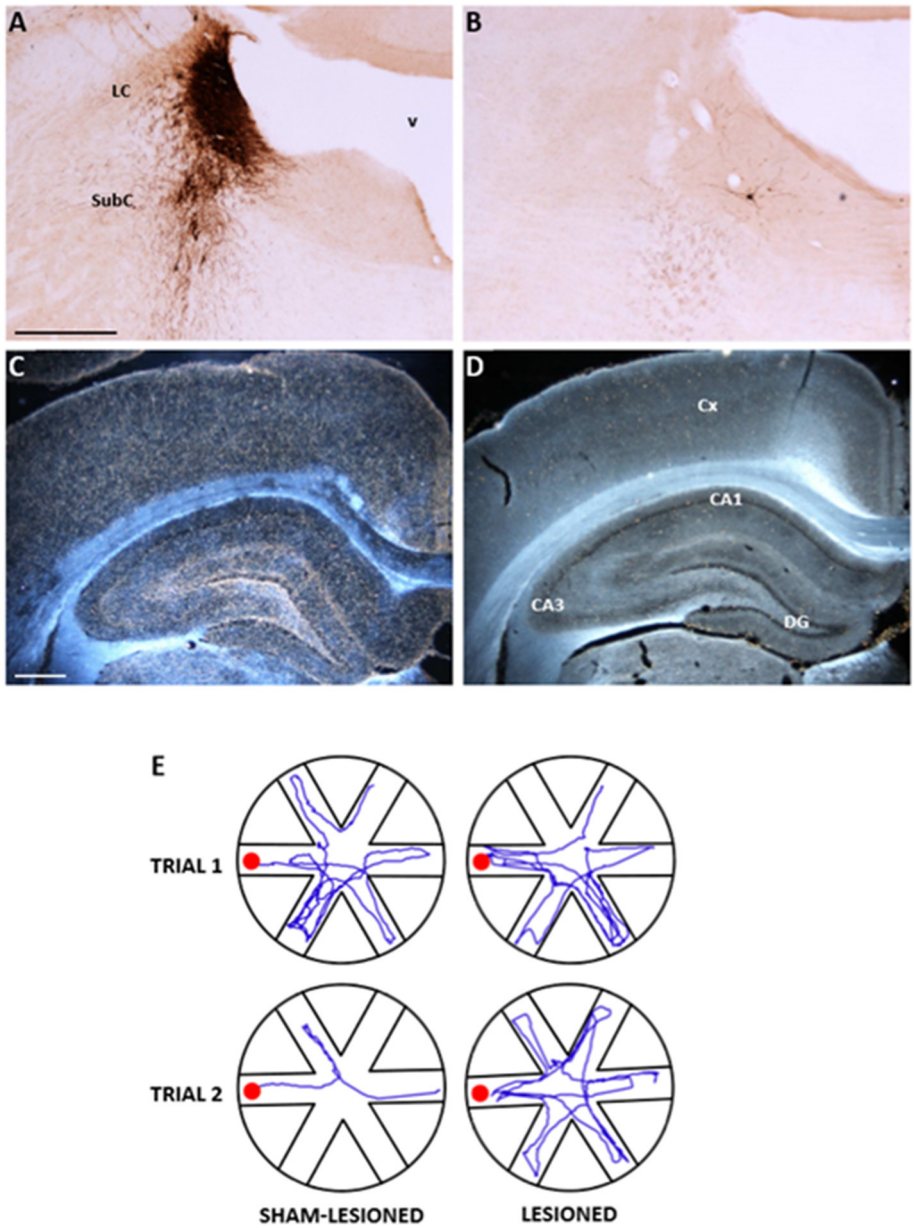

FIGURE 1 | Anatomical and functional effects of the selective noradrenergic lesion in young adult Sprague-Dawley rats. **(A–D)**: Photomicrographs showing the effects of the anti-DBH immunotoxin, injected bilaterally into the LC, on noradrenergic neurons in the LC/SubC **(A,B)** and on the DBH-immunoreactive terminal innervation in the parietal cortex and hippocampus (**C,D**, in dark field). Note in **(B,D)** the nearly complete loss of immunoreactive neurons and fibers induced by the lesion, compared to the normal patterns in the specimens from a sham-lesioned animal **(A,C)**. In **(E)**, the actual swim paths taken by representative sham-lesioned and lesioned animals undergoing the Radial Arm Water Maze (RAWM) task for working memory are illustrated. The sham-lesioned animal rapidly learns the task and significantly improves its performance from the first to the second trial, whereas the lesioned animal does not. LC, locus coeruleus; SubC, subcoeruleus, v fourth ventricle, CA, cornu ammonis of the hippocampus; DG, dentate gyrus. Scale bars in **(A,C)**: 500 μm. Adapted from Coradazzi et al. (2016).

mice), responsible for waste removal (Thrane et al., 2014). Changes in these complex functions of astroglia may lead to a homeostatic failure, leading to disease (Verkhratsky and Parpura, 2015). Hence, primary defect in homeostatic astroglia may lead to a secondary defect in neurons. Interestingly, the role of neuroglial cells in dementia and AD was noted already at least a century ago by A. Alzheimer, who observed glial cells in the proximity of damaged neurons (Alzheimer, 1907, 1910; Strassnig and Ganguli, 2005).

In tissue from post-mortem patients with AD, several morphological observations were made, including astroglial hypertrophy, associated with reactive astrogliosis, the hallmark of which is increased expression of cytoskeletal glial fibrillary acidic protein (GFAP) and S100, a Ca^{2+}-binding protein; these

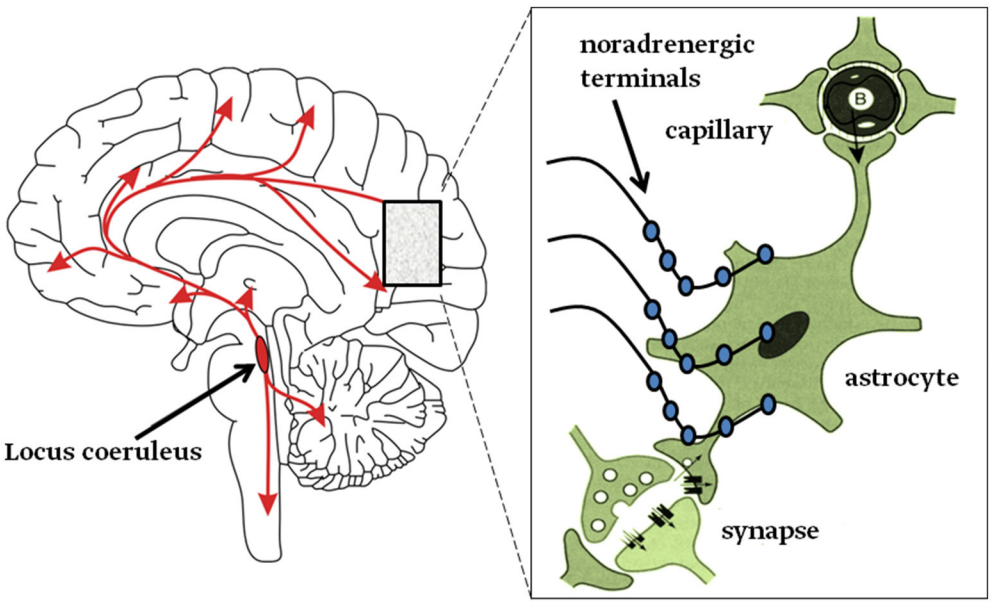

FIGURE 2 | Graphical abstract. **Left**: neurons from the Locus coeruleus (LC) project axons to most, if not all, areas of the brain and into the spinal cord as denoted by the arrows. **Right**: inset magnifies the LC nerve endings with varicosities (swellings on noradrenergic nerve terminals) from which NA is released and mainly activates astroglia (Aoki, 1992; Sherpa et al., 2016). About half of these terminals do not form tight contacts with target cells, resembling synapses (Feinstein et al., 2016).

changes in astrocytes were seen associated with senile plaques (Beach and McGeer, 1988; Griffin et al., 1989; Nagele et al., 2004; Mrak and Griffin, 2005; Verkhratsky et al., 2014). Further, studying patients with AD by imaging methods revealed distinct time- and brain-specific morphological alterations (Rodriguez-Vieitez et al., 2016). Similar changes occurred in an animal mouse model of familial AD as well, including astroglial atrophy in addition to hypertrophy in certain areas of the CNS (Olabarria et al., 2010, 2011; Yeh et al., 2011; Kulijewicz-Nawrot et al., 2012). The appearance of asthenic astrocytes appeared to preced the presence of senile plaques; asthenic astrocytes were at first observed in the entorhinal cortex, an area affected early in AD pathology (Yeh et al., 2011). Ideally, studies of pathological developments associated with neurodegeneration and AD would be best in humans, but these experiments are challenging. Recent attempts to classify protein astrogliopathies, including deposition of amyloid-β, prion protein, tau, α-synuclein, and transactive response DNA-binding protein 43 (TDP-43), demonstrated that these are present in human neurodegenerative diseases (Kovacs et al., 2017). However, animal models seem still very valuable, particularly where many aspects of this pathology can be, to some extent, reproduced, and the time emergence of AD-like characteristic take a much shorter time to develop, providing certain opportunities for studying AD-related neuropathology experimentally. Not only mice, there are several other animal models of AD including nematodes, fruit flies, rabbits, canines, and non-human primates; in each of the models different aspects of AD properties are manifested (reviewed in Woodruff-Pak, 2008). The selective ablation of LC in rats, as presented in previous chapters, offers interesting insights to be explored as a novel animal model of AD and neurodegeneration, not only for functional cognitive impairments (Coradazzi et al., 2016), but also for morphological alterations and aspects of neurogenesis related to astroglia.

Neuron degeneration in the LC during early stages of AD (Heneka et al., 2006) may lead to reduced levels of NA, which is known to be a generic inhibitor of neuroinflammation (De Keyser et al., 2004) and remodeling of the neurovascular unit (del Zoppo, 2009). Therefore, reduced noradrenergic innervation in the CNS may affect the progression of AD through reduced inhibition of neuroinflammation, a tissue remodeling process. This likely operates via a reduced NA contribution of astrocyte adrenergic excitation. Although NA released by the LC neurons acts through α- and β-adrenergic receptors (α/β-ARs), which are expressed in neurons, microglia and astrocytes, but it is the latter cell type that exhibits a high density of ARs, especially the β-ARs (Aoki, 1992) and thus represents a key cell type mediating adrenergic effects on brain tissue. Indeed, activation of α-ARs stimulates Ca^{2+} signaling in astrocytes (Salm and McCarthy, 1989; Kirischuk et al., 1996; Horvat et al., 2016); experiments *in vivo* reported Ca^{2+} waves propagating through astroglial syncytia after stimulating the LC in anesthetized animals (Bekar et al., 2008). In awake animals, electrical stimulation of LC triggered (via activation of $\alpha_?$-ARs) widespread and synchronous astroglial Ca^{2+} signals in practically all astrocytes in the field of study (Ding et al., 2013). This phenomenon may be taken as an event resetting neural networks (Bouret and Sara, 2005). In AD, astrocytic Ca^{2+} signaling is impaired (Lim et al., 2014; Stenovec et al., 2016), which may affect the clearance of Aβ deposits (Mattson, 2004)

and subsequent glutamate toxicity (Mattson and Chan, 2003; Mattson, 2004).

Whenever NA is released, not only α-ARs, but also β-ARs are stimulated, although the effects appear in different time-domains (Horvat et al., 2016). These latter receptors stimulate second messenger cAMP, which affects glycogenolysis (Prebil et al., 2011; Kreft et al., 2012), a likely source of glutamate for memory consolidation (Gibbs et al., 2010). Glycogen, an energy reserve, present in astrocytes, but not in neurons (Barros, 2013; Oe et al., 2016), is likely consumed for processes related to morphological plasticity controlled by β-AR/cAMP signaling in astroglia (Vardjan et al., 2014). Not only in memory formation (Zorec et al., 2015), astroglial β-AR/cAMP-dependent morphological changes are central for astrocytic cell oedema attenuation (Vardjan et al., 2016).

Activation of ARs on astrocytes may also affect neurogenesis through neuronal metabolic support by astroglia. Reduced support due to lower NA levels may in AD result in reduced neurogenesis. Astrocytes are the site of aerobic glycolysis, a special metabolic adaptation, present in tissues exhibiting cell division and morphological plasticity. This non-oxidative utilization of glucose, takes place even in the presence of adequate levels of oxygen; it is also known as "the Warburg effect" (Vander Heiden et al., 2009). It is also a characteristic of cancer cells (Salcedo-Sora et al., 2014), hence aerobic glycolysis seems a universal property needed for tissue enlargement and cell shape remodeling.

Astroglial aerobic glycolysis, with the end product L-lactate, is regulated by NA. During exercise, sensory stimulation, alertness and in some pathophysiological states astroglial L-lactate production is up-regulated, requiering the activation of LC neurons (Dienel and Cruz, 2016; Feinstein et al., 2016). LC neurons respond to L-lactate, generated by astroglia when NA activates ARs on astroglial plasma membrane, with elevated electrical activity, an interesting form of communication between the somata of the two cell-types (Tang et al., 2014). It is possible that astroglial L-lactate may also stimulate LC axons away from the somata; as it was recently demonstarted that transcranial direct current stimulation induces NA-dependent elevation of second messenger Ca^{2+} in astrocytes (Monai et al., 2016). Therefore, degenerated LC neurons in AD fail to adequately stimulate astroglia, a source of necessary support for the metabolic needs of neuronal networks, contributing to attenuated neurogenesis. Hypometabolic manifestation is observed clinically in patients with AD (Rodriguez-Vieitez et al., 2016).

Cholesterol is an important building block of membranes and astroglial aerobic glycolysis is likely linked to cholesterol homeostasis in the brain, the most cholesterol-rich organ in the body (Lütjohann et al., 1996). There is little exchange of cholesterol molecules by circulating lipoproteins, between the brain and systemic circulation, since lipoproteins are unable to pass the blood–brain barrier (BBB). Interestingly, the brain exhibits its own cholesterol synthesis, which occurs mainly in glia (Mauch et al., 2001)). Brain cholesterol is not only synthesized *de novo* in the brain, it is also modified/degraded by enzymatic conversion to 24(*S*)-hydroxycholesterol (Lütjohann et al., 1996), a form that can readily cross the BBB, a major route of cholesterol exit from the brain.

Cholesterol metabolism is linked to the synthesis of the neurosteroids including allopregnanolone, a potent stimulator of neural progenitor cell survival reversing the progress of disease in the 3xTgAD mouse model (Singh et al., 2012). Thus, it is possible to speculate that the hypometabolic state in AD, due to impairment of LC-mediated adrenergic stimulation of astroglia, results in a reduced provision of metabolic intermediates and in attenuated neurosteroid-mediated maintenance of neurogenesis, an avenue that will have to be confirmed experimentally in the future.

FUTURE PROSPECTS AND THERAPY OPTIONS

Based on the above observations of the relationship between central noradrenergic depletion and a series of AD-related changes, including cognitive disturbances, and tissue pathology, it is not surprising that much interest has recently mounted concerning the possibility to restore extracellular NA levels in the brain as a prerequisite to ameliorate cognitive performance as well as to promote cell protection and neurogenesis. Several potential therapeutic venues have been explored so far: one holds that voluntary physical exercise may improve memory by enhancing NA release from LC neurons (Segal et al., 2012), an effect possibly mediated by β-ARs (Van Hoomissen et al., 2004; Ebrahimi et al., 2010). Another study has addressed the possible restorative effects of atomoxetine (a NA reuptake inhibitor) in AD patients undergoing anticholinesterase therapy, reporting no clear-cut cognitive improvements (Mohs et al., 2009), possibly due to a poor effectiveness of the NA uptake inhibitor on LC which is already severely depleted of its neurons as a result of the disease (Braun et al., 2014; Braun and Feinstein, 2017). A similar lack of cognitive improvements has been reported in aged healthy patients following treatment with guanfacine, an α_2-AR agonist (Van Dyck, 2014; http://ClinicalTrials.gov) that, if anything, should reduce, rather than increase NA levels (Starke, 2001). Indeed, α_2-AR antagonists appear to prevent age-related spatial working memory impairments in a transgenic AD mouse model (Scullion et al., 2011). In spite of these inconsistencies, the possibility to ameliorate cognitive performance and cell protection by enhancing noradrenergic neurotransmission remains an exciting prospect: in a recent investigation (Pintus et al., 2018) we have implanted embryonic noradrenergic progenitors bilaterally into the hippocampus of rats whose LC neurons had been almost completely and selectively depleted. We reasoned that if the loss of noradrenergic innervation to the hippocampus was necessary to induce measurable cognitive impairments, its restoration promoted by the implanted embryonic LC neurons should be sufficient to ameliorate/reverse them. As expected (and consistent with our previous findings Coradazzi et al., 2016), the LC lesion induced severe deficits in working memory which were seen fully reversed (up to normal) in transplanted animals and significantly reinstated by a second lesion ablating the implanted neuroblasts. Interestingly,

the transplant-promoted noradrenergic reinnervation also normalized the nuclear expression of the transactive response DNA-binding protein 43 (TDP-43) in various hippocampal subregions, whose cytoplasmic (i.e., pathological) occurrence appeared dramatically increased as a result of the lesions. These findings therefore provide support to the view that cognitive and histopathological changes observed in AD patients may require concurrent loss of ascending regulatory noradrenergic inputs from LC and that NA replenishment may be an effective intervention to slow down and/or reverse cognitive decline and tissue pathology, including neurogenesis. Moreover, the NA replenishment may operate via astroglial adrenergic mechanism that include metabolic and neurotrophic support of neural networks.

CONCLUDING REMARKS

Noradrenergic neurons in the LC and their widespread efferent connections play a central role in normal cognition and their disruption is increasingly believed to be critically associated with severe memory loss and neurodegeneration in general (Wilson et al., 2013; Feinstein et al., 2016; Bharani et al., 2017; Satoh and Iijima, 2017). Notably, the presence of functional and densely present adrenergic receptors on astrocytes (Aoki, 1992), whose activation triggers metabolic and energetic responses supporting synaptic functioning and plasticity (Zorec et al., 2017), strongly suggests that many, if not all, the NA-mediated processes may take place also via an action on astrocyes. Thus, addressing astrocytes as viable targets for neurological diseases related to noradrenergic dysfunction is an interesting issue with fundamental therapeutic implications, warranting further research.

AUTHOR CONTRIBUTIONS

GL, RG, and RZ conceived the concept of paper, wrote and edited the manuscript.

FUNDING

This work was supported by grants to RZ # P3 310, J3 6790, J3 6789 and J3 7605 from the Slovenian Research Agency (ARRS), CipKeBip, COST Action BM1002, EU COST Action CM1207-GLISTEN. GL's work is supported by the Kathleen Foreman-Casali Foundation and the Beneficentia Stiftung.

REFERENCES

Airan, R. D., Meltzer, L. A., Roy, M., Gong, Y., Chen, H., and Deisseroth, K. (2007). High-speed imaging reveals neurophysiological links to behavior in an animal model of depression. *Science* 317, 819–823. doi: 10.1126/science.1144400

Altman, J., and Das, G. D. (1965). Autoradiographic and histological evidence of postnatal hippocampal neurogenesis in rats. *J. Comp. Neurol.* 124, 319–335. doi: 10.1002/cne.901240303

Alzheimer, A. (1907). Über eine eigenartige Erkrankung der Hirnrinde. Versammlung Südwestdeutscher Irrenärzte in Tübingen am 3. November 1906. *Allgemeine Zeitschrift für Psychiatrie und Psychisch-Gerichtliche Medizin*. 64, 146–148.

Alzheimer, A. (1910). "Beiträge zur Kenntnis der pathologischen Neuroglia und ihrer Beziehungen zu den Abbauvorgängen im Nervengewebe," in *Histologische und histopathologische Arbeiten über die Grosshirnrinde mit besonderer Berücksichtigung der pathologischen Anatomie der Geisteskrankheiten,* ed F. Nissl (Jena: Verlag von G. Fischer), 401–562.

Amaral, D. G., and Sinnamon, H. M. (1977). The locus coeruleus: neurobiology of a central noradrenergic nucleus. *Prog. Neurobiol.* 9, 147–196. doi: 10.1016/0301-0082(77)90016-8

Andrés-Benito P., Fernández-Dueñas V., Carmona, M., Escobar, L. A., Torrejón-Escribano, B., Aso, E., et al. (2017). Locus coeruleus at asymptomatic early and middle Braak stages of neurofibrillary tangle pathology. *Neuropathol. Appl. Neurobiol.* 43, 373–392. doi: 10.1111/nan.12386

Aoki, C. (1992). Beta-adrenergic receptors: astrocytic localization in the adult visual cortex and their relation to catecholamine axon terminals as revealed by electron microscopic immunocytochemistry. *J. Neurosci.* 12, 781–792. doi: 10.1523/JNEUROSCI.12-03-00781.1992

Arendt, T., Bruckner, M. K., Morawski, M., Jager, C., and Gertz, H. J. (2015). Early neurone loss in Alzheimer's disease: cortical or subcortical? *Acta Neuropathol. Commun* 3:10. doi: 10.1186/s40478-015-0187-1

Aston-Jones, G., and Cohen, J. D. (2005). An integrative theory of locus coeruleus-norepinephrine function: adaptive gain and optimal performance. *Annu. Rev. Neurosci.* 28, 403–450. doi: 10.1146/annurev.neuro.28.061604.135709

Aztiria, E., Capodieci, G., Arancio, L., and Leanza, G. (2007). Extensive training in a maze task reduces neurogenesis in the adult rat dentate gyrus probably as a result of stress. *Neurosci. Lett.* 416, 133–137. doi: 10.1016/j.neulet.2007.01.069

Barros, L. F. (2013). Metabolic signaling by lactate in the brain. T*rends Neurosci.* 36, 396–404. doi: 10.1016/j.tins.2013.04.002

Barthelemy, I., Martineau, D., Ong, M., Matsunami, R., Ling, N., Benatti, L., et al. (1993). The expression of saporin, a ribosome-inactivating protein from the plant Saponaria officinalis, in *Escherichia coli*. *J. Biol. Chem.* 268, 6541–6458.

Beach, T. G., and McGeer, E. G. (1988). Lamina-specific arrangement of astrocytic gliosis and senile plaques in Alzheimer's disease visual cortex. *Brain Res.* 463, 357–361. doi: 10.1016/0006-8993(88)90410-6

Bekar, L. K., He, W., and Nedergaard, M. (2008). Locus coeruleus alpha-adrenergic-mediated activation of cortical astrocytes in vivo. *Cereb. Cortex* 18, 2789–2795. doi: 10.1093/cercor/bhn040

Benarroch, E. E. (2009). The locus ceruleus norepinephrine system: functional organization and potential clinical significance. *Neurology* 73, 1699–1704. doi: 10.1212/WNL.0b013e3181c2937c

Bharani, K. L., Derex, R., Granholm, A. C., and Ledreux, A. (2017). A noradrenergic lesion aggravates the effects of systemic inflammation on the hippocampus of aged rats. *PLoS ONE* 12:e0189821. doi: 10.1371/journal.pone.0189821

Borodovitsyna, O., Flamini, M., and Chandler, D. (2017). Noradrenergic modulation of cognition in health and disease. *Neural Plast.* 2017:6031478. doi: 10.1155/2017/6031478

Bouret, S., and Sara, S. J. (2004). Reward expectation, orientation of attention and locus coeruleus-medial frontal cortex interplay during learning. *Eur. J. Neurosci.* 20, 791–802. doi: 10.1111/j.1460-9568.2004.03526.x

Bouret, S., and Sara, S. J. (2005). Network reset: a simplified overarching theory of locus coeruleus noradrenaline function. *Trends Neurosci.* 28, 574–582. doi: 10.1016/j.tins.2005.09.002

Braak, H., and Del Tredici, K. (2011a). The pathological process underlying Alzheimer's disease in individuals under thirty. *Acta Neuropathol.* 121, 171–181. doi: 10.1007/s00401-010-0789-4

Braak, H., and Del Tredici, K. (2011b). Alzheimer's pathogenesis: is there neuron-to-neuron propagation? *Acta Neuropathol.* 121, 589–595. doi: 10.1007/s00401-011-0825-z

Braak, H., and Del Tredici, K. (2015). The preclinical phase of the pathological process underlying sporadic Alzheimer's disease. *Brain* 138(Pt 10), 2814–2833. doi: 10.1093/brain/awv236

Braak, H., Thal, D. R., Ghebremedhin, E., and Del Tredici, K. (2011). Stages of the pathologic process in Alzheimer disease: age categories from 1 to 100 years. *J. Neuropathol. Exp. Neurol.* 70, 960–969. doi: 10.1097/NEN.0b013e318232a379

Braun, D., and Feinstein, D. L. (2017). The locus coeruleus neuroprotective drug vindeburnol normalizes behavior in the 5xFAD transgenic mouse model of Alzheimer's disease. *Brain Res.* doi: 10.1016/j.brainres.2017.12.028. [Epub ahead of print].

Braun, D., Madrigal, J. L., and Feinstein, D. L. (2014). Noradrenergic regulation of glial activation: molecular mechanisms and therapeutic implications. C*urr. Neuropharmacol.* 12, 342–352. doi: 10.2174/1570159X12666140828220938

Brezun, J. M., and Daszuta, A. (1999). Depletion in serotonin decreases neurogenesis in the dentate gyrus and the subventricular zone of adult rats. *Neuroscience* 89, 999–1002. doi: 10.1016/S0306-4522(98)00693-9

Cameron, H. A., Woolley, C. S., McEwen, B. S., and Gould, E. (1993). Differentiation of newly born neurons and glia in the dentate gyrus of the adult rat. *Neuroscience* 56, 337–344. doi: 10.1016/0306-4522(93)90335-D

Carlen, M., Cassidy, R. M., Brismar, H., Smith, G. A., Enquist, L. W., and Frisen, J. (2002). Functional integration of adult-born neurons. *Curr. Biol* .12, 606–608. doi: 10.1016/S0960-9822(02)00771-6

Chandler, D. J., Gao, W. J., and Waterhouse, B. D. (2014). Heterogeneous organization of the locus coeruleus projections to prefrontal and motor cortices. *Proc. Natl. Acad. Sci. U.S.A.* 111, 6816–6821. doi: 10.1073/pnas.1320827111

Chan-Palay, V., and Asan, E. (1989). Alterations in catecholamine neurons of the locus coeruleus in senile dementia of the Alzheimer type and in Parkinson's disease with and without dementia and depression. *J. Comp. Neurol.* 287, 373–392. doi: 10.1002/cne.902870308

Chen, Y., Peng, Y., Che, P., Gannon, M., Liu, Y., Li, L., et al. (2014). alpha(2A) adrenergic receptor promotes amyloidogenesis through disrupting APP-SorLA interaction. *Proc. Natl. Acad. Sci. U.S.A.* 111, 17296–172301. doi: 10.1073/pnas.1409513111

Contestabile, A., and Stirpe, F. (1993). Ribosome-inactivating proteins from plants as agents for suicide transport and immunolesioning in the nervous system. *Eur. J. Neurosci.* 5, 1292–1301. doi: 10.1111/j.1460-9568.1993.tb00915.x

Coradazzi, M., Gulino, R., Fieramosca, F., Falzacappa, L. V., Riggi, M., and Leanza, G. (2016). Selective noradrenaline depletion impairs working memory and hippocampal neurogenesis. *Neurobiol. Aging* 48, 93–102. doi: 10.1016/j.neurobiolaging.2016.08.012

Coradazzi, M., Gulino, R., Garozzo, S., and Leanza, G. (2010). Selective lesion of the developing central noradrenergic system: short- and long-term effects and reinnervation by noradrenergic-rich tissue grafts. *J. Neurochem.* 114, 761–771. doi: 10.1111/j.1471-4159.2010.06800.x

De Keyser, J., Zeinstra, E., Mostert, J., and Wilczak, N. (2004). Beta 2-adrenoceptor involvement in inflammatory demyelination and axonal degeneration in multiple sclerosis. *Trends Pharmacol. Sci.* 25, 67–71. doi: 10.1016/j.tips.2003.12.002

del Zoppo, G. J. (2009). Inflammation and the neurovascular unit in the setting of focal cerebral ischemia. *Neuroscience* 158, 972–982. doi: 10.1016/j.neuroscience.2008.08.028

De Strooper, B., and Karran, E. (2016). The cellular phase of Alzheimer's disease. *Cell* 164, 603–615. doi: 10.1016/j.cell.2015.12.056

Dienel, G. A., and Cruz, N. F. (2016). Aerobic glycolysis during brain activation: adrenergic regulation and influence of norepinephrine on astrocytic metabolism. *J. Neurochem.* 38, 14–52 doi: 10.1111/jnc.13630

Ding, F., O'Donnell, J., Thrane, A. S., Zeppenfeld, D., Kang, H., Xie, L., et al. (2013). α1-Adrenergic receptors mediate coordinated Ca^{2+} signaling of cortical astrocytes in awake, behaving mice. *Cell Calcium* 54, 387–394. doi: 10.1016/j.ceca.2013.09.001

Dong, J. H., Wang, Y. J., Cui, M., Wang, X. J., Zheng, W. S., Ma, M. L., et al. (2017). Adaptive activation of a stress response pathway improves learning and memory through Gs and beta-arrestin-1-regulated lactate metabolism. *Biol. Psychiatry* 81, 654–670. doi: 10.1016/j.biopsych.2016.09.025

Dranovsky, A., and Hen, R. (2006). Hippocampal neurogenesis: regulation by stress and antidepressants. *Biol. Psychiatry* 59, 1136–1143. doi: 10.1016/j.biopsych.2006.03.082

Duman, R. S., Malberg, J., and Nakagawa, S. (2001). Regulation of adult neurogenesis by psychotropic drugs and stress. *J. Pharmacol. Exp. Ther.* 299, 401–407.

Ebrahimi, S., Rashidy-Pour, A., Vafaei, A. A., and Akhavan, M. M. (2010). Central beta-adrenergic receptors play an important role in the enhancing effect of voluntary exercise on learning and memory in rat. B*ehav. Brain Res.* 208, 189–193. doi: 10.1016/j.bbr.2009.11.032

Elrod, R., Peskind, E. R., DiGiacomo, L., Brodkin, K. I., Veith, R. C., and Raskind, M. A. (1997). Effects of Alzheimer's disease severity on cerebrospinal fluid norepinephrine concentration. *Am. J. Psychiatry* 154, 25–30. doi: 10.1176/ajp.154.1.25

Eriksson, P. S., Perfilieva, E., Bjork-Eriksson, T., Alborn, A. M., Nordborg, C., Peterson, D. A., et al. (1998). Neurogenesis in the adult human hippocampus. *Nat. Med.* 4, 1313–1317. doi: 10.1038/3305

Feinstein, D. L., Kalinin, S., and Braun, D. (2016). Causes, consequences, and cures for neuroinflammation mediated via the locus coeruleus: noradrenergic signaling system. *J. Neurochem.* 139(Suppl. 2), 154–178. doi: 10.1111/jnc.13447

Forno, L. S., and Alvord, E. C. Jr. (1971). The pathology of Parkinsonism. Part, I. Some new observations and correlations. *Contemp. Neurol. Ser.* 8, 119–130.

Fuller, R. W., Hemrick-Luecke, S. K., and Snoddy, H. D. (1994). Effects of duloxetine, an antidepressant drug candidate, on concentrations of monoamines and their metabolites in rats and mice. *J. Pharmacol. Exp. Ther.* 269, 132–136.

Gannon, M., Che, P., Chen, Y., Jiao, K., Roberson, E. D., and Wang, Q. (2015). Noradrenergic dysfunction in Alzheimer's disease. *Front. Neurosci.* 9:220. doi: 10.3389/fnins.2015.00220

Gannon, M., and Wang, Q. (2018). Complex noradrenergic dysfunction in Alzheimer's disease: Low norepinephrine input is not always to blame. *Brain Res.* doi: 10.1016/j.brainres.2018.01.001. [Epub ahead of print].

Gao, V., Suzuki, A., Magistretti, P. J., Lengacher, S., Pollonini, G., Steinman, M. Q., et al. (2016). Astrocytic beta2-adrenergic receptors mediate hippocampal long-term memory consolidation. *Proc. Natl. Acad. Sci. U.S.A.* 113, 8526–8531. doi: 10.1073/pnas.1605063113

Giaume, C., Kirchhoff, F., Matute, C., Reichenbach, A., and Verkhratsky, A. (2007). Glia: the fulcrum of brain diseases. *Cell Death Differ.* 14, 1324–1335. doi: 10.1038/sj.cdd.4402144

Gibbs, M. E., Hutchinson, D. S., and Summers, R. J. (2010). Noradrenaline release in the locus coeruleus modulates memory formation and consolidation; roles for α- and β-adrenergic receptors. *Neuroscience* 170, 1209–1222. doi: 10.1016/j.neuroscience.2010.07.052

Gould, E., Tanapat, P., McEwen, B. S., Flügge G., and Fuchs, E. (1998). Proliferation of granule cell precursors in the dentate gyrus of adult monkeys is diminished by stress. *Proc. Natl. Acad. Sci. U.S.A.* 95, 3168–3171. doi: 10.1073/pnas.95.6.3168

Griffin, W. S., Stanley, L. C., Ling, C., White, L., MacLeod, V., Perrot, L. J., et al. (1989). Brain interleukin 1 and S-100 immunoreactivity are elevated in Down syndrome and Alzheimer disease. *Proc. Natl. Acad. Sci. U.S.A.* 86, 7611–7615. doi: 10.1073/pnas.86.19.7611

Grudzien, A., Shaw, P., Weintraub, S., Bigio, E., Mash, D. C., and Mesulam, M. M. (2007). Locus coeruleus neurofibrillary degeneration in aging, mild cognitive impairment and early Alzheimer's disease. *Neurobiol. Aging* 28, 327–335. doi: 10.1016/j.neurobiolaging.2006.02.007

Hagena, H., Hansen, N., and Manahan-Vaughan, D. (2016). beta-adrenergic control of hippocampal function: subserving the choreography of synaptic information storage and memory. *Cereb. Cortex* 26, 1349–1364. doi: 10.1093/cercor/bhv330

Haglund, M., Sjöbeck M, M., and Englund, E. (2006). Locus ceruleus degeneration is ubiquitous in Alzheimer's disease: possible implications for diagnosis and treatment. *Neuropathology* 26, 528–532. doi: 10.1111/j.1440-1789.2006.00725.x

Hammerschmidt, T., Kummer, M. P., Terwel, D., Martinez, A., Gorji, A., Pape, H. C., et al. (2013). Selective loss of noradrenaline exacerbates early cognitive dysfunction and synaptic deficits in APP/PS1 mice. *Biol. Psychiatry* 73, 454–463. doi: 10.1016/j.biopsych.2012.06.013

Heneka, M. T., Carson, M. J., El Khoury, J., Landreth, G. E., Brosseron, F., Feinstein, D. L., et al. (2015). Neuroinflammation in Alzheimer's disease. *Lancet Neurol.* 14, 388–405. doi: 10.1016/S1474-4422(15)70016-5

Heneka, M. T., Ramanathan, M., Jacobs, A. H., Dumitrescu-Ozimek, L., Bilkei-Gorzo, A., Debeir, T., et al. (2006). Locus ceruleus degeneration promotes Alzheimer pathogenesis in amyloid precursor protein 23 transgenic mice. *J. Neurosci.* 26, 1343–1354. doi: 10.1523/JNEUROSCI.4236-05.2006

Heneka, M. T., Rodríguez JJ., and Verkhratsky, A. (2010). Neuroglia in neurodegeneration. *Brain Res. Rev.* 63, 189–211. doi: 10.1016/j.brainresrev.2009.11.004

Herregodts, P., Bruyland, M., De Keyser, J., Solheid, C., Michotte, Y., and Ebinger, G. (1989). Monoaminergic neurotransmitters in Alzheimer's disease. An HPLC study comparing presenile familial and sporadic senile cases. *J. Neurol. Sci.* 92, 101–116. doi: 10.1016/0022-510X(89)90179-2

Horvat, A., Zorec, R., and Vardjan, N. (2016). Adrenergic stimulation of single rat astrocytes results in distinct temporal changes in intracellular Ca^{2+} and cAMP-dependent PKA responses. *Cell Calcium*. 59, 156–163. doi: 10.1016/j.ceca.2016.01.002

Iba, M., McBride, J. D., Guo, J. L., Zhang, B., Trojanowski, J. Q., and Lee, V. M. (2015). Tau pathology spread in PS19 tau transgenic mice following locus coeruleus (LC) injections of synthetic tau fibrils is determined by the LC's afferent and efferent connections. *Acta Neuropathol.* 130, 349–362. doi: 10.1007/s00401-015-1458-4

Ishii, T. (1966). Distribution of Alzheimer's neurofibrillary changes in the brain stem and hypothalamus of senile dementia. *Acta Neuropathol.* 6, 181–187. doi: 10.1007/BF00686763

Iversen, L. L., Rossor, M. N., Reynolds, G. P., Hills, R., Roth, M., Mountjoy, C. Q., et al. (1983). Loss of pigmented dopamine-beta-hydroxylase positive cells from locus coeruleus in senile dementia of Alzheimer's type. *Neurosci. Lett.* 39, 95–100. doi: 10.1016/0304-3940(83)90171-4

Jhaveri, D. J., Mackay, E. W., Hamlin, A. S., Marathe, S. V., Nandam, L. S., Vaidya, V. A., et al. (2010). Norepinephrine directly activates adult hippocampal precursors via beta3-adrenergic receptors. *J. Neurosci.* 30, 2795–2806. doi: 10.1523/JNEUROSCI.3780-09.2010

Jhaveri, D. J., Nanavaty, I., Prosper, B. W., Marathe, S., Husain, B. F., Kernie, S. G., et al. (2014). Opposing effects of alpha2- and beta-adrenergic receptor stimulation on quiescent neural precursor cell activity and adult hippocampal neurogenesis. *PLoS ONE* 9:e98736. doi: 10.1371/journal.pone.0098736

Kalaria, R. N., Andorn, A. C., Tabaton, M., Whitehouse, P. J., Harik, S. I., and Unnerstall, J. R. (1989). Adrenergic receptors in aging and Alzheimer's disease: increased beta 2-receptors in prefrontal cortex and hippocampus. *J. Neurochem.* 53, 1772–17781. doi: 10.1111/j.1471-4159.1989.tb09242.x

Kano, M., and Hashimoto, K. (2009). Synapse elimination in the central nervous system. *Curr. Opin. Neurobiol.* 19, 154–161. doi: 10.1016/j.conb.2009.05.002

Khakpour-Taleghani, B., Lashgari, R., Motamedi, F., and Naghdi, N. (2009). Effect of reversible inactivation of locus ceruleus on spatial reference and working memory. *Neuroscience* 158, 1284–1291. doi: 10.1016/j.neuroscience.2008.11.001

Kirischuk, S., Tuschick, S., Verkhratsky, A., and Kettenmann, H. (1996). Calcium signalling in mouse Bergmann glial cells mediated by alpha1-adrenoreceptors and H1 histamine receptors. *Eur. J. Neurosci.* 8, 1198–1208. doi: 10.1111/j.1460-9568.1996.tb01288.x

Kovacs, G. G., Lee, V. M., and Trojanowski, J. Q. (2017). Protein astrogliopathies in human neurodegenerative diseases and aging. *Brain Pathol.* 27, 675–690. doi: 10.1111/bpa.12536

Kreft, M., Bak, L. K., Waagepetersen, H. S., and Schousboe, A. (2012). Aspects of astrocyte energy metabolism, amino acid neurotransmitter homoeostasis and metabolic compartmentation. *ASN Neuro.* 4:e00086. doi: 10.1042/AN20120007

Kulijewicz-Nawrot, M., Verkhratsky, A., Chvátal, A., Syková, E., and Rodríguez, J. J. (2012). Astrocytic cytoskeletal atrophy in the medial prefrontal cortex of a triple transgenic mouse model of Alzheimer's disease. *J. Anat.* 221, 252–262. doi: 10.1111/j.1469-7580.2012.01536.x

Kulkarni, V. A., Jha, S., and Vaidya, V. A. (2002). Depletion of norepinephrine decreases the proliferation, but does not influence the survival and differentiation, of granule cell progenitors in the adult rat hippocampus. *Eur. J. Neurosci.* 16, 2008–2012. doi: 10.1046/j.1460-9568.2002.02268.x

Lapiz, M. D., Mateo, Y., Durkin, S., Parker, T., and Marsden, C. A. (2001). Effects of central noradrenaline depletion by the selective neurotoxin DSP-4 on the behaviour of the isolated rat in the elevated plus maze and water maze. *Psychopharmacology* 155, 251–259. doi: 10.1007/s00213010 0702

Lappi, D. A., Esch, F. S., Barbieri, L., Stirpe, F., and Soria, M. (1985). Characterization of a Saponaria officinalis seed ribosome-inactivating protein: immunoreactivity and sequence homologies. *Biochem. Biophys. Res. Commun.* 129, 934–942. doi: 10.1016/0006-291X(85)91981-3

Leverenz, J. B., Miller, M. A., Dobie, D. J., Peskind, E. R., and Raskind, M. A. (2001). Increased alpha 2-adrenergic receptor binding in locus coeruleus projection areas in dementia with Lewy bodies. *Neurobiol. Aging* 22, 555–561. doi: 10.1016/S0197-4580(01)00221-4

Liddelow, S. A., Guttenplan, K. A., Clarke, L. E., Bennett, F. C., Bohlen, C. J., Schirmer, L., et al. (2017). Neurotoxic reactive astrocytes are induced by activated microglia. *Nature* 541, 481–487. doi: 10.1038/nature21029

Lim, D., Ronco, V., Grolla, A. A., Verkhratsky, A., and Genazzani, A. A. (2014). Glial calcium signalling in Alzheimer's disease. *Rev. Physiol. Biochem. Pharmacol.* 167, 45–65. doi: 10.1007/112_2014_19

Lütjohann, D., Breuer, O., Ahlborg, G., Nennesmo, I., Sidén, A., Diczfalusy, U., et al. (1996). Cholesterol homeostasis in human brain: evidence for an age-dependent flux of 24S-hydroxycholesterol from the brain into the circulation. *Proc. Natl. Acad. Sci. U.S.A.* 93, 9799–9804. doi: 10.1073/pnas.93.18.9799

Mair, R. D., Zhang, Y., Bailey, K. R., Toupin, M. M., and Mair, R. G. (2005). Effects of clonidine in the locus coeruleus on prefrontal- and hippocampal-dependent measures of attention and memory in the rat. *Psychopharmacology* 181, 280–288. doi: 10.1007/s00213-005-2263-x

Mann, D. M., Lincoln, J., Yates, P. O., Stamp, J. E., and Toper, S. (1980). Changes in the monoamine containing neurones of the human CNS in senile dementia. *Br. J. Psychiatry* 136, 533–541. doi: 10.1192/bjp.136.6.533

Mann, D. M., Yates, P. O., and Hawkes, J. (1982). The noradrenergic system in Alzheimer and multi-infarct dementias. *J. Neurol. Neurosurg. Psychiatry* 45, 113–119. doi: 10.1136/jnnp.45.2.113

Marino, M. D., Bourdelat-Parks, B. N., Cameron Liles, L., and Weinshenker, D. (2005). Genetic reduction of noradrenergic function alters social memory and reduces aggression in mice. *Behav. Brain Res.* 161, 197–203. doi: 10.1016/j.bbr.2005.02.005

Markakis, E. A., and Gage, F. H. (1999). Adult-generated neurons in the dentate gyrus send axonal projections to field CA3 and are surrounded by synaptic vesicles. *J. Comp. Neurol.* 406, 449–460. doi: 10.1002/(SICI)1096-9861(19990419)406:4<449::AID-CNE3>3.0.CO;2-I

Martignoni, E., Blandini, F., Petraglia, F., Pacchetti, C., Bono, G., and Nappi, G. (1992). Cerebrospinal fluid norepinephrine, 3-methoxy-4-hydroxyphenylglycol and neuropeptide Y levels in Parkinson's disease, multiple system atrophy and dementia of the Alzheimer type. *J. Neural Transm. Park. Dis. Dement. Sect.* 4, 191–205. doi: 10.1007/BF02260903

Masuda, T., Nakagawa, S., Boku, S., Nishikawa, H., Takamura, N., Kato, A., et al. (2012). Noradrenaline increases neural precursor cells derived from adult rat dentate gyrus through beta2 receptor. *Prog. Neuropsychopharmacol. Biol. Psychiatry* 36, 44–51. doi: 10.1016/j.pnpbp.2011.08.019

Mather, M., and Harley, C. W. (2016). The locus coeruleus: essential for maintaining cognitive function and the aging brain. *Trends Cogn. Sci.* 20, 214–226. doi: 10.1016/j.tics.2016.01.001

Matthews, K. L., Chen, C. P., Esiri, M. M., Keene, J., Minger, S. L., and Francis, P. T. (2002). Noradrenergic changes, aggressive behavior, and cognition in patients with dementia. *Biol. Psychiatry* 51, 407–416. doi: 10.1016/S0006-3223(01)01235-5

Mattson, M. P. (2004). Pathways towards and away from Alzheimer's disease. *Nature* 430, 631–639. doi: 10.1038/nature02621

Mattson, M. P., and Chan, S. L. (2003). Neuronal and glial calcium signaling in Alzheimer's disease. *Cell Calcium* 34, 385–397. doi: 10.1016/S0143-4160(03)00128-3

Mauch, D. H., Nägler, K., Schumacher, S., Göritz, C., Müller, E. C., Otto, A., et al. (2001). CNS synaptogenesis promoted by glia-derived cholesterol. *Science* 294, 1354–1357. doi: 10.1126/science.294.5545.1354

Milstein, J. A., Lehmann, O., Theobald, D. E., Dalley, J. W., and Robbins, T. W. (2007). Selective depletion of cortical noradrenaline by anti-dopamine beta-hydroxylase-saporin impairs attentional function and enhances the effects of guanfacine in the rat. *Psychopharmacology* 190, 51–63. doi: 10.1007/s00213-006-0594-x

Mohapel, P., Leanza, G., Kokaia, M., and Lindvall, O. (2005). Forebrain acetylcholine regulates adult hippocampal neurogenesis and learning. *Neurobiol Aging* 26, 939–946. doi: 10.1016/j.neurobiolaging.2004.07.015

Mohapel, P., Mundt-Petersen, K., Brundin, P., and Frielingsdorf, H. (2006). Working memory training decreases hippocampal neurogenesis. *Neuroscience* 142, 609–613. doi: 10.1016/j.neuroscience.2006.07.033

Mohs, R. C., Shiovitz, T. M., Tariot, P. N., Porsteinsson, A. P., Baker, K. D., and Feldman, P. D. (2009). Atomoxetine augmentation of cholinesterase inhibitor therapy in patients with Alzheimer disease: 6-month, randomized, double-blind, placebo-controlled, parallel-trial study. A*m. J. Geriatr. Psychiatry* 17, 752–759. doi: 10.1097/JGP.0b013e3181aad585

Monai, H., Ohkura, M., Tanaka, M., Oe, Y., Konno, A., Hirai, H., et al. (2016). Calcium imaging reveals glial involvement in transcranial direct current stimulation-induced plasticity in mouse brain. *Nat. Commun.* 7:11100. doi: 10.1038/ncomms11100

Mrak, R. E., and Griffin, W. S. (2005). Glia and their cytokines in progression of neurodegeneration. *Neurobiol. Aging* 26, 349–354. doi: 10.1016/j.neurobiolaging.2004.05.010

Murchison, C. F., Zhang, X. Y., Zhang, W. P., Ouyang, M., Lee, A., and Thomas, S. A. (2004). A distinct role for norepinephrine in memory retrieval. *Cell* 117, 131–143. doi: 10.1016/S0092-8674(04)00259-4

Nagele, R. G., Wegiel, J., Venkataraman, V., Imaki, H., and Wang, K. C. (2004). Contribution of glial cells to the development of amyloid plaques in Alzheimer's disease. *Neurobiol. Aging* 25, 663–674. doi: 10.1016/j.neurobiolaging.2004.01.007

Nazarali, A. J., and Reynolds, G. P. (1992). Monoamine neurotransmitters and their metabolites in brain regions in Alzheimer's disease: a postmortem study. *Cell Mol. Neurobiol.* 12, 581–587. doi: 10.1007/BF00711237

Nedergaard, M., Rodriguez, J. J., and Verkhratsky, A. (2010). Glial calcium and diseases of the nervous system. *Cell Calcium* 47, 140–149. doi: 10.1016/j.ceca.2009.11.010

Oe, Y., Baba, O., Ashida, H., Nakamura, K. C., and Hirase, H. (2016). Glycogen distribution in the microwave-fixed mouse brain reveals heterogeneous astrocytic patterns. G*lia*. doi: 10.1002/glia.23020

Olabarria, M., Noristani, H. N., Verkhratsky, A., and Rodríguez, J. J. (2010). Concomitant astroglial atrophy and astrogliosis in a triple transgenic animal model of Alzheimer's disease. *Glia* 58, 831–838. doi: 10.1002/glia.20967

Olabarria, M., Noristani, H. N., Verkhratsky, A., and Rodríguez, J. J. (2011). Age-dependent decrease in glutamine synthetase expression in the hippocampal astroglia of the triple transgenic Alzheimer's disease mouse model: mechanism for deficient glutamatergic transmission? *Mol. Neurodegener.* 6:55. doi: 10.1186/1750-1326-6-55

Pankratov, Y., and Lalo, U. (2015). Role for astroglial alpha1-adrenoreceptors in gliotransmission and control of synaptic plasticity in the neocortex. *Front. Cell Neurosci.* 9:230. doi: 10.3389/fncel.2015.00230

Parpura, V., Heneka, M. T., Montana, V., Oliet, S. H., Schousboe, A., Haydon, P. G., et al. (2012). Glial cells in (patho)physiology. *J. Neurochem.* 121, 4–27. doi: 10.1111/j.1471-4159.2012.07664.x

Parpura, V., and Zorec, R. (2010). Gliotransmission: exocytotic release from astrocytes. *Brain Res. Rev.* 63, 83–92. doi: 10.1016/j.brainresrev.2009.11.008

Pascual, J., Grijalba, B., Garcia-Sevilla, J. A., Zarranz, J. J., and Pazos, A. (1992). Loss of high-affinity alpha 2-adrenoceptors in Alzheimer's disease: an autoradiographic study in frontal cortex and hippocampus. *Neurosci. Lett.* 142, 36–40. doi: 10.1016/0304-3940(92)90614-D

Paukert, M., Agarwal, A., Cha, J., Doze, V. A., Kang, J. U., and Bergles, D. E. (2014). Norepinephrine controls astroglial responsiveness to local circuit activity. *Neuron* 82, 1263–1270. doi: 10.1016/j.neuron.2014.04.038

Pekny, M., Pekna, M., Messing, A., Steinhauser, C., Lee, J. M., Parpura, V., et al. (2016). Astrocytes: a central element in neurological diseases. *Acta Neuropathol.* 131, 323–345. doi: 10.1007/s00401-015-1513-1

Peterson, A. C., and Li, C. R. (2018). Noradrenergic dysfunction in Alzheimer's and Parkinson's Diseases-an overview of imaging studies. *Front. Aging Neurosci.* 10:127. doi: 10.3389/fnagi.2018.00127

Picklo, M. J., Wiley, R. G., Lappi, D. A., and Robertson, D. (1994). Noradrenergic lesioning with an anti-dopamine beta-hydroxylase immunotoxin. *Brain Res.* 666, 195–200. doi: 10.1016/0006-8993(94)90772-2

Pintus, R., Riggi, M., Cannarozzo, C., Valeri, A., de Leo, G., Romano, M., et al. (2018). Essential role of hippocampal noradrenaline in the regulation of spatial working memory and TDP-43 tissue pathology. *J. Comp. Neurol.* 526, 1131–1147. doi: 10.1002/cne.24397

Prebil, M., Vardjan, N., Jensen, J., Zorec, R., and Kreft, M. (2011). Dynamic monitoring of cytosolic glucose in single astrocytes. *Glia* 59, 903–913. doi: 10.1002/glia.21161

Rodriguez-Vieitez, E., Saint-Aubert, L., Carter, S. F., Almkvist, O., Farid, K., Schöll, M., et al. (2016). Diverging longitudinal changes in astrocytosis and amyloid PET in autosomal dominant Alzheimer's disease. Brain 139(Pt 3):922–936. doi: 10.1093/brain/awv404

Rub, U., Del Tredici, K., Schultz, C., Thal, D. R., Braak, E., and Braak, H. (2001). The autonomic higher order processing nuclei of the lower brain stem are among the early targets of the Alzheimer's disease-related cytoskeletal pathology. *Acta Neuropathol.* 101, 555–564.

Sacchetti, G., Bernini, M., Bianchetti, A., Parini, S., Invernizzi, R. W., and Samanin, R. (1999). Studies on the acute and chronic effects of reboxetine on extracellular noradrenaline and other monoamines in the rat brain. *Br. J. Pharmacol.* 128, 1332–1338.

Salcedo-Sora, J. E., Caamano-Gutierrez, E., Ward, S. A., and Biagini, G. A. (2014). The proliferating cell hypothesis: a metabolic framework for Plasmodium growth and development. T*rends Parasitol.* 30, 170–175. doi: 10.1016/j.pt.2014.02.001

Salm, A. K., and McCarthy, K. D. (1989). Expression of beta-adrenergic receptors by astrocytes isolated from adult rat cortex. *Glia* 2, 346–352.

Sanchez-Padilla, J., Guzman, J. N., Ilijic, E., Kondapalli, J., Galtieri, D. J., Yang, B., et al. (2014). Mitochondrial oxidant stress in locus coeruleus is regulated by activity and nitric oxide synthase. *Nat. Neurosci.* 17, 832–840. doi: 10.1038/nn.3717

Santarelli, L., Saxe, M., Gross, C., Surget, A., Battaglia, F., Dulawa, S., et al. (2003). Requirement of hippocampal neurogenesis for the behavioral effects of antidepressants. *Science* 301, 805–809. doi: 10.1126/science.1083328

Sara, S. J. (2009). The locus coeruleus and noradrenergic modulation of cognition. *Nat. Rev. Neurosci.* 10, 211–223. doi: 10.1038/nrn2573

Satoh, A., and Iijima, K. M. (2017). Roles of tau pathology in the locus coeruleus (LC) in age-associated pathophysiology and Alzheimer's disease pathogenesis: Potential strategies to protect the LC against aging. *Brain Res.* doi: 10.1016/j.brainres.2017.12.027. [Epub ahead of print].

Scullion, G. A., Kendall, D. A., Marsden, C. A., Sunter, D., and Pardon, M. C. (2011). Chronic treatment with the alpha2-adrenoceptor antagonist fluparoxan prevents age-related deficits in spatial working memory in APPxPS1 transgenic mice without altering beta-amyloid plaque load or astrocytosis. N*europharmacology* 60, 223–234. doi: 10.1016/j.neuropharm.2010.09.002

Segal, S. K., Stark, S. M., Kattan, D., Stark, C. E., and Yassa, M. A. (2012). Norepinephrine-mediated emotional arousal facilitates subsequent pattern separation. *Neurobiol Learn. Mem.* 97, 465–469. doi: 10.1016/j.nlm.2012.03.010

Sherpa, A. D., Xiao, F., Joseph, N., Aoki, C., and Hrabetova, S. (2016). Activation of beta-adrenergic receptors in rat visual cortex expands astrocytic processes and reduces extracellular space volume. S*ynapse* 70, 307–316. doi: 10.1002/syn.21908

Shimohama, S., Taniguchi, T., Fujiwara, M., and Kameyama, M. (1986). Biochemical characterization of alpha-adrenergic receptors in human brain and changes in Alzheimer-type dementia. *J. Neurochem.* 47, 1295–1301.

Singh, C., Liu, L., Wang, J. M., Irwin, R. W., Yao, J., Chen, S., et al. (2012). Allopregnanolone restores hippocampal-dependent learning and memory and neural progenitor survival in aging 3xTgAD and nonTg mice. *Neurobiol. Aging* 33, 1493–1506. doi: 10.1016/j.neurobiolaging.2011.06.008

Sontag, T. A., Hauser, J., Kaunzinger, I., Gerlach, M., Tucha, O., and Lange, K. W. (2008). Effects of the noradrenergic neurotoxin DSP4 on spatial memory in the rat. *J. Neural. Transm.* 115, 299–303. doi: 10.1007/s00702-007-0830-5

Sparks, D. L., DeKosky, S. T., and Markesbery, W. R. (1988). Alzheimer's disease. Aminergic-cholinergic alterations in hypothalamus. *Arch. Neurol.* 45, 994–999.

Starke, K. (2001). Presynaptic autoreceptors in the third decade: focus on alpha2-adrenoceptors. *J. Neurochem* 78, 685–693.

Stenovec, M., Trkov, S., Lasič, E., Terzieva, S., Kreft, M., Rodríguez Arellano, J. J., et al. (2016). Expression of familial Alzheimer disease presenilin 1 gene attenuates vesicle traffic and reduces peptide secretion in cultured astrocytes devoid of pathologic tissue environment. *Glia* 64, 317–329. doi: 10.1002/glia.22931

Strassnig, M., and Ganguli, M. (2005). About a peculiar disease of the cerebral cortex: Alzheimer's original case revisited. *Psychiatry* 2, 30–33.

Studelska, D. R., and Brimijoin, S. (1989). Partial isolation of two classes of dopamine beta-hydroxylase-containing particles undergoing rapid axonal transport in rat sciatic nerve. *J. Neurochem* .53, 622–631.

Swanson, L. W., and Hartman, B. K. (1975). The central adrenergic system. An immunofluorescence study of the location of cell bodies and their efferent connections in the rat utilizing dopamine-beta-hydroxylase as a marker. *J. Comp. Neurol.* 163, 467–505.

Szot, P., Miguelez, C., White, S. S., Franklin, A., Sikkema, C., Wilkinson, C. W., et al. (2010). A comprehensive analysis of the effect of DSP4 on the locus coeruleus noradrenergic system in the rat. *Neuroscience* 166, 279–291. doi: 10.1016/j.neuroscience.2009

Szot, P., White, S. S., Greenup, J. L., Leverenz, J. B., Peskind, E. R., and Raskind, M. A. (2006). Compensatory changes in the noradrenergic nervous system in the locus ceruleus and hippocampus of postmortem subjects with Alzheimer's disease and dementia with Lewy bodies. *J. Neurosci.* 26, 467–478. doi: 10.1523/JNEUROSCI.4265-05.2006

Szot, P., White, S. S., Greenup, J. L., Leverenz, J. B., Peskind, E. R., and Raskind, M. A. (2007). Changes in adrenoreceptors in the prefrontal cortex of subjects with dementia: evidence of compensatory changes. *Neuroscience* 146, 471–480. doi: 10.1016/j.neuroscience.2007.01.031

Tang, F., Lane, S., Korsak, A., Paton, J. F., Gourine, A. V., Kasparov, S., et al. (2014). Lactate-mediated glia-neuronal signalling in the mammalian brain. *Nat. Commun.* 5:3284. doi: 10.1038/ncomms4284

Terry, R. D. (2000). Cell death or synaptic loss in Alzheimer disease. *J. Neuropathol. Exp. Neurol* .59, 1118–1189.

Thomas, S. A., and Palmiter, R. D. (1997). Disruption of the dopamine beta-hydroxylase gene in mice suggests roles for norepinephrine in motor function, learning, and memory. *Behav. Neurosci.* 111, 579–589.

Thrane, A. S., Rangroo Thrane, V., and Nedergaard, M. (2014). Drowning stars: reassessing the role of astrocytes in brain edema. *Trends Neurosci.* 37, 620–628. doi: 10.1016/j.tins.2014.08.010

Tohgi, H., Ueno, M., Abe, T., Takahashi, S., and Nozaki, Y. (1992). Concentrations of monoamines and their metabolites in the cerebrospinal fluid from patients with senile dementia of the Alzheimer type and vascular dementia of the Binswanger type. *J. Neural Transm. Par.k Dis. Dement. Sect.* 4, 69–77.

Tomlinson, B. E., Irving, D., and Blessed, G. (1981). Cell loss in the locus coeruleus in senile dementia of Alzheimer type. *J. Neurol Sci.* 49, 419–428.

Van Dyck, C. H. (2014). *Guanfacine Treatment for Prefrontal Cognitive Dysfunction in Elderly Subjects*. Available online at: https://clinicaltrials.gov/ct2/show/NCT00935493

Vander Heiden, M. G., Cantley, L. C., and Thompson, C. B. (2009). Understanding the Warburg effect: the metabolic requirements of cell proliferation. S*cience* 324, 1029–1033. doi: 10.1126/science.1160809

Van Hoomissen, J. D., Holmes, P. V., Zellner, A. S., Poudevigne, A., and Dishman, R. K. (2004). Effects of beta-adrenoreceptor blockade during chronic exercise on contextual fear conditioning and mRNA for galanin and brain-derived neurotrophic factor. *Behav. Neurosci.* 118, 1378–1390.

van Praag, H., Schinder, A. F., Christie, B. R., Toni, N., Palmer, T. D., and Gage, F. H. (2002). Functional neurogenesis in the adult hippocampus. *Nature* 415, 1030–1034. doi: 10.1038/4151030a

Vardjan, N., Horvat, A., Anderson, J. E., Yu, D., Croom, D., Zeng, X., et al. (2016). Adrenergic activation attenuates astrocyte swelling induced by hypotonicity and neurotrauma. G*lia* 64, 1034–1049. doi: 10.1002/glia.22981

Vardjan, N., Kreft, M., and Zorec, R. (2014). Dynamics of β-adrenergic/cAMP signaling and morphological changes in cultured astrocytes. *Glia.*

Vardjan, N., and Zorec, R. (2015). Excitable astrocytes: Ca^{2+}- and cAMP-regulated exocytosis. *Neurochem. Res.* 40, 2414–2414. doi: 10.1007/s11064-015-1545-x

Verkhratsky, A., Marutle, A., Rodríguez-Arellano, J. J., and Nordberg, A. (2014). Glial Asthenia and Functional Paralysis: a new perspective on neurodegeneration and Alzheimer's disease. *Neuroscientist* 21, 552–568. doi: 10.1177/1073858414547132

Verkhratsky, A., and Nedergaard, M. (2014). Astroglial cradle in the life of the synapse. *Philos. Trans. R. Soc. Lond. B. Biol. Sci.* 369:20130595. doi: 10.1098/rstb.2013.0595

Verkhratsky, A., and Nedergaard, M. (2018). Physiology of Astroglia. *Physiol. Rev.* 98, 239–389. doi: 10.1152/physrev.00042.2016

Verkhratsky, A., and Parpura, V. (2015). Astrogliopathology in neurological, neurodevelopmental and psychiatric disorders. *Neurobiol. Dis.* 85, 254–261. doi: 10.1016/j.nbd.2015.03.025

Verkhratsky, A., Zorec, R., Rodriguez, J. J., and Parpura, V. (2016). Astroglia dynamics in ageing and Alzheimer's disease. *Curr. Opin. Pharmacol.* 26, 74–79. doi: 10.1016/j.coph.2015.09.011

Walker, T. L., White, A., Black, D. M., Wallace, R. H., Sah, P., and Bartlett, P. F. (2008). Latent stem and progenitor cells in the hippocampus are activated by neural excitation. *J. Neurosci* .28, 5240–5247. doi: 10.1523/JNEUROSCI.0344-08.2008

Warner-Schmidt, J. L., and Duman, R. S. (2006). Hippocampal neurogenesis: opposing effects of stress and antidepressant treatment. *Hippocampus* 16, 239–249. doi: 10.1002/hipo.20156

Weinshilboum, R. M. (1978). Serum dopamine beta-hydroxylase. *Pharmacol. Rev.* 30, 133–166.

Whitehouse, P. J., Price, D. L., Struble, R. G., Clark, A. W., Coyle, J. T., and Delon, M. R. (1982). Alzheimer's disease and senile dementia: loss of neurons in the basal forebrain. *Science* 215, 1237–1239.

Wiley, R. G., and Kline, I. R. (2000). Neuronal lesioning with axonally transported toxins. *J. Neurosci. Methods* 103, 73–82

Wilson, R. S., Nag, S., Boyle, P. A., Hizel, L. P., Yu, L., Buchman, A. S., et al. (2013). Neural reserve, neuronal density in the locus ceruleus, and cognitive decline. *Neurology* 80, 1202–1208. doi: 10.1212/WNL.0b013e3182897103

Woodruff-Pak, D. S. (2008). Animal models of Alzheimer's disease: therapeutic implications. *J. Alzheimers. Dis.* 15, 507–521.

Wrenn, C. C., Picklo, M. J., Lappi, D. A., Robertson, D., and Wiley, R. G. (1996). Central noradrenergic lesioning using anti-DBH-saporin: anatomical findings. *Brain Res.* 740, 175–184.

Yeh, C. Y., Vadhwana, B., Verkhratsky, A., and Rodríguez, J. J. (2011). Early astrocytic atrophy in the entorhinal cortex of a triple transgenic animal model of Alzheimer's disease. *ASN Neuro* 3, 271–279. doi: 10.1042/AN20110025

Zorec, R., Horvat, A., Vardjan, N., and Verkhratsky, A. (2015). Memory Formation Shaped by Astroglia. *Front. Integr. Neurosci.* 9:56. doi: 10.3389/fnint.2015.00056

Zorec, R., Parpura, V., and Verkhratsky, A. (2018). Astroglial vesicular network: evolutionary trends, physiology and pathophysiology. *Acta Physiol.* 222. doi: 10.1111/apha.12915

Zorec, R., Vardjan, N., and Verkhratsky, A. (2017). "Locus Coeruleus Noradrenergic Neurons and Astroglia in Health and Disease,' in N*oradrenergic Signaling and Astroglia,* eds N. Vardjan and R. Zorec (Oxford: Academic Press), 1–24.

Conflict of Interest Statement: The authors declare that the research was conducted in the absence of any commercial or financial relationships that could be construed as a potential conflict of interest.

frontiers in Molecular Neuroscience

ORIGINAL RESEARCH
published: 13 July 2018
doi: 10.3389/fnmol.2018.00239

Diversity of Astroglial Effects on Aging- and Experience-Related Cortical Metaplasticity

Ulyana Lalo[1], *Alexander Bogdanov*[2] *and Yuriy Pankratov*[1]*

[1]School of Life Sciences, University of Warwick, Coventry, United Kingdom, [2]Institute for Chemistry and Biology, Immanuel Kant Baltic Federal University, Kaliningrad, Russia

Activity-dependent regulation of synaptic plasticity, or metaplasticity, plays a key role in the adaptation of neuronal networks to physiological and biochemical changes in aging brain. There is a growing evidence that experience-related alterations in the mechanisms of synaptic plasticity can underlie beneficial effects of physical exercise and caloric restriction (CR) on brain health and cognition. Astrocytes, which form neuro-vascular interface and can modulate synaptic plasticity by release of gliotransmitters, attract an increasing attention as important element of brain metaplasticity. We investigated the age- and experience-related alterations in astroglial calcium signaling and stimulus-dependence of long-term synaptic plasticity in the neocortex of mice exposed to the mild CR and environmental enrichment (EE) which included ad libitum physical exercise. We found out that astrocytic Ca^{2+}-signaling underwent considerable age-related decline but EE and CR enhanced astroglial signaling, in particular mediated by noradrenaline (NA) and endocannabinoid receptors. The release of ATP and D-Serine from astrocytes followed the same trends of age-related declined and EE-induced increase. Our data also showed that astrocyte-derived ATP and D-Serine can have diverse effects on the threshold and magnitude of long-term changes in the strength of neocortical synapses; these effects were age-dependent. The CR- and EE-induced enhancement of astroglial Ca^{2+}-signaling had more stronger effect on synaptic plasticity in the old (14–18 months) than in the young (2–5 months) wild-type (WT) mice. The effects of CR and EE on synaptic plasticity were significantly altered in both young and aged dnSNARE mice. Combined, our data suggest astrocyte-neuron interactions are important for dynamic regulation of cortical synaptic plasticity. This interaction can significantly decline with aging and thus contributes to the age-related cognitive impairment. On another hand, experience-related increase in the astroglial Ca^{2+}-signaling can ameliorate the age-related decline.

Keywords: ATP release, D-serine, caloric restriction, exocytosis, metaplasticy, CB1 receptors, BCM model

OPEN ACCESS

Edited by:
Alexej Verkhratsky,
University of Manchester,
United Kingdom

Reviewed by:
Frank Kirchhoff,
Saarland University, Germany
Sergey Kasparov,
University of Bristol, United Kingdom

***Correspondence:**
Yuriy Pankratov
y.pankratov@warwick.ac.uk

Received: *16 March 2018*
Accepted: *21 June 2018*
Published: *13 July 2018*

Citation:
Lalo U, Bogdanov A and Pankratov Y (2018) Diversity of Astroglial Effects on Aging- and Experience-Related Cortical Metaplasticity. Front. Mol. Neurosci. 11:239. doi: 10.3389/fnmol.2018.00239

INTRODUCTION

Although an age-related cognitive decline is widely recognized a major societal and scientific problem, fundamental mechanisms of brain longevity are not fully understood. Synaptic plasticity enables the mammalian brain to adapt to environmental challenges during development, adulthood and aging. Nowadays the age-related change in the cognitive functions is viewed not as complete loss of synaptic plasticity but as alteration of its mechanisms (Hillman et al., 2008; Nithianantharajah and Hannan, 2009; van Praag, 2009; Mercken et al., 2012; Merzenich et al., 2014).

Importantly, neural networks and synapses are remarkably responsive to environmental stimuli, physiological modifications, and experience (Hillman et al., 2008; Nithianantharajah and Hannan, 2009; van Praag, 2009; Mercken et al., 2012; Rodríguez et al., 2013; Merzenich et al., 2014). Physical exercise and environmental enrichment (EE) can have beneficial effects on aging brain, both in animal models and human patients (Hillman et al., 2008; Nithianantharajah and Hannan, 2009; van Praag, 2009; Mercken et al., 2012; Merzenich et al., 2014). Also, caloric restriction (CR), usually defined as a reduced intake of calories not causing malnutrition, can have life-extending effects, linked to improvement of brain health and plasticity (Mercken et al., 2012; Park et al., 2012; Madeo et al., 2014; López-Otín et al., 2016).

Aging- and experience-related alterations in synaptic plasticity are closely linked to brain metaplasticity, which is usually defined as "the plasticity of synaptic plasticity." Metaplasticity can occur when priming synaptic or cellular activity or inactivity leads to persistent change in the direction or degree of synaptic plasticity (Abraham and Bear, 1996; Hulme et al., 2013a). Astrocytes are gaining an increasing attention as a very important element of brain cellular networks regulating metaplasticity (Hulme et al., 2013b; Monai et al., 2016; Boué-Grabot and Pankratov, 2017; Singh and Abraham, 2017). Astrocytes form interface between the synapses and brain vasculature (Gourine et al., 2010; Halassa and Haydon, 2010; Araque et al., 2014) and therefore are strategically positioned to couple the enriched mental and physical activity to the brain longevity. Astrocytes can also respond to both high-fat and calorie-restricted diet (Seidel et al., 2006; Lin et al., 2014; Metna-Laurent and Marsicano, 2015).

Importantly, astrocytes can exert bi-directional effects on synaptic plasticity by releasing different gliotransmitters (Pascual et al., 2005; Henneberger et al., 2010; Araque et al., 2014; Pougnet et al., 2014; Rasooli-Nejad et al., 2014; Pankratov and Lalo, 2015; Lalo et al., 2016; Boué-Grabot and Pankratov, 2017; Papouin et al., 2017a). It is conceivable that overall effect of astroglia on plasticity of particular type of synapses would depend on physiological (or pathological) context, i.e., pattern of local neural activity, repertoire of transmitters released from neurons and repertoire of post- and pre-synaptic receptors expressed in the synapse. Such dependence of astroglial modulation of synaptic plasticity on prior activity of network can render an important role for astrocytes in metaplasticity (Hulme et al., 2013b; Monai et al., 2016; Boué-Grabot and Pankratov, 2017; Singh and Abraham, 2017).

The responsiveness of synaptic plasticity to EE, physical activity and CR provides an opportunity to ameliorate the negative consequences of aging on cognitive function. Still, fundamental cellular and molecular mechanisms underlying the impact of CR and exercise on brain metaplasticity remain largely unexplored. There are also many uncertainties in the mechanisms of neuro-glial interaction (Bazargani and Attwell, 2016; Papouin et al., 2017b; Singh and Abraham, 2017; Fiacco and McCarthy, 2018; Savtchouk and Volterra, 2018), particularly in the aging brain (Rodríguez et al., 2014; Verkhratsky et al., 2014, 2017). Until recently, most studies of brain aging have been focused on functional changes in neural networks and alterations in neuronal morphology and gene expression whereas glia-neuron interactions remained largely overlooked. Recent reports of aging-related changes of Ca^{2+} -signaling, morphology and gene expression in astrocytes (Lalo et al., 2011, 2014b; Rodríguez et al., 2014; Verkhratsky et al., 2014, 2017; Soreq et al., 2017) highlighted a crucial importance of study of brain aging and neurodegeneration in the context of complex cellular interactions which maintain synaptic dynamics and homeostasis (De Strooper and Karran, 2016). Still, changes in the glia-driven modulation of synaptic metaplasticity in aging brain remain almost unexplored.

In the present article, we explored role for astroglial Ca^{2+}-signaling and release of gliotransmitters in aging- and environment-related cortical metaplasticity. As a model of impaired astroglial exocytosis, we used dnSNARE mice whose validity, in particular the lack of neuronal expression of dnSNARE, has been recently verified (Pankratov and Lalo, 2015; Sultan et al., 2015; Lalo et al., 2016).

MATERIALS AND METHODS

All animal work has been carried out in accordance with UK legislation (ASPA) and "3R" strategy; all experimental protocols were approved by University of Warwick Ethical Review Committee and Animal Welfare Committee.

Slice and Cell Preparation

Mice of two aged groups, 2–5 (average 3.3) months and 14–18 (average 16.8) months were anesthetized by halothane and then decapitated, in accordance with UK legislation. Brains were removed rapidly after decapitation and placed into ice-cold physiological saline containing (mM): NaCl 130, KCl 3, $CaCl_2$ 0.5, $MgCl_2$ 2.5, NaH_2PO_4 1, $NaHCO_3$ 25, glucose 15, pH of 7.4 gassed with 95% O_2–5% CO_2. Transverse slices (280 μm) were cut at 4^o C and then placed in physiological saline containing (mM): NaCl 130, KCl 3, $CaCl_2$ 2.5, $MgCl_2$ 1, NaH_2PO_4 1, $NaHCO_3$ 22, glucose 15, pH of 7.4 gassed with 95% O_2–5% CO_2 and kept for 1–4 h prior to cell isolation and recording.

Astrocytes were identified by their morphology under DIC observation, EGFP fluorescence (astrocytes from dn-SNARE and GFAP-EGFP mice) or staining with sulforhodamine 101 (astrocytes from WT mice). After recording, the identification of astrocyte was confirmed via functional properties (high potassium conductance, low input resistance, strong activity of glutamate transporters) as described previously (Lalo et al., 2011, 2014a; Rasooli-Nejad et al., 2014; Pankratov and Lalo, 2015).

Electrophysiological Recordings

Whole-cell voltage clamp recordings from cortical neurones and astrocytes cells were made with patch pipettes (4–5 MΩ) filled with intracellular solution (in mM): 110 CsCl, 10 NaCl, 10 HEPES, 5 MgATP, 1 D-Serine, 0.1 EGTA, pH 7.35; Currents were monitored using an MultiClamp 700B patch-clamp amplifier (Axon Instruments, USA) filtered at 2 kHz

and digitized at 4 kHz. Experiments were controlled by Digidata1440A data acquisition board (Axon Instruments, USA) and WinWCP software (Strathclyde University, UK); data were analyzed by self-designed software. Liquid junction potentials were compensated with the patch-clamp amplifier. The series and input resistances were respectively 5–7 MΩ and 600–1100 MΩ; both series and input resistance varied by less than 20% in the cells accepted for analysis.

Field excitatory postsynaptic potentials (fEPSPs) were measured via a glass micropipette filled with extracellular solution (0.5–1 MΩ resistance) placed in neocortical layer II/III. The fEPSPs were evoked by the stimulation of neuronal afferents descending from layers IV–V. For activation of synaptic inputs, axons originating from layer IV–VI neurons were stimulated with a bipolar coaxial electrode (WPI, USA) placed in layer V close to the layer IV border, approximately opposite the site of recording; stimulus duration was 300 μs. The stimulus magnitude was set 3–4 times higher than the minimal stimulus necessary to elicit a response in layer II pyramidal neurons (Rasooli-Nejad et al., 2014; Pankratov and Lalo, 2015; Lalo et al., 2016).

The long-term potentiation/depression (LTP/LTD) was induced by different number of trains of high-frequency theta-burst stimulation (HFS-trains); each train (100 ms-long) consisted of 10 pulses stimulated at 100 Hz, trains were delivered with 200 ms intervals, every 10 trains were separated by 10 s-long intervals.

Multi-photon Fluorescent Ca^{2+}-Imaging in Astrocytes

To monitor the cytoplasmic free Ca^{2+}concentraton ($[Ca^{2+}]_i$) *in situ*, astrocytes of neocortical slices were loaded via 30 min incubation with 1 μM of Rhod-2AM or Oregon Green Bapta-2AM and sulphorhodamine 101 (wild-type (WT) mice) at 33°C. Two-photon images of neurons and astrocytes were acquired at 5 Hz frame-rate using a Zeiss LSM-7MP multi-photon microscope coupled to a SpectraPhysics MaiTai pulsing laser; experiments were controlled by ZEN LSM software (Carl Zeiss, Germany). Images were further analyzed offline using ZEN LSM (Carl Zeiss) and ImageJ (NIH) software. The $[Ca^{2+}]_i$ levels were expressed as ΔF/F ratio averaged over a region of interest (ROI). For analysis of spontaneous Ca^{2+}–transients in astrocytes, three ROIs located over dendrites and one ROI located over the soma were chosen. Overall Ca^{2+}-response to receptors agonists or synaptic stimulation was quantified using an ROI covering the whole cell image.

Measurement of Extracellular Concentration of ATP and D-Serine in the Brain Tissue

The concentration of ATP within cortical slices was measured using microelectrode biosensors obtained from Sarissa Biomedical Ltd (Coventry, UK). A detailed description of the properties of biosensors and recording procedure has been published previously (Frenguelli et al., 2007). Briefly, biosensors consisted of ATP or D-Serine metabolizing enzymes immobilized within a matrix on thin (25 μM) Pt/Ir wire. This allowed insertion of the sensors into the cortical slice and minimized the influence of a layer of dead surface tissue. ATP and D-serine biosensors were used simultaneously. A third, null, biosensor was also used. This sensor is identical to the ATP and D-serine sensors and has a matrix, but lacks enzymes. The signal from the null sensor was subtracted from the signal obtained on the ATP and D-serine sensor. This allows the contribution of any non-specific electroactive substances that bypass the sensor screening layer to be eliminated. Biosensors show a linear response to increasing concentration of ATP and D-Serine and have a rise time less than 10 s (Frenguelli et al., 2007). Biosensors were calibrated with known concentrations (10 μM) of ATP and D-Serine before the slice was present in the perfusion chamber and after the slice had been removed. This allowed compensation of any reduction in sensitivity during the experiment. The integrity of the screening layer was assessed with 10 μM 5-HT. Biosensor signals were acquired at 1 kHz with a 1400 CED interface and analyzed using Spike 6.1 software (Cambridge Electronics Design, Cambridge, UK).

Data Analysis

All data are presented as mean ± SD and the statistical significance of differences between data groups was tested by two-tailed unpaired *t*-test, unless indicated otherwise. For all cases of statistical significance reported, the statistical power of the test was 0.8–0.9. Each neocortical slice was used only for one experiment (e.g., fluorescent recordings in single astrocyte or single LTP induction experiment). The number of experiments/cells reported is therefore equal to the number of slices used. The experimental protocols were allocated randomly so the data in any group were drawn from at least from four animals, typically from 5 to 12 mice. The average ratio of experimental unit per animal was 1.3 for the LTP experiments and 1.5 for biosensor and fluorescent Ca^{2+}-measurements.

The spontaneous transmembrane currents recorded in neurons were analyzed offline using methods described previously (Lalo et al., 2011, 2016). The amplitude distributions of spontaneous and evoked currents were analyzed with the aid of probability density functions and likelihood maximization techniques; all histograms shown were calculated as probability density functions. The amplitude distributions were fitted with either multi-quantal binomial model or bi-modal function consisting of two Gaussians with variable peak location, width and amplitude. Parameters of models were fit using likelihood maximization routine.

RESULTS

Age- and Environment-Related Alterations in Astroglial Ca^{2+}-Signaling

Previously, we have reported the aging-related decline in the density of purinergic and glutamatergic receptors and their contribution to Ca^{2+}-signaling in neocortical astrocytes (Lalo et al., 2011, 2014b). In accordance with decrease in the Ca^{2+}-signaling, the exocytosis of gliotransmitters, such ATP, D-Serine

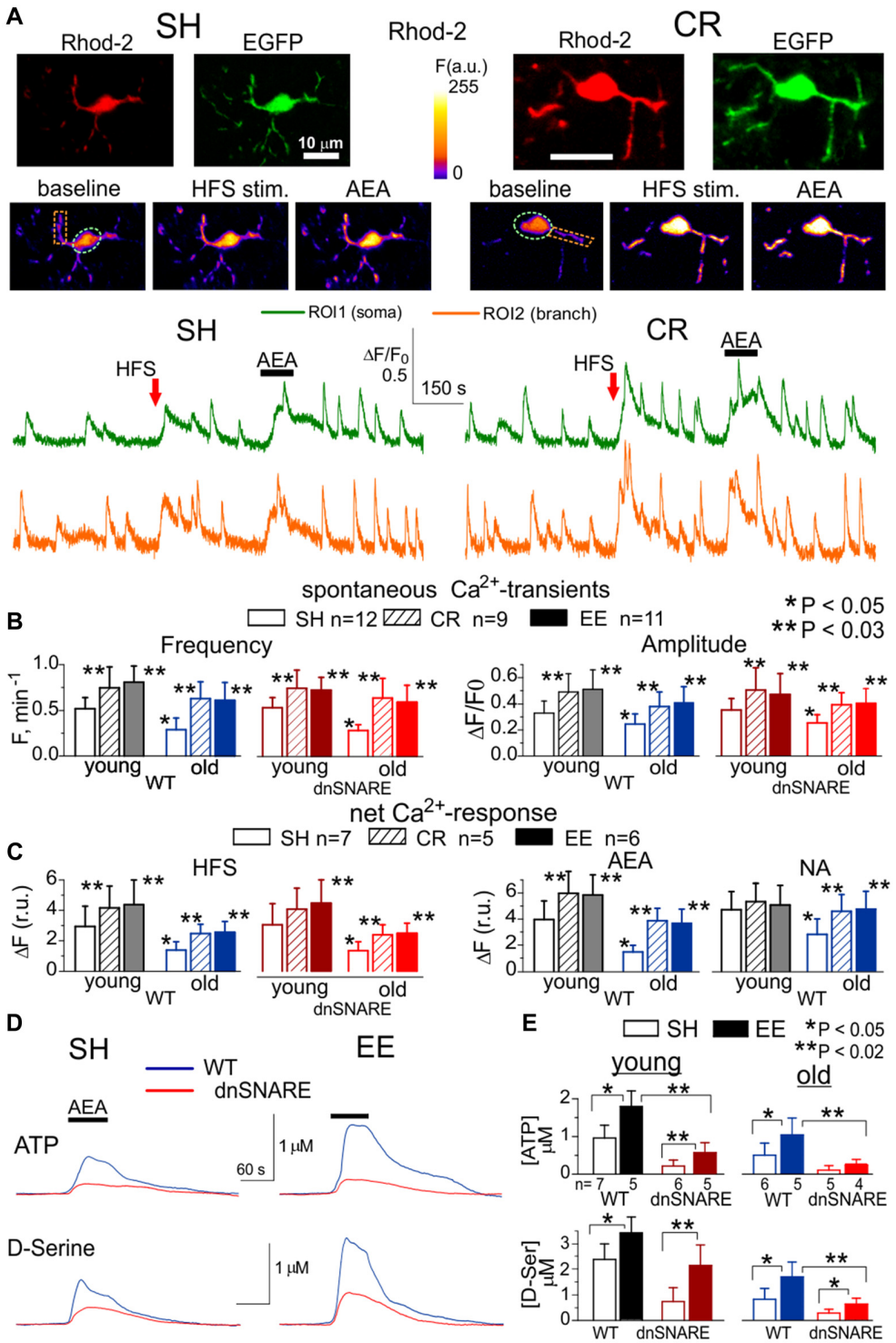

FIGURE 1 | Age- and experience-related changes in the adrenergic Ca^{2+} signaling and release of gliotransmitters in the neocortex. Astroglial Ca^{2+} -signaling **(A–C)** and release of ATP and D-Serine were evaluated in the neocortex of 2–5 month-old (young) and 14–18 month-old mice (old) as described previously in Lalo et al. (2014a), Rasooli-Nejad et al. (2014) and Pankratov and Lalo (2015). The dnSNARE mice and their wild-type (WT) littermates were kept either in standard housing (SH) or exposed to environmental enrichment (EE) or caloric restriction (CR) as described in the text. **(A)** Representative multi-photon images of EGFP fluorescence and presudo-color images of Rhod-2 fluorescence recorded in the astrocytes of old dn-SNARE mouse before and after the 100 ms-long episode of high-frequency stimulation (HFS) of cortical afferents and application of CB1 receptor agonist anandamide (AEA). Graphs below show the time course of Rhod-2 fluorescence

(*Continued*)

FIGURE 1 | Continued
averaged over regions indicated in the fluorescent images. Note the increase in the spontaneous in the Ca^{2+} -elevations and responses to HFS and application of AEA. **(B)** The pooled data on peak amplitude and frequency of the baseline spontaneous Ca^{2+}- transients recorded in astrocytes of WT and dn-SNARE mice of different age and treatment groups. Number and size of spontaneous events were pooled for the whole cell image. **(C)** The pooled data on the net responses to the HFS and application of AEA (500 nM) and noradrenaline (NA, 1 μM). Net response was evaluated as an integral Ca^{2+}-signal measured within 3 min after stimulation, averaged over the whole cell image and normalized to the baseline integral Ca^{2+} signal. Data in the panels **(B,C)** shown as mean ± SD for the number of cells indicated. Note the lack of the difference in the Ca^{2+}-signaling in the WT and dnSNARE mice. Asterisks (*,**) indicate statistical significance of the effect of EE- or CR-treatment (as compared to SH) and difference between the old and young mice of the same treatment group. **(D,E)** AEA-activated release of ATP and D-Serine in the neocortical slices of SH and EE mice was detected using microelectrode sensors as described previously (Lalo et al., 2014a,b; Rasooli-Nejad et al., 2014). **(E)** The representative responses of cortical slices of the old WT and dn-SNARE mice to the application of 500 nM AEA were recorded using microelectrode sensors to ATP and D-Serine placed in the layer II/III. The data are shown as an elevation relative to the resting concentration. **(E)** The pooled data on the peak magnitude of ATP- and D-Serine transients evoked by application of AEA; data shown as mean ± SD for number of experiments indicated. Asterisks (*,**) indicate statistical significance of difference in the magnitude of ATP- and D-serine responses between WT and dn-SNARE mice (unpaired *t*-test) and SH- and EE-mice of similar genotype. The significant reduction in the AEA-evoked responses in the cortical slices from dn-SNARE mice strongly supports the vesicular mechanism of ATP and D-Serine release from astrocytes. Note the decrease in the ATP- and D-Serine transients in the old mice and EE-induced increase.

and Glutamate, from neocortical astrocytes also declined with aging (Lalo et al., 2011, 2014b; Lalo and Pankratov, 2017). In the present work, we tried to elucidate whether EE or CR can mitigate the negative effects of aging. We have focused primarily on receptors for NA and endocannabinoids since recent results highlighted the importance of these receptors for glia-neuron communications (Min and Nevian, 2012; Ding et al., 2013; Paukert et al., 2014; Metna-Laurent and Marsicano, 2015; Pankratov and Lalo, 2015; Oliveira da Cruz et al., 2016). In particular, our data (Rasooli-Nejad et al., 2014; Pankratov and Lalo, 2015) have shown that both α1-adrenoreceptors and CB1 receptors can trigger release of gliotransmitters from neocortical astrocytes.

We explored the difference in the spontaneous and synaptically-evoked cytosolic Ca^{2+}-transients in the neocortical layer 2/3 astrocytes of 2–4 months old (young adults) and 14–18 months old (old) WT and dnSNAREs mice. Astroglial Ca^{2+} signaling was monitored using multi-photon fluorescent microscopy as described previously (Lalo et al., 2014a; Rasooli-Nejad et al., 2014; Pankratov and Lalo, 2015). We compared animals kept under standard housing conditions (SH) vs. animals exposed to the EE from birth (Correa et al., 2012), including *ad libitum* access to running wheel, or kept on mild CR(CR) diet (food intake individually regulated to maintain the body weight loss of 10%–15%) for 4–6 weeks. We also assessed the impact of exogenous activation of adrenergic and eCB receptors on astroglial Ca^{2+} signaling under these conditions (**Figures 1A,B**).

There was no significant difference in the astroglial Ca^{2+}-signaling between dnSNARE mice and their WT littermates. In both WT and dnSNARE mice of SH, the amplitude and frequency of spontaneous Ca^{2+}-transients in the neocortical astrocytes underwent significant decrease with aging. The EE and CR had significant positive effect on the astroglial Ca^{2+}-signaling both in the young and old mice (**Figures 1B,C**). Interestingly, effects of EE and CR on the amplitude and frequency of Ca^{2+}-transients in the old age (60%–95% and 70%–110% correspondingly) were more profound than in the young mice (35%–50% and 30%–45%).

To probe the responses of astrocyte to the stimulation of neighboring synapses, we evaluated astrocytic Ca^{2+}-transients evoked by the short episode of high-frequency stimulation (HFS) of thalamo-cortical afferents, as described previously (Lalo et al., 2011, 2016; Rasooli-Nejad et al., 2014). The HFS-evoked Ca^{2+}-responses followed the similar trends as spontaneous astroglial activity: significant reduction in the old age was opposed by EE- and CR-induced increase (**Figure 1C**).

Similarly to our previous reports (Rasooli-Nejad et al., 2014; Pankratov and Lalo, 2015), activation of CB1 receptors by 500 nM anandamide (AEA) or α1-adrenoreceptors by 1 μM NA evoked profound elevation in the cytosolic Ca^{2+} concentration in the astrocytes of young but not old mice (**Figures 1A,D**). The EE and CR had a moderate effect on the amplitudes of NA- and AEA-evoked responses in the young mice but caused the significant enhancement of astroglial responses in the old mice (**Figure 1D**).

Apart from direct activation of Ca^{2+}-responses, astroglial CB1 receptors and α1-adrenoreceptors are capable to enhance the spontaneous signaling, as reported previously (Min and Nevian, 2012; Rasooli-Nejad et al., 2014; Pankratov and Lalo, 2015). Indeed, application of NA or AEA caused significant increase in the amplitude and frequency of spontaneous Ca^{2+}-transients in the astrocytes of mice of SH (**Figure 1C**). Rather surprisingly, the relative effects of both NA and AEA were much smaller in the EE-mice or CR-mice. This was most likely related to the higher baseline spontaneous activity in astrocytes of EE- and CR-mice as compared to SH.

To evaluate the age-related alterations in gliotransmission, we measured extracellular concentrations of ATP and D-Serine in the neocortical tissue of WT and dnSNARE mice with microelectrode biosensors and activated astrocytes with AEA. In the old age and environment groups, the CB1 receptor-activated elevations in the ATP and D-Serine concentrations were significantly reduced in the dnSNARE mice, supporting the previous data (Lalo et al., 2014a,b; Rasooli-Nejad et al., 2014) on important contribution of astroglial exocytosis in the release of these transmitters. Consistent with changes in the Ca^{2+}-signaling, release of ATP and D-Serine significantly decreased in the old age but was strongly up-regulated by the EE (**Figures 1D,E**). These results closely agree with our previous data on adrenoceptor-activated release of gliotransmitters (Lalo and Pankratov, 2017).

Our results suggest a major role of astrocytes in the release of D-Serine, which is in line with numerous previous

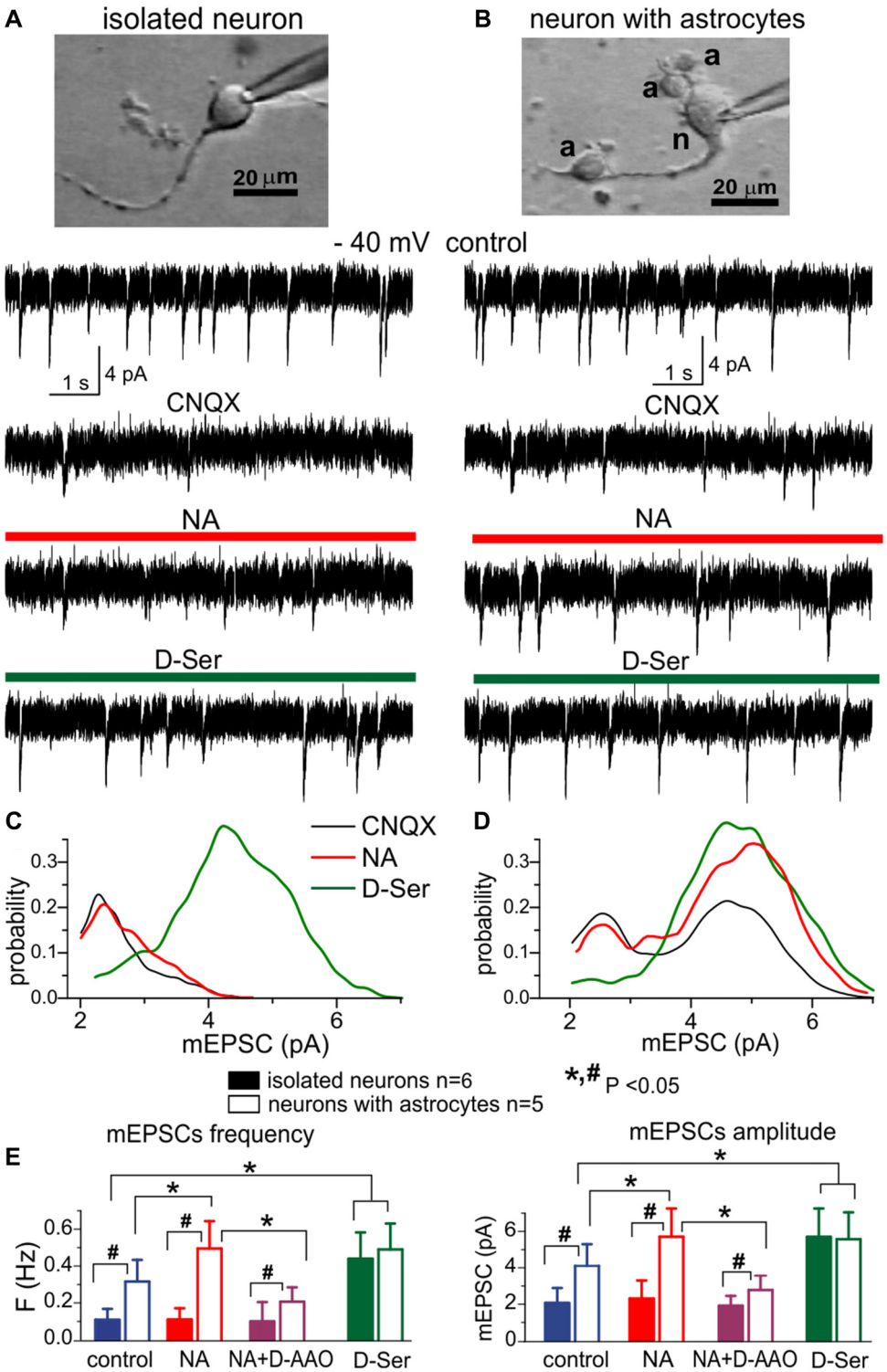

FIGURE 2 | The lack of efficient release of D-Serine from neurons. **(A,C)** Modulation of NMDA receptors by the D-Serine was evaluated in acutely isolated neocortical neurons retaining the functional glutamatergic synapses (Lalo et al., 2006; Lalo and Pankratov, 2017). **(B,D)** Similar recordings were made in the neuron attached to few astrocytes (marked as **"a"**) after dissociation of this neuron-astrocyte "bundle" from neocortex of WT mice; identification of astrocytes was confirmed by their electrophysiological properties after recordings (Lalo et al., 2014a; Rasooli-Nejad et al., 2014; Lalo and Pankratov, 2017). **(A,B)** Representative whole-cell currents recorded at −40 mV in the presence of picrotoxin, TTX, PPADS and 5-BDBD (control) before and after consecutive application of CNQX, (NA, 1 μM) and

(*Continued*)

FIGURE 2 | Continued
exogenous D-Serine (10 μM) after washout of NA. The transient events which can be seen in the neurons **(A,B)** in the control are miniature excitatory synaptic currents, as demonstrated in Lalo et al. (2006) and Lalo and Pankratov (2017). Note that amplitude and frequency of the events recorded in the control in fully isolated neurone are similar to the dissociated neurone with attached astrocytes **(B)**. Inhibition of AMPA receptors with CNQX markedly suppressed the spontaneous activity in the isolated neuron as compared to its counterpart with attached astrocytes **(B)**. The CNQX–insensitive currents were completely eliminated by application D-APV in both cases confirming they were mediated by NMDARs (data are not shown). **(C,D)** The corresponding amplitude distributions (probability density functions) for the spontaneous NMDAR currents recorded in neurons shown in **(A,B)**. **(E)** Pooled data (mean ± SD for number of cells indicated) on the amplitude and frequency of NMDAR-mediated mEPSCs recorded in fully isolated neurons (open bars) and dissociated neurons with attached astrocytes (closed bars) at −40 mV in presence of CNQX (control) and after application of NA alone, NA in presence of D-amino acid oxidase (DAAO, 0.15 U/ml) or exogenous D-Serine. The statistical significance (un-paired *t*-test) of the difference between fully isolated neurons and neurons with astrocytes is indicated by the hash symbol (#); asterisks (*) indicate statistically significance of the effect of NA and D-Serine in comparison to control conditions (−40 mV, CNQX). Note that the amplitude and frequency of NMDAR-mediated mEPSCs in fully isolated neurons were much lower in comparison to the dissociated neuron with astrocytes **(A,E)**. However, mEPSCs in the isolated neurons were restored in the presence of exogenous D-Serine, as evidenced by appearance of events with larger amplitude **(C)**. The most straightforward explanation is that most NMDA receptors on the membrane of fully isolated neurons were not exposed to sufficient concentrations of co-agonist until exogenous D-Serine was applied. Application of NA led to increase in the number of mEPSCs with larger amplitudes **(D)** in the neurons with attached astrocytes but not in fully isolated neurons, suggesting that effect of NA on synaptic transmission is mediated by release of gliotransmitters. The effect of NA on the amplitude and frequency of mEPSCs was strongly attenuated by D-AAO, suggesting the involvement of D-Serine.

reports (Panatier et al., 2006; Henneberger et al., 2010; Sultan et al., 2015; Papouin et al., 2017b). Since the importance and specificity of glial release of D-Serine is hotly debated currently (Wolosker et al., 2016; Papouin et al., 2017b; Savtchouk and Volterra, 2018), we tried to directly assess contribution of neurons and astrocytes in the release of D-serine. For this purpose, we used acutely-isolated neocortical neurons which were devoid of the influence of glial cells (**Figure 2**). We used non-enzymatic vibro-dissociation which retains functional synapses on the dendrites of isolated neurons, which can be verified by the presence of miniature spontaneous synaptic currents (Duguid et al., 2007; Rasooli-Nejad et al., 2014; Lalo et al., 2016; Lalo and Pankratov, 2017). Apart from the pure isolated neurons, the vibro-dissociation technique allows, upon some adjustment, to dissociate neurons with few astrocytes attached. Such neuron-astrocyte "bundle," retaining a certain proportion of intimate contacts between astrocytic and neuronal membranes, could serve as a "minimalistic" model of glia-neuron interaction unit (Rasooli-Nejad et al., 2014; Lalo and Pankratov, 2017).

We recorded the NMDA receptor-mediated spontaneous currents (NMDAR mEPSCs) in the acutely-dissociated neocortical pyramidal neurons at membrane potential of −40 mV in the presence of 100 μM picrotoxin, 30 μM CNQX and 20 μM PPADS (**Figures 2A,B**). To compensate for the putative depletion of neuronal D-Serine content due to intracellular perfusion, intracellular solution was supplemented with 1 mM D-Serine; intracellular concentration of EGTA was set to 0.1 mM. In the absence of external D-Serine or glycine, fully isolated neurons exhibited a low baseline frequency (0.11 ± 0.04 Hz, n = 6) of NMDAR-mediated mEPSCs and the application of NA did not cause notable changes in their amplitude or frequency (**Figures 2A,E**). Application of exogenous D-Serine dramatically increased the average amplitude and notably increased the frequency of mEPSCs. This was accompanied by the shift of mEPSCs amplitudes (**Figure 2C**) towards higher quantal size (from 2.3 ± 0.7 pA to 4.4 ± 1.2 pA, n = 6). In contrast to the fully isolated neurons, the NMDAR mEPSCs recorded in the "neuron-astrocyte bundles," could be observed at relative high frequency (0.32 ± 0.11 Hz) even in the absence of exogenous D-Serine (**Figure 2B**). They had bimodal amplitude distributions with peaks at 2.4 ± 0.8 pA and 4.7 ± 1.4 pA (n = 5). Activation of astrocytes by NA cause a significant increase both in the mean amplitude and frequency of mEPSCs in "neuron-astrocyte bundles" (correspondingly 49 ± 24% and 77 ± 38%, n = 5); which was accompanied by increase in the number of mEPSCs of larger quantal size (**Figure 2D**). Importantly, the NA-induced facilitation of mEPSCs was efficiently blocked by the application of exogenous D-amino acid oxidase (**Figure 2E**), suggesting an involvement of D-Serine in the action of NA. The effect of exogenous D-Serine on NMDAR mEPSCs in neurons with attached astrocytes did not differ considerably from the fully isolated neurons (**Figures 2D,E**).

The most parsimonious explanation of the above results would be a lack of D-Serine (or other co-agonists) in the vicinity of glutamatergic synapses devoid astroglial influence, which drives the amplitude of NMDAR mEPSCs below the threshold of detection. Activation of astrocytes by NA triggers release of D-serine, which diffuses to nearby synapses where it enhances the NMDAR mEPSCs. Application of exogenous D-Serine restores the amplitudes of NMDAR-mediated currents in majority of synapses. Our results argue against the predominant role of neurons in release of D-Serine (Wolosker et al., 2016) and agree with recent transcriptomic data on the expression of serine racemase (*SRR*) gene in cortical astrocytes (Chai et al., 2017) and *in vivo* data on the physiological role for glial-derived D-Serine (Papouin et al., 2017a,b).

Combined, the above results demonstrate that spontaneous and evoked Ca^{2+}-signaling in astrocytes and release of gliotransmitters can undergo significant decrease with aging but can be enhanced by EE or CR. It is also worth to note that astroglial CB1 and adrenergic receptors were capable to activate Ca^{2+}-elevation and release of gliotransmitters even in old mice of SH supporting the notion that glia-neuron communications do not stop with aging. Our data also show a common trend of EE and CR to enhance astroglial signaling mainly in case when it is "weakened," e.g., in the old mice and suggest an existence of "optimal" level of astroglial Ca^{2+}-signaling which may be reached in the younger age.

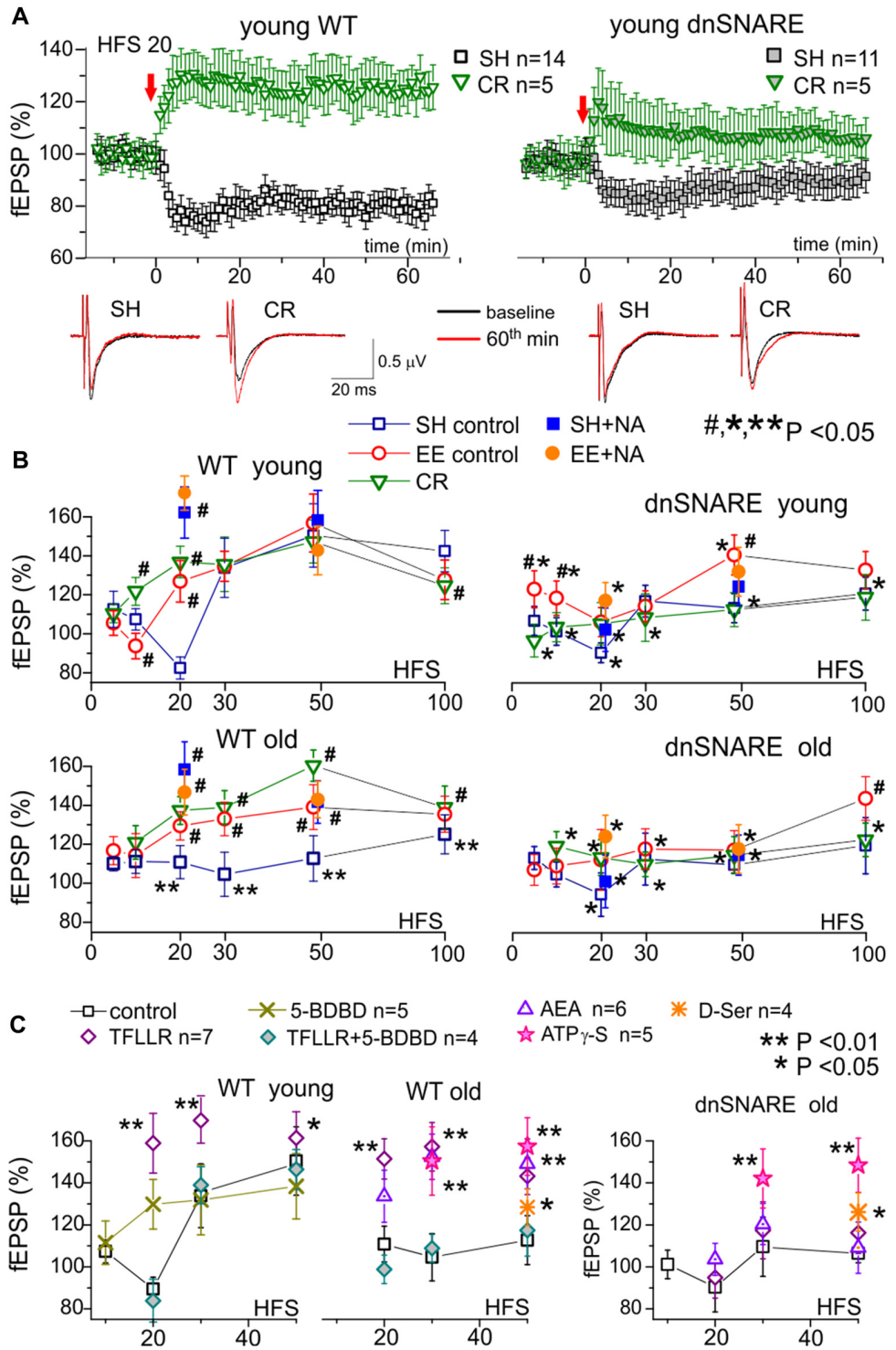

FIGURE 3 | Impact of gliotransmission on synaptic plasticity in the neocortex. Long-term potentiation (LTP) of field excitatory postsynaptic potentials (fEPSPs) was induced in the layer 2/3 of somatosensory cortex of the WT and dnSNARE mice by different number of pulses of high-frequency theta-burst stimulation (100 ms-long trains of 100 Hz pulses delivered with 200 ms intervals, every 10 trains were separated by 10 s-long intervals), as previously described (Lalo et al., 2014a, 2016; Rasooli-Nejad et al., 2014; Pankratov and Lalo, 2015). **(A)** The representative time course of changes in the fEPSP induced by 20 HFS trains delivered at zero time, measured in the young mice of SH and mice exposed to CR. Dots in the graphs represent the average of six consecutive fEPSPs; data are shown as mean ± SD for number of experiments indicated. Data were normalized to the fEPSP slope averaged over 10 min period prior to the HFS. The insets show

(*Continued*)

FIGURE 3 | Continued
the average fEPSP waveforms recorded before and 60 min after the HFS. Note the difference in the effect of CR on long-term depression (LTD)/LTP switch in the WT and dnSNARE mice. **(B)** The stimulus-dependence of the long-term changes in the neocortical fEPSP in the old mice of different genotypes at different conditions. Graphs show the magnitude of LTP/LTD evaluated as relative increase in the fEPSP slope at 60th min, averaged across 10 min time window and plotted against the number of HFS trains delivered. Each data point shows mean ± SD for the following number of experiments/mice used): 10–22 (8–15) for SH, 6–9 (5–6) for EE and 6–7 (4–5) for CR mice. The graphs also show the effect of activation of astrocytes with 1 μM NA [REF] on the LTP induced by 20 and 50 HFS trains; NA was applied for 5 min 2 min prior to HFS. The statistical significance (2-population unpaired *t*-test) for the difference between genotypes, age- and treatment groups was indicated by different symbols as follows: (#)–effect of EE or CR as compared to SH mice of the same genotype and age and the effect of NA as compared to mice of same age, genotype and housing in the control; (*) dnSNARE mice vs. their WT littermates of the same age and housing; (**) old vs. young mice of the same genotype and housing. Note the different pattern of changes in the LTP/LTD between dnSNARE and WT mice and significant effects of EE and CR in the old WT mice. **(C)** The effects of astrocyte-derived ATP on neocortical synaptic plasticity in the young and old mice of SH was evaluated using the same experimental paradigm as in **(A,B)**. The release of gliotransmitters was activated by the agonists of astrocyte-specific PAR-1 receptors (Lalo et al., 2016) TFLLR (10 μM) in the control or after inhibition of neuronal P2 × 4 receptors to ATP with selective antagonist 5-BDBD (5 μM). Alternatively, enhancement of gliotransmitter release was activated via CB1 receptors (Rasooli-Nejad et al., 2014) or mimicked by exogenous application of ATP analog ATPγS (10 μM) or D-Serine (10 μM). All drugs were applied for 5 min 2 min before the LTP induction. Asterisks (* and **) indicate statistical significance of difference in the LTP magnitude as compared to the mice of same age and genotype under control conditions (unpaired *t*-test). Under control conditions, activation of astrocytes with TFLLR significantly increased the LTP in young and old WT but not the dnSNARE mice. Inhibition of P2×4 receptors prevented the TFLLR-induced enhancement of LTP. Contrary to TFLLR-activated release, application of exogenous gliotransmitters had significant effects both in the WT and dnSNARE mice. Combined, these results suggest the importance of astrocyte-derived ATP for modulation of synaptic plasticity in the neocortex.

Impact of Astrocytes on Synaptic Plasticity in the Neocortex

Role for heterosynaptic cortical metaplasticity in brain computation, learning and memory is often studied in the framework of BCM-model (Bienenstock et al., 1982) whose two essential prerequisites are: bidirectional synaptic modification and sliding modification threshold. Accordingly, the general paradigm of BCM model, sub-threshold stimulation should induce long-term depression (LTD) whereas more stronger stimuli should induce potentiation (LTP) and prior stimulation (experience) can shift the LTD/LTP threshold one way or another (Bienenstock et al., 1982; Hulme et al., 2013b).

There is accumulating evidence of both positive and negative effects of astrocytes on the strength of excitatory synapses mediated by glia-derived ATP and adenosine (Hulme et al., 2013b; Boué-Grabot and Pankratov, 2017). Furthermore, our recent data demonstrated that glia-derived ATP can cause down-regulation of NMDA receptors and affect the threshold of LTP induction (Lalo et al., 2016). This effect contrasts with widely accepted positive effect of glia-derived NMDA receptor co-agonist D-Serine on LTP (Henneberger et al., 2010; Papouin et al., 2017a). Hence, one could expect the gliotransmission to be important, if not quintessential, element of cortical metaplasticity. To test this hypothesis, we explored the stimulus-dependence of the LTP of fEPSPs in the neocortical layer 2/3 of WT and dnSNARE mice. The fEPSPs were evoked by the stimulation of neuronal afferents descending from layers IV-V (Rasooli-Nejad et al., 2014; Pankratov and Lalo, 2015; Lalo et al., 2016); LTP was induced by different number of pulses of high-frequency theta-burst stimulation (100 ms-long trains of 100 Hz pulses delivered with 200 ms intervals, every 10 trains were separated by 10 s-long intervals). Similarly to Ca^{2+}-signaling experiments, we compared effects of EE and CR on LTP in the WT and dnSNARE mice (**Figure 3**).

Under control conditions, the long-term plasticity of fEPSPs in the young WT mice exhibited a characteristic stimulus-strength dependence: no potentiation at very weak stimulus, depression at moderate strengths and then potentiation which magnitude grew sharply upon reaching certain threshold but decline slightly in a bell-shaped manner at very strong stimuli. Such dependence goes very well in line with predictions of the BCM theory.

Importantly, impairment of glial exocytosis in the dnSNARE mice dramatically "flattened" the stimulus-dependence inhibiting both the depression at moderate stimuli and potentiation at strong stimuli (**Figure 3B**). The similar "flattened" pattern of LTP/LTD dependence on stimulus strength was observed in the old mice (**Figure 3B**). Taking into account the significant age-related decrease in astroglial Ca^{2+}-signaling, one can suggest that decrease in the Ca^{2+}-dependent release of gliotransmitters (either aging-related or due to dnSNARE expression) strongly attenuates the extent of bi-directional modulation of plasticity of neocortical synapses.

This hypothesis was corroborated by the effects of activation of astrocytes by exogenously applied NA (1 μM) and AEA (200 nM). Previously, we have verified that effects of these agonists on synaptic transmission and plasticity are predominantly related to their ability to activate the astroglial Ca^{2+}-signaling and release of gliotransmitters (Lalo et al., 2014a, 2016; Rasooli-Nejad et al., 2014; Pankratov and Lalo, 2015). The 5 min-long application of NA (started 2 min prior to the induction protocol) significantly increased the magnitude of LTP induced in the neurons of younger WT mice by weak stimulation (20 HFS pulses) and the magnitude of LTP in older mice both at weak and strong (50 HFS pulses) stimuli. The NA-induced LTP enhancement was strongly attenuated in the dnSNARE mice supporting the importance of astroglial exocytosis for this effect. The similar action was shown by application of AEA or agonist of glia-specific PAR-1 receptors (TFLLR, 10 μM; **Figure 3C**).

These data closely agree with our previous results that by astroglial α1-ARs and CB1 receptors can facilitate LTP induction by triggering the release of ATP and D-Serine (Lalo et al., 2014a, 2016; Rasooli-Nejad et al., 2014; Pankratov and Lalo, 2015).

To verify that same molecular mechanisms can rescue the LTP in old mice, we investigated the effect of inhibition of ATP receptors and exogenous application of gliotransmitters (**Figure 3C**). First, selective inhibition of neuronal P2×4 receptors, which are not strongly expressed by neocortical astrocytes (Lalo et al., 2008), by 5-BDBD (5 μM)

decreased both the magnitude and threshold of LTP; similar effects were recently observed in the P2×4 knock-out mice (Lalo et al., 2016). Second, inhibition of P2×4 receptors occluded the positive effects of AEA and TFLLR both in the young and old mice (**Figure 3C**). Finally, application of non-hydrolyzable ATP analog ATP-γS (10 μM) or D-Serine (10 μM) enhanced the LTP in the neocortex of both WT and dnSNARE mice.

Based on these results one could suggest that Ca^{2+} dependent release of ATP and D-Serine from astrocytes may be implicated in cortical metaplasticity by modifying both threshold and magnitude of long-term alterations of synaptic strength. Hence, aging-related decline in gliotransmission can lead to deficit in the LTP which could, in turn, be rescued by enhancement of astroglial signaling, for example by EE or CR (**Figure 1**). This notion was strongly supported by our observations of LTP modifications in the EE- and CR-exposed WT and dnSNARE mice (**Figure 3B**).

In the young WT mice, the main effect of EE and CR was a marked leftward shift in the threshold of LTP induction without increase in the maximal LTP amplitude (**Figure 3B**). So, both EE and CR caused statistically significant alterations in the LTP only at weaker stimuli (10 and 20 HSF). However, in the old WT mice, the EE- and CR-induced enhancement in astroglial signaling was accompanied by the leftward shift in the LTP induction threshold and significant increase in the magnitude of LTP at moderate and strong stimuli. Generally, the exposure of old mice to the EE and CR lead to a "younger" LTP phenotype. In the dnSNARE mice, both young and old, the positive action of CR on the LTP magnitude was effectively occluded strongly suggesting the crucial importance of release of gliotransmitters for CR-related metaplasticity. At the same time, dnSNARE expression had a less straightforward effect on the EE-induced modifications of LTP.

Although there was statistically significant difference in the LTP magnitude between WT and dnSNARE EE-exposed young mice, there also was significant EE-induce increase in the LTP in dnSNARE mice (as compared to SH mice) at most induction protocols. This rather surprising observation of "rescue" of LTP in the young dnSNARE mice by EE have two important implications. First, lack of LTP deficit in the EE dn-SNARE mice strongly argues against the non-selective "leaky" expression of dn-SNARE transgene in neurons. Second, the LTP deficit in the dn-SNARE mice kept in SH clearly demonstrated the physiological relevance of exocytotic release of gliotransmitters from astrocytes. The marked responsiveness of dn-SNARE mice to EE suggested the existence of some compensatory mechanisms which could overcome the deficit in vesicular gliotransmission. The most straightforward explanation might be a mosaic expression of dnSNARE transgene across the astrocyte population (Pascual et al., 2005; Sultan et al., 2015) and EE-induced enhancement of Ca^{2+}-signaling and the release of gliotransmitters from non-dnSNARE astrocytes. In the neocortex and hippocampus, just 50%–60% of astrocytes express dnSNARE (Halassa et al., 2009). Due to the presence of significant proportion of un-affected astrocytes in the dnSNARE mice, the EE-induced enhancement of Ca^{2+}-signaling can, very likely, lead to overall increase of gliotransmitter release even in dnSNARE animals (albeit in a lesser extent than in their WT littermates). Combined with threshold-like behavior of LTP, EE-induced increase in gliotransmitter release can be capable to rescue the LTP in dnSNARE mice. Also, impact of EE on synaptic transmission may involve other mechanisms of neuronal origin, like BDNF/MSK1-dependent homeostatic synaptic scaling (Correa et al., 2012).

We would like to emphasize that the pattern of EE-induced alterations in stimulus-dependence of LTP was different in the young dnSNARE and WT mice. The increase in the LTP both at weak and strong stimuli in the dnSNARE mice contrasted to the alterations of the threshold, but not in the maximal magnitude, in their WT littermates. Furthermore, the EE was not very efficient in the old dnSNARE mice (**Figure 3B**), except at very strong stimulus (100 HFS) suggesting that role of glial exocytosis can increase with age. Hence, one way or another, our data strongly suggest the involvement of glial exocytosis in the EE-induced metaplasticity.

Interestingly, the EE modified the effect of additional action of astrocytes on the LTP. Application of NA caused significant enhancement of LTP in the neocortex of WT mice only at weaker stimulus (20 HFS pulses) but did not have notable effect on the LTP induced by stronger stimulus (50 HFS) in both age groups. One could suggest that exposure to EE, causing increase in astrocytic Ca^{2+} -signaling and gliotransmission, "pre-emptied" the effect of activation of adrenoceptors.

Taken together, the above results strongly support the importance of astroglial Ca^{2+}-signaling and gliotransmission for the bi-directional modulation of synaptic plasticity in the neocortex. Our data also suggest an importance of astroglial eCB and NA receptors for metaplasticity-related effects of aging, EE and CR.

DISCUSSION

During last two decades a plethora of experimental results has been obtained showing that various gliotransmitters can exert different, and sometimes opposing, effects on neuronal signaling (Gordon et al., 2009; Araque et al., 2014; Pougnet et al., 2014; Bazargani and Attwell, 2016; Boué-Grabot and Pankratov, 2017). In particular, release of glutamate and D-serine from astrocytes can enhance the activity of NMDA component of excitatory synapses and thereby the long-term synaptic plasticity (Panatier et al., 2006; Henneberger et al., 2010; Rasooli-Nejad et al., 2014). There is also an evidence of the positive impact of glia-derived ATP on activity and trafficking of AMPA receptors (Boué-Grabot and Pankratov, 2017). Our previous data showed that glia-derived ATP can down-regulate the GABAergic tonic and phasic inhibitory transmission (Lalo et al., 2014a). Hence, one might expect the glia-derived ATP to shift the balance between excitatory and inhibitory synaptic inputs towards excitation and thereby facilitate the induction of LTP. At the same time, our recent data have shown that ATP, acting via postsynaptic P2X receptors, can down-regulate NMDA receptors and decrease the magnitude of LTP (Lalo et al., 2016). Thus, release of ATP and D-Serine from astrocytes can lead to

bi-directional modifications of synaptic strength and thereby play an important role in the mechanisms of brain metaplasticity. Our results present several lines of evidence to support this notion.

We observed that positive effects of EE and CR can counterbalance the aging-related decrease in the Ca^{2+}-signaling and release of gliotransmitters from neocortical astrocytes. The EE- and CR-induced enhancement in astroglial function was accompanied by marked alterations in the stimulus-dependence of the neocortical LTP. These alterations different considerably in the WT and dnSNARE mice supporting the importance of release of gliotransmitters for the beneficial effects of EE and CR on synaptic plasticity in the old age. The EE- and CR-induced enhancement of the LTP in old mice could also be mimicked, irrespective of dnSNARE expression, by short-term application of ATP analog (ATPγS) and D-Serine during LTP induction period, indicating the importance of these gliotransmitters.

Our results also show that additional activation of astrocytes via eCB, adrenergic or PAR-1 receptors during LTP induction protocol can increase the magnitude of the resulting LTP. Importantly, such activation of astrocytes caused significant effect only in cases when LTP magnitude was small, i.e., at weaker stimuli in the younger mice of SH or at stronger stimuli in the old mice. The α1-AR mediated facilitation of LTP was also occluded by the treatments (EE and CR) which already increased astrocytic Ca^{2+}-signaling and LTP.

Combined, our results suggest that activation of astrocytes performs a "balancing act," facilitating the LTP in case of deficit in signaling and gliotransmission but attenuating the LTP magnitude in case of stronger stimuli and higher levels of astroglial activity. A strong dependence of glia-driven modulation, of both the threshold and magnitude of LTP, on the activity of neuronal P2×4 receptors (**Figure 3**, see also Lalo et al., 2016) may imply an important role for ATP receptor-mediated down-regulation of GABA and NMDA receptors in the mechanisms of metaplasticity.

Overall, our observations of LTP modifications in the EE- and CR-exposed WT and dnSNARE mice go in line with our hypothesis that Ca^{2+} dependent release of ATP and D-Serine from astrocytes can affect both threshold and magnitude of long-term alterations of synaptic strength and thereby can be very important for cortical metaplasticity. Our data also indicate that modulation of neocortical plasticity, in particular via glia-neuron communications, can be analyzed in the framework of BCM theory.

It becomes increasingly evident that net effect of activation of astroglial Ca^{2+}-signaling on firing rate or plasticity of neural networks cannot be *a priori* considered as solely positive (or negative). This might explain why some attempts to genetically modify Ca^{2+} signaling in astrocytes did not yield the expected results (Bazargani and Attwell, 2016; Fiacco and McCarthy, 2018; Savtchouk and Volterra, 2018). Our data also suggest that release of gliotransmitters, in particular ATP and D-Serine, can be affected by environment, physical exercise and diet, in addition to the recently reported effects of sleep cycle (Papouin et al., 2017a). A high degree of experience- and environment-related plasticity of astroglial function may further add to the variability of the results obtained in different laboratory settings.

Our results, in particular shown in **Figure 2**, can also be important for the current debate on mechanisms D-Serine release in the brain. Although a large body of evidence, obtained in the last decade using different experimental approaches supports an importance of astroglia in the release of D-Serine and in the D-Serine-mediated modulation of NMDA receptors, an alternative (and rather extreme) view of predominantly neuronal release of D-Serine at physiological conditions has been recently suggested (Wolosker et al., 2016). One should note that notion of predomimant role of neurons in release of D-Serine originates mainly from the data suggesting a high level of expression of SRR in neurons rather than astroglia. However, this contradicts to recent transcriptomic data showing relatively high level of *Srr* gene expression in cortical and hippocampal astrocytes (Chai et al., 2017). There are several other flaws in the "neuronal D-Serine" theory which have been thoroughly addressed by Papouin et al. (2017b).

One should emphasize that even the studies, questioning astroglia-specific expression of serine racemase, do not deny an ability of astrocytes to accumulate D-serine (Wolosker et al., 2016) and a reconciliating theory of cooperation between neuronal and glial release has been recently suggested by Ivanov and Mothet (2018). Whatever is concentration of D-Serine in neurons and astrocytes, their contribution into extracellular D-serine level will depend mainly on efficiency of neuronal vs. glial mechanisms of release. So far, there is a lack direct evidence that neurons possess an efficient mechanism of release of D-serine (Papouin et al., 2017b), with Asc-1 being suggest to be a main pathway (Papouin et al., 2017b). Release of D-serine from strocytes can occur via Ca^{2+}-dependent exocytosis, as an alternative pathway one might also suggest Ca^{2+}-dependent large conductance chloride channels (Woo et al., 2012). These channels have been shown to be permeable to glutamate (Woo et al., 2012) which has even larger molecular size than D-Serine.

Compared to vesicular or channel-mediated release allowing the movement of multiple molecules, transporter, that releases a single molecule per single act of conformational change, is intrinsically slow. So, one could hardly expect the putative Asc-1 transporter-mediated release of D-Serine from neurons to be more than Ca^{2+}-dependent release of D-Serine from astrocytes.

Indeed, our experiments in isolated neurons and neuron-astrocyte "bundles," which allowed to dis-entangle glial and neuronal sources of D-Serine, showed that neuronal release on its own could not provide enough D-Serine to maintain the activity of synaptic NMDAR (**Figure 2**). We would like to stress that our preparation of isolated neurons provide a very good accessibility of synapses to D-amino acid oxidase, however we did not observe any marked effect of DAAO on synaptic NMDAR-mediated currents in conditions when neurons were perfused with 1 mM D-Serine via whole-cell recording pipette. This observation on its own argues against efficient release of D-Serine from neurons. Combined with results of biosensor measurements of D-serine release in

brain slices of WT and dnSNARE mice (**Figure 1D**, see also Rasooli-Nejad et al., 2014), our data strongly support an importance of astrocytes as a source of D-serine at physiological conditions.

Our data on age-related changes in astroglial Ca^{2+}-signaling and release of ATP and D-Serine (**Figure 1**) go in line with accumulating evidence that alterations in extracellular levels of ATP, adenosine and D-Serine can play an important role in physiological and pathological brain aging (Mothet et al., 2006; Orellana et al., 2012; Gundersen et al., 2015; Rodrigues et al., 2015; Piacentini et al., 2017). Our present (**Figures 2**, **3**) and previous data (Lalo et al., 2014b, 2016; Pankratov and Lalo, 2015) on astroglial-driven modulation of synaptic transmission and plasticity supports the recently emerged view that molecular and functional alteration in astrocytes, such as release of gliotransmitters, can precede or even cause, changes in synaptic dynamics and homeostasis during aging and progression of neurodegenerative diseases (De Strooper and Karran, 2016; Soreq et al., 2017). Our results also suggest that widely reported beneficial effects (Hillman et al., 2008; Nithianantharajah and Hannan, 2009; van Praag, 2009; Mercken et al., 2012; Merzenich et al., 2014) of enriched environment on synaptic plasticity and memory in mice and, possibly, effects of active life style in humans, can be mediated by enhancement of release of gliotransmitters, very likely due to increased endocannabinoid and adrenergic Ca^{2+}-signaling in astrocytes. Since both EE and CR upregulated Ca^{2+}signaling in astrocytes and affected synaptic plasticity in the dnSNARE-dependent manner, one can hypothesize that beneficial effects of CR on synaptic plasticity also originate from enhanced gliotransmission and glia-neuron communications. Still, alternative mechanisms of action of CR might be suggested, which can be underlined by various metabolic effects of CR (Mercken et al., 2012; Park et al., 2012; Madeo et al., 2014; López-Otín et al., 2016), for example enhancement mitochondrial function in astrocytes. Specific roles for gliotransmission- and metabolism-related mechanisms in beneficial effects of CR on aging brain are yet to be studied.

To conclude, our results strongly support physiological importance of astroglial cannabinoid and adrenergic signaling and glia-derived ATP for communication between astrocytes and neurons and experience-related modulation of synaptic plasticity across a lifetime.

AUTHOR CONTRIBUTIONS

UL, AB and YP contributed to the design and interpretation of experiments and commented on the manuscript. UL and AB performed experiments and data analysis. YP and UL conceived the study and wrote the manuscript.

FUNDING

This work was supported by grant from Biotechnology and Biological Sciences Research Council (BBSRC) UK (BB/K009192/1) to YP.

ACKNOWLEDGMENTS

We thank Dr. Mark Wall for help with biosensor experiments.

REFERENCES

Abraham, W. C., and Bear, M. F. (1996). Metaplasticity: the plasticity of synaptic plasticity. *Trends Neurosci.* 19, 126–130. doi: 10.1016/s0166-2236(96)80018-x

Araque, A., Carmignoto, G., Haydon, P. G., Oliet, S. H., Robitaille, R., and Volterra, A. (2014). Gliotransmitters travel in time and space. *Neuron* 81, 728–739. doi: 10.1016/j.neuron.2014.02.007

Bazargani, N., and Attwell, D. (2016). Astrocyte calcium signaling: the third wave. *Nat. Neurosci.* 19, 182–189. doi: 10.1038/nn.4201

Bienenstock, E. L., Cooper, L. N., and Munro, P. W. (1982). Theory for the development of neuron selectivity: orientation specificity and binocular interaction in visual cortex. *J. Neurosci.* 2, 32–48. doi: 10.1523/JNEUROSCI.02-01-00032.1982

Boué-Grabot, E., and Pankratov, Y. (2017). Modulation of central synapses by astrocyte-released ATP and postsynaptic P2X receptors. *Neural Plast.* 2017:9454275. doi: 10.1155/2017/9454275

Chai, H., Diaz-Castro, B., Shigetomi, E., Monte, E., Octeau, J. C., Yu, X., et al. (2017). Neural circuit-specialized astrocytes: transcriptomic, proteomic, morphological, and functional evidence. *Neuron* 95, 531.e9–549.e9. doi: 10.1016/j.neuron.2017.06.029

Correa, S. A., Hunter, C. J., Palygin, O., Wauters, S. C., Martin, K. J., McKenzie, C., et al. (2012). MSK1 regulates homeostatic and experience-dependent synaptic plasticity. *J. Neurosci.* 32, 13039–13051. doi: 10.1523/JNEUROSCI.0930-12.2012

De Strooper, B., and Karran, E. (2016). The cellular phase of Alzheimer's disease. *Cell* 164, 603–615. doi: 10.1016/j.cell.2015.12.056

Ding, F., O'Donnell, J., Thrane, A. S., Zeppenfeld, D., Kang, H., Xie, L., et al. (2013). α1-Adrenergic receptors mediate coordinated Ca^{2+} signaling of cortical astrocytes in awake, behaving mice. *Cell Calcium* 54, 387–394. doi: 10.1016/j.ceca.2013.09.001

Duguid, I. C., Pankratov, Y., Moss, G. W., and Smart, T. G. (2007). Somatodendritic release of glutamate regulates synaptic inhibition in cerebellar Purkinje cells via autocrine mGluR1 activation. *J. Neurosci.* 27, 12464–12474. doi: 10.1523/JNEUROSCI.0178-07.2007

Fiacco, T. A., and McCarthy, K. D. (2018). Multiple lines of evidence indicate that gliotransmission does not occur under physiological conditions. *J. Neurosci.* 38, 3–13. doi: 10.1523/JNEUROSCI.0016-17.2017

Frenguelli, B. G., Wigmore, G., Llaudet, E., and Dale, N. (2007). Temporal and mechanistic dissociation of ATP and adenosine release during ischaemia in the mammalian hippocampus. *J. Neurochem.* 101, 1400–1413. doi: 10.1111/j.1471-4159.2007.04425.x

Gordon, G. R., Iremonger, K. J., Kantevari, S., Ellis-Davies, G. C., MacVicar, B. A., and Bains, J. S. (2009). Astrocyte-mediated distributed plasticity at hypothalamic glutamate synapses. *Neuron* 64, 391–403. doi: 10.1016/j.neuron.2009.10.021

Gourine, A. V., Kasymov, V., Marina, N., Tang, F., Figueiredo, M. F., Lane, S., et al. (2010). Astrocytes control breathing through pH-dependent release of ATP. *Science* 329, 571–575. doi: 10.1126/science.1190721

Gundersen, V., Storm-Mathisen, J., and Bergersen, L. H. (2015). Neuroglial transmission. *Physiol. Rev.* 95, 695–726. doi: 10.1152/physrev.00024.2014

Halassa, M. M., Florian, C., Fellin, T., Munoz, J. R., Lee, S. Y., Abel, T., et al. (2009). Astrocytic modulation of sleep homeostasis and cognitive consequences of sleep loss. *Neuron* 61, 213–219. doi: 10.1016/j.neuron.2008.11.024

Halassa, M. M., and Haydon, P. G. (2010). Integrated brain circuits: astrocytic networks modulate neuronal activity and behavior. *Annu. Rev. Physiol.* 72, 335–355. doi: 10.1146/annurev-physiol-021909-135843

Henneberger, C., Papouin, T., Oliet, S. H., and Rusakov, D. A. (2010). Long-term potentiation depends on release of D-serine from astrocytes. *Nature* 463, 232–236. doi: 10.1038/nature08673

Hillman, C. H., Erickson, K. I., and Kramer, A. F. (2008). Be smart, exercise your heart: exercise effects on brain and cognition. *Nat. Rev. Neurosci.* 9, 58–65. doi: 10.1038/nrn2298

Hulme, S. R., Jones, O. D., and Abraham, W. C. (2013a). Emerging roles of metaplasticity in behaviour and disease. *Trends Neurosci.* 36, 353–362. doi: 10.1016/j.tins.2013.03.007

Hulme, S. R., Jones, O. D., Raymond, C. R., Sah, P., and Abraham, W. C. (2013b). Mechanisms of heterosynaptic metaplasticity. *Philos. Trans. R. Soc. Lond. B Biol. Sci.* 369:20130148. doi: 10.1098/rstb.2013.0148

Ivanov, A. D., and Mothet, J. P. (2018). The plastic D-serine signaling pathway: sliding from neurons to glia and vice-versa. *Neurosci. Lett.* doi: 10.1016/j.neulet.2018.05.039 [Epub ahead of print].

Lalo, U., Palygin, O., North, R. A., Verkhratsky, A., and Pankratov, Y. (2011). Age-dependent remodelling of ionotropic signalling in cortical astroglia. *Aging Cell* 10, 392–402. doi: 10.1111/j.1474-9726.2011.00682.x

Lalo, U., Palygin, O., Rasooli-Nejad, S., Andrew, J., Haydon, P. G., and Pankratov, Y. (2014a). Exocytosis of ATP from astrocytes modulates phasic and tonic inhibition in the neocortex. *PLoS Biol.* 12:e1001747. doi: 10.1371/journal.pbio.1001857

Lalo, U., Rasooli-Nejad, S., and Pankratov, Y. (2014b). Exocytosis of gliotransmitters from cortical astrocytes: implications for synaptic plasticity and aging. *Biochem. Soc. Trans.* 42, 1275–1281. doi: 10.1042/BST20140163

Lalo, U., Palygin, O., Verkhratsky, A., Grant, S. G., and Pankratov, Y. (2016). ATP from synaptic terminals and astrocytes regulates NMDA receptors and synaptic plasticity through PSD-95 multi-protein complex. *Sci. Rep.* 6:33609. doi: 10.1038/srep33609

Lalo, U., and Pankratov, Y. (2017). Exploring the Ca^{2+}-dependent synaptic dynamics *in vibro*-dissociated cells. *Cell Calcium* 64, 91–101. doi: 10.1016/j.ceca.2017.01.008

Lalo, U., Pankratov, Y., Kirchhoff, F., North, R. A., and Verkhratsky, A. (2006). NMDA receptors mediate neuron-to-glia signaling in mouse cortical astrocytes. *J. Neurosci.* 26, 2673–2683. doi: 10.1523/JNEUROSCI.4689-05.2006

Lalo, U., Pankratov, Y., Wichert, S. P., Rossner, M. J., North, R. A., Kirchhoff, F., et al. (2008). P2X1 and P2X5 subunits form the functional P2X receptor in mouse cortical astrocytes. *J. Neurosci.* 28, 5473–5480. doi: 10.1523/JNEUROSCI.1149-08.2008

Lin, A. L., Coman, D., Jiang, L., Rothman, D. L., and Hyder, F. (2014). Caloric restriction impedes age-related decline of mitochondrial function and neuronal activity. *J. Cereb. Blood Flow Metab.* 34, 1440–1443. doi: 10.1038/jcbfm.2014.114

López-Otín, C., Galluzzi, L., Freije, J. M., Madeo, F., and Kroemer, G. (2016). Metabolic control of longevity. *Cell* 166, 802–821. doi: 10.1016/j.cell.2016.07.031

Madeo, F., Pietrocola, F., Eisenberg, T., and Kroemer, G. (2014). Caloric restriction mimetics: towards a molecular definition. *Nat. Rev. Drug Discov.* 13, 727–740. doi: 10.1038/nrd4391

Mercken, E. M., Carboneau, B. A., Krzysik-Walker, S. M., and de Cabo, R. (2012). Of mice and men: the benefits of caloric restriction, exercise, and mimetics. *Ageing Res. Rev.* 11, 390–398. doi: 10.1016/j.arr.2011.11.005

Merzenich, M. M., Van Vleet, T. M., and Nahum, M. (2014). Brain plasticity-based therapeutics. *Front. Hum. Neurosci.* 8:385. doi: 10.3389/fnhum.2014.00385

Metna-Laurent, M., and Marsicano, G. (2015). Rising stars: modulation of brain functions by astroglial type-1 cannabinoid receptors. *Glia* 63, 353–364. doi: 10.1002/glia.22773

Min, R., and Nevian, T. (2012). Astrocyte signaling controls spike timing-dependent depression at neocortical synapses. *Nat. Neurosci.* 15, 746–753. doi: 10.1038/nn.3075

Monai, H., Ohkura, M., Tanaka, M., Oe, Y., Konno, A., Hirai, H., et al. (2016). Calcium imaging reveals glial involvement in transcranial direct current stimulation-induced plasticity in mouse brain. *Nat. Commun.* 7:11100. doi: 10.1038/ncomms11100

Mothet, J. P., Rouaud, E., Sinet, P. M., Potier, B., Jouvenceau, A., Dutar, P., et al. (2006). A critical role for the glial-derived neuromodulator D-serine in the age-related deficits of cellular mechanisms of learning and memory. *Aging Cell* 5, 267–274. doi: 10.1111/j.1474-9726.2006.00216.x

Nithianantharajah, J., and Hannan, A. J. (2009). The neurobiology of brain and cognitive reserve: mental and physical activity as modulators of brain disorders. *Prog. Neurobiol.* 89, 369–382. doi: 10.1016/j.pneurobio.2009.10.001

Oliveira da Cruz, J. F., Robin, L. M., Drago, F., Marsicano, G., and Metna-Laurent, M. (2016). Astroglial type-1 cannabinoid receptor (CB1): a new player in the tripartite synapse. *Neuroscience* 323, 35–42. doi: 10.1016/j.neuroscience.2015.05.002

Orellana, J. A., von Bernhardi, R., Giaume, C., and Saez, J. C. (2012). Glial hemichannels and their involvement in aging and neurodegenerative diseases. *Rev. Neurosci.* 23, 163–177. doi: 10.1515/revneuro-2011-0065

Panatier, A., Theodosis, D. T., Mothet, J. P., Touquet, B., Pollegioni, L., Poulain, D. A., et al. (2006). Glia-derived D-serine controls NMDA receptor activity and synaptic memory. *Cell* 125, 775–784. doi: 10.1016/j.cell.2006.02.051

Pankratov, Y., and Lalo, U. (2015). Role for astroglial α1-adrenoreceptors in gliotransmission and control of synaptic plasticity in the neocortex. *Front. Cell. Neurosci.* 9:230. doi: 10.3389/fncel.2015.00230

Papouin, T., Dunphy, J. M., Tolman, M., Dineley, K. T., and Haydon, P. G. (2017a). Septal cholinergic neuromodulation tunes the astrocyte-dependent gating of hippocampal NMDA receptors to wakefulness. *Neuron* 94, 840.e7–854.e7. doi: 10.1016/j.neuron.2017.04.021

Papouin, T., Henneberger, C., Rusakov, D. A., and Oliet, S. H. R. (2017b). Astroglial versus neuronal D-serine: fact checking. *Trends Neurosci.* 40, 517–520. doi: 10.1016/j.tins.2017.05.007

Park, S. J., Ahmad, F., Philp, A., Baar, K., Williams, T., Luo, H., et al. (2012). Resveratrol ameliorates aging-related metabolic phenotypes by inhibiting cAMP phosphodiesterases. *Cell* 148, 421–433. doi: 10.1016/j.cell.2012.01.017

Pascual, O., Casper, K. B., Kubera, C., Zhang, J., Revilla-Sanchez, R., Sul, J. Y., et al. (2005). Astrocytic purinergic signaling coordinates synaptic networks. *Science* 310, 113–116. doi: 10.1126/science.1116916

Paukert, M., Agarwal, A., Cha, J., Doze, V. A., Kang, J. U., and Bergles, D. E. (2014). Norepinephrine controls astroglial responsiveness to local circuit activity. *Neuron* 82, 1263–1270. doi: 10.1016/j.neuron.2014.04.038

Piacentini, R., Li Puma, D. D., Mainardi, M., Lazzarino, G., Tavazzi, B., Arancio, O., et al. (2017). Reduced gliotransmitter release from astrocytes mediates tau-induced synaptic dysfunction in cultured hippocampal neurons. *Glia* 65, 1302–1316. doi: 10.1002/glia.23163

Pougnet, J. T., Toulme, E., Martinez, A., Choquet, D., Hosy, E., and Boué-Grabot, E. (2014). ATP P2X receptors downregulate AMPA receptor trafficking and postsynaptic efficacy in hippocampal neurons. *Neuron* 83, 417–430. doi: 10.1016/j.neuron.2014.06.005

Rasooli-Nejad, S., Palygin, O., Lalo, U., and Pankratov, Y. (2014). Cannabinoid receptors contribute to astroglial Ca^{2+}-signalling and control of synaptic plasticity in the neocortex. *Philos. Trans. R. Soc. Lond. B Biol. Sci.* 369:20140077. doi: 10.1098/rstb.2014.0077

Rodrigues, R. J., Tome, A. R., and Cunha, R. A. (2015). ATP as a multi-target danger signal in the brain. *Front. Neurosci.* 9:148. doi: 10.3389/fnins.2015.00148

Rodríguez, J. J., Terzieva, S., Olabarria, M., Lanza, R. G., and Verkhratsky, A. (2013). Enriched environment and physical activity reverse astrogliodegeneration in the hippocampus of AD transgenic mice. *Cell Death Dis.* 4:e678. doi: 10.1038/cddis.2013.194

Rodríguez, J. J., Yeh, C. Y., Terzieva, S., Olabarria, M., Kulijewicz-Nawrot, M., and Verkhratsky, A. (2014). Complex and region-specific changes in astroglial markers in the aging brain. *Neurobiol. Aging* 35, 15–23. doi: 10.1016/j.neurobiolaging.2013.07.002

Savtchouk, I., and Volterra, A. (2018). Gliotransmission: beyond black-and-white. *J. Neurosci.* 38, 14–25. doi: 10.1523/JNEUROSCI.0017-17.2017

Seidel, B., Bigl, M., Franke, H., Kittner, H., Kiess, W., Illes, P., et al. (2006). Expression of purinergic receptors in the hypothalamus of the rat is modified by reduced food availability. *Brain Res.* 1089, 143–152. doi: 10.1016/j.brainres.2006.03.038

Singh, A., and Abraham, W. C. (2017). Astrocytes and synaptic plasticity in health and disease. *Exp. Brain Res.* 235, 1645–1655. doi: 10.1007/s00221-017-4928-1

Soreq, L., UK Brain Expression Consortium, North American Brain Expression Consortium, Rose, J., Soreq, E., Hardy, J., et al. (2017). Major shifts in glial

regional identity are a transcriptional hallmark of human brain aging. *Cell Rep.* 18, 557–570. doi: 10.1016/j.celrep.2016.12.011

Sultan, S., Li, L., Moss, J., Petrelli, F., Cassé, F., Gebara, E., et al. (2015). Synaptic integration of adult-born hippocampal neurons is locally controlled by astrocytes. *Neuron* 88, 957–972. doi: 10.1016/j.neuron.2015.10.037

van Praag, H. (2009). Exercise and the brain: something to chew on. *Trends Neurosci.* 32, 283–290. doi: 10.1016/j.tins.2008.12.007

Verkhratsky, A., Rodríguez, J. J., and Parpura, V. (2014). Neuroglia in ageing and disease. *Cell Tissue Res.* 357, 493–503. doi: 10.1007/s00441-014-1814-z

Verkhratsky, A., Rodríguez-Arellano, J. J., Parpura, V., and Zorec, R. (2017). Astroglial calcium signalling in Alzheimer's disease. *Biochem. Biophys. Res. Commun.* 483, 1005–1012. doi: 10.1016/j.bbrc.2016.08.088

Wolosker, H., Balu, D. T., and Coyle, J. T. (2016). The rise and fall of the d-serine-mediated gliotransmission hypothesis. *Trends Neurosci.* 39, 712–721. doi: 10.1016/j.tins.2016.09.007

Woo, D. H., Han, K. S., Shim, J. W., Yoon, B. E., Kim, E., Bae, J. Y., et al. (2012). TREK-1 and Best1 channels mediate fast and slow glutamate release in astrocytes upon GPCR activation. *Cell* 151, 25–40. doi: 10.1016/j.cell.2012.09.005

Conflict of Interest Statement: The authors declare that the research was conducted in the absence of any commercial or financial relationships that could be construed as a potential conflict of interest.

frontiers in Molecular Neuroscience

OPINION
published: 02 July 2018
doi: 10.3389/fnmol.2018.00224

Ca^{2+}-Dependent and Ca^{2+}-Independent ATP Release in Astrocytes

Yingfei Xiong[1,2*†], *Suhua Sun*[1†], *Sasa Teng*[1], *Mu Jin*[1,3*] *and Zhuan Zhou*[1*]

[1] State Key Laboratory of Biomembrane and Membrane Biotechnology and Peking-Tsinghua Center for Life Sciences and PKU-IDG/McGovern Institute for Brain Research, Institute of Molecular Medicine, Peking University, Beijing, China, [2] Department of Neurosurgery, Affiliated Hospital of The Air Force Institute of Aeromedicine, Beijing, China, [3] Department of Anesthesiology, Beijing Friendship Hospital, Capital Medical University, Beijing, China

Keywords: glial transmitter, ATP, astrocyte, exocytosis, P2X7, calcium, mechanical stimulation

Edited by:
Alexej Verkhratsky,
University of Manchester,
United Kingdom

Reviewed by:
Yuriy Pankratov,
University of Warwick,
United Kingdom

***Correspondence:**
Yingfei Xiong
yfxiong@139.com
Mu Jin
jinmu0119@tom.com
Zhuan Zhou
zzhou@pku.edu.cn

[†] These authors have contributed equally to this work.

Received: *29 March 2018*
Accepted: *07 June 2018*
Published: *02 July 2018*

Citation:
Xiong Y, Sun S, Teng S, Jin M and Zhou Z (2018) Ca^{2+}-Dependent and Ca^{2+}-Independent ATP Release in Astrocytes. Front. Mol. Neurosci. 11:224. doi: 10.3389/fnmol.2018.00224

Like neurons, astrocytes are abundant in the central nervous system. They contact all types of cells in the brain, communicate with them, and modulate their activity by releasing gliotransmitters, including glutamate, ATP, etc. (Newman, 2003; Halassa and Haydon, 2010; Hamilton and Attwell, 2010; Volterra et al., 2014; Verkhratsky and Nedergaard, 2018), although the role of astrocytes in neurotransmission is still debated (Nedergaard and Verkhratsky, 2012; Fiacco and McCarthy, 2018).

ATP is considered to be a powerful extracellular messenger in both the peripheral and central nervous systems (Edwards et al., 1992; Fields and Stevens, 2000; Burnstock, 2007; Verkhratsky et al., 2009). *Via* activating multiple receptors in glia and neurons, ATP signaling participates in many important functions including cell development and synaptic plasticity (Evans et al., 1992; Newman, 2003; Zhang et al., 2003; Agresti et al., 2005; Abbracchio et al., 2009; Butt, 2011; Wurm et al., 2011; Verkhratsky et al., 2016). However, unlike the mechanism of neurotransmission *via* quantal exocytosis (Katz, 1959, 1969; Augustine and Neher, 1992; Neher, 1998; Sudhof, 2004; Pankratov et al., 2006, 2007; Sudhof and Rothman, 2009), the mechanisms by which ATP is released remain controversial. Because ATP is easily hydrolyzed, monitoring its real-time release is a challenge.

EARLY STUDIES OF NON-QUANTAL ATP RELEASE FROM ASTROCYTES

Early studies usually applied indirect methods such as dye-uptake, ATP analog labeling, and luciferase-luciferin system tests to indirectly detect ATP release (Duan et al., 2003). Based on these studies, ATP was thought to be released through specific channels, such as connexin/pannexin hemichannels, "maxi-anion" channels, and P2X7 receptor channels (**Figure 1A,** Stout et al., 2002; Duan et al., 2003; Bao et al., 2004; Suadicani et al., 2006; Kang et al., 2008; Liu et al., 2008; Iglesias et al., 2009; Bennett et al., 2012). These studies used indirect measurements based on measuring dyes or currents through channels that can pass molecules larger than ATP.

QUANTAL ATP RELEASE UNDER PHYSIOLOGICAL CONDITIONS

Patch-clamp recording *via* sniffer cells (Young and Poo, 1983; Liu et al., 2011) is a powerful tool with which to investigate the ATP release mechanism due to its high spatiotemporal resolution (Hollins and Ikeda, 1997; Pangrsic et al., 2007; Karanauskaite et al., 2009; Lalo et al., 2014; Liu et al., 2014; Lee et al., 2015). By using ATP-sniffer cells, Lalo et al. recorded quantal ATP release in astrocytes freshly isolated from mouse cortex. ATP is released by Ca^{2+}-dependent exocytosis

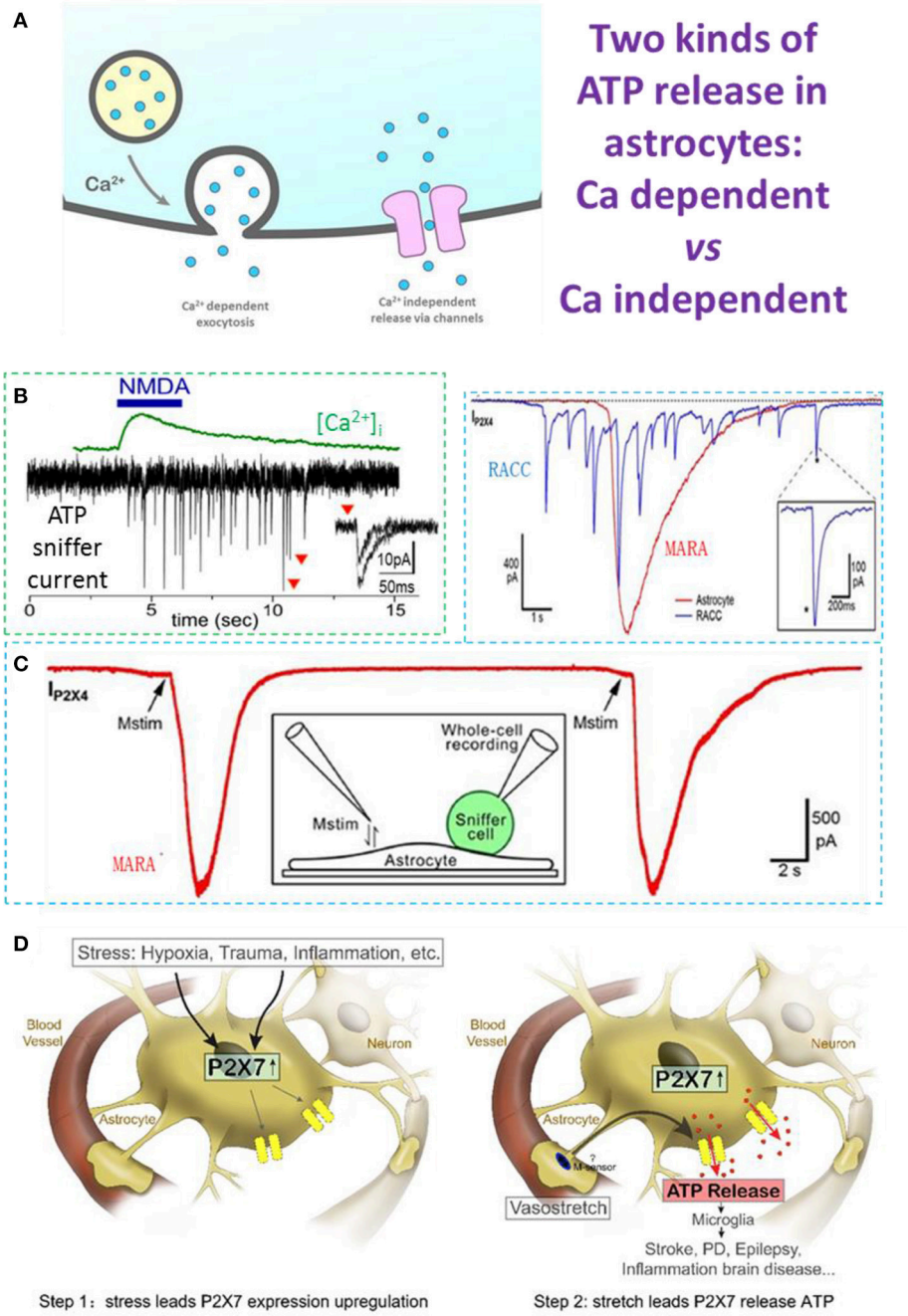

FIGURE 1 | Ca^{2+}-dependent and Ca^{2+}-independent ATP release in astrocytes. **(A)** Two types of ATP release: Ca^{2+}-dependent quantal release and Ca^{2+}-independent non-quantal release. In the Ca^{2+}-dependent pathway, secretory vesicles with packaged ATP are trafficked to the plasma membrane where they dock and fuse with it on arrival of a stimulus; this typically depends on an increase of cytosolic Ca^{2+}. In the Ca^{2+}-independent pathway, ATP is released through channels expressed on the astrocyte plasma membrane, such as the swelling-induced anion channel, connexin hemichannels activated by lower Ca^{2+} concentrations, and ionotropic purinergic receptor channels. **(B)** N-methyl-D-aspartate (NMDA)-induced Ca^{2+}-dependent quantal ATP release from a freshly-isolated astrocyte, recorded by a HEK293-P2X2 sniffer cell. **(C)** Typical MARA current (IP2X4) recorded with an HEK293A sniffer-cell expressing P2X4 (ATP sniffer) on an astrocyte. The astrocyte was stimulated twice and the MARA signal was reproducible. Inset, cartoon of the experimental protocol for MARA recording; Upper right: MARA vs Ca^{2+}-dependent ATP release of burst quantal events from a rat chromaffin cell (RACC). **(D)** Two-step hypothesis of MARA-mediated brain diseases. Left. Step 1: Stress induces upregulation of P2X7 receptor expression in astrocytes. The stressors include hypoxia (i.e., stroke and ischemia), trauma, and CNS diseases associated with inflammation or neurodegeneration. Right. Step 2: Stretch leads to P2X7-mediated ATP release from astrocytes. The abundant ATP is an emergency signal for the neural immune system that recruits and activates microglia in the ATP "hot-spots" and promotes disease. All data adapted from Xiong et al. (2018), except B adapted from Lalo et al. (2014). All data with reproduction permission from the original publishers.

following the activation of metabotropic and ionotropic receptors or direct UV-uncaging. The ATP release is SNARE protein-dependent and is eliminated by pretreatment with bafilomycin, a blocker of vacuolar-type H-ATPase. The kinetics of sniffer-cell responses are consistent with the millisecond time-scale, suggesting that ATP exocytosis is from synaptic-like small vesicles (**Figures 1A,B**). The ATP released from astrocytes (1) activates P2X receptors in neighboring neurons to enhance excitatory signaling, and (2) down-regulates inhibitory synaptic signaling (Lalo et al., 2014).

In addition to the tiny quantal ATP release arising from Ca^{2+}-dependent exocytosis in freshly-isolated astrocytes, an earlier report proposed that Ca^{2+}-dependent lysosome exocytosis is responsible for quantal ATP release in cultured astrocytes (Zhang et al., 2007). They provided three lines of indirect evidence: (1) the uptake of a fluorescent ATP analog, MANT-ATP, into lysosomes; (2) the presence of ATP in biochemically-purified lysosomes; and (3) the real-time visualization of Ca^{2+}-dependent lysosome exocytosis by total internal reflection fluorescence microscopy imaging of a false neurotransmitter (FM2-10). Although these data raised the possibility of quantal ATP release *via* lysosomal exocytosis, direct recording of quantal ATP release from glial lysosomes was absent.

STRETCH-INDUCED CA^{2+}-INDEPENDENT ATP RELEASE THROUGH P2X7 CHANNELS

It was our original goal to record quantal ATP release in cultured hippocampal astrocytes using ATP-sniffer cells. To our surprise, with three independent assays of lysosomal exocytosis, our real-time sniffer recordings clearly denied ATP release by Ca^{2+}-dependent lysosomal exocytosis (Xiong et al., 2018). Instead, following a gentle membrane stretch, Ca^{2+}-independent non-vesicular ATP release occurred in the cultured astrocytes (Xiong et al., 2018). In contrast to the quantal spikes of ATP release in chromaffin cells, the Mechanically-induced ATP Release from Astrocytes (MARA) displays a single spike with distinct kinetic characteristics. MARA is ∼300-fold greater in release content and ∼50 times longer in duration (**Figure 1C**, upper right inset). Mechanistically, MARA-mediated ATP release is (1) Ca^{2+}-independent, (2) not *via* lysosome exocytosis, and (3) mitochondria-dependent (Xiong et al., 2018). The P2X7 receptor channel is essential for MARA-mediated ATP release, because it is profoundly inhibited by Brilliant Blue G, a selective P2X7 antagonist, as well as by RNA interference-based P2X7 knockdown (Xiong et al., 2018). Considering that the open pore of the P2X7 channel allows the permeation of cytosolic molecules of molecular weight ≤900 Da, P2X7 channels should be able to release ATP (507 Da) (Yan et al., 2008; Nagasawa et al., 2009), and other purines, such as AMP, ADP, or adenosine. Together, MARA occurs when mechanical stretch triggers ATP efflux through P2X7 channel pores in "activated" astrocytes expressing P2X7 receptors in culture/*in vitro* or hypoxia/trauma/disease *in vivo* (Nagasawa et al., 2009). Hypoxia might decrease mitochondrial-dependent cytosolic ATP level and partially compensate the MARA signal for the increase in P2X7 expression.

One important open question left by Xiong (Xiong et al., 2018) is the identity of the mechanical sensor by which MARA initiates mechanical-P2X7-ATP release in astrocytes. Since P2X7 itself is not mechanosensor, we hypothesize that a mechanosensor [such as piezo 1 protein (Zhao et al., 2018)] binds P2X7 and "transactivates" mechanical force to activate P2X7 [One recent example of protein-transactivation is that a voltage-sensor channel activates another binding protein of vesicle fusion-pore (Chai et al., 2017)]. Following the discovery of MARA, identification of this sensor is critical for treating possible MARA-mediated brain diseases as proposed below. In addition to P2X7 (Xiong et al., 2018), hemichannels such as connexins (Stout et al., 2002) and large conductance Cl^- channel (Liu et al., 2008) have been reported to mediate the non-vesicular ATP release from astrocytes. At present it is unclear about the relative contributions to ATP release among these channel types, because the stimulations in these studies were different. These ATP-release pathways through different channels may play condition-dependent roles in astrocytes' functions.

A HYPOTHESIS OF MARA IN BRAIN PROTECTION AND DISEASES

In contrast to the Ca^{2+}-dependent quantal ATP release in freshly-isolated astrocytes, the Ca^{2+}-independent ATP release event (MARA) in cultured astrocytes is ∼10,000 times greater (**Figure 1C**). P2X7 is up-regulated under ischemic conditions *in vivo* (Nagasawa et al., 2009), and this could contribute to the release of large amounts of ATP from cellular sources, and in the extracellular space it is quickly hydrolyzed to ADP, AMP, and adenosine, which activate their receptors and play roles in brain protection and damage (Neary et al., 2003; Choo et al., 2013; Rodrigues et al., 2015). On the other hand, the large ATP release *via* MARA would recruit microglia, leading to protective or pathological pathways (Dou et al., 2012). Thus, we propose that MARA could be a mechanism underlying brain diseases such as those associated with hypoxia/ischemia and trauma, as well as other neurological disorders (Parkinson's disease, Alzheimer's disease, and epilepsy) (**Figure 1D**). Our hypothesis is detailed as follows. The first step is MARA genesis, which is dependent on P2X7 receptor expression. The expression level of P2X7 receptors in astrocytes is up-regulated under either of the two conditions: (1) in culture, which is an extremely stressful condition lacking blood and other support for astrocytes (Narcisse et al., 2005; Bartlett et al., 2014; Burnstock, 2017; Xiong et al., 2018); and (2) *in vivo*, when astrocytes suffer stresses, such as hypoxia (i.e., ischemia and stroke), trauma, or some CNS diseases (for example, inflammation and/or neurodegeneration; Ballerini et al., 1996; Narcisse et al., 2005; Nagasawa et al., 2009; Burnstock, 2017). Indeed, few astrocytes express P2X7 receptors in the intact hippocampal slices under physiological conditions (Nagasawa et al., 2009; Xiong et al., 2018). As the P2X7 receptor is a key modulator of aerobic glycolysis, it has an intrinsic ability to reprogram cell metabolism to meet the

needs imposed by adverse environmental conditions (Amoroso et al., 2012). The up-regulation of P2X7 receptors in astrocytes is not only a form of adaptation to stress, but is also a necessary preparation for MARA to execute its repair function in its brain region (**Figure 1D**, step 1). The second step is MARA activation following mechanical stimulation, which could be generated by arterioles *in vivo*. Astrocytes regulate cerebral blood flow to match the metabolic requirements of the brain (Gordon et al., 2008) by eliciting the vasoconstriction or vasodilation of arterioles. A tension change due to such vasoconstriction/dilation is an effective physiological mechanical stimulus (membrane stretch) for astrocytes, which are activated by deformation of their surroundings on a timescale of milliseconds (Janmey and Miller, 2011). Physiological arteriole stretch does not trigger MARA because P2X7 receptors are rare in astrocytes under normal conditions. When stresses such as hypoxia/trauma occur, the expression of astrocytic P2X7 receptors is up-regulated, and if the stress persists and exceeds a threshold, the abnormal changes in arteriole tension directly trigger MARA (**Figure 1D,** step 2). So, noxious stimuli up-regulate the P2X7 receptor expression in astrocytes, and this can be considered as an adaptive change in response to stress and the beginning of pathological damage, because up-regulation of P2X7 receptor expression is the prerequisite for non-quantal ATP release/MARA. When the steady-state is disturbed, MARA occurs and triggers a sustained increase in extracellular ATP, which then acts to alert the presence of a "hot spot." This signal recruits and activates microglia, which scavenge and phagocytize injured cells and cellular debris, increase the susceptibility of neurons to damage, promote astrogliosis, and mount neuroinflammatory responses (Parpura et al., 2012; Rivera et al., 2016). In this sense, both astrocytes and microglia comprise the immune system of the CNS: each of a vast number astrocytes performs an immobile surveillance for its specific location in the brain, signaling stress, while each microglia cell acts as a mobile patrol, responding to the astrocytic "alert" signal—an unusually large increase in extracellular ATP concentration. To a certain extent, MARA from a few astrocytes recruits a few microglia to clear the site and protect the brain. However, when the stress is excessive, MARA from a large number of astrocytes may recruit too many microglia, overkill healthy tissue, and cause irreversible brain damage (disease).

AUTHOR CONTRIBUTIONS

All authors listed have made a substantial, direct and intellectual contribution to the work, and approved it for publication.

ACKNOWLEDGMENTS

We thank Prof. I. C. Bruce (Peking University) for helpful comments, and Xi Wu for art of **Figures 1A** and **D**. This work was supported by the National Natural Science Foundation of China (31330024, 31761133016, 21790394, 31171026, 31327901, 31521062, and 21790390), the National Key Research and Development Program of China (2016YFA0500401), and the National Basic Research Program of China (2012C B518006).

REFERENCES

Abbracchio, M. P., Burnstock, G., Verkhratsky, A., and Zimmermann, H. (2009). Purinergic signalling in the nervous system: an overview. *Trends Neurosci.* 32, 19–29. doi: 10.1016/j.tins.2008.10.001

Agresti, C., Meomartini, M. E., Amadio, S., Ambrosini, E., Volonté, C., Aloisi, F., et al. (2005). ATP regulates oligodendrocyte progenitor migration, proliferation, and differentiation: involvement of metabotropic P2 receptors. *Brain Res. Brain Res. Rev.* 48, 157–165. doi: 10.1016/j.brainresrev.2004.12.005

Amoroso, F., Falzoni, S., Adinolfi, E., Ferrari, D., and Di Virgilio, F. (2012). The P2X7 receptor is a key modulator of aerobic glycolysis. *Cell Death Amp. Dis.* 3:e370. doi: 10.1038/cddis.2012.105

Augustine, G. J., and Neher, E. (1992). Calcium requirements for secretion in bovine chromaffin cells. *J. Physiol.* 450, 247–271. doi: 10.1113/jphysiol.1992.sp019126

Ballerini, P., Rathbone, M. P., Di Iorio, P., Renzetti, A., Giuliani, P., D'alimonte, I., et al. (1996). Rat astroglial P2Z (P2X7) receptors regulate intracellular calcium and purine release. *Neuroreport* 7, 2533–2537. doi: 10.1097/00001756-199611040-00026

Bao, L., Locovei, S., and Dahl, G. (2004). Pannexin membrane channels are mechanosensitive conduits for ATP. *FEBS Lett.* 572, 65–68. doi: 10.1016/j.febslet.2004.07.009

Bartlett, R., Stokes, L., and Sluyter, R. (2014). The P2X7 receptor channel: recent developments and the use of P2X7 antagonists in models of disease. *Pharmacol. Rev.* 66, 638–675. doi: 10.1124/pr.113.008003

Bennett, M. V., Garré, J. M., Orellana, J. A., Bukauskas, F. F., Nedergaard, M., and Saez, J. C. (2012). Connexin and pannexin hemichannels in inflammatory responses of glia and neurons. *Brain Res.* 1487, 3–15. doi: 10.1016/j.brainres.2012.08.042

Burnstock, G. (2007). Physiology and pathophysiology of purinergic neurotransmission. *Physiol. Rev.* 87, 659–797. doi: 10.1152/physrev.00043.2006

Burnstock, G. (2017). Purinergic signalling and neurological diseases: an update. *CNS Neurol. Disord. Drug Targets* 16, 257–265. doi: 10.2174/1871527315666160922104848

Butt, A. M. (2011). ATP: a ubiquitous gliotransmitter integrating neuron-glial networks. *Semin. Cell Dev. Biol.* 22, 205–213. doi: 10.1016/j.semcdb.2011.02.023

Chai, Z., Wang, C., Huang, R., Wang, Y., Zhang, X., Wu, Q., et al. (2017). CaV2.2 gates calcium-independent but voltage-dependent secretion in mammalian sensory neurons. *Neuron* 96, 1317–1326.e1314. doi: 10.1016/j.neuron.2017.10.028

Choo, A. M., Miller, W. J., Chen, Y. C., Nibley, P., Patel, T. P., Goletiani, C., et al. (2013). Antagonism of purinergic signalling improves recovery from traumatic brain injury. *Brain* 136, 65–80. doi: 10.1093/brain/aws286

Dou, Y., Wu, H. J., Li, H. Q., Qin, S., Wang, Y. E., Li, J., et al. (2012). Microglial migration mediated by ATP-induced ATP release from lysosomes. *Cell Res.* 22, 1022–1033. doi: 10.1038/cr.2012.10

Duan, S., Anderson, C. M., Keung, E. C., Chen, Y., Chen, Y., and Swanson, R. A. (2003). P2X7 receptor-mediated release of excitatory amino acids from astrocytes. *J. Neurosci.* 23, 1320–1328. doi: 10.1523/JNEUROSCI.23-04-01320.2003

Edwards, F. A., Gibb, A. J., and Colquhoun, D. (1992). ATP receptor-mediated synaptic currents in the central nervous system. *Nature* 359, 144–147. doi: 10.1038/359144a0

Evans, R. J., Derkach, V., and Surprenant, A. (1992). ATP mediates fast synaptic transmission in mammalian neurons. *Nature* 357, 503–505. doi: 10.1038/357503a0

Fiacco, T. A., and McCarthy, K. D. (2018). Multiple lines of evidence indicate that gliotransmission does not occur under physiological conditions. *J. Neurosci.* 38, 3–13. doi: 10.1523/JNEUROSCI.0016-17.2017

Fields, R. D., and Stevens, B. (2000). ATP: an extracellular signaling molecule between neurons and glia. *Trends Neurosci.* 23, 625–633. doi: 10.1016/S0166-2236(00)01674-X

Gordon, G. R., Choi, H. B., Rungta, R. L., Ellis-Davies, G. C., and MacVicar, B. A. (2008). Brain metabolism dictates the polarity of astrocyte control over arterioles. *Nature* 456, 745–749. doi: 10.1038/nature07525

Halassa, M. M., and Haydon, P. G. (2010). Integrated brain circuits: astrocytic networks modulate neuronal activity and behavior. *Annu. Rev. Physiol.* 72, 335–355. doi: 10.1146/annurev-physiol-021909-135843

Hamilton, N. B., and Attwell, D. (2010). Do astrocytes really exocytose neurotransmitters? *Nat. Rev. Neurosci.* 11, 227–238. doi: 10.1038/nrn2803

Hollins, B., and Ikeda, S. R. (1997). Heterologous expression of a P2x-purinoceptor in rat chromaffin cells detects vesicular ATP release. *J. Neurophysiol.* 78, 3069–3076. doi: 10.1152/jn.1997.78.6.3069

Iglesias, R., Dahl, G., Qiu, F., Spray, D. C., and Scemes, E. (2009). Pannexin 1: the molecular substrate of astrocyte "hemichannels". *J. Neurosci.* 29, 7092–7097. doi: 10.1523/JNEUROSCI.6062-08.2009

Janmey, P. A., and Miller, R. T. (2011). Mechanisms of mechanical signaling in development and disease. *J. Cell Sci.* 124, 9–18. doi: 10.1242/jcs.071001

Kang, J., Kang, N., Lovatt, D., Torres, A., Zhao, Z., Lin, J., et al. (2008). Connexin 43 hemichannels are permeable to ATP. *J. Neurosci.* 28, 4702–4711. doi: 10.1523/JNEUROSCI.5048-07.2008

Karanauskaite, J., Hoppa, M. B., Braun, M., Galvanovskis, J., and Rorsman, P. (2009). Quantal ATP release in rat beta-cells by exocytosis of insulin-containing LDCVs. *Pflugers Arch.* 458, 389–401. doi: 10.1007/s00424-008-0610-6

Katz, B. (1959). Nature of the nerve impulse. *Rev. Mod. Phys* 8, 629–638. doi: 10.1103/RevModPhys.31.466

Katz, B. (1969). The release of neural transmitter substances. *J. Neurol. Neurosurg. Psychiatry* 32:638. doi: 10.1136/jnnp.32.6.638

Lalo, U., Palygin, O., Rasooli-Nejad, S., Andrew, J., Haydon, P. G., and Pankratov, Y. (2014). Exocytosis of ATP from astrocytes modulates phasic and tonic inhibition in the neocortex. *PLoS Biol.* 12:e1001747. doi: 10.1371/journal.pbio.1001747

Lee, J., Chun, Y. E., Han, K. S., Lee, J., Woo, D. H., and Lee, C. J. (2015). $Ca(^{2+})$ Entry is required for mechanical stimulation-induced ATP release from astrocyte. *Exp. Neurobiol.* 24, 17–23. doi: 10.5607/en.2015.24.1.17

Liu, H. T., Toychiev, A. H., Takahashi, N., Sabirov, R. Z., and Okada, Y. (2008). Maxi-anion channel as a candidate pathway for osmosensitive ATP release from mouse astrocytes in primary culture. *Cell Res.* 18, 558–565. doi: 10.1038/cr.2008.49

Liu, T., Li, H., Gounko, N. V., Zhou, Z., Xu, A., Hong, W., et al. (2014). Detection of insulin granule exocytosis by an electrophysiology method with high temporal resolution reveals enlarged insulin granule pool in BIG3-knockout mice. *Am. J. Physiol. Endocrinol. Metab.* 307, E611–E618. doi: 10.1152/ajpendo.00208.2014

Liu, T., Sun, L., Xiong, Y., Shang, S., Guo, N., Teng, S., et al. (2011). Calcium triggers exocytosis from two types of organelles in a single astrocyte. *J. Neurosci.* 31, 10593–10601. doi: 10.1523/JNEUROSCI.6401-10.2011

Nagasawa, K., Escartin, C., and Swanson, R. A. (2009). Astrocyte cultures exhibit P2X7 receptor channel opening in the absence of exogenous ligands. *Glia* 57, 622–633. doi: 10.1002/glia.20791

Narcisse, L., Scemes, E., Zhao, Y., Lee, S. C., and Brosnan, C. F. (2005). The cytokine IL-1beta transiently enhances P2X7 receptor expression and function in human astrocytes. *Glia* 49, 245–258. doi: 10.1002/glia.20110

Neary, J. T., Kang, Y., Willoughby, K. A., and Ellis, E. F. (2003). Activation of extracellular signal-regulated kinase by stretch-induced injury in astrocytes involves extracellular ATP and P2 purinergic receptors. *J. Neurosci.* 23, 2348–2356. doi: 10.1523/JNEUROSCI.23-06-02348.2003

Nedergaard, M., and Verkhratsky, A. (2012). Artifact versus reality–how astrocytes contribute to synaptic events. *Glia* 60, 1013–1023. doi: 10.1002/glia.22288

Neher, E. (1998). Vesicle pools and Ca^{2+} microdomains: new tools for understanding their roles in neurotransmitter release. *Neuron* 20, 389–399. doi: 10.1016/S0896-6273(00)80983-6

Newman, E. A. (2003). New roles for astrocytes: regulation of synaptic transmission. *Trends Neurosci.* 26, 536–542. doi: 10.1016/S0166-2236(03)00237-6

Pangrsic, T., Potokar, M., Stenovec, M., Kreft, M., Fabbretti, E., Nistri, A., et al. (2007). Exocytotic release of ATP from cultured astrocytes. *J. Biol. Chem.* 282, 28749–28758. doi: 10.1074/jbc.M700290200

Pankratov, Y., Lalo, U., Verkhratsky, A., and North, R. A. (2006). Vesicular release of ATP at central synapses. *Pflugers Arch.* 452, 589–597. doi: 10.1007/s00424-006-0061-x

Pankratov, Y., Lalo, U., Verkhratsky, A., and North, R. A. (2007). Quantal release of ATP in mouse cortex. *J. Gen. Physiol.* 129, 257–265. doi: 10.1085/jgp.200609693

Parpura, V., Heneka, M. T., Montana, V., Oliet, S. H., Schousboe, A., Haydon, P. G., et al. (2012). Glial cells in (patho)physiology. *J. Neurochem.* 121, 4–27. doi: 10.1111/j.1471-4159.2012.07664.x

Rivera, A., Vanzulli, I., and Butt, A. M. (2016). A central role for ATP signalling in glial interactions in the CNS. *Curr. Drug Targets* 17, 1829–1833. doi: 10.2174/1389450117666160711154529

Rodrigues, R. J., Tomé, A. R., and Cunha, R. A. (2015). ATP as a multi-target danger signal in the brain. *Front. Neurosci.* 9:148. doi: 10.3389/fnins.2015.00148

Stout, C. E., Costantin, J. L., Naus, C. C., and Charles, A. C. (2002). Intercellular calcium signaling in astrocytes via ATP release through connexin hemichannels. *J. Biol. Chem.* 277, 10482–10488. doi: 10.1074/jbc.M109902200

Suadicani, S. O., Brosnan, C. F., and Scemes, E. (2006). P2X7 receptors mediate ATP release and amplification of astrocytic intercellular Ca^{2+} signaling. *J. Neurosci.* 26, 1378–1385. doi: 10.1523/JNEUROSCI.3902-05.2006

Sudhof, T. C. (2004). The synaptic vesicle cycle. *Annu. Rev. Neurosci.* 27, 509–547. doi: 10.1146/annurev.neuro.26.041002.131412

Sudhof, T. C., and Rothman, J. E. (2009). Membrane fusion: grappling with SNARE and SM proteins. *Science* 323, 474–477. doi: 10.1126/science.1161748

Verkhratsky, A., Krishtal, O. A., and Burnstock, G. (2009). Purinoceptors on neuroglia. *Mol. Neurobiol.* 39, 190–208. doi: 10.1007/s12035-009-8063-2

Verkhratsky, A., Matteoli, M., Parpura, V., Mothet, J. P., and Zorec, R. (2016). Astrocytes as secretory cells of the central nervous system: idiosyncrasies of vesicular secretion. *EMBO J.* 35, 239–257. doi: 10.15252/embj.201592705

Verkhratsky, A., and Nedergaard, M. (2018). Physiology of Astroglia. *Physiol. Rev.* 98, 239–389. doi: 10.1152/physrev.00042.2016

Volterra, A., Liaudet, N., and Savtchouk, I. (2014). Astrocyte Ca^{2+} signalling: an unexpected complexity. *Nat. Rev. Neurosci.* 15, 327–335. doi: 10.1038/nrn3725

Wurm, A., Pannicke, T., Iandiev, I., Francke, M., Hollborn, M., Wiedemann, P., et al. (2011). Purinergic signaling involved in Muller cell function in the mammalian retina. *Prog. Retin. Eye Res.* 30, 324–342. doi: 10.1016/j.preteyeres.2011.06.001

Xiong, Y., Teng, S., Zheng, L., Sun, S., Li, J., Guo, N., et al. (2018). Stretch-induced $Ca(^{2+})$ -independent ATP release in hippocampal astrocytes. *J. Physiol.* 596, 1931–1947. doi: 10.1113/JP275805

Yan, Z., Li, S., Liang, Z., Tomić, M., and Stojilkovic, S. S. (2008). The P2X7 receptor channel pore dilates under physiological ion conditions. *J. Gen. Physiol.* 132, 563–573. doi: 10.1085/jgp.200810059

Young, S. H., and Poo, M. M. (1983). Spontaneous release of transmitter from growth cones of embryonic neurones. *Nature* 305, 634–637. doi: 10.1038/305634a0

Zhang, J. M., Wang, H. K., Ye, C. Q., Ge, W., Chen, Y., Jiang, Z. L., et al. (2003). ATP released by astrocytes mediates glutamatergic activity-dependent heterosynaptic suppression. *Neuron* 40, 971–982. doi: 10.1016/S0896-6273(03)00717-7

Zhang, Z., Chen, G., Zhou, W., Song, A., Xu, T., Luo, Q., et al. (2007). Regulated ATP release from astrocytes through lysosome exocytosis. *Nat. Cell Biol.* 9, 945–953. doi: 10.1038/ncb1620

Zhao, Q., Zhou, H., Chi, S., Wang, Y., Wang, J., Geng, J., et al. (2018). Structure and mechanogating mechanism of the Piezo1 channel. *Nature* 554, 487–492. doi: 10.1038/nature25743

Conflict of Interest Statement: The authors declare that the research was conducted in the absence of any commercial or financial relationships that could be construed as a potential conflict of interest.

frontiers in Molecular Neuroscience

ORIGINAL RESEARCH
published: 28 June 2018
doi: 10.3389/fnmol.2018.00222

Apoptosis of Endothelial Cells Contributes to Brain Vessel Pruning of Zebrafish During Development

Yu Zhang[1,2†], *Bing Xu*[1,2†], *Qi Chen*[1], *Yong Yan*[1,3], *Jiulin Du*[1,2,3*] *and Xufei Du*[1,2*]

[1]*Institute of Neuroscience, State Key Laboratory of Neuroscience, Center for Excellence in Brain Science and Intelligence Technology, Chinese Academy of Sciences, Shanghai, China,* [2]*School of Future Technology, University of Chinese Academy of Sciences, Beijing, China,* [3]*School of Life Science and Technology, ShanghaiTech University, Shanghai, China*

During development, immature blood vessel networks remodel to form a simplified and efficient vasculature to meet the demand for oxygen and nutrients, and this remodeling process is mainly achieved via the pruning of existing vessels. It has already known that the migration of vascular endothelial cells (ECs) is one of the mechanisms underlying vessel pruning. However, the role of EC apoptosis in vessel pruning remains under debate, especially in the brain. Here, we reported that EC apoptosis makes a significant contribution to vessel pruning in the brain of larval zebrafish. Using *in vivo* long-term time-lapse confocal imaging of the brain vasculature in zebrafish larvae, we found that EC apoptosis was always accompanied with brain vessel pruning and about 15% of vessel pruning events were resulted from EC apoptosis. In comparison with brain vessels undergoing EC migration-associated pruning, EC apoptosis-accompanied pruned vessels were longer and showed higher probability that the nuclei of neighboring vessels' ECs occupied their both ends. Furthermore, we found that microglia were responsible for the clearance of apoptotic ECs accompanying vessel pruning, though microglia themselves were dispensable for the occurrence of vessel pruning. Thus, our study demonstrates that EC apoptosis contributes to vessel pruning in the brain during development in a microglial cell-independent manner.

Keywords: apoptosis, endothelial cells, vessel pruning, microglia, zebrafish

OPEN ACCESS

Edited by:
Margaret Su-chun Ho,
ShanghaiTech University, China

Reviewed by:
Marie-Eve Tremblay,
Laval University, Canada
Hari S. Sharma,
Uppsala University, Sweden

***Correspondence:**
Jiulin Du
forestdu@ion.ac.cn
Xufei Du
xufeidu@ion.ac.cn

†These authors have contributed equally to this work.

Received: *27 February 2018*
Accepted: *06 June 2018*
Published: *28 June 2018*

Citation:
Zhang Y, Xu B, Chen Q, Yan Y, Du J and Du X (2018) Apoptosis of Endothelial Cells Contributes to Brain Vessel Pruning of Zebrafish During Development. Front. Mol. Neurosci. 11:222. doi: 10.3389/fnmol.2018.00222

INTRODUCTION

During development, highly ramified immature blood vascular networks undergo extensive remodeling, including refined vessel pruning of selected vessel branches and complete regression of vascular networks, to form an efficient mature vasculature to meet their physiological functions (Adams and Alitalo, 2007; Herbert and Stainier, 2011; Korn and Augustin, 2015; Betz et al., 2016). It is generally thought that vessel pruning is mainly achieved through blood flow fluctuation-induced lateral migration of endothelial cells (ECs) to adjacent unpruned vascular segments (Chen et al., 2012; Kochhan et al., 2013; Franco et al., 2015; Lenard et al., 2015). However, EC apoptosis has been found during the pruning of the cranial division of internal carotid artery (CrDI) in zebrafish (Kochhan et al., 2013) and of the retinal vasculature in mice (Franco et al., 2015). In particular, macrophage-induced EC apoptosis is responsible for the complete regression of the hyaloid vasculature in developing eyes (Lobov et al., 2005). Therefore, the contribution of EC apoptosis to vessel pruning, especially in the brain vasculature, remains unclear.

Microglia, the resident immune cells in the central nervous system (CNS), are specialized macrophages that play crucial roles in mediating immune-related functions (Nayak et al., 2014). Besides being immune mediators, microglia are emerging as important contributors to normal CNS development and function (Paolicelli et al., 2011; Li et al., 2012; Wu et al., 2015). Interestingly, microglia are also shown to be important for the behaviors of vascular tip cells (Fantin et al., 2010; Tammela et al., 2011; Arnold and Betsholtz, 2013), the repair of brain vascular rupture (Liu et al., 2016), and the closure of injured blood-brain barrier (Lou et al., 2016). However, it is still unknown whether microglia participate in brain vascular remodeling during development.

To address whether EC apoptosis and microglia are involved in brain vessel pruning, we performed *in vivo* long-term time-lapse confocal imaging of the brain vasculature in larval zebrafish, and first found that about 15% of brain vessel pruning events were accompanied by EC apoptosis. Furthermore, we demonstrated that microglia were unnecessary for brain vessel pruning but responsible for the clearance of pruned vessel-associated apoptotic ECs. Thus, our findings reveal that microglial cell-independent EC apoptosis is involved in brain vessel pruning of larval zebrafish.

MATERIALS AND METHODS

Zebrafish Husbandry

Adult zebrafish (*Dario rerio*) were maintained in an automatic fish housing system at 28°C following standard protocols (Chen et al., 2012). The *Tg(kdrl:EGFP)s843* (Jin et al., 2005), *Tg(fli1a.ep:DsRedEx)um13* (Covassin et al., 2009), *Tg(fli1a:nEGFP)y7* (Roman et al., 2002) and *Tg(coro1a:DsRedEx)hkz011t* (Li et al., 2012) zebrafish lines were described previously. Zebrafish embryos were raised under a 14 h–10 h light-dark cycle in 10% Hanks' solution that consisted of 140 mM NaCl, 5.4 mM KCl, 0.25 mM Na_2HPO_4, 0.44 mM KH_2PO_4, 1.3 mM $CaCl_2$, 1.0 mM $MgSO_4$ and 4.2 mM $NaHCO_3$ (pH = 7.2). The 0.003% 1-phenyl-2-thiourea (PTU; Sigma, P7629) was added into the Hanks' solution to prevent pigment formation of zebrafish embryos. The zebrafish chorion was removed at 1 day post-fertilization (dpf) with the treatment of 2 mg/ml pronase (Calbiochem, 53702), which was diluted in the Hanks' solution. All animal use and handling procedures were approved by the Institute of Neuroscience, Chinese Academy of Sciences.

In Vivo Confocal Imaging

Imaging was performed on 3–3.5 dpf zebrafish larvae at room temperature (26–28°C). Larvae were embedded in 1% low-melting agarose (Sigma) for imaging without anesthetics. Imaging was carried out under a 40× water immersion objective (N.A., 0.80) with an Olympus Fluoview 1000 confocal microscope (Tokyo, Japan). The *z*-step of imaging was 3 μm. To trace the fate of each vessel segment during development, long-term time-lapse imaging of the brain vasculature of the same larvae was performed with 1-h interval.

Image Analysis

All the images were analyzed by ImageJ (NIH). The pruned vessels were quantified in the whole zebrafish brain. For the quantification of vessel pruning, the vessel segment which initially displayed lumen morphology but with a collapsed shape and disappeared completely later was counted as a pruned vessel. For the quantification of EC apoptosis, the ECs exhibiting typical apoptotic features, such as plasma membrane blebbing and formation of apoptotic bodies, were counted as apoptotic ECs. For the quantification of microglial density, we counted the number of microglia in the whole brain region of the microglial transgenic zebrafish *Tg(coro1a:DsRedEx)* microinjected with control or *pu.1* MO. The microglial engulfment of apoptotic ECs was defined as a process that the microglia migrated to and engulfed the apoptotic ECs and then the apoptotic ECs faded away.

Morpholino Oligonucleotides and Microinjection

Morpholino oligonucleotides (MOs) were purchased from Gene Tools (Philomath, OR, USA). Lyophilized MOs were dissolved in nuclease-free water. The 4 ng *pu.1* MO (5′-GATATACTGATACTCCATTGGTGGT-3′) or equivalent control MO (5′-CCTCTTACCTCAGTTACAATTTATA-3′) were microinjected into one-cell-stage zebrafish embryos.

DAPI Injection

The DAPI (10 nl, 1 mg/ml) was microinjected into the blood circulation system of 3-dpf *Tg(kdrl:EGFP)* larvae through the common cardinal vein. Immediately after the injection, time-lapse imaging was performed to trace pruned vessels with apoptotic ECs.

Immunofluorescence

Whole zebrafish embryos at 3 dpf were fixed in 4% paraformaldehyde for 2 h at room temperature, washed twice in PBS, and then incubated in a blocking solution (5% normal goat serum in PBS 0.2% Triton) overnight at 4°C. The embryos were then incubated in the blocking solution with a rabbit anti-Caspase-3 primary antibody (1:500, ab13847) for 72 h at 4°C. After washing with PBS 0.2% Triton, the embryos were incubated in the blocking solution with a secondary antibody (1:500) and DAPI (1:1000) for 48 h at 4°C. After washing with PBS 0.2% Triton, images were taken with an Olympus Fluoview 1000 confocal microscope (Tokyo, Japan). The dying ECs showing overlapped anti-Caspase-3 staining and DAPI staining are considered as the apoptotic ECs.

Statistical Analysis

Statistical analyses were performed by using GraphPad Prism v6.0 software. The significance of the difference between two groups was determined by using two-tailed unpaired Student's *t*-test. Data were represented as mean ± SEM, and $p < 0.05$ was considered to be statistically significant.

RESULTS

Brain Vessel Pruning Is Accompanied With EC Apoptosis in Larval Zebrafish

To examine whether the apoptosis of ECs contributes to brain vessel pruning, we monitored the development of the brain vasculature in individual larval zebrafish with 1-h interval during 3–3.5 dpf, when most brain vessel pruning events occur (Chen et al., 2012). The brain vasculature was visualized by using the double transgenic line *Tg(fli1a:nEGFP);Tg(fli1a.ep:DsRedEx)*, in which the nucleus and cellular morphology of ECs were labeled by enhanced green fluorescent protein (EGFP) and DsRed, respectively (Chen et al., 2012). Besides the previously reported EC lateral migration-associated vessel pruning, we also found EC death-accompanied vessel pruning, during which the dying EC showed typical morphological features of cell apoptosis, including plasma membrane blebbing and formation of apoptotic bodies (**Figure 1A**). In the total of 55 vessel pruning events observed in 17 larvae, 15% of them (8 out of 55) were accompanied with EC apoptosis (**Figure 1B**). Furthermore, by microinjection of DAPI into the circulation system of *Tg(kdrl:EGFP)* larvae to label the nucleus of ECs, we found that the nucleus of apoptotic ECs condensed and fragmented during vessel pruning (**Figure 1C**).

To demonstrate that the dying ECs with typical apoptotic morphology during vessel pruning are indeed undergoing apoptosis, we first screened out the vessel pruning event accompanied with dying ECs by *in vivo* imaging, and then fixed the embryo immediately to examine the expression of the active Caspase-3, a marker of cell apoptosis (Franco et al., 2015). We found that the dying EC indeed expressed active Caspase-3 and showed nuclear condensation and formation of apoptotic bodies, indicating the existence of EC apoptosis (**Figure 1D**). Taken together, these results demonstrate that EC apoptosis is indeed involved in the vessel pruning of the zebrafish brain vasculature during development.

EC Apoptosis-Accompanied Pruned Vessels Are Longer and Show Higher Probability That Adjacent Vessels' EC Nuclei Occupy Their Both Ends

Compared with pruned vessels with EC lateral migration, we found that EC apoptosis-accompanied pruned vessels showed a higher probability that the nuclei of neighboring vessels' ECs located near the both ends of the pruned vessels (**Figures 2A,B**; pruning with EC apoptosis, 7 out of 9; pruning with EC migration, 3 out of 11). Moreover, EC apoptosis-accompanied pruned vessels were much longer (**Figure 2C**; pruning with EC apoptosis, 85 ± 8 μm; pruning with EC migration, 56 ± 5 μm; $p < 0.01$, two-tailed unpaired Student's *t*-test). These results suggest that the vessel segments with longer length and occupied by the nuclei of neighboring vessels' ECs at their both ends are more likely to be pruned via EC apoptosis rather than EC migration.

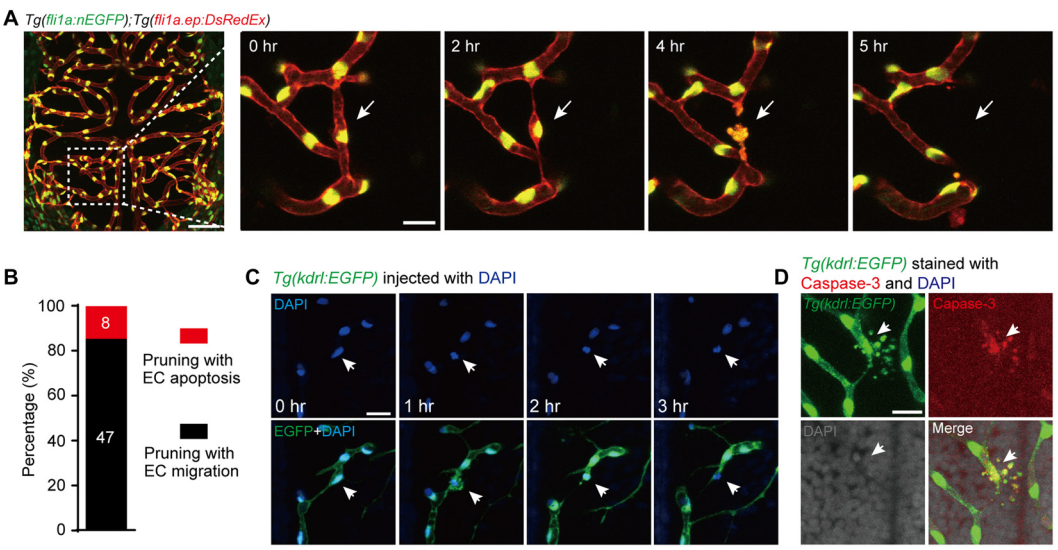

FIGURE 1 | Vessel pruning is accompanied with endothelial cell (EC) apoptosis in the brain of larval zebrafish. **(A)** *In vivo* time-lapse confocal images showing that an EC (arrows) underwent apoptosis on a pruned brain vessel in a *Tg(fli1a:nEGFP);Tg(fli1a.ep:DsRedEx)* larva at 3–3.5 days post-fertilization (dpf), in which EC nuclei were labeled by both enhanced green fluorescent protein (EGFP) and DsRed (yellow). Left, projected confocal image of the whole brain vasculature; Right, time-lapse confocal images of the dashed outlined area in the left. **(B)** Summary of the percentages of EC apoptosis- and migration-accompanied brain vessel pruning (n = 17 larvae). **(C)** *In vivo* time-lapse confocal images showing that an EC (arrows) underwent apoptosis on a brain pruned vessel in a DAPI-injected *Tg(kdrl:EGFP)* larva at 3–3.5 dpf, in which EC nuclei were labeled by DAPI (blue). **(D)** Immunofluorescence images showing that, on a pruned vessel, an EC with typical apoptotic morphology (arrows) expressed Caspase-3. The numbers on the bars **(B)** represent the number of pruned vessels examined. Scales: 50 μm (left in **(A)**, 15 μm (right in **(A)**, 50 μm **(C)** and 15 μm **(D)**.

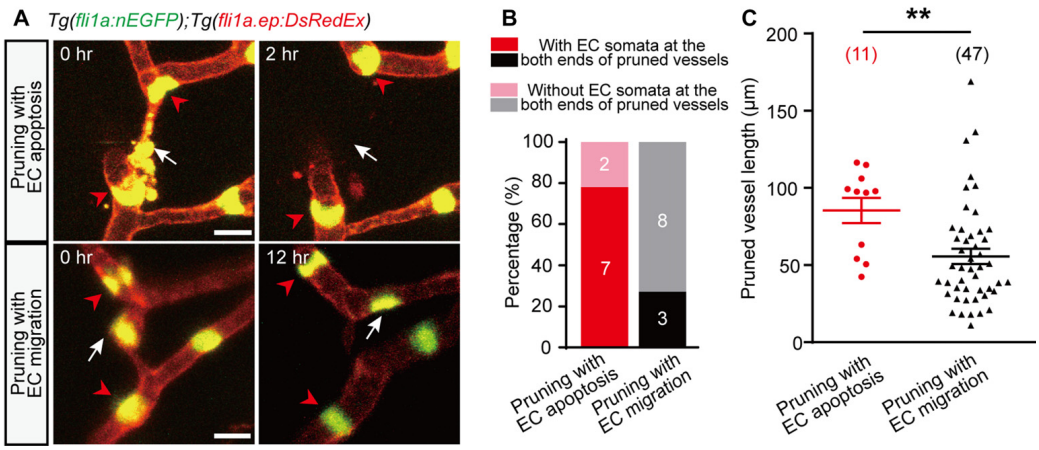

FIGURE 2 | Characterization of EC apoptosis-accompanied pruned vessels. **(A)** *In vivo* time-lapse confocal images showing the relative spatial locations of EC nuclei in pruned and adjacent brain vessels. Top: for an EC apoptosis-accompanied pruned brain vessel, the nuclei of two neighboring vessels' ECs (red arrowheads) located at the both ends of the pruned vessel, respectively (white arrow). Bottom: for an EC migration-accompanied pruned brain vessel, the nuclei of neighboring vessels' ECs (red arrowheads) did not occupy the ends of the pruned vessel (white arrow). **(B)** Summary of data showing that EC apoptosis-accompanied pruning vessels have a higher probability that neighboring vessels' EC nuclei occupy their both ends (7 out of 9, $n = 7$ larvae) than EC migration-accompanied pruning vessels (3 out of 11, $n = 6$ larvae). **(C)** Length of pruned vessels with EC apoptosis ($n = 9$ larvae) or EC migration ($n = 13$ larvae). The numbers on the bars **(B)** or in the brackets **(C)** represent the number of pruned vessels examined. Data are shown as mean ± SEM. $^{**}p < 0.01$ (two-tailed unpaired Student's *t*-test). Scale bar: 10 μm **(A)**.

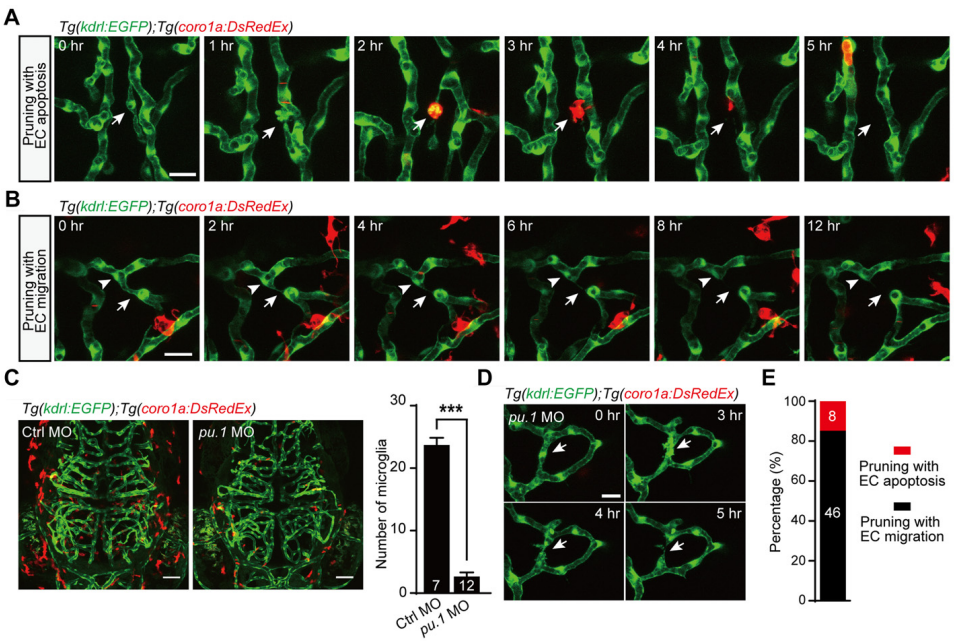

FIGURE 3 | Role of microglia in EC apoptosis-accompanied brain vessel pruning. **(A)** *In vivo* time-lapse confocal images showing that, during EC apoptosis-accompanied vessel pruning, a microglial cell (red) migrated to, engulfed and cleaned the apoptotic EC (white arrow). The *Tg(coro1a:DsRedEx); Tg(kdrl:EGFP)* larvae at 3–3.5 dpf were used. **(B)** *In vivo* time-lapse confocal images showing that, during EC migration-accompanied vessel pruning (white arrow), there was no obvious interaction between microglia (red) and the migrating EC (white arrowhead). **(C)** Representative projected confocal images (left) and summary data (right) showing that knockdown of *pu.1* significantly diminished the number of microglia (red) in the brain at 3 dpf. **(D)** *In vivo* time-lapse confocal images showing that EC apoptosis-accompanied brain vessel pruning (arrow) still occurred in *pu.1* morphants. **(E)** Summary of the percentages of EC apoptosis- and migration-accompanied brain vessel pruning from *pu.1* MO-injected *Tg(coro1a:DsRedEx);Tg(kdrl:EGFP)* ($n = 30$ larvae). The numbers on the bars represent the number of animals **(C)** or pruned vessels **(E)** examined. Data are shown as mean ± SEM. $^{***}p < 0.001$ (two-tailed unpaired Student's *t*-test). Scales: 20 μm **(A,B)**, 50 μm **(C)** and 15 μm **(D)**.

Microglia Engulf Apoptotic ECs but Are Dispensable for Vessel Pruning

As previous studies showed that macrophage-dependent EC apoptosis is responsible for the complete regression of the hyaloid vessel network (Kochhan et al., 2013; Franco et al., 2015), we hypothesized that microglia may be involved in EC apoptosis-accompanied brain vessel pruning. Thus, we performed *in vivo* time-lapse confocal imaging of *Tg(coro1a:DsRedEx);Tg(kdrl:EGFP)* zebrafish larvae, in which DsRed and EGFP were expressed in microglia and ECs, respectively. Interestingly, we found that after the EC on the pruning vessel went into apoptosis, a microglial cell always migrated to and engulfed the apoptotic EC, followed by the completion of vessel pruning (**Figure 3A**). Whereas, in the EC lateral migration-accompanied vessel pruning, we did not find the interaction between microglia and pruned vessels (**Figure 3B**). The fact that the migration of microglia toward pruning vessel is after the EC apoptosis suggests that EC apoptosis is microglial cell-independent. However, microglia contribute to the clearance of the apoptotic ECs.

To further examine whether microglia are essential for EC apoptosis-accompanied vessel pruning, we downregulated the expression of the *pu.1* transcription factor, which is required for macrophage differentiation, through *pu.1* morpholino oligonucleotide (MO; Chen et al., 2012). In the *pu.1* MO-injected *Tg(coro1a:DsRedEx);Tg(kdrl:EGFP)* larvae, microglia were largely diminished (**Figure 3C**; $p < 0.001$, two-tailed unpaired Student's *t*-test). However, in accordance with in normal larvae (see **Figure 1B**), the percentage of EC apoptosis-accompanied brain vessel pruning in microglial cell-deficient fish was also about 15% (**Figures 3D,E**, 8 out of 54). These results indicate that the occurrence of EC apoptosis-accompanied brain vessel pruning is microglial cell-independent, but microglia are responsible for the clearance of apoptotic ECs.

DISCUSSION

Taking advantage of *in vivo* time-lapse imaging on larval zebrafish, in this study we identified, to our knowledge, for the first time that EC apoptosis makes a significant contribution to brain vessel pruning during development in a microglial cell-independent manner. Although unnecessary for EC apoptosis-accompanied vessel pruning, microglia can engulf and clear apoptotic ECs, a behavior that may be important for protecting the brain microenvironment from inflammation.

A previous study showed that the pruning of a defined blood vessel CrDI, which locates along the anterior margin of the eye in zebrafish and contains 3–4 ECs, was accompanied by the death of 1–2 ECs (Kochhan et al., 2013), suggesting that the cell apoptosis are caused by the redundancy of ECs. Franco et al. (2015) reported the association of apoptotic events with regression of long vessels in the retina and hypothesized that cell apoptosis are associated with failure of ECs to integrate into adjacent vessels. Consistently, for the developing brain vasculature, we showed that EC apoptosis-accompanied pruned vessels were longer and more likely to have the nuclei of neighboring vessels' ECs occupying at their both ends. These characteristics may prevent ECs in pruning vessels migrating to and integrating into adjacent vessels, thus leading to EC apoptosis.

In our previous study, we found that vessel pruning in the brain of larval zebrafish occurs preferentially at loop-forming vessels, which usually show inefficient blood flow and are functionally redundant (Chen et al., 2012). Here, EC apoptosis-accompanied vessel pruning also occurred at loop-forming vessels. We speculated that hemodynamic changes in loop-forming vessels will usually trigger the ECs in pruning vessels to migrate and integrate into adjacent unpruned vessels, but if the loop-forming vessels are long in length and occupied by the nuclei of neighboring vessels' ECs at their both ends, the ECs in pruning vessels may be prevented from migration and instead undergo apoptosis.

AUTHOR CONTRIBUTIONS

BX, YZ, JD and XD conceived the project and designed the experiments. BX and YZ carried out the experiments and analyzed the data with QC's and YY's help. BX, YZ, JD and XD wrote the manuscript.

FUNDING

This work was supported by the Key Research Program of Frontier Sciences (QYZDY-SSW-SMC028) of Chinese Academy of Sciences, the National Natural Science Foundation of China (31325011), China Wan-Ren Program, Shanghai Leading Scientist Program, and Yang-Fan Program from Science and Technology Commission of Shanghai Municipality (14YF1406600).

ACKNOWLEDGMENTS

We are grateful to Dr. N. Lawson for providing the *Tg(kdrl:EGFP)* line, Dr. Z. L. Wen for providing the *Tg(coro1a:DsRedEx)* line, and Dr. Q. Jin for providing the *Tg(fli1a:nEGFP)* line.

REFERENCES

Adams, R. H., and Alitalo, K. (2007). Molecular regulation of angiogenesis and lymphangiogenesis. *Nat. Rev. Mol. Cell Biol.* 8, 464–478. doi: 10.1038/nrm2183

Arnold, T., and Betsholtz, C. (2013). The importance of microglia in the development of the vasculature in the central nervous system. *Vasc. Cell* 5:4. doi: 10.1186/2045-824x-5-4

Betz, C., Lenard, A., Belting, H. G., and Affolter, M. (2016). Cell behaviors and dynamics during angiogenesis. *Development* 143, 2249–2260. doi: 10.1242/dev.135616

Chen, Q., Jiang, L., Li, C., Hu, D., Bu, J. W., Cai, D., et al. (2012). Haemodynamics-driven developmental pruning of brain vasculature in zebrafish. *PLoS Biol.* 10:e1001374. doi: 10.1371/journal.pbio.1001374

Covassin, L. D., Siekmann, A. F., Kacergis, M. C., Laver, E., Moore, J. C., Villefranc, J. A., et al. (2009). A genetic screen for vascular mutants in zebrafish

reveals dynamic roles for Vegf/Plcg1 signaling during artery development. *Dev. Biol.* 329, 212–226. doi: 10.1016/j.ydbio.2009.02.031

Fantin, A., Vieira, J. M., Gestri, G., Denti, L., Schwarz, Q., Prykhozhij, S., et al. (2010). Tissue macrophages act as cellular chaperones for vascular anastomosis downstream of VEGF-mediated endothelial tip cell induction. *Blood* 116, 829–840. doi: 10.1182/blood-2009-12-257832

Franco, C. A., Jones, M. L., Bernabeu, M. O., Geudens, I., Mathivet, T., Rosa, A., et al. (2015). Dynamic endothelial cell rearrangements drive developmental vessel regression. *PLoS Biol.* 13:e1002125. doi: 10.1371/journal.pbio.1002125

Herbert, S. P., and Stainier, D. Y. (2011). Molecular control of endothelial cell behaviour during blood vessel morphogenesis. *Nat. Rev. Mol. Cell Biol.* 12, 551–564. doi: 10.1038/nrm3176

Jin, S. W., Beis, D., Mitchell, T., Chen, J. N., and Stainier, D. Y. (2005). Cellular and molecular analyses of vascular tube and lumen formation in zebrafish. *Development* 132, 5199–5209. doi: 10.1242/dev.02087

Kochhan, E., Lenard, A., Ellertsdottir, E., Herwig, L., Affolter, M., Belting, H. G., et al. (2013). Blood flow changes coincide with cellular rearrangements during blood vessel pruning in zebrafish embryos. *PLoS One* 8:e75060. doi: 10.1371/journal.pone.0075060

Korn, C., and Augustin, H. G. (2015). Mechanisms of vessel pruning and regression. *Dev. Cell* 34, 5–17. doi: 10.1016/j.devcel.2015.06.004

Lenard, A., Daetwyler, S., Betz, C., Ellertsdottir, E., Belting, H. G., Huisken, J., et al. (2015). Endothelial cell self-fusion during vascular pruning. *PLoS Biol.* 13:e1002126. doi: 10.1371/journal.pbio.1002126

Li, Y., Du, X. F., Liu, C. S., Wen, Z. L., and Du, J. L. (2012). Reciprocal regulation between resting microglial dynamics and neuronal activity *in vivo*. *Dev. Cell* 23, 1189–1202. doi: 10.1016/j.devcel.2012.10.027

Liu, C., Wu, C., Yang, Q., Gao, J., Li, L., Yang, D., et al. (2016). Macrophages mediate the repair of brain vascular rupture through direct physical adhesion and mechanical traction. *Immunity* 44, 1162–1176. doi: 10.1016/j.immuni.2016.03.008

Lobov, I. B., Rao, S., Carroll, T. J., Vallance, J. E., Ito, M., Ondr, J. K., et al. (2005). WNT7b mediates macrophage-induced programmed cell death in patterning of the vasculature. *Nature* 437, 417–421. doi: 10.1038/nature03928

Lou, N., Takano, T., Pei, Y., Xavier, A. L., Goldman, S. A., and Nedergaard, M. (2016). Purinergic receptor P2RY12-dependent microglial closure of the injured blood-brain barrier. *Proc. Natl. Acad. Sci. U S A* 113, 1074–1079. doi: 10.1073/pnas.1520398113

Nayak, D., Roth, T. L., and McGavern, D. B. (2014). Microglia development and function. *Annu. Rev. Immunol.* 32, 367–402. doi: 10.1146/annurev-immunol-032713-120240

Paolicelli, R. C., Bolasco, G., Pagani, F., Maggi, L., Scianni, M., Panzanelli, P., et al. (2011). Synaptic pruning by microglia is necessary for normal brain development. *Science* 333, 1456–1458. doi: 10.1126/science.1202529

Roman, B. L., Pham, V. N., Lawson, N. D., Kulik, M., Childs, S., Lekven, A. C., et al. (2002). Disruption of acvrl1 increases endothelial cell number in zebrafish cranial vessels. *Development* 129, 3009–3019.

Tammela, T., Zarkada, G., Nurmi, H., Jakobsson, L., Heinolainen, K., Tvorogov, D., et al. (2011). VEGFR-3 controls tip to stalk conversion at vessel fusion sites by reinforcing Notch signalling. *Nat. Cell Biol.* 13, 1202–1213. doi: 10.1038/ncb2331

Wu, Y., Dissing-Olesen, L., MacVicar, B. A., and Stevens, B. (2015). Microglia: dynamic mediators of synapse development and plasticity. *Trends Immunol.* 36, 605–613. doi: 10.1016/j.it.2015.08.008

Conflict of Interest Statement: The authors declare that the research was conducted in the absence of any commercial or financial relationships that could be construed as a potential conflict of interest.

frontiers in Molecular Neuroscience

ORIGINAL RESEARCH
published: 26 June 2018
doi: 10.3389/fnmol.2018.00215

Astrocytic Atrophy Following *Status Epilepticus* Parallels Reduced Ca^{2+} Activity and Impaired Synaptic Plasticity in the Rat Hippocampus

*Alex Plata[1†], Albina Lebedeva[1†], Pavel Denisov[1], Olga Nosova[1], Tatiana Y. Postnikova[2,3], Alexey Pimashkin[1], Alexey Brazhe[4], Aleksey V. Zaitsev[2,5], Dmitri A. Rusakov[1,6] and Alexey Semyanov[1,7,8]**

[1] UNN Institute of Neuroscience, N. I. Lobachevsky State University of Nizhny Novgorod, University of Nizhny Novgorod, Nizhny Novgorod, Russia, [2] Laboratory of Molecular Mechanisms of Neural Interactions, Sechenov Institute of Evolutionary Physiology and Biochemistry, Russian Academy of Sciences, St. Petersburg, Russia, [3] Department of Medical Physics, Peter the Great St. Petersburg Polytechnic University, St. Petersburg, Russia, [4] Department of Biophysics, Faculty of Biology, M. V. Lomonosov Moscow State University, Moscow, Russia, [5] Institute of Experimental Medicine, Almazov National Medical Research Centre, St. Petersburg, Russia, [6] UCL Institute of Neurology, University College London, London, United Kingdom, [7] Department of Molecular Neurobiology, Shemyakin-Ovchinnikov Institute of Bioorganic Chemistry, Russian Academy of Sciences, Moscow, Russia, [8] All-Russian Research Institute of Medicinal and Aromatic Plants, Moscow, Russia

OPEN ACCESS

Edited by:
Alexej Verkhratsky, University of Manchester, United Kingdom

Reviewed by:
Ilya Bezprozvanny, University of Texas Southwestern Medical Center, United States
Robert Zorec, University of Ljubljana, Slovenia

***Correspondence:**
Alexey Semyanov
semyanov@ibch.ru

[†]*These authors have contributed equally to this work.*

Received: *28 February 2018*
Accepted: *30 May 2018*
Published: *26 June 2018*

Citation:
Plata A, Lebedeva A, Denisov P, Nosova O, Postnikova TY, Pimashkin A, Brazhe A, Zaitsev AV, Rusakov DA and Semyanov A (2018) Astrocytic Atrophy Following Status Epilepticus Parallels Reduced Ca^{2+} Activity and Impaired Synaptic Plasticity in the Rat Hippocampus. Front. Mol. Neurosci. 11:215. doi: 10.3389/fnmol.2018.00215

Epilepsy is a group of neurological disorders commonly associated with the neuronal malfunction leading to generation of seizures. Recent reports point to a possible contribution of astrocytes into this pathology. We used the lithium-pilocarpine model of *status epilepticus* (SE) in rats to monitor changes in astrocytes. Experiments were performed in acute hippocampal slices 2–4 weeks after SE induction. Nissl staining revealed significant neurodegeneration in the pyramidal cell layers of hippocampal CA1, CA3 areas, and the hilus, but not in the granular cell layer of the dentate gyrus. A significant increase in the density of astrocytes stained with an astrocyte-specific marker, sulforhodamine 101, was observed in CA1 *stratum (str.) radiatum*. Astrocytes in this area were also whole-cell loaded with a morphological tracer, Alexa Fluor 594, for two-photon excitation imaging. Sholl analyses showed no changes in the size of the astrocytic domain or in the number of primary astrocytic branches, but a significant reduction in the number of distal branches that are resolved with diffraction-limited light microscopy (and are thought to contain Ca^{2+} stores, such as mitochondria and endoplasmic reticulum). The atrophy of astrocytic branches correlated with the reduced size, but not overall frequency of Ca^{2+} events. The volume tissue fraction of nanoscopic (beyond the diffraction limit) astrocytic leaflets showed no difference between control and SE animals. The results of spatial entropy-complexity spectrum analysis were also consistent with changes in ratio of astrocytic branches vs. leaflets. In addition, we observed uncoupling of astrocytes through the gap-junctions, which was suggested as a mechanism for reduced K^+ buffering. However, no significant difference in time-course of synaptically induced K^+ currents in patch-clamped astrocytes argued against possible alterations in K^+ clearance by astrocytes. The magnitude of long-term-potentiation (LTP) was reduced after SE.

Exogenous *D*-serine, a co-agonist of NMDA receptors, has rescued the initial phase of LTP. This suggests that the reduced Ca^{2+}-dependent release of *D*-serine by astrocytes impairs initiation of synaptic plasticity. However, it does not explain the failure of LTP maintenance which may be responsible for cognitive decline associated with epilepsy.

Keywords: astrocyte remodeling, epilepsy, *D*-serine, calcium, plasticity, spatial entropy, spatial complexity, neurodegeneration

INTRODUCTION

Epilepsy is a group of neurological disorders, associated with pathological synchronization of neuronal activity causing seizures. Several cellular mechanisms of this pathology were proposed. The classical view holds that seizures occur because of a shift in the balance between excitation and inhibition in the brain toward excitation (During and Spencer, 1993; DiNuzzo et al., 2014). However, pathological synchronization of excitatory neurons may also result from enhanced inhibition of a relatively small group of inhibitory interneurons, which then synchronously disinhibits numerous excitatory neurons. This is called "rebound" excitation and may make all these cells to fire in synchrony (Paz and Huguenard, 2015). The K^+ hypothesis of epilepsy suggests that extracellular accumulation of this ion in the brain depolarizes neurons and cause epileptiform activity (Green, 1964; Fertziger and Ranck, 1970; Fröhlich et al., 2008). Mutation in astrocytic K^+ channels ($K_{ir}4.1$ type) has been proposed as one of the causes of human epilepsy (Villa and Combi, 2016). Indeed, it has long been reported that periodic elevations of extracellular K^+ concentration could produce long-term changes in neuronal excitability, making the network prone to epileptogenesis (Semyanov and Godukhin, 1997).

An excessive activity of neuronal networks induces excitotoxicity, which leads to neurodegeneration. Hippocampal sclerosis is typically reported in temporal lobe epilepsy (TLE) (Kim, 2001; Blümcke et al., 2002; de Lanerolle and Lee, 2005; Thom, 2014). The loss of neurons is considered as a mechanism for epileptic focus formation and an indication for hippocampus removal in clinic. Neurodegeneration in TLE may also lead to a mild cognitive impairment affecting learning and memory (Hermann and Seidenberg, 2007; Höller and Trinka, 2014). Long-term potentiation (LTP) and depression (LTD) are widely accepted experimental models to explore mechanisms of synaptic memory formation (Bliss and Collingridge, 1993; Ju et al., 2004). Recent studies have demonstrated a significant impairment of long-term synaptic plasticity after SE in different animal models, including a lithium-pilocarpine model of TLE (Zhou et al., 2007; Müller et al., 2013; Cunha et al., 2015; Kryukov et al., 2016; Carpenter-Hyland et al., 2017; Ivanov and Zaitsev, 2017; Postnikova et al., 2017). A reduction or elimination of LTP that can be observed for weeks after SE has frequently been reported (Zhang et al., 2010; Zhou et al., 2011; Suárez et al., 2012). Despite numerous studies, the exact mechanisms of LTP impairment after SE remain unidentified.

The quest for the mechanisms of epileptogenesis have typically been focused on neuronal malfunction, such as altered expression of receptors and channels; extracellular K^+ accumulation synchronizing neuronal populations; a shift in the balance of synaptic excitation and inhibition toward excitation (DiNuzzo et al., 2014). Intriguingly, many of these functions are regulated by astrocytes. Astrocytic uptake of neurotransmitters and extracellular K^+ clearance are key to synaptic function (Cheung et al., 2015; Lebedeva et al., 2018; Verkhratsky and Nedergaard, 2018). Astrocytes control synaptic plasticity in glutamatergic synapses by releasing of *D*-serine, a co-agonist of NMDA receptors (Henneberger et al., 2010, 2012; Papouin et al., 2017). They are involved in uptake and release of GABA, inhibitory neuro- and gliotransmitter (Angulo et al., 2008; Lee et al., 2010; Héja et al., 2012; Kersante et al., 2013; Song et al., 2013). Therefore, astrocytic mechanisms can potentially contribute to epileptogenesis. Indeed, astrocyte control of synaptic NMDA receptors is implicated in the progressive development of TLE (Clasadonte et al., 2013). Astrocytic Ca^{2+}-dependent glutamate release is suggested to trigger synchronous neuronal discharges in rat hippocampal slices following application of a K^+ channel blocker, 4-aminopyridine (4-AP) (Tian et al., 2005). In contrast, some other models of acute epileptiform activity in slices (Mg^{2+}-free solution, picrotoxin, increased extracellular K^+) produce Ca^{2+} oscillations in astrocytes, which are not responsible for paroxysmal activity in neurons (Fellin et al., 2006). Thus, the role of astrocytic Ca^{2+} activity in epileptogenesis remains controversial. Moreover, acute effects have often been obtained in brain slices using convulsants, which may not necessarily reflect changes in astrocytic Ca^{2+} activity after SE.

Another critical aspect of neuron-astrocyte interactions is morphological. Astrocytic processes approach synapses, forming so-called "astrocytic cradle" (Verkhratsky and Nedergaard, 2014). Being highly plastic, perisynaptic astrocytic processes can retract from or extend toward dendritic spines (Bernardinelli et al., 2014a; Heller and Rusakov, 2015). Rearing laboratory animals in complex environment or certain LTP induction protocols appear to increase glial coverage of excitatory synapses (Jones and Greenough, 1996; Lushnikova et al., 2009) whereas some memory consolidation tasks (Ostroff et al., 2014) or experiencing a lactation period (Oliet et al., 2001) appear to decrease it. Suppression of IP_3-dependent Ca^{2+} signaling in astrocytes reduces synaptic coverage (Tanaka et al., 2013). Morphological remodeling of astrocytes following SE has not been systematically studied.

Impairment of K^+ clearance by astrocytes has been proposed as a mechanism for extracellular K^+ accumulation in the epileptic brain (Bedner and Steinhauser, 2013). This may occur due to the redistribution of astrocytic K^+ channels or reduced K^+ buffering

due to astrocyte uncoupling through gap-junctions in epileptic tissue (Wallraff et al., 2006; Bedner et al., 2015). Interestingly, K^+ clearance by astrocytes can be linked to astrocytic Ca^{2+} activity, via Ca^{2+}-dependent K^+ channels (Wang et al., 2012). However, this link has not been considered in the context of epileptogenesis.

Although recent reports have convincingly demonstrated the involvement of astrocytes in epileptogenesis, further analysis of cellular and subcellular mechanisms is still needed. Here we report morphological and physiological changes in astrocytes following SE induced by lithium-pilocarpine injection, as well as their possible association with synaptic plasticity changes. Our quantitative morphological assessment employs a novel approach based on the spatial entropy-complexity spectrum analysis.

MATERIALS AND METHODS

Pilocarpine Model of Epilepsy

All procedures were carried out in accordance with University of Nizhny Novgorod regulations. 3–6 weeks old male Sprague-Dawley (Wistar for LTP experiments) rats were injected with lithium chloride (127 mg/kg, Sigma Aldrich) 20–24 h prior to pilocarpine and methylscopolamine (1 mg/kg, Sigma Aldrich) 20 min prior to pilocarpine. Then pilocarpine (Tocris), 10 mg/kg was injected every 30 min (but no more than 60 mg/kg) to induce SE which characterized with generalized seizures lasting for at least 20 min (Supplementary Figure 1). To reduce mortality, phenazepam 1 mg/kg was injected every 10 min for 30–40 min after 20 min of generalized seizures.

Nissl Staining

Brain tissue was prepared according to routine histologic methods (Singh et al., 2008). Briefly, brains were removed immediately after decapitation, immersed in ethanol 96% and embedded in paraffin after dehydration. Paraffin sections (5 μm) were cut in a coronal plane and stained with Nissl's method. Each sixth staining section was chosen for quantitative analysis for each animal. Images of CA1, CA3, hilus, and dentate gyrus were obtained using an x40 magnification. The neurons were counted per 100 μm for cell layer in each area using the plugin "Cell counter" for ImageJ.

Hippocampal Slice Preparation

The slices were prepared 2–4 weeks after SE. The animals were anesthetized with Isoflurane (1-Chloro-2,2,2-trifluoroethyl difluoromethyl ether) and then decapitated. The rest of the procedure was slightly different for whole cell and field potential recordings.

Preparation for Whole-Cell Recording and Imaging

The brains were exposed, and then chilled with ice-cold solution containing (in mM): 50 sucrose; 87 NaCl; 2.5 KCl; 8.48 MgSO4; 1.24 NaH_2PO_4; 26.2 $NaHCO_3$; 0.5 $CaCl_2$; 22 D-Glucose. Hippocampi from both hemispheres were dissected, isolated, and transverse slices (350 μm) were cut using a vibrating microtome (Microm HM650 V; Thermo Fisher Scientific) and left to recover at 34°C for 1 h in a submerged incubation chamber with "storage" solution containing (in mM): 119 NaCl; 2.5 KCl; 1.3 $MgSO_4$; 1 NaH_2PO_4; 26.2 $NaHCO_3$; 1 $CaCl_2$; 1.6 $MgCl_2$; 22 D-Glucose. Then the slices were transferred to the recording chamber and were continuously perfused with a solution containing (in mM): 119 NaCl; 2.5 KCl; 1.3 $MgSO_4$; 1 NaH_2PO_4; 26.2 $NaHCO_3$; 2.5 $CaCl_2$; 11 D-Glucose. All solutions were saturated with carbogen gas mixture containing 95% O_2 and 5% CO_2. Osmolarity was 295 ± 5 mOsm, pH 7.4. All recordings were done at a temperature of 34°C.

Preparation for Field Potential Recording and LTP Induction

The cerebellum and a small section of the frontal cortex were removed. A flat surface for mounting the brain was created by making a cut on the dorsal surface parallel to the horizontal plane. The brain was then mounted onto the stage of the vibratome, and horizontal sections (400 μm thick) were cut in ice-cold artificial cerebrospinal fluid (ACSF). ACSF composed of (in mM): 126 NaCl, 2.5 KCl, 1.25 NaH_2PO_4, 1 $MgSO_4$, 2 $CaCl_2$, 24 $NaHCO_3$, and 10 D-glucose was saturated with carbogen. The prepared slices were immersed in a chamber with ACSF, which was placed in a temperature-controlled water bath (35°C) for 1 h. After the incubation, the slices were transferred to the recording chamber, where they were kept for 15–20 min prior to the electrophysiological study. In this chamber, hippocampal slices were perfused with a constant flow of oxygenated ACSF at a rate of 5 ml/min at room temperature. One to five slices from each rat were used in the experiment.

Sholl Analysis

Sholl analysis was performed on adaptively thresholded maximal projections of Z-stacks, where each XY-plane has been filtered with anisotropic diffusion filtering. All processing steps were performed using image-funcut library [image-funcut, https://github.com/abrazhe/image-funcut] and other custom-written Python scripts, using Scikit-Image [scikit, http://scikit-image.org/] and Sci-Py [scipy, http://www.scipy.org/] libraries (Van Der Walt et al., 2014). The step-by-step procedure is summarized in Supplementary Figure 2. Sholl metric was calculated automatically as a number of intersections of circles with centers at the soma and increasing radii with the thresholded mask obtained as described above.

Shearlet-Based Estimate of Spatial Complexity and Entropy for 2D Patterns

A spatial pattern can be characterized by a pair of statistical properties, namely entropy and statistical complexity (López-Ruiz et al., 1995). An ordered (e.g., periodic) structure with a single spatial scale and preferred feature orientation will have both low entropy and small statistical complexity, as the structure in any part of the system can be reconstructed from a small area. At the other end of the complexity-entropy spectrum, where the state is disordered with no spatial correlations, the entropy of the system will be maximal, while the complexity will again be low

(the spatial pattern has the same local statistics). Intermediate cases with high statistical complexity are of more interest, as they represent systems with non-trivial regularities and underlying structure embedded in randomness. We developed an algorithm to map local entropy and complexity values for biologically relevant structures using shearlet transform to induce local probability densities of scale and orientation and Jensen-Shannon divergence to define statistical complexity. Below we describe the two points in more detail.

Entropy and Statistical Complexity

Both entropy and complexity (entropic non-triviality) measures for a 2D pattern were defined statistically for a distribution of spatial features, such as orientation, or scale. Here we denoted such a distribution as

$$P := \{P_i\} \tag{1}$$

for a set of features $i = 1 \ldots N$. Then entropy was defined simply as Shannon information entropy

$$S[P] = -\sum_i P_i \, log_2 \, P_i. \tag{2}$$

Entropy will have its maximum for the equiprobable distribution of all features P_e,

$$S[P_e] = S_{\max} = 2N, \tag{3}$$

where N is a number of possible states or features. This allows to introduce normalized entropy:

$$H_s[P] := S[P]/S[P_e], H_s[P] \in [0, ...1] \tag{4}$$

Following (López-Ruiz et al., 1995) we used the disequilibrium-based complexity measure

$$C[P] := Q[P, P_e]H_s[P] \tag{5}$$

i.e., the one based on the statistical distance between the observed (P) and equiprobable (P_e) distributions. Here, following (Lamberti et al., 2004; Rosso et al., 2007), we employed normalized Jensen-Shannon divergence

$$Q_{JS} = J[P, P_e]/J_{\max} \tag{6}$$

as a measure of distance between two distributions, where Jensen-Shannon divergence is defined as

$$J[P, P_e] = S\left[\frac{P + P_e}{2}\right] - \frac{1}{2}(S[P] + S[P_e]). \tag{7}$$

Clearly, $J[P, P_e] = 0$ if $P = P_e$ and reaches its maximum when only one feature, say m, is present, while all others are absent: $P_i = 1|i = m$, and $Pi = 0|i \neq m$.

Shearlet Transform

Shearlet transform provides a convenient probability density function for spatial entropy and complexity estimates, describing local prevalence of structures with some specific scale and orientation. We used fast finite discrete shearlet transform (FFST) described in detail by (Häuser and Steidl, 2013). Here we provide a minimally sufficient description of the FFST and its use in calculation of spatial entropy and complexity.

Discrete shearlet transform was based on convolving the digital 2D image

$$I(x, y) \in R^{(N,N)} \tag{8}$$

with scaled, sheared, and shifted copies of a "mother" shearlet function ψ, thus accounting for different scales and orientations of features contained in the image; one uses the dilation matrix A and shear matrix S to create the sheared, scaled and shifted copies of the mother wavelet ψ_x:

$$\psi_{a,s,t} = a^{-3/4}(Aa^{-1}Ss^{-1}(x - t)). \tag{9}$$

Thus, the scaled and shared copies of ψ pick up dominant anisotropic features at different spatial scales and orientations. In the discrete transform, one uses a fixed number of decomposition scales and shifts as well as scale-dependent number of orientations (more orientations at higher spatial frequencies). Finally, shearlet decomposition of image was given by shearlet coefficients

$$T(I)(j, k, m) = \langle I, \psi_{j,k,m} \rangle \tag{10}$$

where discrete shearlet $\psi_{j,k,m} = \psi_{ajsj,ktm}(x)$ is the shearlet at discrete scale α_j, shear $s_{j,k}$ and shift t_m. Thus, *T(I)* is a set of K images of the same size as *I(x,y)*, where the value at a specific *(x,y)* location in the k-th image represents the shearlet coefficient at some specific scale j and shear s.

Following ideas from wavelet entropy (Rosso et al., 2001) and earlier of spectral entropy of (Powell and Percival, 1979), in each location of the studied 2D image *I(x,y)*, we defined $P(x, y) = Pk(x, y)$ as normalized power of the shearlet coefficients at this point:

$$P_k(x, y) = E_k(x, y)/\sum_j E_j(x, y) \tag{11}$$

thus, interpreting a spectrum of local feature scales and orientations as a density function. Here $(K^*_\sigma \cdot)$ denotes convolution with a Gaussian kernel with scale-dependent standard deviation σ_j.

Volume Fraction (VF) of Astrocytic Leaflets

To calculate the VF of the fine process of the astrocyte, we followed a similar method described by Heller and Rusakov (2015) A line of 45 µm length were drawn from the soma on a single Z plane of the stack. Spatial attention was paid to ensure that fluorescence of soma was not saturated. The estimated VF was calculated with the following:

$$GV(i, j) = (F(i, j) - F_0)/(F_{max} - F_0) \tag{12}$$

where *F(I,j)*—the fluorescent in particular pixel of the line, F_{max}—the fluorescence of soma, F_0–the background fluorescence. F_0 was obtained in image area which had no stained astrocytes.

Astrocyte Coupling Analysis

The astrocytes were loaded with 50 μM Alexa Fluor 594 through the patch pipette for 30 min. then Z-stack two-photon images was obtained (emission band-pass filter 565–610 nm, 512 x 512 pixels). The images were then denoised with block matching 4D (BM4D) free scrip for MATLAB (Maggioni et al., 2013; Danielyan et al., 2014). The distance to neighboring astrocytes coupled to the target astrocyte through gap-junctions was calculated in 3D-space using Pythagorean theorem with custom-written MATLAB script. Fluorescence Intensities of all coupled cells were normalized to fluorescence of soma of the patched astrocyte. The relationship between distance fluorescence of coupled astrocyte and distance to this astrocyte was fitted by monoexponential function to obtain coupling length constant (C_λ) (Anders et al., 2014):

$$I(d) = I_0 exp(-d/C_\lambda), \tag{13}$$

were, d—distance, I_o—the normalized fluorescence intensity of the coupled cell.

Electrophysiological Recordings

Whole-Cell Recording

Whole-cell voltage-clamp and current-clamp were performed with Multiclamp 700B amplifier (Molecular Devices). The CA1 *str.radiatum* astrocytes were visualized with BX51WI (Olympus) or Axio Examiner Z1 (Zeiss) microscope equipped with infrared differential interference contrast. Borosilicate patch pipettes (Resistance 3−5 MΩ) were filled with internal solution containing (in mM): 130 KCH_3SO_3, 10 HEPES, 10 Na_2-phosphocreatine, 8 NaCl, 3 l-ascorbic acid, 2 Mg-GTP (pH adjusted to 7.2, osmolarity of 295 ± 3 mOsm). For simultaneous two-photon imaging, 50 μM Alexa Fluor 594 was added to the internal solution.

Bipolar extracellular tungsten electrode (FHC) was placed in *str. radiatum* between CA1 and CA3 areas. Once whole-cell configuration was obtained, the cell was dialyzed for 5 to 10 min before the start of recording. In voltage clamp recordings the astrocytes were held at−80 mV. Voltage steps were applied to obtain current-voltage (I-V) relationship. In current clamp, current steps were applied to corroborate the absence of membrane excitability. Cycles of 1, 4, and 5 electrical stimuli (100 ms, 50 Hz) were applied to Schaffer collaterals. The intensity of stimulation was set to induce synaptic currents in astrocytes of 20 to 50 pA to a single stimulus. Series and input resistances were continuously monitored by a voltage step of−5 mV after each cycle. Signals were sampled at 5 kHz and filtered at 2.5 kHz.

Passive astrocytes were taken at 100−200 μm from the stimulating electrode. They were identified by small soma (5–10 μm), low resting membrane potential (∼−80 mV), low input resistance (<20 MΩ), and linear I-V relationship. Cells with similar characteristics except for higher input resistance (>50 MΩ) were considered NG2 or complex cells and were excluded from the study.

Membrane currents were analyzed using custom-written MATLAB scrips (MathWorks R2016a). Synaptic currents of 1, 4, and 5 stimuli were baseline subtracted and then averaged. I_K (K^+ current) was measured 200 ms after the stimulus. At this time point I_K was not contaminated by the current mediated by field potential and transporter current. From this point the decay was fitted with mono-exponential function and τ_{decay} calculated. To obtain I_K in response to 5th stimulus, the response to 4 stimuli was subtracted from the response to 4 stimuli.

Field Potential Recording

Field excitatory postsynaptic potentials (fEPSPs) were recorded from CA1 *str. radiatum* using glass microelectrodes (0.2–1.0 MΩ) filled with ACSF. Synaptic responses were evoked with extracellular stimulation of the Schaffer collaterals using a bipolar twisted stimulating electrode made of insulated nichrome wire placed in the *str. radiatum* at the CA1–CA2 border. The stimulation was performed with rectangular paired pulses (duration, 0.1 ms; interstimulus interval, 50 ms) every 20 s via an A365 stimulus isolator (WPI). Responses were amplified using a microelectrode AC amplifier model 1800 (A-M Systems) and were digitized and recorded on a personal computer using ADC/DAC NI USB-6211 (National Instruments) and WinWCP v5.2.2 software by John Dempster (University of Strathclyde). Electrophysiological data were analyzed with the Clampfit 10.2 program (Axon Instruments).

The dependence of field response amplitude on stimulation strength was determined by increasing the current intensity from 25 to 300 μA. For each fEPSP, the amplitude and the slope of the rising phase at a level of 20–80% of the peak amplitude were measured. The presynaptic fiber volley (PrV) was quantified by the peak amplitude. The maximum rise slope of the input-output (I/O) relationships (fEPSP amplitude vs. PrV amplitude) was calculated for every slice by fitting with a sigmoidal Gompertz function (Equation 14) using OriginPro 8 (OriginLab Corporation).

$$y = ae^{-e^{(-k(x-x_c))}}, \tag{14}$$

where a is an asymptote of the maximum fEPSP amplitude; e is Euler's Number ($e = 2.71828\ldots$); k and x_c are positive numbers describing the shape of the curve; x_c is the PrV amplitude at which the maximum slope of the curve is observed; ak/e is a maximum slope of the curve.

The stimulus intensity used in the experiment was chosen so that the amplitude of fEPSP would be 40–50% of the amplitude where the population spike appeared for the first time. The strength of stimulation was unvaried during the experiments, usually being 50–150 μA. The paired-pulse ratio (PPR) was measured as a ratio of the second and first fEPSP amplitude.

The LTP induction was started only if a stable amplitude of the baseline fEPSP had been recorded for 20 min. Three trains of high-frequency stimulation (HFS, 100 pulses at 100 Hz, with an inter-train interval of 20 s protocol) was applied to induce

LTP. The fEPSPs were recorded after induction protocol during 60 min. The baseline fEPSP and the potentiated fEPSP (recorded 47–60 min after HFS) were averaged separately to measure LTP in a slice. Plasticity value was calculated as a ratio of the slope of the rising phase in the averaged potentiated and baseline fEPSP.

Ca^{2+} Imaging

Ca^{2+} activity was recorded with a confocal microscope, Zeiss LSM DuoScan 510, in CA1 *str.radiatum* of acute hippocampal slices pre-incubated with Ca^{2+} dye, Oregon Green 488 BAPTA-1 AM (Invitrogen) and an astrocyte specific marker, sulforhodamine 101 (100 nM, Invitrogen). After the preparation, the slices were transferred to a 3 ml incubation chamber with constantly gassed ACSF containing both dyes. Oregon Green 488 BAPTA-1 AM was initially dissolved to 0.795 mM in 0.8% Pluronic F-127 in DMSO. Then 3 μl of the dye was added to the chamber. After incubation for 40–45 min at 37°C in the dark, the slices were transferred to the recording/imaging chamber for time-lapse imaging (one frame/s). Oregon Green 488 BAPTA1 was excited with a 488 nm argon laser and imaged with an emission band-pass filter 500–530 nm; sulforhodamine 101 was excited with a 543 nm HeNe laser and imaged with an emission band-pass filter 650–710 nm. The imaging was performed for 10 min at 34°C in normal ASCF, then 30 dark noise images were recorded.

The raw imaging data were exported to MATLAB. The median of the dark noise was calculated for each pixel and subtracted from the corresponding pixel intensity value of the fluorescence images. Then denoising was done with the BM3D algorithm (Danielyan et al., 2014). The movement artifacts were corrected with the single-step DFT algorithm (Guizar-Sicairos et al., 2008). The whole Ca^{2+} events (x-y-time 3D Ca^{2+} signals) were detected with the adapted algorithm which we described previously (Wu et al., 2014). Briefly, each pixel of the image series was analyzed independently. Firstly, we roughly estimated a baseline fluorescence F_{0temp} applying 60-s 3rd order Savitzky-Golay polynomial filter which smoothed all Ca^{2+} signals on the fluorescent signal F. Then, we estimated a temporary $(\Delta F/F)_{temp} = (F - F_{0temp}) / F_{0temp}$ to find Ca^{2+} transients exceeding a statistical threshold. Then these transients were excluded from the baseline which was further smoothed with 100-s filter. This filter interpolated the intervals left by the excluded transients, and, thus, we obtained the uninterrupted final baseline F_0 which was used to obtain $\Delta F/F = (F - F_0) / F_0$. Ca^{2+} transients exceeding a statistical threshold were detected and binarized. The active neighboring pixels were grouped into x-y 2D Ca^{2+} events, which were reconstructed into x-y-time 3D Ca^{2+} events. For each Ca^{2+} event the maximal projection (S_{max}), the integral and the duration were calculated. To avoid noise detection the events excluded from further analysis if the integral was less than 4 μm^2 s, or the S_{max} was less than 10 μm^2, or the duration less than 2 s.

The probability density of the events sizes and the durations appeared linear in log-log scale, suggesting that the obtained distributions can be described by a power law. Therefore, the power law fit was applied, and the corresponding exponent was calculated for each slice.

Statistical Analysis

All data are presented as mean ± standard error of mean (SEM). Statistical significance was assessed using non-parametric Mann-Whitney test, parametric Student's *t*-test and repeated measures two-way ANOVA as stated in the text. $P < 0.05$ was considered statistically significant.

RESULTS

Rat hippocampal slices were prepared 2–4 weeks after pilocarpine-induced SE when the animals typically started to develop spontaneous seizures. Nissl staining confirmed statistically significant neurodegeneration in pyramidal layers of three hippocampal regions: CA1, CA3, and hilus (CA1: 7.9 ± 0.36 cells per 100 μm in control, $n = 6$; 6.0 ± 0.4 cells per 100 μm after SE, $n = 6$; $p = 0.02$; CA3: 8.9 ± 0.5 cells per 100 μm in control, $n = 6$; 6.0 ± 0.4 cells per 100 μm after SE, $n = 6$; $p = 0.01$, Mann-Whitney test; hilus: 7.5 ± 0.6 cells per 100 μm in control, $n = 6$; 5.3 ± 0.5 cells per 100 μm after SE, $n = 6$; $p = 0.04$, Mann-Whitney test; **Figures 1A–C**). No significant changes in the cell density were observed in granular cell layer of the dentate gyrus (17.2 ± 1.7 cells per 100 μm in control, $n = 6$; 15.5 ± 0.7 cells per 100 μm after SE, $n = 6$; $p = 0.37$, Mann-Whitney test; **Figure 1D**). Consistent with previously reported astrogliosis, the density of CA1 *str. radiatum* astrocytes stained with an astrocyte-specific marker, sulforhodamine 101, was significantly higher after SE (1.2 ± 0.1 cells per 100 μm^2 in control, $n = 15$; 1.5 ± 0.1 cells per 100 μm^2 after SE, $n = 20$; $p = 0.02$, Mann-Whitney test; **Figures 1E,F**) (Mazzuferi et al., 2010; Pekny et al., 2016). However, this astrogliosis would be considered rather minor.

Then we performed Sholl analysis on two-photon images of astrocytes loaded trough patch pipette with 50 μM Alexa Fluor 594 (morphological tracer, see Materials and Methods, Supplementary Figure 2 and **Figure 2A**). There was no significant difference in the number of primary branches (connected to soma), the peak number of the branches and size of the astrocytic domain in control and SE animals (Supplementary Figure 3). However, the number of distal branches was significantly lower after SE (control, $n = 6$; SE, $n = 6$; two-way repeated measures (RM) ANOVA, $F_{(1,5)} = 6.862$, $p = 0.047$, partial $\eta^2 = 0.578$, with a mean difference of 5.61 ± 2.14; **Figure 2B**). This morphological rearrangement can also be assessed using the analysis of spatial complexity-entropy spectrum (**Figure 2C**). Spatial complexity and spatial entropy are both low in highly ordered or anisotropic systems. As the system loses the order, both entropy and complexity start to increase. When the elements of the systems become randomly distributed ("noise") the entropy is the highest, while the complexity decreases. Remodeling of astrocytic processes after SE significantly increased both entropy and complexity (entropy: 0.51 ± 0.02 in control, $n = 11$; 0.56 ± 0.001 after SE $n = 8$; $p = 0.009$, Mann-Whitney test; complexity 0.343 ± 0.003 in control; 0.352 ± 0.003 after SE; $p = 0.02$, Mann-Whitney test; **Figure 2D**). This finding suggests that astrocytic

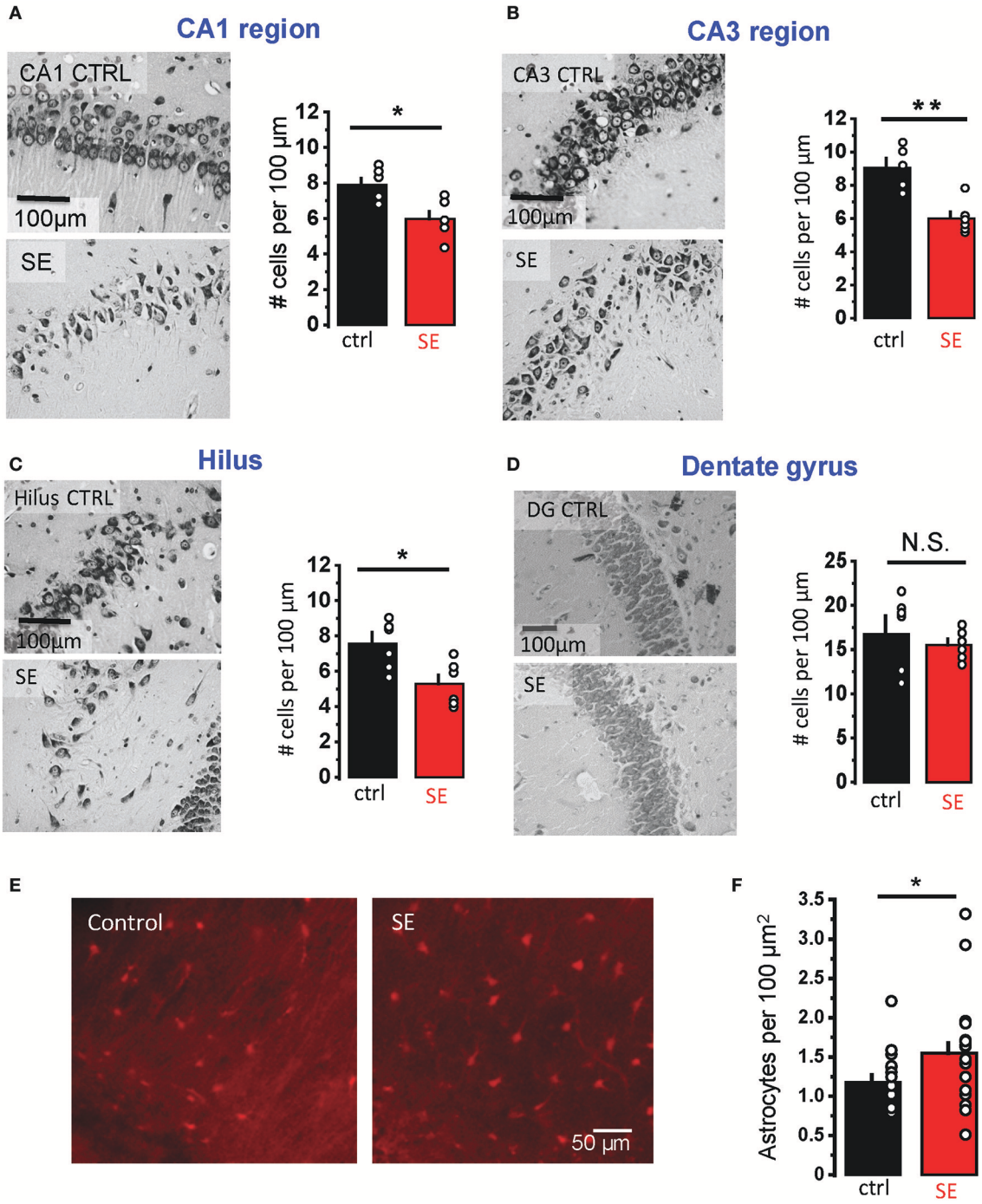

FIGURE 1 | Neurodegeneration and astrogliosis after SE. **(A–D)** Nissl staining showing neurodegeneration in the *str. pyramidale* of CA1 **(A)**, CA3 **(B)**, and hilus **(C)** after SE. No significant neurodegeneration was observed in the granular cell layer of dentate gyrus **(D)**. *Right*, illustrations of stained cells in control (*top*) and SE-rats (*bottom*). *Left*, the summary data from several rats. The cells were counted along the cell layers and normalized to the length of the layers. **(E)** Fluorescent images of astrocytes stained with sulforhodamine 101: in control (*left image*) and SE-rats (*right image*). **(F)** the summary data on several rats. The circles show values in individual rats. The bars with error bars are means ± SEMs. $^{**}p < 0.01$, $^{*}p < 0.05$, N.S. $p > 0.05$ Mann-Whitney test.

processes become less orderly organized after SE. It can be potentially explained by the decrease in the ratio of primary astrocytic branches which are resolved with diffraction-limited light microscopy and thin astrocytic leaflets which appear as a chaotic fluorescent pattern because of their sizes are beyond diffraction-limited light microscopy resolution. To estimate

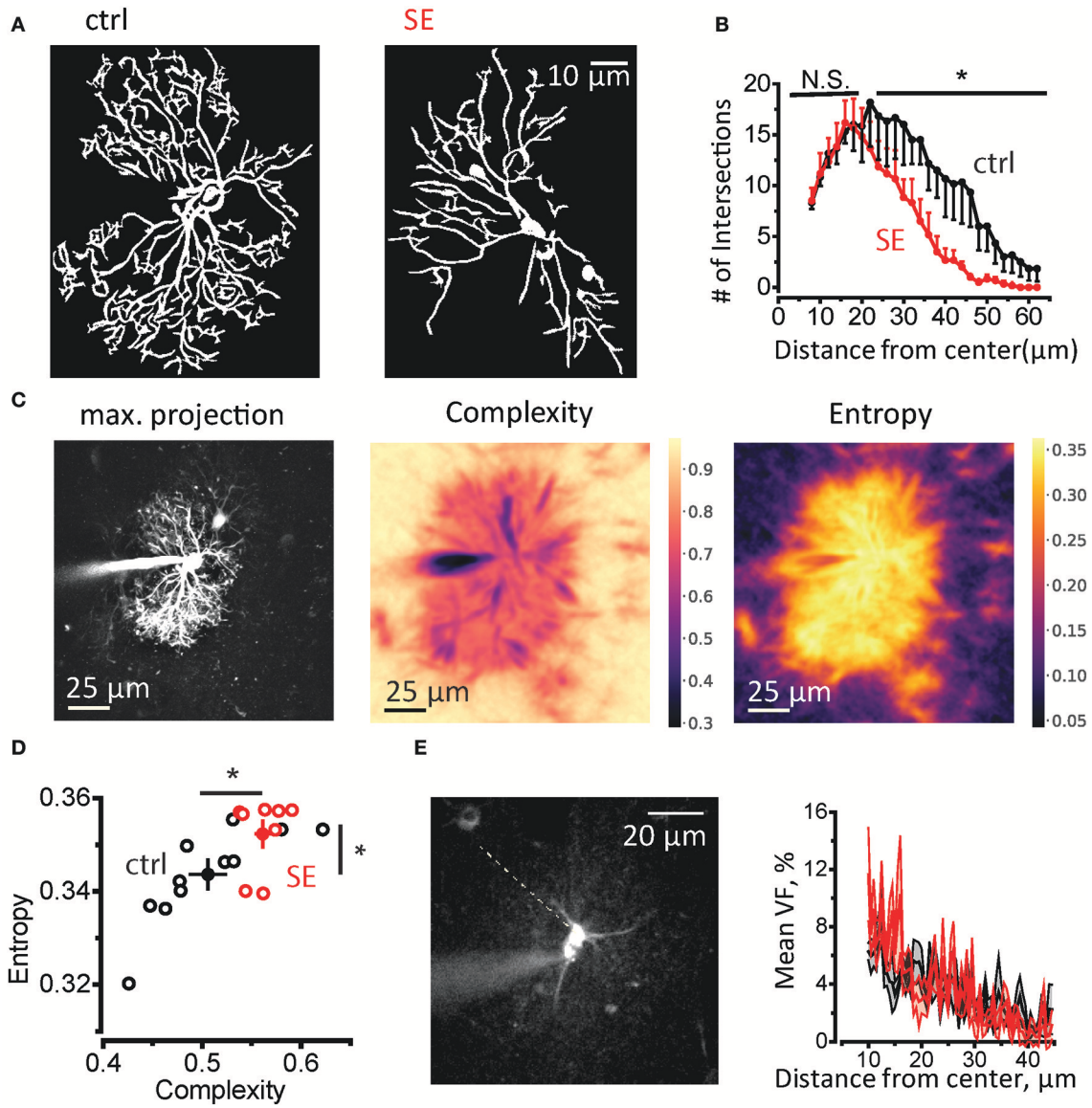

FIGURE 2 | Morphological remodeling of astrocytes after SE. **(A)** Masks of astrocytic branches in control (left) and SE rats (right) which were used for Sholl analysis. The masks were obtained from maximal projections of z-stack of fluorescence images of astrocytes loaded with 50 µM Alexa Fluor 594 through patch pipette. **(B)** The summary data for the number of intersections of circles drawn around center of the astrocyte soma with astrocytic branches. *$p < 0.05$, N.S. $p > 0.05$, two-way ANOVA. **(C)** Spatial entropy-complexity analysis. *Left*, maximal projection of Z-stack of fluorescence images of an astrocyte. *Middle*, The spatial complexity profile of the astrocyte. *Right*, The spatial entropy profile of the astrocyte. **(D)** The summary graph of spatial entropy-complexity pairs of astrocytes on control (black circles) and SE-rats (red circles). Empty circles are individual astrocytes. Filled circles are means ± SEMs. **(E)** Estimation of astrocyte leaflets' VF. *Left,* construction of fluorescence profile across an astrocyte. Dashed line indicates the place there the profile was obtained. It passes through the soma and the area or unresolved processes devoid of identifiable branches. *Right,* the mean ± SEM fluorescent profiles normalized to the fluorescence in soma for control (*black trace*) and SE-rats (*red trace*).

possible changes in leaflets volume fraction, we performed line scan through soma and the area of unresolved astrocytic leaflets avoiding astrocytic branches (**Figure 2E**). This method is based on the assumption that unsaturated fluorescence level in soma corresponds to 100% volume fraction (VF) (Medvedev et al., 2014; Heller and Rusakov, 2015). The ratio between the fluorescence of leaflets area and fluorescence of soma was considered VF of leaflets and did not differ between control and SE rats (mean leaflets VF: 3.4 ± 0.2%, $n = 6$ in control; 3.6 ± 0.2%, $n = 6$ after SE; $p = 0.59$, Mann-Whitney test; **Figure 2E**). The equal VF of leaflets does not, however, rule out their spatial rearrangement after SE which can be only assessed with super-resolution light microscopy or electron microscopy.

Morphological remodeling of astrocytes can be linked to astrocytic uncoupling and disruption of astrocytic syncytium after SE (Wallraff et al., 2006; Bedner et al., 2015). To assess

astrocyte coupling, we monitored diffusion of Alexa Fluor 594 from patched astrocyte to its neighbors through gap-junctions (**Figure 3A**). The number of stained astrocytes was significantly lower after SE compared to control (15.3 ± 2.8, $n = 7$, in control; 6.6 ± 2.9, $n = 8$ after SE; $p = 0.03$ Mann-Whitney test; **Figure 3B**). We also estimated the "strength" of gap-junction connections by the decay of fluorescence measured in somas of coupled astrocytes as a function of distance from the astrocyte loaded with Alexa Fluor 594 through patch pipette. The exponential decay of fluorescence was observed both in control and SE rats (linear relationship in semi-logarithmic scale, **Figure 3C**). Although length constant (λ) tended to be smaller after SE, the difference did not reach significance (λ: 33 ± 5 μm, $n = 7$, in control; 26 ± 5 μm, $n = 6$, after SE, $p = 0.07$, Mann-Whitney test, **Figure 3D**).

Decreased coupling of astrocytes through gap-junctions can lead to reduced spatial buffering of K^+ released during synaptic transmission (Wallraff et al., 2006; Shih et al., 2013; Bedner

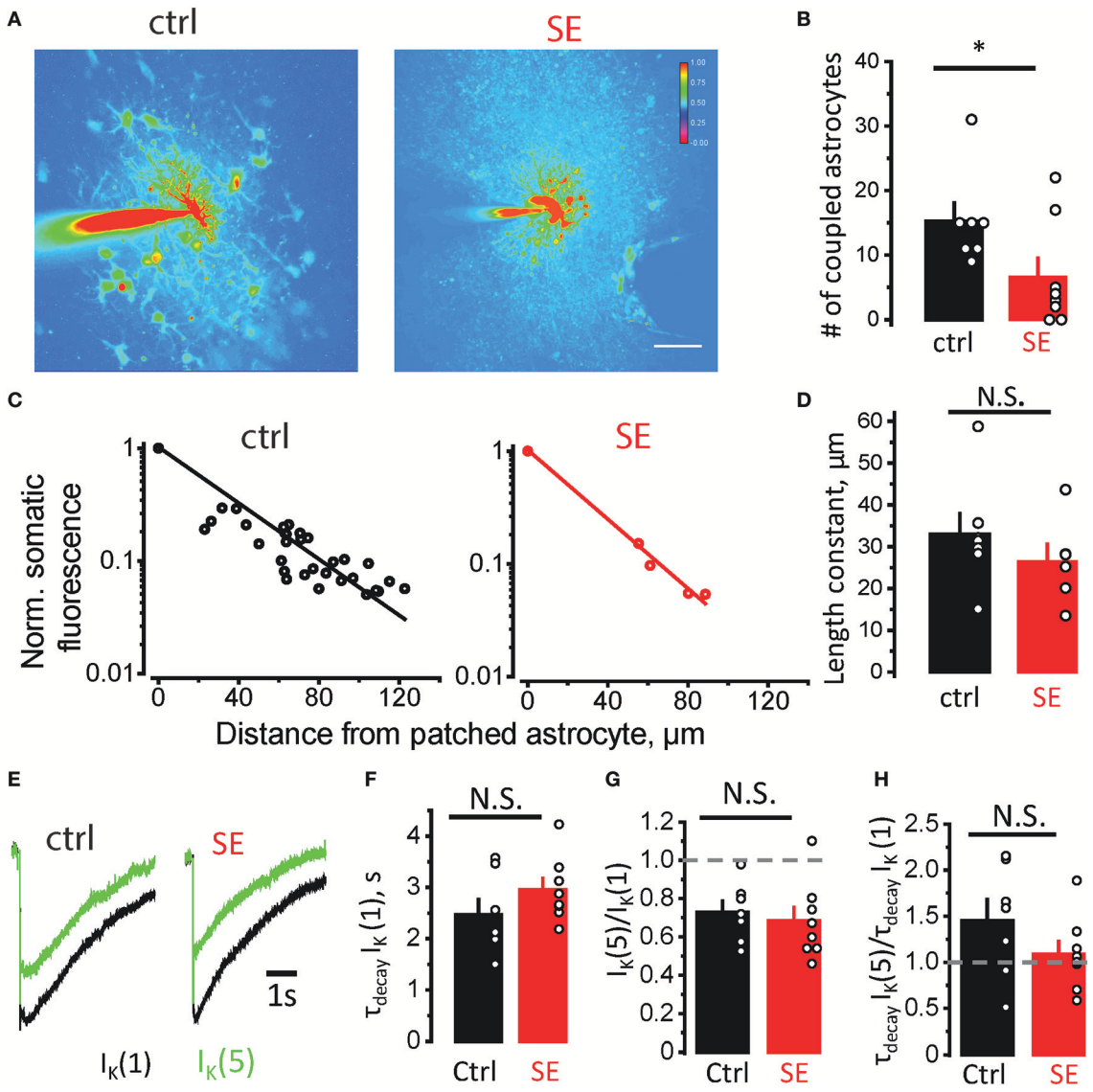

FIGURE 3 | Astrocytic uncoupling through the gap-junctions does not affect K^+ clearance by astrocytes. **(A)** Fluorescence image of an astrocyte stained with 50 μM Alexa Fluor 594 through patch pipette in control (*left*) and SE-rats (*left*). Because the dye goes through gap-junctions, the coupled astrocytes are also stained. The number of stained astrocytes is lower after SE. **(B)** The summary data showing the number of coupled astrocytes in control (*black*) and after SE (*red*). **(C)** Decay of fluorescence in somas of coupled astrocytes with distance from the astrocyte loaded with Alexa Fluor 594. The slope of the linear fit in semi-logarithmic scale determines the length constant. **(D)** The summary data showing the length constant in control (*black*) and after SE (*red*). **(E)** The sample traces of the I_K recorded to the single stimulus [$I_K(1)$, black trace] and to the fifth stimulus [the response to 4 stimuli was subtracted from the response to 5 stimuli, $I_K(5)$, green trace]. **(F)** The summary data of decay time constant of $I_K(1)$ [τ_{decay} $I_K(1)$] in control (*black*) and after SE (*red*). **(G,H)** The summary data of $I_K(5)/I_K(1)$ and τ_{decay} $I_K(5)$/ τ_{decay} $I_K(1)$ ratios, respectively. The circles show values in individual rats. The bars with error bars are means ± SEMs. *p <0.05, N.S. p > 0.05 Mann-Whitney test.

et al., 2015; Cheung et al., 2015; Lebedeva et al., 2018). To address possible changes in K^+ dynamics after SE, we recorded K^+ current (I_K) in CA1 *str.radiatum* astrocytes in response to stimulation of Schaffer collaterals (**Figure 3E**). The astrocytic response consists of three overlapping currents: field potential-induced current, glutamate transporter current, and I_K (Sibille et al., 2014). First two currents are short and typically end within 100 ms, while I_K lasts for several seconds (Afzalov et al., 2013; Lebedeva et al., 2018). Therefore, the amplitude of I_K was measured 200 ms after the stimulus. The I_K was also fitted from this point with mono-exponential function, which was used to calculate the decay time-constant (τ_{decay} I_K). No significant difference was observed in τ_{decay} I_K in response to single stimulus after SE [τ_{decay} $I_K(1)$: 2.5 ± 0.3 s, $n = 7$, in control; 3.0 ± 0.2 s, $n = 8$, after SE; $p = 0.09$, Mann-Whitney test, **Figure 3F**]. This result suggests that K^+ clearance is not affected during single synaptic events after SE, but it may be affected during repeated activity. To address this issue, we stimulated Schaffer collaterals 4 times and 5 times at 50 Hz. Then the response to 4 stimuli was subtracted from the response to 5 stimuli to obtain isolated I_K to 5th stimulus [$I_K(5)$].The ratio of $I_K(5)/I_K(1)$ demonstrated activity-dependent depression of I_K and was not significantly different between control and SE rats [$I_K(5)/I_K(1)$: 0.72 ± 0.06, $n = 7$, in control; 0.68 ± 0.07, $n = 8$, after SE; $p =$ 0.26, Mann-Whitney test, **Figure 3G**]. The ratio of τ_{decay} $I_K(5)/\tau_{decay}$ $I_K(1)$ was also not significantly different between control and SE rats [τ_{decay} $I_K(5)/\tau_{decay}$ $I_K(1)$: 1.45 ± 0.23, $n = 7$, in control; 1.09 ± 0.14, $n = 8$, after SE; $p = 0.14$, Mann-Whitney test, **Figure 3H**]. These findings suggest that possible reduction in K^+ spatial buffering in astrocytic syncytium does not affect K^+ clearance during moderate activity of the neuronal network.

Astrocytic atrophy and uncoupling can affect Ca^{2+} signaling in an astrocytic syncytium. To test this hypothesis, we measured Ca^{2+} signals in CA1 *str. radiatum* stained with membrane-permeable Ca^{2+} dye Oregon Green 488 BAPTA-1, AM (**Figure 4A**). Although this dye predominantly stains astrocytes, we could not rule out the contribution of neuronal responses to a fluorescent signal. Fortunately, astrocyte can generate much slower Ca^{2+} signals than neurons (seconds vs. hundreds of milliseconds) (Bazargani and Attwell, 2016). Such long signals are likely to represent only a proportion of overall Ca^{2+} activity in astrocytes and require Ca^{2+} release from endogenous Ca^{2+} stores. Thus, astrocytic Ca^{2+} events can be separated from neuronal based on their duration (Monai et al., 2016). Time-lapse Ca^{2+} imaging was performed with a confocal microscope at the rate of 1 frame per second. Events lasting ≥ 2 s were considered astrocytic (Supplementary Video). Whole (x-y-time) Ca^{2+} events were identified in local astrocytic syncytium as previously described for single astrocytes (**Figure 4B**) (Wu et al., 2014). The frequency of Ca^{2+} events normalized to the imaged area (frequency density) was not significantly different between control and SE rats (frequency density: 5.3 ± 1.8 s^{-1} mm^{-2}, $n = 7$, in control; 3.8 ± 0.8 s^{-1} mm^{-2}, $n = 7$, after SE; $p = 0.5$, Mann-Whitney test, **Figure 4C**). Consistent with the previous report the distributions of event sizes (S_{max}, maximal projection) and of events durations followed a power law (Wu et al., 2014):

$$P(x) \sim x^{-\alpha}, \tag{15}$$

where P–probability, x–analyzed parameter (S_{max} or duration), α–power law exponent. α defines mean value and standard deviation of the sample. Smaller α suggests that distribution has higher proportion of larger or longer events, and vice versa. To calculate α the sample was log-binned and fitted with power function. The α of S_{max} was significantly larger after SE, suggesting a smaller proportion of large Ca^{2+} events in the distribution [α(S_{max}): 2.7 ± 0.3, $n = 7$, in control; 3.5 ± 0.2, $n = 7$, after SE; $p = 0.015$, Mann-Whitney test, **Figure 4D**]. No significant difference in α of durations was observed after SE [α(durations): 2.75 ± 0.23, $n = 7$, in control; 3.02 ± 0.24, $n = 7$, after SE; $p = 0.15$, Mann-Whitney test, **Figure 4E**]. This finding suggests that morphological changes in astrocytes correlate with reduction of large-sized Ca^{2+} events in astrocytic syncytium after SE.

Ca^{2+} activity in astrocytes is responsible for a number of functions including the release of gliotransmitters such as *D*-serine (Papouin et al., 2017). *D*-serine acts as a co-agonist of NMDA receptors and is required for long-term potentiation (LTP) (Henneberger et al., 2010, 2012). Thus, the decrease of astrocytic Ca^{2+} activity can reduce the amount of *D*-serine released and thus impair LTP after SE (Sherwood et al., 2017). To test this hypothesis, we recorded field (f)EPSPs in CA1 *str.radiatum* in response to stimulation of Shaffer collaterals (**Figure 5A**) The relationship between fEPSP amplitude and stimulus strength has significantly decreased after SE [$F_{(11,297)} = 4.39$, $p < 0.001$, two-way ANOVA; **Figures 5B,C**], but no significant difference in relationship between presynaptic fiber volley (PrV) and stimulus strength was observed [$F_{(11,275)} = 0.37$, $p = 0.97$, two-way ANOVA; **Figures 5B,C**]. The maximum rise slope of the input-output (I/O) relationships (fEPSP amplitude vs. PrV amplitude) was lower after SE (control: 3.32 ± 0.32, $n = 13$, SE: 1.61 ± 0.33, $n = 14$, $p < 0.01$, *t*-test; **Figure 5C**). These results suggest that the number of fibers or excitability of Shaffer collaterals did not change (unless the decreased number of fibers is compensated by their higher excitability), but the number of activated synapses decreased after SE. This result is consistent with neurodegeneration observed after SE. 10 μM *D*-serine changed the relationship between fEPSP amplitude vs. stimulus strength both in control [$F_{(11,231)} = 2.23$, $p < 0.05$, two-way ANOVA; **Figures 5B,C**] and after SE [$F_{(11,330)} = 2.13$, $p < 0.05$, two-way ANOVA; **Figures 5B,C**], however, *post hoc* LSD test did not confirm the effect of *D*-serine at any level of stimulation.

Three trains of high-frequency stimulation (HFS, 100 pulses at 100 Hz, with an inter-train interval of 20 s) were applied to induce LTP (Henneberger et al., 2010). The LTP magnitude was significantly lower after SE compared to control animals (1.73 ± 0.12, $n = 14$, in control 50–60 min after induction; 1.29 ± 0.07, $n = 15$, after SE; $p < 0.01$, *t*-test; **Figures 5D–G**). *D*-serine did not significantly affect the magnitude of LTP in control ($p = 0.48$, *t*-test; **Figures 5D–G**), but restored initial phase of LTP (5–15 min) after SE (1.92 ± 0.17, $n = 13$) to the level of control animals (1.99 ± 0.13, $n = 14$, *t*-test = 0.35, $p = 0.73$). LTP enhancement by exogenous *D*-serine in a later phase of LTP (50–60 min) was not however significant (1.37 ± 0.14, $n = 13$, *t*-test = 0.54, $p = 0.60$, **Figure 5G**).

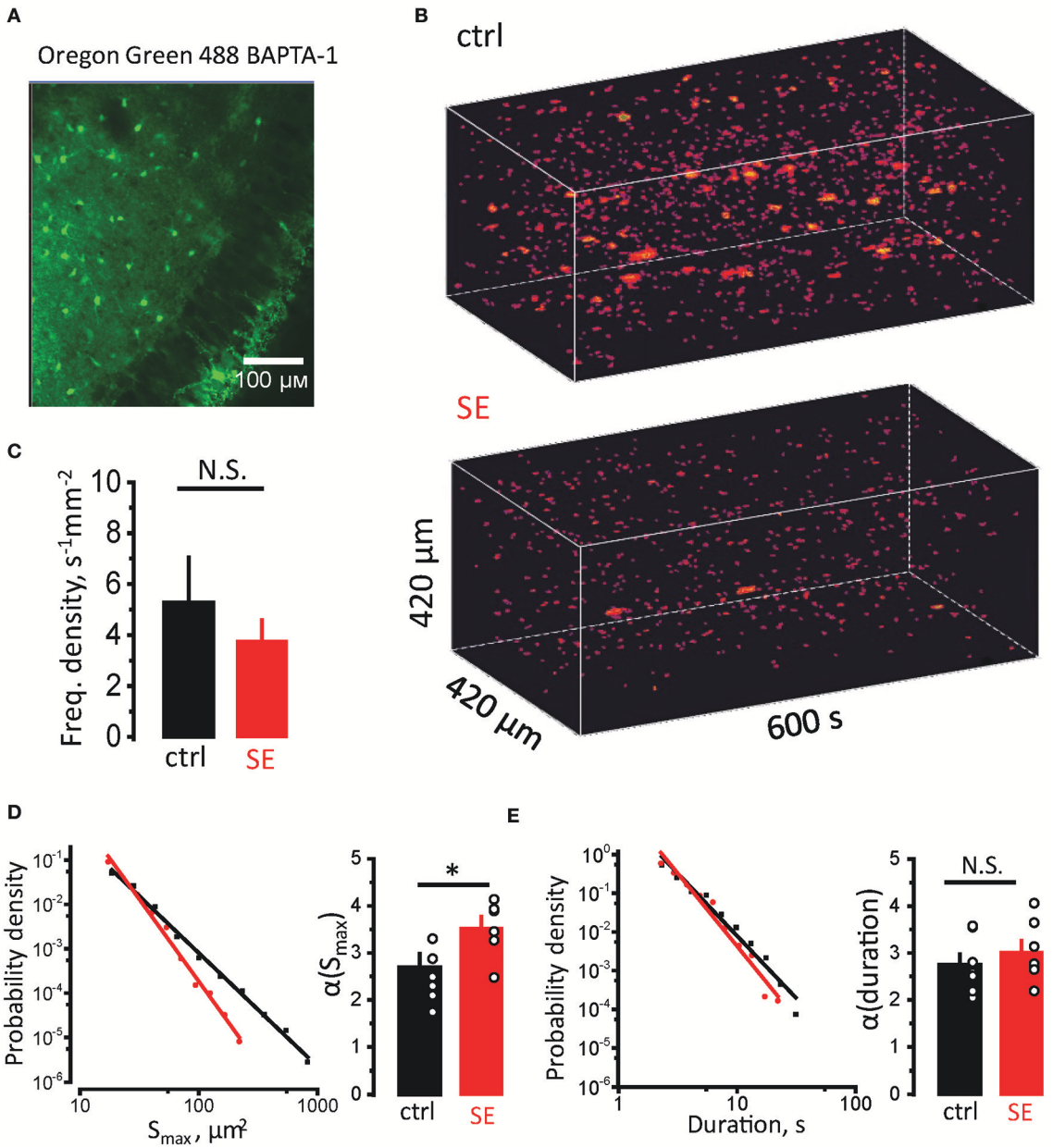

FIGURE 4 | Reduction in sizes of spontaneous Ca^{2+} events in astrocytic syncytium. **(A)** Hippocampal slice stained with Oregon Green 488 BAPTA-1 AM. The image shows that astrocytes in *str.radiatum*, but not neurons in *str.pyramidale* stained. **(B)** 3D reconstruction of Ca^{2+} events in *str.radiatum* astrocytes (x-y-time). *Top,* Time-course of Ca^{2+} events in control slice. *Bottom,* in slice after SE. **(C)** The summary data of the frequency density of astrocytic Ca^{2+} events in control (black) and SE-rats (red). **(D,E)** *Right,* Probability density distributions of S_{max} **(D)** and durations **(E)** of Ca^{2+} events in log–log scale (log-binned data) for all recorded slices. Solid black and red lines are the power function fits for control and SE data, respectively. *Left,* The summary data of the exponents $\alpha(S_{max})$ **(D)** and α(durations) **(E)**. The circles show values in individual rats. The bars with error bars are means ± SEMs. *p <0.05, N.S. p > 0.05 Mann-Whitney test.

Our findings suggest that neurodegeneration 2–4 weeks after pilocarpine-induced SE is accompanied by re-modeling of astrocytes and reduction of their coupling through gap-junctions. It does not affect the ability of astrocytes to clean up extracellular K^+ despite the expected decrease in its spatial buffering. Decreased number of astrocytic branches correlates with reduced sizes of spontaneous Ca^{2+} events in astrocytes. This in turn may be responsible for *D*-serine deficiency and impaired LTP after SE.

DISCUSSION

Astrocytic processes often comprise of thicker astrocytic branches and thinner, nanoscale leaflets (Bernardinelli et al.,

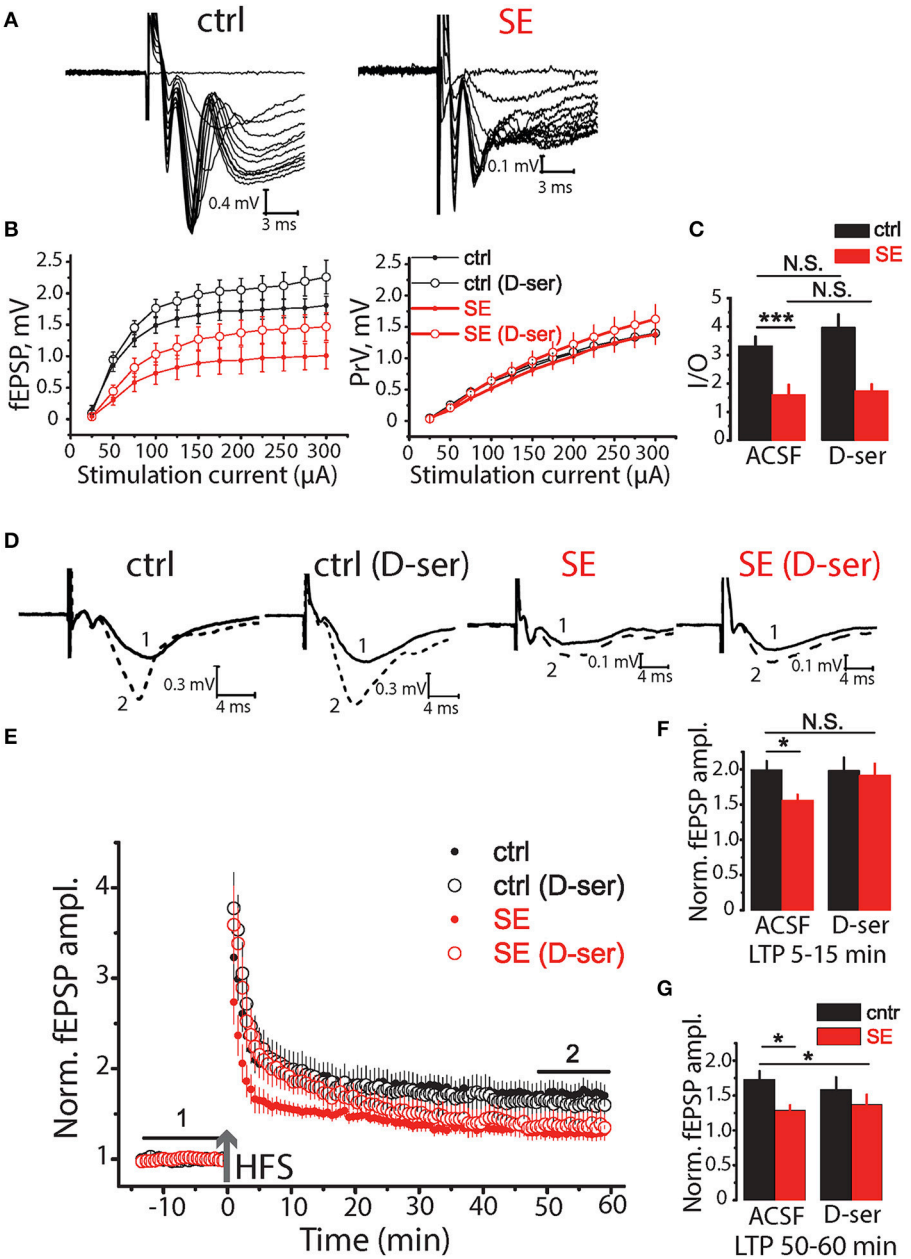

FIGURE 5 | Effects of D-serine on synaptic neurotransmission in the hippocampus of control and SE-rats. **(A)** Representative examples of fEPSPs recorded in the hippocampal CA1 of control (ctrl) and SE-rats (SE). **(B)** Input-output (I/O) curves for the fEPSPs (*left*) and PrV (*right*). **(C)** Bar graphs showing the maximum slope of I/O curves for the fEPSPs. **(D)** Traces are the average of fEPSPs recorded during baseline (1) and 47–60 min after HFS (2). **(E)** LTP induced by HFS in the CA1 region of the hippocampus of control and SE-rats. Note that application of D-serine (D-ser) does not affect the magnitude of LTP in control rats but fully restored initial phase of LTP (5–15 min) in SE-rats. **(F,G)** The summary bar graphs showing significant reductions in LTP after SE as measured by the average normalized fEPSP amplitude and the effect of D-serine on initial **(F)** and later **(G)** phase of LTP. The bars with error bars are means ± SEMs. ***$p < 0.01$ *$p < 0.05$, N.S. $p > 0.05$ t-test.

2014a; Khakh and Sofroniew, 2015). Electron microscopy studies have suggested that thicker astrocytic branches contain endoplasmic reticulum and mitochondria serving as endogenous Ca^{2+} stores (Reichenbach et al., 2010; Patrushev et al., 2013; Bernardinelli et al., 2014b). These structures are thought to be responsible for the amplification of Ca^{2+} signals and their propagation within the astrocyte. The leaflets are thin, sheet-like structures connected to branches. They have the minimal volume of cytoplasm and seem to be largely devoid of organelles. The high surface-to-volume ratio of leaflets ensures the high surface of their plasma membrane within the limited volume of brain tissue (Lehre and Rusakov, 2002). This makes leaflets highly efficient for neurotransmitter uptake and K^+ clearance. Perisynaptic leaflets form an "astrocytic cradle" around synapses

(Verkhratsky and Nedergaard, 2014). Like dendritic spines, astrocytic leaflets are highly plastic; morphological plasticity of perisynaptic leaflets regulates synaptic coverage (Witcher et al., 2007; Reichenbach et al., 2010; Bernardinelli et al., 2014a; Heller and Rusakov, 2015). For example, reduced IP_3-dependent Ca^{2+} activity in astrocytes leads to reduced coverage of spines by astrocytic processes and enhanced glutamate spillover (Tanaka et al., 2013). Changes in the astrocytic environment are also reported following synaptic plasticity (Bernardinelli et al., 2014a).

Our morphological analysis revealed a striking difference between SE and control astrocytes. The Sholl analysis was performed on astrocytic processes identified with two-photon laser scanning microscopy (astrocytic branches $\sim$ $>0.5\,\mu m$ in diameter). Although this analysis did not reveal a difference between the samples in the enclosing radius (size of the astrocytic domain) and number of primary astrocytic branches, a significant reduction in the number of distal astrocytic branches was detected. However, astrocytic leaflets are very thin and are beyond the diffraction-limited light microscopy resolution. To assess possible changes in leaflets VF, we plotted a profile of leaflets fluorescence normalized to the fluorescence of soma (Medvedev et al., 2014; Heller and Rusakov, 2015). This method assumes that, with a $\sim 1\,\mu m$ thick two-photon excitation plane, somatic fluorescence originates from the dye that occupies $\sim$100% of the visualized volume whereas fluorescence of the leaflets area is determined by tissue volume fraction occupied by the cytoplasm of all leaflets in the excitation region. Thus, the ratio between the non-saturated soma fluorescence and the fluorescence of leaflet area is roughly proportional to the VF of leaflets. No significant difference in this ratio was found between astrocytes of SE and control animals. Nevertheless, equal VFs of leaflets do not rule out nanoscopic redistribution of leaflets that affect synaptic coverage.

To get further insights into the spatial organization of astrocytic processes, we advanced a novel, spatial complexity-entropy spectra analysis. This analysis evaluates the nature of order and structure prevalence in a system. Entropy monotonically increases as the system goes from a highly ordered crystalline-like structure to a completely disordered state lacking internal structure. Statistical complexity, on the other hand, changes non-monotonically and reaches a maximum at intermediate levels of entropy, falling near zero for the two extremes of orderliness in a system. Intuitively, the complexity of regular patterns is low due to its predictability and the complexity of a disordered state is low due to the simplicity of its statistical description. Between the two extremes, a given entropy level can correspond to a range of complexity levels. Systems near critical states or in dynamical chaos regimes are characterized by high levels of complexity (Rosso et al., 2007). In such systems, disorder is non-trivial, and the systems contain both structure and randomness. Branching patterns of astrocytic processes are an example of such a non-trivial structure, where large astrocytic branches correspond to locally ordered structures, whereas fine ramifications of leaflets are seen as more complex and chaotic. Thus, entropy-complexity spectra will reflect the ratio between astrocytic branches and leaflets. Consistent with other morphological analysis we observed a shift in entropy-complexity spectra of astrocytes corresponding to a decrease in branches/leaflets ratio.

Astrocytic coupling through gap junctions has been suggested as a mechanism for K^+ "spatial buffering" in the central nervous system (Kofuji and Newman, 2004; Meeks and Mennerick, 2007). K^+ released during action potential propagation and during activation of postsynaptic glutamate receptors is removed by astrocytes through various mechanisms (Walz, 2000; Dallérac et al., 2013; Shih et al., 2013; Pekny et al., 2016; Lebedeva et al., 2018). Once taken by astrocytes, K^+ quickly re-equilibrates within an astrocytic syncytium through gap-junctions which are permeable to this ion. One counterargument to this hypothesis is that intracellular K^+ concentration does not considerably change due to the removal of K^+ from narrow intercellular cleft to the large volume of cytoplasm. To test if astrocytic remodeling and uncoupling through gap-junctions affect K^+ clearance, we recorded I_K in astrocytes in response to synaptic stimulation. No significant difference in the amplitude and the timecourse of I_K was detected between SE and control animals. Thus, in conditions of synchronous synaptic activity, K^+ clearance did not change after SE. It rasises the question whether gap junction suppression could contribute significantly for excessive K^+ accumulation in epileptogenesis.

Astrocytic remodeling may occur as a result of neurodegeneration which is pronounced 2 weeks after SE (Curia et al., 2008). Fewer neurons make fewer synaptic connections which need less astrocytic processes to support them. Reduction in a number of distal astrocytic branches and gap-junction coupling may also decrease Ca^{2+} events spread in single astrocytes and astrocytes syncytium. Spreading of Ca^{2+} events depends on Ca^{2+} release from endogenous stores. When some of the distal astrocytic branches containing Ca^{2+} stores are abolished, Ca^{2+} transients starting in leaflets have less chance to be amplified after SE. Astrocytic gap-junction may play a role in the propagation of Ca^{2+} signals in astrocytic syncytium (Enkvist and Mccarthy, 1992; Höfer et al., 2002; Fujii et al., 2017). When astrocytes become uncoupled, Ca^{2+} events spread may be limited. This, however, does not exclude a possibility of Ca^{2+} activity spread by the release of gliotransmitters (e.g., ATP) (Guthrie et al., 1999; Cotrina et al., 2000). Overall, we found that morphological changes correlated with the reduced spread of Ca^{2+} events in astrocytic syncytium observed after SE. Diminished Ca^{2+} signaling in astrocytes may affect several astrocytic functions such as release of gliotransmitters (Zorec et al., 2012; Araque et al., 2014), Ca^{2+} dependent K^+ clearance (Wang et al., 2012) or outgrow of perisynaptic astrocytic processes (Tanaka et al., 2013; Heller and Rusakov, 2015). This can not only affect signaling in astrocytic syncytium, but also neuronal excitability, activation of extrasynaptic receptors, synaptic transmission, and plasticity (Rusakov et al., 2011; Zorec et al., 2012; Verkhratsky and Nedergaard, 2018).

In the present study, we have demonstrated hippocampal synaptic dysfunctions in pilocarpine-treated rats, as assessed by the reductions in both basal transmission and LTP at Schaffer collateral-CA1 synapses. The decrease in basal transmission is consistent with a reduction in the number of principal neurons

in the CA3 hippocampal area of pilocarpine-treated animals observed earlier by us and other investigators in different hippocampal areas (see for review Curia et al., 2014). LTP induction at Schaffer collateral-CA1 synapses is an NMDA receptor-dependent form of synaptic plasticity (Malenka and Bear, 2004) and, therefore, the impairment of LTP most likely indicates the disturbance in NMDA receptor signaling. NMDA receptor signaling might be disturbed in many ways in epilepsy. For example, it might be affected because of the perturbations in the glutamate-glutamine cycle, such as increased extracellular levels of glutamate, loss of astrocytic glutamine synthetase, and changes in glutaminase and glutamate dehydrogenase, which are frequently encountered in patients with epilepsy (Coulter and Eid, 2012; Eid et al., 2016). Another possible reason is the changes in the production of individual subunits of NMDA receptors, which have been shown in several experimental models of epilepsy including the lithium-pilocarpine model (Di Maio et al., 2013; Müller et al., 2013; Peng et al., 2016; Amakhin et al., 2017). Hippocampal astrocytes in brain slices retain the ability to control LTP within or near their individual territories involving Ca^{2+}-dependent *D*-serine release (Henneberger et al., 2010). This implies that astrocytes are at least capable of regulating local *D*-serine supply and might indeed be able to deliver *D*-serine to specific NMDA receptor populations. Therefore, our next set of experiments was designed to evaluate the role of *D*-serine signaling. We found that application of *D*-serine fully restored the initial phase of LTP (5–15 min) after SE.

Morphological and functional integrity of astrocytes is a key to the healthy brain. Astrocytes occupy non-overlapping or slightly overlapping spatial domains (Bushong et al., 2002) which they fill with highly ramified processes (Khakh and Sofroniew, 2015). Such architecture helps to support neurons metabolically, maintain local homeostasis, synaptic plasticity etc. (Verkhratsky and Nedergaard, 2018). Disruption of the astrocytic domain organization, morphological alterations of astrocytes and changes in the number of these cells are characteristic to many of brain disorders (Verkhratsky et al., 2017). It appears that the changes in astrocytes often precede neurodegeneration and clinical symptoms (Rossi and Volterra, 2009). Astrocytic pathologies can be of several types: (1) changes in the number of astrocytes, e.g., astrogliosis or astrodegeneration; (2) astrocytic remodeling, e.g., atrophy; and (3) reactive astrogliosis. A combination of such astrocytic pathologies might signify of a particular disease or of a stage of the disease (Verkhratsky and Parpura, 2016). Astrocyte degeneration and atrophy have been described in the hSOD1 mouse, an experimental model of amyotrophic lateral sclerosis (Rossi et al., 2008). Astrocytic markers are reduced in the Parkinson's disease (Tong et al., 2015). Region- and stage-specific alterations in astrocytic morphology have been reported in the Alzheimer's disease (Olabarria et al., 2010; Rodríguez-Arellano et al., 2016). Loss of astrocytic domain organization has been observed in the epileptic brain (Oberheim et al., 2008). Here we find that the lithium-pilocarpine model of SE is associated with the atrophy of distal astrocytic branches and with astrocyte uncoupling reported earlier (Bedner et al., 2015). This, in turn, diminishes Ca^{2+} activity in these cells and correlates with the *D*-serine dependent impairment of LTP initiation. However, the LTP maintenance phase failure was not related to the insufficient *D*-serine supply. The maintenance phase could be potentially linked to reduced supply of energy substrates from atrophic astrocytes or to a malfunction of any other metabolic or homeostatic support of synapses. However, this hypothesis requires further experimental testing. Our results demonstrate that the astrocyte remodeling after SE does not affect VF of astrocytic leaflets and K^+ clearance. This indicates that astrocytes can effectively maintain synaptic microenvironment at moderate levels of synaptic activity. However, if astrocytes can prevent the K^+ accumulation during synchronized epileptiform activity remains unclear. In agreement with previous reports we observe astrocyte uncoupling through the gap-junctions (Bedner et al., 2015). This may affect spatial buffering of excessive amounts of K^+ that are released during focal seizures (Fröhlich et al., 2008). In addition, optical methods, which we used, assess the synaptic microenvironment very indirectly. More careful studies on the integrity of "astrocytic cradle" around synapses are required with the use of super-resolution light microscopy or electron microscopy.

ETHICS STATEMENT

All the animal experiments were approved by N. I. Lobachevsky State University of Nizhny Novgorod ethics committee.

AUTHOR CONTRIBUTIONS

APl, AL, PD, ON, and TP performed the experiments, analyzed the data, prepared the figures. AP wrote the MATLAB script for Ca^{2+} analysis. AB wrote the scripts for Sholl analysis and entropy-complexity analysis, analyzed the data, prepared the figures. AZ analyzed the data, prepared the figures. DR planned the experiments. AS planned the experiments, supervised the project. AB, AZ, DR, and AS wrote the paper.

ACKNOWLEDGMENTS

The authors are grateful to Dr. Nikolay Gavrilov for help with 3D visualization of astrocytic Ca^{2+} activity and to Prof. Dmitrii Korzhevskii for help with Nissl staining visualization. The project was supported by COMFI grant 17-00-00412 (K) from RFBR for joint research of AS (grant 17-00-00409), AB (grant 17-00-00407), and AZ (grant 17-00-00408), Wellcome Trust PRF and ERC Advanced (DR).

SUPPLEMENTARY MATERIAL

The Supplementary Material for this article can be found online at: https://www.frontiersin.org/articles/10.3389/fnmol.2018.00215/full#supplementary-material

REFERENCES

Afzalov, R., Pryazhnikov, E., Shih, P. Y., Kondratskaya, E., Zobova, S., Leino, S., et al. (2013). Low micromolar Ba^{2+} potentiates glutamate transporter current in hippocampal astrocytes. *Front. Cell. Neurosci.* 7:135. doi: 10.3389/fncel.2013.00135

Amakhin, D. V., Malkin, S. L., Ergina, J. L., Kryukov, K. A., Veniaminova, E. A., Zubareva, O. E., et al. (2017). Alterations in properties of glutamatergic transmission in the temporal cortex and hippocampus following pilocarpine-induced acute seizures in Wistar rats. *Front. Cell. Neurosci.* 11:264. doi: 10.3389/fncel.2017.00264

Anders, S., Minge, D., Griemsmann, S., Herde, M. K., Steinhäuser, C., and Henneberger, C. (2014). Spatial properties of astrocyte gap junction coupling in the rat hippocampus. *Philos. Trans. R. Soc. Lond. B Biol. Sci.* 369:20130600. doi: 10.1098/rstb.2013.0600

Angulo, M. C., Le Meur, K., Kozlov, A. S., Charpak, S., and Audinat, E. (2008). GABA, a forgotten gliotransmitter. *Prog. Neurobiol.* 86, 297–303. doi: 10.1016/j.pneurobio.2008.08.002

Araque, A., Carmignoto, G., Haydon, P. G., Oliet, S. H., Robitaille, R., and Volterra, A. (2014). Gliotransmitters travel in time and space. *Neuron* 81, 728–739. doi: 10.1016/j.neuron.2014.02.007

Bazargani, N., and Attwell, D. (2016). Astrocyte calcium signaling: the third wave. *Nat. Neurosci.* 19, 182–189. doi: 10.1038/nn.4201

Bedner, P., Dupper, A., Hüttmann, K., Müller, J., Herde, M. K., Dublin, P., et al. (2015). Astrocyte uncoupling as a cause of human temporal lobe epilepsy. *Brain* 138, 1208–1222. doi: 10.1093/brain/awv067

Bedner, P., and Steinhäuser, C. (2013). Altered Kir and gap junction channels in temporal lobe epilepsy. *Neurochem. Int.* 63, 682–687. doi: 10.1016/j.neuint.2013.01.011

Bernardinelli, Y., Muller, D., and Nikonenko, I. (2014a). Astrocyte-synapse structural plasticity. *Neural Plast.* 2014:232105. doi: 10.1155/2014/232105

Bernardinelli, Y., Randall, J., Janett, E., Nikonenko, I., König, S., Jones, E. V., et al. (2014b). Activity-dependent structural plasticity of perisynaptic astrocytic domains promotes excitatory synapse stability. *Curr. Biol.* 24, 1679–1688. doi: 10.1016/j.cub.2014.06.025

Bliss, T. V., and Collingridge, G. L. (1993). A synaptic model of memory: long-term potentiation in the hippocampus. *Nature* 361, 31–39. doi: 10.1038/361031a0

Blümcke, I., Thom, M., and Wiestler, O. D. (2002). Ammon's horn sclerosis: a maldevelopmental disorder associated with temporal lobe epilepsy. *Brain Pathol.* 12, 199–211. doi: 10.1111/j.1750-3639.2002.tb00436.x

Bushong, E. A., Martone, M. E., Jones, Y. Z., and Ellisman, M. H. (2002). Protoplasmic astrocytes in CA1 stratum radiatum occupy separate anatomical domains. *J. Neurosci.* 22, 183–192. doi: 10.1523/JNEUROSCI.22-01-00183.2002

Carpenter-Hyland, E., Bichler, E. K., Smith, M., Sloviter, R. S., and Benveniste, M. (2017). Epileptic pilocarpine-treated rats exhibit aberrant hippocampal EPSP-spike potentiation but retain long-term potentiation. *Physiol. Rep.* 5:e13490. doi: 10.14814/phy2.13490

Cheung, G., Sibille, J., Zapata, J., and Rouach, N. (2015). Activity-dependent plasticity of astroglial potassium and glutamate clearance. *Neural Plast.* 2015:109106. doi: 10.1155/2015/109106

Clasadonte, J., Dong, J., Hines, D. J., and Haydon, P. G. (2013). Astrocyte control of synaptic NMDA receptors contributes to the progressive development of temporal lobe epilepsy. *Proc. Natl. Acad. Sci. U.S.A.* 110, 17540–17545. doi: 10.1073/pnas.1311967110

Cotrina, M. L., Lin, J. H., López-García, J. C., Naus, C. C., and Nedergaard, M. (2000). ATP-mediated glia signaling. *J. Neurosci.* 20, 2835–2844. doi: 10.1523/JNEUROSCI.20-08-02835.2000

Coulter, D. A., and Eid, T. (2012). Astrocytic regulation of glutamate homeostasis in epilepsy. *Glia* 60, 1215–1226. doi: 10.1002/glia.22341

Cunha, A. O., De Oliveira, J. A., Almeida, S. S., Garcia-Cairasco, N., and Leão, R. M. (2015). Inhibition of long-term potentiation in the schaffer-CA1 pathway by repetitive high-intensity sound stimulation. *Neuroscience* 310, 114–127. doi: 10.1016/j.neuroscience.2015.09.040

Curia, G., Longo, D., Biagini, G., Jones, R. S., and Avoli, M. (2008). The pilocarpine model of temporal lobe epilepsy. *J. Neurosci. Methods* 172, 143–157. doi: 10.1016/j.jneumeth.2008.04.019

Curia, G., Lucchi, C., Vinet, J., Gualtieri, F., Marinelli, C., Torsello, A., et al. (2014). Pathophysiogenesis of mesial temporal lobe epilepsy: is prevention of damage antiepileptogenic? *Curr. Med. Chem.* 21, 663–688. doi: 10.2174/09298673206613119152201

Dallérac, G., Chever, O., and Rouach, N. (2013). How do astrocytes shape synaptic transmission? Insights from electrophysiology. *Front. Cell. Neurosci.* 7:159. doi: 10.3389/fncel.2013.00159

Danielyan, A., Wu, Y.-W., Shih, P. Y., Dembitskaya, Y., and Semyanov, A. (2014). Denoising of two-photon fluorescence images with Block-Matching 3D filtering. *Methods* 68, 308–316. doi: 10.1016/j.ymeth.2014.03.010

de Lanerolle, N. C., and Lee, T. S. (2005). New facets of the neuropathology and molecular profile of human temporal lobe epilepsy. *Epilepsy Behav.* 7, 190–203. doi: 10.1016/j.yebeh.2005.06.003

Di Maio, R., Mastroberardino, P. G., Hu, X., Montero, L. M., and Greenamyre, J. T. (2013). Thiol oxidation and altered NR2B/NMDA receptor functions in *in vitro* and *in vivo* pilocarpine models: implications for epileptogenesis. *Neurobiol. Dis.* 49, 87–98. doi: 10.1016/j.nbd.2012.07.013

DiNuzzo, M., Mangia, S., Maraviglia, B., and Giove, F. (2014). Physiological bases of the K+ and the glutamate/GABA hypotheses of epilepsy. *Epilepsy Res.* 108, 995–1012. doi: 10.1016/j.eplepsyres.2014.04.001

During, M. J., and Spencer, D. D. (1993). Extracellular hippocampal glutamate and spontaneous seizure in the conscious human brain. *Lancet* 341, 1607–1610. doi: 10.1016/0140-6736(93)90754-5

Eid, T., Gruenbaum, S. E., Dhaher, R., Lee, T. W., Zhou, Y., and Danbolt, N. C. (2016). The Glutamate-Glutamine Cycle in Epilepsy. *Adv. Neurobiol.* 13, 351–400. doi: 10.1007/978-3-319-45096-4_14

Enkvist, M. O., and Mccarthy, K. D. (1992). Activation of protein kinase C blocks astroglial gap junction communication and inhibits the spread of calcium waves. *J. Neurochem.* 59, 519–526. doi: 10.1111/j.1471-4159.1992.tb09401.x

Fellin, T., Gomez-Gonzalo, M., Gobbo, S., Carmignoto, G., and Haydon, P. G. (2006). Astrocytic glutamate is not necessary for the generation of epileptiform neuronal activity in hippocampal slices. *J. Neurosci.* 26, 9312–9322. doi: 10.1523/JNEUROSCI.2836-06.2006

Fertziger, A. P., and Ranck, J. B. Jr. (1970). Potassium accumulation in interstitial space during epileptiform seizures. *Exp. Neurol.* 26, 571–585. doi: 10.1016/0014-4886(70)90150-0

Fröhlich, F., Bazhenov, M., Iragui-Madoz, V., and Sejnowski, T. J. (2008). Potassium dynamics in the epileptic cortex: new insights on an old topic. *Neuroscientist* 14, 422–433. doi: 10.1177/1073858408317955

Fujii, Y., Maekawa, S., and Morita, M. (2017). Astrocyte calcium waves propagate proximally by gap junction and distally by extracellular diffusion of ATP released from volume-regulated anion channels. *Sci. Rep.* 7:13115. doi: 10.1038/s41598-017-13243-0

Green, J. D. (1964). The hippocampus. *Physiol. Rev.* 44, 561–608. doi: 10.1152/physrev.1964.44.4.561

Guizar-Sicairos, M., Thurman, S. T., and Fienup, J. R. (2008). Efficient subpixel image registration algorithms. *Opt. Lett.* 33, 156–158. doi: 10.1364/OL.33.000156

Guthrie, P. B., Knappenberger, J., Segal, M., Bennett, M. V., Charles, A. C., and Kater, S. B. (1999). ATP released from astrocytes mediates glial calcium waves. *J. Neurosci.* 19, 520–528. doi: 10.1523/JNEUROSCI.19-02-00520.1999

Häuser, S., and Steidl, G. (2013). Convex multiclass segmentation with shearlet regularization. *Int. J. Comput. Math.* 90, 62–81. doi: 10.1080/00207160.2012.688960

Héja, L., Nyitrai, G., Kékesi, O., Dobolyi, A., Szabó, P., Fiáth, R., et al. (2012). Astrocytes convert network excitation to tonic inhibition of neurons. *BMC Biol.* 10:26. doi: 10.1186/1741-7007-10-26

Heller, J. P., and Rusakov, D. A. (2015). Morphological plasticity of astroglia: Understanding synaptic microenvironment. *Glia* 63, 2133–2151. doi: 10.1002/glia.22821

Henneberger, C., Bard, L., and Rusakov, D. A. (2012). D-Serine: a key to synaptic plasticity? *Int. J. Biochem. Cell Biol.* 44, 587–590. doi: 10.1016/j.biocel.2012.01.005

Henneberger, C., Papouin, T., Oliet, S. H., and Rusakov, D. A. (2010). Long-term potentiation depends on release of D-serine from astrocytes. *Nature* 463, 232–236. doi: 10.1038/nature08673

Hermann, B., and Seidenberg, M. (2007). Epilepsy and cognition. *Epilepsy Curr.* 7, 1–6. doi: 10.1111/j.1535-7511.2007.00151.x

Höfer, T., Venance, L., and Giaume, C. (2002). Control and plasticity of intercellular calcium waves in astrocytes: a modeling approach. *J. Neurosci.* 22, 4850–4859. doi: 10.1523/JNEUROSCI.22-12-04850.2002

Höller, Y., and Trinka, E. (2014). What do temporal lobe epilepsy and progressive mild cognitive impairment have in common? *Front. Syst. Neurosci.* 8:58. doi: 10.3389/fnsys.2014.00058

Ivanov, A. D., and Zaitsev, A. V. (2017). NMDAR-independent hippocampal long-term depression impairment after status epilepticus in a lithium-pilocarpine model of temporal lobe epilepsy. *Synapse*. 71:e21982. doi: 10.1002/syn.21982

Jones, T. A., and Greenough, W. T. (1996). Ultrastructural evidence for increased contact between astrocytes and synapses in rats reared in a complex environment. *Neurobiol. Learn. Mem.* 65, 48–56. doi: 10.1006/nlme.1996.0005

Ju, W., Morishita, W., Tsui, J., Gaietta, G., Deerinck, T. J., Adams, S. R., et al. (2004). Activity-dependent regulation of dendritic synthesis and trafficking of AMPA receptors. *Nat. Neurosci.* 7, 244–253. doi: 10.1038/nn1189

Kersante, F., Rowley, S. C. S., Pavlov, I., Gutierrez-Mecinas, M., Semyanov, A., Reul, J. M. H. M., et al. (2013). A functional role for both gamma-aminobutyric acid (GABA) transporter-1 and GABA transporter-3 in the modulation of extracellular GABA and GABAergic tonic conductances in the rat hippocampus. *J. Physiol. Lond.* 591, 2429–2441. doi: 10.1113/jphysiol.2012.246298

Khakh, B. S., and Sofroniew, M. V. (2015). Diversity of astrocyte functions and phenotypes in neural circuits. *Nat. Neurosci.* 18, 942–952. doi: 10.1038/nn.4043

Kim, J. H. (2001). Pathology of epilepsy. *Exp. Mol. Pathol.* 70, 345–367. doi: 10.1006/exmp.2001.2372

Kofuji, P., and Newman, E. A. (2004). Potassium buffering in the central nervous system. *Neuroscience* 129, 1045–1056. doi: 10.1016/j.neuroscience.2004.06.008

Kryukov, K. A., Kim, K. K., Magazanik, L. G., and Zaitsev, A. V. (2016). Status epilepticus alters hippocampal long-term synaptic potentiation in a rat lithium-pilocarpine model. *Neuroreport* 27, 1191–1195. doi: 10.1097/WNR.0000000000000656

Lamberti, P. W., Martin, M. T., Plastino, A., and Rosso, O. A. (2004). Intensive entropic non-triviality measure. *Physica A* 334, 119–131. doi: 10.1016/j.physa.2003.11.005

Lebedeva, A., Plata, A., Nosova, O., Tyurikova, O., and Semyanov, A. (2018). Activity-dependent changes in transporter and potassium currents in hippocampal astrocytes. *Brain Res. Bull.* 136, 37–43. doi: 10.1016/j.brainresbull.2017.08.015

Lee, S., Yoon, B. E., Berglund, K., Oh, S. J., Park, H., Shin, H. S., et al. (2010). Channel-mediated tonic GABA release from glia. *Science* 330, 790–796. doi: 10.1126/science.1184334

Lehre, K. P., and Rusakov, D. A. (2002). Asymmetry of glia near central synapses favors presynaptically directed glutamate escape. *Biophys. J.* 83, 125–134. doi: 10.1016/S0006-3495(02)75154-0

López-Ruiz, R., Mancini, H. L., and Calbet, X. (1995). A statistical measure of complexity. *Phys. Lett. A* 209, 321–326. doi: 10.1016/0375-9601(95)00867-5

Lushnikova, I., Skibo, G., Muller, D., and Nikonenko, I. (2009). Synaptic potentiation induces increased glial coverage of excitatory synapses in CA1 hippocampus. *Hippocampus* 19, 753–762. doi: 10.1002/hipo.20551

Maggioni, M., Katkovnik, V., Egiazarian, K., and Foi, A. (2013). Nonlocal Transform-Domain Filter for Volumetric Data Denoising and Reconstruction. *IEEE Trans. Image Process.* 22, 119–133. doi: 10.1109/TIP.2012.2210725

Malenka, R. C., and Bear, M. F. (2004). LTP and LTD: an embarrassment of riches. *Neuron* 44, 5–21. doi: 10.1016/j.neuron.2004.09.012

Mazzuferi, M., Palma, E., Martinello, K., Maiolino, F., Roseti, C., Fucile, S., et al. (2010). Enhancement of GABA(A)-current run-down in the hippocampus occurs at the first spontaneous seizure in a model of temporal lobe epilepsy. *Proc. Natl. Acad. Sci. U.S.A.* 107, 3180–3185. doi: 10.1073/pnas.0914710107

Medvedev, N., Popov, V., Henneberger, C., Kraev, I., Rusakov, D. A., and Stewart, M. G. (2014). Glia selectively approach synapses on thin dendritic spines. *Philos. Trans. R. Soc. Lond. B Biol. Sci.* 369, 20140047. doi: 10.1098/rstb.2014.0047

Meeks, J. P., and Mennerick, S. (2007). Astrocyte membrane responses and potassium accumulation during neuronal activity. *Hippocampus* 17, 1100–1108. doi: 10.1002/hipo.20344

Monai, H., Ohkura, M., Tanaka, M., Oe, Y., Konno, A., Hirai, H., et al. (2016). Calcium imaging reveals glial involvement in transcranial direct current stimulation-induced plasticity in mouse brain. *Nat. Commun.* 7:11100. doi: 10.1038/ncomms11100

Müller, L., Tokay, T., Porath, K., Kohling, R., and Kirschstein, T. (2013). Enhanced NMDA receptor-dependent LTP in the epileptic CA1 area via upregulation of NR2B. *Neurobiol. Dis.* 54, 183–193. doi: 10.1016/j.nbd.2012.12.011

Oberheim, N. A., Tian, G. F., Han, X., Peng, W., Takano, T., Ransom, B., et al. (2008). Loss of astrocytic domain organization in the epileptic brain. *J. Neurosci.* 28, 3264–3276. doi: 10.1523/JNEUROSCI.4980-07.2008

Olabarria, M., Noristani, H. N., Verkhratsky, A., and Rodríguez, J. J. (2010). Concomitant astroglial atrophy and astrogliosis in a triple transgenic animal model of Alzheimer's disease. *Glia* 58, 831–838. doi: 10.1002/glia.20967

Oliet, S. H., Piet, R., and Poulain, D. A. (2001). Control of glutamate clearance and synaptic efficacy by glial coverage of neurons. *Science* 292, 923–926. doi: 10.1126/science.1059162

Ostroff, L. E., Manzur, M. K., Cain, C. K., and Ledoux, J. E. (2014). Synapses lacking astrocyte appear in the amygdala during consolidation of Pavlovian threat conditioning. *J. Comp. Neurol.* 522, 2152–2163. doi: 10.1002/cne.23523

Papouin, T., Henneberger, C., Rusakov, D. A., and Oliet, S. H. R. (2017). Astroglial versus neuronal D-serine: fact checking. *Trends Neurosci.* 40, 517–520. doi: 10.1016/j.tins.2017.05.007

Patrushev, I., Gavrilov, N., Turlapov, V., and Semyanov, A. (2013). Subcellular location of astrocytic calcium stores favors extrasynaptic neuron-astrocyte communication. *Cell Calcium* 54, 343–349. doi: 10.1016/j.ceca.2013.08.003

Paz, J. T., and Huguenard, J. R. (2015). Microcircuits and their interactions in epilepsy: is the focus out of focus? *Nat. Neurosci.* 18, 351–359. doi: 10.1038/nn.3950

Pekny, M., Pekna, M., Messing, A., Steinhäuser, C., Lee, J. M., Parpura, V., et al. (2016). Astrocytes: a central element in neurological diseases. *Acta Neuropathol.* 131, 323–345. doi: 10.1007/s00401-015-1513-1

Peng, W. F., Ding, J., Li, X., Fan, F., Zhang, Q. Q., and Wang, X. (2016). N-methyl-D-aspartate receptor NR2B subunit involved in depression-like behaviours in lithium chloride-pilocarpine chronic rat epilepsy model. *Epilepsy Res.* 119, 77–85. doi: 10.1016/j.eplepsyres.2015.09.013

Postnikova, T. Y., Zubareva, O. E., Kovalenko, A. A., Kim, K. K., Magazanik, L. G., and Zaitsev, A. V. (2017). Status epilepticus impairs synaptic plasticity in rat hippocampus and is followed by changes in expression of NMDA receptors. *Biochemistry* 82, 282–290. doi: 10.1134/S0006297917030063

Powell, G. E., and Percival, I. C. (1979). A spectral entropy method for distinguishing regular and irregular motion of Hamiltonian systems. *J. Phys. A Math. Gen.* 12, 2053. doi: 10.1088/0305-4470/12/11/017

Reichenbach, A., Derouiche, A., and Kirchhoff, F. (2010). Morphology and dynamics of perisynaptic glia. *Brain Res. Rev.* 63, 11–25. doi: 10.1016/j.brainresrev.2010.02.003

Rodríguez-Arellano, J. J., Parpura, V., Zorec, R., and Verkhratsky, A. (2016). Astrocytes in physiological aging and Alzheimer's disease. *Neuroscience* 323, 170–182. doi: 10.1016/j.neuroscience.2015.01.007

Rossi, D., Brambilla, L., Valori, C. F., Roncoroni, C., Crugnola, A., Yokota, T., et al. (2008). Focal degeneration of astrocytes in amyotrophic lateral sclerosis. *Cell Death Differ.* 15, 1691–1700. doi: 10.1038/cdd.2008.99

Rossi, D., and Volterra, A. (2009). Astrocytic dysfunction: insights on the role in neurodegeneration. *Brain Res. Bull.* 80, 224–232. doi: 10.1016/j.brainresbull.2009.07.012

Rosso, O. A., Blanco, S., Yordanova, J., Kolev, V., Figliola, A., Schürmann, M., et al. (2001). Wavelet entropy: a new tool for analysis of short duration brain electrical signals. *J. Neurosci. Methods* 105, 65–75. doi: 10.1016/S0165-0270(00)00356-3

Rosso, O. A., Larrondo, H. A., Martin, M. T., Plastino, A., and Fuentes, M. A. (2007). Distinguishing noise from chaos. *Phys. Rev. Lett.* 99:154102. doi: 10.1103/PhysRevLett.99.154102

Rusakov, D. A., Zheng, K., and Henneberger, C. (2011). Astrocytes as regulators of synaptic function: a quest for the Ca^{2+} master key. *Neuroscientist* 17, 513–523. doi: 10.1177/1073858410387304

Semyanov, A., and Godukhin, O. (1997). Kindling-like state in rat hippocampal CA1 slices induced by the repeated short-term extracellular K+ increases: The role of L-type Ca^{2+}-channels. *Neurosci. Lett.* 223, 177–180. doi: 10.1016/S0304-3940(97)13436-X

Sherwood, M. W., Arizono, M., Hisatsune, C., Bannai, H., Ebisui, E., Sherwood, J. L., et al. (2017). Astrocytic IP3 Rs: contribution to Ca^{2+} signalling and hippocampal LTP. *Glia* 65, 502–513. doi: 10.1002/glia.23107

Shih, P. Y., Savtchenko, L. P., Kamasawa, N., Dembitskaya, Y., Mchugh, T. J., Rusakov, D. A., et al. (2013). Retrograde synaptic signaling mediated by K+ efflux through postsynaptic NMDA receptors. *Cell Rep.* 5, 941–951. doi: 10.1016/j.celrep.2013.10.026

Sibille, J., Pannasch, U., and Rouach, N. (2014). Astroglial potassium clearance contributes to short-term plasticity of synaptically evoked currents at the tripartite synapse. *J. Physiol.* 592, 87–102. doi: 10.1113/jphysiol.2013.261735

Singh, N. A., Otto, J. F., Dahle, E. J., Pappas, C., Leslie, J. D., Vilaythong, A., et al. (2008). Mouse models of human KCNQ2 and KCNQ3 mutations for benign familial neonatal convulsions show seizures and neuronal plasticity without synaptic reorganization. *J. Physiol.* 586, 3405–3423. doi: 10.1113/jphysiol.2008.154971

Song, I., Volynski, K., Brenner, T., Ushkaryov, Y., Walker, M., and Semyanov, A. (2013). Different transporter systems regulate extracellular GABA from vesicular and non-vesicular sources. *Front. Cell. Neurosci.* 7:23. doi: 10.3389/fncel.2013.00023

Suárez, L. M., Cid, E., Gal, B., Inostroza, M., Brotons-Mas, J. R., Gómez-Domínguez, D., et al. (2012). Systemic injection of kainic acid differently affects LTP magnitude depending on its epileptogenic efficiency. *PLoS ONE* 7:e48128. doi: 10.1371/journal.pone.0048128

Tanaka, M., Shih, P.-Y., Gomi, H., Yoshida, T., Nakai, J., Ando, R., et al. (2013). Astrocytic Ca^{2+} signals are required for the functional integrity of tripartite synapses. *Mol. Brain* 6:6. doi: 10.1186/1756-6606-6-6

Thom, M. (2014). Review: Hippocampal sclerosis in epilepsy: a neuropathology review. *Neuropathol. Appl. Neurobiol.* 40, 520–543. doi: 10.1111/nan.12150

Tian, G. F., Azmi, H., Takano, T., Xu, Q., Peng, W., Lin, J., et al. (2005). An astrocytic basis of epilepsy. *Nat. Med.* 11, 973–981. doi: 10.1038/nm1277

Tong, J., Ang, L. C., Williams, B., Furukawa, Y., Fitzmaurice, P., Guttman, M., et al. (2015). Low levels of astroglial markers in Parkinson's disease: relationship to alpha-synuclein accumulation. *Neurobiol. Dis.* 82, 243–253. doi: 10.1016/j.nbd.2015.06.010

Van Der Walt, S., Schönberger, J. L., Nunez-Iglesias, J., Boulogne, F., Warner, J. D., Yager, N., et al. (2014). scikit-image: image processing in Python. *PeerJ* 2:e453. doi: 10.7717/peerj.453

Verkhratsky, A., and Nedergaard, M. (2014). Astroglial cradle in the life of the synapse. *Philos. Trans. R. Soc. Lond. B Biol. Sci.* 369:20130595. doi: 10.1098/rstb.2013.0595

Verkhratsky, A., and Nedergaard, M. (2018). Physiology of astroglia. *Physiol. Rev.* 98, 239–389. doi: 10.1152/physrev.00042.2016

Verkhratsky, A., and Parpura, V. (2016). Astrogliopathology in neurological, neurodevelopmental and psychiatric disorders. *Neurobiol. Dis.* 85, 254–261. doi: 10.1016/j.nbd.2015.03.025

Verkhratsky, A., Zorec, R., Rodriguez, J. J., and Parpura, V. (2017). Neuroglia: functional paralysis and reactivity in Alzheimer's disease and other neurodegenerative pathologies. *Adv. Neurobiol.* 15, 427–449. doi: 10.1007/978-3-319-57193-5_17

Villa, C., and Combi, R. (2016). Potassium channels and human epileptic phenotypes: an updated overview. *Front. Cell. Neurosci.* 10:81. doi: 10.3389/fncel.2016.00081

Wallraff, A., Köhling, R., Heinemann, U., Theis, M., Willecke, K., and Steinhäuser, C. (2006). The impact of astrocytic gap junctional coupling on potassium buffering in the hippocampus. *J. Neurosci.* 26, 5438–5447. doi: 10.1523/JNEUROSCI.0037-06.2006

Walz, W. (2000). Role of astrocytes in the clearance of excess extracellular potassium. *Neurochem. Int.* 36, 291–300. doi: 10.1016/S0197-0186(99)00137-0

Wang, F., Smith, N. A., Xu, Q., Fujita, T., Baba, A., Matsuda, T., et al. (2012). Astrocytes modulate neural network activity by Ca(2)(+)-dependent uptake of extracellular K(+). *Sci. Signal.* 5, ra26. doi: 10.1126/scisignal.2002334

Witcher, M. R., Kirov, S. A., and Harris, K. M. (2007). Plasticity of perisynaptic astroglia during synaptogenesis in the mature rat hippocampus. *Glia* 55, 13–23. doi: 10.1002/glia.20415

Wu, Y. W., Tang, X., Arizono, M., Bannai, H., Shih, P. Y., Dembitskaya, Y., et al. (2014). Spatiotemporal calcium dynamics in single astrocytes and its modulation by neuronal activity. *Cell Calcium* 55, 119–129. doi: 10.1016/j.ceca.2013.12.006

Zhang, Y., Cai, G. E., Yang, Q., Lu, Q. C., Li, S. T., and Ju, G. (2010). Time-dependent changes in learning ability and induction of long-term potentiation in the lithium-pilocarpine-induced epileptic mouse model. *Epilepsy Behav.* 17, 448–454. doi: 10.1016/j.yebeh.2010.02.008

Zhou, C., Lippman, J. J., Sun, H., and Jensen, F. E. (2011). Hypoxia-induced neonatal seizures diminish silent synapses and long-term potentiation in hippocampal CA1 neurons. *J. Neurosci.* 31, 18211–18222. doi: 10.1523/JNEUROSCI.4838-11.2011

Zhou, J. L., Shatskikh, T. N., Liu, X., and Holmes, G. L. (2007). Impaired single cell firing and long-term potentiation parallels memory impairment following recurrent seizures. *Eur. J. Neurosci.* 25, 3667–3677. doi: 10.1111/j.1460-9568.2007.05598.x

Zorec, R., Araque, A., Carmignoto, G., Haydon, P. G., Verkhratsky, A., and Parpura, V. (2012). Astroglial excitability and gliotransmission: an appraisal of Ca^{2+} as a signalling route. *ASN Neuro* 4:art:e00080. doi: 10.1042/AN20110061

Conflict of Interest Statement: The authors declare that the research was conducted in the absence of any commercial or financial relationships that could be construed as a potential conflict of interest.

frontiers in Molecular Neuroscience

REVIEW
published: 12 June 2018
doi: 10.3389/fnmol.2018.00204

Astroglial Modulation of Hydromineral Balance and Cerebral Edema

Yu-Feng Wang[1]* *and Vladimir Parpura*[2]*

[1]*Department of Physiology, School of Basic Medical Sciences, Harbin Medical University, Harbin, China,* [2]*Department of Neurobiology, The University of Alabama at Birmingham, Birmingham, AL, United States*

Maintenance of hydromineral balance (HB) is an essential condition for life activity at cellular, tissue, organ and system levels. This activity has been considered as a function of the osmotic regulatory system that focuses on hypothalamic vasopressin (VP) neurons, which can reflexively release VP into the brain and blood to meet the demand of HB. Recently, astrocytes have emerged as an essential component of the osmotic regulatory system in addition to functioning as a regulator of the HB at cellular and tissue levels. Astrocytes express all the components of osmoreceptors, including aquaporins, molecules of the extracellular matrix, integrins and transient receptor potential channels, with an operational dynamic range allowing them to detect and respond to osmotic changes, perhaps more efficiently than neurons. The resultant responses, i.e., astroglial morphological and functional plasticity in the supraoptic and paraventricular nuclei, can be conveyed, physically and chemically, to adjacent VP neurons, thereby influencing HB at the system level. In addition, astrocytes, particularly those in the circumventricular organs, are involved not only in VP-mediated osmotic regulation, but also in regulation of other osmolality-modulating hormones, including natriuretic peptides and angiotensin. Thus, astrocytes play a role in local/brain and systemic HB. The adaptive astrocytic reactions to osmotic challenges are associated with signaling events related to the expression of glial fibrillary acidic protein and aquaporin 4 to promote cell survival and repair. However, prolonged osmotic stress can initiate inflammatory and apoptotic signaling processes, leading to glial dysfunction and a variety of brain diseases. Among many diseases of brain injury and hydromineral disorders, cytotoxic and osmotic cerebral edemas are the most common pathological manifestation. Hyponatremia is the most common cause of osmotic cerebral edema. Overly fast

OPEN ACCESS

Edited by:
Christian Henneberger, Universität Bonn, Germany

Reviewed by:
Robert Zorec, University of Ljubljana, Slovenia
Sergey Kasparov, University of Bristol, United Kingdom

***Correspondence:**
Yu-Feng Wang
yufengwang@ems.hrbmu.edu.cn
Vladimir Parpura
vlad@uab.edu

Received: *04 February 2018*
Accepted: *22 May 2018*
Published: *12 June 2018*

Citation:
Wang Y-F and Parpura V (2018) Astroglial Modulation of Hydromineral Balance and Cerebral Edema. Front. Mol. Neurosci. 11:204. doi: 10.3389/fnmol.2018.00204

Abbreviations: Ang II, angiotensin II; ANP, atrial natriuretic peptide; AQP 4, aquaporin 4; BBB, blood-brain barrier; cAMP, cyclic adenosine 3′,5′-monophosphate; CVOs, circumventricular organs; ECM, extracellular matrix; ER, endoplasmic reticulum; ERK 1/2, extracellular signal-regulated kinase 1/2; FAK, focal adhesion kinase; GABA, γ-aminobutyric acid; GFAP, glial fibrillary acidic protein; HB, hydromineral balance; I/R, ischemia/reperfusion; MAPKs, mitogen-activated protein kinases; MNCs, magnocellular neuroendocrine cells; NCX, sodium-calcium exchanger; NKCC1, Na^+, K^+, 2 Cl^- and water cotransporter 1; NO, nitric oxide; NTS, nucleus of the tractus solitarii; OT, oxytocin; OVLT, organum vasculosum of the lamina terminalis; pERK 1/2, phosphorylated ERK 1/2; PKA, protein kinase A; PTN, protein tyrosine nitration; PVN, paraventricular nucleus; RAAS, renin-androgen-aldosterone system; RVD, regulatory volume decrease; RVI, regulatory volume increase; SFO, subfornical organ; SON, supraoptic nucleus; TRP channels, transient receptor potential channels; TRPC, TRP canonical channel; TRPV, TRP vallinoid channel; VP, vasopressin; VRAC, volume-regulated anion channel.

correction of hyponatremia could lead to central pontine myelinolysis. Ischemic stroke exemplifies cytotoxic cerebral edema. In this review, we summarize and analyze the osmosensory functions of astrocytes and their implications in cerebral edema.

Keywords: astrocytes, cerebral edema, osmosensation, osmotransduction, vasopressin

INTRODUCTION

Homeostasis of the internal environment is the prerequisite for normal activity of an organism and heavily depends on the hydromineral balance (HB) of the extracellular fluid. This balance is based on equivalent amounts of water drinking and salt intake vs. their excretion, and is commonly measured by the volume and osmolality of the extracellular fluid (Muhsin and Mount, 2016). Many factors have been implicated in regulation of HB, such as thirst, along with water- and salt-regulating hormones. Among hormones, vasopressin (VP, also called as antidiuretic hormone, ADH) released by hypothalamic neuroendocrine cells has been considered the most sensitive and powerful factor regulating HB (Kinsman et al., 2017). In response to increased osmotic pressure or reduced blood volume, VP release into the brain and blood increases significantly to surge reabsorption of water, thereby maintaining relative fidelity of the osmolality and volume of the brain and blood (Brown, 2016). However, maladapted response of this VP secretion can cause cerebral edema and threaten the life of patients, e.g., due to high intracranial pressure and the resultant brain herniation in hyponatremia (Wang et al., 2011) or ischemic stroke (Jia et al., 2016). Thus, understanding the mechanisms underlying neurohumoral regulation of VP secretion is critically important.

In neurohumoral regulation of VP neuronal activity, one of the most sensitive and important factors is astrocytic plasticity in the osmotic regulatory system (Wang and Zhu, 2014; Jiao et al., 2017). Astrocytes adjacent to neurons in the osmosensory system are sensitive to VP and can also influence VP secretion through their morphological and functional plasticity and produce other hormones that also regulate osmolality, while directly regulating local HB; of note, a variety of astrocytes in other brain areas are sensitive to VP (Simard and Nedergaard, 2004), a subject that is beyond the scope of the present review, however. Nonetheless, under pathological conditions, malfunctions of osmosensory mechanisms in astrocytes worsen hydromineral disorders by affecting the activity of VP neurons and other osmotic regulatory factors; these events lead to brain edema, neural degeneration and irreversible brain damages. In this review, we sum up our current understanding of astrocyte-associated osmosensation, osmotransduction and the resultant changes in the activity of the osmotic regulatory system, along with their implication in diseases involving disorders of HB.

OSMOTIC BALANCE AND ITS NEUROHUMORAL REGULATION

Homeostasis of the internal environment is under constant challenge of the external environment. Factors that can markedly change extracellular and intracellular fluid volume include ingestion and elimination of water and salts, hydromineral distribution across capillaries (e.g., within the blood vs. brain parenchyma/other organs) and, at the cellular level, across the plasma membrane. In response to these challenges, the endocrine system and the autonomic nervous system respond promptly to adaptively modulate the HB by regulating water and salts intake and elimination, as well as their distribution among different compartments of the body.

General Regulation of HB

Hydromineral regulation requires activation of the osmosensory system in conjunction with volemic regulation and is largely determined by a variety of neurohumoral factors. An increase in plasma osmolality draws water from cells and interstitium into the blood, causing dehydration, which activates specific brain osmoreceptors to stimulate drinking and release of VP from VP neurons. VP reduces water loss via increasing water reabsorption in the kidneys. In contrast, hypoosmotic challenge causes opposite reaction by VP neurons and the hydromineral regulation. Hypovolemia, a state of decreased blood volume, stimulates vascular volume sensors that signal brain centers to initiate drinking and VP release; it also stimulates baro/volume receptors in the kidneys to activate the renin-angiotensin (Ang)-aldosterone system (RAAS), which initiates drinking and VP release while increasing Na^+ reabsorption. By contrast, blood volume expansion or hypervolemia can lead to significant increase in plasma concentrations of atrial natriuretic peptide (ANP), oxytocin (OT), prolactin and corticosterone, to eliminate Na^+ and its bound water while suppressing hyperosmotic stimulation of VP secretion. In addition, osmotic challenge can lead to the production of gaseous neurotransmitters, which can affect neuronal secretion; e.g., nitric oxide (NO) inhibits (Stern and Ludwig, 2001), while carbon monoxide stimulates (Reis et al., 2012) VP secretion. The aforementioned factors and events, and likely many more, all work in concert so that the HB is maintained.

To achieve electroneutrality and volume stability of a cell, the sum of osmotically active particles, i.e., osmolytes, in the intracellular space must be equal to that in the extracellular space. As the major extracellular osmolyte, Na^+ in optimal extracellular concentration becomes the reference point for osmoreceptors to control thirst and VP secretion, RAAS activity, levels of natriuretic factors as well as the cell volume. The control over the cell volume is achieved by a chloride shift and by modulating the activity of Na^+/K^+-ATPase (Kurbel, 2008). Movement of water across the cell membranes occurs when an osmotic pressure gradient forms between the intracellular compartment and interstitial fluid. Large amounts of Na^+, Cl^- and HCO_3^- ions are present in the extracellular space

whereas K^+, Mg^{2+} and PO_4^{3-} ions are the major ions in the intracellular compartment. In most cells at rest, the plasma membrane exhibits relatively high permeability for K^+ and water, but not for Na^+ and Cl^-. Consequently, the distribution of fluid across the plasma membrane is determined mainly by the osmotic effect of Na^+ and Cl^-. Whenever osmotic gradients form, following disturbance of the electrochemical balance across the membranes, water will diffuse to the side of higher solute concentration, thereby maintaining intracellular fluid isotonic. The transport of ions and water across cell membranes has been reviewed recently elsewhere (Jia et al., 2016) and, hence, is not further discussed here.

Along with the effect on water balance, VP is also a critical modulator of the arterial diameter, which along with water reabsorption/distribution, determines the effective arterial volume. For instance, in the rat hypothalamic supraoptic nucleus (SON), hyperosmotic stimulation mainly led to vasodilatation followed by vasoconstriction (Du et al., 2015). The initial vasodilatation could be the result of both glial retraction and NO action at the blood vessels, while the later vasoconstriction phase results from VP-mediated activation of V1a VP receptor. By changing the arterial contractility and the blood pressure, VP can maintain irrigation pressure to provide sufficient nutrients to the brain and other important organs (**Figure 1**).

VP Neuronal Activity and its Neural Regulation

VP is an essential regulator of the HB. In the hypothalamus, there are several neuroendocrine nuclei that contain VP neurons. These cells are primarily located in the SON and the paraventricular nucleus (PVN); they are mainly magnocellular neuroendocrine cells (MNCs) releasing VP into the blood and brain. In addition, there are also parvocellular VP neurons in the parvocellular section of the PVN that release VP to regulate the activity of the autonomic nervous system and a variety of brain activities (Hou et al., 2016). In patients with central diabetes insipidus, the lack of VP production causes thirst (polydipsia) and excessive excretion of urine (polyuria) because of a dysfunction in the thirst mechanism, development of hyponatremia and the ensuing complications (Sailer et al., 2017).

The effects of osmotic challenges on VP neuronal activity and VP secretion depend on both external factors and the intrinsic features of these neurons (**Figure 1**). Classically, neural regulation is considered the major factor modulating VP neuronal activity during osmotic challenges (**Figure 1A**). Brain regions around the circumventricular organs (CVOs) and the nucleus of the tractus solitarii (NTS) are the major source of neural inputs and regulation of VP neuronal activity (Wang et al., 2011; McKinley et al., 2015). The CVOs are highly vascularized brain areas lacking a normal/tight blood-brain barrier (BBB). These organs/structures include (but are not limited to) the subfornical organ (SFO), the organum vasculosum of the lamina terminalis (OVLT) and the area postrema. They are the sites allowing communication between the blood plasma and the interstitium of the brain parenchyma, as their fenestrated capillaries are freely permeable to ions and water. Neural inputs

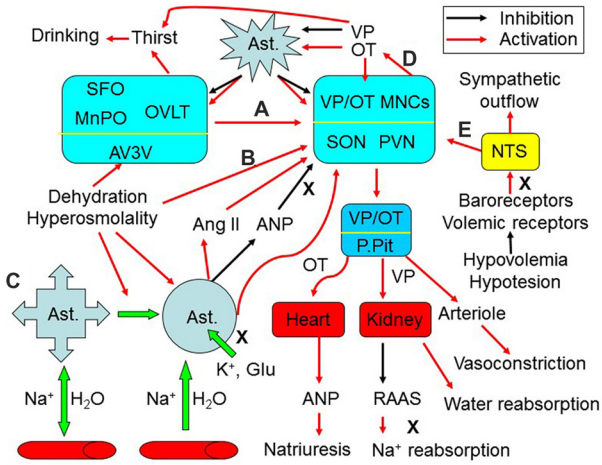

FIGURE 1 | Extrinsic modulation of hydromineral balance (HB). The sketch shows that hyperosmotic stress modulates HB by the following approaches. **(A)** Activating the subfornical organ (SFO), organum vasculosum of the lamina terminalis (OVLT) and the medial preoptic nucleus (MnPO) in the anteroventral-third ventricle (AV3V) area, which in turn activates magnocellular cells. i.e., vasopressin (VP) and oxytocin (OT) neurons in the supraoptic (SON) and paraventricular (PVN) nuclei. **(B)** Changing activity of VP neurons after the osmolality is increased in brain parenchyma. **(C)** Causing retraction of astrocyte (Ast.) processes from the areas surrounding the osmosensory neurons, which increases the excitability of VP neurons by removing the physical barriers between adjacent neurons and by increasing extracellular levels of K^+, glutamate (Glu) and angiotensin II (Ang II), and by reducing extracellular levels of atrial natriuretic peptide (ANP) or brain natriuretic peptide. **(D)** Resultant increases in intrahypothalamic release of OT can activate VP neurons through eliciting the retraction of astrocytic processes, while VP inhibits this retraction by increasing aquaporin expression. **(E)** In addition, hypovolemia or hypotension can increase VP release from the posterior pituitary (P.Pit) by reducing the baroreflex through the nucleus of the tractus solitarii (NTS) and by decreasing activity of the renin–angiotensin–aldosterone system (RAAS), while increasing the sympathetic output. As a result, serum osmotic pressure gets reduced and blood volume/pressure rises through increasing water reabsorption and natriuresis. See text for details.

from the NTS can relay hypovolemic/hypotensive information to the CVOs while directly modulating VP neuronal activity to correct fluid deficits (Miyata, 2015). However, CVOs and the NTS do not regulate the HB directly; rather, they convey osmotic and volemic messages to VP neurons. Among the CVOs, the SFO can sense and integrate hydromineral signals in responses to osmotic, volumetric and cardiovascular challenges, and integrate information from circulating signals of the metabolic status (Hindmarch and Ferguson, 2016). Moreover, VP neurons can also be regulated by other brain regions involved in the integration of circulatory and fluid information (McKinley and McAllen, 2007). Activation of neurons in these brain areas, which include the lateral parabrachial nucleus, the midbrain raphe nuclei, the medial preoptic nucleus and the septum, increases VP neuronal activity in the SON and PVN, and VP secretion that modulates kidney functions and arteriole contractility, along with activation of the anterior cingulate cortex and insula to cause thirst and resultant water drinking (Macchione et al., 2015). The efficiency of the above neuronal inputs on VP neuronal activity depends on astrocytic plasticity

and the neurochemical environment surrounding VP neurons (Wang and Zhu, 2014).

Astrocytic Regulation of HB

In the extrinsic modulation of VP neuronal activity, astrocytic plasticity plays an important role in local and systemic HB (Wang et al., 2011). Astrocytes are the sensors of neuronal activity while detecting humoral information from the blood at the CVOs (Farmer et al., 2016). The responsive changes of astrocytes, i.e., their plasticity, in turn modulate VP neuronal activity, VP secretion and thirst.

Similar to the modulatory role of astrocytes in neuronal activity (Simard and Nedergaard, 2004), astrocytic morphological plasticity is also essential for the integrity of the neurovascular unit. Of note, the neurovascular unit is a functional unit comprised of capillary endothelial cells, along with surrounding neurons, and non-neuronal cells such as pericytes and astrocytes. Malfunction of astrocytes can change the structural integrity of this unit and subsequently disturb the HB across the BBB and the transport of metabolites, ions, varieties of organic molecules and water between the brain and the blood (Wang and Parpura, 2016).

Astrocytic Morphological Plasticity and VP Neuronal Activity

In osmosensation, astrocytes exhibit remarkable morphological plasticity (**Figure 1C**). It was observed that after exposing cell culture to a hypoosmotic solution, astrocytes swell within 30 s and then undergo a regulatory volume decrease (RVD; Eriksson et al., 1992) following the opening of anion channels and release of organic osmolytes. Conversely, when exposed to a hyperosmotic solution, astrocytes shrink first and then exhibit a regulatory volume increase (RVI; Eriksson et al., 1992). This dual morphological plasticity, occurring during acute hypo- or hyper-osmolality, provides astrocytes with unique capacity to keep the extracellular volume stable while differentially regulating extracellular osmolality. Regulatory volume changes could occur in a microdomain specific manner or as a result of intracellular volume redistribution; that is, an expansion of astrocytic processes with a reduced size of astrocytic somata and vice versa (Choe et al., 2016).

Different from the RVI and RVD mentioned above, when exposed to a gradual osmolality decrease, some cells use the mechanism of isovolumetric regulation to adapt to the hypoosmotic challenge without dramatically changing their volume. The apparent isovolumetry is due to the coordinated extrusion of osmolytes, whereby following an early efflux of taurine (2-aminoethanesulfonate$^-$) and Cl^-, a delayed K^+ efflux occurs, as shown in cerebellar astrocytes (Ordaz et al., 2004). These diverse volemic regulatory machineries endow astrocytes with the ability to directly sense and regulate HB in local brain parenchyma.

An example of astrocytic involvement in osmotic regulation is the osmotic response of the SON during osmotic challenges. Plastic change in the morphology of the SON and PVN is a responsive feature to hydromineral disturbance, which is particularly dramatic in the SON during dehydration. As previously reviewed (Hatton, 2002), during dehydration or salt (hypertonic) water drinking, astrocytes show retraction of their processes along with hypertrophic changes in VP neurons. This retraction of astrocytic processes from the surroundings of VP neurons increases the interaction between neurons through interneuronal/dendritic gap junctions and preponderance of synaptic connections, thereby increasing the excitability of VP neurons and promoting synchronous release of VP. To the contrary, hypoosmotic challenges can inhibit VP neuronal activity by evoking the expansion of astrocytic processes, wedging them in between neuronal dendrites and lessening dendritic gap junctional connectivity. These changes reduce direct interactions between adjacent VP neurons, while increasing astrocytic uptake of extracellular K^+ and glutamate; opposite effects are seen during hyperosmotic stress. Correspondingly, VP neurons become more excitable during hyperosmotic stress and inhibited during acute hypoosmotic challenges.

It is worth to notice that during chronic hyperosmotic stimulation, VP release remains at high levels. This is likely due to increased VP synthesis as well as increased release probability of VP packaged in secretory vesicles, along with increased OT-mediated excitation (**Figure 1D**). It has been reported that during chronic hypernatremia, VP and OT mRNA levels increase twofold along with hypertrophy of VP neurons and increased release of VP (Glasgow et al., 2000). Moreover, this condition also causes an activity-dependent depolarizing drift in the chloride reversal potential and abolition of inhibitory pathways, which is prevented by blocking central OT receptors (Kim et al., 2011), suggesting that hyperosmotic stress increased OT receptor signaling that is responsible for the reversal of GABAergic inhibition. Consistently, OT can excite VP neurons (Wang and Hatton, 2006) while exerting autoregulatory effect on OT neuronal activity (Wang et al., 2006; Wang and Hatton, 2007a,b). Thus, the maintenance of high level of VP release during chronic hyperosmotic stimulation is at least partially supported by an increase of OT release. Noteworthy is that the excitatory effect of OT on VP neurons takes minutes to occur, and thus is highly unlikely a direct effect on OT receptors on VP neurons, but most likely an indirect effect due to a retraction of astrocyte processes in the SON caused by OT (Wang and Hatton, 2009; Wang et al., 2017).

Astrocytes of the SON have the ability to change the osmosensory threshold within the local neural circuitry during chronic hypoosmotic challenges, as previously reviewed elsewhere (Wang et al., 2011). That is, the sensitivity of osmosensors to hypoosmotic challenge gradually wears off during continuous stimulation; correspondingly, the initial inhibitory reaction vanishes during prolonged presence of hypoosmotic environment. This notion is partly supported by the recovery of firing rate of VP neurons after initial hypoosmotic inhibition, which is based on dual astrocytic morphological plasticity, i.e., extension and subsequent retraction of astroglial processes during the initial decrease in firing rate of VP neurons followed by its recovery, respectively (Wang et al., 2013a,b).

Taken together, astrocytic morphological plasticity can modulate the activity of osmosensory neurons (OS neurons),

which in turn changes astrocytic plasticity, thereby forming a functional heterocellular network in central osmosensation (**Figure 1**).

Astrocytic Functional Plasticity and VP Neuronal Activity

Accumulating evidence reveals that astrocytes are not just a passive buffer of extracellular environment, but also an active modulator of neuronal activity (**Figure 1C**). Astrocytic modulation of VP neuronal activity is closely related to its ability to take-up neurotransmitters from the extracellular space (Wang et al., 2013a,b) as well as to produce, release and take-up gliotransmitters to modulate interneuronal communication (Parpura et al., 2004; Montana et al., 2006; Ni et al., 2007). As the source of glutamate in the SON (Ponzio et al., 2006), astrocytes can excite OS neurons, including VP neurons during hyperosmotic stimulation. Moreover, the presumed reduction in uptake of β-alanine by astrocytes in the SON can inhibit GABA transporters and subsequently increase extracellular GABA levels (Park et al., 2006; Wang et al., 2013a). Therefore, astrocytes can actively alter the neurochemical environment and modulate the activity of OS neurons. Of note, cultured astrocytes from different brain regions can release various other gliotransmitters using multiple underlying mechanisms and in response not only to hypoosmotic challenge but also to an array of neurotransmitters and modulators (Malarkey and Parpura, 2009). Whether a palette of gliotransmitters, released by astrocytes elsewhere, could be released by astrocytes in the SON in times of osmotic challenge and whether that would lead to modulation of synaptic transmission in the SON remain to be determined.

ASTROCYTIC INTERACTION WITH HORMONES THAT REGULATE OSMOLALITY

While astrocytes can directly regulate thirst and maintain the integrity of neurovascular units, they also directly interact with hormones that regulate osmolality, including VP, Ang II, aldosterone, natriuretic peptide, OT and hormones in the hypothalamic-pituitary-adrenal axis. Thus, astrocytes can modulate the effect of hormones on osmotic regulation of HB (**Figure 1C**).

Astrocytes and VP

It has been reported that hyperosmotic stimulation increases VP release in the brain (Ludwig et al., 2005). VP in the brain can evoke thirst and drinking (Abrão Saad et al., 2004), while increased levels of VP in the blood increase water reabsorption in the kidney by changing water channel activity (Tamma et al., 2017). In addition, VP can antagonize diuresis and natriuretic role of ANP (Lipari et al., 2007), thereby limiting ANP's natriuretic effect. As a result, VP is both an antagonizing agent of hypovolemia or hyperosmolality and a facilitator of hyponatremia; excess release of VP may result in water retention and pathophysiological hyponatremia.

VP is a major facilitator of cell swelling in the brain, which involves several local pathways. VP can increase intracellular osmolality by uptake of Na^+, K^+, 2 Cl^- or by lack of extrusion of Na^+ via activating Na^+, K^+, 2 Cl^- and water cotransporter 1 (NKCC1) or via inhibiting the activity of Na^+/K^+-ATPase, respectively (Hertz et al., 2017). In addition, VP is also a major activator of astrocytic water channel protein, aquaporin 4 (AQP4) by activating V1a type of VP receptor (Niermann et al., 2001). Inhibition of VP1a receptor leads to decrease in AQP-4 expression and prevents brain edema after port-traumatic injury (Marmarou et al., 2014). Thereby, VP could facilitate cell swelling when intracellular osmotic pressure is higher than that of the extracellular fluid.

Astrocytes and RAAS

Along with water reabsorption/excretion mediated by VP secretion, the sodium-retaining function of the RAAS makes a critical contribution to extracellular Na^+ levels and osmolality. In the central nervous system, the RAAS acts mainly through the sensory CVOs, in particular the area postrema, to activate brain neural pathways that elevate blood pressure, release VP and aldosterone, increase renal sympathetic nerve activity, and increase the ingestion of water and Na^+ to restore Na^+ loss to the environment (Geerling and Loewy, 2008). In these processes, Ang II binds to the brain Ang type 1 receptor to stimulate thirst, Na^+ appetite and secretion of VP and OT (Felgendreger et al., 2013; Almeida-Pereira et al., 2016). The prolonged Ang type 1 receptor blockade caused rebound increase in levels of Ang II and VP secretion to compensate for hypovolemia in association with reduced ANP plasma concentrations (Araujo et al., 2013). These findings are in agreement with the classical function of the RAAS in Na^+ balance.

Astrocytes are a major source of the Ang II precursor protein angiotensinogen and Ang II in the brain (Hermann et al., 1988); expression of receptors for Ang was also identified in the rat and monkey astrocytes (Garrido-Gil et al., 2017). Thus, astrocytes could exert self- modulation during osmotic challenges. This notion is supported by the observation that following 7 and 14 days of 2% NaCl (N.B., isotonic solution contains 0.9% NaCl) in drinking water, a significant increase in Ang II precursor, preproangiotensinogen mRNA was detected in astrocytes in regions of the anterior hypothalamus, including the PVN, the medial preoptic area and medial preoptic nucleus, while a decrease was observed in astrocytes in the SON (Ryan and Gundlach, 1997). These results, consistent with a recent report (Dominguez-Meijide et al., 2017), indicate that astrocytes could increase levels of extracellular Ang II to regulate thirst, while Ang II facilitation of VP release is reduced during prolonged hyperosmotic stimulation.

Astrocytes and Natriuretic System

In contrast with the sodium-retaining functions of the RAAS, natriuretic peptides, such as ANP, brain natriuretic peptide, and OT, belong to the "natriuretic system." OT neurons in the hypothalamus can be activated simultaneously with VP neurons during dehydration or hypertonic stimulation. However, OT exerts a natriuretic function, which plays a synergistic role in

maintaining HB with VP-increased water reabsorption following hyperosmotic stimulation. Similar to the modulation of VP neurons in hydromineral disturbance, astrocytic plasticity also strongly influences OT secretion from the SON and PVN (Yuan et al., 2010). In addition, during blood volume expansion, OT is secreted from the posterior pituitary into circulation to activate atrial OT receptors in the heart and promote ANP release. ANP diminishes VP-induced water reabsorption while exerting natriuretic and diuretic actions in the kidney (Gutkowska et al., 2014; Theilig and Wu, 2015), thereby reducing blood volume.

In the brain, ANP-mRNA is present in the hypothalamic suprachiasmatic nucleus, and ANP appears in both the SON and suprachiasmatic nucleus (Lipari et al., 2007). At the cellular level, ANP is present in and exocytotically released from membrane-bound vesicles as shown in cultured rat cortical astrocytes (Krzan et al., 2003; Chatterjee and Sikdar, 2013). Centrally released ANP can inhibit osmotically evoked VP and OT release through presynaptic inhibition of glutamate release from the OVLT. It has been reported that ANP application to rat hypothalamic explants did not affect depolarizing responses of VP neurons to local hypertonicity. However, ANP reversibly abolished the synaptic excitation of MNCs after hypertonic or electrical stimulation of the OVLT (Richard and Bourque, 1996). The inhibition of VP release following activation of ANP neurons can lead to diuresis, and decreased adrenocorticotropin release and blood pressure (Gutkowska et al., 1997). In addition, central ANP release is also increased by glucocorticoids (Lauand et al., 2007) and estradiol (Vilhena-Franco et al., 2011) in response to osmotic/volemic stimulation. Thus, astrocytic ANP can contribute to reducing hydromineral overload under various physiological states.

Other Effects

Hormonal cross talks and receptor-receptor interactions are common phenomena in brain control of HB. For instance, estradiol acts mainly on the VP neurons in response to water deprivation, potentiating VP neuronal activation and VP secretion without altering VP mRNA expression (Vilhena-Franco et al., 2016). Bradykinin, thyrotropin-releasing hormone, neurotensin and opioids (Irazusta et al., 2001), as well as secretin (Bai et al., 2017) and prolactin (Seale et al., 2012), are also implicated in neurohumoral regulation of HB and their expressions are likely regulated by astrocytes. Lastly, astrocytes can participate in the synthesis of many hormones that, under different osmotic conditions, regulate osmolality by differential expression of peptidases involved in the maturation and degradation of peptide (pro)hormones and neuropeptides. For example, in water-loaded rats, prolyl endopeptidase was decreased in the brain cortex (Irazusta et al., 2001). Thus, astrocytes can participate in HB by catabolizing humoral factors as well. These lines of evidence indicate that astrocytes could contribute to the HB through multiple hormones.

OSMOSENSATION BY ASTROCYTES

Homeostasis of the internal environment largely depends on neurohumoral regulation of the central osmosensory system. As reviewed recently (Jiao et al., 2017), the key feature of osmosensation is the activation of mechanoreceptors, particularly vallinoid and canonical types of transient receptor potential channels (TRPV and TRPC, respectively), both of which are highly permeable to Ca^{2+}. Indeed, the activation of these TRP channels increases cytosolic Ca^{2+} levels in osmosensory cells, including VP neurons, and triggers a series of secondary reactions. For example, hypotonic stimulus induces intracellular Ca^{2+} elevations through TRP channels, which then trigger AQP1 translocation and activation (Conner et al., 2012). The activation of TRP channels relies on changes in cell volume, membrane stretch and cytoskeletal reorganization as well as the hydration status of the extracellular matrix (ECM) and activity of integrins in a spatiotemporal dependent manner. In this process, astrocytic plasticity plays a key role since acute hyperosmotic stimulus-induced Fos expression in neurons depends on activation of astrocytes in the SON of rats (Yuan et al., 2010). Moreover, disabling astrocytic plasticity also blocked the rebound excitation of VP neurons in response to hypoosmotic challenges (Wang et al., 2013a,b). Thus, astrocytes could be a prominent component of the osmosensory system and could be more sensitive to the osmotic challenges than neurons are.

Characteristics of Osmosensation

Osmosensation is not a simple result of activation or inactivation of the stretch-activated channels (Cheng et al., 2017). To fully understand the participation of astrocytes in osmosensation, it is necessary to analyze the characteristics of osmosensation by the central osmosensory system.

Osmosensation Is Time-Dependent Process

In an organism, osmosensation is a dynamic process in temporal domain, as outlined below using two examples. (1) Chronic hyperosmotic stress weakens $GABA_A$ receptor-mediated synaptic inhibition of VP and OT secretion in rat hypothalamic MNCs (Kim et al., 2011). That is, hyperosmotic stress caused a profound depolarizing shift in the reversal potential of GABAergic response (E_{GABA}) in MNCs. This E_{GABA} shift was associated with increased expression of NKCC1 in MNCs and was blocked by the NKCC inhibitor bumetanide. (2) In response to hyposmolality challenge, VP neurons in the SON show a transient inhibition of firing activity followed by a rebound excitation (Wang et al., 2013a,b), which can partially account for the rebound increase in VP release after initial inhibition in response to hyponatremic challenges (Yagil and Sladek, 1990). It is likely that the initial osmosensory response involves Ca^{2+}-activated K^+ channels and, the BK and SK types of K^+-selective ion channels (Ohbuchi et al., 2010), leading to elimination of action potentials and to hyperpolarization of membrane potentials, while the latter phase could be a result of RVD-related activation of the volume-regulated anion channel (VRAC) and Cl^- efflux (Muraki et al., 2007; Hübel and Ullah, 2016). Taken together, these findings indicate the presence of a diversity of mechanisms underlying temporal dynamics in osmosensation.

Osmosensation Is Related to the Spatial Location of Osmosensory Cells

Mechanosensitive ion channels could function differently at different loci. For instance, excitation of the OVLT neurons elicited by hyperosmotic stress was not affected by the deletion of TRPV 4 but was abolished in cells lacking TRPV 1 (Ciura et al., 2011). Thus, TRPV1 likely plays a dominant role in OVLT sensation of hyperosmotic stress; however, hyperosmolality-sensitive TRPV4 (Liedtke and Friedman, 2003) could carry out the same function at other loci. Moreover, same TRPV channels at different loci could have different sensitivity to osmotic challenges. For example, cell and cell nuclear sizes in the SON were increased or decreased with hyperosmolality or hypoosmolality, respectively. However, both conditions did not affect those sizes in the medial habenular nucleus *in vivo* (Zhang et al., 2001), although this brain area also expresses TRPV1 and TRPV4 (Ishikura et al., 2015). Furthermore, hyperosmotic glucose or urea solutions activate VP neurons but not CVO neurons (Ho et al., 2007). These findings indicate existence of spatial diversity in osmosensation.

Roles of Various Ion Channels in Osmosensation Might be Interchangeable

In classical view, sensation of osmotic pressure is the matter of activation or inhibition of stretch-activated cation channels, (Prager-Khoutorsky and Bourque, 2015). Besides the TRP channels discussed above, other mechanical ion channels have been implicated in osmosensation, such as TMEM63 proteins found in *Arabidopsis* (Zhao et al., 2016), acid-sensing ion channel 3 in the intervertebral disc (Uchiyama et al., 2007), mammalian TRP ankyrin-1 and TRP melastatin-8 channels (Soya et al., 2014). It is possible that once one ion channel is dysfunctional (Taylor et al., 2008; Ciura et al., 2011), other ion channels with similar responsive features could easily compensate this deficit and thus maintain the osmosensory ability.

Osmoreceptors in Astrocytes

As stated above, the traditional theory of neuron dominance in osmosensation could not entirely explain findings presented above and, thus, the osmosensory ability of astrocytes needs to be considered in the operation of the osmosensory system.

AQP4 and Water Transport

Astrocytic volume change and subsequent morphological plasticity are essential for astrocytic regulation of local HB and VP neuronal activity (Theodosis et al., 2008; Wang and Zhu, 2014), the latter of which heavily relies on AQP4 expression and activity in astrocytes (Wang and Parpura, 2016).

In the rodent brain, AQP4 is the predominant form of specific water channel protein expressed in astrocytes; it is essential for quick water transport between intracellular and extracellular compartments when osmotic gradients are present (Xu et al., 2017). As previously reported, volemic change is essential for osmosensation as it changes the interaction between cytoskeletal elements and osmosensitive TRP channels (Prager-Khoutorsky and Bourque, 2015). Moreover, the expanded astrocyte processes promote releasing gliotransmitters and neuromodulators, metabolizing neural active substance, and transporting content of the interstitial fluid to the blood vessels (Parpura and Verkhratsky, 2012; Zorec et al., 2012) and thus exert the effect of osmosensation while maintaining the HB in the brain. The osmolality-associated AQP4 permeability determines astrocytic morphological plasticity, which can change the activity of their adjacent OS neurons independent of the activity of TRP channels, thereby making individual TRP channel type replaceable in osmosensation.

The participation of AQP4 in osmotic regulation is a dynamic process. It has been observed that the expression of AQP4 increased during chronic hyperosmotic stress (Yang et al., 2013). By contrast, hypoosmotic stimulation increases water influx through AQP4 due to increased osmotic gradient across cell membranes. This latter effect is not due to increase in AQP4 membrane installation but in its permeability to water (Potokar et al., 2013). It is possible, however, that there is a transient increase in AQP4 expression, or a reduction in its catabolism, at the early stage of hypoosmotic stimulation because levels of AQP4 are found to rapidly increase or decrease; these changes are accompanied by expansion and retraction of astrocyte processes in rat SON, respectively (Wang and Hatton, 2009).

Ion Channel Activity

Neurons in the CVOs and the MNCs in the SON and PVN, all important for thirst and urination, are also the target of astrocytic plasticity, which is related to alteration of astrocytic ion channel activity. In addition to the extensively identified astrocyte involvement in osmotic regulation of VP neuronal activity in the SON, astrocytes are also Na^+ sensors. Namely, Na_x, an atypical Na^+ channel and Na^+-level sensor, is found located in perineuronal lamellate processes extending from ependymal cells and astrocytes in the CVOs; astrocytes isolated from the SFO were sensitive to an increase in the extracellular Na^+ level (Noda, 2007).

Another important osmosensory machinery in astrocytes is the expression of TRP channels. Astrocytes are known to express many types of osmosensitive TRP channels. For example, TRPV1 has been identified at thick cellular processes of astrocytes in the CVOs, and intravenous administration of a TRPV1 agonist resiniferatoxin induced Fos expression in astrocytes in the OVLT, SFO and area postrema (Mannari et al., 2013). The resultant Ca^{2+} influx following activation of TRP channels is not only associated with astrocytic volemic change but also related to neuromodulation through releasing glutamate, and this transmitter can modulate neuronal activity at extrasynaptic sites (Parpura et al., 2017). Thus, Na_x channels and TRPV1 channels in astrocytes can sense Na^+ levels in bodily fluids (Noda, 2007), particularly in the blood, as well as in the interstitium of the osmotic regulatory system, and in turn convert hydromineral message to neuronal activity, thereby maintaining the HB. The different types of TRP channel expression in astrocytes and its association with different types of OS neurons endow some of the spatial features of the osmosensory system.

Osmolyte Transport and its Coupling to AQP4

Transporting osmolytes is essential for HB between intra- and extracellular spaces and involves the redistribution of osmolytes through ion transporters and channels.

The function of AQP4 is coordinated with a variety of closely associated osmolyte transporters. As reviewed recently (Wang and Parpura, 2016), AQP4 is colocalized and/or assembled with the TRPV4, Kir4.1/Kir5.1, connexin 43, glutamate transporter-1, metabotropic glutamate receptor 5, and Na^+/K^+-ATPase, mainly at astrocytic endfeet. Along with changes in AQP4 activity, there are also alterations in non-selective cation currents, K^+ and Na^+ transmembrane activity, and glutamate uptake and metabolism. In addition, many other molecules are also involved in this process, including: (1) channels, such as Ca^{2+} release-activated Ca^{2+} channel, voltage gated K^+ channels, sulfonylurea 1/TRP melastatin-4 ion channel; (2) carriers including Na^+, Cl^- cotransporter, NKCC, Na^+/H^+ exchangers, Cl^-/HCO_3^- exchanger, acid-sensing ion channel 1a, Na^+-glucose cotransporter, and glutamate transporters; (3) receptor-coupled channels such as ionotropic AMPA and NMDA types of glutamate receptors, and $GABA_A$ receptor; and (4) Na^+/K^+-ATPase or sodium pump, as reviewed recently (Jia et al., 2016). Lastly, epithelial Na^+ channel (Miller and Loewy, 2013) and VRAC (Hussy et al., 2000) are also involved in astrocyte regulation of HB.

In astrocytes, there is NKCC-mediated $Na^+/K^+/Cl^-$ inward flux evoked by elevated extracellular K^+. The increase in clearance of extracellular K^+ during neuronal excitation is initially performed by Na^+/K^+-ATPase-mediated K^+ uptake into astrocytes; at K^+ concentrations above ∼10 mM this process is aided by uptake of Na^+, K^+ and 2 Cl^- via the cotransporter NKCC1. This activity allows subsequent K^+ release via the inward rectifying K^+ channel Kir4.1, perhaps after syncytial buffering (Walz, 1992), i.e., trans-astrocytic connexin-mediated K^+ transfer. Since the Na^+/K^+-ATPase exchanges 3 Na^+ with 2 K^+, it creates extracellular hypertonicity and cell shrinkage; however, hypertonicity stimulates NKCC1 and can also cause RVI to minimize ionic disequilibrium due to asymmetric Na^+/K^+-ATPase fluxes (Hertz et al., 2013).

Astrocytic ECM

The ECM represents an essential component of osmosensation (Jiao et al., 2017). In response to hydromineral disbalance, the ECM can quickly detect changes in extracellular cation levels and then transmit this message to other components of the osmosensors, including integrins, cell adhesion molecules and cytoskeletal elements. Integrins can transduce hydromineral signals from extracellular to intracellular compartments by activation of TRP channels via integrin-linked kinase and actin, as previously discussed (Jiao et al., 2017). In the SON and PVN, neural cell adhesion molecule, which gets decorated with various amounts of sialic acid, can significantly influence cell adhesion and thus allows astrocyte processes to expand or retract (Theodosis et al., 2008).

The ECM-integrin bonding is modulated by both cell volume and hydration state of the ECM in osmotic stress. Under different osmotic conditions, signaling process modulated by integrin-ECM contacts is either activated or inhibited. As observed in the SON, hyperosmotic stress caused by increasing NaCl concentration can decrease polysialic acid-neural cell adhesion molecule complex content (Schmelzer and Miller, 2002) and increases extracellular volume (Perkins et al., 2017). The changes in the astrocytic ECM (Pierre et al., 2001) could further activate astrocytic TRP channels through integrins (Song and Dityatev, 2018). In contrast, their decrease promotes reactive gliosis or expansion of astrocytic processes that reduces neuronal excitability (Theodosis et al., 2008), at least transiently (Jiao et al., 2017). These features endow astrocytes with the ability to detect osmotic changes in the internal environment. It is likely that changes in extracellular osmolality activate TRP channels, which increases intracellular Ca^{2+}, changes glial fibrillary acidic protein (GFAP) polymerization state and AQP4 distribution at the plasma membrane, leading to astrocytic morphological and functional plasticity.

GFAP Plasticity

The typical morphological feature of astrocytes during hydromineral disturbance is the plastic changes in the expression of GFAP, which determines not only the morphology, but also the function of astrocytes (Wang and Parpura, 2016). As the retraction and expansion of astrocytic processes take place, depolymerization/disassembling and polymerization/assembly of GFAP also occur, correspondingly; these events translocate GFAP-associated functional molecules, such as glutamine synthetase, AQP4 and actin, to (GFAP assembly) and from (GFAP disassembly) astrocyte processes surrounding adjacent neurons, thereby changing the uptake rate of extracellular neurochemical, their transport, conversion and/or release. As a result, neuronal activity is also changed as discussed below.

Hypotonic stimulation of the SON caused transient inhibition of VP neuronal activity (Wang et al., 2013a,b) and VP release (Yagil and Sladek, 1990), which were followed by recovery of the firing activity of VP neurons and rebound of VP secretion. These phenomena were accompanied with an initial increase in GFAP expression followed by a decrease in its expression, and were blocked by gliotoxin, L-aminoadipic acid. Importantly, GFAP increase was accompanied with simultaneous increase in the expression of glutamine synthetase and redistribution of this enzyme toward peripheral processes. This subcellular relocalization of glutamine synthetase to astrocytic processes (vs. soma) reflects upon an increased astrocytic ability to cause a shift in excitation-inhibition by decreasing extracellular concentrations of glutamate (as per increases conversion of glutamate to glutamine in astrocytes) and resulting in suppression of VP neuronal activity. Conversely a subsequent decrease in GFAP was associated with a decrease in membrane installation of GFAP-associated proteins and their functions (Wang et al., 2013a,b), including that of glutamine synthetase, resulting in an increase of extracellular levels of glutamate. Through this GFAP plasticity, astrocytes can adaptively exert their influence on the activity of VP and other OS neurons via differently localizing their functional proteins and changing neurochemical environment.

MECHANISMS UNDERLYING OSMOTRANSDUCTION IN ASTROCYTES

Activation of osmosensory cells is only the beginning of the osmosensory reaction to hydromineral disturbance. Osmosensation in the osmosensory system initiates osmotransduction that is responsible for osmotic adaptation process. The osmotransduction involves a complex set of signaling processes that are responsible for astrocytic plasticity under osmotic stress (**Figures 2A–C**). In this process, changes in GFAP and AQP4 expression are critical events, linked to diverse signaling cascades.

Transduction of Hyperosmotic Signals

Hyperosmotic stress can activate a variety of signaling molecules (**Figure 2B**). We provide a contemporary analysis of the spatiotemporal distribution of signaling molecules and their interactions; this analysis can aid better understanding of signaling cascades responsible for the transduction of different osmotic information in astrocytes. Several lines of evidence reveal that cellular effects of osmotic stress are commonly associated with intracellular Ca^{2+} mobilization and activation of mitogen-activated protein kinases (MAPKs) including c-Jun NH2-terminal kinase, p38 MAPK and extracellular signal-regulated kinase 1/2 (ERK 1/2; **Figures 2A–C**).

ECM-Integrin and Kinase Pathways

When osmotic stress acts on cell surface glycocalyx, integrin-mediated cell-matrix adhesion forms, cytoskeleton reorganizes, and focal adhesion kinase (FAK)-ERK1/2-c-Jun signaling axis gets activated, leading to the upregulation of interstitial collagenase, i.e., matrix metalloproteinase 13 (MMP-13) expression in rats (Horiguchi et al., 2011).

Hyperosmotic activation of the above pathway has dual effect on cellular events. The protective effect of integrins is clearly associated with phosphorylation/activation of FAK (Lunn and Rozengurt, 2004). In astrocytes, it has been reported that ECM binding to integrins can activate FAK, which is colocalized with actin stress fibers at sites of focal adhesion complexes (Rutka et al., 1999). An important downstream signal of FAK is phosphorylated ERK 1/2 (pERK 1/2) that is both essential for the activation of TRP channels during hyperosmotic stimulation (Prager-Khoutorsky and Bourque, 2015) and for GFAP polymerization. As reported, integrin-mediated ECM adhesions and cytoskeleton organization activate the FAK-ERK signaling axis, leading to upregulation of MMP expression and increased cell motility (Shi et al., 2011), a condition favoring astrocyte process retraction during hyperosmotic stimulation (Theodosis et al., 2008). Consistently, FAK signaling can promote organizing filamentous actin into parallel bundles (Rutka et al., 1999), which can interact with GFAP through calponin 3 (Plantier et al., 1999) and fascin (Mondal et al., 2010). Since an increase in this molecular association occurs during astrocyte retraction along with GFAP reduction (Wang and Hatton, 2009), the activation of FAK signaling could account for the astrocyte retraction following hyperosmotic stimulation, at least at the initial stage.

It is worth noting that increase in pERK 1/2 is essential for GFAP polymerization in the SON; however, pERK 1/2 is likely expressed in an undetectable level in astrocytes in the SON during hyperosmotic stimulation (Dine et al., 2014). Thus, the promoting effect of pERK 1/2 on GFAP polymerization could

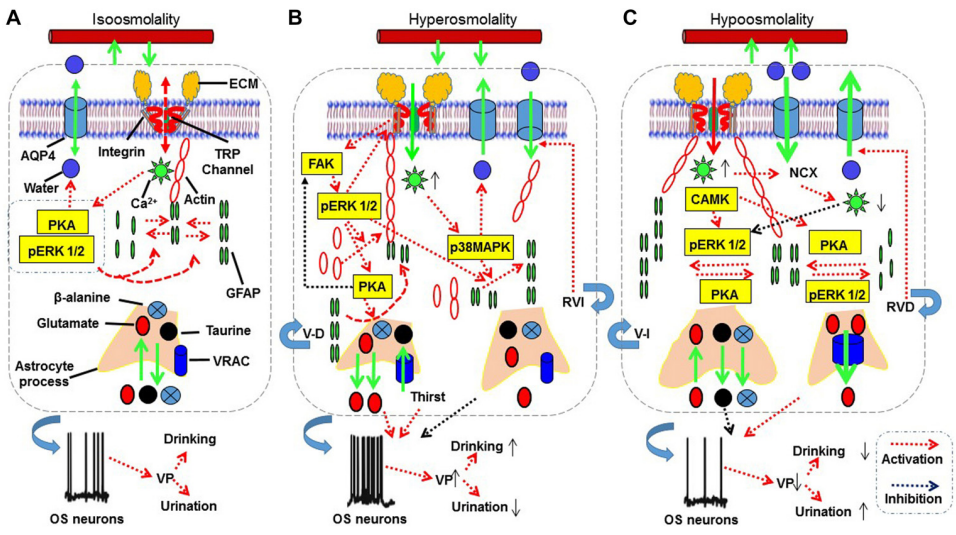

FIGURE 2 | The proposed mechanisms underlying astrocytic sensation and transduction of osmotic signals. **(A–C)** The signaling processes for isosmotic **(A)**, hyperosmotic **(B)** and hypoosmotic **(C)** conditions, respectively. The abbreviations are: AQP4, aquaporin4; CAMK, calmodulin kinase; ECM, extracellular matrix; FAK, focal adhesion kinase; GFAP, glial fibrillary acidic protein; MAPKs, mitogen-activated protein kinases; NCX, sodium-calcium exchanger; OS neuron, osmosensory neurons; pERK 1/2, phosphorylated extracellular signal-regulated kinase 1/2; PKA, protein kinase A; RVD, regulatory volume decrease; RVI, regulatory volume increase; TRP, transient receptor potential; V-D, volume decrease; V-I, volume increase; VRAC, volume-regulated anion channel. See text for details.

be minimal. Alternatively, activation of FAK-ERK 1/2 signaling could be restrained to the somata of astrocytes since pERK 1/2 promotion of GFAP polymerization has strong feature of microdomain-specificity (Wang et al., 2017). Lastly, pERK 1/2 signaling could be an upstream signal of protein kinase A (PKA) that can inhibit FAK activation (Padmanabhan et al., 1999) while increasing AQP4 permeability (Song and Gunnarson, 2012) and GFAP depolymerization in the SON (Wang et al., 2017).

It has been reported that cyclic adenosine 3′,5′-monophosphate (cAMP)-associated signaling is a component of the hyperosmotic signals. Salt-loaded rats had elevated levels of cAMP in the SON within 2 days of drinking 2% NaCl saline. Similarly, increasing medium osmolality from 290 to 325 mOsm/kg increased cAMP levels in the SON in rat explant culture (Carter and Murphy, 1989). Furthermore, increased cAMP promotes bovine VP gene expression (Pardy et al., 1992) through cAMP-PKA-CREB signaling (McCabe and Burrell, 2001). Albeit not directly demonstrated, one might expect that increased levels of cAMP would lead to increased expression-polymerization/assembly of GFAP in the SON, as it has been demonstrated in cultured astrocytes from mouse visual cortex (Gottipati et al., 2012). Taken together, it is very likely that a microdomain specific expression of pERK 1/2 and PKA is responsible for the GFAP-associated astrocytic plasticity during osmotic stress.

Cytosolic Ca^{2+} Levels and Associated Signaling Molecules

A direct effect of activating ECM-integrin signaling is the opening of TRPV channels, which causes increases in intracellular Ca^{2+} level. In turn, Ca^{2+} increase can activate MAPKs through Rho-type small G-protein (Kino et al., 2010), and osmotic stress further promotes couplings of activated Rho-type small G-proteins with c-Jun NH2-terminal kinase-interacting protein 4 to cascade components of the p38 MAPK signaling pathway. This signaling stimulates the expression of nuclear factor of activated T-cells 5, a transcription factor which regulates the expression of genes involved in the osmotic stress (Lee et al., 2011). Moreover, the activation of p38 MAPK also increases AQP4 expression (Salman et al., 2017), particularly following hyperosmotic stimulation (Arima et al., 2003), which facilitates water efflux from intracellular compartment to the extracellular space. Ca^{2+} signaling is also associated with GFAP plasticity (Chatterjee and Sikdar, 2013), which could also been mediated by p38 MAPK in addition to pERK 1/2 (Li et al., 2017). Indeed, in a mouse model of the middle cerebral artery occlusion, p38 MAPK activation was observed in the glial scar area, while in culture hypoxia and scratch injury-induced astrogliosis was attenuated by both p38 inhibition and knockout of p38 MAPK (Roy Choudhury et al., 2014); p38MAPK activation was associated with increased GFAP expression. Since increase in GFAP expression along with its associated astrocytic processes expansion does not occur at the initial stage of hyperosmotic stimulation, the GFAP increase could be a secondary reaction occurring before the RVI. Lastly, Ca^{2+} signaling can contribute to the RVI by antagonizing a PKA-mediated increase in AQP4 permeability (Song and Gunnarson, 2012), which is supposed to further reduce water loss in the presence of higher extracellular osmolality. However, detailed regulation of GFAP reduction and astrocyte retraction following hyperosmotic stimulation remains to be explored.

Pro-inflammatory and Apoptotic Pathway

Chronic and severe hyperosmotic challenges can cause maladaptation of astrocytes and consequently result in detrimental responses of the osmosensory system. Uncontrolled hyperosmotic stress-elicited TRPV1 channel activation increases release of cytokines interleukin-6 and interleukin-8 which could result from transactivation of epidermal growth factor receptor, MAPK, and nuclear factor kappa-light-chain-enhancer of activated B cells activation (Cavet et al., 2011). Moreover, hyperosmotic saline also acts via MMP9 that binds to the low-density lipoprotein receptor-related protein-1, triggers the phosphorylation of ERK 1/2, and induces down-regulation of the perineurial barrier-forming tight junction protein claudin-1 (Hackel et al., 2012). The activation of MAPKs can also evoke cell apoptosis. For example, hyperosmotic stress-induced apoptosis is mediated by p38 MAPK, c-Jun NH2-terminal kinase and activating AP-1 transcription complex, and manifests with acceleration of cytochrome c release and caspase-3 activation (Ben Messaoud et al., 2015). Thus, hyperosmotic stress could cause systemic inflammation and apoptosis if dehydration or hypertonic stress is not corrected promptly.

Hypoosmotic Signals

Under hypoosmotic challenges, cell swelling and the ensuing RVD could involve a series of cellular and molecular events, which lead to adaptive changes in astrocytic morphology (**Figure 2C**).

Cytosolic Ca^{2+}, pERK1/2 and GFAP Plasticity

Hypoosmolality initially causes mild cell swelling that activates Ca^{2+}-permeable cation channels such as TRPV 4 (Benfenati et al., 2007) and leads to transient Ca^{2+} influx into the cells (Sato et al., 2013). The Ca^{2+} influx along with increased membrane stretch triggers Ca^{2+} release from intracellular stores (Borgdorff et al., 2000). This elevation in intracellular Ca^{2+} is essential for an increase in formation of GFAP filaments (González et al., 2007; Salazar et al., 2008) and a hypoosmotic volume increase (Ebner et al., 2006). Hypoosmolality-elicited Ca^{2+}/calmodulin signaling can increase the expression of pERK1/2 that is likely responsible for Ca^{2+}-associated cell swelling because chelation of extracellular Ca^{2+} also abolished pERK 1/2 increases under hypoosmotic conditions, while blocking the phosphorylation of ERK 1/2 significantly reduced cell swelling and the ensuing RVD, as shown in trout hepatocytes (Ebner et al., 2006). Importantly, prolonged hypoosmotic challenge *in vitro* was found to evoke only transient intracellular Ca^{2+} increase that was followed by a long decrease in Ca^{2+} levels (Sánchez-Olea et al., 1993), likely due to the activation of plasmalemmal Na^{+}-Ca^{2+} exchangers as shown in mouse odontoblasts (Sato et al., 2013). In the SON, the pERK1/2-associated GFAP polymerization and the elongation of

astrocytic processes (Wang et al., 2017) appears as a short-lasting (minutes) event, which could be reversed by some subsequent event that causes GFAP depolymerization, such as PKA activation (Wang et al., 2017). The causal association between GFAP depolymerization and hypoosmolality-evoked RVD in chronic hypoosmotic challenges remains to be elucidated.

Cellular Signaling and RVD

Following Ca^{2+} influx and mobilization of intracellular Ca^{2+} store, high cytosolic Ca^{2+} levels lead to further cell swelling and RVD (Mola et al., 2015). In this process, calmodulin kinase plays a key role since intracellular application of monoclonal anti-calmodulin antibody blocked hypoosmotic activation of VRAC opening in rat cerebral astrocytes (Olson et al., 2004). Moreover, p38 MAPK is involved in the occurrence of RVD in hypoosmotic environment (Ebner et al., 2006). Whether these signals are directly linked to RVD remains to be explored.

Interestingly, PKA activation is associated with increased activation of VRAC and efflux of taurine and Cl^- from astrocytes with redistribution of actin network, i.e., its disruption at the somata, while concentrated at foci corresponding to the tips of the cell projections retracted by swelling (Moran et al., 2001). Moreover, actin cytoskeleton and microtubule are important for astrocyte swelling and they may form a barrier for the efflux of taurine and Cl^- since the presence of dense actin network can impede the flow of ions and water (Lange, 2000; Platonova et al., 2015).

Effects of Hypoosmotic Signals on Neuronal Activity

Accompanying the above signaling events and the resultant morphological changes, astrocytes could change neuronal activity through releasing gliotransmitters. The initial hypoosmotic inhibition of VP neuronal activity is associated with the increased availability of extracellular β-alanine, presumably through the reduction in its uptake (Johnston and Stephanson, 1976); the increased level of this non-essential amino acid then inhibits plasmalemmal GABA transporters and subsequently increases extracellular GABA levels (Park et al., 2006). The rebound excitation of VP neurons during hypoosmolality-evoked RVD is associated with the failure of GABAergic inhibition (Wang et al., 2013a) and coordinated D-serine signaling between astrocytes and MNCs in the SON to increase both NMDA receptor activation and VP neuronal activity (Wang et al., 2013b). In addition, the release of ATP from astrocytes during cell swelling could also contribute to the rebound excitation of neurons that are initially inhibited by hypoosmolality (Förster and Reiser, 2016) by activating ATP-sensitive K^+ channel (Thomzig et al., 2003). Lastly, hypoosmotic challenge-evoked taurine release through VRAC is also involved in the transmission of osmotic information. In the SON, taurine is released from astrocytes in an osmolality-dependent manner (Choe et al., 2012) and acts on glycine receptors to inhibit VP neuronal activity (Hussy et al., 2000). However, this effect is reversible during prolonged hypoosmotic challenges (Song and Hatton, 2003). The summary of potential mechanisms underlying astrocyte sensation and transduction of osmotic signals are outlined in **Figure 2**.

ASTROCYTES AND INTRACELLULAR CEREBRAL EDEMA

Cerebral edema is a common outcome when excess fluid is accumulated in the intracellular or extracellular space of the brain due to brain trauma or hydromineral disorder. According to the extent of the BBB disruption, cerebral edema can be divided into two types: (1) Cerebral edema with BBB disruption, which includes both vasogenic and interstitial edemas, featuring extracellular retention of water and Na^+; and (2) Cerebral edema without the BBB disruption, which includes cytotoxic and osmotic edemas, both of which feature intracellular swelling. Astrocytic plasticity is involved in brain edemas. Pathogenesis of vasogenic and interstitial edemas was recently reviewed (Jia et al., 2016; Wang and Parpura, 2016), so was the involvement of maladaptive ion transport in the occurrence of cerebral edema (Stokum et al., 2016); ionic edema is usually associated with cytotoxic edema, where water and ions exit capillaries into the brain interstitium. Thus, in this review we further explore the mechanisms underlying astrocyte-associated cytotoxic edema and osmotic edema.

Hyponatremia and Cerebral Edema

Hyponatremia is the most common clinical electrolyte disorder. When Na^+ plasma concentration falls more than several mmol/L below normal level, hyponatremia occurs (Kleindienst et al., 2016), and is associated with decompensated heart failure, hepatic cirrhosis with ascites formation, renal failure, inappropriate intravenous transfusion, and cancer-associated syndrome of inappropriate antidiuretic hormone secretion. Hyponatremia due to loss of NaCl occurs as a consequence to diarrhea and vomiting, overuse of diuretics, certain types of Na^+-wasting kidney diseases and Addison's disease with reduced aldosterone (Muñoz et al., 2010; Raimann et al., 2017). Hyponatremia creates an abnormal osmotic pressure gradient across the BBB and plasma membrane, which drives movement of water into the brain parenchyma and leads to osmotic cerebral edema (Walcott et al., 2012; Voets and Maas, 2018). The subsequent water intoxication leads to astrocytic swelling and RVD, which further disturb the activity of osmotic regulating system.

Hyponatremia-evoked cerebral edema likely delivers signals through the following process. As reported, excessive Ca^{2+} influx through TRPV4 predisposes Müller glial cells of the retina to activation of Ca^{2+}-dependent proapoptotic signaling pathways (Ryskamp et al., 2011). In glial cells of nematodes, it was also identified that osmotic stress induces massive protein aggregation coupled with unfolded protein response and endoplasmic reticulum (ER) stress (Gankam-Kengne et al., 2017); adequate protein folding is a tightly regulated process that requires proper intracellular ionic strength and it is necessary for normal cell function. Prolonged hyponatremia along with the activation of proapoptotic pathways could similarly cause damages to mammalian astrocytes. During RVD, the reversal of glutamate transporters and anion channel opening could increase glutamate release (Milanese et al., 2009). A sustained low extracellular sodium ion

concentration decreased glutamate uptake by astrocytes and elevated extracellular glutamate concentration (Fujisawa et al., 2016). The release of glutamate from astrocytes can activate extrasynaptic NMDA receptors (Araque et al., 1998) to increase spontaneous synaptic transmission which can lead to an increase in production of NO (Kenny et al., 2018). Prolonged accumulation of NO could cause protein tyrosine nitration (PTN), damage the oxidative phosphorylation and trigger apoptosis in astrocytes (Raju et al., 2015). As a result, astrocyte uptake mechanism, e.g., for glutamate, can be disrupted, leading to the accumulation of the extracellular glutamate, and consequently increased VP neuronal activity and VP secretion as previously reviewed (Wang et al., 2011; Jia et al., 2016). However, since PTN is only possible with NO levels way in excess of what can be expected from either neuronal or epithelial NOS under strong hyperosmotic stimulus, the PTN-associated apoptosis in astrocytes is most likely a result of activation of inducible NOS as discussed in the pathogenesis of cardiac injury (Wang et al., 2018).

It is important to note that MNCs in the SON remain functional during dehydration and ischemic stroke because of down-regulation of NMDA glutamate receptor (Currás-Collazo and Dao, 1999), and neuroprotection by glia and vascular/perivascular cells (Currás-Collazo et al., 2002).

Central Pontine Myelinolysis

Central pontine myelinolysis is an osmotic demyelization syndrome often occurring during overly rapid correction of chronic hyponatremia with hypertonic saline infusion or using VP receptor antagonist. Astrocytes play an essential role in its development. As reported in rat models, massive astrocyte death occurred after rapid correction of hyponatremia. Astrocyte death caused a disruption of the astrocyte-oligodendrocyte network, rapidly upregulated inflammatory cytokines genes, and increased serum S100β, which predicted clinical manifestations and outcome of osmotic demyelination (Gankam Kengne et al., 2011). Treatment of hyponatremia with non-peptide VP receptor antagonists (vaptans) or hypertonic saline resulted in a higher mortality rate, when compared to treatment with urea, because of osmotic breakdown of the BBB, microglia activation, astrocyte demise and demyelination (Gankam Kengne et al., 2015). Moreover, astrocytes in central pontine myelinolysis were small, and exhibited fewer and shorter processes than perilesional astrocytes (Popescu et al., 2013) in addition to the loss of AQP4 in astrocytes within demyelinating lesions (Takagi et al., 2014). The damage of astrocytes is associated with imbalance between protein synthesis and degradation which can induce ER stress and cell death. As reported, rapid correction of chronic hyponatremia induces severe alterations in proteostasis, i.e., the biogenesis, folding, trafficking and degradation of proteins present within and outside the cell. The alterations are characterized by diffuse protein aggregation, ubiquitination and ER stress accompanied by increased autophagic activity and apoptosis in astrocytes within regions previously shown to be demyelinated in later stages of this syndrome (Gankam-Kengne et al., 2017). These results indicate that osmotic demyelination during severe osmotic stress might be a consequence of the failure of proteostasis. Furthermore, these results support a model for the pathophysiology of osmotic brain injury in which rapid correction of hyponatremia triggers apoptosis in astrocytes followed by a loss of trophic communication between astrocytes and oligodendrocytes, secondary inflammation, microglial activation and finally demyelination.

Ischemic Cerebral Edema

The cytotoxic cerebral edema results from disruption in cellular metabolism and cellular retention of sodium and water due to poisoning or hypoxia. Hypoxia-associated cytotoxic cerebral edema is often observed in ischemic cerebral stroke (Jia et al., 2016), traumatic brain injury (Burda et al., 2016), cerebral palsy (Thomas et al., 2004) and cardiac arrest (Hirko et al., 2008). Astrocytes are critical contributors in this process, as typically observed in ischemic stroke (Wang and Parpura, 2016).

In the ischemic cerebral edema, a disruption of ionic and neurotransmitter homeostasis plays a pivotal role, particularly the accumulation of K^+ and glutamate in the extracellular space. The activation of astrocytic NKCC1 by highly increased extracellular K^+ concentrations and hypoxic inhibition of Na^+/K^+-ATPase form conditions promoting influx of $Na^+/K^+/Cl^-$, while inhibiting efflux of K^+ and Cl^- through K^+ and Cl^- co-transporter (Wilson and Mongin, 2018). During reperfusion following initial ischemia in the stroke, with the activation of Na^+/K^+-ATPase, more Na^+ release than K^+ uptake occurs in a 3:2 ratio, which drives NKCC1 to move more ions into the cell, leading to the development of cytotoxic cell swelling (Wang and Parpura, 2016). All these pathological processes are associated with malfunctioned uptake machinery for K^+ and glutamate (Steiner et al., 2012; Yan et al., 2016) and fluid volume transfer through AQP4 (Anderova et al., 2014) by astrocytes during ischemic stroke. Additionally, there is an increased level of extracellular VP during ischemic stroke (Jia et al., 2016). This notion is supported by a clinical observation that continuous intravenous infusion with conivaptan, a non-peptide antagonist of V1a and V2 VP receptors, for 48 h after experimental stroke reduces brain edema and BBB disruption (Zeynalov et al., 2015). Thus, in this process, damaged astrocytes and malfunctioned VP neurons could form a vicious cycle to worsen ischemic brain damages.

The disruption of ionic/neurotransmitter homeostasis is derived from reduced delivery of nutrients to the brain, in particular glucose and oxygen. In this process, disorders of many interacting molecular pathways in astrocytes, particularly TRPV2 activation-associated Ca^{2+} overload, are implicated. As reported in rat cortical astrocytes, oxygen-glucose deprivation followed by reoxygenation treatment enhanced the expression of TRPV2 and increased intracellular Ca^{2+} level (Zhang et al., 2017), which could disrupt normal functions involving mitochondria, ER, and nucleus, leading to cell damage.

Under physiological conditions, mitochondrial activity depends on increases in cytosolic Ca^{2+}, from the extracellular space or from the ER, which is taken up by mitochondria through specialized contact sites between the ER and mitochondria known as mitochondrial-associated ER membranes. The coordination of these Ca^{2+} pools is required to synchronize

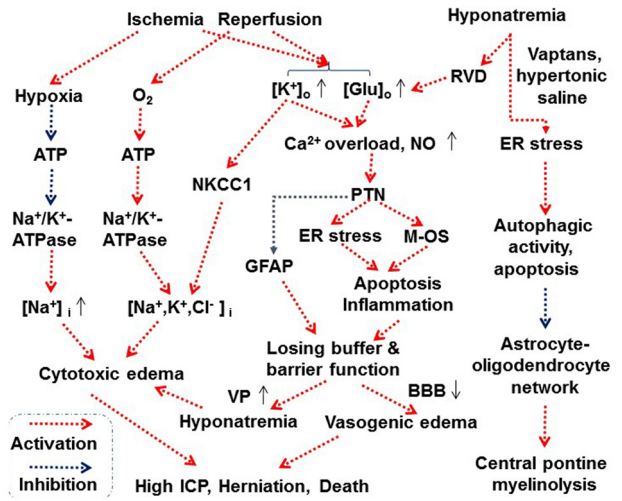

FIGURE 3 | Scheme depicting proposed astrocytes-associated mechanisms underlying cerebral edema. Abbreviations: BBB, blood-brain barrier; ER, endoplasmic reticulum; Glu, glutamate; ICP, intracranial pressure; M-OS, mitochondrial oxidative stress; NKCC1, Na^+, K^+, 2 Cl^- and water cotransporter 1; NO, nitric oxide; PTN, protein tyrosine nitration. See text for details. Other annotations refer to **Figures 1**, **2**.

mitochondrial respiration rates and ATP synthesis to meet physiological demands (Schäfer et al., 2014). However, serious hypoxia and glucose deprivation during ischemic stroke could cause strong mobilization of intracellular Ca^{2+} stores, ER stress, mitochondrial Ca^{2+} overload and oxidative stress in astrocytes (Hori et al., 2002; Ouyang et al., 2011), leading to inflammatory reaction and apoptosis. In this process, abnormal RVD following initial astrocytic swelling could create a hyperosmotic environment (Wang and Parpura, 2016) to cause inflammation (Cavet et al., 2011) and astrocytic apoptosis (Ben Messaoud et al., 2015), leading to irreversible brain damage.

It is worth to notice that a knockout of AQP4 yielded contradictory reports, some claiming reduction in post-traumatic edema (Shi et al., 2012; Wu et al., 2014) while the others just the opposite Hirt et al. (2017). It is possible that AQP4 is differentially involved in different types of cerebral water balance. By slowing the rate of water entry into brain, AQP4-null mice could be protected from cytotoxic brain edema induced by water intoxication, brain ischemia, or meningitis. By contrast, by reducing the rate of water outflow from brain parenchyma, AQP4 deletion could aggravate vasogenic brain edema caused by tumor, cortical freeze, intraparenchymal fluid infusion, or brain abscess (Papadopoulos and Verkman, 2007). However, the detailed mechanisms underlying this controversy remain to be explored. **Figure 3** summarizes the mechanisms underlying astrocytes-associated cerebral edema.

CONCLUSION

Malfunctions of astrocytes have been observed in many diseases in addition to those that are directly associated with hydromineral disorders, such as epilepsy (Losi et al., 2016), neuroinflammatory demyelinating disease (Verkman, 2012), Canavan disease (Clarner et al., 2014), Huntington's disease (Hsiao et al., 2014), amyotrophic lateral sclerosis (Ramírez-Jarquín et al., 2017), and post-traumatic syringomyelia (Najafi et al., 2016). Understanding of the involvement of astrocytes in neurohumoral modulation of HB and astrocytic mechanisms underlying cerebral edema will provide important references for clarification of all the pathogenesis of these diseases. Consequently, specific therapeutic targets might be identified with the perspectives of prevention of disease development and improvement of their prognosis.

AUTHOR CONTRIBUTIONS

Y-FW wrote the first draft. Y-FW and VP designed this topic and edited the manuscript.

FUNDING

This work was supported by the National Natural Science Foundation of China (Grant No. 31471113, Y-FW), the higher education talents funds of Heilongjiang province (Grant No. 002000154, Y-FW) and by the Civitan International McNulty Award (VP).

REFERENCES

Abrão Saad, W., Antonio De Arruda Camargo, L., Sérgio Cerri, P., Simões, S., Abrão Saad, G., Garcia, G., et al. (2004). Influence of arginine vasopressin receptors and angiotensin receptor subtypes on the water intake and arterial blood pressure induced by vasopressin injected into the lateral septal area of the rat. *Auton. Neurosci.* 111, 66–70. doi: 10.1016/j.autneu.2003.08.013

Almeida-Pereira, G., Coletti, R., Mecawi, A. S., Reis, L. C., Elias, L. L., and Antunes-Rodrigues, J. (2016). Estradiol and angiotensin II crosstalk in hydromineral balance: role of the ERK1/2 and JNK signaling pathways. *Neuroscience* 322, 525–538. doi: 10.1016/j.neuroscience.2016.02.067

Anderova, M., Benesova, J., Mikesova, M., Dzamba, D., Honsa, P., Kriska, J., et al. (2014). Altered astrocytic swelling in the cortex of α-syntrophin-negative GFAP/EGFP mice. *PLoS One* 9:e113444. doi: 10.1371/journal.pone.0113444

Araque, A., Sanzgiri, R. P., Parpura, V., and Haydon, P. G. (1998). Calcium elevation in astrocytes causes an NMDA receptor-dependent increase in the frequency of miniature synaptic currents in cultured hippocampal neurons. *J. Neurosci.* 18, 6822–6829. doi: 10.1523/JNEUROSCI.18-17-06822.1998

Araujo, I. G., Elias, L. L., Antunes-Rodrigues, J., Reis, L. C., and Mecawi, A. S. (2013). Effects of acute and subchronic AT1 receptor blockade on cardiovascular, hydromineral and neuroendocrine responses in female rats. *Physiol. Behav.* 122, 104–112. doi: 10.1016/j.physbeh.2013.08.018

Arima, H., Yamamoto, N., Sobue, K., Umenishi, F., Tada, T., Katsuya, H., et al. (2003). Hyperosmolar mannitol simulates expression of aquaporins 4 and 9 through a p38 mitogen-activated protein kinase-dependent pathway in rat astrocytes. *J. Biol. Chem.* 278, 44525–44534. doi: 10.1074/jbc.M304368200

Bai, J. J., Tan, C. D., and Chow, B. K. C. (2017). Secretin, at the hub of water-salt homeostasis. *Am. J. Physiol. Renal Physiol.* 312, F852–F860. doi: 10.1152/ajprenal.00191.2015

Ben Messaoud, N., Katzarova, I., and López, J. M. (2015). Basic properties of the p38 signaling pathway in response to hyperosmotic shock. *PLoS One* 10:e0135249. doi: 10.1371/journal.pone.0135249

Benfenati, V., Amiry-Moghaddam, M., Caprini, M., Mylonakou, M. N., Rapisarda, C., Ottersen, O. P., et al. (2007). Expression and functional characterization of transient receptor potential vanilloid-related channel 4 (TRPV4) in rat cortical astrocytes. *Neuroscience* 148, 876–892. doi: 10.1016/j.neuroscience.2007.06.039

Borgdorff, A. J., Somjen, G. G., and Wadman, W. J. (2000). Two mechanisms that raise free intracellular calcium in rat hippocampal neurons during hypoosmotic and low NaCl treatment. *J. Neurophysiol.* 83, 81–89. doi: 10.1152/jn.2000.83.1.81

Brown, C. H. (2016). Magnocellular neurons and posterior pituitary function. *Compr. Physiol.* 6, 1701–1741. doi: 10.1002/cphy.c150053

Burda, J. E., Bernstein, A. M., and Sofroniew, M. V. (2016). Astrocyte roles in traumatic brain injury. *Exp. Neurol.* 275, 305–315. doi: 10.1016/j.expneurol.2015.03.020

Carter, D. A., and Murphy, D. (1989). Cyclic nucleotide dynamics in the rat hypothalamus during osmotic stimulation: *in vivo* and *in vitro* studies. *Brain Res.* 487, 350–356. doi: 10.1016/0006-8993(89)90839-1

Cavet, M. E., Harrington, K. L., Vollmer, T. R., Ward, K. W., and Zhang, J. Z. (2011). Anti-inflammatory and anti-oxidative effects of the green tea polyphenol epigallocatechin gallate in human corneal epithelial cells. *Mol. Vis.* 17, 533–542.

Chatterjee, S., and Sikdar, S. K. (2013). Corticosterone treatment results in enhanced release of peptidergic vesicles in astrocytes via cytoskeletal rearrangements. *Glia* 61, 2050–2062. doi: 10.1002/glia.22576

Cheng, B., Lin, M., Huang, G., Li, Y., Ji, B., Genin, G. M., et al. (2017). Cellular mechanosensing of the biophysical microenvironment: a review of mathematical models of biophysical regulation of cell responses. *Phys. Life Rev.* 22–23, 88–119. doi: 10.1016/j.plrev.2017.06.016

Choe, K. Y., Olson, J. E., and Bourque, C. W. (2012). Taurine release by astrocytes modulates osmosensitive glycine receptor tone and excitability in the adult supraoptic nucleus. *J. Neurosci.* 32, 12518–12527. doi: 10.1523/JNEUROSCI.1380-12.2012

Choe, K. Y., Prager-Khoutorsky, M., Farmer, W. T., Murai, K. K., and Bourque, C. W. (2016). Effects of salt loading on the morphology of astrocytes in the ventral glia limitans of the rat supraoptic nucleus. *J. Neuroendocrinol.* 28:4. doi: 10.1111/jne.12370

Ciura, S., Liedtke, W., and Bourque, C. W. (2011). Hypertonicity sensing in organum vasculosum lamina terminalis neurons: a mechanical process involving TRPV1 but not TRPV4. *J. Neurosci.* 31, 14669–14676. doi: 10.1523/JNEUROSCI.1420-11.2011

Clarner, T., Wieczorek, N., Krauspe, B., Jansen, K., Beyer, C., and Kipp, M. (2014). Astroglial redistribution of aquaporin 4 during spongy degeneration in a Canavan disease mouse model. *J. Mol. Neurosci.* 53, 22–30. doi: 10.1007/s12031-013-0184-4

Conner, M. T., Conner, A. C., Bland, C. E., Taylor, L. H., Brown, J. E., Parri, H. R., et al. (2012). Rapid aquaporin translocation regulates cellular water flow: mechanism of hypotonicity-induced subcellular localization of aquaporin 1 water channel. *J. Biol. Chem.* 287, 11516–11525. doi: 10.1074/jbc.M111.329219

Currás-Collazo, M. C., and Dao, J. (1999). Osmotic activation of the hypothalamo-neurohypophysial system reversibly downregulates the NMDA receptor subunit, NR2B, in the supraoptic nucleus of the hypothalamus. *Mol. Brain Res.* 70, 187–196. doi: 10.1016/s0169-328x(99)00129-1

Currás-Collazo, M. C., Patel, U. B., and Hussein, M. O. (2002). Reduced susceptibility of magnocellular neuroendocrine nuclei of the rat hypothalamus to transient focal ischemia produced by middle cerebral artery occlusion. *Exp. Neurol.* 178, 268–279. doi: 10.1006/exnr.2002.8032

Dine, J., Ducourneau, V. R., Fenelon, V. S., Fossat, P., Amadio, A., Eder, M., et al. (2014). Extracellular signal-regulated kinase phosphorylation in forebrain neurones contributes to osmoregulatory mechanisms. *J. Physiol.* 592, 1637–1654. doi: 10.1113/jphysiol.2013.261008

Dominguez-Meijide, A., Rodriguez-Perez, A. I., Diaz-Ruiz, C., Guerra, M. J., and Labandeira-Garcia, J. L. (2017). Dopamine modulates astroglial and microglial activity via glial renin-angiotensin system in cultures. *Brain Behav. Immun.* 62, 277–290. doi: 10.1016/j.bbi.2017.02.013

Du, W., Stern, J. E., and Filosa, J. A. (2015). Neuronal-derived nitric oxide and somatodendritically released vasopressin regulate neurovascular coupling in the rat hypothalamic supraoptic nucleus. *J. Neurosci.* 35, 5330–5341. doi: 10.1523/JNEUROSCI.3674-14.2015

Ebner, H. L., Fiechtner, B., Pelster, B., and Krumschnabel, G. (2006). Extracellular signal regulated MAP-kinase signalling in osmotically stressed trout hepatocytes. *Biochim. Biophys. Acta* 1760, 941–950. doi: 10.1016/j.bbagen.2006.03.017

Eriksson, P. S., Nilsson, M., Wågberg, M., Rönnbäck, L., and Hansson, E. (1992). Volume regulation of single astroglial cells in primary culture. *Neurosci. Lett.* 143, 195–199. doi: 10.1016/0304-3940(92)90264-8

Farmer, W. T., Abrahamsson, T., Chierzi, S., Lui, C., Zaelzer, C., Jones, E. V., et al. (2016). Neurons diversify astrocytes in the adult brain through sonic hedgehog signaling. *Science* 351, 849–854. doi: 10.1126/science.aab3103

Felgendreger, L. A., Fluharty, S. J., Yee, D. K., and Flanagan-Cato, L. M. (2013). Endogenous angiotensin II-induced p44/42 mitogen-activated protein kinase activation mediates sodium appetite but not thirst or neurohypophysial secretion in male rats. *J. Neuroendocrinol.* 25, 97–106. doi: 10.1111/j.1365-2826.2012.02376.x

Förster, D., and Reiser, G. (2016). Nucleotides protect rat brain astrocytes against hydrogen peroxide toxicity and induce antioxidant defense via P2Y receptors. *Neurochem. Int.* 94, 57–66. doi: 10.1016/j.neuint.2016.02.006

Fujisawa, H., Sugimura, Y., Takagi, H., Mizoguchi, H., Takeuchi, H., Izumida, H., et al. (2016). Chronic hyponatremia causes neurologic and psychologic impairments. *J. Am. Soc. Nephrol.* 27, 766–780. doi: 10.1681/ASN.2014121196

Gankam-Kengne, F., Couturier, B. S., Soupart, A., Brion, J. P., and Decaux, G. (2017). Osmotic stress-induced defective glial proteostasis contributes to brain demyelination after hyponatremia treatment. *J. Am. Soc. Nephrol.* 28, 1802–1813. doi: 10.1681/ASN.2016050509

Gankam Kengne, F., Couturier, B. S., Soupart, A., and Decaux, G. (2015). Urea minimizes brain complications following rapid correction of chronic hyponatremia compared with vasopressin antagonist or hypertonic saline. *Kidney Int.* 87, 323–331. doi: 10.1038/ki.2014.273

Gankam Kengne, F., Nicaise, C., Soupart, A., Boom, A., Schiettecatte, J., Pochet, R., et al. (2011). Astrocytes are an early target in osmotic demyelination syndrome. *J. Am. Soc. Nephrol.* 22, 1834–1845. doi: 10.1681/ASN.2010111127

Garrido-Gil, P., Rodriguez-Perez, A. I., Fernandez-Rodriguez, P., Lanciego, J. L., and Labandeira-Garcia, J. L. (2017). Expression of angiotensinogen and receptors for angiotensin and prorenin in the rat and monkey striatal neurons and glial cells. *Brain Struct. Funct.* 222, 2559–2571. doi: 10.1007/s00429-016-1357-z

Geerling, J. C., and Loewy, A. D. (2008). Central regulation of sodium appetite. *Exp. Physiol.* 93, 177–209. doi: 10.1113/expphysiol.2007.039891

Glasgow, E., Murase, T., Zhang, B., Verbalis, J. G., and Gainer, H. (2000). Gene expression in the rat supraoptic nucleus induced by chronic hyperosmolality versus hyposmolality. *Am. J. Physiol. Regul. Integr. Comp. Physiol.* 279, R1239–1250. doi: 10.1152/ajpregu.2000.279.4.r1239

González, A., Pariente, J. A., and Salido, G. M. (2007). Ethanol stimulates ROS generation by mitochondria through Ca^{2+} mobilization and increases GFAP content in rat hippocampal astrocytes. *Brain Res.* 1178, 28–37. doi: 10.1016/j.brainres.2007.08.040

Gottipati, M. K., Kalinina, I., Bekyarova, E., Haddon, R. C., and Parpura, V. (2012). Chemically functionalized water-soluble single-walled carbon nanotubes modulate morpho-functional characteristics of astrocytes. *Nano Lett.* 12, 4742–4747. doi: 10.1021/nl302178s

Gutkowska, J., Jankowski, M., and Antunes-Rodrigues, J. (2014). The role of oxytocin in cardiovascular regulation. *Braz. J. Med. Biol. Res.* 47, 206–214. doi: 10.1590/1414-431x20133309

Gutkowska, J., Jankowski, M., Lambert, C., Mukaddam-Daher, S., Zingg, H. H., and Mccann, S. M. (1997). Oxytocin releases atrial natriuretic peptide by combining with oxytocin receptors in the heart. *Proc. Natl. Acad. Sci. U S A* 94, 11704–11709. doi: 10.1073/pnas.94.21.11704

Hackel, D., Krug, S. M., Sauer, R. S., Mousa, S. A., Böcker, A., Pflücke, D., et al. (2012). Transient opening of the perineurial barrier for analgesic drug delivery. *Proc. Natl. Acad. Sci. U S A* 109, E2018–E2027. doi: 10.1073/pnas.1120800109

Hatton, G. I. (2002). Glial-neuronal interactions in the mammalian brain. *Adv. Physiol. Educ.* 26, 225–237. doi: 10.1152/advan.00038.2002

Hermann, K., Phillips, M. I., Hilgenfeldt, U., and Raizada, M. K. (1988). Biosynthesis of angiotensinogen and angiotensins by brain cells in primary culture. *J. Neurochem.* 51, 398–405. doi: 10.1111/j.1471-4159.1988.tb01052.x

Hertz, L., Chen, Y., and Song, D. (2017). Astrocyte cultures mimicking brain astrocytes in gene expression, signaling, metabolism and K^+ uptake and showing astrocytic gene expression overlooked by immunohistochemistry and in situ hybridization. *Neurochem. Res.* 42, 254–271. doi: 10.1007/s11064-016-1828-x

Hertz, L., Xu, J., Song, D., Yan, E., Gu, L., and Peng, L. (2013). Astrocytic and neuronal accumulation of elevated extracellular K^+ with a 2/3 K^+/Na^+ flux ratio-consequences for energy metabolism, osmolarity and higher brain function. *Front. Comput. Neurosci.* 7:114. doi: 10.3389/fncom.2013.00114

Hindmarch, C. C., and Ferguson, A. V. (2016). Physiological roles for the subfornical organ: a dynamic transcriptome shaped by autonomic state. *J. Physiol.* 594, 1581–1589. doi: 10.1113/JP270726

Hirko, A. C., Dallasen, R., Jomura, S., and Xu, Y. (2008). Modulation of inflammatory responses after global ischemia by transplanted umbilical cord matrix stem cells. *Stem Cells* 26, 2893–2901. doi: 10.1634/stemcells.2008-0075

Hirt, L., Fukuda, A. M., Ambadipudi, K., Rashid, F., Binder, D., Verkman, A., et al. (2017). Improved long-term outcome after transient cerebral ischemia in aquaporin-4 knockout mice. *J. Cereb. Blood Flow Metab.* 37, 277–290. doi: 10.1177/0271678x15623290

Ho, J. M., Zierath, D. K., Savos, A. V., Femiano, D. J., Bassett, J. E., McKinley, M. J., et al. (2007). Differential effects of intravenous hyperosmotic solutes on drinking latency and c-Fos expression in the circumventricular organs and hypothalamus of the rat. *Am. J. Physiol. Regul. Integr. Comp. Physiol.* 292, R1690–R1698. doi: 10.1152/ajpregu.00547.2006

Hori, O., Ichinoda, F., Tamatani, T., Yamaguchi, A., Sato, N., Ozawa, K., et al. (2002). Transmission of cell stress from endoplasmic reticulum to mitochondria: enhanced expression of Lon protease. *J. Cell Biol.* 157, 1151–1160. doi: 10.1083/jcb.200108103

Horiguchi, K., Fujiwara, K., Ilmiawati, C., Kikuchi, M., Tsukada, T., Kouki, T., et al. (2011). Caveolin 3-mediated integrin β1 signaling is required for the proliferation of folliculostellate cells in rat anterior pituitary gland under the influence of extracellular matrix. *J. Endocrinol.* 210, 29–36. doi: 10.1530/joe-11-0103

Hou, D., Jin, F., Li, J., Lian, J., Liu, M., Liu, X.-N., et al. (2016). Model roles of the hypothalamo-neurohypophysial system in neuroscience study. *Biochem. Pharmacol.* 5:211. doi: 10.4172/2167-0501.1000211

Hsiao, H.-Y., Chiu, F.-L., Chen, C.-M., Wu, Y.-R., Chen, H.-M., Chen, Y.-C., et al. (2014). Inhibition of soluble tumor necrosis factor is therapeutic in Huntington's disease. *Hum. Mol. Genet.* 23, 4328–4344. doi: 10.1093/hmg/ddu151

Hübel, N., and Ullah, G. (2016). Anions govern cell volume: a case study of relative astrocytic and neuronal swelling in spreading depolarization. *PLoS One* 11:e0147060. doi: 10.1371/journal.pone.0147060

Hussy, N., Deleuze, C., Desarménien, M. G., and Moos, F. C. (2000). Osmotic regulation of neuronal activity: a new role for taurine and glial cells in a hypothalamic neuroendocrine structure. *Prog. Neurobiol.* 62, 113–134. doi: 10.1016/s0301-0082(99)00071-4

Irazusta, J., Silveira, P. F., Gil, J., Varona, A., and Casis, L. (2001). Effects of hydrosaline treatments on prolyl endopeptidase activity in rat tissues. *Regul. Pept.* 101, 141–147. doi: 10.1016/s0167-0115(01)00277-4

Ishikura, T., Suzuki, H., Shoguchi, K., Koreeda, Y., Aritomi, T., Matsuura, T., et al. (2015). Possible involvement of TRPV1 and TRPV4 in nociceptive stimulation-induced nocifensive behavior and neuroendocrine response in mice. *Brain Res. Bull.* 118, 7–16. doi: 10.1016/j.brainresbull.2015.08.004

Jia, S. W., Liu, X. Y., Wang, S. C., and Wang, Y. F. (2016). Vasopressin hypersecretion-associated brain edema formation in ischemic stroke: underlying mechanisms. *J. Stroke Cerebrovasc. Dis.* 25, 1289–1300. doi: 10.1016/j.jstrokecerebrovasdis.2016.02.002

Jiao, R., Cui, D., Wang, S. C., Li, D., and Wang, Y. F. (2017). Interactions of the mechanosensitive channels with extracellular matrix, integrins, and cytoskeletal network in osmosensation. *Front. Mol. Neurosci.* 10:96. doi: 10.3389/fnmol.2017.00096

Johnston, G. A., and Stephanson, A. L. (1976). Inhibitors of the glial uptake of β-alanine in rat brain slices. *Brain Res.* 102, 374–378. doi: 10.1016/0006-8993(76)90895-7

Kenny, A., Plank, M. J., and David, T. (2018). The role of astrocytic calcium and TRPV4 channels in neurovascular coupling. *J. Comput. Neurosci.* 44, 97–114. doi: 10.1007/s10827-017-0671-7

Kim, J. S., Kim, W. B., Kim, Y. B., Lee, Y., Kim, Y. S., Shen, F. Y., et al. (2011). Chronic hyperosmotic stress converts GABAergic inhibition into excitation in vasopressin and oxytocin neurons in the rat. *J. Neurosci.* 31, 13312–13322. doi: 10.1523/JNEUROSCI.1440-11.2011

Kino, T., Segars, J. H., and Chrousos, G. P. (2010). The guanine nucleotide exchange factor brx: a link between osmotic stress, inflammation and organ physiology and pathophysiology. *Expert Rev. Endocrinol. Metab.* 5, 603–614. doi: 10.1586/eem.10.3

Kinsman, B. J., Nation, H. N., and Stocker, S. D. (2017). Hypothalamic signaling in body fluid homeostasis and hypertension. *Curr. Hypertens. Rep.* 19:50. doi: 10.1007/s11906-017-0749-7

Kleindienst, A., Hannon, M. J., Buchfelder, M., and Verbalis, J. G. (2016). Hyponatremia in neurotrauma: the role of vasopressin. *J. Neurotrauma* 33, 615–624. doi: 10.1089/neu.2015.3981

Krzan, M., Stenovec, M., Kreft, M., Pangrsic, T., Grilc, S., Haydon, P. G., et al. (2003). Calcium-dependent exocytosis of atrial natriuretic peptide from astrocytes. *J. Neurosci.* 23, 1580–1583. doi: 10.1523/JNEUROSCI.23-05-01580.2003

Kurbel, S. (2008). Are extracellular osmolality and sodium concentration determined by Donnan effects of intracellular protein charges and of pumped sodium? *J. Theor. Biol.* 252, 769–772. doi: 10.1016/j.jtbi.2008.02.022

Lange, K. (2000). Regulation of cell volume via microvillar ion channels. *J. Cell. Physiol.* 185, 21–35. doi: 10.1002/1097-4652(200010)185:1<21::aid-jcp2>3.3.co;2-4

Lauand, F., Ruginsk, S. G., Rodrigues, H. L., Reis, W. L., de Castro, M., Elias, L. L., et al. (2007). Glucocorticoid modulation of atrial natriuretic peptide, oxytocin, vasopressin and Fos expression in response to osmotic, angiotensinergic and cholinergic stimulation. *Neuroscience* 147, 247–257. doi: 10.1016/j.neuroscience.2007.04.021

Lee, S. D., Choi, S. Y., and Kwon, H. M. (2011). Distinct cellular pathways for resistance to urea stress and hypertonic stress. *Am. J. Physiol. Cell Physiol.* 300, C692–C696. doi: 10.1152/ajpcell.00150.2010

Li, D., Liu, N., Zhao, H. H., Zhang, X., Kawano, H., Liu, L., et al. (2017). Interactions between Sirt1 and MAPKs regulate astrocyte activation induced by brain injury *in vitro* and *in vivo*. *J. Neuroinflammation* 14:67. doi: 10.1186/s12974-017-0841-6

Liedtke, W., and Friedman, J. M. (2003). Abnormal osmotic regulation in *trpv4*$^{-/-}$ mice. *Proc. Natl. Acad. Sci. U S A* 100, 13698–13703. doi: 10.1073/pnas.1735416100

Lipari, E. F., Lipari, A., Dieli, F., and Valentino, B. (2007). ANP presence in the hypothalamic suprachiasmatic nucleus of developing rat. *Ital. J. Anat. Embryol.* 112, 19–25.

Losi, G., Marcon, I., Mariotti, L., Sessolo, M., Chiavegato, A., and Carmignoto, G. (2016). A brain slice experimental model to study the generation and the propagation of focally-induced epileptiform activity. *J. Neurosci. Methods* 260, 125–131. doi: 10.1016/j.jneumeth.2015.04.001

Ludwig, M., Bull, P. M., Tobin, V. A., Sabatier, N., Landgraf, R., Dayanithi, G., et al. (2005). Regulation of activity-dependent dendritic vasopressin release from rat supraoptic neurones. *J. Physiol.* 564, 515–522. doi: 10.1113/jphysiol.2005.083931

Lunn, J. A., and Rozengurt, E. (2004). Hyperosmotic stress induces rapid focal adhesion kinase phosphorylation at tyrosines 397 and 577. Role of Src family kinases and Rho family GTPases. *J. Biol. Chem.* 279, 45266–45278. doi: 10.1074/jbc.M314132200

Macchione, A. F., Beas, C., Dadam, F. M., Caeiro, X. E., Godino, A., Ponce, L. F., et al. (2015). Early free access to hypertonic NaCl solution induces a long-term effect on drinking, brain cell activity and gene expression of adult rat offspring. *Neuroscience* 298, 120–136. doi: 10.1016/j.neuroscience.2015.04.004

Malarkey, E. B., and Parpura, V. (2009). "Mechanisms of transmitter release from astrocytes," in *Astrocytes in (Patho)Physiology of the Nervous System*, eds V. Parpura and P. G. Haydon (New York, NY: Springer), 301–350.

Mannari, T., Morita, S., Furube, E., Tominaga, M., and Miyata, S. (2013). Astrocytic TRPV1 ion channels detect blood-borne signals in the sensory circumventricular organs of adult mouse brains. *Glia* 61, 957–971. doi: 10.1002/glia.22488

Marmarou, C. R., Liang, X., Abidi, N. H., Parveen, S., Taya, K., Henderson, S. C., et al. (2014). Selective vasopressin-1a receptor antagonist prevents brain edema, reduces astrocytic cell swelling and GFAP, V1aR and AQP4 expression after focal traumatic brain injury. *Brain Res.* 1581, 89–102. doi: 10.1016/j.brainres.2014.06.005

McCabe, J. T., and Burrell, A. S. (2001). Alterations of AP-1 and CREB protein DNA binding in rat supraoptic and paraventricular nuclei by acute and repeated hyperosmotic stress. *Brain Res. Bull.* 55, 347–358. doi: 10.1016/s0361-9230(01)00520-2

McKinley, M. J., and McAllen, R. M. (2007). Neuroendocrine self-control: dendritic release of vasopressin. *Endocrinology* 148, 477–478. doi: 10.1210/en.2006-1531

McKinley, M. J., Yao, S. T., Uschakov, A., McAllen, R. M., Rundgren, M., and Martelli, D. (2015). The median preoptic nucleus: front and centre for the regulation of body fluid, sodium, temperature, sleep and cardiovascular homeostasis. *Acta Physiol.* 214, 8–32. doi: 10.1111/apha.12487

Milanese, M., Bonifacino, T., Zappettini, S., Usai, C., Tacchetti, C., Nobile, M., et al. (2009). Glutamate release from astrocytic gliosomes under physiological and pathological conditions. *Int. Rev. Neurobiol.* 85, 295–318. doi: 10.1016/s0074-7742(09)85021-6

Miller, R. L., and Loewy, A. D. (2013). ENaC γ-expressing astrocytes in the circumventricular organs, white matter, and ventral medullary surface: sites for Na^+ regulation by glial cells. *J. Chem. Neuroanat.* 53, 72–80. doi: 10.1016/j.jchemneu.2013.10.002

Miyata, S. (2015). New aspects in fenestrated capillary and tissue dynamics in the sensory circumventricular organs of adult brains. *Front. Neurosci.* 9:390. doi: 10.3389/fnins.2015.00390

Mola, M. G., Sparaneo, A., Gargano, C. D., Spray, D. C., Svelto, M., Frigeri, A., et al. (2015). The speed of swelling kinetics modulates cell volume regulation and calcium signaling in astrocytes: a different point of view on the role of aquaporins. *Glia* 64, 139–154. doi: 10.1002/glia.22921

Mondal, S., Dirks, P., and Rutka, J. T. (2010). Immunolocalization of fascin, an actin-bundling protein and glial fibrillary acidic protein in human astrocytoma cells. *Brain Pathol.* 20, 190–199. doi: 10.1111/j.1750-3639.2008.00261.x

Montana, V., Malarkey, E. B., Verderio, C., Matteoli, M., and Parpura, V. (2006). Vesicular transmitter release from astrocytes. *Glia* 54, 700–715. doi: 10.1002/glia.20367

Moran, J., Morales-Mulia, M., and Pasantes-Morales, H. (2001). Reduction of phospholemman expression decreases osmosensitive taurine efflux in astrocytes. *Biochim. Biophys. Acta* 1538, 313–320. doi: 10.1016/s0167-4889(01)00082-9

Muhsin, S. A., and Mount, D. B. (2016). Diagnosis and treatment of hypernatremia. *Best Pract. Res. Clin. Endocrinol. Metab.* 30, 189–203. doi: 10.1016/j.beem.2016.02.014

Muñoz, A., Riber, C., Trigo, P., and Castejón, F. (2010). Muscle damage, hydration, electrolyte balance and vasopressin concentrations in successful and exhausted endurance horses. *Pol. J. Vet. Sci.* 13, 373–379. doi: 10.1111/j.2042-3306.2010.00211.x

Muraki, K., Shigekawa, M., and Imaizumi, Y. (2007). "Chapter 28-A new insight into the function of TRPV2 in circulatory organs," in *TRP Ion Channel Function in Sensory Transduction and Cellular Signaling Cascades*, eds W. B. Liedtke and S. Heller (Boca Raton, FL: CRC Press/Taylor & Francis).

Najafi, E., Stoodley, M. A., Bilston, L. E., and Hemley, S. J. (2016). Inwardly rectifying potassium channel 4.1 expression in post-traumatic syringomyelia. *Neuroscience* 317, 23–35. doi: 10.1016/j.neuroscience.2016.01.001

Ni, Y., Malarkey, E. B., and Parpura, V. (2007). Vesicular release of glutamate mediates bidirectional signaling between astrocytes and neurons. *J. Neurochem.* 103, 1273–1284. doi: 10.1111/j.1471-4159.2007.04864.x

Niermann, H., Amiry-Moghaddam, M., Holthoff, K., Witte, O. W., and Ottersen, O. P. (2001). A novel role of vasopressin in the brain: modulation of activity-dependent water flux in the neocortex. *J. Neurosci.* 21, 3045–3051. doi: 10.1523/JNEUROSCI.21-09-03045.2001

Noda, M. (2007). Hydromineral neuroendocrinology: mechanism of sensing sodium levels in the mammalian brain. *Exp. Physiol.* 92, 513–522. doi: 10.1113/expphysiol.2006.035659

Ohbuchi, T., Yokoyama, T., Saito, T., Suzuki, H., Fujihara, H., Katoh, A., et al. (2010). Modulators of BK and SK channels alter electrical activity *in vitro* in single vasopressin neurons isolated from the rat supraoptic nucleus. *Neurosci. Lett.* 484, 26–29. doi: 10.1016/j.neulet.2010.08.010

Olson, J. E., Li, G. Z., Wang, L., and Lu, L. (2004). Volume-regulated anion conductance in cultured rat cerebral astrocytes requires calmodulin activity. *Glia* 46, 391–401. doi: 10.1002/glia.20014

Ordaz, B., Tuz, K., Ochoa, L. D., Lezama, R., Peña-Segura, C., and Franco, R. (2004). Osmolytes and mechanisms involved in regulatory volume decrease under conditions of sudden or gradual osmolarity decrease. *Neurochem. Res.* 29, 65–72. doi: 10.1023/b:nere.0000010434.06311.18

Ouyang, Y. B., Xu, L. J., Emery, J. F., Lee, A. S., and Giffard, R. G. (2011). Overexpressing GRP78 influences Ca^{2+} handling and function of mitochondria in astrocytes after ischemia-like stress. *Mitochondrion* 11, 279–286. doi: 10.1016/j.mito.2010.10.007

Padmanabhan, J., Clayton, D., and Shelanski, M. L. (1999). Dibutyryl cyclic AMP-induced process formation in astrocytes is associated with a decrease in tyrosine phosphorylation of focal adhesion kinase and paxillin. *J. Neurobiol.* 39, 407–422. doi: 10.1002/(sici)1097-4695(19990605)39:3<407::aid-neu7>3.0.co;2-s

Papadopoulos, M. C., and Verkman, A. S. (2007). Aquaporin-4 and brain edema. *Pediatr. Nephrol.* 22, 778–784. doi: 10.1007/s00467-006-0411-0

Pardy, K., Adan, R. A., Carter, D. A., Seah, V., Burbach, J. P., and Murphy, D. (1992). The identification of a cis-acting element involved in cyclic 3′,5′-adenosine monophosphate regulation of bovine vasopressin gene expression. *J. Biol. Chem.* 267, 21746–21752.

Park, J. B., Skalska, S., and Stern, J. E. (2006). Characterization of a novel tonic γ-aminobutyric acidA receptor-mediated inhibition in magnocellular neurosecretory neurons and its modulation by glia. *Endocrinology* 147, 3746–3760. doi: 10.1210/en.2006-0218

Parpura, V., and Verkhratsky, A. (2012). Astrocytes revisited: concise historic outlook on glutamate homeostasis and signaling. *Croat. Med. J.* 53, 518–528. doi: 10.3325/cmj.2012.53.518

Parpura, V., Fisher, E. S., Lechleiter, J. D., Schousboe, A., Waagepetersen, H. S., Brunet, S., et al. (2017). Glutamate and ATP at the interface between signaling and metabolism in astroglia: examples from pathology. *Neurochem. Res.* 42, 19–34. doi: 10.1007/s11064-016-1848-6

Parpura, V., Scemes, E., and Spray, D. C. (2004). Mechanisms of glutamate release from astrocytes: gap junction "hemichannels", purinergic receptors and exocytotic release. *Neurochem. Int.* 45, 259–264. doi: 10.1016/s0197-0186(03)00290-0

Perkins, K. L., Arranz, A. M., Yamaguchi, Y., and Hrabetova, S. (2017). Brain extracellular space, hyaluronan, and the prevention of epileptic seizures. *Rev. Neurosci.* 28, 869–892. doi: 10.1515/revneuro-2017-0017

Pierre, K., Bonhomme, R., Dupouy, B., Poulain, D. A., and Theodosis, D. T. (2001). The polysialylated neural cell adhesion molecule reaches cell surfaces of hypothalamic neurons and astrocytes via the constitutive pathway. *Neuroscience* 103, 133–142. doi: 10.1016/s0306-4522(00)00536-4

Plantier, M., Fattoum, A., Menn, B., Ben-Ari, Y., Der Terrossian, E., and Represa, A. (1999). Acidic calponin immunoreactivity in postnatal rat brain and cultures: subcellular localization in growth cones, under the plasma membrane and along actin and glial filaments. *Eur. J. Neurosci.* 11, 2801–2812. doi: 10.1046/j.1460-9568.1999.00702.x

Platonova, A., Ponomarchuk, O., Boudreault, F., Kapilevich, L. V., Maksimov, G. V., Grygorczyk, R., et al. (2015). Role of cytoskeleton network in anisosmotic volume changes of intact and permeabilized A549 cells. *Biochim. Biophys. Acta* 1848, 2337–2343. doi: 10.1016/j.bbamem.2015.07.005

Ponzio, T. A., Ni, Y., Montana, V., Parpura, V., and Hatton, G. I. (2006). Vesicular glutamate transporter expression in supraoptic neurones suggests a glutamatergic phenotype. *J. Neuroendocrinol.* 18, 253–265. doi: 10.1111/j.1365-2826.2006.01410.x

Popescu, B. F., Bunyan, R. F., Guo, Y., Parisi, J. E., Lennon, V. A., and Lucchinetti, C. F. (2013). Evidence of aquaporin involvement in human central

pontine myelinolysis. *Acta Neuropathol. Commun.* 1:40. doi: 10.1186/2051-5960-1-40

Potokar, M., Stenovec, M., Jorgacevski, J., Holen, T., Kreft, M., Ottersen, O. P., et al. (2013). Regulation of AQP4 surface expression via vesicle mobility in astrocytes. *Glia* 61, 917–928. doi: 10.1002/glia.22485

Prager-Khoutorsky, M., and Bourque, C. W. (2015). Mechanical basis of osmosensory transduction in magnocellular neurosecretory neurones of the rat supraoptic nucleus. *J. Neuroendocrinol.* 27, 507–515. doi: 10.1111/jne.12270

Raimann, J. G., Tzamaloukas, A. H., Levin, N. W., and Ing, T. S. (2017). Osmotic pressure in clinical medicine with an emphasis on dialysis. *Semin. Dial.* 30, 69–79. doi: 10.1111/sdi.12537

Raju, K., Doulias, P. T., Evans, P., Krizman, E. N., Jackson, J. G., Horyn, O., et al. (2015). Regulation of brain glutamate metabolism by nitric oxide and S-nitrosylation. *Sci. Signal.* 8:ra68. doi: 10.1126/scisignal.aaa4312

Ramírez-Jarquín, U. N., Rojas, F., van Zundert, B., and Tapia, R. (2017). Chronic infusion of SOD1G93A astrocyte-secreted factors induces spinal motoneuron degeneration and neuromuscular dysfunction in healthy rats. *J. Cell. Physiol.* 232, 2610–2615. doi: 10.1002/jcp.25827

Reis, W. L., Biancardi, V. C., Son, S., Antunes-Rodrigues, J., and Stern, J. E. (2012). Enhanced expression of heme oxygenase-1 and carbon monoxide excitatory effects in oxytocin and vasopressin neurones during water deprivation. *J. Neuroendocrinol.* 24, 653–663. doi: 10.1111/j.1365-2826.2011.02249.x

Richard, D., and Bourque, C. W. (1996). Atrial natriuretic peptide modulates synaptic transmission from osmoreceptor afferents to the supraoptic nucleus. *J. Neurosci.* 16, 7526–7532. doi: 10.1523/JNEUROSCI.16-23-07526.1996

Roy Choudhury, G., Ryou, M. G., Poteet, E., Wen, Y., He, R., Sun, F., et al. (2014). Involvement of p38 MAPK in reactive astrogliosis induced by ischemic stroke. *Brain Res.* 1551, 45–58. doi: 10.1016/j.brainres.2014.01.013

Rutka, J. T., Muller, M., Hubbard, S. L., Forsdike, J., Dirks, P. B., Jung, S., et al. (1999). Astrocytoma adhesion to extracellular matrix: functional significance of integrin and focal adhesion kinase expression. *J. Neuropathol. Exp. Neurol.* 58, 198–209. doi: 10.1097/00005072-199902000-00009

Ryan, M. C., and Gundlach, A. L. (1997). Differential regulation of angiotensinogen and natriuretic peptide mRNAs in rat brain by osmotic stimulation: focus on anterior hypothalamus and supraoptic nucleus. *Peptides* 18, 1365–1375. doi: 10.1016/s0196-9781(97)00192-7

Ryskamp, D. A., Witkovsky, P., Barabas, P., Huang, W., Koehler, C., Akimov, N. P., et al. (2011). The polymodal ion channel transient receptor potential vanilloid 4 modulates calcium flux, spiking rate, and apoptosis of mouse retinal ganglion cells. *J. Neurosci.* 31, 7089–7101. doi: 10.1523/JNEUROSCI.0359-11.2011

Sailer, C., Winzeler, B., and Christ-Crain, M. (2017). Primary polydipsia in the medical and psychiatric patient: characteristics, complications and therapy. *Swiss Med. Wkly.* 147:w14514. doi: 10.4414/smw.2017.14514

Salazar, M., Pariente, J. A., Salido, G. M., and Gonzalez, A. (2008). Ebselen increases cytosolic free Ca^{2+} concentration, stimulates glutamate release and increases GFAP content in rat hippocampal astrocytes. *Toxicology* 244, 280–291. doi: 10.1016/j.tox.2007.12.002

Salman, M. M., Sheilabi, M. A., Bhattacharyya, D., Kitchen, P., Conner, A. C., Bill, R. M., et al. (2017). Transcriptome analysis suggests a role for the differential expression of cerebral aquaporins and the MAPK signalling pathway in human temporal lobe epilepsy. *Eur. J. Neurosci.* 46, 2121–2132. doi: 10.1111/ejn.13652

Sánchez-Olea, R., Pasantes-Morales, H., and Schousboe, A. (1993). Neurons respond to hyposmotic conditions by an increase in intracellular free calcium. *Neurochem. Res.* 18, 147–152. doi: 10.1007/bf01474677

Sato, M., Sobhan, U., Tsumura, M., Kuroda, H., Soya, M., Masamura, A., et al. (2013). Hypotonic-induced stretching of plasma membrane activates transient receptor potential vanilloid channels and sodium-calcium exchangers in mouse odontoblasts. *J. Endod.* 39, 779–787. doi: 10.1016/j.joen.2013.01.012

Schäfer, M. K., Pfeiffer, A., Jaeckel, M., Pouya, A., Dolga, A. M., and Methner, A. (2014). Regulators of mitochondrial Ca^{2+} homeostasis in cerebral ischemia. *Cell Tissue Res.* 357, 395–405. doi: 10.1007/s00441-014-1807-y

Schmelzer, A. E., and Miller, W. M. (2002). Effects of osmoprotectant compounds on NCAM polysialylation under hyperosmotic stress and elevated pCO_2. *Biotechnol. Bioeng.* 77, 359–368. doi: 10.1002/bit.10175

Seale, A. P., Watanabe, S., and Grau, E. G. (2012). Osmoreception: perspectives on signal transduction and environmental modulation. *Gen Comp Endocrinol* 176, 354–360. doi: 10.1016/j.ygcen.2011.10.005

Shi, W. Z., Qi, L. L., Fang, S. H., Lu, Y. B., Zhang, W. P., and Wei, E. Q. (2012). Aggravated chronic brain injury after focal cerebral ischemia in aquaporin-4-deficient mice. *Neurosci. Lett.* 520, 121–125. doi: 10.1016/j.neulet.2012.05.052

Shi, Z. D., Wang, H., and Tarbell, J. M. (2011). Heparan sulfate proteoglycans mediate interstitial flow mechanotransduction regulating MMP-13 expression and cell motility via FAK-ERK in 3D collagen. *PLoS One* 6:e15956. doi: 10.1371/journal.pone.0015956

Simard, M., and Nedergaard, M. (2004). The neurobiology of glia in the context of water and ion homeostasis. *Neuroscience* 129, 877–896. doi: 10.1016/j.neuroscience.2004.09.053

Song, I., and Dityatev, A. (2018). Crosstalk between glia, extracellular matrix and neurons. *Brain Res. Bull.* 136, 101–108. doi: 10.1016/j.brainresbull.2017.03.003

Song, Y., and Gunnarson, E. (2012). Potassium dependent regulation of astrocyte water permeability is mediated by cAMP signaling. *PLoS One* 7:e34936. doi: 10.1371/journal.pone.0034936

Song, Z., and Hatton, G. I. (2003). Taurine and the control of basal hormone release from rat neurohypophysis. *Exp. Neurol.* 183, 330–337. doi: 10.1016/s0014-4886(03)00105-5

Soya, M., Sato, M., Sobhan, U., Tsumura, M., Ichinohe, T., Tazaki, M., et al. (2014). Plasma membrane stretch activates transient receptor potential vanilloid and ankyrin channels in Merkel cells from hamster buccal mucosa. *Cell Calcium* 55, 208–218. doi: 10.1016/j.ceca.2014.02.015

Steiner, E., Enzmann, G. U., Lin, S., Ghavampour, S., Hannocks, M. J., Zuber, B., et al. (2012). Loss of astrocyte polarization upon transient focal brain ischemia as a possible mechanism to counteract early edema formation. *Glia* 60, 1646–1659. doi: 10.1002/glia.22383

Stern, J. E., and Ludwig, M. (2001). NO inhibits supraoptic oxytocin and vasopressin neurons via activation of GABAergic synaptic inputs. *Am. J. Physiol. Regul. Integr. Comp. Physiol.* 280, R1815–R1822. doi: 10.1152/ajpregu.2001.280.6.r1815

Stokum, J. A., Gerzanich, V., and Simard, J. M. (2016). Molecular pathophysiology of cerebral edema. *J. Cereb. Blood Flow Metab.* 36, 513–538. doi: 10.1177/0271678X15617172

Takagi, H., Sugimura, Y., Suzuki, H., Iwama, S., Izumida, H., Fujisawa, H., et al. (2014). Minocycline prevents osmotic demyelination associated with aquaresis. *Kidney Int.* 86, 954–964. doi: 10.1038/ki.2014.119

Tamma, G., Di Mise, A., Ranieri, M., Geller, A., Tamma, R., Zallone, A., et al. (2017). The V2 receptor antagonist tolvaptan raises cytosolic calcium and prevents AQP2 trafficking and function: an *in vitro* and *in vivo* assessment. *J. Cell. Mol. Med.* 21, 1767–1780. doi: 10.1111/jcmm.13098

Taylor, A. C., McCarthy, J. J., and Stocker, S. D. (2008). Mice lacking the transient receptor vanilloid potential 1 channel display normal thirst responses and central Fos activation to hypernatremia. *Am. J. Physiol. Regul. Integr. Comp. Physiol.* 294, R1285–R1293. doi: 10.1152/ajpregu.00003.2008

Theilig, F., and Wu, Q. (2015). ANP-induced signaling cascade and its implications in renal pathophysiology. *Am. J. Physiol. Renal Physiol.* 308, F1047–F1055. doi: 10.1152/ajprenal.00164.2014

Theodosis, D. T., Poulain, D. A., and Oliet, S. H. (2008). Activity-dependent structural and functional plasticity of astrocyte-neuron interactions. *Physiol. Rev.* 88, 983–1008. doi: 10.1152/physrev.00036.2007

Thomas, R., Salter, M. G., Wilke, S., Husen, A., Allcock, N., Nivison, M., et al. (2004). Acute ischemic injury of astrocytes is mediated by Na-K-Cl cotransport and not Ca^{2+} influx at a key point in white matter development. *J. Neuropathol. Exp. Neurol.* 63, 856–871. doi: 10.1093/jnen/63.8.856

Thomzig, A., Prüss, H., and Veh, R. W. (2003). The Kir6.1-protein, a pore-forming subunit of ATP-sensitive potassium channels, is prominently expressed by giant cholinergic interneurons in the striatum of the rat brain. *Brain Res.* 986, 132–138. doi: 10.1016/s0006-8993(03)03222-0

Uchiyama, Y., Cheng, C. C., Danielson, K. G., Mochida, J., Albert, T. J., Shapiro, I. M., et al. (2007). Expression of acid-sensing ion channel 3 (ASIC3) in nucleus pulposus cells of the intervertebral disc is regulated by p75NTR and ERK signaling. *J. Bone Miner. Res.* 22, 1996–2006. doi: 10.1359/jbmr.070805

Verkman, A. S. (2012). Aquaporins in clinical medicine. *Annu. Rev. Med.* 63, 303–316. doi: 10.1146/annurev-med-043010-193843

Vilhena-Franco, T., Mecawi, A. S., Elias, L. L., and Antunes-Rodrigues, J. (2011). Oestradiol potentiates hormone secretion and neuronal activation in response to hypertonic extracellular volume expansion in ovariectomised

rats. *J. Neuroendocrinol.* 23, 481–489. doi: 10.1111/j.1365-2826.2011.02133.x

Vilhena-Franco, T., Mecawi, A. S., Elias, L. L., and Antunes-Rodrigues, J. (2016). Oestradiol effects on neuroendocrine responses induced by water deprivation in rats. *J. Endocrinol.* 231, 167–180. doi: 10.1530/joe-16-0311

Voets, P. J. G. M., and Maas, R. P. P. W. M. (2018). Extracellular volume depletion and resultant hypotonic hyponatremia: a novel translational approach. *Math. Biosci.* 295, 62–66. doi: 10.1016/j.mbs.2017.11.005

Walcott, B. P., Kahle, K. T., and Simard, J. M. (2012). Novel treatment targets for cerebral edema. *Neurotherapeutics* 9, 65–72. doi: 10.1007/s13311-011-0087-4

Walz, W. (1992). Role of Na/K/Cl cotransport in astrocytes. *Can. J. Physiol. Pharmacol.* 70, S260–S262. doi: 10.1139/y92-270

Wang, Y. F., and Hatton, G. I. (2006). Mechanisms underlying oxytocin-induced excitation of supraoptic neurons: prostaglandin mediation of actin polymerization. *J. Neurophysiol.* 95, 3933–3947. doi: 10.1152/jn.01267.2005

Wang, Y. F., and Hatton, G. I. (2007a). Dominant role of βγ subunits of G-proteins in oxytocin-evoked burst firing. *J. Neurosci.* 27, 1902–1912. doi: 10.1523/JNEUROSCI.5346-06.2007

Wang, Y. F., and Hatton, G. I. (2007b). Interaction of extracellular signal-regulated protein kinase 1/2 with actin cytoskeleton in supraoptic oxytocin neurons and astrocytes: role in burst firing. *J. Neurosci.* 27, 13822–13834. doi: 10.1523/JNEUROSCI.4119-07.2007

Wang, Y. F., and Hatton, G. I. (2009). Astrocytic plasticity and patterned oxytocin neuronal activity: dynamic interactions. *J. Neurosci.* 29, 1743–1754. doi: 10.1523/JNEUROSCI.4669-08.2009

Wang, Y.-F., Liu, L.-X., and Yang, H.-P. (2011). Neurophysiological involvement in hypervolemic hyponatremia-evoked by hypersecretion of vasopressin. *Transl. Biomed.* 2:3. doi: 10.3823/425

Wang, S. C., Meng, D., Yang, H.-P., Wang, X., Shuwei, J., Wang, P., et al. (2018). Pathological basis of cardiac arrhythmias: vicious cycle of immune-metabolic dysregulation. *Cardiovasc. Disord. Med.* 3, 1–7. doi: 10.15761/cdm.1000158

Wang, Y. F., and Parpura, V. (2016). Central role of maladapted astrocytic plasticity in ischemic brain edema formation. *Front. Cell. Neurosci.* 10:129. doi: 10.3389/fncel.2016.00129

Wang, Y. F., Ponzio, T. A., and Hatton, G. I. (2006). Autofeedback effects of progressively rising oxytocin concentrations on supraoptic oxytocin neuronal activity in slices from lactating rats. *Am. J. Physiol. Regul. Integr. Comp. Physiol.* 290, R1191–R1198. doi: 10.1152/ajpregu.00725.2005

Wang, P., Qin, D., and Wang, Y. F. (2017). Oxytocin rapidly changes astrocytic GFAP plasticity by differentially modulating the expressions of pERK 1/2 and protein kinase A. *Front. Mol. Neurosci.* 10:262. doi: 10.3389/fnmol.2017.00262

Wang, Y. F., Sun, M. Y., Hou, Q., and Hamilton, K. A. (2013a). GABAergic inhibition through synergistic astrocytic neuronal interaction transiently decreases vasopressin neuronal activity during hypoosmotic challenge. *Eur. J. Neurosci.* 37, 1260–1269. doi: 10.1111/ejn.12137

Wang, Y. F., Sun, M. Y., Hou, Q., and Parpura, V. (2013b). Hyposmolality differentially and spatiotemporally modulates levels of glutamine synthetase and serine racemase in rat supraoptic nucleus. *Glia* 61, 529–538. doi: 10.1002/glia.22453

Wang, Y. F., and Zhu, H. (2014). Mechanisms underlying astrocyte regulation of hypothalamic neuroendocrine neuron activity. *Sheng Li Ke Xue Jin Zhan* 45, 177–184.

Wilson, C. S., and Mongin, A. A. (2018). The signaling role for chloride in the bidirectional communication between neurons and astrocytes. *Neurosci. Lett.* doi: 10.1016/j.neulet.2018.01.012 [Epub ahead of print].

Wu, Q., Zhang, Y. J., Gao, J. Y., Li, X. M., Kong, H., Zhang, Y. P., et al. (2014). Aquaporin-4 mitigates retrograde degeneration of rubrospinal neurons by facilitating edema clearance and glial scar formation after spinal cord injury in mice. *Mol. Neurobiol.* 49, 1327–1337. doi: 10.1007/s12035-013-8607-3

Xu, M., Xiao, M., Li, S., and Yang, B. (2017). Aquaporins in nervous system. *Adv. Exp. Med. Biol.* 969, 81–103. doi: 10.1007/978-94-024-1057-0_5

Yagil, C., and Sladek, C. D. (1990). Osmotic regulation of vasopressin and oxytocin release is rate sensitive in hypothalamoneurohypophysial explants. *Am. J. Physiol.* 258, R492–R500. doi: 10.1152/ajpregu.1990.258.2.r492

Yan, W., Zhao, X., Chen, H., Zhong, D., Jin, J., Qin, Q., et al. (2016). β-Dystroglycan cleavage by matrix metalloproteinase-2/-9 disturbs aquaporin-4 polarization and influences brain edema in acute cerebral ischemia. *Neuroscience* 326, 141–157. doi: 10.1016/j.neuroscience.2016.03.055

Yang, M., Gao, F., Liu, H., Yu, W. H., Zhuo, F., Qiu, G. P., et al. (2013). Hyperosmotic induction of aquaporin expression in rat astrocytes through a different MAPK pathway. *J. Cell. Biochem.* 114, 111–119. doi: 10.1002/jcb.24308

Yuan, H., Gao, B., Duan, L., Jiang, S., Cao, R., Xiong, Y. F., et al. (2010). Acute hyperosmotic stimulus-induced Fos expression in neurons depends on activation of astrocytes in the supraoptic nucleus of rats. *J. Neurosci. Res.* 88, 1364–1373. doi: 10.1002/jnr.22297

Zeynalov, E., Jones, S. M., Seo, J. W., Snell, L. D., and Elliott, J. P. (2015). Arginine-vasopressin receptor blocker conivaptan reduces brain edema and blood-brain barrier disruption after experimental stroke in mice. *PLoS One* 10:e0136121. doi: 10.1371/journal.pone.0136121

Zhang, B., Glasgow, E., Murase, T., Verbalis, J. G., and Gainer, H. (2001). Chronic hypoosmolality induces a selective decrease in magnocellular neurone soma and nuclear size in the rat hypothalamic supraoptic nucleus. *J. Neuroendocrinol.* 13, 29–36. doi: 10.1111/j.1365-2826.2001.00593.x

Zhang, Y., Hong, G., Lee, K. S., Hammock, B. D., Gebremedhin, D., Harder, D. R., et al. (2017). Inhibition of soluble epoxide hydrolase augments astrocyte release of vascular endothelial growth factor and neuronal recovery after oxygen-glucose deprivation. *J. Neurochem.* 140, 814–825. doi: 10.1111/jnc.13933

Zhao, X., Yan, X., Liu, Y., Zhang, P., and Ni, X. (2016). Co-expression of mouse TMEM63A, TMEM63B and TMEM63C confers hyperosmolarity activated ion currents in HEK293 cells. *Cell Biochem. Funct.* 34, 238–241. doi: 10.1002/cbf.3185

Zorec, R., Araque, A., Carmignoto, G., Haydon, P. G., Verkhratsky, A., and Parpura, V. (2012). Astroglial excitability and gliotransmission: an appraisal of Ca^{2+} as a signalling route. *ASN Neuro* 4:e00080. doi: 10.1042/AN20110061

Conflict of Interest Statement: The authors declare that the research was conducted in the absence of any commercial or financial relationships that could be construed as a potential conflict of interest.

frontiers in Molecular Neuroscience

ORIGINAL RESEARCH
published: 18 May 2018
doi: 10.3389/fnmol.2018.00162

Dynamic Calcium Release From Endoplasmic Reticulum Mediated by Ryanodine Receptor 3 Is Crucial for Oligodendroglial Differentiation

Tao Li, Lingyun Wang, Teng Ma, Shouyu Wang, Jianqin Niu, Hongli Li and Lan Xiao**

Chongqing Key Laboratory of Neurobiology, Department of Histology and Embryology, Third Military Medical University, Chongqing, China

Increased intracellular Ca^{2+} in oligodendrocyte progenitor cells (OPCs) is important to initiate their differentiation, but the intracellular Ca^{2+} channel involved in this process remains unclear. As a Ca^{2+}-induced Ca^{2+} release (CICR) channel that mediates endoplasmic reticulum (ER) Ca^{2+} release, the role of ryanodine receptors (RyRs) in oligodendroglial development is unexplored. In the present study, we observed that among the three mammalian isoforms, oligodendroglial lineage cells selectively expressed RyR3. Strong RyR3-positive signal was distributed all over the cytoplasm and processes in OPCs and/or immature OLs (imOLs), whereas it gradually decreased and was located mainly around the perinuclear region in mature oligodendrocytes (OLs). In addition, RyR3-mediated intracellular Ca^{2+} waves following caffeine stimulation were correlated with the expression pattern of RyR3, in which high flat Ca^{2+} fluctuations and oscillatory Ca^{2+} waves were more frequently recorded in OPCs and/or imOLs than in OLs. Through further functional exploration, we demonstrated that pretreatment with the RyR antagonist ryanodine could neutralize the increase in intracellular Ca^{2+} induced by OPC differentiation and reduce the number of mature OLs. Moreover, gene-level knockdown of RyR3 by lentivirus in OPCs resulted in inhibition of OPC differentiation. Taken together, our results provide new insight into the crucial role of RyR3-mediated ER Ca^{2+} release in the regulation of OPC differentiation and/or myelination.

Keywords: oligodendrocyte progenitor cells (OPCs), oligodendrocytes (OLs), ryanodine receptor 3 (RyR3), Ca^{2+} release, differentiation, caffeine

OPEN ACCESS

Edited by:
Alexej Verkhratsky, University of Manchester, United Kingdom

Reviewed by:
Carlos Matute, University of the Basque Country (UPV/EHU), Spain
Alla B. Salmina, Krasnoyarsk State Medical University named after Prof. V.F.Voino-Yasenetski, Russia

****Correspondence:***
Hongli Li
lihongli@tmmu.edu.cn
Lan Xiao
xiaolan35@hotmail.com

Received: *30 November 2017*
Accepted: *30 April 2018*
Published: *18 May 2018*

Citation:
Li T, Wang L, Ma T, Wang S, Niu J, Li H and Xiao L (2018) Dynamic Calcium Release From Endoplasmic Reticulum Mediated by Ryanodine Receptor 3 Is Crucial for Oligodendroglial Differentiation. Front. Mol. Neurosci. 11:162. doi: 10.3389/fnmol.2018.00162

INTRODUCTION

In the CNS, myelinating oligodendrocytes (OLs) originate from oligodendrocyte progenitor cells (OPCs) after passing through a series of distinct developmental stages, i.e., OPCs, immature OLs (imOLs) and mature OLs (Stangel and Hartung, 2002). As impairment of OL differentiation has been considered to be the major cause of remyelination failure, which occurs in numerous

Abbreviations: CICR, Ca^{2+}-induced Ca^{2+} release; CNPase, 2′,3′-cyclic nucleotide-3′-phosphodiesterase; ER, endoplasmic reticulum; imOL, immature oligodendrocyte; MBP, myelin basic protein; OL, oligodendrocyte; OPC, oligodendrocyte progenitor cell; PDGFRα, platelet-derived growth factor receptor α; RyR, ryanodine receptor; VOCC, voltage-operated Ca^{2+} channel.

demyelination diseases such as multiple sclerosis (MS; Wolswijk, 1998; Chang et al., 2002; Kuhlmann et al., 2008), promoting OPC differentiation into mature OLs becomes a promising approach for myelin repair. However, the mechanism regulating oligodendroglial differentiation remains to be elucidated. As a critical functional pattern of non-excitable glia cells, Ca^{2+} signaling is essential for oligodendroglial differentiation and myelination (Kirischuk et al., 1995; Cohen et al., 1996; Yoo et al., 1999; Soliven, 2001; Fulton et al., 2010; Cheli et al., 2015; Friess et al., 2016; Baraban et al., 2018; Krasnow et al., 2018). For instance, inhibition of the voltage-operated Ca^{2+} entry in OPCs repressed their maturation and the myelin forming ability (Cheli et al., 2015). Increasing resting intracellular Ca^{2+} through membrane depolarization could facilitate MBP synthesis in OPCs (Friess et al., 2016). Newest studies further provided *in vivo* data showing that the Ca^{2+} transients in OLs could regulate retraction and elongation of the developing myelin sheath (Baraban et al., 2018; Krasnow et al., 2018). However, the Ca^{2+} channels involved in oligodendroglial differentiation is believed to be important but remains largely unexplored.

It is known that endoplasmic reticulum (ER) is the major intracellular Ca^{2+} pool (Meldolesi and Pozzan, 1998) and that ER Ca^{2+} release is driven mainly by inositol-1,4,5,-trisphosphate receptors (IP3Rs) and ryanodine receptors (RyRs; Koulen and Thrower, 2001). In OPCs, both IP3R2 and ryanodine receptor 3 (RyR3) can mediate highly localized Ca^{2+} release, of the types called "puffs" and "sparks", respectively (Haak et al., 2001), but only IP3R2 is able to initiate Ca^{2+} waves under pharmacological treatments (Haak et al., 2001). However, the functions of those channels during oligodendroglial development remain unclear. Series of studies demonstrate that, compared with IP3Rs, the opening of which requires both Ca^{2+} and IP3 (Moraru et al., 1999; Foskett et al., 2007), RyRs are Ca^{2+}-induced Ca^{2+} release (CICR) channels that can be triggered merely by a low concentration of Ca^{2+} ($\sim$1 μM; Meissner et al., 1986, 1997; Bezprozvanny et al., 1991), and this CICR function has been shown to powerfully amplify small inward Ca^{2+} currents in NG2 glial cells (Haberlandt et al., 2011). Therefore, we propose that RyR3 is likely a critical bridge for the formation of intracellular Ca^{2+} signaling and thus participates in the regulation of oligodendroglial development.

In the present study, we sought to characterize the expression and function of RyRs during OPC differentiation. Our results showed that RyR3 was selectively expressed and widely distributed in the soma and processes of the oligodendroglial lineage cells and that its expression level was downregulated following OPC differentiation. Using confocal Ca^{2+} imaging, we found that the ER Ca^{2+} release after caffeine stimulation was much stronger in OPCs and imOLs than in mature OLs. Moreover, inhibiting the function of RyR3 either pharmacologically or by gene knockdown suppressed the differentiation of OPCs. Our results revealed a critical role for RyR3-mediated Ca^{2+} signaling in oligodendroglial differentiation that may provide new insight into therapeutic approaches for demyelinating diseases.

MATERIALS AND METHODS

OPC Culture

Cortical OPCs were purified as previously described (Niu et al., 2012b). Briefly, the mixed glial cells were isolated from cortex of postnatal day 1–3 neonatal Sprague-Dawley (SD) rats and enriched in OPC growth medium followed by two passages to enrich cell numbers. OPC proliferation medium was DMEM/F12 + 1% N2 supplement + PDGFAA. OPCs were induced to differentiate by replacing the medium with OPC differentiation medium: DMEM/F12 + 1% N2 supplement + 5 mg/mL N-acetyl-L-cysteine (Amresco) + 1% fetal bovine serum + 5 mg/mL insulin.

Reagents used were as follows: Dulbecco's modified Eagle's medium/F12 (DMEM/F12; Hyclone, SH30023), N2 supplement (Invitrogen, 17502048), fetal bovine serum (FBS; Hyclone, SV30087), insulin (Sigma, I6634), N-acetyl-l-cysteine (NAC; AMRESCO, 0LA0011), PDGFAA (Peprotech, 100-13A). The SD rats related procedures were performed in accordance with the guidelines approved by the Laboratory Animal Welfare and Ethics Committee of the Third Military Medical University (Niu et al., 2016).

Confocal Ca^{2+} Imaging Measurements

OPCs were grown and differentiated in glass-bottom dish and loaded with the fluorescent Ca^{2+} sensitive dye Fluo-3AM (5 μM, Invitrogen) for 20 min at 37°C in a modified imaging buffer containing (in mM): NaCl, 135; KCl, 3; $MgCl_2$, 2; Glucose, 8; HEPES, 10 and $CaCl_2$, 2 (pH adjusted to 7.4 with NaOH). The dye-loaded cells were washed twice and maintained for at least 20 min at RT in fresh imaging buffer to allow complete dye de-esterification. Ca^{2+} wave and fluorescence images were real-time recorded for at least 15 min in all experiments, using a confocal laser-scanning microscope (FluoView FV1000, Olympus, Japan) with the UplanFl40× objective (N.A. 0.95). The image acquisition frequency is 100–180 ms/image. Cell morphology was detected using differential interference contrast (DIC) under confocal microscopy. Ca^{2+} concentrations were measured by exciting Fluo-3 AM at 488 nm.

Intracellular Ca^{2+} responses in OPCs, imOLs and mature OLs were recorded with caffeine (20 mM, Sigma, Ca^{2+} free) stimulation in a Ca^{2+} free imaging buffer. For spontaneous Ca^{2+} recordings, OPCs were grown in proliferation medium or differentiation medium for 6 h with or without ryanodine treatment (50 μM, TOCRIS, 1329, 10 min). Fluo-3 loading and cell washing was followed by applying normal proliferating medium (Pro-medium) or differentiating medium (Diff-medium) for the following recording.

Cell Processing and Immunocytochemistry

Cells were grown on coverslips, fixed in cold 4% paraformaldehyde for 20 min, rinsed with 0.01 M PBS, blocked with 1% bovine serum albumin (BSA) and 0.2% Triton-X100 for 30 min and then incubated with primary antibodies diluted in 1% BSA overnight at 4°C and then by fluorophore-conjugated secondary antibodies at room temperature (RT) for 2 h. Cell

nuclei were stained with 4′,6-diamidino-2-phenylindole (DAPI, Thermo Fisher) for 10 min.

In this study, the following antibodies were used: mouse polyclonal anti-Olig2 (1:500, Millipore, MABN50), rabbit polyclonal anti-RyR3 (1:200, Millipore, AB9082), and goat anti-myelin basic protein (MBP; 1:500, Santa Cruz, sc13914). The secondary antibodies were as follows: Alexa 568-labeled donkey anti-mouse (1:1000, Invitrogen), Alexa 488-labeled donkey anti-goat (1:1000, Invitrogen), Alexa 568-labeled donkey anti-goat (1:1000, Invitrogen), Alexa 568-labeled donkey anti-rabbit (1:1000, Invitrogen) and Cy5-labeled rabbit anti-mouse (1:500, Jackson ImmunoResearch).

Image Acquisition and Quantification

Fluorescent images were captured using an Axio Imager M2 fluorescence microscope (Zeiss, Oberkochen, Germany) or a confocal laser-scanning microscope (Olympus, IV 1000, Shinjuku, Tokyo) with excitation wavelengths appropriate for Alexa Fluor 488 (488 nm), 596 (568 nm), 647 (628 nm) or DAPI (380 nm). Digital images of the oligodendroglial lineage cells in the supplemental figure were acquired with an Olympus IX51 microscope with an Olympus C-7070 camera (Tokyo). For the statistical analysis, randomly selected images in at least three representative fields were acquired from each sample. Detection and quantification were performed using ImageJ software (National Institutes of Health, NIH).

Western Blot Analysis

The cells were lysed using RIPA lysis buffer (Beyotime, P0013B) with freshly added 1% phenylmethylsulfonyl fluoride (PMSF, Amresco, O754) solution. Protein concentration was determined using Coomassie brilliant Blue G-250. SDS-PAGE and Western blotting were carried out as reported previously (Niu et al., 2012a). Proteins were transferred to polyvinylidene difluoride (PVDF) membranes and visualized by chemiluminescence (ECL Plus, GE Healthcare, Marlborough, MA, USA) after incubation with the antibodies. β-actin was used as the loading control. Quantification of band intensity was performed using ImageJ software. The primary antibodies included the following: rabbit polyclonal anti-RyR3 (1:1000, Millipore), rabbit polyclonal anti-platelet-derived growth factor receptor α (PDGFRα; 1:1000, Santa Cruz, sc-338), mouse anti-2′,3′-cyclic nucleotide-3′-phosphodiesterase (CNPase; 1:1000, Abcam, ab6319), goat anti-MBP (1:1000, Santa Cruz) and mouse anti-β-actin (1:2000, Santa Cruz, sc-47778). The secondary antibodies included the following: goat anti-mouse-HRP (1:2000, Santa Cruz, sc-2094), goat anti-rabbit-HRP (1:2000, Santa Cruz, sc-2313) and rabbit anti-goat-HRP (1:2000, Santa Cruz, sc-2020).

RT-PCR Analysis

Total ribonucleic acid (RNA) was isolated from different stages of OPC cultures (OPC differentiated for 1 day, 2 days, or 4 days using TRIzol (Life Technologies). Real-time polymerase chain reaction (RT-PCR) was performed with the C1000 Touch™ Real-time PCR Detection System (Bio-Rad) and GoTaq® qPCR Master Mix (Promega, Sunnyvale, CA, USA). The amplification procedure and melt curve analysis were performed using three independent replicates for each sample.

The oligonucleotide primers used were as follows:

	Forward	Reverse	Tm
RyR1	GAGGGTGATGAAGATGAGAAC	TCCCGCCCGAAGATGTC	60°C
RyR2	GCTGGCCCTGTTTGTTG	ATCCATGCCCAGTAACTCGCT	61.3°C
RyR3	CTGTGTGGTGGGCTATTACTG	TGCTTTGGCCTCTTCTACTG	58.3°C
MBP	GAGACCCTCACAGCGACAC	ATCCAGAGCGGCTGTCTC	59°C
β-actin	CGTTGTACATCCGTAAAGACC	CATCGCACTCCTGCTTGCT	58°C

Lentivirus Mediated shRNA Interference

The shRNA lentivirus was purchased from Obio Technology, Shanghai. Targeted sequence in rat RyR3 gene is: AGATGCTAATTGCATCTC. The primary lentivirus solution was diluted in several gradient concentrations (1:10, 1:100, 1:300, 1:500, 1:1000) to check the best work concentration (normal oligodendroglial viability and good interference efficiency). The lentivirus was diluted 1:300 in the differentiation medium with a primary concentration of $8.67*10^8$ transducing units (TU)/ml for the interference group (shRyR3) and $6.71*10^8$ TU/ml for the control group (shCTL). Lentivirus was removed after transfection for 16 h. OPC were further differentiated for another 32 h and fixed.

Antisense Oligonucleotides

Phosphodiester ODNs protected by terminal phosphorothioate double substitution (capped ODNs) against possible exonuclease-mediated degradation were purchased from Tib-Molbiol (Sigma). The sequences are as follows: anti-RyR3: 5′-A*G*ATGCTAATTGCATC*T*C-3′ (*indicates the phosphorothioate residues) and an 18-mer fully degenerated ODN (dODN), 5′-N*N*NNNNNNNNNNNNNN*N*N-3′ (where N is G, C, A, or T), which was used as a control ODN. ODNs were transported using an artificial cationic lipid (DOTAP; Sigma) to enhance both uptake and stability. Antisense ODNs (aODNs) or dODNs were pre-incubated at 37°C for 30 min. Differentiated OLs were collected on day 3.

Statistics Analysis

All experiments were repeated at least three times. Data are shown as the means ± SEM. Statistical analyses of three groups were performed using one-way analysis of variance (ANOVA) followed by Tukey's *post hoc* test. Comparisons between two experimental groups were made using Student's *t*-test (GraphPad Prism 6). A probability of $p < 0.05$ was considered significant.

RESULTS

Oligodendrocytes Selectively Express RyR3, Which Is Downregulated During Differentiation

Similar to our previous studies (Niu et al., 2012b), different stages of oligodendroglial cells in our culture system were identified based on morphological features using DIC and immunostaining for stage-specific markers. Normally, OPCs

have small, round cell bodies with a bipolar morphology (Supplementary Figure S1). After 2 days in the differentiation medium, imOLs with 3–5 primary processes and a sparse arborization predominate this stage (Supplementary Figure S1). After 4 days of differentiation, mainly mature OLs characterized by multipolar processes and a rich arborization were observed (Supplementary Figure S1). These features indicate the accuracy of our culture model for studying the developmental schedule of the OL lineage.

To determine the RyR subtypes expressed in OLs, we first analyzed the mRNA levels in OL lineage cells. We found that only RyR3, the known "brain type", was detected in OL lineage cells. In parallel experiments, RyR3 mRNA was also found in astrocytes, RyR2 mRNA was found in astrocytes and rat brain tissue, and RyR1 mRNA was only found in brain tissue (**Figure 1B**). Interestingly, the RyR3 mRNA level gradually decreased during OPC differentiation, and this downregulation tendency was further confirmed by western blot analysis (**Figures 1C,D**).

Next, we clarified the RyR3 distribution pattern in OL lineage cells by immunostaining. It has been shown that RyR3 is the subtype of ryanodine receptors expressed in OPCs. Specifically, RyR3 is located throughout the cell body and processes of OPCs, except in the region of the nuclear membrane (Haak et al., 2001). Our present results also revealed the enrichment of RyR3 in the processes and non-nuclear area of OPCs and imOLs, while in mature OLs, RyR3 was mainly located in the cell body and primary processes (**Figure 1A**).

Taken together, these results reveal a spatiotemporal regulated expression pattern of RyR3 in OL lineage cells, indicating its potential in regulating OL development.

ER Ca^{2+} Release Following Caffeine Stimulation Is Stage Specific During OPC Differentiation

Although OPCs are reported to have spontaneous oscillatory-like Ca^{2+} activity with peak and plateau transients, while mature OLs show "flat" Ca^{2+} signaling (Niu et al., 2016), the ER Ca^{2+} channels in OPCs (RyR3 and IP_3R2) are relatively quiescent in comparison to those in neurons (Haak et al., 2001). To better study the RyR channel function, we took advantage of the classical RyR agonist caffeine (20 mM, 0 Ca^{2+}; Zucchi and Ronca-Testoni, 1997) and real-time recorded the intracellular Ca^{2+} concentration with confocal microscopy. The Ca^{2+} release peaks are significantly higher in OPC and imOLs than in mature OLs (**Figure 2D**). More importantly, three typical Ca^{2+} responses were recorded in OL lineage cells

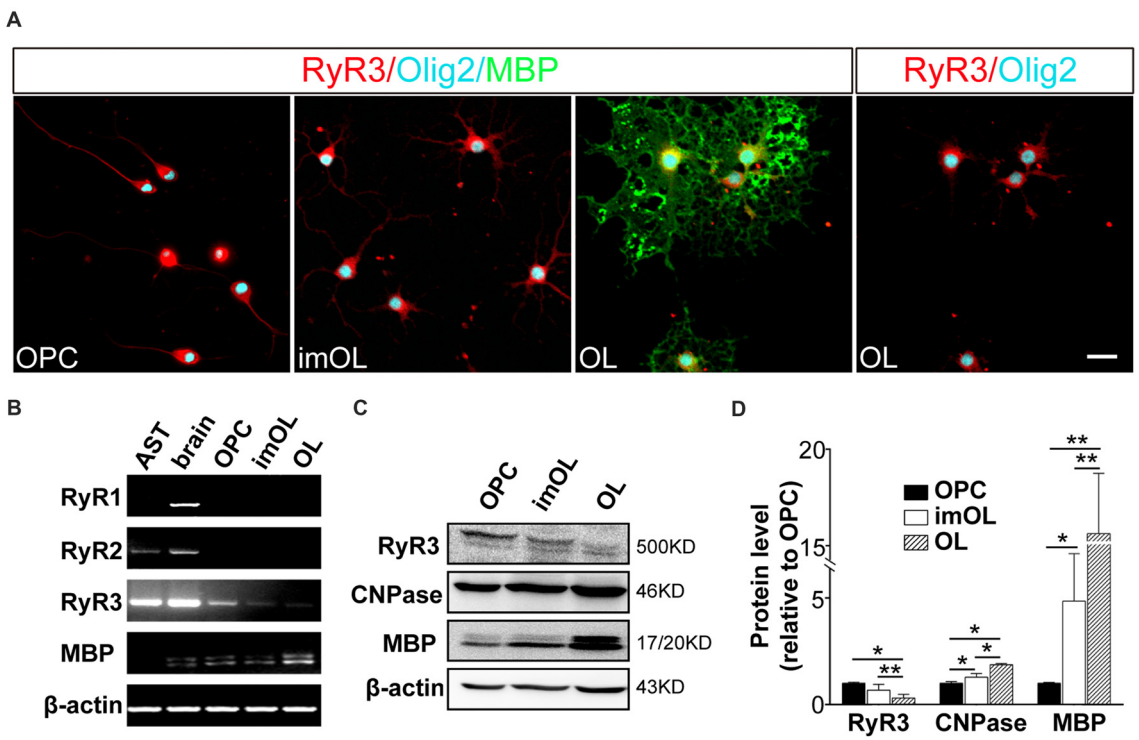

FIGURE 1 | Oligodendroglial cells selectively express ryanodine receptor 3 (RyR3), which is downregulated during differentiation. **(A)** Immunofluorescence staining of RyR3, Olig2 (oligodendroglial lineage marker) and myelin basic protein (MBP; mature OL marker) in three stages of cultured OL lineage cells. RyR3 was strongly distributed all over the cytoplasm and processes in oligodendrocyte progenitor cells (OPCs) and immature oligodendrocytes (imOLs), while in mature OLs, RyR3 signal was mainly located in the cell body and showed lower expression in the primary processes. Scale bar 20 μm. **(B)** mRNA levels of RyRs in OL lineage cells, astrocytes (AST) and rat brain tissue. **(C,D)** Western blot analysis showed increased levels of myelin proteins (CNPase, MBP) and decreased levels of RyR3 protein during OPC development (*$p < 0.05$, **$p < 0.01$).

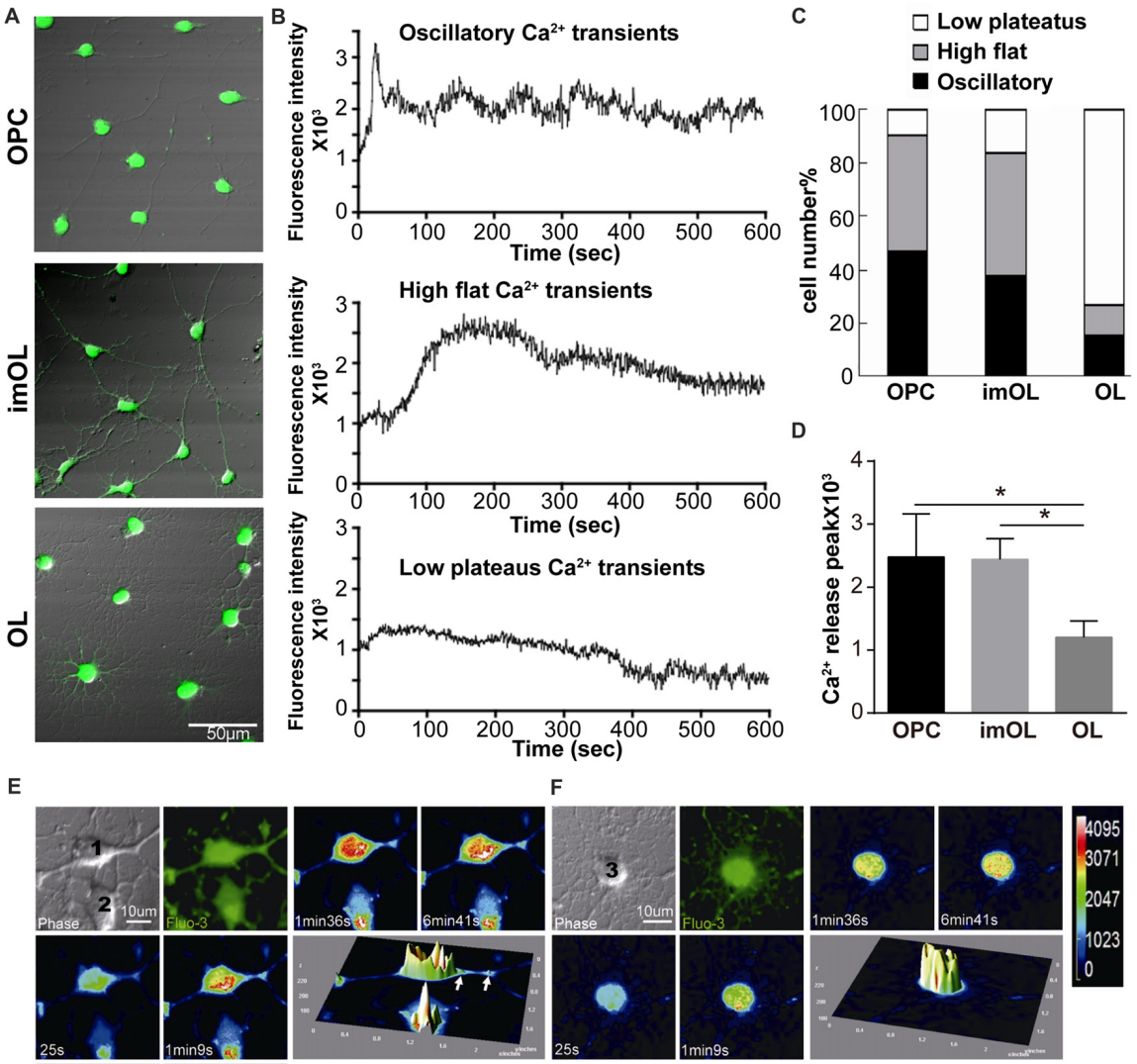

FIGURE 2 | Endoplasmic reticulum (ER) Ca^{2+} release following caffeine stimulation is stage specific during OPC differentiation. **(A)** Differential interference contrast (DIC) with Fluo-3 fluorescence of three stages of OL lineage cells, showing typical shape of OPC, imOL and OL. Note that the pictures were acquired at the end point of Ca^{2+} imaging to ensure the morphology of the oligodendroglial cells, thus Fluo-3 fluorescence was extremely strong. **(B)** Representative examples of Ca^{2+} response following caffeine stimulation. Note that the start point in the x-axis is not the beginning point of recording, baseline recording is omitted from the curve. **(C)** OPCs and imOLs, which tend to respond with oscillatory Ca^{2+} transients and high flat Ca^{2+} transients, reacted stronger than OLs, which tend to respond with low plateaus Ca^{2+} transients. **(D)** OPC and imOL had significantly higher Ca^{2+} release peaks after caffeine stimulation compared with mature OLs (*$p < 0.05$). Time-lapse Ca^{2+} imaging induced by caffeine (20 mM, 0 Ca^{2+}) in an OPC (1) **(E)** and a mature OL **(F)**. Four successive scans were selected from a series of images obtained within 10 min. Transient fluorescence fluctuations, representing local Ca^{2+} release events, were indicated by the pseudocolored peaks in the OPC cell body and processes (arrows), but they occurred only in the soma in mature OLs. The pseudocolor bar in **(F)** showed the fluorescence intensity of different colors.

after caffeine stimulation, showing stage-specific characteristics (**Figures 2A,B**). The high flat Ca^{2+} response following caffeine application was mainly found in OPCs (53.7%, n = 65) and imOLs (54.8%, n = 72). Likely, the oscillatory Ca^{2+} transients were present at a higher ratio in OPCs (35.5%, n = 65) and imOLs (27.9%, n = 72) than in mature OLs (10.5%, n = 76). The low plateaus Ca^{2+} response was the dominant reaction of mature OLs (76.3%, n = 76) but was barely found in OPCs and imOLs (**Figure 2C**). Notably, the millimolar concentration of caffeine was previously demonstrated to be an inhibitor of the IP3R channel in glioblastoma (1–10 mM; Kang et al., 2010), cerebellar microsomes (10–50 mM; Brown et al., 1992), B lymphocytes (1–25 mM) and other cells (Sei et al., 2001). In our present study, while the corresponding Ca^{2+} influx was abolished by using a Ca^{2+}-free extracellular solution, the caffeine (20 mM)-induced Ca^{2+} transient is likely due to release of Ca^{2+} from ER mediated mainly by RyR3 channel. We assume that this stage-specific response is probably correlated to the downregulated expression of RyR3 during OL development.

Given that RyR3 is not homogeneously distributed in the cell body and cell processes (Haak et al., 2001), especially in mature OLs, as we showed in **Figure 1A**, we wonder whether there is a regional difference in the Ca^{2+} response. By transforming the time-lapse Ca^{2+} imaging into pseudocolor changes and 3D surface plots with Image J software, we found that OPCs respond rapidly and strongly in both the soma and processes (**Figure 2E**), whereas only somal regions showed a slow and weak Ca^{2+} response in mature OLs (**Figure 2F**). Thus, the Ca^{2+} response pattern is highly correlated with the expression level and distribution of RyR3 in OL lineage cells.

At this point, we clarified the spatiotemporal regulated expression pattern of RyR3 and its expression-correlated functional pattern after caffeine stimulation. Our results indicate that RyR3-mediated Ca^{2+} signaling actively participates in the developmental regulation of OL lineage cells. The role of RyR3 under physiological conditions requires further exploration.

Inhibition of RyR3 Function by Ryanodine Suppresses OPC Differentiation

As Ca^{2+} signaling is essential for OPC differentiation and myelination, especially the initiation of OPC differentiation (Cheli et al., 2015; Friess et al., 2016), we next investigated whether there is active Ca^{2+} signaling at the initial stage of OPC differentiation. Spontaneous Ca^{2+} signaling was recorded in OPCs cultured in the proliferation medium and in OPCs that had been cultured in differentiation medium for 6 h. Consistent with our previous research (Niu et al., 2016), approximately 38.5% of OPCs presented occasional Ca^{2+} elevation (n = 18), which was characterized by a gradual increase in the Ca^{2+} concentration to a peak and a subsequently

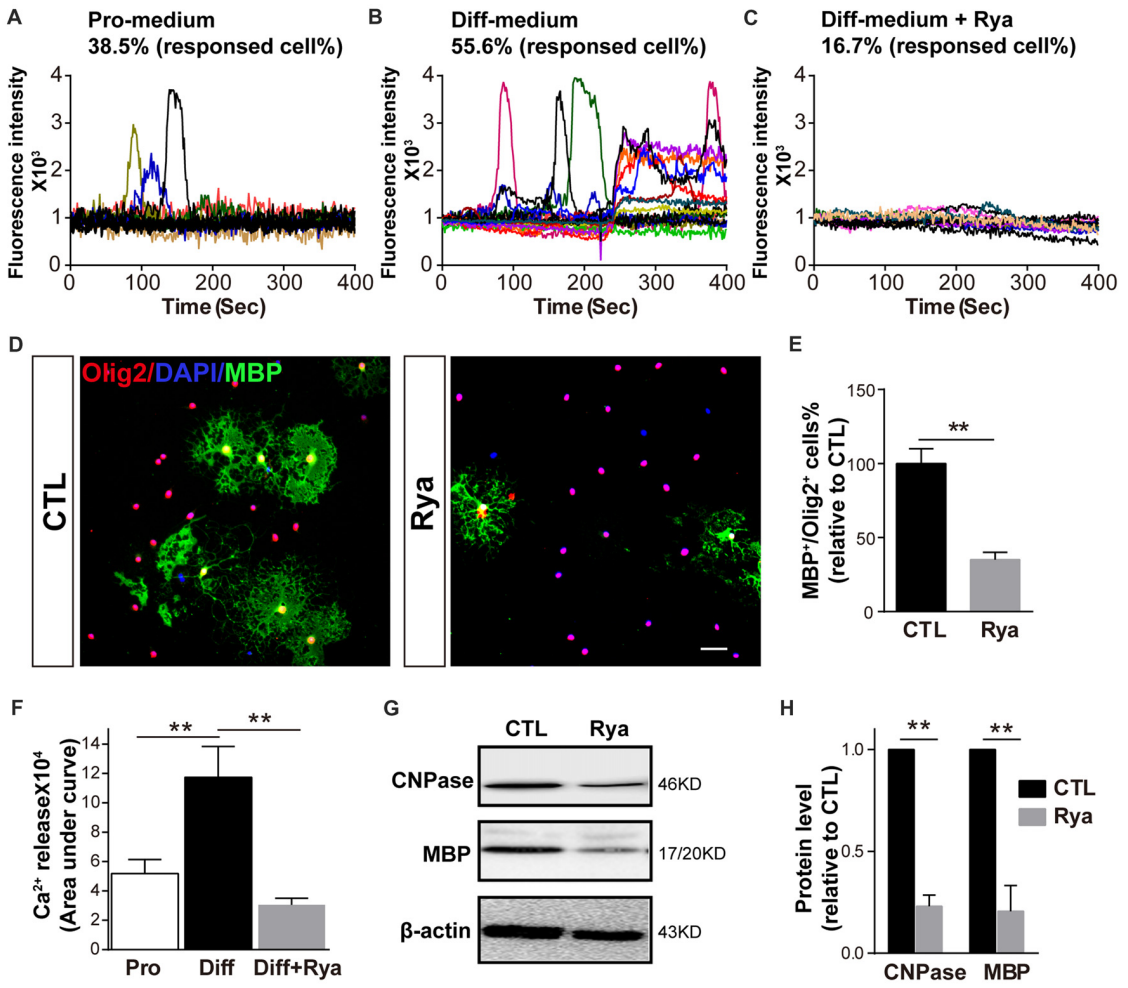

FIGURE 3 | Inhibition of RyR3 by ryanodine suppresses OPC differentiation. **(A)** Ca^{2+} recording of OPCs in proliferation medium (Pro-medium) showing random spontaneous waves. **(B)** OPCs cultured in differentiation medium (Diff-medium) for 6 h showed frequently higher peak waves, which could be inhibited by ryanodine (Rya) **(C)**. **(F)** The total amount of Ca^{2+} release, reflected by the area under curve, was greater in early differentiating OPCs than in proliferating OPCs (**$p < 0.05$), and the release activity in early differentiating OPCs was greatly reduced by ryanodine (**$p < 0.05$). **(D,E)** There were fewer MBP-positive mature OLs after treatment with ryanodine (50 μM) for 72 h. Scale bar 50 μm. **(G,H)** Western blot analysis showed the same inhibitory effect of ryanodine on OPC differentiation (**$p < 0.05$).

decreasing Ca^{2+} signal (**Figure 3A**). Meanwhile, in OPCs that were induced to initiate differentiation, spontaneous Ca^{2+} activity was observed in 55.6% of cells (n = 20). Those Ca^{2+} activities appeared at higher frequency; moreover, the elevation of Ca^{2+} signaling was more persistent in certain individual cells (**Figure 3B**). It has been reported that ryanodine, a RyR-specific blocker, locks the RyR channel into a "closed state" at higher concentrations (>50 μM; Meissner, 1986; Lai et al., 1989; McGrew et al., 1989). Thus, we used 50 μM ryanodine as an antagonist to block RyR3. The differentiation-related Ca^{2+} activity was dramatically inhibited (n = 24; **Figures 3C,F**). The amount of Ca^{2+} release reflected as the area under curve was markedly greater in early differentiating OPCs than in proliferating OPCs (**Figure 3F**). This result indicates that RyR3-mediated Ca^{2+} release from the ER is a critical process during OPC differentiation. To further verify the function of RyR3 in oligodendroglial differentiation, we treated OPCs with ryanodine (50 μM) and measured the number of mature OLs by immunofluorescence staining after 3 days of differentiation. The number of MBP-positive OLs was significantly decreased in the ryanodine-treated group (**Figures 3D,E**). Importantly, cell viabilities of OPC cultures were not affected by ryanodine treatment as reflected by the nuclear number, which is consistent with previous works (Matyash et al., 2002; Ruiz et al., 2010). Western blot results showed decreased protein levels of MBP and CNPase, which also reflected the inhibition of oligodendroglial maturation (**Figures 3G,H**). Thus, our results demonstrate that RyR3-mediated Ca^{2+} signaling does participate in the differentiation of OPCs.

Knockdown of RyR3 in OPCs Results in Inhibition of OPC Differentiation

To further detect the role of RyR3 in OPC differentiation, we performed lentivirus-mediated gene knockdown of RyR3, which more precisely targets RyR3. OPCs were induced to differentiate after infection with an RNA interference lentivirus (shRyR3) or a control lentivirus (shCTL). After differentiation for 48 h, we observed efficient infection of both lentiviruses, visualized as the GFP expression in the cytoplasm (**Figure 4A**). Immunofluorescence staining for Olig2 (OL lineage marker) and MBP (mature OL marker) showed that the percentage of MBP-positive OLs was significantly decreased and most of the MPB-positive cells showed smaller process areas, and less flat membrane structures after RyR3 knockdown (**Figures 4A,B**), indicating the blockage of OPC differentiation in the absence of RyR3-mediated Ca^{2+} signaling. Cell viability after lentivirus treatment was guaranteed by the unchanged Olig2 positive cell number. As antisense oligonucleotides (aODNs) have the ability to selectively reduce the mRNA level of RyR3 (Galeotti et al., 2008), we also applied aODNs in OPC cultures and confirmed that aODNs reduced the protein level of RyR3. Consistent with the shRNA effect, aODN treatment similarly reduced the number of mature OLs (data not shown) and the levels of MBP (**Figures 4C,D**). Taken together, these observations reveal that gene-level knockdown of RyR3 induces loss of

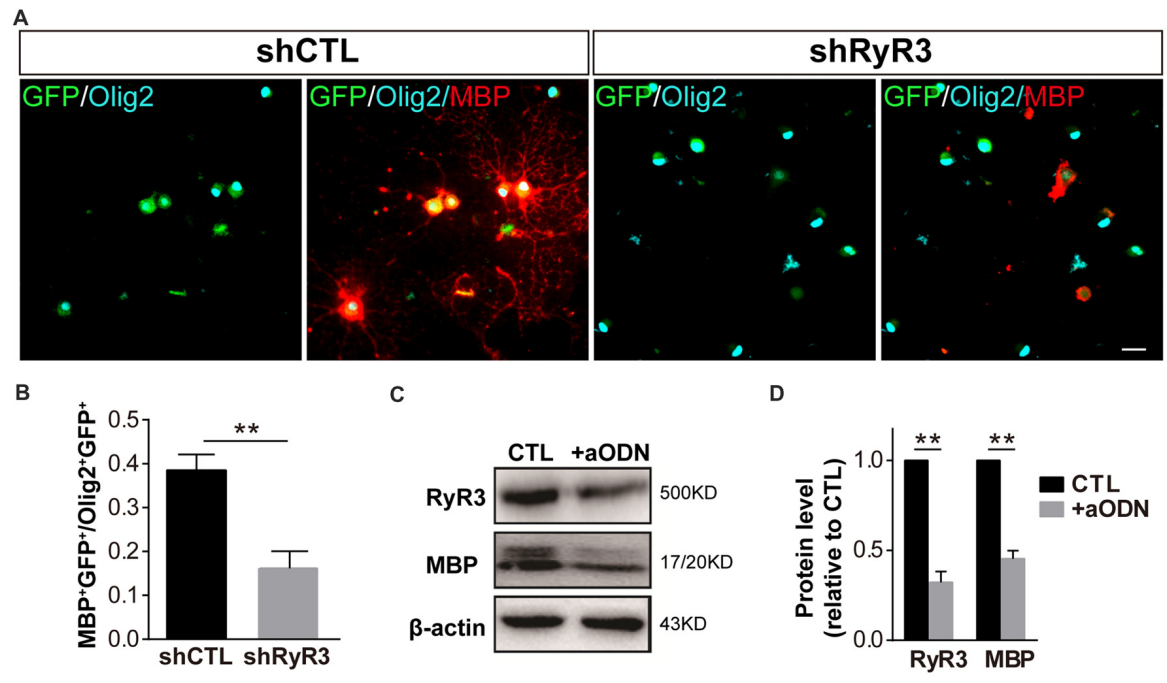

FIGURE 4 | Knockdown of RyR3 in OPCs results in inhibition of OPC differentiation. **(A,B)** Gene knockdown of RyR3 with shRNA interference mediated by lentivirus infection showed fewer MBP-positive mature OLs after 48 h of differentiation. GFP was expressed in lentivirus-infected cells (**$p < 0.05$). Scale bar 20 μm. **(C,D)** Knockdown of RyR3 in OPCs by antisense oligonucleotide (+aODN) resulted in less expression of myelin basic protein (MBP; **$p < 0.05$).

RyR3 channel function in OPCs, finally resulting in inhibition of OPC differentiation, implying that RyR3-mediated Ca^{2+} signaling plays an essential role during OPC differentiation.

DISCUSSION

In non-excitable oligodendroglial cells, how intracellular Ca^{2+} signaling is regulated and how it contributes to oligodendroglial differentiation remains unclear. In our present study, we systematically analyzed the expression and function of the ER Ca^{2+} release channel—RyR3. We found that RyR3 is the only RyR expressed in oligodendroglial cells and dynamically regulated during OPC differentiation. Importantly, inhibition of RyR3 resulted in blockage of OPC differentiation (**Figure 5**). Our results not only demonstrate the essential role of RyR3-mediated Ca^{2+} signaling for oligodendroglial differentiation but also improve our understanding of the intracellular Ca^{2+} channel function in oligodendroglial lineage cells, which has barely been studied before.

RyRs (RyR1–3) are major Ca^{2+} channels responsible for ER Ca^{2+} release, and RyR-mediated transient increase and oscillations of intracellular Ca^{2+} has been considered to be particularly important for cell functions (Zalk et al., 2007; Fulton et al., 2010; Suzuki et al., 2012). In oligodendroglial lineage cells, the RyR functionality was suggested to correlate with their developmental stages both *in vivo* and *in vitro* (Simpson et al., 1998), but the isoform of RyRs involved in this process has not been identified. Among RyRs, RyR3 is abundantly distributed in the CNS, and it functions in the activation and migration of astrocytes (Fill and Copello, 2002; Matyash et al., 2002; Galeotti et al., 2008; Lanner et al., 2010). In oligodendroglial lineage cells, only RyR3 was selectively expressed in cultured rat cortex OPCs (Haak et al., 2001), while another study demonstrated that three isoforms of RyRs (RyR1–3) were expressed in cultured rat optic nerve-derived mature OLs (Ruiz et al., 2010). Here, using rat cortex-derived OPC cultures, we confirmed the selective expression of RyR3 in oligodendroglial lineage cells and further determined the spatiotemporal expression pattern of RyR3 during oligodendroglial differentiation. Additionally, we found that enrichment of RyR3 in OPCs and imOLs corresponded to the stronger Ca^{2+} responses in those cell types than in mature OLs following caffeine stimulation. Interestingly, a previous study in myotubes has revealed that embryonic myotubes, which express RyR3, have considerably more variability in the size and kinetics of their Ca^{2+} sparks than do adult cells, which lose RyR3 expression (Ward et al., 2000). Therefore, expression of RyR3 in OPCs and imOLs likely enabled them to be more hyperactive in terms of Ca^{2+}

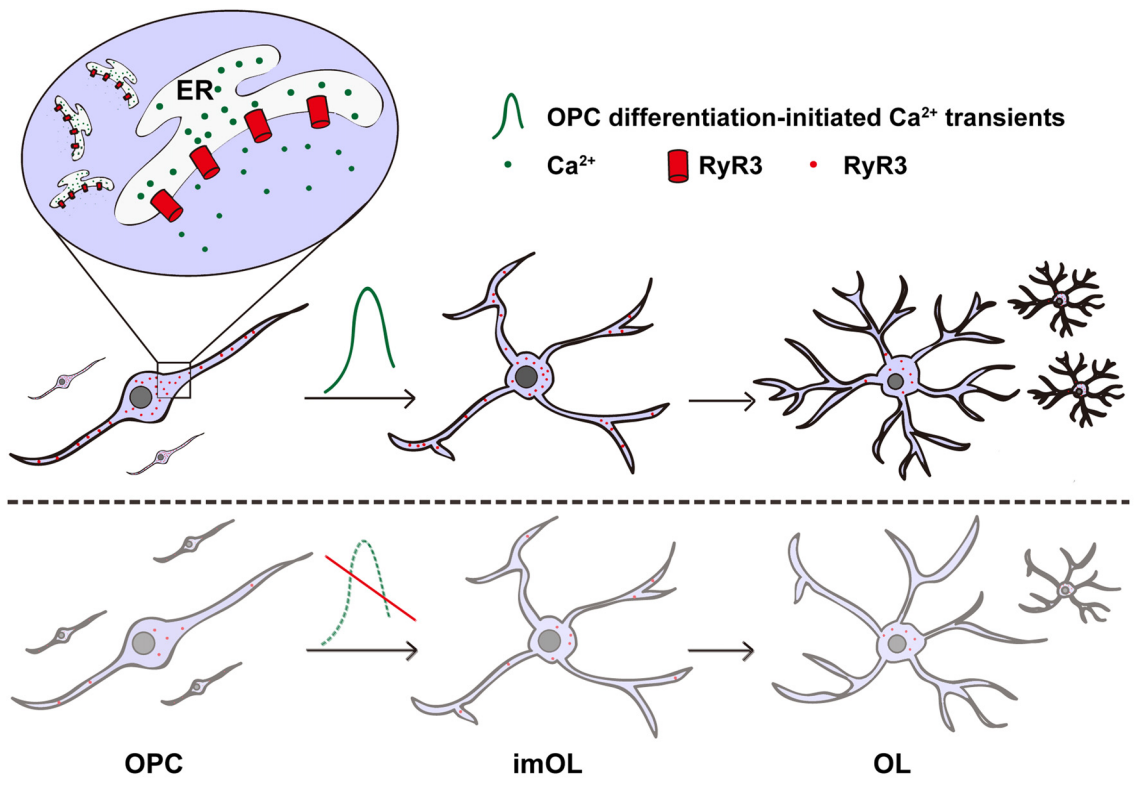

FIGURE 5 | Scheme illustrating the contribution of RyR3-mediated Ca^{2+} signaling during oligodendroglial development. RyR3, a Ca^{2+}-induced Ca^{2+} release (CICR) channel located on the ER membrane during oligodendroglial differentiation, note that it is widely distributed in the cell body and processes of OPC/imOLs but down-regulated and restricted in the cell body of mature OLs. The initiation of OPC differentiation requires hyperactive Ca^{2+} signaling mediated by RyR3. RyR3 knockdown or blockage of RyR3-mediated Ca^{2+} signaling in OPCs results in inhibition of OPC differentiation.

transients and thus program them into the differentiating state.

Previous studies showed that Ca^{2+} responses to depolarization in OPCs were more active than those in mature OLs, and this phenomenon was mainly explained by the downregulation of L-type voltage-operated Ca^{2+} channels (VOCCs) following OPC maturation (Berger et al., 1992; Takeda et al., 1995; Paez et al., 2010; Zhang et al., 2014). Considering that RyR-mediated CICR is a critical amplification point for depolarization-induced intracellular Ca^{2+} elevation (Verkhratsky and Petersen, 2002; Pouvreau et al., 2007; Haberlandt et al., 2011), our results suggested that RyR3-mediated Ca^{2+} release from the ER is also an important contributor to the dynamic intracellular responses during OPC differentiation.

Consistent with a previous study (Simpson et al., 1998), we found that RyR3 was enriched in the entire processes of OPCs and imOLs but was absent in the leading processes of mature OLs, indicating that RyR3-mediated local Ca^{2+} signaling may contribute to enabling the process elongation and/or movements of OPCs (Paez et al., 2007) and to initiating cell differentiation (Friess et al., 2016). In agreement with this, we provide evidence showing that RyR3 knockdown results in failure of oligodendroglial differentiation, indicating that CICR may critically contribute to OPC differentiation.

Even if it has not been studied in this work, we speculate that in physiological *in vivo* condition, the Ca^{2+} signals triggering the opening of RyR3 are likely originated from the nearby neurons. Large amount of evidences have shown that neuronal action potentials could regulate myelin development, the candidate mediators are the neurotransmitters (glutamate, ATP, adenosine...) which could trigger Ca^{2+} influx in oligodendroglial cells and possibly evoke the following CICR through RyR3 (Butt, 2006; Spitzer et al., 2016; Sun et al., 2016; Krasnow et al., 2018). Moreover, axonal activity-induced increases in extracellular K^+ are sufficient to depolarize VOCCs in nearby oligodendroglial cells to produce a significant rise in intracellular Ca^{2+} which also need CICR to form the final Ca^{2+} signal (Cheli et al., 2015). Importantly, RyR3 and IP3R2 are usually co-localized in OPCs, and interactions between them determine the spatial and temporal characteristics of Ca^{2+} signaling (Haak et al., 2001). Although a relative higher concentration of caffeine that was applied in our current study has been shown to stimulate RyR but inhibit the IP3R Ca^{2+} channel in several cell types (Brown et al., 1992; Sei et al., 2001; Kang et al., 2010), we could not exclude the role of IP3R2 in the Ca^{2+} signaling formation in oligodendroglial differentiation. Channel-specific antagonists or a genetic approach may be needed in our future studies.

In summary, we provide direct evidence showing that RyR3-mediated ER Ca^{2+} release is dynamically regulated and plays an essential role in initiating OPC differentiation (**Figure 5**). Our results supplement the current understanding of the function of intracellular Ca^{2+} channels in oligodendroglia and may provide valuable insights into therapeutic strategies for demyelinating diseases.

AUTHOR CONTRIBUTIONS

LX, HL and TL designed experiments and wrote the manuscript. TL, LW, TM and SW conducted the experiments. TL, LW and JN collected and analyzed the data.

FUNDING

This work was supported by National Natural Science Foundation of China (31271467, 81471297), Natural Science Foundation of Chongqing (CSTCKJCXLJRC07) to LX and China Scholarship Council ([2015]3022) to TL.

SUPPLEMENTARY MATERIAL

The Supplementary Material for this article can be found online at: https://www.frontiersin.org/articles/10.3389/fnmol.2018.00162/full#supplementary-material

REFERENCES

Baraban, M., Koudelka, S., and Lyons, D. A. (2018). Ca^{2+} activity signatures of myelin sheath formation and growth *in vivo*. *Nat. Neurosci.* 21, 19–23. doi: 10.1038/s41593-017-0040-x

Berger, T., Schnitzer, J., Orkand, P. M., and Kettenmann, H. (1992). Sodium and calcium currents in glial cells of the mouse corpus callosum slice. *Eur. J. Neurosci.* 4, 1271–1284. doi: 10.1111/j.1460-9568.1992.tb00153.x

Bezprozvanny, I., Watras, J., and Ehrlich, B. E. (1991). Bell-shaped calcium-response curves of $Ins(1,4,5)P_3$- and calcium-gated channels from endoplasmic reticulum of cerebellum. *Nature* 351, 751–754. doi: 10.1038/351751a0

Brown, G. R., Sayers, L. G., Kirk, C. J., Michell, R. H., and Michelangeli, F. (1992). The opening of the inositol 1,4,5-trisphosphate-sensitive Ca^{2+} channel in rat cerebellum is inhibited by caffeine. *Biochem. J.* 282, 309–312. doi: 10.1042/bj2820309

Butt, A. M. (2006). Neurotransmitter-mediated calcium signalling in oligodendrocyte physiology and pathology. *Glia* 54, 666–675. doi: 10.1002/glia.20424

Chang, A., Tourtellotte, W. W., Rudick, R., and Trapp, B. D. (2002). Premyelinating oligodendrocytes in chronic lesions of multiple sclerosis. *N. Engl. J. Med.* 346, 165–173. doi: 10.1056/nejmoa010994

Cheli, V. T., Santiago González, D. A., Spreuer, V., and Paez, P. M. (2015). Voltage-gated Ca^{2+} entry promotes oligodendrocyte progenitor cell maturation and myelination *in vitro*. *Exp. Neurol.* 265, 69–83. doi: 10.1016/j.expneurol.2014.12.012

Cohen, R. I., Molina-Holgado, E., and Almazan, G. (1996). Carbachol stimulates c-fos expression and proliferation in oligodendrocyte progenitors. *Brain Res. Mol. Brain Res.* 43, 193–201. doi: 10.1016/s0169-328x(96)00176-3

Fill, M., and Copello, J. A. (2002). Ryanodine receptor calcium release channels. *Physiol. Rev.* 82, 893–922. doi: 10.1152/physrev.00013.2002

Foskett, J. K., White, C., Cheung, K. H., and Mak, D. O. (2007). Inositol trisphosphate receptor Ca^{2+} release channels. *Physiol. Rev.* 87, 593–658. doi: 10.1152/physrev.00035.2006

Friess, M., Hammann, J., Unichenko, P., Luhmann, H. J., White, R., and Kirischuk, S. (2016). Intracellular ion signaling influences myelin basic protein synthesis in oligodendrocyte precursor cells. *Cell Calcium* 60, 322–330. doi: 10.1016/j.ceca.2016.06.009

Fulton, D., Paez, P. M., Fisher, R., Handley, V., Colwell, C. S., and Campagnoni, A. T. (2010). Regulation of L-type Ca^{++} currents and process morphology in white matter oligodendrocyte precursor cells by golli-myelin proteins. *Glia* 58, 1292–1303. doi: 10.1002/glia.21008

Galeotti, N., Vivoli, E., Bartolini, A., and Ghelardini, C. (2008). A gene-specific cerebral types 1, 2, and 3 RyR protein knockdown induces an antidepressant-like effect in mice. *J. Neurochem.* 106, 2385–2394. doi: 10.1111/j.1471-4159.2008.05581.x

Haak, L. L., Song, L. S., Molinski, T. F., Pessah, I. N., Cheng, H., and Russell, J. T. (2001). Sparks and puffs in oligodendrocyte progenitors: cross talk between ryanodine receptors and inositol trisphosphate receptors. *J. Neurosci.* 21, 3860–3870. doi: 10.1523/JNEUROSCI.21-11-03860.2001

Haberlandt, C., Derouiche, A., Wyczynski, A., Haseleu, J., Pohle, J., Karram, K., et al. (2011). Gray matter NG2 cells display multiple Ca^{2+}-signaling pathways and highly motile processes. *PLoS One* 6:e17575. doi: 10.1371/journal.pone.0017575

Kang, S. S., Han, K. S., Ku, B. M., Lee, Y. K., Hong, J., Shin, H. Y., et al. (2010). Caffeine-mediated inhibition of calcium release channel inositol 1,4,5-trisphosphate receptor subtype 3 blocks glioblastoma invasion and extends survival. *Cancer Res.* 70, 1173–1183. doi: 10.1158/0008-5472.CAN-09-2886

Kirischuk, S., Scherer, J., Möller, T., Verkhratsky, A., and Kettenmann, H. (1995). Subcellular heterogeneity of voltage-gated Ca^{2+} channels in cells of the oligodendrocyte lineage. *Glia* 13, 1–12. doi: 10.1002/glia.440130102

Koulen, P., and Thrower, E. C. (2001). Pharmacological modulation of intracellular Ca^{2+} channels at the single-channel level. *Mol. Neurobiol.* 24, 65–86. doi: 10.1385/mn:24:1-3:065

Krasnow, A. M., Ford, M. C., Valdivia, L. E., Wilson, S. W., and Attwell, D. (2018). Regulation of developing myelin sheath elongation by oligodendrocyte calcium transients *in vivo*. *Nat. Neurosci.* 21, 24–28. doi: 10.1038/s41593-017-0031-y

Kuhlmann, T., Miron, V., Cui, Q., Wegner, C., Antel, J., and Brück, W. (2008). Differentiation block of oligodendroglial progenitor cells as a cause for remyelination failure in chronic multiple sclerosis. *Brain* 131, 1749–1758. doi: 10.1093/brain/awn096

Lai, F. A., Misra, M., Xu, L., Smith, H. A., and Meissner, G. (1989). The ryanodine receptor-Ca^{2+} release channel complex of skeletal muscle sarcoplasmic reticulum. Evidence for a cooperatively coupled, negatively charged homotetramer. *J. Biol. Chem.* 264, 16776–16785.

Lanner, J. T., Georgiou, D. K., Joshi, A. D., and Hamilton, S. L. (2010). Ryanodine receptors: structure, expression, molecular details, and function in calcium release. *Cold Spring Harb. Perspect. Biol.* 2:a003996. doi: 10.1101/cshperspect.a003996

Matyash, M., Matyash, V., Nolte, C., Sorrentino, V., and Kettenmann, H. (2002). Requirement of functional ryanodine receptor type 3 for astrocyte migration. *FASEB J.* 16, 84–86. doi: 10.1096/fj.01-0380fje

McGrew, S. G., Wolleben, C., Siegl, P., Inui, M., and Fleischer, S. (1989). Positive cooperativity of ryanodine binding to the calcium release channel of sarcoplasmic reticulum from heart and skeletal muscle. *Biochemistry* 28, 1686–1691. doi: 10.1021/bi00430a039

Meissner, G. (1986). Ryanodine activation and inhibition of the Ca^{2+} release channel of sarcoplasmic reticulum. *J. Biol. Chem.* 261, 6300–6306.

Meissner, G., Darling, E., and Eveleth, J. (1986). Kinetics of rapid Ca^{2+} release by sarcoplasmic reticulum. Effects of Ca^{2+}, Mg^{2+}, and adenine nucleotides. *Biochemistry* 25, 236–244. doi: 10.1021/bi00349a033

Meissner, G., Rios, E., Tripathy, A., and Pasek, D. A. (1997). Regulation of skeletal muscle Ca^{2+} release channel (ryanodine receptor) by Ca^{2+} and monovalent cations and anions. *J. Biol. Chem.* 272, 1628–1638. doi: 10.1074/jbc.272.3.1628

Meldolesi, J., and Pozzan, T. (1998). The endoplasmic reticulum Ca^{2+} store: a view from the lumen. *Trends Biochem. Sci.* 23, 10–14. doi: 10.1016/s0968-0004(97)01143-2

Moraru, I. I., Kaftan, E. J., Ehrlich, B. E., and Watras, J. (1999). Regulation of type 1 inositol 1,4,5-trisphosphate-gated calcium channels by InsP3 and calcium: simulation of single channel kinetics based on ligand binding and electrophysiological analysis. *J. Gen. Physiol.* 113, 837–849. doi: 10.1085/jgp.113.6.837

Niu, J., Li, T., Yi, C., Huang, N., Koulakoff, A., Weng, C., et al. (2016). Connexin-based channels contribute to metabolic pathways in the oligodendroglial lineage. *J. Cell Sci.* 129, 1902–1914. doi: 10.1242/jcs.178731

Niu, J., Mei, F., Wang, L., Liu, S., Tian, Y., Mo, W., et al. (2012a). Phosphorylated olig1 localizes to the cytosol of oligodendrocytes and promotes membrane expansion and maturation. *Glia* 60, 1427–1436. doi: 10.1002/glia.22364

Niu, J., Wang, L., Liu, S., Li, C., Kong, J., Shen, H. Y., et al. (2012b). An efficient and economical culture approach for the enrichment of purified oligodendrocyte progenitor cells. *J. Neurosci. Methods* 209, 241–249. doi: 10.1016/j.jneumeth.2012.05.032

Paez, P. M., Fulton, D. J., Spreur, V., Handley, V., and Campagnoni, A. T. (2010). Multiple kinase pathways regulate voltage-dependent Ca^{2+} influx and migration in oligodendrocyte precursor cells. *J. Neurosci.* 30, 6422–6433. doi: 10.1523/JNEUROSCI.5086-09.2010

Paez, P. M., Spreuer, V., Handley, V., Feng, J. M., Campagnoni, C., and Campagnoni, A. T. (2007). Increased expression of golli myelin basic proteins enhances calcium influx into oligodendroglial cells. *J. Neurosci.* 27, 12690–12699. doi: 10.1523/JNEUROSCI.2381-07.2007

Pouvreau, S., Royer, L., Yi, J., Brum, G., Meissner, G., Rios, E., et al. (2007). Ca^{2+} sparks operated by membrane depolarization require isoform 3 ryanodine receptor channels in skeletal muscle. *Proc. Natl. Acad. Sci. U S A* 104, 5235–5240. doi: 10.1073/pnas.0706530104

Ruiz, A., Matute, C., and Alberdi, E. (2010). Intracellular Ca^{2+} release through ryanodine receptors contributes to AMPA receptor-mediated mitochondrial dysfunction and ER stress in oligodendrocytes. *Cell Death Dis.* 1:e54. doi: 10.1038/cddis.2010.31

Sei, Y., Gallagher, K. L., and Daly, J. W. (2001). Multiple effects of caffeine on Ca^{2+} release and influx in human B lymphocytes. *Cell Calcium* 29, 149–160. doi: 10.1054/ceca.2000.0175

Simpson, P. B., Holtzclaw, L. A., Langley, D. B., and Russell, J. T. (1998). Characterization of ryanodine receptors in oligodendrocytes, type 2 astrocytes, and O-2A progenitors. *J. Neurosci. Res.* 52, 468–482. doi: 10.1002/(sici)1097-4547(19980515)52:4<468::aid-jnr11>3.0.co;2-#

Soliven, B. (2001). Calcium signalling in cells of oligodendroglial lineage. *Microsc. Res. Tech.* 52, 672–679. doi: 10.1002/jemt.1051

Spitzer, S., Volbracht, K., Lundgaard, I., and Káradóttir, R. T. (2016). Glutamate signalling: a multifaceted modulator of oligodendrocyte lineage cells in health and disease. *Neuropharmacology* 110, 574–585. doi: 10.1016/j.neuropharm.2016.06.014

Stangel, M., and Hartung, H. P. (2002). Remyelinating strategies for the treatment of multiple sclerosis. *Prog. Neurobiol.* 68, 361–376. doi: 10.1016/s0301-0082(02)00105-3

Sun, W., Matthews, E. A., Nicolas, V., Schoch, S., and Dietrich, D. (2016). NG2 glial cells integrate synaptic input in global and dendritic calcium signals. *Elife* 5:e16262. doi: 10.7554/elife.16262

Suzuki, M., Nagai, Y., Wada, K., and Koike, T. (2012). Calcium leak through ryanodine receptor is involved in neuronal death induced by mutant huntingtin. *Biochem. Biophys. Res. Commun.* 429, 18–23. doi: 10.1016/j.bbrc.2012.10.107

Takeda, M., Nelson, D. J., and Soliven, B. (1995). Calcium signaling in cultured rat oligodendrocytes. *Glia* 14, 225–236. doi: 10.1002/glia.440140308

Verkhratsky, A., and Petersen, O. H. (2002). The endoplasmic reticulum as an integrating signalling organelle: from neuronal signalling to neuronal death. *Eur. J. Pharmacol.* 447, 141–154. doi: 10.1016/s0014-2999(02)01838-1

Ward, C. W., Schneider, M. F., Castillo, D., Protasi, F., Wang, Y., Chen, S. R., et al. (2000). Expression of ryanodine receptor RyR3 produces Ca^{2+} sparks in dyspedic myotubes. *J. Physiol.* 525, 91–103. doi: 10.1111/j.1469-7793.2000.t01-2-00091.x

Wolswijk, G. (1998). Chronic stage multiple sclerosis lesions contain a relatively quiescent population of oligodendrocyte precursor cells. *J. Neurosci.* 18, 601–609. doi: 10.1523/JNEUROSCI.18-02-00601.1998

Yoo, A. S., Krieger, C., and Kim, S. U. (1999). Process extension and intracellular Ca^{2+} in cultured murine oligodendrocytes. *Brain Res.* 827, 19–27. doi: 10.1016/s0006-8993(99)01282-2

Zalk, R., Lehnart, S. E., and Marks, A. R. (2007). Modulation of the ryanodine receptor and intracellular calcium. *Annu. Rev. Biochem.* 76, 367–385. doi: 10.1146/annurev.biochem.76.053105.094237

Zhang, Y., Chen, K., Sloan, S. A., Bennett, M. L., Scholze, A. R., O'Keeffe, S., et al. (2014). An RNA-sequencing transcriptome and splicing database of glia, neurons, and vascular cells of the cerebral cortex. *J. Neurosci.* 34, 11929–11947. doi: 10.1523/JNEUROSCI.1860-14.2014

Zucchi, R., and Ronca-Testoni, S. (1997). The sarcoplasmic reticulum Ca^{2+} channel/ryanodine receptor: modulation by endogenous effectors, drugs and disease states. *Pharmacol. Rev.* 49, 1–51.

Conflict of Interest Statement: The authors declare that the research was conducted in the absence of any commercial or financial relationships that could be construed as a potential conflict of interest.

frontiers in Neuroscience

PROTOCOLS
published: 15 May 2018
doi: 10.3389/fnins.2018.00324

A Novel Method to Image Macropinocytosis *in Vivo*

*Lunhao Chen[1,2], Daxiao Cheng[1], Jiachen Chu[1,3], Ting Zhang[1], Zhuoer Dong[4], Huifang Lou[1], Liya Zhu[1] and Yijun Liu[1]**

[1] Department of Neurobiology, Key Laboratory of Medical Neurobiology, Ministry of Health of China, Zhejiang Provincial Key Laboratory of Neurobiology, Zhejiang University School of Medicine, Hangzhou, China, [2] Department of Orthopedic Surgery, The First Affiliated Hospital, Zhejiang University School of Medicine, Hangzhou, China, [3] Department of Physiology, Johns Hopkins University School of Medicine, Baltimore, MD, United States, [4] Middle School Attached to Northwestern Polytechnical University, Xi'an, China

Here we described an experimental protocol for *in vivo* imaging of macropinocytosis and subsequent intracellular events. By microinjection, we delivered fluorescence dextrans together with or without ATPγS into transparent *Drosophila* melanogaster embryos. Using a confocal microscope for live imaging, we monitored the generation of dextran-positive macropinosomes and subsequent intracellular events. Our protocol provides a continent and reliable way for investigating macropinocytosis and its underlying mechanisms, especially when combined with genetic strategies.

Keywords: macropinocytosis, live imaging, *Drosophila*, embryo, hemocyte, *in vivo*

OPEN ACCESS

Edited by:
Margaret Su-chun Ho, ShanghaiTech University, China

Reviewed by:
Gang Chen, Nantong University, China
Wei Zhou, Huazhong University of Science and Technology, China

****Correspondence:***
Yijun Liu
yjliu@zju.edu.cn

Specialty section:
This article was submitted to Neurogenesis, a section of the journal Frontiers in Neuroscience

Received: *28 February 2018*
Accepted: *25 April 2018*
Published: *15 May 2018*

Citation:
Chen L, Cheng D, Chu J, Zhang T, Dong Z, Lou H, Zhu L and Liu Y (2018) A Novel Method to Image Macropinocytosis in Vivo. Front. Neurosci. 12:324. doi: 10.3389/fnins.2018.00324

INTRODUCTION

In eukaryotic cells, macropinocytosis is the most efficient way to internalize extracellular fluid through plasma membrane-formed large vacuoles called macropinosomes (Racoosin and Swanson, 1993; Swanson and Watts, 1995; Lim and Gleeson, 2011). As an ancient cellular behavior, macropinocytosis is essential for many physiological and pathological processes, such as nutrients uptake, pathogen capture, antigen presentation, and tumorigenesis (Kerr and Teasdale, 2009; Diken et al., 2011; Liu and Roche, 2015; Bloomfield and Kay, 2016). Sharing similar intracellular mechanism, macropinocytosis is thought to be largely homologous to phagocytosis, neuronal bulk endocytosis and other actin-driven endocytosis (Bloomfield and Kay, 2016).

Macropinocytosis provides a non-selective route to internalize extracellular fluids. In cancer cells, macropinocytosis is utilized for nutrient uptake to support metabolic needs and promote tumor growth (Commisso et al., 2013). Several infectious pathogens, such as bacteria, virus and protozoa, opportunistically hijack macropinocytosis to invade host cells and evade immune responses (Haraga et al., 2008; Gobeil et al., 2013). Observation of macropinocytosis will provide insight into the underlying regulatory molecular mechanisms and enable the physiological control of macropinocytosis for drug delivery in anti-cancer or -infection therapies. However, most observations of macropinocytosis were obtained from *in vitro* experiments or unicellular organisms (Chubb et al., 2000; Chen et al., 2015), e.g., *Dictyostelium* amoebae, instead of naturalistic models that do not fully reflect the complexity of *in vivo* situations, limiting their application. Therefore, considerable gaps remain in the knowledge of the relevance of macropinocytosis, especially the lack of optical imaging approaches, in living organisms. It is essential to develop consistent and reliable methods for *in vivo* macropinocytosis studies.

Most *Drosophila* melanogaster (fruit fly) genes are evolutionarily conserved with human and other mammals (Reiter and Bier, 2002). With its short life cycle and genetic amenability, *Drosophila* provides attractive model systems for various researches (Brand and Perrimon, 1993). After

removal of chorions, *Drosophila* embryos become transparent, but still tolerance to subsequent operations for live imaging, rendering this model feasible for *in vivo* cell behavioral and cell biological studies.

In the present study, we described a protocol for *in vivo* studies of macropinocytosis. By microinjection, fluorescence-labeled dextrans were delivered into *Drosophila* embryos. Engulfed by *Drosophila* hemocytes, which resemble mammalian macrophages, fluorescent dextrans were internalized with associated membrane, resulting in formation and subsequent transportation of macropinosomes. For microscopic methods, macropinocytosis was fluorescently visualized and monitored in live embryos. This method provides a novel way for observation of the organization and subsequent processing of macropinosomes *in vivo*, and an ideal model for revealing the underlying mechanisms of macropinocytosis.

MATERIALS AND METHODS

Drosophila Stocks

A stable line *srp-Gal4;UAS-GFP* was used to visualize hemocytes with green fluorescent protein (GFP) in embryos. F1 embryos were crossed from *Srp-Gal4* and *UAS-tau-GFP* for microtubule labeling in the hemocytes. All crosses were raised on standard *Drosophila* medium at 25°C with 12:12 h light/dark cycle. The *Drosophila* line *srp-gal4; UAS-GFP line* is a kindly gift from Prof. Henry Sun.

Regents and Equipment

Injection Solutions

Hank's Balanced Salt Solution (HBSS, Invitrogen, Carlsbad, CA, USA) was used for dilution of fluorescent dextrans and adenosine 5=-O-(3-thio) triphosphate (ATPγS, Sigma-Aldrich, St. Louis, MO, USA) to the final concentration of 5 mg/ml and 1 mM, respectively. Cascade blue labeled 3-kDa fluorescent dextran (CB3S), tetramethylrhodamine (TRITC) labeled 3-, 10-, 40-, and 70-kDa fluorescent dextrans (TRD3S, TRD10S, TRD40S, and TRD70S) were all purchased from Invitrogen.

Heptane Glue

To stick and stabilize embryos for subsequent injection, heptane glue was prepared as previously described (Brust-Mascher and Scholey, 2009). In brief, one pack of double sticky tapes were unrolled and dissolved with 50 ml heptane (Ourche, China). Seal the bottle and mild shake the solution for at least 12 h until it is clear and sticky.

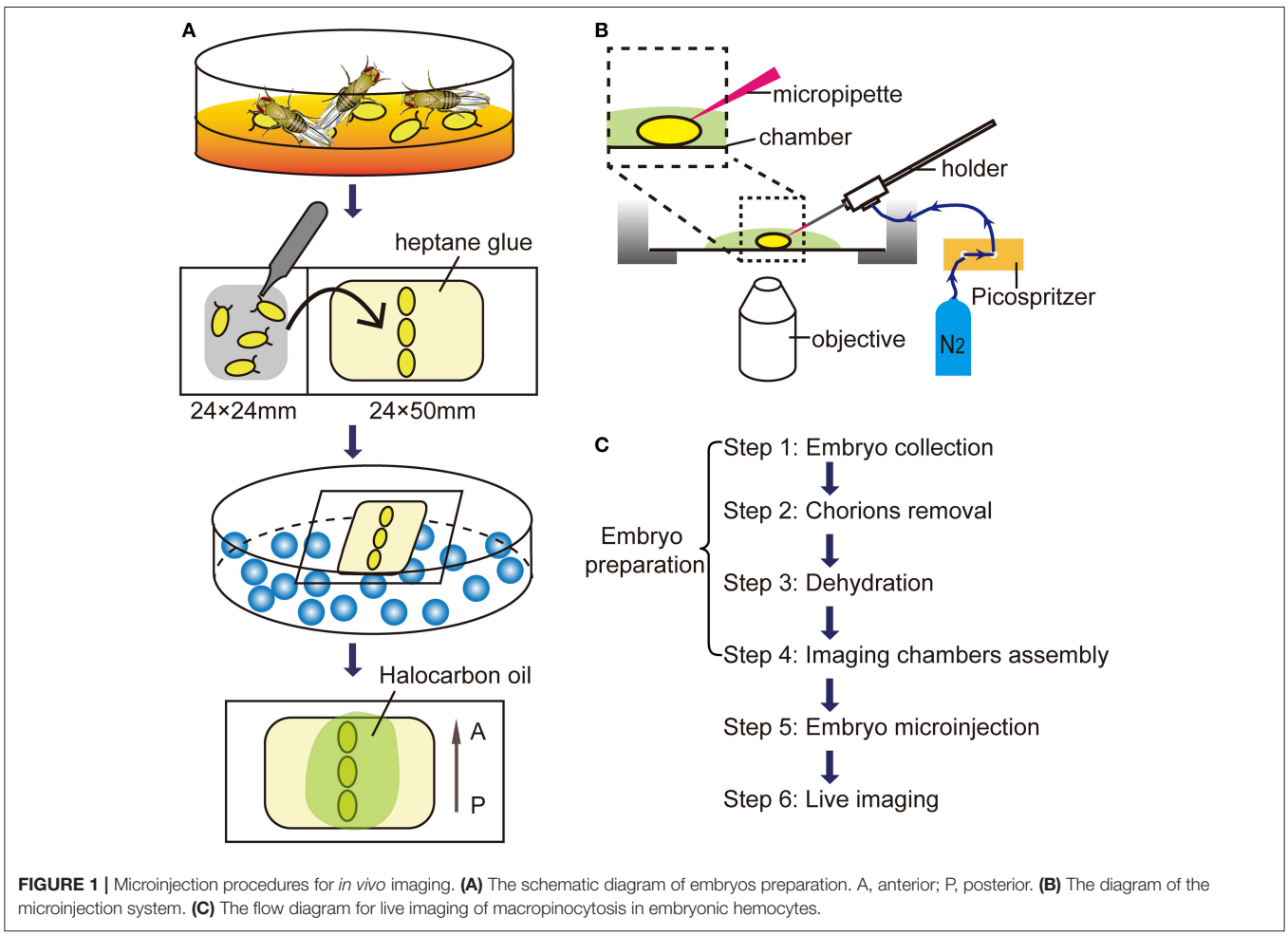

FIGURE 1 | Microinjection procedures for *in vivo* imaging. **(A)** The schematic diagram of embryos preparation. A, anterior; P, posterior. **(B)** The diagram of the microinjection system. **(C)** The flow diagram for live imaging of macropinocytosis in embryonic hemocytes.

Juice Agar Plates

Combine 2 g agar with 100 ml fruit juice, add ddH_2O to a final volume of 250 ml. Boil in microwave and pour the solution into 60 mm diameter Petri dishes and cool down at room temperature for 1 h. Scatter some dry yeast on the surface before use.

Micropipettes

Micropipettes for microinjection of dextrans are pre-pulled from borosilicate glass tubes (outer diameter: 1.0 mm, inner diameter: 0.5 mm, BF100-50-15, Sutter Instrument, Novato, CA, USA) by a micropipette puller (P-97, Sutter Instrument) to form a tip of ∼5 μm in diameter. A microforge (MF-830, Narishige, Japan) was used for quality control.

Glass Coverslips

24*24 mm and 55*24 mm coverslips with thickness 0.13–0.16 mm were used (Stars, China).

Microinjection Preparation

The microinjection system was adapted from micropipette assay system for microglia migration as described previously (Wu et al., 2014). In short, the nitrogen cylinder was connected with Picospritzer (Picospritzer III, Parker Hannifin, Cleveland, OH, USA) and set the output pressure to 0.1 MPa. Connect the "OUTPUT" signal of the electronic stimulator with the micropipette holder and attach the holder to the micromanipulator (MP-225, Sutter Instrument). Set the pulse "DURATION" at 50–100 ms. About 1-2 μl injection solution with or without ATPγS was filled into the micropipette by a 1 ml syringe and make sure without any air bubbles. By local micropipette ejection (Lohof et al., 1992), injection solution is pulse-ejected into embryos controlled by pressing the "MANUAL" button.

Embryos Preparation (Figure 1A)

Step 1. Embryos Collection

100-200 adult *Drosophila* were transferred into an embryo collection cage (Brust-Mascher and Scholey, 2009) and adapt for 1 day before collection. When collection starts, change juice plates and collect newborn embryos per hr. Collected embryos were incubated for at least 5 h until hemocytes matured and GFP expression (Tepass et al., 1994; Miller et al., 2002).

Step 2. Chorions removal

Under a stereoscopic microscope (SZ51, Olympus, Japan), chorions were carefully removed from embryos by rolling them on the double sticky tape by fine tweezers (0208-5-PO, Dumont, Swiss). After removal of chorions, transparent embryos without chorions were paralleled arranged and attached on a coverslip with heptane glue.

Step 3. Dehydration

Put embryos with the coverslip into a dryer which bottom filled with allochroic silicates (Sinopharm, China). Embryos were dehydrated for ∼5 min to prevent leakage of body fluids.

Step 4. Imaging chambers assembly

Transfer dehydrated embryos to an imaging chamber with a cover glass bottom. A droplet (about 20 μl) of Halocarbon oil 700 (H8898, Sigma-Aldrich) was added to each embryo providing appropriate humidity and enough oxygen.

TABLE 1 | Troubleshooting table.

Problem	Possible reason	Solution
Embryos are carried away during inserting.	Embryos are glued not enough.	Prepare thicker heptane glue to stable embryos.
	The tip is not sharp enough.	Adjust the tip size of micropipettes during preparation.
Body fluids flow out during injection.	Not enough Dehydration.	Prolong dehydration to 6-7 min.
	The flow from the micropipette tip is too high.	Use the micropipette with an appropriate tip size.
		Reduce the output pressure or the pulse duration.
Dextran-positive macropinosomes cannot be seen after 30 min of injection.	The micropipette tip is sealed or its tip is too small.	Replace the micropipette with a newly-made one. Use the micropipette with an appropriate tip size.
	Air bubbles are trapped in the micropipette tip.	Gently flick the micropipette to discharge bubbles or reload the injection solution.
	Large dextrans are filtered during diffusion.	Use small dextrans. 3 kDa-dextran is recommended.
	Embryos are not healthy enough.	Use another healthy embryo.
		Operate embryos as quickly as possible.
High background in the extracellular space	The micropipette tip is too large.	Adjust the tip size of micropipettes.
	The output pressure is too high or pulse duration is too long.	Reduce the output pressure or the pulse duration.

Embryo Microinjection

Assembly the injection equipment and imaging chambers as shown in the **Figure 1B**. Under a confocal microscope (FV1200, Olympus) with a 60x/NA 1.2 water objective, move the micropipette tip to the abdominal level of embryos by the micromanipulator. Carefully move the embryo against the micropipette tip and make sure the tip sticking into the embryo at the center of the optic field. Wait for 30 sec and press the "MANUAL" button to operate a single pulse of 10-ms duration. The total injection volume is about 20–30 nl.

Live Imaging

After the dextran injection, 3D Time-lapse imaging was captured using 60x water dipping objectives, stacks of images were

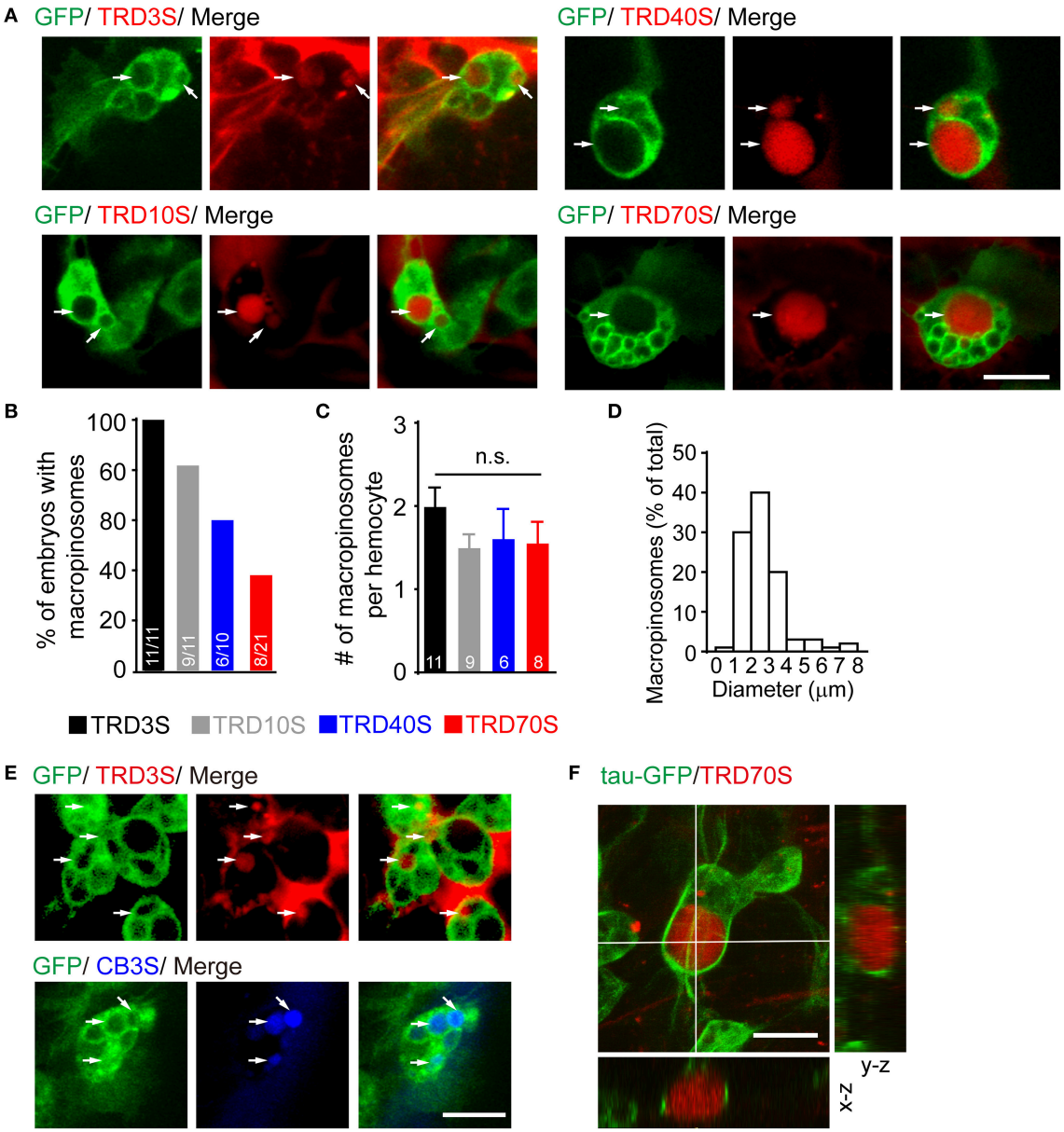

FIGURE 2 | ATPγS induced macropinosomes in *Drosophila* embryonic hemocytes. **(A)** Hemocytes (green) uptook fluorescent dextrans ranged from 3-kDa (TRD3S) to 70-kDa (TRD70S) dextrans and generated macropinosomes (arrows). **(B)** Success rates were defined as the percentage of embryos where hemocytes with macropinosomes 1.5 h after completion of different-sized dextrans injected. **(C)** Numbers (#) of macropinosomes in each hemocyte. *P*-values were calculated using one-way ANOVA among groups; n.s.: non-significant. **(D)** The size-distribution pattern of macropinosomes containing TRD3S ($n = 100$ macropinosomes, from 11 embryos). **(E)** Both TRITC labeled (red, TRD3S) and cascade blue labeled (blue, CB3S) dextrans were feasible to be uptaken by GFP-positive hemocytes (green), and formed macropinosomes (arrows). **(F)** In-depth 3D reconstruction analysis of ATPγS induced macropinosomes using a spatial deconvolution. Note that TRD70S dextran (red) labeled macropinosomes (red) and their surrounding GFP-positive microtubule-structures (green). Images were displayed in x-y (top), x-z (bottom), and y-z (right) projections. Scale bars, 10 μm.

acquired with a step size of 1 μm for a depth of 10 μm below embryo surface. Time-lapse movies were then generated between 3D stacks for 90 min without an interval. The time-lapse stack images were reconstructed and analyzed using Imaris software (Bitplane AG) and Image J (National Institute of Health, USA) software. The flow chart from embryo collection to live imaging was illustrated in **Figure 1C**.

Statistical Analysis

Statistical analysis was performed with STATA software (Version 13.0, Stata Corp, USA). Data are presented as means ± standard errors of the means (SEM). Statistical comparisons were assessed using student *t*-test or one-way ANOVA among three groups or above. Differences were considered to be significant at a P level of <0.05.

Troubleshooting

Troubleshooting advices can be found in **Table 1**.

RESULTS

Using our embryo microinjection method, we first sought to determine whether embryonic hemocytes were capable for evoking macropinocytosis. After induction by ATPγS, a non-hydrolysable ATP analog, macropinocytosis was observed using a confocal microscope. Five standard rules are followed to identify formed macropinosomes; (1) dextran-positive; (2) approximately pellet and ellipse-shaped; (3) surrounded by GFP-positive cytoplasm;(4) larger than 0.2 μm in diameter; (5) fluorescence intensities of macropinosomes are comparable with or higher than that of the extracellular space.

In our observation, responding to injected ATPγS, GFP-positive hemocytes efficiently engulfed large volumes of extracellular fluids containing fluorescent-labeled dextran with diverse molecular weights and different fluorophores (**Figures 2A,E**). However, macropinosomes were seen in almost 100% of embryos after 3-kDa dextran injection, whereas only 81.8, 60.0, and 38.1% of embryos generated macropinosomes after injection of 10, 40, and 70-kDa dextran, respectively (**Figure 2B**). To clarify whether hemocytes have equal ability to uptake dextrans with different sizes, we measured the number of macropinosomes in each hemocyte. Our result shows that about 2 macropinosomes were generated in each hemocyte and there were no statistically significant differences among hemocytes uptake 3-kDa to 70-kDa dextrans (**Figure 2C**). In addition, our result showed that dextran-positive pinosomes were heterogeneous in sizes, ranging from 0.2 to 10 μm, and approximately 90% of the macropinosomes were 1 to 4 μm in diameter (**Figure 2D**). Combined with genetic strategies, e.g., GAL4/UAS system, this model is appropriate for molecular studies, especially in endocytosis and its subsequent events. For instance, using hemocyte-specific promoter *srp-Gal4* to drive GFP fused tubulin-associated protein tau (tau-GFP), microtubule-filaments could be visualized and further analyzed in formation and trafficking of nascent macropinosomes (**Figure 2F**).

To clarify whether ATPγS was necessary for hemocytes to induce macropinosomes in our system. We injected 3 or 70-kD dextrans without ATPγS into embryonic hemocyte and observed spontaneous macropinocytosis in GFP positive hemocytes. Compared with ATPγS induced macropinosomes, spontaneous macropinosomes were much smaller (**Figure 3**), raising the difficulty for *in vivo* observation. Therefore, we recommend ATPγS induction to promote macropinocytosis in this model.

To further test whether this method is suitable for monitoring the cellular and subcellular events of macropinocytosis, we injected fluorescence-labeled dextrans together with ATPγS into the embryos with GFP-labeled hemocytes. As shown in **Figure 4A**, GFP-hemocyte extracellular dextrans were internalized along with cell surface ruffling and generated TRD70S-positive macropinosomes. Using low molecular weight TRITC-dextrans, TRD3S, we monitored the intracellular events of ATPγS-induced macropinosomes. During a 15 min observation period, dextran-containing macropinosomes transported in the cell body of a migrating hemocytes, indicating the method is reliable for cellular events and cell behavioral recordings (**Figure 4B**).

DISCUSSION

Adenosine triphosphate, or ATP, is the principal molecule for intracellular energy transfer in cells. Extracellular ATP is also an essential messenger for several physiologic and pathological processes (Lim and Gleeson, 2011; Li et al., 2013; Cisneros-Mejorado et al., 2015). Sensed by purinergic receptors, extracellular ATP activates intracellular signaling pathway and induces membrane ruffling and macropinocytosis (Grimmer et al., 2002; Li et al., 2013).

Here, we present an ATP analog microinjection-based system for *in vivo* observation of macropinocytosis and its subsequent cellular events. In our observation, ATPγS are

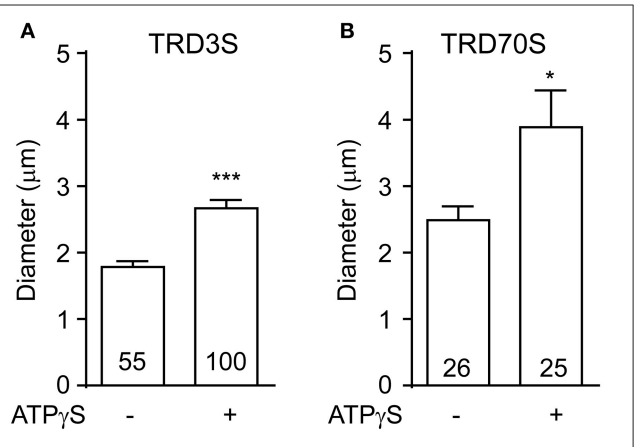

FIGURE 3 | ATPγS stimulation increased the vesicle size of macropinosomes. The diameter of macropinosomes were analyzed at 1.5 h after TRD3S **(A)** or TRD70S **(B)** injected. *P*-values of significance (indicated with asterisks, $*p < 0.05$, $***p < 0.001$) were calculated using student *t*-test.

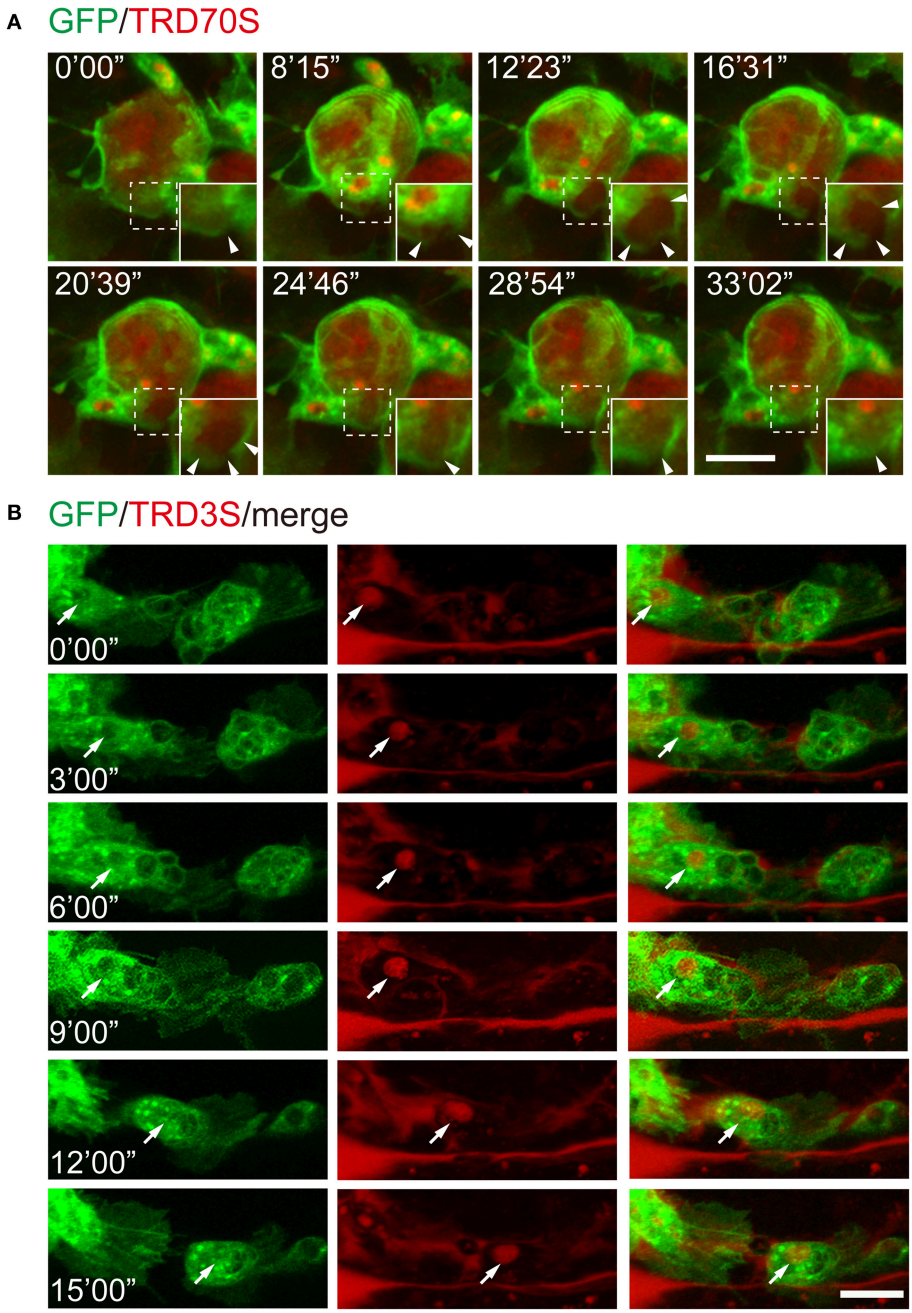

FIGURE 4 | Recording of cellular and subcellular behaviors using the ATPγS microinjection-based imaging system. **(A)** Dynamic changes of macropinosomes, from formation to fusion. Note that macropinosomes (red) were formed from the surface membrane ruffles and internalized after enclosure (arrowheads). The newly formed macropinosomes were indicated by dashed boxes and corresponding enlarged parts were presented at right corners. **(B)** TRD3S macropinosomes (red) transported within migrating hemocytes (green). The arrow indicates the location of a trafficking vesicle. Scale bars, 10 μm.

capable to induce larger macropinosomes engulfed by *Drosophila* embryonic hemocytes using different molecular weights of dextrans (**Figures 2**, **3**). In addition, small dextrans are more efficient for labeling macropinosomes. Moreover, this method is feasible to investigate cellular events of macropinosomes, such as generation, fusion, and trafficking (**Figure 4**).

Although macropinocytosis is a nonselective process in cell culture systems, natural structures in living tissues may filter molecules and cause different diffusion properties in different size dextrans. Therefore, we tried to find out which size of dextran would be suitable for our system. In our experiment, dextrans ranged from 3-kDa to 70-kDa were all capable of

labeling macropinosomes. However, small dextran (TRD3S) labeled macropinosomes could be seen in almost 100% of injected embryos, whereas large dextran (TRD70S) could only successfully label macropinosomes in about 40% of embryos under same conditions (**Figure 2B**). These data suggest that small molecules are more efficient for labeling macropinosomes in our system. In addition, although induced by different-sized dextrans, each hemocyte generated approximate numbers of macropinosomes. Taken together, application of larger dextran will reduce the success rate of induction without changing the uptake ability of hemocytes. It also suggests a potential filter effect of extracellular matrix in live tissues.

There are some difference of macropinocytosis between *in vivo* and *in vitro* systems. In previously studies, cultured macrophages and microglia exhibit impressive capabilities in internalization of extracellular fluids by macropinosomes (Racoosin and Swanson, 1993; Chen et al., 2015; Canton et al., 2016; Fu et al., 2016), which could generate within 1 min followed by centripetally migration and rapid shrink (Racoosin and Swanson, 1993; Lee and Knecht, 2002). It is a relatively short window to observe each phase. By contrast, *in vivo* macropinocytosis takes longer to generate macropinosomes in about 30 min (**Figure 3A**), providing enough time for observation. In addition, primary macrophages and the Drosophila hemocyte S2 cell line generate macropinosomes with high density (Gupta et al., 2009; Canton et al., 2016), raising the difficulty for observation of each vesicle. In contrast, no more than 5 macropinosomes were observed in our *in vivo* model. The sparse labeling provides a convenient approach to distinguish and monitor macropinosomes.

Combined with genetic tools and other strategies, this method is suitable to investigate molecular functions in macropinocytosis. For instance, using *srp-GAL4;UAS-tau-GFP* transgenic *Drosophila*, microtubules were visualized around ATPγS induced macropinosomes (**Figure 2F**). Together with previous *in vitro* studies (Gilberti and Knecht, 2015), our results provide essential *in vivo* cues supporting that microtubule-associated structures may regulate macropinosomes formation and subsequent processes.

To expend applications, the method could be used to: (1) reveal the underlying mechanism in macropinocytosis; (2) uncover the way by which macrophages/microglia used for pathogens internalization; (3) develop new approaches for drug delivery via macropinocytosis. Taken together, this method provides novel sights for *in vivo* investigation of macropinocytosis and associated processes.

ETHICS STATEMENT

This study was carried out in accordance with the recommendations of the Guidance for the Care and Use of Laboratory Animals at Zhejiang University. The protocol was approved by the Institutional Animal Care and Use Committee at Zhejiang University.

AUTHOR CONTRIBUTIONS

LC and YL designed the research. LC, DC, JC, TZ, ZD, and YL performed the experiments together; LC, JC, and YL wrote the paper; LZ and HL helped with animal raising and experimental preparation; LC with JC analyzed the data; YL supervised the entire study. All authors discussed the results and commented on the manuscript.

ACKNOWLEDGMENTS

We thank Prof. Henry Sun and Prof. Yongqing Zhang for providing transgenic fly stocks. We are grateful to the Core Facilities of Zhejiang University Institute of Neuroscience for technical assistance. This work was supported by grants from the Major State Basic Research Program of China (2016YFA0501000), the National Natural Science Foundation of China (31501128, 31490590, and 31490592).

REFERENCES

Bloomfield, G., and Kay, R. R. (2016). Uses and abuses of macropinocytosis. *J. Cell Sci.* 129, 2697–2705. doi: 10.1242/jcs.176149

Brand, A. H., and Perrimon, N. (1993). Targeted gene expression as a means of altering cell fates and generating dominant phenotypes. *Development* 118, 401–415.

Brust-Mascher, I., and Scholey, J. M. (2009). Microinjection techniques for studying mitosis in the *Drosophila melanogaster* syncytial embryo. *J. Vis. Exp.* 31:1382. doi: 10.3791/1382

Canton, J., Schlam, D., Breuer, C., Gutschow, M., Glogauer, M., and Grinstein, S. (2016). Calcium-sensing receptors signal constitutive macropinocytosis and facilitate the uptake of NOD2 ligands in macrophages. *Nat. Commun.* 7:11284. doi: 10.1038/ncomms11284

Chen, C., Li, H. Q., Liu, Y. J., Guo, Z. F., Wu, H. J., Li, X., et al. (2015). A novel size-based sorting mechanism of pinocytic luminal cargoes in microglia. *J. Neurosci.* 35, 2674–2688. doi: 10.1523/JNEUROSCI.4389-14.2015

Chubb, J. R., Wilkins, A., Thomas, G. M., and Insall, R. H. (2000). The Dictyostelium RasS protein is required for macropinocytosis, phagocytosis and the control of cell movement. *J. Cell Sci.* 113, 709–719.

Cisneros-Mejorado, A., Perez-Samartin, A., Gottlieb, M., and Matute, C. (2015). ATP signaling in brain: release, excitotoxicity and potential therapeutic targets. *Cell. Mol. Neurobiol.* 35, 1–6. doi: 10.1007/s10571-014-0092-3

Commisso, C., Davidson, S. M., Soydaner-Azeloglu, R. G., Parker, S. J., Kamphorst, J. J., Hackett, S., et al. (2013). Macropinocytosis of protein is an amino acid supply route in Ras-transformed cells. *Nature* 497, 633–637. doi: 10.1038/nature12138

Diken, M., Kreiter, S., Selmi, A., Britten, C. M., Huber, C., Tureci, O., et al. (2011). Selective uptake of naked vaccine RNA by dendritic cells is driven by macropinocytosis and abrogated upon DC maturation. *Gene Ther.* 18, 702–708. doi: 10.1038/gt.2011.17

Fu, P., Tang, R., Yu, Z., Li, C., Chen, X., Xie, M., et al. (2016). Rho-associated kinase inhibitors promote microglial uptake via the ERK signaling pathway. *Neurosci. Bull.* 32, 83–91. doi: 10.1007/s12264-016-0013-1

Gilberti, R. M., and Knecht, D. A. (2015). Macrophages phagocytose nonopsonized silica particles using a unique microtubule-dependent pathway. *Mol. Biol. Cell* 26, 518–529. doi: 10.1091/mbc.E14-08-1301

Gobeil, L. A., Lodge, R., and Tremblay, M. J. (2013). Macropinocytosis-Like HIV-1 internalization in macrophages is CCR5 dependent and leads to efficient

but delayed degradation in endosomal compartments. *J. Virol.* 87, 735–745. doi: 10.1128/Jvi.01802-12

Grimmer, S., van Deurs, B., and Sandvig, K. (2002). Membrane ruffling and macropinocytosis in A431 cells require cholesterol. *J. Cell Sci.* 115(Pt 14), 2953–2962. doi: 10.1016/j.yexcr.2007.02.012

Gupta, G. D., Swetha, M. G., Kumari, S., Lakshminarayan, R., Dey, G., and Mayor, S. (2009). Analysis of endocytic pathways in Drosophila cells reveals a conserved role for GBF1 in internalization via GEECs. *PLoS ONE* 4:e6768. doi: 10.1371/journal.pone.0006768

Haraga, A., Ohlson, M. B., and Miller, S. I. (2008). Salmonellae interplay with host cells. *Nat. Rev. Microbiol.* 6, 53–66. doi: 10.1038/nrmicro1788

Kerr, M. C., and Teasdale, R. D. (2009). Defining macropinocytosis. *Traffic* 10, 364–371. doi: 10.1111/j.1600-0854.2009.00878.x

Lee, E., and Knecht, D. A. (2002). Visualization of actin dynamics during macropinocytosis and exocytosis. *Traffic* 3, 186–192. doi: 10.1034/j.1600-0854.2002.030304.x

Li, H. Q., Chen, C., Dou, Y., Wu, H. J., Liu, Y. J., Lou, H. F., et al. (2013). P2Y4 receptor-mediated pinocytosis contributes to amyloid beta-induced self-uptake by microglia. *Mol. Cell. Biol.* 33, 4282–4293. doi: 10.1128/MCB.00544-13

Lim, J. P., and Gleeson, P. A. (2011). Macropinocytosis: an endocytic pathway for internalising large gulps. *Immunol. Cell Biol.* 89, 836–843. doi: 10.1038/icb.2011.20

Liu, Z., and Roche, P. A. (2015). Macropinocytosis in phagocytes: regulation of MHC class-II-restricted antigen presentation in dendritic cells. *Front. Physiol.* 6:1. doi: 10.3389/fphys.2015.00001

Lohof, A. M., Quillan, M., Dan, Y., and Poo, M. M. (1992). Asymmetric modulation of cytosolic cAMP activity induces growth cone turning. *J. Neurosci.* 12, 1253–1261. doi: 10.1523/jneurosci.12-04-01253.1992

Miller, J. M., Oligino, T., Pazdera, M., Lopez, A. J., and Hoshizaki, D. K. (2002). Identification of fat-cell enhancer regions in *Drosophila melanogaster*. *Insect Mol. Biol.* 11, 67–77. doi: 10.1139/g95-065

Racoosin, E. L., and Swanson, J. A. (1993). Macropinosome maturation and fusion with tubular lysosomes in macrophages. *J. Cell Biol.* 121, 1011–1020. doi: 10.1083/jcb.121.5.1011

Reiter, L. T., and Bier, E. (2002). Using Drosophila melanogaster to uncover human disease gene function and potential drug target proteins. *Exp. Opin. Ther. Targets* 6, 387–399. doi: 10.1517/14728222.6.3.387

Swanson, J. A., and Watts, C. (1995). Macropinocytosis. *Trends Cell Biol.* 5, 424–428.

Tepass, U., Fessler, L. I., Aziz, A., and Hartenstein, V. (1994). Embryonic origin of hemocytes and their relationship to cell death in *Drosophila*. *Development* 120, 1829–1837.

Wu, H. J., Liu, Y. J., Li, H. Q., Chen, C., Dou, Y., Lou, H. F., et al. (2014). Analysis of microglial migration by a micropipette assay. *Nat. Protoc.* 9, 491–500. doi: 10.1038/nprot.2014.015

Conflict of Interest Statement: The authors declare that the research was conducted in the absence of any commercial or financial relationships that could be construed as a potential conflict of interest.

frontiers in Molecular Neuroscience

REVIEW
published: 14 May 2018
doi: 10.3389/fnmol.2018.00158

Microglial Lectins in Health and Neurological Diseases

Jian Jing Siew[1,2] *and Yijuang Chern*[1,2]*

[1]Taiwan International Graduate Program in Molecular Medicine, National Yang-Ming University and Academia Sinica, Taipei, Taiwan, [2]Institute of Biomedical Sciences, Academia Sinica, Taipei, Taiwan

Microglia are the innate sentinels of the central nervous system (CNS) and are responsible for the homeostasis and immune defense of the CNS. Under the influence of the local environment and cell-cell interaction, microglia exhibit a multidimensional and context-dependent phenotypes that can be cytotoxic and neuroprotective. Recent studies suggest that microglia express multitudinous types of lectins, including galectins, Siglecs, mannose-binding lectins (MBLs) and other glycan binding proteins. Because most studies that examine lectins focus on the peripheral system, the functions of lectins have not been critically investigated in the CNS. In addition, the types of brain cells that contribute to the altered levels of lectins present in diseases are often unclear. In this review, we will discuss how galectins, Siglecs, selectins and MBLs contribute to the dynamic functions of microglia. The interacting ligands of these lectins are complex glycoconjugates, which consist of glycoproteins and glycolipids that are expressed on microglia or surrounding cells. The current understanding of the heterogeneity and functions of glycans in the brain is limited. Galectins are a group of pleotropic proteins that recognize both β-galactoside-containing glycans and non- β-galactoside-containing proteins. The function and regulation of galectins have been implicated in immunomodulation, neuroinflammation, apoptosis, phagocytosis and oxidative bursts. Most Siglecs are expressed at a low level on the plasma membrane and bind to sialic acid residues for immunosurveillance and cell-cell communication. Siglecs are classified based on their inhibitory and activatory downstream signaling properties. Inhibitory Siglecs negatively regulate microglia activation upon recognizing the intact sialic acid patterns and vice versa. MBLs are expressed upon infection in cytoplasm and can be secreted in order to recognize molecules containing terminal mannose as an innate immune defense machinery. Most importantly, multiple studies have reported dysregulation of lectins in neurological disorders. Here, we reviewed recent studies on microglial lectins and their functions in CNS health and disease, and suggest that these lectin families are novel, potent therapeutic targets for neurological diseases.

Keywords: microglia, galectin, Siglec, selectin, mannose-binding lectin, neurological disease, neurodegeneration

OPEN ACCESS

Edited by:
Margaret Su-chun Ho, ShanghaiTech University, China

Reviewed by:
Marina Bentivoglio, University of Verona, Italy
Savina Apolloni, Fondazione Santa Lucia (IRCCS), Italy

***Correspondence:**
Yijuang Chern
bmychern@ibms.sinica.edu.tw

Received: *27 January 2018*
Accepted: *25 April 2018*
Published: *14 May 2018*

Citation:
Siew JJ and Chern Y (2018) Microglial Lectins in Health and Neurological Diseases. Front. Mol. Neurosci. 11:158. doi: 10.3389/fnmol.2018.00158

INTRODUCTION

The central nervous system (CNS) consists of neurons and glial cells such as microglia, astrocytes and oligodendrocytes. Microglia are the CNS counterpart of macrophages and differ from other types of glial cells in terms of their origin, morphology and functions (Kettenmann et al., 2011). They are widely distributed throughout the brain and spinal cord, and constitute 5%–10% of total brain cells depending on the region (Lawson et al., 1990).

Microglia play multiple roles in healthy and diseased brains. During development, microglia regulate the number of neuronal cells by triggering programmed cell death and actively phagocytose the apoptotic neurons (de la Rosa and de Pablo, 2000; Bessis et al., 2007). In addition, microglia are capable of promoting neurogenesis by secreting trophic factors (such as nerve growth factor (NGF) and insulin-like growth factor 1 (IGF-1; Frielingsdorf et al., 2007; Thored et al., 2009). In addition to regulating the number of neurons, microglia also strengthen and prune excessive synapses to ensure that neuronal circuits are connected correctly (Paolicelli et al., 2011). Hence, microglia have been implicated in synaptic plasticity.

As the immune sentinels of the CNS, microglia are responsible for detecting and swiftly responding to infection, injury, molecules released by damaged cells and misfolded proteins (Davalos et al., 2005; Nimmerjahn et al., 2005). In this context, microglia are believed to play exacerbating roles in the inflammatory response of neurological diseases, including multiple sclerosis (MS; Politis et al., 2012), ischemic stroke (Patel et al., 2013), Alzheimer's disease (AD; Fuhrmann et al., 2010), Parkinson's disease (PD; Subramaniam and Federoff, 2017), amyotrophic lateral sclerosis (ALS; Brites and Vaz, 2014), Huntington's disease (HD; Hsiao et al., 2014) and virus infection in the brain (Cenker et al., 2017). Hence, elucidating the machinery that regulates the multidimensional phenotypes of microglia is critical for understanding neurological diseases and developing effective therapeutic interventions.

Microglia express various types of lectins that functionally regulate their dynamic phenotypes. These lectins include galectins, Siglecs, C-type lectins (such as mannose-binding lectins, MBLs) and other glycan binding proteins. Some of these lectins are expressed constitutively, while others are expressed upon stimulation. For instance, microglia generally do not express galectin-3, but its expression can be up-regulated by inflammatory mediators (Burguillos et al., 2015). Galectins have multiple cellular localizations and different functions. For instance, galectin-1, -3 and -9 have been reported to exist in the nucleus, cytoplasm, plasma membrane and extracellular matrix. The cell types in the CNS that express galectins and their cellular localization and functions are summarized in **Table 1**. Contrary to galectins, all CNS Siglecs (except Siglec-4) are localized on the plasma membrane of microglia. Details about the CNS Siglecs are summarized in **Table 2**. Similar to Siglecs, selectins are localized on the plasma membrane of endothelial cells. In contrast, MBL is found in the cytoplasm of all brain cells in disease conditions and can be secreted into the extracellular matrix. Details on these C-type lectins are summarized in **Table 3**. The cell surface contains a complex layer of glycosylated molecules, such as glycoproteins and glycolipids that are recognized by these lectins and store important information for cell-cell communication and response (Brandley and Schnaar, 1986; Groves, 2013; Letschert et al., 2014). Classification of lectins is based on the homology of amino acid sequences and specificity of glycan structures. Their functions have been reviewed in detail elsewhere (Varki et al., 2009; Fujimoto et al., 2014).

TABLE 1 | Summary of galectins in central nervous system (CNS).

Type	Ligands	Cell type/Subcellular location		Functions	References
Galectin-1	β-Galactosides	Microglia Astrocytes Neurons	• Nucleus • Cytoplasm • Plasma membrane • Extracellular	• Suppression of microglial activation • Regulation of neurogenesis • Regulation of oligodendrocyte proliferation	Sakaguchi et al. (2006, 2007) and Starossom et al. (2012)
Galectin-3	β-Galactosides	Microglia	• Nucleus • Cytoplasm • Plasma membrane • Extracellular	• Microglial activation • Promotion of neuroinflammation • Suppression of neuroinflammation • Regulation of oligodendrocyte differentiation	Jiang et al. (2009), Lerman et al. (2012) and James et al. (2016)
Galectin-4	β-Galactosides	Neurons	• Plasma membrane	• Axonal growth • Axonal transport • Suppression of axonal myelination	Cao and Guo (2016)
Galectin-8	β-Galactosides	Microglia Others	• High levels in hippocampus and choroid plexus • Other brain regions • CSF	• Immunosuppression	Stancic et al. (2011), John and Mishra (2016) and Pardo et al. (2017)
Galectin-9	β-Galactosides	Microglia Astrocytes	• Nucleus • Cytoplasm • Plasma membrane • Extracellular	• Modulation of neuroinflammation	Stancic et al. (2011), Lerman et al. (2012) and Steelman et al. (2013)

TABLE 2 | Summary of Siglecs in CNS.

Type	Ligands	Cell type/ Subcellular location		Functions	References
Siglec-1 (sialoadhesin, CD169)	α2–3, α2–6 sialic acid residues	Microglia	• Plasma membrane	• Cell-cell interaction	Macauley et al. (2014) and Groh et al. (2016)
Siglec-3 (CD33)	α2–6, α2–3 sialic acid residues	Microglia	• Plasma membrane	• Modulation of microglial phagocytosis activity	Griciuc et al. (2013) and Macauley et al. (2014)
Siglec-4 (MAG)	α2–3, α2–6 sialic acid residues	On myelin sheath, produced by oligodendrocytes	• Inner-most, myelin periaxonal membrane	• Myelin-axon interaction, maintaining long-term axon stability	Sun et al. (2004), Huang et al. (2012) and Macauley et al. (2014)
Siglec-E	α2–3, α2–6, α2–8 sialic acid residues	Microglia	• Plasma membrane	• Inhibition of inflammation, ROS production and phagocytosis	Claude et al. (2013) and Macauley et al. (2014)
Siglec-F	α2–3 sialic acid residues	Microglia	• Plasma membrane	• Inhibition of phagocytosis	Wielgat and Braszko (2012) and Macauley et al. (2014)
Siglec-H	Abnormal sialic acid residues in glioma	Microglia	• Plasma membrane	• Promotion of phagocytosis	Kopatz et al. (2013) and Macauley et al. (2014)
Siglec-11	α2–8 sialic acid residues	Microglia	• Plasma membrane	• Inhibition of inflammation and phagocytosis	Wang and Neumann (2010), Wang X. et al. (2012) and Macauley et al. (2014)
Siglec-16	α2–8 sialic acid residues	Microglia	• Plasma membrane	• No functional data	Wang X. et al. (2012) and Macauley et al. (2014)

TABLE 3 | Summary of C-type lectins in CNS.

Type	Ligands	Cell type/Subcellular location		Functions	References
E-Selectin	Sialyl-Lewis X terminal	Endothelial cells	• Plasma membrane	• Facilitate the adhesion of neutrophils	Jin et al. (2010)
P-Selectin	Sialyl-Lewis X terminal	Endothelial cells	• Plasma membrane	• Facilitate the adhesion of neutrophils	Atkinson et al. (2006) and Jin et al. (2010)
Mannose-binding lectin	Terminal mannose, fucose, GlcNAc	Microglia Astrocytes Oligodendrocytes Neuron	• Cytoplasm • Extracellular	• Innate immune defense	Singh et al. (2011)

In this review, we focus on the role of lectins and how they affect the functions of microglia in the CNS. **Tables 1–3** summarizes the major lectins that have been reported in the CNS so far.

GALECTINS

Galectins represent a family of lectins characterized by conserved carbohydrate-recognition domains (CRDs) and bind to β-galactosides with different specificities and affinities (Liu and Rabinovich, 2005). Through the conserved CRDs, 15 galectins have been identified; they can be categorized into three groups: (1) proto, or one CRD; (2) tandem repeats, or two distinct CRDs in tandem; and (3) chimera, consisting of CRD with unusual tandem repeat of glycine- and proline-rich short stretches (Kasai and Hirabayashi, 1996). The prototype galectins include galectins-1, -2, -5, -7, -10, -11, -13, -14 and -15, while the tandem repeats type consists of galectins -4, -6, -8, -9 and -12; and galectin-3 is the only galectin classified as chimera type. Among these galectins, only galectins -1, -2, -3, -4, -7, -8, -9, -10, -12 and -13 are expressed in humans (Chang et al., 2017). Furthermore, many of these galectins have differentially spliced forms that may be expressed in different tissues. For instance, galectins-8 and -9 have seven and three isoforms, respectively (Zhang et al., 2009; Troncoso et al., 2014). In particular, the galectin-9M and 9S isoforms positively promote the expression of E-selectin, while the galectin-9L isoform suppresses the level of E-selectin (Zhang et al., 2009). These isoforms are critical in regulating important cellular activity. The mechanisms involved in coordinating the expression of these isoforms and the functions they serve are still in need of extensive exploration. To date, no specific surface receptor for galectins has been reported. Nonetheless, galectins can bind to and interact with various glycoproteins and cell membrane glycoconjugates via their carbohydrate moieties and trigger a cascade of transmembrane signaling events (Liu and Rabinovich, 2005; Wan and Liu, 2016). In addition, galectins have non-carbohydrate binding partners and function intracellularly to regulate gene transcription, mRNA splicing, cell growth, apoptosis and immune responses (Liu et al., 2002; Wang J. L. et al., 2012). For instance, intracellular galectin-1 and galectin-3 interact with Gemin4 to facilitate the assembly of spliceosomes (Park et al., 2001). The functions of galectins in the peripheral system have been extensively studied. To date, only galectins-1, -3, -4, -8 and -9 have been found in the CNS. **Table 4** summarizes the role of galectins in neurological disorders.

Galectins and Myelination

During the maturation of neurons, axons are myelinated in a specific manner that leaves certain parts of the segments

TABLE 4 | Summary of the role of galectins in neurological disease.

Neurological conditions	Type of galectin	Disease-associated features	References
Multiple sclerosis	Galectin-1	• Astrocytes produce galectin-1 to deactivate microglia through the p38, CREB and NF-κB pathways. • The function of galectin-1 produced by MS microglia is unknown.	Starossom et al. (2012)
	Galectin-3	• Modulation of immune cell infiltration into the CNS • Up-regulation of inflammatory cytokines and down-regulation of anti-inflammatory cytokines in dendritic and T cells. • Inhibition of neural cell proliferation	Jiang et al. (2009) and James et al. (2016)
	Galectin-8	• Up-regulated in microglia. • Immunosuppression in the periphery, unknown effects in the brain.	Stancic et al. (2011) and Pardo et al. (2017)
	Galectin-9	• Up-regulated in CSF of secondary progressive MS patients and microglia, its function is not clear. • Located in the cytosol of microglia in inactive lesions. • Located in the nuclei and cytosol of microglia in active lesions.	Stancic et al. (2011) and Burman and Svenningsson (2016)
Stroke and ischemia	Galectin-3	• Up-regulated in the microglia, promotes proliferation. • Promotes the production of IGF-1. • Suppression of IL6 inflammatory cytokine. • Acts as the ligand of TLR4 to promote inflammatory responses.	Lalancette-Hébert et al. (2007, 2012) and Burguillos et al. (2015)
Traumatic brain injury	Galectin-3	• Up-regulated in the corpus callosum and is associated with the production of NGF. • Up-regulated in the cortex and hippocampus and promotes inflammation.	Venkatesan et al. (2010) and Yip et al. (2017)
Amyotrophic Lateral Sclerosis (ALS)	Galectin-1	• Up-regulated in the spinal cord at the end stage.	Lerman et al. (2012)
	Galectin-3	• Up-regulated in the microglia and suppresses inflammation and oxidative damage in the spinal cord.	Lerman et al. (2012)
	Galectin-9	• Up-regulated in the spinal cord at the symptomatic stage	Lerman et al. (2012)
Parkinson's disease	Galectin-3	• Up-regulated in the microglia to promote phagocytosis of α-synuclein and secretion of inflammatory cytokines.	Boza-Serrano et al. (2014)
Prion disease	Galectin-3	• Up-regulated in the medulla and pons. • Up-regulation associated with impairment of lysosomal function and autophagy.	Riemer et al. (2004) and Mok et al. (2007)

unmyelinated; these unmyelinated nodes are marked by contactin-1 (Çolakoğlu et al., 2014; **Figure 1**). Beginning in development, the expression of galectin-4 is different in each cortical layer and brain region. Galectin-4 is absent in the striatum and cortical layer VI, which are heavily myelinated, while its level remains high in cortical layers II to III, which contain neurons with less myelination at the mature stage. In particular, galectin-4 is found to cover these unmyelinated segments, colocalize with contactin-1 and inhibit oligodendrocytes from depositing myelin on these segments (Díez-Revuelta et al., 2017). Additionally, galectin-4 is secreted by neurons and inhibits the maturation of oligodendrocytes (Stancic et al., 2012). In contrast, astrocytes and microglia are involved in regulating and supporting myelination in different manners. In particular, astrocytes promote the proliferation of oligodendrocytes, while microglia induce the differentiation of oligodendrocytes, as demonstrated by culturing oligodendrocytes with conditioned medium from the two cell types (Pang et al., 2013). In addition, galectin-1, which is secreted mainly by astrocytes, shift microglia from an inflammatory to an anti-inflammatory status, which subsequently drives oligodendrocytes toward the myelination process (Starossom et al., 2012; Miron et al., 2013; Sirko et al., 2015). In parallel with these findings, galectin-3 controls the integrity of myelin *in vivo*, as demonstrated by the loosely wrapped myelin structures in galectin-3-depleted mice (Pasquini et al., 2011). Furthermore, in the cuprizone-induced demyelination mouse model, the level of galectin-3 is increased in microglia, which promotes the differentiation of oligodendrocytes for remyelination. The abovementioned machinery is impaired in galectin-3-depleted mice (Hoyos et al., 2014, 2016).

Galectins in Multiple Sclerosis (MS)

MS is a chronic inflammatory and autoimmune neurological disease marked by damage to the myelin that surrounds the axons in the CNS (Goldenberg, 2012). The pathogenesis of MS can be divided into two processes: (1) the overactivated immune system damages the myelin sheath and axon; and (2) remyelination is impaired (Dendrou et al., 2015). Both microglia and macrophages are chronically activated throughout the progression of MS and contribute to the inflammatory and demyelination processes (Fischer et al., 2012). Importantly, galectins-1, -3, -8 and -9 are reported to be up-regulated in human MS white matter samples. Immunohistochemical staining reveals that galectin-1 is up-regulated in microglia and macrophages, while its quantity is decreased in the astrocytes, at the lesioned area. The reduction of astrocytic galectin-1 may be due to the enhanced release of galectin-1 by astrocytes and may play an important role in MS progression. Conversely, the levels of galectins-8 and -9 are increased in microglia and macrophages located in active MS lesions. Interestingly,

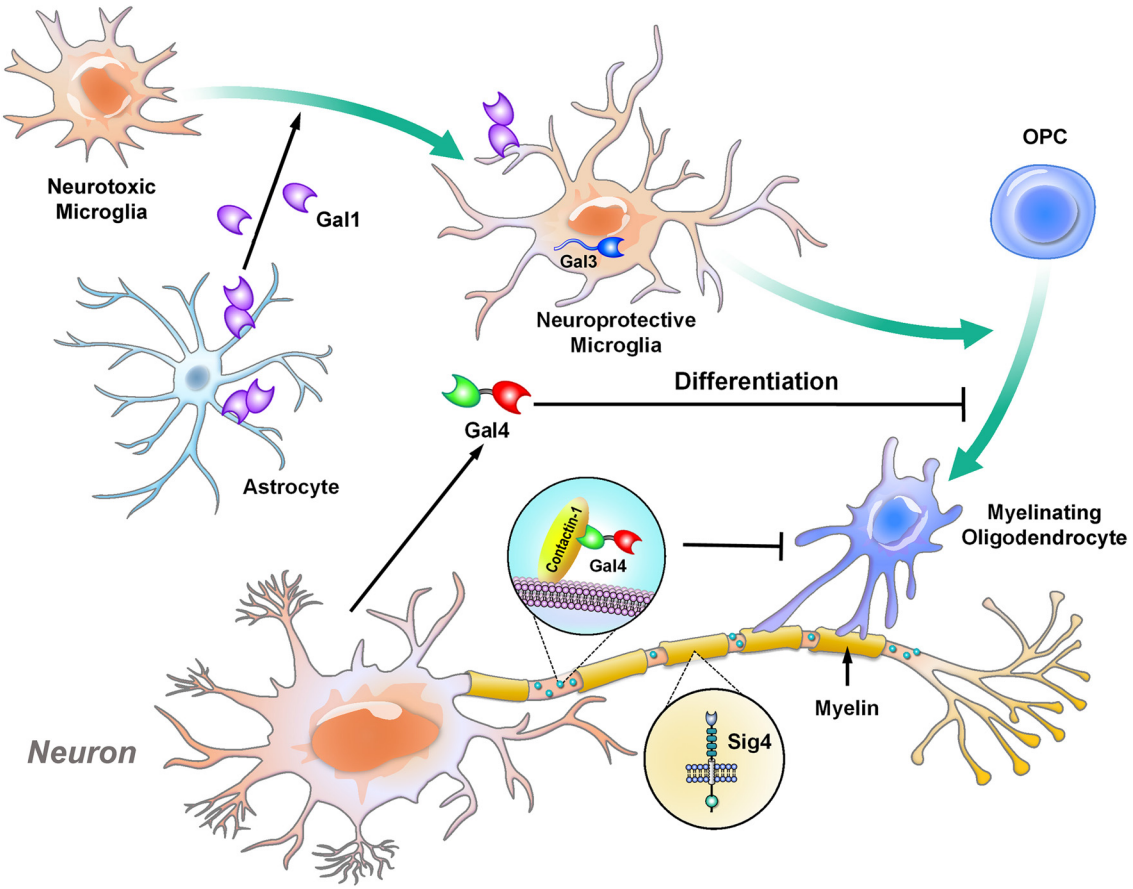

FIGURE 1 | Galectins and Siglec-4 contribute to the glia-mediated regulation of neuronal myelination. Oligodendrocytes are the cells responsible for myelination in the central nervous system (CNS). Under normal conditions, galectin-4 is delivered to the unmyelinated axonal regions and co-localizes with contactin-1 (a marker for nodes of Ranvier). The presence of galectin-4 inhibits oligodendrocytes from myelinating the region (Çolakoğlu et al., 2014). In addition, soluble galectin-4 inhibits the maturation of oligodendrocytes (Stancic et al., 2012). Siglec-4 is produced by oligodendrocytes and is expressed in the myelin sheath (Sun et al., 2004; Huang et al., 2012). Astrocytes and microglia promote the proliferation and differentiation, respectively, of oligodendrocytes. In particular, astrocytes secrete galectin-1 to drive microglia toward neuroprotective phenotype, while these microglia trigger the differentiation of oligodendrocytes in a galectin-3-dependent manner (Hoyos et al., 2014, 2016). Gal, galectin; Sig, Siglec.

galectin-9 alters cellular localization in MS microglia upon activation. In inactive lesion, galectin-9 is located in the cytoplasmic region of microglia, while it is present in both the nuclei and the cytosol of microglia in active lesions (Stancic et al., 2011). The functional relevance of this nuclear localization of galectin-9 remains elusive and requires further investigation.

To date, the most widely used animal model for the study of MS pathogenesis has been the experimental autoimmune encephalomyelitis (EAE) model (Steinman and Zamvil, 2006). In the EAE model, the expression of galectin-1 is up-regulated, with the highest level at the peak of the disease. Further analysis shows that galectin-1 is highly expressed in astrocytes (GFAP+ cells) and moderately expressed in a subset of T cells (CD4+ cells) and microglia/macrophages (CD11b+ cells) during the acute phase. Interestingly, astrocytes, but not other cell types, continue to express galectin-1 during the chronic phase. One of the specific binding targets of the secreted galectin-1 consists of the core 2 O-glycans of CD45 on the cell surface of microglia. Treatment of the pro-inflammatory microglia with galectin-1 inhibits the activation of the p38, CREB and NF-κB pathways (**Figure 2**). In the absence of galectin-1, MS progresses much more rapidly. More microglia with inflammatory phenotype and much more severe demyelination can be observed in the galectin-1 depleted EAE model (Starossom et al., 2012). These studies suggest a beneficial role of galectin-1 in the EAE model.

The level of galectin-3 is also up-regulated in the phagocytosing microglia in areas of demyelination in the EAE model (Reichert and Rotshenker, 1999; Stancic et al., 2011). Further studies suggested that the onset and severity of EAE were markedly reduced in galectin-3 KO mice (Jiang et al., 2009). In a demyelination experimental model of MS, generated by infection with Theiler's murine encephalomyelitis virus (TMEV), the level of galectin-3 is also up-regulated in microglia residing in the subventricular zone

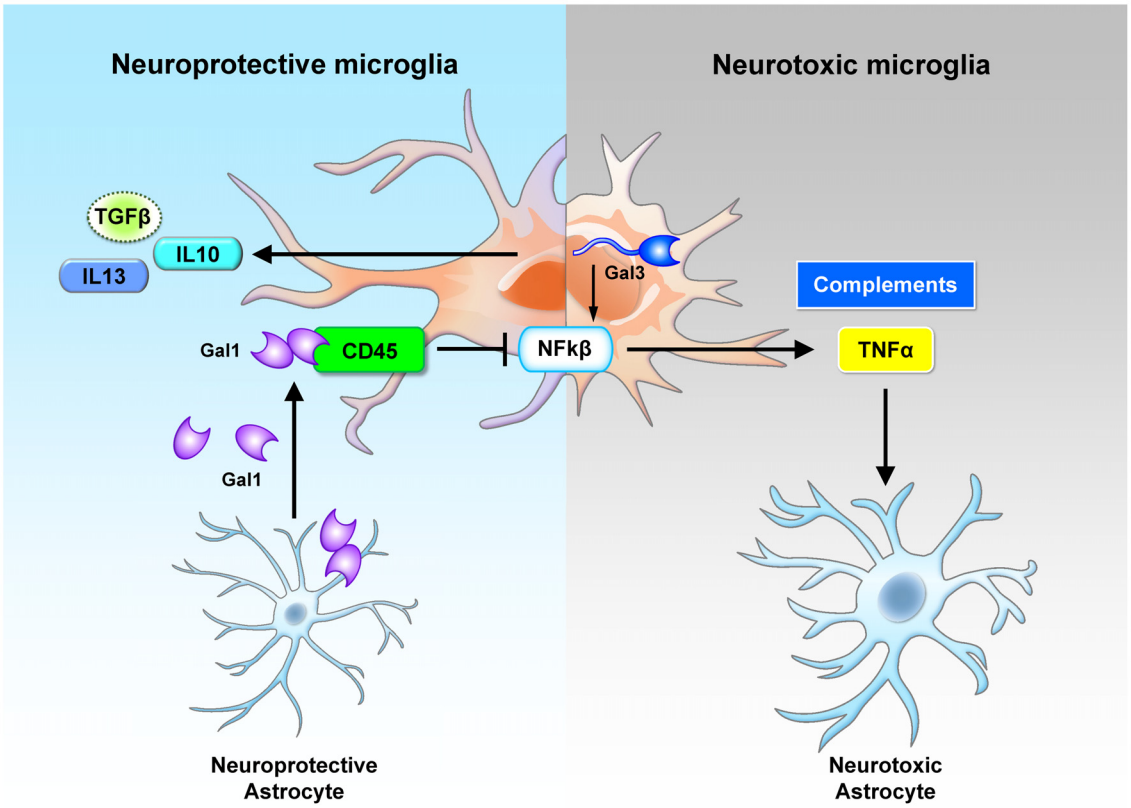

FIGURE 2 | Cross-regulation between astrocytes and microglia by galectin-1 and galectin-3. Neuroprotective astrocytes secrete galectin-1 to inhibit the neurotoxic activation of microglia. The secreted galectin-1 binds with CD45 on the microglia surface, suppresses NF-κB activation and promotes the polarization of neuroprotective microglia (Starossom et al., 2012). Neurotoxic microglia express various types of lectins. In particular, the up-regulated galectin-3 promotes inflammation response through NF-κB activation (Boza-Serrano et al., 2014). These microglial cells secrete inflammatory cytokines (TNFα) and complements that trigger the activation of neurotoxic astrocytes (Liddelow et al., 2017). Gal, galectin; Sig, Siglec.

(the neurogenetic niche that is markedly inflamed in MS and its murine models) and the cerebral cortex. In this model, genetic removal of galectin-3 greatly normalizes the immune response observed in the SVZ, reduces the migration of immune cells into the SVZ, and increases the number of progenitors in the corpus callosum (James et al., 2016). These lines of evidence suggest that galectin-3 may play an essential role in MS.

Galectin-8 can be detected in the cerebrospinal fluid (CSF) of MS patients. Genetic removal of galectin-8 hastens the onset of the disease and worsens the progression. Daily treatment with galectin-8 significantly delays the disease progression of EAE. In particular, galectin-8 inhibits the activity of Th17-positive cells to induce inflammation by influencing cells toward apoptosis (Pardo et al., 2017). Similarly, galectin-9 can also be detected in the CSF of secondary progressive MS patients (Burman and Svenningsson, 2016). Compared to the peripheral nervous system, the roles of galectin-8 and galectin-9 in the CNS (such as their expression profiles and their functions in different brain cells) have not been extensively explored and are worth further investigation.

Galectins in Stroke and Ischemia

Galectin-3 is up-regulated in microglia after stroke and induces the expression of IGF-1 (Lalancette-Hébert et al., 2007). Importantly, galectin-3 interacts directly with IGF-1 to promote post-ischemic microglial proliferation. These microglia are suggested to serve as the reservoir of neurotrophic factors, such as IGF-1. Genetic depletion of galectin-3 significantly reduces microglial activation and proliferation; these effects are associated with larger ischemic lesion size, decreased IGF-1 levels and neuronal death. Moreover, there is a twofold increase in IL6 in the ischemic brains of galectin-3-depleted mice (Lalancette-Hébert et al., 2012). These studies suggest that the presence of galectin-3 promotes alternative activation of microglia toward an anti-inflammatory status after stroke. Nonetheless, in a separate study, secreted galectin-3 was shown to act as a ligand for the toll-like receptor 4 (TLR4) and promote inflammatory response in a murine neuroinflammatory LPS model and in the brain of stroke patients. Compared to wild-type controls, galectin-3-knockout (KO) mice have elevated neuronal survival in the hippocampus after ischemia, suggesting that galectin-3 prolongs microglia at the pro-inflammatory

status (Burguillos et al., 2015). Consistent with a detrimental role, galectin-3 is found to be up-regulated in the CA1 and CA2 hippocampal regions following transient ischemia. The expression of galectin-3 in these regions is associated with neuronal death and can be prevented by intra-ischemic hypothermia treatment (Satoh et al., 2011; Hisamatsu et al., 2016). Moreover, in the permanent middle cerebral artery occlusion (pMCAO) model, the lack of galectin-3 rescues significant neuronal loss. Treatment with sera collected from pMCAO-treated WT mice also induces increased death of enteric neurons compared with sera collected from pMCAO-treated galectin-3 KO mice. The death of these neurons can be prevented by inhibition of TAK1 and AMPK (transforming growth factor and beta-activated kinase 1 and AMP activated kinase, respectively; Cheng et al., 2016). Collectively, the inflammatory roles of galectin-3 are diverse and may depend on the following factors: the type of ischemic insult, the stage of disease/trauma and the subcellular localization.

Galectins in Traumatic Brain Injury (TBI)

Traumatic Brain Injury (TBI) is clinically categorized into three groups, namely, mild, moderate and severe. Its effects can be further divided into primary and secondary injuries. Primary injuries (such as direct damage to the brain parenchyma that may shear axons) are usually irreversible. On the other hand, secondary injuries are the detrimental effects resulting from the primary injury (such as inflammation and ischemia; Blennow et al., 2016). In response to TBI, in order to restore the normal brain environment, microglia rapidly migrate to the site of injury to remove damaged and dead cells. In a mouse closed-skull model of TBI, the level of galectin-3 increased in the corpus callosum for about 1 month following injury, with the peak at 24 h after injury. The galectin-3- positive microglia engulf damaged axons and produce NGF that facilitates the repair of damaged neurons (Venkatesan et al., 2010). In another study using the controlled cortical impact (CCI) model of head injury, galectin-3 is also up-regulated in the microglia but binds with TLR4 to promote inflammation in the cortex and hippocampus. Treatment with a galectin-3-neutralizing antibody reduces the expression of pro-inflammatory genes *IL1β*, *IL6* and *NOS2* while promoting the expression of *Ym1*, *Arg1* and *TGFβ*. Consistent with a damaging role of galectin-3, galectin-3-deficient mice show less neuronal death and microglial activation in a CCI model (Yip et al., 2017). These data suggest that the role of microglial galectin-3 in TBI can be complex depending on the severity and type of trauma.

Galectins in Amyotrophic Lateral Sclerosis (ALS)

ALS is a rare, progressive and fatal neurodegenerative disease. Multiple genes have been identified as being associated with familial ALS, but those genes explain only approximately 10% of cases. Nearly 90% of ALS cases are sporadic (Abhinav et al., 2007). Up-regulation of plasma galectin-3 is detected in ALS patients with limb onset or disease duration longer than 12 months. The level of plasma galectin-3 is correlated with the duration of disease. Female patients exhibit higher increase of galectin-3 in the plasma than male patients, although the reason is still unknown (Yan et al., 2016). A study using the B6SJL SOD1(G93A) transgenic mouse model of familial ALS (Smittkamp et al., 2008) revealed that microglia undergo a transition stage from the protective phenotype in early-stage ALS to the detrimental phenotype in end-stage ALS. Furthermore, early-stage microglia promote the survival of motor neurons in a co-culture system, while end-stage microglia trigger neuronal death (Liao et al., 2012).

In particular, galectin-1 is increased in the spinal cord of SOD1 mice, while galectins-3 and -9 are increased in SOD1 mice and sporadic ALS patients. The alterations in these galectins during ALS progression are different. Specifically, the amount of galectin-3 can be detected in microglia of spinal cord at the presymptomatic stage, and its level continues to increase until the end stage. Conversely, the expression of galectin-9 is increased at the symptomatic stage, while the levels of galectin-1 is up-regulated only at the end stage (Lerman et al., 2012). The types of cells that contribute to the higher levels of galectin-1 and -9 in the spinal cord are currently unknown.

Nonetheless, it is of great interest to observe that treatment of SOD1 mice with recombinant galectin-1 significantly enhances the survival of motor neurons, delays the onset of disease, improves motor performance, and prolongs the lifespan of ALS mice. Because galectin-1 treatment has no specific effect on isolated primary neurons, the therapeutic effect of galectin-1 may be mediated by non-neuronal cells (Chang-Hong et al., 2005). In particular, microglia and macrophages are among the target cells of galectin-1. For example, treatment with galectin-1 induces macrophages to produce an axonal regeneration-promoting factor that is critical to the survival of degenerating motor neurons (Horie et al., 2004). Overall, although the underlying mechanism remain to be clarified, galectin-1 is a potential therapeutic target for ALS.

Another interesting drug target for ALS is galectin-3. Genetic depletion of galectin-3 in SOD1 mice accelerates disease progression (i.e., a shorter life span and faster motor function impairment) with a significant increase in microglial activation, along with higher inflammatory response and oxidative damage (Lerman et al., 2012). In the CNS of healthy rats, the basal expression of galectin-3 is relatively higher in the spinal cord than in the cortex. Flow cytometry analysis detects at least two major populations of microglia (namely, galectin-3- positive and negative) in the spinal cord of SOD1(G93A) rats after disease onset. Compared to microglia in wild-type rats, microglia in the spinal cord of SOD1(G93A) rats express significantly higher levels of galectin-3 from early to late stage of the disease. The levels of both neurotoxic and neuroprotective molecules (i.e., TNFα, IL6, arginase-1, IL10 and BDNF) in the late stage of the disease are lower, compared with in the early stage. Intriguingly, these alterations only appeared in the spinal cord but not in the cortex, suggesting that the function of galectin-3 and the features of microglia are different in the spinal cord and cortex (Nikodemova et al., 2014). Collectively, these findings suggest that microglial galectin-3 plays a protective role in ALS, which appears different from most of the neurodegenerative diseases where the role of

galectin-3 has been investigated so far; further investigation is required.

Galectin-3 in Parkinson's Disease (PD)

The pathology of PD is characterized by the degeneration of dopaminergic neurons in the substantia nigra and widespread Lewy bodies that contain α-synuclein (α-Syn) aggregates. Accumulated evidence suggest that neurons can release α-Syn to neighboring astrocytes and microglia (Kim et al., 2013). Microglia would take up α-Syn either by phagocytosis or endocytosis. Treatment of a BV2 microglial cell line with different forms of α-Syn (monomer and aggregates) promotes microglial activation as assessed by the levels of iNOS and pro-inflammatory cytokines (TNFα, IL2 and IL12). Importantly, knockdown of galectin-3 or treatment with a galectin-3 inhibitor abolishes the effect of α-Syn on the release of iNOS and pro-inflammatory cytokines. Inhibition of galectin-3 reduces the phagocytic capability of microglia to take up exogenous α-Syn, while treatment with recombinant galectin-3 promotes phagocytosis. Injection of oligomeric forms of α-Syn into the olfactory bulb also significantly enhances the expression of galectin-3 and the phagocytotic activity of microglia. These findings suggest that exposure of microglia to α-Syn causes up-regulation of galectin-3 and subsequently enhances phagocytosis (Boza-Serrano et al., 2014).

The glycan binding targets of galectin (i.e., β-galactosides) are located in the plasma membrane outer leaflet and the luminal side of the intracellular vesicles. Cytosolic galectins (e.g., galectin-3) therefore have no access to β-galactosides. In a neuronal model (SY5Y cells), treatments with α-Syn trigger the formation of galectin-3 puncta because the endocytosed α-Syn cannot be effectively degraded and triggers cellular stress (e.g., elevated ROS), leading to vesicle rupture (Flavin et al., 2017). Exposure of surface glycans from the ruptured vesicular membranes to the cytoplasm recruits galectin-3, which forms galectin-3 puncta (Freeman et al., 2013; Flavin et al., 2017). Such endosomal and lysosomal ruptures not only expose the internal compartment of the vesicles but also release into the cytoplasm substances (e.g., cathepsin B) that need to be confined inside the vesicle, potentially inducing the mitochondrial dysfunction and inflammation that are the common features of PD. It is likely that cell-to-cell transmission of cytosolic protein aggregates (e.g., α-Syn) may induce cellular stress that causes vesicle rupture and the formation of galectin-3 puncta as illustrated in **Figure 3**. Similar to galectin-8 (Thurston et al., 2012), galectin-3 may serve as a cellular danger receptor that senses detrimental conditions

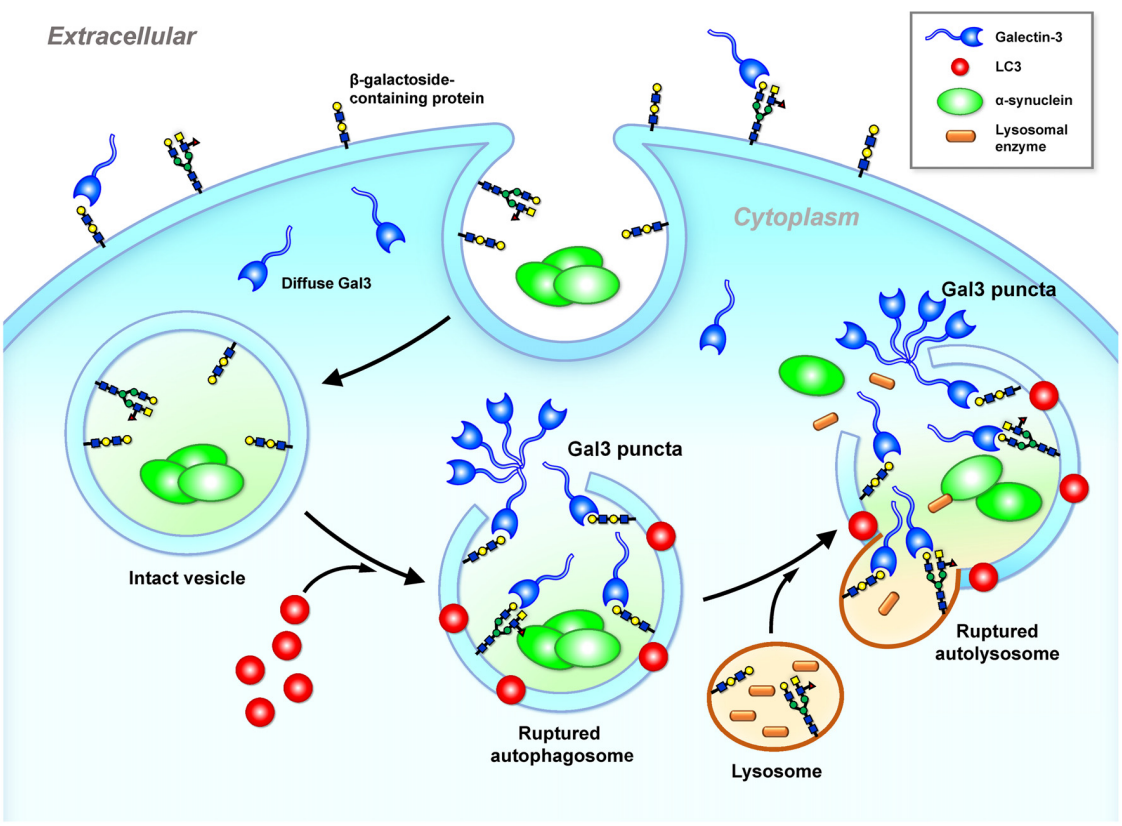

FIGURE 3 | Galectin-3 is a sensor of ruptured intracellular vesicles. Galectin-3 recognizes and binds to β-galactosides. β-galactosides containing proteins are located in the plasma membrane outer leaflet and the luminal side of intact intracellular vesicles (e.g., lysosome, autophagosome and autolysosome). Once these vesicles leak or rupture under stress, galectin-3 gains access and binds to β-galactosides located inside of ruptured vesicles and forms puncta (Freeman et al., 2013; Flavin et al., 2017). Gal3, galectin-3; α-Syn, α-synuclein.

during neuronal degeneration. Further investigation is required to determine whether the formation of galectin-3 puncta at these ruptured vesicles affects cellular functions.

Galectin-3 in Prion Diseases

Prion diseases consist of a group of neurodegenerative disorders that are caused by misfolded proteins called prions. Prions are infectious and the disease can occur in a sporadic, genetic or acquired manner. Genetic prion disease is caused by the mutation of prion-related protein gene (*PRPN*; Geschwind, 2015). In the scrapie-infected mouse model of prion disease, gene array analysis of the brain reveals 114 altered mRNA levels, and many of the identified genes were related to immune and stress responses. Among the genes with altered expression, the mRNA of galectin-3 is significantly up-regulated in the medulla and pons (Riemer et al., 2004). In a separate study, the protein level of galectin-3 was also found to be increased in scrapie-infected brains. Because galectin-3 KO mice with scrapie infection survive longer than the scrapie-infected wild-type mice and because the levels of a lysosomal activation marker (LAMP-2) and autophagy-related proteins (i.e., Beclin-1 and Atg5) are significantly decreased in the scrapie-infected galectin-3 KO mice, it is possible that galectin-3 may play a detrimental role by damaging the integrity of lysosomes and suppressing autophagy in prion disease (Mok et al., 2007).

SIGLECS

Siglecs (sialic acid-binding immunoglobulin-like lectins) represent the best-characterized subgroup of I-type lectins, which contain the immunoglobulin domain that recognizes structural diversity of carbohydrates (Crocker et al., 2007). In general, Siglecs are expressed on plasma membrane, containing an amino terminal V-set immunoglobulin domain that binds sialic acid and a number of C2-set immunoglobulin domains. As their full name suggests, Siglecs recognize sialic acid residues (best described as N-acetyl-neuraminic acids, Neu5Ac) that are presented on glycoproteins and glycolipids with distinct yet overlapping specificities. The presence of C-2 α-hydroxyl group at the terminal of sialic acid enables covalent linkage to other hydroxyl groups on the C-3 and C-6 positions to form the α2–3 and α2–6 linkages, respectively. Enzymes that are responsible for generating such linkages are named sialyltransferases. There are multiples types of sialyltransferases that produce a variety of linkages that can be recognized by Siglecs with different specificities.

Currently, up to 16 Siglecs have been identified and can be categorized based on their sequence similarity, conservation among murine and human and the regulatory properties (i.e., inhibitory or activatory; for review, see Pillai et al., 2012; Macauley et al., 2014). In brief, Siglec-1 (sialoadhesin), Siglec-2 (CD22), Siglec-4 (myelin-associated glycoprotein, MAG) and Siglec-15 are conserved across mammals. Conversely, a variety of Siglecs-3 (CD33)- related Siglecs have been found across mammals. The human CD33-related Siglecs include Siglecs-3, -5, -6, -7, -8, -9, -10, -11, -12, -14 and -16, while the murine CD33-related Siglecs consist of Siglecs-3, -E, -F, -G and -H (Macauley et al., 2014). Most Siglecs (excluding Siglec-1 and MAG) contain immunoreceptor tyrosine-based inhibitory motifs (ITIMs) at the cytoplasmic regions to recruit SH2 domain-containing protein tyrosine phosphatase SHP1 and SHP2; these Siglecs are classified as inhibitory Siglecs. On the other hand, Siglecs-14, -15 and -16 contain the immunoreceptor tyrosine-based activation motifs (ITAMs) on the adaptor of DAP12 to recruit spleen tyrosine kinase (SYK); these Siglecs are classified as activatory Siglecs.

Siglecs are expressed specifically on the cells from hematopoietic lineage, with the exceptions of MAG on oligodendrocytes and Siglec-6 on placental trophoblasts (Macauley et al., 2014). Knowledge of Siglecs is collected mainly from the peripheral system, while Siglecs that are reported to exist in the CNS include sialoadhesin, CD33, MAG, Siglec-E, Siglec-F, Siglec-H, Siglec-11 and Siglec-16. Siglecs are generally absent or scarce under normal physiological condition and are induced to express by various stimuli that activate microglia. These Siglecs, with exception of MAG that is located in oligodendrocytes, are expressed on microglia in the brain. **Table 5** summarizes the role of Siglecs in neurological disorders.

Siglec-1 (Sialoadhesin, CD169) During the Breakdown of the BBB

Siglec-1 does not have the ITIM or ITAM at its cytoplasmic regions but contains a long immunoglobulin domain that allows the binding domain to reach a distal site from the membrane. Therefore, Siglec-1 is thought to be important for cell-cell adhesion and cell-pathogen recognition (Crocker et al., 1994). Siglec-1 is present in peripheral blood mononuclear phagocytes. Nevertheless, its expression in microglia is rather controversial and may be due to the exposure to plasma proteins upon the breakdown of the blood-brain barrier (BBB) during brain trauma (e.g., TBI model, Perry et al., 1992). Similarly, during retinal degeneration, activated microglia may express Siglec-1 after the

TABLE 5 | Summary of the role of Siglecs in neurological disease.

Neurological conditions	Type of Siglec	Disease-associated features	References
Traumatic brain injury	Siglec-1	• Up-regulated in the microglia upon exposure to plasma proteins, unclear function.	Perry et al. (1992)
Ceriod lipofuscinoses	Siglec-1	• Up-regulated in the microglia of the optic nerve. • Serves as an APC and interacts with CD8+ T cells to promote inflammation.	Groh et al. (2016)
Alzheimer's disease	CD33	• Up-regulated in the microglia to suppress phagocytosis of Aβ.	Bradshaw et al. (2013) and Griciuc et al. (2013)
Brain tumor	Siglec-H	• Phagocytosis of glioma cells	Kopatz et al. (2013)
Amyotrophic lateral sclerosis	Siglec-H	• Up-regulated over time in the spinal cord of SOD1 mice, uncharacterized function.	Chiu et al. (2013)

breakdown of the blood-retinal barrier (Hughes et al., 2003). Whether these Siglec-1-expressing microglia are originated in the brain or blood-derived cells (i.e., macrophages) that migrate into the brain and their functions are not clear at this time.

In ceroid lipofuscinosis (CLN), a disease that is characterized by lysosomal storage dysfunction, neurodegeneration and early death, the expression of Siglec-1 is significantly up-regulated. These Siglec-1-expressing microglia serve as antigen-presenting cells (APCs) to interact with CD8+ T cells and promote the pathology of the disease. In Siglec-1-deficient CLN mice, microglia express significantly lower inflammatory cytokines (e.g., IL1β and TNFα) and higher level of anti-inflammatory cytokines (e.g., TGFβ). In addition, Siglec-1-deficient CLN mice exhibit reduced axonal degeneration and longer lifespan, supporting a harmful role of Siglec-1 (Groh et al., 2016). Hence, antagonizing the function of Siglec-1 appears as a potential therapeutic approach during the breakdown of the BBB from disease or injury.

Siglec-3 (CD33) in AD

AD is a chronic neurodegenerative disorder that affects up to 30% of the population over 65 years old (Masters et al., 2015). The pathology of the disease is characterized by intracellular neurofibrillary tangles and failure to clear extracellular amyloid-β (Aβ) peptides from the brain. Most patients with AD have the sporadic form, while a small portion of patients carry genes that cause ineffective clearing of Aβ. Recent genome-wide association studies have identified CD33 as a genetic risk factor of AD (Hollingworth et al., 2011; Naj et al., 2011). The risk allele *rs3865444* is associated with higher expression of CD33 on the cell surface without affecting the number of microglial cells. Moreover, these CD33-immunoreactive microglia exhibit a positive correlation with Aβ aggregates and plaque burden in the brain of AD patients (Bradshaw et al., 2013; Griciuc et al., 2013). Further *in vitro* studies confirmed the presence of CD33 with the risk allele *rs3865444*, which significantly suppresses the phagocytosis capability of microglia. Interestingly, the levels of CD33 with the minor allele of *rs3865444* single nucleotide polymorphism (SNP) are markedly reduced. Similarly, primary microglia derived from CD33 KO mice showed greater uptake of Aβ than the control cells, while the rates of Aβ degradation are unaffected. Moreover, the KO of CD33 in the APP/PS1 mouse model significantly reduces Aβ plaques in the cortex and hippocampus (Griciuc et al., 2013). Therefore, tuning the capability of microglia to take up and degrade Aβ through inhibition of CD33 activity may provide a novel therapeutic intervention for AD. The regulation of microglial phagocytosis by CD33 is summarized in **Figure 4**.

Siglec-H in Brain Tumors

Siglec-H is expressed only in murine microglia and plasmacytoid dendritic cells (pDCs), while they are absent in human monocytes (Zhang et al., 2006; Kopatz et al., 2013). In contrast to most Siglecs, Siglec-H is an activatory Siglec with complex functions. Siglec-H suppresses the downstream signaling of TLR9 to produce interferon-α in pDCs (Takagi et al., 2011; Puttur et al., 2013). Although Siglec-H is known to be expressed in microglia, its ligands and functions are only now being discovered, as it does not bind to the typical sialic acid-containing glycoproteins or glycolipids of healthy cells (Varki and Angata, 2006; Varki, 2009). Treatment of a microglial cell line and primary microglia with interferon-γ significantly enhances inflammatory phenotypes (e.g., up-regulation of iNOS, CXCL10 and TNFα) and up-regulation of Siglec-H. These Siglec-H-enriched microglia exhibit high phagocytosis activity that can be suppressed by down-regulation of Siglec-H. Importantly,

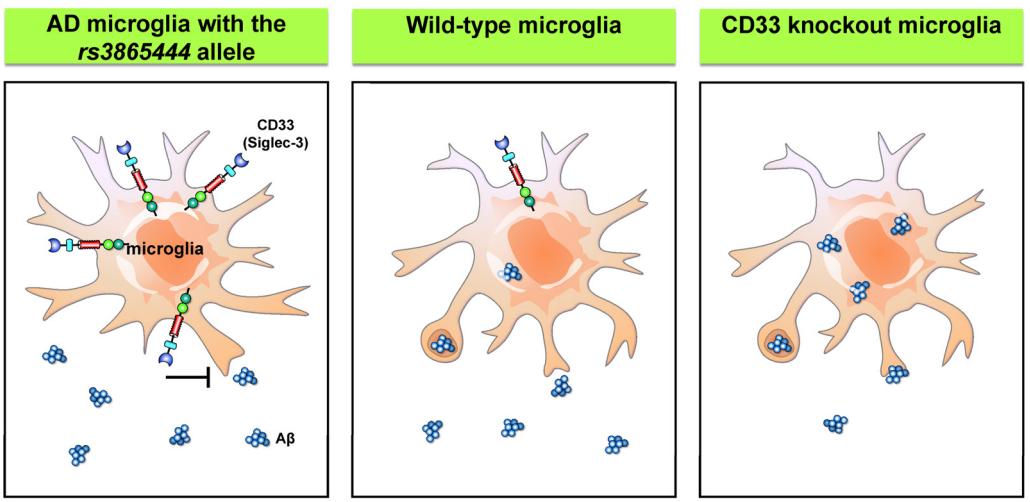

FIGURE 4 | Siglecs regulate microglial phagocytosis. Wild-type microglia express a low level of CD33/Siglec 3, a member of the Siglec family. The risk allele *rs3865444* was originally identified in patients with Alzheimer's disease (AD) and is associated with higher levels of CD33 that suppress the microglial phagocytosis. Conversely, knockdown of CD33 significantly improves the phagocytosis capability of microglia (Hollingworth et al., 2011; Naj et al., 2011; Griciuc et al., 2013). Aβ, amyloid β.

Siglec-H binds to and triggers the engulfment of glioma cell lines (namely, GL261 and SMA560) but not normal astrocytes, splenocytes, or fibroblasts. It is possible that microglial Siglec-H may function to monitor the surface sialylation profiles present on tumor cells in the brain (Kopatz et al., 2013). These studies identified the functions of Siglec-H in the brain. However, whether enhancing Siglec-H activity is a potent approach to target brain tumor required further investigation.

Siglec-H in ALS

Microglia share many markers with peripheral monocytes and macrophages. Transcriptome analysis reveals that Siglec-H is the third highest gene (out of 29 identified genes) that can distinguish microglia from monocytes and macrophages. The level of Siglec-H is also up-regulated in the spinal cord of an ALS mouse model (SOD1; Chiu et al., 2013). The function of Siglec-H in ALS remains unclear.

C-TYPE LECTINS

C-type lectins are a group of proteins that bind to glycan in a calcium-dependent manner. The proteins contain a C-type lectin domain (CTLD), which is also present in many proteins that do not recognize or bind to any glycan. C-type lectins and protein with CTLD are found in all organism and can be categorized to at least 17 groups based on their domain architecture, such as selectins, collectins, etc. The classification of C-type lectins and their roles in the peripheral immunity have been reviewed extensively elsewhere (Sancho and Reis e Sousa, 2012; Dambuza and Brown, 2015; Yan et al., 2015). In this review, we focus on a few C-type lectins (**Table 6**) that have been implicated in neurological disorder.

Selectins

Selectins are single-chain transmembrane glycoproteins of the cell adhesion molecule family. They are highly homologous proteins, which contain a CTLD, an epidermal growth factor-like domain, a few consensus repeats composed of sushi domain, a transmembrane domain and an intracellular cytoplasmic tail. The CTLD of selectins recognizes sialyl Lewis X antigens (sialylated and fucosylated glycoprotein and glycolipid structures; Ley, 2003; Angiari and Constantin, 2013). Three types of selectins (i.e., E-, L- and P-Selectins) have being identified so far. In the brain, selectins (particularly the E- and P-type) are located in endothelial cells and are responsible for controlling leukocyte infiltration and the BBB permeability during trauma or acute inflammation (Tang et al., 1996; Carvalho-Tavares et al., 2000; Bernardes-Silva et al., 2001). This is an important aspect because accumulation and adhesion of leukocytes to the endothelial cells are the critical steps that cause cell death at the ischemic regions (Kataoka et al., 2004; Langer and Chavakis, 2009).

In the animal model of focal cerebral ischemia and reperfusion injury, E-Selectins are induced and expressed on the endothelial cells (Wang et al., 1995; Zhang et al., 1996). Because E-Selectins bind sialyl Lewis X glycans enriched in neutrophils (Lasky, 1992) and the administration of sialyl Lewis X significantly decreases the recruitment of neutrophils to the ischemic region and decrease the infarct volume (Zhang et al., 1996), E-Selectins appear to be an important component of ischemia pathogenesis. Another intriguing observation is that the polysialylated E-Selectin Ligand-1 (ESL1, a ligand for E-Selectins) was found to be enriched in the Golgi compartments of microglia. Brain injuries translocate ESL1 to the cell surfaces and therefore trigger the binding of E-Selectins with microglia (Werneburg et al., 2016). Binding of E-Selectins to myeloid cells (i.e., neutrophils) has been demonstrated to regulate cell homing to sites of inflammation (Mondal et al., 2016), while the effect of binding of E-Selectins to microglia remains to be determined.

The expression of P-Selectin in endothelial cells is also up-regulated in a complement C3-dependent manner in an ischemia mouse model (Atkinson et al., 2006). Both P-Selectin deficiency and P-Selectin inhibition protect mice from the cerebral injury following ischemia (Zhou et al., 2000; Atkinson et al., 2006). Up-regulation of P-Selectin also contributes to the transient breakdown of BBB following ischemia (Jin et al., 2010). It is interesting to note that the level of P-Selectin is significantly up-regulated in the experimental subarachnoid hemorrhage (eSAH) model as well. The presence of P-Selectins on endothelial cells recruit neutrophils and microglia to the site of injury. It is likely that these microglia are activated by the inflammatory cytokines released by the neutrophils promoted

TABLE 6 | Summary of the role of C-type lectins in neurological disease.

Neurological conditions	Type of C-type lectin	Disease-associated features	References
Stroke and ischemia	E-Selectin	• Facilitates the adhesion of neutrophils to endothelial cells and promotes cell damage.	Zhang et al. (1996) and Jin et al. (2010)
	P-Selectin	• Facilitates the adhesion of neutrophils to endothelial cells and promotes the activation of complement. • Contributes to the breakdown of the BBB.	Atkinson et al. (2006) and Jin et al. (2010)
	Mannose-binding lectin	• Up-regulated and contributes to cerebral infarction. • Contributes to complement activation and promotes inflammation.	Cervera et al. (2010), Morrison et al. (2011), Orsini et al. (2012) and De Blasio et al. (2017)
Subarachnoid hemorrhage	P-Selectin	• Recruits neutrophils and subsequently activates microglia through intravascular inflammation.	Atangana et al. (2017)
HIV infection	Mannose-binding lectin	• Up-regulated in microglia, astrocytes, oligodendrocytes and neurons. • Expression is associated with MCP-1, which may trigger inflammation.	Singh et al. (2011)

by intravascular inflammation (Schneider et al., 2015; Atangana et al., 2017). In addition, induction of eSAH in mice lacking the P-Selectin glycoprotein ligand-1 (PSGL1; a P-Selectin ligand) results in significant reductions in the endothelial-neutrophil interactions, the number of activated microglia and the extent of neuronal death (Atangana et al., 2017). Collectively, these studies suggest that P-Selectin is likely to play a detrimental role in neurological traumas by facilitating the microglia-mediated neuroinflammation. **Figure 5** summarizes the roles of E-selectins and P-selectins in brain ischemia.

Mannose-Binding Lectins (MBLs)

MBLs, also called mannan-binding lectins, are from the collectin class of the C-type lectin family and are important components of the innate immune system. These proteins contain a cysteine-rich N-terminal region, a collagenous domain, a short α-helical coiled-coil domain and a CRD at the C-terminal. It is important to note that CRDs of MBL recognize glycans on the surface of pathogens as well as cryptic self-antigens that are modified in disease conditions or injuries (Ip et al., 2009). They exist in oligomeric forms (i.e., from dimer to hexamer) and recognizes mannose, fucose and N-acetyl-glucosamine (GlcNAc), but not sialic acid and galactose (Drickamer, 1992; Weis et al., 1992; Yokota et al., 1995). MBLs participate in a range of biological functions including the recognition of pathogen invasion, activation of complement system, phagocytosis and mediation of inflammatory signaling (Ip et al., 2009; Auriti et al., 2017).

Activation of complement system is one of the main causes for brain damage during ischemia and stroke. MBL has been implicated to participate in the activation of complement system via the lectin pathway (Morrison et al., 2011). MBL-KO mice are protected from transient and permanent ischemic injuries with the reduction of infarct volume and sensorimotor impairments. Blocking MBL using an anti-MBL-A antibody also produce similar results (Orsini et al., 2012; Longhi et al., 2014). Consistently, ischemic stroke patients, who have MBL-low genotypes and lower MBL in their serum, are associated with a favorable stroke outcome and decreased levels of proinflammatory cytokines (e.g., TNFα and IL6). These patients with lower MBL levels (<100 ng/ml) are likely to recover from movement disabilities in less than 3 months (Cervera et al., 2010; Osthoff et al., 2011). Collectively, effective inhibition of MBL may reduce the damage caused by ischemic stroke.

In patients infected by HIV, viruses can enter the CNS and continue to replicate within the brain. Infection of HIV in the

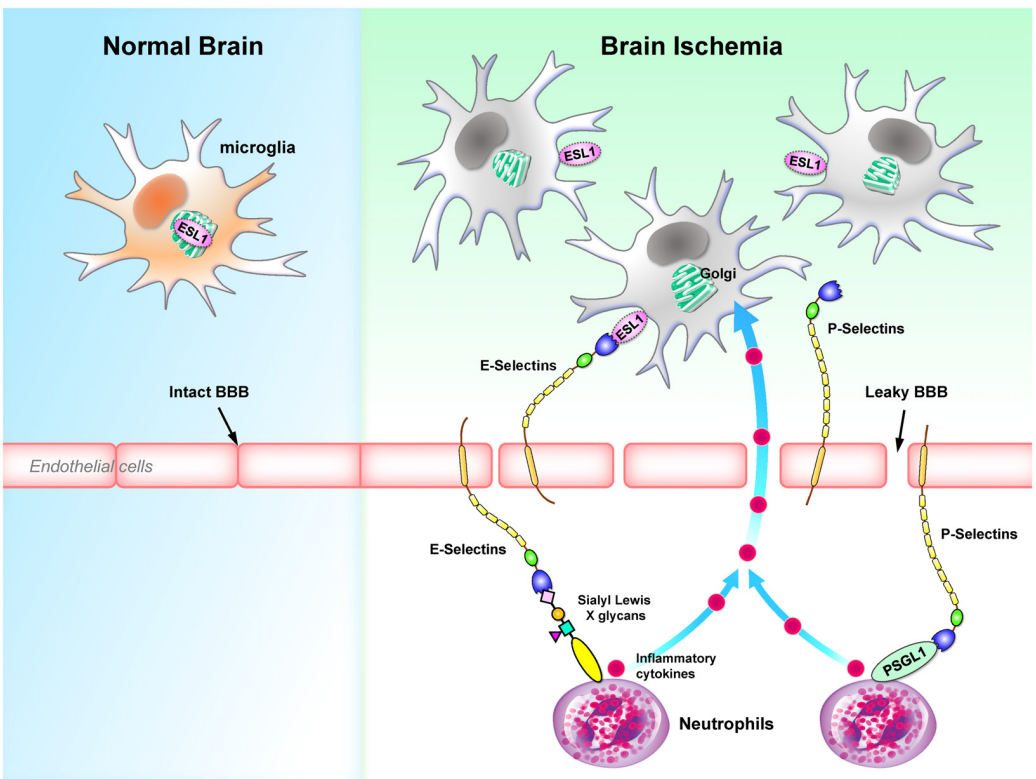

FIGURE 5 | Selectins regulates microglial activation and homing to sites of inflammation during brain ischemia. E-selectins and P-selectins that bind to Sialyl Lewis X glycans are up-regulated in endothelial cells during brain ischemia. Binding of selectins serves as a homing mechanism to retain Sialyl Lewis X glycans-containing cells close to endothelial cells. In particular, ESL1 located in the Golgi compartments of microglia is translocated to the plasma membrane and binds to E-selectins on the surface of endothelial cells (Werneburg et al., 2016). In contrast, P-selectins cause a transient leakage of BBB (Jin et al., 2010). P-selectins bind to PSGL1 on neutrophils, which secrete inflammatory cytokines and further activate microglia in the CNS (Schneider et al., 2015; Atangana et al., 2017). BBB, blood-brain barrier; ESL1, E-selectin ligand-1; PSGL1, P-selectin glycoprotein ligand-1.

brain therefore causes a chronic inflammatory response and a spectrum of neurological dysfunction (Saylor et al., 2016). By studying post-mortem brain tissues, it was shown that the expression of MBL is up-regulated in the HIV- infected brains. Interestingly, the expression of MBL is detected in all brain cells, including microglia, astrocytes, oligodendrocytes and neurons. In particular, axons in the HIV-infected brain show high levels of MBL, while the level of MBL is associated with the level of monocytes chemoattractant protein-1 (MCP-1 or CCL2; Singh et al., 2011). MCP-1 is the key chemokine that triggers the migration of microglia or macrophages (Deshmane et al., 2009; Hinojosa et al., 2011). Hence, the expression of MBL is suggested to be associated with the activation of complement and neuroinflammation, which subsequently cause neuronal damage in the HIV-infected brain.

CONCLUSION AND FUTURE PERSPECTIVES

Accumulated evidence suggest that dysregulation of lectins is a critical pathogenetic factor in neurological diseases. The altered expressions of lectins on microglia affect the phenotypes of microglia (Yip et al., 2017). Importantly, the aberrant expression of lectins on the surrounding cells can also trigger the activation of microglia (Atangana et al., 2017). These may independently or synergistically lead to the chronic pathogenic inflammatory response that causes neuronal dysfunctions or death. Likewise, these activated microglia may also secrete inflammatory cytokines and complement that will influence the activity of astrocytes to produce neurotoxic factors (Liddelow et al., 2017).

One major area that still requires clarification is the specific type of cells that express these lectins. Many lectins are not expressed in the healthy CNS, nevertheless are induced to express or up-regulated in disease condition. It is crucial to identify the specific types of cells that show aberrant expression of lectins and their functional effect on the cells themselves or the surrounding cells. For instance, galectin-3 is expressed virtually on activated microglia in various neurological disorders *in vivo*, while it is expressed in various cell lines derived from brain glial cells *in vitro* (Pasquini et al., 2011). These studies raise the questions of why cell lines express galectin-3 even under normal conditions. There is a possibility that galectin-3 is involved in the immortalization and proliferation of cell lines, as it does in tumor cells (i.e., pancreatic cancer cells, thyroid carcinoma cells; Song et al., 2012; Cardoso et al., 2016). At the same time, it is also of interest to investigate whether other glial cells (astrocytes and oligodendrocytes) in abnormal conditions also express galectin-3 *in vivo*. Meanwhile, Galectin-4 is expressed in non-myelinated region of axons and Siglec-4 is expressed specifically on oligodendrocytes to regulate myelination (**Figure 1**). Contrary to Galectins that can be expressed in various types of cells, all CD33-related Siglecs are expressed specifically on myeloid- origin cells, namely, microglia in the CNS. Selectins are mainly on endothelial cells and their expressions directly affects the integrity of BBB and the activity of nearby microglia. MBL has been reported to increase in stroke and ischemia, while the sources of MBL are elusive. It is unclear whether MBLs are produced by brain cells or migrate from the peripheral nervous system due to the leakage of the BBB. Interestingly, in HIV-infected brain, all brain cells show positive signals for MBL, indicating brain cells are capable of producing MBL upon stimulation. Further understandings on how lectins affect microglia and its interaction with other brain cells certainly would broaden our view on neurodegenerative diseases and raise new questions as well. Are these lectins druggable targets for neurological disease? Would pharmacological inhibition or activation of these lectins be effective in treating neurological diseases? Notably, these inhibitors/activators also need to have the capacity to cross the BBB to treat brain disorders.

The concept of lectin-based therapeutics deploys the specific targets of lectins or the delivery of drugs that interacts with lectins to the target site. For example, Galectin-3 has been implicated in numerous neurological disorders and diseases in the peripheral nervous system. Pharmacological suppression of galectin-3 appears to be a promising approach. Specifically, TD139 that binds to galectin-3 and inhibit its functions have passed the clinical phase Ib/IIa trials for treating idiopathic pulmonary fibrosis (http://ClinicalTrials.gov identifier, NCT02257177). Although this development is encouraging, the ability of TD139 to cross the BBB is poor and therefore limits its application to neurological diseases with abnormal up-regulation of Gal3. Further modification of TD139 to increase its permeability across the BBB may pave the way for the development of therapeutic intervention for brain diseases.

On the other hand, lectin-based therapeutics may enhance the exposure of drugs to the targeted cells/sites, and reduce the dosage and side effects. Moreover, internalization of drug also increases the uptake of therapeutic agents with low cellular permeability. The decoration of drug enveloped with surface sialic acid ligands can directly activate Siglecs downstream signaling or deploy their internalization properties. For example, nanoparticles coated with di(α2–8) N-acetylneuraminic acid effectively target Siglec-7 and Siglec-9 to exert anti-inflammatory effects of macrophages in a human *ex vivo* lung perfusion model (Spence et al., 2015). Furthermore, liposomal nanoparticles that are coated with high-affinity CD22 ligands result in substantial uptake of the nanoparticles by B cell lymphomas that express the endocytic receptor CD22 (Chen et al., 2012).

Collectively, emerging studies have shown that modulating the lectins activity via direct interference in the lectin itself or the receptor-ligand interaction in CNS is a promising area for further exploration. Currently, treatment of neurological disorders using a lectin-based approach has not been envisaged, likely owing to an incomplete understanding of the roles of lectins in the CNS and the limited ability of drugs to cross the BBB. A greater understanding of microglial lectins may facilitate the development of novel therapeutic interventions for patients with neurological disorders.

AUTHOR CONTRIBUTIONS

JJS designed and wrote the manuscript. YC designed and edited the manuscript.

FUNDING

This work was supported by Academia Sinica and Ministry of Science and Technology, Taiwan (MOST 103-2321-B-001068, MOST 106-0210-01-15-02, MOST 107-0210-01-19-01).

ACKNOWLEDGMENTS

We are grateful to the Medical Art Room of Institute of Biomedical Sciences at Academia Sinica for the assistance in preparing the illustration.

REFERENCES

Abhinav, K., Stanton, B., Johnston, C., Hardstaff, J., Orrell, R. W., Howard, R., et al. (2007). Amyotrophic lateral sclerosis in South-East England: a population-based study. The South-East England register for amyotrophic lateral sclerosis (SEALS Registry). *Neuroepidemiology* 29, 44–48. doi: 10.1159/000108917

Angiari, S., and Constantin, G. (2013). Selectins and their ligands as potential immunotherapeutic targets in neurological diseases. *Immunotherapy* 5, 1207–1220. doi: 10.2217/imt.13.122

Atangana, E., Schneider, U. C., Blecharz, K., Magrini, S., Wagner, J., Nieminen-Kelha, M., et al. (2017). Intravascular inflammation triggers intracerebral activated microglia and contributes to secondary brain injury after experimental subarachnoid hemorrhage (eSAH). *Transl. Stroke Res.* 8, 144–156. doi: 10.1007/s12975-016-0485-3

Atkinson, C., Zhu, H., Qiao, F., Varela, J. C., Yu, J., Song, H., et al. (2006). Complement-dependent P-selectin expression and injury following ischemic stroke. *J. Immunol.* 177, 7266–7274. doi: 10.4049/jimmunol.177.10.7266

Auriti, C., Prencipe, G., Moriondo, M., Bersani, I., Bertaina, C., Mondì, V., et al. (2017). Mannose-binding lectin: biologic characteristics and role in the susceptibility to infections and ischemia-reperfusion related injury in critically Ill neonates. *J. Immunol. Res.* 2017:7045630. doi: 10.1155/2017/7045630

Bernardes-Silva, M., Anthony, D. C., Issekutz, A. C., and Perry, V. H. (2001). Recruitment of neutrophils across the blood-brain barrier: the role of E- and P-selectins. *J. Cereb. Blood Flow Metab.* 21, 1115–1124. doi: 10.1097/00004647-200109000-00009

Bessis, A., Béchade, C., Bernard, D., and Roumier, A. (2007). Microglial control of neuronal death and synaptic properties. *Glia* 55, 233–238. doi: 10.1002/glia.20459

Blennow, K., Brody, D. L., Kochanek, P. M., Levin, H., McKee, A., Ribbers, G. M., et al. (2016). Traumatic brain injuries. *Nat. Rev. Dis. Primers* 2:16084. doi: 10.1038/nrdp.2016.84

Boza-Serrano, A., Reyes, J. F., Rey, N. L., Leffler, H., Bousset, L., Nilsson, U., et al. (2014). The role of Galectin-3 in α-synuclein-induced microglial activation. *Acta Neuropathol. Commun.* 2:156. doi: 10.1186/s40478-014-0156-0

Bradshaw, E. M., Chibnik, L. B., Keenan, B. T., Ottoboni, L., Raj, T., Tang, A., et al. (2013). CD33 Alzheimer's disease locus: altered monocyte function and amyloid biology. *Nat. Neurosci.* 16, 848–850. doi: 10.1038/nn.3435

Brandley, B. K., and Schnaar, R. L. (1986). Cell-surface carbohydrates in cell recognition and response. *J. Leukoc. Biol.* 40, 97–111. doi: 10.1002/jlb.40.1.97

Brites, D., and Vaz, A. R. (2014). Microglia centered pathogenesis in ALS: insights in cell interconnectivity. *Front. Cell. Neurosci.* 8:117. doi: 10.3389/fncel.2014.00117

Burguillos, M. A., Svensson, M., Schulte, T., Boza-Serrano, A., Garcia-Quintanilla, A., Kavanagh, E., et al. (2015). Microglia-secreted galectin-3 acts as a toll-like receptor 4 ligand and contributes to microglial activation. *Cell Rep.* 10, 1626–1638. doi: 10.1016/j.celrep.2015.02.012

Burman, J., and Svenningsson, A. (2016). Cerebrospinal fluid concentration of Galectin-9 is increased in secondary progressive multiple sclerosis. *J. Neuroimmunol.* 292, 40–44. doi: 10.1016/j.jneuroim.2016.01.008

Cao, Z. Q., and Guo, X. L. (2016). The role of galectin-4 in physiology and diseases. *Protein Cell* 7, 314–324. doi: 10.1007/s13238-016-0262-9

Cardoso, A. C., Andrade, L. N., Bustos, S. O., and Chammas, R. (2016). Galectin-3 determines tumor cell adaptive strategies in stressed tumor microenvironments. *Front. Oncol.* 6:127. doi: 10.3389/fonc.2016.00127

Carvalho-Tavares, J., Hickey, M. J., Hutchison, J., Michaud, J., Sutcliffe, I. T., and Kubes, P. (2000). A role for platelets and endothelial selectins in tumor necrosis factor-α-induced leukocyte recruitment in the brain microvasculature. *Circ. Res.* 87, 1141–1148. doi: 10.1161/01.res.87.12.1141

Cenker, J. J., Stultz, R. D., and McDonald, D. (2017). Brain microglial cells are highly susceptible to HIV-1 infection and spread. *AIDS Res. Hum. Retroviruses* 33, 1155–1165. doi: 10.1089/aid.2017.0004

Cervera, A., Planas, A. M., Justicia, C., Urra, X., Jensenius, J. C., Torres, F., et al. (2010). Genetically-defined deficiency of mannose-binding lectin is associated with protection after experimental stroke in mice and outcome in human stroke. *PLoS One* 5:e8433. doi: 10.1371/journal.pone.0008433

Chang, W. A., Tsai, M. J., Kuo, P. L., and Hung, J. Y. (2017). Role of galectins in lung cancer. *Oncol. Lett.* 14, 5077–5084. doi: 10.3892/ol.2017.6882

Chang-Hong, R., Wada, M., Koyama, S., Kimura, H., Arawaka, S., Kawanami, T., et al. (2005). Neuroprotective effect of oxidized galectin-1 in a transgenic mouse model of amyotrophic lateral sclerosis. *Exp. Neurol.* 194, 203–211. doi: 10.1016/j.expneurol.2005.02.011

Chen, W. C., Sigal, D. S., Saven, A., and Paulson, J. C. (2012). Targeting B lymphoma with nanoparticles bearing glycan ligands of CD22. *Leuk. Lymphoma* 53, 208–210. doi: 10.3109/10428194.2011.604755

Cheng, X., Boza-Serrano, A., Turesson, M. F., Deierborg, T., Ekblad, E., and Voss, U. (2016). Galectin-3 causes enteric neuronal loss in mice after left sided permanent middle cerebral artery occlusion, a model of stroke. *Sci. Rep.* 6:32893. doi: 10.1038/srep32893

Chiu, I. M., Morimoto, E. T., Goodarzi, H., Liao, J. T., O'Keeffe, S., Phatnani, H. P., et al. (2013). A neurodegeneration-specific gene-expression signature of acutely isolated microglia from an amyotrophic lateral sclerosis mouse model. *Cell Rep.* 4, 385–401. doi: 10.1016/j.celrep.2013.06.018

Claude, J., Linnartz-Gerlach, B., Kudin, A. P., Kunz, W. S., and Neumann, H. (2013). Microglial CD33-related Siglec-E inhibits neurotoxicity by preventing the phagocytosis-associated oxidative burst. *J. Neurosci.* 33, 18270–18276. doi: 10.1523/jneurosci.2211-13.2013

Çolakoğlu, G., Bergstrom-Tyrberg, U., Berglund, E. O., and Ranscht, B. (2014). Contactin-1 regulates myelination and nodal/paranodal domain organization in the central nervous system. *Proc. Natl. Acad. Sci. U S A* 111, E394–E403. doi: 10.1073/pnas.1313769110

Crocker, P. R., Mucklow, S., Bouckson, V., McWilliam, A., Willis, A. C., Gordon, S., et al. (1994). Sialoadhesin, a macrophage sialic acid binding receptor for haemopoietic cells with 17 immunoglobulin-like domains. *EMBO J.* 13, 4490–4503.

Crocker, P. R., Paulson, J. C., and Varki, A. (2007). Siglecs and their roles in the immune system. *Nat. Rev. Immunol.* 7, 255–266. doi: 10.1038/nri2056

Dambuza, I. M., and Brown, G. D. (2015). C-type lectins in immunity: recent developments. *Curr. Opin. Immunol.* 32, 21–27. doi: 10.1016/j.coi.2014.12.002

Davalos, D., Grutzendler, J., Yang, G., Kim, J. V., Zuo, Y., Jung, S., et al. (2005). ATP mediates rapid microglial response to local brain injury *in vivo*. *Nat. Neurosci.* 8, 752–758. doi: 10.1038/nn1472

De Blasio, D., Fumagalli, S., Longhi, L., Orsini, F., Palmioli, A., Stravalaci, M., et al. (2017). Pharmacological inhibition of mannose-binding lectin ameliorates neurobehavioral dysfunction following experimental traumatic brain injury. *J. Cereb. Blood Flow Metab.* 37, 938–950. doi: 10.1177/0271678x16647397

de la Rosa, E. J., and de Pablo, F. (2000). Cell death in early neural development: beyond the neurotrophic theory. *Trends Neurosci.* 23, 454–458. doi: 10.1016/s0166-2236(00)01628-3

Dendrou, C. A., Fugger, L., and Friese, M. A. (2015). Immunopathology of multiple sclerosis. *Nat. Rev. Immunol.* 15, 545–558. doi: 10.1038/nri3871

Deshmane, S. L., Kremlev, S., Amini, S., and Sawaya, B. E. (2009). Monocyte chemoattractant protein-1 (MCP-1): an overview. *J. Interferon Cytokine Res.* 29, 313–326. doi: 10.1089/jir.2008.0027

Díez-Revuelta, N., Higuero, A. M., Velasco, S., Peñas-de-la-Iglesia, M., Gabius, H. J., and Abad-Rodríguez, J. (2017). Neurons define non-myelinated axon segments by the regulation of galectin-4-containing axon membrane domains. *Sci. Rep.* 7:12246. doi: 10.1101/115758

Drickamer, K. (1992). Engineering galactose-binding activity into a C-type mannose-binding protein. *Nature* 360, 183–186. doi: 10.1038/360183a0

Fischer, M. T., Sharma, R., Lim, J. L., Haider, L., Frischer, J. M., Drexhage, J., et al. (2012). NADPH oxidase expression in active multiple sclerosis lesions in relation to oxidative tissue damage and mitochondrial injury. *Brain* 135, 886–899. doi: 10.1093/brain/aws012

Flavin, W. P., Bousset, L., Green, Z. C., Chu, Y., Skarpathiotis, S., Chaney, M. J., et al. (2017). Endocytic vesicle rupture is a conserved mechanism of cellular invasion by amyloid proteins. *Acta Neuropathol.* 134, 629–653. doi: 10.1007/s00401-017-1722-x

Freeman, D., Cedillos, R., Choyke, S., Lukic, Z., McGuire, K., Marvin, S., et al. (2013). α-synuclein induces lysosomal rupture and cathepsin dependent reactive oxygen species following endocytosis. *PLoS One* 8:e62143. doi: 10.1371/journal.pone.0062143

Frielingsdorf, H., Simpson, D. R., Thal, L. J., and Pizzo, D. P. (2007). Nerve growth factor promotes survival of new neurons in the adult hippocampus. *Neurobiol. Dis.* 26, 47–55. doi: 10.1016/j.nbd.2006.11.015

Fuhrmann, M., Bittner, T., Jung, C. K., Burgold, S., Page, R. M., Mitteregger, G., et al. (2010). Microglial Cx3cr1 knockout prevents neuron loss in a mouse model of Alzheimer's disease. *Nat. Neurosci.* 13, 411–413. doi: 10.1038/nn.2511

Fujimoto, Z., Tateno, H., and Hirabayashi, J. (2014). Lectin structures: classification based on the 3-D structures. *Methods Mol. Biol.* 1200, 579–606. doi: 10.1007/978-1-4939-1292-6_46

Geschwind, M. D. (2015). Prion diseases. *Continuum* 21, 1612–1638. doi: 10.1212/CON.0000000000000251

Goldenberg, M. M. (2012). Multiple sclerosis review. *P T* 37, 175–184.

Griciuc, A., Serrano-Pozo, A., Parrado, A. R., Lesinski, A. N., Asselin, C. N., Mullin, K., et al. (2013). Alzheimer's disease risk gene CD33 inhibits microglial uptake of amyloid β. *Neuron* 78, 631–643. doi: 10.1016/j.neuron.2013.04.014

Groh, J., Ribechini, E., Stadler, D., Schilling, T., Lutz, M. B., and Martini, R. (2016). Sialoadhesin promotes neuroinflammation-related disease progression in two mouse models of CLN disease. *Glia* 64, 792–809. doi: 10.1002/glia.22962

Groves, J. T. (2013). Cell membranes: glycans' imprints. *Nat. Mater.* 12, 96–97. doi: 10.1038/nmat3555

Hinojosa, A. E., Garcia-Bueno, B., Leza, J. C., and Madrigal, J. L. (2011). CCL2/MCP-1 modulation of microglial activation and proliferation. *J. Neuroinflammation* 8:77. doi: 10.1186/1742-2094-8-77

Hisamatsu, K., Niwa, M., Kobayashi, K., Miyazaki, T., Hirata, A., Hatano, Y., et al. (2016). Galectin-3 expression in hippocampal CA2 following transient forebrain ischemia and its inhibition by hypothermia or antiapoptotic agents. *Neuroreport* 27, 311–317. doi: 10.1097/wnr.0000000000000538

Hollingworth, P., Harold, D., Sims, R., Gerrish, A., Lambert, J. C., Carrasquillo, M. M., et al. (2011). Common variants at ABCA7, MS4A6A/MS4A4E, EPHA1, CD33 and CD2AP are associated with Alzheimer's disease. *Nat. Genet.* 43, 429–435. doi: 10.1038/ng.803

Horie, H., Kadoya, T., Hikawa, N., Sango, K., Inoue, H., Takeshita, K., et al. (2004). Oxidized galectin-1 stimulates macrophages to promote axonal regeneration in peripheral nerves after axotomy. *J. Neurosci.* 24, 1873–1880. doi: 10.1523/jneurosci.4483-03.2004

Hoyos, H. C., Marder, M., Ulrich, R., Gudi, V., Stangel, M., Rabinovich, G. A., et al. (2016). The role of galectin-3: from oligodendroglial differentiation and myelination to demyelination and remyelination processes in a cuprizone-induced demyelination model. *Adv. Exp. Med. Biol.* 949, 311–332. doi: 10.1007/978-3-319-40764-7_15

Hoyos, H. C., Rinaldi, M., Mendez-Huergo, S. P., Marder, M., Rabinovich, G. A., Pasquini, J. M., et al. (2014). Galectin-3 controls the response of microglial cells to limit cuprizone-induced demyelination. *Neurobiol. Dis.* 62, 441–455. doi: 10.1016/j.nbd.2013.10.023

Hsiao, H. Y., Chiu, F. L., Chen, C. M., Wu, Y. R., Chen, H. M., Chen, Y. C., et al. (2014). Inhibition of soluble tumor necrosis factor is therapeutic in Huntington's disease. *Hum. Mol. Genet.* 23, 4328–4344. doi: 10.1093/hmg/ddu151

Huang, J. Y., Wang, Y. X., Gu, W. L., Fu, S. L., Li, Y., Huang, L. D., et al. (2012). Expression and function of myelin-associated proteins and their common receptor NgR on oligodendrocyte progenitor cells. *Brain Res.* 1437, 1–15. doi: 10.1016/j.brainres.2011.12.008

Hughes, E. H., Schlichtenbrede, F. C., Murphy, C. C., Sarra, G. M., Luthert, P. J., Ali, R. R., et al. (2003). Generation of activated sialoadhesin-positive microglia during retinal degeneration. *Invest. Ophthalmol. Vis. Sci.* 44, 2229–2234. doi: 10.1167/iovs.02-0824

Ip, W. K., Takahashi, K., Ezekowitz, R. A., and Stuart, L. M. (2009). Mannose-binding lectin and innate immunity. *Immunol. Rev.* 230, 9–21. doi: 10.1111/j.1600-065X.2009.00789.x

James, R. E., Hillis, J., Adorján, I., Gration, B., Mundim, M. V., Iqbal, A. J., et al. (2016). Loss of galectin-3 decreases the number of immune cells in the subventricular zone and restores proliferation in a viral model of multiple sclerosis. *Glia* 64, 105–121. doi: 10.1002/glia.22906

Jiang, H. R., Al Rasebi, Z., Mensah-Brown, E., Shahin, A., Xu, D., Goodyear, C. S., et al. (2009). Galectin-3 deficiency reduces the severity of experimental autoimmune encephalomyelitis. *J. Immunol.* 182, 1167–1173. doi: 10.4049/jimmunol.182.2.1167

Jin, A. Y., Tuor, U. I., Rushforth, D., Kaur, J., Muller, R. N., Petterson, J. L., et al. (2010). Reduced blood brain barrier breakdown in P-selectin deficient mice following transient ischemic stroke: a future therapeutic target for treatment of stroke. *BMC Neurosci.* 11:12. doi: 10.1186/1471-2202-11-12

John, S., and Mishra, R. (2016). mRNA transcriptomics of galectins unveils heterogeneous organization in mouse and human brain. *Front. Mol. Neurosci.* 9:139. doi: 10.3389/fnmol.2016.00139

Kasai, K., and Hirabayashi, J. (1996). Galectins: a family of animal lectins that decipher glycocodes. *J. Biochem.* 119, 1–8. doi: 10.1093/oxfordjournals.jbchem.a021192

Kataoka, H., Kim, S. W., and Plesnila, N. (2004). Leukocyte-endothelium interactions during permanent focal cerebral ischemia in mice. *J. Cereb. Blood Flow Metab.* 24, 668–676. doi: 10.1097/01.wcb.0000117812.35136.5b

Kettenmann, H., Hanisch, U. K., Noda, M., and Verkhratsky, A. (2011). Physiology of microglia. *Physiol. Rev.* 91, 461–553. doi: 10.1152/physrev.00011.2010

Kim, C., Ho, D. H., Suk, J. E., You, S., Michael, S., Kang, J., et al. (2013). Neuron-released oligomeric α-synuclein is an endogenous agonist of TLR2 for paracrine activation of microglia. *Nat. Commun.* 4:1562. doi: 10.1038/ncomms2534

Kopatz, J., Beutner, C., Welle, K., Bodea, L. G., Reinhardt, J., Claude, J., et al. (2013). Siglec-h on activated microglia for recognition and engulfment of glioma cells. *Glia* 61, 1122–1133. doi: 10.1002/glia.22501

Lalancette-Hébert, M., Gowing, G., Simard, A., Weng, Y. C., and Kriz, J. (2007). Selective ablation of proliferating microglial cells exacerbates ischemic injury in the brain. *J. Neurosci.* 27, 2596–2605. doi: 10.1523/JNEUROSCI.5360-06.2007

Lalancette-Hébert, M., Swarup, V., Beaulieu, J. M., Bohacek, I., Abdelhamid, E., Weng, Y. C., et al. (2012). Galectin-3 is required for resident microglia activation and proliferation in response to ischemic injury. *J. Neurosci.* 32, 10383–10395. doi: 10.1523/JNEUROSCI.1498-12.2012

Langer, H. F., and Chavakis, T. (2009). Leukocyte-endothelial interactions in inflammation. *J. Cell. Mol. Med.* 13, 1211–1220. doi: 10.1111/j.1582-4934.2009.00811.x

Lasky, L. A. (1992). Selectins: interpreters of cell-specific carbohydrate information during inflammation. *Science* 258, 964–969. doi: 10.1126/science.1439808

Lawson, L. J., Perry, V. H., Dri, P., and Gordon, S. (1990). Heterogeneity in the distribution and morphology of microglia in the normal adult mouse brain. *Neuroscience* 39, 151–170. doi: 10.1016/0306-4522(90)90229-w

Lerman, B. J., Hoffman, E. P., Sutherland, M. L., Bouri, K., Hsu, D. K., Liu, F. T., et al. (2012). Deletion of galectin-3 exacerbates microglial activation and accelerates disease progression and demise in a SOD1(G93A) mouse model of amyotrophic lateral sclerosis. *Brain Behav.* 2, 563–575. doi: 10.1002/brb3.75

Letschert, S., Gohler, A., Franke, C., Bertleff-Zieschang, N., Memmel, E., Doose, S., et al. (2014). Super-resolution imaging of plasma membrane glycans. *Angew. Chem. Int. Ed. Engl.* 53, 10921–10924. doi: 10.1002/anie.201406045

Ley, K. (2003). The role of selectins in inflammation and disease. *Trends Mol. Med.* 9, 263–268. doi: 10.1016/s1471-4914(03)00071-6

Liao, B., Zhao, W., Beers, D. R., Henkel, J. S., and Appel, S. H. (2012). Transformation from a neuroprotective to a neurotoxic microglial phenotype in a mouse model of ALS. *Exp. Neurol.* 237, 147–152. doi: 10.1016/j.expneurol.2012.06.011

Liddelow, S. A., Guttenplan, K. A., Clarke, L. E., Bennett, F. C., Bohlen, C. J., Schirmer, L., et al. (2017). Neurotoxic reactive astrocytes are induced by activated microglia. *Nature* 541, 481–487. doi: 10.1038/nature21029

Liu, F. T., Patterson, R. J., and Wang, J. L. (2002). Intracellular functions of galectins. *Biochim. Biophys. Acta* 1572, 263–273. doi: 10.1016/s0304-4165(02)00313-6

Liu, F. T., and Rabinovich, G. A. (2005). Galectins as modulators of tumour progression. *Nat. Rev. Cancer* 5, 29–41. doi: 10.1038/nrc1527

Longhi, L., Orsini, F., De Blasio, D., Fumagalli, S., Ortolano, F., Locatelli, M., et al. (2014). Mannose-binding lectin is expressed after clinical and experimental traumatic brain injury and its deletion is protective. *Crit. Care Med.* 42, 1910–1918. doi: 10.1097/CCM.0000000000000399

Macauley, M. S., Crocker, P. R., and Paulson, J. C. (2014). Siglec-mediated regulation of immune cell function in disease. *Nat. Rev. Immunol.* 14, 653–666. doi: 10.1038/nri3737

Masters, C. L., Bateman, R., Blennow, K., Rowe, C. C., Sperling, R. A., and Cummings, J. L. (2015). Alzheimer's disease. *Nat. Rev. Dis. Primers* 1:15056. doi: 10.1038/nrdp.2015.56

Miron, V. E., Boyd, A., Zhao, J. W., Yuen, T. J., Ruckh, J. M., Shadrach, J. L., et al. (2013). M2 microglia and macrophages drive oligodendrocyte differentiation during CNS remyelination. *Nat. Neurosci.* 16, 1211–1218. doi: 10.1038/nn.3469

Mok, S. W., Riemer, C., Madela, K., Hsu, D. K., Liu, F. T., Gultner, S., et al. (2007). Role of galectin-3 in prion infections of the CNS. *Biochem. Biophys. Res. Commun.* 359, 672–678. doi: 10.1016/j.bbrc.2007.05.163

Mondal, N., Stolfa, G., Antonopoulos, A., Zhu, Y., Wang, S. S., Buffone, A. Jr., et al. (2016). Glycosphingolipids on human myeloid cells stabilize E-selectin-dependent rolling in the multistep leukocyte adhesion cascade. *Arterioscler. Thromb. Vasc. Biol.* 36, 718–727. doi: 10.1161/ATVBAHA.115.306748

Morrison, H., Frye, J., Davis-Gorman, G., Funk, J., McDonagh, P., Stahl, G., et al. (2011). The contribution of mannose binding lectin to reperfusion injury after ischemic stroke. *Curr. Neurovasc. Res.* 8, 52–63. doi: 10.2174/156720211794520260

Naj, A. C., Jun, G., Beecham, G. W., Wang, L. S., Vardarajan, B. N., Buros, J., et al. (2011). Common variants at MS4A4/MS4A6E, CD2AP, CD33 and EPHA1 are associated with late-onset Alzheimer's disease. *Nat. Genet.* 43, 436–441. doi: 10.1038/ng.801

Nikodemova, M., Small, A. L., Smith, S. M., Mitchell, G. S., and Watters, J. J. (2014). Spinal but not cortical microglia acquire an atypical phenotype with high VEGF, galectin-3 and osteopontin, and blunted inflammatory responses in ALS rats. *Neurobiol. Dis.* 69, 43–53. doi: 10.1016/j.nbd.2013.11.009

Nimmerjahn, A., Kirchhoff, F., and Helmchen, F. (2005). Resting microglial cells are highly dynamic surveillants of brain parenchyma *in vivo*. *Science* 308, 1314–1318. doi: 10.1126/science.1110647

Orsini, F., Villa, P., Parrella, S., Zangari, R., Zanier, E. R., Gesuete, R., et al. (2012). Targeting mannose-binding lectin confers long-lasting protection with a surprisingly wide therapeutic window in cerebral ischemia. *Circulation* 126, 1484–1494. doi: 10.1161/CIRCULATIONAHA.112.103051

Osthoff, M., Katan, M., Fluri, F., Schuetz, P., Bingisser, R., Kappos, L., et al. (2011). Mannose-binding lectin deficiency is associated with smaller infarction size and favorable outcome in ischemic stroke patients. *PLoS One* 6:e21338. doi: 10.1371/journal.pone.0021338

Pang, Y., Fan, L. W., Tien, L. T., Dai, X., Zheng, B., Cai, Z., et al. (2013). Differential roles of astrocyte and microglia in supporting oligodendrocyte development and myelination *in vitro*. *Brain Behav.* 3, 503–514. doi: 10.1002/brb3.152

Paolicelli, R. C., Bolasco, G., Pagani, F., Maggi, L., Scianni, M., Panzanelli, P., et al. (2011). Synaptic pruning by microglia is necessary for normal brain development. *Science* 333, 1456–1458. doi: 10.1126/science.1202529

Pardo, E., Cárcamo, C., Uribe-San Martin, R., Ciampi, E., Segovia-Miranda, F., Curkovic-Pena, C., et al. (2017). Galectin-8 as an immunosuppressor in experimental autoimmune encephalomyelitis and a target of human early prognostic antibodies in multiple sclerosis. *PLoS One* 12:e0177472. doi: 10.1371/journal.pone.0177472

Park, J. W., Voss, P. G., Grabski, S., Wang, J. L., and Patterson, R. J. (2001). Association of galectin-1 and galectin-3 with Gemin4 in complexes containing the SMN protein. *Nucleic Acids Res.* 29, 3595–3602. doi: 10.1093/nar/29.17.3595

Pasquini, L. A., Millet, V., Hoyos, H. C., Giannoni, J. P., Croci, D. O., Marder, M., et al. (2011). Galectin-3 drives oligodendrocyte differentiation to control myelin integrity and function. *Cell Death Differ.* 18, 1746–1756. doi: 10.1038/cdd.2011.40

Patel, A. R., Ritzel, R., McCullough, L. D., and Liu, F. (2013). Microglia and ischemic stroke: a double-edged sword. *Int. J. Physiol. Pathophysiol. Pharmacol.* 5, 73–90.

Perry, V. H., Crocker, P. R., and Gordon, S. (1992). The blood-brain barrier regulates the expression of a macrophage sialic acid-binding receptor on microglia. *J. Cell Sci.* 101, 201–207.

Pillai, S., Netravali, I. A., Cariappa, A., and Mattoo, H. (2012). Siglecs and immune regulation. *Annu. Rev. Immunol.* 30, 357–392. doi: 10.1146/annurev-immunol-020711-075018

Politis, M., Giannetti, P., Su, P., Turkheimer, F., Keihaninejad, S., Wu, K., et al. (2012). Increased PK11195 PET binding in the cortex of patients with MS correlates with disability. *Neurology* 79, 523–530. doi: 10.1212/WNL.0b013e3182635645

Puttur, F., Arnold-Schrauf, C., Lahl, K., Solmaz, G., Lindenberg, M., Mayer, C. T., et al. (2013). Absence of Siglec-H in MCMV infection elevates interferon α production but does not enhance viral clearance. *PLoS Pathog.* 9:e1003648. doi: 10.1371/journal.ppat.1003648

Reichert, F., and Rotshenker, S. (1999). Galectin-3/MAC-2 in experimental allergic encephalomyelitis. *Exp. Neurol.* 160, 508–514. doi: 10.1006/exnr.1999.7229

Riemer, C., Neidhold, S., Burwinkel, M., Schwarz, A., Schultz, J., Krätzschmar, J., et al. (2004). Gene expression profiling of scrapie-infected brain tissue. *Biochem. Biophys. Res. Commun.* 323, 556–564. doi: 10.1016/j.bbrc.2004.08.124

Sakaguchi, M., Imaizumi, Y., and Okano, H. (2007). Expression and function of galectin-1 in adult neural stem cells. *Cell. Mol. Life Sci.* 64, 1254–1258. doi: 10.1007/s00018-007-6476-5

Sakaguchi, M., Shingo, T., Shimazaki, T., Okano, H. J., Shiwa, M., Ishibashi, S., et al. (2006). A carbohydrate-binding protein, Galectin-1, promotes proliferation of adult neural stem cells. *Proc. Natl. Acad. Sci. U S A* 103, 7112–7117. doi: 10.1073/pnas.0508793103

Sancho, D., and Reis e Sousa, C. (2012). Signaling by myeloid C-type lectin receptors in immunity and homeostasis. *Annu. Rev. Immunol.* 30, 491–529. doi: 10.1146/annurev-immunol-031210-101352

Satoh, K., Niwa, M., Goda, W., Binh, N. H., Nakashima, M., Takamatsu, M., et al. (2011). Galectin-3 expression in delayed neuronal death of hippocampal CA1 following transient forebrain ischemia and its inhibition by hypothermia. *Brain Res.* 1382, 266–274. doi: 10.1016/j.brainres.2011.01.049

Saylor, D., Dickens, A. M., Sacktor, N., Haughey, N., Slusher, B., Pletnikov, M., et al. (2016). HIV-associated neurocognitive disorder—pathogenesis and prospects for treatment. *Nat. Rev. Neurol.* 12:309. doi: 10.1038/nrneurol.2016.53

Schneider, U. C., Davids, A. M., Brandenburg, S., Müller, A., Elke, A., Magrini, S., et al. (2015). Microglia inflict delayed brain injury after subarachnoid hemorrhage. *Acta Neuropathol.* 130, 215–231. doi: 10.1007/s00401-015-1440-1

Singh, K. K., Nathamu, S., Adame, A., Alire, T. U., Dumaop, W., Gouaux, B., et al. (2011). Expression of mannose binding lectin in HIV-1-infected brain: implications for HIV-related neuronal damage and neuroAIDS. *Neurobehav. HIV Med.* 3, 41–52. doi: 10.2147/nbhiv.s19969

Sirko, S., Irmler, M., Gascon, S., Bek, S., Schneider, S., Dimou, L., et al. (2015). Astrocyte reactivity after brain injury-: the role of galectins 1 and 3. *Glia* 63, 2340–2361. doi: 10.1002/glia.22898

Smittkamp, S. E., Brown, J. W., and Stanford, J. A. (2008). Time-course and characterization of orolingual motor deficits in B6SJL-Tg(SOD1–G93A)1Gur/J mice. *Neuroscience* 151, 613–621. doi: 10.1016/j.neuroscience.2007.10.017

Song, S., Ji, B., Ramachandran, V., Wang, H., Hafley, M., Logsdon, C., et al. (2012). Overexpressed galectin-3 in pancreatic cancer induces cell proliferation and invasion by binding Ras and activating Ras signaling. *PLoS One* 7:e42699. doi: 10.1371/journal.pone.0042699

Spence, S., Greene, M. K., Fay, F., Hams, E., Saunders, S. P., Hamid, U., et al. (2015). Targeting Siglecs with a sialic acid-decorated nanoparticle abrogates inflammation. *Sci. Transl. Med.* 7:303ra140. doi: 10.1126/scitranslmed.aab3459

Stancic, M., Slijepcevic, D., Nomden, A., Vos, M. J., de Jonge, J. C., Sikkema, A. H., et al. (2012). Galectin-4, a novel neuronal regulator of myelination. *Glia* 60, 919–935. doi: 10.1002/glia.22324

Stancic, M., van Horssen, J., Thijssen, V. L., Gabius, H. J., van der Valk, P., Hoekstra, D., et al. (2011). Increased expression of distinct galectins in multiple sclerosis lesions. *Neuropathol. Appl. Neurobiol.* 37, 654–671. doi: 10.1111/j.1365-2990.2011.01184.x

Starossom, S. C., Mascanfroni, I. D., Imitola, J., Cao, L., Raddassi, K., Hernandez, S. F., et al. (2012). Galectin-1 deactivates classically activated microglia and protects from inflammation-induced neurodegeneration. *Immunity* 37, 249–263. doi: 10.1016/j.immuni.2012.05.023

Steelman, A. J., Smith, R. III., Welsh, C. J., and Li, J. (2013). Galectin-9 protein is up-regulated in astrocytes by tumor necrosis factor and promotes encephalitogenic T-cell apoptosis. *J. Biol. Chem.* 288, 23776–23787. doi: 10.1074/jbc.M113.451658

Steinman, L., and Zamvil, S. S. (2006). How to successfully apply animal studies in experimental allergic encephalomyelitis to research on multiple sclerosis. *Ann. Neurol.* 60, 12–21. doi: 10.1002/ana.20913

Subramaniam, S. R., and Federoff, H. J. (2017). Targeting microglial activation states as a therapeutic avenue in Parkinson's disease. *Front. Aging Neurosci.* 9:176. doi: 10.3389/fnagi.2017.00176

Sun, J., Shaper, N. L., Itonori, S., Heffer-Lauc, M., Sheikh, K. A., and Schnaar, R. L. (2004). Myelin-associated glycoprotein (Siglec-4) expression is progressively and selectively decreased in the brains of mice lacking complex gangliosides. *Glycobiology* 14, 851–857. doi: 10.1093/glycob/cwh107

Takagi, H., Fukaya, T., Eizumi, K., Sato, Y., Sato, K., Shibazaki, A., et al. (2011). Plasmacytoid dendritic cells are crucial for the initiation of inflammation and T cell immunity *in vivo*. *Immunity* 35, 958–971. doi: 10.1016/j.immuni.2011.10.014

Tang, T., Frenette, P. S., Hynes, R. O., Wagner, D. D., and Mayadas, T. N. (1996). Cytokine-induced meningitis is dramatically attenuated in mice deficient in endothelial selectins. *J. Clin. Invest.* 97, 2485–2490. doi: 10.1172/jci118695

Thored, P., Heldmann, U., Gomes-Leal, W., Gisler, R., Darsalia, V., Taneera, J., et al. (2009). Long-term accumulation of microglia with proneurogenic phenotype concomitant with persistent neurogenesis in adult subventricular zone after stroke. *Glia* 57, 835–849. doi: 10.1002/glia.20810

Thurston, T. L., Wandel, M. P., von Muhlinen, N., Foeglein, A., and Randow, F. (2012). Galectin 8 targets damaged vesicles for autophagy to defend cells against bacterial invasion. *Nature* 482, 414–418. doi: 10.1038/nature10744

Troncoso, M. F., Ferragut, F., Bacigalupo, M. L., Cárdenas Delgado, V. M., Nugnes, L. G., Gentilini, L., et al. (2014). Galectin-8: a matricellular lectin with key roles in angiogenesis. *Glycobiology* 24, 907–914. doi: 10.1093/glycob/cwu054

Varki, A. (2009). Natural ligands for CD33-related Siglecs? *Glycobiology* 19, 810–812. doi: 10.1093/glycob/cwp063

Varki, A., and Angata, T. (2006). Siglecs—the major subfamily of I-type lectins. *Glycobiology* 16, 1R–27R. doi: 10.1093/glycob/cwj008

Varki, A., Etzler, M. E., Cummings, R. D., and Esko, J. D. (2009). "Discovery and classification of glycan-binding proteins," in *Essentials of Glycobiology*, 2nd Edn. eds A. Varki, R. D. Cummings, J. D. Esko, H. H. Freeze, P. Stanley, C. R. Bertozzi, et al. (New York, NY: Cold Spring Harbor), 1–22.

Venkatesan, C., Chrzaszcz, M., Choi, N., and Wainwright, M. S. (2010). Chronic upregulation of activated microglia immunoreactive for galectin-3/Mac-2 and nerve growth factor following diffuse axonal injury. *J. Neuroinflammation* 7:32. doi: 10.1186/1742-2094-7-32

Wan, L., and Liu, F.-T. (2016). Galectin-3 and inflammation. *Glycobiol. Insights* 6, 1–9. doi: 10.4137/gbi.s13921

Wang, J. L., Haudek, K. C., Voss, P. G., Patterson, R. J., and Arnoys, E. J. (2012). "Intracellular galectins: platforms for assembly of macromolecular complexes," in *Galectins and Disease Implications for Targeted Therapeutics*, eds A. A. Klyosov and P. G. Traber (Washington, DC: ACS Symposium Series), 81–93. doi: 10.1021/bk-2012-1115.ch004

Wang, X., Mitra, N., Cruz, P., Deng, L., NISC Comparative Sequencing Program, Varki, N., et al. (2012). Evolution of siglec-11 and siglec-16 genes in hominins. *Mol. Biol. Evol.* 29, 2073–2086. doi: 10.1093/molbev/mss077

Wang, Y., and Neumann, H. (2010). Alleviation of neurotoxicity by microglial human Siglec-11. *J. Neurosci.* 30, 3482–3488. doi: 10.1523/JNEUROSCI.3940-09.2010

Wang, X., Yue, T. L., Barone, F. C., and Feuerstein, G. Z. (1995). Demonstration of increased endothelial-leukocyte adhesion molecule-1 mRNA expression in rat ischemic cortex. *Stroke* 26, 1665–1668; discussion 1668–1669. doi: 10.1161/01.str.26.9.1665

Weis, W. I., Drickamer, K., and Hendrickson, W. A. (1992). Structure of a C-type mannose-binding protein complexed with an oligosaccharide. *Nature* 360, 127–134. doi: 10.1038/360127a0

Werneburg, S., Buettner, F. F., Erben, L., Mathews, M., Neumann, H., Muhlenhoff, M., et al. (2016). Polysialylation and lipopolysaccharide-induced shedding of E-selectin ligand-1 and neuropilin-2 by microglia and THP-1 macrophages. *Glia* 64, 1314–1330. doi: 10.1002/glia.23004

Wielgat, P., and Braszko, J. J. (2012). The participation of sialic acids in microglia-neuron interactions. *Cell. Immunol.* 273, 17–22. doi: 10.1016/j.cellimm.2011.12.002

Yan, H., Kamiya, T., Suabjakyong, P., and Tsuji, N. M. (2015). Targeting C-type lectin receptors for cancer immunity. *Front. Immunol.* 6:408. doi: 10.3389/fimmu.2015.00408

Yan, J., Xu, Y., Zhang, L., Zhao, H., Jin, L., Liu, W. G., et al. (2016). Increased expressions of plasma galectin-3 in patients with amyotrophic lateral sclerosis. *Chin. Med. J.* 129, 2797–2803. doi: 10.4103/0366-6999.194656

Yip, P. K., Carrillo-Jimenez, A., King, P., Vilalta, A., Nomura, K., Chau, C. C., et al. (2017). Galectin-3 released in response to traumatic brain injury acts as an alarmin orchestrating brain immune response and promoting neurodegeneration. *Sci. Rep.* 7:41689. doi: 10.1038/srep41689

Yokota, Y., Arai, T., and Kawasaki, T. (1995). Oligomeric structures required for complement activation of serum mannan-binding proteins. *J. Biochem.* 117, 414–419. doi: 10.1093/jb/117.2.414

Zhang, R. L., Chopp, M., Zhang, Z. G., Phillips, M. L., Rosenbloom, C. L., Cruz, R., et al. (1996). E-selectin in focal cerebral ischemia and reperfusion in the rat. *J. Cereb. Blood Flow Metab.* 16, 1126–1136. doi: 10.1097/00004647-199611000-00006

Zhang, J., Raper, A., Sugita, N., Hingorani, R., Salio, M., Palmowski, M. J., et al. (2006). Characterization of Siglec-H as a novel endocytic receptor expressed on murine plasmacytoid dendritic cell precursors. *Blood* 107, 3600–3608. doi: 10.1182/blood-2005-09-3842

Zhang, F., Zheng, M., Qu, Y., Li, J., Ji, J., Feng, B., et al. (2009). Different roles of galectin-9 isoforms in modulating E-selectin expression and adhesion function in LoVo colon carcinoma cells. *Mol. Biol Rep.* 36, 823–830. doi: 10.1007/s11033-008-9251-2

Zhou, T., Li, X., Wu, P., Zhang, D., Zhang, M., Chen, N., et al. (2000). Effect of anti-P-selectin monoclonal antibody on renal ischemia/reperfusion injury in rats. *Chin. Med. J.* 113, 790–793.

Conflict of Interest Statement: The authors declare that the research was conducted in the absence of any commercial or financial relationships that could be construed as a potential conflict of interest.

frontiers in Molecular Neuroscience

ORIGINAL RESEARCH
published: 08 May 2018
doi: 10.3389/fnmol.2018.00148

Enhancement of Astroglial Aerobic Glycolysis by Extracellular Lactate-Mediated Increase in cAMP

Nina Vardjan[1,2], Helena H. Chowdhury[1,2], Anemari Horvat[1], Jelena Velebit[1,2], Maja Malnar[2], Marko Muhič[1], Marko Kreft[1,2,3], Špela G. Krivec[1,2], Saša T. Bobnar[1,2], Katarina Miš[4], Sergej Pirkmajer[4], Stefan Offermanns[5], Gjermund Henriksen[6,7], Jon Storm-Mathisen[8], Linda H. Bergersen[9,10] and Robert Zorec[1,2]**

[1] Laboratory of Neuroendocrinology - Molecular Cell Physiology, Institute of Pathophysiology, Faculty of Medicine, University of Ljubljana, Ljubljana, Slovenia, [2] Laboratory of Cell Engineering, Celica Biomedical, Ljubljana, Slovenia, [3] Department of Biology, Biotechnical Faculty, University of Ljubljana, Ljubljana, Slovenia, [4] Laboratory for Molecular Neurobiology, Institute of Pathophysiology, Faculty of Medicine, University of Ljubljana, Ljubljana, Slovenia, [5] Department of Pharmacology, Max Planck Institute for Heart and Lung Research, Bad Nauheim, Germany, [6] Nuclear and Energy Physics, Department of Physics, The Faculty of Mathematics and Natural Sciences, University of Oslo, Oslo, Norway, [7] Norwegian Medical Cyclotron Centre Ltd., Oslo, Norway, [8] Division of Anatomy, Department of Molecular Medicine, CMBN/SERTA Healthy Brain Ageing Centre, Institute of Basic Medical Sciences, Faculty of Medicine, University of Oslo, Oslo, Norway, [9] Institute of Oral Biology, Faculty of Dentistry, University of Oslo, Oslo, Norway, [10] Center for Healthy Aging, Faculty of Health and Medical Sciences, University of Copenhagen, Copenhagen, Denmark

OPEN ACCESS

Edited by:
Margaret Su-chun Ho, ShanghaiTech University, China

Reviewed by:
Selva Baltan, Cleveland Clinic Lerner College of Medicine, United States
Yu-Feng Wang, Harbin Medical University, China

***Correspondence:**
Nina Vardjan
nina.vardjan@mf.uni-lj.si
Robert Zorec
robert.zorec@mf.uni-lj.si

Received: *15 February 2018*
Accepted: *16 April 2018*
Published: *08 May 2018*

Citation:
Vardjan N, Chowdhury HH, Horvat A, Velebit J, Malnar M, Muhič M, Kreft M, Krivec ŠG, Bobnar ST, Miš K, Pirkmajer S, Offermanns S, Henriksen G, Storm-Mathisen J, Bergersen LH and Zorec R (2018) Enhancement of Astroglial Aerobic Glycolysis by Extracellular Lactate-Mediated Increase in cAMP. Front. Mol. Neurosci. 11:148. doi: 10.3389/fnmol.2018.00148

Besides being a neuronal fuel, L-lactate is also a signal in the brain. Whether extracellular L-lactate affects brain metabolism, in particular astrocytes, abundant neuroglial cells, which produce L-lactate in aerobic glycolysis, is unclear. Recent studies suggested that astrocytes express low levels of the L-lactate GPR81 receptor ($EC_{50} \approx 5$ mM) that is in fat cells part of an autocrine loop, in which the G_i-protein mediates reduction of cytosolic cyclic adenosine monophosphate (cAMP). To study whether a similar signaling loop is present in astrocytes, affecting aerobic glycolysis, we measured the cytosolic levels of cAMP, D-glucose and L-lactate in single astrocytes using fluorescence resonance energy transfer (FRET)-based nanosensors. In contrast to the situation in fat cells, stimulation by extracellular L-lactate and the selective GPR81 agonists, 3-chloro-5-hydroxybenzoic acid (3Cl-5OH-BA) or 4-methyl-*N*-(5-(2-(4-methylpiperazin-1-yl)-2-oxoethyl)-4-(2-thienyl)-1,3-thiazol-2-yl)cyclohexanecarboxamide (Compound 2), like adrenergic stimulation, elevated intracellular cAMP and L-lactate in astrocytes, which was reduced by the inhibition of adenylate cyclase. Surprisingly, 3Cl-5OH-BA and Compound 2 increased cytosolic cAMP also in GPR81-knock out astrocytes, indicating that the effect is GPR81-independent and mediated by a novel, yet unidentified, excitatory L-lactate receptor-like mechanism in astrocytes that enhances aerobic glycolysis and L-lactate production via a positive feedback mechanism.

Keywords: astrocytes, aerobic glycolysis, L-lactate receptor, cAMP, L-lactate

INTRODUCTION

Aerobic glycolysis, non-oxidative metabolism of glucose despite the presence of adequate levels of oxygen, a phenomenon termed "the Warburg effect," is an inefficient way to generate energy in the form of ATP. The advantage of this process, however, appears to be in providing intermediates for the biosynthesis of lipids, nucleic acids, and amino acids (Vander Heiden et al., 2009).

These are needed for making new cells during division, such as in cancer cells and in developing normal cells, and for cells engaged in morphological reshaping, such as neural cells in the central nervous system (CNS; Goyal et al., 2014).

At least in the brain, aerobic glycolysis appears to be regulated. For example, during alerting, sensory stimulation, exercise, and pathophysiological conditions, L-lactate production and release are upregulated. Although it is still unclear how this takes place at the cellular level, the process likely involves noradrenergic neurons from *locus coeruleus* (LC; Dienel and Cruz, 2016). L-lactate can be produced from glycogen stored in astrocytes, an abundant glial cell type in the CNS, and can be used by neurons and oligodendrocytes, which seem to require L-lactate in addition to D-glucose for their optimal function, including memory formation (Cowan et al., 2010; Barros, 2013; Gao et al., 2016; Dong et al., 2017), myelin production, and the sustenance of long axons (Lee et al., 2012; Rinholm and Bergersen, 2012). In addition, L-lactate is considered to be neuroprotective against various types of brain damage (Castillo et al., 2015) and is required for cancer cell survival (Roland et al., 2014).

These effects suggest that L-lactate not only acts as a fuel but also has extracellular signaling roles (Chen et al., 2005; Barros, 2013; Roland et al., 2014). L-lactate modulates the activity of primary cortical neurons through a receptor-mediated pathway (Bozzo et al., 2013), and the activation of astrocytes by LC neurons results in the release of L-lactate, which back-excites LC neurons and stimulates the further release of noradrenaline (NA; Tang et al., 2014). These effects are supported by the observation that the monocarboxylate transporter 2 (MCT2), transporting L-lactate, is selectively co-located with glutamate receptors at the postsynaptic membranes of fast-acting excitatory synapses (Bergersen et al., 2001). Interestingly, L-lactate appears to promote gene expression that mediates *N*-methyl-D-aspartate (NMDA)-related neuronal plasticity (Yang et al., 2014) and the expression of membrane metabolite receptors at the plasma membrane (Castillo et al., 2015). L-lactate is known to mediate cerebral vasodilatation, causing increased brain blood flow (Gordon et al., 2007, 2008).

The notion of multiple signaling roles of L-lactate and its widespread diffusion in tissues led to the concept of L-lactate being a "volume transmitter" of metabolic information (Chen et al., 2005) and perhaps also a gliotransmitter (Tang et al., 2014) in the brain.

L-lactate signaling may occur through several mechanisms, including the modulation of prostaglandin action (Gordon et al., 2008), redox regulation (Brooks, 2009), and the activation of the L-lactate-sensitive receptors, such as G_i-protein coupled receptors GPR81 (Lauritzen et al., 2014) or the yet unidentified plasma membrane receptors (Tang et al., 2014).

The L-lactate selectivity of the GPR81 receptor ($EC_{50} \approx 5$ mM for rat GPR81; Liu et al., 2009), also known as hydroxycarboxylic acid receptor 1 (HCA_1 or HCAR1), was discovered in adipose tissues (reported EC_{50} range from 1 to 5 mM; Cai et al., 2008; Liu et al., 2009), where GPR81 is highly expressed and down-regulates the formation of cytosolic cyclic adenosine monophosphate ($[cAMP]_i$) by coupling to G_i-protein and inhibiting the cAMP producing enzyme adenylate cyclase (AC), thereby in an autocrine loop inhibiting lipolysis and promoting energy storage (Ahmed et al., 2010). Whether a similar signaling loop is present in astrocytes is not known and was explored in this study. Quantitative RT-PCR analysis of human, rat, and mouse brain tissue revealed the presence of mRNA GPR81 in the brain, although at very low levels compared to adipose tissue (Liu et al., 2009). Consistent with RT-PCR analysis, RNA sequencing transcriptome databases revealed the presence of GPR81 mRNA in individual types of mouse brain cells, including astrocytes (Zhang et al., 2014; Sharma et al., 2015). Immunohistochemical studies on mouse brain tissue slices also suggested the presence of the GPR81 receptor in neurons, endothelial cells, and at low density of expression in astrocytes, in particular in membranes of perivascular astrocytic processes and not so much in perisynaptic processes of astrocytes (Lauritzen et al., 2014; Morland et al., 2017). The mechanism of how L-lactate via activation of a GPR81 receptor would modulate $[cAMP]_i$, cytosolic levels of D-glucose ($[glucose]_i$) and L-lactate ($[lactate]_i$) in brain, in particular in astrocytes that are actively involved in the regulation of brain metabolism and produce L-lactate, is currently unknown.

In contrast to the situation in adipocytes, where the GPR81 receptor agonist decreases $[cAMP]_i$ (Ahmed et al., 2010), we show here by fluorescence resonance energy transfer (FRET) microscopy on single astrocytes expressing FRET-nanosensors for cAMP and L-lactate that very high levels of extracellular L-lactate and the agonist for the L-lactate GPR81 receptor 3-chloro-5-hydroxybenzoic acid (3Cl-5OH-BA; Dvorak et al., 2012) elevate $[cAMP]_i$ and $[lactate]_i$ in astrocytes, as does the activation of adrenergic receptors (ARs). The 3Cl-5OH-BA-dependent elevation in $[lactate]_i$ and the extracellular L-lactate-mediated rise in $[cAMP]_i$, both act through the activation of AC in astrocytes, as demonstrated by the use of an AC inhibitor. Interestingly, in astrocytes from the L-lactate specific GPR81 receptor knock-out (KO) mice, 3Cl-5OH-BA still elevated $[cAMP]_i$, indicating that the supposedly selective GPR81 agonist also activates a second, yet unidentified excitatory L-lactate receptor-like mechanism. Pretreatment of rat astrocytes with the sub-effective doses of 3Cl-5OH-BA reduced the L-lactate-induced elevation in $[cAMP]_i$, suggesting that 3Cl-5OH-BA and L-lactate at least to some extent bind to the same yet unidentified receptor. A new generation GPR81 selective high affinity agonist lead compound, Compound 2 (4-methyl-N-(5-(2-(4-methylpiperazin-1-yl)-2-oxoethyl)-4-(2-thienyl)-1,3-thiazol-2-yl)cyclohexanecarboxamide; Sakurai et al., 2014) reproduced the cAMP enhancing effects of L-lactate and 3Cl-5OH-BA, further supporting the existence of an unidentified L-lactate receptor. The new excitatory L-lactate receptor-mediated mechanism ("metabolic excitability") may participate in maintaining high $[lactate]_i$ in cells exhibiting aerobic glycolysis, such as in astrocytes (Mächler et al., 2016), contributing to the elevated levels of extracellular L-lactate in comparison to the plasma levels (Abi-Saab et al., 2002). While generating metabolic intermediates required for cell division and morphological plasticity, this regulation presumably facilitates the exit of L-lactate into the extracellular space, where it can become an autocrine and paracrine signal. Since relatively high concentrations of L-lactate (20 mM, but not 2 mM) are required

for the increase in second messenger cAMP (the predicted brain physiological concentrations of L-lactate are up to 2 mM), the putative novel facilitatory L-lactate receptor-like mechanism may have a role under conditions of very high extracellular L-lactate that may occur during extreme exercise (Osnes and Hermansen, 1972; Matsui et al., 2017) or neuronal activity (for example during seizures; During et al., 1994). Such a scenario may also be relevant if local fluctuations of extracellular L-lactate concentration exist in brain microdomains (Morland et al., 2015; Mosienko et al., 2015).

MATERIALS AND METHODS

Cell Culture, Transfection, and Reagents

Primary cultures of astrocytes were prepared from cortices of 2–3 and 1–4 days old rat and wild type (WT) or GPR81 KO mice pups, respectively, as described previously (Schwartz and Wilson, 1992), and grown in high-glucose (25 mM) Dulbecco's Modified Eagle's Medium containing 10% fetal bovine serum, 1 mM sodium pyruvate, 2 mM L-glutamine, and 25 μg/ml penicillin-streptomycin at 37°C in 95% air–5% CO_2 until reaching 70–80% confluency. Confluent cultures were shaken at 225 rpm overnight, and the medium was changed the next morning; this was repeated three times. After the third overnight shaking, the cells were trypsinized and put in flat tissue culture tubes with 10 cm^2 growth area. After reaching confluency, the cells were trypsinized and plated on 22-mm diameter glass cover slips coated with poly- L-lysine. By using quantitative PCR, we verified that astrocytes from the GPR81 KO animals were devoid of the GPR81 RNA transcript. The purity of rat astrocytes was determined immunocytochemically using antibodies against the astrocytic marker GFAP (Abcam, Cambridge, United Kingdom) and >94% of imaged cultured cells were GFAP-positive (Stenovec et al., 2016). 3T3-L1 fibroblasts (ATCC-LGC Standards, VA, United States) were grown in high-glucose Dulbecco's Modified Eagle's Medium containing 10% fetal bovine serum and 2 mM L-glutamine. BT474 cancer cells (BT-474 Clone 5; ATCC® CRL-3247™; ATCC-LGC Standards) were grown in Hybri-Care medium (ATCC® 46-X™; ATCC-LGC Standards) supplemented with 1.5 g/L sodium bicarbonate and 10% fetal bovine serum. 3T3-L1 and BT474 cells were grown in culture flasks with 25 cm^2 growth area at 37°C in 95% air–5% CO_2. After reaching 70–80% confluency, cells were trypsinized and plated on 22-mm diameter glass cover slips coated with poly- L-lysine.

After 24–72 h, transfection with plasmids carrying FRET-based nanosensors was performed with FuGENE® 6 transfection reagent according to manufacturer's instructions (Promega Co., Madison, WI, United States). Transfection medium contained no serum or antibiotics.

GPR81 KO and WT mice (Ahmed et al., 2010) in C57Bl/6N background were bred in Oslo from founder mice obtained from Stefan Offermanns, Max-Planck-Institute for Heart and Lung Research, Department of Pharmacology, D-61231 Bad Nauheim, Germany. The experimental animals were cared for in accordance with the International Guiding Principles for Biomedical Research Involving Animals developed by the Council for International Organizations of Medical Sciences and the Animal Protection Act (Official Gazette RS, No. 38/13). The experimental protocol was approved by The Administration of the Republic of Slovenia for Food Safety, Veterinary and Plant Protection (Republic of Slovenia, Ministry of Agriculture, Forestry and Food, Ljubljana), Document No. U34401-47/2014/7, signed by Barbara Tomše, DVM. All experiments were performed on rat astrocytes isolated from at least two different animals. All chemicals were from Sigma-Aldrich (St. Louis, MO, USA) unless otherwise noted.

FRET Measurements of $[cAMP]_i$ and PKA Activity

Cells expressing the FRET-based cAMP nanosensor Epac1-camps (Nikolaev et al., 2004) or the PKA nanosensor AKAR2 (Zhang et al., 2005) were examined 24–48 h after transfection with a Plan NeoFluoar 40×/1.3 NA oil differential interference contrast (DIC) immersion objective (Carl Zeiss, Jena, Germany) using a Zeiss LSM510 META confocal microscope (Carl Zeiss, Jena, Germany). Cells were excited at 458 nm, and images (512 × 512) were acquired every 3.5 s using lambda stack acquisition. Emission spectra were collected from the META detector in 8 channels (lambda stack) ranging from 470 nm to 545 nm, each with a 10.7-nm width. Two-channel [cyan fluorescent protein (CFP) and yellow fluorescent protein (YFP)] images were generated using the analytical software Extract channels (Zeiss LSM510 META, Carl Zeiss, Jena, Germany). Channels with emission spectra at 470 and 481 nm and emission spectra at 513, 524, and 534 nm were extracted to the CFP and YFP channels, respectively. YFP and CFP fluorescence intensities were quantified within a region of interest (ROI) selected for individual cells expressing Epac1-camps or AKAR2 using the LSM510 META software.

In some experiments, astrocytes expressing the Epac1-camps FRET nanosensor, were examined 24 h after transfection with a fluorescence microscope Zeiss Axio Observer.A1 (Zeiss, Oberkochen, Germany) with a CCD camera and monochromator Polychrome V (Till Photonics, Graefelfing, Germany) as a monochromatic source of light with a wavelength 436 nm/10 nm. Dual emission intensity ratios were recorded using an image splitter (Optical Insights, Tucson, AZ, United States) and two emissions filters (465/30 nm for CFP and 535/30 nm for YFP). Images were acquired every 3.5 s with an exposure time of 0.1 s. CFP and YFP fluorescence intensities were obtained from the integration of ROI over the entire cell using Life Acquisition software (Till Photonics, Graefelfing, Germany).

In the graphs, the FRET ratio signal was reported as the ratio of the CFP/YFP (Epac1-camps) and YFP/CFP (AKAR2) fluorescence signals after subtracting the background fluorescence from the signals using Excel (Microsoft, Seattle, WA, United States). The values of the FRET signals were normalized to 1.0. An increase in the FRET ratio signal reflects an increase in the $[cAMP]_i$ and the PKA activity.

Initially, astrocytes were kept in extracellular solution (10 mM Hepes/NaOH, pH 7.2, 10 mM D-glucose, 131.8 mM NaCl, 1.8 mM $CaCl_2$, 2 mM $MgCl_2$, and 5 mM KCl) or extracellular

solution with sodium bicarbonate (10 mM Hepes/NaOH, pH 7.2, 10 mM D-glucose, 131.8 mM NaCl, 1.8 mM $CaCl_2$, 2 mM $MgCl_2$, 5 mM KCl, 0.5 mM $NaH_2PO_4 \times H_2O$, and 5 mM $NaHCO_3$) and were then treated with various reagents following a 100-s baseline: 1 μM NA, 10 μM isoprenaline (ISO), 2 or 20 mM L-lactate (osmolality was adjusted by lowering NaCl in extracellular solution containing sodium bicarbonate) and 0.5 mM 3Cl-5OH-BA. In some experiments cell were after initial a 100-s baseline pretreated with 100 μM 2′,5′-dideoxyadenosine (DDA) or 50 μM 3Cl-5OH-BA for 450 s and then stimulated with 20 mM L-lactate in the presence of DDA or 3Cl-5OH-BA, respectively. The 4-methyl-*N*-(5-(2-(4-methylpiperazin-1-yl)-2-oxoethyl)-4-(2-thienyl)-1,3-thiazol-2-yl)cyclohexanecarboxamide (Compound 2; Sakurai et al., 2014) was custom synthesized (ABX advanced biochemical compounds, D-01454 Radeberg, Germany). After the initial 90–100-s baseline, WT and GPR81 KO astrocytes were treated with GPR81 receptor agonist 3Cl-5OH-BA (0.5 mM) or Compound 2 (50 nM) and recorded for another 300 s. In control experiments, astrocytes were treated only with extracellular solution (Vehicle). Extracellular solution osmolality was ∼300 mOsm, measured with a freezing point osmometer (Osmomat030, Gonotech GmbH, Germany).

FRET Measurements of $[glucose]_i$ and $[lactate]_i$

Astrocytes, 3T3-L1 embryonic preadipocyte fibroblast cells and BT474 cancer cells expressing the FRET-based glucose nanosensor FLII^{12}Pglu-700μδ6[1] (Takanaga et al., 2008; Prebil et al., 2011) or the FRET-based lactate nanosensor Laconic (San Martin et al., 2013) were examined 16–48 h after transfection with a fluorescence microscope (Zeiss Axio Observer.AI, Zeiss, Oberkochen, Germany), with a CCD camera and monochromator Polychrome V (Till Photonics, Graefelfing, Germany) as a monochromatic source of light with a wavelength 436 nm/10 nm. Dual emission intensity ratios were recorded using an image splitter (Optical Insights, Tucson, AZ, United States) and two emission filters; 465/30 nm for ECFP or mTFP and 535/30 nm for EYFP or Venus. Images were acquired every 10 s with an exposure time of 0.1 s. The background fluorescence was subtracted from individual EYFP or Venus and ECFP or mTFP fluorescence signals. The FRET ratio signals, EYFP/ECFP (FLII^{12}Pglu-700μδ6) and mTFP/Venus (Laconic), were obtained from the integration of the ratio signal over the entire cell using Life Acquisition software (Till Photonics, Graefelfing, Germany). The values of the FRET signals were normalized to 1.0. An increase in the FRET ratio signal reflects increases in the $[glucose]_i$ and $[lactate]_i$.

Initially, cells were kept in extracellular solution with sodium bicarbonate (10 mM Hepes/NaOH, pH 7.2, 3 mM D-glucose, 135.3 mM NaCl, 1.8 mM $CaCl_2$, 2 mM $MgCl_2$, 5 mM KCl, 0.5 mM $NaH_2PO_4 \times H_2O$, and 5 mM $NaHCO_3$), and were then treated with various reagents following a 200-s baseline: 200 μM ISO, 200 μM NA, 2 or 20 mM L-lactate, 0.5 mM 3Cl-5OH-BA, and 6 mM α-cyano-4-hydroxycinnamate (CHC). In some experiments, cells were, after an initial 200 s-baseline, pretreated with 100 μM DDA for 450 s and then stimulated with 0.5 mM 3Cl-5OH-BA in the presence of DDA. Extracellular solution osmolality was ∼300 mOsm, measured with a freezing point osmometer (Osmomat030, Gonotech GmbH, Germany).

[1]www.addgene.org

Extraction of mRNA and Quantitative Real-Time PCR (qPCR)

Rat, WT mouse, and GPR81 KO mouse astrocytes were cultured in six-well plates. Total RNA was extracted from cultured astrocytes with the RNeasy Mini Plus Kit (Qiagen, Hilden, Germany). cDNA was synthesized from total RNA using the High-Capacity cDNA Reverse Transcription Kit (Applied Biosystems, Thermo Fisher Scientific, Vilnius, Lithuania). qPCR was performed on ABI PRISM SDS 7500 (Applied Biosystems, Thermo Fisher Scientific) in a 96-well format using TaqMan Universal PCR Master Mix (Applied Biosystems, Thermo Fisher Scientific, Foster City, United States) and gene expression assays for GPR81 (Rn03037047_sH) and 18S rRNA (TaqMan Endogenous Control). Standard quality controls were performed in line with the MIQE Guidelines (Bustin et al., 2009). Expression level of GPR81 mRNA was calculated as gene expression ratio (GPR81 mRNA/18S rRNA) according to the equation: $E_{18S\ rRNA}^{Ct,18S\ rRNA} / E_{GPR81}^{Ct,GPR81}$, where E is the PCR efficiency and C_t is the threshold cycle for the reference (18S rRNA) or the target (GPR81) gene (Ruijter et al., 2009; Tuomi et al., 2010). PCR efficiency was estimated using the LinRegPCR program (Ruijter et al., 2009; Tuomi et al., 2010).

Statistical Analysis

Single-exponential increase to maximum functions [$F = F_0 + c \times (1 - \exp(-t/\tau))$] were fitted to the diagrams with FRET ratio signals using SigmaPlot. The time constant (τ) and the FRET ratio signal amplitudes (c) were determined from the fitted curves. F is the FRET ratio signal at time t, F_0 is the baseline FRET ratio signal, c is FRET ratio signal amplitude of $F - F_0$, and τ is the time constant of the individual exponential component. In some experiments, the initial rate of the FRET signal increase (ΔFRET/Δtime) after the addition of various reagents was calculated as the slope of the linear regression function [ΔFRET (%) = slope (%/min) × Δtime (min)] fitting the initial FRET signal decrease or increase. In these experiments, the amplitude of the ΔFRET (%) was determined by subtracting the mean FRET ratio signal of the first 100 s from the last 100 s upon stimulation or *vice versa*, if the FRET signal increased.

The average traces of the predominant responses are presented in the figures for individual stimuli; all other responses are listed in **Table 1**. Unless stated otherwise, the Student's t-test was performed to determine statistical significance. $P < 0.05$ was considered to be significant.

RESULTS

We studied here how extracellular L-lactate and agonists of the L-lactate GPR81 receptor affect cAMP signaling and

TABLE 1 | Responsiveness of astrocytes to adrenergic and L-lactate receptor activation.

FRET nanosensor		Stimulus	*n* (%) increase	*n* (%) decrease	*n* (%) transient decrease	*n* (%) unresponsive	*n* all
Rat astrocytes							
cAMP		ISO (10 μM)	8 (100%)	0 (0%)	0 (0%)	0 (0%)	8
		NA (1 μM)	16 (100%)	0 (0%)	0 (0%)	0 (0%)	16
		L-lactate (20 mM)	7 (36.8%)	3 (15.8%)	0 (0%)	9 (47.4%)	19
		3Cl-5OH-BA (0.5 mM)	9 (42.9%)	2 (9.5%)	0 (0%)	10 (47.6%)	21
PKA		L-lactate (2 mM)	0 (0%)	0 (0%)	0 (0%)	7 (100%)	7
		L-lactate (20 mM)	8 (57.1%)	1 (7.1%)	0 (0%)	5 (35.7%)	14
		3Cl-5OH-BA (0.5 mM)	9 (56.3%)	2 (12.5%)	0 (0%)	5 (31.3%)	16
Glucose		ISO (200 μM)	5 (16.1%)	0 (%)	0 (0%)	26 (83.9%)	31
		NA (200 μM)	8 (40%)	0 (%)	0 (0%)	12 (60%)	20
		L-lactate (2 mM)	0 (0%)	0 (0%)	0 (0%)	11 (100%)	11
		L-lactate (20 mM)	3 (15%)	4 (20.0%)	13 (65.0%)	0 (0%)	20
		3Cl-5OH-BA (0.5 mM)	1 (5.3%)	13 (68.4%)	1 (5.3%)	4 (21.1%)	19
Lactate		ISO (200 μM)	10 (63%)	0 (0%)	0 (0%)	6 (27%)	16
		NA (200 μM)	8 (88.9%)	0 (0%)	0 (0%)	1 (11.1%)	9
		L-lactate (20 mM)	14 (93.3%)	0 (0%)	0 (0%)	1 (6.7%)	15
		3Cl-5OH-BA (0.5 mM)	14 (100%)	0 (0%)	0 (0%)	0 (0%)	14
Mouse astrocytes							
cAMP	WT	3Cl-5OH-BA (0.5 mM)	11 (68.8)	0 (0)	0 (0)	5 (31.2)	16
		Compound 2 (50 nM)	10 (66.7%)	0 (0)	0 (0)	5 (33.3%)	15
	KO GPR81	3Cl-5OH-BA (0.5 mM)	11 (73.3)	0 (0)	0 (0)	4 (26.7)	15
		Compound 2 (50 nM)	11 (100%)	0 (0)	0 (0)	0 (0)	11

ISO, isoprenaline; NA, noradrenaline; 3Cl-5OH-BA, 3-chloro-5-hydroxybenzoic acid; Compound 2, 4-methyl-N-(5-(2-(4-methylpiperazin-1-yl)-2-oxoethyl)-4-(2-thienyl)-1,3-thiazol-2-yl)cyclohexanecarboxamide; n, number of cells studied. The increase or decrease in the FRET ratio signal was set by determining a threshold of 3 standard deviations of the average signal measured prior to the application of agents (baseline), as described (Horvat et al., 2016). The frequency of unresponsive cells did not differ in KO group compared to WT group, when treated with 3Cl-5OH-BA (P = 0.78). The frequency of unresponsive cells was significantly lower in KO group compared to WT group, when treated with Compound 2 (P = 0.03; chi-square statistic).

changes in the intracellular levels of metabolites in isolated astrocytes, which can express the GPR81 receptor (Lauritzen et al., 2014; Sharma et al., 2015) and mRNA for GPR81 can be measured in these cells (Supplementary Figure S1). Real-time FRET imaging of cultured cortical astrocytes, expressing FRET-nanosensors for cAMP, glucose, and lactate was performed.

Extracellular L-Lactate and GPR81 Lactate Receptor Agonists Increase $[cAMP]_i$ in Astrocytes

We performed real-time monitoring of $[cAMP]_i$ while extracellular L-lactate or the GPR81 lactate receptor agonist 3Cl-5OH-BA (Dvorak et al., 2012; Liu et al., 2012) were applied. Using the FRET-nanosensor for cAMP Epac1-camps, in 7 (37%) out of 19 cells an increase in $[cAMP]_i$ was measured when a high concentration of L-lactate (20 mM) was applied (**Figure 1A**). Decreased $[cAMP]_i$ was measured only in 3 (16%) cells out of 19 (**Table 1**). Although GPR81 receptor in adipocytes is coupled to G_i-proteins decreasing $[cAMP]_i$ (Ahmed et al., 2010), the observed L-lactate-mediated elevation in $[cAMP]_i$ in 37% of cells studied might be due to the activation of a G_s-protein coupled to L-lactate GPR81 receptor, as a similar rise in $[cAMP]_i$ was recorded in astrocytes by adding the selective GPR81 receptor agonist 3Cl-5OH-BA (0.5 mM, **Figure 1B**); 9 (43%) of 21 cells responded with an increase (**Figure 1B**) and 2 (10%) with a small decrease in $[cAMP]_i$ (**Table 1**). Inhibition of AC activity by 100 μM DDA (Vardjan et al., 2014) reduced the 20 mM extracellular L-lactate-induced increase in $[cAMP]_i$ by ∼50 % (**Figure 3A**), indicating that in the majority of astrocytes, extracellular L-lactate activates the cAMP pathways via binding to receptors that activate AC.

To verify whether the 3Cl-5OH-BA-induced increase in $[cAMP]_i$ is mediated via the GPR81 lactate receptor, we used isolated astrocytes from the GPR81 KO mice (Ahmed et al., 2010). Interestingly, even in GPR81 KO astrocytes, the application of 3Cl-5OH-BA (0.5 mM), like in WT astrocytes, elicited an increase in $[cAMP]_i$ (**Figure 2** and **Table 1**). Similar results were obtained by using a much higher affinity GPR81 receptor agonist Compound 2 (Sakurai et al., 2014; histograms in **Figures 2C,D**; **Table 1**), suggesting that these agonists activate in astrocytes a second, yet unidentified receptor-like mechanism, thus resembling the unidentified L-lactate receptor in neurons, coupled to G_s-protein increasing the production of cAMP (Tang et al., 2014).

To see if L-lactate and GPR81 agonist 3Cl-5OH-BA target the same, yet unidentified receptor-like mechanism, sharing the binding on the receptor, we pretreated rat astrocytes with

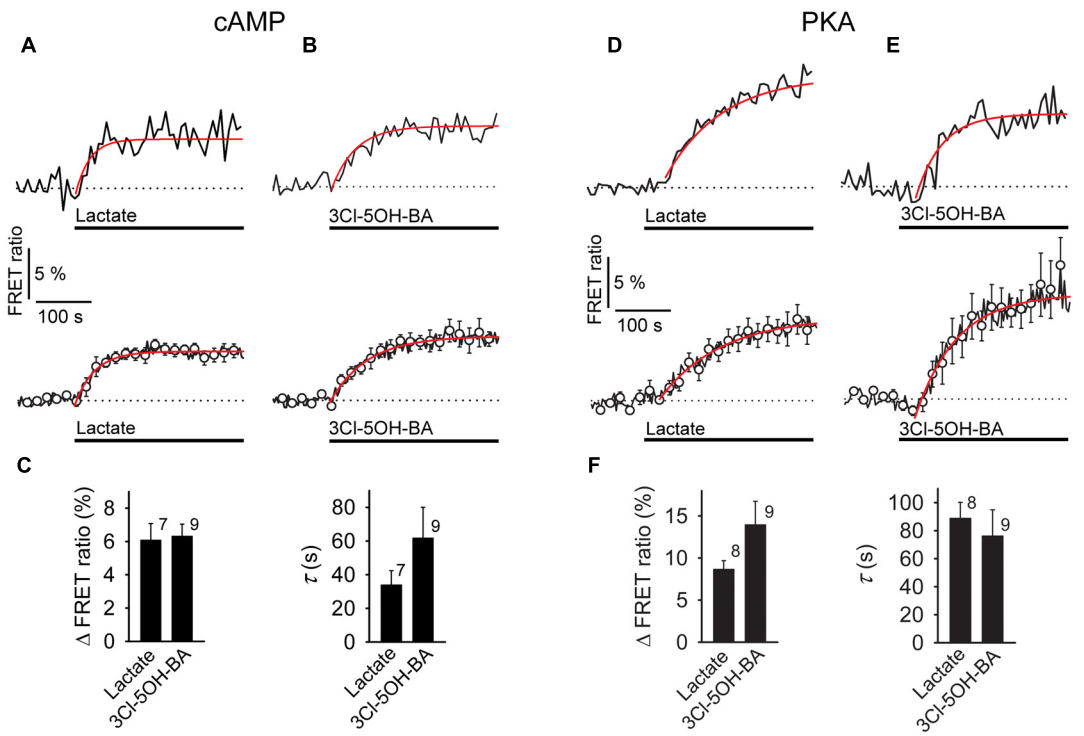

FIGURE 1 | Application of L-lactate and 3Cl-5OH-BA increases $[cAMP]_i$ and the intracellular PKA activity in rat astrocytes. **(A,B)** Representative (above) and mean time-course (below) of the Epac1-camps FRET ratio signal upon the addition of **(A)** L-lactate (20 mM) and **(B)** 3Cl-5OH-BA (0.5 mM), a selective agonist of the GPR81 receptor. Data are expressed as percentages of the inverse FRET ratio signal (CFP/YFP) relative to the baseline values. Single exponential rise functions were fitted to the curves: (**A**, above) *FRET ratio* = [0.98 ± 0.01] + [0.06 ± 0.01] × (1 – exp(–*t*/[25.00 ± 5.63 s])), (**A**, below) *FRET ratio* = [1.00 ± 0.00] + [0.05 ± 0.00] × (1 – exp(–*t*/[35.71 ± 2.55 s])), and (**B**, above) *FRET ratio* = [0.94 ± 0.00] + [0.06 ± 0.01] × (1 – exp(–*t*/[41.49 ± 5.85 s])), (**B**, below) *FRET ratio* = [1.00 ± 0.00] + [0.07 ± 0.00] × (1 – exp(*t*/[66.67 ± 4.42 s])). Note that the addition of L-lactate and 3Cl-5OH-BA increased the FRET ratios, indicating increases in $[cAMP]_i$. Each data point represents the mean ± s.e.m. **(C)** Mean changes in the FRET ratio (ΔFRET ratio) and mean time-constants (τ) upon L-lactate and 3Cl-5OH-BA stimulation. Changes in FRET ratio are expressed as percentages relative to the initial values. The numbers by the bars depict the number of cells analyzed. Data are shown as the means ± s.e.m. **(D,E)** Representative (above) and mean time-course (below) of the AKAR2 FRET ratio signal upon addition of **(D)** L-lactate (20 mM) and **(E)** 3Cl-5OH-BA (0.5 mM). Data are expressed as percentages of the FRET ratio signals (YFP/CFP) relative to the baseline ratio values. Single exponential rise functions were fitted to the curves: (**A**, above) *FRET ratio* = [1.01 ± 0.00] + [0.10 ± 0.00] × (1 – exp(–*t*/[90.91 ± 8.26 s])), (**A**, below) *FRET ratio* = [1.00 ± 0.00] + [0.08 ± 0.00] × (1 – exp(–*t*/[111.11 ± 9.91 s])), and (**B**, above) *FRET ratio* = [0.97 ± 0.01] + [0.10 ± 0.01] × (1 – exp(–*t*/[47.62 ± 4.54 s])), (**B**, below) *FRET ratio* = [0.98 ± 0.00] + [0.12 ± 0.00] × (1 – exp(–*t*/[71.43 ± 5.10 s])). Note that the addition of L-lactate and 3Cl-5OH-BA increased the FRET ratios, indicating increased PKA activity. Each data point represents the mean ± s.e.m. **(F)** Mean changes in the FRET ratio (ΔFRET ratio) and mean time-constants (τ) upon L-lactate and 3Cl-5OH-BA stimulation. The numbers by the bars depict the number of cells analyzed. Data shown are in the format of the mean ± s.e.m. Data for every set of experiment was acquired from at least two different animals.

the sub-effective dose of GPR81 receptor agonist 3Cl-5OH-BA (50 μM). The application of 50 μM 3Cl-5OH-BA is ineffective in increasing $[cAMP]_i$ in astrocytes, since the application of 3Cl-5OH-BA results in a FRET ratio signal change (1.63 ± 0.38 %, $n = 13$), not significantly different to the vehicle-induced response in controls (1.01 ± 0.46 %, $n = 13$, $P = 0.31$). However, the sub-effective dose of 3Cl-5OH-BA (50 μM) reduced the L-lactate-induced elevation in $[cAMP]_i$ (Supplementary Figure S4), indicating that in addition to interacting with the GPR81 lactate receptor, this supposedly selective GPR81 receptor agonist (Dvorak et al., 2012), binds like L-lactate to the yet unidentified receptor in astrocytes.

Furthermore, to evaluate whether the L-lactate receptor-like mechanism elevates $[cAMP]_i$ and consequently also activates the cAMP-effector protein kinase A (PKA) we used the AKAR2, PKA activation nanosensor (Zhang et al., 2005). Significant increase in PKA activity was recorded (**Figures 1D,E**) when astrocytes were exposed to 20 mM L-lactate in 57% of 14 cells or to 0.5 mM 3Cl-5OH-BA in 56% of 16 cells (**Table 1**). The differences in the responsiveness of cells between Epac1-camps and AKAR2 nanosensors (∼40% vs. ∼60%, respectively) may be due to a higher sensitivity of the AKAR2 nanosensor, since Epac1-camps can only detect $[cAMP]_i$ that is >100 nM (Börner et al., 2011). No changes in PKA activity were observed, when a 10-fold lower concentration of L-lactate (2 mM) was applied to cells (Supplementary Figure S5). The time-course and the extent of increase in the PKA activity were similar for both types of stimuli, L-lactate and 3Cl-5OH-BA (**Figure 1F**). We observed a delay between the addition of L-lactate or 3Cl-5OH-BA and subsequent increase in AKAR2 FRET ratio signal,

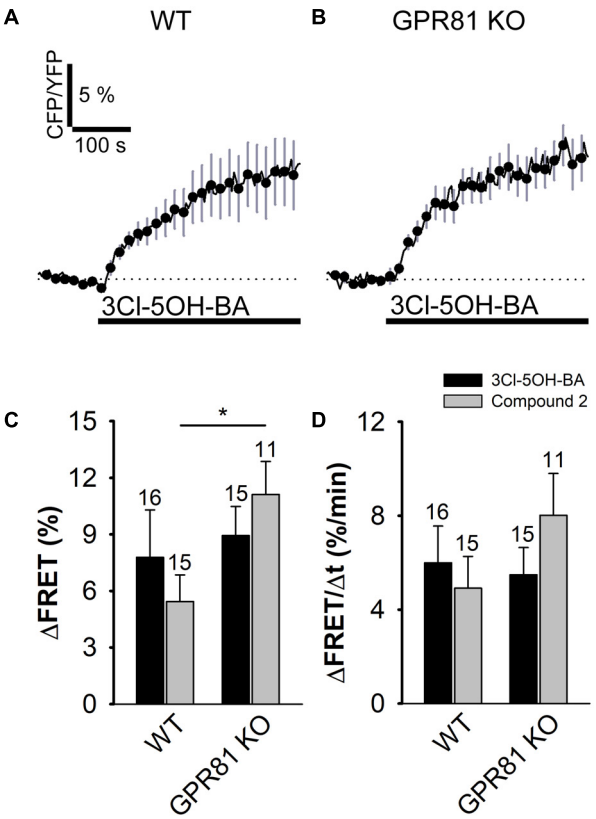

FIGURE 2 | Stimulation with 3Cl-5OH-BA and Compound 2 elicits persistent increase in $[cAMP]_i$ in WT and GPR81 KO mice astrocytes expressing the FRET nanosensor Epac1-camps. **(A,B)** Mean normalized time-courses of the Epac1-camps FRET ratio signal after stimulation with 3Cl-5OH-BA (0.5 mM) in **(A)** WT (n = 16) and **(B)** GPR81 KO (n = 15) cultured mouse astrocytes at t = 100 s (black lines). Changes in the FRET ratio signal are expressed as percentages of the inverse FRET ratio signal (CFP/YFP) relative to the baseline values. The monophasic exponential increase in the FRET signal (represented by the CFP/YFP ratio) after 3Cl-5OH-BA stimulation reflects an increase in $[cAMP]_i$. Each data point represents mean ± s.e.m. **(C,D)** Mean changes in the Epac1-camps FRET ratio signal (ΔFRET; **C**) and initial rates of the FRET ratio signal increase (ΔFRET/Δt; **D**) after the addition of 3Cl-5OH-BA (black bars) and Compound 2 (gray bars) in WT and GPR81 KO astrocytes. Numbers by the error bars depict the number of cells analyzed. (*$P < 0.05$; Mann Whitney U test) Data for every set of experiment was acquired from at least two different animals except for Compound 2.

determined from the intersection of the reference baseline with the exponential curve (time of delay was 35 ± 7 s (20 mM L-lactate) vs. 49 ± 7 s (0.5 mM 3Cl-5OH-BA); P = 0.19), consistent with PKA activation occurring downstream of cAMP production.

The observation that a 10-fold lower concentrations of 3Cl-5OH-BA (50 μM vs. 500 μM) and L-lactate (2 mM vs. 20 mM) does not affect cAMP levels and PKA activity in astrocytes, respectively, indicates that astrocytes respond to extracellular 3Cl-5OH-BA and L-lactate in a concentration-dependent manner, further suggesting that these two agonists in astrocytes cause a rise in cAMP via activation of an excitatory receptor-like mechanism in the plasma membrane.

Extracellular L-Lactate and GPR81 Receptor Agonist Trigger Similar Increases in $[lactate]_i$ in Astrocytes and Cancer Cells as Adrenergic Stimulation via Adenylate Cyclase Activation

Brain-based aerobic glycolysis (Goyal et al., 2014) is upregulated by noradrenergic stimuli affecting astrocyte metabolism (Dienel and Cruz, 2016). It has been reported that AR stimulation elevates astrocytic $[cAMP]_i$ (Vardjan et al., 2014; Horvat et al., 2016) and also intracellular concentration in free glucose ($[glucose]_i$; Prebil et al., 2011). We show here using lactate FRET nanosensor Laconic (San Martin et al., 2013) that astrocytes respond to AR activation also with an increase in intracellular L-lactate (Supplementary Figure S2) from its basal to the new steady state levels.

Although we have observed that in all studied astrocytes exposed to ISO (n = 8) and NA (n = 16) the $[cAMP]_i$ increased, the elevations in $[glucose]_i$ were only rarely observed, when cells were treated with selective β-AR agonist ISO [5 (16%) of the 31 cells]. The percentage of responsive cells, however, increased by twofold, when cells were exposed to NA, nonselective AR agonist [8 (40%) of the 20 cells; **Table 1**] and when cells were treated with selective α_1-AR agonist (data not shown), implying the role of Ca^{2+} in the elevation of $[glucose]_i$. In contrast to measurements of $[glucose]_i$, the majority of astrocytes (63%) responded to ISO application with an elevation in $[lactate]_i$ (10 out of 16 cells); 89% of astrocytes (8 out of 9 cells) responded with enhanced $[lactate]_i$ to stimulation by NA (Supplementary Figure S2C, **Table 1**). The time-course of the measured $[cAMP]_i$ increase was faster compared to that of $[glucose]_i$ and $[lactate]_i$ (Supplementary Figure S3).

Since L-lactate and GPR81 agonist 3Cl-5OH-BA (**Figure 1**), like β-AR agonists (Supplementary Figure S2; Vardjan et al., 2014; Horvat et al., 2016) increase $[cAMP]_i$ and PKA activity in astrocytes, we further examined whether extracellular L-lactate or the GPR81 agonist 3Cl-5OH-BA affect $[glucose]_i$ and $[lactate]_i$ in astrocytes. **Figure 4** shows that both extracellular L-lactate (20 mM) and 3Cl-5OH-BA (0.5 mM) decreased $[glucose]_i$ in the majority of studied cells. In the former case, the decrease was transient (65% of 20 cells responded), but the change was persistent in the latter case, where 68% of 19 cells responded. Interestingly, these treatments elevated $[lactate]_i$ in 93% of 15 cells (L-lactate) and in all 14 (100%) cells in case of 3Cl-5OH-BA (**Figures 3B** (left panel), **5**). The increase in $[lactate]_i$ was faster when the cells were exposed to extracellular L-lactate than 3Cl-5OH-BA, likely due to the entry of L-lactate into the cytosol through the plasma membrane MCTs. The extent of $[lactate]_i$ elevation was more than twofold higher upon the addition of L-lactate vs. 3Cl-5OH-BA (**Figure 5C**), which was expected due to L-lactate entry into the cytoplasm via the MCTs and possibly channels (Sotelo-Hitschfeld et al., 2015).

A few cells responded with a $[glucose]_i$ increase to L-lactate or 3Cl-5OH-BA stimulation [3 (15%) and 1 (5%) cells, respectively], but no cell responded with a decrease in $[lactate]_i$ to these stimuli.

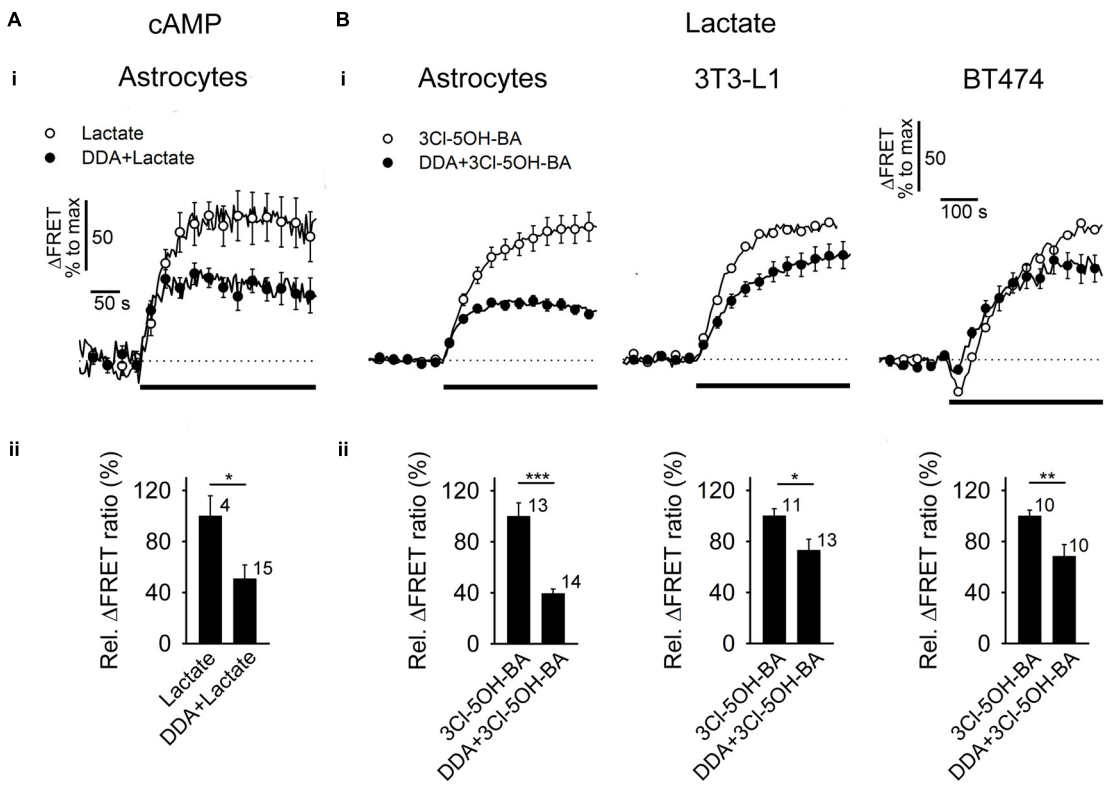

FIGURE 3 | Inhibition of AC reduces the L-lactate- and 3Cl-5OH-BA-induced increase in $[cAMP]_i$ and $[lactate]_i$ **(A,B**, panels **i)** Mean time-courses of FRET ratio signal changes normalized to the maximum signal change for **(A,i)** Epac1-camps upon addition of 20 mM L-lactate and **(B,i)** Laconic upon addition of 0.5 mM 3Cl-5OH-BA (black lines) in the absence (white circles) and presence (black circles) of 100 μM DDA, an inhibitor of AC. Each data point represents mean ± s.e.m. (**A,B**, panels **ii)** Mean relative changes in FRET ratio (Rel. ΔFRET ratio) upon L-lactate **(A)** and **(B)** 3Cl-5OH-BA stimulation in the absence and presence of DDA. Relative ΔFRET values (%) were calculated by dividing individual ΔFRET values with the average ΔFRET value upon L-lactate or 3Cl-5OH-BA stimulation. Note that the inhibition of AC by DDA causes ∼50 % reduction in L-lactate-induced increase in $[cAMP]_i$ in astrocytes and a ∼30–60% reduction in 3Cl-5OH-BA-induced increase in $[lactate]_i$ in astrocytes, 3T3-L1 and BT474 cells. In BT474 cells the application of 3Cl-5OH-BA initiated a transient reduction in $[lactate]_i$ that was diminished in the presence of DDA. Numbers adjacent to black bars represent number of cells. Data are in the format of the mean ± s.e.m (*$P < 0.05$, **$P < 0.01$, ***$P < 0.001$). Data for every set of experiment was acquired from at least two different animals.

As in the case of the cAMP-dependent PKA activity ($n = 7$), the addition of 2 mM L-lactate had no significant effect on $[glucose]_i$ ($n = 11$; Supplementary Figure S5), further indicating that astrocytes respond to extracellular L-lactate in a concentration-dependent manner.

Taken together these results show that in astrocytes, extracellular L-lactate and 3Cl-5OH-BA trigger an elevation in $[lactate]_i$, likely via the cAMP-mediated activation of glucose consumption, as decreased $[glucose]_i$ was recorded in the majority of the 3Cl-5OH-BA-treated cells. Moreover, inhibition of AC by 100 μM DDA (Vardjan et al., 2014), reduced the 3Cl-5OH-BA-induced increase in $[lactate]_i$ in astrocytes. We have observed inhibition of 3Cl-5OH-BA-induced increase in $[lactate]_i$ with DDA also in 3T3-L1 embryonic murine cells with genetic trait as seen in human ectodermal cancers (Leibiger et al., 2013) and in human mammary ductal carcinoma BT474 cells (**Figure 3B**). Both cell lines were shown to be positive for the GPR81 receptor (Liu et al., 2009; Staubert et al., 2015), indicating that AC activation by a membrane receptor is responsible for the increase in $[lactate]_i$ in cells that exhibit aerobic glycolysis such as astrocytes and cancer cells (Supplementary Table S1).

Receptor-Regulated Increase in the Rate of Aerobic Glycolysis in Astrocytes

Aerobic glycolysis in the brain is likely mediated by astrocytes, since these cells strongly favor L-lactate as the end glycolytic product whether or not oxygen is present (Halim et al., 2010). To measure the glycolytic rate in these cells, we estimated the maximal initial rate of $[lactate]_i$ increase in the presence of CHC (6 mM), a non-specific inhibitor of membrane MCTs (MCTs 1-4). In the absence of L-lactate exchange through the plasma membrane, the predominant pathway available for cytosolic L-lactate accumulation is considered to be glycolytic L-lactate production. Although cytosolic L-lactate may be transported to mitochondria for oxidation in astrocytes (Passarella et al., 2008), in the presence of MCT blockers the initial rate of cytosolic L-lactate accumulation, measured as $\Delta FRET/\Delta t$, is comparable to that of the initial rate of aerobic glycolysis. **Figure 6A**, ii

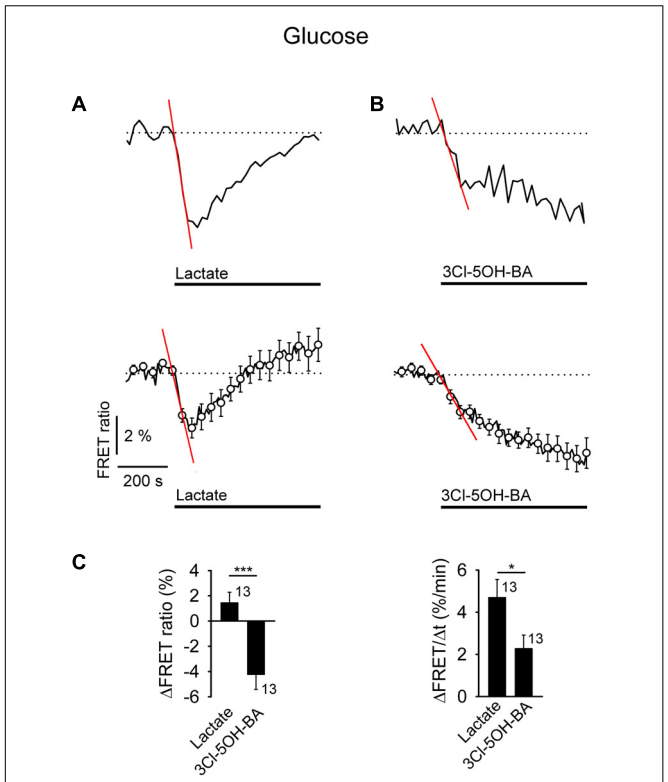

FIGURE 4 | Application of L-lactate and 3Cl-5OH-BA decreases $[glucose]_i$ in astrocytes. **(A,B)** Representative (above) and mean time-course (below) of FLII^{12}Pglu-700μδ6 FRET ratio signal, reporting $[glucose]_i$, upon the addition of **(A)** L-lactate (20 mM) and **(B)** 3Cl-5OH-BA (0.5 mM). Data are expressed as the percentages of the FRET ratio signals (EYFP/ECFP) relative to the baseline ratio values. The initial rate of change in $[glucose]_i$ was determined by fitting the regression lines to the signal decreases; $\Delta FRET\ (\%) = -k\ (\%/min) \times \Delta t\ (min)$, where t is the time and the k–slope is the initial ΔFRET decline: $k_{(A,above)} = 4.94 \pm 0.28$ %/min, $k_{(A,below)} = 2.90 \pm 0.36$ %/min, and $k_{(B,above)} = 2.32 \pm 0.29$ %/min, $k_{(B,below)} = 1.05 \pm 0.11$ %/min. Note that the addition of L-lactate transiently decreased the FRET ratio, while the 3Cl-5OH-BA persistently decreased the FRET ratio. Each data point represents the mean ± s.e.m. **(C)** Mean changes in the FRET ratio (ΔFRET ratio; left) and initial rates in the FRET ratio decrease (ΔFRET/Δt; right) upon L-lactate and 3Cl-5OH-BA stimulation. Numbers adjacent to the bars depict the number of cells analyzed. Data shown are in the format of the mean ± s.e.m (*$P < 0.05$, ***$P < 0.001$). Data for every set of experiment was acquired from at least two different animals.

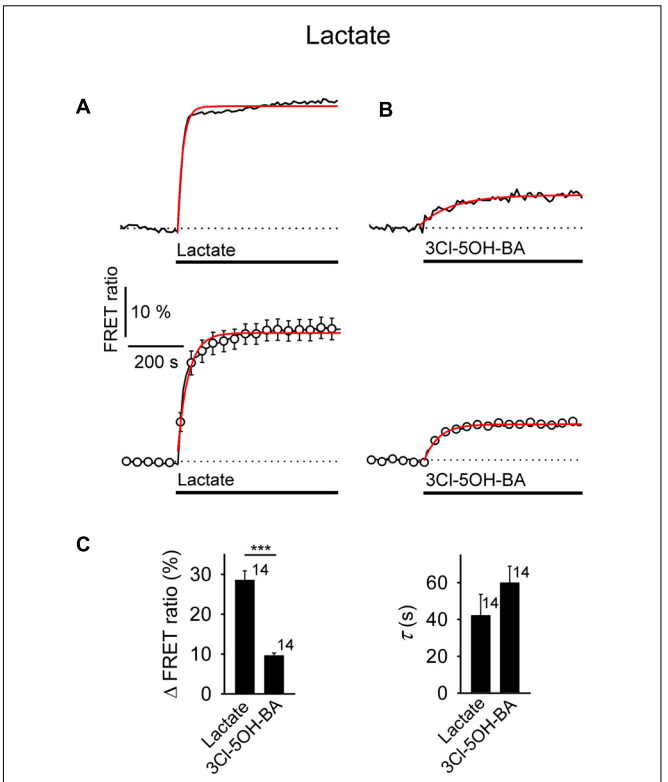

FIGURE 5 | Comparison of increases in $[lactate]_i$ by extracellular L-lactate and 3Cl-5OH-BA in astrocytes. **(A,B)** Representative (above) and mean time-course (below) of the Laconic FRET ratio signal upon the addition of **(A)** L-lactate (20 mM) and **(B)** 3Cl-5OH-BA (0.5 mM). Data are expressed as the percentages of FRET ratio signals (mTFP/Venus) relative to the baseline ratio values. Single exponential rise functions were fitted to the curves: (**A**, above) FRET ratio = [0.81 ± 0.02] + [0.44 ± 0.02] × (1 − exp(−t/[18.80 ± 1.10 s])), (**A**, below) FRET ratio = [1.02 ± 0.01] + [0.24 ± 0.01] × (1 − exp(−t / [39.06 ± 2.44 s])), and (**B**, above) FRET ratio = [1.00 ± 0.00] + [0.06 ± 0.00] × (1 − exp(−t/[116.28 ± 14.87 s])), (**B**, below) FRET ratio = [0.98 ± 0.00] + [0.09 ± 0.00] × (1 − exp(−t/[54.05 ± 2.34 s])). Note that the addition of L-lactate and 3Cl-5OH-BA increased the FRET ratios, indicating an increase in $[lactate]_i$. Each data point represents the mean ± s.e.m. **(C)** Mean changes in the FRET ratio (ΔFRET ratio; left) and mean time-constants (τ; right) upon L-lactate and 3Cl-5OH-BA stimulation. Numbers by the error bars depict the number of cells analyzed. Data shown are in the format of the mean ± s.e.m (***$P < 0.001$). Data for every set of experiment was acquired from at least two different animals.

shows that upon the addition of CHC, the initial maximal rate of the $[lactate]_i$ increase was 3.2 ± 0.6 %/min ($P < 0.001$), which was consistent with previous results (Sotelo-Hitschfeld et al., 2015). It appears that this effect is not an artifact, as vehicle addition did not affect the $[lactate]_i$ (**Figure 6B**; $P = 0.18$). With the addition of 3Cl-5OH-BA (0.5 mM), the rate of $[lactate]_i$ increase was approximately twofold higher than the resting rate of glycolysis. NA (200 μM) appeared as a weaker stimulus of $[lactate]_i$ increase in comparison to 3Cl-5OH-BA (0.5 mM) (**Figure 6B**) at the concentrations of respective agonists used. The strongest effect on the measured rate in the $[lactate]_i$ increase was recorded when extracellular L-lactate (20 mM) was applied. This was expected, as L-lactate can enter the cytoplasm via the MCTs. Consistent with this finding, when L-lactate was added in the presence of the MCT blocker CHC, the increase in $[lactate]_i$ was strongly attenuated in comparison to the conditions in the absence of CHC (data not shown).

Taken together, the results indicate that in astrocytes, extracellular L-lactate mediates an increase in $[cAMP]_i$ that stimulates aerobic glycolysis and elevates $[lactate]_i$ via a receptor-mediated pathway involving AC.

DISCUSSION

Here we studied whether extracellular L-lactate affects aerobic glycolysis via G-protein coupled L-lactate receptors, such as

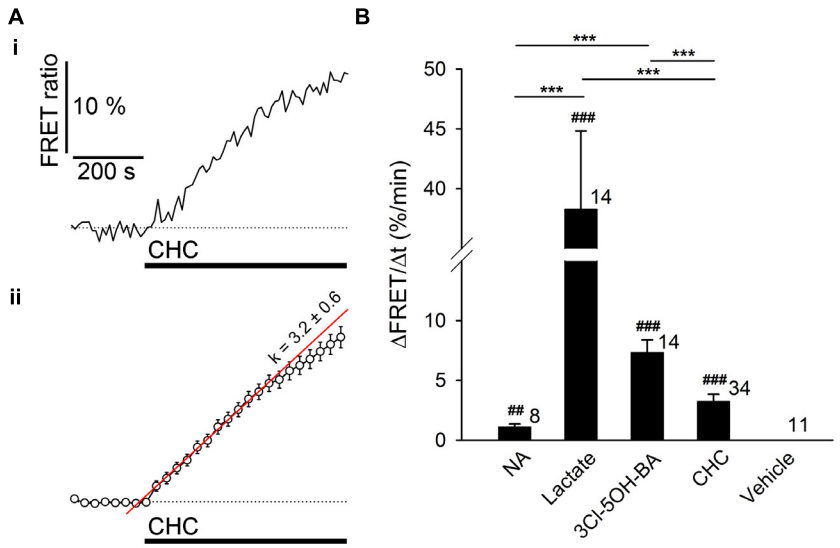

FIGURE 6 | The resting rate of glycolysis and lactate production is modulated by noradrenaline and 3Cl-5OH-BA in astrocytes. **(A)** Representative **(i)** and mean **(ii)** time-course of Laconic FRET ratio signal upon addition of 6 mM CHC. Data are expressed as the percentage of the FRET ratio signal (mTFP/Venus) relative to the baseline ratio values. Note that the increased FRET ratio indicates an increase in $[lactate]_i$. Each data point in **(ii)** represents mean ± s.e.m. The initial rate of change in $[lactate]_i$ was determined by fitting the regression lines to the initial rise of the curves. The regression line in **(ii)** has the form of: $\Delta FRET\ (\%) = k\ (\%/min) \times \Delta t\ (min) + \Delta FRET_0$, where t is time, $\Delta FRET_0$ is $\Delta FRET$ at the time of stimulus, and the k-slope is the initial $\Delta FRET$ rise: $k = 3.2 \pm 0.6$ %/min. **(B)** Comparison of mean maximal initial rates in FRET ratio changes ($\Delta FRET/\Delta t$) upon the addition of NA (200 μM), L-lactate (20 mM), 3Cl-5OH-BA (0.5 mM), CHC (6 mM), and vehicle (control) in astrocytes. Maximal initial rates are expressed as percent change of FRET ratio per minute. Numbers by the error bars depict the number of cells analyzed. $^{***}P < 0.001$ one-way ANOVA comparison between different types of stimuli; $^{\#\#}P < 0.01$, $^{\#\#\#}P < 0.001$ one-sample t-test. Data for every set of experiment was acquired from at least two different animals.

the GPR81 receptor in astrocytes (Lauritzen et al., 2014; Sharma et al., 2015). The main finding of this study is that extracellular L-lactate in astrocytes activates AC, elevates $[cAMP]_i$, and accelerates aerobic glycolysis. Interestingly, by using the selective agonists for the GPR81 receptor, such as 3Cl-5OH-BA (Dvorak et al., 2012; Liu et al., 2012) or Compound 2 (Sakurai et al., 2014), the results revealed that even in the absence of the GPR81 receptor expression in astrocytes from GPR81 KO mice, elevations in $[cAMP]_i$ were still recorded, indicating that in addition to the GPR81 receptors, these agonists activate also a yet unidentified L-lactate receptor-like mechanism.

L-Lactate and Adrenergic Receptor Stimulation Increases $[lactate]_i$ in Astrocytes

Genes associated with aerobic glycolysis are mainly expressed in neocortical areas where neuronal cell plasticity is taking place (Goyal et al., 2014). In these areas, astrocytes are considered the primary site of aerobic glycolysis, and the primary source of L-lactate release. The results of this study demonstrate that the activation of astrocytic receptors by extracellular L-lactate (20 mM) or the GPR81 lactate receptor agonist 3Cl-5OH-BA (0.5 mM) (Dvorak et al., 2012) increases $[lactate]_i$ within 1 min to a relatively high and stable level.

If the L-lactate-mediated increase in $[cAMP]_i$ is present *in vivo* it may contribute to the maintenance of the L-lactate gradient between astrocytes and neurons (Mächler et al., 2016) and also the gradient between the extracellular L-lactate in the brain and in the plasma (Abi-Saab et al., 2002). A positive feedback mechanism involving L-lactate as an extracellular signal that controls L-lactate production and subsequent L-lactate release from astrocytes (**Figure 7**) may be important during neuronal activity, when $[lactate]_i$ may rapidly decline in astrocytes due to its facilitated exit through lactate MCTs and putative ion channels (Sotelo-Hitschfeld et al., 2015) and/or its diffusion through the gap junctions in astroglial syncytia (Hertz et al., 2014). Thus, in the absence of a positive feedback mechanism, the L-lactate concentration gradient may dissipate, reducing the availability of L-lactate as a metabolic fuel for neurons (Barros, 2013; Mosienko et al., 2015) and thereby limiting the support for neural network activity.

Experiments in slices have revealed that optical activation of astrocytes in LC triggers the release of L-lactate from astrocytes, which then excites LC neurons and triggers the widespread release of NA, likely in a receptor-dependent manner involving AC and PKA activation (Tang et al., 2014). It has been proposed that astrocytes also release L-lactate at the axonal varicosities of the noradrenergic neurons, where it facilitates the release of NA from the varicosities (Tang et al., 2014). However, whether NA released from the LC neurons affects astrocyte L-lactate production has not been studied directly.

The real-time $[lactate]_i$ monitoring in this study revealed that AR activation by NA can elicit a sustained increase in

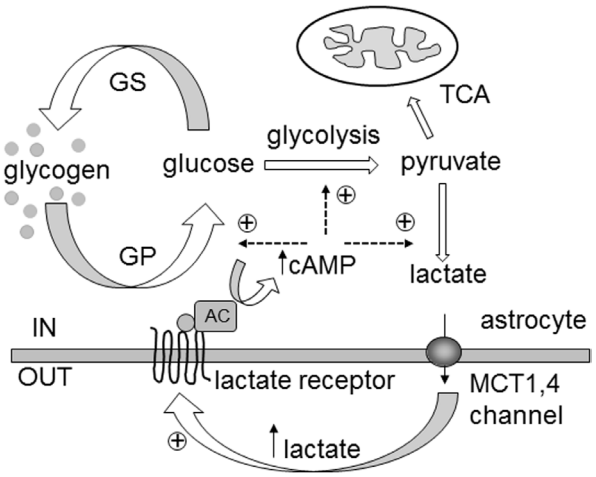

FIGURE 7 | Extracellular L-lactate controls cytosolic lactate synthesis via yet unidentified receptors coupled to adenylate cyclase activity and cytosolic cAMP increase in astrocytes. In the brain, L-lactate is formed in the cytoplasm of astrocytes (IN) and is released through monocarboxylate transporters (MCTs) 1,4 and/or lactate-permeable channels. Extracellularly (OUT), L-lactate can be transported to neighboring cells as a fuel. However, it can also act as a signaling molecule by binding to the L-lactate receptors of neighboring cells, stimulating adenylate cyclase activity (AC) and an increase in cAMP synthesis. Elevated cytosolic cAMP levels facilitate glycogen degradation by activating glycogen phosphorylase (GP) and glycolysis with L-lactate as the end product. In the absence of the L-lactate positive feedback mechanism ("metabolic excitability"), the L-lactate tissue concentration gradient could be dissipated, reducing the availability of L-lactate as a metabolic fuel, when local energy demands, especially in the brain, are high. This model shares similarities with the 'autocrine lactate loop' acting (oppositely) on $[cAMP]_i$ through GPR81 receptor in adipocytes (Ahmed et al., 2010). GS, glycogen synthase; TCA, tricarboxylic acid cycle. Glucose denotes phosphorylated and free glucose.

$[lactate]_i$ in astrocytes, with an average time constant of ∼100 s (Supplementary Figure S2). The increase in $[lactate]_i$ is predominantly a consequence of increased L-lactate production in aerobic glycolysis, although changes in L-lactate fluxes across the plasma membrane or astrocytic consumption of L-lactate in oxidative metabolic pathway could also partly contribute to the new L-lactate steady state levels (San Martin et al., 2013).

The increased $[lactate]_i$ likely leads to L-lactate exiting astrocytes, which, *in vivo*, may back-excite LC neurons and further stimulate NA release (Tang et al., 2014). Such bidirectional communication between astrocytes and neurons may be part of a tissue-coordinated astrocyte activity, which can be studied by monitoring widespread LC-mediated Ca^{2+} signaling in astrocytes in awake-behaving mice *in vivo* (Ding et al., 2013; Paukert et al., 2014). Consistent with this possibility, cultured primary cortical neurons respond to extracellular L-lactate and the GPR81 lactate receptor agonists with a decrease in spontaneous Ca^{2+}-spiking activity that is concentration-dependent, with 50% inhibitory concentration (IC_{50}) of ∼4 mM L-lactate (Bozzo et al., 2013), which is close to the sensitivity of the GPR81 receptor for L-lactate (Liu et al., 2012).

Extracellular L-Lactate-Induced Increase in $[lactate]_i$ Involves Receptor-Like Mediated Adenylate Cyclase Activation and cAMP Production

In astrocytes, similar to the activation of β-ARs (Vardjan et al., 2014; Horvat et al., 2016), extracellular L-lactate (20 mM) and GPR81 lactate receptor agonist 3Cl-5OH-BA (0.5 mM) elevate $[cAMP]_i$ (**Figures 1A,B**), as independently confirmed by monitoring the increase in activity of cAMP effector PKA (**Figures 1D,E**), but do not elevate $[Ca^{2+}]_i$ (data not shown). Thus, extracellular L-lactate in astrocytes likely stimulates a plasma membrane L-lactate sensitive receptor, such as the recently identified GPR81 receptor in brain astrocytes, which was linked to downregulation of cAMP synthesis (Lauritzen et al., 2014). To exclude the possibility that the addition of extracellular L-lactate acidifies the cytoplasm, thus affecting the fluorescence of fluorophores in a FRET nanosensor, especially the fluorescence of YFP (Patterson et al., 2001), which declines with acidification, producing an artifact that can be read as an increase in cAMP, we used two different types of FRET nanosensors to monitor cAMP activity; Epac1-camps (Nikolaev et al., 2004), and AKAR2 (Zhang et al., 2005), which report cAMP activity in opposite directions, as decrease and increase in YFP/CFP ratio, respectively. While in Epac1-camps transfected cells the L-lactate application induced a reduction in the YFP/CFP ratio, AKAR2-transfected cells responded to L-lactate with the increase in YFP/CFP ratio. Since the readouts from the Epac1-camps and AKAR2 YFP/CFP signals are in opposite directions it is highly unlikely that the observed YFP/CFP responses are due to acidification of the cytoplasm and not a consequence of cAMP activity. Furthermore, if the responses in cAMP and PKA activity would simply be due to a pH-dependent artifact, then we would have recorded signals that would be in phase with the application of L-lactate. This was not the case. As the PKA response was significantly delayed, it is more likely that delayed PKA activity is due to an elevation of cAMP, followed by the cAMP-mediated activation of PKA.

Interestingly, in both mouse WT and GPR81 KO astrocytes an increase in $[cAMP]_i$ was detected (**Table 1**), suggesting that the observed effects of L-lactate and 3Cl-5OH-BA on cAMP signaling and metabolism in astrocytes are GPR81 independent. These results indicate the existence of a yet unidentified receptor-like mechanism of L-lactate production, activated with L-lactate as well as with the GPR81 selective agonists, 3Cl-5OH-BA (**Figure 1**) and Compound 2 (**Figure 2**; Sakurai et al., 2014). The unidentified receptor-like mechanism exhibits a relatively low 3Cl-5OH-BA affinity (we could not observe any response using 50 μM concentration) in comparison with the GPR81 lactate receptor (EC_{50} = 17 μM for 3Cl-5OH-BA) (Dvorak et al., 2012). Pretreatment of rat astrocytes with the 50 μM (subeffective) dose of 3Cl-5OH-BA reduced the L-lactate-induced elevations in $[cAMP]_i$, indicating that this GPR81 receptor agonist may share with L-lactate the binding site on a yet unidentified receptor stimulating L-lactate production in astrocytes.

The synthesis of cAMP upon receptor activation is likely achieved via activation of AC, as was suggested for LC neurons, where extracellular L-lactate has been considered to activate AC

and PKA, although the receptor triggering cAMP elevation in LC neurons is unknown (Tang et al., 2014; Mosienko et al., 2015). The application of DDA, an AC inhibitor, reduced the L-lactate-mediated increase in $[cAMP]_i$ and also the 3Cl-5OH-BA-induced increase in $[lactate]_i$ (**Figure 3**). An AC-dependent activity by the 3Cl-5OH-BA-induced increase in $[lactate]_i$ appears to be taking place also in 3T3-L1 and BT474 cells, indicating that the Warburg effect-bearing cells regulate L-lactate synthesis via receptors (Supplementary Table S1).

A 10-fold lower L-lactate concentration (2 mM) did not affect $[cAMP]_i$ or $[glucose]_i$, implying a role of L-lactate receptor-like mechanism *in vivo* only at relatively elevated extracellular L-lactate levels, as likely takes place during exercise (Matsui et al., 2017). During abnormal conditions (e.g., hypoxia, hyperglycemia, seizures) the local resting extracellular L-lactate concentration of 0.1–2 mM in the narrow brain interstices (in humans 5 mM; Abi-Saab et al., 2002) can increase ∼10- to 20-fold to values >10 mM (Barros, 2013; Mosienko et al., 2015). Moreover, L-lactate production in the normal brain might occur in microdomains, which could create higher-than-average local concentrations (Morland et al., 2015; Mosienko et al., 2015).

In a few rat astrocytes (up to 16%, **Table 1**), the addition of 3Cl-5OH-BA, but not AR agonists, resulted in small sustained decreases in $[cAMP]_i$ and PKA activity (**Table 1**), indicating that in these cells, L-lactate preferentially activates receptors coupled to the G_i-proteins to downregulate cAMP, i.e., the coupling originally identified for GPR81 receptor (Ahmed et al., 2010). In mouse WT and GPR81 KO astrocytes, however, the decrease in $[cAMP]_i$ was not detected (**Table 1**). The observed heterogeneity in the recorded L-lactate receptor-mediated cAMP responses may be species specific and/or due to molecular and functional heterogeneity of the astrocytes (Zhang and Barres, 2010), determined by the neuron-specific circuits (Chai et al., 2017).

The time-constants of the increases in $[cAMP]_i$ and $[lactate]_i$ were similar (58 s vs. 60 s, respectively; $P = 0.90$) upon 3Cl-5OH-BA application. However, upon AR activation, the increase in $[cAMP]_i$ was approximately fivefold faster than that for the $[lactate]_i$ increase (20 s vs. 105 s, respectively; $P < 0.001$; Supplementary Figure S2). The observed difference could be due to the distinct molecular coupling mechanisms between the respective receptors and the cAMP pathway generating distinct cAMP pools inside cells (compartmentalized cAMP signaling; Pidoux and Taskén, 2010), but altogether, the results indicate that lactate production depends on cAMP and occurs downstream of cAMP synthesis.

Taken together, these results show that the activation of not only ARs but also L-lactate receptor-like mechanism can accelerate L-lactate production in astrocytes via cAMP signaling, suggesting the existence of a yet unidentified excitatory L-lactate receptor in astrocytes. These findings diverge from the previously reported results in CHO-K1 cells (Cai et al., 2008), primary cortical neurons (Bozzo et al., 2013), homogenized mouse adipose tissue slices (Ahmed et al., 2010), and rat hippocampal slices (Lauritzen et al., 2014). In these tissues L-lactate (presumably via activation of the L-lactate GPR81 receptor) was considered to inhibit cAMP and subsequent L-lactate production.

L-Lactate Receptor-Like Mechanisms Increase Intracellular L-Lactate More Potently Than Adrenergic Receptors

In astrocytes the NA-mediated glycogen breakdown and $[glucose]_i$ increase (Prebil et al., 2011) may regulate the extent of aerobic glycolysis, a metabolic process favored in astrocytes (Gandhi et al., 2009; Barros, 2013). Intracellular $[glucose]_i$ is (i) a function of glucose uptake from the extracellular space, (ii) is affected by glycogen degradation (Prebil et al., 2011), and (iii) involves the activity of glucose-6-phosphatase, present in astrocytes (Ghosh et al., 2005; Sharma et al., 2015), which converts glucose-6-phosphate to free glucose.

Glycogenolysis in astroglial cells is considered to be mainly regulated by β-ARs, although α_2-ARs may also enhance it (Subbarao and Hertz, 1990; Hertz et al., 2010). Consistent with this possibility, the responsiveness of astrocytes to β-AR stimulation was lower than to α-/β-AR agonist NA when $[lactate]_i$ was measured [63% (ISO) and 90% (NA), respectively, **Table 1**]. Upon the addition of 3Cl-5OH-BA, in contrast to adrenergic stimulation, a sustained decrease in $[glucose]_i$ was recorded, indicating that D-glucose is rapidly consumed upon 3Cl-5OH-BA-mediated L-lactate receptor-like mechanism of activation (**Figure 4**). However, extracellular L-lactate triggered only a transient decrease in D-glucose, likely due to its interference with cytoplasmic L-lactate-sensitive enzymes (Costa Leite et al., 2007).

To estimate the extent by which the ARs and L-lactate receptors modulate the rate of aerobic glycolysis, we monitored $[lactate]_i$ at rest in the presence of blocked L-lactate membrane transport. The addition of CHC, an inhibitor of several MCTs, resulted in a persistent increase in $[lactate]_i$ (**Figure 6**). If it is assumed that L-lactate cannot exit cells under these conditions, the putative L-lactate-permeable channels are inactive (Sotelo-Hitschfeld et al., 2015), and L-lactate is not substantially metabolized (Passarella et al., 2008) then the rate of change in $[lactate]_i$ reflects the resting rate of aerobic glycolysis in astrocytes. The addition of NA accelerated the rate of glycolysis to only ∼30% of the resting rate, whereas in the presence of 3Cl-5OH-BA, the glycolytic rate was increased by >600% relative to the NA-induced response (**Figure 6**). Although the effectiveness of the agonists used and their affinities for respective receptors may not be easily compared, these results suggest that L-lactate via receptor-like mechanism activates glycolysis more potently vs. ARs in astrocytes.

The results of this work bring new insights that in astrocytes L-lactate receptor-like mechanisms increase the rate of aerobic glycolysis, which manifests itself in increased $[lactate]_i$. This metabolite can exit astrocytes to further accelerate L-lactate signaling at autocrine and paracrine sites. Hence, designating this process as "metabolic excitability" appears appropriate, as it may provide the means for maintaining a high and stable source of L-lactate levels in astrocytes, as measured *in vivo* (Mächler et al., 2016) and likely contributes to the difference between the brain

extracellular fluid and plasma levels of L-lactate (Abi-Saab et al., 2002).

AUTHOR CONTRIBUTIONS

NV conceived and co-directed the study, performed experiments, analyzed data, and wrote the manuscript. HHC, AH, JV, MMu, STB, KM, and SP performed experiments and analyzed data. MMa and ŠGK performed experiments. MK analyzed data. GH designed and provided custom synthesized Compound 2. LHB and JS-M provided GPR81 KO mouse pups (founder mice from SO's lab). SO generated the GPR81 KO mouse line. RZ conceived and directed the study and wrote the manuscript. All authors read and contributed to the completion of the draft manuscript.

FUNDING

This study was funded by Slovenian Research Agency (P3 310, J3 4051, J3 4146, L3 3654; J3 3236, J3 6790, J3 6789, and J3 7605), the Centre of Excellence for Integrated Approaches in Chemistry and Biology of Proteins (CIPKEBIP), COST Nanomechanics of Intermediate Filament Networks (Nanonet), COST Mouse Ageing, COST CM1207 – GLISTEN, and the Research Council of Norway and the University of Oslo.

ACKNOWLEDGMENTS

The authors thank Drs. W. B. Frommer for providing FLII^{12}Pglu-700μδ6 (Addgene plasmid # 17866), M. Lohse for providing Epac1-camps, Roger Y. Tsien for providing AKAR2, and L. F. Barros for providing Laconic.

SUPPLEMENTARY MATERIAL

The Supplementary Material for this article can be found online at: https://www.frontiersin.org/articles/10.3389/fnmol.2018.00148/full#supplementary-material

REFERENCES

Abi-Saab, W. M., Maggs, D. G., Jones, T., Jacob, R., Srihari, V., Thompson, J., et al. (2002). Striking differences in glucose and lactate levels between brain extracellular fluid and plasma in conscious human subjects: effects of hyperglycemia and hypoglycemia. *J. Cereb. Blood Flow Metab.* 22, 271–279. doi: 10.1097/00004647-200203000-00004

Ahmed, K., Tunaru, S., Tang, C., Muller, M., Gille, A., Sassmann, A., et al. (2010). An autocrine lactate loop mediates insulin-dependent inhibition of lipolysis through GPR81. *Cell Metab.* 11, 311–319. doi: 10.1016/j.cmet.2010.02.012

Barros, L. F. (2013). Metabolic signaling by lactate in the brain. *Trends Neurosci.* 36, 396–404. doi: 10.1016/j.tins.2013.04.002

Bergersen, L., Waerhaug, O., Helm, J., Thomas, M., Laake, P., Davies, A. J., et al. (2001). A novel postsynaptic density protein: the monocarboxylate transporter MCT2 is co-localized with delta-glutamate receptors in postsynaptic densities of parallel fiber-Purkinje cell synapses. *Exp. Brain Res.* 136, 523–534. doi: 10.1007/s002210000600

Börner, S., Schwede, F., Schlipp, A., Berisha, F., Calebiro, D., Lohse, M. J., et al. (2011). FRET measurements of intracellular cAMP concentrations and cAMP analog permeability in intact cells. *Nat. Protoc.* 6, 427–438. doi: 10.1038/nprot.2010.198

Bozzo, L., Puyal, J., and Chatton, J. Y. (2013). Lactate modulates the activity of primary cortical neurons through a receptor-mediated pathway. *PLoS One* 8:e71721. doi: 10.1371/journal.pone.0071721

Brooks, G. A. (2009). Cell-cell and intracellular lactate shuttles. *J. Physiol.* 587, 5591–5600. doi: 10.1113/jphysiol.2009.178350

Bustin, S. A., Benes, V., Garson, J. A., Hellemans, J., Huggett, J., Kubista, M., et al. (2009). The MIQE guidelines: minimum information for publication of quantitative real-time PCR experiments. *Clin. Chem.* 55, 611–622. doi: 10.1373/clinchem.2008.112797

Cai, T. Q., Ren, N., Jin, L., Cheng, K., Kash, S., Chen, R., et al. (2008). Role of GPR81 in lactate-mediated reduction of adipose lipolysis. *Biochem. Biophys. Res. Commun.* 377, 987–991. doi: 10.1016/j.bbrc.2008.10.088

Castillo, X., Rosafio, K., Wyss, M. T., Drandarov, K., Buck, A., Pellerin, L., et al. (2015). A probable dual mode of action for both L- and D-lactate neuroprotection in cerebral ischemia. *J. Cereb. Blood Flow Metab.* 35, 1561–1569. doi: 10.1038/jcbfm.2015.115

Chai, H., Diaz-Castro, B., Shigetomi, E., Monte, E., Octeau, J. C., Yu, X., et al. (2017). Neural circuit-specialized astrocytes: transcriptomic, proteomic, morphological, and functional evidence. *Neuron* 95, 531–549.e9. doi: 10.1016/j.neuron.2017.06.029

Chen, X., Wang, L., Zhou, Y., Zheng, L. H., and Zhou, Z. (2005). "Kiss-and-run" glutamate secretion in cultured and freshly isolated rat hippocampal astrocytes. *J. Neurosci.* 25, 9236–9243. doi: 10.1523/JNEUROSCI.1640-05.2005

Costa Leite, T., Da Silva, D., Guimarães Coelho, R., Zancan, P., and Sola-Penna, M. (2007). Lactate favours the dissociation of skeletal muscle 6-phosphofructo-1-kinase tetramers down-regulating the enzyme and muscle glycolysis. *Biochem. J.* 408, 123–130. doi: 10.1042/BJ20070687

Cowan, C. M., Shepherd, D., and Mudher, A. (2010). Insights from *Drosophila* models of Alzheimer's disease. *Biochem. Soc. Trans.* 38, 988–992. doi: 10.1042/BST0380988

Dienel, G. A., and Cruz, N. F. (2016). Aerobic glycolysis during brain activation: adrenergic regulation and influence of norepinephrine on astrocytic metabolism. *J. Neurochem.* 138, 14–52. doi: 10.1111/jnc.13630

Ding, F., O'donnell, J., Thrane, A. S., Zeppenfeld, D., Kang, H., Xie, L., et al. (2013). α1-Adrenergic receptors mediate coordinated Ca2+ signaling of cortical astrocytes in awake, behaving mice. *Cell Calcium* 54, 387–394. doi: 10.1016/j.ceca.2013.09.001

Dong, J. H., Wang, Y. J., Cui, M., Wang, X. J., Zheng, W. S., Ma, M. L., et al. (2017). Adaptive activation of a stress response pathway improves learning and memory through Gs and beta-arrestin-1-regulated lactate metabolism. *Biol. Psychiatry* 81, 654–670. doi: 10.1016/j.biopsych.2016.09.025

During, M. J., Fried, I., Leone, P., Katz, A., and Spencer, D. D. (1994). Direct measurement of extracellular lactate in the human hippocampus during spontaneous seizures. *J. Neurochem.* 62, 2356–2361. doi: 10.1046/j.1471-4159.1994.62062356.x

Dvorak, C. A., Liu, C., Shelton, J., Kuei, C., Sutton, S. W., Lovenberg, T. W., et al. (2012). Identification of hydroxybenzoic acids as selective lactate receptor (GPR81) agonists with antilipolytic effects. *ACS Med. Chem. Lett.* 3, 637–639. doi: 10.1021/ml3000676

Gandhi, G. K., Cruz, N. F., Ball, K. K., and Dienel, G. A. (2009). Astrocytes are poised for lactate trafficking and release from activated brain and for supply of glucose to neurons. *J. Neurochem.* 111, 522–536. doi: 10.1111/j.1471-4159.2009.06333.x

Gao, V., Suzuki, A., Magistretti, P. J., Lengacher, S., Pollonini, G., Steinman, M. Q., et al. (2016). Astrocytic β2-adrenergic receptors mediate hippocampal long-term memory consolidation. *Proc. Natl. Acad. Sci. U.S.A.* 113, 8526–8531. doi: 10.1073/pnas.1605063113

Ghosh, A., Cheung, Y. Y., Mansfield, B. C., and Chou, J. Y. (2005). Brain contains a functional glucose-6-phosphatase complex capable of endogenous glucose production. *J. Biol. Chem.* 280, 11114–11119. doi: 10.1074/jbc.M410894200

Gordon, G., Mulligan, S., and Macvicar, B. (2007). Astrocyte control of the cerebrovasculature. *Glia* 55, 1214–1221. doi: 10.1002/glia.20543

Gordon, G. R., Choi, H. B., Rungta, R. L., Ellis-Davies, G. C., and Macvicar, B. A. (2008). Brain metabolism dictates the polarity of astrocyte control over arterioles. *Nature* 456, 745–749. doi: 10.1038/nature07525

Goyal, M. S., Hawrylycz, M., Miller, J. A., Snyder, A. Z., and Raichle, M. E. (2014). Aerobic glycolysis in the human brain is associated with development and neotenous gene expression. *Cell Metab.* 19, 49–57. doi: 10.1016/j.cmet.2013.11.020

Halim, N. D., Mcfate, T., Mohyeldin, A., Okagaki, P., Korotchkina, L. G., Patel, M. S., et al. (2010). Phosphorylation status of pyruvate dehydrogenase distinguishes metabolic phenotypes of cultured rat brain astrocytes and neurons. *Glia* 58, 1168–1176. doi: 10.1002/glia.20996

Hertz, L., Gibbs, M. E., and Dienel, G. A. (2014). Fluxes of lactate into, from, and among gap junction-coupled astrocytes and their interaction with noradrenaline. *Front. Neurosci.* 8:261. doi: 10.3389/fnins.2014.00261

Hertz, L., Lovatt, D., Goldman, S. A., and Nedergaard, M. (2010). Adrenoceptors in brain: cellular gene expression and effects on astrocytic metabolism and [Ca(2+)]i. *Neurochem. Int.* 57, 411–420. doi: 10.1016/j.neuint.2010.03.019

Horvat, A., Zorec, R., and Vardjan, N. (2016). Adrenergic stimulation of single rat astrocytes results in distinct temporal changes in intracellular Ca(2+) and cAMP-dependent PKA responses. *Cell Calcium* 59, 156–163. doi: 10.1016/j.ceca.2016.01.002

Lauritzen, K. H., Morland, C., Puchades, M., Holm-Hansen, S., Hagelin, E. M., Lauritzen, F., et al. (2014). Lactate receptor sites link neurotransmission, neurovascular coupling, and brain energy metabolism. *Cereb. Cortex* 24, 2784–2795. doi: 10.1093/cercor/bht136

Lee, Y., Morrison, B. M., Li, Y., Lengacher, S., Farah, M. H., Hoffman, P. N., et al. (2012). Oligodendroglia metabolically support axons and contribute to neurodegeneration. *Nature* 487, 443–448. doi: 10.1038/nature11314

Leibiger, C., Kosyakova, N., Mkrtchyan, H., Glei, M., Trifonov, V., and Liehr, T. (2013). First molecular cytogenetic high resolution characterization of the NIH 3T3 cell line by murine multicolor banding. *J. Histochem. Cytochem.* 61, 306–312. doi: 10.1369/0022155413476868

Liu, C., Kuei, C., Zhu, J., Yu, J., Zhang, L., Shih, A., et al. (2012). 3,5-Dihydroxybenzoic acid, a specific agonist for hydroxycarboxylic acid 1, inhibits lipolysis in adipocytes. *J. Pharmacol. Exp. Ther.* 341, 794–801. doi: 10.1124/jpet.112.192799

Liu, C., Wu, J., Zhu, J., Kuei, C., Yu, J., Shelton, J., et al. (2009). Lactate inhibits lipolysis in fat cells through activation of an orphan G-protein-coupled receptor, GPR81. *J. Biol. Chem.* 284, 2811–2822. doi: 10.1074/jbc.M806409200

Mächler, P., Wyss, M. T., Elsayed, M., Stobart, J., Gutierrez, R., Von Faber-Castell, A., et al. (2016). In Vivo evidence for a lactate gradient from astrocytes to neurons. *Cell Metab.* 23, 94–102. doi: 10.1016/j.cmet.2015.10.010

Matsui, T., Omuro, H., Liu, Y. F., Soya, M., Shima, T., Mcewen, B. S., et al. (2017). Astrocytic glycogen-derived lactate fuels the brain during exhaustive exercise to maintain endurance capacity. *Proc. Natl. Acad. Sci. U.S.A.* 114, 6358–6363. doi: 10.1073/pnas.1702739114

Morland, C., Andersson, K. A., Haugen, O. P., Hadzic, A., Kleppa, L., Gille, A., et al. (2017). Exercise induces cerebral VEGF and angiogenesis via the lactate receptor HCAR1. *Nat. Commun.* 8:15557. doi: 10.1038/ncomms15557

Morland, C., Lauritzen, K. H., Puchades, M., Holm-Hansen, S., Andersson, K., Gjedde, A., et al. (2015). The lactate receptor, G-protein-coupled receptor 81/hydroxycarboxylic acid receptor 1: expression and action in brain. *J. Neurosci. Res.* 93, 1045–1055. doi: 10.1002/jnr.23593

Mosienko, V., Teschemacher, A. G., and Kasparov, S. (2015). Is L-lactate a novel signaling molecule in the brain? *J. Cereb. Blood Flow Metab.* 35, 1069–1075. doi: 10.1038/jcbfm.2015.77

Nikolaev, V. O., Bünemann, M., Hein, L., Hannawacker, A., and Lohse, M. J. (2004). Novel single chain cAMP sensors for receptor-induced signal propagation. *J. Biol. Chem.* 279, 37215–37218. doi: 10.1074/jbc.C400302200

Osnes, J. B., and Hermansen, L. (1972). Acid-base balance after maximal exercise of short duration. *J. Appl. Physiol.* 32, 59–63. doi: 10.1152/jappl.1972.32.1.59

Passarella, S., De Bari, L., Valenti, D., Pizzuto, R., Paventi, G., and Atlante, A. (2008). Mitochondria and L-lactate metabolism. *FEBS Lett.* 582, 3569–3576. doi: 10.1016/j.febslet.2008.09.042

Patterson, G., Day, R. N., and Piston, D. (2001). Fluorescent protein spectra. *J. Cell Sci.* 114, 837–838.

Paukert, M., Agarwal, A., Cha, J., Doze, V. A., Kang, J. U., and Bergles, D. E. (2014). Norepinephrine controls astroglial responsiveness to local circuit activity. *Neuron* 82, 1263–1270. doi: 10.1016/j.neuron.2014.04.038

Pidoux, G., and Taskén, K. (2010). Specificity and spatial dynamics of protein kinase A signaling organized by A-kinase-anchoring proteins. *J. Mol. Endocrinol.* 44, 271–284. doi: 10.1677/JME-10-0010

Prebil, M., Vardjan, N., Jensen, J., Zorec, R., and Kreft, M. (2011). Dynamic monitoring of cytosolic glucose in single astrocytes. *Glia* 59, 903–913. doi: 10.1002/glia.21161

Rinholm, J. E., and Bergersen, L. H. (2012). Neuroscience: the wrap that feeds neurons. *Nature* 487, 435–436. doi: 10.1038/487435a

Roland, C. L., Arumugam, T., Deng, D., Liu, S. H., Philip, B., Gomez, S., et al. (2014). Cell surface lactate receptor GPR81 is crucial for cancer cell survival. *Cancer Res.* 74, 5301–5310. doi: 10.1158/0008-5472.CAN-14-0319

Ruijter, J. M., Ramakers, C., Hoogaars, W. M., Karlen, Y., Bakker, O., Van Den Hoff, M. J., et al. (2009). Amplification efficiency: linking baseline and bias in the analysis of quantitative PCR data. *Nucleic Acids Res.* 37:e45. doi: 10.1093/nar/gkp045

Sakurai, T., Davenport, R., Stafford, S., Grosse, J., Ogawa, K., Cameron, J., et al. (2014). Identification of a novel GPR81-selective agonist that suppresses lipolysis in mice without cutaneous flushing. *Eur. J. Pharmacol.* 727, 1–7. doi: 10.1016/j.ejphar.2014.01.029

San Martin, A., Ceballo, S., Ruminot, I., Lerchundi, R., Frommer, W. B., and Barros, L. F. (2013). A genetically encoded FRET lactate sensor and its use to detect the Warburg effect in single cancer cells. *PLoS One* 8:e57712. doi: 10.1371/journal.pone.0057712

Schwartz, J., and Wilson, D. (1992). Preparation and characterization of type 1 astrocytes cultured from adult rat cortex, cerebellum, and striatum. *Glia* 5, 75–80. doi: 10.1002/glia.440050111

Sharma, K., Schmitt, S., Bergner, C. G., Tyanova, S., Kannaiyan, N., Manrique-Hoyos, N., et al. (2015). Cell type- and brain region-resolved mouse brain proteome. *Nat. Neurosci.* 18, 1819–1831. doi: 10.1038/nn.4160

Sotelo-Hitschfeld, T., Niemeyer, M. I., Mächler, P., Ruminot, I., Lerchundi, R., Wyss, M. T., et al. (2015). Channel-mediated lactate release by K^+-stimulated astrocytes. *J. Neurosci.* 35, 4168–4178. doi: 10.1523/JNEUROSCI.5036-14.2015

Staubert, C., Broom, O. J., and Nordstrom, A. (2015). Hydroxycarboxylic acid receptors are essential for breast cancer cells to control their lipid/fatty acid metabolism. *Oncotarget* 6, 19706–19720. doi: 10.18632/oncotarget.3565

Stenovec, M., Trkov, S., Lasiè, E., Terzieva, S., Kreft, M., Rodríguez Arellano, J. J., et al. (2016). Expression of familial Alzheimer disease presenilin 1 gene attenuates vesicle traffic and reduces peptide secretion in cultured astrocytes devoid of pathologic tissue environment. *Glia* 64, 317–329. doi: 10.1002/glia.22931

Subbarao, K. V., and Hertz, L. (1990). Effect of adrenergic agonists on glycogenolysis in primary cultures of astrocytes. *Brain Res.* 536, 220–226. doi: 10.1016/0006-8993(90)90028-A

Takanaga, H., Chaudhuri, B., and Frommer, W. B. (2008). GLUT1 and GLUT9 as major contributors to glucose influx in HepG2 cells identified by a high sensitivity intramolecular FRET glucose sensor. *Biochim. Biophys. Acta* 1778, 1091–1099. doi: 10.1016/j.bbamem.2007.11.015

Tang, F., Lane, S., Korsak, A., Paton, J. F., Gourine, A. V., Kasparov, S., et al. (2014). Lactate-mediated glia-neuronal signalling in the mammalian brain. *Nat. Commun.* 5:3284. doi: 10.1038/ncomms4284

Tuomi, J. M., Voorbraak, F., Jones, D. L., and Ruijter, J. M. (2010). Bias in the Cq value observed with hydrolysis probe based quantitative PCR can be corrected with the estimated PCR efficiency value. *Methods* 50, 313–322. doi: 10.1016/j.ymeth.2010.02.003

Vander Heiden, M. G., Cantley, L. C., and Thompson, C. B. (2009). Understanding the Warburg effect: the metabolic requirements of cell proliferation. *Science* 324, 1029–1033. doi: 10.1126/science.1160809

Vardjan, N., Kreft, M., and Zorec, R. (2014). Dynamics of β-adrenergic/cAMP signaling and morphological changes in cultured astrocytes. *Glia* 62, 566–579. doi: 10.1002/glia.22626

Yang, J., Ruchti, E., Petit, J. M., Jourdain, P., Grenningloh, G., Allaman, I., et al. (2014). Lactate promotes plasticity gene expression by potentiating NMDA signaling in neurons. *Proc. Natl. Acad. Sci. U.S.A.* 111, 12228–12233. doi: 10.1073/pnas.1322912111

Zhang, J., Hupfeld, C. J., Taylor, S. S., Olefsky, J. M., and Tsien, R. Y. (2005). Insulin disrupts beta-adrenergic signalling to protein kinase A in adipocytes. *Nature* 437, 569–573. doi: 10.1038/nature04140

Zhang, Y., and Barres, B. A. (2010). Astrocyte heterogeneity: an underappreciated topic in neurobiology. *Curr. Opin. Neurobiol.* 20, 588–594. doi: 10.1016/j.conb.2010.06.005

Zhang, Y., Chen, K., Sloan, S. A., Bennett, M. L., Scholze, A. R., O'keeffe, S., et al. (2014). An RNA-sequencing transcriptome and splicing database of glia, neurons, and vascular cells of the cerebral cortex. *J. Neurosci.* 34, 11929–11947. doi: 10.1523/JNEUROSCI.1860-14.2014

Conflict of Interest Statement: The authors declare that the research was conducted in the absence of any commercial or financial relationships that could be construed as a potential conflict of interest.

frontiers in Molecular Neuroscience

ORIGINAL RESEARCH
published: 15 March 2018
doi: 10.3389/fnmol.2018.00057

Lipoprotein Lipase Is a Feature of Alternatively-Activated Microglia and May Facilitate Lipid Uptake in the CNS During Demyelination

Kimberley D. Bruce[1], Sachi Gorkhali[1], Katherine Given[2], Alison M. Coates[3], Kristen E. Boyle[4], Wendy B. Macklin[2] and Robert H. Eckel[1]*

[1]*Division of Endocrinology, Metabolism, & Diabetes, Department of Medicine, University of Colorado Denver Anschutz Medical Campus, Aurora, CO, United States,* [2]*Department of Cell and Developmental Biology, University of Colorado School of Medicine, Aurora, CO, United States,* [3]*School of Health Sciences, Sansom Institute for Health Research, University of South Australia, Adelaide, SA, Australia,* [4]*Department of Pediatrics, Section of Nutrition, University of Colorado School of Medicine, Aurora, CO, United States*

Severe demyelinating disorders of the central nervous system (CNS) such as multiple sclerosis (MS), can be devastating for many young lives. To date, the factors resulting in poor remyelination and repair are not well understood, and reparative therapies that benefit MS patients have yet to be developed. We have previously shown that the activity and abundance of Lipoprotein Lipase (LPL)—the rate-limiting enzyme in the hydrolysis of triglyceride-rich lipoproteins—is increased in Schwann cells and macrophages following nerve crush injury in the peripheral nervous system (PNS), suggesting that LPL may help scavenge myelin-derived lipids. We hypothesized that LPL may play a similar role in the CNS. To test this, mice were immunized with $MOG_{35–55}$ peptide to induce experimental allergic encephalomyelitis (EAE). LPL activity was increased ($p < 0.05$) in the brain at 30 days post-injection, coinciding with partial remission of clinical symptoms. Furthermore, LPL abundance and activity was up-regulated ($p < 0.05$) at the transition between de- and re-myelination in lysolecithin-treated *ex vivo* cerebellar slices. Since microglia are the key immune effector cells of the CNS we determined the role of LPL in microglia. Lipid uptake was decreased ($p < 0.001$) in LPL-deficient BV-2 microglial cells compared to WT. In addition, LPL-deficient cells showed dramatically reduced expression of anti-inflammatory markers, YM1 (−22 fold, $p < 0.001$), and arginase 1 (Arg1; −265 fold, $p < 0.001$) and increased expression of pro-inflammatory markers, such as iNOS compared to WT cells (+53 fold, $p < 0.001$). This suggests that LPL is a feature of reparative microglia, further supported by the metabolic and inflammatory profile of LPL-deficient microglia. Taken together, our data strongly suggest that LPL expression is a novel feature of a microglial phenotype that supports remyelination and repair through the clearance of lipid debris. This mechanism may be exploited to develop future reparative therapies for MS and primary neurodegenerative disorders (Alzheimer's disease (AD) and Parkinson's disease).

Keywords: lipoprotein lipase (LPL), microglia, multiple sclerosis, myelination, lipid metabolism

OPEN ACCESS

Edited by:
Vladimir Parpura,
University of Alabama at Birmingham, United States

Reviewed by:
Björn Spittau,
Universitätsmedizin Rostock, Germany
Xiaolai Zhou,
Cornell University, United States

****Correspondence:***
Kimberley D. Bruce
kimberley.bruce@ucdenver.edu

Received: *22 November 2017*
Accepted: *12 February 2018*
Published: *15 March 2018*

Citation:
Bruce KD, Gorkhali S, Given K, Coates AM, Boyle KE, Macklin WB and Eckel RH (2018) Lipoprotein Lipase Is a Feature of Alternatively-Activated Microglia and May Facilitate Lipid Uptake in the CNS During Demyelination. Front. Mol. Neurosci. 11:57. doi: 10.3389/fnmol.2018.00057

INTRODUCTION

Multiple sclerosis (MS) is the most common cause of neurological disability in young adults, affecting approximately 2.3 million people worldwide. The majority of MS patients show a relapsing-remitting (RR-MS) clinical phenotype, in which oligodendrocyte precursor cells (OPCs) attempt to remyelinate areas of myelin damage. However, as the disease progresses these attempts fail, leading to severe secondary progressive MS (P-MS; Antel et al., 2012). Despite recent advances in our understanding of the pathophysiology of MS, the factors resulting in poor remyelination and repair are not well understood. Consequently, much needed reparative therapies that benefit MS patients have yet to be developed.

Microglia are the key immune effector cells of the central nervous system (CNS), where they have essential functions such as synaptic pruning by engulfment of neuronal terminals (Hong and Stevens, 2016), and phagocytosis of dying cells and myelin debris (Ransohoff and Perry, 2009). CNS microglia have been repeatedly implicated in the pathophysiology of MS (Ransohoff and El Khoury, 2015). On one hand, CNS microglia may be considered "classically activated" and be associated with the production of neurotoxic molecules and pro-inflammatory cytokines that are detrimental to the repair processes (Becher et al., 2001; Heppner et al., 2005). In contrast, "alternatively activated" reparative microglia provide neurotrophic and immunosuppressive factors that counteract pathological processes and may help facilitate remyelination (Schwartz and Moalem, 2001; Hohlfeld, 2008). Although the plethora of intermediate microglial phenotypes associated within a disease process make it difficult to categorize microglial sub-populations into defined activation states, it is a useful starting point to investigate the basic mechanisms by which microglia participate in demyelination and remyelination. In MS, appropriately activated microglia may help clear debris after myelin damage (Lampron et al., 2015), expedite extracellular matrix deposition, facilitate regeneration, and offer trophic support to OPCs (Varin and Gordon, 2009). In support of this notion, when debris clearance by microglia is impeded, regeneration is delayed (Neumann et al., 2009). However, the microglial factors that actively facilitate these processes are unknown.

In peripheral tissues such as adipose tissue and skeletal/cardiac muscle the canonical function of lipoprotein lipase (LPL)—hydrolysis of triglyceride-rich lipoproteins—is well defined. However, the role of LPL in cells of the CNS is not well understood. Nonetheless, previous work from our laboratory and others have shown that LPL is expressed in several regions of the nervous system including the brain, spinal cord and peripheral nerves, with the highest expression observed in the hippocampus and spinal cord (Eckel and Robbins, 1984; Goldberg et al., 1989; Bessesen et al., 1993). Our studies show that in the peripheral nervous system (PNS), LPL is expressed in Schwann cells, macrophages, and dorsal root ganglia neurons, and its abundance and activity is increased following nerve crush injury (Huey et al., 2002; Nunes and Sousa, 2008). This increase in LPL is associated with macrophage infiltration, suggesting that LPL may be part of an acute response to scavenge and reutilize myelin-derived lipids in degenerating peripheral nerves (Huey et al., 2002). However, this has yet to be empirically determined.

A number of recent reports have highlighted LPL as a key feature of reparative CNS microglia. Single cell analysis of disease-associated-microglia (DAM) in a murine model of Alzheimer's disease (AD), shows that LPL is markedly increased in a unique microglial sub-type associated with phagocytosis and protection in advanced stages of AD (Keren-Shaul et al., 2017). In addition, in a cuprizone model of demyelination, LPL gene expression was elevated during demyelination, and tailed-off once remyelination was complete, suggesting that LPL is novel feature of a microglial phenotype that actively supports remyelination and repair (Olah et al., 2012). Despite these important observations the mechanisms underlying the role of LPL in CNS microglia have not been determined.

Here, we hypothesize that LPL may support repair through the clearance of myelin-derived lipids. In the current study we utilize *in vivo*, *ex vivo* and *in vitro* systems to demonstrate that LPL is increased during the onset of remyelination, is associated with an anti-inflammatory reparative microglial phenotype, and may facilitate the uptake of myelin-derived lipids in the CNS.

MATERIALS AND METHODS

Animals

This study was carried out in accordance with University of Colorado Institutional Animal Care and Use Committee (IACUC) guidelines IACUC for animal use, which are in agreement with the NIH Guide for the Care and Use of Laboratory Animals. Animal protocols were approved by the University of Colorado IACUC. Male C57Bl/6J wild-type mice 8–10 weeks-old were obtained from Jackson Labs (Bar Harbor, Maine, ME, USA). Mice were individually housed and maintained at ∼20°C with a 12-h light/dark cycle and given unrestricted access to standard laboratory diet (Diet 8640; Harlan Teklad, Madison, WI, USA) and water. Paralyzed mice were afforded easier access to food and water to prevent dehydration.

Antigens

The peptide used in this study was the immunodominant $MOG_{35–55}$ peptide (MEVGWYRSPFSRVVHLYRNGK; Mendel et al., 1995). The purity was assessed by HPLC (>97% pure) and amino acid composition was verified by mass spectrometry (Peptides International, Louisville, KY, USA). $MOG_{35–55}$ peptide batches for *in vivo* work were all from one preparation. They were stored insoluble until required and then dissolved in saline to a concentration of 150 μg/μl. The unused portions were stored at 4°C for a maximum of 3 months.

Induction of Experimental Autoimmune Encephalitis (EAE)

Mice were injected subcutaneously at two sites on the femoral region with 200 μl of a mixture of $MOG_{35–55}$ peptide emulsified 1:1 with Freund's complete adjuvant (Difco Laboratories, Detroit, MI, USA). MOG treated mice were also boosted

with pertussis toxin (List Laboratories, Campbell, CA, USA; 200 ng) I.P. on both the day of injection and also 48 h later. Control mice were injected with equal volumes of CFA and given saline instead of pertussis toxin. Tissues were harvested at days 10, 20, 30 and 60 post injection after the animals had been fasted for 4 h before being anesthetized with Avertin (2,2,2-tribromoethanol, 32 mg; Aldrich, Milwaukee, WI, USA).

Clinical Evaluation

Individual mice were observed daily for clinical signs of disease for up to 60 days after immunization. Mice were scored according to the following scale: 0, no detectable signs of experimental allergic encephalomyelitis (EAE); 0.5, incomplete tail paralysis; 1, complete limp tail; 2, hind limb weakness and unsteady gait; 3, complete hind limb paralysis; 4, total paralysis of both forelimbs and hind limbs; 5, moribund; 6, death (Okuda et al., 2002). Body weights and food intake was also measured daily. The data were plotted as daily mean clinical score for all animals in a particular treatment group.

General Cell Culture Conditions and Reagents

Immortalized BV-2 murine microglia cells were kindly donated by Dr. Peter Grace (University of Colorado, Boulder). BV-2 cells were grown in Dulbecco's modified Eagle's medium (DMEM) containing 10% fetal bovine serum (FBS) and 1% penicillin/streptomycin (P/S) and maintained at 37°C with 5% CO_2 (unless otherwise stated). Cells were grown to 70%–90% confluency for all experiments (unless otherwise specified).

LPL Targeting by shRNA

LPL was knocked down (KD) in BV-2 microglia using shRNA targeting, as previously described (Libby et al., 2015). In brief, for stable KD of LPL, 12 μg of control (202) or LPL shRNA (553) lentiviral vector was transfected into HEK 293FT cells along with 10.8 μg pΔ8.9 and 1.2 μg VSV-G using 45 μL Lipofectamine 2000. Virus was packaged for 48 h in 6 mL media, and two rounds of BV-2 transduction were performed. Stably-transduced cells were then selected for 3 days by growth in medium containing 5 μg/mL puromycin.

Real-Time RT PCR

Total RNA was isolated from BV-2 cells using RNeasy Plus Mini Kit (Qiagen, Valencia, CA, USA) according to the manufacturer's instructions. cDNA was prepared from 1 μg of total RNA using verso cDNA synthesis kit (Thermo Scientific, Lithuania). Relative gene expression levels quantified by real-time PCR using SYBR Select Master Mix (Applied Biosystems, Foster City, CA, USA). Primers were designed using the NCBI primer-blast tool and specific primers were designed to cross exon boundaries where available. The sequences for all primers used in the study are shown in **Table 1**. All PCR was performed with the following cycling conditions: 50°C for 2 min, 95°C for 10 min, followed by 40 cycles of 95°C for 15 s and 60 for 1 min using the StepOnePlus instrument (Applied Biosystem, Foster City, CA, USA) with complementary StepOne™ Software v2.3. Comparative Ct method was used to determine relative target gene expression and data were normalized to an average of the references genes Ubc and GAPDH.

Western Blots

BV-2 cells were grown to 90% confluency and total protein was harvested using RIPA buffer (150 nM NaCl, 1% Triton X-100, 0.5% Sodium Deoxycholate, 0.1% SDS, 50 mM Tris pH 8.0, and Complete Protease Inhibitor Cocktail). Insoluble cell debris were removed by centrifugation, and protein containing supernatants were retained. Protein quantification was performed using the Peirce™ BCA protein Assay kit (Thermo). Twenty-five microgram of total protein extracts were run on 12% Separating Gel and transferred to nitrocellulose membrane. The membrane was blocked in skim milk and incubated with a proprietary anti-mouse anti-LPL primary antibody raised in rabbit at a concentration of 3 μg/ml 397-1 (397-1, NeoBiolab, Cambridge, MA, USA) and 1 μg/ml mouse anti-GAPDH (MAB374, Millipore, Billerica, MA, USA) overnight at 4°C. Membranes were then incubated with secondary antibodies IRDye 800RD goat anti-rabbit and IRDye 680RD donkey anti-mouse (Li-Cor, Nebraska, NE, USA) at 1:10,000 dilution. Protein bands were visualized using the Li-COR Odyssey with complementary software (Image studio).

LPL Enzymatic Activity

The enzymatic activity of cell-surface heparin-released LPL was measured using a phospholipid (PL)/^{3}H-triolein substrate with human serum as a source of ApoC2 as described previously (Jensen et al., 2008).

LPS Stimulation

BV-2-553 and BV-2-202 and primary adult microglia were stimulated with 1 μg/ml lipopolysaccharide (LPS) in DMEM containing 1% FBS and 1% P/S media for 24 h. Gene expression and LPL activity assays were then conducted.

Lipid Uptake Experiments

Lipid Uptake Experiments were performed as previously described (Libby et al., 2015), with limited modifications. The assay was performed by preparing a synthetic PL/TG emulsion containing a ^{3}H triolein tracer. The emulsion was prepared by combining and sonicating the following: 5 mg ^{1}H triolein, 0.25 mg L-phosphatidylcholine, a trace amount of ^{3}H triolein (12.5 μCi total) tracer (NET431001MC, Perkin Elmer, Waltham, MA, USA), 0.9 mL water, 2 mL 1 M tris–HCl (pH 8.0), 800 μL FFA-free BSA (MP Biomedical), and 300 μL KRP. After sonication, the substrate was diluted into DMEM to a final concentration of 50 μM, and 100 μM triolein. Purified human ApoC2 (MyBioSource, SanDiego, CA, USA) was added to a final concentration of 5 μg/mL. Substrate was applied to over-night serum-starved BV-2-553 and BV-2-202 cells for 2 h. Cells were washed with 0.1% FFA-free BSA and lysed in 1 mL of RIPA buffer. Eight-hundred microliter of each lysis fraction was subjected to scintillation counting, while the rest was used for protein normalization.

TABLE 1 | Primer Sequences.

Gene	Accession	Forward	Reverse
LPL	NM_008509	ATGGATGGACGGTAACGGGAATGT	TGGATAATGTTGCTGGGCCCGATA
Arg1	NM_007482.3	GGTCTGTGGGGAAAGCCAAT	AACTGCCAGACTGTGGTCTC
YM1	NM_009892.3	GTACCCTGGGTCTCGAGGAA	CCTTGGAATGTCTTTCTCCACAG
iNOS	NM_010927.4	GGTGAAGGGACTGAGCTGTT	ACGTTCTCCGTTCTCTTGCAG
IGF-1	NM_010512.5	CTCAGAAGTCCCCGTCCCTA	ATTTTCTGCTCCGTGGGAGG
CCL3	NM_011337.2	CCATATGGAGCTGACACCCC	TCAGGAAAATGACACCTGGCT
IL-6	NM_031168.2	CTCTGCAAGAGACTTCCATCCA	GACAGGTCTGTTGGGAGTGG
IL-12	NM_001159424.2	TTCTCACCGTGCACATCCAA	GAGGAGGTAGCGTGATTGACA
MSR1	NM_031195.2	GGGAGTGTAGGCGGATCAAG	ATAGTAGGGTGCTCTGCCCA
CD36	NM_001159558.1	AGAATTCTCAGCTGCTCCGC	ACACATTTCAGAAGGCAGCAAC
VLDLR	NM_013703.2	TCAACTGCCCTTCTCGAACC	AGCCATCAACACAGTCTCGG
LDLR	NM_010700.3	CCAATCGACTCACGGGTTCA	TCACACCAGTTCACCCCTCT

Uptake of DiI Labeled Liposomes

Synthetic PL/TG chylomicrons were prepared as described above in the absence of radiolabeled triolein. PL containing vesicles were prepared by drying an 80:20 molar ratio of phosphatidylcholine (PC, Avanti) and phosphatidylserine (PS, Avanti) under nitrogen. HBS was added to the dried lipid for 1 h prior to sonication. Ten microliter of a 3 mg/ml solution of 1′-dioctadecyl-3,3,3′3′-tetramethylindocarbocyanine perchlorate (DiI) was added to 1 ml of either SC's or PL vesicles and incubated in the dark for 10 min at 37°C. Free label was removed with ultracentrifugation at 24,000 *g* for 10 min. After resuspension in sterile PBS, labeled liposomes were added to cells for 16 h (overnight) at a final concentration of 250 μg/ml.

Conditioned Media Experiments

Conditioned media (CM) was harvested from either BV-2-553 or BV-2-202 cells grown in DMEM containing 1% FBS for 72 h reaching 90% confluency. Following aspiration, the media was briefly centrifuged to remove cellular debris, and media was either used immediately for experiments or flash frozen and stored at −80°C.

Neuro-Discovery Array

Semi-quantitative analysis of cytokines and cell signaling proteins from BV-2-CM was performed using the RayBio® C-series Mouse Neuro Discovery Array C1 (RayBiotech, Norcross, GA, USA) according to manufacturer's instructions. In brief, membranes were incubated with 1 ml of CM (described above) overnight at 4°C, while the biotinylated antibody and streptavidin incubation steps were performed at 2 h at room temperature (RT). The array was then visualized using chemiluminescence detection.

Cerebellar Slice Culture, Lysolecithin and Conditioned Media Treatment

Sagittal cerebellar slices (300 μm) were prepared from PLP-eGFP mice (Mallon et al., 2002) at P10–P12 and cultured on MilliCell 0.4 μm membrane inserts (Millipore, Billerica, MA, USA) for 7 days in slice media (25% HBSS, 25% heat-inactivated horse serum, 50% MEM, 125 mM HEPES, 28 mM D-Glucose, 2 mM L-Glutamine; Sheridan and Dev, 2012). Slices were incubated at 37°C at 5% CO_2 and slice media was changed within 24 h after preparation, then every 3–4 days following. Lysolecithin (Lyso; Sigma) was prepared as a 5 mg/ml stock and stored at −20°C until use. To prepare a working solution, lysolecithin stock was diluted in slice media at 0.5 mg/ml and sterile filtered. Treatments (Slice media or lysolecithin) were applied both on top (50 μl) and below (250 μl) the membrane insert that contained the slice for 17 h at 37°C at 5% CO_2. After 17 h, slices were washed twice with slice media and then incubated in control media or CM from BV-2 microglia.

Slice Fixation and Immunostaining

After treatment, cerebellar slices were rinsed twice with PBS and fixed in 4% paraformaldehyde in PBS for 20 min. For immunohistochemistry, slices were rinsed in PBS and permeabilized in 1.5% or 10% (for myelin proteins) Triton X-100 in PBS for 20 min. Slices were rinsed, blocked with 5% normal donkey serum (NDS) in PBSTx (0.3%) for 1 h, and incubated with primary antibodies overnight at RT. Following three washes in PBS, secondary antibodies (Jackson ImmunoResearch) were applied 1:800 overnight at RT, slices were washed three times in PBS and mounted in Fluoromount G (Southern Biotech). The following primary antibodies were used: Rb α glial fibrillary acidic protein, GFAP (Sigma, G3893), Rb α Calbindin (Millipore, AB1778), Ms α myelin-associated glycoprotein, Myelin associated glycoprotein (MAG; Millipore, MAB1567), Rb α myelin-oligodendrocyte glycoprotein, MOG (Abcam, ab32760), Ms α myelin basic protein, MBP (Covance, SMI 94), Ckn α Neurofilament-H (Neuromics, CH22104), Gt α Iba1 (Abcam, ab5076), Rb α NG2 proteoglycan, GP α NG2 proteoglycan (gifts from Dr. William Stallcup, Burnham Institute), and Rb α Olig2 (a gift from Dr. Charles Stiles, Harvard University).

Immunocytochemistry of BV-2 Cells

BV-2-202 and BV-2-553 cells were grown to about 40% confluency on a coverslip. Media was then replaced with CM from BV-2-202 cells, BV-2-553 cells or regular control media for 24 h. Cells were fixed in 4% paraformaldehyde for 20 min at RT and incubated with 1 μg/ml of rabbit anti-Iba1 primary antibody (Wako, Osaka, Japan) overnight at 4°C. Cells were then incubated in Alexa Fluor® goat anti-rabbit 488 (Molecular Probes, Eugene, OR, USA) secondary antibody at 1:400 for

1 h at RT. Vectashield mounting media with DAPI (Vector Laboratories, Inc., Burlingame, CA, USA) was used to mount coverslip onto slide and stain nuclei. Confocal laser scanning microscopy (Olympus FV1000, Olympus, Tokyo, Japan, using Olympus Fluoview Software), was used to image the cells. Exposure parameters were identical in all slides.

For DiI labeled lipid uptake experiments the average fluorescence per cell was determined by measuring the mean fluoresce in $N = 10$ induvial cells from each experimental group using the cell magic wand plugin for ImageJ.

Primary Microglia Isolation

Primary microglia were isolated from adult brains of $Cx3CR1^{CreER}$ (Jackson Labs) which express a Cre-ERT2 and EYFP in microglia as previously described with very limited modifications (Lee and Tansey, 2013). Care was taken to dissociate cells with large, medium and small-sized hole polished Pasteur pipettes.

Immunohistochemistry of Primary Microglial Cells

Primary microglia cells were plated on poly-D-lysine coated glass coverslips and cultured for 2 days. Cells were washed with HBSS 1× and fixed in 4% paraformaldehyde at RT for 20 min. Cells were blocked for 1 h with 10% normal goat serum (NGS) in PBST. Cells were incubated with 1 µl Anti-Iba1, rabbit (Wako) for 16 h at 4°C. The cells were washed 3× with PBS. Secondary goat anti-rabbit 488 was diluted 1:400, cells were incubated for 1 h at RT. Coverslips were mounted with Vectashield Anti Fade Mounting Media with DAPI, and slides were imaged using confocal Olympus FV1000.

Metabolomics

Cell pellets (10^6 cells) were stored at −80°C and were extracted in ice-cold lysis/extraction buffer (methanol:acetonitrile:water 5:3:2 v/v). Amino acids (Nemkov et al., 2017), and other metabolites (Nemkov et al., 2015), were quantified in cell extracts as previously described.

Fatty Acid Oxidation (FAO) Assays

Fatty Acid Oxidation (FAO) assays were performed as described with limited modifications (Boyle et al., 2017). Control and LPL KD BV-2 microglia were incubated at 37°C in sealed 24-well plates containing differentiation media containing 0.25 µCi/ml [^{14}C]oleate and 0.25 µCi/ml [^{14}C]palmitate (PerkinElmer Life Sciences, Waltham, MA, USA), with 200 µM, 1:1 "cold" oleate:palmitate. After a 2 h incubation, the rate of FAO was determined by measuring the $^{14}CO_2$ released from the media following acidification. Measures were performed in quintuplet and data were corrected for total protein content, determined by BCA assay (Pierce Biotechnology, Inc., Waltham, MA, USA).

Statistical Analysis

The difference between mean values for each experimental group were determined by either an ANOVA (for three or more experimental groups) followed by *post hoc* analysis with Bonferroni correction for multiple comparisons, or unpaired *t*-test (for experiments with two experimental groups), since data showed Gaussian distribution.

RESULTS

LPL Activity Is Increased at the Interphase of De- and Remyelination

EAE is a CNS autoimmune disease that has been used to investigate human demyelinating diseases such as MS (Johns et al., 1995). EAE has been well characterized in rodents using both recombinant and synthetic myelin proteins including MOG or MOG peptides (Amor et al., 1994; Johns et al., 1995; Frausto et al., 2007). To induce EAE we chose the MOG_{35-55} peptide as a suitable antigen since MS patients predominantly generate anti-MOG antibodies (Goudonnet et al., 1990). Following immunization with MOG_{35-55} or vehicle, mice were scored daily for severity of clinical symptoms. By 20 days post immunization MOG_{35-55} mice had symptoms ranging from a limp tail (score of 1) to completely paralyzed hind limbs (score of 3) while the control mice showed no symptoms of paralysis. The control mice continued to show no signs of paralysis from 1 day through to 60 days after treatment while the MOG-treated mice had relapsing remitting symptoms (**Figure 1A**). At 20 days (when clinical symptoms were at their peak in the MOG group) and 30 days (when clinical symptoms reached a nadir in the MOG group), LPL activity was measured in whole brain tissue (**Figure 1B**). Interestingly, while there was no difference in LPL activity in the brain at 20 days, LPL activity was increased in the brain by 30 days ($P < 0.01$), suggesting that increased LPL activity was associated with the initiation of improved symptoms.

To further understand the dynamics of LPL function during active demyelination and subsequent remyelination, we measured LPL enzymatic activity and expression in lysolecithin-treated *ex vivo* organotypic slice cultures of mouse cerebellum. The *ex vivo* slice culture system closely resembles the *in vivo* environment of the CNS, with the added benefit of ease of high throughput experimental treatments (Harlow et al., 2015). In this system, short term treatment with lysolecithin produces dramatic demyelination in brain slices *ex vivo* (Birgbauer et al., 2004). Twenty-four hours after lysolecithin removal there is continued demyelination and a significant reduction of the myelin markers, MBP, MOG and cyclic nucleotide phosphodiesterase (CNPase; Birgbauer et al., 2004). Several days after lysolecithin treatment these markers began to increase, concomitant with the initiation of remyelination. Here we show that heparin-releasable LPL enzymatic activity from the surface of cerebellar slices was significantly increased after 2 days of recovery in normal medium (**Figure 1C**), suggesting that LPL is most active and abundant at the end of demyelination and the initiation of remyelination. In addition, LPL expression was significantly increased by 7 days post-lysolecithin treatment (**Figure 1D**), which is consistent with the recovery of myelin markers, MAG and proteolipid protein1 (PLP1) by 7 days (**Figures 1E–J**).

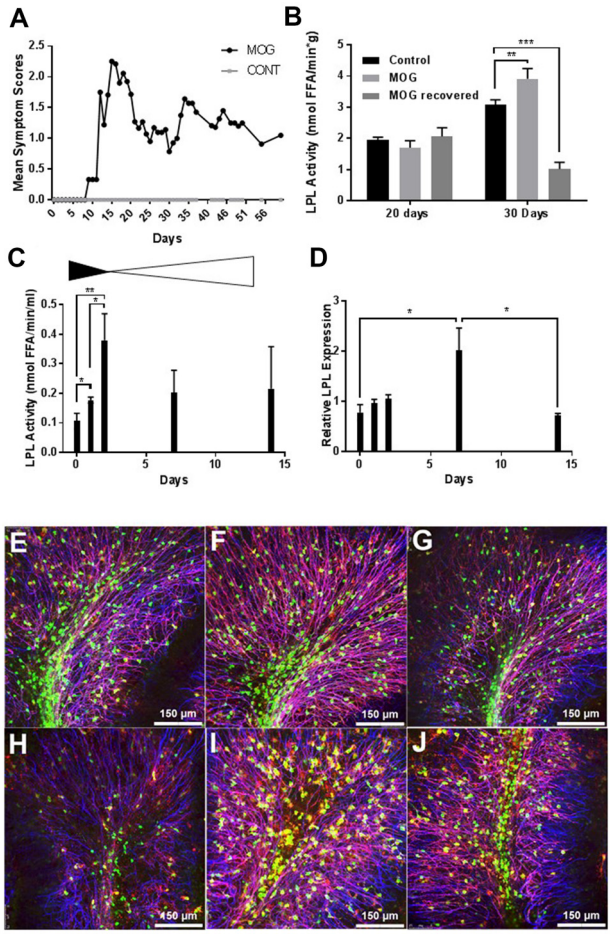

FIGURE 1 | Lipoprotein lipase (LPL) is increased during de- and re-myelination. **(A)** Mean symptom scores of MOG treated (N = 10) and Control (N = 20) mice**. (B)** LPL activity in brain tissue at 20 and 30 days MOG post injection from Control (N = 20), MOG-treated (symptomatic; N = 10), and MOG-recovered (MOG-treated but asymptomatic following an initial bout of symptoms, N = 3)**. (C)** LPL enzymatic activity in cerebellar slice cultures at 0, 1, 2, 7 and 14 days post LPC treatment (N = 3 per group, per time point). **(D)** LPL gene expression in cerebellar slice cultures at 0, 1, 2, 7 and 14 days post LPC treatment (N = 3 per group, per time point). **(E–J)** Lysolecithin-mediated demyelination of *ex vivo* cerebella brain slices (N = 3 per group, per time point). Blue—neurofilament (NFH), Green—PLPeGFP, Red—myelin associated glycoprotein (MAG). **(E–G)** No Lysolecithin control, 1, 4 and 7 days. **(H–J)** 1, 4 and 7 days post Lysolecithin treatment. $^{*}P < 0.05$ vs. CONT (at corresponding time point). $^{**}P < 0.01$ vs. CONT (at corresponding time point). $^{***}P < 0.001$ vs. CONT (at corresponding time point).

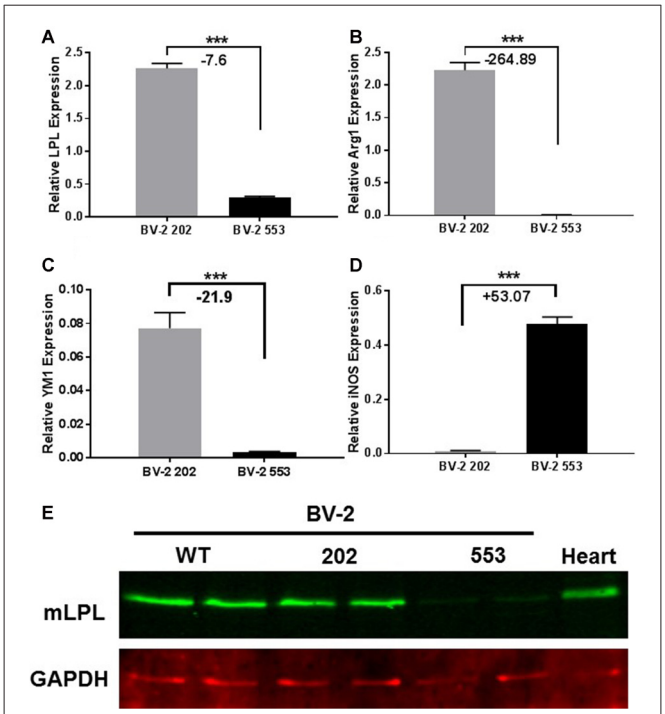

FIGURE 2 | Characterization of LPL knock down (KD) cells. **(A–D)** Gene expression in microglial BV-2 KD (553) vs. control (202) cells (N = 4 per group). **(E)** Western blot analysis showing reduced LPL protein expression in BV-2 553 cells. $^{***}P < 0.001$ vs. CONT.

The Loss of LPL in BV-2 Microglia Polarizes BV-2 Microglia to a Pro-inflammatory Phenotype

Since CNS microglia have been repeatedly implicated in myelination dynamics (Sun et al., 2017), and recent reports have highlighted the pivotal role of microglial LPL in remyelination and primary neurodegenerative disorders (Olah et al., 2012; Keren-Shaul et al., 2017), we utilized BV-2 microglia to investigate the role of LPL within these cells. BV-2 cells are an immortalized mouse microglial cell line that retains many of the morphological and functional characteristics of microglia, with the ability to stably alter the levels of LPL expression and activity (Blasi et al., 1990; Bocchini et al., 1992; Wen et al., 2006; Fu et al., 2017). We stably KD LPL expression in BV-2 cells using an LPL shRNA lentiviral vector, previously validated in our laboratory, to generate BV-2 553 (LPL KD) cells (Libby et al., 2015). An empty lentiviral vector was used to generate BV-2 202 (control) cells. Comparative gene expression between LPL KD and control cells showed a dramatic decrease in LPL KD cells in the expression of genes classically associated with an "M2" or "alternatively activated" phenotype. For example, the enzyme arginase 1 (Arg1), which converts arginine to polyamines and contributes to wound healing and repair (Munder, 2009; Cherry et al., 2014), showed a −265-fold reduction in LPL KD cells (**Figure 2B**). Similarly, chitinase-like 3 (YM1), a secretory lectin that binds heparin sulfate and prevents degradation of extracellular matrix proteins showed a −22-fold reduction in gene expression in LPL KD cells (**Figure 2C**). In contrast, iNOS expression, commonly associated with an M1-like microglial phenotype was markedly elevated in LPL KD cells (+53 fold; **Figure 2D**). Taken together, these data strongly suggest that microglial LPL expression is a feature of alternatively activated microglia.

To further understand the inflammatory phenotype of BV-2 cells lacking LPL, the relative abundance of cytokines and chemokines in CM from LPL KD and control cells was determined. Monocyte chemoattractant protein (MCP-1), which

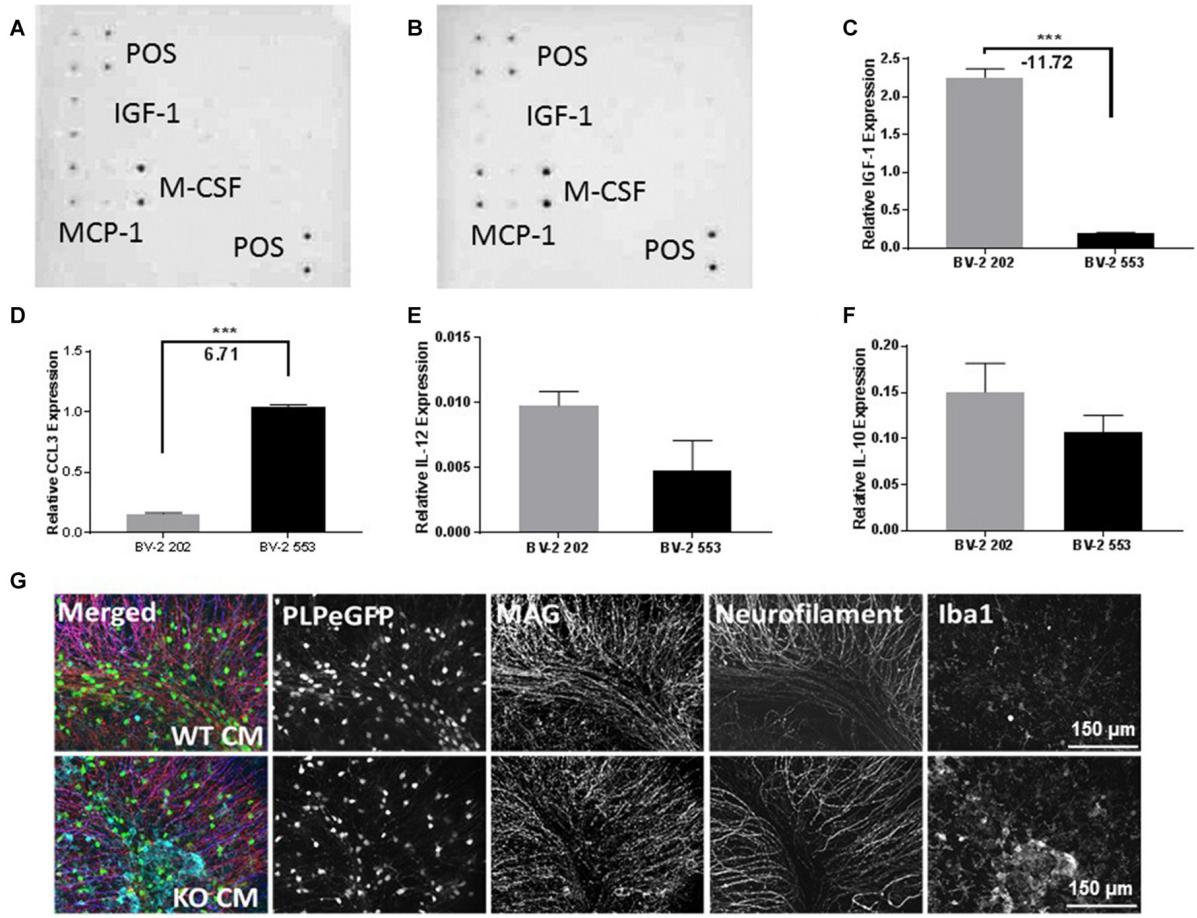

FIGURE 3 | Chemokine and cytokine production in LPL KD microglia. Ray biotech mouse neuro array was used to determine differences in chemokine expression in media from **(A)** BV-2 202 or **(B)** BV-2 553 cells. **(C–F)** Comparative gene expression between control (BV-2 202) and LPL KD (BV-2 553) cells ($N = 4$ per group). **(G)** *Ex vivo* brain slices following incubation with conditioned media (CM) from either control (WT CM) or LPL KD (KD CM) for 24 h, characterizing Plp-eGFP MAG, neurofilament or Iba1 expression ($N = 3$ per group). $^{***}P < 0.001$ vs. CONT.

is associated with microglial migration and proliferation, but not pro-inflammation (Hinojosa et al., 2011), was detected at a similar abundance in both control (**Figure 3A**), and LPL KD (**Figure 3B**) cells. Similarly, macrophage colony stimulating factor (M-CSF) was secreted at similar levels by both cell lines (**Figures 3A,B**). In contrast, insulin-like growth factor 1 (IGF-1), which is thought to play a role in the trophic support and development of neurons, was only detected in CM from control cells (**Figures 3A,B**). Since these findings were only semi-quantitative, we also used real-time PCR to quantify the level of IGF-1 gene expression in LPL KD vs. control cells. IGF-1 mRNA was significantly reduced (−12 fold) in LPL KD cells (**Figure 3C**). The expression of additional genes associated with a pro-inflammatory phenotype was also measured. Macrophage inflammatory protein (MIP)-1alpha (CCL3), associated with neuro-inflammation in the CNS (Zhu et al., 2016), was increased (+6.7 fold) in LPL KD cells (**Figure 3D**) compared to control. However, the expression of IL-12 and IL-10 were not significantly different between LPL KD and control cells (**Figures 3E,F**). To establish whether microglia-CM from either control cells or cells lacking LPL could elicit an inflammatory response *ex vivo*, brain slices were cultured with CM for 24 h. Histological analysis revealed that while myelin markers remained unchanged between groups, the expression of Iba1, associated with classically activated microglia, was increased in slices treated with CM from LPL KD cells (**Figure 3G**).

It is well established that LPS can stimulate an inflammatory response in BV-2 microglia (Orihuela et al., 2016; Sun et al., 2017). Since our data suggest that LPL is a feature of reparative microglia, we hypothesized that LPS-mediated microglial polarization would influence LPL dynamics. Following LPS treatment, both the enzymatic activity (**Figure 4A**) and mRNA expression (**Figure 4B**) of LPL were significantly reduced. Although the profile of the BV-2 microglia resembles that of primary microglia, it is important to assess the role of LPL in primary microglial cultures. Therefore, to test the dynamics of LPL following microglial polarization, primary microglia were isolated from adult brain (**Figure 4C**) and incubated with LPS for 24 h. Following LPS stimulation LPL gene expression was significantly reduced (**Figure 4D**).

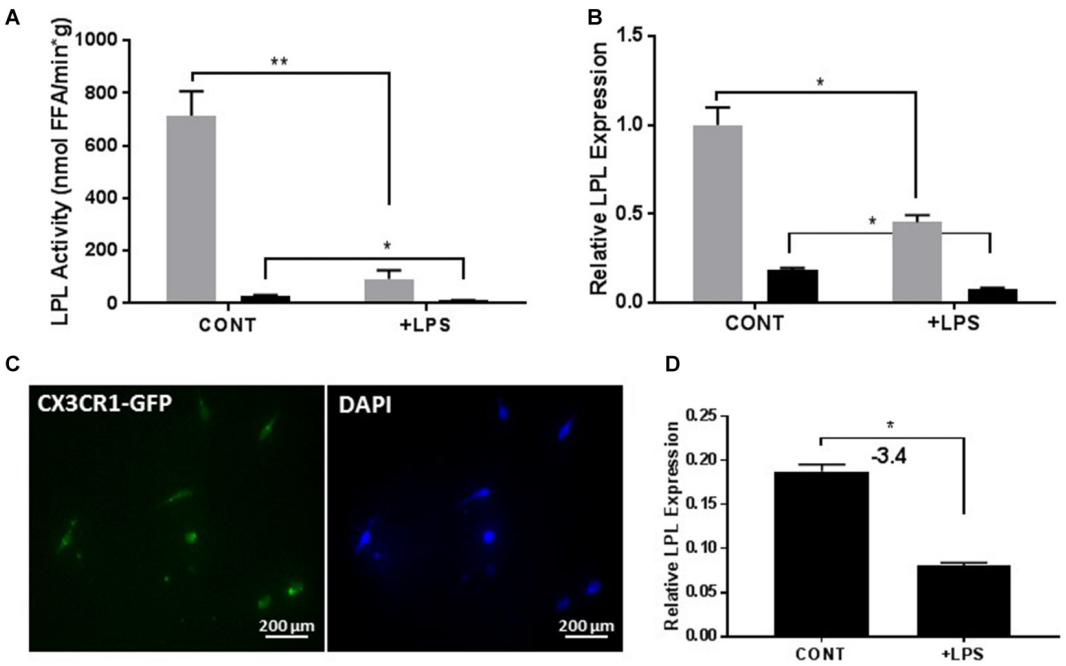

FIGURE 4 | Lipopolysaccharide (LPS) activation reduces LPL expression and activity in both immortalized cells (*N* = 4 per group; **A,B**) and primary microglial cells from adult brain (**C,D**; *N* = 3 per group). $^{*}P < 0.05$ vs. CONT. $^{**}P < 0.01$ vs. CONT.

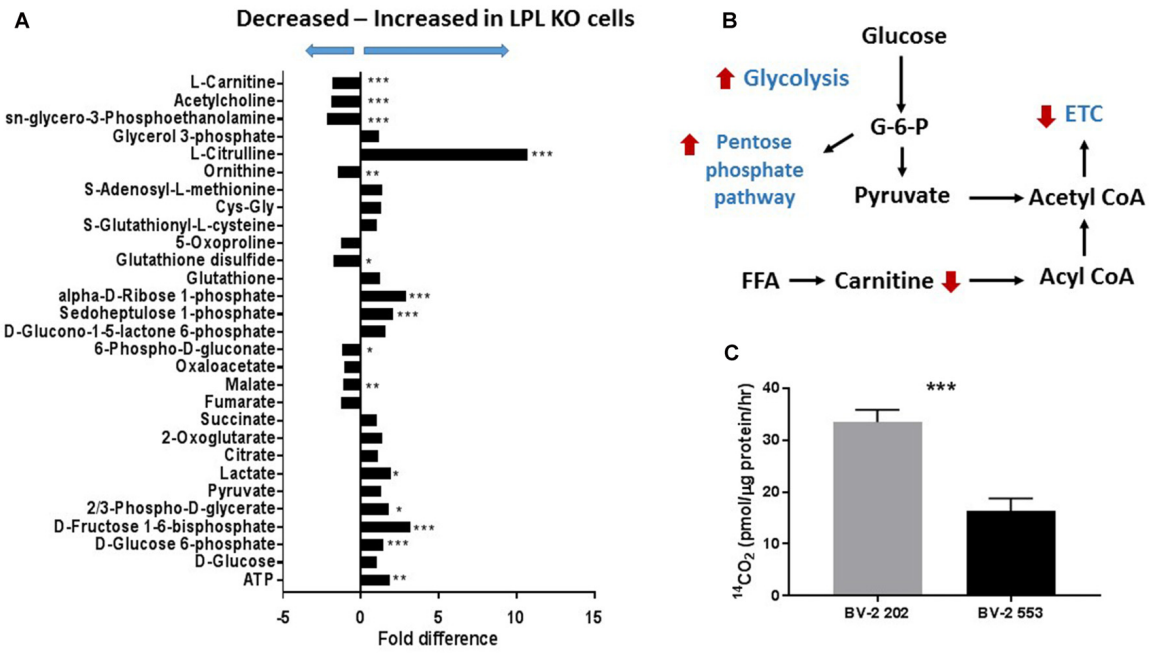

FIGURE 5 | Glycolysis is increased and fatty acid oxidation (FAO) is decreased in BV-2 microglial cells lacking LPL. **(A)** Global metabolomics in control and LPL KD BV-2 microglia (*N* = 3 per group). **(B)** Schematic representation of metabolic reprogramming following depletion of LPL in microglia. **(C)** FAO in control vs. LPL KD BV-2 microglia (*N* = 6 per group). $^{*}P < 0.05$ vs. CONT. $^{**}P < 0.01$ vs. CONT. $^{***}P < 0.001$ vs. CONT.

Although microglial activation states are complex, it is likely that microglial polarization resembles that of M1/M2 macrophages (Orihuela et al., 2016). In brief, metabolic functions in reparative (M2-like) macrophages is

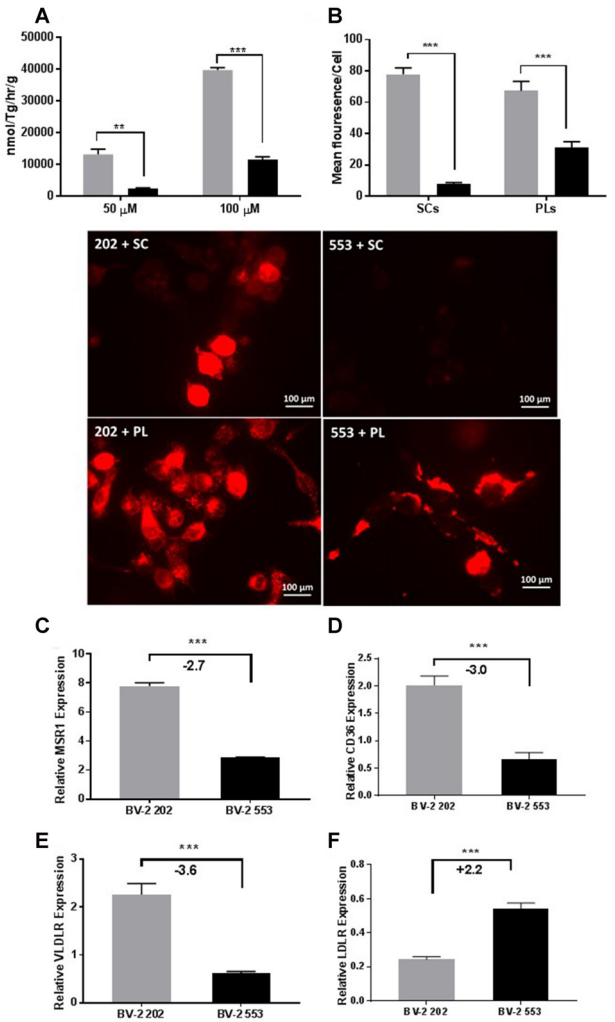

FIGURE 6 | LPL is involved in lipid and lipoprotein uptake in microglia. **(A)** Intracellular uptake of radiolabeled synthetic lipid vesicles containing 50 or 100 μM Triolein Tg. **(B)** Uptake/phagocytosis of 1′-dioctadecyl-3,3,3′3′-tetramethylindocarbocyanine perchlorate (DiI) labeled synthetic chylomicrons (SC) and phospholipid liposomes (PLs; $N = 3$ per group). **(C–F)** Expression of scavenger and lipoprotein receptors in BV-2 202 vs. 553 cells ($N = 4$ per group). $^{**}P < 0.01$ vs. CONT. $^{***}P < 0.001$ vs. CONT.

characterized by FA oxidation (FAO; Odegaard and Chawla, 2011), comparatively lower glucose consumption as compared to M1 macrophages, and arginine metabolism is shifted towards ornithine and polyamines (Mills et al., 2000). By contrast, acutely activated M1-like macrophages are shifted towards increased glycolysis (Rodríguez-Prados et al., 2010), activation of the pentose phosphate pathway (PPP; Haschemi et al., 2012), and the conversion of L-arginine to L-citrulline by iNOS. To further understand the involvement of microglial LPL in the metabolic reprogramming associated with polarization we performed global metabolomics in control and LPL KD BV-2 cells (**Figure 5A**). We found that glucose metabolism, PPP metabolism and L-citrulline were significantly increased in LPL KD cells (**Figure 5A**), consistent with the metabolic changes associated with M1-like polarization (**Figure 5B**). We also found that FAO was increased in control cells vs. LPL KD cells, consistent with the metabolic profile of M2-like macrophages (**Figure 5C**).

Lipoprotein Lipase Is Involved in Microglial Lipid Uptake

Several studies have implicated LPL in phagocytosis and repair. However, to date the precise mechanisms have not been determined. To test whether microglial LPL is involved in the uptake of free fatty acids (FFA), either control or LPL KD cells were incubated with synthetic TG-rich chylomicrons (SCs) containing radiolabeled FFAs. After incubation, the amount of intracellular radiolabeled FFA was quantified. FFA uptake was significantly increased in LPL expressing control microglia (**Figure 6A**). To address whether uptake was dependent on enzymatic hydrolysis by LPL, SCs were labeled with DiI and the internalization of intact (non-hydrolyzed) DiI labeled SC was visualized by fluorescence microscopy. SC uptake was undetectable in cells lacking LPL (**Figure 6B**). Since low-density lipoproteins are scarce in the brain we next asked whether LPL was involved in the uptake of myelin associated phospholipids (PLs). BV-2 cells were incubated with DiI labeled liposomes containing PC and PS. Although BV-2 cells lacking LPL internalized PLs, this was much greater in the control cells (**Figure 6B**). Taken together these data suggest that microglia LPL is involved in the uptake, and phagocytosis of lipids. Therefore, we measured the expression of factors associated with phagocytosis. We found that MSR1, CD36, and VLDLR expression was markedly reduced in LPL KD cells (**Figures 6C–E**); however, LDLR, which is the major importer of ApoE containing lipoproteins in the brain, was significantly increased (**Figure 6F**).

Conditioned Media From LPL KD Cells Inhibits Remyelination and Repair

To determine whether LPL directly plays a role in the remyelination process, *ex vivo* brain slices were demyelinated with lysolecithin and then allowed to recover in CM from LPL-secreting control cells and cells lacking LPL (**Figure 7**). After a 7-day recovery period, cells treated with lysolecithin, but then incubated in optimal slice media showed normal tissue morphology and expression of myelin markers. In slices treated with CM from control cells, the slice morphology was comparable to control, and there was no change in myelin marker expression. However, brain slices treated with CM from LPL KD cells showed a somewhat necrotic morphology with diffuse myelin marker staining and a significant reduction in neurofilament expression, suggesting that re-myelination was incomplete in this condition.

DISCUSSION

MS is a relatively common (1:1000 in susceptible populations) debilitating disease that can affect an individual for much of

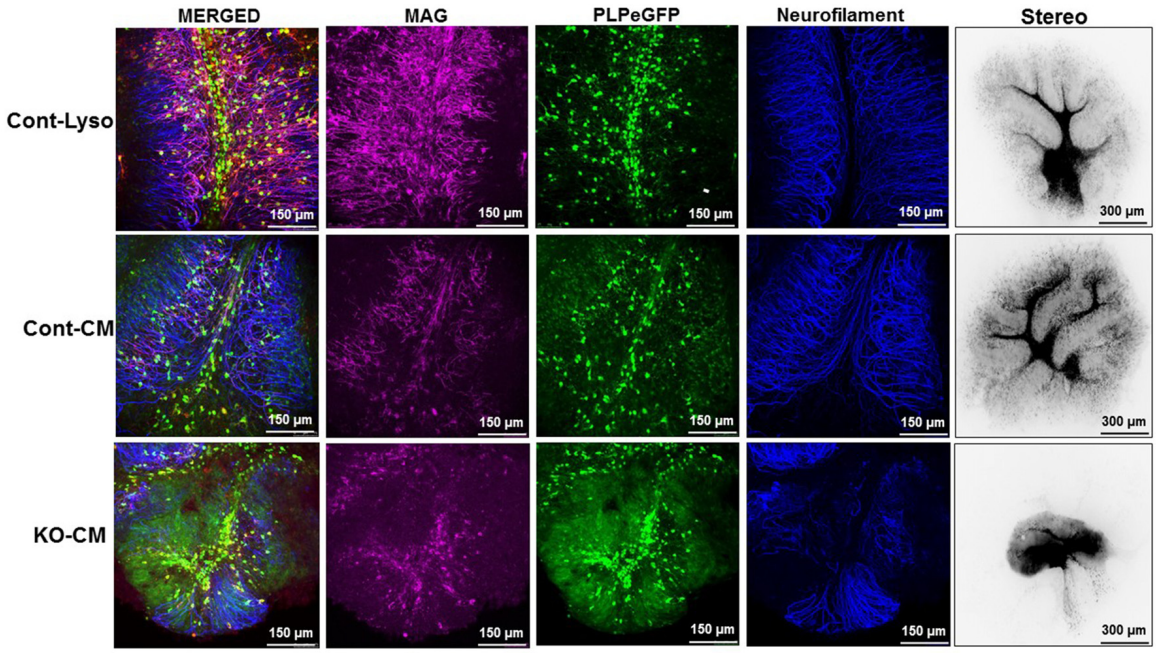

FIGURE 7 | CM from LPL KD cells prevents normal remyelination processes. *Ex vivo* cerebellar slices were demyelinated by overnight treatment (17 h) with lysolecithin. The next day slices were incubated with either standard slice media, or CM and allowed to recover for 7 days.

their life. During the RR-MS stage of the disease there is a discrete balance between de- and remyelination. In P-MS, these attempts to remyelinate fail leading to neurodegeneration and progressive disability. Understanding the dynamics of de- and remyelination may be key to identifying potential targets for MS treatments. Microglial function plays a key role in the remyelination process. The production of cytokines/chemokines from the appropriate microglial phenotype can stimulate the proliferation of OPCs to promote remyelination (Voss et al., 2012). In addition, microglial-phagocytosis of myelin debris plays in important role in the initiation of remyelination (Neumann et al., 2009). However, to date the factors involved in these processes remain elusive. Here we show for the first time that LPL, a lipid-processing enzyme with known roles in hydrolytic and non-hydrolytic lipid uptake, was a feature of an "alternatively activated" microglial phenotype associated with phagocytosis and remyelination.

In the present study we have demonstrated that LPL is increased at the initiation of remyelination in both *in vivo* and *ex vivo* model systems (**Figure 1**). Using the EAE model of demyelination we showed that LPL activity in the brain is significantly increased at 30 days following immunization. This time point correlates with a nadir in clinical symptoms, suggesting that LPL expression is associated with the partial remyelination observed in RR-MS. In further support of this notion, we have shown that LPL abundance and enzymatic activity is increased at the interphase of de- and remyelination in an *ex vivo* model of demyelination. These observations are consistent with findings from a cuprizone model of de- and remyelination in which LPL was identified as a key feature of a microglial phenotype that actively supports remyelination (Olah et al., 2012). Since cuprizone models of de- and remyelination have been used to identify the central role of debris clearance in these processes (Voss et al., 2012), these data suggest that LPL is a feature of a scavenging microglial phenotype that promotes regeneration.

Microglia play an important role in remyelination and regeneration process through their ability to clear debris, and their expression and secretion of cytokines and growth factors. Our data robustly show that cells lacking LPL polarize to a pro-inflammatory phenotype characterized by the expression of iNOS, inflammatory cytokines, and a metabolic shift towards glycolysis—similar to that of M1-like macrophages. In contrast, cells that express LPL maintain an alternately activated phenotype that is characterized by elevated Arg1 expression, IGF-1 production and increased FAO. The switch in expression between Arg1 and iNOS is particularly indicative of microglial polarization, since both Arg1 and iNOS use the same substrate (arginine) to either produce polyamines for wound healing and matrix deposition (Arg1; Munder, 2009), or nitric oxidase production contributing to inflammation (iNOS; Morris, 2007). Thus, Arg1 vs. iNOS represents a useful switch to an M2 vs. M1 phenotype. In the present study we show that the loss of LPL markedly increases iNOS expression while reducing Arg1 expression, suggesting a polarization towards an M1-like phenotype (**Figure 2**). In further support we show that L-citrulline, a product in the synthesis of NO by iNOS (Chaturvedi et al., 2007), was markedly increased in cells lacking LPL (**Figure 5**). Although defined phenotypic boundaries likely do not represent the full microglial spectra observed in

complex disease states such as MS, the expression of these genes serve as useful categorical markers. In addition, the expression of chemokines and growth factors are also useful markers of microglial status. Therefore, it is of interest that microglial cells lacking LPL have significantly reduced IGF-1 secretion and expression (**Figure 3**), which has been classically associated with M2-like macrophages. Recent studies have shown that IGF-1 plays a key role in the CNS, where it exerts a trophic effect on neurogenesis and neuronal survival (Russo et al., 2005). Moreover, microglia are an important source of IGF-1, and its production is linked to microglial inflammatory status (Suh et al., 2013). Interestingly, reduced IGF-1 has been observed in AD (Alvarez et al., 2007), and in patients with MS (Shahbazi et al., 2017). Recent studies using rodent models of local lysolecithin induced demyelination have shown that intrathecal IGF-1 administration promotes remyelination (Hlavica et al., 2017). Taken together, these observations suggest that LPL expression promotes a microglial polarization towards an anti-inflammatory and reparative phenotype associated with IGF-1 production, a key factor that links microglial function to repair and remyelination in MS.

Our findings prompt the question; how does modulated LPL expression mediate microglial polarization? Since LPL depletion is associated with a shift towards glycolysis and away from FAO, it is likely that LPL loss causes a shift in lipid availability, substrate metabolism, and polarization towards an M1-like classically activated phenotype. In contrast, cells harboring endogenous LPL levels may have sufficient lipid-uptake, facilitating the shift towards FAO that is associated with M2-like alternatively activated and reparative microglia. Precisely why increased FAO is important for reparative microglial remains to be tested, but one may speculate that FAO provides the additional energy supply required for long-term reparative processes.

In support of the notion that LPL facilitates microglial lipid uptake, we have also shown that microglia lacking LPL are less able to take up FFAs from synthetic chylomicrons than cells expressing endogenous levels of LPL (**Figure 6**). These data are consistent with the canonical function of LPL—the hydrolysis of TG-rich lipoproteins—and suggests that microglial LPL may play a similar role in the CNS. Since TG-rich lipoproteins are scarce in the CNS, we hypothesized that LPL may facilitate the up-take of myelin-associated lipids. The phospholipids PC and PS are major components of myelin with pleotropic roles in the pathogenesis of MS (Ho et al., 2012). In the present study we show that LPL is involved in the uptake of PC and PS containing liposomes (**Figure 6**), highlighting the role of microglial LPL in myelin phagocytosis. It is well established that the phagocytosis and clearance of myelin debris is important for the remyelination process (Neumann et al., 2009). For example, ineffective microglial function in CXC3CR1 knockout mice has been shown to impair debris clearance and subsequent remyelination (Lampron et al., 2015). In addition, many recent reports have highlighted the potential role of microglial-LPL in phagocytosis and myelin clearance (Olah et al., 2012; Ma et al., 2013; Keren-Shaul et al., 2017). Although the precise mechanism regarding the mode of phagocytosis remains to be determined, recent data from mice deficient in Triggering receptor expressed on myeloid cells 2 (TREM 2)—a microglial immunoreceptor associated with phagocytosis and whose loss-of-function mutations in humans cause presenile dementia—have shown that LPL is markedly reduced in this model, suggesting that LPL is involved in TREM 2-mediated phagocytosis (Cantoni et al., 2015). In addition, the mechanism underlying the role of LPL in phagocytosis may be similar to its non-hydrolytic, or endocytotic bridging function. LPL can facilitate lipid-uptake through simultaneous interaction with lipoproteins, heparin sulfate proteoglycans (HSPG), or cell surface receptors such as lipoprotein receptors (Makoveichuk et al., 2004). Conversely, it is well established that lipoprotein receptors have a duel function in immune cells, and may also serve as scavenging receptors to facilitate phagocytosis. For example, the low density lipoprotein receptor-related protein-1 (LRP1) functions as a scavenger receptors for myelin debris (Fernandez-Castaneda et al., 2013). It is thus plausible to speculate that LPL may simultaneously bind to lipid-rich myelin debris and cell surface lipoprotein receptors to expedite myelin clearance and remyelination.

Collectively, our observations suggest that microglial LPL exerts simultaneous benefits for repair and remyelination. On one hand the presence of LPL is associated with a reparative microglial phenotype, the production of important neurotropic factors, and the maintenance of appropriate substrate availability for metabolic polarization towards and M2-like phenotype. In addition, microglial LPL is directly involved in the internalization of myelin associated lipids. In summary, our findings highlight the importance of LPL in demyelinating disorders and are the first to demonstrate that microglial-LPL is directly involved in reparative processes needed for remyelination. We anticipate that the role of LPL in debris clearance and uptake may be exploited to develop future therapies for demyelinating disorders such as MS, and also primary neurodegenerative disease.

AUTHOR CONTRIBUTIONS

KDB, WBM and RHE designed the experiments. KDB, SG, KG and AMC performed the experiments; analyzed the data. KDB, KEB, WBM and RHE interpreted data. KDB wrote the manuscript and all authors edited the manuscript.

ACKNOWLEDGMENTS

The funding for the animal work was provided by a Pilot Award from the National Multiple Sclerosis Society. *In vitro* and *ex vivo* work was funded by the Colorado Clinical and Translational Sciences Institute (CCTSI: CNS-Pilot Basic Research Team Award, CNSBT-15-92). We would like to acknowledge Ms. Leslie Knaub and Mr. Dalan Jensen for technical assistance with these studies. We would also like to acknowledge and thank Ms. Sarah Gehrke in the University of Colorado School of Medicine Metabolomics Core for technical assistance.

REFERENCES

Alvarez, A., Cacabelos, R., Sanpedro, C., García-Fantini, M., and Aleixandre, M. (2007). Serum TNF-α levels are increased and correlate negatively with free IGF-I in Alzheimer disease. *Neurobiol. Aging* 28, 533–536. doi: 10.1016/j.neurobiolaging.2006.02.012

Amor, S., Groome, N., Linington, C., Morris, M. M., Dornmair, K., Gardinier, M. V., et al. (1994). Identification of epitopes of myelin oligodendrocyte glycoprotein for the induction of experimental allergic encephalomyelitis in SJL and Biozzi AB/H mice. *J. Immunol.* 153, 4349–4356.

Antel, J., Antel, S., Caramanos, Z., Arnold, D. L., and Kuhlmann, T. (2012). Primary progressive multiple sclerosis: part of the MS disease spectrum or separate disease entity? *Acta Neuropathol.* 123, 627–638. doi: 10.1007/s00401-012-0953-0

Becher, B., Durell, B. G., Miga, A. V., Hickey, W. F., and Noelle, R. J. (2001). The clinical course of experimental autoimmune encephalomyelitis and inflammation is controlled by the expression of CD40 within the central nervous system. *J. Exp. Med.* 193, 967–974. doi: 10.1084/jem.193.8.967

Bessesen, D. H., Richards, C. L., Etienne, J., Goers, J. W., and Eckel, R. H. (1993). Spinal cord of the rat contains more lipoprotein lipase than other brain regions. *J. Lipid Res.* 34, 229–238.

Birgbauer, E., Rao, T. S., and Webb, M. (2004). Lysolecithin induces demyelination *in vitro* in a cerebellar slice culture system. *J. Neurosci. Res.* 78, 157–166. doi: 10.1002/jnr.20248

Blasi, E., Barluzzi, R., Bocchini, V., Mazzolla, R., and Bistoni, F. (1990). Immortalization of murine microglial cells by a v-raf/v-myc carrying retrovirus. *J. Neuroimmunol.* 27, 229–237. doi: 10.1016/0165-5728(90)90073-v

Bocchini, V., Mazzolla, R., Barluzzi, R., Blasi, E., Sick, P., and Kettenmann, H. (1992). An immortalized cell line expresses properties of activated microglial cells. *J. Neurosci. Res.* 31, 616–621. doi: 10.1002/jnr.490310405

Boyle, K. E., Friedman, J. E., Janssen, R. C., Underkofler, C., Houmard, J. A., and Rasouli, N. (2017). Metabolic inflexibility with obesity and the effects of fenofibrate on skeletal muscle fatty acid oxidation. *Horm. Metab. Res.* 49, 50–57. doi: 10.1055/s-0042-111517

Cantoni, C., Bollman, B., Licastro, D., Xie, M., Mikesell, R., Schmidt, R., et al. (2015). TREM2 regulates microglial cell activation in response to demyelination *in vivo*. *Acta Neuropathol.* 129, 429–447. doi: 10.1007/s00401-015-1388-1

Chaturvedi, R., Asim, M., Lewis, N. D., Algood, H. M., Cover, T. L., Kim, P. Y., et al. (2007). L-arginine availability regulates inducible nitric oxide synthase-dependent host defense against Helicobacter pylori. *Infect. Immun.* 75, 4305–4315. doi: 10.1128/iai.00578-07

Cherry, J. D., Olschowka, J. A., and O'Banion, M. K. (2014). Neuroinflammation and M2 microglia: the good, the bad, and the inflamed. *J. Neuroinflammation* 11:98. doi: 10.1186/1742-2094-11-98

Eckel, R. H., and Robbins, R. J. (1984). Lipoprotein lipase is produced, regulated and functional in rat brain. *Proc. Natl. Acad. Sci. U S A* 81, 7604–7607. doi: 10.1073/pnas.81.23.7604

Fernandez-Castaneda, A., Arandjelovic, S., Stiles, T. L., Schlobach, R. K., Mowen, K. A., Gonias, S. L., et al. (2013). Identification of the low density lipoprotein (LDL) receptor-related protein-1 interactome in central nervous system myelin suggests a role in the clearance of necrotic cell debris. *J. Biol. Chem.* 288, 4538–4548. doi: 10.1074/jbc.M112.384693

Frausto, R. F., Crocker, S. J., Eam, B., Whitmire, J. K., and Whitton, J. L. (2007). Myelin oligodendrocyte glycoprotein peptide-induced experimental allergic encephalomyelitis and T cell responses are unaffected by immunoproteasome deficiency. *J. Neuroimmunol.* 192, 124–133. doi: 10.1016/j.jneuroim.2007.09.024

Fu, W., Vukojevic, V., Patel, A., Soudy, R., MacTavish, D., Westaway, D., et al. (2017). Role of microglial amylin receptors in mediating β amyloid (Aβ)-induced inflammation. *J. Neuroinflammation* 14:199. doi: 10.1186/s12974-017-0972-9

Goldberg, I. J., Soprano, D. R., Wyatt, M. L., Vanni, T. M., Kirchgessner, T. G., and Schotz, M. C. (1989). Localization of lipoprotein lipase mRNA in selected rat tissues. *J. Lipid Res.* 30, 1569–1577.

Goudonnet, H., Magdalou, J., Mounie, J., Naoumi, A., Viriot, M. L., Escousse, A., et al. (1990). Differential action of thyroid hormones and chemically related compounds on the activity of UDP-glucuronosyltransferases and cytochrome P-450 isozymes in rat liver. *Biochim. Biophys. Acta* 1035, 12–19. doi: 10.1016/0304-4165(90)90167-u

Harlow, D. E., Saul, K. E., Komuro, H., and Macklin, W. B. (2015). Myelin proteolipid protein complexes with αv integrin and AMPA receptors *in vivo* and regulates AMPA-dependent oligodendrocyte progenitor cell migration through the modulation of cell-surface GluR2 expression. *J. Neurosci.* 35, 12018–12032. doi: 10.1523/JNEUROSCI.5151-14.2015

Haschemi, A., Kosma, P., Gille, L., Evans, C. R., Burant, C. F., Starkl, P., et al. (2012). The sedoheptulose kinase CARKL directs macrophage polarization through control of glucose metabolism. *Cell Metab.* 15, 813–826. doi: 10.1016/j.cmet.2012.04.023

Heppner, F. L., Greter, M., Marino, D., Falsig, J., Raivich, G., Hövelmeyer, N., et al. (2005). Experimental autoimmune encephalomyelitis repressed by microglial paralysis. *Nat. Med.* 11, 146–152. doi: 10.1038/nm1177

Hinojosa, A. E., Garcia-Bueno, B., Leza, J. C., and Madrigal, J. L. (2011). CCL2/MCP-1 modulation of microglial activation and proliferation. *J. Neuroinflammation* 8:77. doi: 10.1186/1742-2094-8-77

Hlavica, M., Delparente, A., Good, A., Good, N., Plattner, P. S., Seyedsadr, M. S., et al. (2017). Intrathecal insulin-like growth factor 1 but not insulin enhances myelin repair in young and aged rats. *Neurosci. Lett.* 648, 41–46. doi: 10.1016/j.neulet.2017.03.047

Ho, P. P., Kanter, J. L., Johnson, A. M., Srinagesh, H. K., Chang, E. J., Purdy, T. M., et al. (2012). Identification of naturally occurring fatty acids of the myelin sheath that resolve neuroinflammation. *Sci. Transl. Med.* 4:137ra73. doi: 10.1126/scitranslmed.3003831

Hohlfeld, R. (2008). Neurotrophic cross-talk between the nervous and immune systems: relevance for repair strategies in multiple sclerosis? *J. Neurol. Sci.* 265, 93–96. doi: 10.1016/j.jns.2007.03.012

Hong, S., and Stevens, B. (2016). Microglia: phagocytosing to clear, sculpt, and eliminate. *Dev. Cell* 38, 126–128. doi: 10.1016/j.devcel.2016.07.006

Huey, P. U., Waugh, K. C., Etienne, J., and Eckel, R. H. (2002). Lipoprotein lipase is expressed in rat sciatic nerve and regulated in response to crush injury. *J. Lipid Res.* 43, 19–25.

Jensen, D. R., Knaub, L. A., Konhilas, J. P., Leinwand, L. A., MacLean, P. S., and Eckel, R. H. (2008). Increased thermoregulation in cold-exposed transgenic mice overexpressing lipoprotein lipase in skeletal muscle: an avian phenotype? *J. Lipid Res.* 49, 870–879. doi: 10.1194/jlr.M700519-jlr200

Johns, T. G., Kerlero de Rosbo, N., Menon, K. K., Abo, S., Gonzales, M. F., and Bernard, C. C. (1995). Myelin oligodendrocyte glycoprotein induces a demyelinating encephalomyelitis resembling multiple sclerosis. *J. Immunol.* 154, 5536–5541.

Keren-Shaul, H., Spinrad, A., Weiner, A., Matcovitch-Natan, O., Dvir-Szternfeld, R., Ulland, T. K., et al. (2017). A unique microglia type associated with restricting development of Alzheimer's disease. *Cell* 169, 1276.e17–1290.e17. doi: 10.1016/j.cell.2017.05.018

Lampron, A., Larochelle, A., Laflamme, N., Préfontaine, P., Plante, M. M., Sanchez, M. G., et al. (2015). Inefficient clearance of myelin debris by microglia impairs remyelinating processes. *J. Exp. Med.* 212, 481–495. doi: 10.1084/jem.20141656

Lee, J. K., and Tansey, M. G. (2013). Microglia isolation from adult mouse brain. *Methods Mol. Biol.* 1041, 17–23. doi: 10.1007/978-1-62703-520-0_3

Libby, A. E., Wang, H., Mittal, R., Sungelo, M., Potma, E., and Eckel, R. H. (2015). Lipoprotein lipase is an important modulator of lipid uptake and storage in hypothalamic neurons. *Biochem. Biophys. Res. Commun.* 465, 287–292. doi: 10.1016/j.bbrc.2015.08.026

Ma, Y., Bao, J., Zhao, X., Shen, H., Lv, J., Ma, S., et al. (2013). Activated cyclin-dependent kinase 5 promotes microglial phagocytosis of fibrillar β-amyloid by up-regulating lipoprotein lipase expression. *Mol. Cell. Proteomics* 12, 2833–2844. doi: 10.1074/mcp.M112.026864

Makoveichuk, E., Castel, S., Vilaró, S., and Olivecrona, G. (2004). Lipoprotein lipase-dependent binding and uptake of low density lipoproteins by THP-1 monocytes and macrophages: possible involvement of lipid rafts. *Biochim. Biophys. Acta* 1686, 37–49. doi: 10.1016/j.bbalip.2004.08.015

Mallon, B. S., Shick, H. E., Kidd, G. J., and Macklin, W. B. (2002). Proteolipid promoter activity distinguishes two populations of NG2-positive cells throughout neonatal cortical development. *J. Neurosci.* 22, 876–885.

Mendel, I., Kerlero de Rosbo, N., and Ben-Nun, A. (1995). A myelin oligodendrocyte glycoprotein peptide induces typical chronic experimental autoimmune encephalomyelitis in H-2b mice: fine specificity and T cell receptor V β expression of encephalitogenic T cells. *Eur. J. Immunol.* 25, 1951–1959. doi: 10.1002/eji.1830250723

Mills, C. D., Kincaid, K., Alt, J. M., Heilman, M. J., and Hill, A. M. (2000). M-1/M-2 macrophages and the Th1/Th2 paradigm. *J. Immunol.* 164, 6166–6173. doi: 10.4049/jimmunol.164.12.6166

Morris, S. M. Jr. (2007). Arginine metabolism: boundaries of our knowledge. *J. Nutr.* 137, 1602S–1609S. doi: 10.1093/jn/137.6.1602s

Munder, M. (2009). Arginase: an emerging key player in the mammalian immune system. *Br. J. Pharmacol.* 158, 638–651. doi: 10.1111/j.1476-5381.2009.00291.x

Nemkov, T., D'Alessandro, A., and Hansen, K. C. (2015). Three-minute method for amino acid analysis by UHPLC and high-resolution quadrupole orbitrap mass spectrometry. *Amino Acids* 47, 2345–2357. doi: 10.1007/s00726-015-2019-9

Nemkov, T., Hansen, K. C., and D'Alessandro, A. (2017). A three-minute method for high-throughput quantitative metabolomics and quantitative tracing experiments of central carbon and nitrogen pathways. *Rapid Commun. Mass Spectrom.* 31, 663–673. doi: 10.1002/rcm.7834

Neumann, H., Kotter, M. R., and Franklin, R. J. (2009). Debris clearance by microglia: an essential link between degeneration and regeneration. *Brain* 132, 288–295. doi: 10.1093/brain/awn109

Nunes, A. F., and Sousa, M. M. (2008). Transthyretin knockout mouse nerves have increased lipoprotein lipase and sphingolipid content following crush. *Neurosci. Lett.* 446, 83–87. doi: 10.1016/j.neulet.2008.09.054

Odegaard, J. I., and Chawla, A. (2011). Alternative macrophage activation and metabolism. *Annu. Rev. Pathol.* 6, 275–297. doi: 10.1146/annurev-pathol-011110-130138

Okuda, Y., Okuda, M., and Bernard, C. C. (2002). Gender does not influence the susceptibility of C57BL/6 mice to develop chronic experimental autoimmune encephalomyelitis induced by myelin oligodendrocyte glycoprotein. *Immunol. Lett.* 81, 25–29. doi: 10.1016/s0165-2478(01)00339-x

Olah, M., Amor, S., Brouwer, N., Vinet, J., Eggen, B., Biber, K., et al. (2012). Identification of a microglia phenotype supportive of remyelination. *Glia* 60, 306–321. doi: 10.1002/glia.21266

Orihuela, R., McPherson, C. A., and Harry, G. J. (2016). Microglial M1/M2 polarization and metabolic states. *Br. J. Pharmacol.* 173, 649–665. doi: 10.1111/bph.13139

Ransohoff, R. M., and El Khoury, J. (2015). Microglia in health and disease. *Cold Spring Harb. Perspect. Biol.* 8:a020560. doi: 10.1101/cshperspect.a020560

Ransohoff, R. M., and Perry, V. H. (2009). Microglial physiology: unique stimuli, specialized responses. *Annu. Rev. Immunol.* 27, 119–145. doi: 10.1146/annurev.immunol.021908.132528

Rodríguez-Prados, J. C., Través, P. G., Cuenca, J., Rico, D., Aragonés, J., Martín-Sanz, P., et al. (2010). Substrate fate in activated macrophages: a comparison between innate, classic and alternative activation. *J. Immunol.* 185, 605–614. doi: 10.4049/jimmunol.0901698

Russo, V. C., Gluckman, P. D., Feldman, E. L., and Werther, G. A. (2005). The insulin-like growth factor system and its pleiotropic functions in brain. *Endocr. Rev.* 26, 916–943. doi: 10.1210/er.2004-0024

Schwartz, M., and Moalem, G. (2001). Beneficial immune activity after CNS injury: prospects for vaccination. *J. Neuroimmunol.* 113, 185–192. doi: 10.1016/s0165-5728(00)00447-1

Shahbazi, M., Abdolmohammadi, R., Ebadi, H., and Farazmandfar, T. (2017). Novel functional polymorphism in IGF-1 gene associated with multiple sclerosis: a new insight to MS. *Mult. Scler. Relat. Disord.* 13, 33–37. doi: 10.1016/j.msard.2017.02.002

Sheridan, G. K., and Dev, K. K. (2012). S1P1 receptor subtype inhibits demyelination and regulates chemokine release in cerebellar slice cultures. *Glia* 60, 382–392. doi: 10.1002/glia.22272

Suh, H. S., Zhao, M. L., Derico, L., Choi, N., and Lee, S. C. (2013). Insulin-like growth factor 1 and 2 (IGF1, IGF2) expression in human microglia: differential regulation by inflammatory mediators. *J. Neuroinflammation* 10:37. doi: 10.1186/1742-2094-10-37

Sun, D., Yu, Z., Fang, X., Liu, M., Pu, Y., Shao, Q., et al. (2017). LncRNA GAS5 inhibits microglial M2 polarization and exacerbates demyelination. *EMBO Rep.* 18, 1801–1816. doi: 10.15252/embr.201643668

Varin, A., and Gordon, S. (2009). Alternative activation of macrophages: immune function and cellular biology. *Immunobiology* 214, 630–641. doi: 10.1016/j.imbio.2008.11.009

Voss, E. V., Skuljec, J., Gudi, V., Skripuletz, T., Pul, R., Trebst, C., et al. (2012). Characterisation of microglia during de- and remyelination: can they create a repair promoting environment? *Neurobiol. Dis.* 45, 519–528. doi: 10.1016/j.nbd.2011.09.008

Wen, W., Sanelli, T., Ge, W., Strong, W., and Strong, M. J. (2006). Activated microglial supernatant induced motor neuron cytotoxicity is associated with upregulation of the TNFR1 receptor. *Neurosci. Res.* 55, 87–95. doi: 10.1016/j.neures.2006.02.004

Zhu, X., Wei, D., Chen, O., Zhang, Z., Xue, J., Huang, S., et al. (2016). Upregulation of CCL3/MIP-1α regulated by MAPKs and NF-κB mediates microglial inflammatory response in LPS-induced brain injury. *Acta Neurobiol. Exp.* 76, 304–317. doi: 10.21307/ane-2017-029

Conflict of Interest Statement: The authors declare that the research was conducted in the absence of any commercial or financial relationships that could be construed as a potential conflict of interest.

frontiers in Cellular Neuroscience

ORIGINAL RESEARCH
published: 06 March 2018
doi: 10.3389/fncel.2018.00055

In Utero Administration of Drugs Targeting Microglia Improves the Neurodevelopmental Outcome Following Cytomegalovirus Infection of the Rat Fetal Brain

*Robin Cloarec[1,2†], Sylvian Bauer[1†], Natacha Teissier[3,4], Fabienne Schaller[1,5], Hervé Luche[6], Sandra Courtens[1], Manal Salmi[1], Vanessa Pauly[7], Emilie Bois[3,4], Emilie Pallesi-Pocachard[1,8], Emmanuelle Buhler[1,5], François J. Michel[1,9], Pierre Gressens[3,4], Marie Malissen[6], Thomas Stamminger[10], Daniel N. Streblow[11], Nadine Bruneau[1] and Pierre Szepetowski[1]**

[1] INMED, French National Institute of Health and Medical Research INSERM U1249, Aix-Marseille University, Marseille, France, [2] Neurochlore, Marseille, France, [3] French National Institute of Health and Medical Research INSERM U1141, Paris Diderot University, Sorbonne Paris Cité, Paris, France, [4] PremUP, Paris, France, [5] PPGI Platform, INMED, Marseille, France, [6] Centre National de la Recherche Scientifique CNRS UMS3367, CIPHE (Centre D'Immunophénomique), French National Institute of Health and Medical Research INSERM US012, PHENOMIN, Aix-Marseille University, Marseille, France, [7] Laboratoire de Santé Publique EA 3279, Faculté de Médecine Centre d'Evaluation de la Pharmacodépendance-Addictovigilance de Marseille (PACA-Corse) Associé, Aix-Marseille University, Marseille, France, [8] PBMC platform, INMED, Marseille, France, [9] InMAGIC platform, INMED, Marseille, France, [10] Institute for Clinical and Molecular Virology, University of Erlangen-Nuremberg, Erlangen, Germany, [11] Vaccine and Gene Therapy Institute, Oregon Health and Science University, Portland, OR, United States

OPEN ACCESS

Edited by:
Alexej Verkhratsky, University of Manchester, United Kingdom

Reviewed by:
Andrew MacLean, Tulane University School of Medicine, United States
Marina Bentivoglio, University of Verona, Italy

***Correspondence:**
Pierre Szepetowski
pierre.szepetowski@inserm.fr

† These authors have contributed equally to this work.

Received: *29 November 2017*
Accepted: *16 February 2018*
Published: *06 March 2018*

Citation:
Cloarec R, Bauer S, Teissier N, Schaller F, Luche H, Courtens S, Salmi M, Pauly V, Bois E, Pallesi-Pocachard E, Buhler E, Michel FJ, Gressens P, Malissen M, Stamminger T, Streblow DN, Bruneau N and Szepetowski P (2018) In Utero Administration of Drugs Targeting Microglia Improves the Neurodevelopmental Outcome Following Cytomegalovirus Infection of the Rat Fetal Brain. Front. Cell. Neurosci. 12:55. doi: 10.3389/fncel.2018.00055

Congenital cytomegalovirus (CMV) infections represent one leading cause of neurodevelopmental disorders. Recently, we reported on a rat model of CMV infection of the developing brain *in utero*, characterized by early and prominent infection and alteration of microglia—the brain-resident mononuclear phagocytes. Besides their canonical function against pathogens, microglia are also pivotal to brain development. Here we show that CMV infection of the rat fetal brain recapitulated key postnatal phenotypes of human congenital CMV including increased mortality, sensorimotor impairment reminiscent of cerebral palsy, hearing defects, and epileptic seizures. The possible influence of early microglia alteration on those phenotypes was then questioned by pharmacological targeting of microglia during pregnancy. One single administration of clodronate liposomes in the embryonic brains at the time of CMV injection to deplete microglia, and maternal feeding with doxycyxline throughout pregnancy to modify microglia in the litters' brains, were both associated with dramatic improvements of survival, body weight gain, sensorimotor development and with decreased risk of epileptic seizures. Improvement of microglia activation status did not persist postnatally after doxycycline discontinuation; also, active brain infection remained unchanged by doxycycline. Altogether our data indicate that early microglia alteration, rather than brain CMV load *per se*, is instrumental in influencing survival and the neurological

outcomes of CMV-infected rats, and suggest that microglia might participate in the neurological outcome of congenital CMV in humans. Furthermore this study represents a first proof-of-principle for the design of microglia-targeted preventive strategies in the context of congenital CMV infection of the brain.

Keywords: cytomegalovirus, microglia, rat model, fetal brain, neurological outcome

INTRODUCTION

Perinatal and congenital infections cause morbidity and mortality throughout the world. Some pathogens are of considerable public health impact, such as *Toxoplasma gondii*, rubella, human immunodeficiency virus, Zika virus, and human cytomegalovirus (CMV). CMVs belong to the *Herpesviridae* family. In humans, congenital CMV infection can cause severe neurological diseases and defects (Adler and Nigro, 2013). These include microcephaly, polymicrogyria, hearing loss, cerebral palsy, epileptic seizures and intellectual disability, as well as the as-yet elusive influence on the emergence of schizophrenia, autism or epilepsy. Despite the incidence and the medical and socioeconomical burden of congenital CMV, which represents about 1% of all live births, the pathophysiological mechanisms underlying the emergence of neurodevelopmental disorders remain elusive (Cheeran et al., 2009). In the absence of effective preventive or curative therapies, understanding the pathogenesis is mandatory before strategies for early interventions can be designed and tested. The pathophysiology of congenital CMV disease is inherently complicated and involves different stages, from maternal CMV primary infection or reactivation and the associated maternal immune responses, to infection and dissemination within the developing brain—not to mention the crossing of the placental and blood-brain barriers.

Insights into the early events following CMV infection of the developing brain are particularly needed. CMVs are generally species-specific; thus, the development of relevant animal models has been, and will continue to be, critical to our understanding of the mechanisms involved in CMV congenital brain disease (Britt et al., 2013; Cekinovic et al., 2014). Whereas multiple routes (intracranial, intraperitoneal or intraplacental) and developmental timepoints (antenatal or neonatal) of CMV inoculation were used, and despite the lack of materno-fetal transmission of CMV infection in rodents, convergent insights into the alteration of innate and adaptive immune responses have emerged from such models (Kosmac et al., 2013; Sakao-Suzuki et al., 2014; Bradford et al., 2015; Slavuljica et al., 2015; Cloarec et al., 2016; Seleme et al., 2017). The production of cytokines by glial cells, the recruitment of peripheral immune cells, and the altered status of microglia, are all likely to influence neuropathogenesis. Microglia are targeted by CMV during human congenital disease (Teissier et al., 2014) and in murine models of intraplacental or neonatal infections (Kosugi et al., 2002; Sakao-Suzuki et al., 2014). Recently, we reported on a rat model of CMV infection of the developing brain displaying prominent infection of brain myelomonocytic cells and early alteration of microglia (Cloarec et al., 2016). Microglial cells originate from erythromyeloid progenitors located in the yolk sac during embryogenesis (Ginhoux et al., 2010) and represent the resident mononuclear phagocytes of the brain (Ginhoux et al., 2013; Ginhoux and Jung, 2014). These cells play crucial roles not only in immune defense, maintenance of the neural environment, injury, and repair, but also in neurogenesis, synaptogenesis, synaptic pruning, connectivity, and modulation of synaptic and neuronal activity (Frost and Schafer, 2016). Importantly, early microglial responses might well combat against CMV infection; but these responses might likely have detrimental effects by interacting with important neurodevelopmental processes.

To which extent and to which direction—favorable or detrimental—early microglia alteration would influence the emergence and severity of neurodevelopmental phenotypes in the developing brain *in utero* in the context of CMV infection represent an important pathophysiological question. Herein, we have tested whether early pharmacological targeting of microglia during pregnancy impacts postnatal neurological manifestations in our previously reported rat model of CMV infection of the embryonic brain (Cloarec et al., 2016) and have identified a critical role for microglia.

MATERIALS AND METHODS

Experimental Design

In this study, we explored whether neuroimmune events associated with brain CMV infection *in utero* could be involved in the emergence of postnatal neurological consequences. We first explored whether infected rats would display phenotypes related to the human pathology. We then tested two independent methods in order to target microglia: (1) doxycycline treatment, which is known to attenuate microglia activation in the developing brain (Cunningham et al., 2013) and (2) liposomes containing clodronate to deplete microglia by uptake and release into the cytosol of a non-hydrolysable ATP analog leading to cell death. Finally, we determined whether animals would still display postnatal neurological consequences following each treatment.

Ethical Statement

Animal experimentations were performed in accordance with the French legislation and in compliance with the European Communities Council Directives (2010/63/UE). Depending on the age of the animals, euthanasia were performed after anesthesia with 4% isoflurane with overdose of pentobarbital (120 mg/kg) or with decapitation. This study was approved under the French department of agriculture and the local veterinary authorities by the Animal Experimentation Ethics Committee (*Comité d'Ethique en Expérimentation Animale)* n°14 under licenses n°01010.02 and n°2016100715494790.

CMV Infection and Pharmacological Treatments

Wistar rats (Janvier Labs, France) were raised and mated at INMED Post Genomic Platform (PPGI) animal facility. Rat CMV recombinant Maastricht strain (RCMV-Δ145-147-gfp) with a green fluorescent protein (GFP) expression cassette, and its production, purification and titration, were reported previously (Baca Jones et al., 2009). *In utero* intracerebroventricular (icv) injections were performed at embryonic day 15 (E15) as previously described (Salmi et al., 2013; Cloarec et al., 2016) in embryos from timed pregnant rats that were anaesthetized with ketamine (100 mg/kg)/xylazine (10 mg/kg). Microglia were depleted *in vivo* with clodronate liposomes icv (0.5 μL/injection, Encapsula Nanosciences) co-injected with 1.75 10^3 pfu of rat CMV; alternatively, phosphate-buffered saline (PBS)-containing liposomes (0.5 μL/injection) were co-injected as a control (untreated condition). Microglia status was modified in the embryos *in vivo* with doxycycline *per os* given to the mother throughout pregnancy (200 mg/kg in food pellet chow, Safe).

Immunohistochemistry Experiments

Immunohistochemistry experiments on coronal brain sections (50–100 μm, vibratome, Microm; 14 μm, cryostat, Leica) were carried out as described previously (Cloarec et al., 2016) with the following primary (anti-Iba1: 1/500, Wako; anti-Cd68, Ed1 clone: 1/200, Millipore) and secondary (Alexa Fluor 568 or 647-conjugated goat anti-rabbit or anti-mouse IgGs; Life Technologies) antibodies. Hoescht 33258 (1:2000, Sigma) was used for nuclei staining.

For tissue clearing experiments (see next subsection), whole infected brains were first immunostained as follows. Tissue samples were dehydrated in methanol/1X PBS series: 20, 40, 60, 80, 100 × 2 for 1h each at room temperature (RT) and then incubated overnight at RT on a platform shaker in a solution of PBSG-T [PBS 1X containing 0.2% gelatin (Sigma-Aldrich), 0.5% Triton X-100 (Sigma-Aldrich) and 0.02% Sodium-Azide (Sigma-Aldrich)]. Next, samples were transferred to PBSG-T containing anti-GFP antibodies (AVES, 1:2,000) and placed at 37°C, with rotation at 100 rpm, for 10 days. This was followed by six washes of 1 h in PBSG-T at RT. Samples were then incubated in secondary antibodies (Donkey anti-chicken Alexa-Fluor 647, Jackson ImmunoResearch, 1:500) diluted in PBSG-T for 2 days at 37°C. After six washes of 1 h in PBSG-T at RT, samples were stored at 4°C in PBS until clearing.

Tissue Clearing

Tissue clearing was performed according to previously reported 3DISCO and iDISCO+ clearing procedures (Erturk et al., 2012; Belle et al., 2014, 2017; Renier et al., 2014) with slight modifications. Briefly, all incubation steps were performed at RT in a fume hood using a 15 ml centrifuge tube (TPP, Dutscher). Samples were first dehydrated in a graded series (20, 40, 60, 80, and 100%) of methanol (Sigma-Aldrich) for 1 h. This was followed by a delipidation step of 20 min in dichloromethane (DCM; Sigma-Aldrich). Samples were transferred to 100% DCM and finally cleared overnight at RT in dibenzylether (DBE; Sigma-Aldrich).

Quantitative Reverse Transcription Polymerase Chain Reaction (qRT-PCR)

Total RNA samples were extracted from whole CMV-infected brains at P1 using TRIZOL reagent (Life Technology). cDNA was synthesized from 1 μg of total RNA using Quantitect Reverse Transcription Kit according to manufacturer protocol (Qiagen). RT-PCRs were carried out using SYBR-Green chemistry (Roche Diagnostics) and Roche amplification technology (Light Cycler 480). PCR primers were designed for GFP transcripts (forward: 5′-gggcacaagctggagtaca; reverse: 5′-cttgatgccgttcttctgc) and for control gene *Rpl19* (ribosomal protein L19) (Cloarec et al., 2016). Primer pairs were optimized to ensure specific amplification of the PCR product and the absence of any primer dimer. Quantitative PCR standard curves were set up for all analyses.

Microscopy, Cell Counting, and Image Analyses

Images of brain sections were acquired with a Stereo Microscope Olympus SZX16 equipped with digital camera DP73, or a Zeiss Axio Imager Z2 microscope with structured illumination (ApoTome) equipped with Zeiss AxioCam MRm camera and processed using Axiovision software, or with a confocal laser scanning microscope Leica TCS SP5X equipped with a white light laser, a 405 nm diode for ultra-violet excitation, and 2 HyD detectors. For cell counting analyses on immunostained brain sections, at least three adjacent brain sections were analyzed throughout the entire z-dimension for each sample using confocal microscopy, according to previously reported procedures (Cloarec et al., 2016) and as further detailed in Supplementary Materials. A phagocytic activation index (PAI) was defined as the ratio of $Iba1^+$ $Ed1^+$ cells to the total number of $Iba1^+$ cells. ImageJ software was used to quantify fluorescence areas on coronal brain sections selected according to their coordinates, as indicated in the rat brain atlas (Khazipov et al., 2015), excluding the meninges. Percentage of fluorescence area of a given brain section was obtained by normalizing to the total area of this brain section.

Whole-brain imaging after tissue clearing was performed using ImspectorPro software (LaVision BioTec) with a binocular stereomicroscope (MXV10, Olympus) equipped with a 2X objective (MVPLAPO, Olympus) used at magnifications 0.8X. A laser (NKT Photonics SuperK extrem) with a 640/30 nm emision filtre and two cylindrical lenses was used to generate a light sheet. Samples were placed in an imaging chamber made of 100% quartz (LaVision BioTec) filled with DBE and illuminated from the side by the laser. Images were acquired with an Andor NEO sCMOS camera (2,560 × 2,160 pixel size, LaVision BioTec). The Z-step size between each image was fixed at 3 μm. 3D (three-dimensional)-images, quantifications and movies were generated using Imaris x64 software (version 8.4.1, Bitplane). Stack images were first converted to Imaris file (.ims) using ImarisFileConverter. 3D reconstruction of the sample was performed using "volume rendering." Brain segmentation was performed using "surface" tool by creating a mask around each volume to remove meninges and peripheral tissue containing antibody aggregates, allowing GFP intensity quantification only

in brain parenchyma. GFP mean intensity obtained was then normalized to the total volume of segmented brain. 3D pictures and movies were generated using the "snapshot" and "animation" tools.

Flow Cytometry

Leukocytes from brains obtained from anesthetized P1 or P7 pups were isolated as previously described (Cloarec et al., 2016). Approximately, 1–3 $\times$ 10^6 leukocytes were incubated with Zombie NIR Fixable Viability kit (1:200; Biolegend) for 20 min at RT. Fc receptors were blocked using mouse anti-rat CD32 antibody (FcγII receptor, clone D34-485) for 10 min. at 4°C to reduce nonspecific binding. Blocked cell samples were stained with antibodies against combinations of cell surface markers as previously described (Cloarec et al., 2016). An average of 1.3 $\times$ 10^5 living singlet cells were analyzed per brain equivalent on a BD LSRFortessa cell cytometer and raw data were analyzed using FACSDiva V8.0 software (BD Biosciences).

Phenotyping

Acquisition of classical developmental righting and cliff aversion reflexes was monitored daily between postnatal day 1 (P1) and P20 as further detailed in Supplementary Materials. The presence of hindlimb paralysis was determined visually in animals that had a postural misplacement and immobility of their hindlimbs. Generalized tonic-clonic epileptic seizures (GTCS) were detected visually, usually after animal handling, especially during cage changing and behavioral testing. They consisted in a classical behavioral sequence including (i) movement arrest and loss of postural equilibrium (ii) hypertonic posture of the trunk, limbs and tail, symmetrically, and (iii) repeated, large clonic movements of all limbs, often with respiratory arrest, incontinence, motor automatisms such as chewing and grooming, terminated by a catatonic phase. Auditory experiments were performed and monitored as detailed in Supplementary Figure 1.

Data Analysis and Statistics

Data were expressed as means ± s.e.m. unless otherwise stated. Non-parametric Mann Whitney test (two-tailed) followed by Bonferroni correction, if needed, and non-parametric Kruskall-Wallis test were used to detect heterogeneous distribution between groups followed by Dunn's post-hoc test for multiple comparisons. Univariate Cox analysis and Fisher's exact test (two-tailed) were used to compare between survival distributions and rates. Parametric Student's *t*-test was used to compare between body weight gains, whereas Chi-square test with Bonferroni correction and mixed model for repeated data were used for all other phenotypic comparisons between groups of animals. Generalized mixed models allow incorporating correlations while observations are collected over time. The group of animal was entered as a covariate and the time point (time when measures were repeated) was introduced as a random effect with autogressive covariance structure to account for the within-subjects correlations, assuming that two measurements timely close to each other are closely correlated, and less correlated when they get farther apart. As we are modeling binary data, we specified the binomial distribution and the logit function as the link one using the PROC GLIMMIX with sas 9.4. Significance threshold was set at 0.05 unless otherwise stated in the figure legends.

RESULTS

CMV Infection of the Rat Fetal Brain Leads to Postnatal Mortality and to Neurological Manifestations

To determine whether CMV infection and the accompanying immune responses in the developing rat brain could be associated with the emergence of postnatal consequences, recalling those seen in the corresponding human congenital disorder, recombinant rat CMV expressing GFP was injected icv in embryos from timed-pregnant rats at E15 as previously described (Cloarec et al., 2016).

During the period of evaluation, i.e., until P20, CMV infection significantly decreased postnatal survival as compared with control animals, which were injected icv with the vehicle (MEM) ($p = 0.0017$) (**Figures 1A**, **2**; Supplementary Table 1). Indeed, 70.4% (38 out of 54 pups) of CMV-infected newborns died in the first three postnatal weeks, compared to 2.9% (one out of 34) controls ($p < 10^{-4}$, Chi2 test). In contrast, antenatal mortality was not affected as no significant difference was observed in the ratio of live animals at birth (72.8%, $n = 103$) as compared to controls (68.5%, $n = 54$) (Fisher's exact test, two-tailed). Body weight was similar at P1 between CMV-infected (7.20 g ± 0.10) and control (7.40 g ± 0.11) newborns (Student's *t*-test), but CMV infection *in utero* significantly impacted the postnatal evolution of body weight gain ($p < 10^{-4}$) (**Figure 1B**; Supplementary Table 1).

Congenital CMV infection is the leading cause of non-hereditary congenital sensorineural hearing loss (Smith et al., 2005). In order to assess whether CMV infection *in utero* causes hearing loss in rats, auditory tests were performed at P40. Hearing thresholds were significantly higher for clicks ($p = 0.0146$) and for 24 kHz bursts ($p = 0.0017$) in the CMV infected group compared to the control group (Supplementary Figure 1; Supplementary Table 1). As hearing loss caused by congenital CMV infection may be progressive in children, we aimed at evaluating hearing thresholds in CMV-infected animals at later ages. However, a significant deterioration of hearing thresholds was also detected in control (MEM-injected) rats between P40 and P60 (data not shown); this restrained us from performing such a longitudinal analysis in CMV-infected rats as the deterioration of hearing thresholds seen in control rats would likely preclude reliable interpretation of the overall data.

Human congenital CMV infection is also well known to be a contributing cause of cerebral palsy, a group of disorders involving variable degree of sensorimotor disabilities (Colver et al., 2014). Sensorimotor development was evaluated by daily monitoring pups between P1 and P20 for the acquisition of the classic righting and cliff aversion reflexes (Rousset et al., 2013). The righting reflex consisted in assessing the ability of rodent pups to coordinate the necessary movement to roll over from

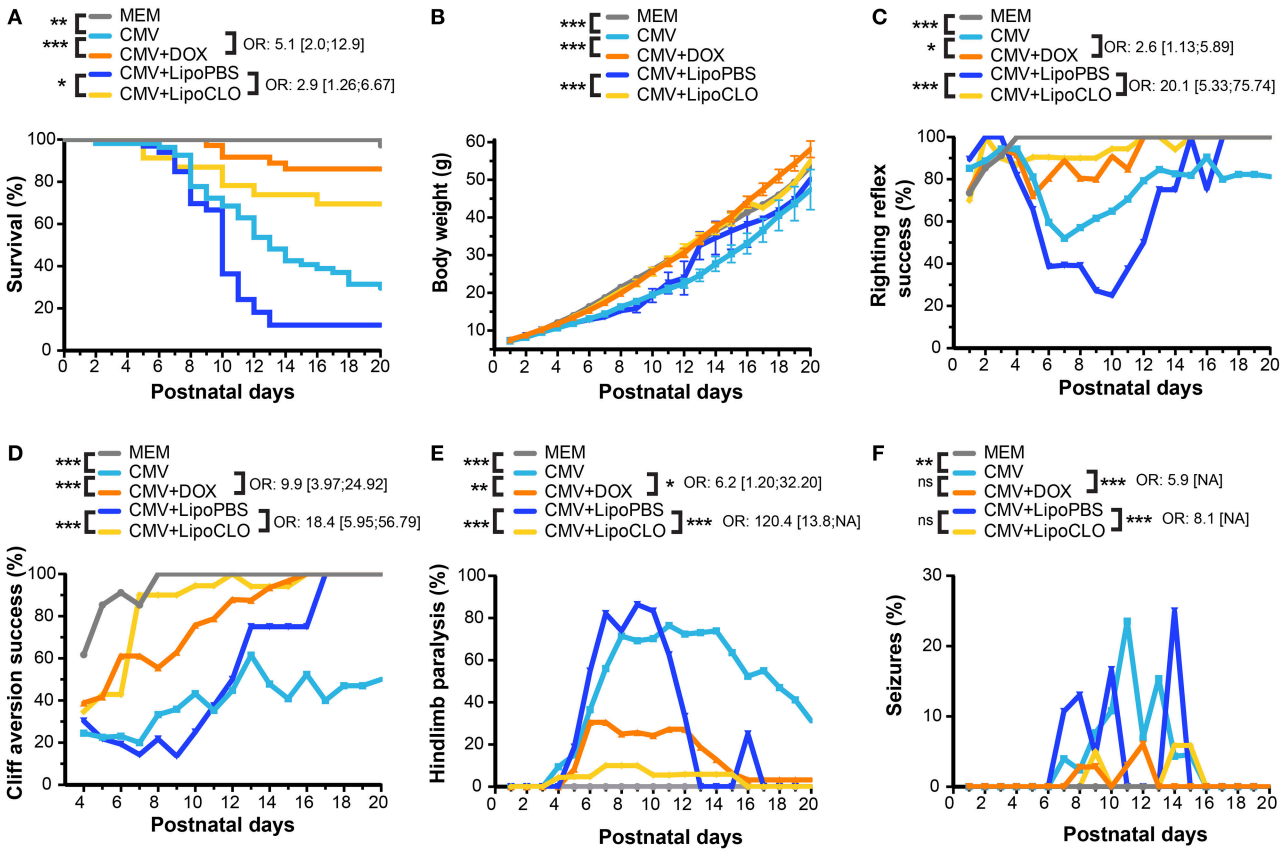

FIGURE 1 | CMV infection of the embryonic rat brain causes decreased survival and neurodevelopmental defects that can be prevented *in utero* by microglia-targeted drug-based strategies. Phenotypic investigations (see **Figure 2**) in the three first postnatal weeks in pups previously subjected to the following procedures during pregnancy: vehicle intraventricularly (icv) (MEM; $n = 34$, four litters); CMV icv, pregnant rat fed with doxycycline (DOX) during pregnancy (CMV+DOX; $n = 36$, four litters); CMV icv, untreated pregnant rat (CMV; $n = 54$, six litters); CMV with clodronate liposomes icv (CMV+LipoCLO; $n = 23$, two litters); CMV with PBS liposomes icv (CMV+LipoPBS; $n = 33$, four litters). Sex ratio did not differ between the five groups at birth ($p = 0.15$, Chi-square test). **(A)** Kaplan-Meier survival curves indicated significant decreased survival in the CMV vs. MEM group, and significant rescues in the CMV+DOX and CMV+LipoCLO groups vs. their untreated counterparts (CMV and CMV+LipoPBS, respectively). **(B)** Cumulative body weight decreased significantly in the CMV vs. MEM group. Significant improvements were seen in the CMV+DOX and CMV+LipoCLO groups vs. their untreated counterparts (CMV and CMV+LipoPBS, respectively). **(C,D)** The proportion of animals succeeding to the righting reflex **(C)** or the cliff aversion reflex **(D)** sensorimotor tests decreased significantly in the CMV vs. MEM group, and significantly improved in the CMV+DOX vs. CMV group, and in the CMV+LipoCLO vs. CMV+LipoPBS group. **(E,F)** Hindlimb paralysis **(E)** and generalized tonic-clonic epileptic seizures (GTCS) **(F)** occurred significantly more frequently in the CMV vs. MEM group. This improved significantly in the CMV+DOX vs. untreated CMV group and in the CMV+LipoCLO vs. untreated CMV+LipoPBS group. Note that because the most severely affected pups were at higher risk to death, a misleading effect of apparent improvement with time could be perceived from curve shapes even for untreated conditions. Left sides of the cohorts legend: univariate Cox analysis **(A)**, mixed model for repeated data **(B–D)**, or Chi2 test with Bonferroni correction **(E,F)**. Right sides of the cohorts legend: odds ratio (OR) ± confidence intervals correspond to the risks in the untreated vs. their corresponding treated groups: postnatal mortality **(A)**; failure at test **(C,D)**; hindlimb paralysis **(E)**; GTCS **(F)**. ***$p < 0.001$; **$p < 0.01$; *$p < 0.05$; ns, not significant, for all figure panels, except **(E,F)** where ***$p < 0.0002$; **$p < 0.002$. NA, not available.

their backs onto their paws. A significant proportion of CMV-infected pups showed inability to right, as compared with MEM-injected pups, which all performed the test successfully ($p < 10^{-4}$; **Figures 1C**, **2**; Supplementary Figure 2A; Supplementary Table 1). In the cliff aversion test, pups were placed with their forepaws overhanging the edge of a board and the time required to turn away from the edge was recorded. Control MEM-injected rats showed a clear performance improvement from P4 as all succeeded the test after P8 (**Figures 1D**, **2**; Supplementary Table 1). In contrast, a significant proportion of CMV-infected pups was unable to complete the cliff aversion test all along the first three postnatal weeks ($p < 10^{-4}$; **Figure 1D**, **2**; Supplementary Figure 2B; Supplementary Table 1). Hindlimb paralysis was detected in the first three postnatal weeks in 83.3% of CMV-infected pups, likely preventing animals from turning away from the cliff. Hindlimb paralysis was not seen in any non-infected pup ($p < 10^{-4}$; **Figures 1E**, **2**; Supplementary Table 1).

Patients with human congenital CMV are also at high risk of postnatal epileptic seizures (Suzuki et al., 2008). Consistently, 24.1% of CMV-infected rat pups exhibited GTCS at least once in the first three postnatal weeks whereas none of MEM-injected pups ever showed any GTCS ($p = 0.002$; **Figure 1F**, **2**; Supplementary Table 1). Interestingly, a clear relationship between epileptic seizures and death was observed wherein 85%

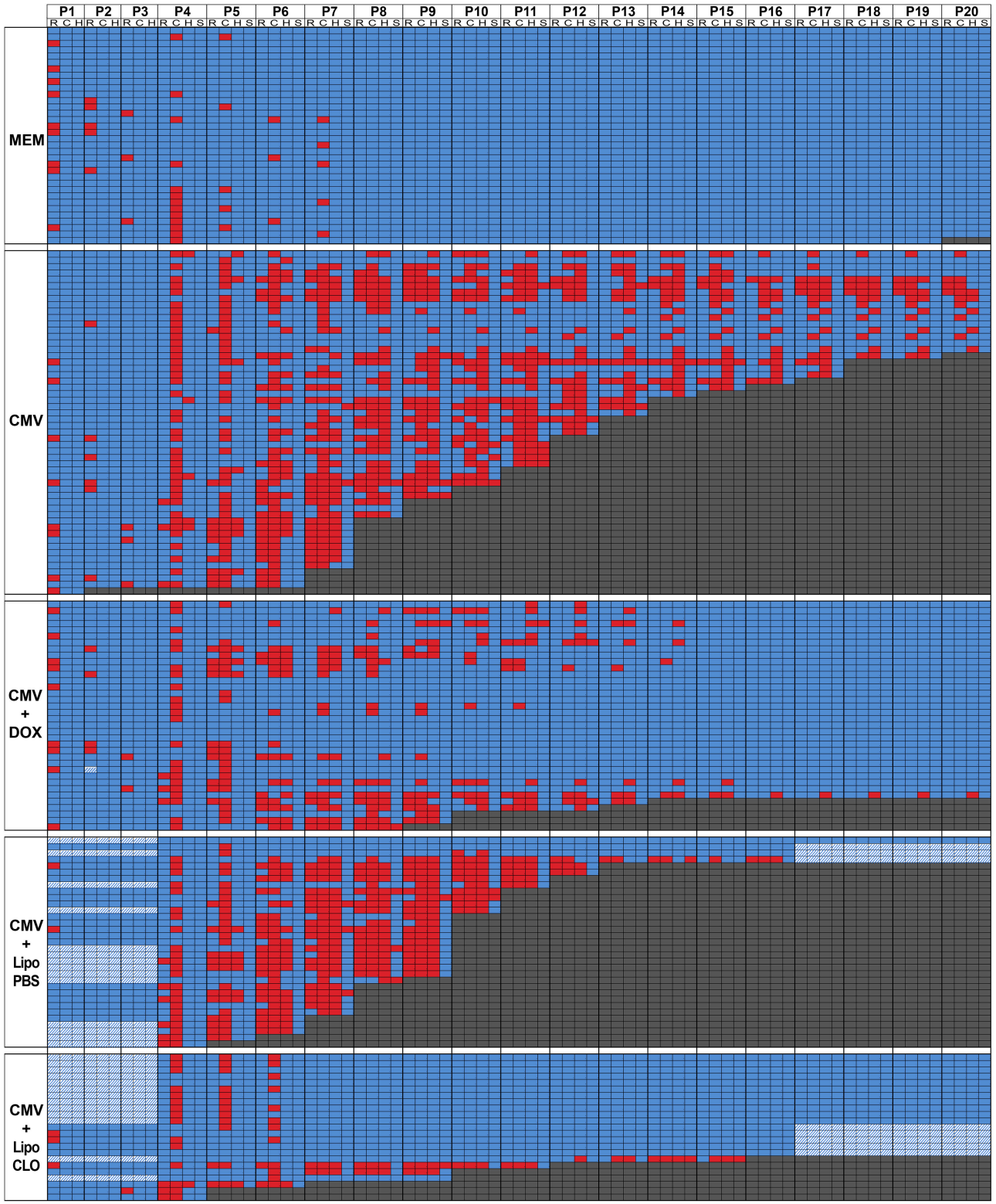

FIGURE 2 | Overview of day-per-day phenotype assessment in the first three postnatal weeks. Color-encoded overview of postnatal test evaluations and observations performed as from postnatal day P1 (see also **Figure 1**; Supplementary Table 1). Five experimental cohorts of rats were analyzed postnatally: i/control embryos were injected intraventricularly (icv) with vehicle at E15 (MEM; $n = 34$ from four litters); ii/embryos were injected icv with rat CMV at E15 and were born from dams fed with

(Continued)

FIGURE 2 | control chow all over pregnancy (CMV; $n = 54$ from six litters); iii/embryos were injected icv with rat CMV at E15 and were born from dams fed with doxycycline-supplemented chow all over pregnancy (CMV+DOX; $n = 36$ from four litters); iv/embryos were injected icv with rat CMV and with control (PBS) liposomes at E15 (CMV+LipoPBS; $n = 33$ from 4 litters); v/embryos were injected icv with rat CMV and with clodronate liposomes at E15 (CMV+LipoCLO; $n = 23$ from 2 litters). The table shows color-encoded results for each individual pup evaluated on a daily basis (P1 to P20 columns) for the phenotypic parameters as detailed below. Performances at the righting (R sub-column) and cliff aversion (C sub-column) reflexes were measured from P1 or from P4, respectively; performances to right (R) or to turn away from the cliff (C) were color-encoded following a binary rule (blue: success; red: failure). For righting reflex evaluation, rat pups were placed in a supine position, and the time required to flip to the prone position was measured. For the cliff aversion reflex, animals were placed with their forepaws overhanging the edge of a board; the time required to turn >90° away from the edge was recorded. For both tests, a maximum observation time of 30 s. was used. Each pup was also monitored daily for the appearance of hindlimb paralysis (H sub-column) and of generalized tonic-clonic seizures (GTCS) (S sub-column); the data were color-encoded following a binary rule where blue reflected the absence of either event, whereas red indicated the occurrence of paralysis or seizure. When pups died, this was also annotated on the table and color-encoded in dark gray. Hatched cells: data unavailable.

of seizing rats deceased, as compared to 37% of non-seizing rats ($p < 10^{-4}$, Chi2 test). Similarly, 72% of rats with hindlimb paralysis deceased during the period of evaluation, as compared to 13% of non-paralyzed rats ($p < 10^{-4}$).

Acute icv Injection of Clodronate Liposomes *in Utero* Depletes Microglia and Improves the Postnatal Outcome

The consequences of rat CMV infection as described above, recapitulated several cardinal clinical features of the human pathology. The early and prominent infection and alteration of microglia upon CMV infection of the developing rat brain *in utero* (Cloarec et al., 2016) suggested that microglia might contribute to the pathophysiology of congenital CMV. In order to evaluate the possible impact of microglia on the emergence of the neurological and other developmental defects, experiments were designed to target microglia with drugs during pregnancy.

In a first series of experiments, microglia were acutely depleted with clodronate liposomes co-injected icv together with rat CMV at E15. Immunohistochemistry experiments confirmed that clodronate liposomes triggered a significant decrease in the total number of $Iba1^+$ microglial cells in the dorsolateral part of the striatal wall of the lateral ventricles taken as the region of interest (ROI) at P1 (112.3 cells/ROI ± 9.37), as compared to the condition where PBS liposomes were used (558.5 cells/ROI ± 128.3; $p = 0.0022$; **Figure 3A**; Supplementary Table 2). A significant decrease in the absolute number of phagocytically active, $Iba1^+$ $Ed1(CD68)^+$ microglia was also oberved (clodronate liposomes: 27.17 cells/ROI ± 2.80; PBS liposomes: 141 cells/ROI ± 23.82) ($p = 0.0022$). This was associated with a dramatic reduction of CMV spreading, since GFP^+ infected cells were barely visible within the brains of treated embryos. The reduction in CMV infection was confirmed by quantifying the percentage of fluorescent areas in coronal brain sections taken from treated and untreated pups at P1 ($p = 0.0022$; **Figure 3B**; Supplementary Table 3).

Microglia depletion and reduction of brain CMV infection were associated with a significant improvement of survival and neurodevelopmental outcomes. Postnatal mortality was reduced by 2.9 fold ($p = 0.012$) in clodronate-treated, CMV-infected pups, relative to untreated, infected pups (**Figures 1A**, **2**; Supplementary Table 1). Indeed, 69.6% (16 out of 23 newborns) of clodronate-treated, CMV-infected newborns survived at P16, as compared to 12.1% (4 out of 33) of untreated, CMV-infected newborns ($p < 10^{-4}$, Chi2 test). A similar significant increase in body weight gain was observed in the clodronate-treated pups ($p < 10^{-4}$; **Figure 1B**; Supplementary Table 1).

CMV-infected pups treated with clodronate liposomes *in utero* also performed significantly better at the righting and the cliff aversion reflexes when compared to infected pups, which had received control (PBS) liposomes *in utero* (**Figures 1C,D**, **2**; Supplementary Figure 2; Supplementary Table 1). With clodronate the odds in favor of success to righting and to cliff aversion tests were at 20.1:1 and 18.4:1, respectively ($p < 10^{-4}$ for both). Hindlimb paralysis also improved significantly ($p < 10^{-4}$) with clodronate liposomes (17% of rat pups) as compared with control liposomes (88%) (**Figures 1E**, **2**; Supplementary Table 1). There was a dramatic, 120.4-fold decrease in the risk to hindlimb paralysis in clodronate-treated CMV-infected rats ($p < 10^{-4}$). Epileptic seizures also occurred less frequently in the first three weeks of life upon treatment with clodronate liposomes (8.7% of rats experiencing at least one seizure), as compared to PBS liposomes (24.2% of epileptic rats) but this difference did not reach statistical significance ($p = 0.14$) (**Figures 1F**, **2**; Supplementary Table 1). However, when the risk of seizures was considered, it decreased significantly by 8.1-fold in clodronate-treated, CMV-infected rats when compared to their PBS-liposomes counterparts ($p < 10^{-4}$).

Hence a single injection of clodronate liposomes at the time of CMV icv infection not only led to depletion of microglia and to a dramatic reduction of active CMV infection in the rat developing brain, but the treatment also led to a stunning improvement of survival, body weight gain, sensorimotor development and epileptic seizures in early postnatal life.

Chronic Administration of Doxycycline to Pregnant Mothers Improves Microglia Phenotype

Tetracyclines can efficiently modify microglia status in the brains of rat pups after chronic maternal administration during pregnancy (Cunningham et al., 2013). Tetracyclines impact on microglia phenotype independently of their canonical antibacterial action (Tikka et al., 2001). In order to confirm the possible role of microglia in the emergence of phenotypes associated with brain CMV infection, doxycycline, a second-generation, lipophilic tetracycline that crosses blood-brain and placental barriers, was administered *per os* to pregnant dams from E0 to birth. The effects of doxycycline treatment on

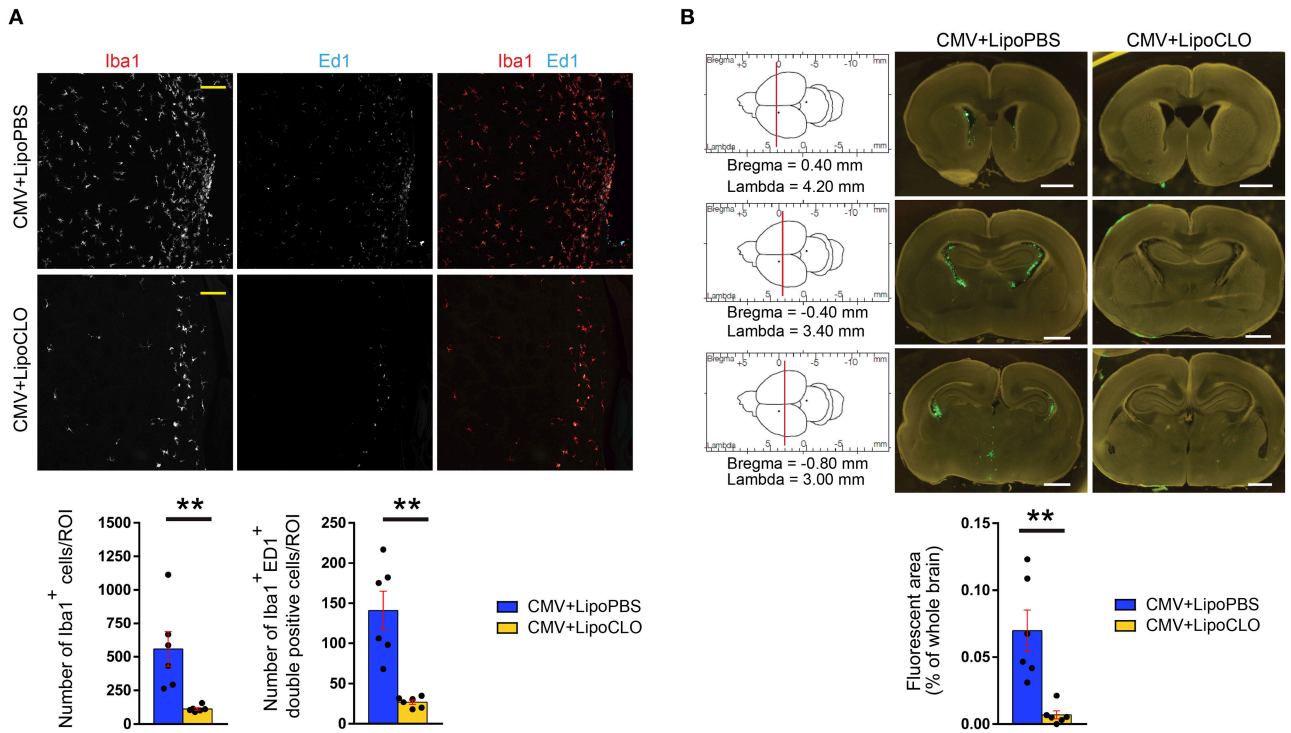

FIGURE 3 | Clodronate liposomes deplete microglia and reduce CMV spreading in the developing brain. Recombinant rat CMV allowing expression of GFP (green) in the infected cells was injected icv in rat embryos at E15 together with either clodronate liposomes (LipoCLO) to deplete microglia, or PBS liposomes (LipoPBS) as control. **(A)** LipoCLO decreased the number of Iba1$^+$ microglia (red) and of Iba1$^+$, Ed1$^+$ (cyan) phagocytically active microglia. Three to four adjacent coronal brain sections were analyzed by confocal microscopy throughout the entire z-dimension ($n = 6$ brains in each condition). ROI: region of interest (775 × 775 μm^2). Bar: 100 μm. Mann-Whitney test, two-tailed, with Bonferroni correction. $^{**}p < 0.005$. **(B)** LipoCLO reduced rat CMV infection of the brain. Brains were analyzed at P1 using fluorescent binocular microscopy. Three sections were selected according to their coordinates in the rostrocaudal axis (left). CMV infection decreased dramatically after treatment with LipoCLO ($n = 6$ brains in each condition), as quantified by measuring the proportion of fluorescent (GFP) areas. Bar: 1 mm. Mann-Whitney test, two-tailed. $^{**}p < 0.01$.

microglia phenotype was tested by immunohistochemistry in the dorsolateral part of the striatal wall of the lateral ventricles, a region where active CMV infection was frequently detected (Cloarec et al., 2016), and by multicolor flow cytometry analysis of the whole brain.

In line with previously reported experiments (Cloarec et al., 2016), rat CMV infection at E15 led to a significant increase in the proportion of phagocytically active, Iba1$^+$ Ed1(CD68)$^+$ microglia/macrophages cells at P1. Indeed, the phagocytic activation index (PAI), defined as the ratio of Iba1$^+$ Ed1$^+$ cells to the total number of Iba1$^+$ cells, was significantly increased (42.74% ± 6.16) as compared with control (MEM-injected) rats (PAI = 14.28% ± 4.29) (p = 0.0174), and was significantly improved by doxycycline (17.32% ± 6.44; $p = 0.0321$) (**Figure 4A**; Supplementary Table 2). Consistent data were obtained when whole brains were analyzed at P1 by flow cytometry (**Figure 4B**; Supplementary Table 4). As previously reported (Cloarec et al., 2016), a significant increase in the proportion of major histocompatibility (MHC) class II-positive microglia (fraction IV: CD45$^{low/int}$, CD11b/c$^+$, RT1B$^+$) was detected in CMV-infected brains (13.98% ± 2.12) as compared with controls (0.73% ± 0.05; $p <$ 0.0001). This increase in activated microglia was significantly counteracted in doxycycline-treated, CMV-infected pups (5.66% ± 1.13) ($p = 0.0483$). The proportions of other types of CD45$^+$ hematopoietic cells were not changed by doxycycline (**Figure 4B**; Supplementary Figure 3; Supplementary Table 4). Importantly, the favorable impact of the doxycycline *in utero* treatment on reactive microglia seen at P1 did not last after treatment discontinuation. The proportion of reactive, CD45$^{low/int}$, CD11b/c$^+$, RT1B$^+$ microglia (fraction IV) at P7 were similar in treated (55.76% ± 4.60) and in untreated (58.93% ± 5.54) CMV-infected rats (**Figure 4C**; Supplementary Figure 3; Supplementary Table 4).

The consequences of *in utero* treatment with doxycycline on brain CMV infection *per se* were also evaluated. Independent series of brains were submitted to tissue clearing using the iDisco method (Renier et al., 2014). Fluorescence-based 3D quantification of the infected areas of whole brains showed no difference between treated and untreated rats at P1 (**Figure 5A**; Supplementary Table 3; Supplementary Videos 1, 2). Consistently, no significant difference in GFP gene expression was found by qRT-PCR between treated and untreated CMV-infected brains at P1 (**Figure 5B**; Supplementary Table 5). Moreover, the proportions of CMV-infected, GFP$^+$ cells as detected by flow cytometry analysis performed on CD45$^+$

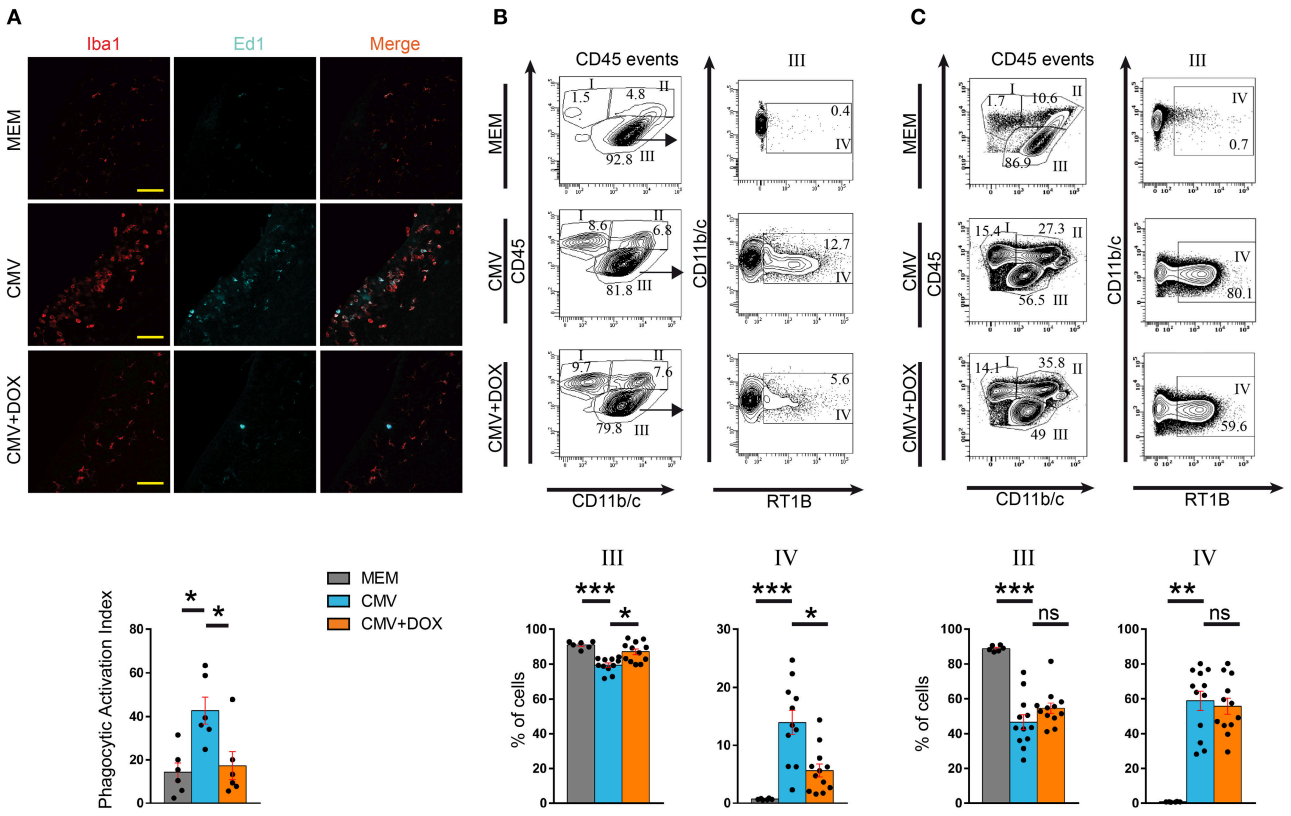

FIGURE 4 | CMV infection of the embryonic rat brain leads to altered microglia phenotype, which is rescued by maternal feeding with doxycycline throughout pregnancy. **(A)** Microglia status in the lateral ventricles was assessed on coronal sections observed by confocal microscopy at P1 by quantifying microglial cells (red, Iba1$^+$) and phagocytically active microglial cells (Iba1$^+$, red; Cd68/Ed1$^+$, cyan). Those values were then used to calculate the phagocytic activation index (PAI) defined as the ratio of the number of Iba1$^+$, Ed1$^+$ activated cells to the total number of Iba1$^+$ cells. PAI increased in the CMV vs. the MEM group. Doxycycline (CMV+DOX) significantly counteracted PAI increase ($n = 6$ brains in each condition). ROI: region of interest (387 × 200 μm^2). Bar: 50 μm. Kruskall-Wallis test followed by Dunn's *post-hoc* test. *$p < 0.05$. **(B,C)** Flow cytometry analysis of leukocytes collected at P1 **(B)** and P7 **(C)**. Total leukocytes (CD45 events) were gated for CD45 and Cd11b/c, thus defining fractions I (lymphocytic cells), II (myelo-monocytic cells) and III (resident microglial cells) (see also Supplementary Figure 3). Fraction III corresponding to CD45$^{low/int}$, CD11b/c$^+$ microglial cells was further characterized for RT1B expression to identify reactive microglia (RT1B$^+$; fraction IV). Representative flow cytometry plots and the corresponding quantifications are shown for each group. **(B)** At P1, the increased proportion of reactive microglia triggered by CMV infection was significantly counteracted by doxycycline ($n = 6$ MEM; $n = 11$ CMV; $n = 12$ CMV+DOX). **(C)** At P7, i.e., 7 days after discontinuation of doxycycline, the decreased proportion of total microglial cells (fraction III) and, within that fraction, the increased proportion of reactive microglia (fraction IV) triggered by CMV infection, were not counteracted by doxycycline treatment given *in utero* ($n = 6$ MEM; $n = 12$ CMV; $n = 12$ CMV+DOX). Kruskall Wallis test followed by Dunn's post test. ***$p < 0.001$; **$p < 0.01$; *$p < 0.05$; ns, not significant.

hematopoietic cells isolated from CMV-infected brains at P1, were not significantly different between doxycycline-treated and untreated pups (**Figure 5C**; Supplementary Table 4). Also, no significant difference in GFP$^+$ infected cells was found by flow cytometry at P7 between doxycycline-treated and untreated pups. Hence the early and transient impact of doxycycline on microglia phenotype was not accompanied by a parallel decrease in CMV infection of the brain.

Chronic Doxycycline Administration to the Mother Throughout Pregnancy Improves the Postnatal Outcome

Owing to the transient improvement of microglia status upon maternal administration of doxycycline during pregnancy, we then tested whether this would in turn impact the postnatal outcomes. In doxycycline-treated, CMV-infected pups, survival rate improved significantly as compared to infected pups from untreated dams (**Figure 1A**, **2**; Supplementary Table 1). CMV-infected pups treated with doxycycline *in utero* had a risk 5.1 lower to postnatal death in the first three postnatal weeks, than their untreated, CMV-infected counterparts ($p = 0.0006$). At P20, 86.1% ($n = 31$ out of 36 newborns) of infected pups from doxycycline-treated dams had survived as compared to 29.6% ($n = 16$ out of 54 newborns) of infected pups from untreated dams ($p < 0.001$, Chi2 test). Significant improvement in body weight gain was also observed in CMV-infected pups after doxycycline treatment *in utero* ($p < 10^{-4}$; **Figure 1B**; Supplementary Table 1).

Whereas no rescue could be obtained at P40 on hearing threshold after doxycycline treatment (Supplementary Figure 1; Supplementary Table 1), responses to sensorimotor tests (righting and cliff aversion reflexes) improved significantly

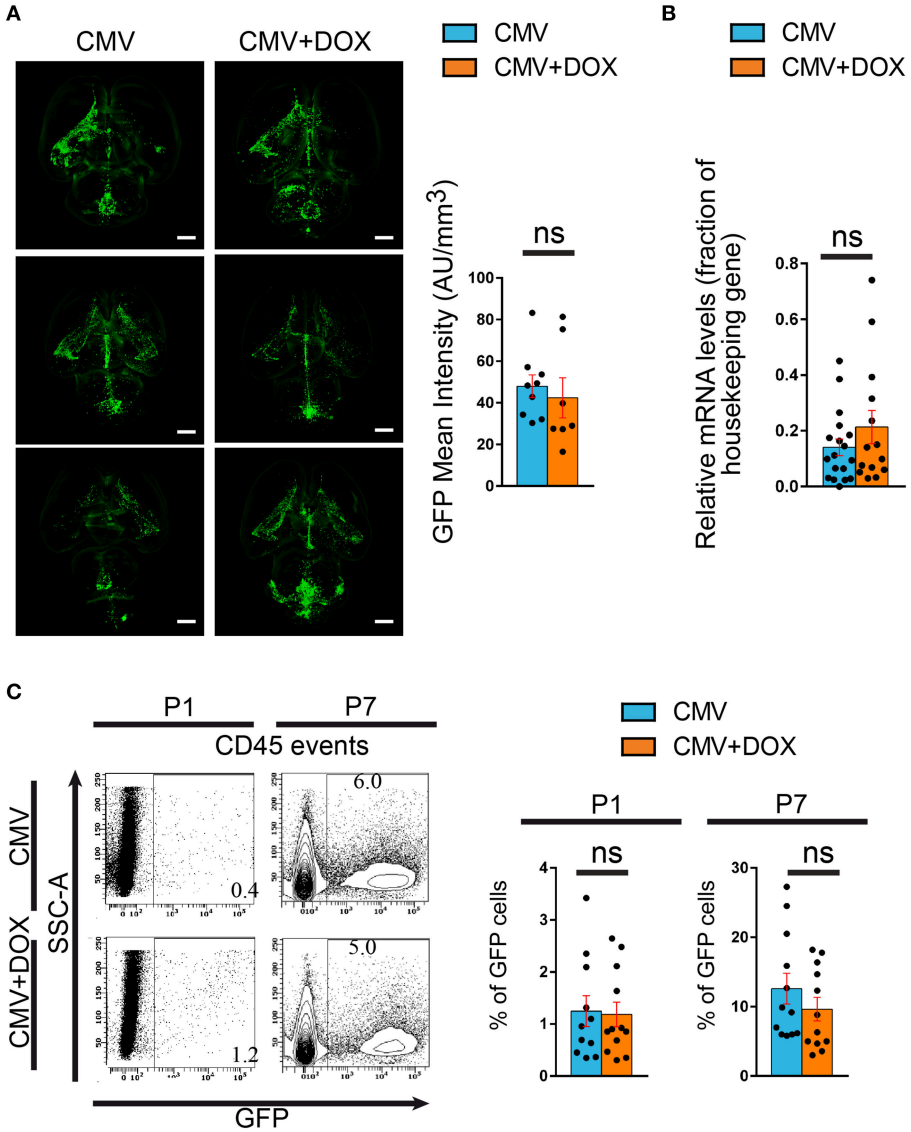

FIGURE 5 | Maternal feeding with doxycycline throughout pregnancy does not impact rat CMV infection of the brain. Green fluorescent protein (GFP) expression was used to monitor infection of the pups' brains by rat CMV with three independent methods. **(A)** Tissue clearing. Whole brains from P1 rat pups were submitted to tissue clearing and GFP expression was quantified by measuring mean fluoresence intensity normalized to each corresponding total brain volume. Representative examples of clarified brains are shown (light sheet microscopy) (see also Supplementary Videos 1, 2). No significant difference was found between the CMV+DOX group ($n = 7$) and its untreated counterpart (CMV; $n = 9$). Bar: 2 mm. Mann Whitney test, two-tailed. ns, not significant. **(B)** qRT-PCR. Relative mRNA expression of GFP was assessed by quantitative RT-PCR in CMV-infected brains at P1, using *RPL-19* as reference gene. No difference was found between the CMV+DOX group ($n = 14$) and its untreated counterpart (CMV; $n = 18$). Values of fold change represent averages from triplicate measurements for each sample. Mann Whitney test, two-tailed. ns: not significant. **(C)** Flow cytometry. Relative proportion of GFP^+, CMV-infected cells was estimated by flow cytometry analysis of $CD45^+$ cells isolated from CMV-infected brains at P1 and at P7. No difference was found between the CMV+DOX group ($n = 12$) and its untreated counterpart (CMV; $n = 11$). SSC, side-scattered light. Mann Whitney test, two-tailed. Ns, not significant.

($p = 0.025$ and $p < 10^{-4}$, respectively) in infected pups treated with doxycycline *in utero* (success to righting: odds ratio 2.6:1; success to cliff aversion: odds ratio 9.9:1) (**Figures 1C,D**, **2**; Supplementary Figure 2; Supplementary Table 1).

Hindlimb paralysis was also observed less frequently after doxycycline administration (**Figures 1E**, **2**; Supplementary Table 1). Hence, 50% ($n = 18$ out of 36) of doxycycline-treated, CMV-infected pups displayed paralysis during the first three postnatal weeks, as compared to 83.3% ($n = 45$ out of 54) in the untreated counterparts ($p = 0.001$). Consistently, the risk of hindlimb paralysis reduced by 6.2 fold ($p = 0.03$). Whereas the proportion of epileptic, CMV-infected rats decreased, albeit not significantly ($p = 0.12$), upon treatment with doxycycline (11%) as compared with untreated, infected rats (24%), the risk

of epileptic seizures during the period of evaluation decreased significantly by 5.9-fold in CMV-infected rats receiving doxycycline *in utero* ($p < 10^{-4}$; **Figures 1F**, **2**; Supplementary Table 1).

Hence, while doxycycline administration during pregnancy did not significantly modify the amount of active CMV infection in the developing brain after birth, it led to a transient modification of microglia phenotype that was associated with long-term favorable effects on survival, body weight gain and neurodevelopmental outcomes.

DISCUSSION

Phenotypes in the Rat and in Humans

Studies on different rodent models that showed similarities with the human disease at the neuroanatomical, cellular and molecular levels, have suggested that neuroimmune alterations might play an important pathophysiological role. In a rat model of CMV infection of the developing brain *in utero*, we reported recently the detection of early neuroimmune anomalies including microglia alteration (Cloarec et al., 2016). Utilizing this model, we herein demonstrate altered postnatal oucomes in CMV infected neonates including increased postnatal lethality, decreased body weight gain, early-onset epileptic seizures, sensorimotor impairment reminiscent of cerebral palsy, and hearing defects. Despite the fact that maternal, placental and peripheral embryonic events were purposedly bypassed by directly infecting the embryonic brain *in utero*, this model recapitulated several fundamental phenotypic features of the human pathology following CMV infection. Moreover, the postnatal outcomes varied dramatically among the rat pups, as in the human disease. This indicates that in addition to the aforementioned upstream factors, the somehow unpredictable and highly diverse outcome of congenital CMV infection might rely, at least partly, on fetal brain-related events. The consequences of CMV infections of the brain on the future neurological phenotypes had been hardly addressed in rodent models until recently. Auditory features associated with inflammation of the inner ear recalling the hearing losses seen in human congenital infections were recently reported in a neonatal mouse model (Bradford et al., 2015). Also, early and long-term neurological dysfunctions including acquisition of the righting and cliff aversion reflexes as well as motor performances and social behavior have been reported very recently in a murine model of neonatal infection (Ornaghi et al., 2017). Interestingly, in the present rat model of rat CMV infection *in utero*, more dramatic neurological consequences were observed, probably because CMV was inoculated directly into the ventricles and at an earlier developmental stage.

Targeting Microglia With Doxycycline and Clodronate

Generally, microglia-targeted rescue strategies had already been successfully used in a range of models for various postnatal neurological insults and disorders, such as neonatal excitotoxic brain damage (Dommergues et al., 2003), experimental autoimmune encephalitis (Ponomarev et al., 2011), cerebral palsy (Kannan et al., 2012), or Alzheimer disease (Hong et al., 2016). In the present model of prenatal cerebral infection, two previously reported microglia-targeted drug-based strategies both led to the successful rescue of the neurological phenotypes. While the respective modes of action of clodronate liposomes on the one hand, and doxycycline on the other hand, are unrelated at the molecular and subcellular levels, we cannot firmly exclude the possibility that they would both have influenced the phenotypes by microglia-independent, off-target mechanisms. Doxycycline might have other biological consequences (Yrjanheikki et al., 1999) such as a broader anti-inflammatory action on other immune and non-immune cells (Yrjanheikki et al., 1998). Hence, it was shown in a murine model of multiple sclerosis that minocycline, another second-generation tetracycline, can decrease leukocytes infiltration into the spinal cord (Brundula et al., 2002). However, in our model doxycycline did not modify the different fractions corresponding to the non-microglial immune cells detected in the CMV-infected brains (e.g., monocytes/macrophages, dendritic cells, T cells and B cells), as analyzed by flow cytometry (see Supplementary Figure 3). Moreover tetracyclines have already been used to decrease microglia activation in NMDA-induced excitotoxicity (Tikka et al., 2001), experimental autoimmune encephalitis (Popovic et al., 2002), or epileptogenesis (Abraham et al., 2012).

Influence of Early Microglia Alteration on the Postnatal Phenotypes

Whereas clodronate liposomes led to microglia depletion associated with a dramatic decrease in brain CMV infection, doxycycline promoted microglia modification while leaving CMV infection of the brain unchanged. Moreover, the early improvement of microglia was associated with long-term beneficial effects. Indeed, the effect of doxycycline on microglia was transient and was no longer detected at P7. Despite this observation, the favorable impact on the clinical phenotypes lasted long after treatment was stopped. This suggests that the early alteration of microglia following CMV infection had long-term detrimental effects on the neurological and other outcome. Although we cannot exclude the existence of more subtle changes such as a modification in the distribution of CMV in different brain areas, our data indicate that early microglia alteration, rather than CMV infection and viral cytopathic effects *per se*, promoted the emergence of most neurological and other postnatal manifestations. The relationship between CMV load and the occurrence and severity of CMV-related phenotypes has indeed been challenged in a murine model of neonatal CMV infection (Kosmac et al., 2013; Seleme et al., 2017) and in human congenital CMV (Revello et al., 1999; Boppana et al., 2013). Our data are congruent with recent reports on inflammatory processes in CMV infection of the murine neonatal brain (Kosmac et al., 2013; Bradford et al., 2015; Kawasaki et al., 2015; Slavuljica et al., 2015; Seleme et al., 2017).

The microglia-targeted strategies used in the present study led to significant improvements of sensorimotor impairments and of epilepsy. The alteration and possible role of microglia in epileptic disorders and in cerebral palsy have already been discussed

(Fleiss and Gressens, 2012; Vezzani et al., 2012; Devinsky et al., 2013). The presence of hearing impairment in the present model might be difficult to interpret. First, a progressive deterioration of auditory performances was seen in the control rats; this is consistent with previous reports on the existence of age-related hearing loss in control Wistar rats (Alvarado et al., 2014), which was likely related with the lack of strial melanin in albino rodents (Ohlemiller, 2009). Second, a detrimental effect of doxycycline on the development of the auditory system cannot be excluded, notably given its known potential auditory toxicity. Third, whereas hearing loss caused by murine neonatal CMV infection was recently associated with persistent inflammation of the inner ear (Bradford et al., 2015), the lack of significant improvement after doxycycline treatment *in utero* might indicate that microglia does not play an important role in hearing impairment in our model.

Microglia in Brain Development and in Neurodevelopmental Disorders

A crucial pathogenic impact of early microglia alteration in the context of congenital CMV is consistent with the role of microglia in the development, the functioning and the pathology of the central nervous system (Prinz and Priller, 2014). Microglia undergo several programmed changes during brain development in rodents (Matcovitch-Natan et al., 2016), impact synaptic transmission, as well as synapse formation and elimination. Microglia also shape embryonic and postnatal brain circuits (Paolicelli et al., 2011; Schafer et al., 2012). The alteration of microglia by CMV infection early during brain development might well have disrupted the timing of such developmental programs, leading to altered development of neuronal networks and the subsequent detrimental neurological outcome. As an example, susceptibility to epileptic seizures could be caused by several microglia-dependent processes, such as the alteration of migration and neocortical laminar distribution of interneurons, the altered control of synaptic development and regulation, or an increased glutamate release (Paolicelli and Ferretti, 2017). As a matter of fact, the transient improvement of microglia status as obtained here with doxycycline was sufficient to obtain dramatic improvements of the neurological phenotypes. Prenatal alteration of microglia and the accompanying microglia priming can have long-term consequences on synaptic functioning (Roumier et al., 2008) and could participate in the susceptibility to neurodevelopmental disorders occurring as consequences of viral infections of the developing brain.

Besides Microglia

Whereas early microglia improvement was sufficient to impact significantly the prenatal phenotypes, this of course does not exclude the important roles likely played in parallel by other components of the neuroimmune system, either at the molecular level such as cytokines and chemokines, or at the cellular level such as infiltrating monocytes or lymphocytes. Hence, the role of T lymphocytes infiltration in CMV infection has been proposed (Bantug et al., 2008); T cells control viral spread within the brain and are pivotal in resolving acute CMV infection of the neonatal murine brain (Slavuljica et al., 2015). However, the amount of T cells was not impacted by doxycycline in the present model, which is consistent with the lack of any significant change in CMV infection observed here after doxycycline treatment. Similarly, doxycycline did not modify the proportions of dendritic cells or monocytes within the infected brains. Other types of glial cells such as astrocytes are also likely to play a pathophysiological role, as reported in other models of CMV infection (Lokensgard et al., 2016; Ornaghi et al., 2017), and notably given the known reciprocal interactions between microglia and astrocytes.

Besides CMV

Apart from congenital CMV, microglia infection and alteration can occur in a wide range of viral encephalitis. Microglia might participate in neuronal damage seen in encephalitis caused by Japanese encephalitis virus (Thongtan et al., 2012). Microglia status might inform on neuronal dysfunctioning following murine leukemia virus-induced encephalopathy (Xue et al., 2010). Microglia might also participate in HIV-associated cognitive and behavioral impairments (Hong and Banks, 2015). $Il34^{-/-}$ mice with fewer microglia were protected from synaptic defects triggered by West Nile virus infection (Vasek et al., 2016). Interestingly also, acute administration of minocycline prevented against long-term behavioral outcome in a model of temporal lobe epilepsy caused by infection with Theiler's virus (Barker-Haliski et al., 2016). Whether microglia-targeted strategies could be successfully applied to these and other congenital infections of the brain remains to be demonstrated.

From the Rat Model to the Human Disease

Although extrapolation to the corresponding human pathology should be approached with caution, it is tempting to speculate that microglia might also play an important role in human neurological disease following congenital CMV infection. As a matter of fact, microglial nodules and infected microglial cells were detected in human CMV-infected fetal brains (Teissier et al., 2014). While different innovative strategies to combat against CMV infection and its consequences have been proposed recently in complementary rodent models (see Ornaghi et al., 2017), microglia represent another promising target for various neuropathological conditions (Cartier et al., 2014) Strategies directed toward the immune system have already been proposed with the use of corticosteroids in a mouse model of neonatal CMV infection (Kosmac et al., 2013) and with the administration of immunoglobulins to prevent against human CMV congenital infection (Revello et al., 2014). Pharmacological interventions *in utero* have already been successful in rodent models of motor impairment (Yamada et al., 2009) and of epilepsy (Salmi et al., 2013). The use of doxycycline in pregnancy could also be revisited in line with its potential benefits (Cross et al., 2016). Generally risk reduction of fetal infection and subsequent disease still remains a crucial issue (Hamilton et al., 2014). Together with progress in fetal medicine (Bianchi, 2012) and in the identification of reliable biomarkers to predict severity (Desveaux et al., 2016), the present study, which now warrants confirmation and expansion using complementary rodent models of CMV infection and other microglia modifying tools, represents a first

proof-of-principle for the future design of microglia-targeted strategies to prevent against the severe neurological outcome of congenital CMV infection of the brain.

CONCLUDING REMARKS

In conclusion, we have shown here that the neurological and other phenotypes caused by CMV infection of the rat brain *in utero*, are caused by the early activation of microglia, rather than by the virus load by itself, at least in this model - suggesting that microglia might also influence the corresponding human disease.

AUTHOR CONTRIBUTIONS

RC and SB performed most experiments and data analyzes, with equal contribution. NT supervised, performed and validated auditory tests and participated in the overall strategy. FS performed most *in utero* injections. HL supervised and participated in flow cytometry. SC performed a subset of immunohistochemistry, confocal microscopy and image analyzes. MS participated in immunohistochemistry and pilot rescue experiments at the initial stages of the project. VP designed and performed most statistical analyzes. EBo performed and analyzed auditory tests. EP-P performed and analyzed qRT-PCR. EBu supervised *in utero* injections and performed a subset of them. FM headed the InMAGIC imaging platform and participated in images acquisition and analyzes. PG participated in the follow-up of the project and in the overall strategy. MM provided strong scientific support on flow cytometry analyzes. TS and DS provided and purified the RCMV strain and provided strong expertise in virology. NB provided scientific support and advices all along the duration of the project and participated in the overall strategy. PS was the project leader. He decided on the overall strategy, directed the follow-up of experiments, supervised data analysis, and wrote the manuscript with help of RC and SB. All authors contributed the final version of the manuscript.

FUNDING

This work was supported by INSERM (Institut National de la Santé et de la Recherche Médicale), by ANR (Agence Nationale de la Recherche) grant EPILAND to PS (ANR-2010-BLAN-1405 01), and by the PACA (Provence-Alpes-Côte d'Azur) Regional Council (CERVIR to PS, and IM3D3C grants). TS was supported by the Deutsche Forschungsgemeinschaft (SFB796). This work was also carried out within the FHU EPINEXT thanks to the support of the AMIDEX project (ANR-11-IDEX-0001-02) funded by the Investissements d'Avenir French Governement program managed by the French National Research Agency (ANR).

ACKNOWLEDGMENTS

We thank P. Grenot at CIPHE, F. Bader, and S. Corby at INMED animal core facilities, B. Riffault at Neurochlore for his help in iDisco experiments, and H. Child at Oxford University for his help as a trainee *via* the BIOTRAIL international student exchange program.

SUPPLEMENTARY MATERIAL

The Supplementary Material for this article can be found online at: https://www.frontiersin.org/articles/10.3389/fncel.2018.00055/full#supplementary-material

REFERENCES

Abraham, J., Fox, P. D., Condello, C., Bartolini, A., and Koh, S. (2012). Minocycline attenuates microglia activation and blocks the long-term epileptogenic effects of early-life seizures. *Neurobiol. Dis.* 46, 425–430. doi: 10.1016/j.nbd.2012.02.006

Adler, S. P., and Nigro, G. (2013). "Clinical cytomegalovirus research: congenital infection," in *Cytomegaloviruses: From Molecular Pathogenesis to Intervention*, Vol. 2, ed M. J. Reddehase (Mainz: Caister Academic Press), 55–73.

Alvarado, J. C., Fuentes-Santamaria, V., Gabaldon-Ull, M. C., Blanco, J. L., and Juiz, J. M. (2014). Wistar rats: a forgotten model of age-related hearing loss. *Front. Aging Neurosci.* 6:29. doi: 10.3389/fnagi.2014.00029

Baca Jones, C. C., Kreklywich, C. N., Messaoudi, I., Vomaske, J., Mccartney, E., Orloff, S. L., et al. (2009). Rat cytomegalovirus infection depletes MHC II in bone marrow derived dendritic cells. *Virology* 388, 78–90. doi: 10.1016/j.virol.2009.02.050

Bantug, G. R., Cekinovic, D., Bradford, R., Koontz, T., Jonjic, S., and Britt, W. J. (2008). CD8+ T lymphocytes control murine cytomegalovirus replication in the central nervous system of newborn animals. *J. Immunol.* 181, 2111–2123. doi: 10.4049/jimmunol.181.3.2111

Barker-Haliski, M. L., Vanegas, F., Mau, M. J., Underwood, T. K., and White, H. S. (2016). Acute cognitive impact of antiseizure drugs in naive rodents and corneal-kindled mice. *Epilepsia* 57, 1386–1397. doi: 10.1111/epi.13476

Belle, M., Godefroy, D., Couly, G., Malone, S. A., Collier, F., Giacobini, P., et al. (2017). Tridimensional visualization and analysis of early human development. *Cell* 169, 161–173 e112. doi: 10.1016/j.cell.2017.03.008

Belle, M., Godefroy, D., Dominici, C., Heitz-Marchaland, C., Zelina, P., Hellal, F., et al. (2014). A simple method for 3D analysis of immunolabeled axonal tracts in a transparent nervous system. *Cell Rep.* 9, 1191–1201. doi: 10.1016/j.celrep.2014.10.037

Bianchi, D. W. (2012). From prenatal genomic diagnosis to fetal personalized medicine: progress and challenges. *Nat. Med.* 18, 1041–1051. doi: 10.1038/nm.2829

Boppana, S. B., Ross, S. A., and Fowler, K. B. (2013). Congenital cytomegalovirus infection: clinical outcome. *Clin Infect Dis* 57(Suppl. 4), S178–S181. doi: 10.1093/cid/cit629

Bradford, R. D., Yoo, Y. G., Golemac, M., Pugel, E. P., Jonjic, S., and Britt, W. J. (2015). Murine CMV-induced hearing loss is associated with inner ear inflammation and loss of spiral ganglia neurons. *PLoS Pathog.* 11:e1004774. doi: 10.1371/journal.ppat.1004774

Britt, W.J., Cekinovic, D., and Jonjic, S. (2013). "Murine model of neonatal cytomegalovirus infection," in *Cytomegaloviruses: From Molecular Pathogenesis to Intervention*, Vol. 2, ed. M. J. Reddehase (Mainz: Caister Academic Press), 119–141.

Brundula, V., Rewcastle, N. B., Metz, L. M., Bernard, C. C., and Yong, V. W. (2002). Targeting leukocyte MMPs and transmigration: minocycline as a potential therapy for multiple sclerosis. *Brain* 125, 1297–1308. doi: 10.1093/brain/awf133

Cartier, N., Lewis, C. A., Zhang, R., and Rossi, F. M. (2014). The role of microglia in human disease: therapeutic tool or target? *Acta Neuropathol.* 128, 363–380. doi: 10.1007/s00401-014-1330-y

Cekinovic, D., Lisnic, V. J., and Jonjic, S. (2014). Rodent models of congenital cytomegalovirus infection. Methods *Mol. Biol.* 1119, 289–310. doi: 10.1007/978-1-62703-788-4_16

Cheeran, M. C., Lokensgard, J. R., and Schleiss, M. R. (2009). Neuropathogenesis of congenital cytomegalovirus infection: disease mechanisms and prospects for intervention. *Clin. Microbiol. Rev.* 22, 99–126, Table of Contents. doi: 10.1128/CMR.00023-08

Cloarec, R., Bauer, S., Luche, H., Buhler, E., Pallesi-Pocachard, E., Salmi, M., et al. (2016). Cytomegalovirus infection of the rat developing brain in utero prominently targets immune cells and promotes early microglial activation. *PLoS ONE* 11:e0160176. doi: 10.1371/journal.pone.0160176

Colver, A., Fairhurst, C., and Pharoah, P. O. (2014). Cerebral palsy. *Lancet* 383, 1240–1249. doi: 10.1016/S0140-6736(13)61835-8

Cross, R., Ling, C., Day, N. P., Mcgready, R., and Paris, D. H. (2016). Revisiting doxycycline in pregnancy and early childhood–time to rebuild its reputation? *Expert Opin. Drug Saf.* 15, 367–382. doi: 10.1517/14740338.2016.1133584

Cunningham, C. L., Martinez-Cerdeno, V., and Noctor, S. C. (2013). Microglia regulate the number of neural precursor cells in the developing cerebral cortex. *J. Neurosci.* 33, 4216–4233. doi: 10.1523/JNEUROSCI.3441-12.2013

Desveaux, C., Klein, J., Leruez-Ville, M., Ramirez-Torres, A., Lacroix, C., Breuil, B., et al. (2016). Identification of Symptomatic Fetuses Infected with Cytomegalovirus Using Amniotic Fluid Peptide Biomarkers. *PLoS Pathog.* 12:e1005395. doi: 10.1371/journal.ppat.1005395

Devinsky, O., Vezzani, A., Najjar, S., De Lanerolle, N. C., and Rogawski, M. A. (2013). Glia and epilepsy: excitability and inflammation. *Trends Neurosci.* 36, 174–184. doi: 10.1016/j.tins.2012.11.008

Dommergues, M. A., Plaisant, F., Verney, C., and Gressens, P. (2003). Early microglial activation following neonatal excitotoxic brain damage in mice: a potential target for neuroprotection. *Neuroscience* 121, 619–628. doi: 10.1016/S0306-4522(03)00558-X

Erturk, A., Becker, K., Jahrling, N., Mauch, C. P., Hojer, C. D., Egen, J. G., et al. (2012). Three-dimensional imaging of solvent-cleared organs using 3DISCO. *Nat. Protoc.* 7, 1983–1995. doi: 10.1038/nprot.2012.119

Fleiss, B., and Gressens, P. (2012). Tertiary mechanisms of brain damage: a new hope for treatment of cerebral palsy? *Lancet Neurol.* 11, 556–566. doi: 10.1016/S1474-4422(12)70058-3

Frost, J. L., and Schafer, D. P. (2016). Microglia: architects of the developing nervous system. *Trends Cell Biol.* 26, 587–597. doi: 10.1016/j.tcb.2016.02.006

Ginhoux, F., Greter, M., Leboeuf, M., Nandi, S., See, P., Gokhan, S., et al. (2010). Fate mapping analysis reveals that adult microglia derive from primitive macrophages. *Science* 330, 841–845. doi: 10.1126/science.1194637

Ginhoux, F., and Jung, S. (2014). Monocytes and macrophages: developmental pathways and tissue homeostasis. *Nat. Rev. Immunol.* 14, 392–404. doi: 10.1038/nri3671

Ginhoux, F., Lim, S., Hoeffel, G., Low, D., and Huber, T. (2013). Origin and differentiation of microglia. *Front. Cell. Neurosci.* 7:45. doi: 10.3389/fncel.2013.00045

Hamilton, S. T., Van Zuylen, W., Shand, A., Scott, G. M., Naing, Z., Hall, B., et al. (2014). Prevention of congenital cytomegalovirus complications by maternal and neonatal treatments: a systematic review. *Rev. Med. Virol.* 24, 420–433. doi: 10.1002/rmv.1814

Hong, S., and Banks, W. A. (2015). Role of the immune system in HIV-associated neuroinflammation and neurocognitive implications. *Brain Behav. Immun.* 45, 1–12. doi: 10.1016/j.bbi.2014.10.008

Hong, S., Beja-Glasser, V. F., Nfonoyim, B. M., Frouin, A., Li, S., Ramakrishnan, S., et al. (2016). Complement and microglia mediate early synapse loss in Alzheimer mouse models. *Science* 352, 712–716. doi: 10.1126/science.aad8373

Kannan, S., Dai, H., Navath, R. S., Balakrishnan, B., Jyoti, A., Janisse, J., et al. (2012). Dendrimer-based postnatal therapy for neuroinflammation and cerebral palsy in a rabbit model. *Sci. Transl. Med.* 4:130ra146. doi: 10.1126/scitranslmed.3003162

Kawasaki, H., Kosugi, I., Sakao-Suzuki, M., Meguro, S., Arai, Y., Tsutsui, Y., et al. (2015). Cytomegalovirus initiates infection selectively from high-level beta1 integrin-expressing cells in the brain. *Am. J. Pathol.* 185, 1304–1323. doi: 10.1016/j.ajpath.2015.01.032

Khazipov, R., Zaynutdinova, D., Ogievetsky, E., Valeeva, G., Mitrukhina, O., Manent, J. B., et al. (2015). Atlas of the postnatal rat brain in stereotaxic coordinates. *Front. Neuroanat.* 9:161. doi: 10.3389/fnana.2015.00161

Kosmac, K., Bantug, G. R., Pugel, E. P., Cekinovic, D., Jonjic, S., and Britt, W. J. (2013). Glucocorticoid treatment of MCMV infected newborn mice attenuates CNS inflammation and limits deficits in cerebellar development. *PLoS Pathog.* 9:e1003200. doi: 10.1371/journal.ppat.1003200

Kosugi, I., Kawasaki, H., Arai, Y., and Tsutsui, Y. (2002). Innate immune responses to cytomegalovirus infection in the developing mouse brain and their evasion by virus-infected neurons. *Am. J. Pathol.* 161, 919–928. doi: 10.1016/S0002-9440(10)64252-6

Lokensgard, J. R., Mutnal, M. B., Prasad, S., Sheng, W., and Hu, S. (2016). Glial cell activation, recruitment, and survival of B-lineage cells following MCMV brain infection. *J. Neuroinflamm.* 13:114. doi: 10.1186/s12974-016-0582-y

Matcovitch-Natan, O., Winter, D. R., Giladi, A., Vargas Aguilar, S., Spinrad, A., Sarrazin, S., et al. (2016). Microglia development follows a stepwise program to regulate brain homeostasis. *Science* 353:aad8670. doi: 10.1126/science.aad8670

Ohlemiller, K. K. (2009). Mechanisms and genes in human strial presbycusis from animal models. *Brain Res.* 1277, 70–83. doi: 10.1016/j.brainres.2009.02.079

Ornaghi, S., Hsieh, L. S., Bordey, A., Vergani, P., Paidas, M. J., and Van Den Pol, A. N. (2017). Valnoctamide inhibits cytomegalovirus infection in developing brain and attenuates neurobehavioral dysfunctions and brain abnormalities. *J. Neurosci.* 37, 6877–6893. doi: 10.1523/JNEUROSCI.0970-17.2017

Paolicelli, R. C., Bolasco, G., Pagani, F., Maggi, L., Scianni, M., Panzanelli, P., et al. (2011). Synaptic pruning by microglia is necessary for normal brain development. *Science* 333, 1456–1458. doi: 10.1126/science.1202529

Paolicelli, R. C., and Ferretti, M. T. (2017). Function and dysfunction of microglia during brain development: consequences for synapses and neural circuits. *Front. Synaptic Neurosci.* 9:9. doi: 10.3389/fnsyn.2017.00009

Ponomarev, E. D., Veremeyko, T., Barteneva, N., Krichevsky, A. M., and Weiner, H. L. (2011). MicroRNA-124 promotes microglia quiescence and suppresses EAE by deactivating macrophages via the C/EBP-alpha-PU.1 pathway. *Nat. Med.* 17, 64–70. doi: 10.1038/nm.2266

Popovic, N., Schubart, A., Goetz, B. D., Zhang, S. C., Linington, C., and Duncan, I. D. (2002). Inhibition of autoimmune encephalomyelitis by a tetracycline. *Ann. Neurol.* 51, 215–223. doi: 10.1002/ana.10092

Prinz, M., and Priller, J. (2014). Microglia and brain macrophages in the molecular age: from origin to neuropsychiatric disease. *Nat. Rev. Neurosci.* 15, 300–312. doi: 10.1038/nrn3722

Renier, N., Wu, Z., Simon, D. J., Yang, J., Ariel, P., and Tessier-Lavigne, M. (2014). iDISCO: a simple, rapid method to immunolabel large tissue samples for volume imaging. *Cell* 159, 896–910. doi: 10.1016/j.cell.2014.10.010

Revello, M. G., Lazzarotto, T., Guerra, B., Spinillo, A., Ferrazzi, E., Kustermann, A., et al. (2014). A randomized trial of hyperimmune globulin to prevent congenital cytomegalovirus. *N. Engl. J. Med.* 370, 1316–1326. doi: 10.1056/NEJMoa1310214

Revello, M. G., Zavattoni, M., Baldanti, F., Sarasini, A., Paolucci, S., and Gerna, G. (1999). Diagnostic and prognostic value of human cytomegalovirus load and IgM antibody in blood of congenitally infected newborns. *J. Clin. Virol.* 14, 57–66. doi: 10.1016/S1386-6532(99)00016-5

Roumier, A., Pascual, O., Bechade, C., Wakselman, S., Poncer, J. C., Real, E., et al. (2008). Prenatal activation of microglia induces delayed impairment of glutamatergic synaptic function. *PLoS ONE* 3:e2595. doi: 10.1371/journal.pone.0002595

Rousset, C. I., Kassem, J., Aubert, A., Planchenault, D., Gressens, P., Chalon, S., et al. (2013). Maternal exposure to lipopolysaccharide leads to transient motor dysfunction in neonatal rats. *Dev. Neurosci.* 35, 172–181. doi: 10.1159/000346579

Sakao-Suzuki, M., Kawasaki, H., Akamatsu, T., Meguro, S., Miyajima, H., Iwashita, T., et al. (2014). Aberrant fetal macrophage/microglial reactions to cytomegalovirus infection. *Ann. Clin. Trans. Neurol.* 1, 570–588. doi: 10.1002/acn3.88

Salmi, M., Bruneau, N., Cillario, J., Lozovaya, N., Massacrier, A., Buhler, E., et al. (2013). Tubacin prevents neuronal migration defects and epileptic activity caused by rat Srpx2 silencing in utero. *Brain* 136, 2457–2473. doi: 10.1093/brain/awt161

Schafer, D. P., Lehrman, E. K., Kautzman, A. G., Koyama, R., Mardinly, A. R., Yamasaki, R., et al. (2012). Microglia sculpt postnatal neural circuits in an activity and complement-dependent manner. *Neuron* 74, 691–705. doi: 10.1016/j.neuron.2012.03.026

Seleme, M. C., Kosmac, K., Jonjic, S., and Britt, W. J. (2017). Tumor necrosis factor alpha-induced recruitment of inflammatory mononuclear cells leads to inflammation and altered brain development in murine cytomegalovirus-infected newborn mice. *J. Virol.* 91:pii: e01983-16. doi: 10.1128/JVI.01983-16

Slavuljica, I., Kvestak, D., Huszthy, P. C., Kosmac, K., Britt, W. J., and Jonjic, S. (2015). Immunobiology of congenital cytomegalovirus infection of the central nervous system-the murine cytomegalovirus model. *Cell. Mol. Immunol.* 12, 180–191. doi: 10.1038/cmi.2014.51

Smith, R. J., Bale, J. F. Jr., and White, K. R. (2005). Sensorineural hearing loss in children. *Lancet* 365, 879–890. doi: 10.1016/S0140-6736(05)71047-3

Suzuki, Y., Toribe, Y., Mogami, Y., Yanagihara, K., and Nishikawa, M. (2008). Epilepsy in patients with congenital cytomegalovirus infection. *Brain Dev.* 30, 420–424. doi: 10.1016/j.braindev.2007.12.004

Teissier, N., Fallet-Bianco, C., Delezoide, A. L., Laquerriere, A., Marcorelles, P., Khung-Savatovsky, S., et al. (2014). Cytomegalovirus-induced brain malformations in fetuses. *J. Neuropathol. Exp. Neurol.* 73, 143–158. doi: 10.1097/NEN.0000000000000038

Thongtan, T., Thepparit, C., and Smith, D. R. (2012). The involvement of microglial cells in Japanese encephalitis infections. *Clin. Dev. Immunol.* 2012:890586. doi: 10.1155/2012/890586

Tikka, T., Fiebich, B. L., Goldsteins, G., Keinanen, R., and Koistinaho, J. (2001). Minocycline, a tetracycline derivative, is neuroprotective against excitotoxicity by inhibiting activation and proliferation of microglia. *J. Neurosci.* 21, 2580–2588. Available online at: http://www.jneurosci.org/content/21/8/2580.long

Vasek, M. J., Garber, C., Dorsey, D., Durrant, D. M., Bollman, B., Soung, A., et al. (2016). A complement-microglial axis drives synapse loss during virus-induced memory impairment. *Nature* 534, 538–543. doi: 10.1038/nature18283

Vezzani, A., Auvin, S., Ravizza, T., and Aronica, E. (2012). "Glia-neuronal interactions in ictogenesis and epileptogenesis: role of inflammatory mediators," in *Jasper's Basic Mechanisms of the Epilepsies. 4th Edn.,* eds J. L. Noebels, M. Avoli, M. A. Rogawski (Bethesda, MD: National Center for Biotechnology Information).

Xue, Q. S., Yang, C., Hoffman, P. M., and Streit, W. J. (2010). Microglial response to murine leukemia virus-induced encephalopathy is a good indicator of neuronal perturbations. *Brain Res.* 1319, 131–141. doi: 10.1016/j.brainres.2009.12.089

Yamada, M., Yoshida, Y., Mori, D., Takitoh, T., Kengaku, M., Umeshima, H., et al. (2009). Inhibition of calpain increases LIS1 expression and partially rescues *in vivo* phenotypes in a mouse model of lissencephaly. *Nat. Med.* 15, 1202–1207. doi: 10.1038/nm.2023

Yrjanheikki, J., Keinanen, R., Pellikka, M., Hokfelt, T., and Koistinaho, J. (1998). Tetracyclines inhibit microglial activation and are neuroprotective in global brain ischemia. *Proc. Natl. Acad. Sci. U.S.A.* 95, 15769–15774. doi: 10.1073/pnas.95.26.15769

Yrjanheikki, J., Tikka, T., Keinanen, R., Goldsteins, G., Chan, P. H., and Koistinaho, J. (1999). A tetracycline derivative, minocycline, reduces inflammation and protects against focal cerebral ischemia with a wide therapeutic window. *Proc. Natl. Acad. Sci. U.S.A.* 96, 13496–13500. doi: 10.1073/pnas.96.23.13496

Conflict of Interest Statement: RC has been a recipient of an INSERM/PACA Ph.D. fellowship and a recipient of a FRM Ph.D. fellowship (FDT20140930813), during which he performed all his experiments and data analyzes except the iDisco experiments, which he performed and analyzed while being a Neurochlore employee. A patent application has been filed and submitted to the European Patent Office via the Tech Transfer office at INSERM.

The other authors declare that the research was conducted in the absence of any commercial or financial relationships that could be construed as a potential conflict of interest.

frontiers in Cellular Neuroscience

ORIGINAL RESEARCH
published: 28 February 2018
doi: 10.3389/fncel.2018.00049

Caffeine and Modafinil Ameliorate the Neuroinflammation and Anxious Behavior in Rats during Sleep Deprivation by Inhibiting the Microglia Activation

*Meetu Wadhwa, Garima Chauhan, Koustav Roy, Surajit Sahu†, Satyanarayan Deep†, Vishal Jain, Krishna Kishore, Koushik Ray, Lalan Thakur and Usha Panjwani**

Defence Institute of Physiology & Allied Sciences (DIPAS), Defence Research and Development Organization (DRDO), New Delhi, India

OPEN ACCESS

Edited by:
Alexej Verkhratsky, University of Manchester, United Kingdom

Reviewed by:
Rodrigo A. Cunha, University of Coimbra, Portugal
Leanne Stokes, University of East Anglia, United Kingdom

****Correspondence:***
Usha Panjwani
neurophysiolab.dipas@gmail.com

†Present address:
Surajit Sahu, INSERM U901 INMED, Marseille, France
Satyanarayan Deep, Department of Neurology, University of New Mexico, Albuquerque, NM, United States

Received: *31 December 2017*
Accepted: *15 February 2018*
Published: *28 February 2018*

Citation:
Wadhwa M, Chauhan G, Roy K, Sahu S, Deep S, Jain V, Kishore K, Ray K, Thakur L and Panjwani U (2018) Caffeine and Modafinil Ameliorate the Neuroinflammation and Anxious Behavior in Rats during Sleep Deprivation by Inhibiting the Microglia Activation. Front. Cell. Neurosci. 12:49. doi: 10.3389/fncel.2018.00049

Background: Sleep deprivation (SD) plagues modern society due to the professional demands. It prevails in patients with mood and neuroinflammatory disorders. Although growing evidence suggests the improvement in the cognitive performance by psychostimulants during sleep-deprived conditions, the impending involved mechanism is rarely studied. Thus, we hypothesized that mood and inflammatory changes might be due to the glial cells activation induced modulation of the inflammatory cytokines during SD, which could be improved by administering psychostimulants. The present study evaluated the role of caffeine/modafinil on SD-induced behavioral and inflammatory consequences.

Methods: Adult male Sprague-Dawley rats were sleep deprived for 48 h using automated SD apparatus. Caffeine (60 mg/kg/day) or modafinil (100 mg/kg/day) were administered orally to rats once every day during SD. Rats were subjected to anxious and depressive behavioral evaluation after SD. Subsequently, blood and brain were collected for biochemical, immunohistochemical and molecular studies.

Results: Sleep deprived rats presented an increased number of entries and time spent in closed arms in elevated plus maze test and decreased total distance traveled in the open field (OF) test. Caffeine/modafinil treatment significantly improved these anxious consequences. However, we did not observe substantial changes in immobility and anhedonia in sleep-deprived rats. Caffeine/modafinil significantly down-regulated the pro- and up-regulated the anti-inflammatory cytokine mRNA and protein expression in the hippocampus during SD. Similar outcomes were observed in blood plasma cytokine levels. Caffeine/modafinil treatment significantly decreased the microglial immunoreactivity in DG, CA1 and CA3 regions of the hippocampus during SD, however, no significant increase in immunoreactivity of astrocytes was observed. Sholl analysis

Abbreviations: DAB, Diaminobenzidine; ELISA, Enzyme-linked immunosorbent assay; EPM, Elevated plus maze; FST, Forced swim test; GFAP, Glial fibrillary acidic protein; Iba-1, Ionized calcium-binding adapter molecule I; OF, Open field; PBS, Phosphate buffered saline; PFA, Paraformaldehyde; PBST, Phosphate buffered saline containing tween-20/tritonX-100; SD, Sleep deprivation.

signified the improvement in the morphological alterations of astrocytes and microglia after caffeine/modafinil administration during SD. Stereological analysis demonstrated a significant improvement in the number of ionized calcium binding adapter molecule I (Iba-1) positive cells (different states) in different regions of the hippocampus after caffeine or modafinil treatment during SD without showing any significant change in total microglial cell number. Eventually, the correlation analysis displayed a positive relationship between anxiety, pro-inflammatory cytokines and activated microglial cell count during SD.

Conclusion: The present study suggests the role of caffeine or modafinil in the amelioration of SD-induced inflammatory response and anxious behavior in rats.

Highlights

- SD induced mood alterations in rats.
- Glial cells activated in association with the changes in the inflammatory cytokines.
- Caffeine or modafinil improved the mood and restored inflammatory changes during SD.
- SD-induced anxious behavior correlated with the inflammatory consequences.

Keywords: sleep deprivation, mood changes, microglia, cytokines, neuroinflammation, caffeine, modafinil

INTRODUCTION

Insufficient sleep is one of the most common and significant health problem worldwide associated with the immune system modulation (Dworak et al., 2011) and mood decline (Babson et al., 2010; Alkadhi et al., 2013). Documented evidence support the high prevalence of anxiety and depression with an associated link to inflammation in several pathological conditions like rheumatoid arthritis, kidney disease and bowel disease conditions (Kang et al., 2011). Cytokines play a crucial role in inflammation, neurobehavioral and emotional deficits. During the inflammatory challenge, microglial cells get activated and affect the release of cytokines (pro-inflammatory cytokines increase and anti-inflammatory cytokines decrease), often coinciding with behavioral manifestations (Kang et al., 2014; Wohleb et al., 2014b).

There are growing lines of evidence showing bi-directional communication between the sleep and immune system. Sleep influences the immune system and vice versa (Zielinski and Krueger, 2011). The pro-inflammatory cytokines such as interleukin-1β (IL-1β), TNF-α, IL-6 are found to be increased upon sleep deprivation (SD) in humans as well as experimental animals. Glial cells comprise the innate immune cells of the brain. Once activated, these cells imbalance the cytokine levels leading to behavioral abnormalities. However, their role under sleep-deprived conditions is remained unclear (Wisor et al., 2011; Alkadhi et al., 2013). It had reported that insufficient sleep decreases the mental performance and increases the risk of immune dysfunctions (Carey et al., 2011). Pro-inflammatory cytokines are associated with SD and mood disorders, however, the underlying mechanism is poorly understood (Rönnbäck and Hansson, 2004; Abelaira et al., 2013; Hong et al., 2016).

Caffeine and modafinil are widely consumed psychoactive drugs in the world showing beneficial effects on cognitive performance. Caffeine acts as a non-selective adenosine antagonist showing stimulant activity and prevents the deterioration of the cognitive performance (Daly, 2007; Nehlig, 2010; Sanday et al., 2013; Cappelletti et al., 2015). Concurrently, modafinil acts as a cognitive enhancer after directly binding to dopamine transporter and elevates the level of serotonin (Minzenberg and Carter, 2008; Rasetti et al., 2010). Caffeine or modafinil are thought to improve the mood (Cunha and Agostinho, 2010; Boele et al., 2013). Available literature suggests the dose-dependent effect of caffeine on mood showing an anxiolytic effect at low or moderate doses and anxiogenic effects at higher doses (Rusconi et al., 2014; Yamada et al., 2014).

Human and animal studies have shown improved memory performance after SD upon taking caffeine and modafinil (McGaugh et al., 2009; Cunha and Agostinho, 2010). Caffeine/modafinil administration prevents the neuroinflammation mediating memory disturbance in animal models of Alzheimer's, Parkinson's, stress, diabetes, convulsions, or alcohol-induced amnesia (Brothers et al., 2010; Raineri et al., 2012; Gyoneva et al., 2014a). However, neither the detailed mechanisms underlying neuroinflammation mediated emotional regulation during SD nor the effectiveness of the psychostimulants agents has been established yet. Therefore, we selected the two well-known psychostimulants viz., caffeine and modafinil; to assess the mood changes, astrocytes and microglial cells investigation along with the inflammatory cytokine levels during SD. Additionally, the predicted mechanism was investigated by the correlation analysis between the behavioral and inflammatory test parameters.

MATERIALS AND METHODS

Animals

Adult male Sprague-Dawley rats of 6–8 weeks old and approximately 220 ± 10 g body weight were used for the present study. Rats were housed in the clean cages made up of plexiglass material in the animal house at a temperature of 25 ± 2°C and humidity of 55 ± 2% RH with 12 h light and dark cycles with food and water *ad libitum*. All the experimental protocols were approved by the Institutional Animal Ethics Committee (IAEC, IAEC/DIPAS/2015-19) of Government of India, in accordance with the Committee for the Purpose of Control and Supervision of Experiments on Animals (CPCSEA) guidelines. Animal handling was done regularly to make them habituate to the experimenter. Experiments were conducted during the light period of the day. All efforts were done to minimize the number of rats used and to avoid unnecessary pain to the animal.

Chemicals and Reagents

Analytical grade chemicals were procured from Sigma Chemicals (Sigma-Aldrich, St. Louis, MO, USA) unless otherwise mentioned. The Enzyme-Linked Immunosorbent Assay (ELISA) kits were purchased from BD Biosciences Laboratory Ltd. (USA) and R and D Systems, Minneapolis, MN, USA. Antibodies (primary and secondary) were procured from Sigma-Aldrich, St. Louis, MO, USA, Abcam, Cambridge, MA, USA and Millipore, CA, USA.

Experimental Design

Initially, behavioral screening of rats was done, in which the body weight, food intake, aggressiveness and stereotype behavior were evaluated. This was done to ensure that rats were not suffering from any impairment, after that the animals were divided randomly into different groups: cage control with vehicle treatment (CC+Veh); cage control with caffeine treatment (CC+Caf); cage control with modafinil treatment (CC+Mod); sleep deprived for 48 h with vehicle treatment (SD+Veh); sleep deprived for 48 h and caffeine treatment (SD+Caf); sleep deprived for 48 h and modafinil treatment (SD+Mod). The rats underwent the vehicle and drugs treatment during the control and sleep deprived conditions for 48 h. Each group had five rats, and the behavioral study took place between 8:00 AM and 11:00 AM. We used a different set of rats in each behavioral paradigm. Animals were euthanized immediately after the behavioral test during the light period of the day and evaluated for the biochemical and immunohistochemical analyses. The schematic experimental design of the present study is shown in **Figure 1**.

Sleep Deprivation Procedure

Briefly, the male Sprague-Dawley rats were sleep deprived for 48 h in the automated SD apparatus according to the well-established SD protocol of our lab (Wadhwa et al., 2015; Chauhan et al., 2016). The exposure paradigm made the rats awake on providing the SD stimulus such as sound, light, and vibration. There was a proper provision of ventilation, food and water during the SD exposure. The control rats were kept under controlled conditions (temperature, humidity and light) in the animal house facility.

Drug Administration

Caffeine (Sigma-Aldrich, St. Louis, MO, USA, 60 mg/kg/day, dissolved in physiological saline, administered orally) and

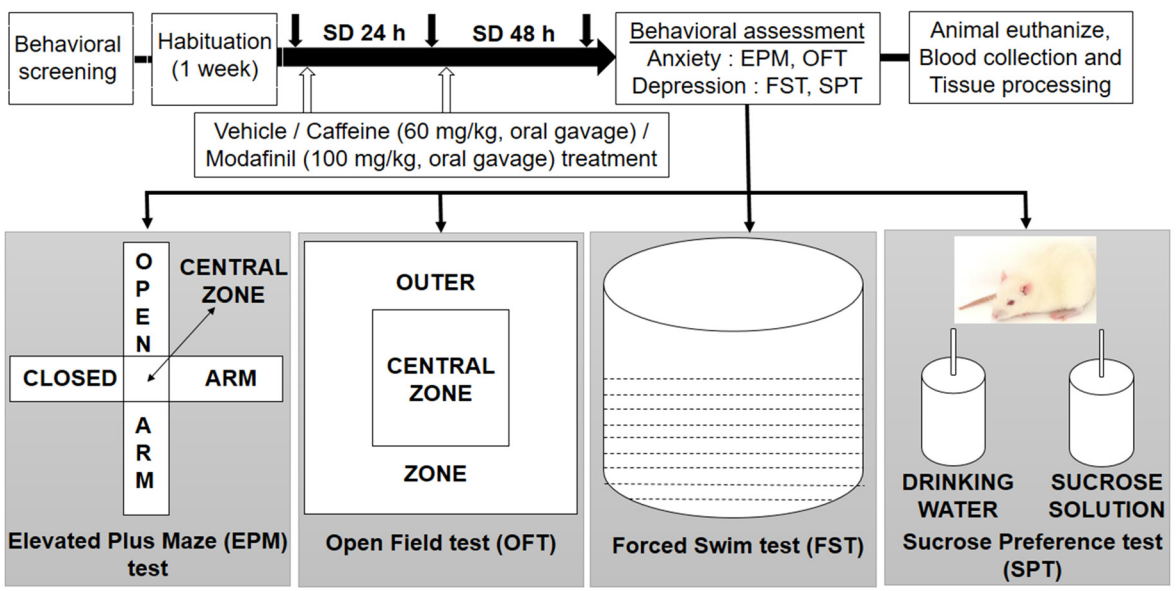

FIGURE 1 | Schematic design of the experiment.

modafinil (Modalert, Sun Pharma, India; 100 mg/kg/day, suspended in physiological saline, treated orally) dose were based upon our previous study (Sahu et al., 2013; Wadhwa et al., 2015), however, the tested doses of caffeine were higher and did not mimic habitual caffeine consumption. Caffeine or modafinil was given to the rats as an oral gavage, once a day in the morning time, during 48 h of SD.

Body Weight and Food Intake

To evaluate the physiological consequences, we monitored the body weight and food intake of both control and experimental rats regularly in the morning (1 week before the initiation of the experiments). The food was maintained at a constant amount (150 g) per animal, and every morning (8:00–9:00 AM), the remaining food was measured. At the same time, the body weight of each animal was noted down.

Behavioral Testing

We utilized a battery of behavioral tests that measure anxiety and depressive-like behavior including the open field (OF, locomotor activity, exploratory behavior), elevated plus maze (EPM, locomotor activity, exploratory behavior, anxiety), forced swim test (FST, behavioral "despair") and sucrose preference test (SPT, anhedonia). Each behavioral analysis was carried out with 15 rats in each experimental group.

Elevated Plus Maze Apparatus and Test Procedure

The EPM test is used to assess the level of anxiety in rodents. The EPM test apparatus consisted of plus shape design with four arms (two open and two closed, perpendicular to each other) having an open roof. The apparatus was about 40–70 cm elevated from the floor. Briefly, the rat was placed at the junction of the open and closed arms, facing the open arm opposite to the experimenter for 5 min. At the end of the test, rats were removed from the apparatus and placed back to their home cage. The test apparatus was properly cleaned with alcohol and dried with cotton before testing another rat. An overhead camera in association with ANY-maze software (Stoelting Co, Wood Dale, IL, USA) was properly arranged for the tracking and automatically recording the number of entries and time spent by the rat in the open and closed arms. The anxious behavior was evaluated by calculating the proportion of the time spent (time spent into the open arms divided by the total time spent in the open/closed arms) and the proportion of the number of entries (entries into the open arms divided by the total entries into the open/closed arms).

Open field apparatus and test procedure

OF test is a well-known method to assess the spontaneous locomotor activity in rats. The OF maze was divided into two zones: central and peripheral zone, using the square drawn on the maze. The apparatus consisted of a rectangular area of 81 × 81 cm surrounded by a 28 cm high wall. The field was lit with white light (23W) fixed 100 cm above the field. The rat was placed in the center of the OF, and its activity during the subsequent 5 min was recorded using ANY-Maze tracking software (Stoelting Co, Wood Dale, IL, USA). The test apparatus was properly cleaned with alcohol and dried with cotton before testing another rat to exclude any cues and smell.

Forced swim apparatus and test procedure

The FST was used to assess the depression in rodents. It is based on the assumption that an animal will try to escape, if the rat fails, the animal eventually stops trying and gives up. The FST apparatus is a vertical plexiglas cylinder (40 cm high; 20 cm in diameter) filled with 30 cm deep water (24–30°C). Briefly, the rat was placed in a cylindrical container of water from which it cannot escape, for 5 min. The rat was properly dried after removal from the water with a clean towel. The water was replaced regularly with fresh water to avoid the accumulation of the urine and fecal material. ANY-maze software (Stoelting Co, Wood Dale, IL, USA) was used to determine the test parameters.

Sucrose preference test procedure

The anhedonia, indicator of depression, means the lack of interest in rewarding stimuli. In this task, we assessed the animal interest in seeking out a sweet, rewarding drink in plain drinking water. This test was carried out in the animal's home cage. Briefly, rats were initially habituated to the presence of two bottles; one containing 2% sucrose solution and another drinking water for 2 days in their home cage. During this phase, rats had the free access to both bottles. The intake of normal drinking water and sucrose solution was measured daily, and the positions of bottles were regularly interchanged to reduce biases. On the completion of 48 h SD, the rats were presented the same two bottles (one containing water and another containing sucrose solution) and measured the intake of water and sucrose solution. Sucrose preference index was calculated as a ratio of the volume of sucrose intake over the total volume of fluid intake.

Blood Collection and Tissue Processing

After the scheduled period of SD exposure and the behavioral assessment, the blood was collected from left ventricle under anesthesia (ketamine 80 mg/kg-xylazine 20 mg/kg) in the vacutainer tube containing the sodium heparin as an anticoagulant. The blood was centrifuged at 3500 rpm at 4°C for 10–15 min, and plasma was separated. The rats were euthanized, and the brain was extracted out immediately. The hippocampi were isolated, washed with cold 0.1 M phosphate buffer saline (PBS) solution. The hippocampus was snap frozen in liquid nitrogen and then stored at −80°C until the time of analysis. Later, the samples were homogenized with the help of Polytron homogenizer (Remi Pvt. Limited) with 1× PBS and protease inhibitor cocktail containing inhibitors with broad specificity for serine, cysteine, acid proteases and aminopeptidases. After homogenization, the solution was centrifuged at 10,000 rpm for 10 min at 4°C, and the supernatant was isolated out for the cytokines assay.

Cytokine Levels Estimation

The ELISA is a specific and highly sensitive method for the quantification of cytokines. Plasma samples and hippocampal supernatant (100 μl, 1:50 dilution in assay buffer) were assayed

for ILs (IL-1β, IL-6, IL-4, IL-10) and TNF-α using commercial ELISA kits. The assays were performed as per the manufacturer's protocols.

Evaluation of RNA Expression Levels of Secretory Cytokines in Hippocampus by Real-Time PCR (RT-PCR)

Isolation of the total RNA from hippocampal tissue was done using TRIZOL reagent (Sigma-Aldrich, St. Louis, MO, USA) according to the previously described protocol (Rio et al., 2010). RNA level was quantified using a Nanodrop (Thermo Fisher Scientific, Waltham, MA, USA) by measuring absorbance at 260 and 280 nm. The purity of RNA was checked by denaturing agarose gel electrophoresis and ethidium bromide staining. RNA was reverse-transcribed to cDNA using an RT2 first strand cDNA Synthesis Kit (QIAGEN Sciences, Germantown, MD, USA), according to the manufacturer's instruction. Relative quantitative analysis of the gene expression of interleukins and TNF for each group was done by employing RT^2 Profiler inflammatory cytokines and receptor array (QIAGEN Sciences, Germantown, MD, USA) using RT^2 SYBR® Green qPCR master mix (QIAGEN Sciences, Germantown, MD, USA). The analysis was performed by the comparative $2^{-\Delta\Delta CT}$ method as previously described. The gene expression analysis was done using software available online at www.sabiosciences.com, after normalization of each gene (Ct) to the housekeeping genes.

Immunohistochemistry

Transcardial perfusion and fixation were performed using 4% paraformaldehyde (PFA) in 0.1 M PBS (pH = 7.4). Brains were cryosectioned after processing with graded sucrose solution (10%, 20% and 30%) respectively dissolved in PBS (0.1 M, pH 7.4) using cryostat (Leica, Germany). Coronal sections of 30 μm thickness were taken in tissue culture plate and stored at 4°C in sodium azide solution to prevent fungal growth. The sections were processed for immunoreactivity of glial fibrillary acidic protein (GFAP) and ionized calcium binding adapter molecule I (Iba-1) proteins. Briefly, the sections were washed in PBS containing 0.1% Tween-20 or Triton X-100 (PBST) twice for 5 min each, subsequently; the antigen retrieval was done by incubating the sections with sodium citrate buffer for 10–15 min in boiling water bath. Sections were incubated with blocking buffer (5% goat serum for GFAP; 3% bovine serum albumin (BSA) for Iba-1) diluted in PBS for 2 h at room temperature, followed by washing with PBST. Prior to primary antibody labeling of an Iba-1 protein, there was an additional step of permeabilization in which the sections were treated with 0.25% Triton X-100 for 20–30 min followed by PBST washing thrice for 5 min each. The sections were then probed with rabbit anti-GFAP antibody and goat anti-Iba-1 antibody prepared in blocking solution for 40 h at 4°C. Sections were subsequently incubated with biotinylated goat anti-rabbit and rabbit anti-goat antibody for 2 h at room temperature, followed by three washings in PBST (5 min each). Finally, the sections were developed with diaminobenzidine (DAB) tetrahydrochloride solution.

Imaging and Analysis

The immune-stained sections were observed under Olympus (Melville, NY, USA) BX51TF microscope and images were taken from the DG, CA1 and CA3 regions of the dorsal hippocampus of the brain. We performed sholl analysis for the morphological evaluation of astrocytes and microglial cells. The cell quantification was performed using stereo investigator program. Similarly, immunoreactivity of astrocytes and microglial cells was quantified with the help of ImageJ software.

Statistical Analysis

All the data are expressed as Means ± SEM. Physiological, behavioral, biochemical, immunohistochemical and molecular data were analyzed by Two-way ANOVA followed by Tukey *post hoc* test with multiple comparisons. Pearson's correlation test was applied for correlation analysis. Data presented as mean percentage of control value used for graphical representation has been mentioned with graphs. All statistical analysis was done using GraphPad Prism 7.03 Software. The significance level of $p < 0.05$ was considered to be statistically significant.

RESULTS

Caffeine or Modafinil Treatment Improved the Physiological Consequences during SD

To assess the physiological changes in rats during SD, their body weight and food intake were recorded. We did not notice changes in body weight gain in the caffeine or modafinil treated control groups compared to vehicle-treated control rats, but a significant decrease in body weight was observed in vehicle-treated sleep-deprived rats as compared to vehicle treated control group rats. Administration of caffeine or modafinil to SD exposed rats significantly improved the body weight as compared to vehicle-treated SD group ($F_{(dFn,\ dFd);\ (2,114)} = 76.28$; $p < 0.0001$; **Supplementary Figure S1A**). However, changes in food intake among the different groups was non-significant ($F_{(2,114)} = 0.8429$; $p = 0.4331$; **Supplementary Figure S1B**).

Caffeine/Modafinil Administration Produced Anxiolytic Effect during SD

Sleep deprived rats showed anxious behavior while caffeine or modafinil treatment to SD exposed rats improved the anxious behavior of sleep-deprived rats as shown in the track plot of rats during EPM and OF test (**Figures 2A,D**). The proportion of the number of entries and the proportion of the time spent in the open arms were significantly reduced in sleep-deprived rats treated with vehicle compared to vehicle treated control rats Caffeine or modafinil treatment during SD significantly improved the proportion of the number of entries ($F_{(2,114)} = 17.4$; $p < 0.0001$) and the proportion of the time spent in the open arms ($F_{(2,114)} = 25.19$; $p < 0.0001$) compared to SD exposed rats (**Figures 2B,C**).

Similarly, in the OF test, the total distance traveled in the OF was significantly reduced in sleep-deprived rats. However, caffeine or modafinil administration significantly

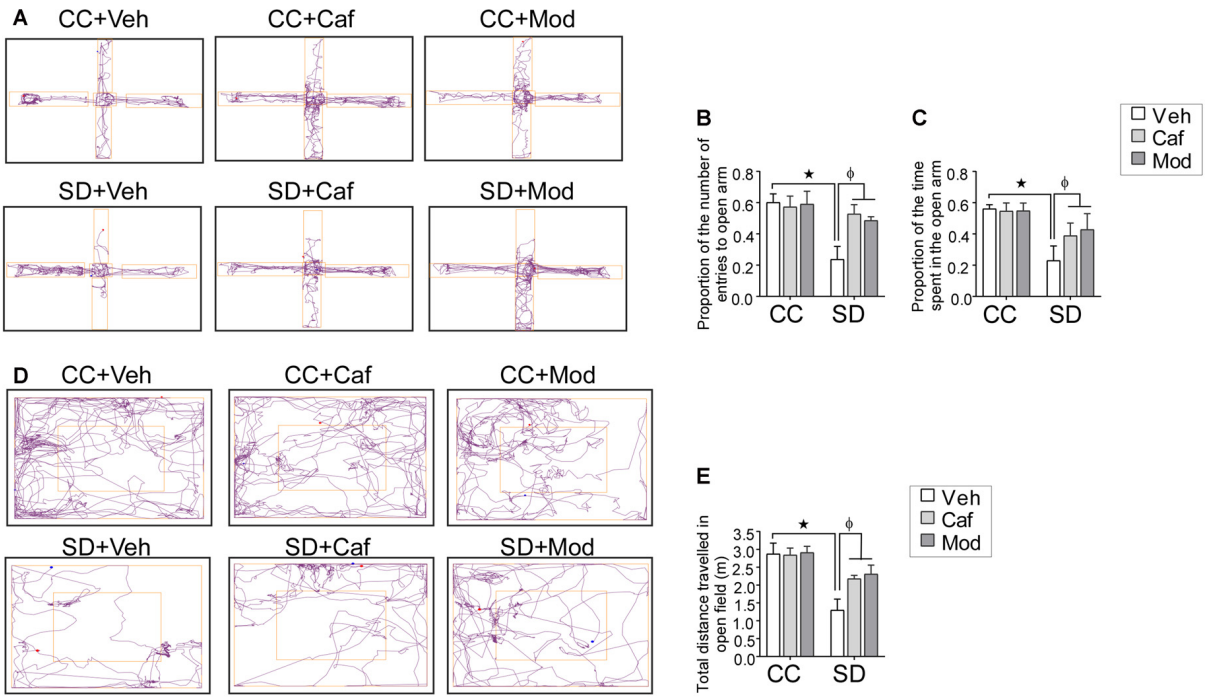

FIGURE 2 | Assessment of the anxious behavior following caffeine/modafinil treatment during sleep deprivation (SD). **(A)** Track plot of the rats during elevated plus maze (EPM) test and the study parameters: **(B)** proportion of the number of entries in the open arms; **(C)** proportion of the time spent in the open arms. **(D)** Track plot of the rats during open field (OF) test; **(E)** total distance traveled in the OF. $^{*}p < 0.05$ when compared to control treated with vehicle; $^{\Phi}p < 0.05$ when compared to sleep deprived treated with vehicle. Two way ANOVA followed by Tukey *post hoc* test with multiple comparison was used.

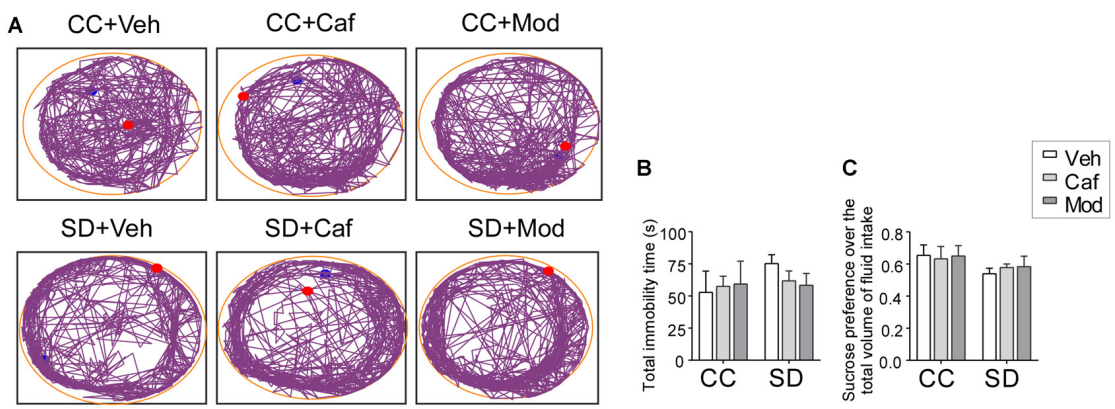

FIGURE 3 | Assessment of the depressive behavior following caffeine/modafinil treatment during SD. **(A)** Track plot of the rats during forced swim test (FST) test; **(B)** total immobility time; **(C)** sucrose preference over the total volume of fluid intake. Two way ANOVA followed by Tukey *post hoc* with multiple comparison test was applied for statistical comparison between groups. Blue dot represented the starting point and the red dot represented the end point of the test.

improved/increased the total distance traveled in the OF in SD exposed animals compared to sleep-deprived rats ($F_{(2,114)} = 14.91$; $p = 0.0001$; **Figure 2E**). However, change in vehicle or caffeine, or modafinil treated control rats in EPM and OF test was comparable.

Caffeine or Modafinil Treatment Recovered the Depressive Behavior during SD

A non-significant increase in the immobility time was observed in SD exposed animals compared to control animals. Data showed that caffeine/modafinil treatment during SD

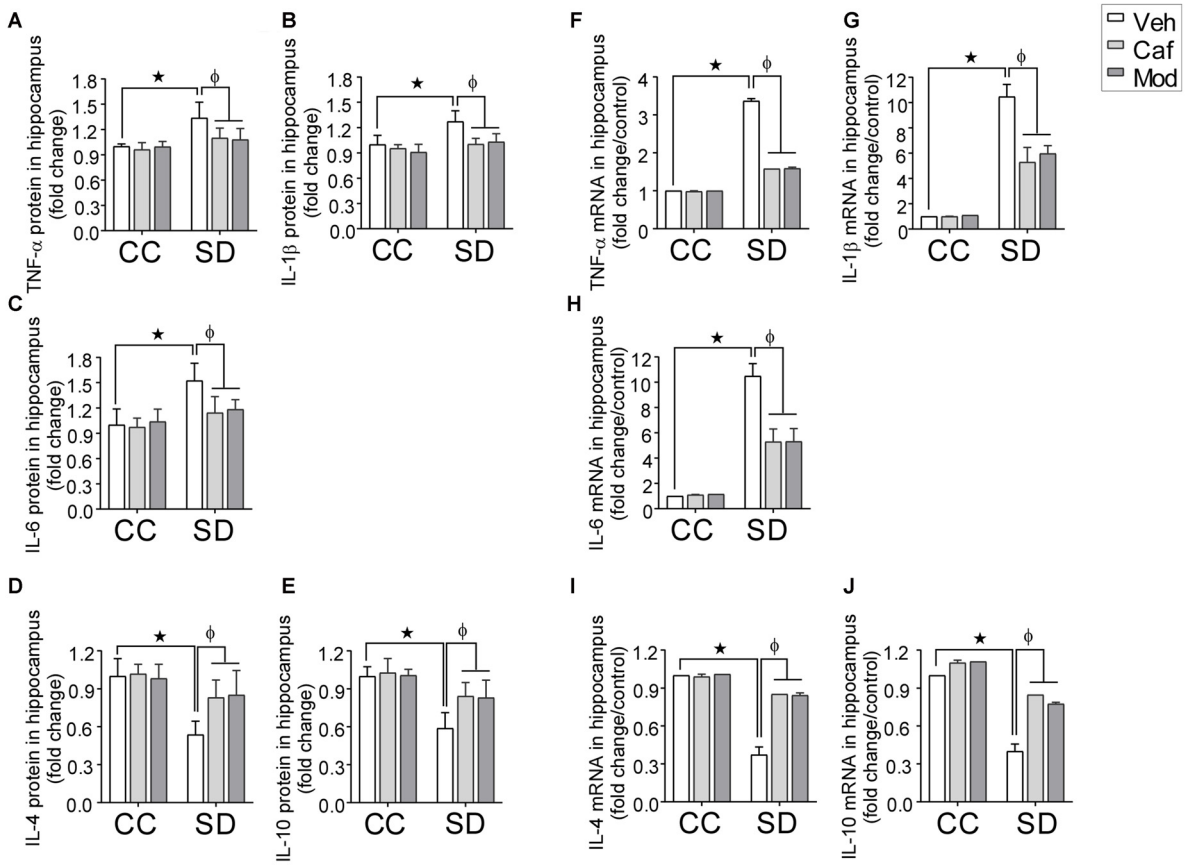

FIGURE 4 | Fold changes in the inflammatory cytokines in hippocampus during caffeine/modafinil administration following SD. The concentration of cytokine levels were measured in picograms per milliliter and expressed as the fold changes in TNF-α **(A,F)**; interleukin-1β (IL-1β) **(B,G)**; IL-6 **(C,H**; pro-inflammatory cytokines), IL-4 **(D,I)**; IL-10 **(E,J**; anti-inflammatory cytokines) in the hippocampus. $^{*}p < 0.05$ when compared to control treated with vehicle; $^{\phi}p < 0.05$ when compared to sleep deprived treated with vehicle. Two way ANOVA followed by Tukey *post hoc* test with multiple comparison were used for the statistical evaluation.

non-significantly improved the immobility time in SD exposed rats ($F_{(2,54)} = 1.274$; $p = 0.2881$; **Figures 3A,B**).

Similar to FST, sucrose preference index was non-significantly reduced in rats subjected to SD compared to control, while caffeine/modafinil administration following SD exposure non-significantly improved the sucrose solution intake compared to the sleep-deprived group ($F_{(2,54)} = 0.6609$; $p = 0.5205$; **Figure 3C**). Also, we did not find a significant difference in the vehicle or caffeine or modafinil-treated control rats.

Caffeine/Modafinil Administration Maintained the Cytokines Profiling during SD

A significant fold increase in the pro-inflammatory cytokines (TNF-α, IL-1β and IL-6) and decrease in the anti-inflammatory cytokines (IL-4 and IL-10) in the hippocampus of rats subjected to SD as compared to control was observed. However, caffeine or modafinil administered during SD significantly decreased the pro-inflammatory: TNF-α ($F_{(2,84)} = 10.17$; $p = 0.0001$; **Figure 4A**); IL-1β ($F_{(2,84)} = 3.693$; $p = 0.0290$; **Figure 4B**); IL-6 ($F_{(2,84)} = 4.168$; p = $P = 0.0188$; **Figure 4C**) and increased the anti-inflammatory cytokines: IL-4 ($F_{(2,84)} = 22.09$; $p < 0.0001$; **Figure 4D**); IL-10 ($F_{(2,84)} = 5.933$; $p = 0.0039$; **Figure 4E**) in the hippocampus as compared to vehicle-treated sleep deprived rats.

Subsequently, in plasma, we found a significant fold increase in the pro-inflammatory cytokines and decrease in the anti-inflammatory cytokines insleep deprived rats as compared to control, that were restored by caffeine or modafinil treatment during SD. The respective figures were: TNF-α ($F_{(2,84)} = 20.32$; $p < 0.0001$; **Supplementary Figure S2A**); IL-1β ($F_{(2,84)} = 27.67$; $p < 0.0001$; **Supplementary Figure S2B**); IL-6 ($F_{(2,84)} = 15.39$; $p < 0.0001$; **Supplementary Figure S2C**); IL-4 ($F_{(2,84)} = 18.52$; $p < 0.0001$; **Supplementary Figure S2D**); IL-10 ($F_{(2,84)} = 15.2$; $p < 0.0001$; **Supplementary Figure S2E**).

Real time PCR study showed that caffeine or modafinil administration during SD significantly down-regulated the mRNA expression of TNF-α ($F_{(2,12)} = 2007$; $p < 0.0001$; **Figure 4F**); IL-1β ($F_{(2,12)} = 27.41$, $p < 0.0001$; **Figure 4G**); IL-6

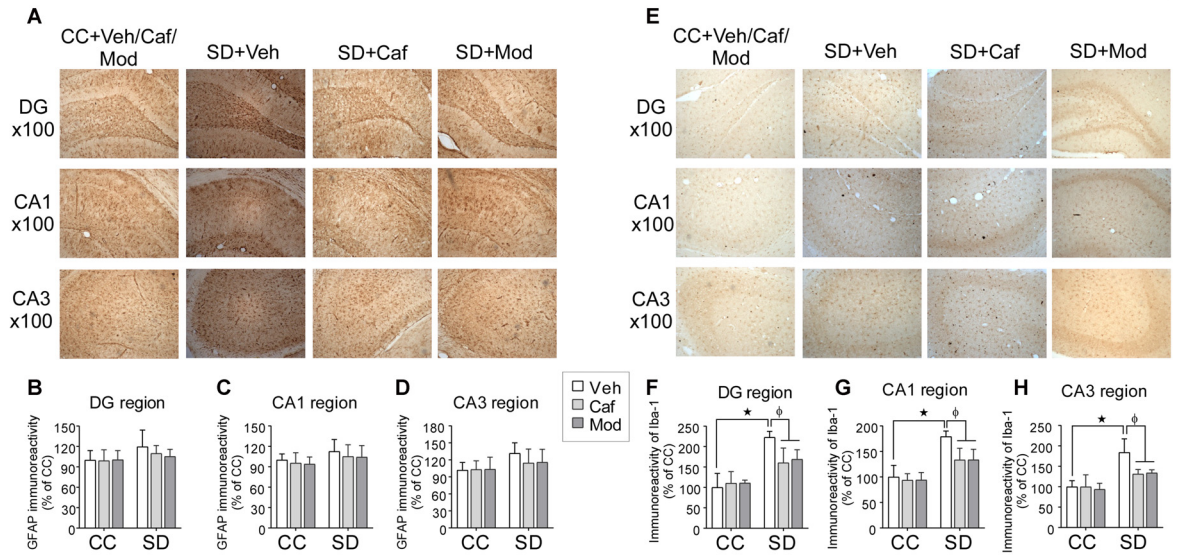

FIGURE 5 | Caffeine or modafinil treatment inhibited the glial cell immunoreactivity in rat hippocampus following SD. **(A)** Representable image of astrocytes expression in DG, CA1 and CA3 regions of the hippocampus. Glial fibrillary acidic protein (GFAP) immunoreactivity quantification in **(B)** DG region; **(C)** CA1 region; **(D)** CA3 region of the hippocampus. **(E)** Representable image of microglial cells expression in DG, CA1 and CA3 regions of the hippocampus. Ionized calcium binding adapter molecule I (Iba-1) cell immunoreactivity quantification in **(F)** DG region; **(G)** CA1 region; **(H)** CA3 region of the hippocampus. $^{*}p < 0.05$ when compared to control treated with vehicle; $^{\phi}p < 0.05$ when compared to sleep deprived treated with vehicle. Two way ANOVA followed by Tukey *post hoc* multiple comparison test was applied for statistical comparison between groups and for the graphical representation, values expressed mean percentage of Control ± SEM.

($F_{(2,12)} = 28.36$; $p < 0.0001$; **Figure 4H**), and up-regulated the mRNA expression of IL-4 ($F_{(2,12)} = 153.9$; $p < 0.0001$; **Figure 4I**), IL-10 ($F_{(2,12)} = 76.56$; $p < 0.0001$; **Figure 4J**) during SD.

Caffeine or Modafinil Treatment Down-regulated the Astrocyte and Microglial Cells Immunoreactivity Following SD

Astrocytes and microglial cells activation were evaluated by studying the immunohistochemical changes in the expression of GFAP and Iba-1 protein in different regions of the dorsal hippocampus. Changes in the expression of astrocytes among different groups in DG, CA1 and CA3 region of the dorsal hippocampus was shown in **Figure 5A**. We found no significant increase in the relative mean pixel intensity of GFAP positive cells (astrocytes immunoreactivity) in DG, CA1 and CA3 region of the hippocampus, belonged to SD exposed rats compared to control rats. Caffeine or modafinil treatment non-significantly decrease the astrocytes immunoreactivity in DG ($F_{(2,84)} = 0.6826$; $p = 0.5081$; **Figure 5B**); CA1 ($F_{(2,84)} = 0.2293$; $p = 0.7956$; **Figure 5C**), and CA3 ($F_{(2,84)} = 0.1089$; $p = 0.8970$; **Figure 5D**) region of dorsal hippocampus compared to sleep deprived vehicle-treated rats.

Similarly, the vehicle and drugs treated rats showed changes in the expression of microglial cell in different hippocampal regions as shown in **Figure 5E**. We found a significant increase in the relative mean pixel intensity of microglial cell in SD exposed rats compared to control rats. Caffeine or modafinil treatment during SD significantly decreased the immunoreactivity of microglial cell in DG ($F_{(2,84)} = 44.32$; $p < 0.0001$; **Figure 5F**); CA1 ($F_{(2,84)} = 30.26$; $p < 0.0001$; **Figure 5G**), and CA3 ($F_{(2,84)} = 25.97$; $p < 0.0001$; **Figure 5H**) region of the hippocampus in comparison with vehicle-treated SD rats. Furthermore, no significant change in the immunoreactivity of GFAP and Iba-1 positive cells was observed following treatment of caffeine or modafinil to control rats compared to vehicle-treated control rats.

Caffeine or Modafinil Administration Efficiently Improved the Astrocyte and Microglial Cells Morphology Following SD

Representable intersectional and segmented images of the resting, intermediate and activated stage of astrocyte and the microglial cell was shown in **Figures 6A,B**. Astrocyte and microglial cells morphology were investigated by the following parameters such as soma density, soma area, sum inters, mean inters, ramification index and glial cell size/length among different groups in DG, CA1 and CA3 region of the dorsal hippocampus.

Administration of caffeine/modafinil significantly improved the SD-induced changes in the morphology of astrocytes in DG, CA1 and CA3 region of the hippocampus (**Figures 6C–H**; **Table 1**). Subsequently, microglial cell showed significantly increase in soma density, soma area and a decrease in sum inters, mean inters, ramification index, microglia length following SD while after caffeine or modafinil treatment during SD, the above consequences were significantly improved (**Figures 6I–N**; **Table 1**). Statistically non-significant morphological changes

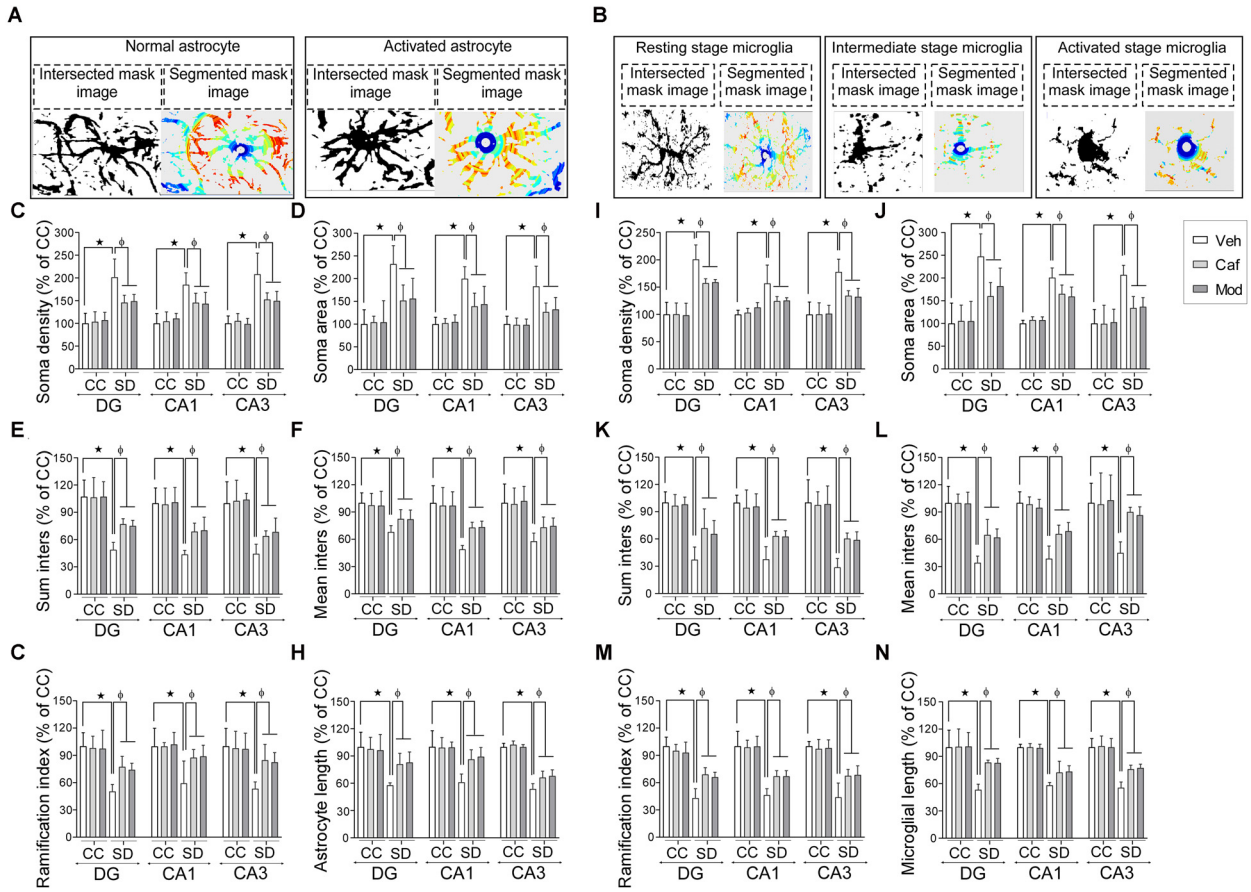

FIGURE 6 | Caffeine or modafinil administration altered the morphology of astrocytes and microglia towards the resting state in rat hippocampus during SD. Representable image (intersection and segmented mask) of **(A)** normal and activated astrocyte; **(B)** resting, intermediate and activated stage microglial cell. Changes in the **(C)** soma density; **(D)** soma area; **(E)** sum inters; **(F)** mean inters; **(G)** ramification index; **(H)** astrocyte length of astrocytes in DG, CA1 and CA3 regions of the hippocampus. Changes in the **(I)** soma density; **(J)** soma area; **(K)** sum inters; **(L)** mean inters; **(M)** ramification index; **(N)** microglial length of microglia cells. $^{*}p < 0.05$ when compared to control treated with vehicle; $^{\Phi}p < 0.05$ when compared to sleep deprived treated with vehicle. Two way ANOVA followed by Tukey *post hoc* test with multiple comparison was applied for statistical comparison between groups and for the graphical representation, values expressed mean percentage of Control ± SEM.

were observed in the vehicle and drugs treated control rats hippocampus.

Caffeine or Modafinil Treatment Maintained the Microglial Cells Numbers during SD

We found a significant decrease in resting stage microglial cell in DG and CA3 region of the hippocampus, while the activated microglial cell numbers were significantly increased in DG, CA1 and CA3 region of the hippocampus. No significant change was observed in the intermediate state microglia cell count during SD. Caffeine or modafinil treatment during SD significantly increased the resting stage microglial cell and decreased activated microglial cell count, given during SD in DG (resting ($F_{(2,84)}$ = 22.65; $p < 0.0001$; Boia et al., 2017); intermediate ($F_{(2,84)}$ = 0.1197; p = 0.8874); activated ($F_{(2,84)}$ = 33.82; $p < 0.0001$); **Figure 7A**), CA1 (resting ($F_{(2,84)}$ = 4.741; p = 0.0112); intermediate ($F_{(2,84)}$ = 0.03004; p = 0.9704); activated ($F_{(2,84)}$ = 44.26; $p < 0.0001$); **Figure 7B**), and CA3 (resting ($F_{(2,84)}$ = 11.15; $p < 0.0001$); intermediate ($F_{(2,84)}$ = 0.09492; p = 0.9095); activated ($F_{(2,30)}$ = 3.636; $p < 0.0001$; **Figure 7C**).

Although, trivial increase in total microglial cell count in SD-vehicle group was observed, caffeine or modafinil treatment also showed in consequential improvement in DG ($F_{(2,84)}$ = 0.1095; p = 0.8964; **Figure 7D**); CA1 ($F_{(2,84)}$ = 0.5845; p = 0.5597; **Figure 7E**), and CA3 ($F_{(2,84)}$ = 0.8691; p = 0.4231; **Figure 7F**) region of the hippocampus.

Changes in Mood Was Correlated to Microglial Activation Induced Up-regulated Level of Pro-inflammatory Cytokines during SD

The interaction between the anxiety parameters, pro-inflammatory cytokines and activated microglia cell

TABLE 1 | Astrocyte and microglia morphology during sleep deprivation (SD) and caffeine/modafinil administration.

	$F_{(dFn,dFd)}; p < 0.0001$		
Parameter	**DG region**	**CA1 region**	**CA3 region**
Astrocyte morphology			
Soma density	$F_{(2,84)} = 30.53$*	$F_{(2,84)} = 22.83$*	$F_{(2,84)} = 24.37$*
Soma area	$F_{(2,84)} = 18.27$*	$F_{(2,84)} = 24.6$*	$F_{(2,84)} = 19.5$*
Sum inters	$F_{(2,84)} = 14.53$*	$F_{(2,84)} = 13.03$*	$F_{(2,84)} = 10.18$*
Mean inters	$F_{(2,84)} = 20.42$*	$F_{(2,84)} = 13.4$*	$F_{(2,84)} = 12.76$*
Ramification index	$F_{(2,84)} = 14.24$*	$F_{(2,84)} = 11.37$*	$F_{(2,84)} = 16.81$*
Astrocyte length	$F_{(2,84)} = 20.14$*	$F_{(2,84)} = 28.86$*	$F_{(2,84)} = 23.1$*
Microglia morphology			
Soma density	$F_{(2,84)} = 9.216$*	$F_{(2,84)} = 54.27$*	$F_{(2,84)} = 25.22$*
Soma area	$F_{(2,84)} = 18.24$*	$F_{(2,84)} = 47.28$*	$F_{(2,84)} = 27.67$*
Sum inters	$F_{(2,84)} = 17.21$*	$F_{(2,84)} = 30.28$*	$F_{(2,84)} = 30.85$*
Mean inters	$F_{(2,84)} = 21.58$*	$F_{(2,84)} = 45.18$*	$F_{(2,84)} = 18.76$*
Ramification index	$F_{(2,84)} = 62.23$*	$F_{(2,84)} = 12.55$*	$F_{(2,84)} = 27.44$*
Microglial length	$F_{(2,84)} = 19.53$*	$F_{(2,84)} = 32.63$*	$F_{(2,84)} = 34.45$*

*Two way ANOVA followed by Tukey post hoc test with multiple comparison was applied for statistical comparison. *$p < 0.05$ is significantly different compared to control.*

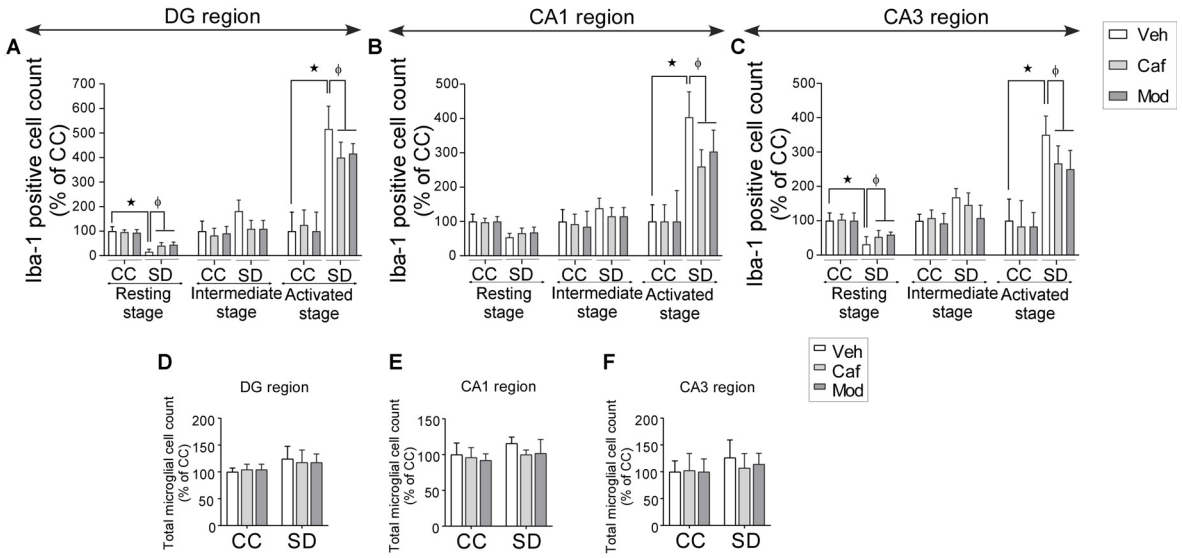

FIGURE 7 | Caffeine or modafinil improved the microglial cell numbers following SD. Changes in the microglial cell count at different stages (resting, intermediate and activated) in **(A)** DG region; **(B)** CA1 region; **(C)** CA3 region of the hippocampus. Total microglial cell count in **(D)** DG region; **(E)** CA1 region; **(F)** CA3 region of the hippocampus. *$p < 0.05$ when compared to control treated with vehicle; $^{\phi}p < 0.05$ when compared to sleep deprived treated with vehicle. Two way ANOVA followed by Tukey *post hoc* test with multiple comparison was applied for statistical comparison between groups and for the graphical representation, values expressed mean percentage of Control ± SEM.

count was evaluated by the correlation analysis to validate the findings.

There was a significant correlation between the proportion of the number of entries in the open arms and the number of activated microglial cell count ($r^2 = 0.5634$; $p < 0.0001$; **Figure 8A**); proportion of the time spent in the open arms and the number of activated microglial cell count ($r^2 = 0.5958$; $p < 0.0001$; **Figure 8B**), and the total distance traveled in the OF and the number of activated microglial cell count ($r^2 = 0.3979$; $p < 0.0001$; **Figure 8C**).

A significant correlation was observed between the proportion of the number of entries in the open arms and TNF-α level in hippocampus ($r^2 = 0.331$; $p < 0.0001$; **Figure 8D**); proportion of the time spent in the open arms and TNF-α level in hippocampus ($r^2 = 0.4472$; $p < 0.0001$; **Figure 8E**), and the total distance traveled in the OF and TNF-α level in hippocampus ($r^2 = 0.3734$; $p < 0.0001$; **Figure 8F**). Similarly, correlation analysis showed significant correlation between the proportion of the number of entries in the open arms and IL-1β level in hippocampus ($r^2 = 0.2514$; $p < 0.0001$; **Figure 8G**); proportion of the time spent in the open arms and IL-1β level in hippocampus ($r^2 = 0.2457$; $p < 0.0001$; **Figure 8H**) and the total distance traveled in the OF and IL-1β level in hippocampus ($r^2 = 0.26$; $p < 0.0001$; **Figure 8I**).

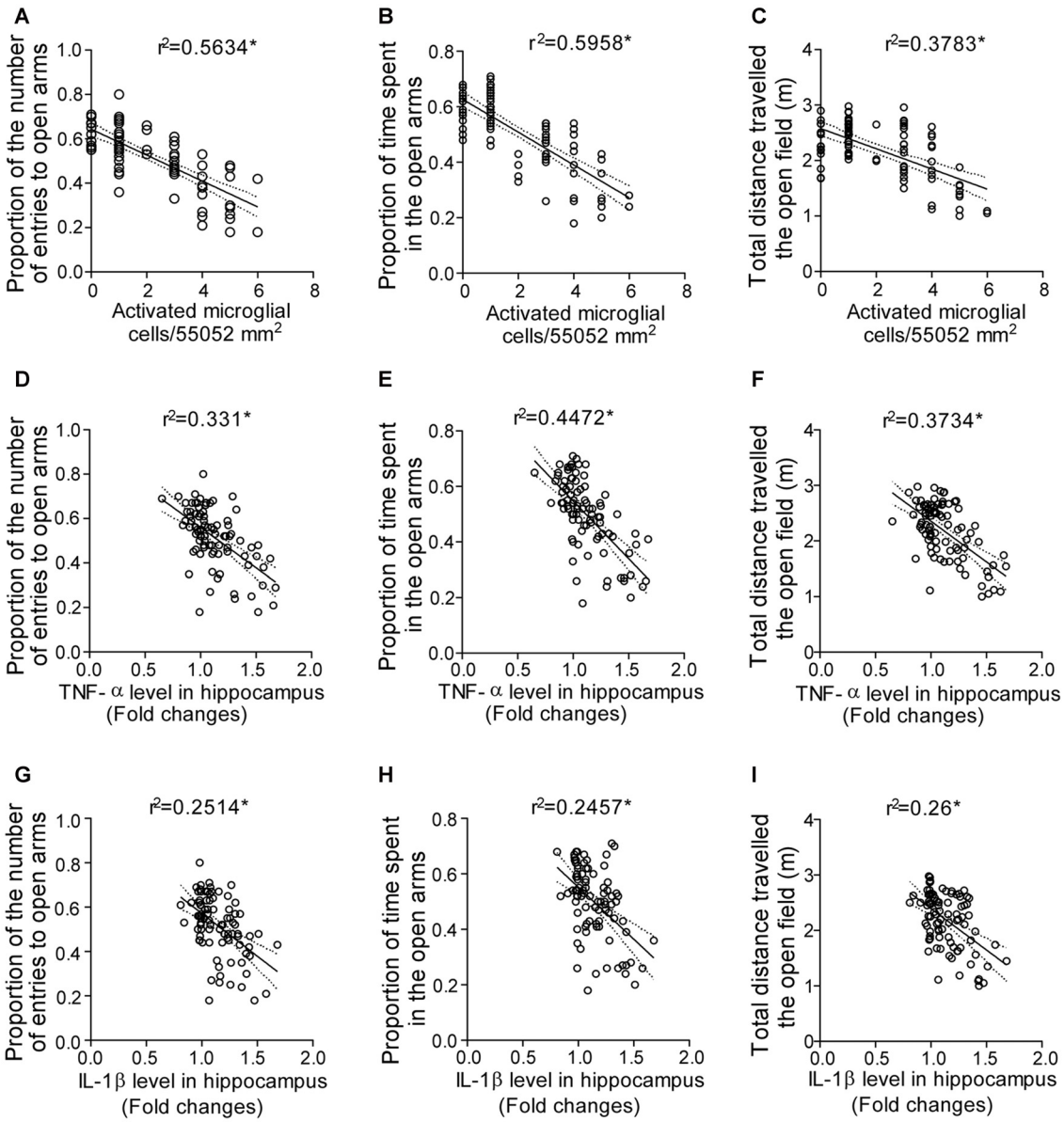

FIGURE 8 | Correlation analysis predicting the interaction between the anxious behavior, pro-inflammatory cytokines and activated microglia cell during SD. Interaction between the anxious behavior and activated microglial cell as shown by correlation between **(A)** proportion of the number of entries in the open arms and activated microglial cell count in the hippocampus; **(B)** proportion of the time spent in the open arms and activated microglial cell count in the hippocampus; **(C)** total distance traveled in the OF and activated microglial cell count in the hippocampus. Finally, the interaction between the anxious behavior and pro-inflammatory cytokine levels as shown by correlation between **(D)** proportion of the number of entries in the open arms and TNF-α level in hippocampus; **(E)** proportion of the time spent in the open arms and TNF-α level in hippocampus; **(F)** total distance traveled in the OF and TNF-α level in hippocampus; **(G)** proportion of the number of entries in the open arms and IL-1β level in hippocampus; **(H)** proportion of the time spent in the open arms and IL-1β level in hippocampus; **(I)** total distance traveled in the OF and IL-1β level in hippocampus. Pearson's test was applied for correlation analysis. $p < 0.05$ was considered to be statistically significant.

DISCUSSION

SD affected depressive/anxiety-like behavior and neuroinflammatory reactivity. Sleep deprived rats were more anxious in the EPM and OF test. However, caffeine or modafinil treatment increased OF activity, and thus reversed the effects of SD. Moreover, caffeine or modafinil decreased the time in closed but increased the time in open arms. Finally, pro-inflammatory cytokine levels were increased following SD and caffeine/modafinil decreased the pro-inflammatory and increased anti-inflammatory cytokine levels. As anticipated, the hippocampus of SD rats had higher glial immunoreactivity and altered morphology, and this effect was more pronounced in the microglial cells number, while psychostimulant drugs

improved the above consequences. However, the tested doses of caffeine were higher and did not mimic habitual caffeine consumption. Together, our data highlight the influence of SD on neuroinflammatory responsiveness, and the importance of considering these factors in animal tests of depression/anxiety behaviors.

Caffeine or Modafinil Treatment Improved the Physiological Consequences during SD

Normal sleep is necessary for health and sleep disruption influences the physiological function (Kumar and Kalonia, 2007). Food intake and mood are related to each other, depending on the stress, food intake may decrease or increase (Singh, 2014). There is a controversial relationship between the body weight, food intake and sleep. There are reports on body weight reduction during SD (Mavanji et al., 2013), weight gain attenuation with no change in food intake during SD (Barf et al., 2012), at the same time increase in food intake with decreases in body weight (Koban and Stewart, 2006). Animal studies had shown that increased cytokine levels reduce food intake and body weight during neuroinflammatory conditions (Park et al., 2011a; Zombeck et al., 2013). In contrast to previous studies, we observed a decrease in body weight of sleep-deprived rats, which was improved after caffeine/modafinil treatment.

Caffeine or Modafinil Administration Produced Anxiolytic Effect and Recovered from the Depressive Behavior during SD

Under stressful conditions, the anxiety index has been found to be increased (Pechlivanova et al., 2012). Additionally, there are various reports of anxiogenic behavior in rodents as shown by EPM (decrease in time spent in open arms) and OF (impaired locomotor activity) test with body weight loss during SD (Silva et al., 2004; Garcia et al., 2011; Alkadhi et al., 2013; Matzner et al., 2013). Caffeine has a dose-dependent effect on anxious behavior. The previous findings revealed the behavioral observations that low (10 mg/kg) or moderate (20 mg/kg) dose of caffeine administration had shown reduction in anxiety behavior revealed by increased locomotor activity (Poletaeva and Oleinik, 1975; Antoniou et al., 1998), while increased dose of caffeine showed anxiogenic effect (Kayir and Uzbay, 2006) as predicted by the decrease or increase time and entry in open arms in rodents. Caffeine had shown to decrease the anxiety level during bright light stress conditions (Hughes et al., 2014) and chronic unpredictable stress conditions in rodents (Kaster et al., 2015). Like rodent studies, caffeine administration showed mood improvement in humans also (Smith et al., 2006). There are also reports available showing no effects of caffeine on anxiety (Khor et al., 2013). Similar to caffeine, modafinil showed anxiolytic effect shown by increased locomotor activity in humans (van Vliet et al., 2006) as well as rodents (Siwak et al., 2000; Quisenberry et al., 2013). This data is in consistent with the previous reports showing anxiogenic behavior during SD and caffeine or modafinil treatment improved the anxiety state during SD in rats, although the exact mechanism is still unclear.

There is a close association of the anxiety and depression with the disturbance in the normal sleep-wake cycle (Grønli et al., 2004; Jakubcakova et al., 2012; Kostyalik et al., 2014), immune system activation, assessed by decreased preference for a sweetness increased immobility time (Park et al., 2011b; Jangra et al., 2014). Imbalance in the cytokines level upon immune system activation has been found to be responsible for depression, predicted by a decrease in sucrose preference and increase in immobility (Ballok and Sakic, 2008; Braun et al., 2012). Inflammatory stimulation such as lipopolysaccharide model (Sayd et al., 2014) and Poly I:C administration (Missault et al., 2014), increased the pro-inflammatory cytokine (IL-1β, TNF-α and IL-6) levels and induced depressive symptoms. Furthermore, sickness behavior had also been found to be associated with the increased levels of the pro-inflammatory cytokine (Bluthé et al., 1995; Konsman et al., 2002; Dantzer, 2004; Vichaya et al., 2016, 2017). The incidence of anhedonia (decreased intake of sweet solution) had been reported in humans after SD (Petrovsky et al., 2014). Previous studies indicate a positive effect of caffeine on depressive symptoms shown by reduced immobility in rats (Vieira et al., 2008; Rusconi et al., 2014). Caffeine administration had been reported to alleviate the depressive behavior and memory dysfunction during chronic stress in a study by Kaster group (Kaster et al., 2015). Furthermore, inability in the reversal of the mood deficits in helpless mice during caffeine intake was reported (Machado et al., 2017). Human studies had shown improvement after modafinil treatment given during depression (Price and Taylor, 2005; Frye et al., 2007). Similar to humans, modafinil showed improvement in body weight along with mobility during stress in rats (Regenthal et al., 2009). In the paradigm used for our study, SD rats showed an increase in immobility and decrease the preference for sucrose solution, but the changes observed were not significant. Our data revealed non-significant decrease in immobility and increased sucrose preference after caffeine/modafinil treatment during SD.

Caffeine or Modafinil Administration Maintained the Inflammatory Profile during SD

The increase in the cytokine levels with decreased food and water intake had been reported in neuroinflammatory models of rodents (Zombeck et al., 2013). The anxiogenic and depressive effect of cytokines shown by a preference for closed arms than open arms reduced immobility and decreased sucrose preference validated by knock-out and cytokines administration studies (Pan et al., 2013). One rodent study on maternal obesity reported an elevated level of pro-inflammatory cytokines along with mood disorder (Kang et al., 2014); another neuroinflammatory study on lupus-prone mice described anxious behavior along with an increased pro-inflammatory cytokine level (Ballok and Sakic, 2008). The previous report suggested the beneficial effects of caffeine on MDMA induced a behavioral and neuroinflammatory response (Ruiz-Medina et al., 2013). Caffeine administration showed the ability to control the behavioral alterations in neuroinflammatory disease models such as Parkinson's (Chen et al., 2001; Joghataie et al., 2004) and Alzheimer's (Arendash et al., 2006; Dall'Igna et al., 2007). Caffeine treatment also restored the memory performance and

glial cells reactivity in a rodent model of diabetes (Duarte et al., 2012) and Machado-Joseph disease (Gonçalves et al., 2013). Our data showed the increased level of pro-inflammatory and decreased levels of anti-inflammatory cytokine in hippocampus and plasma during SD. Caffeine or modafinil treatment improved the cytokine levels in the hippocampus and plasma during SD.

Astrocytes, immunocompetent cells of the brain, becomes activated and secretes several neurotoxic substances along with an enhanced GFAP protein expression (astrogliosis protein marker). This enhanced GFAP expression relates to the astrocytes activation severity. Astrocytes activation assessed by GFAP expression was increased along with increased cytokine levels during inflammatory stimulation by LPS administration (Brahmachari et al., 2006; Park et al., 2011a; Norden et al., 2016). Microglial activation marker (Iba-1) showed increased expression associated with anxiety in maternal obesity model (Kang et al., 2014), pollutants exposure (Bolton et al., 2012) in rodents. The association between the mood alterations and glial cells reactivity under the perspective of the purinergic neuromodulation had been recently studied (Rial et al., 2016). Caffeine decreases the glial cells activation along with the reducing production of pro-inflammatory cytokines due to the localization of the adenosine receptors on microglia (Sonsalla et al., 2012). In rodents, caffeine treatment has been reported to decrease the astrocytes activity (Ardais et al., 2014) and microglial activation during rodent models of neuroinflammation such as maneb and paraquat (Yadav et al., 2012) and MDMA (Ruiz-Medina et al., 2013). Our results also highlight the influence of SD on the immunoreactivity of astrocytes and microglia (increased) and caffeine or modafinil treatment down-regulated the immunoreactivity of astrocytes and microglia during SD.

We also observed the morphological changes in the astrocytes and microglia in the hippocampus of sleep-deprived rats and caffeine or modafinil administration during SD improved these changes during SD. Results of this study get supported from the previous studies of social defeat, showing elevated cytokine levels in the brain associated with anxiety (Wohleb et al., 2014a,b). Along with morphological changes, we observed increased cell numbers of activated microglial cells and decreased cell count of resting stage microglial cell during SD, while caffeine or modafinil treatment following SD improved the resting and activated microglial cells count. Previous findings dictated the modulatory role of adenosine A2A receptor system in neuroprotection by controlling the microglia inducing neuroinflammation (Dai et al., 2010; Rebola et al., 2011; Gyoneva et al., 2014b). In a previous study on stroke model, increased activated microglial cells, morphological alteration of microglia along with anxiety and depression-like behavior was reported (Nemeth et al., 2014). A recent study enlightened an interplay between the microglial cells alterations and anxiety disorders, regulated by adenosine A2A receptor (Caetano et al., 2017). Stressful conditions trigger the increased release of adenosine and ATP, in which the adenosine modulation system in association with glial cells afford maximum neuroprotection (Cunha, 2016). Caffeine attenuated the activated microglial cell count in the hippocampus on LPS stimulation (Brothers et al., 2010) and high cholesterol diet-induced model of neuroinflammation (Chen et al., 2008). Caffeine administration prevented the microglia activation induced neuroinflammation in the transient retinal ischemic model in rodents (Boia et al., 2017). Similarly, modafinil treatment prevented the glial cells activation shown by increased resting and decrease activated stage cell with improvement in immunoreactivity in a neuroinflammatory model in rodents (Raineri et al., 2012). It was observed that microglial cells activation induced the increased level of pro-inflammatory cytokines, which further influenced the normal mood of rats towards anxious state during SD. The use of only male Sprague Dawley rats is a limitation of the present study as recent survey suggested the relation of sleep patterns with caffeine is different in males and females (Frozi et al., 2018).

CONCLUSION

The present study demonstrated that inhibition of microglial cells by caffeine or modafinil treatment modulated the cytokine levels with increased the anti-inflammatory cytokines and ameliorates the anxious behavior) during SD. Our data suggested that caffeine/modafinil are the effective therapeutic agents against SD-induced neuroinflammation and anxiety behavior.

AUTHOR CONTRIBUTIONS

UP and MW designed the study and wrote the manuscript. MW performed the experiments and analyzed the data. KRay, LT, GC, KRoy, SS, SD and VJ helped in the manuscript writing. GC, KRoy and VJ helped in the immunohistochemistry of glial proteins and cytokines level measurement. SS and SD helped in the behavioral and RT-PCR experiments. UP, KRay, KK and LT contributed in procurement and facilitated the instruments and other facilities. All authors read and approved the final manuscript.

FUNDING

This study was funded by the Defence Research and Development Organization (DRDO), and the first author is the recipient of Department of Science and Technology, Ministry of Science and Technology (DST-INSPIRE) fellowship.

ACKNOWLEDGMENTS

We are thankful to Director, DIPAS, for supporting and facilitating the research work. Dr. Dipti Prasad and Dr. Ekta Kohli, Neurobiology division are acknowledged for extending the behavioral facility for the study. We are thankful to Dr. Zahid Mohammad Ashraf, Genomics Division, for extending us to use RT-PCR instrument facility.

SUPPLEMENTARY MATERIAL

The Supplementary Material for this article can be found online at: https://www.frontiersin.org/articles/10.3389/fncel.2018.00049/full#supplementary-material

FIGURE S1 | Caffeine or modafinil treatment improved the sleep deprivation (SD)-induced physiological changes in rats. Changes in **(A)** body weight; **(B)** food intake. $^{*}p < 0.05$ when compared to control treated with vehicle; $^{\phi}p < 0.05$, when compared to sleep deprived treated with vehicle. Two way ANOVA followed by Tukey *post hoc* test with multiple comparison was applied for statistical comparison between groups and for the graphical representation, values expressed mean percentage of Control ± SEM.

FIGURE S2 | Fold changes in the inflammatory cytokines in plasma during caffeine/modafinil administration following SD. Fold changes in **(A)** TNF-α; **(B)** IL-1β; **(C)** IL-6 (pro-inflammatory cytokines); **(D)** IL-4; **(E)** IL-10 (anti-inflammatory cytokines) in plasma. $^{*}p < 0.05$ when compared to control treated with vehicle; $^{\phi}p < 0.05$ when compared to sleep deprived treated with vehicle. Two way ANOVA followed by Tukey *post hoc* test with multiple comparison was applied for statistical analysis.

REFERENCES

Abelaira, H. M., Reus, G. Z., and Quevedo, J. (2013). Animal models as tools to study the pathophysiology of depression. *Rev. Bras. Psiquiatr.* 35, S112–S120. doi: 10.1590/1516-4446-2013-1098

Alkadhi, K., Zagaar, M., Alhaider, I., Salim, S., and Aleisa, A. (2013). Neurobiological consequences of sleep deprivation. *Curr. Neuropharmacol.* 11, 231–249. doi: 10.2174/1570159x11311030001

Antoniou, K., Kafetzopoulos, E., Papadopoulou-Daifoti, Z., Hyphantis, T., and Marselos, M. (1998). D-amphetamine, cocaine and caffeine: a comparative study of acute effects on locomotor activity and behavioural patterns in rats. *Neurosci. Biobehav. Rev.* 23, 189–196. doi: 10.1016/s0149-7634(98)00020-7

Ardais, A. P., Borges, M. F., Rocha, A. S., Sallaberry, C., Cunha, R. A., and Porciúncula, L. O. (2014). Caffeine triggers behavioral and neurochemical alterations in adolescent rats. *Neuroscience* 270, 27–39. doi: 10.1016/j.neuroscience.2014.04.003

Arendash, G. W., Schleif, W., Rezai-Zadeh, K., Jackson, E. K., Zacharia, L. C., Cracchiolo, J. R., et al. (2006). Caffeine protects Alzheimer's mice against cognitive impairment and reduces brain β-amyloid production. *Neuroscience* 142, 941–952. doi: 10.1016/j.neuroscience.2006.07.021

Babson, K. A., Trainor, C. D., Feldner, M. T., and Blumenthal, H. (2010). A test of the effects of acute sleep deprivation on general and specific self-reported anxiety and depressive symptoms: an experimental extension. *J. Behav. Ther. Exp. Psychiatry* 41, 297–303. doi: 10.1016/j.jbtep.2010.02.008

Ballok, D. A., and Sakic, B. (2008). Purine receptor antagonist modulates serology and affective behaviors in lupus-prone mice: evidence of autoimmune-induced pain? *Brain Behav. Immun.* 22, 1208–1216. doi: 10.1016/j.bbi.2008.06.002

Barf, R. P., Van Dijk, G., Scheurink, A. J., Hoffmann, K., Novati, A., Hulshof, H. J., et al. (2012). Metabolic consequences of chronic sleep restriction in rats: changes in body weight regulation and energy expenditure. *Physiol. Behav.* 107, 322–328. doi: 10.1016/j.physbeh.2012.09.005

Bluthé, R. M., Beaudu, C., Kelley, K. W., and Dantzer, R. (1995). Differential effects of IL-1ra on sickness behavior and weight loss induced by IL-1 in rats. *Brain Res.* 677, 171–176. doi: 10.1016/0006-8993(95)00194-u

Boele, F. W., Douw, L., De Groot, M., Van Thuijl, H. F., Cleijne, W., Heimans, J. J., et al. (2013). The effect of modafinil on fatigue, cognitive functioning and mood in primary brain tumor patients: a multicenter randomized controlled trial. *Neuro Oncol.* 15, 1420–1428. doi: 10.1093/neuonc/not102

Boia, R., Elvas, F., Madeira, M. H., Aires, I. D., Rodrigues-Neves, A. C., Tralhão, P., et al. (2017). Treatment with A_{2A} receptor antagonist KW6002 and caffeine intake regulate microglia reactivity and protect retina against transient ischemic damage. *Cell Death Dis.* 8:e3065. doi: 10.1038/cddis.2017.451

Bolton, J. L., Smith, S. H., Huff, N. C., Gilmour, M. I., Foster, W. M., Auten, R. L., et al. (2012). Prenatal air pollution exposure induces neuroinflammation and predisposes offspring to weight gain in adulthood in a sex-specific manner. *FASEB J.* 26, 4743–4754. doi: 10.1096/fj.12-210989

Brahmachari, S., Fung, Y. K., and Pahan, K. (2006). Induction of glial fibrillary acidic protein expression in astrocytes by nitric oxide. *J. Neurosci.* 26, 4930–4939. doi: 10.1523/jneurosci.5480-05.2006

Braun, T. P., Grossberg, A. J., Veleva-Rotse, B. O., Maxson, J. E., Szumowski, M., Barnes, A. P., et al. (2012). Expression of myeloid differentiation factor 88 in neurons is not requisite for the induction of sickness behavior by interleukin-1β. *J. Neuroinflammation* 9:229. doi: 10.1186/1742-2094-9-229

Brothers, H. M., Marchalant, Y., and Wenk, G. L. (2010). Caffeine attenuates lipopolysaccharide-induced neuroinflammation. *Neurosci. Lett.* 480, 97–100. doi: 10.1016/j.neulet.2010.06.013

Caetano, L., Pinheiro, H., Patrício, P., Mateus-Pinheiro, A., Alves, N. D., Coimbra, B., et al. (2017). Adenosine A_{2A} receptor regulation of microglia morphological remodeling-gender bias in physiology and in a model of chronic anxiety. *Mol. Psychiatry* 22, 1035–1043. doi: 10.1038/mp.2016.173

Cappelletti, S., Piacentino, D., Sani, G., and Aromatario, M. (2015). Caffeine: cognitive and physical performance enhancer or psychoactive drug? *Curr. Neuropharmacol.* 13, 71–88. doi: 10.2174/1570159x13666141210215655

Carey, M. G., Al-Zaiti, S. S., Dean, G. E., Sessanna, L., and Finnell, D. S. (2011). Sleep problems, depression, substance use, social bonding, and quality of life in professional firefighters. *J. Occup. Environ. Med.* 53, 928–933. doi: 10.1097/jom.0b013e318225898f

Chauhan, G., Ray, K., Sahu, S., Roy, K., Jain, V., Wadhwa, M., et al. (2016). Adenosine A1 receptor antagonist mitigates deleterious effects of sleep deprivation on adult neurogenesis and spatial reference memory in rats. *Neuroscience* 337, 107–116. doi: 10.1016/j.neuroscience.2016.09.007

Chen, X., Gawryluk, J. W., Wagener, J. F., Ghribi, O., and Geiger, J. D. (2008). Caffeine blocks disruption of blood brain barrier in a rabbit model of Alzheimer's disease. *J. Neuroinflammation* 5:12. doi: 10.1186/1742-2094-5-12

Chen, J. F., Xu, K., Petzer, J. P., Staal, R., Xu, Y. H., Beilstein, M., et al. (2001). Neuroprotection by caffeine and A_{2A} adenosine receptor inactivation in a model of Parkinson's disease. *J. Neurosci.* 21:RC143.

Cunha, R. A. (2016). How does adenosine control neuronal dysfunction and neurodegeneration? *J. Neurochem.* 139, 1019–1055. doi: 10.1111/jnc.13724

Cunha, R. A., and Agostinho, P. M. (2010). Chronic caffeine consumption prevents memory disturbance in different animal models of memory decline. *J. Alzheimers Dis.* 20, S95–S116. doi: 10.3233/jad-2010-1408

Dai, S. S., Zhou, Y. G., Li, W., An, J. H., Li, P., Yang, N., et al. (2010). Local glutamate level dictates adenosine A_{2A} receptor regulation of neuroinflammation and traumatic brain injury. *J. Neurosci.* 30, 5802–5810. doi: 10.1523/JNEUROSCI.0268-10.2010

Dall'Igna, O. P., Fett, P., Gomes, M. W., Souza, D. O., Cunha, R. A., and Lara, D. R. (2007). Caffeine and adenosine A_{2A} receptor antagonists prevent β-amyloid (25–35)-induced cognitive deficits in mice. *Exp. Neurol.* 203, 241–245. doi: 10.1016/j.expneurol.2006.08.008

Daly, J. W. (2007). Caffeine analogs: biomedical impact. *Cell Mol. Life Sci.* 64, 2153–2169. doi: 10.1007/s00018-007-7051-9

Dantzer, R. (2004). Cytokine-induced sickness behaviour: a neuroimmune response to activation of innate immunity. *Eur. J. Pharmacol.* 500, 399–411. doi: 10.1016/j.ejphar.2004.07.040

Duarte, J. M., Agostinho, P. M., Carvalho, R. A., and Cunha, R. A. (2012). Caffeine consumption prevents diabetes-induced memory impairment and synaptotoxicity in the hippocampus of NONcZNO10/LTJ mice. *PLoS One* 7:e21899. doi: 10.1371/journal.pone.0021899

Dworak, M., Kim, T., Mccarley, R. W., and Basheer, R. (2011). Sleep, brain energy levels and food intake: relationship between hypothalamic ATP concentrations, food intake and body weight during sleep-wake and sleep deprivation in rats. *Somnologie* 15, 111–117. doi: 10.1007/s11818-011-0524-y

Frozi, J., De Carvalho, H. W., Ottoni, G. L., Cunha, R. A., and Lara, D. R. (2018). Distinct sensitivity to caffeine-induced insomnia related to age. *J. Psychopharmacol.* 32, 89–95. doi: 10.1177/0269881117722997

Frye, M. A., Grunze, H., Suppes, T., McElroy, S. L., Keck, P. E. Jr., Walden, J., et al. (2007). A placebo-controlled evaluation of adjunctive modafinil in the treatment of bipolar depression. *Am. J. Psychiatry* 164, 1242–1249. doi: 10.1176/appi.ajp.2007.06060981

Garcia, A. M., Cardenas, F. P., and Morato, S. (2011). The effects of pentylenetetrazol, chlordiazepoxide and caffeine in rats tested in the elevated plus-maze depend on the experimental illumination. *Behav. Brain Res.* 217, 171–177. doi: 10.1016/j.bbr.2010.09.032

Gonçalves, N., Simões, A. T., Cunha, R. A., and De Almeida, L. P. (2013). Caffeine and adenosine A_{2A} receptor inactivation decrease striatal neuropathology in a lentiviral-based model of Machado-Joseph disease. *Ann. Neurol.* 73, 655–666. doi: 10.1002/ana.23866

Grønli, J., Murison, R., Bjorvatn, B., Sørensen, E., Portas, C. M., and Ursin, R. (2004). Chronic mild stress affects sucrose intake and sleep in rats. *Behav. Brain Res.* 150, 139–147. doi: 10.1016/s0166-4328(03)00252-3

Gyoneva, S., Davalos, D., Biswas, D., Swanger, S. A., Garnier-Amblard, E., Loth, F., et al. (2014a). Systemic inflammation regulates microglial responses to tissue damage *in vivo*. *Glia* 62, 1345–1360. doi: 10.1002/glia.22686

Gyoneva, S., Shapiro, L., Lazo, C., Garnier-Amblard, E., Smith, Y., Miller, G. W., et al. (2014b). Adenosine A_{2A} receptor antagonism reverses inflammation-induced impairment of microglial process extension in a model of Parkinson's disease. *Neurobiol. Dis.* 67, 191–202. doi: 10.1016/j.nbd.2014.03.004

Hong, H., Kim, B. S., and Im, H. I. (2016). Pathophysiological role of neuroinflammation in neurodegenerative diseases and psychiatric disorders. *Int. Neurourol. J.* 20, S2–S7. doi: 10.5213/inj.1632604.302

Hughes, R. N., Hancock, N. J., Henwood, G. A., and Rapley, S. A. (2014). Evidence for anxiolytic effects of acute caffeine on anxiety-related behavior in male and female rats tested with and without bright light. *Behav. Brain Res.* 271, 7–15. doi: 10.1016/j.bbr.2014.05.038

Jakubcakova, V., Flachskamm, C., Landgraf, R., and Kimura, M. (2012). Sleep phenotyping in a mouse model of extreme trait anxiety. *PLoS One* 7:e40625. doi: 10.1371/journal.pone.0040625

Jangra, A., Lukhi, M. M., Sulakhiya, K., Baruah, C. C., and Lahkar, M. (2014). Protective effect of mangiferin against lipopolysaccharide-induced depressive and anxiety-like behaviour in mice. *Eur. J. Pharmacol.* 740, 337–345. doi: 10.1016/j.ejphar.2014.07.031

Joghataie, M. T., Roghani, M., Negahdar, F., and Hashemi, L. (2004). Protective effect of caffeine against neurodegeneration in a model of Parkinson's disease in rat: behavioral and histochemical evidence. *Parkinsonism Relat. Disord.* 10, 465–468. doi: 10.1016/j.parkreldis.2004.06.004

Kang, A., Hao, H., Zheng, X., Liang, Y., Xie, Y., Xie, T., et al. (2011). Peripheral anti-inflammatory effects explain the ginsenosides paradox between poor brain distribution and anti-depression efficacy. *J. Neuroinflammation* 8:100. doi: 10.1186/1742-2094-8-100

Kang, S. S., Kurti, A., Fair, D. A., and Fryer, J. D. (2014). Dietary intervention rescues maternal obesity induced behavior deficits and neuroinflammation in offspring. *J. Neuroinflammation* 11:156. doi: 10.1186/s12974-014-0156-9

Kaster, M. P., Machado, N. J., Silva, H. B., Nunes, A., Ardais, A. P., Santana, M., et al. (2015). Caffeine acts through neuronal adenosine A_{2A} receptors to prevent mood and memory dysfunction triggered by chronic stress. *Proc. Natl. Acad. Sci. U S A* 112, 7833–7838. doi: 10.1073/pnas.1423088112

Kayir, H., and Uzbay, I. T. (2006). Nicotine antagonizes caffeine- but not pentylenetetrazole-induced anxiogenic effect in mice. *Psychopharmacology* 184, 464–469. doi: 10.1007/s00213-005-0036-1

Khor, Y. M., Soga, T., and Parhar, I. S. (2013). Caffeine neuroprotects against dexamethasone-induced anxiety-like behaviour in the Zebrafish (Danio rerio). *Gen. Comp. Endocrinol.* 181, 310–315. doi: 10.1016/j.ygcen.2012.09.021

Koban, M., and Stewart, C. V. (2006). Effects of age on recovery of body weight following REM sleep deprivation of rats. *Physiol. Behav.* 87, 1–6. doi: 10.1016/j.physbeh.2005.09.006

Konsman, J. P., Parnet, P., and Dantzer, R. (2002). Cytokine-induced sickness behaviour: mechanisms and implications. *Trends Neurosci.* 25, 154–159. doi: 10.1016/s0166-2236(00)02088-9

Kostyalik, D., Vas, S., Kátai, Z., Kitka, T., Gyertyán, I., Bagdy, G., et al. (2014). Chronic escitalopram treatment attenuated the accelerated rapid eye movement sleep transitions after selective rapid eye movement sleep deprivation: a model-based analysis using Markov chains. *BMC Neurosci.* 15:120. doi: 10.1186/s12868-014-0120-8

Kumar, A., and Kalonia, H. (2007). Protective effect of *Withania somnifera* Dunal on the behavioral and biochemical alterations in sleep-disturbed mice (Grid over water suspended method). *Indian J. Exp. Biol.* 45, 524–528.

Machado, N. J., Simões, A. P., Silva, H. B., Ardais, A. P., Kaster, M. P., Garção, P., et al. (2017). Caffeine reverts memory but not mood impairment in a depression-prone mouse strain with up-regulated adenosine A_{2A} receptor in hippocampal glutamate synapses. *Mol. Neurobiol.* 54, 1552–1563. doi: 10.1007/s12035-016-9774-9

Matzner, P., Hazut, O., Naim, R., Shaashua, L., Sorski, L., Levi, B., et al. (2013). Resilience of the immune system in healthy young students to 30-hour sleep deprivation with psychological stress. *Neuroimmunomodulation* 20, 194–204. doi: 10.1159/000348698

Mavanji, V., Teske, J. A., Billington, C. J., and Kotz, C. M. (2013). Partial sleep deprivation by environmental noise increases food intake and body weight in obesity-resistant rats. *Obesity* 21, 1396–1405. doi: 10.1002/oby.20182

McGaugh, J., Mancino, M. J., Feldman, Z., Chopra, M. P., Gentry, W. B., Cargile, C., et al. (2009). Open-label pilot study of modafinil for methamphetamine dependence. *J. Clin. Psychopharmacol.* 29, 488–491. doi: 10.1097/JCP.0b013e3181b591e0

Minzenberg, M. J., and Carter, C. S. (2008). Modafinil: a review of neurochemical actions and effects on cognition. *Neuropsychopharmacology* 33, 1477–1502. doi: 10.1038/sj.npp.1301534

Missault, S., Van den Eynde, K., Vanden Berghe, W., Fransen, E., Weeren, A., Timmermans, J. P., et al. (2014). The risk for behavioural deficits is determined by the maternal immune response to prenatal immune challenge in a neurodevelopmental model. *Brain Behav. Immun.* 42, 138–146. doi: 10.1016/j.bbi.2014.06.013

Nehlig, A. (2010). Is caffeine a cognitive enhancer? *J. Alzheimers Dis.* 20, S85–S94. doi: 10.3233/JAD-2010-091315

Nemeth, C. L., Reddy, R., Bekhbat, M., Bailey, J., and Neigh, G. N. (2014). Microglial activation occurs in the absence of anxiety-like behavior following microembolic stroke in female, but not male, rats. *J. Neuroinflammation* 11:174. doi: 10.1186/s12974-014-0174-7

Norden, D. M., Trojanowski, P. J., Villanueva, E., Navarro, E., and Godbout, J. P. (2016). Sequential activation of microglia and astrocyte cytokine expression precedes increased Iba-1 or GFAP immunoreactivity following systemic immune challenge. *Glia* 64, 300–316. doi: 10.1002/glia.22930

Pan, W., Wu, X., He, Y., Hsuchou, H., Huang, E. Y., Mishra, P. K., et al. (2013). Brain interleukin-15 in neuroinflammation and behavior. *Neurosci. Biobehav. Rev.* 37, 184–192. doi: 10.1016/j.neubiorev.2012.11.009

Park, S. E., Dantzer, R., Kelley, K. W., and McCusker, R. H. (2011a). Central administration of insulin-like growth factor-I decreases depressive-like behavior and brain cytokine expression in mice. *J. Neuroinflammation* 8:12. doi: 10.1186/1742-2094-8-12

Park, S. E., Lawson, M., Dantzer, R., Kelley, K. W., and McCusker, R. H. (2011b). Insulin-like growth factor-I peptides act centrally to decrease depression-like behavior of mice treated intraperitoneally with lipopolysaccharide. *J. Neuroinflammation* 8:179. doi: 10.1186/1742-2094-8-179

Pechlivanova, D. M., Tchekalarova, J. D., Alova, L. H., Petkov, V. V., Nikolov, R. P., and Yakimova, K. S. (2012). Effect of long-term caffeine administration on depressive-like behavior in rats exposed to chronic unpredictable stress. *Behav. Pharmacol.* 23, 339–347. doi: 10.1097/FBP.0b013e3283564dd9

Petrovsky, N., Ettinger, U., Hill, A., Frenzel, L., Meyhöfer, I., Wagner, M., et al. (2014). Sleep deprivation disrupts prepulse inhibition and induces psychosis-like symptoms in healthy humans. *J. Neurosci.* 34, 9134–9140. doi: 10.1523/JNEUROSCI.0904-14.2014

Poletaeva, I. I., and Oleinik, V. M. (1975). The effect of phenamine and caffeine on the ability to extrapolate in rats. *Zh. Vyssh. Nerv. Deiat. Im. I P Pavlova* 25, 529–534.

Price, C. S., and Taylor, F. B. (2005). A retrospective chart review of the effects of modafinil on depression as monotherapy and as adjunctive therapy. *Depress. Anxiety* 21, 149–153. doi: 10.1002/da.20075

Quisenberry, A. J., Prisinzano, T. E., and Baker, L. E. (2013). Modafinil alone and in combination with low dose amphetamine does not establish conditioned place preference in male Sprague-Dawley rats. *Exp. Clin. Psychopharmacol.* 21, 252–258. doi: 10.1037/a0031832

Raineri, M., Gonzalez, B., Goitia, B., Garcia-Rill, E., Krasnova, I. N., Cadet, J. L., et al. (2012). Modafinil abrogates methamphetamine-induced neuroinflammation and apoptotic effects in the mouse striatum. *PLoS One* 7:e46599. doi: 10.1371/journal.pone.0046599

Rasetti, R., Mattay, V. S., Stankevich, B., Skjei, K., Blasi, G., Sambataro, F., et al. (2010). Modulatory effects of modafinil on neural circuits regulating emotion and cognition. *Neuropsychopharmacology* 35, 2101–2109. doi: 10.1038/npp.2010.83

Rebola, N., Simões, A. P., Canas, P. M., Tomé, A. R., Andrade, G. M., Barry, C. E., et al. (2011). Adenosine A_{2A} receptors control neuroinflammation and consequent hippocampal neuronal dysfunction. *J. Neurochem.* 117, 100–111. doi: 10.1111/j.1471-4159.2011.07178.x

Regenthal, R., Koch, H., Köhler, C., Preiss, R., and Krügel, U. (2009). Depression-like deficits in rats improved by subchronic modafinil. *Psychopharmacology* 204, 627–639. doi: 10.1007/s00213-009-1493-8

Rial, D., Lemos, C., Pinheiro, H., Duarte, J. M., Gonçalves, F. Q., Real, J. I., et al. (2016). Depression as a glial-based synaptic dysfunction. *Front. Cell. Neurosci.* 9:521. doi: 10.3389/fncel.2015.00521

Rio, D. C., Ares, M. Jr., Hannon, G. J., and Nilsen, T. W. (2010). Purification of RNA using TRIzol (TRI reagent). *Cold Spring Harb. Protoc.* 2010:pdb.prot5439. doi: 10.1101/pdb.prot5439

Rönnbäck, L., and Hansson, E. (2004). On the potential role of glutamate transport in mental fatigue. *J. Neuroinflammation* 1:22. doi: 10.1186/1742-2094-1-22

Ruiz-Medina, J., Pinto-Xavier, A., Rodríguez-Arias, M., Miñarro, J., and Valverde, O. (2013). Influence of chronic caffeine on MDMA-induced behavioral and neuroinflammatory response in mice. *Psychopharmacology* 226, 433–444. doi: 10.1007/s00213-012-2918-3

Rusconi, A. C., Valeriani, G., Carluccio, G. M., Majorana, M., Carlone, C., Raimondo, P., et al. (2014). [Coffee consumption in depressive disorders: it's not one size fits all]. *Riv. Psichiatr.* 49, 164–171. doi: 10.1708/1600.17452

Sahu, S., Kauser, H., Ray, K., Kishore, K., Kumar, S., and Panjwani, U. (2013). Caffeine and modafinil promote adult neuronal cell proliferation during 48 h of total sleep deprivation in rat dentate gyrus. *Exp. Neurol.* 248, 470–481. doi: 10.1016/j.expneurol.2013.07.021

Sanday, L., Zanin, K. A., Patti, C. L., Fernandes-Santos, L., Oliveira, L. C., Longo, B. M., et al. (2013). Role of state-dependent learning in the cognitive effects of caffeine in mice. *Int. J. Neuropsychopharmacol.* 16, 1547–1557. doi: 10.1017/S1461145712001551

Sayd, A., Antón, M., Alén, F., Caso, J. R., Pavón, J., Leza, J. C., et al. (2014). Systemic administration of oleoylethanolamide protects from neuroinflammation and anhedonia induced by LPS in rats. *Int. J. Neuropsychopharmacol.* 18:pyu111. doi: 10.1093/ijnp/pyu111

Silva, R. H., Kameda, S. R., Carvalho, R. C., Takatsu-Coleman, A. L., Niigaki, S. T., Abilio, V. C., et al. (2004). Anxiogenic effect of sleep deprivation in the elevated plus-maze test in mice. *Psychopharmacology* 176, 115–122. doi: 10.1007/s00213-004-1873-z

Singh, M. (2014). Mood, food, and obesity. *Front. Psychol.* 5:925. doi: 10.3389/fpsyg.2014.00925

Siwak, C. T., Gruet, P., Woehrlé, F., Schneider, M., Muggenburg, B. A., Murphey, H. L., et al. (2000). Behavioral activating effects of adrafinil in aged canines. *Pharmacol. Biochem. Behav.* 66, 293–300. doi: 10.1016/s0091-3057(00)00188-x

Smith, A. P., Christopher, G., and Sutherland, D. (2006). Effects of caffeine in overnight-withdrawn consumers and non-consumers. *Nutr. Neurosci.* 9, 63–71. doi: 10.1080/10284150600582927

Sonsalla, P. K., Wong, L. Y., Harris, S. L., Richardson, J. R., Khobahy, I., Li, W., et al. (2012). Delayed caffeine treatment prevents nigral dopamine neuron loss in a progressive rat model of Parkinson's disease. *Exp. Neurol.* 234, 482–487. doi: 10.1016/j.expneurol.2012.01.022

van Vliet, S. A., Jongsma, M. J., Vanwersch, R. A., Olivier, B., and Philippens, I. H. (2006). Behavioral effects of modafinil in marmoset monkeys. *Psychopharmacology* 185, 433–440. doi: 10.1007/s00213-006-0340-4

Vichaya, E. G., Molkentine, J. M., Vermeer, D. W., Walker, A. K., Feng, R., Holder, G., et al. (2016). Sickness behavior induced by cisplatin chemotherapy and radiotherapy in a murine head and neck cancer model is associated with altered mitochondrial gene expression. *Behav. Brain Res.* 297, 241–250. doi: 10.1016/j.bbr.2015.10.024

Vichaya, E. G., Vermeer, D. W., Christian, D. L., Molkentine, J. M., Mason, K. A., Lee, J. H., et al. (2017). Neuroimmune mechanisms of behavioral alterations in a syngeneic murine model of human papilloma virus-related head and neck cancer. *Psychoneuroendocrinology* 79, 59–66. doi: 10.1016/j.psyneuen.2017.02.006

Vieira, C., De Lima, T. C., Carobrez Ade, P., and Lino-de-Oliveira, C. (2008). Frequency of climbing behavior as a predictor of altered motor activity in rat forced swimming test. *Neurosci. Lett.* 445, 170–173. doi: 10.1016/j.neulet.2008.09.001

Wadhwa, M., Sahu, S., Kumari, P., Kauser, H., Ray, K., and Panjwani, U. (2015). Caffeine and modafinil given during 48 h sleep deprivation modulate object recognition memory and synaptic proteins in the hippocampus of the rat. *Behav. Brain Res.* 294, 95–101. doi: 10.1016/j.bbr.2015.08.002

Wisor, J. P., Schmidt, M. A., and Clegern, W. C. (2011). Evidence for neuroinflammatory and microglial changes in the cerebral response to sleep loss. *Sleep* 34, 261–272. doi: 10.1093/sleep/34.3.261

Wohleb, E. S., McKim, D. B., Shea, D. T., Powell, N. D., Tarr, A. J., Sheridan, J. F., et al. (2014a). Re-establishment of anxiety in stress-sensitized mice is caused by monocyte trafficking from the spleen to the brain. *Biol. Psychiatry* 75, 970–981. doi: 10.1016/j.biopsych.2013.11.029

Wohleb, E. S., Patterson, J. M., Sharma, V., Quan, N., Godbout, J. P., and Sheridan, J. F. (2014b). Knockdown of interleukin-1 receptor type-1 on endothelial cells attenuated stress-induced neuroinflammation and prevented anxiety-like behavior. *J. Neurosci.* 34, 2583–2591. doi: 10.1523/JNEUROSCI.3723-13.2014

Yadav, S., Gupta, S. P., Srivastava, G., Srivastava, P. K., and Singh, M. P. (2012). Role of secondary mediators in caffeine-mediated neuroprotection in maneb- and paraquat-induced Parkinson's disease phenotype in the mouse. *Neurochem. Res.* 37, 875–884. doi: 10.1007/s11064-011-0682-0

Yamada, K., Kobayashi, M., and Kanda, T. (2014). Involvement of adenosine A_{2A} receptors in depression and anxiety. *Int. Rev. Neurobiol.* 119, 373–393. doi: 10.1016/B978-0-12-801022-8.00015-5

Zielinski, M. R., and Krueger, J. M. (2011). Sleep and innate immunity. *Front. Biosci.* 3, 632–642. doi: 10.2741/s176

Zombeck, J. A., Fey, E. G., Lyng, G. D., and Sonis, S. T. (2013). A clinically translatable mouse model for chemotherapy-related fatigue. *Comp. Med.* 63, 491–497.

Conflict of Interest Statement: The authors declare that the research was conducted in the absence of any commercial or financial relationships that could be construed as a potential conflict of interest.

frontiers in Molecular Neuroscience

PERSPECTIVE
published: 21 February 2018
doi: 10.3389/fnmol.2018.00048

Revisit the Candidacy of Brain Cell Types as the Cell(s) of Origin for Human High-Grade Glioma

*Fangjie Shao and Chong Liu**

Department of Pathology and Pathophysiology, Zhejiang University School of Medicine, Hangzhou, China

High-grade glioma, particularly, glioblastoma, is the most aggressive cancer of the central nervous system (CNS) in adults. Due to its heterogeneous nature, glioblastoma almost inevitably relapses after surgical resection and radio-/chemotherapy, and is thus highly lethal and associated with a dismal prognosis. Identifying the cell of origin has been considered an important aspect in understanding tumor heterogeneity, thereby holding great promise in designing novel therapeutic strategies for glioblastoma. Taking advantage of genetic lineage-tracing techniques, performed mainly on genetically engineered mouse models (GEMMs), multiple cell types in the CNS have been suggested as potential cells of origin for glioblastoma, among which adult neural stem cells (NSCs) and oligodendrocyte precursor cells (OPCs) are the major candidates. However, it remains highly debated whether these cell types are equally capable of transforming in patients, given that in the human brain, some cell types divide so slowly, therefore may never have a chance to transform. With the recent advances in studying adult NSCs and OPCs, particularly from the perspective of comparative biology, we now realize that notable differences exist among mammalian species. These differences have critical impacts on shaping our understanding of the cell of origin of glioma in humans. In this perspective, we update the current progress in this field and clarify some misconceptions with inputs from important findings about the biology of adult NSCs and OPCs. We propose to re-evaluate the cellular origin candidacy of these cells, with an emphasis on comparative studies between animal models and humans.

Keywords: cell of origin, high-grade glioma, glioblastoma, adult neural stem cells (NSCs), oligodendrocyte precursor cells (OPC), genetically engineered mouse models (GEMMs), lineage tracing

OPEN ACCESS

Edited by:
Margaret Su-chun Ho, ShanghaiTech University, China

Reviewed by:
Mirko H. H. Schmidt, Universitätsmedizin der Johannes Gutenberg-Universität Mainz, Germany
Francois M. Vallette, Institut National de la Santé et de la Recherche Médicale (INSERM), France

***Correspondence:**
Chong Liu
chongliu77@zju.edu.cn

Received: *27 November 2017*
Accepted: *05 February 2018*
Published: *21 February 2018*

Citation:
Shao F and Liu C (2018) Revisit the Candidacy of Brain Cell Types as the Cell(s) of Origin for Human High-Grade Glioma. Front. Mol. Neurosci. 11:48. doi: 10.3389/fnmol.2018.00048

INTRODUCTION

Adult gliomas are the most common cancers of the central nervous system (CNS) (Louis, 2006; Perry and Wesseling, 2016). Despite many years of efforts in both basic research and clinical practice, the prognosis of malignant gliomas, particularly the most advanced one, glioblastoma multiforme (GBM), remains dismal. This lack of progress is largely associated with high inter- and intra-tumoral heterogeneity. Tumor tissues from not only different patients, but also from the same ones, can be stratified into distinct morphopathological groups or molecular subtypes (Verhaak et al., 2010; Snuderl et al., 2011; Brennan et al., 2013; Kim J. et al., 2015; Wang et al., 2016, 2017). Such heterogeneity is generally considered as the main reason for drug resistance and high recurrence rate during treatment.

A cell of origin is the normal progenitor from which all the neoplastic cells of a given type of cancer develop (Visvader, 2011; Chaffer and Weinberg, 2015). Identification of the cell of origin can give critical insights into the principles dictating tumor heterogeneity, therefore holding great promise in understanding the cancer etiology, and facilitating the design of effective therapeutic strategies. In this *Perspective*, we review the current progress in the research of the cell of origin of glioma. Together with new findings in NSCs and OPCs from both rodents and large-brained mammals including humans, we propose to carefully re-evaluate the candidacy of several popular cell types that have been believed as the potential cells of origin of glioma in humans.

CNS CELL TYPES RELEVANT TO GLIOMA ETIOLOGY: THEIR LINEAGE RELATIONSHIP AND SOME IMPORTANT UPDATES

Knowing the properties of neural cell types and their lineage relationship will help understanding their potential contributions to the etiology of human glioma. Neural cells in the adult CNS are grossly classified as neurons, astrocytes, oligodendrocyte precursor cells (OPCs), and oligodendrocytes. In addition to these lineage-committed progenitor and mature cells, specialized stem cells, termed adult neural stem cells (NSCs) exist within restricted regions such as the subventricular zone (SVZ) next to the lateral ventricle, and the subgranular zone (SGZ) of the hippocampus (Ming and Song, 2011), in the adult brain. Both SVZ adult NSCs and OPCs have been implicated as the major candidates for glioma cell of origin, therefore, deserving a little more discussion.

Adult Neural Stem Cells (NSCs)

Adult NSCs (also termed B1 cells), which were best studied in rodents, have been generally believed to be able to persistently self-renew, and give rise to multiple neuronal and glial cell types (Alvarez-Buylla et al., 2001). Recent progresses in NSC biology, however, may suggest a quite different scenario. By using a temporal Histone 2B-EGFP marking system or barcoded retroviral labeling-based clonal analysis, two groups independently reported that postnatal B1 cells are derived from embryonic NSCs that divide during mid-fetal development and then remain quiescent until they reactivate, thus generating progeny in the postnatal brain (Fuentealba et al., 2015; Furutachi et al., 2015). Surprisingly, clonal analysis unraveled that postnatally, a single B1 cell neither divides repeatedly to produce generations of olfactory bulb (OB) neurons, nor gives rise to cortical glial cells and OB neurons simultaneously, raising an interesting possibility that adult NSCs may not systematically self-renew (Fuentealba et al., 2015) (see also **Figure 1A**). Therefore, although adult NSCs exhibit remarkable self-renewal potential and differentiation plasticity in culture (Doetsch et al., 1999; Codega et al., 2014), it remains highly debated whether, in the brain, they conform to the hardwired definition of tissue stem cells, as seen in the case of hematopoietic or intestinal stem cells (Batlle and Clevers, 2017).

Oligodendrocyte Precursor Cells (OPCs)

Oligodendrocyte precursor cells were initially thought to function solely as transient forms of glial progenitors, to generate mature oligodendrocytes. Nevertheless, recent studies show that even though some OPCs indeed differentiate, many of them retain the ability to self-renew (Nishiyama et al., 2009; Vigano and Dimou, 2016) (see also **Figure 1A**). By using a sensitive DNA-labeling approach to mark cells undergoing proliferation, Yeung et al. (2014) showed that all OPCs in the adult mouse brain were dividing. Strikingly, Garcia-Marques et al. (2014 observed that at the clonal level, a single OPC could give rise to up to 400 cells in the adult mouse brain, therefore unequivocally demonstrating that OPCs are a *bona fide* self-renewable cell population *in vivo*. Given that OPCs make up 5–10% of all cells in the brain (Dawson et al., 2003), using the absolute number as the criteria, OPCs should be viewed as the largest proliferation pool in the mammalian brain. In addition to self-renewal, OPCs have been reported to exhibit some lineage plasticity. Despite being a matter of intensive debate, OPCs were shown to be able to differentiate into astrocytes and/or neurons *in vivo* (Rivers et al., 2008; Zhu et al., 2008, 2011; Richardson et al., 2011), and can be reprogrammed into the NSC-like status *in vitro* (Kondo and Raff, 2000), thus resembling NSCs in ways stronger than those previously considered (Richardson et al., 2011).

THE RESEARCH PROGRESS OF GLIOMA CELLULAR ORIGINS

NSCs as the Cell of Origin: Evidence and Concerns

Adult NSCs have been widely viewed as the most possible cell of origin for high-grade glioma, given their prominent property to self-renew, and the remarkable plasticity to differentiate into multiple neural cell types (Doetsch et al., 1999; Alvarez-Buylla et al., 2001; Stiles and Rowitch, 2008). In addition, cancer stem cells (CSCs) isolated from human GBMs share many markers normally expressed by NSCs (such as Nestin, GFAP, CD133, and Sox2), and are able to form renewable NSC-like spheres in culture (Singh et al., 2004; Bao et al., 2006). Furthermore, mouse and human NSCs can be transformed *in vitro*; they gain the capacity to develop into gliomas after implantation into host mice (Bachoo et al., 2002; Duan et al., 2015). Importantly, delivery of DNA or viral vehicles into the embryonic, neonatal, or adult SVZ (the brain structure where NSCs reside) to introduce over-expression of oncogenes and/or knockout/knockdown of tumor suppressor genes could efficiently generate high-grade glioma in mice (Alcantara Llaguno et al., 2009; Marumoto et al., 2009; Breunig et al., 2015; Zuckermann et al., 2015). Intriguingly, human glioblastomas were frequently diagnosed next to the SVZ, further supporting the possibility that they originated from NSCs (Barami et al., 2009). More direct evidence was obtained from

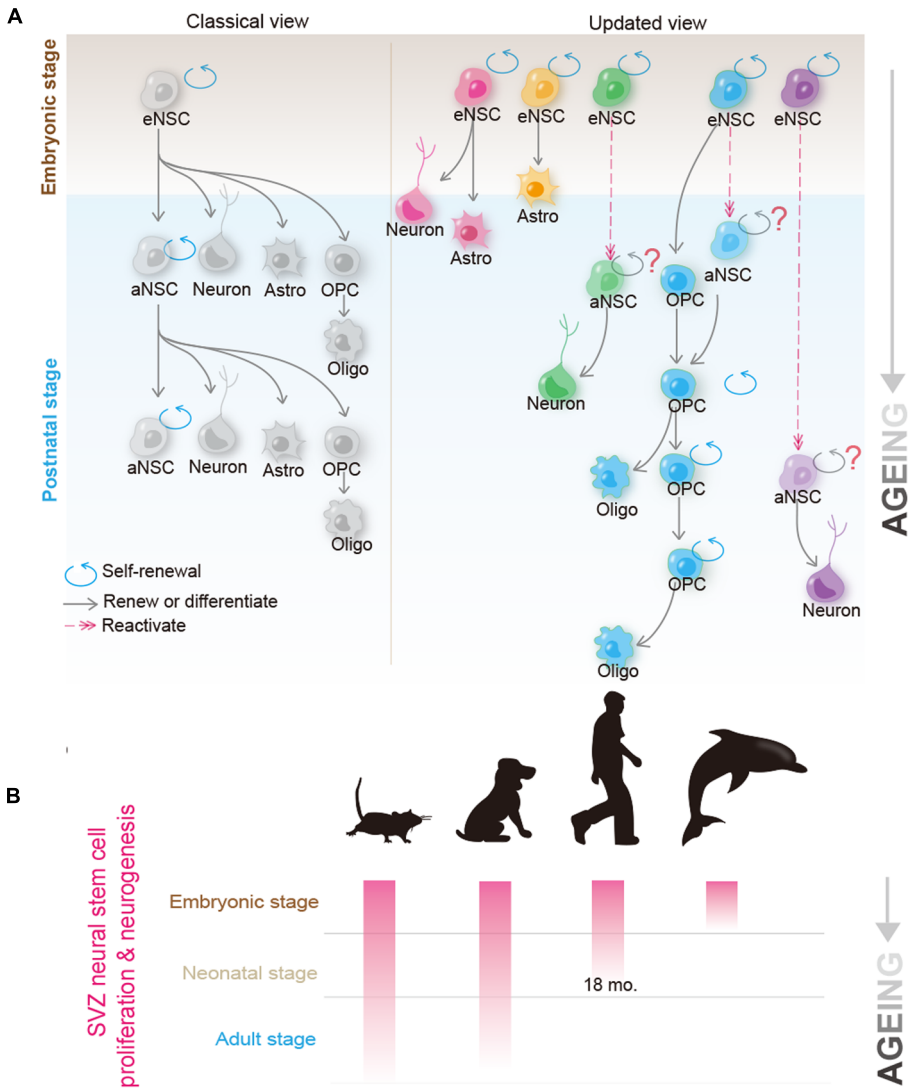

FIGURE 1 | Recent progress in the biology of neural stem cells (NSCs) and oligodendrocyte precursor cells (OPCs) provides new insights into their candidacy as the cell of origin for human glioblastoma. **(A)** Classical (left) and the updated (right) view of the NSC behavior in the brain. In the classical view, it was believed that a single NSC can repeatedly self-renew for many generations and give rise to new NSCs; at the same time, it possesses the potential to differentiate into neurons, astrocyte and OPCs. OPCs can further differentiate into mature oligodendrocytes. Recent studies using mouse models suggest that adult B1 cells (adult form of NSCs) are derived from eNSCs that actively proliferate at ~E14.5. These embryonic NSCs remain quiescent until they are reactivated at the adult stage. Though as a whole population, adult NSCs continuously proliferate and give rise to olfactory bulb (OB) neurons and glial cells, they are extremely heterogeneous at the single cell level. Clonal analysis revealed that a single adult NSC can either give rise to OB neurons or glial cells (such as astrocytes and oligodendrocytes), but rarely to both cell types. Furthermore, many, if not all, adult NSCs cannot bud off OB neurons and simultaneously self-renew, raising the question of whether adult NSCs conform to the hardwired definition of self-renewable tissue stem cells (Fuentealba et al., 2015; Furutachi et al., 2015). On the other hand, despite OPCs originally being derived from NSCs during early development, and adult NSCs contributing to the OPC pool to some extent, in the normal brain, most adult OPCs are generated from the locally resident OPCs. Clonal analysis further revealed that adult OPCs can self-renew continuously (Garcia-Marques et al., 2014; Yeung et al., 2014). **(B)** Neurogenic and proliferative activities of SVZ NSCs in rodent, dog, human, and dolphin. Please note that neurogenic activity disappears in human at ~18 months, and is completely absent in dolphin postnatally; however, both species can suffer from GBM at adulthood. Kindly refer to the main text for further details.

the lineage-tracing experiment by using genetically engineered mouse models (GEMMs). Taking advantage of NSC-specific genetic tools such as hGFAP-Cre, Nestin-Cre, or Nestin-Cre^{ER}, Parada and his colleagues showed that mouse NSCs are capable of transforming into high-grade gliomas after the loss of *Trp53*, *NF1* and/or *PTEN* (Zhu et al., 2005; Chen et al., 2012; Alcantara Llaguno et al., 2015).

While these multiple lines of evidence demonstrate that NSCs are capable of transforming into malignancy, several important issues should be understood. Firstly, as already mentioned, recent findings about NSC biology challenges the concept that a single SVZ aNSC can repeatedly self-renew, therefore greatly decreasing the possibility for an aNSC to accumulate mutations, as previously assumed. Secondly, the stem cell feature of CSCs

need not necessarily be inherited from tissue stem cells; it can also be regained through the de-differentiation of lineage-committed progenitors or mature cells (Batlle and Clevers, 2017). Thirdly, many claimed that NSC cellular markers are not specific to NSCs. For example, the most widely used NSC marker Nestin, an intermediate filament protein expressed in radial glia and adult B1 cells, is prominently expressed in reactive astrocytes (Ernst and Christie, 2006). Although partial overlaps between brain tumor locations and the NSC niche is a good argument to support the fact that gliomas originate from adult NSCs in patients, a recent work revealed that the SVZ may merely function as a niche toward which glioma cells prefer to migrate (Qin et al., 2017).

An additional dimension of complexity comes from the nature of NSCs *per se*. As NSCs can readily differentiate into fate-committed precursors such as OPCs or mature astrocytes, it is unclear whether NSCs, after acquiring initial mutations, directly transform, or they must proceed through the status of lineage-committed cell types prior to the final transformation. In fact, by using a single-cell resolution genetic mouse model termed mosaic analysis with double markers (MADM), we have shown that introducing *p53* and *NF1* mutations into NSCs did not evidently change the proliferation rate of pre-cancerous adult NSCs, but drastically promoted the over-expansion of descendant OPCs, arguing against a direct transformation of NSCs, at least in the context of this mutation combination (Liu et al., 2011).

OPCs as the Cell of Origin: Evidence and Some Updates

Oligodendrocyte precursor cells have been proposed as an important cell of origin for glioma since they were first identified. As already mentioned, OPCs represent the largest proliferation pool in the brain, and exhibit remarkable self-renewal capacity both *in vitro* and *in vivo*, and are therefore suitable, as cells of origin, to accumulate genetic mutations. In fact, NG2, one of the most commonly used OPC cell marker, was initially isolated from a rat glioma model (Stallcup, 1981). In addition to NG2, we and others showed that many cellular markers typically expressed in OPCs, such as Olig2, PDGFRa, and O4, were also expressed in most, if not all, human malignant gliomas (Shoshan et al., 1999; Ligon et al., 2004, 2007; Rebetz et al., 2008; Ledur et al., 2016; Shao et al., 2017). Furthermore, over-expression of the oncogenic form of EGFR (EGFRvIII) under the promoter S100b, a non-stem cell marker (Raponi et al., 2007), induced gliomas recapitulating the pathological features of human oligodendroglioma (Weiss et al., 2003; Persson et al., 2010). Moreover, overexpression of PDGF-BB alone, or when combined with p53 and Pten deactivation, was shown to be able to effectively transform rat and mouse OPCs into lower-grade oligodendrogliomas or high-grade gliomas (Assanah et al., 2006; Lindberg et al., 2009; Lei et al., 2011; Lu et al., 2016). More direct evidence to support the OPC-origin of high-grade gliomas comes from fate-mapping experiments. By using OPC-specific NG2-Cre or NG2-Cre^{ERT} transgenic mouse lines, we and others have provided convincing evidence that OPCs, after acquiring *Trp53* and *NF1* mutations, can be directly transformed into malignant gliomas resembling the proneural subtype of GBM, whenever the mutations were introduced in early or adult stage (Liu et al., 2011; Galvao et al., 2014; Alcantara Llaguno et al., 2015).

The data from our group show that OPC-like tumor cells are universally present in all human malignant gliomas, and share remarkable similarities in many aspects with their counterparts found in mouse genetic models, in which OPCs are the defined cells of origin (Ledur et al., 2016; Shao et al., 2017). These lines of evidence collectively lead to a reasonable assumption that OPCs are important glioma cells of origin in patients.

Mature Astrocytes and Neurons as the Cells of Origin: An Unsettled Issue

Whether mature astrocytes and/or neurons are able to directly transform remains highly debated. Chow et al. (2011) utilized GFAP-Cre^{ER} to introduce Trp53, Pten and/or Rb1 mutations into astrocytes and induced high-grade astrocytomas in adult mice. Also using GFAP-Cre^{ER}, Vitucci et al. (2017) observed that murine astrocytes could transform into high-grade glioma mimicking human mesenchymal, proneural, and neural GBMs. By using Cre-activatable lentiviral vehicles that encoded shRNA against Trp53 and NF1, Friedmann-Morvinski et al. (2012) reported high incidence of GBMs when they transfected such lentiviral particles into the brains of hGFAP-Cre, Synapsin I-Cre or CamK2a-Cre transgenic mice. Therefore, the authors claimed that both mature astrocytes and neurons can function as the cells of origin for GBMs through dedifferentiation. Nevertheless, as most claimed astrocyte-specific markers such as GFAP are also expressed in NSCs (Chaker et al., 2016), and those for neurons like Synapsin-1 are also expressed in OPCs [(Cahoy et al., 2008; Zhang et al., 2014) and personal observations], further validation is necessary to exclude the possibility of targeting NSCs and/or OPCs when attempting to manipulate mature astrocytes or neurons. Highly specific genetic tools are warranted to clarify this fundamental issue.

HUMAN RELEVANCE: NEW DATA AND THE INSIGHT FROM COMPARATIVE STUDIES

Most of our current knowledge on glioma cell of origin was derived from the observations on animal models, mostly GEMM-based cancer models. One fundamental question we must confront is that how much of the landscape depicted thus far can be directly extrapolated to human cases. Despite the overall anatomical structures and developmental principles of the CNS being highly conserved among mammals, notable differences, particularly in the properties of adult NSCs, do exist among species. Recognizing these differences has important impacts on shaping our understandings of the glioma cell of origin in humans.

Adult NSCs May Not Be a Major Player in the Pathogenesis of Glioblastoma in Human or Other Large-Brained Animals

Unlike in rodents, where NSCs and neural progenitors proliferate continuously to form new neurons, in large-brained mammals, such as humans, SVZ neurogenesis declines drastically during postnatal life (Lipp and Bonfanti, 2016; Paredes et al., 2016), and fully disappears at around 18 months (Sanai et al., 2011), long before high-grade gliomas are diagnosed. Consistent with this observation, by measuring the turnover rate of nuclear bomb test-derived ^{14}C in genomic DNA, Bergmann et al. (2012, 2015) showed that there is virtually no postnatal neurogenesis in the human OB.

Direct evidence to support a lack of marked levels of neurogenesis or self-renewal of NSCs in the adult human SVZ comes from immunohistological studies, where proliferative cells were rarely found in the SVZ in adults (Wang et al., 2011; Dennis et al., 2016). Furthermore, the density of dividing cells in the SVZ is comparable to or even lower than that in other regions such as the corpus callosum (Shao et al. personal observations). Despite the suggestion that certain pathological conditions such as ischemic stroke may activate NSCs in the adult human brain (Jin et al., 2006; Marti-Fabregas et al., 2010), this conclusion was disproved by the ^{14}C turnover assay (Huttner et al., 2014). Regardless the potential of adult NSCs to be activated *in vivo* after injury, no definitive evidence yet shows an association of human glioma pathogenesis with any pathological lesions.

Comparative studies between species provide deeper insights into questioning the relevance of adult NSCs in glioma pathogenesis (as summarized in **Figure 1B**). Unlike humans, but quite similar to rodents, dogs possess SVZ neurogenesis that persists into adulthood (Malik et al., 2012). Therefore, one may expect a much higher incidence of gliomagenesis in dogs, if adult NSCs indeed play critical roles in initiating glioma. Contrary to this speculation, epidemiological studies suggest that the incidence of spontaneous brain tumors in dogs is remarkably similar to that in humans, i.e., approximately 20 in 100,000 per year (Dobson et al., 2002; Hicks et al., 2017). On the other hand, aquatic mammals such as dolphins, which lack a functional periventricular germinal layer postnatally and any detectable dividing cells within the SVZ (Parolisi et al., 2017), can surely suffer from glioblastoma (Diaz-Delgado et al., 2015). These findings, together with those in rodent NSCs, contradict the argument that adult NSCs play major roles in initiating gliomagenesis.

Adult OPCs May Function as an Important Cell of Origin with Strong Human Relevance

Unlike the great variations of cellular behaviors of adult NSCs, the renewal capacity of OPCs are largely conserved across species. For instance, immunohistological studies show that, although sparse, OPCs are the major cycling cells in the adult human brain (Geha et al., 2010). In line with this observation, ^{14}C data revealed that gray matter oligodendrocytes do not reach a plateau until the fourth decade of life, even after which the annual turnover remains as high as 2.5% (Yeung et al., 2014). These results in collection clearly demonstrate that OPCs undergo substantial renewal in the adult human brain.

Interestingly, the proliferation rate of OPCs are significantly elevated in epileptic patients (Geha et al., 2010). As epilepsies are frequently associated with glioma patients (Iuchi et al., 2015; Englot et al., 2016), these observations raise an intriguing possibility that aberrant neuronal activity may directly contribute to OPC self-renewals and, most likely, to oncogenic transformation. This hypothesis has been recently substantiated by showing that artificially enhancing the neuronal activity in GEMMs through optogenetic approaches can stimulate the proliferation of normal resident OPCs and engrafted human GBM cells (Gibson et al., 2014; Venkatesh et al., 2015).

Therefore, although comprehensive studies are warranted to systematically characterize the relative proliferating capacities of OPCs and NSCs/NPCs in the adult human brain *in situ*, given that OPCs retain a relatively decent level of self-renewal activity, and significantly outnumber NSCs in the adult human brain, they remain a highly probable candidate for the cell of origin of human GBMs.

THE RELATIONSHIP BETWEEN CELL(s) OF ORIGIN AND CANCER STEM CELLS (CSCs)

It should be noted that the "CSC" is a functional definition that can only be assessed by the capacity of a cancer cell to initiate new tumors. Some studies identified CSCs from the NSC-derived GBM mouse models and showed that these NSC-derived CSCs resemble normal NSCs in certain ways such as the expression of Nestin (Zheng et al., 2008; Alcantara Llaguno et al., 2009; Chen et al., 2012). However, the cells functioning as CSCs may not have to be derived and/or resemble normal NSCs. By using S100b- promoter-driven EGFRViii transgene, Persson et al. (2010) clearly showed that oligodendroglioma can be initiated from non NSCs, and the CSCs in this model can be identified and isolated based on their expression of NG2 (CSPG4), an OPC marker. We showed that CSCs derived from OPC-originated HGGs expressed NG2 as well as other OPC markers (such as PDGFRa and Olig2) and that the OPC feature is essential for the maintenance of the stemness of these CSCs (Liu et al., 2011; Ledur et al., 2016). Interestingly, OPC-originated CSCs gained the capacity to form spheres and to express Nestin. This latter observation implicates that Nestin is a marker for the stemness but not the cell identity in this particular case. In the human cases, NG2 have been used to enrich CSCs from oligodendrogliomas (Persson et al., 2010) and at least some GBMs (Persson et al., 2010; Al-Mayhani et al., 2011). Our own study showed that human primary GBM cell lines maintained under culture conditions that favor the enrichment of OPC-like tumor cells have enhanced malignancy (Ledur et al., 2016). In addition to OPCs, Schmid et al. (2016) provided the evidence that

TABLE 1 | Pathological features and molecular signatures of currently reported GEMMs for gliomas.

Putative cell of origin	Mutations	Approach	Molecular subtype	Pathology	Reference
NSC	Ras, Akt	RCAS/tv-a system	NA	GBM	Holland et al., 2000
	Ink4a, Arf, EGFR	Retrovirus	NA	High-grade gliomas	Bachoo et al., 2002
	H-Ras, AKT	Lentivirus + GFAP-Cre mice	NA	GBM	Marumoto et al., 2009
	Trp53, Nf1, and/or Pten	Adenovirus + Nestin-CreER	NA	A	Alcantara Llaguno et al., 2009
	PTEN, Trp53	Adenovirus-Cre	NA	High-grade gliomas	Jacques et al., 2010
	Ras; Erbb2; Pdgfra	Plasmid DNA + Electroporation	Proneural, Neural, Mesenchymal	AA, AO, AOA, GBM	Breunig et al., 2015
	Trp53, Pten, Nf1	CRISPR/Cas9 + Electroporation	NA	GBM	Zuckermann et al., 2015
	Trp53, NF1	hGFAP-Cre	NA	A, AA, GBM	Zhu et al., 2005
	Trp53, Pten	hGFAP-Cre	NA	Malignant gliomas	Zheng et al., 2008
	Nf1, Trp53, Pten	hGFAP-Cre	NA	Malignant gliomas	Chen et al., 2012
	K-Ras	BLBP-Cre	NA	Gliomatosis	Munoz et al., 2013
	Trp53, Nf1, and/or Pten	Nestin-CreER	NA	GBM	Alcantara Llaguno et al., 2015
OPC	PDGF	Retrovirus	NA	GBM	Assanah et al., 2006
	PDGF-B	RCAS/tv-a system	NA	O	Lindberg et al., 2009
	Pten, Trp53	Retrovirus + PDGF-IRES-Cre	Proneural	GBM	Lei et al., 2011
	TAZ, PDGFB	RCAS/N-tva system	Mesenchymal	Gliomas	Bhat et al., 2011
	NF1, PDGFA	RCAS/tv-a system	Mesenchymal	GBM	Ozawa et al., 2014
	PDGFB	RCAS/tv-a system	Mesenchymal	GBM	Ozawa et al., 2014
	Arf	RCAS/tv-a system	NA	A	Lindberg et al., 2014
	Ink4a, Arf	RCAS/tv-a system	NA	A	Lindberg et al., 2014
	Arf, PDGF-B	RCAS/tv-a system	NA	O	Lindberg et al., 2014
	Ink4a, Arf, PDGF-B	RCAS/tv-a system	NA	O	Lindberg et al., 2014
	Pten, Trp53	Retrovirus + PDGFB-IRES-Cre	Proneural	GBM	Lu et al., 2016
	Pten, Trp53, Olig2	Retrovirus + PDGFB-IRES-Cre	Classical	GBM	Lu et al., 2016
	Trp53	S100β-v-erbB	NA	O	Weiss et al., 2003
	ink/arf	S100β-v-erbB	NA	AO	Weiss et al., 2003
	Trp53	S100β-v-erbB	OPC like	O, GBM	Persson et al., 2010
	Trp53, NF1	NG2-Cre	Proneural	Malignant gliomas	Liu et al., 2011
	Trp53, NF1	NG2-CreER	Proneural	Malignant gliomas	Galvao et al., 2014
	Trp53, Nf1, and/or Pten	NG2-CreER	NA	Malignant gliomas	Alcantara Llaguno et al., 2015
Astrocyte	Ink4a, Arf, EGFR	Retrovirus	NA	High-grade gliomas	Bachoo et al., 2002
	Trp53, NF1	Lentivirus + GFAP-Cre mice	Mesenchymal	GBM	Friedmann-Morvinski et al., 2012
	Trp53, Pten	GFAP-CreER	Proneural, Neural, Mesenchymal	AA, GBM	Chow et al., 2011
	Trp53, Pten, Rb1	GFAP-CreER	Proneural, Neural, Mesenchymal	AA, AOA, GBM	Chow et al., 2011
	$TgGZT_{121}$, $Kras^{G12D}$, Pten	GFAP-CreER	Mesenchymal, Proneural, Neural	GBM	Vitucci et al., 2017
Neuron	Trp53, NF1	Lentivirus + Synapsin I-Cre or CamK2a-Cre mice	Mesenchymal	Malignant gliomas	Friedmann-Morvinski et al., 2012

A, astrocytoma; O, oligodendroglioma; AA, anaplastic astrocytoma; AO, anaplastic oligodendroglioma; AOA, anaplastic oligoastrocytoma; GBM, glioblastoma multiforme.

mature astrocytes could dedifferentiate into glioma CSCs upon transformation. Therefore, CSCs in gliomas can definitely be developed from the non-CSC cell types. The detailed lineage relationship between NSCs, lineage-committed progenitors, mature cells and CSCs remains to be fully elucidated in the future studies.

THE RELATIONSHIP BETWEEN CELLS OF ORIGIN, TUMOR SUBTYPES AND HETEROGENEITY

Cumulative evidence suggests that the same cell of origin can give rise to the GBMs manifesting different molecular features and that distinct types of cells of origin can evolve in parallel to give rise to tumors resembling similar molecular features (see also **Table 1**).

For instance, OPCs have been previously considered to mainly give rise to oligodendrogliomas and proneural subtype of GBMs (Weiss et al., 2003; Lei et al., 2011; Liu et al., 2011; Galvao et al., 2014). However, recent studies demonstrate that they can also serve as the cell of origin for astrocytoma (Lindberg et al., 2014) and other subtypes of GBMs, depending on the mutations initially introduced (Carro et al., 2009; Bhat et al., 2011, 2013; Lu et al., 2016). In particular, removal of Olig2 switches OPC-derived proneural subtype of GBMs into the classical subtype. Over-expression of TAZ or suppression of NF1, instead, readily induces OPC-derived GBMs into the mesenchymal subtype (Bhat et al., 2011; Ozawa et al., 2014). Similar observations were also obtained in astrocyte-originated GBMs, where the same GEMM can give rise to tumors with highly heterogeneous profiles (Chow et al., 2011; Schmid et al., 2016).

Importantly, the evolution routes of a defined cell of origin may also affect the molecular features of brain tumors. The recurrent GBMs from the same patients frequently switched their molecular features when compared to their primary tumor counterparts (Kim H. et al., 2015; Kim J. et al., 2015; Wang et al., 2016). Therefore, the molecular signature of a particular transformed tumor may not always reliably predict its cell of origin.

FUTURE PERSPECTIVES

Owing to genetic lineage tracing techniques and other advanced biological methods, tremendous progress has been made in understanding the glioma cell of origin during the past decade. Now, a consensus has been made that several important cell types, particularly NSCs and OPCs, are capable of transforming at least in GEMMs. However, many fundamental questions remain unanswered. For instance, is there a universal cell type functioning as the cell of origin for all gliomas in humans? Or alternatively, do different cell types give rise to gliomas with distinct pathological identities? Can different mutations drive the same cell of origin to follow the same or distinct routes toward the final transformation? When exactly do human gliomas form? GEMMs will surely continue to serve as the most important tools to address these fundamental questions. Nevertheless, we should be aware of the difference between GEMMs and patients. Newer methods and the concept of comparative pathology could help us identify what really initiates this devastating form of cancer in humans.

AUTHOR CONTRIBUTIONS

FS and CL wrote the manuscript. FS prepared the figure and the table.

FUNDING

This work was supported by the National Key Research and Development Program of China, Stem Cell and Translational Research (2016YFA0101201 to CL), Science Foundation for Distinguished Young Scientists of Zhejiang Province (LR17H160001 to CL), National Natural Science Foundation of China (81673035 to CL), and Thousand Talent Program for Young Outstanding Scientists, China (to CL).

ACKNOWLEDGMENTS

We thank Drs. Weijun Yang and Yingjie Wang for their critical comments.

REFERENCES

Alcantara Llaguno, S., Chen, J., Kwon, C.-H., Jackson, E. L., Li, Y., Burns, D. K., et al. (2009). Malignant astrocytomas originate from neural stem/progenitor cells in a somatic tumor suppressor mouse model. *Cancer Cell* 15, 45–56. doi: 10.1016/j.ccr.2008.12.006

Alcantara Llaguno, S. R., Wang, Z., Sun, D., Chen, J., Xu, J., Kim, E., et al. (2015). Adult lineage-restricted CNS progenitors specify distinct glioblastoma subtypes. *Cancer Cell* 28, 429–440. doi: 10.1016/j.ccell.2015.09.007

Al-Mayhani, M. T., Grenfell, R., Narita, M., Piccirillo, S., Kenney-Herbert, E., Fawcett, J. W., et al. (2011). NG2 expression in glioblastoma identifies an actively proliferating population with an aggressive molecular signature. *Neuro Oncol.* 13, 830–845. doi: 10.1093/neuonc/nor088

Alvarez-Buylla, A., Garcia-Verdugo, J. M., and Tramontin, A. D. (2001). A unified hypothesis on the lineage of neural stem cells. *Nat. Rev. Neurosci.* 2, 287–293. doi: 10.1038/35067582

Assanah, M., Lochhead, R., Ogden, A., Bruce, J., Goldman, J., and Canoll, P. (2006). Glial progenitors in adult white matter are driven to form malignant gliomas by platelet-derived growth factor-expressing retroviruses. *J. Neurosci.* 26, 6781–6790. doi: 10.1523/Jneurosci.0514-06.2006

Bachoo, R. M., Maher, E. A., Ligon, K. L., Sharpless, N. E., Chan, S. S., You, M. J. J., et al. (2002). Epidermal growth factor receptor and Ink4a/Arf: convergent mechanisms governing terminal differentiation and transformation along the neural stem cell to astrocyte axis. *Cancer Cell* 1, 269–277. doi: 10.1016/S1535-6108(02)00046-6

Bao, S. D., Wu, Q. L., Mclendon, R. E., Hao, Y. L., Shi, Q., Hjelmeland, A. B., et al. (2006). Glioma stem cells promote radioresistance by preferential activation of the DNA damage response. *Nature* 444, 756–760. doi: 10.1038/nature05236

Barami, K., Sloan, A. E., Rojiani, A., Schell, M. J., Staller, A., and Brem, S. (2009). Relationship of gliomas to the ventricular walls. *J. Clin. Neurosci.* 16, 195–201. doi: 10.1016/j.jocn.2008.03.006

Batlle, E., and Clevers, H. (2017). Cancer stem cells revisited. *Nat. Med.* 23, 1124–1134. doi: 10.1038/nm.4409

Bergmann, O., Liebl, J., Bernard, S., Alkass, K., Yeung, M. S., Maggie, S. Y., et al. (2012). The age of olfactory bulb neurons in humans. *Neuron* 74, 634–639. doi: 10.1016/j.neuron.2012.03.030

Bergmann, O., Spalding, K. L., and Frisen, J. (2015). Adult neurogenesis in humans. *Cold Spring Harb. Perspect. Biol.* 7:a018994. doi: 10.1101/cshperspect.a018994

Bhat, K. P. L., Balasubramaniyan, V., Vaillant, B., Ezhilarasan, R., Hummelink, K., Hollingsworth, F., et al. (2013). Mesenchymal differentiation mediated by NF-κB promotes radiation resistance in glioblastoma. *Cancer Cell* 24, 331–346. doi: 10.1016/j.ccr.2013.08.001

Bhat, K. P. L., Salazar, K. L., Balasubramaniyan, V., Wani, K., Heathcock, L., Hollingsworth, F., et al. (2011). The transcriptional coactivator TAZ regulates mesenchymal differentiation in malignant glioma. *Genes Dev.* 25, 2594–2609. doi: 10.1101/gad.176800.111

Brennan, C. W., Verhaak, R. G. W., Mckenna, A., Campos, B., Noushmehr, H., Salama, S. R., et al. (2013). The somatic genomic landscape of glioblastoma. *Cell* 155, 462–477. doi: 10.1016/j.cell.2013.09.034

Breunig, J. J., Levy, R., Antonuk, C. D., Molina, J., Dutra-Clarke, M., Park, H., et al. (2015). Ets factors regulate neural stem cell depletion and gliogenesis in Ras pathway glioma. *Cell Rep.* 12, 258–271. doi: 10.1016/j.celrep.2015.06.012

Cahoy, J. D., Emery, B., Kaushal, A., Foo, L. C., Zamanian, J. L., Christopherson, K. S., et al. (2008). A transcriptome database for astrocytes, neurons, and oligodendrocytes: a new resource for understanding brain development and function. *J. Neurosci.* 28, 264–278. doi: 10.1523/Jneurosci.4178-07.2008

Carro, M. S., Lim, W. K., Alvarez, M. J., Bollo, R. J., Zhao, X., Snyder, E. Y., et al. (2009). The transcriptional network for mesenchymal transformation of brain tumours. *Nature* 463, 318–325. doi: 10.1038/nature08712

Chaffer, C. L., and Weinberg, R. A. (2015). How does multistep tumorigenesis really proceed? *Cancer Discov.* 5, 22–24. doi: 10.1158/2159-8290.cd-14-0788

Chaker, Z., Codega, P., and Doetsch, F. (2016). A mosaic world: puzzles revealed by adult neural stem cell heterogeneity. *Wiley Interdiscip. Rev. Dev. Biol.* 5, 640–658. doi: 10.1002/wdev.248

Chen, J., Li, Y. J., Yu, T. S., Mckay, R. M., Burns, D. K., Kernie, S. G., et al. (2012). A restricted cell population propagates glioblastoma growth after chemotherapy. *Nature* 488, 522–526. doi: 10.1038/nature11287

Chow, L. M. L., Endersby, R., Zhu, X. Y., Rankin, S., Qu, C. X., Zhang, J. Y., et al. (2011). Cooperativity within and among Pten, p53, and Rb pathways induces high-grade astrocytoma in adult brain. *Cancer Cell* 19, 305–316. doi: 10.1016/j.ccr.2011.01.039

Codega, P., Silva-Vargas, V., Paul, A., Maldonado-Soto, A. R., Deleo, A. M., Pastrana, E., et al. (2014). Prospective identification and purification of quiescent adult neural stem cells from their in vivo niche. *Neuron* 82, 545–559. doi: 10.1016/j.neuron.2014.02.039

Dawson, M. R. L., Polito, A., Levine, J. M., and Reynolds, R. (2003). NG2-expressing glial progenitor cells: an abundant and widespread population of cycling cells in the adult rat CNS. *Mol. Cell. Neurosci.* 24, 476–488. doi: 10.1016/S1044-7431(03)00210-0

Dennis, C. V., Suh, L. S., Rodriguez, M. L., Kril, J. J., and Sutherland, G. T. (2016). Human adult neurogenesis across the ages: an immunohistochemical study. *Neuropathol. Appl. Neurobiol.* 42, 621–638. doi: 10.1111/nan.12337

Diaz-Delgado, J., Sacchino, S., Suarez-Bonnet, A., Sierra, E., Arbelo, M., Espinosa, A., et al. (2015). High-grade astrocytoma (glioblastoma multiforme) in an Atlantic spotted dolphin (*Stenella frontalis*). *J. Comp. Pathol.* 152, 278–282. doi: 10.1016/j.jcpa.2014.12.016

Dobson, J. M., Samuel, S., Milstein, H., Rogers, K., and Wood, J. L. N. (2002). Canine neoplasia in the UK: estimates of incidence rates from a population of insured dogs. *J. Small Anim. Pract.* 43, 240–246. doi: 10.1111/j.1748-5827.2002.tb00066.x

Doetsch, F., Caille, I., Lim, D. A., Garcia-Verdugo, J. M., and Alvarez-Buylla, A. (1999). Subventricular zone astrocytes are neural stem cells in the adult mammalian brain. *Cell* 97, 703–716. doi: 10.1016/S0092-8674(00)80783-7

Duan, S. L., Yuan, G. H., Liu, X. M., Ren, R. T., Li, J. Y., Zhang, W. Z., et al. (2015). PTEN deficiency reprogrammes human neural stem cells towards a glioblastoma stem cell-like phenotype. *Nat. Commun.* 6:10068. doi: 10.1038/ncomms10068

Englot, D. J., Chang, E. F., and Vecht, C. J. (2016). Epilepsy and brain tumors. *Handb. Clin. Neurol.* 134, 267–285. doi: 10.1016/b978-0-12-802997-8.00016-5

Ernst, C., and Christie, B. R. (2006). The putative neural stem cell marker, nestin, is expressed in heterogeneous cell types in the adult rat neocortex. *Neuroscience* 138, 183–188. doi: 10.1016/j.neuroscience.2005.10.065

Friedmann-Morvinski, D., Bushong, E. A., Ke, E., Soda, Y., Marumoto, T., Singer, O., et al. (2012). Dedifferentiation of neurons and astrocytes by oncogenes can induce gliomas in mice. *Science* 338, 1080–1084. doi: 10.1126/science.1226929

Fuentealba, L. C., Rompani, S. B., Parraguez, J. I., Obernier, K., Romero, R., Cepko, C. L., et al. (2015). Embryonic origin of postnatal neural stem cells. *Cell* 161, 1644–1655. doi: 10.1016/j.cell.2015.05.041

Furutachi, S., Miya, H., Watanabe, T., Kawai, H., Yamasaki, N., Harada, Y., et al. (2015). Slowly dividing neural progenitors are an embryonic origin of adult neural stem cells. *Nat. Neurosci.* 18, 657–665. doi: 10.1038/nn.3989

Galvao, R. P., Kasina, A., Mcneill, R. S., Harbin, J. E., Foreman, O., Verhaak, R. G. W., et al. (2014). Transformation of quiescent adult oligodendrocyte precursor cells into malignant glioma through a multistep reactivation process. *Proc. Natl. Acad. Sci. U.S.A.* 111, E4214–E4223. doi: 10.1073/pnas.1414389111

Garcia-Marques, J., Nunez-Llaves, R., and Lopez-Mascaraque, L. (2014). NG2-glia from pallial progenitors produce the largest clonal clusters of the brain: time frame of clonal generation in cortex and olfactory bulb. *J. Neurosci.* 34, 2305–2313. doi: 10.1523/Jneurosci.3060-13.2014

Geha, S., Pallud, J., Junier, M.-P., Devaux, B., Leonard, N., Chassoux, F., et al. (2010). $NG2^{+}$/$Olig2^{+}$ cells are the major cycle-related cell population of the adult human normal brain. *Brain Pathol.* 20, 399–411. doi: 10.1111/j.1750-3639.2009.00295.x

Gibson, E. M., Purger, D., Mount, C. W., Goldstein, A. K., Lin, G. L., Wood, L. S., et al. (2014). Neuronal activity promotes oligodendrogenesis and adaptive myelination in the mammalian brain. *Science* 344:1252304. doi: 10.1126/science.1252304

Hicks, J., Platt, S., Kent, M., and Haley, A. (2017). Canine brain tumours: a model for the human disease? *Vet. Comp. Oncol.* 15, 252–272. doi: 10.1111/vco.12152

Holland, E. C., Celestino, J., Dai, C., Schaefer, L., Sawaya, R. E., and Fuller, G. N. (2000). Combined activation of Ras and Akt in neural progenitors induces glioblastoma formation in mice. *Nat. Genet.* 25, 55–57. doi: 10.1038/75596

Huttner, H. B., Bergmann, O., Salehpour, M., Racz, A., Tatarishvili, J., Lindgren, E., et al. (2014). The age and genomic integrity of neurons after cortical stroke in humans. *Nat. Neurosci.* 17, 801–803. doi: 10.1038/nn.3706

Iuchi, T., Hasegawa, Y., Kawasaki, K., and Sakaida, T. (2015). Epilepsy in patients with gliomas: incidence and control of seizures. *J. Clin. Neurosci.* 22, 87–91. doi: 10.1016/j.jocn.2014.05.036

Jacques, T. S., Swales, A., Brzozowski, M. J., Henriquez, N. V., Linehan, J. M., Mirzadeh, Z., et al. (2010). Combinations of genetic mutations in the adult neural stem cell compartment determine brain tumour phenotypes. *EMBO J.* 29, 222–235. doi: 10.1038/emboj.2009.327

Jin, K. L., Wang, X. M., Xie, L., Mao, X. O., Zhu, W., Wang, Y., et al. (2006). Evidence for stroke-induced neurogenesis in the human brain. *Proc. Natl. Acad. Sci. U.S.A.* 103, 13198–13202. doi: 10.1073/pnas.0603512103

Kim, H., Zheng, S., Amini, S. S., Virk, S. M., Mikkelsen, T., Brat, D. J., et al. (2015). Whole-genome and multisector exome sequencing of primary and post-treatment glioblastoma reveals patterns of tumor evolution. *Genome Res.* 25, 316–327. doi: 10.1101/gr.180612.114

Kim, J., Lee, I. H., Cho, H. J., Park, C. K., Jung, Y. S., Kim, Y., et al. (2015). Spatiotemporal evolution of the primary glioblastoma genome. *Cancer Cell* 28, 318–328. doi: 10.1016/j.ccell.2015.07.013

Kondo, T., and Raff, M. (2000). Oligodendrocyte precursor cells reprogrammed to become multipotential CNS stem cells. *Science* 289, 1754–1757. doi: 10.1126/science.289.5485.1754

Ledur, P. F., Liu, C., He, H., Harris, A. R., Minussi, D. C., Zhou, H. Y., et al. (2016). Culture conditions tailored to the cell of origin are critical for maintaining native properties and tumorigenicity of glioma cells. *Neuro Oncol.* 18, 1413–1424. doi: 10.1093/neuonc/now062

Lei, L., Sonabend, A. M., Guarnieri, P., Soderquist, C., Ludwig, T., Rosenfeld, S., et al. (2011). Glioblastoma models reveal the connection between adult glial progenitors and the proneural phenotype. *PLoS One* 6:e20041. doi: 10.1371/journal.pone.0020041

Ligon, K. L., Alberta, J. A., Kho, A. T., Weiss, J., Kwaan, M. R., Nutt, C. L., et al. (2004). The oligodendroglial lineage marker OLIG2 is universally expressed in diffuse gliomas. *J. Neuropathol. Exp. Neurol.* 63, 499–509. doi: 10.1093/jnen/63.5.499

Ligon, K. L., Huillard, E., Mehta, S., Kesari, S., Liu, H. Y., Alberta, J. A., et al. (2007). Olig2-regulated lineage-restricted pathway controls replication competence in neural stem cells and malignant glioma. *Neuron* 53, 503–517. doi: 10.1016/j.neuron.2007.01.009

Lindberg, N., Jiang, Y., Xie, Y., Bolouri, H., Kastemar, M., Olofsson, T., et al. (2014). Oncogenic signaling is dominant to cell of origin and dictates astrocytic

or oligodendroglial tumor development from oligodendrocyte precursor cells. *J. Neurosci.* 34, 14644–14651. doi: 10.1523/jneurosci.2977-14.2014

Lindberg, N., Kastemar, M., Olofsson, T., Smits, A., and Uhrbom, L. (2009). Oligodendrocyte progenitor cells can act as cell of origin for experimental glioma. *Oncogene* 28, 2266–2275. doi: 10.1038/onc.2009.76

Lipp, H. P., and Bonfanti, L. (2016). Adult neurogenesis in mammals: variations and confusions. *Brain Behav. Evol.* 87, 205–221. doi: 10.1159/000446905

Liu, C., Sage, J. C., Miller, M. R., Verhaak, R. G. W., Hippenmeyer, S., Vogel, H., et al. (2011). Mosaic analysis with double markers reveals tumor cell of origin in glioma. *Cell* 146, 209–221. doi: 10.1016/j.cell.2011.06.014

Louis, D. N. (2006). Molecular pathology of malignant gliomas. *Annu. Rev. Pathol. Mech. Dis.* 1, 97–117. doi: 10.1146/annurev.pathol.1.110304.100043

Lu, F. H., Chen, Y., Zhao, C. T., Wang, H. B., He, D. Y., Xu, L. L., et al. (2016). Olig2-dependent reciprocal shift in PDGF and EGF receptor signaling regulates tumor phenotype and mitotic growth in malignant glioma. *Cancer Cell* 29, 669–683. doi: 10.1016/j.ccell.2016.03.027

Malik, S. Z., Lewis, M., Isaacs, A., Haskins, M., Van Winkle, T., Vite, C. H., et al. (2012). Identification of the rostral migratory stream in the canine and feline brain. *PLoS One* 7:e36016. doi: 10.1371/journal.pone.0036016

Marti-Fabregas, J., Romaguera-Ros, M., Gomez-Pinedo, U., Martinez-Ramirez, S., Jimenez-Xarrie, E., Marín, R., et al. (2010). Proliferation in the human ipsilateral subventricular zone after ischemic stroke. *Ann. Neurosci.* 17, 134–135. doi: 10.5214/ans.0972-7531.1017308

Marumoto, T., Tashiro, A., Friedmann-Morvinski, D., Scadeng, M., Soda, Y., Gage, F. H., et al. (2009). Development of a novel mouse glioma model using lentiviral vectors. *Nat. Med.* 15, 110–116. doi: 10.1038/nm.1863

Ming, G. L., and Song, H. J. (2011). Adult neurogenesis in the mammalian brain: significant answers and significant questions. *Neuron* 70, 687–702. doi: 10.1016/j.neuron.2011.05.001

Munoz, D. M., Singh, S., Tung, T., Agnihotri, S., Nagy, A., Guha, A., et al. (2013). Differential transformation capacity of neuro-glial progenitors during development. *Proc. Natl. Acad. Sci. U.S.A.* 110, 14378–14383. doi: 10.1073/pnas.1303504110

Nishiyama, A., Komitova, M., Suzuki, R., and Zhu, X. Q. (2009). Polydendrocytes (NG2 cells): multifunctional cells with lineage plasticity. *Nat. Rev. Neurosci.* 10, 9–22. doi: 10.1038/nrn2495

Ozawa, T., Riester, M., Cheng, Y. K., Huse, J. T., Squatrito, M., Helmy, K., et al. (2014). Most human non-GCIMP glioblastoma subtypes evolve from a common proneural-like precursor glioma. *Cancer Cell* 26, 288–300. doi: 10.1016/j.ccr.2014.06.005

Paredes, M. F., Sorrells, S. F., Garcia-Verdugo, J. M., and Alvarez-Buylla, A. (2016). Brain size and limits to adult neurogenesis. *J. Comp. Neurol.* 524, 646–664. doi: 10.1002/cne.23896

Parolisi, R., Cozzi, B., and Bonfanti, L. (2017). Non-neurogenic SVZ-like niche in dolphins, mammals devoid of olfaction. *Brain Struct. Funct.* 222, 2625–2639. doi: 10.1007/s00429-016-1361-3

Perry, A., and Wesseling, P. (2016). Histologic classification of gliomas. *Handb. Clin. Neurol.* 134, 71–95. doi: 10.1016/b978-0-12-802997-8.00005-0

Persson, A. I., Petritsch, C., Swartling, F. J., Itsara, M., Sim, F. J., Auvergne, R., et al. (2010). Non-stem cell origin for oligodendroglioma. *Cancer Cell* 18, 669–682. doi: 10.1016/j.ccr.2010.10.033

Qin, E. Y., Cooper, D. D., Abbott, K. L., Lennon, J., Nagaraja, S., Mackay, A., et al. (2017). Neural precursor-derived pleiotrophin mediates subventricular zone invasion by glioma. *Cell* 170, 845.e19–859.e19. doi: 10.1016/j.cell.2017.07.016

Raponi, E., Agenes, F., Delphin, C., Assard, N., Baudier, J., Legraverend, C., et al. (2007). S100B expression defines a state in which GFAP-expressing cells lose their neural stem cell potential and acquire a more mature developmental stage. *Glia* 55, 165–177. doi: 10.1002/glia.20445

Rebetz, J., Tian, D., Persson, A., Widegren, B., Salford, L. G., Englund, E., et al. (2008). Glial progenitor-like phenotype in low-grade glioma and enhanced CD133-expression and neuronal lineage differentiation potential in high-grade glioma. *PLoS One* 3:e1936. doi: 10.1371/journal.pone.0001936

Richardson, W. D., Young, K. M., Tripathi, R. B., and Mckenzie, I. (2011). NG2-glia as multipotent neural stem cells: fact or fantasy? *Neuron* 70, 661–673. doi: 10.1016/j.neuron.2011.05.013

Rivers, L. E., Young, K. M., Rizzi, M., Jamen, F., Psachoulia, K., Wade, A., et al. (2008). PDGFRA/NG2 glia generate myelinating oligodendrocytes and piriform projection neurons in adult mice. *Nat. Neurosci.* 11, 1392–1401. doi: 10.1038/nn.2220

Sanai, N., Nguyen, T., Ihrie, R. A., Mirzadeh, Z., Tsai, H. H., Wong, M., et al. (2011). Corridors of migrating neurons in the human brain and their decline during infancy. *Nature* 478, 382–386. doi: 10.1038/nature10487

Schmid, R. S., Simon, J. M., Vitucci, M., Mcneill, R. S., Bash, R. E., Werneke, A. M., et al. (2016). Core pathway mutations induce de-differentiation of murine astrocytes into glioblastoma stem cells that are sensitive to radiation but resistant to temozolomide. *Neuro Oncol.* 18, 962–973. doi: 10.1093/neuonc/nov321

Shao, F. J., Jiang, W. H., Gao, Q. Q., Li, B. Z., Sun, C. R., Wang, Q. Y., et al. (2017). Frozen tissue preparation for high-resolution multiplex histological analyses of human brain specimens. *J. Neurooncol.* 135, 21–28. doi: 10.1007/s11060-017-2547-0

Shoshan, Y., Nishiyama, A., Chang, A. S., Mork, S., Barnett, G. H., Cowell, J. K., et al. (1999). Expression of oligodendrocyte progenitor cell antigens by gliomas: implications for the histogenesis of brain tumors. *Proc. Natl. Acad. Sci. U.S.A.* 96, 10361–10366. doi: 10.1073/pnas.96.18.10361

Singh, S. K., Hawkins, C., Clarke, I. D., Squire, J. A., Bayani, J., Hide, T., et al. (2004). Identification of human brain tumour initiating cells. *Nature* 432, 396–401. doi: 10.1038/nature03128

Snuderl, M., Fazlollahi, L., Le, L. P., Nitta, M., Zhelyazkova, B. H., Davidson, C. J., et al. (2011). Mosaic amplification of multiple receptor tyrosine kinase genes in glioblastoma. *Cancer Cell* 20, 810–817. doi: 10.1016/j.ccr.2011.11.005

Stallcup, W. B. (1981). The Ng2 antigen, a putative lineage marker - immunofluorescent localization in primary cultures of rat-brain. *Dev. Biol.* 83, 154–165. doi: 10.1016/S0012-1606(81)80018-8

Stiles, C. D., and Rowitch, D. H. (2008). Glioma stem cells: a midterm exam. *Neuron* 58, 832–846. doi: 10.1016/j.neuron.2008.05.031

Venkatesh, H. S., Johung, T. B., Caretti, V., Noll, A., Tang, Y. J., Nagaraja, S., et al. (2015). Neuronal activity promotes glioma growth through neuroligin-3 secretion. *Cell* 161, 803–816. doi: 10.1016/j.cell.2015.04.012

Verhaak, R. G. W., Hoadley, K. A., Purdom, E., Wang, V., Qi, Y., Wilkerson, M. D., et al. (2010). Integrated genomic analysis identifies clinically relevant subtypes of glioblastoma characterized by abnormalities in PDGFRA, IDH1, EGFR, and NF1. *Cancer Cell* 17, 98–110. doi: 10.1016/j.ccr.2009.12.020

Vigano, F., and Dimou, L. (2016). The heterogeneous nature of NG2-glia. *Brain Res.* 1638, 129–137. doi: 10.1016/j.brainres.2015.09.012

Visvader, J. E. (2011). Cells of origin in cancer. *Nature* 469, 314–322. doi: 10.1038/nature09781

Vitucci, M., Irvin, D. M., Mcneill, R. S., Schmid, R. S., Simon, J. M., Dhruv, H. D., et al. (2017). Genomic profiles of low-grade murine gliomas evolve during progression to glioblastoma. *Neuro Oncol.* 19, 1237–1247. doi: 10.1093/neuonc/nox050

Wang, C. M., Liu, F., Liu, Y. Y., Zhao, C. H., You, Y., Wang, L., et al. (2011). Identification and characterization of neuroblasts in the subventricular zone and rostral migratory stream of the adult human brain. *Cell Res.* 21, 1534–1550. doi: 10.1038/cr.2011.83

Wang, J. G., Cazzato, E., Ladewig, E., Frattini, V., Rosenbloom, D. I. S., Zairis, S., et al. (2016). Clonal evolution of glioblastoma under therapy. *Nat. Genet.* 48, 768–776. doi: 10.1038/ng.3590

Wang, Q. H., Hu, B. L., Hu, X., Kim, H., Squatrito, M., Scarpace, L., et al. (2017). Tumor evolution of glioma-intrinsic gene expression subtypes associates with immunological changes in the microenvironment. *Cancer Cell* 32, 42.e6–56.e6. doi: 10.1016/j.ccell.2017.06.003

Weiss, W. A., Burns, M. J., Hackett, C., Aldape, K., Hill, J. R., Kuriyama, H., et al. (2003). Genetic determinants of malignancy in a mouse model for oligodendroglioma. *Cancer Res.* 63, 1589–1595.

Yeung, M. S. Y., Zdunek, S., Bergmann, O., Bernard, S., Salehpour, M., Alkass, K., et al. (2014). Dynamics of oligodendrocyte generation and myelination in the human brain. *Cell* 159, 766–774. doi: 10.1016/j.cell.2014.10.011

Zhang, Y., Chen, K., Sloan, S. A., Bennett, M. L., Scholze, A. R., O'keeffe, S., et al. (2014). An RNA-sequencing transcriptome and splicing database of glia,

neurons, and vascular cells of the cerebral cortex. *J. Neurosci.* 34, 11929–11947. doi: 10.1523/jneurosci.1860-14.2014

Zheng, H. W., Ying, H. Q., Yan, H. Y., Kimmelman, A. C., Hiller, D. J., and Chen, A. J. (2008). p53 and Pten control neural and glioma stem/progenitor cell renewal and differentiation. *Nature* 455, 1129–1133. doi: 10.1038/nature07443

Zhu, X. Q., Bergles, D. E., and Nishiyama, A. (2008). NG2 cells generate both oligodendrocytes and gray matter astrocytes. *Development* 135, 145–157. doi: 10.1242/dev.004895

Zhu, X. Q., Hill, R. A., Dietrich, D., Komitova, M., Suzuki, R., and Nishiyama, A. (2011). Age-dependent fate and lineage restriction of single NG2 cells. *Development* 138, 745–753. doi: 10.1242/dev.047951

Zhu, Y., Guignard, F., Zhao, D. W., Liu, L., Burns, D. K., Mason, R. P., et al. (2005). Early inactivation of p53 tumor suppressor gene cooperating with NF1 loss induces malignant astrocytoma. *Cancer Cell* 8, 119–130. doi: 10.1016/j.ccr.2005.07.004

Zuckermann, M., Hovestadt, V., Knobbe-Thomsen, C. B., Zapatka, M., Northcott, P. A., Schramm, K., et al. (2015). Somatic CRISPR/Cas9-mediated tumour suppressor disruption enables versatile brain tumour modelling. *Nat. Commun.* 6:7391. doi: 10.1038/ncomms8391

Conflict of Interest Statement: The authors declare that the research was conducted in the absence of any commercial or financial relationships that could be construed as a potential conflict of interest.

frontiers in Cellular Neuroscience

MINI REVIEW
published: 16 February 2018
doi: 10.3389/fncel.2018.00036

It's All about Timing: The Involvement of Kir4.1 Channel Regulation in Acute Ischemic Stroke Pathology

*Meagan Milton and Patrice D. Smith**

Department of Neuroscience, Carleton University, Ottawa, ON, Canada

An acute ischemic stroke is characterized by the presence of a blood clot that limits blood flow to the brain resulting in subsequent neuronal loss. Acute stroke threatens neuronal survival, which relies heavily upon proper function of astrocytes. Neurons are more susceptible to cell death when an astrocyte is unable to carry out its normal functions in supporting the neuron in the area affected by the stroke (Rossi et al., 2007; Takano et al., 2009). For example, under normal conditions, astrocytes initially swell in response to changes in extracellular osmotic pressure and then reduce their regulatory volume in response to volume-activated potassium (K^+) and chloride channels (Vella et al., 2015). This astroglial swelling may be overwhelmed, under ischemic conditions, due to the increased levels of glutamate and extracellular K^+ (Lai et al., 2014; Vella et al., 2015). The increase in extracellular K^+ contributes to neuronal damage and loss through the initiation of harmful secondary cascades (Nwaobi et al., 2016). Reducing the amount of extracellular K^+ could, in theory, limit or prevent neuronal damage and loss resulting in an improved prognosis for individuals following ischemic stroke. Kir4.1, an inwardly rectifying K^+ channel, has demonstrated an ability to regulate the rapid reuptake of this ion to return the cell to basal levels allowing it to fire again in rapid transmission (Sibille et al., 2015). Despite growing interest in this area, the underlying mechanism suggesting that neuroprotection could occur through modification of the Kir4.1 channel's activity has yet to be described. The purpose of this review is to examine the current literature and propose potential underlying mechanisms involving Kir4.1, specially the mammalian target of rapamycin (mTOR) and/or autophagic pathways, in the pathogenesis of ischemic stroke. The hope is that this review will instigate further investigation of Kir4.1 as a modulator of stroke pathology.

Keywords: Kir4.1, ischemia, astrocytes, autophagy, mammalian target of rapamycin

OPEN ACCESS

Edited by:
Alexej Verkhratsky,
University of Manchester,
United Kingdom

Reviewed by:
Johannes Hirrlinger,
Leipzig University, Germany
Mario Valentino,
University of Malta, Malta

****Correspondence:***
Patrice D. Smith
patrice.smith@carleton.ca

Received: *27 November 2017*
Accepted: *30 January 2018*
Published: *16 February 2018*

Citation:
Milton M and Smith PD (2018) It's All about Timing: The Involvement of Kir4.1 Channel Regulation in Acute Ischemic Stroke Pathology. Front. Cell. Neurosci. 12:36. doi: 10.3389/fncel.2018.00036

GENERAL PROPERTIES OF KIR4.1

Kir4.1, initially named BIR10, was first identified by the Adelman's group (Bond et al., 1994). It is predominately expressed on glial cells and is responsible for developmental regulation of extracellular K^+ dynamics (described below) (D'Adamo et al., 2011, 2013). Research has demonstrated that the channel forms both homomeric Kir4.1-Kir4.1 tetramers and heteromeric Kir4.1-Kir5.1 tetramers (Hibino et al., 2010; D'Adamo et al., 2011, 2013). The two types of tetramers have different sensitivities to pH. Between 6.5 and 8.0, the homomeric Kir4.1 channel is inhibited,

whereas the heteromeric Kir4.1-Kir5.1 is suppressed significantly (Pessia et al., 2001; D'Adamo et al., 2011, 2013). In addition, Kir4.1 and Kir5.1 are coexpressed on locus coeruleus neurons where they appear to be involved in neuronal carbon dioxide (CO_2) chemosensitivity (D'Adamo et al., 2011). Taken together, these results suggest that pH, CO_2, and Kir5.1 subunits modulate Kir4.1 activity.

Previous research has demonstrated that Kir4.1 channels are implicated in the pathophysiology of several disease/disorders. Abnormalities, specifically missense variations, within this channel have been linked to epilepsy (Hibino et al., 2010; D'Adamo et al., 2013). For example, a missense variation in Kir4.1 (T262S) was found to be the reason that DBA/2 mice are more susceptible to induced seizures than C57BL/6 mice (Ferraro et al., 2004; D'Adamo et al., 2013). In patients with either focal or generalized epilepsy, the R271C mutation in the Kir4.1 channel has been associated with a resistance to seizures (Ferraro et al., 2004; D'Adamo et al., 2013). Another condition, autism spectrum disorders (ASD), is associated with Kir4.1 channel mutations. In children with ASD, two specific mutations (R18Q and V84M) within the Kir4.1 channel have been identified. R18Q has been associated with several ASD symptoms, such as absence of speech and severe social interaction deficits, whereas the V84M appears to confer an increased expression of poor social gaze and withdrawal behaviors that are also characteristic of ASD (Sicca et al., 2011; Guglielmi et al., 2015). Kir4.1 abnormalities are also believed to underlie the comorbidity between epilepsy and ASD (D'Adamo et al., 2013; Guglielmi et al., 2015). Finally, Kir4.1 activity appears to be altered in response to ischemia (Nwaobi et al., 2016). Research has shown that Kir4.1 expression and Kir-mediated currents are reduced from day 1 to day 14 post-injury following global and focal ischemia (Pivonkova et al., 2010; Steiner et al., 2012). Furthermore, Kir4.1 channels appear more at the soma of the astrocyte rather than on the astrocytic processes when these reductions occur (Stewart et al., 2010; Nwaobi et al., 2016). It has been suggested that this shift changes Kir4.1 focus to proliferation instead of K^+ spatial buffering (Nwaobi et al., 2016).

THE ROLE OF KIR4.1 IN ASTROCYTIC FUNCTIONING

Within the central nervous system, astrocytes are involved in controlling ion and water homeostasis, moving metabolite and waste products, and participating in the formation of the blood-brain barrier (Takano et al., 2009; Nwaobi et al., 2016). These biophysical properties appear to be affected by Kir4.1; specifically, the homeostasis of extracellular K^+, the regulation of extracellular glutamate, and the mediation of water and volume levels are three of the processes that Kir4.1 is involved (Nwaobi et al., 2016). First, K^+ spatial buffering is a process carried out by astrocytes to ensure that extracellular K^+ concentrations are regulated following an action potential (Nwaobi et al., 2016). An action potential may increase local K^+ concentrations by 1 mM under normal neuronal activity or by >10–12 mM under ischemic conditions (Moody et al., 1974; Ransom et al., 2000). The increased K^+ concentrations prevent the neuron from firing in response to further stimulation and in the case of ischemic conditions, contribute to neuronal loss (Nwaobi et al., 2016). Thus, it is important for K^+ to be removed from the extracellular space through a mechanism such as the Kir4.1 channel. This is supported by the fact that at the sites of local accumulation, Kir4.1 has been shown to allow K^+ influx to return the extracellular K^+ concentrations to baseline. Recent work has demonstrated that local extracellular K^+ concentrations were greater following the blockage of Kir4.1 using barium (Ransom et al., 2000; Larsen et al., 2014; Nwaobi et al., 2016). Furthermore, previous work has shown a slower recovery rate of extracellular K^+ concentrations and enhanced undershoot recovery following brainstem stimulation in glial-conditional Kir4.1 knock out animals (Neusch et al., 2006). Taken together, these results implicate the Kir4.1 channel's involvement in extracellular K^+ homeostasis and neuronal survival following ischemia.

Second, astrocytes are involved in glutamate uptake through two transporters, GLAST (EAAT1) and GLT-1 (EAAT2), in an energetically unfavorable process (Rothstein et al., 1996). Sodium, hydrogen and K^+ electrochemical gradients work in concert with the two transporters to bring glutamate into the astrocyte in an efficient manner (Barbour et al., 1988; Nwaobi et al., 2016). With respect to extracellular K^+, high concentrations decrease K^+ unbinding and depolarize the glial membrane reducing the amount of glutamate reuptake resulting in an increase in neuronal excitability (Barbour et al., 1988). The contribution of Kir4.1 to astrocytic glutamate uptake has been previously studied. Researchers found a 33.1 and 57.0 percent decrease in glutamate uptake following pharmacological inhibition and siRNA-mediated Kir4.1 knockdown in cortical astrocytes (Kucheryavykh et al., 2007). The authors attributed these decreases to be the result of a loss in the hyperpolarized resting membrane potential of the astrocyte. In addition, a TBOA (*threo*-beta-benzyloxyaspartate)-sensitive glutamate uptake reduction of >50 percent was seen in Kir4.1 knockout animals when compared to wild-type animals (Nwaobi et al., 2016). The results support Kir4.1's role in glutamate uptake by allowing the astrocyte to maintain a K^+ electrochemical gradient that promotes K^+ unbinding and glial depolarization.

Lastly, a third property of astrocytes that appears to involve Kir4.1 functioning is water and volume regulation. Aquaporins, specifically aquaporin 4 (AQP4), are found at the astroglial endfeet where they are responsible for bringing water into specific cells and removing excess water to alleviate swelling to prevent cell lysis (Vella et al., 2015). Under conditions of water and/or food deprivation, AQP4 has demonstrated an ability to alter its expression levels in order to maintain the brain's normal water content and prevent cell loss (Ye et al., 2016). Studies examining the relationship between Kir4.1 and AQP4 have found that they co-localize with one another. For

Abbreviations: AKT, protein kinase B; AMPA, α-amino-3-hydroxy-5-methyl-4-isoxazolepropionic acid; ASD, autism spectrum disorders; ATG, autophagy-related gene; ATP, adenosine triphosphate; AQP4, aquaporin 4; CO_2, carbon dioxide; GLAST, L-glutamate/L-aspartate transporter; GLT-1, glutamate transporter 1; K^+, potassium; KA, kainite receptor; mTOR, mammalian target of rapamycin; mTORC1, mammalian target of rapamycin complex 1; NMDA, *N*-methyl-D-aspartate; PI3K, phosphatidylinositol 3 kinase.

example, one study demonstrated that co-immunoprecipitates between the two were found in Müller cells and that loss or mislocalization of Kir4.1 in the post-ischemic retina played a role in glial cell swelling (Pannicke et al., 2004). However, a follow-up study was able to induce the same cell swelling through the inhibition, using physostigmine, of Kir4.1 to prevent K^+ efflux without changing AQP4 expression or function (Nwaobi et al., 2016). This suggests that changing Kir4.1 channel's activity alone, through the application of different pharmacological agents, could reduce the amount of cell lysis or autophagic cell death seen in ischemic conditions.

In addition, due to the interaction between Kir4.1 and APQ4 channels, an important factor that may modulate Kir4.1 activity is water movement through different compartments. With a specific focus on glutamate, a review published by Rothman and Olney (1986) described how neurotoxicity results in the simultaneous build-up of intracellular sodium, K^+, and water that may lead to lysis/autophagic injury. Glutamate, a neurotransmitter impacted by K^+ gradients and Kir4.1 as described above, acts on many different receptors to exert its effects. The two most important ones for the purpose of this review are α-amino-3-hydroxy-5-methyl-4-isoxazolepropionic acid (AMPA) and kainite (KA) receptors. These two receptors are highly permeable to sodium and K^+ (Chen et al., 1998). Over-activation of these receptors, as well as the *N*-methyl-D-aspartate (NMDA) receptor, results in response to brain ischemia (Rothman and Olney, 1987; Coyle and Puttfarcken, 1993). The over-activation leads to excessive ion influx, osmotic swelling, free radical generation, and cell death (Rothman and Olney, 1987; Coyle and Puttfarcken, 1993). Specifically, Rothman and Olney (1986) found that the recovery of water regulation might also reverse the lysis/autophagic injury. Based on these findings, water accumulation may also be considered a "stressor" that damages organelles. Due to the Kir4.1 channel's interaction with APQ4, and its involvement in water/volume regulation, further studies are required to examine how levels of intracellular K^+ contribute to such conditions and how the proposed mTOR pathway involving Kir4.1 (described below; **Figure 1**) is linked to cell survival.

POTENTIAL MECHANISMS INVOLVED IN MEDIATING KIR4.1 FUNCTIONAL BENEFITS

Kir4.1 channel activity following ischemia and its contribution to the biophysical properties of astrocytes has previously been described. How Kir4.1 is involved in preventing neuronal loss following ischemia through an intrinsic pathway has yet to be outlined. Specifically, it is possible that Kir4.1 may play a role in the activation of the mammalian target of rapamycin complex 1 (mTORC1). mTORC1 is one of two mTOR complexes that contains a kinase mTOR component (Heras-Sandoval et al., 2014). It is mediated upstream by the phosphatidylinositol 3 kinase/protein kinase B (PI3K/AKT) pathway that is involved in cell survival and the inhibition of apoptosis (Heras-Sandoval et al., 2014). Furthermore, researchers have shown that mTORC1 is involved in the negative regulation of autophagy (Noda and Ohsumi, 1998; Schmelzle and Hall, 2000; Cuyàs et al., 2014).

Autophagy involves the breakdown of damaged organelles and misfolded proteins *via* a stress-induced catabolic pathway that maintains proper cellular homeostasis (Heras-Sandoval et al., 2014; Sahni et al., 2017). Autophagy does not seem to always result in cell survival. Autophagic programmed cell death occurs in response to stressors, such as water accumulation or nutrient deprivation, due to induced autophagy (Heras-Sandoval et al., 2014). Induced autophagy has been shown to occur in response to altered expression of autophage-related gene (Atg) 5 and 6 within the cell leading to cellular lysis (Amelio et al., 2011; Majid, 2014). Research has also demonstrated that autophagy is impacted significantly more in nutrient-deprived situations, such as K^+-deprivation, as the process is associated with energy re-usage in cells (Ye et al., 2016; Sahni et al., 2017). For example, within cerebellar granule cells, K^+-deprivation has not only induced autophagy but has been linked to programmed cell death as conditions move into K^+-starvation (K^+ reduced to 5 mM) (Canu et al., 2005; Kaasik et al., 2005; Sahni et al., 2017). Kir4.1 is dependent on adenosine triphosphate (ATP) (Nwaobi et al., 2016). Under K^+-starvation, Kir4.1 may be inactive as a result of ATP depletion in response to brain ischemia and low pH due to the acidosis that occurs in response to ischemia (Pessia et al., 2001; Hu and Song, 2017). As a result, Kir4.1 is no longer activated in a PI3K-dependent manner (as suggested below) and mTORC1 no longer prevents autophagic cell death.

The point at which PI3K attempts to activate Kir4.1 appears to be dependent on timing. This may be because recent evidence has pointed not only to the dual role of autophagy following ischemia (Chen et al., 2014; Majid, 2014) but implicates the potential role of K^+ in preventing autophagy (Canu et al., 2005; Kaasik et al., 2005; Sahni et al., 2017). Initially, Koike et al. (2008) demonstrated that the induction of autophagy, following hypoxia-ischemia injury, results in neuronal death. On the other hand, Carloni et al. (2010) described a pro-survival signaling complex involving autophagy to prevent neuronal death. More recently, it was suggested that the role autophagy plays following ischemia is determined by the time at which it is induced (Chen et al., 2014). Ravikumar et al. (2010) stated that a protective role for autophagy might be seen during ischemic preconditioning, whereas following ischemia/reperfusion the process might aggravate cerebral ischemic injury. Based on these findings, He et al. (2012) hypothesized that inducing autophagy at different time points during early and late stage ischemia may account for the different outcomes. For example, infarct size was reduced significantly and eliminated water content increases in the brain after treatment with 3-MA (a known autophagy inhibitor) prior to reperfusion (Chen et al., 2014). On the other hand, Carloni et al. (2010) found that treatment with rapamycin decreased brain injury and increased autophagy when administered prior to hypoxia-ischemia. Furthermore, the neuroprotective effects of ischemic postconditioning, previously described as being mimicked (Yan et al., 2011), are weakened when rapamycin is applied at the onset of reperfusion rather than at the onset of hypoxia-ischemia (Gao et al., 2012).

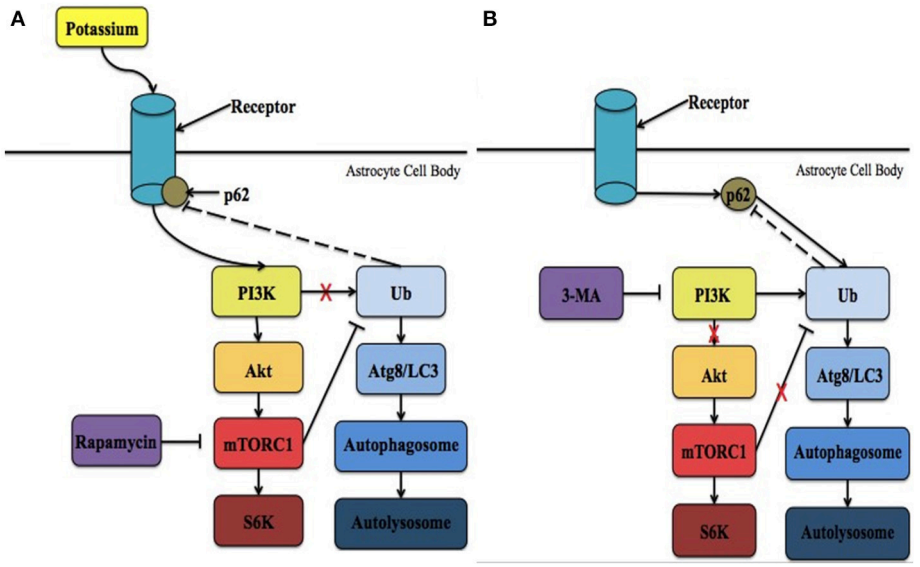

FIGURE 1 | The proposed intrinsic mechanism involving Kir4.1 in neuronal survival following ischemia. **(A)** Following ischemia, the levels of extracellular potassium increase significantly. PI3K is recruited to activate Kir4.1 leading to the initiation of mTORC1 and the overall mTOR pathway. In addition, it is possible that p62 is recruited to regulate Kir4.1. As a result, more cells in the ischemic penumbra survive and brain injury is reduced. Treatment with rapamycin has been demonstrated to reduce these effects. **(B)** During potassium starvation Kir4.1 is not activated due to ATP-depletion and mTORC1 no longer negatively regulates autophagy. Instead, autophagic cell death via protein breakdown in the autolysosome is initiated in a PI3K-dependent manner. Under these conditions, p62 interacts with ubiquitin (Ub) and binds with Atg8/LC3 within the phagophore. Lysosomes then interact with the autophagosome to form the autolysosome. 3-MA is an inhibitor of the PI3K pathway that prevents the initiation of autophagic cell death. Ubiquitin is the only molecule that is depicted as potentially feeding back in the mechanism, however, many other molecules are known to feedback in both the mTOR and autophagic pathways, respectively.

The mammalian target of rapamycin (mTOR) pathways is one of several cellular pathways that are involved in the maintenance of neuronal survival. It is also inhibited by rapamycin. As mentioned above, the timing at which PI3K attempts to activate Kir4.1, resulting in mTORC1 activation, may determine which pathway is activated leading to either cell survival or death. It is possible that targeting Kir4.1 activity prior to reperfusion may increase PI3K activity, and subsequent AKT phosphorylation, resulting in the activation of the mTORC1. It is important to note that the channel's involvement in the mTOR pathway has only been previously implicated by a single study. Zaika et al. (2016) showed that using insulin and insulin-like growth factor-1, within the cortical collecting duct, activates the heteromeric Kir4.1/Kir5.1 channel in a phosphoinositide 3-kinase (PI3K)-dependent manner. It is possible that Kir4.1 works through the mTOR pathway to prevent the induction of autophagy, through its PI3K-dependent activation (Zaika et al., 2016), following the onset reperfusion leading to the reduction of infarct size and a decrease in water content. This hypothesis is supported by the fact that during the onset of reperfusion ATP levels are high (Murphy and Steenbergen, 2008; Kalogeris et al., 2012), which corresponds to the time when Kir4.1 is optimally activated (Takumi et al., 1995; Kucheryavykh et al., 2009) and APQ4 levels remain unaltered (Shin et al., 2011). On the other hand, when energy levels are low, corresponding to Kir4.1 inactivation, the PI3K/AKT pathway is less active leading to the adoption of a quiescent state by the cells (Cheung and Rando, 2013). Thus, it is hypothesized that Kir4.1 is activated in PI3K-dependent manner, leading to cell survival through the mTOR pathway. Future research could focus on determining the upstream effectors within this intrinsic pathway and suggests that Kir4.1 represents a potential therapeutic target for the treatment of ischemic insult. The two potential mechanisms involved in mediating Kir4.1 functional benefits are summarized in **Figure 1**.

It is also important to note that p62, an adapter molecule in autophagy, may also play a role in this pathway. Voltage-gated K^+ channels (K_v) are regulated by p62 (Sahni et al., 2017). It has been previously demonstrated that PKCζ interacts with p62 to increase the phosphorylation of the β subunit of K_v ($K_v\beta$) (Puls et al., 1997; Ishii et al., 2013). As a result, K_v channels, specifically $K_v1.5$, are inhibited under acute hypoxia (Ishii et al., 2013). While Kir4.1 is not a voltage-gated channel, as it lacks a voltage-sensing domain, PKC isoforms have been shown to modulate both inwardly rectifying and voltage-gated channels (Dini et al., 2006). For example, the heteromeric Kir4.1-Kir5.1 channel is inhibited in a PKC-dependent manner (Rojas et al., 2007). Assuming p62 and Kir4.1 do interact, the timing at which p62 attempts to interact with Kir4.1 may determine which pathway is activated leading to either cell survival or death. Immediately following ischemic onset, p62 may be recruited to regulate Kir4.1, which is activated in a PI3K-dependent manner, leading to cell survival through the mTOR pathway (**Figure 1A**). Thus, it is possible that targeting Kir4.1 prior to reperfusion, with

different pharmacological agents, may increase the likelihood of p62 associating with Kir4.1 and subsequent cell survival. On the other hand, the point at which p62 attempts to interact with Kir4.1 would be dependent on timing. This is because as more ATP is used, Kir4.1 is no longer active and p62 would be able to associate with ubiquitin to initiate autophagic cell death under nutrient-deprived situations (**Figure 1B**). Future research should examine whether or not the homomeric Kir4.1 channel is inhibited by PKC isoforms, specifically PKCζ, and if there is an interaction between Kir4.1 and p62.

CONCLUSION

Previous evidence points to an intrinsic pathway, involving the regulation of Kir4.1, within the central nervous system that regulates neuronal survival. Further understanding of this pathway within astrocytes, and how it impacts neuronal viability (example: the impact on autophagy), could improve treatment options following ischemia. In this regard, further research is critical to identifying the potential role of Kir4.1 channel, and its subsequent effectors, in ischemia in order to guide the development of novel treatment options for stroke. These treatment strategies could be focused on altering Kir4.1 channel activity, which may be useful in improving the clinical outcomes after ischemic stroke.

AUTHOR CONTRIBUTIONS

All authors listed have made a substantial, direct, and intellectual contribution to the work, and approved it for publication.

REFERENCES

Amelio, I., Melino, G., and Knight, R. A. (2011). Cell death pathology: cross-talk with autophagy and its clinical implications. *Biochem. Biophys. Res. Commun.* 414, 277–281. doi: 10.1016/j.bbrc.2011.09.080

Barbour, B., Brew, H., and Attwell, D. (1988). Electrogenic glutamate uptake in glial cells is activated by intracellular potassium. *Nature* 335, 433–435. doi: 10.1038/335433a0

Bond, C. T., Pessia, M., Xia, X. M., Lagrutta, A., Kavanaugh, M. P., and Adelman, J. P. (1994). Cloning and expression of a family of inward rectifier potassium channels. *Recept. Channels* 2, 183–191.

Canu, N., Tufi, R., Serafino, A. L., Amadoro, G., Ciotti, M. T., and Calissano, P. (2005). Role of the autophagic-lysosomal system on low potassium-induced apoptosis in cultured cerebellar granule cells. *J. Neurochem.* 92, 1228–1242. doi: 10.1111/j.1471-4159.2004.02956.x

Carloni, S., Girelli, S., Scopa, C., Buonocore, G., Longini, M., and Balduini, W. (2010). Activation of autophagy and Akt/CREB signaling play an equivalent role in the neuroprotective effect of rapamycin in neonatal hypoxia-ischemia. *Autophagy* 6, 366–377. doi: 10.4161/auto.6.3.11261

Chen, Q., Olney, J. W., Lukasiewicz, P. D., Almli, T., and Romano, C. (1998). Fenamates protect neurons against ischemic and excitotoxic injury in chick embryo retina. *Neurosci. Lett.* 242, 163–166. doi: 10.1016/S0304-3940(98)00081-0

Chen, W., Sun, Y., Liu, K., and Sun, X. (2014). Autophagy: a double-edged sword for neuronal survival after cerebral ischemia. *Neural Regen. Res.* 9, 1210–1216. doi: 10.4103/1673-5374.135329

Cheung, T. H., and Rando, T. A. (2013). Molecular regulation of stem cell quiescence. *Nat. Rev. Mol. Cell Biol.* 14, 329–340. doi: 10.1038/nrm3591

Coyle, J. T., and Puttfarcken, P. (1993). Oxidative stress, glutamate, and neurodegenerative disorders. *Science* 262, 689–695. doi: 10.1126/science.7901908

Cuyàs, E., Corominas-Faja, B., Joven, J., and Menendez, J. A. (2014). "Cell cycle regulation by the nutrient-sensing mammalian target of rapamycin (mTOR) pathway," in *Cell Cycle Control: Mechanisms and Protocols*, eds E. Noguchi and M. C. Gadaleta. (New York, NY: Springer), 113–144.

D'Adamo, M. C., Catacuzzeno, L., Di Giovanni, G., Franciolini, F., and Pessia, M. (2013). K^+ channelepsy: progress in the neurobiology of potassium channels and epilepsy. *Front. Cell. Neurosci.* 7:134. doi: 10.3389/fncel.2013.00134

D'Adamo, M. C., Shang, L., Imbrici, P., Brown, S. D., Pessia, M., and Tucker, S. J. (2011). Genetic inactivation of Kcnj16 identifies Kir5.1 as an important determinant of neuronal PCO2/pH sensitivity. *J. Biol. Chem.* 286, 192–8.

Dini, G., Ilkanich, E. V., and Janigro, D. (2006). "Potassium channels, cell cycle, and tumorigenesis in the central nervous system," in *The Cell Cycle in the Central Nervous System*, ed D. Janigro, (Totowa, NJ: Humana Press), 177–191.

Ferraro, T. N., Golden, G. T., Smith, G. G., Martin, J. F., Lohoff, F. W., Gieringer, T. A., et al. (2004). Fine mapping of a seizure susceptibility locus on mouse Chromosome 1: nomination of Kcnj10 as a causative gene. *Mamm. Genome* 15, 239–251. doi: 10.1007/s00335-003-2270-3

Gao, L., Jiang, T., Guo, J., Liu, Y., Cui, G., Gu, L., et al. (2012). Inhibition of autophagy contributes to ischemic postconditioning-induced neuroprotection against focal cerebral ischemia in rats. *PLoS ONE* 7:e46092. doi: 10.1371/journal.pone.0046092

Guglielmi, L., Servettini, I., Caramia, M., Catacuzzeno, L., Franciolini, F., D'Adamo, M. C., et al. (2015). Update on the implication of potassium channels in autism: K(+) channelautism spectrum disorder. *Front. Cell. Neurosci.* 9:34. doi: 10.3389/fncel.2015.00034

He, S., Wang, C., Dong, H., Xia, F., Zhou, H., Jiang, X., et al. (2012). Immune-related GTPase M (IRGM1) regulates neuronal autophagy in a mouse model of stroke. *Autophagy* 8, 1621–1627. doi: 10.4161/auto.21561

Heras-Sandoval, D., Pérez-Rojas, J. M., Hernández-Damián, J., and Pedraza-Chaverri, J. (2014). The role of PI3K/AKT/mTOR pathway in the modulation of autophagy and the clearance of protein aggregates in neurodegeneration. *Cell. Signal.* 26, 2694–2701. doi: 10.1016/j.cellsig.2014.08.019

Hibino, H., Inanobe, A., Furutani, K., Murakami, S., Findlay, I., and Kurachi, Y. (2010). Inwardly rectifying potassium channels: their structure, function, and physiological roles. *Physiol. Rev.* 90, 291–366. doi: 10.1152/physrev.00021.2009

Hu, H. J., and Song, M. (2017). Disrupted ionic homeostasis in ischemic stroke and new therapeutic targets. *J. Stroke Cerebrovasc. Dis.* 26, 2706–2719. doi: 10.1016/j.jstrokecerebrovasdis.2017.09.011

Ishii, T., Warabi, E., Siow, R. C., and Mann, G. E. (2013). Sequestosome1/p62: a regulator of redox-sensitive voltage-activated potassium channels, arterial remodeling, inflammation, and neurite outgrowth. *Free Radic. Biol. Med.* 65, 102–116. doi: 10.1016/j.freeradbiomed.2013.06.019

Kaasik, A., Rikk, T., Piirsoo, A., Zharkovsky, T., and Zharkovsky, A. (2005). Up-regulation of lysosomal cathepsin L and autophagy during neuronal death induced by reduced serum and potassium. *Eur. J. Neurosci.* 22, 1023–1031. doi: 10.1111/j.1460-9568.2005.04279.x

Kalogeris, T., Baines, C. P., Krenz, M., and Korthuis, R. J. (2012). Cell biology of ischemia/reperfusion injury. *Int Rev Cell Mol Biol.* 298:229–317. doi: 10.1016/B978-0-12-394309-5.00006-7

Koike, M., Shibata, M., Tadakoshi, M., Gotoh, K., Komatsu, M., Waguri, S., et al. (2008). Inhibition of autophagy prevents hippocampal pyramidal neuron death after hypoxic-ischemic injury. *Am. J. Pathol.* 172, 454–469. doi: 10.2353/ajpath.2008.070876

Kucheryavykh, L. Y., Kucheryavykh, Y. V, Inyushin, M., Shuba, Y. M., Sanabria, P., Cubano, L. A., et al. (2009). Ischemia increases TREK-2 channel expression in astrocytes: relevance to glutamate clearance. *Open Neurosci. J.* 3, 40–47. doi: 10.2174/1874082000903010040

Kucheryavykh, Y. V., Kucheryavykh, L. Y., Nichols, C. G., Maldonado, H. M., Baksi, K., Reichenbach, A., et al. (2007). Downregulation of Kir4.1 inward rectifying potassium channel subunits by RNAi impairs potassium transfer and glutamate uptake by cultured cortical astrocytes. *Glia* 55, 274–281. doi: 10.1002/glia.20455

Lai, T. W., Zhang, S., and Wang, Y. T. (2014). Excitotoxicity and stroke: identifying novel targets for neuroprotection. *Prog. Neurobiol.* 115, 157–188. doi: 10.1016/j.pneurobio.2013.11.006

Larsen, B. R., Assentoft, M., Cotrina, M. L., Hua, S. Z., Nedergaard, M., Kaila, K., et al. (2014). Contributions of the Na^+/K^+-ATPase, NKCC1, and Kir4.1 to hippocampal K^+ clearance and volume responses. *Glia* 62, 608–622. doi: 10.1002/glia.22629

Majid, A. (2014). Neuroprotection in stroke : past, present, and future. *ISRN Neurol.* 2014:515716. doi: 10.1155/2014/515716

Moody, W. J., Futamachi, K. J., and Prince, D. A. (1974). Extracellular potassium activity during epileptogenesis. *Exp. Neurol.* 42, 248–263. doi: 10.1016/0014-4886(74)90023-5

Murphy, E., and Steenbergen, C. (2008). Mechanisms underlying acute protection from cardiac ischemia-reperfusion injury. *Physiol. Rev.* 88, 581–609. doi: 10.1152/physrev.00024.2007

Neusch, C., Papadopoulos, N., Müller, M., Maletzki, I., Winter, S. M., Hirrlinger, J., et al. (2006). Lack of the Kir4.1 channel subunit abolishes K^+ buffering properties of astrocytes in the ventral respiratory group: impact on extracellular K^+ regulation. *J. Neurophysiol.* 95, 1843–1852. doi: 10.1152/jn.00996.2005

Noda, T., and Ohsumi, Y. (1998). Tor, a phosphatidylinositol kinase homologue, controls autophagy in yeast. *J. Biol. Chem.* 273, 3963–3966. doi: 10.1074/jbc.273.7.3963

Nwaobi, S. E., Cuddapah, V. A., Patterson, K. C., Randolph, A. C., and Olsen, M. L. (2016). The role of glial-specific Kir4.1 in normal and pathological states of the CNS. *Acta Neuropathol.* 132, 1–21. doi: 10.1007/s00401-016-1553-1

Pannicke, T., Iandiev, I., Uckermann, O., Biedermann, B., Kutzera, F., Wiedemann, P., et al. (2004). A potassium channel-linked mechanism of glial cell swelling in the postischemic retina. *Mol. Cell. Neurosci.* 26, 493–502. doi: 10.1016/j.mcn.2004.04.005

Pessia, M., Imbrici, P., D'Adamo, M. C., Salvatore, L., and Tucker, S. J. (2001). Differential pH sensitivity of Kir4.1 and Kir4.2 potassium channels and their modulation by heteropolymerisation with Kir5.1. *J. Physiol.* 532, 359–367. doi: 10.1111/j.1469-7793.2001.0359f.x

Pivonkova, H., Benesova, J., Butenko, O., Chvatal, A., and Anderova, M. (2010). Impact of global cerebral ischemia on K+ channel expression and membrane properties of glial cells in the rat hippocampus. *Neurochem. Int.* 57, 783–794. doi: 10.1016/j.neuint.2010.08.016

Puls, A., Schmidt, S., Grawe, F., and Stabel, S. (1997). Interaction of protein kinase C ζ with ZIP, a novel protein kinase C-binding protein. *Proc. Natl. Acad. Sci. U.S.A.* 94, 6191–6196. doi: 10.1073/pnas.94.12.6191

Ransom, C. B., Ransom, B. R., and Sontheimer, H. (2000). Activity-dependent extracellular K^+ accumulation in rat optic nerve: the role of glial and axonal Na^+ pumps. *J. Physiol.* 522(Pt 3), 427–442. doi: 10.1111/j.1469-7793.2000.00427.x

Ravikumar, B., Sarkar, S., Davies, J. E., Futter, M., Garcia-Arencibia, M., Green-Thompson, Z. W., et al. (2010). Regulation of mammalian autophagy in physiology and pathophysiology. *Physiol. Rev.* 90, 1383–1435. doi: 10.1152/physrev.00030.2009

Rojas, A., Cui, N., Su, J., Yang, L., Muhumuza, J. P., and Jiang, C. (2007). Protein kinase C dependent inhibition of the heteromeric Kir4.1–Kir5.1 channel. *Biochim. Biophys. Acta* 1768, 2030–2042. doi: 10.1016/j.bbamem.2007.04.008

Rossi, D. J., Brady, J. D., and Mohr, C. (2007). Astrocyte metabolism and signaling during brain ischemia. *Nat. Neurosci.* 10, 1377–1386. doi: 10.1038/nn2004

Rothman, S. M., and Olney, J. W. (1986). Glutamate and the pathophysiology of hypoxic–ischemic brain damage. *Ann. Neurol.* 19, 105–111. doi: 10.1002/ana.410190202

Rothman, S. M., and Olney, J. W. (1987). Excitotoxity and the NMDA receptor. *Trends Neurosci.* 10, 299–302. doi: 10.1016/0166-2236(87)90177-9

Rothstein, J. D., Dykes-Hoberg, M., Pardo, C. A., Bristol, L. A., Jin, L., Kuncl, R. W., et al. (1996). Knockout of glutamate transporters reveals a major role for astroglial transport in excitotoxicity and clearance of glutamate. *Neuron* 16, 675–686. doi: 10.1016/S0896-6273(00)80086-0

Sahni, S., Bae, D. H., Jansson, P. J., and Richardson, D. R. (2017). The mechanistic role of chemically diverse metal ions in the induction of autophagy. *Pharmacol. Res.* 119, 118–127. doi: 10.1016/j.phrs.2017.01.009

Schmelzle, T., and Hall, M. N. (2000). TOR, a central controller of cell growth. *Cell* 103, 253–262. doi: 10.1016/S0092-8674(00)00117-3

Shin, J. A., Choi, J. H., Choi, Y. H., and Park, E. M. (2011). Conserved aquaporin 4 levels associated with reduction of brain edema are mediated by estrogen in the ischemic brain after experimental stroke. *Biochim. Biophys. Acta - Mol. Basis Dis.* 1812, 1154–1163. doi: 10.1016/j.bbadis.2011.05.004

Sibille, J., Dao Duc, K., Holcman, D., and Rouach, N. (2015). The neuroglial potassium cycle during neurotransmission: role of Kir4.1 channels. *PLOS Comput. Biol.* 11:e1004137. doi: 10.1371/journal.pcbi.1004137

Sicca, F., Imbrici, P., D'Adamo, M. C., Moro, F., Bonatti, F., Brovedani, P., et al. (2011). Autism with seizures and intellectual disability: possible causative role of gain-of-function of the inwardly-rectifying K^+ channel Kir4.1. *Neurobiol. Dis.* 43, 239–247. doi: 10.1016/j.nbd.2011.03.016

Steiner, E., Enzmann, G. U., Lin, S., Ghavampour, S., Hannocks, M. J., Zuber, B., et al. (2012). Loss of astrocyte polarization upon transient focal brain ischemia as a possible mechanism to counteract early edema formation. *Glia* 60, 1646–1659. doi: 10.1002/glia.22383

Stewart, T. H., Eastman, C. L., Groblewski, P. A., Fender, J. S., Verley, D. R., Cook, D. G., et al. (2010). Chronic dysfunction of astrocytic inwardly rectifying K^+ channels specific to the neocortical epileptic focus after fluid percussion injury in the rat. *J. Neurophysiol.* 104, 3345–3360. doi: 10.1152/jn.00398.2010

Takano, T., Oberheim, N., Cotrina, M. L., and Nedergaard, M. (2009). Astrocytes and ischemic injury. *Stroke* 40, S8–S12. doi: 10.1161/STROKEAHA.108.533166

Takumi, T., Ishii, T., Horio, Y., Morishige, K. I., Takahashi, N., Yamada, M., et al. (1995). A novel ATP-dependent inward rectifier potassium channel expressed predominantly in glial cells. *J. Biol. Chem.* 270, 16339–16346. doi: 10.1074/jbc.270.27.16339

Vella, J., Zammit, C., Di Giovanni, G., Muscat, R., and Valentino, M. (2015). The central role of aquaporins in the pathophysiology of ischemic stroke. *Front. Cell. Neurosci.* 9:108. doi: 10.3389/fncel.2015.00108

Yan, W., Zhang, H., Bai, X., Lu, Y., Dong, H., and Xiong, L. (2011). Autophagy activation is involved in neuroprotection induced by hyperbaric oxygen preconditioning against focal cerebral ischemia in rats. *Brain Res.* 1402, 109–121. doi: 10.1016/j.brainres.2011.05.049

Ye, Q., Wu, Y., Gao, Y., Li, Z., Li, W., and Zhang, C. (2016). The "selfish brain" is regulated by aquaporins and autophagy under nutrient deprivation. *Mol. Med. Rep.* 13, 3842–3848. doi: 10.3892/mmr.2016.4988

Zaika, O., Palygin, O., Tomilin, V., Mamenko, M., Staruschenko, A., and Pochynyuk, O. (2016). Insulin and IGF-1 activate Kir4.1/5.1 channels in cortical collecting duct principal cells to control basolateral membrane voltage. *Am. J. Physiol. Ren. Physiol.* 310, F311–F321. doi: 10.1152/ajprenal.00436.2015

Conflict of Interest Statement: The authors declare that the research was conducted in the absence of any commercial or financial relationships that could be construed as a potential conflict of interest.

frontiers in Molecular Neuroscience

ORIGINAL RESEARCH
published: 24 January 2018
doi: 10.3389/fnmol.2018.00004

Function of B-Cell CLL/Lymphoma 11B in Glial Progenitor Proliferation and Oligodendrocyte Maturation

*Chih-Yen Wang[1], Yuan-Ting Sun[2], Kuan-Min Fang[1], Chia-Hsin Ho[1], Chung-Shi Yang[3] and Shun-Fen Tzeng[1]**

[1] *Institute of Life Sciences, College of Bioscience and Biotechnology, National Cheng Kung University, Tainan, Taiwan,* [2] *Department of Neurology, National Cheng Kung University Hospital, College of Medicine, National Cheng Kung University, Tainan, Taiwan,* [3] *Institute of Biomedical Engineering and Nanomedicine, National Health Research Institutes, Zhunan, Taiwan*

B-cell CLL/lymphoma 11B (Bcl11b) – a C2H2 zinc finger transcriptional factor – is known to regulate neuronal differentiation and function in the development of the central nervous system (CNS). Although its expression is reduced during oligodendrocyte (OLG) differentiation, its biological role in OLGs remains unknown. In this study, we found that the downregulation of Bcl11b gene expression in glial progenitor cells (GPCs) by lentivirus-mediated gene knockdown (KD) causes a reduction in cell proliferation with inhibited expression of stemness-related genes, while increasing the expression of cell cyclin regulator p21. In contrast, OLG specific transcription factors (Olig1) and OLG cell markers, including myelin proteolipid protein (PLP) and myelin oligodendrocyte glycoprotein (MOG), were upregulated in Bcl11b-KD GPCs. Chromatin immunoprecipitation (ChIP) analysis indicated that Bcl11b bound to the promoters of Olig1 and PLP, suggesting that Bcl11b could act as a repressor for Olig1 and PLP, similar to its action on p21. An increase in the number of GC^+- or PLP^+- OLGs derived from Bcl11b-KD GPCs or OLG precursor cells was also observed. Moreover, myelin basic protein (MBP) expression in OLGs derived from Bcl11b-KD GPCs was enhanced in hippocampal neuron co-cultures and in cerebellar brain-slice cultures. The *in vivo* study using a lysolecithin-induced demyelinating animal model also indicated that larger amounts of MBP^+-OLGs and PLP^+-OLGs derived from implanted Bcl11b-KD GPCs were present at the lesioned site of the white matter than in the scramble group. Taken together, our results provide insight into the functional role of Bcl11b in the negative regulation of GPC differentiation through the repression of OLG differentiation-associated genes.

Main Points:

(1) Bcl11b regulates glial progenitor proliferation via inhibition of cell cycle regulator p21.
(2) Bcl11b downregulation in glial progenitors promotes their differentiation into mature oligodendrocytes *in vitro* and *in vivo*.
(3) Bcl11b could bind to the promotor regions of cell cycle regulator p21, Olig1, and PLP1 to control the proliferation and differentiation of glial progenitors.

Keywords: Bcl11b, glia, oligodendrocytes, glial progenitors, differentiation and proliferation

Edited by:
Margaret Su-chun Ho, ShanghaiTech University, China

Reviewed by:
Shin Hyeok Kang, Temple University, United States
Christoph Wiegreffe, University of Ulm, Germany

****Correspondence:***
Shun-Fen Tzeng
stzeng@mail.ncku.edu.tw

Received: *09 October 2017*
Accepted: *03 January 2018*
Published: *24 January 2018*

Citation:
Wang C-Y, Sun Y-T, Fang K-M, Ho C-H, Yang C-S and Tzeng S-F (2018) Function of B-Cell CLL/Lymphoma 11B in Glial Progenitor Proliferation and Oligodendrocyte Maturation. Front. Mol. Neurosci. 11:4. doi: 10.3389/fnmol.2018.00004

INTRODUCTION

Oligodendrocytes (OLGs), myelin-producing glia cells in the CNS, not only support the structure and energy metabolism of axons, but also facilitate the propagation of action potentials by extending their cellular processes to form multilayered myelin sheaths (Nave and Werner, 2014; Kremer et al., 2016). OLGs have been known to arise from OLG precursor cells (OPCs) during development and in adults (Herrera et al., 2001; Zuchero and Barres, 2013; Mayoral and Chan, 2016; Yang et al., 2017). In general, in the early phase of OLG differentiation, pre-myelinating OLGs with numerous complex elongating processes are generated from OPCs, and express O4, 2′,3′-cyclic-nucleotide 3′-phosphodiesterase (CNPase) and galactocerebroside (GC) (Zhang, 2001). The pre-myelinating OLGs further differentiate into mature myelinating OLGs, which are able to encircle axons with their extensions to form compact multilayered myelin consisting of lipids and myelin-associated proteins (Czepiel et al., 2015). The major myelin proteins in the CNS are MBP and PLP. Meanwhile, MOG and myelin-associated glycoprotein (MAG) only constitute 1% of all CNS myelin proteins (Nave and Werner, 2014). The differentiation of OPCs toward mature OLGs is controlled by extrinsic and transcriptional programs. It is well-documented that a pair of basic helix-loop-helix (bHLH) transcriptional factors, together with Olig1, Olig2, and Sox10, are required for OLG specification and maturation (Lu et al., 2002; Stolt et al., 2002; Zuchero and Barres, 2013). In addition, axonal/glial secreted factors and neuronal activity are important for OLG maturation and myelination (Emery, 2010; Zuchero and Barres, 2013). The progenitors isolated from embryonic and postnatal CNS tissues have been reported to give rise to astrocytes in serum-containing medium, but differentiate into OLGs in defined medium (Raff et al., 1983; Yang et al., 2011, 2017). For this reason, such bipotential progenitor cells have been termed as glial progenitor cells (GPCs). Accordingly, GPCs and OPCs are widely used as the culture models to study the molecular regulation of oligodendrocyte differentiation.

B-cell chronic lymphocytic leukemia/lymphoma 11B (Bcl11b), also named Ctip2, is a C2H2 zinc finger protein, originally discovered in T lymphoblastic leukemia (Bernard et al., 2001), and identified as a tumor suppressor in hematopoietic malignancies. The molecule can regulate cell-cycle progression by acting as a repressor for the expression of cyclin dependent kinase (CDK) inhibitors, such as p21 (Cherrier et al., 2009; Grabarczyk et al., 2010; Karanam et al., 2010; Chen et al., 2012). Expressed Bcl11b has been found in mouse brain regions, including the neocortex, hippocampus, and striatum (Arlotta et al., 2005, 2008; Chen et al., 2008; Simon et al., 2012), and is involved in the development of mouse cortical-projection neurons and striatal neurons (Arlotta et al., 2005, 2008; Chen et al., 2008). Findings indicating that proliferating progenitors and post-mitotic dentate granule cells in the dentate gyrus declined in Bcl11b mouse mutants during postnatal development point to the important role of Bcl11b in the regulation of progenitor proliferation (Simon et al., 2012). Moreover, the lack of Bcl11b-impaired post-mitotic neuron differentiation in the hippocampus of a developing mouse (Simon et al., 2012) demonstrates that progenitor cell proliferation and differentiation in the developing CNS depend on Bcl11b expression. Despite Bcl11b expression being significantly higher in neurons than that detected in OPCs (Zhang et al., 2014), its levels in newly formed OLGs and myelinating OLGs were much lower than in OPCs. However, the involvement of Bcl11b in glial differentiation has not yet been identified.

In this study, we provide evidence in a rat model for the Bcl11b-mediated regulation of OLG maturation by using commercially available rat GPCs and OPCs prepared from rat embryonic cortex. To determine the functional role of Bcl11b in GPCs/OPCs and OLGs, lentivirus-mediated knockdown of Bcl11b (Bcl11b-KD) was first performed to effectively reduce Bcl11b expression in GPCs. The downregulation of Bcl11b not only suppressed GPC cell proliferation, but also reduced their stemness markers. Interestingly, Bcl11b-KD increased the expression of OLG cell markers (PLP and MOG), as well as the number of OLGs in the cultures. Moreover, MBP expression in OLGs derived from Bcl11b-KD GPCs was increased in the presence of neurons, which possibly could enhance neuronal interaction with OLGs from the Bcl11b-KD GPCs. These observations were also verified by implanting Bcl11b-KD GPCs into the lysolecithin-treated corpus callosum of adult rat brains. We also infer that the manipulation of Bcl11b expression in GPCs/OPCs could foster their differentiation toward mature OLGs in demyelinating CNS tissues.

MATERIALS AND METHODS

Materials

Media (DMEM/F12, MEM, Neurobasal medium), GlutaMAX^{TM}, StemPro® NSC SFM, B27 supplement, N2 supplement, poly-L-ornithine (PLO), and Lipofectamine 2000 were purchased from Invitrogen. Horse serum (HS) was obtained from HyClone Laboratories. Apotransferrin, biotin, bovine serum albumin (BSA), 5-bromo-2′-deoxyuridine (BrdU), cytosine arabinoside (Ara-C), diethylpyrocarbonate (DEPC), hydrocortisone, insulin, *N*-acetyl-cysteine (NAC), poly-D-lysine (PDL), sodium ampicillin, sodium pyruvate, sodium selenite, triiodothyronine (T3), and lysolecithin were obtained from Sigma. Ciliary neurotrophic factor (CNTF), epidermal growth factor (EGF), fibroblast growth factor-2 (FGF-2), and platelet derived growth factor-AA (PDGF-AA) were obtained from ProSpec. The antibodies used in this study are listed in **Table 1**.

Cell Culture

Rat glial progenitor cells (GPCs)

Glial progenitor cells prepared from cortical tissues of newborn Sprague-Dawley (SD) rats were purchased from Invitrogen (Cat no. N7746100). The cells, after passages, were seeded onto PLO-coated 100 mm petri dishes and maintained in the growth medium (GM) provided by the vendor (Wang et al., 2017). To induce the differentiation of GPCs into OLGs, the cultures were

TABLE 1 | The antibodies used in the study.

Antibodies	Manufacturer	Immunogen	Working dilution
Monoclonal mouse anti-APC (clone CC1)	Calbiochem (OP80)	Recombinant protein consisting of amino acids 1–226 of APC	1:50 (IF)
Monoclonal rat anti-Bcl11b	Abcam (ab18465)	Fusion protein of human Ctip2 amino acids 1–150 [25B6]	1:500 (WB)
Polyclonal rabbit anti-Bcl11b	Abcam (ab28448)	Synthetic peptide within residues 850–950 of human Bcl11b	1:200 (IF for rat brain)
Polyclonal rabbit anti-Bcl11b	Novus (NBP2-33549)	Recombinant protein: QGNPQHLSQRELITPEADHVEAAILEE DEGLEIEEPSGLGLMVGGPDPDLLTCG	1:200 (IF for mouse brain)
Monoclonal mouse anti-CNP	Covance (SMI-91R)	46 and 48 kDa subunit of 94 kDa myelin CNPase dimer (SMI-91)	1:2000 (WB) 1:200 (IF)
Monoclonal mouse anti-GAPDH	Millipore (MAB374)	Glyceraldehyde-3-phosphate dehydrogenase from rabbit muscle	1:2000 (WB)
Polyclonal rabbit anti-GC	Millipore (MAB342)	Synaptic plasma membranes from bovine hippocampus	1:200 (WB)
Monoclonal mouse anti-GFP	Millipore (MAB2510)	Bacterially expressed GFP fusion protein	1:200 (IF)
Polyclonal rabbit anti-GFP	Millipore (MAB3080)	Highly purified native GFP from Aequorea victoria	1:200 (IF)
Monoclonal mouse anti-MBP	Calbiochem (NE1018)	Purified human myelin basic protein with amino acids 70–89	1:1000 (WB) 1:200 (IF)
Polyclonal rabbit anti-MOG	Abcam (ab32760)	Synthetic peptide as within residues 200 to C-terminal of rat myelin oligodendrocyte glycoprotein	1:1000 (WB) 1:200 (IF)
Polyclonal rabbit anti-NG2	Millipore (AB5320)	Immunoaffinity purified NG2 Chondroitin Sulfate Proteoglyacan from rat	1:200 (IF)
Polyclonal goat anti-NF200	Millipore (AB5539)	Purified bovine neurofilament-heavy	1:500 (IF)
Polyclonal rabbit anti-OLIG2	Millipore (AB9610)	Recombinant mouse Olig2	1:200 (IF)
Monoclonal mouse anti-p21	Calbiochem (OP79)	Recombinant mouse p21 protein (clone 22)	1:1000 (WB)
Rabbit antiserum anti-PDGFaR	Upstate (06-216)	GST-fusion protein corresponding to the 110 C-terminal amino acid residues of mouse PDGF type A receptor	1:200 (IF)
Polyclonal rabbit anti-PLP	Abcam (ab28486)	Synthetic peptide as amino acids 109–128 of mouse myelin PLP	1:1000 (WB) 1:200 (IF)

IF, immunofluorescence; WB, western blot.

maintained for 5 days in OLG differentiation medium (DM), which contains basal components in the GM without growth factors.

Rat oligodendrocyte progenitor cells (OPCs)

Oligodendrocyte progenitor cells were prepared by modifying the protocol in (Fancy et al., 2012). Animal use followed the National Institutes of Health (NIH) Guidelines for Animal Research (Guide for the Care and Use of Laboratory Animals) and was approved by the National Cheng Kung University Institutional Animal Care and Use Committee, Tainan, Taiwan (IACUC approval number: 103060). Briefly, cortical tissues from SD rat embryos at 14.5 days were dissected and passed through a 40-μm pore filter. The cells were replated onto petri dishes without PDL coating, and cultured for 5–7 days in oligosphere medium – consisting of DMEM/F12 medium, 2% B27, 1% N2 supplement, 10 ng/ml FGF2, 10 ng/ml EGF, and 10 ng/ml PDGF-AA. After the formation of oligospheres, the OPCs were dissociated and plated onto PDL-coated dishes in growth medium (GM), as previously described (Wang et al., 2017). The cells were maintained for 5 days in OLG differentiation medium (DM) containing DMEM medium, 4 mM L-glutamine, 1 mM sodium pyruvate, 0.1% BSA, 50 μg/ml apotransferrin, 5 μg/ml insulin, 30 nM sodium selenite, 10 nM biotin, 10 nM hydrocortisone, 15 nM T3, 10 ng/ml CNTF, and 5 μg/ml NAC.

Rat hippocampal neurons

Hippocampal tissues were isolated from newborn SD rat, and digested by 0.25% trypsin solution containing DNase at 37°C for 30 min. The hippocampal cells were seeded onto PDL-coated coverslips (1×10^4 cells/coverslip) in Neurobasal medium with 2% B27, 0.25% GlutaMAX^{TM} and 10% HS. After a period of 1 h, the medium was replaced by Neurobasal medium with 2% B27 and 0.25% GlutaMAX^{TM}. Ara-C (1 mM) was added to the culture at day 4 to inhibit glia cell proliferation.

Lentivirus-Mediated shRNA Targeting Bcl11b

Previously, we found that the constructs of lentiviral vectors made in Biosettia (San Diego, CA, United States) were highly efficient in the inhibition of Bcl11b (NM_001277287) in rat

glioma cells (Liao et al., 2016). Thus, we used the same lentiviral vector constructs for this study: pLV-mU6-EF1a-GFP-Puro-scramble (lenti-ctrl); and, pLV-mU6-EF1a-GFP-Puro-shBcl11b-916 (lenti-shBcl11b). The shRNA sequences are shown in **Table 2**. For gene transduction, GPCs/OPCs (1×10^6 cells/dish) were seeded onto 60-mm petri dishes in GM, and lentiviruses (300 μl/dish) carrying shRNA against Bcl11b and scramble lentiviruses were separately added into the medium for 24 h. The shRNA genes were allowed to express for 48 h, and the transfectants were selected in the presence of puromycin (3 μg/ml), also for 48 h. The efficiency of the lentiviral particles for Bcl11b downregulation in the GPCs was confirmed by quantitative polymerase chain reaction (QPCR) and western blotting. GPCs infected by lenti-ctrl were referred to as 'scramble,' while cells infected by lenti-Bcl11b-KD were called 'Bcl11b-KD'.

Quantitative Real-Time Polymerase Chain Reaction

The RNA (1 μg/sample) isolated from the GPCs and OPCs was reacted with M-MLV reverse transcriptase (Invitrogen) to generate cDNA, and then incubated with SYBR Green reagents (Roche) and specific primers (**Table 2**). The expression level of GAPDH was used as an internal control. StepOne Software v2.1 (Applied Biosystems) was used to determine the cycle-threshold (Ct) fluorescence values. The expression level of the target genes relative to the internal control was presented as $2^{-\Delta CT}$, where $\Delta CT = (Ct_{target} - Ct_{GAPDH})$.

TABLE 2 | Primer sequences for QPCR analysis and Sequences for shRNA against rat Bcl11b.

Gene	Sequence
Rat Bcl11b (NM_001277287)	Forward (5′→3′): GCAGTCCAACCTAACCTGTGTC Reverse (5′→3′): GGGTGCCTTAATCAACCCTCAG
Rat CD133 (NM_021751)	Forward (5′→3′): CCAGCGGCAGAAGCAGAACGA Reverse (5′→3′): GTCAGGAGAGCCCGCAAGTCT
Rat Sox2 (NM_001109181)	Forward (5′→3′): CACAACTCGGAGATCAGCAA Reverse (5′→3′): CGGGGCCGGTATTTATAATC
Rat Bmi-1 (NM_001107368)	Forward (5′→3′): GCGTTACTTGGAGACCAGCA Reverse (5′→3′): CTTTCCGATCCGACCTGCTT
Rat Hes1 (NM_024360)	Forward (5′→3′): TACCCCAGCCAGTGTCAACA Reverse (5′→3′): TCCATGATAGGCTTTGATGACTTTC
Rat Hey1 (NM_001191845)	Forward (5′→3′): AGCGCAGACGAGAATGGAAA Reverse (5′→3′): CGCTTCTCGATGATGCCTCT
Rat Hey2 (NM_130417)	Forward (5′→3′): CTTGACAGAAGTGGCGAGGT Reverse (5′→3′): CATTGGGTTGGAGCAGGGAT
Rat p21 (NM_080782)	Forward (5′→3′): TGGACAGTGAGCAGTTGAGC Reverse (5′→3′): ACACGCTCCCAGACGTAGTT
Rat Olig1 (NM_021770)	Forward (5′→3′): GAGGGGCCTCTTTCCTTGTC Reverse (5′→3′): ACCGAGCTTCACAAGCCTAC
Rat Olig2 (NM_001100557)	Forward (5′→3′): GCTTAACAGAGACCCGAGCC Reverse (5′→3′): GTGGCGATCTTGGAGAGCTT
Rat MBP (NM_001025291)	Forward (5′→3′): GTGGGGGTAAGAGAAACGCA Reverse (5′→3′): CGAACACTCCTGTGGAACGA
Rat PLP (NM_030990)	Forward (5′→3′):GGCGACTACAAGACCACCAT Reverse (5′→3′):AATGACACACCCGCTCCAAA
Rat NFATc3 (NM_001108447)	Forward (5′→3′):TCTGACTTGGAACACCAGCC Reverse (5′→3′): AAGCAGTCAGAGCAGTTGGT
Rat MOG (NM_022668)	Forward (5′→3′): CCCAGCGCTTCAACATTACG Reverse (5′→3′): GCACCTAGCTTGTTTGTGTCTG
Rat GAPDH (NM_017008)	Forward (5′→3′): TCTACCCACGGCAAGTTC Reverse (5′→3′): GATGTTAGCGGGATCTCG
Scramble shRNA	GCAGTTATCTGGAAGATCAGGTTGGATCCAAC CTGATCTTCCAGATAACTGC
shBcl11b-916 (NM_001277287: nt637-656)	AAAAGAGCCTTCCAGCTACATTTGTTGGATCCA ACAAATGTAGCTGGAAGGCTC

Immunofluorescence

After harvesting, the cells were fixed in 4% paraformaldehyde for 10 min, and incubated in PBS containing 0.1% Triton-X100 for 30 min. The cultures then were incubated overnight at 4°C with primary antibodies (**Table 1**). To stain galactoceramide (GC), a major glycolipid of myelin, the cultures were directly incubated with anti-GC antibody after fixation with 4% paraformaldehyde, but without permeabilization by 0.1% Triton-X100. Alternatively, to carry out double immunofluorescence for NF200 (or GFP) and MBP (or PLP), the cultures were incubated with anti-NF200 (or anti-GFP) at 4°C overnight, and then with anti-MBP (or anti-PLP) at RT for 3 h. After reacting with the primary antibodies, appropriate secondary antibodies and FITC-avidin were added to the cultures at RT for 1 h and for 45 min, respectively. The immunostained cells were photographed under a Nikon E800 epifluorescence microscope equipped with a CCD camera and also under an Olympus FluoView laser scanning confocal microscope (FV1000, Japan).

Evaluation of Oligodendrocytic Differentiation

In addition to the morphological observations of OLG differentiation from GPCs or OPCs, OLG differentiation was evaluated by measurement of OLG cell-marker expression intensity, as described previously (Wang et al., 2017). MetaXpress software (Molecular Devices; Sunnyvale, CA, United States) and NIH ImageJ analysis software were used. Five randomly selected images (5–10 cells per image) were captured from each immunostained culture using the above-mentioned epifluorescence microscope with a 40X objective lens. The experiments were repeated in triplicate, and 70–100 cells in total per group were counted. The number of processes and branches per cell, the average length of the processes, and the total length of the outgrowing processes per cell in each field were quantified. The immunofluorescent intensity per cell and the number of immunostained cells in each field were also measured. The results are presented as the percentage of the data obtained from the Bcl11b-KD culture versus data from the scramble culture.

Western Blot Analysis

GPCs and OPCs were replated at a density of 1×10^6 cells/60-mm onto petri dishes for various experiments. After harvesting, the total protein content (100 μg) was extracted from the cultures and lysis buffered in 1% NP-40, 1% Triton-X100, and 0.1% SDS, which it was loaded onto 10% SDS polyacrylamide gel. After electrophoresis, the protein was transferred to a nitrocellulose membrane and immunoblotted overnight at 4°C with primary antibodies (**Table 1**). The immunoblotted

membrane was incubated with secondary antibodies conjugated with peroxidase for 60 min at RT. The signal was detected by chemiluminescence using the ECL-Plus detection system (PerkinElmer Life Sciences).

Cell Growth Assays

MTT colorimetric assay, gliosphere formation assay, and colony formation assay were performed as described previously (Fang et al., 2014). GPCs and OPCs were maintained in GM either for different time periods (MTT assay), or for 7 days (gliosphere and colony formation assays). The cell proliferation of the GPCs in GM after 48 h was also examined using BrdU incorporation assay via the addition of BrdU (10 μM) into the culture 12 h before harvesting, following the previously described procedure (Wang et al., 2015). The number of gliospheres, colonies, and $BrdU^+$ cells in the culture were counted using ImageJ analysis software (NIH, United States).

TABLE 3 | Primer sequences for ChIP-QPCR analysis.

Promoter	Sequence
Rat *p21* (+2862 ~ +2944) [Gene ID: 114851]	Forward (5′→3′): GCCCCTTTCTAGCTGTCTGG Reverse (5′→3′): GCTCCTTCACCCATCCCTG
Rat *Olig1* (−1864 ~ −1763) [Gene ID: 60394]	Forward (5′→3′): CGTACCGCTTATGTGCAGGG Reverse (5′→3′): ACCCTACATTCCTAGCCATCG
Rat *Olig1* (−1487 ~ −1264) [Gene ID: 60394]	Forward (5′→3′): CTGATAGCTGTGAGGGTGAAG Reverse (5′→3′): CCCAGATGCTGGGAATACAA
Rat *Olig1* (−1121 ~ −1030) [Gene ID: 60394]	Forward (5′→3′): TGAGCCAGCCACTAAAAGACA Reverse (5′→3′): CTTCATCCTGGGGTGTCTGC
Rat *Olig1* (−575 ~ −502) [Gene ID: 60394]	Forward (5′→3′): CAAAAGCTAACAAGTCCCGATCA Reverse (5′→3′): CGCAGTTCAGTCGTTAAAACACC
Rat *Olig1* (−399 ~ −261) [Gene ID: 60394]	Forward (5′→3′): CAGCTACAGCAGTTCCCAGT Reverse (5′→3′): CTAGTTCAGCGGGTCATGCT
Rat *Olig1* (−240 ~ −147) [Gene ID: 60394]	Forward (5′→3′): GCCCTATAAAGCTCCCTCCC Reverse (5′→3′): CAGCCAGAGTTGCCAGAGAT
Rat *Plp* (−1521 ~ −1423) [Gene ID: 24943]	Forward (5′→3′): GATCAGTGGGAGTGTGCAGG Reverse (5′→3′): CACTCTCCCCTGTCCCCTAA
Rat *Plp* (−1173 ~ −1065) [Gene ID: 24943]	Forward (5′→3′): AGTCCCAGAGATGCTCCTGA Reverse (5′→3′): GAGGGGAATCAAGCAGCCAA
Rat *Plp* (−982 ~ −862) [Gene ID: 24943]	Forward (5′→3′): GCTGCACTTTCGTAACAGGC Reverse (5′→3′): AGGTAGTAGCTTCCCAGGGT
Rat *Plp* (−625 ~ −433) [Gene ID: 24943]	Forward (5′→3′): TCTTGAGCCTGGTCACACAC Reverse (5′→3′): AGTTGGCCTTGACCATGGAA
Rat *Plp* (−368 ~ −266) [Gene ID: 24943]	Forward (5′→3′): TCCTCACCAGGGCTACCATT Reverse (5′→3′): AGGGGTCCTTAAATCCTCCCA
Rat *Plp* (−40 ~ −109) [Gene ID: 24943]	Forward (5′→3′): TTTAAGGGGGTTGGCTGTCA Reverse (5′→3′): AGTCTGTTTTGCGGCTGACT

Chromatin Immunoprecipitation

A chromatin immunoprecipitation (ChIP) assay kit (Millipore) was employed, the experimental procedure for which was based on the manual provided by the vendor. Briefly, GPCs were seeded at a density of 1×10^7 cells/100-mm petri dish for 2 days in GM. After 1% formaldehyde was added into the medium, the cells were removed and suspended in a cell-lysis buffer. After centrifugation, the resulting cell pellet was resuspended in a nuclear-lysis buffer for 10 min. The sample was then sonicated to produce DNA fragments at lengths of 200–600 bp, followed by incubation with anti-Bcl11b antibodies (or isotype IgG as negative control) and protein A/G magnetic beads at 4°C overnight. DNA-protein complexes were collected and treated by proteinase K at 62°C for 2 h. After DNA purification, the DNA fragments that potentially interacted with Bcl11b were analyzed by QPCR using specific primers (**Table 3**). Results from samples that had reacted with mouse isotype IgG (IgG) are referred to as negative control.

Assessments of *in Vitro* Co-culture of GPCs and Neurons

After hippocampal neurons were cultured for 7 days, GPCs at the density of 1×10^4 cells per coverslip were added into the hippocampal culture, and maintained in Neurobasal medium with 2% B27, 0.25% GlutaMAX™ and T3 (30 ng/ml) for 7 days. The hippocampal neuron-OLG co-cultures were subjected to double immunofluorescence for NF200 and MBP. The assessments followed the methods described in our previous study (Wang et al., 2017). The intensity of MBP fluorescence, which overlapped with a neuronal fiber featuring immunoreactivity to NF200, was quantified using NIH ImageJ analysis software. Additionally, to further verify the overlap of the MBP^+-OLG process with the NF200-immunostained fiber, the cultures were subjected to confocal imaging analysis to acquire a z-stack reconstructed from 7 sequential images at 1-μm intervals. 3D images, including x-z and y-z views, were obtained from the same z-stack to identify the overlapping regions of MBP- and NF200-immunostaining.

Cerebellar Slice Culture

The *ex vivo* cerebellar slice culture was modified and performed according to a previous study (Lee et al., 2015). Briefly, the rat sagittal-cerebellar slices at P7 were dissected at a thickness of 350 μm using a Microslicer™ DTK-1000 vibratory tissue slicer. The tissue slices were then plated on Millicell-CM culture inserts (Millipore, 0.4 μm) and maintained on the surface of the slice culture medium (50% MEM with Earle's salts, 35% Earle's balanced salt solution, 15% heat-inactivated horse serum, 1% GlutaMAX™) at 37°C for 9 days. The scramble and Bcl11b-KD GPCs were seeded onto a cerebellar slice at a number of 1×10^5 cells/slice. After 48 h, the scramble GPCs/cerebellar slice and Bcl11b-KD GPCs/cerebellar slice cultures were fixed with 4% paraformaldehyde and permeabilized by 0.3% Triton X-100 in PBS, followed by immunofluorescence for MBP and NF200.

GPC Transplantation Followed by Lysolecithin Injection

Adult male SD rats (250 ± 30 g) were anesthetized by intraperitoneal injection of chloral hydrate (50 mg/kg) and placed in a stereotaxic frame (Stoelting). A midline incision was made and the underlying tissue removed using a scalpel. A hole was drilled in the exposed skull by a dentist drill fitted with a 0.9 mm diameter carbide dental burr at 2 mm to the right of the sagittal suture. A Hamilton syringe with a 25-gauge needle was inserted 2.5 mm into the brain (corpus callosum). The fluid (5 μl) containing 1% lysolecithin was slowly injected into the brain. After injection, the needle was maintained in place for 2 min to prevent leakage. At 3 days post injection (dpi), the hole was re-exposed, and 1×10^5 GPCs in 5 μl PBS were injected into the brain at the same position. At 14 dpi, the rats were sacrificed and their brains removed. The brain tissues were fixed in 4% paraformaldehyde, and then cryoprotected in 30% (w/v) sucrose in PBS. The tissues were embedded in Tissue Tek OCT (Electron Microscopy Sciences), sectioned with a 15-μm thickness, and then subjected to immunofluorescence as described above.

Statistical Analysis

The statistical significance of the differences between the two groups of data was analyzed by a two-tailed unpaired Student's *t*-test, with all data expressed as means ± SEM. In all comparisons, differences were statistically significant at $p < 0.05$.

RESULTS

Reduced Stemness and Proliferation of Glial Progenitor Cells by Downregulation of Bcl11b Expression under the Growth Condition

The findings indicated that Bcl11b is highly expressed in mouse cortical neurons and hippocampal dentate gyrus granule neurons (Arlotta et al., 2005; Simon et al., 2012). Here, through immunofluorescence, we showed that Bcl11b expression was co-localized to $CC1^+$-OLGs in the corpus callosum, as well as $Olig2^+$-OLG lineage cells and $NG2^+$-glial progenitor cells (GPCs) in the subventricular zone (SVZ) of the rat brain (Supplementary Figure S1). *In vitro* examination showed that Bcl11b was produced in $A2B5^+$- and $NG2^+$-rat GPCs (Supplementary Figure S2A). Bcl11b expression was also detectable in $CNPase^+$-OLGs generated from rat GPCs (Supplementary Figure S2A). The mRNA levels of Bcl11b in neurons and distinct glial cells were also confirmed using primary cultures. Although Bcl11b showed considerable expression in neurons, OPCs were found to express only a moderate level of Bcl11b (Supplementary Figure S2B).

To determine the function of Bcl11b in GPCs and OLGs, we performed lentivirus-mediated shRNA delivery against Bcl11b expression (Bcl11b-KD) in GPCs. Lenti-Bcl11b shRNA efficiently downregulated Bcl11b mRNA expression (**Figure 1A**) and protein production (**Figure 1B**) in GPCs compared to what we

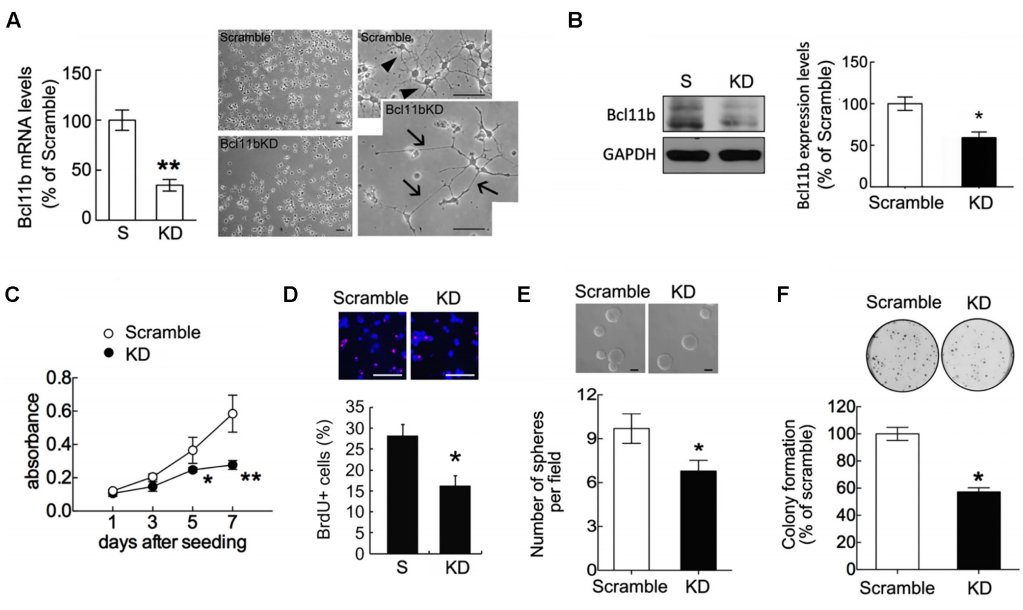

FIGURE 1 | Reduction in GPC cell proliferation after Bcl11b gene downregulation. GPCs were infected by lenti-ctrl (scramble) and lenti-shBcl11b (Bcl11b-KD) as described in section "Materials and Methods." The efficiency of Bcl11b downregulation in Bcl11b-KD GPCs was confirmed using QPCR for the measurement of Bcl11b mRNA expression **(A)** and western blot assay for Bcl11b protein production **(B)**. The phase-contrast images with low (left-panel) and high (right-panel) magnification were taken to examine the morphological change of GPCs after Bcl11b-KD **(A)**. Arrows in **(A)** indicate elongating processes extending from Bcl11b-KD GPCs compared to those of scramble GPCs (arrowheads). Scramble and Bcl11b-KD GPCs maintained in GM were subjected to MTT analysis **(C)**, BrdU incorporation assay **(D)**, sphere formation **(E)**, and colony formation assays **(F)**. Data are presented as means ± SEM of repeated independent experiments (n = 3–4). *$p < 0.05$, **$p < 0.01$ vs. scramble. Scale bar in **(A)** and **(D)** 50 μm; in **(E)** 100 μm.

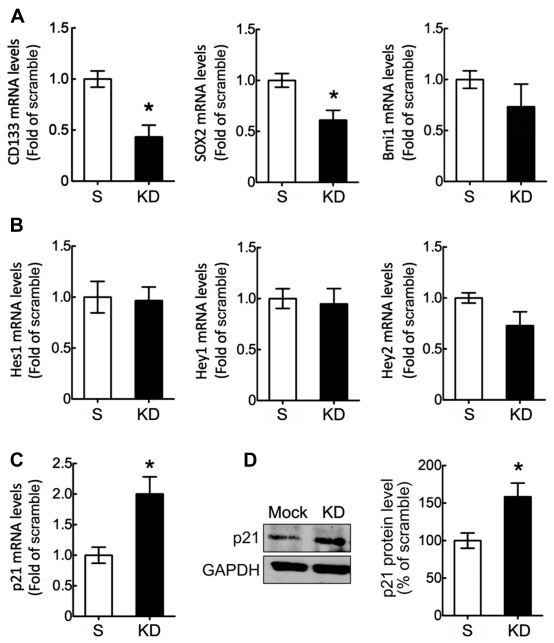

FIGURE 2 | Downregulation of stemness-related genes in GPCs by Bcl11b knockdown. Scramble and Bcl11b-KD GPCs were maintained in GM for 48 h, and then subjected to QPCR analysis for the measurement of stemness-associated genes including CD133, Sox2, and Bmi1 **(A)**, as well as the effector genes (Hes1, Hey1, and Hey 2) of Notch signaling **(B)**. The expression of p21 mRNA in scramble and Bcl11b-KD GPCs was examined using QPCR **(C)**. Moreover, total proteins were extracted from scramble and Bcl11b-KD GPCs in GM for 48 h, and then subjected to western blotting **(D)** to measure p21 protein production. The intensity of immunoreactive bands corresponding to p21 and GAPDH as a loading control was quantified by ImageJ software. Data shown in **(A–D)** are presented as means ± SEM of the three independent experiments. $^*p < 0.05$ vs. the scramble.

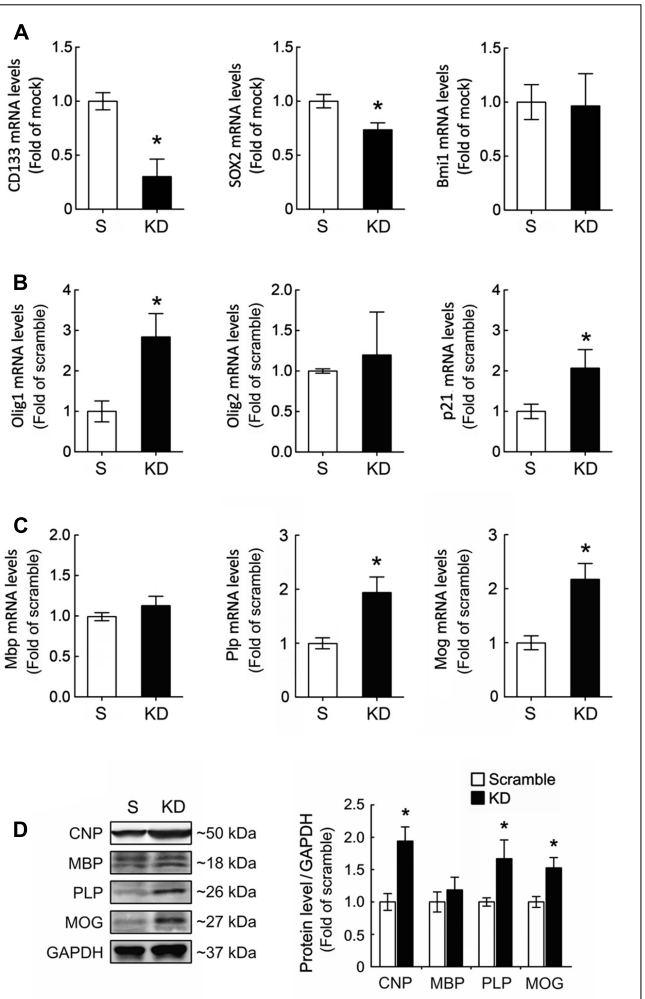

FIGURE 3 | Upregulation of Olig1 and p21 expression in GPCs after Bcl11b gene downregulation. **(A)** Scramble and Bcl11b-KD GPCs were cultured in DM for 48 h, and then subjected to QPCR analysis for the measurement of stemness-associated genes, CD133, Sox2, and Bmi1. **(B,C)** Moreover, transcription factor-associated OLG differentiation (i.e., Olig1 and Olig2), p21, and myelin-related genes were examined by QPCR analysis. **(D)** In addition, total proteins were extracted from scramble and Bcl11b-KD GPCs cultured in DM for 5 days, and then subjected to western blot analysis for the examination of OLG cell markers, CNPase, MBP, PLP, and MOG. The intensity of immunoreactive bands shown in the right panel was quantified by ImageJ software, and normalized by the level of GAPDH that is as a loading control. Data are presented as means ± SEM of the three independent experiments. $^*p < 0.05$ vs. the scramble.

observed in GPCs infected by lenti-ctrl (scramble). In addition, it was observed that the morphology of the GPCs had altered into a shape with elongated processes after Bcl11b-shRNA transduction (**Figure 1A**, arrows). The examination of GPC cell growth at different times by MTT analysis or after 24 h by BrdU incorporation assay indicated that GPC cell growth was reduced in the GM after Bcl11b downregulation (**Figures 1C,D**). Moreover, the ability of GPCs to form glial spheres and colonies declined after Bcl11b-KD (**Figures 1E,F**).

Based on our previous findings that Bcl11b-KD reduced the expression of stemness-related genes (Sox2 and Bmi1) in glioma cells (Liao et al., 2016), we also examined the expression of stemness-related genes in the scramble and Bcl11b-KD cultures. As shown in **Figure 2**, the expression of Sox2 – but not of Bmi1 – was reduced in Bcl11b-KD GPCs compared to that detected in the scramble culture. Moreover, we found that CD133, a stem-cell marker, was downregulated in the GPCs after Bcl11b-KD (**Figure 2A**). These data reveal that Bcl11b actively participates in the regulation of GPC cell proliferation. Findings in a separate study indicated that Bcl11b can trigger early differentiation of epidermal keratinocytes by binding to the Notch1 promoter to promote the expression of Notch1 (Zhang et al., 2012). Thus, we examined the expression of Notch downstream genes (Hes1, Hey1, and Hey2) in the GPCs cultured in GM for 48 h. The results indicated that the change in the expression of the three genes was insignificant in both the scramble and Bcl11b-KD GPCs (**Figure 2B**).

Given that Bcl11b can bind to the Sp1 promoter binding site of the cell cycle repressor p21 to cause p21 gene silencing (Cherrier et al., 2009), the p21 mRNA expression in Bcl11b-KD GPCs was compared to that detected in the scramble GPCs. The results showed that p21 mRNA expression and its protein

production were significantly increased in the GPCs after Bcl11b-KD (**Figures 2C,D**). These results suggest that the reduced cell proliferation of GPCs in GM might be due to the increased effect of p21 after Bcl11b downregulation.

Upregulation of OLG-Specific Gene Expression in GPCs after Bcl11b Gene Knockdown

Our findings, as indicated above, raise the question of whether Bcl11b-KD induced the cell death of GPCs or instructed the GPCs toward the differentiation of OLGs. Since the cell death of GPCs with Bcl11b-KD in GM or in DM was not observed (data not shown), we next evaluated the differentiation ability of GPCs after Bcl11b-KD. When GPCs were cultured in DM for 48 h to induce OLG differentiation, the expression of stemness-related genes (i.e., CD133 and Sox2) was significantly reduced compared to the scramble culture (**Figure 3A**). No change was observed in Bmi1 expression after Bcl11b-KD. Examination of Olig1 and Olig2, two critical bHLH transcription factors specific for OLG differentiation, indicated that Bcl11b-KD caused the upregulation of Olig1, but not of Olig2 (**Figure 3B**). This also provides evidence that Bcl11b-KD can promote OLG lineage specification. Moreover, an increase in p21 gene expression was observed when Bcl11b-KD GPCs were cultured in DM (**Figure 3B**). Furthermore, our results showed that Bcl11b-KD induced upregulated gene and protein expression of myelin proteolipid protein (PLP) and myelin oligodendrocyte glycoprotein (MOG), which are myelin proteins in mature OLGs (**Figures 3C,D**). However, MBP mRNA and protein expression was not affected by Bcl11b-KD (**Figures 3C,D**). In addition, the protein level of CNPase, a myelin-associated enzyme and a marker for OLG differentiation, was upregulated in the Bcl11b-KD culture (**Figure 3D**). These results reveal that Bcl11b-KD in the GPCs increased the expression of crucial proteins associated with the progression of the OLG lineage.

Interaction of Bcl11b with the Promoter Regions of Olig1 and PLP

It has been reported that Bcl11b is associated with the Sp1 binding sites containing the p21 promoter, and acts as a repressor for p21 expression (Cherrier et al., 2009). Through ChIP analysis, we verified that Bcl11b can bind to the Sp1 sequence located at the p21 promoter in the scramble GPCs (**Figure 4**). This finding reflects our observations of an increased expression of p21 in the GPCs after Bcl11b-KD (**Figure 2**). Through the ChIP method combined with high-throughput sequencing, the potential DNA binding sequences of Bcl11b have been identified (Tang et al., 2011). Accordingly, we used a nucleotide blast search for these potential Bcl11b binding sites on the Olig1 and Plp1 promoters, for which 6 and 7 potential segments were predicated for Bcl11b binding to within 2000 nt upstream sequences of the Olig1 and Plp1 promoters, respectively (**Figure 4**). To examine if Bcl11b can interact with the promoter of Olig1, ChIP experiments were performed using 6 designed primer pairs for the Bcl11b binding sites at the Olig1 promoter in both the scramble and Bcl11b-KD cultures (**Figure 4A**). The ChIP assay using anti-Bcl11b in combination with QPCR indicated that Bcl11b had a strong interaction with the segment ($-1487 \sim -1264$ bp) encompassing two predicted Bcl11b binding sites located at the Olig1 promoter (**Figure 4A**). This interaction, however, declined in Bcl11b-KD GPCs. In addition, Bcl11b was able to bind to the sequence at $-625 \sim -433$ bp of the Plp1 promoter in both cultures (**Figure 4B**), despite reduced binding being observed in Bcl11b-KD GPCs. Taken together, these findings, in conjunction with the results that Bcl11b-KD caused the upregulation of Olig1 and PLP in the GPCs, suggest

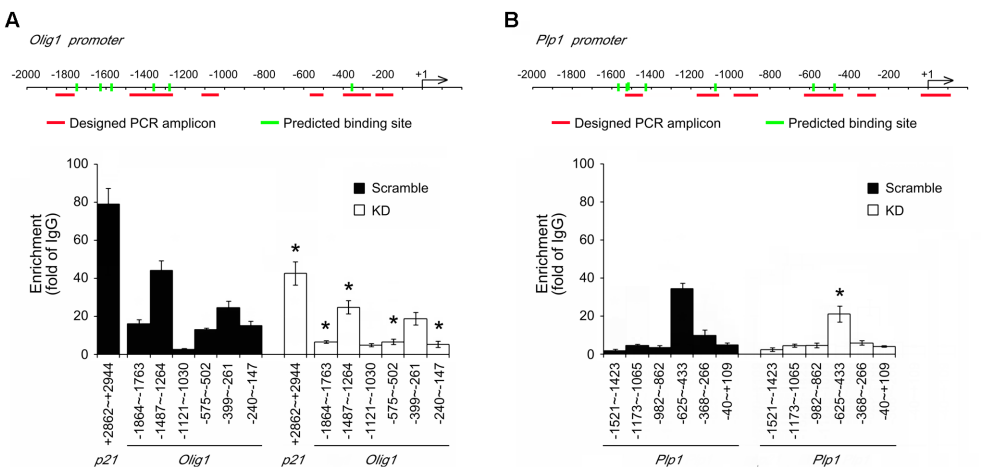

FIGURE 4 | Identification of potential Bcl11b binding regions located in Olig1 and Plp1 promoters. ChIP assay was conducted as described in Section "Materials and Methods" to verify the predicted Bcl11b binding sites located at the promoter regions of Olig1, Plp1 and p21. The predicted Bcl11b binding sites are labeled as green rods. The primers that match to the flanking regions indicated by red lines in Olig1 **(A)** and Plp1 **(B)** promoters were designed and synthesized. ChIP products prepared from scramble and Bcl11b-KD GPCs were analyzed by QPCR using the synthesized primers. The data shown in **(A,B)** are normalized over those obtained from IgG samples. Interaction of Bcl11b and p21 promoter is referred to be a positive control. Data are presented as means ± SEM of the four independent experiments. $^*p < 0.05$ vs. the scramble.

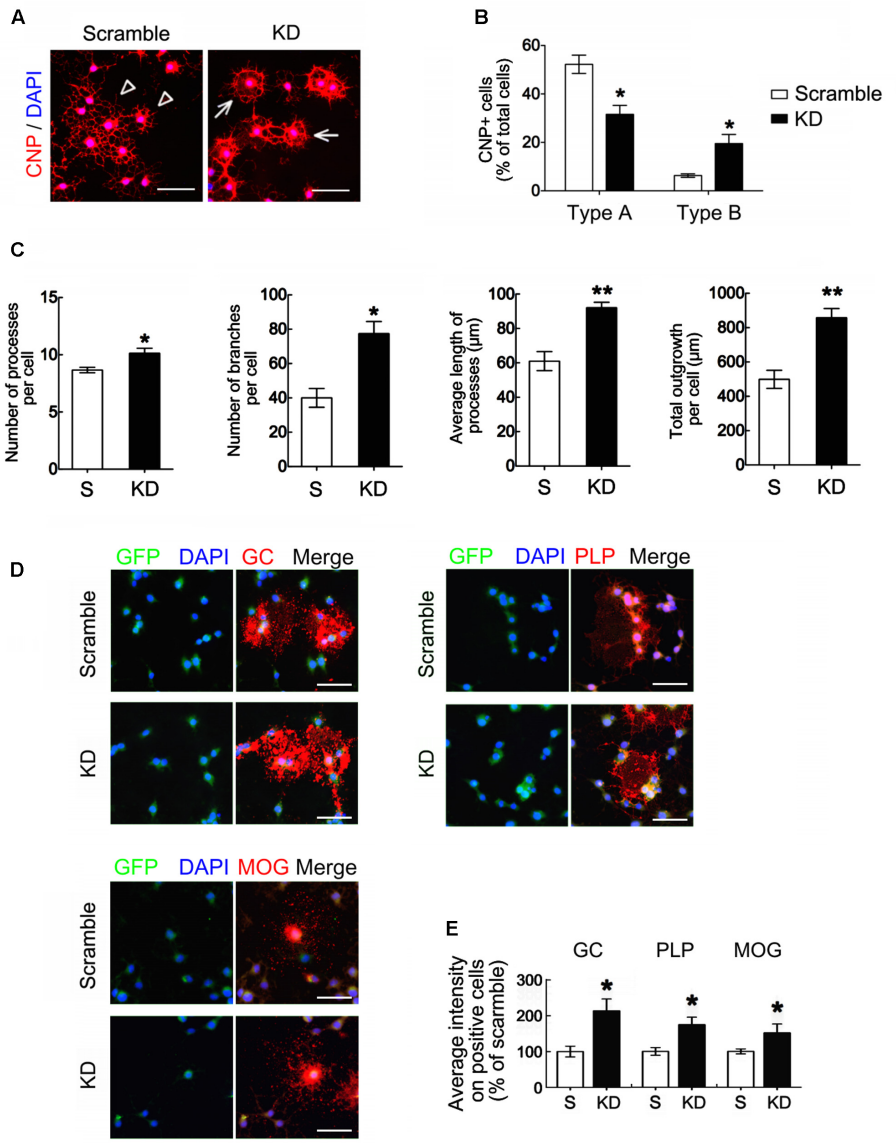

FIGURE 5 | Oligodendrocyte differentiation and maturation enhanced by Bcl11b gene knockdown. **(A,B)** Scramble and Bcl11b-KD GPCs were seeded and maintained in DM for 5 days. The cultures were subjected to immunofluorescence using anti-CNPase antibody **(A)**. Arrowheads indicate the differentiated cells with branching processes (type A). Arrows point to the cells extending the processes to form a ring-shaped network (type B). $CNPase^{+}$-Type A and $CNPase^{+}$-Type B cells in scramble and Bcl11b-KD cultures were quantified using ImageJ software **(B)**. **(C)** The images taken from scramble and Bcl11b-KD cultures were further analyzed by MetaXpress software to measure the number of cell processes per cell, the branching numbers per cell, the average length per process, and the total process length per cell. **(D,E)** Scramble and Bcl11b-KD cultures were subjected to double immunofluorescence for GC, PLP, and MOG, combined with GFP as well as DAPI nuclear counterstaining **(D)**. The immunofluorescent intensity of each immunoreactive cell in the cultures was measured using ImageJ software **(E)**. Data are presented as means ± SEM of at least three independent experiments (n = 70–100 cells per group). *$p < 0.05$ vs. the scramble. Scale bar in **(A,D)**, 50 μm.

that Bcl11b might act as a transcriptional repressor of these genes.

Enhanced Differentiation of GPCs toward OLGs by the Downregulation of Bcl11b Gene Expression

We used immunofluorescence to compare the morphological differences between the OLGs generated from the scramble GPCs and those from the Bcl11b-KD GPCs. The cultures were maintained in DM for 5 days to stimulate the differentiation of OLGs from GPCs. Through CNPase immunostaining, we observed that the OLGs generated from the scramble GPCs and those from the Bcl11b-KD GPCs had a shape with either multi-polar interconnected fine processes, termed as Type A (**Figure 5A**, arrowheads), or formed a ring-like structure of complex interwoven thick processes, named as Type B (**Figure 5A**, arrows). The process thickness was

1.60 ± 0.13 μm for Type A, and 3.10 ± 0.31 μm for Type B (Type A vs. Type B, $p < 0.001$). The number of CNPase$^+$-OLGs with the Type B shape was significantly higher in the Bcl11b-KD culture than in the scramble culture (**Figure 5B**). These results indicate that Bcl11b-KD changed the morphology of the OLGs derived from GPCs toward a more complex and mature shape. In addition, Bcl11b-KD increased the number of OLG processes and process branches per cell (**Figure 5C**). Increases in the average length of the cell processes and in the total process length per cell were observed (**Figure 5C**). In addition, a stronger GC immunoreactivity was observed in the OLGs derived from the Bcl11b-KD GPCs (**Figures 5D,E**). MOG and PLP immunofluorescence also showed enhanced differentiation of Bcl11b-KD GPCs toward mature OLGs when these cells were cultured in DM over 5 days.

We also used neural stem cells (NSCs) prepared from rat cortical tissues at E14 to generate OPCs. The efficiency of Bcl11b-KD in the OPCs by lentiviruses was examined (**Figures 6A,B**). Note that there was approximately 95% PDGFRα$^+$-cells in the scramble and Bcl11b-KD cultures maintained in GM (Supplementary Figure S3A). Bcl11b-KD causes decreased cell growth and sphere formation of the OPCs, which is comparable with the results from the GPCs (**Figures 6C,D**). Moreover, the findings were verified by Ki67 immunostaining, which showed lower amount of Ki67$^+$/GFP$^+$-cells in the Bcl11b-KD culture than that seen in the scramble culture (Supplementary Figure S3B). The morphology of CNPase$^+$-OLGs differentiated from the scramble NSCs is shown in **Figure 6E** (arrowheads). In comparison, the CNPase$^+$-OLGs generated from the NSCs that received Bcl11b-KD, showed elongated processes with a complex structure (**Figure 6E**, arrows). The total outgrowth length per CNPase$^+$-OLG from the Bcl11b-KD NSCs was greater than that of the CNPase$^+$-OLGs generated from the scramble culture (**Figure 6F**). In addition, the GC$^+$-OLGs had visible cell processes extending from their cell bodies (**Figure 6E**, arrows), and were more numerous in the Bcl11b-KD culture than in the scramble culture (**Figure 6F**). Increased GC immunoreactivity and GC$^+$-cell number in the Bcl11b-KD cultures were also observed (**Figures 6G,H**). Moreover, PLP$^+$-OLGs derived from Bcl11b-KD NSCs displayed a cell form with more complex processes (**Figure 6E**, arrows) compared to those observed in the scramble culture (**Figure 6E**, arrowheads). Furthermore, although an increase in PLP immunoreactivity and the number of PLP$^+$ cells was detected in the Bcl11b-KD culture (**Figures 6G,H**), Bcl11b-KD did not change the expression of MBP. These results demonstrate that the downregulation of Bcl11b gene expression in GPCs and NSCs caused an upregulation of GC and PLP, and promoted the differentiation of premyelinating OLGs.

A co-culture of GPCs with rat hippocampal neurons was established to further evaluate the effect of Bcl11b on OLG maturation. The co-culture was incubated for 7 days, and then subjected to double immunofluorescence for the identification of OLGs and neurons using anti-MBP and anti-NF200, respectively. The results displayed NF200$^+$-neuronal fibers covered by MBP$^+$-cell processes extending from the Bcl11b-KD OLGs (**Figures 7A,B**, arrows). By comparison, NF200$^+$-neuronal fibers were not covered to the same degree by the scramble OLGs (**Figures 7A,B**, arrows). Quantitative analysis also showed that the intensity of the MBP immunofluorescence overlapping onto the NF200$^+$-neuronal fibers in the Bcl11b-KD co-culture was higher than that in the scramble co-culture (**Figure 7B**). The 3D reconstruction imaging (xy, xz, and yz planes) from the serial confocal images further verified the intensive MBP immunoreactivity overlaid onto the NF200$^+$-neuronal fibers in the Bcl11b-KD co-culture (**Figure 7C**, arrows). In contrast, weak MBP immunofluorescence spotted around the NF200$^+$-neuronal fibers was seen in the scramble GPC/neuronal co-culture (**Figure 7C**, arrows). Moreover, the Bcl11b-KD GPCs were seeded onto *ex vivo* cerebellar-slice cultures for further examination. The Bcl11b-KD GPC/cerebellar tissue-slice co-culture displayed more MBP$^+$ processes over NF200$^+$ fibers compared to that in the scramble culture (**Figure 7D**). These observations further confirm that Bcl11b downregulation can progress OLG maturation.

Differentiation of Bcl11b-KD OLGs *in Vivo*

An *in vivo* model of focal demyelination that was induced by the injection of lysolecithin into the corpus callosum of adult rats was performed (**Figure 8A**). In this model, demyelination was detected at 3 dpi through examination of MBP$^+$-debris at the injection site (**Figure 8B**, arrows), while the dense MBP immunoreactivity remained in the corpus callosum receiving-vehicle injection (**Figure 8B**, arrowheads). To further examine the differentiation of GPCs at the demyelinated site, the scramble and Bcl11b-KD GPCs were separately implanted into the corpus callosum 3 days after the lysolecithin injection (**Figure 8C**). OLGs derived from the implanted GPCs were identified by double immunofluorescence for GFP and MBP. The GFP$^+$-scramble cells were found primarily at the injection site at 11 dpi (**Figure 8C**, arrowheads), whereas some of GFP$^+$/MBP$^+$-cells were found around the injection site in the Bcl11b-KD group (**Figure 8C**, arrows). The cell processes with intense MBP and PLP immunostaining were further detected in the GFP$^+$ Bcl11b-KD GPCs in the corpus callosum (**Figure 8D**, arrows). In contrast, the GFP$^+$-scramble cells expressed less MBP immunostaining (**Figure 8D**, arrowheads). The intensity of MBP and PLP immunostaining in the GFP$^+$-OLGs in the corpus callosum was higher when receiving Bcl11b-KD GPCs than with the scramble group (**Figure 8E**). In addition, the proportion of MBP and PLP expressing cells with respect to GFP$^+$-OLGs was also increased by Bcl11b-KD (**Figure 8E**). Notably, the amount of CC1$^+$/GFP$^+$-OLGs derived from Bcl11b-KD GPCs was higher than that observed in the scramble group (Supplementary Figures S4A,C), although the total amount of GFP$^+$-cells at the adjacent area to the injection site in the Bcl11b-KD group was lower than that analyzed in the scramble group (Supplementary Figure S4B), These results demonstrate that Bcl11b-KD GPCs effectively generate mature OLGs in the demyelinating region of the brain.

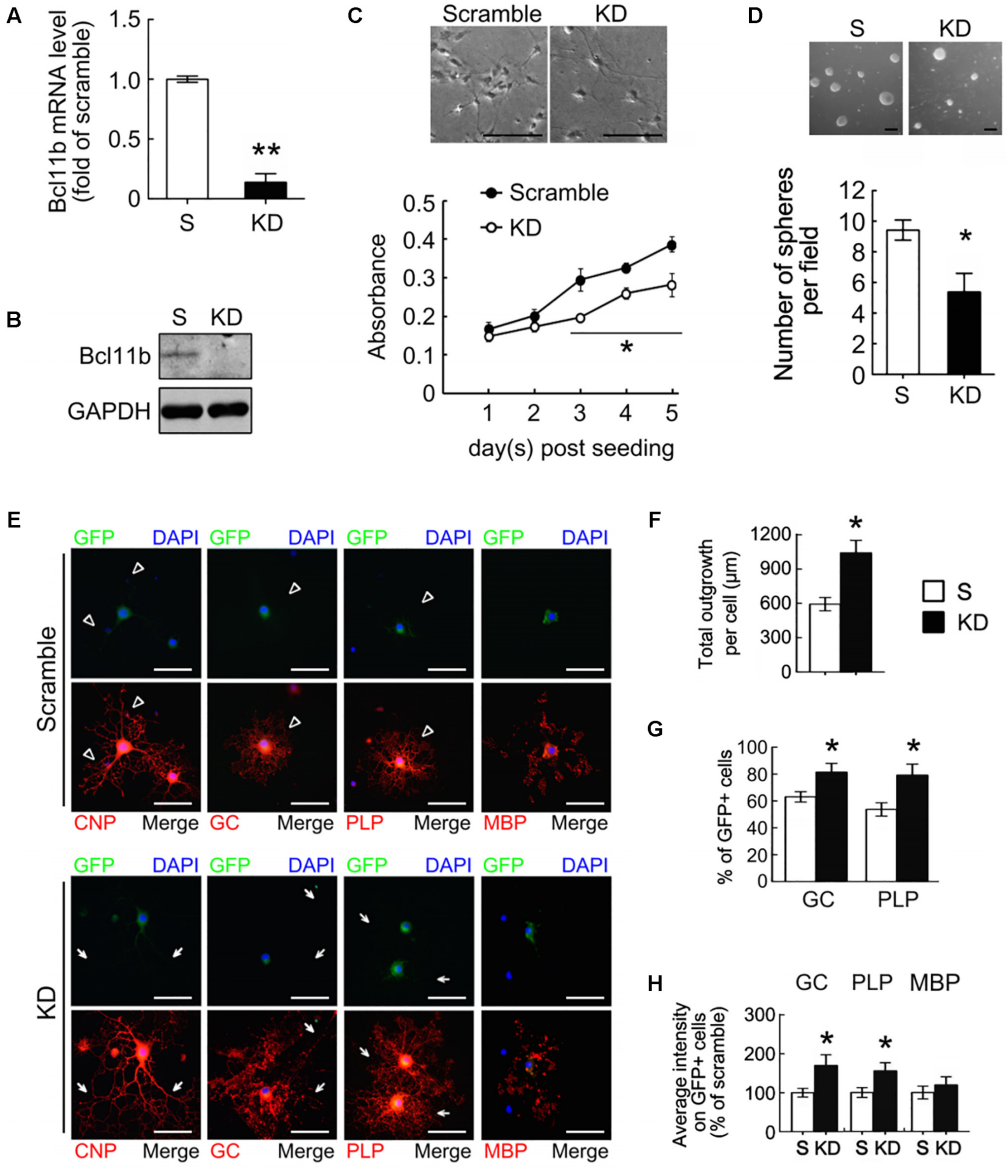

FIGURE 6 | Oligodendrocyte differentiation from OPCs promoted by Bcl11b gene knockdown. OPCs were derived from primary NSCs as described in Materials and Methods. OPCs were infected by lenti-ctrl (scramble) and lenti-sh-Bcl11b (Bcl11b-KD) and maintained in GM with puromycin for 2 days. The efficiency of Bcl11b-KD was measured by QPCR **(A)** and western blot **(B)**. The scramble- and Bcl11b-KD OPCs maintained in GM were subjected to MTT analysis **(C)**, and the sphere formation assay **(D)**. In addition, the scramble- and Bcl11b-KD OPCs were cultured in DM to generate OLGs for 5 days, followed by immunofluorescence for CNPase, GC, PLP, and MBP **(E)**. The total length of CNPase$^+$-cell processes per OLG cultures was analyzed **(F)**. Moreover, the percentage of GC$^+$-OLGs and PLP$^+$-OLGs in the scramble and Bcl11b-KD was measured **(G)**. Moreover, the intensity of immunofluorescence for GC, PLP, and MBP in each cell was measured by ImageJ software. The results show the average fluorescence intensity of Bcl11b-KD cells over those of scramble cells **(H)**. Data are presented as means ± SEM of at least three independent experiments (n = 70–100 cells per group for **F,G**). *$p < 0.05$ vs. the scramble. Scale bar in **(C,D)**, 100 μm; in **(E)**, 50 μm.

DISCUSSION

Here, we show that Bcl11b expression can be detected in the GPCs within the SVZ of rat and mouse brains (Supplementary Figure S1). Moreover, Bcl11b expression declines in OLGs generated from OPCs. Further the *in vitro* study demonstrated that the downregulation of Bcl11b in GPCs caused the upregulation of the cell cycle inhibitor p21, and increased premyelinating OLGs generated from the GPCs. In addition, we report that Bcl11b might function as a transcriptional repressor for Olig1 and PLP to downregulate their gene expression in GPCs. The observations from the co-culture system of GPCs with hippocampal neurons and with the *ex vivo* cerebellar slice cultures also indicated that MBP expression can be upregulated in OLGs derived from Bcl11b-KD GPCs. The *in vivo* study using a chemically induced demyelinating animal model indicated

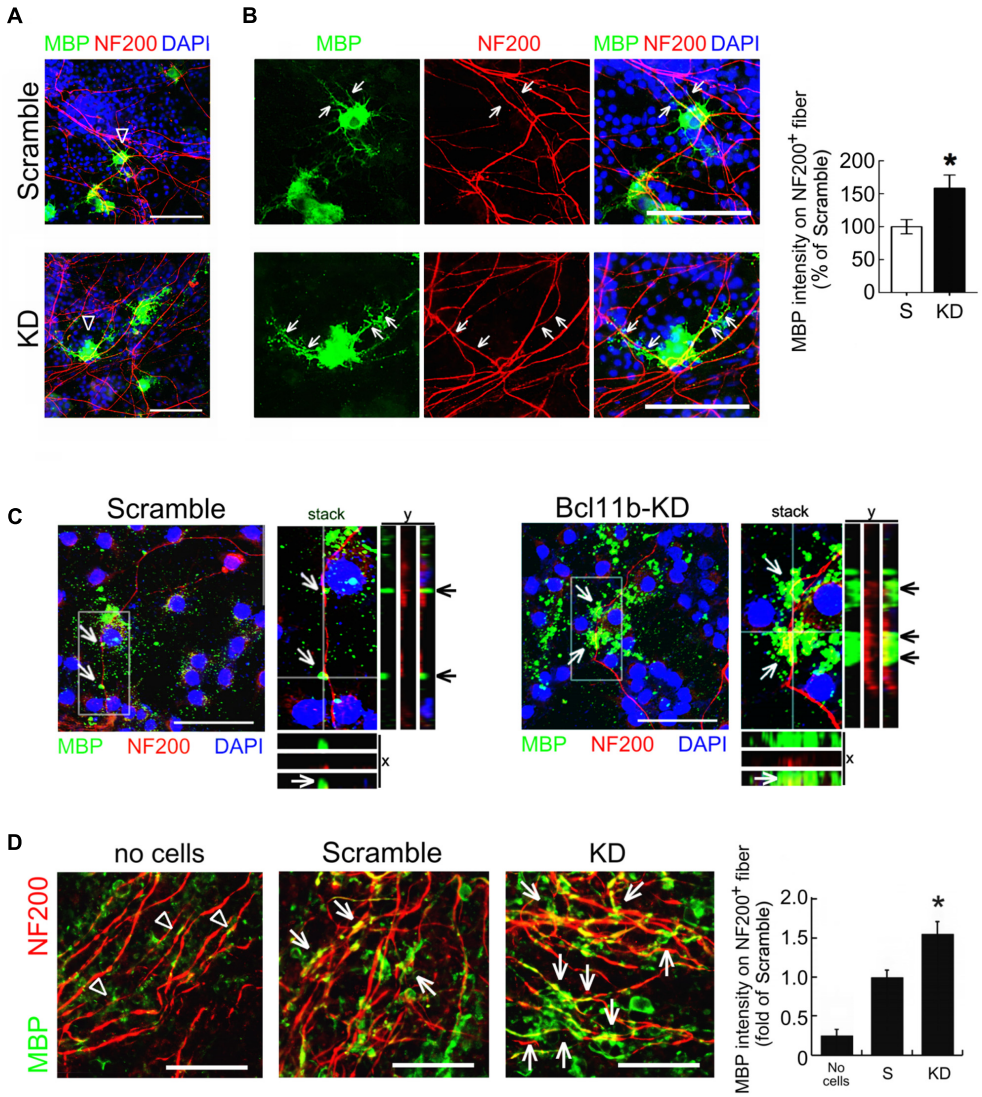

FIGURE 7 | Increased premyelinating processes of Bcl11b-KD GPCs along neuronal fibers. **(A)** Hippocampal neurons were co-cultured for 7 days with scramble and Bcl11b-KD GPCs. The cultures were then subjected to double immunofluorescence using anti-NF200 (red) and anti-MBP (green) antibodies. **(B)** The images with a higher magnification display the representative regions indicated by arrowheads in **(A)**. Arrows indicate the hippocampal fibers overlapping with MBP^+-processes extending from scramble OLGs and Bcl11b-KD OLGs, respectively. The intensity of MBP immunostaining overlapping to $NF200^+$- hippocampal fibers (arrowheads and arrows) in the scramble and Bcl11b-KD culture was quantified. **(C)** 3D-confocal imaging analysis was conducted to show the overlapping of MBP^+-OLG processes (green) to $NF200^+$-neuronal fibers (red). Arrows indicate the MBP immunostaining co-localized with $NF200^+$-regions in the longitudinal *y-z* and transverse x–z views from a z-stack image. **(D)** Scramble and Bcl11b-KD GPCs were seeded onto rat cerebellar slice culture for 7 days. The cultures were then subjected to double immunofluorescence for MBP (green) and NF200 (red). The immunoreactive intensity of MBP overlapping to $NF200^+$ fiber (arrows) was quantified by ImageJ software (right panel). Note that MBP^+-cell debris was observed in the culture without the addition of GPCs (arrowheads). Data are presented as means ± SEM of three independent experiments (n = 20–30 cells per group). $^*p < 0.05$ vs. scramble. Scale bar, 50 μm.

that Bcl11b downregulation can promote implanted GPCs to differentiate into OLGs in the demyelinating region. These findings demonstrate the positive role of Bcl11b in the cell growth of GPCs and OPCs, but point to its negative effect on the progression of the OLG lineage to maturation.

Bcl11b has been reported to act as a transcriptional repressor to silence the expression of p21 (Cherrier et al., 2009). Our previous study using human and rat glioma cells also showed that p21 expression was upregulated after the downregulation of Bcl11b expression in glioma cell lines, suggesting that Bcl11b is an important regulator for glioma cell expansion through the repression of p21 action (Liao et al., 2016). The results from the present study showing that the proliferation of GPCs in GM was suppressed after Bcl11b-KD along with the upregulation of p21, also indicate that Bcl11b is involved in the maintenance of GPC stemness via the repression of p21 expression. Given that the ablation of p21 gene expression is known to inhibit OLG differentiation (Zezula et al., 2001),

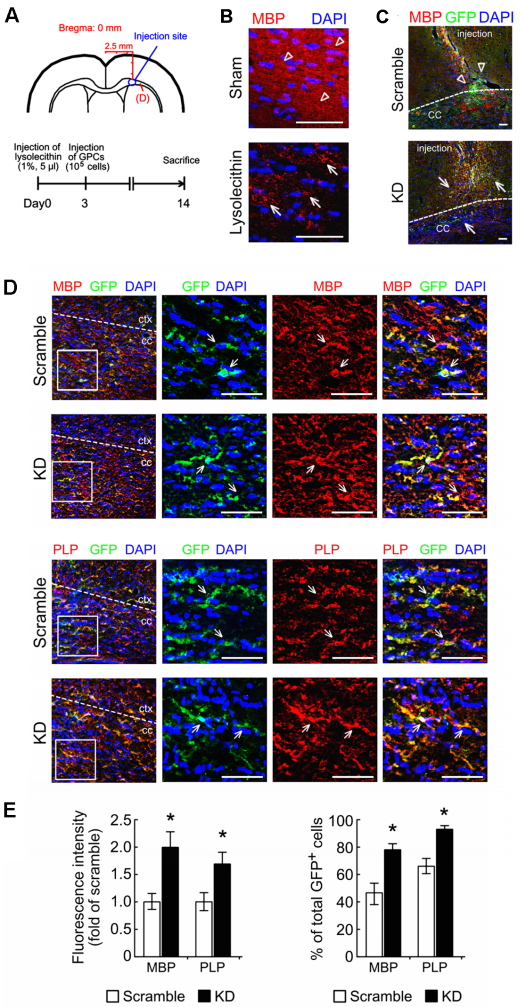

FIGURE 8 | Improved differentiation of OLGs derived from Bcl11b-KD GPCs under a demyelinating condition. **(A)** The diagrams show the injection site of lysolecithin and GPCs just above the corpus callosum (CC, upper panel), and indicate the time points (lower panel) for the injection of 1% lysolecithin at Day 0 and GPCs (scramble and Bcl11b-KD GPCs) at Day 3. The animals were sacrificed at Day 14 after lysolecithin injection to investigate the differentiation of implanted GPCs into OLGs at the demyelinating CC regions labeled by **(D)**. **(B)** The brain sections that were prepared from animals having received lysolecithin injection were subjected to MBP immunostaining (red) and DAPI nuclear counterstaining (blue). The sham-operated group was only receiving vehicle. MBP^+ debris was clearly observed in lysolecithin-injected CC (arrows). Diffuse and dense MBP staining was seen in the sham-operated group. **(C)** The brain sections receiving lysolecithin injection were subjected to double immunofluorescence for GFP (green) and MBP (red) to identify OLGs derived from implanted GPCs at the injection site. **(D)** By double immunofluorescence, GFP^+/MBP^+-OLGs (upper panel) and GFP^+/PLP^+-OLGs (lower panel) derived from implanted scramble and Bcl11b-KD GPCs in the CC adjacent to the injection site **(A)** were indicated by arrows. **(E)** To examine OLGs derived from implanted GPCs in the CC, the immunoreactive intensity of MBP and PLP in GFP^+-cells shown in **(D)** was measured by ImageJ software. The results are shown as the fold of the scramble group. The results are shown as the percentage of double immunostained OLGs (GFP^+/MBP^+, GFP^+/PLP^+) over the total number of GFP^+-cells in the field. Data in **(E)** are presented as means ± SEM from at least 3 animals in each group. The dash lines shown in **(C)** designate the border between cortex and CC. $^*p < 0.05$ vs. scramble. Scale bar, 50 μm.

the upregulation of p21 after Bcl11b-KD might be involved in the differentiation of GPCs into OLGs. In addition, although Sox2 as a transcription factor is required for the self-renewal of OPCs, it blocks OLG differentiation (Zhao et al., 2015). Our observations that Bcl11b-KD attenuated the expression of Sox2 in GPCs under the condition of GM or DM, raise the possibility that the downregulation of Bcl11b might facilitate OLG differentiation from GPCs. Indeed, the expression of OLG markers (CNPase, PLP, and MOG) can be increased in Bcl11b-KD GPCs or Bcl11b-KD OPCs, demonstrating that a decline in Bcl11b expression can promote GPC differentiation into mature OLGs.

It has been reported that neuronal progenitor proliferation and post-mitotic neuron differentiation in the hippocampus declined in Bcl11b mutant mice during development (Simon et al., 2012). In addition, the deficiency of Bcl11b can cause postmitotic vomeronasal sensory neurons to selectively undergo cell apoptosis (Enomoto et al., 2011). A lack of Bcl11b functionality has been reported to cause inefficient differentiation of spiny neurons in striatal medium, with reduced expression of mature striatal markers (Arlotta et al., 2008). Here, we show that the downregulation of Bcl11b expression in GPCs and OPCs can reduce their proliferation under the growth condition, but promote the OLG lineage progression. Our results, in conjunction with findings on neuronal development, demonstrate that functional Bcl11b is required for neural progenitor cell proliferation. Despite the expression of Bcl11b in rat and mouse OLGs located in the white matter being different, it remains to be further investigated if OLG differentiation could be impaired in the absence of functional Bcl11b.

Several Bcl11b binding sites have been assumed to occur at the promoters of striatal genes (Desplats et al., 2008). It has also been reported that the expression of Olig1, one of the key transcription factors for OLG differentiation, was induced in Bcl11b-deficient neurons (Enomoto et al., 2011). These findings, together with our observations of an increased expression of Olig1 in OLGs derived from Bcl11b-KD GPCs, raise the possibility that Bcl11b might be involved in the regulation of OLG-specific gene expression. By searching a transcription factor prediction database for potential Bcl11b binding sites in 2-kb long promoter regions of rat OLG-specific genes (Olig1, Olig2, MBP, and PLP), we validated six and seven (predicted) Bcl11b binding sites located at the Olig1 and PLP promoters, respectively. Our results from the ChIP assay further confirm that Bcl11b exhibits high binding affinity to the specific promoter regions of Olig1 ($-1487 \sim -1264$) and PLP ($-625 \sim -433$). Although the 2-kb long promoter regions of MBP contain 3 predicted binding sites with Bcl11b, the binding affinity of Bcl11b derived from the MBP promoters was extremely weak (data not shown). This is in accordance with our observation that MBP transcription was not affected by Bcl11b-KD. In other words, Bcl11b most likely acts as a transcriptional repressor of Olig1 and PLP, but not of MBP. Yet, the regulation of these genes by Bcl11b could also be due to the action of Bcl11b-induced chromatin remodeling via its interaction with nucleosome remodeling as well as histone deacetylase (NuRD) complex and SWI/SNF complex, which has been found in the control of T cells

and neural development (Cismasiu et al., 2005; Topark-Ngarm et al., 2006; Son and Crabtree, 2014). Taken together, Bcl11b potentially deters the differentiation of GPCs into OLGs through the repression of Olig1 and PLP. Accordingly, the reduction of Bcl11b can decrease its inhibition in the expression of these two molecules, and subsequently promote OLG differentiation and maturation. Nevertheless, the upstream regulators that can mediate Bcl11b expression during OLG development remain to be determined.

Proteolipid protein is not only required for the stabilization of the myelin membrane and axonal structure (Uschkureit et al., 2000), but is also involved in the transportation of myelin membranes in the OLG secretory pathway (Nave and Werner, 2014). Thus, the upregulation of PLP expression in OLGs derived from Bcl11b-KD GPCs could promote the maintenance of OLG interaction with neuronal fibers in hippocampal neuron co-cultures and cerebellar-slice systems, as well as in chemically induced demyelination of the corpus callosum. Sox10 can directly induce MBP expression (Liu et al., 2007), or cooperate with Olig1 to increase MBP expression (Li et al., 2007). However, based on our *in vitro* study, we found no change in the Sox10 gene expression after Bcl11b-KD. This may explain why MBP gene expression and its protein production did not increase in our *in vitro* study. Yet, MBP expression has been known to be upregulated in the presence of neurons and neuronal factors (Bologa et al., 1986; Jensen et al., 2000; Simons and Trajkovic, 2006). Here, we provide important evidence that MBP expression in OLGs derived from Bcl11b-KD GPCs was increased under the condition of hippocampal neuron co-culture and cerebellar-slice culture. In addition, our *in vivo* results demonstrate that an increase in MBP immunoreactivity was detected in OLGs derived from implanted Bcl11b-KD GPCs toward the demyelination of white matter regions. These *ex vivo* and *in vivo* results further revealed that the downregulation of Bcl11b expression can facilitate glial progenitors to induce OLG maturation. Moreover, in response to neuronal signals, OLGs derived from GPCs, in tandem with the downregulation of Bcl11b expression, could possibly foster myelination.

CONCLUSION

Bcl11b is essential for maintaining the proliferation of glial progenitors and their stemness properties. Reduced expression of Bcl11b in glial progenitors can contribute to the differentiation of GPCs toward mature OLGs. Moreover, our *in vitro* and *in vivo* findings provide important information for the development of an effective cell therapeutic strategy for demyelinating disorders via the downregulation of Bcl11b expression.

AUTHOR CONTRIBUTIONS

Study concept and design: C-YW and S-FT. Acquisition of data: C-YW, K-MF, and C-HH. Analysis and interpretation of data: C-YW, Y-TS, and S-FT. Drafting of the manuscript: C-YW, Y-TS, and S-FT. Critical revision of the article for important intellectual content: C-YW and S-FT. Statistical analysis: C-YW and K-MF. Obtained funding: C-SY and S-FT. Technical and material support: C-SY and S-FT.

FUNDING

This project was supported by the Ministry of Science and Technology, Taiwan (NSC 102-2314-B-006-058, MOST 103-2314-B-006-007-MY3 and MOST 105-2811-B-006-010).

ACKNOWLEDGMENTS

The authors thank Ms. Yun Ting Hsieh for technical assistance.

SUPPLEMENTARY MATERIAL

The Supplementary Material for this article can be found online at: https://www.frontiersin.org/articles/10.3389/fnmol.2018.00004/full#supplementary-material

REFERENCES

Arlotta, P., Molyneaux, B. J., Chen, J., Inoue, J., Kominami, R., and Macklis, J. D. (2005). Neuronal subtype-specific genes that control corticospinal motor neuron development in vivo. *Neuron* 45, 207–221. doi: 10.1016/j.neuron.2004.12.036

Arlotta, P., Molyneaux, B. J., Jabaudon, D., Yoshida, Y., and Macklis, J. D. (2008). Ctip2 controls the differentiation of medium spiny neurons and the establishment of the cellular architecture of the striatum. *J. Neurosci.* 28, 622–632. doi: 10.1523/JNEUROSCI.2986-07.2008

Bernard, O. A., Busson-LeConiat, M., Ballerini, P., Mauchauffe, M., Della Valle, V., Monni, R., et al. (2001). A new recurrent and specific cryptic translocation, t(5;14)(q35;q32), is associated with expression of the Hox11L2 gene in T acute lymphoblastic leukemia. *Leukemia* 15, 1495–1504. doi: 10.1038/sj.leu.2402249

Bologa, L., Aizenman, Y., Chiappelli, F., and de Vellis, J. (1986). Regulation of myelin basic protein in oligodendrocytes by a soluble neuronal factor. *J. Neurosci. Res.* 15, 521–528. doi: 10.1002/jnr.490150409

Chen, B., Wang, S. S., Hattox, A. M., Rayburn, H., Nelson, S. B., and McConnell, S. K. (2008). The Fezf2-Ctip2 genetic pathway regulates the fate choice of subcortical projection neurons in the developing cerebral cortex. *Proc. Natl. Acad. Sci. U.S.A.* 105, 11382–11387. doi: 10.1073/pnas.0804918105

Chen, S., Huang, X., Chen, S., Yang, L., Shen, Q., Zheng, H., et al. (2012). The role of BCL11B in regulating the proliferation of human naive T cells. *Hum. Immunol.* 73, 456–464. doi: 10.1016/j.humimm.2012.02.018

Cherrier, T., Suzanne, S., Redel, L., Calao, M., Marban, C., Samah, B., et al. (2009). p21(WAF1) gene promoter is epigenetically silenced by CTIP2 and SUV39H1. *Oncogene* 28, 3380–3389. doi: 10.1038/onc.2009.193

Cismasiu, V. B., Adamo, K., Gecewicz, J., Duque, J., Lin, Q., and Avram, D. (2005). BCL11B functionally associates with the NuRD complex in T lymphocytes to repress targeted promoter. *Oncogene* 24, 6753–6764. doi: 10.1038/sj.onc.1208904

Czepiel, M., Boddeke, E., and Copray, S. (2015). Human oligodendrocytes in remyelination research. *Glia* 63, 513–530. doi: 10.1002/glia.22769

Desplats, P. A., Lambert, J. R., and Thomas, E. A. (2008). Functional roles for the striatal-enriched transcription factor, Bcl11b, in the control of striatal

gene expression and transcriptional dysregulation in Huntington's disease. *Neurobiol. Dis.* 31, 298–308. doi: 10.1016/j.nbd.2008.05.005

Emery, B. (2010). Regulation of oligodendrocyte differentiation and myelination. *Science* 330, 779–782. doi: 10.1126/science.1190927

Enomoto, T., Ohmoto, M., Iwata, T., Uno, A., Saitou, M., Yamaguchi, T., et al. (2011). Bcl11b/Ctip2 controls the differentiation of vomeronasal sensory neurons in mice. *J. Neurosci.* 31, 10159–10173. doi: 10.1523/JNEUROSCI.1245-11.2011

Fancy, S. P., Glasgow, S. M., Finley, M., Rowitch, D. H., and Deneen, B. (2012). Evidence that nuclear factor IA inhibits repair after white matter injury. *Ann. Neurol.* 72, 224–233. doi: 10.1002/ana.23590

Fang, K. M., Yang, C. S., Lin, T. C., Chan, T. C., and Tzeng, S. F. (2014). Induced interleukin-33 expression enhances the tumorigenic activity of rat glioma cells. *Neuro Oncol.* 16, 552–566. doi: 10.1093/neuonc/not234

Grabarczyk, P., Nahse, V., Delin, M., Przybylski, G., Depke, M., Hildebrandt, P., et al. (2010). Increased expression of bcl11b leads to chemoresistance accompanied by G1 accumulation. *PLOS ONE* 5:e12532. doi: 10.1371/journal.pone.0012532

Herrera, J., Yang, H., Zhang, S. C., Proschel, C., Tresco, P., Duncan, I. D., et al. (2001). Embryonic-derived glial-restricted precursor cells (GRP cells) can differentiate into astrocytes and oligodendrocytes *in vivo*. *Exp. Neurol.* 171, 11–21. doi: 10.1006/exnr.2001.7729

Jensen, M. B., Poulsen, F. R., and Finsen, B. (2000). Axonal sprouting regulates myelin basic protein gene expression in denervated mouse hippocampus. *Int. J. Dev. Neurosci.* 18, 221–235. doi: 10.1016/S0736-5748(99)00091-X

Karanam, N. K., Grabarczyk, P., Hammer, E., Scharf, C., Venz, S., Gesell-Salazar, M., et al. (2010). Proteome analysis reveals new mechanisms of Bcl11b-loss driven apoptosis. *J. Proteome Res.* 9, 3799–3811. doi: 10.1021/pr901096u

Kremer, D., Gottle, P., Hartung, H. P., and Kury, P. (2016). Pushing forward: remyelination as the new frontier in CNS diseases. *Trends Neurosci.* 39, 246–263. doi: 10.1016/j.tins.2016.02.004

Lee, H. K., Laug, D., Zhu, W., Patel, J. M., Ung, K., Arenkiel, B. R., et al. (2015). Apcdd1 stimulates oligodendrocyte differentiation after white matter injury. *Glia* 63, 1840–1849. doi: 10.1002/glia.22848

Li, H., Lu, Y., Smith, H. K., and Richardson, W. D. (2007). Olig1 and Sox10 interact synergistically to drive myelin basic protein transcription in oligodendrocytes. *J. Neurosci.* 27, 14375–14382. doi: 10.1523/JNEUROSCI.4456-07.2007

Liao, C. K., Fang, K. M., Chai, K., Wu, C. H., Ho, C. H., Yang, C. S., et al. (2016). Depletion of B cell CLL/lymphoma 11B gene expression represses glioma cell growth. *Mol. Neurobiol.* 53, 3528–3539. doi: 10.1007/s12035-015-9231-1

Liu, Z., Hu, X., Cai, J., Liu, B., Peng, X., Wegner, M., et al. (2007). Induction of oligodendrocyte differentiation by Olig2 and Sox10: evidence for reciprocal interactions and dosage-dependent mechanisms. *Dev. Biol.* 302, 683–693. doi: 10.1016/j.ydbio.2006.10.007

Lu, Q. R., Sun, T., Zhu, Z., Ma, N., Garcia, M., Stiles, C. D., et al. (2002). Common developmental requirement for Olig function indicates a motor neuron/oligodendrocyte connection. *Cell* 109, 75–86. doi: 10.1016/S0092-8674(02)00678-5

Mayoral, S. R., and Chan, J. R. (2016). The environment rules: spatiotemporal regulation of oligodendrocyte differentiation. *Curr. Opin. Neurobiol.* 39, 47–52. doi: 10.1016/j.conb.2016.04.002

Nave, K. A., and Werner, H. B. (2014). Myelination of the nervous system: mechanisms and functions. *Annu. Rev. Cell Dev. Biol.* 30, 503–533. doi: 10.1146/annurev-cellbio-100913-013101

Raff, M. C., Miller, R. H., and Noble, M. (1983). A glial progenitor cell that develops *in vitro* into an astrocyte or an oligodendrocyte depending on culture medium. *Nature* 303, 390–396. doi: 10.1038/303390a0

Simon, R., Brylka, H., Schwegler, H., Venkataramanappa, S., Andratschke, J., Wiegreffe, C., et al. (2012). A dual function of Bcl11b/Ctip2 in hippocampal neurogenesis. *EMBO J.* 31, 2922–2936. doi: 10.1038/emboj.2012.142

Simons, M., and Trajkovic, K. (2006). Neuron-glia communication in the control of oligodendrocyte function and myelin biogenesis. *J. Cell Sci.* 119, 4381–4389. doi: 10.1242/jcs.03242

Son, E. Y., and Crabtree, G. R. (2014). The role of BAF (mSWI/SNF) complexes in mammalian neural development. *Am. J. Med. Genet. C Semin. Med. Genet.* 166C, 333–349. doi: 10.1002/ajmg.c.31416

Stolt, C. C., Rehberg, S., Ader, M., Lommes, P., Riethmacher, D., Schachner, M., et al. (2002). Terminal differentiation of myelin-forming oligodendrocytes depends on the transcription factor Sox10. *Genes Dev.* 16, 165–170. doi: 10.1101/gad.215802

Tang, B., Di Lena, P., Schaffer, L., Head, S. R., Baldi, P., and Thomas, E. A. (2011). Genome-wide identification of Bcl11b gene targets reveals role in brain-derived neurotrophic factor signaling. *PLOS ONE* 6:e23691. doi: 10.1371/journal.pone.0023691

Topark-Ngarm, A., Golonzhka, O., Peterson, V. J., Barrett, B. Jr., Martinez, B., Crofoot, K., et al. (2006). CTIP2 associates with the NuRD complex on the promoter of p57KIP2, a newly identified CTIP2 target gene. *J. Biol. Chem.* 281, 32272–32283. doi: 10.1074/jbc.M602776200

Uschkureit, T., Sporkel, O., Stracke, J., Bussow, H., and Stoffel, W. (2000). Early onset of axonal degeneration in double (plp−/−mag−/−) and hypomyelinosis in triple (plp−/−mbp−/−mag−/−) mutant mice. *J. Neurosci.* 20, 5225–5233.

Wang, C. Y., Deneen, B., and Tzeng, S. F. (2017). MicroRNA-212 inhibits oligodendrocytes during maturation by down-regulation of differentiation-associated gene expression. *J. Neurochem.* 143, 112–125. doi: 10.1111/jnc.14138

Wang, C. Y., Yang, S. H., and Tzeng, S. F. (2015). MicroRNA-145 as one negative regulator of astrogliosis. *Glia* 63, 194–205. doi: 10.1002/glia.22743

Yang, J., Cheng, X., Qi, J., Xie, B., Zhao, X., Zheng, K., et al. (2017). EGF enhances oligodendrogenesis from glial progenitor cells. *Front. Mol. Neurosci.* 10:106. doi: 10.3389/fnmol.2017.00106

Yang, Y., Lewis, R., and Miller, R. H. (2011). Interactions between oligodendrocyte precursors control the onset of CNS myelination. *Dev. Biol.* 350, 127–138. doi: 10.1016/j.ydbio.2010.11.028

Zezula, J., Casaccia-Bonnefil, P., Ezhevsky, S. A., Osterhout, D. J., Levine, J. M., Dowdy, S. F., et al. (2001). p21cip1 is required for the differentiation of oligodendrocytes independently of cell cycle withdrawal. *EMBO Rep.* 2, 27–34. doi: 10.1093/embo-reports/kve008

Zhang, L. J., Bhattacharya, S., Leid, M., Ganguli-Indra, G., and Indra, A. K. (2012). Ctip2 is a dynamic regulator of epidermal proliferation and differentiation by integrating EGFR and Notch signaling. *J. Cell Sci.* 125, 5733–5744. doi: 10.1242/jcs.108969

Zhang, S. C. (2001). Defining glial cells during CNS development. *Nat. Rev. Neurosci.* 2, 840–843. doi: 10.1038/35097593

Zhang, Y., Chen, K., Sloan, S. A., Bennett, M. L., Scholze, A. R., O'Keeffe, S., et al. (2014). An RNA-sequencing transcriptome and splicing database of glia, neurons, and vascular cells of the cerebral cortex. *J. Neurosci.* 34, 11929–11947. doi: 10.1523/JNEUROSCI.1860-14.2014

Zhao, C., Ma, D., Zawadzka, M., Fancy, S. P., Elis-Williams, L., Bouvier, G., et al. (2015). Sox2 sustains recruitment of oligodendrocyte progenitor cells following CNS demyelination and primes them for differentiation during remyelination. *J. Neurosci.* 35, 11482–11499. doi: 10.1523/JNEUROSCI.3655-14.2015

Zuchero, J. B., and Barres, B. A. (2013). Intrinsic and extrinsic control of oligodendrocyte development. *Curr. Opin. Neurobiol.* 23, 914–920. doi: 10.1016/j.conb.2013.06.005

Conflict of Interest Statement: The authors declare that the research was conducted in the absence of any commercial or financial relationships that could be construed as a potential conflict of interest.

frontiers in Cellular Neuroscience

ORIGINAL RESEARCH
published: 20 December 2017
doi: 10.3389/fncel.2017.00411

Proteomic and Metabolomic Analyses of Vanishing White Matter Mouse Astrocytes Reveal Deregulation of ER Functions

*Lisanne E. Wisse[1‡], Renske Penning[2‡], Esther A. Zaal[2], Carola G. M. van Berkel[1], Timo J. ter Braak[1], Emiel Polder[1], Justin W. Kenney[3†], Christopher G. Proud[3†], Celia R. Berkers[2], Maarten A. F. Altelaar[2], Dave Speijer[4], Marjo S. van der Knaap[1] and Truus E. M. Abbink[1]**

[1] Pediatrics, VU University Medical Center, Amsterdam, Netherlands, [2] Biomolecular Mass Spectrometry and Proteomics Group, Utrecht Institute for Pharmaceutical Sciences, Bijvoet Center for Biomolecular Research, Utrecht University, Utrecht, Netherlands, [3] Centre for Biological Sciences, University of Southampton, Southampton, United Kingdom, [4] Medical Biochemistry, Academic Medical Center, Amsterdam, Netherlands

OPEN ACCESS

Edited by:
Margaret Su-Chun Ho,
ShanghaiTech University, China

Reviewed by:
Johannes Hirrlinger,
Leipzig University, Germany
Jinchong Xu,
Johns Hopkins University,
United States

***Correspondence:**
Truus E. M. Abbink
g.abbink@vumc.nl

†Present address:
Justin W. Kenney,
The Hospital for Sick Children,
Toronto, ON, Canada
Christopher G. Proud,
South Australian Health and Medical Research Institute, School of Biological Sciences, University of Adelaide, Adelaide, SA, Australia

‡These authors have contributed equally to this work.

Received: 11 September 2017
Accepted: 07 December 2017
Published: 20 December 2017

Citation:
Wisse LE, Penning R, Zaal EA, van Berkel CGM, ter Braak TJ, Polder E, Kenney JW, Proud CG, Berkers CR, Altelaar MAF, Speijer D, van der Knaap MS and Abbink TEM (2017) Proteomic and Metabolomic Analyses of Vanishing White Matter Mouse Astrocytes Reveal Deregulation of ER Functions. Front. Cell. Neurosci. 11:411. doi: 10.3389/fncel.2017.00411

Vanishing white matter (VWM) is a leukodystrophy with predominantly early-childhood onset. Affected children display various neurological signs, including ataxia and spasticity, and die early. VWM patients have bi-allelic mutations in any of the five genes encoding the subunits of the eukaryotic translation factor 2B (eIF2B). eIF2B regulates protein synthesis rates under basal and cellular stress conditions. The underlying molecular mechanism of how mutations in eIF2B result in VWM is unknown. Previous studies suggest that brain white matter astrocytes are primarily affected in VWM. We hypothesized that the translation rate of certain astrocytic mRNAs is affected by the mutations, resulting in astrocytic dysfunction. Here we subjected primary astrocyte cultures of wild type (wt) and VWM (*2b5^{ho}*) mice to pulsed labeling proteomics based on stable isotope labeling with amino acids in cell culture (SILAC) with an L-azidohomoalanine (AHA) pulse to select newly synthesized proteins. AHA was incorporated into newly synthesized proteins in wt and *2b5^{ho}* astrocytes with similar efficiency, without affecting cell viability. We quantified proteins synthesized in astrocytes of wt and *2b5^{ho}* mice. This proteomic profiling identified a total of 80 proteins that were regulated by the eIF2B mutation. We confirmed increased expression of PROS1 in *2b5^{ho}* astrocytes and brain. A DAVID enrichment analysis showed that approximately 50% of the eIF2B-regulated proteins used the secretory pathway. A small-scale metabolic screen further highlighted a significant change in the metabolite 6-phospho-gluconate, indicative of an altered flux through the pentose phosphate pathway (PPP). Some of the proteins migrating through the secretory pathway undergo oxidative folding reactions in the endoplasmic reticulum (ER), which produces reactive oxygen species (ROS). The PPP produces NADPH to remove ROS. The proteomic and metabolomics data together suggest a deregulation of ER function in *2b5^{ho}* mouse astrocytes.

Keywords: vanishing white matter, eIF2B, AHA, SILAC, astrocytes, metabolomics, endoplasmic reticulum

INTRODUCTION

Vanishing white matter (VWM) is one of the more prevalent leukodystrophies (van der Knaap et al., 1999). Patients with VWM display chronic neurological deterioration and additionally episodes of stress-provoked rapid and severe deterioration. Neuropathology of post-mortem brain shows cystic degeneration of the cerebral white matter with lack of appropriate astrogliotic scar formation, profound lack of myelin, increased numbers of oligodendrocyte precursor cells and immature astrocytes. The morphology of especially astrocytes in cerebral white matter is abnormal. They look coarse and have fewer, thicker processes than normal (van der Knaap et al., 2006; Bugiani et al., 2011). A small proportion of the oligodendrocytes look foamy (Wong et al., 2000).

Recessive mutations in the eukaryotic translation factor 2B (eIF2B) cause VWM (Leegwater et al., 2001; van der Knaap et al., 2002). eIF2B is an enzyme composed of five different subunits (eIF2Bα-ε), encoded by five genes (*EIF2B1-5*). Mutations reduce the activity of eIF2B (van Kollenburg et al., 2006; Horzinski et al., 2009; Liu et al., 2011).

The eIF2B complex functions as a guanine nucleotide exchange factor (GEF), mediating the exchange of GDP for GTP on eIF2. eIF2-GTP binds to methionine-charged initiator tRNA (Met-tRNA$^{Met}_i$), thereby forming the ternary complex eIF2.GTP.Met-tRNA$^{Met}_i$. The ternary complex together with the small ribosomal subunit binds the 5′-end of the mRNA and scans the 5′-untranslated region (5′-UTR) until it encounters a start codon in a suitable context, whereupon translation of the open reading frame (ORF) starts. Simultaneously, GTP on eIF2 is hydrolyzed to GDP which makes the complex inactive (Konieczny and Safer, 1983; Kleijn et al., 1998; Proud, 2001). GEF activity is needed to recharge eIF2 with GTP.

Translation initiation is a complex process, involving multiple eukaryotic initiation factors (eIFs) (Voorma et al., 1994; Sonenberg and Hinnebusch, 2009). Translation initiation efficiency is profoundly influenced by the nucleotides flanking the start codon (usually AUG), the Kozak consensus sequence (Kozak, 1987). Purines at the −3 and +4 position relative to the AUG start codon are most important in determining translation initiation efficiency (Kozak, 1987; Noderer et al., 2014). The architecture of the 5′-UTR with regard to various sequences, structural motifs and length also determines the translation efficiency of an mRNA (Hinnebusch et al., 2016). eIF2B mutations are expected to reduce ternary complex levels and thus overall mRNA translation. However, this reduced activity can actually enhance translation of certain mRNAs with 5′-upstream open reading frames (uORFs) in their 5′-UTR. uORFs can inhibit translation of the main ORF (mORF) and translation of these mORFs depends on translation reinitiation, which is regulated by ternary complex levels (Meijer and Thomas, 2002; Hinnebusch et al., 2016).

A VWM mouse model, homozygous for the Arg191His mutation in the eIF2Bε subunit has been developed, representative of the human disease (*2b5^{ho}* mice) (Dooves et al., 2016). The Arg191His mutation corresponds to the Arg195His mutation in patients. This mutation reduces eIF2B activity *in vitro* and gives a severe VWM phenotype (Fogli et al., 2004; Li et al., 2004). Astrocytes in brains of *2b5^{ho}* mice are positive for the immaturity marker nestin. *In vitro* experiments show that *2b5^{ho}* astrocytes inhibit maturation of wild type (wt) oligodendrocytes (Dooves et al., 2016).

The mechanism by which mutations in eIF2B lead to astrocytic dysfunction and disease remains unclear. Here we aim to improve understanding of the molecular mechanism underlying VWM. We expected that mutant eIF2B would *not* have a general effect on mRNA translation but rather affects translation of a small number of specific mRNAs, leading to disruption of cellular balances and dysfunction of astrocytes in particular. To identify these translational differences, we subjected adult mouse astrocytes to high-resolution quantitative proteomics after a pulse labeling with AHA (L-azidohomoalanine) combined with SILAC (stable isotope-labeling by amino acids in cell culture) (Dieterich et al., 2006; Eichelbaum et al., 2012; Kenney et al., 2016).

MATERIALS AND METHODS

Mice

All experiments were carried out under the Dutch and European law with approval of the local Institutional Animal Care and Use Committee (IACUC) of the VU University (Amsterdam, Netherlands). Wt and *2b5^{ho}* animals were used. All animals were weaned at P21 and had *ad libitum* access to food and water. The mice were housed with a 12 h light and dark cycle.

Astrocyte Culture

Four-month-old mice were sacrificed by cervical dislocation. Brains were taken out and the olfactory bulbs, cerebella and forebrains were removed. Astrocytes from the remaining structures (gray and white matter structures, including striatum, hippocampi and basal nuclei) were isolated. Brain tissue was minced with a scalpel in Hank's balanced salt solution (HBSS) without magnesium and calcium (Gibco) at 4°C. The tissue was dissociated with a papain solution containing 20 mM PIPES (pH 7.4), 120 mM NaCl, 5 mM KCl, 1.1 mM EDTA, 5.5 mM L-cysteine-HCl, 40 U/ml DNase and 20 U/ml papain for 30 min at 37°C. Cells were plated in poly-L-ornithine (PLO)-coated flasks and cultured in DMEM/F12 with 15% fetal bovine serum (FBS) (Hyclone), 1% sodium pyruvate (Gibco), 100U penicillin, 100 μg/ml streptomycin (Gibco) and 10 μg/ml gentamicin (Gibco). The cells were passaged twice before they were used for experiments. All chemicals were purchased from Sigma–Aldrich unless otherwise stated. Every experiment was replicated in independent cultures derived from different mice (number of experiments is indicated in figure legends as, e.g., $n = 3$).

Rate of Protein Synthesis Assay

Astrocytes were plated in 6 cm dishes (∼250,000 cells/dish) and cultured until 80–90% confluent. Cells were starved for methionine for 15 min in AHA medium [DMEM/F12 without methionine, lysine, arginine and phenol red (Thermo Fisher Scientific)] supplemented with 91.3 mg/L L-lysine, 147.5 mg/L

L-arginine, dialysed FBS and phenol red, after which AHA (Bachem) was added to AHA medium for the indicated time in a final concentration of 2 mM. Cells were harvested in lysis buffer composed of 50 mM Tris pH 7.5, 100 mM NaCl, 0.5 mM EDTA and 0.5% sodium dodecyl sulfate (SDS).

The newly synthesized proteins were labeled using the Click-iT® Protein buffer kit according to the manufacturer's protocol (Invitrogen). In short, the AHA molecules in the cell lysate were coupled to biotin. Proteins were precipitated by subsequent addition of six volumes of methanol, 1.5 volume of chloroform and 4 volumes of water. The protein pellet was dissolved in 50 mM Tris-HCl pH 7.5 with 1% SDS before subjection to Western blot analysis. Samples were loaded on 12% Criterion™ TGX Stain-Free™ Protein Gels (Bio-Rad), allowing detection of total protein load. Biotinylated AHA-labeled proteins were stained with 400 ng/ml streptavidin (680 nm) and visualized at 700 nm in an Odyssey system (Odyssey® Fc, LI-COR). The amount of AHA-staining was corrected for the total protein load determined by Gel Doc™ EZ System (Bio-Rad).

Cell Viability Assay

Astrocytes were plated in ½ area 96 well plates (∼5000 cells/well) and cultured for 2 days in AHA-SILAC medium (Thermo Fisher Scientific, custom-made DMEM/F12 without methionine, arginine, lysine and phenol red), with addition of 15% dialyzed serum, 0.005% phenol red, SILAC amino acids (94.2 mg/L [$^{13}C_6$] L-lysine 152 mg/L [$^{13}C_6$] L-arginine or 96 mg/L [$^{13}C_6$, $^{15}N_4$] L-lysine and 154.3 mg/L [$^{13}C_6$, $^{15}N_4$] L-arginine) and 17.2 mg/L L-methionine. The cells were starved for methionine from 15 min and cultured with 2 mM AHA (Bachem) or methionine overnight in half well area plates. Cell viability (ATP levels, CellTiter-Glo) was measured according to manufacturer's instructions (Promega). In short, cells were kept at room temperature for 30 min. CellTiter-Glo was added in the same volume as the culture medium. The plate was shaken for 2 min and left standing for 10 min before measuring luminescence with a Victor2 plate reader (PerkinElmer Life Sciences).

AHA Enrichment and On-Bead Digestion

Astrocytes were plated in 10 cm dishes (∼750,000 cells/dish) and cultured until 80% confluent. The culture medium was replaced with AHA-SILAC medium. Cells were grown for 4 days. SILAC labels were reversed in biological duplicates. Cells were subsequently starved for methionine for 15 min and AHA was added as described in the previous section. Astrocytes were further cultured for 2 h or otherwise indicated. The cells were subsequently washed with cold PBS and lysed in urea lysis buffer (supplied with the Click-IT Protein enrichment Kit, Invitrogen).

For the protein analysis of secreted proteins conditioned medium samples from wt and *2b5^{ho}* astrocytes (2 h) were concentrated using Amicon® Ultra-15 centrifuge filter tubes (3 kDa, Merck). Samples were diluted with urea lysis buffer to a volume of 400 µl per sample.

The AHA-labeled proteins from cell lysates as well as from the conditioned medium were enriched using the Click-iT® Protein Enrichment Kit according to the manufacturer's protocol (Invitrogen) with some minor modifications. In short, the AHA-labeled proteins were bound to the resin (16 h), following an iodoacetamide treatment and several washing steps. The AHA-labeled proteins bound to the resin were dissolved in 50 mM ammonium bicarbonate with 3 M urea. Digestion was performed at 37°C by adding 0.1 µg Lys-C for 4 h followed by addition of 1 µg trypsin overnight. The peptides were separated from the resin by briefly centrifuging them through a 0.8 ml spin columns (Thermo Fisher Scientific). The flow through contains the peptides. Peptide samples were stored at −80°C until further use. See also **Figure 1** for an overview of the enrichment procedure.

LC-MS/MS Analysis

Peptides were analyzed using a Q Exactive™ Hybrid Quadrupole-Orbitrap™ Mass Spectrometer (Thermo Fisher Scientific), which was connected to a 1290 Infinity II LC System (Agilent). The trap column was made of C18 (Dr. Maisch Reprosil) material and the analytical column was a 50 cm, 50 µm inner diameter Poroshell C18 (Agilent) column. Both the trap and analytical columns were packed in-house. Solvent A consisted of 0.1% formic acid (Merck) in deionized water (Merck) and Solvent B of 0.1% formic acid in 80% acetonitrile (Biosolve). Peptides were first trapped at 50 µl/min with solvent A and then eluted with solvent B in a 120 min gradient at 100 nl/min: 0–10 min, 100% solvent A; 10.1–105 min, 13–40% solvent B; 105–108 min, 40–100% solvent B; 108–109 min, 100% solvent B; 109–110 min, 0–100% solvent A; 110–120 min, 100% solvent A. The Orbitrap was operated in a data-dependent manner, with the following settings: ESI voltage, 1700 V; inlet capillary temperature 320°C; full-scan automatic gain control (AGC) target, 3×10^6 ions at 35000 resolution; scan range, 350–1500 *m*/*z*; Orbitrap full-scan maximum injection time, 250 ms; MS2 scan AGC target, 5×10^4 ions at 17500 resolution; maximum injection, 120 ms; normalized collision energy, 25; dynamic exclusion time, 30; isolation window 1.5 *m*/*z*; 10 MS2 scans per full scan.

Data Processing

The LC-MS/MS data were processed with MaxQuant (v1.5.2.8) and MS2 spectra were searched with the Andromeda search engine against the mouse proteome in UniProt (17155 entries, downloaded on 2015-10-27). Enzyme specificity was set to Trypsin/P and two missed cleavages were allowed. SILAC labels (K6/8, R6/10), methionine for AHA substitution and methionine oxidation were set as variable modifications and cysteine carbamidomethylation was set as fixed modification. Minimum peptide length was 7 amino acids. Mass tolerance was set to 20 ppm for peptide masses and 0.6 Da for fragmentation masses. The false discovery rate (FDR) threshold was set to 1% for identifications. Minimal ratio count was set to 2 for protein quantification and the functions "match between runs" and "requantify" were enabled. Data were further analyzed in Perseus (v1.5.0.0). Protein groups were kept for further analysis if they were detected in at least three of the biological replicates.

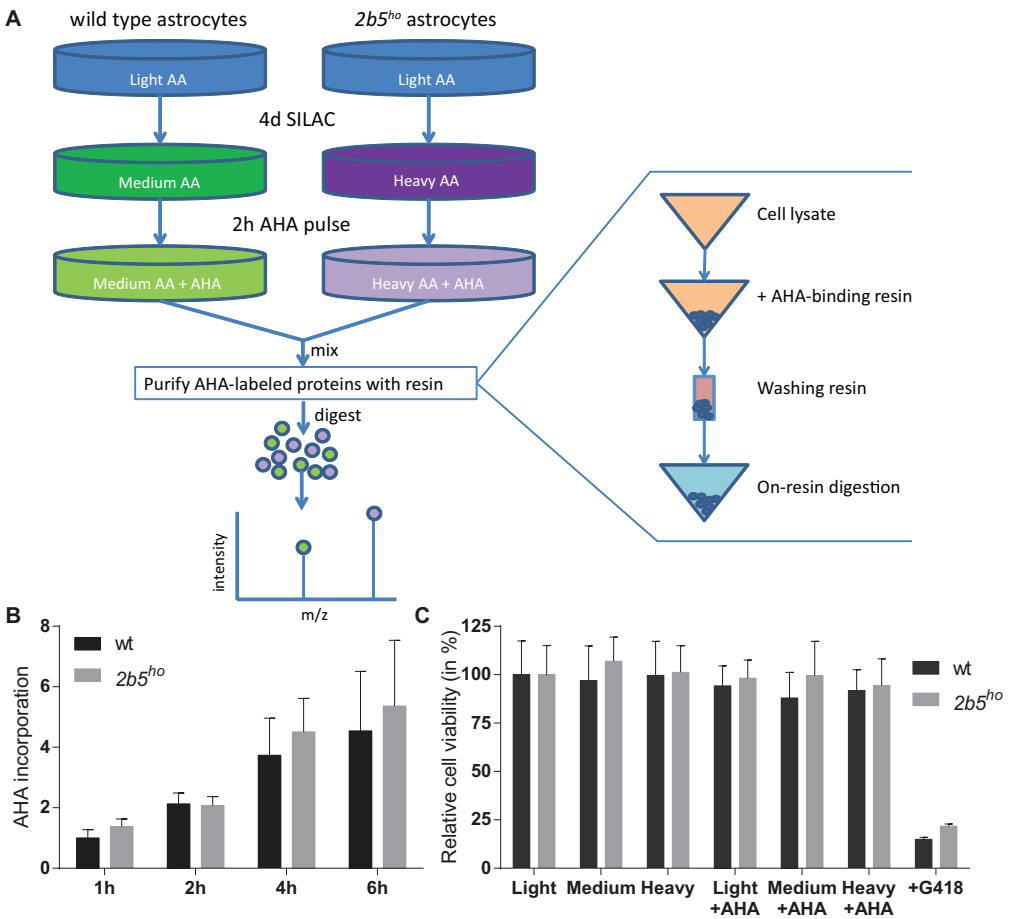

FIGURE 1 | L-azidohomoalanine (AHA) incorporation rates are similar between wt and *2b5*^{ho} astrocytes and assay conditions do not affect wt and *2b5*^{ho} cell viability. **(A)** Overview of the enrichment protocol. Heavy refers to labeling with [$^{13}C_6$, $^{15}N_4$] L-lysine and [$^{13}C_6$, $^{15}N_4$] L-arginine, while medium refers to labeling with [$^{13}C_6$] L-lysine and [$^{13}C_6$] L-arginine. **(B)** Astrocytes were treated with AHA for 1–6 h to determine a suitable AHA labeling time to measure newly synthesized proteins as well as confirm a similar AHA incorporation between wt and *2b5*^{ho} astrocytes. The graph shows the mean + SD (n = 3) and the 1-h-incorporation in wt cells was set to 1. **(C)** Astrocytes were grown in normal (light) or SILAC culture medium (medium or heavy) for 2 days with or without a 16-h AHA pulse. Cell viability was determined by measuring intracellular ATP levels (CellTiter-glo, Promega). As a positive control for the assay, cells were grown in the presence of G418. The graph shows the mean ± SD (n = 3).

A t-test was performed and protein groups were considered significant if the p-value was <0.05.

Signal Peptide Analysis

To assess the presence of an N-terminal signal peptide in the proteins, we subjected the proteins from the proteomic screen to the SignalP 4.1 server (Bendtsen et al., 2004; Petersen et al., 2011). For all UniProt IDs the FASTA files were downloaded from the UniProt website and all Fasta files are automatically subjected to the SignalP 4.1 server. The presence or absence of a signal peptide for each UniProt ID was predicted with the SignalP 4.1 algorithms and the results were saved to Excel. The UniProt IDs linked back to the list of all identified protein names. Biomart was used to identify proteins containing a transmembrane domain. The number of proteins with a signal peptide was calculated for the proteins, the synthesis of which was affected by eIF2Bε^{Arg191His} as well as for the other proteins that are not regulated by the same mutation. Next the number of regulated proteins with a signal peptide were subdivided in 'upregulated' and 'downregulated'.

In Silico Analysis of mRNA Features of eIF2Bε^{Arg191His}-Regulated Proteins

The sequences of the mRNA variants encoding the proteins identified in the AHA-SILAC proteomes were downloaded from the NCBI database including the start and stop codon location. The 5′-UTR features "uORFs, %GC and thermodynamic stability (ΔG in kcal/mol)" were determined for all mRNAs (Babendure et al., 2006). We compared each mRNA characteristic for all proteins found in the AHA-SILAC proteomic screen and compared the characteristics for the proteins regulated by eIF2Bε^{Arg191His} and non-regulated proteins. The 5′-UTR length,

%GC and ΔG from mRNAs encoding the proteins found in the AHA-SILAC proteomes were analyzed per protein. When a protein is potentially translated from more than 1 mRNA variant (taken from the NCBI database), we counted and analyzed all features of all mRNA variants per protein and plotted all as a proportional representation per protein so that the analysis was not skewed by proteins with multiple variants. 5′-UTR lengths of less than 13 nucleotides were omitted from analyses as AUG codons less than 13 nt from the cap are inefficient to initiate translation (Hinnebusch, 2011). The % of GC in the 5′-UTRs was calculated. To calculate the thermodynamic stability, the free energy (ΔG) of 5′-UTRs was determined using UNAFold[1], which predicts thermodynamic stability. The uORF was defined as upstream AUG/CUG/GUG/UUG/ACG with a purine (A/G) at the -3 position and a guanine at the +4 position (Ingolia et al., 2011; Ferreira et al., 2013; Noderer et al., 2014). Scripts used for the analyses are found at: https://github.com/LisanneWisse/UORF or https://github.com/LisanneWisse/RefSeq.

DAVID Analysis

Overrepresentation of specific pathways was analyzed with DAVID [based on gene ontology (GO)-terms] between the proteins that are affected by the eIF2Bε^{Arg191His} mutation and all the proteins found in the AHA-SILAC proteome (Huang et al., 2009a,b).

Cell Lysates for Western Blot Experiments

Astrocytes were plated in 10 cm dishes (∼750,000 cells/dish) and cultured until 80% confluent. Cells were washed with cold PBS, collected by scraping in PBS and pelleted by centrifugation (5 min, 1000 × *g*, 4°C). The method is based on the protocol described[2]. Cells were lysed in harvesting buffer containing 10 mM HEPES pH 7.9, 50 mM NaCl, 0.5 M sucrose, 0.1 mM EDTA, 0.5% Triton, 1 mM DTT, phosphatase inhibitors (0.5 mM activated $NaVO_3$, 25 mM β-glycerophosphate, 50 mM NaF) and protease inhibitors (Roche). Lysates were centrifuged (10 min 500 × *g*, 4°C) and the supernatant was used for Western blot analyses.

Whole Brain Lysates for qPCR and Western Blot Experiments

Mice were sacrificed by cervical dislocation at 4 months of age. Brains were removed, snap-frozen in liquid nitrogen and stored at −80°C until further use. Lysates were prepared by grinding the brain samples with a pestle and mortar under liquid nitrogen. The powder was lysed in cytoplasmic lysis buffer (20 mM Tris pH 7.4, 100 mM KAc, 3 mM $MgAc_2$, 2 mM DTT, 1.5% IGEPAL, 1.5% sodium deoxycholate (SODC), 1x HALT (protease and phosphatase inhibitory cocktail, Thermo Fisher Scientific]. The samples were homogenized with a pestle followed by trituration through a 23G needle. The samples were centrifuged (10 min, 10.000 × *g*, 4°C) and the supernatant was aliquoted into pre-chilled microfuge tubes. Protein concentrations were determined using a Quick Start™ Bradford Protein Assay (Bio-Rad). For RNA isolation, TRIzol™ Reagent (Invitrogen) was added to 50 μl of the supernatant and total RNA was isolated as described under RNA isolation and cDNA synthesis.

Western Blot

For cell lysates approximately 10 μg and for brain lysates 50–60 μg of protein was loaded on a 12% SDS-polyacrylamide gel with 2,2,2-trichloroethanol (TCE) which allow detection of total protein load (Ladner et al., 2004). Proteins were transferred onto a PVDF membrane (Bio-Rad). Membranes were blocked in 5% (w/v) milk powder and stained with the antibody against PROS1 (16910-1-AP, Proteintech) or SLC3A2 (LS-C334231, LSBio) overnight (16 h) at 4°C. Membranes were washed with TBS-Tween20 (0.1%) and incubated with an HRP-conjugated secondary goat anti-rabbit IgG antibody (Dako, P0448) for 2 h at room temperature. The membranes were washed three times with TBS-Tween (0.1%) and once with TBS, incubated with SuperSignal™ West Femto (Thermo Fisher Scientific) and imaged (Odyssey® Fc, LI-COR). Protein expression was corrected for total amount of protein determined by Gel Doc™ EZ System (Bio-Rad).

RNA Isolation, cDNA Synthesis and qPCR

Astrocytes were washed twice with PBS and collected in TRIzol™ Reagent (Invitrogen). RNA was isolated according to the manufacturer's protocol. In short, 1/5 volume chloroform was added to the TRIzol™ Reagent. The samples were centrifuged (10 min, 12000 × *g*, 4°C) and the water layer was transferred to a fresh tube. Half a volume of isopropanol and 1/250 volume of linear acrylamide (Ambion) was added and the samples were centrifuged for 20 min at 4°C and 12000 × *g*. The pellet was washed twice with 70% ethanol and resuspended in non-DEPC treated water (Ambion). RNA was precipitated with 175 mM sodium acetate (pH 5.2) and 70% ethanol and incubated for 30 min at −20°C. The samples were centrifuged (30 min, 4°C, 12000 × *g*) and the pellets were washed twice with 70% ethanol and resuspended in non-DEPC-treated water.

RNA quality and quantity were determined by measuring the A260 and A280 (NanoDrop 2000, Thermo Fisher Scientific). cDNA was synthesized in a 20 μl reverse transcription reaction: 1x first strand buffer (Invitrogen), random hexamers (0.02 μg/μl; Qiagen), oligoDT (0.02 μg/μl; Qiagen), dNTPs (1 mM each; Roche), DTT (1 mM; Invitrogen), RNaseOUT (0.25 U/μl; Invitrogen), Superscript III (5 U/μl; Invitrogen) and 1.5 μg total RNA were incubated for 2 h at 50°C. RNAseH (62.5 U/μl; Invitrogen) was added and incubated for 30 min at 37°C followed by 15 min at 70°C.

mRNA levels were determined with qPCR using a LightCycler® 480 II Instrument (Roche). For each 10 μl sample a mixture of LightCycler® 480 SYBR Green I Master (Roche), primers (1 pmol/μl) and cDNA (0.1 μl) was used. Used primers are listed in **Table 1**. *Gapdh* mRNA was used as reference.

[1]http://unafold.rna.albany.edu//?q=DINAMelt/Quickfold

[2]http://ron.cimr.cam.ac.uk/protocols/NucCyto.html

TABLE 1 | Primers used for qPCR.

Gene name	Forward (5′->3′)	Reverse (5′->3′)
Gapdh	GTGCTGAGTATGTCGTGGAG	TCGTGGTTCACACCCATCAC
Akt	AAGAAGGAGGTCATCGTCGC	GGTCGTGGGTCTGGAATGAG
Gas6	CTAAAACTATCCCCAGACAT	GGTACAAGGACTTCACGCTCT
Nrxn1	CCCCACAAAGGAACCCATCA	GTTGGCTAACCCACCTGAGC
Sorcs1	GGGACATCAGCCGAGTCATC	AACACCGCCACCAGGATATG
Fndc3c1	AGAGCGAGGCTTTTGGAGAA	TGGCACTGTTGGAGGTATTTCA
Pros1	TCCCTGGAGGCTACTCTTGTT	AGGTCCAAGGAAAGGCACAC
Scrn1	TGTCTGTCTTGCCTCAGAACA	TTTTGGCTGGGTCATCGTCA
Fgfr1	GCCAGACAACTTGCCGTATG	TCCGATAGAGTTACCCGCCA
Txnip	GTCTCAGCAGTGCAAACAGAC	CCTTCACCCAGTAGTCTACGC
Ddr1	CTGCTGCTTCTCATCATCGC	GTCAGCTCCTCCTCCAACAC
Slc3a2	GAAAGCTGATGAATGCACCC	CAATTTGCTGCAGGTCAGAG
Sec31A	GAGAGTCCTGCTGCTGAAGAG	AGACCGTCAATATCCCCACT

Constructs

Construct to Determine Secretion

The pNL1.3 plasmid (Promega) expresses the nanoluciferase protein with an *N*-terminal signal peptide from interleukin-6 (IL-6; Secluc). The signal peptide promotes secretion of the nanoluciferase into the culture medium. The pNL1.3-*Gapdh* construct contains the promoter including 5′-UTR of *Gapdh,* which was inserted in the pNL1.3 vector using an infusion reaction, according to the manufacturer's protocol (In-Fusion® HD Cloning Kit, Clontech). The PCR-amplified sequence of the constructs was confirmed by sequence analysis.

Constructs to Determine Translation

The pNL1.1 plasmids express the nanoluciferase protein (Nluc). Promoter and 5′-UTR sequences of candidate genes were taken from NCBI and Ensembl databases (**Table 2**). Infusion primers were designed to amplify promoter (approximately 2000 bps upstream of the transcription start site) and 5′-UTR-encoding sequences using the primer design tool on the Clontech website. Internal primers were designed to merge the *Gapdh* promoter region and the 5′-UTR of the candidate.

The promoter and 5′-UTR sequences were amplified using the infusion primers and the overlapping internal primers on gDNA from mouse liver or cDNA from cultured mouse astrocytes (**Table 2**) according to the manufacturer's protocol (ClonAmp, In-Fusion HD, Clontech). For the chimeric constructs comprising the murine *Gapdh* core promoter and 5′-UTR of the candidate mRNA a triple infusion reaction was performed with the pNL1.1 vector, the amplified promoter product and the amplified 5′-UTR product (**Table 2**). All promoter and 5′-UTR sequences were inserted into the pNL1.1 vector (Promega) using an infusion reaction according to the manufacturer's protocol (In-Fusion® HD Cloning Kit, Clontech). The resulting plasmids are listed in **Table 2**. PCR-amplified sequences of all constructs were confirmed by sequence analysis.

Construct Used As Internal Control

The pGL3 plasmid expresses the firefly luciferase protein (Fluc). The murine *Gapdh* promoter and 5′-UTR were digested from the pNL1.1 vector with KpnI and NcoI, purified from agarose gel (High Pure PCR Cleanup, Roche) and inserted into an empty pGL3 vector digested with the same restriction enzyme using a T4 DNA ligase (Promega). The resulting plasmid pGL3-*Gapdh* was used as internal standard in transfection studies. PCR-amplified sequence of the constructs was confirmed by sequence analysis.

Measurement of Secretion and Secretory Pathway Flux

Astrocytes were plated in half-area 96 well plates (∼3000 cells/dish, CELLSTRAR) to 80% confluency. pNL1.3-Gapdh (80 ng) was transfected into the cells using 0.24 μl FuGENE® 6 according to the manufacturer's protocol (Promega). Luciferase activity in cells and culture medium was measured using the protocol of Promega and a Wallac 1420 Victor2 Microplate Reader (Perkin Elmer). The ratio of extracellular/intracellular luciferase activity determines the relative secretion.

Transfections

Astrocytes were plated in half-area 96 well plates (∼3000 cells/dish, CELLSTAR). Each pNL1.1 promoter/5′-UTR construct (40 ng) was co-transfected with internal control pGL3-*Gapdh* (20 ng) using FuGENE® 6 Transfection Reagent (0.24 μl) according to the manufacturer's protocol. Luciferase activity was measured using the protocol of Promega and a GloMax® Discover System (Promega). The ratio Nluc:Fluc determines the expression of Nluc corrected for well-by-well differences.

Metabolomics

Astrocytes were cultured in 6 cm dishes (∼250,000 cells/dish) until 70% confluent. Medium was replaced 72 and 24 h before harvesting. At the time of harvesting culture medium was removed from the cells and stored at −80°C until analysis. Cells were washed with ice-cold PBS and metabolites were extracted from cells in 0.5 ml lysis buffer containing methanol/acetonitrile/dH_2O (2:2:1). Samples were spun at 16.000 × *g* for 15 min at 4°C. Supernatants were collected for LC-MS analysis. 10 μl of conditioned medium was added to 1 mL of lysis buffer containing methanol/acetonitrile/H_2O (2:2:1) and prepared as above.

LC-MS analysis was performed on an Exactive mass spectrometer (Thermo Fisher Scientific) coupled to a Dionex Ultimate 3000 autosampler and pump (Thermo Fisher Scientific). The MS operated in polarity-switching mode with spray voltages of 4.5 and −3.5 kV. Metabolites were separated using a SeQuant® ZIC®-pHILIC HPLC Columns (2.1 mm × 150 mm, 5 μm, guard column 2.1 mm × 20 mm, 5 μm; Merck) using a linear gradient of acetonitrile and eluent A [20 mM $(NH_4)_2CO_3$, 0.1% NH_4OH in ULC/MS grade water (Biosolve)]. Flow rate was set at 150 μl/min. Metabolites were identified and quantified using LCQUAN^{TM} Quantitative Software (Thermo Fisher Scientific) on the basis of exact mass within 5 ppm and further validated by concordance with retention times of standards. Metabolites were quantified

using LCQUAN^{TM} Quantitative Software (Thermo Fisher Scientific). Peak intensities were normalized based on median peak intensity.

Statistical Analyses

The program Factor was used to correct for differences between experiments (qPCR, Western blot, cell viability) but not between other conditions (genotype, treatments) (Ruijter et al., 2006). Statistical analysis of qPCR, Western blot and cell viability experiments were performed with a two way ANOVA followed by a Sidaks multiple comparison test, using GraphPad Prism software. Statistical analysis of the transfection data was performed using a *T*-test per construct.

A Chi-square analysis was used to measure significant differences in the presence of signal peptides, transmembrane regions and SP-targeting proteins as well as for the analysis on the 5′-UTR features using GraphPad Prism software.

The secretion assay was statistically tested with a multilevel analysis in SPSS. Differences were significant when $p < 0.05$.

TABLE 2 | Primer sequences used for cloning.

Gene number	Construct name	Primer	Sequence
NM_008084	pNL1.3-*Gapdh*	Infusion FW primer	TGGCCTAACTGGCCGGTACCTGCTGTGTCACTACCGAAGAACAACGAGGAGAAGAT
		Infusion RV primer	GGCTAGCGAGCTCAGGTACCTTTGTCTACGGGACGAGGCTGGCACTGCACAAGAAG
NM_008084	pNL1.1-*Gapdh*	Infusion FW primer	TGGCCTAACTGGCCGGTACCTGCTGTGTCACTACCGAAGAACAACGAGGAGAAGAT
		Infusion RV primer	AGTGTGAAGACCATGGTTTGTCTACGGGACGAGGCTGGCACTGCACAAGAAG
NM_011173	pNL1.1-*Pros1*	Infusion FW primer	TGGCCTAACTGGCCGGTACCAACTGGCTTCTTTGTGGTG
		Infusion RV primer	AGTGTGAAGACCATGGCTGAGAGGATGGCCGGG
NM_019521	pNL1.1-*Gas6*	Infusion FW primer	TGGCCTAACTGGCCGGTACCGGACAGGCACTCTTTGGA
		Infusion RV primer	AGTGTGAAGACCATGGCGAGGCCGGTGCCGGG
NM_027268	pNL1.1-*Scrn1*	Infusion FW primer	TGGCCTAACTGGCCGGTACCCTTTTTTGATTCTGGAAA
		Infusion RV primer	AGTGTGAAGACCATGCTGCCAAGCAGCCGGCT
NM_010206.3	pNL1.1-*Fgfr1*	Infusion FW primer	TGGCCTAACTGGCCGGTACCCAGGGCAAGGATATTGCTA
		Infusion RV primer	AGTGTGAAGACCATGCCAGTTCTGCGGTTAGAG
		Internal primer FW	ACCGCAGCGCCAAGTGAG
		Internal primer RV	CTCACTTGGCGCTGCGGT
NM_011173	pNL1.1-*Pros1* 5′UTR	Infusion FW primer	TGGCCTAACTGGCCGGTACCTGCTGTGTCACTACCGAAGAACAACGAGGAGAAGAT
		Infusion RV primer	AGTGTGAAGACCATGGCTGAGAGGATGGCCGG
		Internal primer FW	GGGTCCAAAGAGAGGGAGGAGCTCGGGCTGGGCCGCGGCAG
		Internal primer RV	TCCTCCCTCTCTTTGGACCCGCCTCATTTT
NM_019521	pNL1.1-*Gas6* 5′UTR	Infusion FW primer	TGGCCTAACTGGCCGGTACCTGCTGTGTCACTACCGAAGAACAACGAGGAGAAGAT
		Infusion RV primer	AGTGTGAAGACCATGGCGAGGCCGGTGCCGGGG
		Internal primer FW	GGGTCCAAAGAGAGGGAGGAACCCGCTGCCTCCTTCACGGC
		Internal primer RV	TCCTCCCTCTCTTTGGACCCGCCTCATTTT
NM_010206.3	pNL1.1-*Fgfr1* 5′UTR	Infusion FW primer	TGGCCTAACTGGCCGGTACCTGCTGTGTCACTACCGAAGAACAACGAGGAGAAGAT
		Infusion RV primer	AGTGTGAAGACCATGCCAGTTCTGCGGTTAGA
		Internal primer FW	GGGTCCAAAGAGAGGGAGGAGCACAGCGCTCGGAGCGCTCC
		Internal primer RV	GGAGCGCTCCGAGCGCTGTGCTCCTCCCTCTCTTTGGACCC
NM_020252.3	pNL1.1-*Nrxn1* 5′UTR	Infusion FW primer	TGGCCTAACTGGCCGGTACCTGCTGTGTCACTACCGAAGAACAACGAGGAGAAGAT
		Infusion RV primer	AGTGTGAAGACCATGCTCGGGGCTGGGGTGCG
		Internal primer FW	GGGTCCAAAGAGAGGGAGGACCTTTTTCCCTCTCCTCCTCC
		Internal primer RV	GGAGGAGGAGAGGGAAAAAGGTCCTCCCTCTCTTTGGACCC
NM_021377	pNL1.1-*Sorcs1* 5′UTR	Infusion FW primer	TGGCCTAACTGGCCGGTACCTGCTGTGTCACTACCGAAGAACAACGAGGAGAAGAT
		Infusion RV primer	AGTGTGAAGACCATGTCTGGAGCGTAGAGAAG
		Internal primer FW	GGGTCCAAAGAGAGGGAGGAAGCCTGGGCGAGCGGCAGGCA
		Internal primer RV	TCCTCCCTCTCTTTGGACCCGCCTCATTTT
NM_001198833	pNL1.1-*Ddr1* 5′UTR	Infusion FW primer	TGGCCTAACTGGCCGGTACCTGCTGTGTCACTACCGAAGAACAACGAGGAGAAGAT
		Infusion RV primer	AGTGTGAAGACCATGGCTCTCCGGGGCGGACC
		Internal primer FW	GGGTCCAAAGAGAGGGAGGATGGCTCCTCTCCCCGGAACAG
		Internal primer RV	TCCTCCCTCTCTTTGGACCCGCCTCATTTT
NM_011173	pNL1.1-*Pros1* promoter	Infusion FW primer	TGGCCTAACTGGCCGGTACCAACTGGCTTCTTTGTGGTG
		Infusion RV primer	AGTGTGAAGACCATGGTTTGTCTACGGGACGAGGCTGGCACTGCACAAGAAG
		Internal primer FW	TGGCTGCTCCGCCCGCCCGCGGGGAAATGAGAGAGGCCCA
		Internal primer RV	GCGGGCGGGCGGAGCAGCCA

RESULTS

AHA-SILAC Incorporation Is Not Affected by Mutations in eIF2B and Does Not Affect Astrocyte Viability

L-azidohomoalanine incorporation was measured in wt and *2b5*^{ho} astrocytes to investigate if the general protein synthesis rate is affected by the homozygous Arg191His mutation in eIF2Bε (**Figure 1**). Label incorporation increased linearly for a period of 4 h (**Figure 1B**). The incorporation occurred with similar kinetics in *2b5*^{ho} and wt astrocytes (**Figure 1B**), indicating that the eIF2Bε Arg191His mutation did not significantly affect protein synthesis rate. The viability of both wt and *2b5*^{ho} astrocytes was not influenced by AHA or SILAC treatment (**Figure 1C**). Expression of stress-related mRNAs was unaffected by the AHA-labeling protocol (Supplementary Figure 1). These results allow further proteomic analyses with an AHA incorporation pulse of 2 h.

Pulsed Labeling Proteomics of Astrocytes Reveals 80 Proteins Regulated by the eIF2Bε Arg191His Mutation

The AHA proteomic labeling approach was performed to identify and quantify proteins that are differentially translated in *2b5*^{ho} astrocytes. SILAC-labeled wt and *2b5*^{ho} astrocytes were subjected to AHA labeling for 2 h. After AHA labeling cells were harvested and subjected to bead-based enrichment using a Click-iT chemistry approach. Bound proteins were digested and resulting peptides were analyzed by LC-MS/MS. In four biological replicates, we identified a total of 2888 proteins across both wt and *2b5*^{ho} astrocytes. 1240 proteins were detected in at least 3 out of 4 biological replicates for both wt and *2b5*^{ho} astrocytes and used for further analysis. Accumulation of 72 proteins was increased and of eight proteins decreased in the *2b5*^{ho} AHA-proteome ($p < 0.05$, student's *T*-test) (**Figure 2A** and Supplementary File 1).

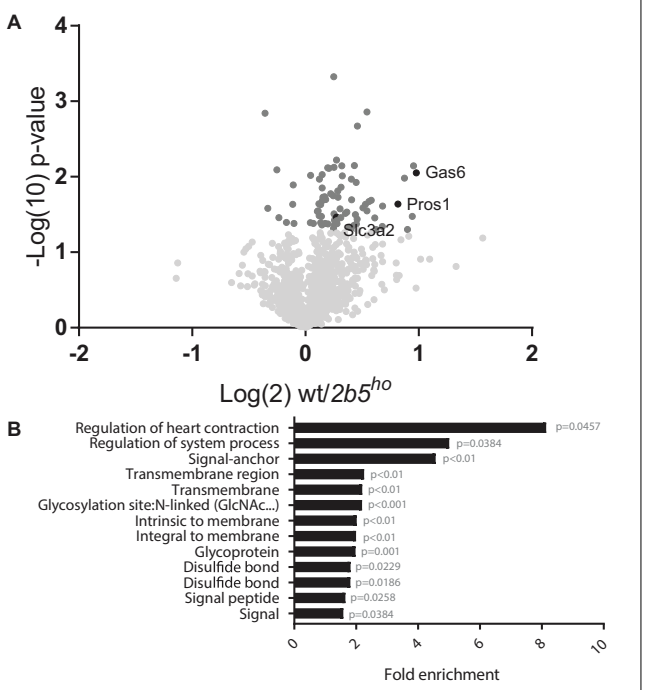

FIGURE 2 | Volcano plot of all 1240 proteins from the proteomic screen and DAVID analysis of the 80 proteins regulated by eIF2Bε^{Arg191His} identifies a difference in proteins that migrate through the secretory pathway. **(A)** In the volcano plot the proteins in darker gray have a *p*-value < 0.05 and are considered significantly differently synthesized between wt and *2b5*^{ho} astrocyte cultures. The *p*-values are plotted as Log(10) and $p < 0.05$ corresponds to -Log10 > 1.12. The fold change between wt and *2b5*^{ho} is plotted as Log(2) and a fold change of >2 corresponds to Log(2) > 1. 80 proteins are significantly different between wt and *2b5*^{ho} astrocytes of which 72 are increased and 8 are decreased in *2b5*^{ho} astrocytes. The proteins SLC3A2, PROS1, and GAS6 are highlighted in black. **(B)** The figure shows the overrepresentation analysis (*p*-value < 0.05) between the significantly different proteins with the proteins found in the proteome as a background. The pathway analysis reveals an overrepresentation of proteins with a signal peptide, transmembrane domain, *N*-linked glycosylation site(s) and/or disulfide bond(s). These terms together pinpoint targeting of proteins to the secretory pathway, some of which are post-translationally modified, as being affected by this mutation.

eIF2Bε^{Arg191His}-Regulated Proteins Localize Predominantly to the Plasma Membrane or Extracellular Space

We performed a DAVID pathway analysis to investigate if the eIF2Bε^{Arg191His}-regulated proteins share common functions, localizations or other features. This analysis showed enrichment for *N*-terminally glycosylated proteins, membrane proteins, proteins with disulfide bonds as well as proteins that contain a signal peptide among the set of eIF2Bε^{Arg191His}-regulated

TABLE 3 | Analysis of the proteins that are synthesized and migrate in the secretory pathway (SP).

AHA-SILAC data set*)	% of proteins with a signal peptide (absolute #)	% of proteins with a transmembrane domain (absolute #)	% of SP-targeting proteins (absolute #)
All proteins (1240)	19.1% (237)	14.3% (177)	25.6% (317)
Regulated (80)	33.8% (27)	30.0% (24)	47.5% (38)
Upregulated (72)	37.5% (27)	33.3% (24)	52.7% (38)
Downregulated (8)	0% (0)	0% (0)	0% (0)

**All proteins, proteins measured in wt and 2b5^{ho} astrocytes; regulated, proteins that differ significantly in intracellular accumulation between wt and 2b5^{ho} astrocytes (divided in upregulated and downregulated).*

proteins (**Figure 2B**). This outcome suggests that many regulated proteins follow the secretory pathway. Since signal peptides and transmembrane domains are associated with targeting to the secretory pathway (von Heijne, 1990; Petersen et al., 2011; Borgese, 2016), we tested all 1240 identified proteins for signal peptides or transmembrane domains. Signal peptides were found in 237 proteins and transmembrane domains in 177. The number of proteins predicted to pass through the secretory pathway was significantly enriched in the *2b5*^{ho} proteome (**Table 3**). 27 out of the 80 regulated proteins harbor a signal peptide and 24 have at least one transmembrane domain; 13 of the proteins harbor both a signal peptide and a transmembrane domain (in total 38 proteins out of 80). Intriguingly, the proteins annotated as migrating through the secretory pathway were all upregulated in *2b5*^{ho} astrocytes. It is possible that these proteins accumulate more in *2b5*^{ho} astrocytes during the 2-h labeling pulse due to a secretory pathway flux difference and not to an actual increase in translation rate. To investigate this, we analyzed the AHA-enriched secretome from wt and *2b5*^{ho} cultures after a 2-h AHA labeling. We detected 22 labeled proteins in the secretome, of which three (APOE, CST3 and POSTN) were significantly reduced in the *2b5*^{ho} astrocyte-conditioned medium. Intracellularly, APOE and POSTN were not changed by eIF2Bε^{Arg191His}. CST3 was significantly increased intracellularly in *2b5*^{ho} astrocytes. No other protein from the original 27 eIF2Bε^{Arg191His}-regulated proteins with a signal peptide was detected in the secretomes of wt and *2b5*^{ho} astrocytes. To further address the hypothesis that *2b5*^{ho} astrocytes have an altered secretory pathway flux, we evaluated the flux of proteins migrating through the secretory pathway with a reporter assay. The assay showed robust secretion of the Secluc reporter (Supplementary Figure 2) and secretion differences between wt and *2b5*^{ho} astrocytes were not detected (**Figure 3**).

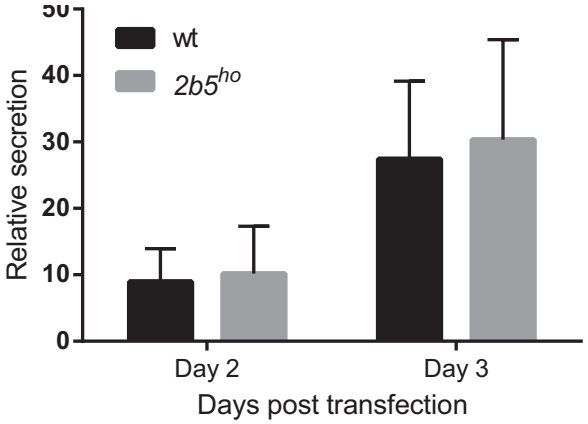

FIGURE 3 | The secretion of Secluc nanoluciferase via the secretory pathway is not affected in *2b5*^{ho} astrocyte cultures. Astrocytes were transfected with a luciferase reporter construct that expresses nanoluciferase fused to the IL-6 signal peptide. Luciferase activity was measured 2 and 3 days post transfection in cell lysates and cell culture medium. The ratio of extracellular:intracellular luciferase activity was determined as a measure for secretion through the secretory pathway. In the absence of the signal peptide, the extracellular luciferase activity was similar to the background signal (Supplementary Figure 2). The graph shows the mean ± SD (three independent cultures, six wells per culture).

Validation of eIF2Bε^{Arg191His}-Regulated Proteins

To investigate if the proteins that were found in the screen are indeed differentially expressed at the translational level, we selected eleven candidates that are either increased or decreased in wt vs. *2b5*^{ho} cultures. We quantified their mRNA levels to discriminate whether differences in protein amounts are regulated at the transcriptional or the translational level. Only one of the selected candidates differed in mRNA expression between wt and *2b5*^{ho} astrocytes (**Figure 4A**), suggesting that the increased accumulation of the other 10 proteins was not due to increased transcription or mRNA stability. Of the 11 candidates two were further investigated at the protein level by Western blot. We found that PROS1 and SLC3A2 were indeed significantly increased at the total protein level (**Figure 4B**). This result confirms the data from the proteomic screen and also demonstrates increased accumulation of these candidate proteins.

We next investigated several targets in mouse brain. At the mRNA level seven out of nine targets were similar between wt and *2b5*^{ho} brains (Supplementary Figure 3A). Two proteins were further assessed using Western blot (Supplementary Figure 3B). SLC3A2 protein abundance was also increased in brain lysates; however, this correlated with increased *Slc3a2* mRNA levels, suggesting transcriptional regulation in brain. PROS1 protein abundance was also increased in brain lysates, but *Pros1* mRNA abundance was not. This finding suggests translational upregulation of PROS1 both in cell culture and brain.

In Silico Analysis of mRNAs

eIF2B plays an essential role in the regulation of protein synthesis. For this reason, we investigated if the mRNAs of the eIF2Bε^{Arg191His}-regulated proteins share specific features that could explain the translational regulation by eIF2B. We investigated the 5′-UTRs for length, structural stability (%GC and ΔG) and number of uORFs with a Kozak sequence. The 5′-UTR length was significantly increased for mRNAs encoding eIF2Bε^{Arg191His}-regulated proteins (**Figure 5**). Of note, the mRNAs for the eight proteins *decreased* in the eIF2Bε^{Arg191His}-regulated proteome have relatively short 5′-UTRs (29-343 bases, median 133). This analysis showed that the eIF2Bε^{Arg191His} mutation differentially influences expression of proteins translated from mRNAs with *short* 5′-UTRs (<150 bases), which were underrepresented, compared to those with lengthy 5′-UTRs (>550 nucleotides), which were overrepresented; those translated from mRNAs with short 5′-UTRs, if regulated, tend to go down in expression in the mutant cells. The %GC in the 5′-UTRs did not significantly differ between eIF2Bε^{Arg191His}-regulated proteins and other proteins (**Figure 5**). The thermodynamic stability (ΔG in kcal/mole) of the 5′-UTR seemed to be higher for mRNAs encoding the eIF2Bε^{Arg191His}-regulated proteins, although not significantly (**Figure 5**). The

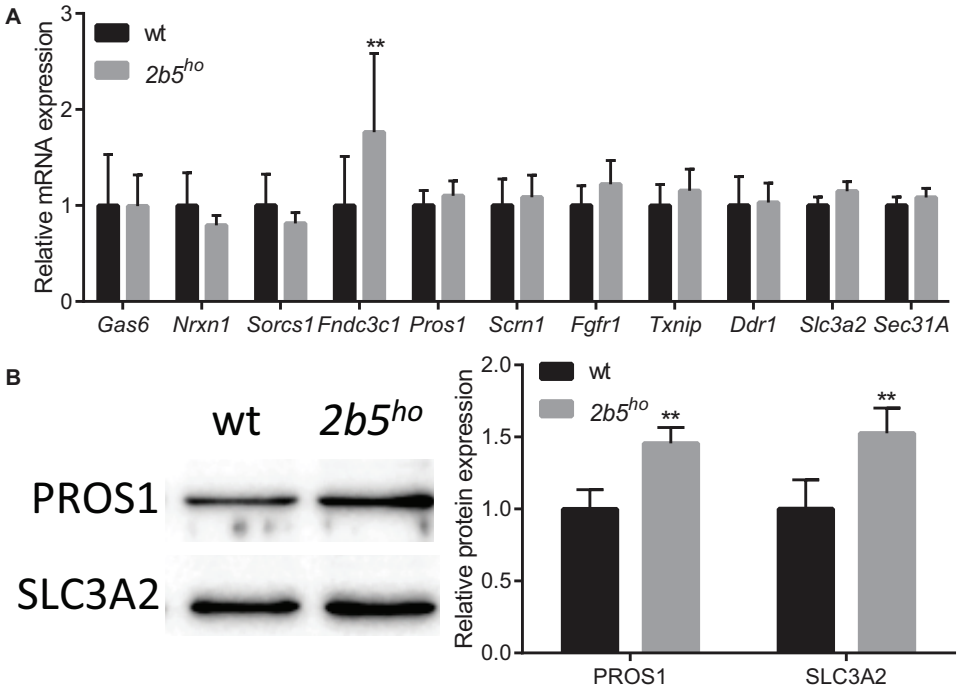

FIGURE 4 | mRNA and protein levels of candidate proteins in astrocyte cultures. **(A)** mRNA levels of the investigated candidate were investigated with qPCR. The mRNA levels were similar between wt and *2b5*^{ho} astrocytes ($n \geq 5$), with the exception of the *Fndc3c1* mRNA, which was increased in *2b5*^{ho} astrocytes. **(B)** The total protein levels of PROS1 and SLC3A2 were determined by Western blot. The graph shows the mean ± SD. The protein levels were increased in *2b5*^{ho} cultures compared to wt cultures ($n \geq 3$). $^{**}p < 0.01$. Post-translational modifications were overall not affected in *2b5*^{ho} astrocytes. Western blot analyses did not show whether PROS1 in astrocytes was post-translationally modified or not. Staining of all proteins (loading control) is shown in Supplementary Figure 4.

overall number of uORFs did not significantly differ for mRNA encoding the eIF2Bε^{Arg191His}-regulated proteins compared to the non-regulated proteins (**Figure 5**). However, mRNAs with high numbers of uORFs (8 or more) were clearly overrepresented in the group of significantly altered proteins.

Translation Efficiency Was Assessed in Reporter Assays

We investigated the potential translational regulation of some eIF2Bε^{Arg191His}-regulated proteins using reporter constructs encoding nanoluciferase driven by promoter sequences (including the 5′-UTR) of the candidates GAS6, PROS1, SCRN1 and FGFR1. A *Gapdh* promoter construct was included as non-regulated control. Transfection of each construct yielded similar luciferase expression in wt and *2b5*^{ho} cultures (**Figure 6**). Transfection of the pNL1.1-*Fgfr1* promoter construct did not yield a reliable level of nanoluciferase (approximately two–threefold over the background signal in non-transfected cells) and was therefore omitted from analysis. The levels of nanoluciferase activity expressed with the other constructs were still low in comparison to the *Gapdh*-promoter-driven expression. Because expression could be increased by replacing the candidate promoter with the *Gapdh* promoter, we therefore constructed *Gapdh*-candidate chimeras. With these chimeras we tested the 5′-UTR efficiency of candidates GAS6, SORCS1, PROS1, FGFR1, NRXN1, and DDR1 in wt and *2b5*^{ho} cultures. Neither the pNL1.1-*Fgfr1*-5′-UTR nor the pNL1.1-*Nrxn1*-5′-UTR constructs yielded quantifiable nanoluciferase expression. These constructs were omitted from further analyses. The expression from the chimeric promoter-5′-UTR constructs of *Gas6* and *Pros1* was increased by the *Gapdh* core promoter in both wt and *2b5*^{ho} cells. Still, none of these constructs yielded an increased nanoluciferase expression in *2b5*^{ho} compared to wt astrocytes (**Figure 6**).

Metabolic Screen of Astrocytes Conditioned Medium and Lysates

Because the proteomic data only gave small differences, the VWM phenotype remained difficult to explain. Tiny differences in protein levels and post-translational modifications occasionally lead to metabolic shifts. Thus we checked whether they affected cellular metabolism, using a mass spectrometry-based metabolic screen. We measured intra- and extracellular metabolites 24 and 72 h after replacing the culture medium. We looked at general energy consumption by measuring the uptake and secretion of metabolites from the culture medium (**Figure 7A**). As expected, both cultures had taken up glutamate (Martin-Jimenez et al., 2017) and aspartate (which use the same transporters) (Bender et al., 1997), reflecting specific astrocyte function. The uptake of glutamate and aspartate did not influence their intracellular levels (Supplementary File 2). Also, both wt and *2b5*^{ho} cultures showed uptake of pyruvate. Astrocytes convert

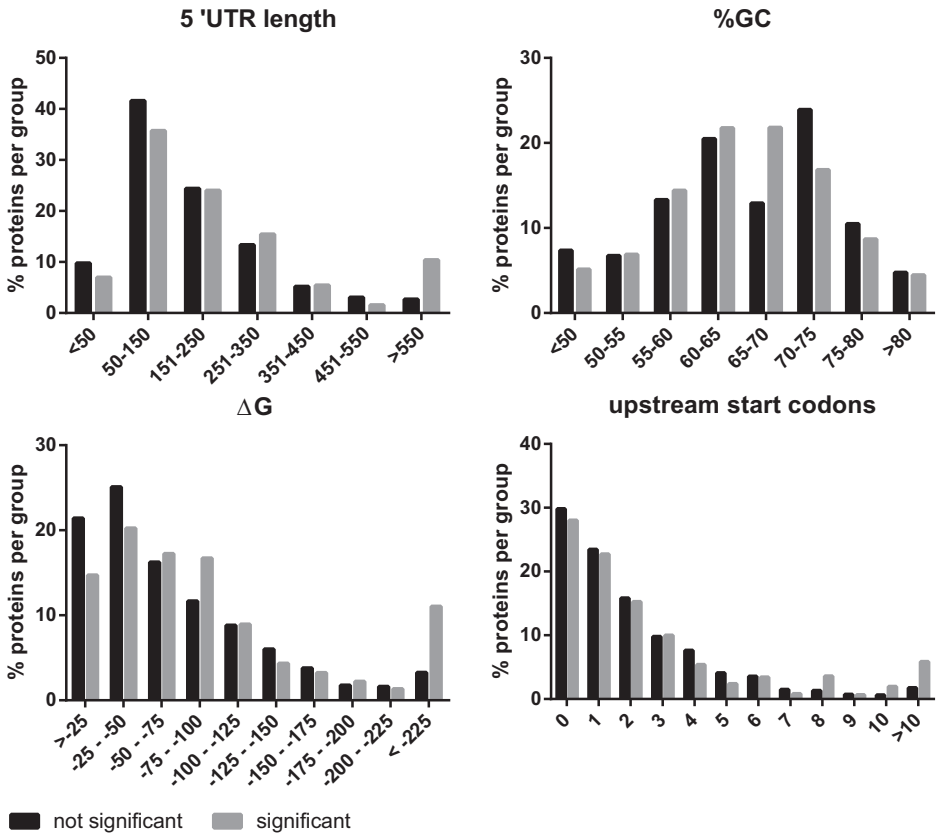

FIGURE 5 | *In silico* 5′UTR analysis of the eIF2B^{Arg191His}-regulated proteins. The 5′UTRs of the mRNAs encoding the proteins regulated by eIF2Bε^{Arg191His} mRNAs are significantly longer than of those encoding non-regluated proteins. They have an overall similar percentage GC content to the non regulated proteins. However, they seem to tend to higher ΔG's. These findings combined are indicative of relatively structured 5′-UTRs in the mRNAs of eIF2Bε^{Arg191His}-regulated proteins. The number of uORFs is similar between the significant and not significant proteins, though mRNAs with very high numbers (8 or more) of predicted uORFs are overrepresented in the group of significantly altered proteins.

pyruvate into lactate and glutamate/aspartate into glutamine, *cis*-aconitate and α-ketoglutarate (Martin-Jimenez et al., 2017). Indeed, the wt as well as the *2b5^{ho}* cultures secreted lactate, glutamine, *cis*-aconitate and α-ketoglutarate (**Figure 7A**). In addition, we investigated intracellular metabolites (**Figure 7B**). 6P-gluconate, an intermediate of the pentose phosphate pathway (PPP), was detected in *2b5^{ho}* but not in wt cells at both time points (**Figure 7B**). A fluctuation over time in NADPH levels was observed. The remaining metabolites tested did not show consistent differences over time between wt and *2b5^{ho}* astrocytes (**Figure 7B** and Supplementary File 2).

DISCUSSION

Here we aimed to identify whether specific proteins are translationally regulated by eIF2Bε^{Arg191His} in astrocytes. We used primary astrocyte cultures of the *2b5^{ho}* mouse model. Both wt and *2b5^{ho}* cells display an astrocyte morphology, synthesize CD44, nestin and vimentin (Supplementary Figure 5 and File 1), supporting astrocyte identity. We first established that cultures of primary astrocytes are suitable for sensitive labeling of newly synthesized proteins. Consistent with previous studies (Howden et al., 2013; Genheden et al., 2015), we found that AHA-labeling did not affect murine astrocyte viability for at least 16 h. No differences in AHA-labeling efficiency were observed between wt and *2b5^{ho}* astrocytes. These results confirm that the pulsed AHA-SILAC labeling protocol is suitable to study differences in proteins synthesized in wt and *2b5^{ho}* astrocytes, enabling us to investigate whether the Arg191His mutation in eIF2Bε affects translation of specific mRNAs.

We identified 80 proteins that accumulate differentially in wt vs. *2b5^{ho}* astrocyte cultures upon a 2 h AHA pulse. The majority (72 out of 80) is upregulated in *2b5^{ho}* astrocytes. We investigated the proteomic results by qPCR (11 candidates) and Western blot (4 candidates) (**Figure 4**). The tested antibodies detecting PROS1 and SLC3A2 showed consistent differences between wt and *2b5^{ho}* while TXNIP gave variable results and SCRN1 was not detected. Changes observed at the proteomic level were not due to altered mRNA levels, indicating that differences arose at the translational level. PROS1 and SLC3A2 protein levels were also increased in *2b5^{ho}* mouse brain lysates, supporting the findings in astrocyte cultures. Of these, *Pros1* was not increased at the mRNA level.

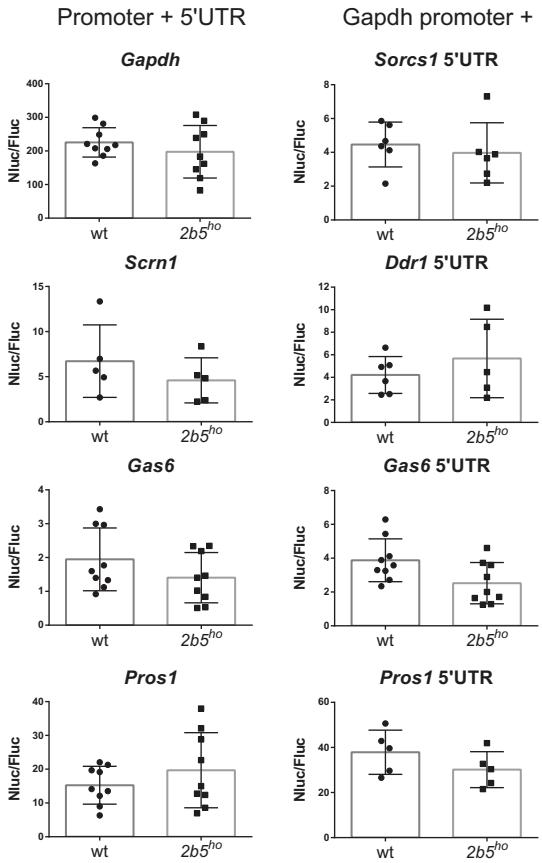

FIGURE 6 | *In vitro* analyses of candidate gene expression regulation do not reveal difference in promoter or 5′-UTR efficiency in wt and *2b5*^{ho} astrocytes. pNL1.1- *Scrn1*, *-Gas6* and *-Pros1* constructs and pNL1.1-*Sorcs1*, *-Ddr1*, *-Gas6* and *-Pros1* 5′UTR constructs were transfected into wt and *2b5*^{ho} astrocytes. Nanoluciferase activity was measured 3 days post transfection and corrected for firefly luciferase activity expressed from the pGL3-*Gapdh* internal standard. Every culture is shown as a single dot and bars represent the mean ± SD (n = 5–9). Replacement of the authentic *Pros1* or *Gas6* promoter by the *Gapdh* promoter increased the nanoluciferase expression by approximately twofold. pNL1.1-*Gapdh* was used as reference non-regulated promoter.

Our analyses indicate significant enrichment for proteins containing a signal peptide and motifs for *N*-glycosylation and disulfide bond formation in *2b5*^{ho} astrocytes (**Figure 2B**). These motifs highlight involvement of the endoplasmic reticulum (ER), the first organelle of the secretory pathway (Farhan and Rabouille, 2011). Approximately 50% of the eIF2Bε^{Arg191His}-regulated proteins were predicted to use the secretory pathway, suggesting an increased flux in *2b5*^{ho} astrocytes. The analysis of the secretome after 2 h AHA labeling as well as a standardized secretion assay did not indicate a difference in general secretion between wt and *2b5*^{ho} astrocytes. The increased amount of proteins using the secretory pathway observed in the proteomic screen may still indicate a deregulation of ER function. The secreted luciferase reporter used in the standardized secretion assay was not modified in the ER. Protein modifications could be further investigated by expressing a reporter protein that is, e.g., *N*-glycosylated, actively folded by chaperones and/or subjected to extensive disulfide bond formation in ER and Golgi. However, transfections with such reporter constructs probably do not yield protein levels sufficient to quantify the small differences in these processes. Overexpression of such reporters will overburden the ER and induce an unfolded protein response, compromising ER function, preventing reliable conclusions.

Next we investigated if the mRNAs for eIF2Bε^{Arg191His}-regulated proteins contain uORFs as reduced eIF2B activity increases translation of mRNAs with one or more uORFs in the 5′-UTR (Meijer and Thomas, 2002). *In silico* analyses of the 5′-UTR sequences of the candidates did not reveal obvious overall differences in uORF numbers. Nonetheless, mRNAs with high numbers of uORFs (8 or more) were clearly overrepresented in the group of significantly altered proteins (**Figure 5**). Thus, when eIF2B activity is reduced, protein synthesis of those mRNAs may be enhanced due to inefficient initiation on inhibitory uORFs, stimulating initiation on the "normal" start codon of the mORF (Meijer and Thomas, 2002). Our analyses highlighted some overrepresentation for mRNAs with (especially) long 5′-UTRs and probably higher ΔG in *2b5*^{ho} astrocytes (**Figure 5**). These length and ΔG observations suggest greater dependence on RNA helicase activity during translation initiation of eIF2Bε^{Arg191His}-regulated proteins (Sen et al., 2016). To further characterize the 5′-UTR efficiency in wt and *2b5*^{ho} astrocytes, we performed transient transfection assays for several candidates, some of which were longer than 700 nucleotides (*Fgfr1* and *Nrxn1*). Unfortunately, transfection of the *Fgfr1* and *Nrxn1* constructs did not yield reliable expression, which precluded testing whether they are translated more efficiently in *2b5*^{ho} than in wt astrocytes. The transfection assay is not robust enough to detect differences that were picked up with the pulsed AHA-SILAC proteomics and *in silico* 5′UTR analyses.

PROS1 was shown to be upregulated in both *2b5*^{ho} astrocytes and brain without increased mRNA level. In brain, PROS1 is expressed by astrocytes and microglia (Zhang et al., 2014). Interestingly, PROS1 and GAS6 (which was also found to be upregulated) bind the same class of receptors (Hafizi and Dahlback, 2006). PROS1 and GAS6 enhance myelination and support oligodendrocyte survival in mice *in vitro* and *in vivo* (Tsiperson et al., 2010; Gruber et al., 2014; Goudarzi et al., 2016; Akkermann et al., 2017). Recently, PROS1 was described to function in neural stem cells (NSCs) as a regulator for NSC quiescence, proliferation and NSC development into neurons or astrocytes (Zelentsova et al., 2016).

Other proteins enriched in the eIF2Bε^{Arg191His}-regulated proteome are implicated in astrocyte development. For example NRXN1 (Zeng et al., 2013) and SORCS1, that transports NRXN1, can induce differentiation toward astrocytes (Savas et al., 2015). Moreover TGFβ2 (Park et al., 2012) and its binding partners, ERBIN and latent TGFβ-binding protein 3 (LTBP3) are increased during astrocyte differentiation (Robertson et al., 2015). All these results suggest that *2b5*^{ho} astrocytes have a slightly altered differentiation state as shown before in *2b5*^{ho} mice and VWM patients (Bugiani et al., 2011; Dooves et al., 2016).

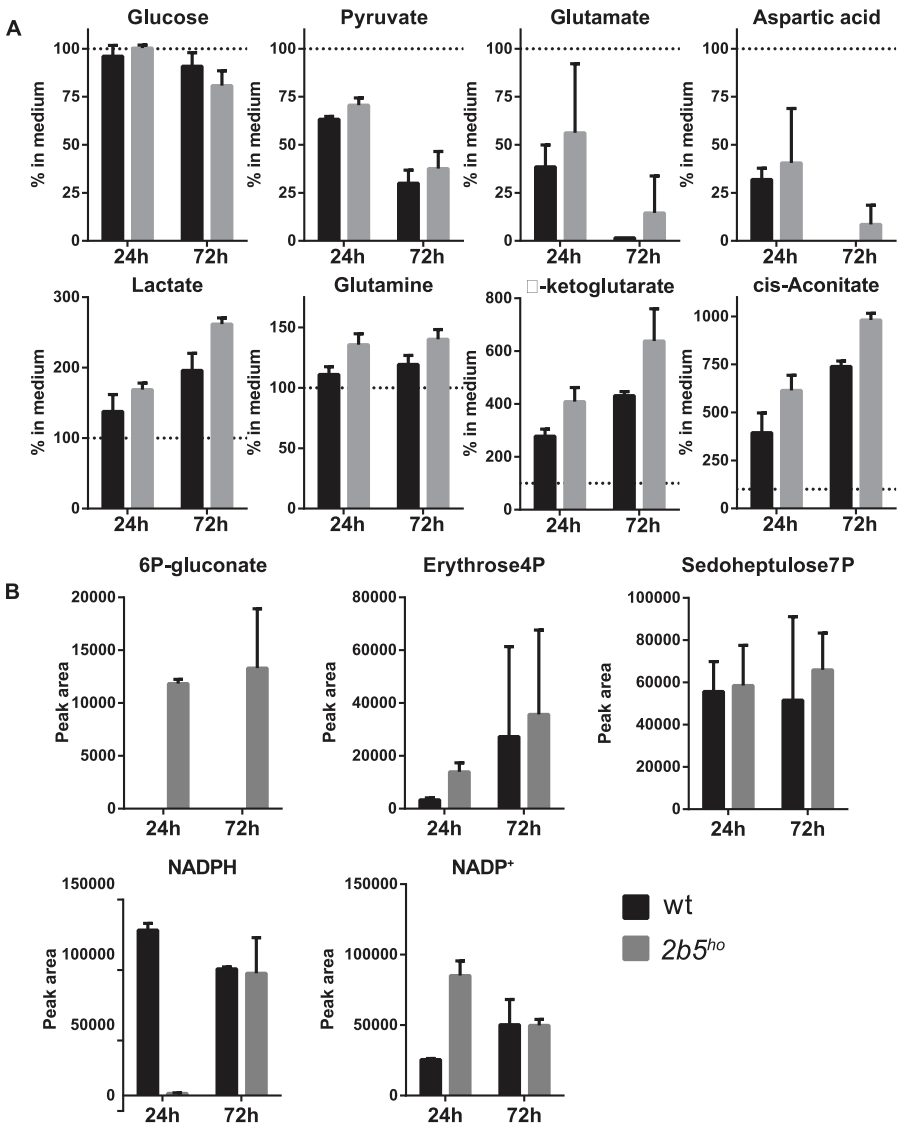

FIGURE 7 | Intracellular and extracellular metabolic analysis after 24 and 72 h of culture showed increased levels of intracellular levels of a pentose phosphate pathway intermediate (6P-gluconate). The astrocytes were cultured until 70% confluent. Media of the cultures were replaced with fresh medium. The cells as well as the media were collected after 24 and 72 h. The graphs show the mean ± SD. **(A)** The metabolite concentrations in the culture media of wt and *2b5*^{ho} astrocytes were compared to unconditioned media ($n = 2$). Glucose levels and pyruvate levels in conditioned medium of wt and *2b5*^{ho} astrocytes were decreased as well as glutamate and aspartate levels. Lactate, glutamine, *cis*-aconitate and α-ketoglutarate were increased in the conditioned medium of both cultures. **(B)** 6P-gluconate levels were consistently detected in *2b5*^{ho} cultures but not in wt cultures (24 and 72 h after replacing the culture medium). Four other metabolites of the pentose phosphate pathway were detected in the metabolic screen (erythrose-4P and sedoheptulose-7P, NADPH and NADP^{+}), but these were not consistently altered between wt and *2b5*^{ho} cultures.

To investigate other functional changes, we compared the metabolomes of wt and *2b5*^{ho} cells. We detected glutamate uptake in both cultures, which is a typical function of astrocytes, (Martin-Jimenez et al., 2017). This observation further confirms the astrocytic identity of the cultured cells. The most consistent difference observed was an increase in 6P-gluconate, an intermediate of the PPP. The PPP shunt is an alternative route for the metabolism of glucose which can supply ribose for nucleotide production in the non-oxidative part and NADPH in the oxidative part of the pathway. The reducing equivalents provided by NADPH are used both for biosynthesis and repair of oxidative damage (Stincone et al., 2015). The oxidative intermediate 6P-gluconate was increased in *2b5*^{ho} astrocytes while the non-oxidative intermediates sedoheptulose 7-phosphate and erythrose 4-phosphate were not consistent over time. These results suggest an increased activity of the PPP, especially at earlier time points. Interestingly, the observed PPP signature has been found in lung cancer cells in response to

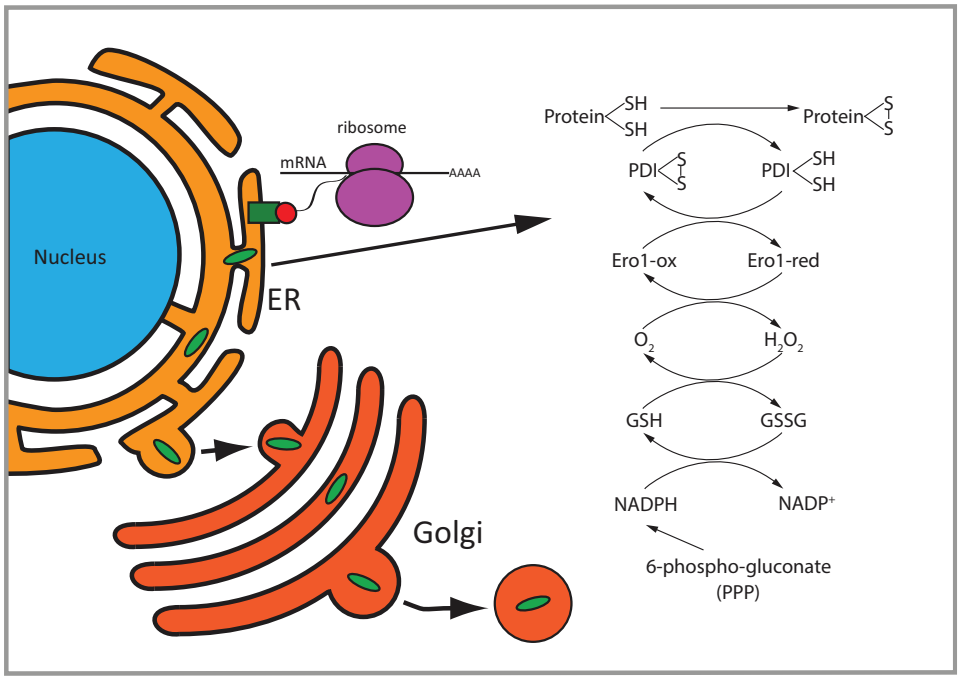

FIGURE 8 | Overview of differentially regulated functions in *2b5*^{ho} astrocytes. Proteins with a signal peptide or transmembrane domain enter the ER to be folded. Proteins going through the secretory pathway that are subjected to *N*-glycosylation and disulfide bond formation are enriched in the set of eIF2B$\varepsilon^{Arg191His}$-regulated proteins. Disulfide bridge formation through oxidation of these proteins can induce H_2O_2. 6-Phospho-gluconate is involved in the production of NADPH which can be used to remove H_2O_2. PDI, protein disulfide isomerase; GSH, reduced glutathione; GSSG, oxidized glutathione; Ero1-ox, oxidized Ero1; Ero1-red, reduced Ero1; PPP, pentose phosphate pathway.

reduced 6P-gluconate dehydrogenase (6PGDH) activity leading to reactive oxygen species (ROS) production (Patra and Hay, 2014).

Could there be a link between the two main observations, i.e., the deregulated transport of some proteins in the ER and the increased 6P-gluconate concentrations? We think this is likely; although PPP is cytosolic, there are links to the ER. Part of the pathway appears to be associated with the ER (Stockwell et al., 2012) and NADPH produced by the PPP might be needed to combat ROS formation, which can be produced in the ER by processes related to oxidative protein folding. On the basis of the combined proteomic and metabolomic findings, we hypothesize that *2b5*^{ho} astrocytes may accumulate ROS as a result of an increased flux of proteins (e.g., requiring correct disulfide bond formation) through the secretory pathway (**Figures 2**, **8**). Correct disulfide bond formation is dependent on protein disulfide isomerases (PDIs) and Ero1 in the ER (Bechtel and Weerapana, 2017). This process can result in H_2O_2 as by-product and increased PPP flux might compensate by producing NADPH (Espinosa-Diez et al., 2015). 6P-gluconate is the only metabolite in the metabolic screen that was changed in *2b5*^{ho} astrocytes and it is not completely clear whether this reflects increased production or decreased breakdown or a combination of both. There are indications that G6PDH is the only NADPH-producing enzyme activated upon oxidative stress and therefore it has been called "guardian of the cell redox potential" (Filosa et al., 2003). Lack of consistent changes over time in NADPH in *2b5*^{ho} astrocytes suggest that the balance between H_2O_2 and NADPH in steady state is "successfully" compensated (**Figure 8**). On the basis of our results we cannot discriminate between a compensated system or a deregulated system, the latter leading to pathology (Bechtel and Weerapana, 2017).

CONCLUSION

The 80 proteins differentially detected in the AHA-SILAC proteome are most likely translationally regulated as their mRNA levels are similar. Regulation thus must occur via increased synthesis or accumulation in *2b5*^{ho} astrocytes. We observed that the function of some of these differentially affected proteins is linked to astrocyte differentiation, which is known to be disturbed in VWM. As we would expect from deregulated protein synthesis in *2b5*^{ho} cells, the regulated proteins differ from their non-regulated counterparts in aspects of their 5′-UTRs. Altered synthesis may lead to an increase of proteins in the ER and secretory pathway without an overt effect on overall secretion. Possibly, increased demands of protein folding in the ER may result in generation of H_2O_2 or other ROS by-products (Espinosa-Diez et al., 2015). Thus, the increased synthesis of proteins that undergo disulfide formation and elevated 6P-gluconate might point to increased ROS in astrocytes, which may affect their function (**Figure 8**).

AUTHOR CONTRIBUTIONS

Substantial contributions to the conception or design of the work: LW, RP, CP, MvdK, and TA. The acquisition, analysis: LW, RP, EZ, CvB, TtB, and EP. Interpretation of data for the work: LW, RP, EZ, JK, CP, CB, MA, DS, and TA. Drafting the work or revising it critically for important intellectual content: LW, RP, EZ, CvB, TtB, EP, JK, CP, CB, MA, DS, MvdK, and TA. Final approval of the version to be published: LW, RP, EZ, CvB, TtB, EP, JK, CP, CB, MA, DS, MvdK, and TA. Agreement to be accountable for all aspects of the work in ensuring that questions related to the accuracy or integrity of any part of the work are appropriately investigated and resolved: LW, RP, EZ, CvB, TtB, EP, JK, CP, CB, MA, DS, MvdK, and TA.

FUNDING

LW, TA, TtB, EP, and MvdK are supported by ZonMw (TOP grant 91211005), Fonds NutsOHRA (1204-032), Hersenstichting Project grant (BGWS2014(1)-04), the Phelps Foundation (grant 2011.040). MA and RP are supported by Netherlands Organization for Scientific Research (NWO) as part of the National Roadmap Large-scale Research Facilities of the Netherlands, Proteins@Work (project number 184.032.201) and a VIDI grant (723.012.102) CB and EZ are supported by VENI grant (project 722.013.009) from the Netherlands Organization for Scientific Research (NWO).

ACKNOWLEDGMENTS

The authors thank Adri Thomas (University of Utrecht, Netherlands) for critical reading of the manuscript. They thank Anton den Hoed for the writing of the scripts used for the 5′UTR analysis. They thank I. G. Metgod and C. M. T. Beertsen (Department of Clinical Chemistry, VU University Medical Center, Amsterdam, Netherlands) for use of the Wallac 1420 Victor2 Microplate Reader. They thank R. Groen (Department of Hematology, VU University Medical Center, Amsterdam, Netherlands) for use of the GloMax® Discover System. They thank Sander Bobeldijk for facilitating the ΔG calculations.

SUPPLEMENTARY MATERIAL

The Supplementary Material for this article can be found online at: https://www.frontiersin.org/articles/10.3389/fncel.2017.00411/full#supplementary-material

REFERENCES

Akkermann, R., Aprico, A., Perera, A. A., Bujalka, H., Cole, A. E., Xiao, J., et al. (2017). The TAM receptor Tyro3 regulates myelination in the central nervous system. *Glia* 65, 581–591. doi: 10.1002/glia.23113

Babendure, J. R., Babendure, J. L., Ding, J. H., and Tsien, R. Y. (2006). Control of mammalian translation by mRNA structure near caps. *RNA* 12, 851–861. doi: 10.1261/rna.2309906

Bechtel, T. J., and Weerapana, E. (2017). From structure to redox: the diverse functional roles of disulfides and implications in disease. *Proteomics* 17:1600391. doi: 10.1002/pmic.201600391

Bender, A. S., Woodbury, D. M., and White, H. S. (1997). The rapid L- and D-aspartate uptake in cultured astrocytes. *Neurochem. Res.* 22, 721–726. doi: 10.1023/A:1027358211472

Bendtsen, J. D., Jensen, L. J., Blom, N., Von Heijne, G., and Brunak, S. (2004). Feature-based prediction of non-classical and leaderless protein secretion. *Protein Eng. Des. Sel.* 17, 349–356. doi: 10.1093/protein/gzh037

Borgese, N. (2016). Getting membrane proteins on and off the shuttle bus between the endoplasmic reticulum and the Golgi complex. *J. Cell Sci.* 129, 1537–1545. doi: 10.1242/jcs.183335

Bugiani, M., Boor, I., van Kollenburg, B., Postma, N., Polder, E., van Berkel, C., et al. (2011). Defective glial maturation in vanishing white matter disease. *J. Neuropathol. Exp. Neurol.* 70, 69–82. doi: 10.1097/NEN.0b013e318203ae74

Dieterich, D. C., Link, A. J., Graumann, J., Tirrell, D. A., and Schuman, E. M. (2006). Selective identification of newly synthesized proteins in mammalian cells using bioorthogonal noncanonical amino acid tagging (BONCAT). *Proc. Natl. Acad. Sci. U.S.A.* 103, 9482–9487. doi: 10.1073/pnas.0601637103

Dooves, S., Bugiani, M., Postma, N. L., Polder, E., Land, N., Horan, S. T., et al. (2016). Astrocytes are central in the pathomechanisms of vanishing white matter. *J. Clin. Invest.* 126, 1512–1524. doi: 10.1172/JCI83908

Eichelbaum, K., Winter, M., Berriel Diaz, M., Herzig, S., and Krijgsveld, J. (2012). Selective enrichment of newly synthesized proteins for quantitative secretome analysis. *Nat. Biotechnol.* 30, 984–990. doi: 10.1038/nbt.2356

Espinosa-Diez, C., Miguel, V., Mennerich, D., Kietzmann, T., Sanchez-Perez, P., Cadenas, S., et al. (2015). Antioxidant responses and cellular adjustments to oxidative stress. *Redox Biol.* 6, 183–197. doi: 10.1016/j.redox.2015.07.008

Farhan, H., and Rabouille, C. (2011). Signalling to and from the secretory pathway. *J. Cell Sci.* 124(Pt 2), 171–180. doi: 10.1242/jcs.076455

Ferreira, J. P., Overton, K. W., and Wang, C. L. (2013). Tuning gene expression with synthetic upstream open reading frames. *Proc. Natl. Acad. Sci. U.S.A.* 110, 11284–11289. doi: 10.1073/pnas.1305590110

Filosa, S., Fico, A., Paglialunga, F., Balestrieri, M., Crooke, A., Verde, P., et al. (2003). Failure to increase glucose consumption through the pentose-phosphate pathway results in the death of glucose-6-phosphate dehydrogenase gene-deleted mouse embryonic stem cells subjected to oxidative stress. *Biochem. J.* 370, 935–943. doi: 10.1042/bj20021614

Fogli, A., Schiffmann, R., Bertini, E., Ughetto, S., Combes, P., Eymard-Pierre, E., et al. (2004). The effect of genotype on the natural history of eIF2B-related leukodystrophies. *Neurology* 62, 1509–1517. doi: 10.1212/01.WNL.0000123259.67815.DB

Genheden, M., Kenney, J. W., Johnston, H. E., Manousopoulou, A., Garbis, S. D., and Proud, C. G. (2015). BDNF stimulation of protein synthesis in cortical neurons requires the MAP kinase-interacting kinase MNK1. *J. Neurosci.* 35, 972–984. doi: 10.1523/JNEUROSCI.2641-14.2015

Goudarzi, S., Rivera, A., Butt, A. M., and Hafizi, S. (2016). Gas6 promotes oligodendrogenesis and myelination in the adult central nervous system and after lysolecithin-induced demyelination. *ASN Neuro* 8:1759091416668430. doi: 10.1177/1759091416668430

Gruber, R. C., Ray, A. K., Johndrow, C. T., Guzik, H., Burek, D., de Frutos, P. G., et al. (2014). Targeted GAS6 delivery to the CNS protects axons from damage during experimental autoimmune encephalomyelitis. *J. Neurosci.* 34, 16320–16335. doi: 10.1523/JNEUROSCI.2449-14.2014

Hafizi, S., and Dahlback, B. (2006). Gas6 and protein S. Vitamin K-dependent ligands for the Axl receptor tyrosine kinase subfamily. *FEBS J.* 273, 5231–5244. doi: 10.1111/j.1742-4658.2006.05529.x

Hinnebusch, A. G. (2011). Molecular mechanism of scanning and start codon selection in eukaryotes. *Microbiol. Mol. Biol. Rev.* 75, 434–467. doi: 10.1128/MMBR.00008-11

Hinnebusch, A. G., Ivanov, I. P., and Sonenberg, N. (2016). Translational control by 5′-untranslated regions of eukaryotic mRNAs. *Science* 352, 1413–1416. doi: 10.1126/science.aad9868

Horzinski, L., Huyghe, A., Cardoso, M. C., Gonthier, C., Ouchchane, L., Schiffmann, R., et al. (2009). Eukaryotic initiation factor 2B (eIF2B) GEF

activity as a diagnostic tool for EIF2B-related disorders. *PLOS ONE* 4:e8318. doi: 10.1371/journal.pone.0008318

Howden, A. J., Geoghegan, V., Katsch, K., Efstathiou, G., Bhushan, B., Boutureira, O., et al. (2013). QuaNCAT: quantitating proteome dynamics in primary cells. *Nat. Methods* 10, 343–346. doi: 10.1038/nmeth.2401

Huang, D. W., Sherman, B. T., and Lempicki, R. A. (2009a). Bioinformatics enrichment tools: paths toward the comprehensive functional analysis of large gene lists. *Nucleic Acids Res.* 37, 1–13. doi: 10.1093/nar/gkn923

Huang, D. W., Sherman, B. T., and Lempicki, R. A. (2009b). Systematic and integrative analysis of large gene lists using DAVID bioinformatics resources. *Nat. Protoc.* 4, 44–57. doi: 10.1038/nprot.2008.211

Ingolia, N. T., Lareau, L. F., and Weissman, J. S. (2011). Ribosome profiling of mouse embryonic stem cells reveals the complexity and dynamics of mammalian proteomes. *Cell* 147, 789–802. doi: 10.1016/j.cell.2011.10.002

Kenney, J. W., Genheden, M., Moon, K. M., Wang, X., Foster, L. J., and Proud, C. G. (2016). Eukaryotic elongation factor 2 kinase regulates the synthesis of microtubule-related proteins in neurons. *J. Neurochem.* 136, 276–284. doi: 10.1111/jnc.13407

Kleijn, M., Scheper, G. C., Voorma, H. O., and Thomas, A. A. (1998). Regulation of translation initiation factors by signal transduction. *Eur. J. Biochem.* 253, 531–544. doi: 10.1046/j.1432-1327.1998.2530531.x

Konieczny, A., and Safer, B. (1983). Purification of the eukaryotic initiation factor 2-eukaryotic initiation factor 2B complex and characterization of its guanine nucleotide exchange activity during protein synthesis initiation. *J. Biol. Chem.* 258, 3402–3408.

Kozak, M. (1987). At least six nucleotides preceding the AUG initiator codon enhance translation in mammalian cells. *J. Mol. Biol.* 196, 947–950. doi: 10.1016/0022-2836(87)90418-9

Ladner, C. L., Yang, J., Turner, R. J., and Edwards, R. A. (2004). Visible fluorescent detection of proteins in polyacrylamide gels without staining. *Anal. Biochem.* 326, 13–20. doi: 10.1016/j.ab.2003.10.047

Leegwater, P. A., Vermeulen, G., Konst, A. A., Naidu, S., Mulders, J., Visser, A., et al. (2001). Subunits of the translation initiation factor eIF2B are mutant in leukoencephalopathy with vanishing white matter. *Nat. Genet.* 29, 383–388. doi: 10.1038/ng764

Li, W., Wang, X., Van Der Knaap, M. S., and Proud, C. G. (2004). Mutations linked to leukoencephalopathy with vanishing white matter impair the function of the eukaryotic initiation factor 2B complex in diverse ways. *Mol. Cell. Biol.* 24, 3295–3306. doi: 10.1128/MCB.24.8.3295-3306.2004

Liu, R., van der Lei, H. D., Wang, X., Wortham, N. C., Tang, H., van Berkel, C. G., et al. (2011). Severity of vanishing white matter disease does not correlate with deficits in eIF2B activity or the integrity of eIF2B complexes. *Hum. Mutat.* 32, 1036–1045. doi: 10.1002/humu.21535

Martin-Jimenez, C. A., Salazar-Barreto, D., Barreto, G. E., and Gonzalez, J. (2017). Genome-scale reconstruction of the human astrocyte metabolic network. *Front. Aging Neurosci.* 9:23. doi: 10.3389/fnagi.2017.00023

Meijer, H. A., and Thomas, A. A. (2002). Control of eukaryotic protein synthesis by upstream open reading frames in the 5'-untranslated region of an mRNA. *Biochem. J.* 367(Pt 1), 1–11. doi: 10.1042/bj20011706

Noderer, W. L., Flockhart, R. J., Bhaduri, A., Diaz de Arce, A. J., Zhang, J., Khavari, P. A., et al. (2014). Quantitative analysis of mammalian translation initiation sites by FACS-seq. *Mol. Syst. Biol.* 10:748. doi: 10.15252/msb.20145136

Park, J. H., Choi, M. R., Park, K. S., Kim, S. H., Jung, K. H., and Chai, Y. G. (2012). The characterization of gene expression during mouse neural stem cell differentiation in vitro. *Neurosci. Lett.* 506, 50–54. doi: 10.1016/j.neulet.2011.10.046

Patra, K. C., and Hay, N. (2014). The pentose phosphate pathway and cancer. *Trends Biochem. Sci.* 39, 347–354. doi: 10.1016/j.tibs.2014.06.005

Petersen, T. N., Brunak, S., von Heijne, G., and Nielsen, H. (2011). SignalP 4.0: discriminating signal peptides from transmembrane regions. *Nat. Methods* 8, 785–786. doi: 10.1038/nmeth.1701

Proud, C. G. (2001). Regulation of eukaryotic initiation factor eIF2B. *Prog. Mol. Subcell. Biol.* 26, 95–114. doi: 10.1007/978-3-642-56688-2_4

Robertson, I. B., Horiguchi, M., Zilberberg, L., Dabovic, B., Hadjiolova, K., and Rifkin, D. B. (2015). Latent TGF-beta-binding proteins. *Matrix Biol.* 47, 44–53. doi: 10.1016/j.matbio.2015.05.005

Ruijter, J. M., Thygesen, H. H., Schoneveld, O. J., Das, A. T., Berkhout, B., and Lamers, W. H. (2006). Factor correction as a tool to eliminate between-session variation in replicate experiments: application to molecular biology and retrovirology. *Retrovirology* 3:2. doi: 10.1186/1742-4690-3-2

Savas, J. N., Ribeiro, L. F., Wierda, K. D., Wright, R., DeNardo-Wilke, L. A., Rice, H. C., et al. (2015). The sorting receptor SorCS1 regulates trafficking of neurexin and AMPA receptors. *Neuron* 87, 764–780. doi: 10.1016/j.neuron.2015.08.007

Sen, N. D., Zhou, F., Harris, M. S., Ingolia, N. T., and Hinnebusch, A. G. (2016). eIF4B stimulates translation of long mRNAs with structured 5' UTRs and low closed-loop potential but weak dependence on eIF4G. *Proc. Natl. Acad. Sci. U.S.A.* 113, 10464–10472. doi: 10.1073/pnas.1612398113

Sonenberg, N., and Hinnebusch, A. G. (2009). Regulation of translation initiation in eukaryotes: mechanisms and biological targets. *Cell* 136, 731–745. doi: 10.1016/j.cell.2009.01.042

Stincone, A., Prigione, A., Cramer, T., Wamelink, M. M., Campbell, K., Cheung, E., et al. (2015). The return of metabolism: biochemistry and physiology of the pentose phosphate pathway. *Biol. Rev. Camb. Philos. Soc.* 90, 927–963. doi: 10.1111/brv.12140

Stockwell, S. R., Platt, G., Barrie, S. E., Zoumpoulidou, G., Te Poele, R. H., Aherne, G. W., et al. (2012). Mechanism-based screen for G1/S checkpoint activators identifies a selective activator of EIF2AK3/PERK signalling. *PLOS ONE* 7:e28568. doi: 10.1371/journal.pone.0028568

Tsiperson, V., Li, X., Schwartz, G. J., Raine, C. S., and Shafit-Zagardo, B. (2010). GAS6 enhances repair following cuprizone-induced demyelination. *PLOS ONE* 5:e15748. doi: 10.1371/journal.pone.0015748

van der Knaap, M. S., Breiter, S. N., Naidu, S., Hart, A. A., and Valk, J. (1999). Defining and categorizing leukoencephalopathies of unknown origin: MR imaging approach. *Radiology* 213, 121–133. doi: 10.1148/radiology.213.1.r99se01121

van der Knaap, M. S., Leegwater, P. A., Konst, A. A., Visser, A., Naidu, S., Oudejans, C. B., et al. (2002). Mutations in each of the five subunits of translation initiation factor eIF2B can cause leukoencephalopathy with vanishing white matter. *Ann. Neurol.* 51, 264–270. doi: 10.1002/ana.10112

van der Knaap, M. S., Pronk, J. C., and Scheper, G. C. (2006). Vanishing white matter disease. *Lancet Neurol.* 5, 413–423. doi: 10.1016/S1474-4422(06)70440-9

van Kollenburg, B., Thomas, A. A., Vermeulen, G., Bertrand, G. A., van Berkel, C. G., Pronk, J. C., et al. (2006). Regulation of protein synthesis in lymphoblasts from vanishing white matter patients. *Neurobiol. Dis.* 21, 496–504. doi: 10.1016/j.nbd.2005.08.009

von Heijne, G. (1990). The signal peptide. *J. Membr. Biol.* 115, 195–201.

Voorma, H. O., Thomas, A. A., and Van Heugten, H. A. (1994). Initiation of protein synthesis in eukaryotes. *Mol. Biol. Rep.* 19, 139–145. doi: 10.1007/BF00986956

Wong, K., Armstrong, R. C., Gyure, K. A., Morrison, A. L., Rodriguez, D., Matalon, R., et al. (2000). Foamy cells with oligodendroglial phenotype in childhood ataxia with diffuse central nervous system hypomyelination syndrome. *Acta Neuropathol.* 100, 635–646. doi: 10.1007/s004010000234

Zelentsova, K., Talmi, Z., Abboud-Jarrous, G., Sapir, T., Capucha, T., Nassar, M., et al. (2016). Protein S regulates neural stem cell quiescence and neurogenesis. *Stem Cells* 35, 679–693. doi: 10.1002/stem.2522

Zeng, L., Zhang, P., Shi, L., Yamamoto, V., Lu, W., and Wang, K. (2013). Functional impacts of NRXN1 knockdown on neurodevelopment in stem cell models. *PLOS ONE* 8:e59685. doi: 10.1371/journal.pone.0059685

Zhang, Y., Chen, K., Sloan, S. A., Bennett, M. L., Scholze, A. R., O'Keeffe, S., et al. (2014). An RNA-sequencing transcriptome and splicing database of glia, neurons, and vascular cells of the cerebral cortex. *J. Neurosci.* 34, 11929–11947. doi: 10.1523/JNEUROSCI.1860-14.2014

Conflict of Interest Statement: The authors declare that the research was conducted in the absence of any commercial or financial relationships that could be construed as a potential conflict of interest.

frontiers in Molecular Neuroscience

ORIGINAL RESEARCH
published: 21 November 2017
doi: 10.3389/fnmol.2017.00383

miR-145-5p/Nurr1/TNF-α Signaling-Induced Microglia Activation Regulates Neuron Injury of Acute Cerebral Ischemic/Reperfusion in Rats

Xuemei Xie[1,2], *Li Peng*[1,2], *Jin Zhu*[1,2], *Yang Zhou*[1,2], *Lingyu Li*[1,2], *Yanlin Chen*[1,2], *Shanshan Yu*[1,2] *and Yong Zhao*[1,2]*

[1]Department of Pathology, Chongqing Medical University, Chongqing, China, [2]Key Laboratory of Neurobiology, Chongqing Medical University, Chongqing, China

Nurr1 is a member of the nuclear receptor 4 family of orphan nuclear receptors that is decreased in inflammatory responses and leads to neurons death in Parkinson's disease. Abnormal expression of Nurr1 have been attributed to various signaling pathways, but little is known about microRNAs (miRNAs) regulation of Nurr1 in ischemia/ reperfusion injury. To investigate the post transcriptional regulatory networks of Nurr1, we used a miRNA screening approach and identified miR-145-5p as a putative regulator of Nurr1. By using computer predictions, we identified and confirmed a miRNA recognition element in the 3′UTR of Nurr1 that was responsible for miR-145-5p-mediated suppression. We next demonstrated that overexpression of Nurr1 inhibited TNF-α expression in microglia by trans-repression and finally attenuated ischemia/reperfusion-induced inflammatory and cytotoxic response of neurons. Results of further *in vivo* study revealed that anti-miR-145-5p administration brought about increasing expression of Nurr1 and reduction of infarct volume in acute cerebral ischemia. Administration of anti-miR-145-5p promotes neurological outcome of rats post MCAO/R. It might be an effective therapeutic strategy to relieve neurons injury upon ischemia/reperfusion of rats through interrupting the axis signaling of miR-145-5p- Nurr1-TNF-α in acute phase.

Keywords: Mir-145-5p, Nurr1, TNF-α, cerebral, ischemic/reperfusion

OPEN ACCESS

Edited by:
Margaret Su-chun Ho, ShanghaiTech University, China

Reviewed by:
Mohammad Badruzzaman Khan, Medical College of Georgia, Augusta University, United States
Dennis Qing Wang, Third Affiliated Hospital of Sun Yat-sen University, China

***Correspondence:**
Yong Zhao
zhaoyong668@cqmu.edu.cn

Received: *21 August 2017*
Accepted: *03 November 2017*
Published: *21 November 2017*

Citation:
Xie X, Peng L, Zhu J, Zhou Y, Li L, Chen Y, Yu S and Zhao Y (2017) miR-145-5p/Nurr1/TNF-α Signaling-Induced Microglia Activation Regulates Neuron Injury of Acute Cerebral Ischemic/Reperfusion in Rats. Front. Mol. Neurosci. 10:383. doi: 10.3389/fnmol.2017.00383

INTRODUCTION

Cerebral ischemia/reperfusion (I/R) injury-induced neuronal cell death is the most difficult problem to solve in clinical stroke (Al-Mufti et al., 2017). Activated microglia have been reported to act as sensors that detect abnormal metabolic changes following I/R, including reactive oxygen species and inflammatory cytokines (Yuan et al., 2014; Fumagalli et al., 2015). Microglia can release excessive proinflammatory cytokines and/or cytotoxic factors, such as tumor necrosis factor-α (TNF-α), interleukin-1β (IL-1β) and nitric oxide (NO), which have been shown to contribute to neuronal damage (Yuan et al., 2014; Roqué et al., 2016; Gullo et al., 2017). Therefore, suppressing overreaction of the microglial inflammatory response may be an efficacious therapeutic strategy to alleviate progression of stroke.

Nurr1 (NR4A2) is a member of the nuclear receptor 4 family of orphan nuclear receptors (Kim et al., 2015; Zou et al., 2017), and has been studied extensively in Parkinson's disease recently. Nurr1 has been shown to inhibit expression of proinflammatory neurotoxic mediators by docking to NF-κB-p65 on target inflammatory gene promoters in microglia (Saijo et al., 2009; Kim et al., 2015). Contra-directional coupling of Nur77 and Nurr1 are involved in neurodegeneration or injury by regulating endoplasmic reticulum stress and mitochondrial impairment (Gao et al., 2016; Wei et al., 2016). Cystatin C induces VEGF expression and attenuates PC12 cell degeneration by regulating p-PKC-α/p-ERK1/2-NURR1 signaling and inducing autophagy in Parkinson's disease (Zou et al., 2017). Taken together, these findings indicate that Nurr1 could be a promising therapeutic target in neuronal diseases. However, the specific functions and/or mechanisms of Nurr1 in I/R injury are still unknown.

Increasing recent evidence suggests important roles for microRNAs (miRNAs) in molecular processes of cerebral ischemia pathogenesis, which involve fast post-transcriptional effects and simultaneous regulation of various target genes (Ouyang et al., 2015; Minhas et al., 2017). Although several miRNAs have been reported to target Nurr1 in cancer cells (Yang et al., 2012; Wu et al., 2015; Beard et al., 2016), interaction between miRNAs and Nurr1 in cerebral I/R injury is still poorly understood.

In the present study, we therefore sought to determine: (1) how Nurr1 level and Nurr1-related microRNAs change in the brain of MCAO/R rats, an *in vivo* model; (2) in *in vitro* studies, what are the post-transcriptional regulatory network of Nurr1 and the specific mechanisms of Nurr1 on microglia activation; (3) in an *in vivo* study, whether miR-145-5p/Nurr1/TNF-α signal exerts neuron injury function upon cerebral ischemia-reperfusion in rats.

MATERIALS AND METHODS

Experimental Animals and Ethics Statement

About 170 adult male Sprague-Dawley (SD) rats (weight between 250–300 g, 60–80 d) were purchased from the Laboratory Animal Centre of Chongqing Medical University used for the *in vivo* study. Brain tissues from newborn SD rats (0–24 h) were used to culture primary neurons of cerebral cortex and glia cells. This study has been carried out within an appropriate ethical framework. All experimental procedures were performed in accordance with the National Institutes of Health (NIH) Guide for the Care and Use of Laboratory Animals and approved by Biomedical Ethics Committee of Chongqing Medical University. Maximum efforts have been made to minimize the number of animals used and their suffering. Adult male Sprague-Dawley rats were used that is exempted from ethics approval.

Cell Culture of Primary Microglia and Neurons and OGD/R Treatment

Primary glial cells were isolated from the cerebrum and cerebellum of rats (1-day-old) and placed in 6-well plates at a density of 1.2×10^6 cells/ml of DMEM supplemented with 10% fetal bovine serum (FBS), non-essential amino acids, and insulin. Plates were then placed in a humidified incubator with 5% CO_2/balanced with air (result: 20% O_2) at 37°C with medium change per 48 h. Microglia were isolated from the mixed glial population after confluent (about 2 weeks) by a method previously described (Jose et al., 2014). Microglia cultures with more than 96% purity were used for the study.

Primary neurons were obtained from the cerebral cortex of 1 day-old rats and cultured as described in our previous studies (Zhou et al., 2015; Chen et al., 2016). Approximately 2.0×10^6 cells per 2 mL of Neurobasal Medium containing 1% penicillin (Pen, 100 U/mL) and 1% streptomycin (Strep, 100 U/mL), and 2% B27 supplement were seeded per well. Neurons were cultured in a humidified incubator with 5% CO_2 at 37°C. After 6–7 days of culture *in vitro*, cells were examined to ensure more than 90% purity of neurons which could be used for further study.

The thorough method of OGD/R was conducted as previously described (Tauskela et al., 2003). Briefly, microglia/neurons were washed and cultured with glucose-free DMEM, which had been previously equilibrated with 1% O_2 + 5% CO_2 + 94% N_2 at 37°C for 2.0 h in an incubator. Cells were exposed to hypoxia by placing them in an incubator filled with a gas mixture of 1% O_2 + 5% CO_2 + 94% N_2 for 1.5 h at 37°C. The glucose-free DMEM were then changed back to their special mediums and cultures were returned to the normal incubator for recovery times of 0.5 h, 1.0 h, 2 h, 6 h or 12.0 h. An appropriate time of reoxygenation was selected for subsequent studies. Cells exposed to normoxia were used as negative control.

Coculture of Microglia and Neurons

Primary microglia were seeded onto Transwell permeable support membrane inserts (Corning, NY, USA) at a density 1.0×10^6/well in DMEM medium supplemented with 10% FBS and allowed to settle and grow for 24 h, which constituted the upper chamber in a 2-chambered microglia-neuronal cell coculture system. The cultured neurons were seeded into the bottom of 6-well plates at a density of 2.0×10^6 cells/well in specific Neurobasal medium as described above until confluence at 24 h. These neurons were then cocultured with microglia-containing inserts for 48 h in the following conFigureuration: (1) neurons incubated with empty inserts lacking microglia (neurons only); (2) neurons incubated with inserts containing microglia that had not been exposed to OGD/R (microglia normoxia (nor.) + neurons); and (3) neurons incubated with inserts containing activated microglia that had been previously exposed to OGD/R for 2 h (microglia OGD/R 2 h + neurons). Following coculture, the two coculture chambers were disassembled, and exposed neurons were washed with PBS and harvested for micro-RNA, mRNA, and/or cell viability analysis (Chen et al., 2012, 2016).

Construction of Middle Cerebral Artery Occlusion and Reperfusion (MCAO/R) Model for *in Vivo* Experiments

SD rats were fed and housed under standard conditions before operation, and the room temperature was monitored at 24–28°C throughout the surgical procedure. MCAO model of rats were construct by method of intraluminal vascular occlusion as previously described in our laboratory (Chen et al., 2012, 2016). All the surgical procedures were performed successfully under anesthesia with 3.5% chloral hydrate (350 mg/Kg, intraperitoneal injection). The nylon filament with its tip rounded (diameter 0.24–0.28 mm), determined by the animal weight, was inserted into the middle cerebral artery for 1.5 h. Reperfusion of the ischemic artery was established by withdrawal of the filament until the tip cleared the lumen of the external carotid artery. Regional cerebral blood flow was monitored by an ultrasonic blood flow meter during the operation.

A successful occlusion and reperfusion of MCAO model was evaluated by methods of Neurological Outcome Assays and infarction volume assays as described in references (Lourbopoulos et al., 2008; Wang et al., 2014). Rats of sham-operated were subjected to the same surgical procedures as MCAO/R group except for occlusion of the external carotid artery. Animals which had blood reperfusion below 70% or died during reperfusion were excluded from analysis.

After MCAO, the experimental rats in each group (n = 5) were euthanized randomly at the end of reperfusion for 2, 6, 12, 24 and 48 h to detect the alterations of various index. SD rats were divided randomly into 15 groups. Before suffered MCAO/R, the groups were: null group, scramble group, anti-miR-145-5p group, miR-145-5p mimic group, Nurr1-siRNA group, Nurr1 activation plasmid group (Nurr1; intra-cerebroventricular injection). After MCAO/R, the groups were: sham-operated (sham) group, MCAO/R group, null + MCAO/R group, scramble + MCAO/R group, anti-miR-145-5p + MCAO/R group, miR-145-5p mimic + MCAO/R group, Nurr1-siRNA + MCAO/R group, Nurr1 + MCAO/R group. miR-145-5p mimic and anti-miR-145-5p were administered to the animals before they underwent any surgery via intracerebroventricular infusion.

Neurological Outcome Assays

Two different assays were used to assess the neurological deficit of the rat on days 1, 7 and 14 after MCAO/R after the induction of stroke. A modified Neurological Severity Score (mNSS) was applied, three motor tests and two sensory tests were included, which are evaluated by total score 18 (Lourbopoulos et al., 2008; Wang et al., 2014). The scores are added up to a score between 12 (severe impairment) and 6 (no neurological impairment). Additionally, the foot fault test was performed to assay fine motor skills and proprioception. The amount of foot faults was computed via ((number of left forelimb faults) + (number of left hindlimb faults))/((total number of left forelimb steps) + (total number of left hindlimb steps)) (Lourbopoulos et al., 2008; Wang et al., 2014).

Infarct Volume Analysis

SD rats were sacrificed upon different treatment, and the brain tissue was prepared into 3 mm sections for 2,3,5-triphenyltetrazolium chloride (TTC) staining (Sigma-Aldrich, St. Louis, MO, USA). Cerebral tissue sections were incubated with 2% TCC solution in the dark room at 37°C for 5 min; the tissue sections were then fixed in 4% paraformaldehyde. The living brain tissues was bright red, however the ischemic or necrotic tissues were pale. The digital images were further analyzed by Sigma Scan Pro 5.0 Software. The real infarct volume (cortex, striatum and hemisphere), after excluding edema, was calculated by subtraction of the ipsilateral non-infarcted regional volume from the contralateral regional volume. The real infarct volume was then divided by the contralateral regional volume as a percent of the contralateral region (McCarter et al., 2017).

RNA Extraction, Reverse Transcription and RT-qPCR

Total RNA and miRNA in the brain tissues or primary cultured cells were extracted using TRIzol® with miRcute miRNA isolation kits (Tiangen Biotech, Beijing, China). The concentration and integrity of sample RNA were determined using Nanodrop ND-1000 spectrophotometry (Nanodrop Tech, Rockland, DE, USA) and denaturing agarose gel electrophoresis. The cDNA was obtained by reverse transcription with an miRcute miRNA First-Strand cDNA Synthesis kit (Tiangen Biotech, Beijing, China). The RT-qPCR was performed using iQ5 RT-qPCR detection system (Bio-Rad Laboratories, Inc., Hercules, CA, USA).

Quantitation of Nurr1 and TNF-α mRNAs was performed using SYBR green assay (Zhou et al., 2015). Specific primer sequences were designed and generated by Sangon Biotech (Shanghai, China). For miRNA detection, the cDNA was obtained by reverse transcription with an miRcute miRNA First-Strand cDNA Synthesis kit (Tiangen Biotech, Beijing, China). Stem-loop qRT-PCR reactions were performed according to manufacturer's protocols using miRNA specific stem-loop primers (Sangon Biotech, Shanghai, Co., Ltd.). Real-Time PCR reactions were conducted on a PCR amplifier (CFX-96 Content Real-time System). The endogenous control of both mRNAs and miRNAs was Ribosomal RNA (18S rRNA) for the quantitative PCR (qPCR) assays because it is known to expressed stably in cerebral ischemic conditions (Sepramaniam et al., 2010; Liu F. J. et al., 2015).

miRNA Profiling

A miRNA microarray was performed according to the MicroRNA Expression Profiling Assay Guide (Illumina Inc., San Diego, CA, USA). The extracted RNA from the cerebral cortex of rats was labeled with Hy3 dye at 3′-end using the miRCURY LNA Power Labeling Kit (Illumina Inc.) in the 500 ng intact total RNA sample (Liu C. et al., 2015). The labeled miRNAs were hybridized to the BeadChip for 16–18 h, according to manufacturer's instructions (Illumina Inc.). The microarray chips were then

washed and scanned by InnoScan700, microarray scanner and analyzed by GenomeStudio™ Gene Expression Module v1.0 software (Illumina Inc.). The p value < 0.01 was considered to be accurately detected and selected for further analysis.

miRNA Target Prediction and Mutagenesis

Six miRNA target-prediction algorithms were used to identify putative miRNA regulators of Nurr1: http://www.mirbase.org/; http://mirtar.mbc.nctu.edu.tw/human/index.php; http://www.targetscan.org; http://www.microrna.org; http://mirdb.org/cgi-bin/search.cgi; and http://pictar.mdc-berlin.de/. By using these algorithms, a putative seed region was determined and mutated using site-directed mutagenesis (Mutagenex, Inc., Piscataway, NJ, USA; Jeyaseelan et al., 2008). Reporter constructs containing either the wild-type or mutated 3′UTR were used to demonstrate miR-145-5p specificity in the Nurr1 3′UTR.

Cloning of Nurr1 3′UTR and Dual Luciferase Reporter Assay

The 3′UTR of *Nurr1* was amplified by PCR using gene specific primers and cloned into firefly-luciferase-expressing vector pMIR-REPORT (Ambion, Austin, TX, USA). HEK293T cell was used in this study for its high transfection efficiency (>90%; Karra and Dahm, 2010). Briefly, HEK293T cells were cultured in 24-well plates and transfected with 40 nM anti- or mimic microRNAs for 3 h followed by 200 ng/well of pMIR-REPORT constructs for 3–5 h. Before lysed for measurement of luciferase activity, cells were then left to recover in CO_2 incubator at 37°C for 48 h. The effect of miRNA binding with 3′UTR of Nurr1 quantified using Dual luciferase assay according to manufacturer's protocol (Cat # E1910; Promega, USA). Transfection efficiencies were normalized to those of cells by co-transfecting with the Renilla-luc-expressing vector pRL-CMV (Cat # E2261; Promega, Madison, WI, USA) at 5 ng/well.

Gene Transfection and siRNA Interference Experiments *in Vivo* and *in Vitro*

The pcDNA-Nurr1 overexpression lentivirus was constructed and packaged by Neuron Biotech (Shanghai, China). The Nurr1-siRNA, scramble siRNA and siRNA reagent system were purchased from Santa Cruz Biotechnology Inc. (Cat # sc-36111). For *in vitro* assays, the confluent microglia and neuron were transfected with pcDNA- Nurr1 using Lipofectamine 2000 (Invitrogen, Carlsbad, CA, USA) according to the manufacturer's instructions. The siRNA interference of Nurr1 was performed according to the manufacturer's instructions. Cells transfected with empty vectors (EV) and un-transfected cells (Null) served as negative control groups. Sustained Nurr1 overexpression or down-regulation were confirmed by qRT-PCR and western blot analysis 72 h after transfection. Scramble siRNA and Nurr1-siRNA were dissolved in RNase-free water to a final concentration of 2 μg/μL, and injected ipsilaterally into the left lateral cerebral ventricle 48 h before MCAO.

Cell Viability Analysis

The cultured neurons with different treatments were grown in 96-well plates separately at a density of 2.0×10^5 cells/mL and then harvested to analyze cell viability using The Cell Titer 96 Aqueous One Solution cell proliferation assay with 3-(4,5-dimethylthiazol-2-yl)-2,5-diphenyltetrazolium bromide (MTS; Cat # G3582, Promega, USA). Absorbance was measured at 490 nm using a microplate reader.

Chromatin Immunoprecipitation (ChIP) Assay

ChIP assay were performed using EZChIP kit which contains all necessary reagents to perform 22 individual (ChIP) reactions using inexpensive protein G agarose beads (Cat # 17-371, EZ-ChIP™, Merck Millipore, USA). Briefly, for each experimental condition, 2×10^7 rat primary microglia were needed. Cells were cross-linked for 10 min with 1% formaldehyde. Samples were incubated with Anti-Nurr1 antibody [N1404]—ChIP Grade (ab41917; Cat # ab41917, 1:100, Abcam, Cambridge, MA, USA; 1:100 in ChIP dilution buffer - 0.01% SDS, 1.1% Triton X-100, 1.2 mM EDTA, 16.7 mM Tris-HCl (pH 8.1), 167 mM NaCl, proteanase inhibitor cocktail) for 16 h at 4°C. A 150-bp region of the rat proximal TNF-α promoter was amplified spanning the NF-κB site. Protein binding was detected using RT-qPCR.

Immunofluorescence Staining

Fresh freeze brain sections (10 μm) were incubated with 10% normal goat serum/0.3% Triton-X 100 diluted in PBS blocking solution at 37°C for 1 h. Slides were then incubated with the following corresponding primary antibodies: Polyclonal rabbit anti-rat Nurr1 (1:100 dilution; sc-991, Santa Cruz, CA, USA) and monoclonal mouse anti-goat CD68 (1:50 dilution; Cat # ab1211, Abcam, Cambridge, MA, USA) overnight at 4°C. Following incubation, slides were then washed in 0.1 M PBS and incubated for 1 h with the following secondary antibodies: goat anti-rabbit Immunoglobulin G (1:100 dilution; zhongshanjinqiao, China) and goat anti-mouse Immunoglobulin G (1:200 dilution; zhongshanjinqiao, China). DAPI was used to stain the nuclei (Sigma-Aldrich). All the sections were visualized under a Nikon ECLIPSE Ti fluorescence microscope, loaded with a CoolSNAP photometrics camera at 400× magnification.

Western Immunoblot Analysis

Cell lysis buffer of cultured neurons and the rat cortex supplemented with proteinase inhibitors were used to extract total protein. The quantified proteins were separated by 8% SDS-PAGE and transferred onto polyvinylidene fluoride (PVDF) membranes. The membranes were subsequently blocked with 5% skim-milk for 2.0 h at room temperature and incubated in primary antibody overnight at 4°C. Dilutions for primary antibodies were as follows: Polyclonal rabbit anti-Nurr1 and anti-TNF-α (1:500 dilution; 6945S, Cell Signaling Technology, USA), Polyclonal mouse anti-β-actin (1:5000, ABclonal, Wuhan, China, AC004) and anti-IL1β (1:1000, Bioworld technology, USA). The membranes were then incubated with appropriate secondary antibodies at 37°C for 2 h (dilution 1:5000, Sangon Biotech, Shanghai, Co., Ltd.). The density of bands was detected

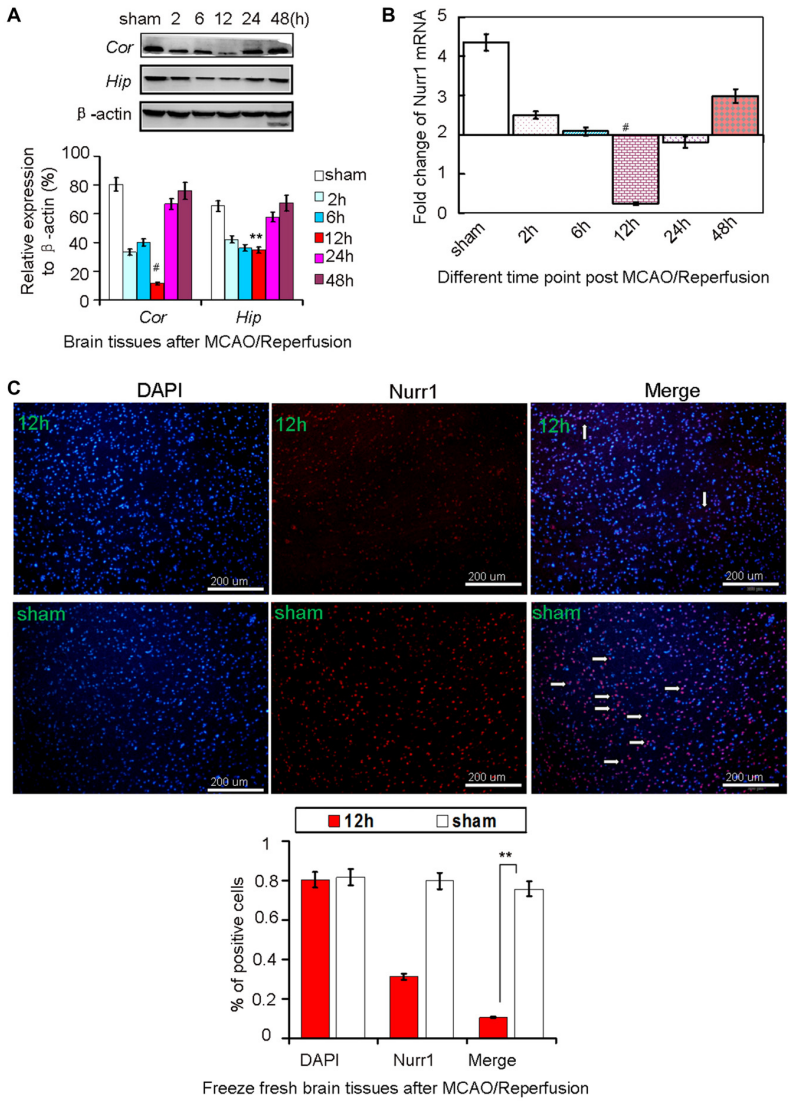

FIGURE 1 | Nurr1 expression at 2, 6, 12, 24 and 48 h after MCAO/R. **(A)** Nurr1 protein was measured by Western blot at each time point upon cerebral ischemia/reperfusion. The gray intensities of the bands were quantified using ImageJ software and presented as percentage of β-actin (internal control, %). Nurr1 expression decreased sharply and reached a minimum at 12 h in cerebral cortex (*Cor*) and hippocampus (*Hip*) of rats. **(B)** Nurr1 mRNA was measured by RT-qPCR and presented as relative expression (mean ± SD, $n = 3$). **(C)** Nurr1 protein expression was significantly declined in the infarct side of cortex by immunofluorescence staining from fresh freeze brain sections 12 h after MCAO/R. $^{**}p < 0.01$, $^{\#}p < 0.001$.

using an enhanced chemiluminescence system (Cat # 32132, Pierce™ ECL Plus Western Blotting Substrate ECL Plus, USA), and the gray value of bands was quantified using ImageJ analysis software. The relative expression quantity of protein was scored as the ratio of target protein intensity to β-actin staining intensity.

Statistical Analysis

All data are expressed as mean ± SD. One-way analysis of variance (ANOVA) followed by Bonferroni test was used to compare results among all groups. The Spearman's correlation test was used to examine the correlations of relative expression levels between protein and miRNA. The SPSS 17.0 software package was used to execute all statistics. All experiments were independently repeated at least three times. p-values < 0.05 were considered statistically significant.

RESULTS

Nurr1 Expression Decreased in Both the Cerebral Cortex and Hippocampus of Rats after MCAO/R

Every three rats were euthanized randomly in each group at different time point and different treatment after MCAO/R. Rats

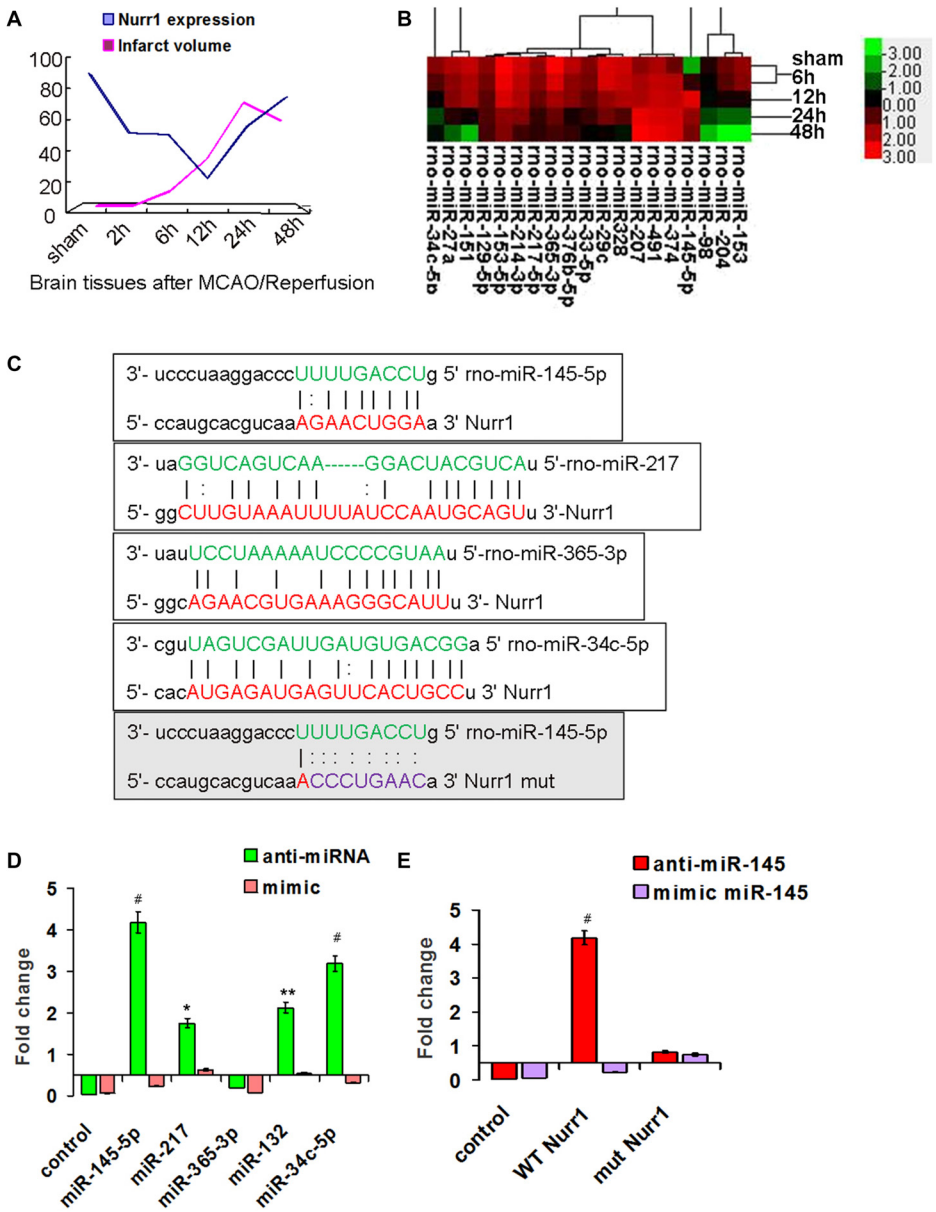

FIGURE 2 | Screening for miRNAs that directly target the 3′UTR of Nurr1. **(A)** The infarct volume was negatively correlated with Nurr1 expression some extent by Pearson correlation test, but was not statistically significant (correlation coefficient −0.457, $P = 0.362$). **(B)** Heat map of predicted miRNAs expression in cerebral cortex tissue from sham and MCAO/R animals (one-way analysis of variance (ANOVA), $p < 0.05$). **(C)** The predicted binding sites of selected miRNAs (in green color) to the 3′UTR of Nurr1 (in red color) is mapped in this figure. Nucleotides which were altered for mutational studies are marked in gray color of background. **(D)** Quantitation of the effects of anti miRNAs and miRNA mimics interaction with the 3′UTR of Nurr1. **(E)** Quantitation of the effects of anti-miR-145-5p and miR-145-5p mimic interactions with the normal binding sites (WT) and mutated binding sites (mut) in 3′UTR of Nurr1. $^{*}p < 0.05$, $^{**}p < 0.01$, $^{\#}p < 0.001$.

in the sham group were used as negative control. Approximately 138 rats were euthanized in the whole study, with the 82.4% (138/170) survival rate of the animals after MCAO surgery. Both mRNA and protein levels of Nurr1 decreased from the start of ischemic stroke, reached a minimum at 12 h, and then increased until 48 h (**Figures 1A,B**). Similarly, Nurr1 expression significantly decreased on the infarct side of the cortex and hippocampus of fresh frozen brain tissue sections as shown by immunofluroescence assays (**Figure 1C**). In addition, brain tissues were stained with 2,3,5-triphenyl-tetrazolium chloride (TTC) to measure infarct size on the ipsilateral side. Infarct size peaked at ∼24 h and then decreased progressively until 48 h after occlusion (**Figure 2A**). Infarct volume was negatively correlated with Nurr1 expression in the cortex, but this was not statistically significant using the Pearson correlation test (correlation coefficient −0.457, $P = 0.362$).

TABLE 1 | microRNAs that potentially regulate Nurr1 through its 3′UTR by bioinformatic analysis prediction in three foremost databases in this field.

miRNA	Mature sequence	Target Score of Nurr1 prediction			Other target genes
		MIRDB	TARGETSCAN (Pct)	MICRORNA (mirSVR)	
>rno-miR-145-5p	GUCCAGUUUUCCCAGGAAUCCCU	81	0.30	−1.03	SRGAP2, Abhd17c, Ebf3, Add3, Ythdf2, Kcna4, Elmo1, Snx8, Abhd17b, Cbfb, Ino80, Ap1g1, Rev3l, Scamp3, Mdfic, Spop, Zfyve9, Mpzl2, Prkx, Pikfyve, Angpt2, RGD1562865, Zbtb6, Cachd1, Zfhx4, Zfyve26, Dusp6, Actg1, Fam135a, H1f0, H2afx, Spsb4, Lox, Rapgef2, Gosr2, Coro2b, Snx27, Cdo1, Spats2, Nol9, Csmd3
>rno-miR-365-3p	UAAUGCCCCUAAAAAUCCUUAU	–	0.28	−0.55	Ing3, Fads1, Casp6, Usp48, Sgk1, Eltd1, Adm, Pax6, Ublcp1, Mrs2, Crbn, Gcom1, MGC112830, Ets1, Rgs1, Tcp11l2, Otc, Tyms, Pebp1, Inhbe, Larp1b, Igf1, Csk, Ubfd1, Dcun1d5, Prkab2, Acsm5, Plcb4, Cpox, Arrb2, Fgfbp1, Nat15, Mare, IL10, Grb7, Galt, Nphs1, Aldob
>rno-miR-214-3p	ACAGCAGGCACAGACAGGCAG	–	<0.1	−0.28	Zbtb20, Luzp1, Atp2a3, Camta1, Smarcd1, Naa15, Endod1, Sec24c, P2rx6, Ldoc1, Pla2g3, Cpsf4, Psmd11, Ammecr1l, Myo18a, Zfand3, Numa1, Ccdc167, Tspan9, Sema4d, Phf6, Zbtb39, Ppih, Itpk1, Atp11c, Pter, Slc8a1, Wnt2, Diaph1, Naa50, Qsox1, Nfatc2, Plekhj1, Ezh1, Hr, Ctdsp1, Fbln5, Nomo1, Slc45a4, Lhx6, Socs7
>rno-miR-33-5p	GUGCAUUGUAGUUGCAUUGCA	57	<0.1	−0.99	Abca1, Zfp281, Crot, Pdgfra, Ywhah, Hadhb, Sec24c, Arid5b, Scn8a, Cacna1c, Mdm4, Rb1cc1, Slc25a25, Cntln, Fbxw7, Naa15, Tmem33, Tmem86a, Ctnnd1, Map3k3, Dpy19l1, Slitrk5, Gpr158, Zfp286a, Abi1, Tph2, Sgcb, Braf, Txk, Pof1b, Fv1, B3galt2, Enc1, Cdk14, Tbc1d9b, Nfatc2, Plekhj1, Ezh1, Hr, Ctdsp1, Fbln5
>rno-miR-217-5p	UACUGCAUCAGGAACUGACUGG	75	0.20	−1.02	Acer3, Zfp711, Usp6nl, Ppm1d, Atp1b1, Med17, Bai3, RGD1566359, Thoc2, Ezh2, Hivep3, Slc38a2, Ubl3, Kctd9, Dennd6a, Anln, Extl2, Stt3a, Yipf6, Tmem47, Fn1, Yaf2, Ythdc1, RGD1307830, Appbp2, Gpm6a, Bicd1, Atp11c, Tm9sf3, Zfyve20, Zbtb5, Morf4l2, Tet2, Ptpn21, Foxo1, Kcnh5, Klhl29, Wdr48, Ube4a, Hnrnpa3, Tmed10, Esco1, Slc45a2, Wapal, Ehmt1, Kctd5, RGD1311595, Myef2
>rno-miR-34c-5p	AGGCAGUGUAGUUAGCUGAUUGC	–	0.62	–	Ttc19, Vamp2, Notch1, Rras, E2f5, Tmem79, Arhgap1, Fam76a, Osgin2, Zfhx4, Ctnnd2, Frk, Soga1, Ap1s2, Fam167a, Ubp1, Camta1, Ppp1r11, Gmfb, Slc44a2, Ptpn4, Svop, Mycn, Zfp644, Map1a, Baalc, Pogz, Eml5, Tbl1xr1, Pitpnc1, Shkbp1, Dgkz, Taf5, Ranbp10, Myrf, Pip5k1a, Akap6, Slc35g2, Asic2, Strn3, Zer1, Daam1
>rno-miR-129-5p	CUUUUUGCGGUCUGGGCUUGC	88	<0.1	−1.20	Prkcb, Rbms3, Cib2, Zbtb20, Zfp281, Hmg1l1, Ube2k, Sc5d, Ctdspl2, Rai14, Ccdc43, Eif4g3, Kctd4, Ago3, Mdm4, Sun2, Rims2, Ythdf1, Tnpo1, Ap3b1, Fam63b, Sacm1l, Pdp2, RGD1559786, Ube4b, Klhl32, Nr2c2, Zfp36l1, Gapt, Wdr61, Duoxa1, Ets1, Pou3f1, Tmub2, Ptp4a1, Nrg2, RGD1307621, Paqr5, Add3, Kctd1

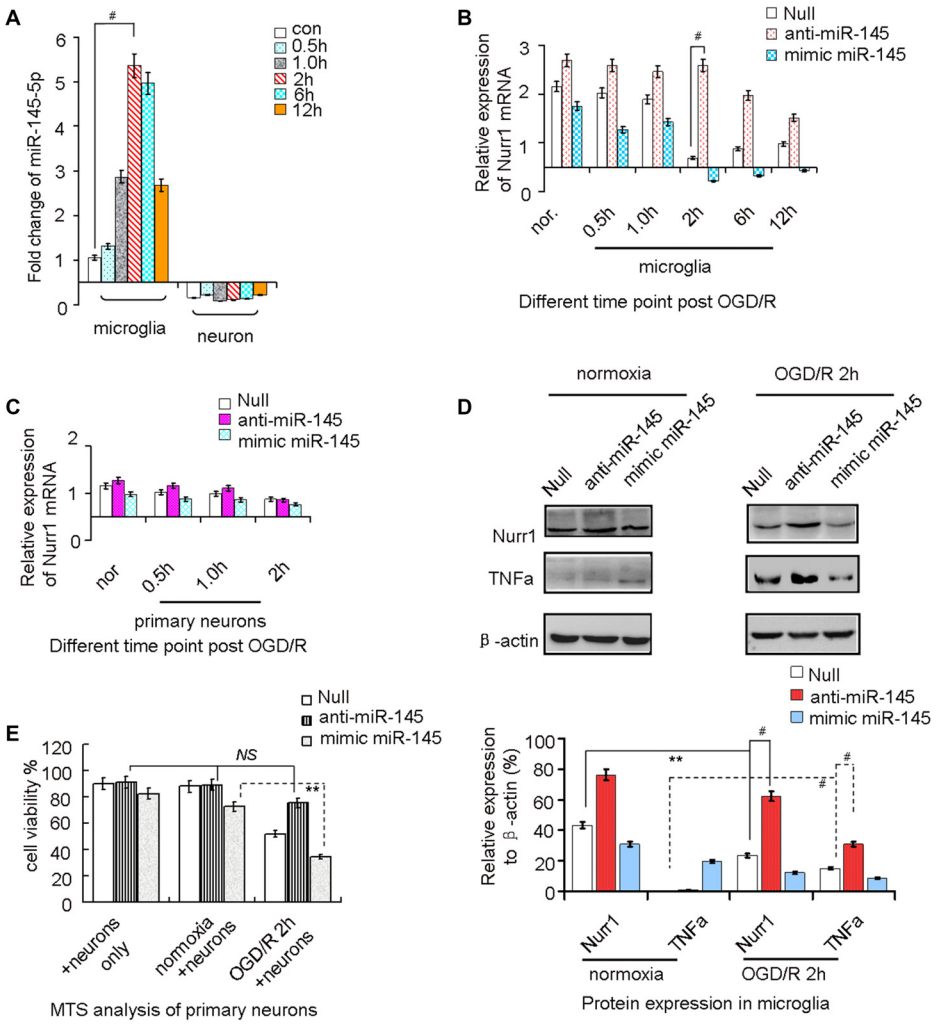

FIGURE 3 | miR-145-5p regulates endogenous Nurr1 levels in microglia. Microglia cultured in normoxia (nor.) and un-transfected (the null group) served as negative controls. **(A)** miR-145-5p expression increased from the onset of OGD/R and peaked at 2 h in microglia ($p < 0.001$), but did not change significantly in primary neurons. **(B)** Transfection anti-miR-145-5p induced an sharply increasing of Nurr1 mRNA post OGD/R 2 h in microglia ($p < 0.001$). **(C)** No obvious changes of Nurr1 mRNA were observed in primary neurons subjected to OGD/R, independent of anti-miR-145-5p or miR-145-5p mimic administration. **(D)** By Western blot assay, Nurr1 protein decreased and TNF-α increased significantly after OGD/R 2 h in microglia. miR-145-5p mimic administration significantly reduced Nurr1 protein level after OGD/R 2 h. **(E)** By MTS analysis of neurons, cell viability of primary neurons cocultured with microglia OGD/R 2 h with anti-miR-145-5p transfection did not show significant increase of cell death when compared to microglia normoxia group or neurons only group (NS: non-significance; $p > 0.05$). Oppositely, administration of miR-145-5p mimic increases neurons death notably in microglia after OGD/R 2 h than those co-cultured with microglia control ($p < 0.01$). $^{**}p < 0.01$, $^{\#}p < 0.001$.

Screening for miRNAs that Directly Target the 3′UTR of Nurr1

miRNA expression was measured in our miRNA profiling analysis of rat cortex samples at different time point after MCAO/R (**Figure 2B**). Eleven miRNAs, including miR-145-5p, miR-34c-5p, miR-365-3p, miR-214-3p, miR-151, miR-27a, miR-153-5p, miR-365-3p, miR-33-5p, miR-217-5p and miR-129-5p, were differentially and significantly expressed ($P < 0.05$; **Figure 2B**). Among them, seven putative relevant miRNAs were screened by bioinformatic analysis of databases to identify miRNAs that regulate Nurr1 directly through its 3′UTR (**Table 1**). The predicted binding sites of the selected miRNAs are shown in **Figure 2C**.

The 3′UTR of Nurr1 and miRNA binding sites were cloned to construct firefly luciferase reporter plasmids (pMIR-REPORT). Plasmids were cotransfected independently with the respective anti- or mimic miRNAs into HEK293T cells. Results showed that the miR-145-5p mimic clearly decreased the luminescence reporter signal to a greater extent ($P < 0.001$; **Figure 2D**), as did miR-132 and miR-34c-5p, which were previously shown to directly target Nurr1. However,

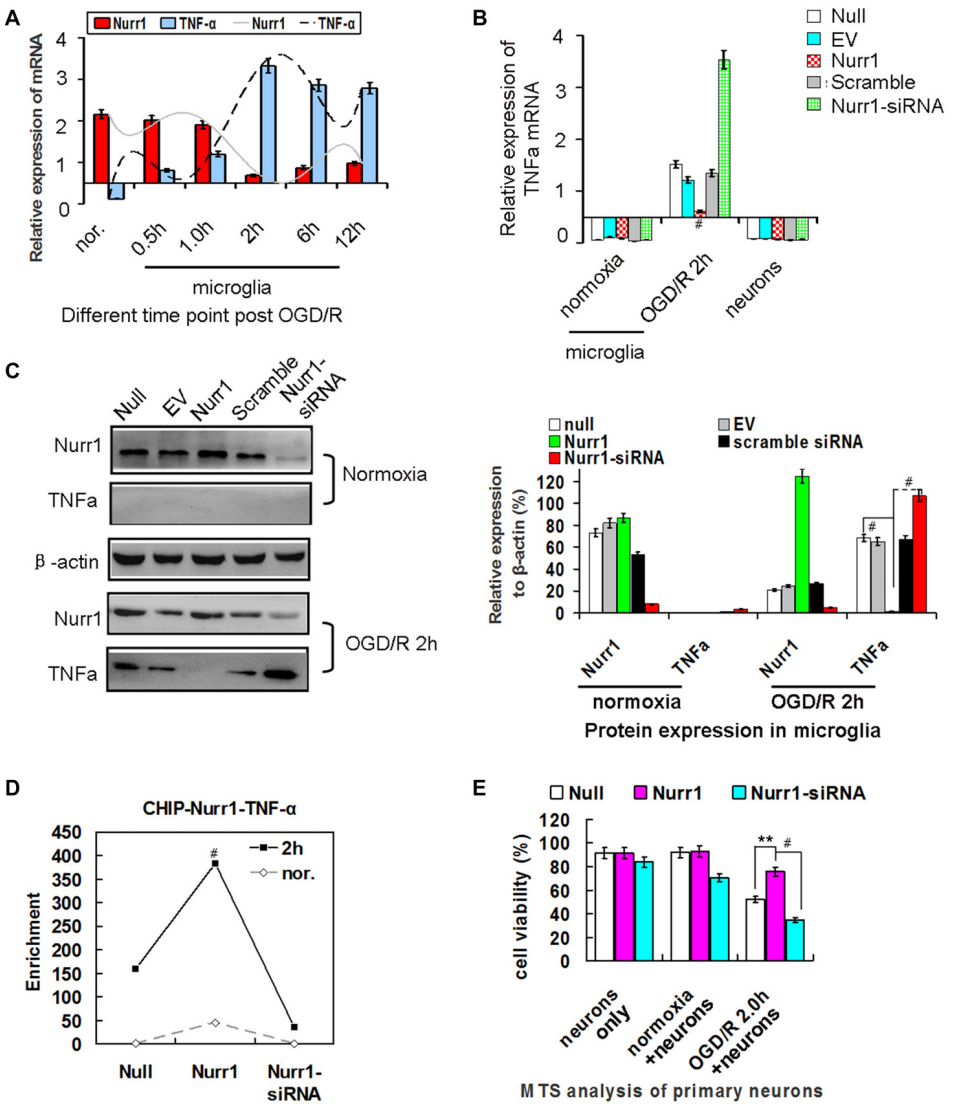

FIGURE 4 | Nurr1 overexpression suppresses TNF-α expression in microglia. **(A)** Quantitation of Nurr1 and TNF-α mRNA in primary microglia which were subjected to OGD/R 0.5 h, 1.0 h, 2 h, 6.0 h and 12 h, respectively. TNF-α mRNA increased from the onset of OGD/R and peaked at OGD/R 2 h in microglia ($p < 0.001$). However, Nurr1 mRNA showed an opposite trend at different time point of OGD/R. **(B)** Overexpression of Nurr1 led to significant attenuation of TNF-α mRNA, otherwise Nurr1-siRNA led to sharply increase of TNF-α expression after OGD/R 2 h in microglia. However, these significant changes of TNF-α mRNA expression were not observed in microglia with normooxia culturing (microglia nor. group) or neurons only group. **(C)** After OGD/R 2 h in microglia, Nurr1 overexpression by pcDNA-Nurr1 transfection significantly inhibited TNF-α protein expression ($p < 0.001$). Oppositely, Nurr1 knockdown by siRNA interference significantly restored TNF-α protein expression ($p < 0.001$). **(D)** *ChIP* assay of Nurr1 on the TNF-α promoter in response to OGD/R 2 h in microglia cells. Nurr1 overexpression by plasmid transfection increased Nurr1 occupancy at the TNF-α promoter, especially when TNF-α expression reached great amount post OGD/R 2 h. Data are displayed as fold enrichment over control IgG. **(E)** By MTS analysis of neurons, neurons viability co-cultured with microglia OGD/R 2 h which were transfected with Nurr1 overexpression plasmid showed significant lower ratio of cell death than the null ($p < 0.01$) and Nurr1-siRNA group ($p < 0.001$). However, no obvious changes of cell viability were observed in groups of neurons only and neurons+microglia normoxia after overexpression or knockdown Nurr1 expression. $^{**}p < 0.01$, $^{\#}p < 0.001$.

miR-217 exhibited a lower significant interaction when compared with miR-145-5p and miR-34c-5p (**Figure 2D**). Mutations of the miR-145-5p and Nurr1 recognition sites in the 3′UTR abolished their interaction (**Figure 2E**). These results suggest that miR-145-5p modulates Nurr1 through its 3′UTR.

miR-145-5p Regulates Endogenous Nurr1 Levels in Microglia

miR-145-5p expression increased from the onset of OGD/R, peaked at 2 h, and then progressively decreased until 12 h in microglia (**Figure 3A**). However, no significant changes of miR-145-5p expression were observed at different time points

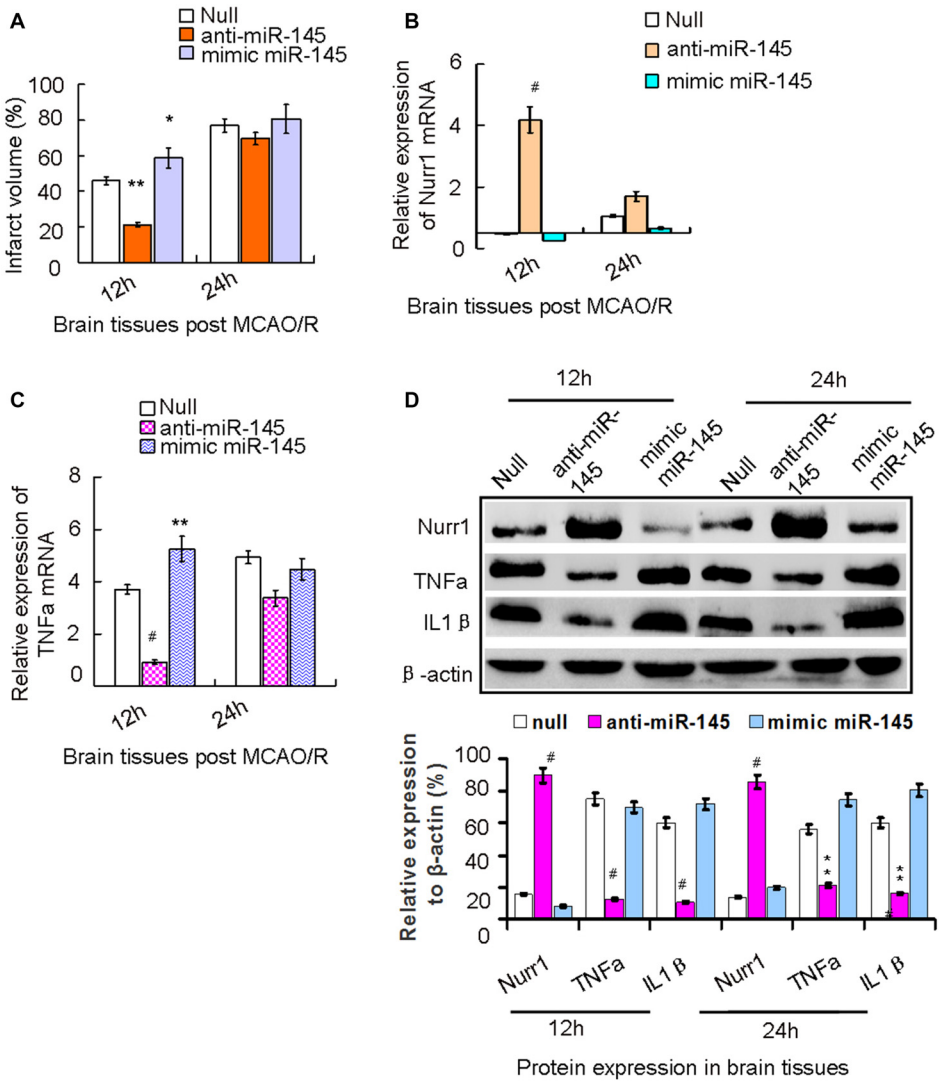

FIGURE 5 | The axis signaling of miR-145-5p-Nurr1-TNF-α in acute *MCAO/R* model of rats by *in vivo* expriments. Infarct volume was plotted as the percentage of ipsilateral cerebral. **(A)** After 12 h of MCAO/R, administration of anti-miR-145-5p *in vivo* via ICV injection to ischemic rats immediately reduced Infarct volume by 39.05% ($p < 0.01$). While administration of miR-145-5p mimic increased infarct volume by 15.05% when compared to the null group ($p < 0.05$). However, these changes of infarct volume were not observed significantly at 24 h. **(B)** By RT-qPCR analysis, Nurr1 mRNA expression significantly increased in anti-miR-145-5p injection samples ($p < 0.001$) whereas decreased after administration of mimic miR-145-5p ($p < 0.05$). **(C)** In contrast, TNF-α mRNA expression significantly decreased in anti-miR-145-5p injection samples post 12 h of MCAO/R ($p < 0.001$) whereas significantly increased when administration of miR-145-5p mimic ($p < 0.01$). However, these significant changes of TNF-α mRNA expression were not observed in samples post 24 h of MCAO/R. **(D)** By western blot analysis, both TNF-α and IL1β expression levels were significantly suppressed by Nurr1 overexpression with administration of anti-miR-145-5p at 12 h and 24 h post-MCAO/R, and vice versa. $^{*}p < 0.05$, $^{**}p < 0.01$, $^{\#}p < 0.001$.

of OGD/R in primary neurons (**Figure 3A**). Nurr1 mRNA levels were reduced from the onset of OGD/R and peaked at 2 h in microglia (**Figure 3B**). Administration of anti-miR-145-5p induced a sharp increase of Nurr1 mRNA levels in comparison with the null group at each time point of OGD/R in microglia (**Figure 3B**) but not in primary neurons (**Figure 3C**).

After OGD/R 2 h induction of miR-145-5p overexpression in microglia, the Nurr1 protein was clearly reduced when compared with cells in the normoxia group (**Figure 3D**). In particular, expression of TNF-α, which was reported to be transrepressed by Nurr1, displayed a pattern of expression opposite that of Nurr1 under treatment with the miR-145-5p mimic or anti-miR-145-5p (**Figure 3D**). Cell viability assessed by MTS analysis showed that primary neuronal cells co-cultured with microglia transfected with anti-miR-145-5p post OGD/R 2 h did not exhibit significant cell death when compared with the normoxia group (**Figure 3E**). Conversely, a noticeable increase in neuronal cell death was observed in those co-cultured with miR-145-5p mimic-transfected

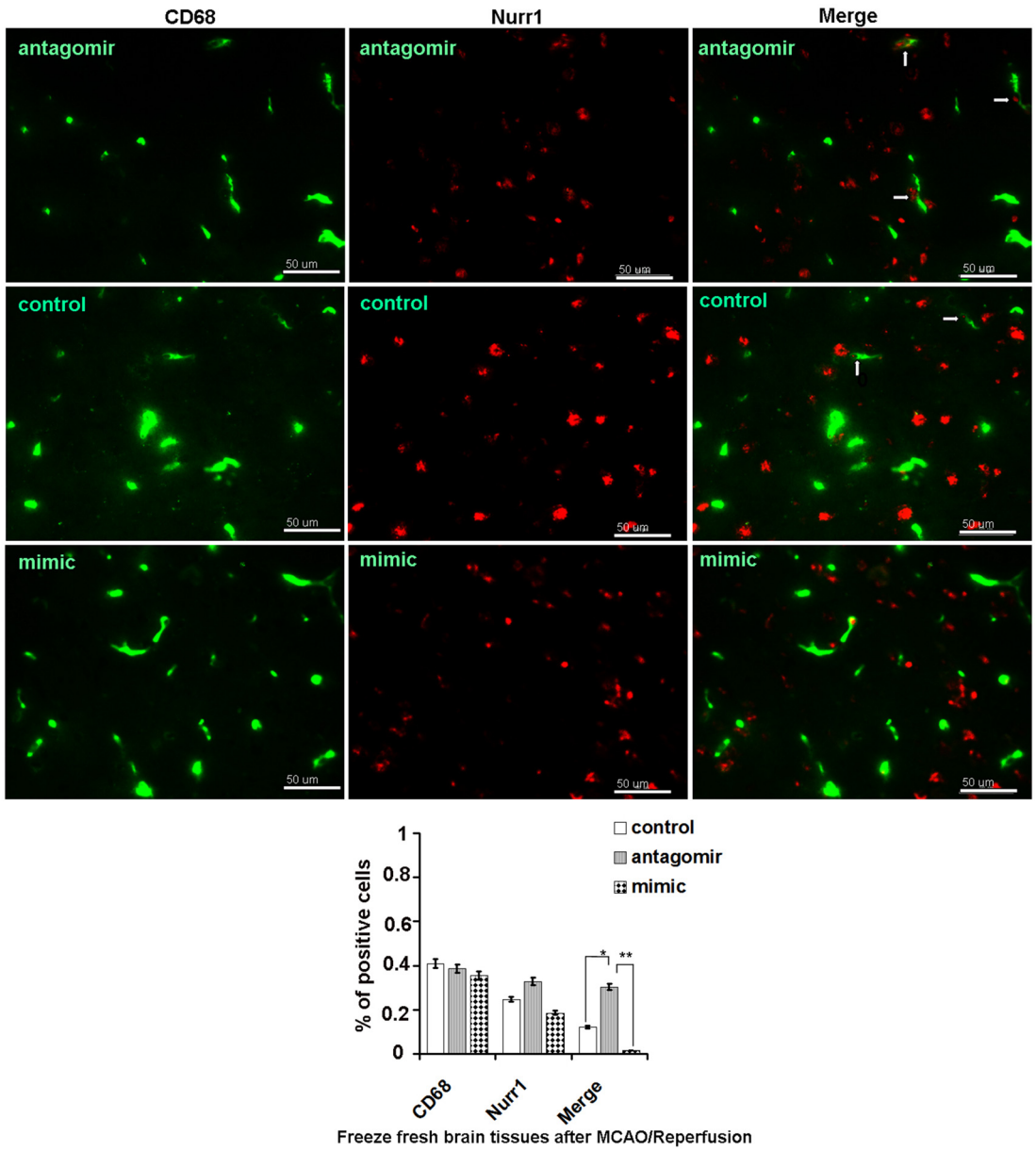

FIGURE 6 | Nurr1 expression in active microglia with administration of miR-145-5p in peri-infarct areas post 12 h of MCAO/R. Double immunofluorescence staining shows more expression of Nurr1 in active microglia with administration of anti-miR-145-5p, and little expression of Nurr1 with administration of miR-145-5p mimic in the peri-infarct areas bordering with intact tissues post 12 h of MCAO/R. Scale bars = 50 μm. Arrows indicate co-localization of CD68 and Nurr1 in active microglia. $^{*}p < 0.05$, $^{**}p < 0.01$.

microglia (**Figure 3E**). These experiments suggest that enhanced levels of miR-145-5p inhibit neuronal viability by regulating expression of Nurr1 and TNF-α in microglia after OGD/R.

Overexpression of Nurr1 Suppresses TNF-α Expression

It was previously reported that Nurr1 induces transrepression of TNF-α by binding to its promoter in Parkinson's disease (Saijo et al., 2009). Herein, we sought to determine the effects of aberrant expression of Nurr1 on TNF-α expression in microglia and primary neurons subjected to OGD/R at different time. Results of qRT-PCR analysis showed that TNF-α mRNA expression increased and peaked at 2 h of OGD/R in microglia which is opposite to Nurr1 mRNA levels (**Figure 4A**), but not in primary neurons (data not shown). Upon treatment with the Nurr1 activation plasmid, overexpression of Nurr1 significantly attenuated TNF-α mRNA and protein expression. Conversely, an increase in TNF-α expression was observed after treatment with Nurr1-siRNA after OGD/R 2 h in microglia (**Figures 4B,C**).

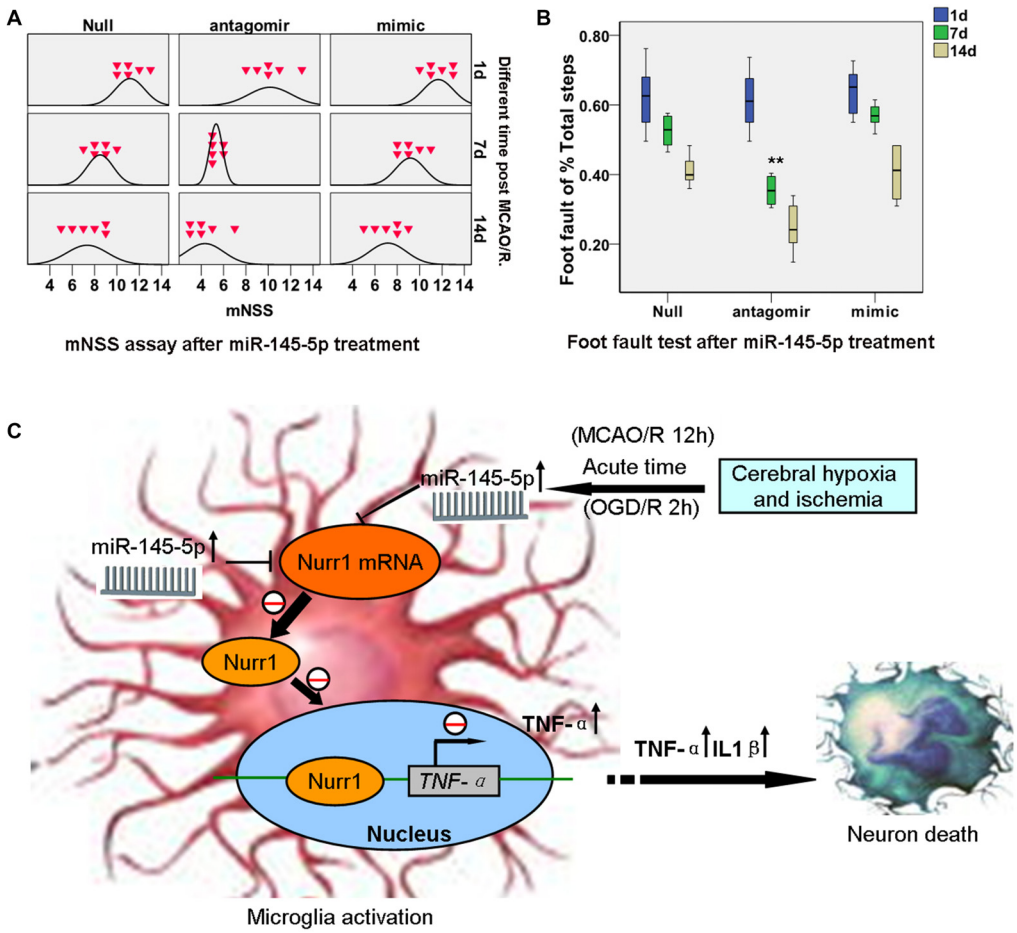

FIGURE 7 | miR-145-5p interruption facilitates neurological outcome of rats post MCAO/R. Modified Neurological Severity Score (mNSS) and foot fault tests were assessed on days 1, 7 and 14 after MCAO/R. **(A)** mNSS in antago-miR-145-5p animals were significantly decreased at both 7d and 14d after MCAO/R ($p < 0.05$). **(B)** Foot fault test, for the front left and hind left limbs were significantly lower in antagomiR-145-5p animals than that of miR-145-5p mimic and null animals. $n = 54$ for the combination group. **(C)** The graphical summary. Here, we describe a novel miR-145-5p regulatory mechanism of Nurr1 that can act downstream of TNF-α activation. In acute cerebral ischemia (MCAO/R 12 h) of rats and OGD/R 2 h of microglia, Nurr1 inhibits TNF-α expression by binding promoter of *TNF-α* gene. This regulatory effect is inhibited by Nurr1 protein decline that induced by miR-145-5p overexpression. Blocking the abnormal activation of miR-145-5p-Nurr1-TNF-α axis signaling can relieve neurons death upon MCAO/R of rats in acute time. $^{**}p < 0.01$.

However, no significant changes were observed in primary neurons (**Figure 4B**).

To assess whether Nurr1 binds to the *TNF-α* gene promoter, we performed a chromatin immunoprecipitation (ChIP) assay in microglia. As shown in **Figure 4D**, Nurr1 plasmid transfection increased Nurr1 occupancy at the TNF-α promoter, especially when TNF-α expression reached a high level after OGD/R 2 h. Furthermore, neuronal cells co-cultured with microglia after OGD/R 2 h with Nurr1-siRNA transfection showed significant cell death and could be rescued by Nurr1 overexpression after transfection with the Nurr1 plasmid (**Figure 4E**). In contrast, knockdown or overexpression of Nurr1 did not alter cell viability independent of OGD/R in the primary neuron culture only group (**Figure 4E**). These data demonstrate that lower expression of Nurr1 relieves transrepression of TNF-α in microglia and inhibits cell growth in primary neurons after OGD/R 2 h.

Abnormal Inactivation of Nurr1-Mediated Transrepression on TNF-α by miR-145-5p Overexpression Accelerates Inflammatory Injury in Acute MCAO/R of Rats

We demonstrated that increasing expression of miR-145-5p peaked at 12 h in our rat MCAO/R model (**Figure 2A**). We next administered the miR-145-5p mimic and anti-miR-145-5p *in vivo* via ICV injection into ischemic rats immediately after MCAO. Mean infarct volumes were measured at 12 h and 24 h post-MCAO/R. Administration of anti-miR-145-5p reduced infarct volume by 24.05% at 12 h, whereas administration of the miR-145-5p mimic increased infarct volume by 11.05% (**Figure 5A**). Administration of anti-miR-145-5p significantly increased Nurr1 mRNA expression (**Figure 5B**) and reduced TNF-α mRNA expression at 12 h post-MCAO/R (**Figure 5C**) but not at 24 h post-MCAO/R.

Accordingly, Nurr1 protein expression increased 4.53- and 3.42-fold upon treatment with anti-miR-145-5p at 12 h and 24 h post-MCAO/R, respectively (**Figure 5D**). Both TNF-α and IL-1β protein levels were significantly up-regulated at both 12 h and 24 h post-MCAO/R, and they were successfully suppressed by Nurr1 overexpression induced by administration of anti-miR-145-5p (**Figure 5D**). Accordingly, Nurr1 expression increased significantly upon anti-miR-145-5p treatment vs. miR-145-5p mimic treatment in active microglia in peri-infarct areas post 12 h of MCAO/R using immunofluorescence (**Figure 6**). These data reveal that lower expression of Nurr1 induced by miR-145-5p upregulation increases infarct volume at an early stage of cerebral ischemia of rats by activating TNF-α and IL-1β proinflammatory signals.

miR-145-5p Interruption Facilitates Neurological Outcome of Rats Post MCAO/R

Significant functional deficits were observed in the mNSS for animals subjected to mimic miR-145-5p administration compared to anti-miR-145-5p animals at both 7d and 14d after injury ($p < 0.05$; **Figure 7A**). For foot fault tests, the percentages of front left, hind left, total left, and total foot faults at 7d and 14d after injury after anti-miR-145-5p was significantly lower, compared to that of null and mimic miR-145-5p animals ($p < 0.05$; **Figure 7B**). However, in the mNSS and foot fault tests were not significantly different between the null and miR-145-5p mimic administration animals ($p > 0.05$).

DISCUSSION

The present study utilized a coculture model system in which neurotoxicity was induced by activated microglia post OGD/R 2 h. We showed several lines of evidence that Nurr1 plays an important role in protecting neurons from inflammation-induced neurotoxicity by inhibiting expression of inflammatory genes in microglia. Firstly, clear reductions in both Nurr1 mRNA and protein expression were detected in microglia post OGD/R 2 h and accompanied by a substantial elevation in TNF-α gene expression (**Figures 4A,C**). Furthermore, Nurr1 overexpression induced by Nurr1 plasmid indeed leaded to inhibition of TNF-α mRNA and protein expression in microglia post OGD/R 2 h (**Figures 4B,C**). Secondly, reduction of Nurr1 expression induced by OGD/R 2 h in microglia resulted in increased neuronal cell death that could be rescued by Nurr1 plasmid transfection (**Figure 4E**). Thirdly, ChIP assay demonstrated that Nurr1 was recruited to the TNF-α promoter following OGD/R 2 h treatment and was further enhanced by Nurr1 overexpression (**Figure 4D**), indicating that it was acting locally to repress transcription. This finding is consistent with previous studies showing that reduced Nurr1 expression results in death of tyrosine hydroxylase-expressing neurons in Parkinson's disease by targeting the TNF-α gene promoter in microglia (Saijo et al., 2009; Kim et al., 2015). Finally, Nurr1 declined sharply in brain tissues at 12 h following MCAO/R, and lower Nurr1 expression was partly correlated with infarct volume 12–24 h post MCAO/R by *in vivo* assays (**Figure 2A**).

Results of our study strongly indicate transcript factor Nurr1 protects neurons from ischemia-induced inflammation injury, at least in part, through transrepression of TNF-α in activated microglia post OGD/R. These are supported by several recent studies: (1) up-regulation of VEGF and Nurr1 strongly promote DAergic neuronal survival after Cystatin C treatment, which might be involved in p-PKC-α/p-ERK1/2-Nurr1 signaling and autophagy (Zou et al., 2017). (2) The interaction between Nurr1 and Foxa2 protects midbrain dopamine neurons against various toxic insults, while their expression are absent during aging and degenerative processes (Oh et al., 2015). (3) The Glial cell line-derived neurotrophic factor (GDNF) was found to protect neurons in cerebral ischemia, and Nurr1 was up-regulated by GDNF in the process of dendritic and electrical maturation of neuron cells (Cortés et al., 2017).

The important roles of changes in miRNA expression in ischemic brain injury have been discovered recently using miRNA profiling techniques in a rat MCAO/R model (Dharap et al., 2009; Di et al., 2014). In the present study, miR-145-5p mimic clearly decreased Nurr1 expression in HEK293T ($P < 0.001$), as did miR-132 and miR-34c-5p, which was consistent with the previous study that miR-34c-5p directly regulated Nurr1 in HCT116 cells (Beard et al., 2016) and miR-132 targeted Nurr1 in differentiation of dopamine neurons (Yang et al., 2012). However, miR-217 exhibited a lower significant interaction when compared with miR-145-5p and miR-34c-5p (**Figure 2D**). Further mutation of the miR-145-5p and Nurr1 recognition sites in the 3′UTR abolished their interaction in HEK293T cells as detected by luciferase reporter assay (**Figure 2E**). However, Nurr1 expression is not regulated by miR-365-3p. These data demonstrate that it was essential to elucidate the specific relation between miR-145-5p and Nurr1 in rat model of cerebral I/R injury.

miR-145-5p has been shown to be up-regulated in the pathological process of vascular neointimal lesion formation (Saugstad, 2010; Li et al., 2012), cardiomyocyte survival (Chen et al., 2015), and H_2O_2-induced neuronal injury (Gan et al., 2012). Here, we observed that miR-145-5p expression sharply increased in the cortex of rats 12 h post MCAO/R (**Figure 2B**) and in isolated primary microglia post OGD/R 2 h (**Figure 3A**). Modulation of miR-145-5p expression affects cell viability under *in vitro* ischemic conditions, and this occurs via regulation of Nurr1 (**Figures 3D,E**). Administration of miR-145-5p mimic in primary microglia post OGD/R significantly reduced TNF-α expression and IL-1β by enhancing Nurr1 expression, which subsequently improved neuronal cell viability (**Figures 3E**, **4E**). As expected, anti-miR-145-5p administration via ICV injection reduced infarct volume by 24.05% at 12 h post MCAO/R in rats (**Figure 5A**). Whatever, more researches must be performed to elucidate the specific effects of miR-145-5p on cerebral I/R injury in human blood or cerebrospinal fluid.

CD68 is specifically expressed in microglia in ischemic stroke brain (Szalay et al., 2016). By immunofluorescence assay, massive

Nurr1 expression was observed in active microglia after anti-miR-145-5p treatment (**Figure 6**). Our findings are in agreement with a previous report, which demonstrated that antagomir-145 infusion resulted in a decreased area of infarction at 1 day of reperfusion by increasing SOD2 protein expression (Gan et al., 2012). It is noteworthy that 24 h after MCAO/R in rats, miR-145-5p inhibition could not reduce infarct volume despite the significant increase in Nurr1 (**Figure 5A**). Furthermore, significant functional improvement were observed in the mNSS and foot fault tests for animals subjected to mimic miR-145-5p administration compared to anti-miR-145-5p animals after cerebral I/R injury (**Figures 7A,B**). This indicates that the supression of miR-145-5p, which decreased neuron cell death by increasing TNF-α-mediated inflammation, might be insufficient to provide protective effects under these conditions. Therefore, it is still worth exploring function and mechanism(s) of miR-145-5p/Nurr1/TNF-α Signaling in human stoke in the near future.

CONCLUSION

In summary, our study identified and confirmed a novel regulation of Nurr1 by miR-145-5p in both *in vitro* and *in vivo* cerebral ischemic conditions. The hypothetic mechanisms were examined in isolated primary microglia and neurons post OGD/R by *in vitro* study (**Figure 7C**). I/R-induced miR-145-5p overexpression suppresses Nurr1 protein expression and attenuates Nurr1 transrepression of the *TNF*-α promoter in microglia (OGD/R 2 h), which then causes TNF-α-related neuronal injury. Additional *in vivo* studies have shown that administration of anti-miR-145-5p could increase Nurr1 expression and reduce subsequent infarct volume in acute cerebral ischemia (MCAO/R 12 h). It may be an effective therapeutic strategy of reducing neuronal injury following MCAO/R in rats by blocking abnormal activation of miR-145-5p/Nurr1/TNF-α axis signaling in the acute phase.

AUTHOR CONTRIBUTIONS

XX and YoZ conceived and designed the experiments. XX, LP and YaZ conducted the experiments. XX and LL analyzed the results. LP, YC, JZ, SY and XX contributed materials and analysis tools. XX wrote the article. YoZ is the corresponding author. All authors reviewed the manuscript.

ACKNOWLEDGMENTS

This study was supported by the Natural Science Foundation of China, grant 81271460; the Natural Science Foundation of Chongqing Education Committee, grant KJ1500230; and the Science and Technology Innovation Programs for Postgraduates of Chongqing, grant CYB16103.

REFERENCES

Al-Mufti, F., Amuluru, K., Roth, W., Nuoman, R., El-Ghanem, M., and Meyers, P. M. (2017). Cerebral ischemic reperfusion injury following recanalization of large vessel occlusions. *Neurosurgery* doi: 10.1093/neuros/nyx341 [Epub ahead of print].

Beard, J. A., Tenga, A., Hills, J., Hoyer, J. D., Cherian, M. T., Wang, Y. D., et al. (2016). The orphan nuclear receptor NR4A2 is part of a p53-microRNA-34 network. *Sci. Rep.* 6:25108. doi: 10.1038/srep25108

Chen, R., Chen, S., Liao, J., Chen, X., and Xu, X. (2015). MiR-145 facilitates proliferation and migration of endothelial progenitor cells and recanalization of arterial thrombosis in cerebral infarction mice via JNK signal pathway. *Int. J. Clin. Exp. Pathol.* 8, 13770–13776.

Chen, X., Liu, Y., Zhu, J., Lei, S., Dong, Y., Li, L., et al. (2016). GSK-3β downregulates Nrf2 in cultured cortical neurons and in a rat model of cerebral ischemia-reperfusion. *Sci. Rep.* 6:20196. doi: 10.1038/srep20196

Chen, Y., Wu, X., Yu, S., Lin, X., Wu, J., Li, L., et al. (2012). Neuroprotection of tanshinone IIA against cerebral ischemia/reperfusion injury through inhibition of macrophage migration inhibitory factor in rats. *PLoS One* 7:e40165. doi: 10.1371/journal.pone.0040165

Cortés, D., Carballo-Molina, O. A., Castellanos-Montiel, M. J., and Velasco, I. (2017). The non-survival effects of glial cell line-derived neurotrophic factor on neural cells. *Front. Mol. Neurosci.* 10:258. doi: 10.3389/fnmol.2017.00258

Dharap, A., Bowen, K., Place, R., Li, L. C., and Vemuganti, R. (2009). Transient focal ischemia induces extensive temporal changes in rat cerebral microRNAome. *J. Cereb. Blood Flow Metab.* 29, 675–687. doi: 10.1038/jcbfm.2008.157

Di, Y., Lei, Y., Yu, F., Changfeng, F., Song, W., and Xuming, M. (2014). MicroRNAs expression and function in cerebral ischemia reperfusion injury. *J. Mol. Neurosci.* 53, 242–250. doi: 10.1007/s12031-014-0293-8

Fumagalli, S., Perego, C., Pischiutta, F., Zanier, E. R., and De Simoni, M. G. (2015). The ischemic environment drives microglia and macrophage function. *Front. Neurol.* 6:81. doi: 10.3389/fneur.2015.00081

Gan, C. S., Wang, C. W., and Tan, K. S. (2012). Circulatory microRNA-145 expression is increased in cerebral ischemia. *Genet. Mol. Res.* 11, 147–152. doi: 10.4238/2012.January.27.1

Gao, H., Chen, Z., Fu, Y., Yang, X., Weng, R., Wang, R., et al. (2016). Nur77 exacerbates PC12 cellular injury *in vitro* by aggravating mitochondrial impairment and endoplasmic reticulum stress. *Sci. Rep.* 6:34403. doi: 10.1038/srep34403

Gullo, F., Ceriani, M., D'Aloia, A., Wanke, E., Constanti, A., Costa, B., et al. (2017). Plant polyphenols and exendin-4 prevent hyperactivity and TNF-α release in LPS-treated *in vitro* neuron/astrocyte/microglial networks. *Front. Neurosci.* 11:500. doi: 10.3389/fnins.2017.00500

Jeyaseelan, K., Lim, K. Y., and Armugam, A. (2008). MicroRNA expression in the blood and brain of rats subjected to transient focal ischemia by middle cerebral artery occlusion. *Stroke* 39, 959–966. doi: 10.1161/STROKEAHA.107.500736

Jose, S., Tan, S. W., Ooi, Y. Y., Ramasamy, R., and Vidyadaran, S. (2014). Mesenchymal stem cells exert anti-proliferative effect on lipopolysaccharide-stimulated BV2 microglia by reducing tumour necrosis factor-α levels. *J. Neuroinflammation* 11:149. doi: 10.1186/s12974-014-0149-8

Karra, D., and Dahm, R. (2010). Transfection techniques for neuronal cells. *J. Neurosci.* 30, 6171–6177. doi: 10.1523/JNEUROSCI.0183-10.2010

Kim, C. H., Han, B. S., Moon, J., Kim, D. J., Shin, J., Rajan, S., et al. (2015). Nuclear receptor Nurr1 agonists enhance its dual functions and improve behavioral deficits in an animal model of Parkinson's disease. *Proc. Natl. Acad. Sci. U S A* 112, 8756–8761. doi: 10.1073/pnas.1509742112

Li, R., Yan, G., Li, Q., Sun, H., Hu, Y., Sun, J., et al. (2012). MicroRNA-145 protects cardiomyocytes against hydrogen peroxide (H_2O_2)-induced apoptosis through targeting the mitochondria apoptotic pathway. *PLoS One* 7:e44907. doi: 10.1371/journal.pone.0044907

Liu, F. J., Kaur, P., Karolina, D. S., Sepramaniam, S., Armugam, A., Wong, P. T., et al. (2015). MiR-335 regulates hif-1α to reduce cell death in both mouse cell line and rat ischemic models. *PLoS One* 10:e0128432. doi: 10.1371/journal.pone.0128432

Liu, C., Zhao, L., Han, S., Li, J., and Li, D. (2015). Identification and functional analysis of microRNAs in mice following focal cerebral ischemia injury. *Int. J. Mol. Sci.* 16, 24302–24318. doi: 10.3390/ijms161024302

Lourbopoulos, A., Karacostas, D., Artemis, N., Milonas, I., and Grigoriadis, N. (2008). Effectiveness of a new modified intraluminal suture for temporary middle cerebral artery occlusion in rats of various weight. *J. Neurosci. Methods* 173, 225–234. doi: 10.1016/j.jneumeth.2008.06.018

McCarter, K. D., Li, C., Jiang, Z., Lu, W., Smith, H. C., Xu, G., et al. (2017). Effect of low- dose alcohol consumption on inflammation following transient focal cerebral ischemia in rats. *Sci. Rep.* 7:12547. doi: 10.1038/s41598-017-12720-w

Minhas, G., Mathur, D., Ragavendrasamy, B., Sharma, N. K., Paanu, V., and Anand, A. (2017). Hypoxia in CNS pathologies: emerging role of mirna-based neurotherapeutics and yoga based alternative therapies. *Front. Neurosci.* 11:386. doi: 10.3389/fnins.2017.00386

Oh, S. M., Chang, M. Y., Song, J. J., Rhee, Y. H., Joe, E. H., Lee, H. S., et al. (2015). Combined Nurr1 and Foxa2 roles in the therapy of Parkinson's disease. *EMBO Mol. Med.* 7, 510–525. doi: 10.15252/emmm.201404610

Ouyang, Y. B., Stary, C. M., White, R. E., and Giffard, R. G. (2015). The use of microRNAs to modulate redox and immune response to stroke. *Antioxid. Redox Signal.* 22, 187–202. doi: 10.1089/ars.2013.5757

Roqué, P. J., Dao, K., and Costa, L. G. (2016). Microglia mediate diesel exhaust particle-induced cerebellar neuronal toxicity through neuroinflammatory mechanisms. *Neurotoxicology* 56, 204–214. doi: 10.1016/j.neuro.2016.08.006

Saijo, K., Winner, B., Carson, C. T., Collier, J. G., Boyer, L., Rosenfeld, M. G., et al. (2009). A Nurr1/CoREST pathway in microglia and astrocytes protects dopaminergic neurons from inflammation-induced death. *Cell* 137, 47–59. doi: 10.1016/j.cell.2009.01.038

Saugstad, J. A. (2010). MicroRNAs as effectors of brain function with roles in ischemia and injury, neuroprotection, and neurodegeneration. *J. Cereb. Blood Flow Metab.* 30, 1564–1576. doi: 10.1038/jcbfm.2010.101

Sepramaniam, S., Armugam, A., Lim, K. Y., Karolina, D. S., Swaminathan, P., Tan, J. R., et al. (2010). MicroRNA 320a functions as a novel endogenous modulator of aquaporins 1 and 4 as well as a potential therapeutic target in cerebral ischemia. *J. Biol. Chem.* 285, 29223–29230. doi: 10.1074/Jbc.M110.144576

Szalay, G., Martinecz, B., Lénárt, N., Környei, Z., Orsolits, B., Judák, L., et al. (2016). Microglia protect against brain injury and their selective elimination dysregulates neuronal network activity after stroke. *Nat. Commun.* 7:11499. doi: 10.1038/ncomms11499

Tauskela, J. S., Brunette, E., Monette, R., Comas, T., and Morley, P. (2003). Preconditioning of cortical neurons by oxygen-glucose deprivation: tolerance induction through abbreviated neurotoxic signaling. *Am. J. Physiol. Cell Physiol.* 285, C899–C911. doi: 10.1152/ajpcell.00110.2003

Wang, X., Fan, X., Yu, Z., Liao, Z., Zhao, J., Mandeville, E., et al. (2014). Effects of tissue plasminogen activator and annexin A2 combination therapy on long-term neurological outcomes of rat focal embolic stroke. *Stroke* 45, 619–622. doi: 10.1161/STROKEAHA.113.003823

Wei, X., Gao, H., Zou, J., Liu, X., Chen, D., Liao, J., et al. (2016). Contra-directional coupling ofNur77 and nurr1in neurodegeneration: a novel mechanism for memantine-induced anti-inflammation and anti-mitochondrial impairment. *Mol. Neurobiol.* 53, 5876–5892. doi: 10.1007/s12035-015-9477-7

Wu, S., Sun, H., Zhang, Q., Jiang, Y., Fang, T., Cui, I., et al. (2015). MicroRNA-132 promotes estradiol synthesis in ovarian granulosa cells via translational repression of Nurr1. *Reprod. Biol. Endocrinol.* 13:94. doi: 10.1186/s12958-015-0095-z

Yang, D., Li, T., Wang, Y., Tang, Y., Cui, H., Tang, Y., et al. (2012). miR-132 regulates the differentiation of dopamine neurons by directly targeting Nurr1 expression. *J. Cell Sci.* 125, 1673–1682. doi: 10.1242/jcs.086421

Yuan, Y., Zha, H., Rangarajan, P., Ling, E. A., and Wu, C. (2014). Anti-inflammatory effects of Edaravone and Scutellarin in activated microglia in experimentally induced ischemia injury in rats and in BV-2 microglia. *BMC Neurosci.* 15:125. doi: 10.1186/s12868-014-0125-3

Zhou, Y., Zhou, Y., Yu, S., Wu, J., Chen, Y., and Zhao, Y. (2015). Sulfiredoxin-1 exerts anti-apoptotic and neuroprotective effects against oxidative stress-induced injury in rat cortical astrocytes following exposure to oxygen-glucose deprivation and hydrogen peroxide. *Int. J. Mol. Med.* 36, 43–52. doi: 10.3892/ijmm.2015.2205

Zou, J., Chen, Z., Wei, X., Chen, Z., Fu, Y., Yang, X., et al. (2017). Cystatin C as a potential therapeutic mediator against Parkinson's disease via VEGF-induced angiogenesis and enhanced neuronal autophagy in neurovascular units. *Cell Death Dis.* 8:e2854. doi: 10.1038/cddis.2017.240

Conflict of Interest Statement: The authors declare that the research was conducted in the absence of any commercial or financial relationships that could be construed as a potential conflict of interest.

frontiers in Molecular Neuroscience

ORIGINAL RESEARCH
published: 17 October 2017
doi: 10.3389/fnmol.2017.00324

CHL1 Is Expressed and Functions as a Malignancy Promoter in Glioma Cells

Zhai Yang[1†], Qing Xie[1†], Cheng-Liang Hu[1], Qiong Jiang[1], Hui-Fan Shen[1], Melitta Schachner[1,2] and Wei-Jiang Zhao[1]**

[1]Center for Neuroscience, Shantou University Medical College, Shantou, China, [2]Keck Center for Collaborative Neuroscience and Department of Cell Biology and Neuroscience, Rutgers University, Piscataway, NJ, United States

The cell adhesion molecule with homology to L1CAM (close homolog of L1) (CHL1) is a member of the cell adhesion molecule L1 (L1CAM) gene family. Although CHL1 expression and function have been reported in several tumors, the roles of CHL1 in the development of glioma remain unclear. In the present study, we investigated the effects of CHL1 on proliferation indexes and activation of Akt1 and Erk signaling by siRNA in U-87 MG human glioblastoma and human U251 and SHG-44 glioma cells. We found that siRNA targeting CHL1 significantly down-regulated the expression of CHL1 mRNA and protein accompanied by reduced cell proliferation and transmigration invasion in all three cell lines. Down-regulating CHL1 expression also reduced cell survival, as measured by the Bax/Bcl-2 ratio, and increased activation of caspase-3. In subcutaneous U-87 MG cell xenograft tumors in nude mice, intratumoral administration of siRNA targeting CHL1 treatment significantly down-regulated CHL1 expression *in vivo*, accompanied by increased levels of activated caspase-3. Our combined results confirmed for the first time that in contrast to findings about CHL1 in most other cancer types, CHL1 functions in promoting cell proliferation, metastasis and migration in human glioma cells both *in vitro* and *in vivo*. These results indicate that CHL1 is a therapeutic target in the clinical management of glioma/glioblastoma.

Keywords: glioma, glioma cell lines, close homolog of L1 cell adhesion molecule (CHL1), siRNA, malignancy

OPEN ACCESS

Edited by:
Vladimir Parpura, University of Alabama at Birmingham, United States

Reviewed by:
Marcus Semtner, Max Delbrück Center for Molecular Medicine (HZ), Germany
Yonghe Wu, Deutsches Krebsforschungszentrum (DKFZ), Germany

****Correspondence:***
Melitta Schachner
schachner@stu.edu.cn
Wei-Jiang Zhao
neuromancn@aliyun.com

[†]These authors have contributed equally to this work.

Received: *13 June 2017*
Accepted: *25 September 2017*
Published: *17 October 2017*

Citation:
Yang Z, Xie Q, Hu C-L, Jiang Q, Shen H-F, Schachner M and Zhao W-J (2017) CHL1 Is Expressed and Functions as a Malignancy Promoter in Glioma Cells. Front. Mol. Neurosci. 10:324. doi: 10.3389/fnmol.2017.00324

INTRODUCTION

Gliomas are a set of highly invasive glial cell-derived tumors that originate in the central nervous system, and they account for 40% to 50% of all intracranial tumors (Gabriel et al., 2014). Despite advancements in surgery, chemotherapy and radiation oncology technology, the average survival time is 9.7 months. In addition, patients with lowly differentiated astroglioma and glioblastoma exhibit high recurrence, high mortality and low cure rates, and the 5-year survival rate remains less than 5% (Sathornsumetee et al., 2007; Nakazato, 2008; Jemal et al., 2010). All these clinical data suggest that the development of glioma is a multifactor-based process in which a series of molecules are involved.

We previously reported that cell adhesion molecule L1 (L1CAM) is involved in regulating tumor progression and invasion under the modulation of Neuregulin-1 (Nrg1), suggesting the roles of L1 family members in glioma development (Zhao and Schachner, 2013). The close homolog of cell adhesion molecule L1 (CHL1) belongs to the transmembrane adhesion molecule

of the immunoglobulin superfamily and exhibits biological functions similar to that of L1. CHL1 contains an N-terminal signal sequence, six immunoglobulin (Ig)-like domains, five fibronectin type III repeat (FN III) sequences, a transmembrane domain and a conserved intracellular domain containing the sequence that functions in the cell skeleton protein anykrin recognition sequence (FIGAY; Holm et al., 1996; Zhang et al., 1998; Maness and Schachner, 2007). CHL1 was identical to melanoma cell adhesion molecule (MCAM), which was previously reported as one of the extravillous trophoblasts (EVT) markers (Higuchi et al., 2003). CHL1 is located within or near the uveal melanoma susceptibility locus UVM2 at 3p25 (Tschentscher et al., 2003). In addition, CHL1 interacts genetically with both CTF7/ECO1 and CTF18/CHL12 to modulate sister-chromatid cohesion (Skibbens, 2004).

The cleavage and release of the CHL1 extracellular domain initiates autocrine signaling and reduces cellular adhesion to promote cell motility (Katic et al., 2014). In the central nervous system, CHL1 promotes Purkinje and granule cell survival and granule cell migration during cerebellar development (Jakovcevski et al., 2009). In *Caenorhabditis elegans*, the chl-1 gene is required for normal development and fertility, whereas CHL1 mutations can lead to lineage-independent cell proliferation defects (Chung et al., 2011). CHL1 dysfunction has been implicated in abnormal thalamocortical circuitry, schizophrenia and autism (Morag et al., 2011). Mutations in the coding region of CHL1 are involved in the etiology of schizophrenia in both Chinese and Japanese populations (Sakurai et al., 2002; Chen et al., 2005). Patients with heterozygous deletion of CHL1 gene can suffer cognitive impairment (Tassano et al., 2014). Research on the roles of CHL1 in tumorigenesis has gradually attracted attention (He et al., 2013). Overexpression of CHL1 was also observed in serous epithelial ovarian cancers (EOCs; Manderson et al., 2009). However, single-nucleotide polymorphism (SNP)-mass array demonstrated the absence and down-regulation of CHL1 expression in primary esophageal squamous cell carcinoma (ESCC) tumors and ESCC cell lines (Qin et al., 2008). Down-regulation/silencing of CHL1 is present in a majority of primary tumors, and its up-regulation is associated with invasive/metastatic growth. In one study, frequent down-regulation of CHL1 was detected in 11 types of cancer, mainly including breast, kidney, colon, thyroid, and stomach. In contrast, only five types (lung, ovary, uterus, liver and trachea) of cancer exhibited frequent up-regulation (Senchenko et al., 2011). These combined data indicated that the functional expression of CHL1 is tumor phenotype dependent. However, CHL1 expression in the development, metastasis, and progression of gliomas both *in vitro* and *in vivo* remains unclear.

To address this issue, we systematically investigated the roles of CHL1 in glioma behaviors mainly using siRNA targeting CHL1 in glioma cells. We evaluated the roles of CHL1 in cell proliferation, metastasis, colony formation, and AKT1 and ERK signaling in these cells. Finally, siRNA targeting CHL1 was intratumorally administered to U-87 MG cell-derived subcutaneous xenografts to further confirm the observations *in vitro*. In summary, CHL1 is vitally involved in the regulation of the occurrence and development of glioma. Targeting the role of CHL1 may represent a promising therapeutic means for the management of glioma.

MATERIALS AND METHODS

Animals

Nude mice were purchased from Beijing Vital River Animal Center (Beijing, China). All the procedures related to handling, care, and treatment in the present research were performed according to the guidelines approved by Institutional Animal Care and Use Committees (IACUC) of Shantou University Medical College.

Cell Culture and CHL1 siRNA Transfection

Normal human astro glia cell HEB cell line and human glioma cell lines U251 and SHG44 and human glioblastoma U-87 MG cell line (Chinese Type Culture Collection, Shanghai, China) were cultured in Dulbecco's modified Eagle's medium (DMEM, Thermo Scientific HyClone, Beijing, China) supplemented with 50 U/ml of a penicillin/streptomycin mixture (Solarbio Biotech Corp. Beijing, China) and 10% fetal bovine serum (Sijiqing Biotech Corp, Hangzhou, China). All cells were routinely grown in 75-cm^2 cell culture plates (Corning Inc., Corning, NY, USA) at 37°C with 5% CO_2 in a humidified atmosphere. The cells were collected in logarithmic phase for the following experiments. On the day before transfection, cells were digested by trypsin (0.25%, Solarbio Biotech Corp., Beijing, China), counted and seeded in a six-well plate at an optimal concentration. When the cells achieved 80% confluence, the medium was changed with serum-free DMEM, and cells were incubated overnight. Control siRNA or siRNA targeting CHL1 (10 nM for both; **Table 1**) complexed with Entranster^{TM}-R4000 (Cat. No. 4000-3, Engreen, Beijing, China) was transfected into three cell lines. In the vehicle control group, cells were treated with the same volume of transfection reagent. The efficiency of CHL1 siRNA was confirmed by RT-PCR and Western blot.

Cell Viability Assay

U251, SHG44 and U-87 MG cells were seeded onto the 96-well plate at 5000 cells/well in 200 μl of DMEM supplemented with 10% FBS. These cells were transfected with control siRNA or siRNA targeting CHL1 or treated with transfection reagent as mentioned above. Transfected and non-transfected cells were incubated under the conditions of 5% CO_2, saturated humidity, and 37°C for 24, 48, 72, and 96 h. Then, 20 μl

TABLE 1 | Sequences for random control siRNA and siRNAs against CHL1.

siRNA	Sequence	
	Sense (5′-3′)	Anti-sense (5′-3′)
Random control	UUCUCCGAACG UGUCACGUtt	ACGUGACACGUU CGGAGAAtt
CHL1	GGAGCUAAUUU GACCAUAUtt	AUAUGGUCAAAUU AGCUCCtt

of 5 mg/ml MTT (Beyotime, Jiangsu, China) was added to each well, and cells were further cultured for 4 h. Then, the culture medium was removed, and 150 μl of dimethyl sulfoxide (DMSO, Sigma) was added. The optical density was measured at 570 nm using a multiwell spectrophotometer (Infinite M1000, Tecan, Switzerland). Cell growth curves were plotted using the average absorbance at 570 nm from triplicate samples of three independent experiments.

Colony Formation Assay

Forty-eight hours after transfection, U251, SHG44 and U-87 MG cells were seeded onto six-well plates at a density of 500 cells/well in triplicate. After 14 days of culture, cells were fixed with methanol, stained with 0.5% crystal violet, and visualized under a phase-contrast light microscope (Olympus, IX51, Japan). Cells were then lysed in 1% SDS, and the colony formation was indexed by the optical density measured at 564 nm using a multiwell spectrophotometer (Infinite M1000, Tecan, Switzerland).

Cell Senescence Assay

CHL1 siRNA was tested in U251, SHG44 and U-87 MG cells to assess the effect of CHL1 on cell senescence. Cells (1×10^5 cells/well) in culture medium were allowed to adhere overnight to 24-well plates. When 80% confluence was achieved, the medium was aspirated and replaced with fresh medium containing RNA-siRNA-mate complexes (10 nM of either the control or CHL1 siRNA per well). The cells were further cultured for 48 h. Cells treated with the same volume of siRNA-mate were used as the vehicle control. After 48 h of treatment, the cells were fixed. β-galactosidase/X-Gal complex was added to each well and incubated overnight at 37°C according to the manufacturer's protocol (Beyotime, Jiangsu, China). Cell senescence was indexed by the activation of β-galactosidase reflected by the development of deep blue color of X-Gal (Dimri et al., 1995). Photographs were obtained from at least five random bright-field areas. The percentage of deep blue-stained cells was counted to indicate the senescence response of cells to CHL1 down-regulation.

Transwell Migration Assay

Given that L1 potentiates the migration of glioma cells, we hypothesized that CHL1 may also possess similar functions. We then tested the potential role of CHL1 for inducing glioma cell migration using the Transwell migration assay (Zhao and Schachner, 2013). For the Transwell migration assay, U-87 MG, SHG44, and U251 cells were pretreated individually with the vehicle control, CHL1 siRNA, and random control siRNA in DMEM for 48 h. The culture medium was then aspirated, and cells were resuspended in DMEM and seeded onto the upper chamber (1×10^5 per well) of each Transwell insert consisting of a filter (Becton Dickinson Labware, Franklin Lakes, NJ, USA) with 8-μm pores. The underside of the filter was pretreated with 100 μg/mL fibronectin in PBS (Millipore) to ensure the attachment of the migrated cells to this side of the filter. The lower chamber was loaded with 500 μl of DMEM only. At 18 h after plating, the cells that had failed to move to the underside of the filter were removed using a cotton-tipped applicator. The cells retained on the underside of the filter were rinsed 3× with PBS and fixed in 4% paraformaldehyde in PBS. The migrated cells were stained with 0.1% crystal violet in acetic acid to determine their morphology. The crystal violet staining was evaluated at 200× magnification with bright field microscopy. The number of cells in each field was counted using Image Tool II software.

Xenograft Studies

For subcutaneous implantation, 10 4-week-old female BALB/c nude mice (Vital River, Beijing, China) were randomly divided into control siRNA group ($n = 5$) and siRNA targeting CHL1 group ($n = 5$). Mice were anesthetized with 100 $mg \cdot kg^{-1}$ ketamine, and 5×10^5 U-87 MG cells were injected into the right flank near the upper extremity. After 4 weeks, tumor length and width were measured with calipers in cephalad-to-caudad and left-to-right dimensions, and measurements continued at one-day intervals. Tumor volume was calculated each day using the formula: volume = length × width^2 × 0.5 and expressed in mm^3. When the tumor volume reached approximately 150 mm^3, control siRNA or CHL1-siRNA complexed with Entranster^{TM}-*in vivo* were intratumorally injected at 2 mg/kg for the 1st time and at 4 mg/kg 7 days after the 1st injection (EngreenBiosystem Co. Ltd., Beijing, China) was undertaken. The second intratumoral injection was performed on the 7th day after the 1st intratumoral injection. After the 16th day of measurements, mice were anesthetized and euthanized by decapitation to remove the tumors.

RNA Isolation and Reverse Transcriptase PCR (RT-PCR) Analysis

Total RNA from glioma cells was extracted using RNAiso extraction kit (Tiangen, Beijing, China) according to the manufacturer's protocol, and reverse transcription was performed using StarScrip II First-strand cDNA Synthesis Mix (GenStar, Beijing, China). A 35-cycle PCR using the following conditions was performed (except for the GAPDH primer set): 94°C for 2 min, 94°C for 30 s, 59°C for 20 s, 74°C for

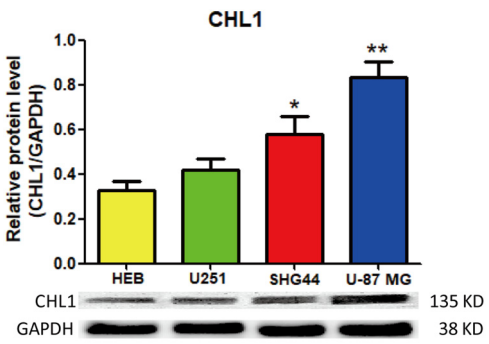

FIGURE 1 | Western blot analysis of the protein levels of CHL1 detected in normal human glial HEB cells and 3 glioma/glioblastoma cell lines. CHL1 was weakly expressed in normal human HEB glial cells. Its levels in all the 3 glioma/glioblastoma cells were higher than that in normal human HEB glial cells, with the statistical significance detected in SHG44 cells (*$p < 0.05$ vs. HEB cells) and U-87 MG cells (**$p < 0.01$ vs. HEB cells). $n = 3$ for each group. Student's *t*-test for independent samples was used.

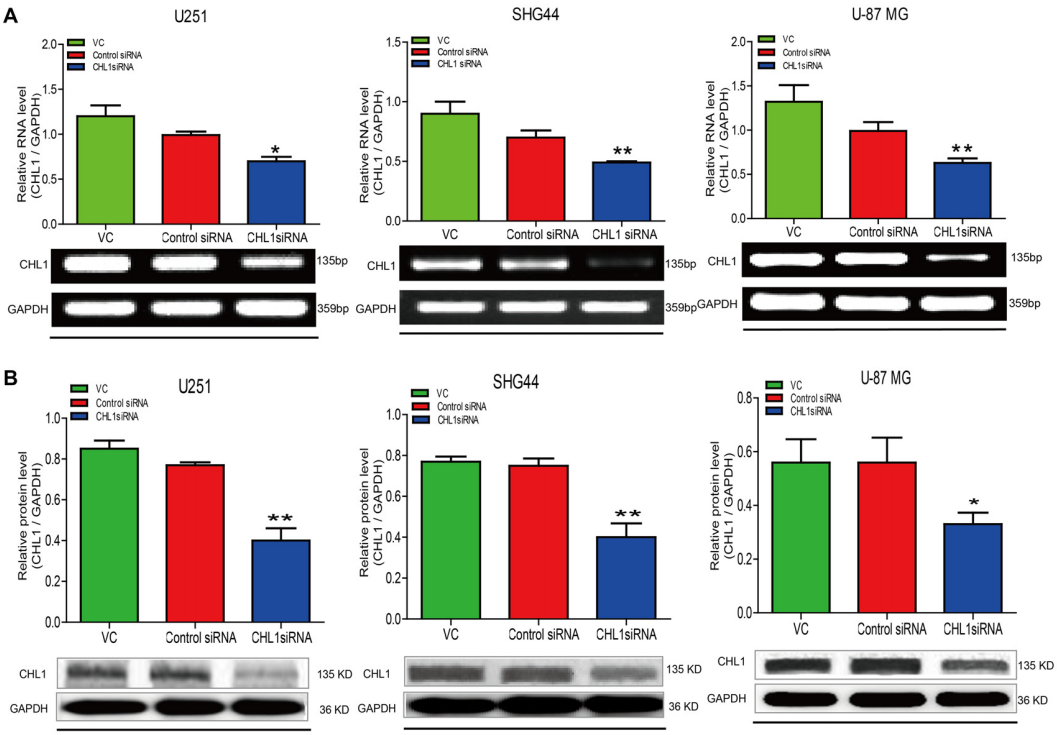

FIGURE 2 | Treatment of siRNA targeting CHL1 in three human glioma cell lines. Total RNA was isolated from U251, SHG44 and U-87 MG cells treated with vehicle control (vc), control siRNA (control siRNA) or siRNA targeting CHL1 (CHL1 siRNA). RT-PCR and Western blot analysis were then used to measure both relative mRNA and protein levels of CHL1. **(A)** RT-PCR analysis of the mRNA levels of CHL1 in U251, SHG44 and U-87 MG cells treated with vehicle control (vc), control siRNA and siRNA targeting CHL1, and **(B)** Western blot analysis of the protein levels of CHL1 detected in U251, SHG44 and U-87 MG cells treated with vehicle control (vc), control siRNA and siRNA targeting CHL1. Data are presented as means ± standard error of the mean (SEM) ($n = 3$, $^*p < 0.05$; $^{**}p < 0.01$, independent Student's *t*-test).

40 s and a final extension step at 72°C for 10 min. For GAPDH cDNA amplification, 28 reaction cycles were employed. We subjected 5 μl of the PCR products to gel electrophoresis using a 2.0% agarose gel (Gene Choice) containing Gelred (1:10,000; Biotium, Hayward, CA, USA). The bands were identified under UV light. The primers used for PCR for detecting the mRNA expression were listed as follows: hCHL1-forward primer: 5′-TCAAAGGAAGCCTTCGGTCC-3′ and hCHL1-reverse primer: 5′-TAGATCCAGCGTAGGCACCA-3′; GAPDH forward primer: 5′-TATAAATTGAGCCCGCAGCC-3′ and GAPDH reverse primer: 5′-TTCCCGTTCTCAGCCTTGAC-3′. The signal intensity was quantified using Image Tool II software via average densitometry multiplied by the number of pixel (National Institutes of Health, Bethesda, MD, USA). The relative mRNA level of a protein was indexed by its signal intensity to that of GAPDH.

Western Blot Analysis

The cells and tumor samples were lysed in a RIPA buffer mixture (Solarbio Biotech, Beijing, China) supplemented with PMSF (1:200, Solarbio Biotech). The cell lysates were centrifuged at 14,000× *g* for 15 min at 4°C, and the supernatants were collected for Western blot analysis (Zhao W. and Ren, 2011; Zhao W. J. and Ren, 2011). Equivalent quantities of the lysates from the cells were heated at 95°C in 20% sample loading buffer (0.125 M Tris-HCl, pH 6.8, 20% glycerol, 10% SDS, 0.1% bromophenol blue and 5% β-mercaptoethanol), resolved using an 8% SDS-PAGE and electroblotted onto polyvinylidenedifluoride membranes (PVDF, Millipore, Billerica, MA, USA). Non-specific protein binding sites were blocked with 5% BSA diluted in Tris-buffered saline (TBS, pH 7.3) buffer containing 0.05% Tween-20 (TBST). Membranes were incubated with a rat anti-human CHL1 antibody that specifically targets the extracellular domain of CHL1 (1:500, R&D Systems, cat. no. MAB2126, Minneapolis, MN, USA), mouse monoclonal anti-Bcl-2 antibody (1:1000, cat. no. sc-7382, Santa Cruz, CA, USA), rabbit polyclonal anti-Bax antibody (1:1000, cat. no. sc-526, Santa Cruz), rabbit polyclonal anti-PCNA antibody (1:1000, cat. no. sc-7907, Santa Cruz), rabbit polyclonal anti-caspase-3 antibody (1:1000, cat. no. sc-7148, Santa Cruz), mouse monoclonal anti phosphorylated extracellular signal regulated kinase 1/2 (anti-pErk1/2) antibody (1:1000, cat. no. sc-7383, Santa Cruz), mouse monoclonal anti-Erk1/2 antibody (1:1000, cat. no. sc-135900, Santa Cruz), mouse monoclonal anti-pAkt1 antibody (1:1000, cat. no. sc-81433, Santa Cruz), mouse monoclonal anti-Akt1 antibody (1:1000, cat. no. sc-55523, Santa Cruz) and mouse monoclonal anti-glyceraldehyde-3-phosphate dehydrogenase (GADPH) antibody (1:1000, cat. no. sc-365062, Santa Cruz) overnight at 4°C.

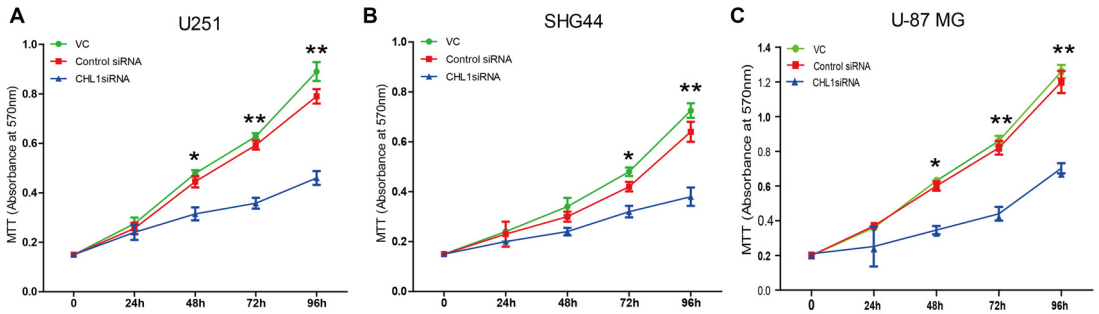

FIGURE 3 | Knockdown of CHL1 affects the proliferation and survival of U251, SHG44 and U-87 MG glioma cells. Cells were seeded on 96-well plates in triplicate, and proliferation rates were measured by MTT assay to evaluate the effect of CHL1 on the proliferation of U251, SHG44 and U-87 MG glioma/glioblastoma cells. **(A–C)** Changes of the proliferation rate in U251 **(A)**, SHG44 **(B)**, and U-87 MG **(C)** cells treated with vehicle control (vc), control siRNA (control siRNA) or siRNA targeting CHL1 (CHL1 siRNA). The data were expressed as the means ± SEM of three independent experiments (*$p < 0.05$ and **$p < 0.01$ vs. either vehicle control or control siRNA; independent Student's *t*-test).

After washing the membrane with TBST three times at room temperature (5 min each wash), the membranes were further incubated with horseradish peroxidase conjugated goat anti mouse secondary antibody (1:1000, cat. no. BA1051, Boster Biological Technology, Wuhan, China), anti rabbit secondary antibody (1:1000, cat. no. BA1055, Boster Biological Technology), or rabbit anti-rat secondary antibody (1:1000, cat. no. BA1058, Boster Biological Technology) for 1 h. Subsequently, the membranes were washed with TBST three times (5 min each wash) at room temperature. The immunoreactive bands were visualized using an enhanced chemiluminescence kit (Bio Rad Laboratories, Richmond, CA, USA) and an imaging system (Alpha Innotech, San Leandro, CA, USA). The signal intensity was quantified using Image Tool II software via average densitometry multiplied by the number of pixels (National Institutes of Health, Bethesda, MD, USA). The relative expression level of the protein under study was indicated by the ratio of its signal intensity to that of GAPDH.

Immunohistochemical Analysis

Immunohistochemical staining of paraffin sections was performed as described (Zhao et al., 2009). The human U-87 MG glioma cell xenograft tissues were cryosectioned at 8 μm thickness. Antigen retrieval was performed using 10 mM citrate buffer (pH 6.0), and endogenous peroxidase clearance was performed by incubation in 3% H_2O_2. Then, sections were blocked with 10% normal goat serum in PBS at room temperature for 30 min, and samples were subjected to incubation with the following primary antibodies: rat anti-human CHL1 antibody (1:100, cat. no. MAB2126, R&D Systems), rabbit polyclonal anti-PCNA antibody (1:200, cat. no. sc-7907, Santa Cruz), rabbit polyclonal anti-caspase-3 antibody (1:200, cat. no. sc-7148, Santa Cruz), rabbit polyclonal anti-GFAP antibody (1:500, cat. no. BA0056, Boster Biological Technology) at 4°C overnight. Bound antibody was visualized using the AEC method. Counterstaining was performed with Mayer's hematoxylin. H&E (Zhongshan Goldbridge Biotechnology Co., LTD, Beijing, China) and immunohistochemical stainings were analyzed using a Jiangnan light microscope (DN-10B, Jiangnan, Nanjing, Jiangsu).

STATISTICAL ANALYSIS

In vitro experiments were repeated at least three times using independent culture preparations. All data are presented as group mean values with standard error of the mean (SEM). Statistical analyses were performed using SPSS (Statistical Package for the Social Sciences) 10.0 software (SPSS, Chicago, IL, USA). The data from CHL1 siRNA group were compared with those from either vehicle control or control siRNA group by using Student's *t*-test for independent samples. *p*-values < 0.05 were considered statistically significant.

RESULTS

Comparison of the Protein Levels of CHL1 in 3 Glioma/Glioblastoma Cell Lines with that in Normal Human Glia HEB Cells

We first used Western blot to evaluate and compare the expression of CHL1 protein in HEB and three human glioma/glioblastoma cell lines. As demonstrated in **Figure 1**, CHL1 was weakly expressed in normal human HEB glial cells. Its levels in all the 3 glioma/glioblastoma cells were higher than that in normal human HEB glial cells, with the statistical significance detected in SHG44 cells ($p < 0.05$ vs. HEB cells) and U-87 MG cells ($p < 0.01$ vs. HEB cells). Western blot of CHL1 using samples from all the four cell lines on the uncut PVDF membrane suggests that the CHL1 antibody used in the present study is highly specific (**Supplementary Figure S1**).

Down-Regulation of CHL1 Expression Affects Glioma Cell Proliferation and Survival

We then explored whether glioma cell oncogenicity is dependent upon CHL1. We reduced CHL1 expression using Entranster^{TM}-

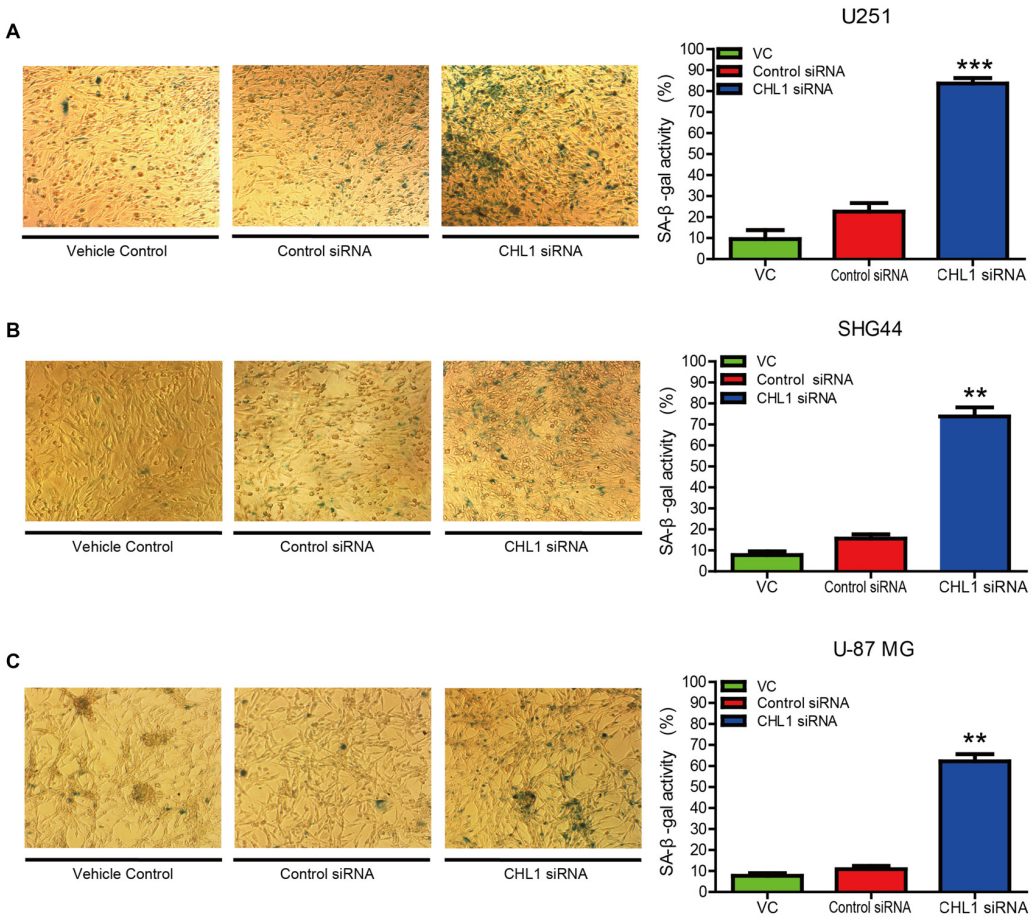

FIGURE 4 | Knockdown of CHL1 affects the senescence of glioma/glioblastoma cells *in vitro*. **(A–C)** U251 **(A)**, SHG44 **(B)** and U-87 MG **(C)** cells were seeded onto 24-well plates and treated with vehicle control, control siRNA and siRNA targeting CHL1, and senescent cells were then detected by senescence-associated β-galactosidase staining (200×). The data were expressed as the means ± SEM from four independent experiments (**$p < 0.01$; ***$p < 0.001$ vs. either vehicle control or control siRNA; Independent Student's *t*-test).

R4000-mediated CHL1-siRNA transfection inU251, SHG44 and U-87 MG glioma cells to specifically knock down endogenous CHL1 expression. CHL1 expression was significantly suppressed by siRNA targeting CHL1 mRNA and protein levels in all three cell lines investigated (**Figures 2A,B**). As seen from the MTT assay, compared with the vehicle control group and negative control group, knocking down CHL1 significantly reduced the viability of U251 cells at 48, 72 and 96 h ($p < 0.05$ vs. controls at 48 h, and $p < 0.01$ vs. controls at 72 h and 96 h; **Figure 3**). A similar pattern of cell viability inhibition in response to CHL1 knockdown was observed in both SHG44 glioma and U-87 MG glioblastoma cells, with remarkable viability inhibition observed at both 72 h and 96 h time points ($p < 0.01$ vs. controls at both time points; **Figure 3**). These results suggested that CHL1 is involved in the viability of glioma/glioblastoma cells.

Reducing CHL1 Expression Promotes Cell Senescence

To investigate whether down-regulation of CHL1 leads to cell senescence, we performed senescence staining via a β-galactosidase activity assay. After glioma cells were transfected with CHL1 siRNA or negative control siRNA, cells were fixed and stained for β-galactosidase activity using the X-Gal substrate at 37°C for 24 h. In the vehicle control with U251 cells, 10.16% of the total cells were X-Gal-positive, whereas the average percentage of X-Gal-positive cells upon treatment with negative control siRNA and CHL1 siRNA were 21.67% and 82.46%, respectively. Thus, knocking down CHL1 expression induced a significant increase in SA-β-gal-positive senescent cells compared with the vehicle control and negative control siRNA ($p < 0.001$ for both; **Figure 4A**). Similarly, SHG44 and U-87 MG cells were also sensitive to CHL1 knockdown-induced senescence. Both the CHL1 knockdown groups (74.89% and 61.27% for SHG44 and U-87 MG cells, respectively; **Figures 4B,C**) exhibited a remarkable increase in the number of SA-β-gal-positive cells compared with vehicle control (9.87% and 8.36% for SHG44 and U-87 MG cells, respectively; $p < 0.01$ vs. vehicle control for both cell lines; **Figures 4B,C**) and negative control siRNA (17.56% and 10.53% for SHG44 and U-87 MG

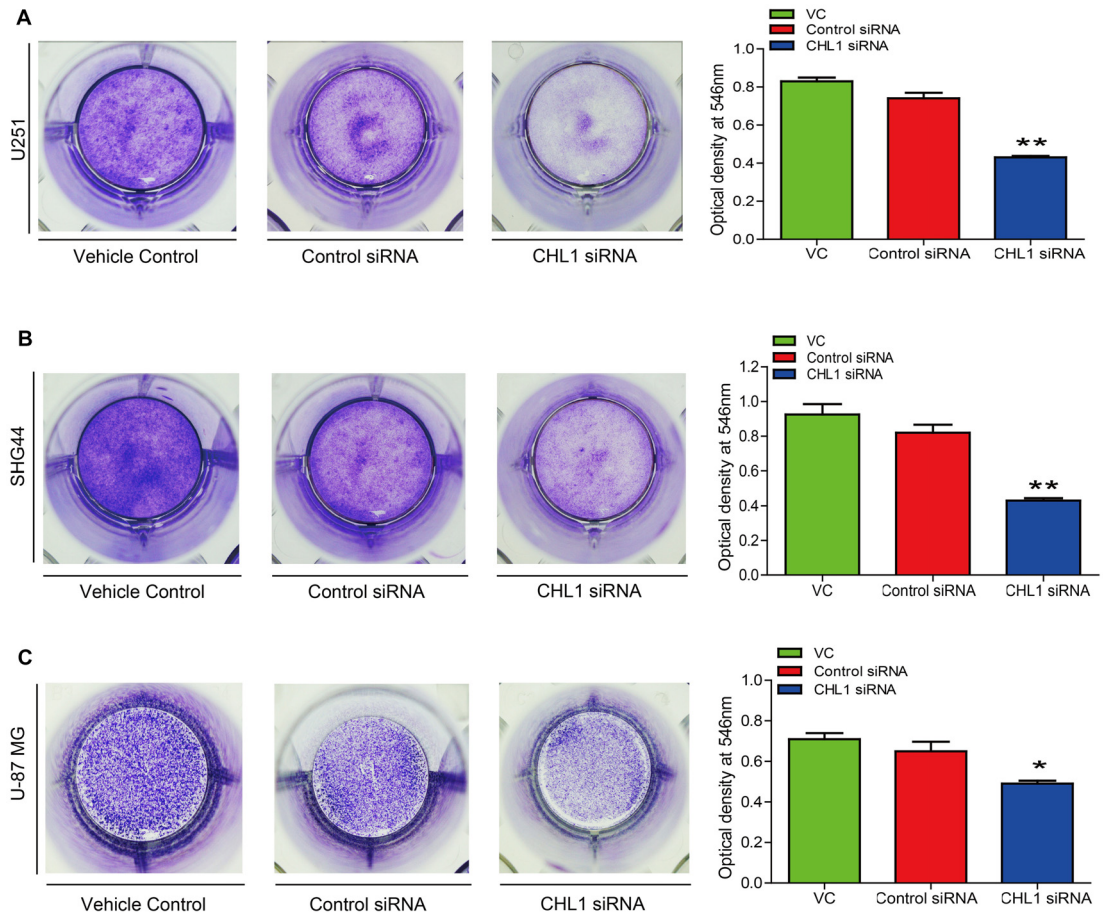

FIGURE 5 | Knockdown of CHL1 reduced colony formation capacity of glioma/glioblastoma cells *in vitro*. Cell colony was stained by crystal violet, which was then dissolved in 1% SDS and the optical density was measured at 546 nm under a microplate reader. **(A)** The colony formation assay revealed that knockdown of CHL1 reduced the colony formation of U251 cells, as was revealed by the optical density detected at 546 nm from three independent experiments (*$p < 0.05$; **$p < 0.01$ vs. either vehicle control or control siRNA). **(B,C)** Similar results were found in SHG44 **(B)** and U-87 MG **(C)** cells for the colony formation experiment. The data were expressed as the means ± SEM from 4 independent experiments (*$p < 0.05$ and **$p < 0.01$ vs. both vehicle control and control siRNA; independent Student's *t*-test).

cells, respectively; $p < 0.01$ vs. negative control for both cell lines; **Figures 4B,C**). These results indicated that knocking down CHL1 expression significantly promoted glioma cell senescence.

Knockdown of CHL1 Expression Inhibits Glioma Cell Colony Formation *in Vitro*

To test whether knocking down CHL1 expression suppresses colony formation, we performed a colony formation assay using U251, SHG44 and U-87 MG cells. After 14 days, the cells were stained with crystal violet and imaged to analyze colony formation rates. Then, crystal violet was dissolved in 1% SDS, and the optical density was measured at 546 nm using a microplate reader. The results demonstrated that CHL1 down-regulation induced a significant reduction in the colony formation rate compared with the negative control siRNA in U251 cell line ($p < 0.05$, **Figure 5A**). Similarly, SHG44 and U-87 MG cell lines with CHL1 knocked down also exhibited a remarkable decrease in the colony formation compared with the negative control siRNA group ($p < 0.01$, **Figures 5B,C**).

Knockdown of Expression Inhibits Cell Invasion *in Vitro*

The number of invading U251 cells in the CHL1-siRNA-transfected group was 100 ± 9, which was significantly lower than that in the groups of cell streated with either the vehicle control or the negative control siRNA (312 ± 11 and 276 ± 8, respectively; $p < 0.05$ for both comparisons (**Figure 6A**). In addition, the numbers of invading SHG44 and U-87 MG cells in the CHL1-siRNA-transfected groups were also significantly decreased compared with cells treated with vehicle or negative control siRNA (84 ± 6 vs. 239 ± 7 and 224 ± 4 for SHG44 cells and 54 ± 5 vs. 187 ± 6 and 205 ± 3 for U-87 MG cells, respectively; $p < 0.001$ for comparisons in SHG44 cells, and $p < 0.01$ for both comparisons in U-87 MG cells; **Figures 6B,C**).

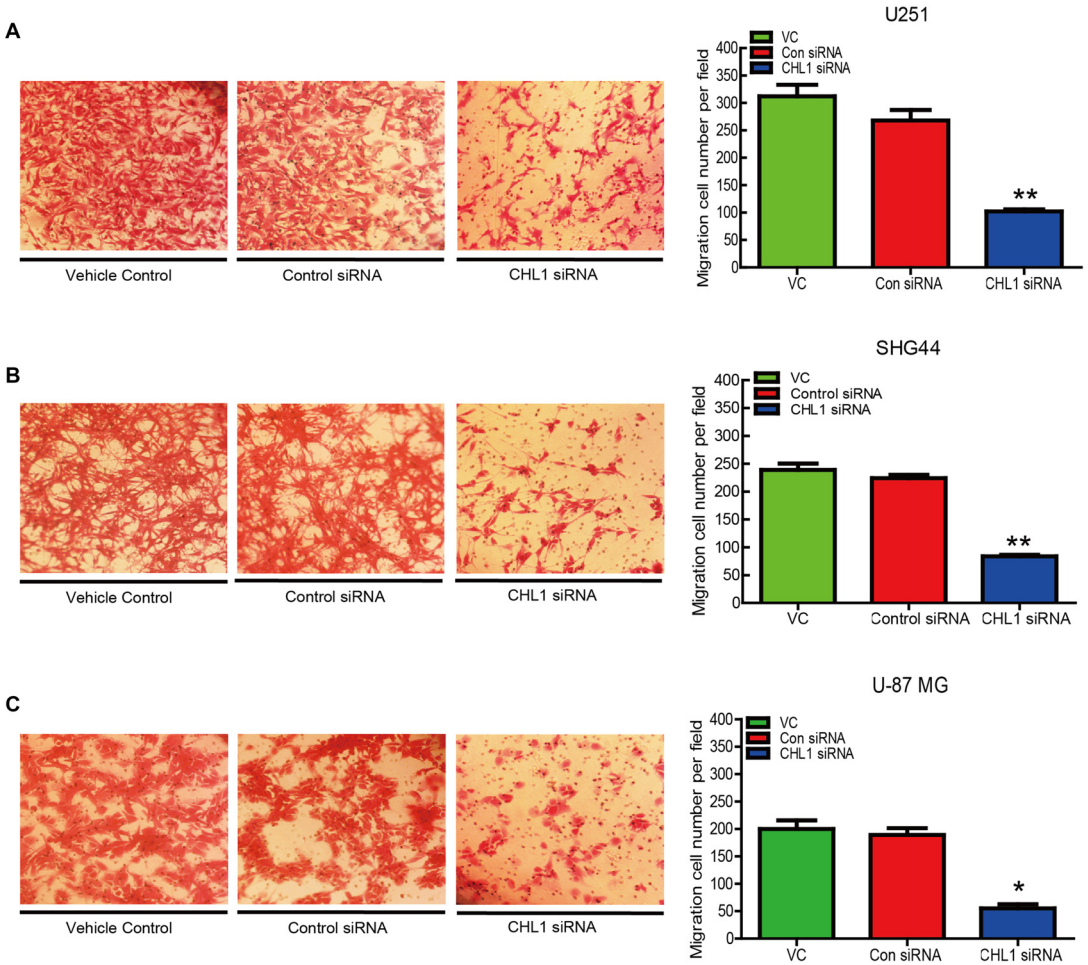

FIGURE 6 | Knockdown of CHL1 suppressed the migration of glioma/glioblastoma cells *in vitro*. Transwell migration assays were carried out using U251 **(A)**, SHG44 **(B)** and U-87 MG **(C)** cells transfected with CHL siRNA. Representative fields containing migrated cells attached to the underside of the membrane were presented. The migration ability was indexed by the relative number of migrated cells from three independent experiments. The data were expressed as the means ± SEM from 3 independent experiments (*$p < 0.05$; **$p < 0.01$ vs. both vehicle control and control siRNA (independent Student's *t*-test).

Knockdown of Expression Affects Cell Survival/Apoptosis Signaling Pathways in Glioma Cells

To confirm the results of the MTT assay, Western blot was performed to determine the expression of the apoptosis-related proteins Bcl-2, Bax, active caspase-3 and PCNA in the three human glioma cell lines. We found that 48 h post transfection, the ratio of Bax to Bcl-2 was up-regulated in three siRNA-CHL1-transfected cell lines compared with cells treated with vehicle control or the negative control siRNA ($p < 0.001$ for both comparisons in U251 cells, and $p < 0.01$ for both comparisons in regarding SHG44 and U-87 MG cells; **Figure 7A**). In addition, active caspase-3 protein levels were significantly increased in all 3 siRNA-CHL1-transfected cell lines compared with cells treated with the negative control or vehicle control ($p < 0.05$ for both comparisons in both SHG44 and U-87 MG cells, and $p < 0.01$ for both comparisons in U251 cells; **Figure 7B**). In addition, PCNA was examined as a possible proliferation indicator in glioma cells. The results demonstrated that PCNA protein levels were significantly reduced in three siRNA-CHL1-transfected cell lines compared with cells treated with vehicle control or negative control siRNA ($p < 0.05$ for both comparisons in SHG44 cells, and $P < 0.01$ for both comparisons in both U251 and U-87 MG cells; **Figure 7C**). Taken together, these results indicated that CHL1-dependent anti-apoptosis in glioma cells may be partially mediated by regulation of the death receptor signaling pathway composed of Bax, Bcl-2 and active caspase-3.

Effects of siRNA Targeting CHL1 on Main Signaling Pathways in Human Glioma Cells

Accumulating evidence indicates that the Ras/MAPK/ERK and PI3/AKT signaling pathways contribute to cell growth, proliferation, and survival (Asati et al., 2016). Western blot analysis was performed to determine pErk and pAkt

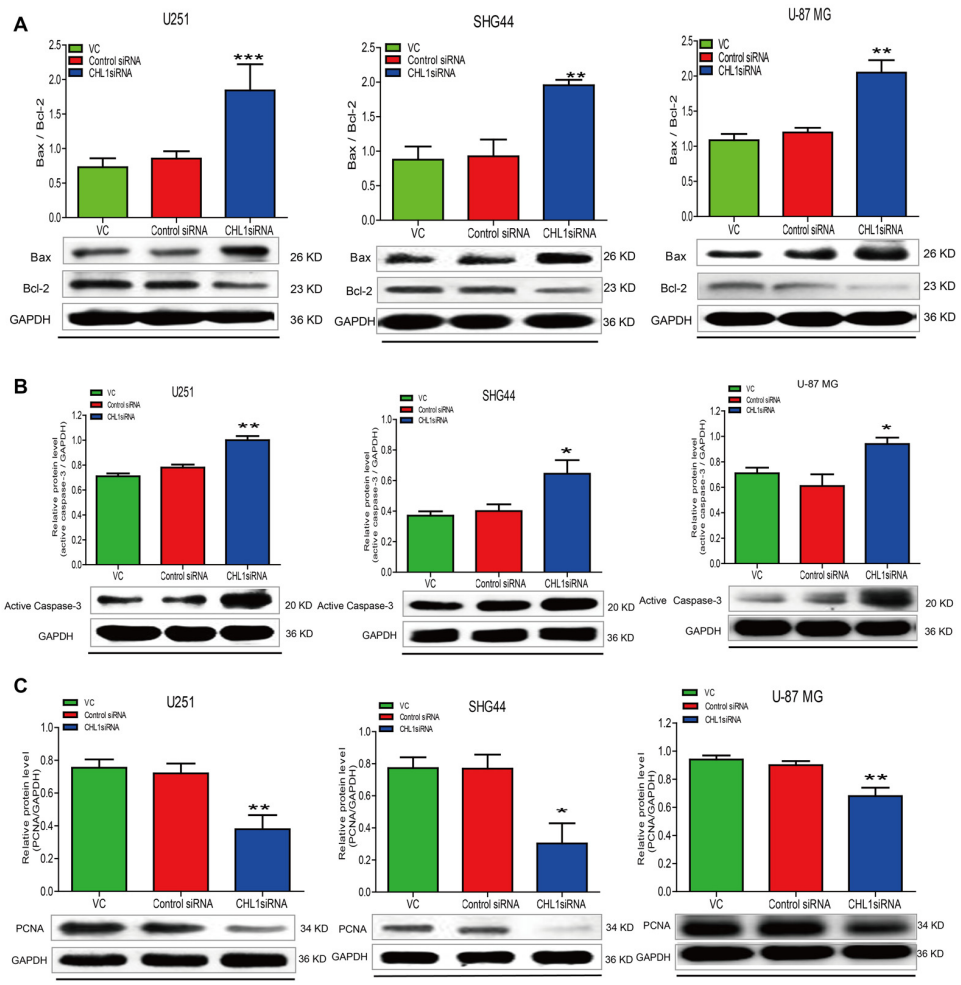

FIGURE 7 | Knockdown of CHL1 affects apoptosis signaling molecules in glioma/glioblastoma cells. U251, SHG44 and U-87 MG cells were seeded onto 48-well plates and treated with vehicle control, control siRNA and siRNA targeting CHL1, respectively. Western blot analysis was performed to determine the levels the apoptosis-related proteins, including changes of the ratio of Bax to Bcl-2 (Bax/Bcl-2) **(A)**, active caspase-3 **(B)** and PCNA **(C)** in glioma/glioblastoma cells. GAPDH was used as the loading control. The data were expressed as the means ± SEM from three independent experiments (*$p < 0.05$; **$p < 0.01$; ***$p < 0.001$ vs. either vehicle control or control siRNA; independent Student's *t*-test).

levels in U251, SHG44 and U-87 MG cells in response to CHL1 siRNA treatment for 48 h. We found that 48 h post transfection, pAkt/AKT levels were significantly decreased in three CHL1 siRNA-transfected human glioma cell lines compared with cells transfected with negative control siRNA ($p < 0.05$ for both comparisons in both SHG44 and U-87 MG cells and $p < 0.01$ for both comparisons in U251 cells (**Figure 8**). However, CHL1 knockdown exhibited no apparent effect on pErk/ERK protein levels at 48 h compared with treatment with either the vehicle control or the negative control siRNA ($p > 0.05$ for both comparisons in all three cell lines).

CHL1 Regulates U-87 MG Glioma Cell Growth *in Vivo*

We established subcutaneous xenografts of U-87 MG glioblastoma cells in nude mice. To determine whether the tumor formation of glioblastoma oncogenicity is dependent upon CHL1, we reduced CHL1 expression using CHL1-siRNA combined with Entranster^{TM}-*in vivo*, which was intratumorally injected to specifically knockdown endogenous CHL1 expression *in vivo*. Intratumoral injection of siRNA targeting CHL1 significantly reduces the fold increases in tumor volume at most time points post siRNA transfection ($p < 0.05$ vs. control siRNA at 3, 5, 7, 10, 11, 12 and 13 day points post 1st siRNA injection; $p < 0.01$ vs. control siRNA at 4, 6, and 9 day points post the 1st siRNA injection; **Figures 9A–C**). The final tumor volume in mice treated with siRNA targeting CHL1 was lower than that in mice treated with control siRNA, although no statistical significance was detected (1689.41 ± 239.46 vs. 1877.50 ± 325.11 mm^3, $p = 0.2768$ vs. control siRNA, **Figure 9D**). However, the total increased tumor volume in mice treated with siRNA targeting CHL1 was significantly lower than that in mice treated with control siRNA ($p < 0.05$ vs.

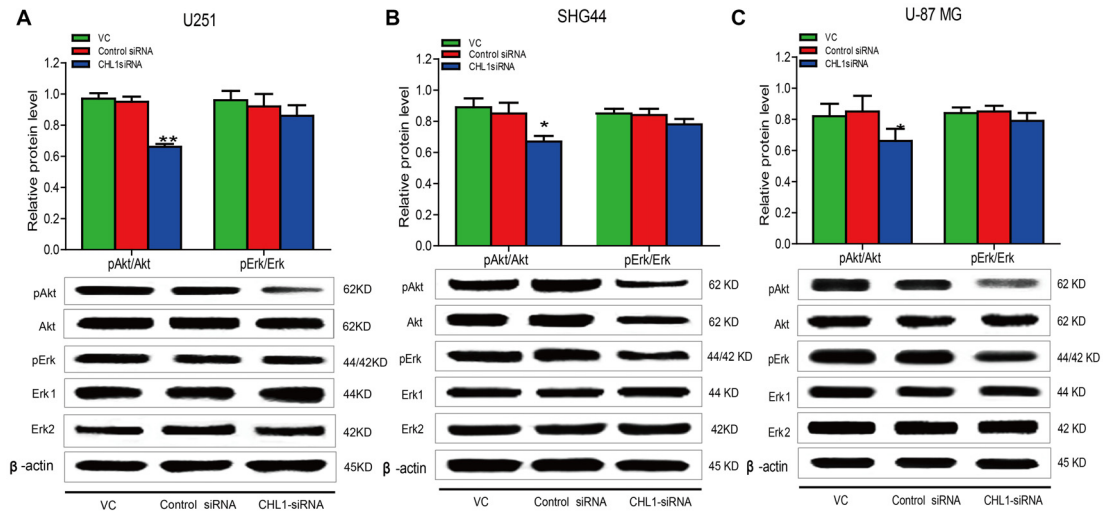

FIGURE 8 | Knockdown of CHL1 reduced the phosphorylation levels of ERK and AKT. Western blot was used to analyze the levels of pAkt and pErk in three cell lines after treatment with vehicle control, negative control and CHL1 siRNA for 48 h. pAkt and pErk protein levels in U251 **(A)**, SHG44 **(B)** and U-87 MG cells **(C)** were presented. GAPDH was used as a loading control. The data were expressed as the means ± SEM from 3 independent experiments (*$p < 0.05$ and **$p < 0.01$ vs. both vehicle control and control siRNA; independent Students *t*-test).

control siRNA, data not shown). These results demonstrate that reducing CHL1 expression can partially inhibit the growth of glioma *in vivo*.

Morphological Changes in Subcutaneous Xenografts of U-87 MG Cells in Response to CHL1 Transfection

H&E staining and immunohistochemical staining were performed to analyze changes in the xenograft tumor in response to CHL1 down-regulation. The results demonstrated that the staining intensities of CHL1, PCNA and GFAP were apparently reduced, whereas active caspase-3 intensity was apparently increased (**Figure 10**).

DISCUSSION

Despite recent progress in the treatment of melanoma and other tumors, treatment of glioma remains disappointing. Traditional therapeutic means, including radiotherapy and chemotherapy, and neurosurgical removal do not completely eradicate the tumor, and recurrence often occurs (Sathornsumetee et al., 2007). L1 is among the most intensively studied cell adhesion molecules in glioma investigation. Inhibition of L1 expression by siRNA and administration of L1 ectodomain-binding antibodies reduced the migration of glioblastoma cells *in vitro* (Izumoto et al., 1996) and disrupted glioma stem cell proliferation, leading to apoptosis (Bao et al., 2008). Reducing L1 expression *in vivo* also suppressed tumor growth and increased the survival of tumor-bearing animals (Cheng et al., 2011).

The overexpression of cell adhesion molecules, including L1, and specific inhibition of the function of these molecules suggests target-directed and promising therapeutic methods for glioma (Skibbens, 2004; Wolterink et al., 2010). The mAbs specifically reacting with L1CAM efficiently prolong survival and reduce tumor burden in a model of SKOV3ip cells in CD1 nude mice. Antibody-based functional impairment of L1 also altered the expression of cellular genes associated with apoptosis and tumor growth (Wolterink et al., 2010). Additional reports demonstrated that cell adhesion molecule VCAM-1-positive glioblastoma tumor stem cells (GTSC) possess a high rate of proliferation as measured by PCNA expression (Zarnescu et al., 2011). However, neural cell adhesion molecule (NCAM) levels were down-regulated as the malignancy of astrocytomas increased, and this effect is inversely correlated with PCNA (Huang et al., 2001). These data suggested that different cell adhesion molecule members may function differentially in the development of glioma and promoted us to explore the potential roles of CHL1 in promoting glioma cell migration, proliferation and metastasis.

Similar to L1, CHL1 also plays major roles in axonal guidance in the developing brain and mediates the maintenance and remodeling of neural circuits in the adult brain (Sakurai et al., 2002; Hitt et al., 2012). In the present work, CHL1 was lowly expressed in human astroglia cells, but was highly expressed in human glioma cell lines, suggesting its potential roles in the development of glioma. To date, paradoxical data about the roles of CHL1 under the tumorigenic conditions were reported in non-neuronal cell-derived tumors. He et al. (2013) reported that CHL1 is down-regulated in human breast cancer and is related to lower grade. Down-regulating CHL1 expression results in increased proliferation and invasion, and CHL1 deficiency also promotes tumor formation *in vivo*. Knocking down CHL1 expression by miR-10a increased colony formation activity, migration and invasion of human cervical cancer cells, whereas over-expression of CHL1 abolished the effects of

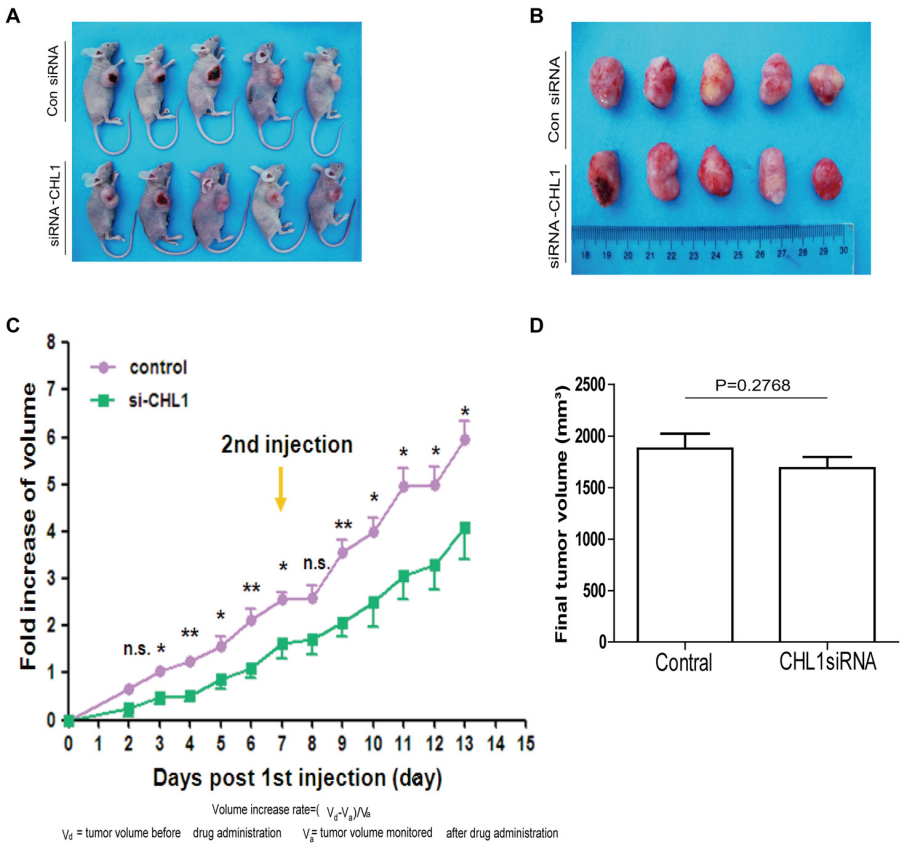

FIGURE 9 | CHL1 regulates growth of U-87 MG glioma cells *in vivo*. **(A,B)** Two weeks after the 1st intratumoral injection, all mice were killed by cervical dislocation. The *in situ* tumors and the dissected tumor tissues were photographed. **(C)** The fold increase of volume at each day points post the 1st intratumoral injection of either control siRNA or CHL1 siRNA complexed with the Entranster^{TM}-*in vivo*. **(D)** Column diagram showing the final average tumor volumes from both control siRNA and CHL1 siRNA-treated group (n = 5, p = 0.2768 vs. the control siRNA group) (*$p < 0.05$; **$p < 0.01$ vs. control siRNA; Independent Student's t-test).

miR-10a (Long et al., 2012). In addition, miR-182 promotes cell proliferation and invasion through direct suppression of CHL1 in papillary thyroid carcinoma (PTC; Zhu et al., 2014). miR-590-5p is up-regulated in human cervical cancer and promotes cervical cancer cell growth, cell invasion and colony formation by negatively regulating CHL1 at the posttranscriptional level (Chu et al., 2014). In addition, CHL1 negatively modulates the proliferation and neuronal differentiation of neural progenitor cells (NPCs) by CHL1/ERK1/2 MAPK signaling (Huang et al., 2011). Although CHL1 functions as a putative tumor suppressor during primary tumor growth and is silenced to facilitate *in situ* tumor growth, re-expression of CHL1 on the edge of the tumor mass may promote local invasive growth and enable further metastatic spread in ovary, colon and breast cancers (Senchenko et al., 2011). In addition, CHL1 facilitates the identification of two major histological types of renal cancer as a potentially novel specific biomarker in early pathogenesis (Senchenko et al., 2011). In pituitary adenoma (PA), differential expression of CHL1 may potentially predict a recurrence phenotype (Marko et al., 2012). Senescence is a stress response that stably blocks proliferation and functions as a tumor suppressor in aging and precancerous cells (Collado and Serrano, 2010; Wagner et al., 2015). The lysosomal-β-galactosidase gene is the source of senescence associated-β-galactosidase activity, and that level of lysosomal-β-galactosidase protein increase during senescence (Lee et al., 2006). The presence of senescence in response to CHL1 knockdown indicates the potential role of CHL1 in promoting cell survival during the development of glioma.

The discrepancy of our findings with those observed in non-glia-derived tumors may be due to the fact that glioma cells express a variety of molecules that interact with CHL1. CHL1 also potentiates integrin-dependent haptotactic cell migration toward the extracellular matrix via a potential integrin interaction motif Asp-Gly-Glu-Ala (DGEA) in the sixth immunoglobulin domain (Buhusi et al., 2003). CHL1–CHL1 homophilic interactions inhibit the neurite outgrowth-promoting functions of CHL1, whereas integrins in cis- and trans-configurations are conducive to heterophilic CHL1 interactions (Buhusi et al., 2003; Demyanenko et al., 2004; Jakovcevski et al., 2007, 2009). Observations indicate that homophilic CHL1 trans-interactions regulate differentiation of neuronal progenitor cells at early postnatal stages, whereas heterophilic trans-interactions of CHL1 with vitronectin, integrins and the plasminogen activator system regulate neuritogenesis and neuronal cell migration at a

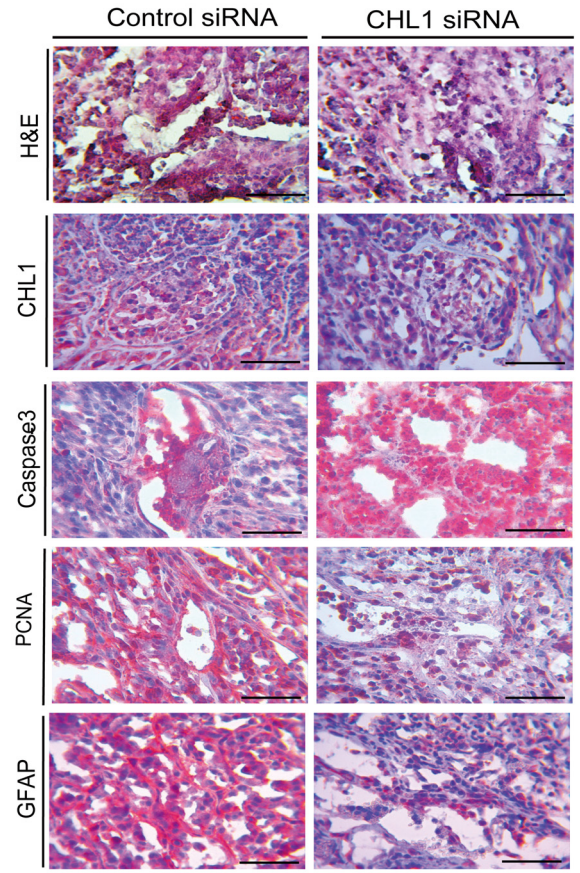

FIGURE 10 | H&E staining and immunohistochemical staining analyses for the CHL1, caspase-3, PCNA and GFAP molecules in glioblastoma xenograft tissues from both control siRNA and CHL1 siRNA-treated groups. Scale bars represent 25 μm.

later stage of cerebellar morphogenesis (Hillenbrand et al., 1999; Katic et al., 2014).

The activation of the AKT and ERK signaling pathways plays an important role in the regulation of cell apoptosis, invasion and metastasis of gliomas. Feng et al. (2010) reported that TAM was present in the rat C6 glioma cell line through activation of PI3K/Akt, JNK and ERK signaling pathways to mediate the physiological processes of glioma cell apoptosis. Studies by Li et al. (2013) reported that a DC electric field can activate the AKT and ERK signaling pathways in U251 glioma cells, thus affecting the direction of tumor migration. Wu et al. (2010) found that PI3K-dependent activation of Erk1/2 signaling pathway up-regulates CHL1 expression in the primary culture of astrocytes. Whether the effect of CHL1 on glioma is closely related to the ERK and AKT signaling pathways has not been reported. We demonstrate that downregulation of CHL1 reduces the activation of Akt1 with no apparent effect on Erk1/2 activation. This finding suggests that the modulating role of CHL1 on glioma behaviors may be partially mediated by Akt1 signaling.

Intratumoral injection represents a promising therapeutic method for tumor management via directly introducing siRNA or other forms of RNA into the tumor tissue. Unlike traditional xenografts of cells with a targeting molecule knocked down, *in vivo* knockdown is more similar to the clinical setting. Zheng et al. (2015) introduced shRNA against LunX into lung cancer tissue *in vivo*, which successfully disrupted local invasion, micrometastasis formation and metastatic colonization of lung cancer cells, thus inhibiting the initial and final steps of the invasion-metastasis cascade. Using an *in vivo* tumorigenicity assay, Wang et al. (2012) reported that daily intratumoral injection of let-7a-mimics in nude mice suppresses NIRF expression and reduces tumor growth. Although intratumoral injection of siRNA targeting CHL1 in the present study reduces the volume increase of glioma xenografts, the growth inhibition efficacy is limited. This effect may be partially attributed to low siRNA transfection and expansion due to the high intensity of cell proliferation in the glioma tissue, which is different from that of lung cancer. Increases in the siRNA transfection efficiency may lead to a more promising therapeutic result.

In summary, our work preliminarily demonstrated the roles of CHL1 in the development of gliomas, which may provide a scientific basis for the molecular targeting treatment of gliomas.

AUTHOR CONTRIBUTIONS

ZY and QX performed most of the experiments, analyzed the data, and drafted the sections of Materials and Methods, and Results. C-LH was responsible for figure processing and adjusting the format of the draft. QJ and H-FS assisted the performance of some experiments. MS provided suggestions and comments for the project and contributed to writing of the manuscript. W-JZ conceived and designed the experiments, undertook some of the experiments, wrote the manuscript and revised the article critically and approved the final version to be submitted.

ACKNOWLEDGMENTS

The authors are grateful to the National Natural Science Foundation of China (Grant Nos. 81471279 and 81171138 to W-JZ) for support. The authors are also grateful to the Li Kashing Foundation (Grant No. LD030601 to MS). This work was also supported by a Talent grant of Shantou University Medical College (Grant No. 250122 0118 to W-JZ).

SUPPLEMENTARY MATERIAL

The Supplementary Material for this article can be found online at: https://www.frontiersin.org/articles/10.3389/fnmol.2017.00324/full#supplementary-material

FIGURE S1 | Specificity testing for CHL1 antibody on an uncut PVDF membrane.

REFERENCES

Asati, V., Mahapatra, D. K., and Bharti, S. K. (2016). PI3K/Akt/mTOR and Ras/Raf/MEK/ERK signaling pathways inhibitors as anticancer agents: structural and pharmacological perspectives. *Eur. J. Med. Chem.* 109, 314–341. doi: 10.1016/j.ejmech.2016.01.012

Bao, S., Wu, Q., Li, Z., Sathornsumetee, S., Wang, H., McLendon, R. E., et al. (2008). Targeting cancer stem cells through L1CAM suppresses glioma growth. *Cancer Res.* 68, 6043–6048. doi: 10.1158/0008-5472.CAN-08-1079

Buhusi, M., Midkiff, B. R., Gates, A. M., Richter, M., Schachner, M., and Maness, P. F. (2003). Close homolog of L1 is an enhancer of integrin-mediated cell migration. *J. Biol. Chem.* 278, 25024–25031. doi: 10.1074/jbc.M303084200

Chen, Q. Y., Chen, Q., Feng, G. Y., Lindpaintner, K., Chen, Y., Sun, X., et al. (2005). Case-control association study of the close homologue of L1 (CHL1) gene and schizophrenia in the Chinese population. *Schizophr. Res.* 73, 269–274. doi: 10.1016/j.schres.2004.06.001

Cheng, L., Wu, Q., Guryanova, O. A., Huang, Z., Huang, Q., Rich, J. N., et al. (2011). Elevated invasive potential of glioblastoma stem cells. *Biochem. Biophys. Res. Commun.* 406, 643–648. doi: 10.1016/j.bbrc.2011.02.123

Chu, Y., Ouyang, Y., Wang, F., Zheng, A., Bai, L., Han, L., et al. (2014). MicroRNA-590 promotes cervical cancer cell growth and invasion by targeting CHL1. *J. Cell. Biochem.* 115, 847–853. doi: 10.1002/jcb.24726

Chung, G., O'Neil, N. J., and Rose, A. M. (2011). CHL-1 provides an essential function affecting cell proliferation and chromosome stability in *Caenorhabditis elegans*. *DNA Repair* 10, 1174–1182. doi: 10.1016/j.dnarep.2011.09.011

Collado, M., and Serrano, M. (2010). Senescence in tumours: evidence from mice and humans. *Nat. Rev. Cancer* 10, 51–57. doi: 10.1038/nrc2772

Demyanenko, G. P., Schachner, M., Anton, E., Schmid, R., Feng, G., Sanes, J., et al. (2004). Close homolog of L1 modulates area-specific neuronal positioning and dendrite orientation in the cerebral cortex. *Neuron* 44, 423–437. doi: 10.1016/j.neuron.2004.10.016

Dimri, G. P., Lee, X., Basile, G., Acosta, M., Scott, G., Roskelley, C., et al. (1995). A biomarker that identifiessenescenthumancells in culture and in aging skin *in vivo*. *Proc. Natl. Acad. Sci. U S A* 92, 9363–9367. doi: 10.1073/pnas.92.20.9363

Feng, Y., Huang, J., Ding, Y., Xie, F., and Shen, X. (2010). Tamoxifen-induced apoptosis of rat C6 glioma cells via PI3K/Akt, JNK and ERK activation. *Oncol. Rep.* 24, 1561–1567. doi: 10.3892/or_00001018

Gabriel, A., Batey, J., Capogreco, J., Kimball, D., Walters, A., Tubbs, R. S., et al. (2014). Adult brain cancer in the U.S. black population: a surveillance, epidemiology, and end results (SEER) analysis of incidence, survival and trends. *Med. Sci. Monit.* 20, 1510–1517. doi: 10.12659/MSM.890762

He, L. H., Ma, Q., Shi, Y. H., Ge, J., Zhao, H. M., Li, S. F., et al. (2013). CHL1 is involved in human breast tumorigenesis and progression. *Biochem. Biophys. Res. Commun.* 438, 433–438. doi: 10.1016/j.bbrc.2013.07.093

Higuchi, T., Fujiwara, H., Egawa, H., Sato, Y., Yoshioka, S., Tatsumi, K., et al. (2003). Cyclic AMP enhances the expression of an extravillous trophoblast marker, melanoma cell adhesion molecule, in choriocarcinoma cell JEG3 and human chorionic villous explant cultures. *Mol. Hum. Reprod.* 9, 359–366. doi: 10.1093/molehr/gag044

Hillenbrand, R., Molthagen, M., Montag, D., and Schachner, M. (1999). The close homologue of the neural adhesion molecule L1 (CHL1): patterns of expression and promotion of neurite outgrowth by heterophilic interactions. *Eur. J. Neurosci.* 11, 813–826. doi: 10.1046/j.1460-9568.1999.00496.x

Hitt, B., Riordan, S. M., Kukreja, L., Eimer, W. A., Rajapaksha, T. W., and Vassar, R. (2012). β-Site amyloid precursor protein (APP)-cleaving enzyme 1 (BACE1)-deficient mice exhibit a close homolog of L1 (CHL1) loss-of-function phenotype involving axon guidance defects. *J. Biol. Chem.* 287, 38408–38425. doi: 10.1074/jbc.M112.415505

Holm, J., Hillenbrand, R., Steuber, V., Bartsch, U., Moos, M., Lübbert, H., et al. (1996). Structuralfeatures of a close homologue of L1 (CHL1) in the mouse: a new member of the L1 family of neural recognition molecules. *Eur. J. Neurosci.* 8, 1613–1629. doi: 10.1111/j.1460-9568.1996.tb01306.x

Huang, C. X., Hu, S. X., and Chen, B. (2001). Expression of the neural cell adhesion molecule in human astrocytomas. *Hunan Yi Ke Da Xue Xue Bao* 26, 543–545.

Huang, X., Zhu, L. L., Zhao, T., Wu, L. Y., Wu, K. W., Schachner, M., et al. (2011). CHL1 negatively regulates the proliferation and neuronal differentiation of neural progenitor cells through activation of the ERK1/2 MAPK pathway. *Mol. Cell. Neurosci.* 46, 296–307. doi: 10.1016/j.mcn.2010.09.013

Izumoto, S., Ohnishi, T., Arita, N., Hiraga, S., Taki, T., and Hayakawa, T. (1996). Gene expression of neural cell adhesion molecule L1 in malignant gliomas and biological significance of L1 in glioma invasion. *Cancer Res.* 56, 1440–1444.

Jakovcevski, I., Siering, J., Hargus, G., Karl, N., Hoelters, L., Djogo, N., et al. (2009). Close homologue of adhesion molecule L1 promotes survival of Purkinje and granule cells and granule cell migration during murine cerebellar development. *J. Comp. Neurol.* 513, 496–510. doi: 10.1002/cne.21981

Jakovcevski, I., Wu, J., Karl, N., Leshchyns'ka, I., Sytnyk, V., Chen, J., et al. (2007). Glial scar expression of CHL1, the close homolog of the adhesion molecule L1, limits recovery after spinal cord injury. *J. Neurosci.* 27, 7222–7233. doi: 10.1523/JNEUROSCI.0739-07.2007

Jemal, A., Siegel, R., Xu, J., and Ward, E. (2010). Cancer statistics, 2010. *CA Cancer J. Clin.* 60, 277–300. doi: 10.3322/caac.20073

Katic, J., Loers, G., Kleene, R., Karl, N., Schmidt, C., Buck, F., et al. (2014). Interaction of the cell adhesion molecule CHL1 with vitronectin, integrins and the plasminogen activator inhibitor-2 promotes CHL1-induced neurite outgrowth and neuronal migration. *J. Neurosci.* 34, 14606–14623. doi: 10.1523/JNEUROSCI.3280-13.2014

Lee, B. Y., Han, J. A., Im, J. S., Morrone, A., Johung, K., Goodwin, E. C., et al. (2006). Senescence-associated β-galactosidase is lysosomal β-galactosidase. *Aging Cell* 5, 187–195. doi: 10.1111/j.1474-9726.2006.00199.x

Li, F., Chen, T., Hu, S., Lin, J., Hu, R., and Feng, H. (2013). Superoxide mediates direct current electric field-induced directional migration of glioma cells through the activation of AKT and ERK. *PLoS One* 8:e61195. doi: 10.1371/journal.pone.0061195

Long, M. J., Wu, F. X., Li, P., Liu, M., Li, X., and Tang, H. (2012). MicroRNA-10a targets CHL1 and promotes cell growth, migration and invasion in human cervical cancer cells. *Cancer Lett.* 324, 186–196. doi: 10.1016/j.canlet.2012.05.022

Manderson, E. N., Birch, A. H., Shen, Z., Mes-Masson, A. M., Provencher, D., and Tonin, P. N. (2009). Molecular genetic analysis of a cell adhesion molecule with homology to L1CAM, contactin 6 and contactin 4 candidate chromosome 3p26pter tumor suppressor genes in ovarian cancer. *Int. J. Gynecol. Cancer* 19, 513–525. doi: 10.1111/IGC.0b013e3181a3cd38

Maness, P. F., and Schachner, M. (2007). Neural recognition molecules of the immunoglobulin superfamily: signaling transducers of axon guidance and neuronal migration. *Nat. Neurosci.* 10, 19–26. doi: 10.1038/nn0207-263b

Marko, N. F., Coughlan, C., and Weil, R. J. (2012). Towards an integrated molecular and clinical strategy to predict early recurrence in surgically resected non-functional pituitary adenomas. *J. Clin. Neurosci.* 19, 1535–1540. doi: 10.1016/j.jocn.2012.01.038

Morag, A., Pasmanik-Chor, M., Oron-Karni, V., Rehavi, M., Stingl, J. C., and Gurwitz, D. (2011). Genome-wide expression profiling of human lymphoblastoid cell lines identifies CHL1 as a putative SSRI antidepressant response biomarker. *Pharmacogenomics* 12, 171–184. doi: 10.2217/pgs.10.185

Nakazato, Y. (2008). The 4th edition of WHO classification of tumours of the central nervous system published in 2007. *No Shinkei Geka* 36, 473–491.

Qin, Y. R., Fu, L., Sham, P. C., Kwong, D. L., Zhu, C. L., Chu, K. K., et al. (2008). Single-nucleotide polymorphism-mass array reveals commonly deleted regions at 3p22 and 3p14.2 associate with poor clinical outcome in esophageal squamous cell carcinoma. *Int. J. Cancer* 123, 826–830. doi: 10.1002/ijc.23577

Sakurai, K., Migita, O., Toru, M., and Arinami, T. (2002). An association between a missense polymorphism in the close homologue of L1 (CHL1, CALL) gene and schizophrenia. *Mol. Psychiatry* 7, 412–415. doi: 10.1038/sj.mp.4000973

Sathornsumetee, S., Rich, J. N., and Reardon, D. A. (2007). Diagnosis and treatment of high-grade astrocytoma. *Neurol. Clin.* 25, 1111–1139. doi: 10.1016/j.ncl.2007.07.004

Senchenko, V. N., Krasnov, G. S., Dmitriev, A. A., Kudryavtseva, A. V., Anedchenko, E. A., Braga, E. A., et al. (2011). Differential expression of

CHL1 gene during development of major human cancers. *PLoS One* 6:e15612. doi: 10.1371/journal.pone.0015612

Skibbens, R. V. (2004). Chl1p, a DNA helicase-like protein in budding yeast, functions in sister-chromatid cohesion. *Genetics* 166, 33–42. doi: 10.1534/genetics.166.1.33

Tassano, E., Biancheri, R., Denegri, L., Porta, S., Novara, F., Zuffardi, O., et al. (2014). Heterozygous deletion of CHL1 gene: detailed array-CGH and clinical characterization of a new case and review of the literature. *Eur. J. Med. Genet.* 57, 626–629. doi: 10.1016/j.ejmg.2014.09.007

Tschentscher, F., Hüsing, J., Hölter, T., Kruse, E., Dresen, I. G., Jöckel, K. H., et al. (2003). Tumor classification based on gene expression profiling shows that uveal melanomas with and without monosomy 3 represent two distinct entities. *Cancer Res.* 10, 2578–2584.

Wagner, J., Damaschke, N., Yang, B., Truong, M., Guenther, C., McCormick, J., et al. (2015). Overexpression of the novel senescence marker β-galactosidase (GLB1) in prostate cancer predicts reduced PSA recurrence. *PLoS One* 10:e0124366. doi: 10.1371/journal.pone.0124366

Wang, F., Zhang, P., Ma, Y., Yang, J., Moyer, M. P., Shi, C., et al. (2012). NIRF is frequently upregulated in colorectal cancer and its oncogenicity can be suppressed by let-7a microRNA. *Cancer Lett.* 314, 223–231. doi: 10.1016/j.canlet.2011.09.033

Wolterink, S., Moldenhauer, G., Fogel, M., Kiefel, H., Pfeifer, M., Lüttgau, S., et al. (2010). Therapeutic antibodies to human L1CAM: functional characterization and application in a mouse model for ovarian carcinoma. *Cancer Res.* 70, 2504–2515. doi: 10.1158/0008-5472.CAN-09-3730

Wu, J., Wrathall, J. R., and Schachner, M. (2010). Phosphatidylinositol 3-kinase/protein kinase Cdelta activation induces close homolog of adhesion molecule L1 (CHL1) expression in cultured astrocytes. *Glia* 58, 315–328. doi: 10.1002/glia.20925

Zarnescu, O., Brehar, F. M., Bleotu, C., and Gorgan, R. M. (2011). Co-localization of PCNA, VCAM-1 and caspase-3 with nestin in xenografts derived from human anaplastic astrocytoma and glioblastoma multiforme tumor spheres. *Micron* 42, 793–800. doi: 10.1016/j.micron.2011.04.005

Zhang, X., Davis, J. Q., Carpenter, S., and Bennett, V. (1998). Structural requirements for association of neurofascin with ankyrin. *J. Biol. Chem.* 273, 30785–30794. doi: 10.1074/jbc.273.46.30785

Zhao, W. J., and Ren, S. G. (2011). Endogenous neuregulin-1 expression in the anterior pituitary of female Wistar-Furth rats during the estrous cycle. *Nan Fang Yi Ke Da Xue Xue Bao* 31, 921–927.

Zhao, W., and Ren, S. G. (2011). Neuregulin-1 (Nrg1) is mainly expressed in rat pituitarygonadotroph cells and possibly regulates prolactin (PRL) secretionin a juxtacrine manner. *J. Neuroendocrinol.* 23, 1252–1262. doi: 10.1111/j.1365-2826.2011.02223.x

Zhao, W. J., and Schachner, M. (2013). Neuregulin 1 enhances cell adhesion molecule l1 expression in human glioma cells and promotes their migration as a function of malignancy. *J. Neuropathol. Exp. Neurol.* 72, 244–255. doi: 10.1097/NEN.0b013e3182863dc5

Zhao, W., Shen, H., Yuan, F., Li, G., Sun, Y., Shi, Z., et al. (2009). Induction stage-dependent expression of vascular endothelial growth factor and aquaporin-1 in diethylstilbestrol-treated rat pituitary. *Eur. J. Histochem.* 53, 53–60. doi: 10.4081/ejh.2009.53

Zheng, X., Cheng, M., Fu, B., Fan, X., Wang, Q., Yu, X., et al. (2015). Targeting LUNX inhibits non-small cell lung cancer growth and metastasis. *Cancer Res.* 75, 1080–1090. doi: 10.1158/0008-5472.CAN-14-1831

Zhu, H., Fang, J., Zhang, J., Zhao, Z., Liu, L., Wang, J., et al. (2014). miR-182 targets CHL1 and controls tumor growth and invasion in papillary thyroid carcinoma. *Biochem. Biophys. Res. Commun.* 450, 857–862. doi: 10.1016/j.bbrc.2014.06.073

Conflict of Interest Statement: The authors declare that the research was conducted in the absence of any commercial or financial relationships that could be construed as a potential conflict of interest.

frontiers in Molecular Neuroscience

REVIEW
published: 04 October 2017
doi: 10.3389/fnmol.2017.00316

MeCP2 Deficiency in Neuroglia: New Progress in the Pathogenesis of Rett Syndrome

Xu-Rui Jin[1,2], *Xing-Shu Chen*[1]* *and Lan Xiao*[1]*

[1] Department of Histology and Embryology, Faculty of Basic Medicine, Collaborative Program for Brain Research, Third Military Medical University, Chongqing, China, [2] The Cadet Brigade of Clinic Medicine, Third Military Medical University, Chongqing, China

Rett syndrome (RTT) is an X-linked neurodevelopmental disease predominantly caused by mutations of the methyl-CpG-binding protein 2 (MeCP2) gene. Generally, RTT has been attributed to neuron-centric dysfunction. However, increasing evidence has shown that glial abnormalities are also involved in the pathogenesis of RTT. Mice that are MeCP2-null specifically in glial cells showed similar behavioral and/or neuronal abnormalities as those found in MeCP2-null mice, a mouse model of RTT. MeCP2 deficiency in astrocytes impacts the expression of glial intermediate filament proteins such as fibrillary acidic protein (GFAP) and S100 and induces neuron toxicity by disturbing glutamate metabolism or enhancing microtubule instability. MeCP2 deficiency in oligodendrocytes (OLs) results in down-regulation of myelin gene expression and impacts myelination. While MeCP2-deficient microglia cells fail in response to environmental stimuli, release excessive glutamate, and aggravate impairment of the neuronal circuit. In this review, we mainly focus on the progress in determining the role of MeCP2 in glial cells involved in RTT, which may provide further insight into a therapeutic intervention for RTT.

Keywords: Rett syndrome (RTT), MeCP2, astrocyte, oligodendrocyte, microglia

OPEN ACCESS

Edited by:
Alexej Verkhratsky,
University of Manchester,
United Kingdom

Reviewed by:
Xiaolu Zhang,
Northern Jiangsu People's Hospital,
China
Michele Papa,
Università degli Studi della Campania
"Luigi Vanvitelli" Caserta, Italy

***Correspondence:**
Xing-Shu Chen
xingshuchen2011@163.com
Lan Xiao
xiaolan35@hotmail.com

Received: *30 April 2017*
Accepted: *19 September 2017*
Published: *04 October 2017*

Citation:
Jin X-R, Chen X-S and Xiao L (2017) MeCP2 Deficiency in Neuroglia: New Progress in the Pathogenesis of Rett Syndrome. Front. Mol. Neurosci. 10:316. doi: 10.3389/fnmol.2017.00316

INTRODUCTION

Rett Syndrome (RTT) is an X-linked autism spectrum disorder that affects 1 in every 10,000–15,000 newborns in the United States (Chahrour and Zoghbi, 2007). It is specially characterized by a period of seemingly normal development that lasts for 6–18 months after birth. Subsequently, microcephaly and stereotypic hand wringing start to appear (Nomura, 2005) and more special symptoms appear as the age increases, such as a loss of motor coordination, ataxia, gait apraxia, seizures, poor sleep efficiency or parkinsonian features (Roze et al., 2007). In an overwhelming majority (more than 95%) of RTT patients, the syndrome is caused by mutations in a gene called methyl-CpG-binding protein 2 (MeCP2), a transcriptional corepressor that can bind to methylated CpG islands and complex with Sin3 homolog A (Sin3A) and histone deacetylases (HDACs) to regulate gene expression (Lyst and Bird, 2015). Moreover, different mutations are associated with disease severity, and there are approximately 30 types of mutations that can cause RTT. Patients with the R270X mutation and frame shift deletions in a $(CCACC)_n$-rich region present with the most typical symptoms (Bienvenu et al., 2000).

Generally, the symptoms of RTT are attributed to neuronal dysfunction. Substantial evidence shows that neuronal, morphological and functional abnormalities are involved in RTT pathogenesis. For instance, MeCP2-deficient neurons have an abnormal morphology (e.g., fewer dendritic spines and reduced arborization) (Zhou et al., 2006; Smrt et al., 2007;

Palmer et al., 2008). The number of synapses is decreased in hippocampi of MeCP2-null mice and conversely, the change was elevated in MeCP2-overexpressing mice (Johnston et al., 2001; Chao et al., 2007; Banerjee et al., 2012). Moreover, the re-expression of *MECP2* in MeCP2-null neurons effectively rescued behavioral abnormalities in mice (Luikenhuis et al., 2004).

However, increasing evidence has shown that white matter damage and/or glial cell (i.e., astrocyte, oligodendrocyte and microglia) dysfunction induced by a change in the DNA methylation state is also involved in the pathogenesis of RTT (Ballas et al., 2009; Maezawa and Jin, 2010; Okabe et al., 2012; Durand et al., 2013; Nguyen et al., 2013). Recently, it was reported that MeCP2-null astrocytes are incapable of supporting the normal development of co-cultured wild-type (WT) neurons (Williams et al., 2014). MeCP2-null microglia and astrocytes have been reported to be toxic to neurons through non-cell autonomous mechanisms, including a slower rate of glutamate (Glu) clearance and release of excessive Glu, as well as glial connexin (Maezawa et al., 2009; Maezawa and Jin, 2010). This latter finding proposes a viewpoint that RTT is not simply a disease of neurons alone, but a complex disease in which glial cells might play a vital role in the pathological process. Hence, we will attempt to summarize the progress of glial abnormalities involved in the pathogenesis of RTT in this review.

MeCP2 AND RTT

MeCP2 is one of the members of the methyl-CpG-binding domain protein (MBD) family, which is functionally involved in chromatin remodeling or transcriptional regulation. There are two crucial domains in MeCP2:, one is MBD and another is the transcriptional repression domain (TRD), which can recruit different protein partners, such as HDACs and Sin3A, to form a transcriptional repression complex and regulate target gene expression (Du et al., 2015) (**Figure 1**). The *MeECP2* gene consists of four exons (exon 1–4) and three introns (intron 1–3) and is located on the X chromosome. The transcriptional level of MeCP2 exon 1 (E1) is much higher than other exons in the brain, and mutations in MeCP2 E1 are sufficient to cause RTT (Fichou et al., 2009). Furthermore, the MeCP2 isoform has a time-specific expression pattern during brain development. MeCP2 E1 in the mouse hippocampus was detected as early as at E14, whereas MeCP2 E2 was detected at E18 (Olson et al., 2014). Generally, *MECP2* was believed to bind to methylated CpG islands; however, a recent study showed that MeCP2 can bind to non-CG methylated DNA and influence the transcription of disease-relevant genes in the adult mouse brain (Chen et al., 2015; Luo and Ecker, 2015) (**Figure 1**). Those results provide insight into the molecular mechanism of MECP2 in the delayed onset of RTT.

Generally, almost 95% of RTT patients carry mutations in the MeCP2 gene, and recent findings demonstrated that two additional genes, cyclin-dependent kinase like 5 (CDKL5) (Evans et al., 2005) and fork head box G1 (FOXG1), can also be involved in the pathogenesis of this syndrome (Mencarelli et al., 2010). Furthermore, CDKL5 has been shown to have the ability to promote the release of MeCP2 from DNA by phosphorylating MeCP2 (Mari et al., 2005; Bertani et al., 2006), while a direct functional relationship between these two molecules in RTT is controversial.

MeCP2 DEFICIENCY AND NEURONAL DYSFUNCTION

The function of MeCP2 in brain is multifarious, including modulation of neurogenesis, synaptic development and maintenance of neural circuits (Chahrour and Zoghbi, 2007; Banerjee et al., 2012; Lyst and Bird, 2015). It was demonstrated that MeCP2 is essential for neurogenesis in Xenopus embryos, and deficiency of MeCP2 resulted in a decreased number of neuronal precursors (Stancheva et al., 2003). *In vitro*, MeCP2 mutant mesenchymal stem cells presented impaired neural differentiation and increased the rate of senescence (Squillaro et al., 2012). MeCP2-deficient neurons have decreased numbers of axons and dendrites (Nguyen et al., 2012), and the neurite complexity was reduced in cultured MeCP2-null embryonic primary cortical neurons (Vacca et al., 2016), indicating that MeCP2 plays a crucial role in modulating neuronal differentiation and terminal maturation. Recent studies have revealed that MeCP2 is also involved in neuronal cell fate specification and migration (Feldman et al., 2016). It was found that neural progenitor cells (NPCs) lacking MeCP2 exhibited delayed corticogenesis with respect to abnormal migration of NPCs from the subventricular and ventricular zones into the cortical plate (Bedogni et al., 2016).

Some of the abnormal social behaviors of patients with RTT, such as anxiety and autistic features, are thought to be caused by MeCP2 deficiency in the neurons of certain special brain areas, including the forebrain, hypothalamus and basolateral amygdala (Armstrong et al., 1998; Gemelli et al., 2006; Fyffe et al., 2008; Chao et al., 2010; Williams et al., 2014). *MECP2* conditional knockout in glutamatergic neurons, but not in inhibitory neurons, leads to more serious RTT-like symptoms in mice (Meng et al., 2016). It has been shown that the balance between Glu excitatory synapses and GABAergic (gamma-amino butyric acid) inhibitory synapses is disrupted in RTT (Nelson and Valakh, 2015). MeCP2 knockdown reduces the excitatory synapse number and attenuates synaptic scale-up by reducing the expression of metabotropic glutamate receptor 2 (GluR2), and there is a major down-regulation of GABAergic inhibitory synapses in MeCP2 knockout mice (He et al., 2014; Kang et al., 2014). Thus, correcting the abnormal MeCP2 level by adding the gene back or over-expressing is a valid method to study the function of MeCP2 and treatment for RTT. For instance, dendritic abnormalities and behavioral changes can be ameliorated by reactivation of MeCP2 expression in MeCP2-null mice (Armstrong et al., 1998; Stearns et al., 2007; Robinson et al., 2012). Recently, MECP2 gene therapy by intracisternal injection of transgenic adeno-associated virus 9 (AAV9/hMECP2) has been shown to extend survival of MeCP2-deficient ($Mecp^{2-/y}$) mice without apparent toxicity (Matagne et al., 2017; Sinnett et al., 2017). Moreover, as RTT

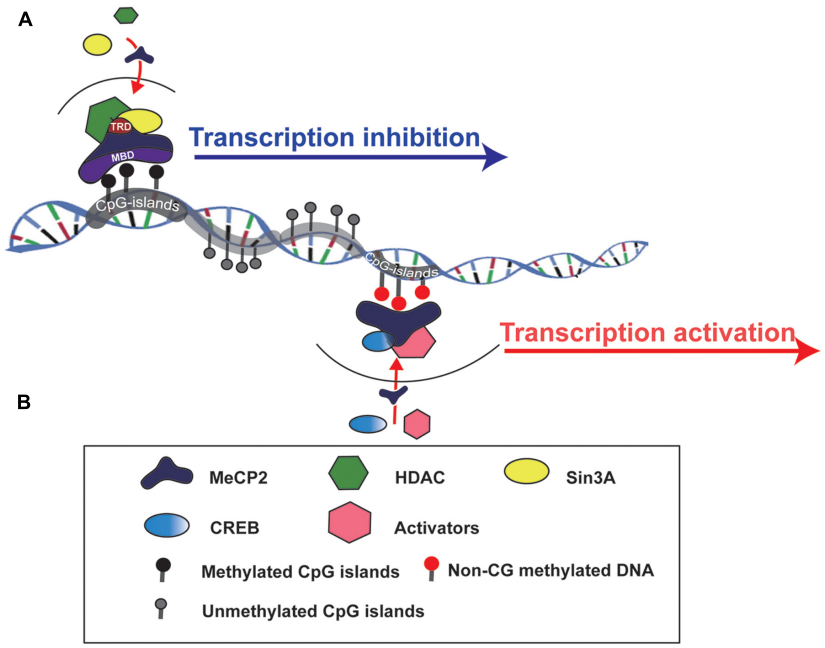

FIGURE 1 | Schematic to show how MeCP2 regulates target gene expression. **(A)** MeCP2 recruits a transcriptional corepressor complex containing Sin3A and histone deacetylase (HDAC) to methylated CpG islands and results in target gene transcription inhibition. TRD, transcriptional repression domain; MBD, methyl-CpG-binding domain. **(B)** MeCP2 is able to active gene transcription by recruiting CREB and other transcriptional factors to non-CG methylted DNA regions.

is always caused by heterozygous mutations in an X-linked gene and there exists a prevalent wild-type MeCP2 allele on the inactive X chromosome, reactivation of the inactive X chromosome-linked wild-type allele may represent another way to rescue MeCP2 deficiency. Recently, several trans-acting X-chromosome inactivation factors (XCIFs) have been identified and the inhibitor of two XCIFs (PDPK1, AURKA) has been demonstrated to exhibit reactive expression of the WT MeCP2 allele on the inactive X chromosome, which can be considered as a potential therapy for RTT (Bhatnagar et al., 2014).

In addition to RTT, evidence has shown that MeCP2 regulates the expression of its downstream genes, such as brain-derived neurotrophic factor (BDNF) (Chen et al., 2003) and ubiquitin-protein ligase E3A (UBE3a), the latter being involved in Angelman syndrome (Makedonski et al., 2005). In addition, MeCP2 also regulates the expression of distal-less homeobox 5/6 (Dlx5/6) genes, which are necessary for spinal skeletal development and are related to definite symptoms of RTT patients, such as scoliosis and microcephaly (Nakashima et al., 2010).

MeCP2 DEFICIENCY AND GLIAL CELL DYSFUNCTION

Glial cells are non-excitable cells that are functional support neurons and maintain the stability of neuronal structure and function. In the central nervous system (CNS), glial cells mainly include astrocytes, OLs and microglia. Previous studies have revealed that MeCP2 is present in a majority of neurons but is absent from glial cells (Shahbazian et al., 2002). However, increasing evidence suggests that the abnormality of MeCP2 also plays an important role in white matter damage and/or glial dysfunction in RTT (Ballas et al., 2009; Maezawa and Jin, 2010; Okabe et al., 2012; Durand et al., 2013; Nguyen et al., 2013). Mice with MeCP2 loss specifically in glial cells presented Rett-like symptoms due to neuronal toxicity via a non-cell autonomous mechanism, and the restoration of MeCP2 in glial cells can rescue some of these defects (Lioy et al., 2011; Nguyen et al., 2013; Cronk et al., 2015). Evidence from magnetic resonance spectroscopy (MRS) indicated an increased glia-to-neuron ratio in the white matter of RTT patients along with ongoing axonal damage and glial abnormalities (Khong et al., 2002). The contribution of MeCP2 deficiency to dysfunction of different types of glial cells varies in RTT pathogenesis.

MeCP2 IN ASTROCYTES

Astrocytes are the most abundant of all glial cell types and are well known for supporting neurons and maintaining brain function. Although the expression level of MeCP2 in astrocytes is lower, it is important for astrocyte differentiation and function. After *MECP2* was specifically knocked out in neural stem cells (NSCs), these NSCs tend to differentiate into more astrocytes (Andoh-Noda et al., 2015). While the growth rate of MeCP2-deficient astrocytes is significantly slower and more interleukin (IL)-1β and IL-6 are released in response to immune stimulation *in vitro*, no obvious morphological change was found in those cells (De Filippis et al., 2012). MeCP2-deficient astrocytes that were

differentiated from induced pluripotent stem cell (iPSC) lines from RTT patients have negative regulatory effects on neuronal morphology and function (Williams et al., 2014). Moreover, subsequent studies found that MeCP2-null astrocytes have certain abnormalities in target gene regulation and are toxic to neurons mainly due to abnormal Glu metabolism. Similarly, it was shown that a state of MeCP2 deficiency can spread in the brain of MeCP2$^{-/+}$ mice via a non-cell autonomous mechanism (Maezawa et al., 2009). This suggests that abnormal astrocytes are able to deteriorate the function of neurons, which speeds up the process of RTT. It was found that preferential re-expression of Mecp2 in astrocytes dramatically improved RTT symptoms and the lifetimes of MeCP2-deficient mice (Kifayathullah et al., 2010; Lioy et al., 2011; Zachariah et al., 2012).

Target Gene Dysregulation in MeCP2-Null Astrocytes

The expression of astroglial marker genes GFAP and S100β was significantly higher in MeCP2-null astrocytes than that in WT astrocytes (Forbes-Lorman et al., 2014). It was noted that *MECP2* small interference RNA (siRNA) increased the expression of GFAP in the female amygdala (Forbes-Lorman et al., 2014). These observations suggest that GFAP and S100β genes are suppressed by MeCP2. Although the mechanism by which MeCP2 regulates these two genes is unclear, evidence has shown that MeCP2 E1 can couple with the Sin3A/HDAC complex, which can bind to the GFAP promoter and regulate GFAP transcription. On embryonic day 11.5 (E11.5), the promoter of the GFAP gene is highly methylated, which may facilitate assembly of MeCP2-Sin3A/HDAC complexes and suppress GFAP gene transcription. On E14, the promoter of the GFAP gene is demethylated, which may lead to the disintegration of this complex and results in GFAP gene expression. In the early stages of astrocyte differentiation, MeCP2 also has a vital effect by binding to the promoter of the S100β gene, while this binding is gradually reduced in the later stages, as demethylation of a specific CpG site occurs (Cheng et al., 2011; Forbes-Lorman et al., 2014).

In addition to astroglial marker genes, many other target genes such as solute carrier family member 38, member 1 (Slc38a1), neuronal regeneration-related protein (Nrep), and nuclear receptor subfamily 2, group F, member 2 (Nr2f2) are also regulated by MeCP2. Slc38a1 is a rate-limiting transporter of glutamine (Gln) across the plasma membrane, Nrep is a transcriptional factor that is involved in glial mobility and neoplasia, and Nr2f2 is a transcription factor that is necessary for glial differentiation from NSCs (Mackenzie and Erickson, 2004; Yasui et al., 2013; Delepine et al., 2015). In addition, Nr2f2 can regulate some target genes including those encoding chromogranin B (Chgb), chemokine (C-C motif) ligand 2 (CCL2), and lipocalin 2 (LCN2). Chgb is a highly efficient system that is directly involved in monoamine accumulation. In MeCP2-deficient mice, the expression of Nr2f2 is up-regulated, which may down-regulate Chgb and cause excess monoamine accumulation in the extracellular fluid and impair neurons. This finding suggests that influence of MeCP2 deficiency can be aggravated through a downstream target gene cascade in astrocytes (Kloukina-Pantazidou et al., 2013; Delepine et al., 2015). Interestingly, in response to LPS stimulation, MeCP2-deficient astrocytes released fewer cytokines such as IL-1β and IL-6 (Maezawa et al., 2009).

Microtubule Instability in MeCP2-Null Astrocytes

Cellular morphology, division, migration and intracellular transportation of vesicles are controlled by microtubules (MTs), which assemble from α- and β-tubulin dimers. The acetylation modification of tubulin is deemed to be a characteristic of stable MTs (Palazzo et al., 2003). In *Mecp2*$^{308/y}$ and *Mecp2* p. Arg294* iPSC-derived astrocytes, the level of acetylated tubulin is reduced, and histone deacetylase 6 (HDAC6) is overexpressed (Delepine et al., 2016). A similar result was also reported in MeCP2-deficient fibroblasts and MeCP2-null neurons (Gold et al., 2015). MT growth speed of Mecp2$^{308/y}$ astrocytes was higher, and MT polymerization was significantly increased. Moreover, MT-dependent lysosome vesicle mobility was obviously increased in both *Mecp2*$^{308/y}$ and *Mecp2* p.Arg294* iPSC-derived astrocytes; however, the percentage of highly directional vesicles was reduced (Delepine et al., 2016). A special type of directional vesicle cellular transport can regulate Glu uptake, which suggests an abnormal Glu uptake rate may be associated with MT-dependent vesicle mobility in RTT (Li et al., 2015). The aforementioned phenomenon was related to the decreased expression of stathmin 2 (STMN2), which could inhibit MT polymerization (Nectoux et al., 2012). Moreover, expression of TUBA1B, which encodes the ubiquitous α-tubulin, is down-regulated in brain tissue of patients with RTT (Abuhatzira et al., 2009). These findings suggest a role of MeCP2 as an activator for MT-associated genes. Molecularly, a recent study revealed a potential mechanism by which sumoylated MeCP2 releases CREB from the repressor complex and increases the transcription of CREB-regulated genes such as BDNF (Tai et al., 2016). Interestingly, sumoylation of MeCP2 was found to be decreased in RTT, and further study is warranted to examine the sumoylation status of MeCP2 in glial cells of RTT. In addition, epothilone D, a brain-penetrating MT-stabilizing natural product, can rescue MT growth velocity, and epothilone D corrects the abnormal behavioral symptoms of *Mecp2*$^{308/y}$ mice (Delepine et al., 2016). Treatment via targeting MTs seems to be a new approach for RTT therapy. Notably, when co-cultured with MeCP2-deficient fibroblasts, MT stability of WT human fibroblasts is reduced (Delepine et al., 2013). All of this evidence suggests that MT impairment seems to be a common phenomenon of MeCP2 deficiency.

Abnormal Glutamate Metabolism in MeCP2-Deficient Astrocytes

Glutamate is an important signaling molecule in the CNS. At a high extracellular concentration, it is a potent cytotoxin that

can induce both neuronal and glial death through excitotoxicity or oxidative stress. Extracellular glutamate concentration is maintained at an appropriate level predominantly by active transport mediated by excitatory amino acid transporters (EAATs) of astrocytes (Lehmann et al., 2009). Normally, when astrocytes are incubated with high levels of extracellular Glu, EAAT1/EAAT2 expression is rapidly decreased. However, when the down-regulation of EAAT1/2 was impaired, EAAT1/EAAT2 expression had no obvious changes in MeCP2-null astrocytes (Okabe et al., 2012). Regarding the underlying mechanism, it was found that HDAC I and II served as repressors for EAAT2 promoter activity (Karki et al., 2014), thus, MeCP2 deficiency may fail to recruit HDACs to inhibit EAAT gene expression upon environment stimulation. Notably, the Glu clearance rate of MeCP2-null astrocytes was lower than that of WT astrocytes *in vitro* (Okabe et al., 2012). Moreover, the glutamine synthetase (GS) protein was significantly higher in MeCP2-null astrocytes than that in WT astrocytes (Okabe et al., 2012). All of this evidence seems to support the concept that both Glu clearance and production are abnormal in MeCP2-deficient astrocytes, and that these abnormalities may contribute to the pathological process of RTT (**Figure 2**).

Spread of MeCP2 Deficiency in Astrocytes

An interesting phenomenon is that MeCP2 expression in *Mecp2*$^{-/+}$ mice is much lower at 7 months than that at 1 month, when proliferation rates of astrocytes are higher. *In vitro*, MeCP2 expression was significantly decreased in WT astrocytes that were co-cultured with MeCP2-deficient astrocytes for a long period, indicating that MeCP2 deficiency can spread among astrocytes progressively and eventually lead to a dysfunctional brain (Maezawa et al., 2009). Recent studies have shown that MeCP2 deficiency can spread among astrocytes via connexin, especially connexin 43 (Cx43)-mediated gap junction. When Cx43 was knocked down with siRNA, the spread of MeCP2 deficiency was significantly reduced (Maezawa et al., 2009). This finding suggests that astroglial Cx may be a new target for preventing the phenotype of RTT.

Abnormal Astrocytes May Be the Main Contributor to the Disordered Breathing Pattern

RTT symptoms always include a severely disordered breathing pattern and reduced CO_2 sensitivity. In the respiratory control center, highly chemosensitive astrocytes can respond to the physiological decrease in pH with a vigorous increase in intracellular Ca^{2+} and release of ATP (Gourine et al., 2010). MeCP2 deficiency in astrocytes induced an obvious depression of the ventilatory responses to an increased level of CO_2, which is similar to global MeCP2-null mice (Zhang et al., 2011). Additionally, although neurons constitute the respiratory control network and determine the ventilatory response to CO_2, MeCP2 mutation selectively in neurons leads to an absolute lower depression of the CO_2 response than MeCP2 loss in astrocytes (Fyffe et al., 2008; Garg et al., 2015).

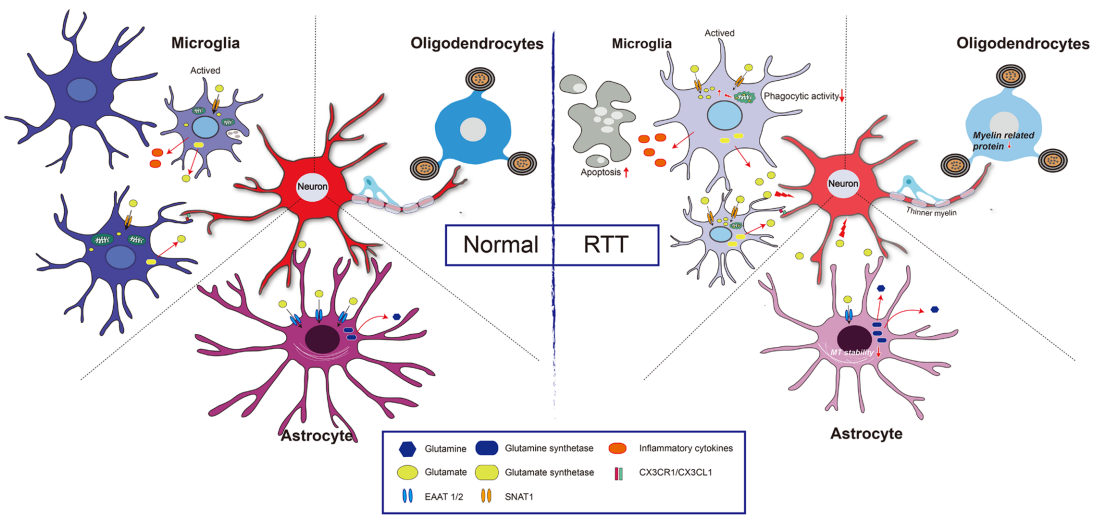

FIGURE 2 | Glia and neuron interaction under pathologic condition of RTT. Normal: Extracellular glutamate (Glu) can be uptake by excitatory amino acid transporter 1 and 2 (EAAT1/2) in astrocyte and sodium-coupled neutral amino acid transporter 1 (SNAT1) in microglial cell, and is utilized by glutamine synthetase to reduce its toxicity to neuron. Both astrocytes and microglia can be active upon stimulation, and the active microglia has capacity of phagocytosis. Furthermore, CX3CR1 (a chemokine receptor in microglial cell) and its neuronal ligand CX3CL1 mediates neuron-microglia interaction. Myelinating oligodendrocyte is important to maintain axonal integrity. RTT: MeCP2 deficiency in astrocytes leads to a decreased expression of EAAT1/2, and increased expression of glutamine synthetase, which results in a high concentration of extracellular Glu, and thus impairs neuronal activity. Additionally, those astrocytes present decreases microtubule stability. In microglia, MeCP2 deficiency results in decreased phagocytic activity and overloads of Glu due to upregulation of SNAT1. The MeCP2-deficient in oligodendrocyte results in thinner myelin due to down-regulation of myelin-related genes.

After re-expression of MeCP2 in astrocytes, the respiratory phenotype is rescued (Garg et al., 2015), suggesting that the disordered breathing pattern may be caused by abnormal astrocytes in RTT patients. However, recent evidence suggests that RTT-like breathing abnormality was only developed in 20% of *Mecp2*$^{+/-}$ mice (Johnson et al., 2015). Imaging of calcium signaling in ventral medullary astrocytes reveals that these phenomena may be related to a reduction in the ability of MeCP2-deficient astrocytes to sense $P_{CO2}/[H^+]$ and that the CO_2-induced $[Ca^{2+}]_i$ response is impaired. Additionally, the ATP response of MeCP2-deficient astrocytes is not affected. Normally, ATP propagates astrocytic Ca^{2+} excitation, depolarizes chemoreceptor neurons, and induces adaptive increases in breathing. This evidence suggests that the most apparent deficiency of the MeCP2-null astrocyte is the ability to sense physiological increases in CO_2, while the downstream signaling pathway can still be activated by ATP (Bissonnette and Knopp, 2008; Zhang et al., 2011; Turovsky et al., 2015).

MeCP2 IN MICROGLIA

Mecp2 Regulates Microglial Activation

Microglia are considered to be resident myeloid-derived cells distributed throughout the brain and account for over 10% of CNS cells (Kawabori and Yenari, 2015). Microglial activation can occur in response to stimuli such as glucocorticoids, hypoxia, and inflammation (Kiernan et al., 2016). In Mecp2-null mice, microglial cells are relatively small but become larger in response to environmental stimuli compared to those of wild-type mice, and these microglial cells are lost with disease progression. Moreover, the expression of glucocorticoid-induced transcriptional signature genes and a subset of hypoxia-inducible genes were up-regulated in Mecp2-deficient microglia, suggesting the regulatory role of MeCP2 in microglia activation (Cronk et al., 2015) (**Figure 2**). From another point of view, a gene array study confirmed that the function of differentially expressed genes, as MeCP2 deficiency is strongly related to regulating the activation states of microglia (Zhao et al., 2017). In addition, studies have shown that bone marrow transplantation increases the number of microglia in the brain (Derecki et al., 2012). MeCP2-null mice that were transplanted with WT bone marrow partly restored behavior and functional abnormalities (Derecki et al., 2012). However, another study reached the opposite conclusion that WT marrow transplantation did not positively influence MeCP2-null mice (Wang et al., 2015). The beneficial effect declined when the phagocytic activity of these transplanted cells was inhibited and the ability to clear apoptotic targets was reduced. This result indicated that the phagocytic activity of microglia is impaired in MeCP2-null microglia and that a non-cell autonomous mechanism is involved in spreading the MeCP2-deficient state (Maezawa and Jin, 2010). In contrast to microglia, the MeCP2 knockout of myeloid-derived cells led to the release of more tumor necrosis factor-α (TNF-α) and inflammatory cytokines, such as IL-6, TNF-α, and IL-3 (O'Driscoll et al., 2015).

Mutant MECP2 in Microglia Impairs the Neuronal Circuit

In the developing CNS, microglia have been demonstrated to play an important role in shaping neuronal circuit structure by microglia-synapse interactions or removing excess synapses, and an etiology of disrupted synaptic function can be detected in mouse models of RTT (Johnston et al., 2001; Noutel et al., 2011). Recent research offered a new viewpoint of the effect of MECP2-defective microglia on the neuronal circuit. It was reported that in MECP2-null mice, microglia contribute to RTT pathogenesis by excessively engulfing and thereby eliminating, which is concomitant with synaptic loss at the end stages of the disease (Schafer et al., 2016). Intriguingly, gain or loss of Mecp2 expression specifically in microglia cannot induce the abovementioned phenomena (Schafer et al., 2016), indicating that abnormalities in microglia may accelerate the pathological process by impairing the neuronal circuit as a secondary effect, not the primary cause, of RTT. In addition, the result of another research study also implicitly demonstrated this point that restoring the expression of Mecp2 in myeloid cells by bone marrow transplantation made no sense in the Mecp2-null mouse (Wang et al., 2015).

A recent study showed that ablating CX3CR1, a chemokine receptor of microglia mediating neuron–microglia interaction by pairing with its neuronal ligand CX3CL1, can rescue the negative effect of *MeCP2*-deficient microglia on neurons. After blocking the interaction, the survival of MECP2-null mice was remarkably improved and behavioral abnormalities were partly restored. These results indicated that blocking intercellular interaction in brains of RTT patients might be a novel therapeutic approach for RTT (Horiuchi et al., 2016).

MeCP2-Deficient Microglia Leads to Neurotoxicity

Activation of glutamate receptors and the expression level of Glu transporters are important for maintaining the plasticity of glutamatergic synapses (Groc et al., 2006; Yuan and Bellone, 2013). MeCP2-deficient microglia released a fivefold higher level of Glu, which was associated with neurotoxic or synaptotoxic activity, as the neuronal abnormality can be partially restored by blocking the NMDA receptor (Maezawa and Jin, 2010). In addition, normal neurons co-cultured with MeCP2 mutant microglia exhibited functional and morphological disorder such as thinner and shorter dendrites and a reduced number of excitatory synapses, because the microtubule was disrupted by a decrease in MAP2 and acetylated tubulin (Maezawa and Jin, 2010; Cronk et al., 2015; Jin et al., 2015). Moreover, the level of the connexin channel protein Cx32, which can release Glu, was significantly up-regulated in MeCP2-null microglia, and the blockade of Cx32 can partially ameliorate the excessive release of Glu (Maezawa and Jin, 2010).

From the perspective of bioenergetics, MeCP2 loss in microglia led to mitochondrial dysfunction by impairing Glu homeostasis (Jin et al., 2015). In MeCP2-deficient microglia, the overexpression of the Glu transporter sodium-coupled neutral amino acid transporter 1 (SNAT1) promoted microglial uptake

TABLE 1 | A summary of the abnormal features in glial cells induced by MeCP2 abnormalities.

MECP2 abnormalities	Features			PMID
	Astrocyte	Oligodendrocyte	Microglia	
Mecp2 *tm1.1Bird*	Slower growth rate, reduced cytokine release			19386901
	Increased MT growth velocity, decreased MT stability			23351786
	Decreased CO_2 sensitivity			PMC4532534
	Increased glutamate production			22532851
		Down-regulation of SNAT1, glutamate overproduction, less ATP production		25673846
		Up-regulation of glucocorticoid-induced transcription and hypoxia-inducible gene expression		25902482
		Be activated but subsequently depleted with disease progression		25902482
			Toxic to neurons by increasing glutamate production and release, up-regulation of Cx32 expression	20392956
$Mecp2^{308/y}$	Atrophy			22157810
	Down-regulation of Nr2f2 expression			26208914
	Down-regulation of Stathmin expression, increased MT growth velocity, decreased MT stability			22252744, 26604147
		Up-regulation of MAG expression in corpus callosum, down-regulation of PLP expression in cerebellum		20697302
		Down-regulation of CNP expression in subcortical white matter and hippocampus		22334035
Mecp2p.Arg294*	Increased MT growth velocity, decreased MT stability and vesicular transport			26604147
$Mecp2^{loxJ/y}$/NG2Cre		Down-regulation of PLP and MBP expression		24285883
		Thinner myelin sheet		
			More active and developed severe hind limb clasping phenotypes	
Mecp2 siRNA	Up-regulation of GFAP, S100β and BDNF expression			24269336, 19386901
		Up-regulation of MBP, PLP, MOG and MOBP expression		26140854

of Glu; the excessive Glu was translated into the mitochondria, coupled with the rising mitochondrial reactive oxygen and damaged the mitochondria (Jin et al., 2015). As a consequence, adenosine triphosphate (ATP) production is significantly reduced in MeCP2-deficient microglia, and this ATP reduction leads to a greater potential for the apoptosis of abnormal microglia (Jin et al., 2015) (**Figure 2**).

MeCP2 IN OLIGODENDROGLIA

Oligodendrocytes are the myelinating cells in the brain that maintain nerve impulse conduction and provide nutrition for axons (recently reviewed in Bergles and Richardson, 2016). There are several markers that distinguish the oligodendroglial cells at different stages. OL progenitor cells (OPCs) are positive for platelet-derived growth factor receptor α (PDGFR-α) or neural antigen 2 (NG2); immature OLs are O4-positive, and mature OLs express myelin-associated glycoprotein (MAG), proteolipid protein (PLP), CNP and myelin basic protein (MBP) (He and Lu, 2013).

Some studies have found the expression of MeCP2 in oligodendroglial lineage cells (KhorshidAhmad et al., 2016), which may be associated with oxidative damage of white matter that occurred in the early stages of RTT (Durand et al., 2013). In MeCP2-null mice, although the OL morphology is unchanged, the expression of myelin-related genes is partially changed in some specific regions. For example, in the frontal cortex of MeCP2-null mice, no changes in global expression levels of the MBP, MAG and PLP were found, but MAG expression was significantly increased in the corpus callosum, while PLP expression was significantly decreased in the cerebellum (Vora et al., 2010). Furthermore, in *Mecp2*$^{308/y}$-mutant mice, GFAP, Cx43, Cx45, Cx40 and Cx32 were unchanged, but the CNP expression level was decreased (Wu et al., 2012). Additionally, cultured OLs with MeCP2 knocked down exhibited an increase in myelin genes, including MBP, PLP, myelin oligodendrocyte glycoprotein (MOG), myelin-associated oligodendrocyte basic protein (MOBP) and Ying Yang 1 (YY1) (KhorshidAhmad et al., 2016), indicating MeCP2 is a negative regulator for myelin protein expression (Sharma et al., 2015). As a co-repressor of MeCP2, HDACs have also been found to be functionally involved in oligodendroglial development (Huang et al., 2015). Moreover, when MeCP2 was specifically knocked out in NG2^{+} OPCs, the mice displayed more active behaviors, with severe hind limb-clasping phenotypes (Nguyen et al., 2013). The PLP and MBP expression levels were lower in those mice, and thinner myelin was present. After restoring the expression of MeCP2 in the OPCs, the ethological abnormality was significantly corrected in both female and male mice (Nguyen et al., 2013) (**Figure 2**). It is noteworthy that MeCP2 re-expression in OPCs, compared with that in astrocytes or microglia cells, shows more potent ability to prolong the lifespan of MeCP2$^{stop/y}$ mice (Nguyen et al., 2013). However, the expression of myelin protein (MBP) was mildly or not rescued (CNP, MOG, or PLP) after re-expression of MeCP2 in oligodendrocytes in otherwise MeCP2-null mice, suggesting that a likely non-cell autonomous mechanism regulated the expression of OL-related genes (Nguyen et al., 2013). This mechanism is maybe related to the excessive Glu released by other glial cell types, such as astrocytes or microglia, because

excessive Glu might partly restore the development of OLs through activating *n*-methyl-D-aspartic acid (NMDA) receptors in MeCP2-null brains (Lundgaard et al., 2013). In addition, white matter damage in RTT patients has been related to impaired nuclear factor kappa-B (NF-κB) signaling: there were additional copies of the inhibitor of the kappa light polypeptide gene, kinase gamma (IKBKG) enhancer in B-cells of patients with Xq28 duplications, and three of the five presented white matter anomalies in brain MRI (Philippe et al., 2013).

PERSPECTIVES

In this review, we summarized glial abnormalities induced by MeCP2 deficiency and how these cells are toxic to neurons and disturb the neural circuit (**Table 1**). The mice with MeCP2-null specifically in glial cells showed behavioral and neural synaptic abnormalities that are similar to those in MeCP2-null mice, and re-expression of MeCP2 in glial cells can restore those abnormalities and prolong the life span of MeCP2-null mice. Additionally, we discussed the role of MeCP2 in glial cells to gain a better understanding of the pathology process of RTT and ultimately a new glial-target strategy for RTT treatment. For instance, Glu metabolism abnormalities may be a predominant component of the RTT pathology process, especially in glial cells. Some drugs such as riluzole, a glutamatergic modulator that has been approved for treating amyotrophic lateral sclerosis (ALS) by primarily rectifying extensive Glu levels, may also be utilized to treat RTT. Moreover, the regulatory mechanism of MeCP2 in the oligodendroglial development involved in RTT pathogenesis is understudied.

AUTHOR CONTRIBUTIONS

X-RJ and X-SC wrote the manuscript, LX designed and revised the manuscript.

ACKNOWLEDGMENTS

This work was supported by grants from the National Natural Science Foundation of China (31100771), Natural Science Foundation Project of CQ CSTC (2016jcyjA0600, CSTCKJCXLJRC07), and Postdoctoral Foundation of CQ CSTC (2011018).

REFERENCES

Abuhatzira, L., Shemer, R., and Razin, A. (2009). MeCP2 involvement in the regulation of neuronal alpha-tubulin production. *Hum. Mol. Genet.* 18, 1415–1423. doi: 10.1093/hmg/ddp048

Andoh-Noda, T., Akamatsu, W., Miyake, K., Matsumoto, T., Yamaguchi, R., Sanosaka, T., et al. (2015). Differentiation of multipotent neural stem cells derived from Rett syndrome patients is biased toward the astrocytic lineage. *Mol. Brain* 8:31. doi: 10.1186/s13041-015-0121-2

Armstrong, D. D., Dunn, K., and Antalffy, B. (1998). Decreased dendritic branching in frontal, motor and limbic cortex in Rett syndrome compared with trisomy 21. *J. Neuropathol. Exp. Neurol.* 57, 1013–1017. doi: 10.1097/00005072-199811000-00003

Ballas, N., Lioy, D. T., Grunseich, C., and Mandel, G. (2009). Non-cell autonomous influence of MeCP2-deficient glia on neuronal dendritic morphology. *Nat. Neurosci.* 12, 311–317. doi: 10.1038/nn.2275

Banerjee, A., Castro, J., and Sur, M. (2012). Rett syndrome: genes, synapses, circuits, and therapeutics. *Front. Psychiatry* 3:34. doi: 10.3389/fpsyt.2012.00034

Bedogni, F., Cobolli Gigli, C., Pozzi, D., Rossi, R. L., Scaramuzza, L., Rossetti, G., et al. (2016). Defects during Mecp2 null embryonic cortex development precede the onset of overt neurological symptoms. *Cereb. Cortex* 26, 2517–2529. doi: 10.1093/cercor/bhv078

Bergles, D. E., and Richardson, W. D. (2016). Oligodendrocyte development and plasticity. *Cold Spring Harb. Perspect. Biol.* 8:a020453. doi: 10.1101/cshperspect.a020453

Bertani, I., Rusconi, L., Bolognese, F., Forlani, G., Conca, B., De Monte, L., et al. (2006). Functional consequences of mutations in CDKL5, an X-linked gene involved in infantile spasms and mental retardation. *J. Biol. Chem.* 281, 32048–32056. doi: 10.1074/jbc.M606325200

Bhatnagar, S., Zhu, X., Ou, J., Lin, L., Chamberlain, L., Zhu, L. J., et al. (2014). Genetic and pharmacological reactivation of the mammalian inactive X chromosome. *Proc. Natl. Acad. Sci. U.S.A.* 111, 12591–12598. doi: 10.1073/pnas.1413620111

Bienvenu, T., Carrie, A., De Roux, N., Vinet, M. C., Jonveaux, P., Couvert, P., et al. (2000). MECP2 mutations account for most cases of typical forms of Rett syndrome. *Hum. Mol. Genet.* 9, 1377–1384. doi: 10.1093/hmg/9.9.1377

Bissonnette, J. M., and Knopp, S. J. (2008). Effect of inspired oxygen on periodic breathing in methy-CpG-binding protein 2 (Mecp2) deficient mice. *J. Appl. Physiol.* 104, 198–204. doi: 10.1152/japplphysiol.00843.2007

Chahrour, M., and Zoghbi, H. Y. (2007). The story of Rett syndrome: from clinic to neurobiology. *Neuron* 56, 422–437. doi: 10.1016/j.neuron.2007.10.001

Chao, H. T., Chen, H., Samaco, R. C., Xue, M., Chahrour, M., Yoo, J., et al. (2010). Dysfunction in GABA signalling mediates autism-like stereotypies and Rett syndrome phenotypes. *Nature* 468, 263–269. doi: 10.1038/nature09582

Chao, H. T., Zoghbi, H. Y., and Rosenmund, C. (2007). MeCP2 controls excitatory synaptic strength by regulating glutamatergic synapse number. *Neuron* 56, 58–65. doi: 10.1016/j.neuron.2007.08.018

Chen, L., Chen, K., Lavery, L. A., Baker, S. A., Shaw, C. A., Li, W., et al. (2015). MeCP2 binds to non-CG methylated DNA as neurons mature, influencing transcription and the timing of onset for Rett syndrome. *Proc. Natl. Acad. Sci. U.S.A.* 112, 5509–5514. doi: 10.1073/pnas.1505909112

Chen, W. G., Chang, Q., Lin, Y., Meissner, A., West, A. E., Griffith, E. C., et al. (2003). Derepression of BDNF transcription involves calcium-dependent phosphorylation of MeCP2. *Science* 302, 885–889. doi: 10.1126/science.1086446

Cheng, P. Y., Lin, Y. P., Chen, Y. L., Lee, Y. C., Tai, C. C., Wang, Y. T., et al. (2011). Interplay between SIN3A and STAT3 mediates chromatin conformational changes and GFAP expression during cellular differentiation. *PLOS ONE* 6:e22018. doi: 10.1371/journal.pone.0022018

Cronk, J. C., Derecki, N. C., Ji, E., Xu, Y., Lampano, A. E., Smirnov, I., et al. (2015). Methyl-CpG binding protein 2 regulates microglia and macrophage gene expression in response to inflammatory stimuli. *Immunity* 42, 679–691. doi: 10.1016/j.immuni.2015.03.013

De Filippis, B., Fabbri, A., Simone, D., Canese, R., Ricceri, L., Malchiodi-Albedi, F., et al. (2012). Modulation of RhoGTPases improves the behavioral phenotype and reverses astrocytic deficits in a mouse model of Rett syndrome. *Neuropsychopharmacology* 37, 1152–1163. doi: 10.1038/npp.2011.301

Delepine, C., Meziane, H., Nectoux, J., Opitz, M., Smith, A. B., Ballatore, C., et al. (2016). Altered microtubule dynamics and vesicular transport in mouse and human MeCP2-deficient astrocytes. *Hum. Mol. Genet.* 25, 146–157. doi: 10.1093/hmg/ddv464

Delepine, C., Nectoux, J., Bahi-Buisson, N., Chelly, J., and Bienvenu, T. (2013). MeCP2 deficiency is associated with impaired microtubule stability. *FEBS Lett.* 587, 245–253. doi: 10.1016/j.febslet.2012.11.033

Delepine, C., Nectoux, J., Letourneur, F., Baud, V., Chelly, J., Billuart, P., et al. (2015). Astrocyte transcriptome from the Mecp2(308)-truncated mouse model of rett syndrome. *Neuromol. Med.* 17, 353–363. doi: 10.1007/s12017-015-8363-9

Derecki, N. C., Cronk, J. C., Lu, Z., Xu, E., Abbott, S. B., Guyenet, P. G., et al. (2012). Wild-type microglia arrest pathology in a mouse model of Rett syndrome. *Nature* 484, 105–109. doi: 10.1038/nature10907

Du, Q., Luu, P. L., Stirzaker, C., and Clark, S. J. (2015). Methyl-CpG-binding domain proteins: readers of the epigenome. *Epigenomics* 7, 1051–1073. doi: 10.2217/epi.15.39

Durand, T., De Felice, C., Signorini, C., Oger, C., Bultel-Ponce, V., Guy, A., et al. (2013). F(2)-Dihomo-isoprostanes and brain white matter damage in stage 1 Rett syndrome. *Biochimie* 95, 86–90. doi: 10.1016/j.biochi.2012.09.017

Evans, J. C., Archer, H. L., Colley, J. P., Ravn, K., Nielsen, J. B., Kerr, A., et al. (2005). Early onset seizures and Rett-like features associated with mutations in CDKL5. *Eur. J. Hum. Genet.* 13, 1113–1120. doi: 10.1038/sj.ejhg.5201451

Feldman, D., Banerjee, A., and Sur, M. (2016). Developmental dynamics of Rett syndrome. *Neural Plast.* 2016:6154080. doi: 10.1155/2016/6154080

Fichou, Y., Nectoux, J., Bahi-Buisson, N., Rosas-Vargas, H., Girard, B., Chelly, J., et al. (2009). The first missense mutation causing Rett syndrome specifically affecting the MeCP2_e1 isoform. *Neurogenetics* 10, 127–133. doi: 10.1007/s10048-008-0161-1

Forbes-Lorman, R. M., Kurian, J. R., and Auger, A. P. (2014). MeCP2 regulates GFAP expression within the developing brain. *Brain Res.* 1543, 151–158. doi: 10.1016/j.brainres.2013.11.011

Fyffe, S. L., Neul, J. L., Samaco, R. C., Chao, H. T., Ben-Shachar, S., Moretti, P., et al. (2008). Deletion of Mecp2 in Sim1-expressing neurons reveals a critical role for MeCP2 in feeding behavior, aggression, and the response to stress. *Neuron* 59, 947–958. doi: 10.1016/j.neuron.2008.07.030

Garg, S. K., Lioy, D. T., Knopp, S. J., and Bissonnette, J. M. (2015). Conditional depletion of methyl-CpG-binding protein 2 in astrocytes depresses the hypercapnic ventilatory response in mice. *J. Appl. Physiol.* 119, 670–676. doi: 10.1152/japplphysiol.00411.2015

Gemelli, T., Berton, O., Nelson, E. D., Perrotti, L. I., Jaenisch, R., and Monteggia, L. M. (2006). Postnatal loss of methyl-CpG binding protein 2 in the forebrain is sufficient to mediate behavioral aspects of Rett syndrome in mice. *Biol. Psychiatry* 59, 468–476. doi: 10.1016/j.biopsych.2005.07.025

Gold, W. A., Lacina, T. A., Cantrill, L. C., and Christodoulou, J. (2015). MeCP2 deficiency is associated with reduced levels of tubulin acetylation and can be restored using HDAC6 inhibitors. *J. Mol. Med.* 93, 63–72. doi: 10.1007/s00109-014-1202-x

Gourine, A. V., Kasymov, V., Marina, N., Tang, F., Figueiredo, M. F., Lane, S., et al. (2010). Astrocytes control breathing through pH-dependent release of ATP. *Science* 329, 571–575. doi: 10.1126/science.1190721

Groc, L., Gustafsson, B., and Hanse, E. (2006). AMPA signalling in nascent glutamatergic synapses: there and not there! *Trends Neurosci.* 29, 132–139. doi: 10.1016/j.tins.2006.01.005

He, L., and Lu, Q. R. (2013). Coordinated control of oligodendrocyte development by extrinsic and intrinsic signaling cues. *Neurosci. Bull.* 29, 129–143. doi: 10.1007/s12264-013-1318-y

He, L. J., Liu, N., Cheng, T. L., Chen, X. J., Li, Y. D., Shu, Y. S., et al. (2014). Conditional deletion of Mecp2 in parvalbumin-expressing GABAergic cells results in the absence of critical period plasticity. *Nat. Commun.* 5:5036. doi: 10.1038/ncomms6036

Horiuchi, M., Smith, L., Maezawa, I., and Jin, L. W. (2016). CX3CR1 ablation ameliorates motor and respiratory dysfunctions and improves survival of a Rett syndrome mouse model. *Brain Behav. Immun.* 60, 106–116. doi: 10.1016/j.bbi.2016.02.014

Huang, N., Niu, J., Feng, Y., and Xiao, L. (2015). Oligodendroglial development: new roles for chromatin accessibility. *Neuroscientist* 21, 579–588. doi: 10.1177/1073858414565467

Jin, L. W., Horiuchi, M., Wulff, H., Liu, X. B., Cortopassi, G. A., Erickson, J. D., et al. (2015). Dysregulation of glutamine transporter SNAT1 in Rett syndrome microglia: a mechanism for mitochondrial dysfunction and neurotoxicity. *J. Neurosci.* 35, 2516–2529. doi: 10.1523/JNEUROSCI.2778-14.2015

Johnson, C. M., Cui, N., Zhong, W., Oginsky, M. F., and Jiang, C. (2015). Breathing abnormalities in a female mouse model of Rett syndrome. *J. Physiol. Sci.* 65, 451–459. doi: 10.1007/s12576-015-0384-5

Johnston, M. V., Jeon, O. H., Pevsner, J., Blue, M. E., and Naidu, S. (2001). Neurobiology of Rett syndrome: a genetic disorder of synapse development. *Brain Dev.* 23(Suppl. 1), S206–S213. doi: 10.1016/S0387-7604(01)00351-5

Kang, S. K., Kim, S. T., Johnston, M. V., and Kadam, S. D. (2014). Temporal- and location-specific alterations of the GABA recycling system in Mecp2 KO mouse brains. *J. Cent. Nerv. Syst. Dis.* 6, 21–28. doi: 10.4137/JCNSD.S14012

Karki, P., Webb, A., Smith, K., Johnson, J Jr, Lee, K., Son, D. S., et al. (2014). Yin Yang 1 is a repressor of glutamate transporter EAAT2, and it mediates manganese-induced decrease of EAAT2 expression in astrocytes. *Mol. Cell. Biol.* 34, 1280–1289. doi: 10.1128/MCB.01176-13

Kawabori, M., and Yenari, M. A. (2015). The role of the microglia in acute CNS injury. *Metab. Brain Dis.* 30, 381–392. doi: 10.1007/s11011-014-9531-6

Khong, P. L., Lam, C. W., Ooi, C. G., Ko, C. H., and Wong, V. C. (2002). Magnetic resonance spectroscopy and analysis of MECP2 in Rett syndrome. *Pediatr. Neurol.* 26, 205–209. doi: 10.1016/S0887-8994(01)00385-X

KhorshidAhmad, T., Acosta, C., Cortes, C., Lakowski, T. M., Gangadaran, S., and Namaka, M. (2016). Transcriptional regulation of brain-derived neurotrophic factor (BDNF) by methyl CpG binding protein 2 (MeCP2): a novel mechanism for re-myelination and/or myelin repair involved in the treatment of multiple sclerosis (MS). *Mol. Neurobiol.* 53, 1092–1107. doi: 10.1007/s12035-014-9074-1

Kiernan, E. A., Smith, S. M., Mitchell, G. S., and Watters, J. J. (2016). Mechanisms of microglial activation in models of inflammation and hypoxia: implications for chronic intermittent hypoxia. *J. Physiol.* 594, 1563–1577. doi: 10.1113/JP271502

Kifayathullah, L. A., Arunachalam, J. P., Bodda, C., Agbemenyah, H. Y., Laccone, F. A., and Mannan, A. U. (2010). MeCP2 mutant protein is expressed in astrocytes as well as in neurons and localizes in the nucleus. *Cytogenet. Genome. Res.* 129, 290–297. doi: 10.1159/000315906

Kloukina-Pantazidou, I., Chrysanthou-Piterou, M., Havaki, S., and Issidorides, M. R. (2013). Chromogranin A and vesicular monoamine transporter 2 immunolocalization in protein bodies of human locus coeruleus neurons. *Ultrastruct. Pathol.* 37, 102–109. doi: 10.3109/01913123.2012.750410

Lehmann, C., Bette, S., and Engele, J. (2009). High extracellular glutamate modulates expression of glutamate transporters and glutamine synthetase in cultured astrocytes. *Brain Res.* 1297, 1–8. doi: 10.1016/j.brainres.2009.08.070

Li, D., Herault, K., Zylbersztejn, K., Lauterbach, M. A., Guillon, M., Oheim, M., et al. (2015). Astrocyte VAMP3 vesicles undergo Ca2+ -independent cycling and modulate glutamate transporter trafficking. *J. Physiol.* 593, 2807–2832. doi: 10.1113/JP270362

Lioy, D. T., Garg, S. K., Monaghan, C. E., Raber, J., Foust, K. D., Kaspar, B. K., et al. (2011). A role for glia in the progression of Rett's syndrome. *Nature* 475, 497–500. doi: 10.1038/nature10214

Luikenhuis, S., Giacometti, E., Beard, C. F., and Jaenisch, R. (2004). Expression of MeCP2 in postmitotic neurons rescues Rett syndrome in mice. *Proc. Natl. Acad. Sci. U.S.A.* 101, 6033–6038. doi: 10.1073/pnas.0401626101

Lundgaard, I., Luzhynskaya, A., Stockley, J. H., Wang, Z., Evans, K. A., Swire, M., et al. (2013). Neuregulin and BDNF induce a switch to NMDA receptor-dependent myelination by oligodendrocytes. *PLOS Biol.* 11:e1001743. doi: 10.1371/journal.pbio.1001743

Luo, C., and Ecker, J. R. (2015). Epigenetics. Exceptional epigenetics in the brain. *Science* 348, 1094–1095. doi: 10.1126/science.aac5832

Lyst, M. J., and Bird, A. (2015). Rett syndrome: a complex disorder with simple roots. *Nat. Rev. Genet.* 16, 261–275. doi: 10.1038/nrg3897

Mackenzie, B., and Erickson, J. D. (2004). Sodium-coupled neutral amino acid (System N/A) transporters of the SLC38 gene family. *Pflugers. Arch.* 447, 784–795. doi: 10.1007/s00424-003-1117-9

Maezawa, I., and Jin, L. W. (2010). Rett syndrome microglia damage dendrites and synapses by the elevated release of glutamate. *J. Neurosci.* 30, 5346–5356. doi: 10.1523/JNEUROSCI.5966-09.2010

Maezawa, I., Swanberg, S., Harvey, D., Lasalle, J. M., and Jin, L. W. (2009). Rett syndrome astrocytes are abnormal and spread MeCP2 deficiency through gap junctions. *J. Neurosci.* 29, 5051–5061. doi: 10.1523/JNEUROSCI.0324-09.2009

Makedonski, K., Abuhatzira, L., Kaufman, Y., Razin, A., and Shemer, R. (2005). MeCP2 deficiency in Rett syndrome causes epigenetic aberrations at the PWS/AS imprinting center that affects UBE3A expression. *Hum. Mol. Genet.* 14, 1049–1058. doi: 10.1093/hmg/ddi097

Mari, F., Azimonti, S., Bertani, I., Bolognese, F., Colombo, E., Caselli, R., et al. (2005). CDKL5 belongs to the same molecular pathway of MeCP2 and it is responsible for the early-onset seizure variant of Rett syndrome. *Hum. Mol. Genet.* 14, 1935–1946. doi: 10.1093/hmg/ddi198

Matagne, V., Ehinger, Y., Saidi, L., Borges-Correia, A., Barkats, M., Bartoli, M., et al. (2017). A codon-optimized Mecp2 transgene corrects breathing deficits and improves survival in a mouse model of Rett syndrome. *Neurobiol. Dis.* 99, 1–11. doi: 10.1016/j.nbd.2016.12.009

Mencarelli, M. A., Spanhol-Rosseto, A., Artuso, R., Rondinella, D., De Filippis, R., Bahi-Buisson, N., et al. (2010). Novel FOXG1 mutations associated with the congenital variant of Rett syndrome. *J. Med. Genet.* 47, 49–53. doi: 10.1136/jmg.2009.067884

Meng, X., Wang, W., Lu, H., He, L. J., Chen, W., Chao, E. S., et al. (2016). Manipulations of MeCP2 in glutamatergic neurons highlight their contributions to Rett and other neurological disorders. *Elife* 5:e14199. doi: 10.7554/eLife.14199

Nakashima, N., Yamagata, T., Mori, M., Kuwajima, M., Suwa, K., and Momoi, M. Y. (2010). Expression analysis and mutation detection of DLX5 and DLX6 in autism. *Brain Dev.* 32, 98–104. doi: 10.1016/j.braindev.2008.12.021

Nectoux, J., Florian, C., Delepine, C., Bahi-Buisson, N., Khelfaoui, M., Reibel, S., et al. (2012). Altered microtubule dynamics in Mecp2-deficient astrocytes. *J. Neurosci. Res.* 90, 990–998. doi: 10.1002/jnr.23001

Nelson, S. B., and Valakh, V. (2015). Excitatory/inhibitory balance and circuit homeostasis in autism spectrum disorders. *Neuron* 87, 684–698. doi: 10.1016/j.neuron.2015.07.033

Nguyen, M. V., Du, F., Felice, C. A., Shan, X., Nigam, A., Mandel, G., et al. (2012). MeCP2 is critical for maintaining mature neuronal networks and global brain anatomy during late stages of postnatal brain development and in the mature adult brain. *J. Neurosci.* 32, 10021–10034. doi: 10.1523/JNEUROSCI.1316-12.2012

Nguyen, M. V., Felice, C. A., Du, F., Covey, M. V., Robinson, J. K., Mandel, G., et al. (2013). Oligodendrocyte lineage cells contribute unique features to Rett syndrome neuropathology. *J. Neurosci.* 33, 18764–18774. doi: 10.1523/JNEUROSCI.2657-13.2013

Nomura, Y. (2005). Early behavior characteristics and sleep disturbance in Rett syndrome. *Brain Dev.* 27(Suppl. 1), S35–S42. doi: 10.1016/j.braindev.2005.03.017

Noutel, J., Hong, Y. K., Leu, B., Kang, E., and Chen, C. (2011). Experience-dependent retinogeniculate synapse remodeling is abnormal in MeCP2-deficient mice. *Neuron* 70, 35–42. doi: 10.1016/j.neuron.2011.03.001

O'Driscoll, C. M., Lima, M. P., Kaufmann, W. E., and Bressler, J. P. (2015). Methyl CpG binding protein 2 deficiency enhances expression of inflammatory cytokines by sustaining NF-kappaB signaling in myeloid derived cells. *J. Neuroimmunol.* 283, 23–29. doi: 10.1016/j.jneuroim.2015.04.005

Okabe, Y., Takahashi, T., Mitsumasu, C., Kosai, K., Tanaka, E., and Matsuishi, T. (2012). Alterations of gene expression and glutamate clearance in astrocytes derived from an MeCP2-null mouse model of Rett syndrome. *PLOS ONE* 7:e35354. doi: 10.1371/journal.pone.0035354

Olson, C. O., Zachariah, R. M., Ezeonwuka, C. D., Liyanage, V. R., and Rastegar, M. (2014). Brain region-specific expression of MeCP2 isoforms correlates with DNA methylation within Mecp2 regulatory elements. *PLOS ONE* 9:e90645. doi: 10.1371/journal.pone.0090645

Palazzo, A., Ackerman, B., and Gundersen, G. G. (2003). Cell biology: Tubulin acetylation and cell motility. *Nature* 421:230. doi: 10.1038/421230a

Palmer, A., Qayumi, J., and Ronnett, G. (2008). MeCP2 mutation causes distinguishable phases of acute and chronic defects in synaptogenesis and maintenance, respectively. *Mol. Cell. Neurosci.* 37, 794–807. doi: 10.1016/j.mcn.2008.01.005

Philippe, O., Rio, M., Malan, V., Van Esch, H., Baujat, G., Bahi-Buisson, N., et al. (2013). NF-kappaB signalling requirement for brain myelin formation is shown by genotype/MRI phenotype correlations in patients with Xq28 duplications. *Eur. J. Hum. Genet.* 21, 195–199. doi: 10.1038/ejhg.2012.140

Robinson, L., Guy, J., Mckay, L., Brockett, E., Spike, R. C., Selfridge, J., et al. (2012). Morphological and functional reversal of phenotypes in a mouse model of Rett syndrome. *Brain* 135, 2699–2710. doi: 10.1093/brain/aws096

Roze, E., Cochen, V., Sangla, S., Bienvenu, T., Roubergue, A., Leu-Semenescu, S., et al. (2007). Rett syndrome: an overlooked diagnosis in women with stereotypic hand movements, psychomotor retardation, Parkinsonism, and dystonia? *Mov. Disord.* 22, 387–389. doi: 10.1002/mds.21276

Schafer, D. P., Heller, C. T., Gunner, G., Heller, M., Gordon, C., Hammond, T., et al. (2016). Microglia contribute to circuit defects in Mecp2 null mice independent of microglia-specific loss of Mecp2 expression. *Elife* 5:e15224. doi: 10.7554/eLife.15224

Shahbazian, M. D., Antalffy, B., Armstrong, D. L., and Zoghbi, H. Y. (2002). Insight into Rett syndrome: MeCP2 levels display tissue- and cell-specific differences and correlate with neuronal maturation. *Hum. Mol. Genet.* 11, 115–124. doi: 10.1093/hmg/11.2.115

Sharma, K., Singh, J., Pillai, P. P., and Frost, E. E. (2015). Involvement of MeCP2 in regulation of myelin-related gene expression in cultured rat oligodendrocytes. *J. Mol. Neurosci.* 57, 176–184. doi: 10.1007/s12031-015-0597-3

Sinnett, S. E., Hector, R. D., Gadalla, K. K. E., Heindel, C., Chen, D., Zaric, V., et al. (2017). Improved MECP2 gene therapy extends the survival of MeCP2-null mice without apparent toxicity after intracisternal delivery. *Mol. Ther. Methods Clin. Dev.* 5, 106–115. doi: 10.1016/j.omtm.2017.04.006

Smrt, R. D., Eaves-Egenes, J., Barkho, B. Z., Santistevan, N. J., Zhao, C., Aimone, J. B., et al. (2007). Mecp2 deficiency leads to delayed maturation and altered gene expression in hippocampal neurons. *Neurobiol. Dis.* 27, 77–89. doi: 10.1016/j.nbd.2007.04.005

Squillaro, T., Alessio, N., Cipollaro, M., Melone, M. A., Hayek, G., Renieri, A., et al. (2012). Reduced expression of MECP2 affects cell commitment and maintenance in neurons by triggering senescence: new perspective for Rett syndrome. *Mol. Biol. Cell* 23, 1435–1445. doi: 10.1091/mbc.E11-09-0784

Stancheva, I., Collins, A. L., Van Den Veyver, I. B., Zoghbi, H., and Meehan, R. R. (2003). A mutant form of MeCP2 protein associated with human Rett syndrome cannot be displaced from methylated DNA by notch in *Xenopus* embryos. *Mol. Cell.* 12, 425–435. doi: 10.1016/S1097-2765(03)00276-4

Stearns, N. A., Schaevitz, L. R., Bowling, H., Nag, N., Berger, U. V., and Berger-Sweeney, J. (2007). Behavioral and anatomical abnormalities in Mecp2 mutant mice: a model for Rett syndrome. *Neuroscience* 146, 907–921. doi: 10.1016/j.neuroscience.2007.02.009

Tai, D. J., Liu, Y. C., Hsu, W. L., Ma, Y. L., Cheng, S. J., Liu, S. Y., et al. (2016). MeCP2 SUMOylation rescues Mecp2-mutant-induced behavioural deficits in a mouse model of Rett syndrome. *Nat. Commun.* 7:10552. doi: 10.1038/ncomms10552

Turovsky, E., Karagiannis, A., Abdala, A. P., and Gourine, A. V. (2015). Impaired CO2 sensitivity of astrocytes in a mouse model of Rett syndrome. *J. Physiol.* 593, 3159–3168. doi: 10.1113/JP270369

Vacca, M., Tripathi, K. P., Speranza, L., Aiese Cigliano, R., Scalabri, F., Marracino, F., et al. (2016). Effects of Mecp2 loss of function in embryonic cortical neurons: a bioinformatics strategy to sort out non-neuronal cells variability from transcriptome profiling. *BMC Bioinformat.* 17(Suppl. 2):14. doi: 10.1186/s12859-015-0859-7

Vora, P., Mina, R., Namaka, M., and Frost, E. E. (2010). A novel transcriptional regulator of myelin gene expression: implications for neurodevelopmental disorders. *Neuroreport* 21, 917–921. doi: 10.1097/WNR.0b013e32833da500

Wang, J., Wegener, J. E., Huang, T. W., Sripathy, S., De Jesus-Cortes, H., Xu, P., et al. (2015). Wild-type microglia do not reverse pathology in mouse models of Rett syndrome. *Nature* 521, E1–E4. doi: 10.1038/nature14671

Williams, E. C., Zhong, X., Mohamed, A., Li, R., Liu, Y., Dong, Q., et al. (2014). Mutant astrocytes differentiated from Rett syndrome patients-specific iPSCs have adverse effects on wild-type neurons. *Hum. Mol. Genet.* 23, 2968–2980. doi: 10.1093/hmg/ddu008

Wu, W., Gu, W., Xu, X., Shang, S., and Zhao, Z. (2012). Downregulation of CNPase in a MeCP2 deficient mouse model of Rett syndrome. *Neurol. Res.* 34, 107–113. doi: 10.1179/016164111X13214359296301

Yasui, D. H., Xu, H., Dunaway, K. W., Lasalle, J. M., Jin, L. W., and Maezawa, I. (2013). MeCP2 modulates gene expression pathways in astrocytes. *Mol. Autism* 4:3. doi: 10.1186/2040-2392-4-3

Yuan, T., and Bellone, C. (2013). Glutamatergic receptors at developing synapses: the role of GluN3A-containing NMDA receptors and GluA2-lacking AMPA receptors. *Eur. J. Pharmacol.* 719, 107–111. doi: 10.1016/j.ejphar.2013.04.056

Zachariah, R. M., Olson, C. O., Ezeonwuka, C., and Rastegar, M. (2012). Novel MeCP2 isoform-specific antibody reveals the endogenous MeCP2E1 expression

in murine brain, primary neurons and astrocytes. *PLOS ONE* 7:e49763. doi: 10.1371/journal.pone.0049763

Zhang, X., Su, J., Cui, N., Gai, H., Wu, Z., and Jiang, C. (2011). The disruption of central CO2 chemosensitivity in a mouse model of Rett syndrome. *Am. J. Physiol. Cell Physiol.* 301, C729–C738. doi: 10.1152/ajpcell.00334.2010

Zhao, D., Mokhtari, R., Pedrosa, E., Birnbaum, R., Zheng, D., and Lachman, H. M. (2017). Transcriptome analysis of microglia in a mouse model of Rett syndrome: differential expression of genes associated with microglia/macrophage activation and cellular stress. *Mol. Autism* 8:17. doi: 10.1186/s13229-017-0134-z

Zhou, Z., Hong, E. J., Cohen, S., Zhao, W. N., Ho, H. Y., Schmidt, L., et al. (2006). Brain-specific phosphorylation of MeCP2 regulates activity-dependent Bdnf transcription, dendritic growth, and spine maturation. *Neuron* 52, 255–269. doi: 10.1016/j.neuron.2006.09.037

Conflict of Interest Statement: The authors declare that the research was conducted in the absence of any commercial or financial relationships that could be construed as a potential conflict of interest.

frontiers in Neuroscience

ORIGINAL RESEARCH
published: 06 September 2017
doi: 10.3389/fnins.2017.00500

Plant Polyphenols and Exendin-4 Prevent Hyperactivity and TNF-α Release in LPS-Treated *In vitro* Neuron/Astrocyte/Microglial Networks

Francesca Gullo[1], Michela Ceriani[1], Alessia D'Aloia[2], Enzo Wanke[2], Andrew Constanti[3], Barbara Costa[1†] and Marzia Lecchi[1†]*

[1] Department of Biotechnology and Biosciences and Milan Center for Neuroscience, University of Milano-Bicocca, Milan, Italy, [2] Department of Biotechnology and Biosciences, University of Milano-Bicocca, Milan, Italy, [3] Department of Pharmacology, School of Pharmacy, University College London, London, United Kingdom

OPEN ACCESS

Edited by:
Alexej Verkhratsky, University of Manchester, United Kingdom

Reviewed by:
Darius Widera, University of Reading, United Kingdom
Varun Kesherwani, University of Nebraska Medical Center, United States

***Correspondence:**
Marzia Lecchi
marzia.lecchi1@unimib.it

† These authors jointly supervised this work.

Specialty section:
This article was submitted to Neurodegeneration, a section of the journal Frontiers in Neuroscience

Received: *22 May 2017*
Accepted: *23 August 2017*
Published: *06 September 2017*

Citation:
Gullo F, Ceriani M, D'Aloia A, Wanke E, Constanti A, Costa B and Lecchi M (2017) Plant Polyphenols and Exendin-4 Prevent Hyperactivity and TNF-α Release in LPS-Treated In vitro Neuron/Astrocyte/Microglial Networks. Front. Neurosci. 11:500. doi: 10.3389/fnins.2017.00500

Increasing evidence supports a decisive role for neuroinflammation in the neurodegenerative process of several central nervous system (CNS) disorders. Microglia are essential mediators of neuroinflammation and can regulate a broad spectrum of cellular responses by releasing reactive oxygen intermediates, nitric oxide, proteases, excitatory amino acids, and cytokines. We have recently shown that also in *ex-vivo* cortical networks of neurons, astrocytes and microglia, an increased level of tumor necrosis factor-alpha (TNF-α) was detected a few hours after exposure to the bacterial endotoxin lipopolysaccharide (LPS). Simultaneously, an atypical "seizure-like" neuronal network activity was recorded by multi-electrode array (MEA) electrophysiology. These effects were prevented by minocycline, an established anti-inflammatory antibiotic. We show here that the same inhibitory effect against LPS-induced neuroinflammation is exerted also by natural plant compounds, polyphenols, such as curcumin (CU, curcuma longa), crocin (CR, saffron), and resveratrol (RE, grape), as well as by the glucagon like peptide-1 receptor (GLP-1R) agonist exendin-4 (EX-4). The drugs tested also caused *per-se* early transient (variable) changes of network activity. Since it has been reported that LPS-induced neuroinflammation causes rearrangements of glutamate transporters in astrocytes and microglia, we suggest that neural activity could be putatively increased by an imbalance of glial glutamate transporter activity, leading to prolonged synaptic glutamatergic dysregulation.

Keywords: sterile inflammation, LPS, TNF-α, GLP-1, plant polyphenols, exendin-4 (EX-4), neocortical cultures, multi-electrode array (MEA)

INTRODUCTION

Microglia are an integral part of central nervous system (CNS) networks, forming the innate defensive system, and their pathological potential has been extensively investigated (Kettenmann et al., 2011). In different pathologies, microglia acquire distinct functional states and, during the disease progression, modify and change their activated phenotype. Activated microglia specifically

interact with neurons and influence their survival either in a positive or in a negative direction. They can physically contact injured neurons and remove synapses, a process termed synaptic stripping (Kettenmann et al., 2013). Conceptually, microglial cells not only can affect neural networks through removal of cellular and subcellular elements and secreting cytokines, trophic factors, and neurotransmitters (Kettenmann et al., 2011), but also by receiving messages; in fact, they express a variety of receptors for neurotransmitters, neuropeptides, and neuromodulators. Thus they have also the capacity to sense neuronal activity (Pocock and Kettenmann, 2007).

Current pharmacological interventions against neuroinflammation have symptomatic benefits to certain degrees, but do not prevent progressive neurodegeneration. More recently, it has been shown that some natural substances protect the substantia nigra dopaminergic neurons (involved in the onset of Parkinson's disease) through their anti-inflammatory action. Among these are some polyphenols such as curcumin, CU (Ojha et al., 2012), resveratrol, RE (Zhang et al., 2010; Gao et al., 2014; Lofrumento et al., 2014), and peptide molecules such as exendin-4, EX-4 (Kim et al., 2009; Athauda and Foltynie, 2016). Moreover, also crocin, CR, extracted from saffron, resulted in an effective protection from macular degeneration, a retinal disease principally related to oxidative stress and chronic inflammation (Nam et al., 2010; Marangoni et al., 2013). In many of these reports, sterile inflammation was induced, microglia-released cytokine concentration increased, but the properties of neuronal network activity were never explored.

By using low concentrations of the purified bacterial endotoxin lipopolysaccharide (LPS) over 6–8 h, we reproduced *in vitro* a "sterile" CNS neuroinflammation in a 10,000-cell network of neurons, astrocytes and microglia, grown on a multielectrode array (MEA) dish, where neurons were regularly bursting for weeks (Gullo et al., 2014). We found that an "atypical" neuronal excitability took place causing long-lasting bursts resembling epileptiform seizures. These slow changes of neuronal excitability were accompanied by a simultaneous increase in microglia-released tumor necrosis factor-alpha (TNF-α) concentration, suggesting a crucial role of microglia, but not of astrocytes, in this process. Both these effects were blocked by pre-treatment with minocycline, an anti-inflammatory antibiotic drug, which was inactive when applied alone.

Here, we wished to examine whether the action of minocycline on our neuron/astrocyte/microglial co-culture system could be reproduced by the above mentioned natural molecules as anti-inflammatory tools. By simultaneously using an electrophysiological recording technique, such as microelectrode arrays (MEA), and TNF-α ELISA assays, we found that all of these molecules, depending on the concentration used, were transiently able to modify the balanced network activity and to imitate the blocking effects of minocycline against LPS neuroinflammation. Furthermore, all of the agents tested resulted in an anti-inflammatory action at concentrations lower than those generally reported in the literature.

MATERIALS AND METHODS

Cell Cultures

Primary cultures of cortical neurons were prepared from post-natal mice (P1–P3) as previously described (Gullo et al., 2009). All the procedures concerning animal handling and sacrifice followed the Principles of Laboratory Animal Care (2010/63/UE Directive), and were approved by the University of Milan-Bicocca Ethics Committee and the Italian Ministry of Health (D.Lgs 26/2014). Briefly, the cerebral cortex (excluding the hippocampus) was removed from decapitated mice, cut into 1 mm^3 pieces, and digested by trypsin (0.15%) and DNAse (10 μg/ml) at 37°C for 20 min. After enzyme digestion, cells were mechanically dissociated by means of trituration, and plated at densities of 600–900 × 10^3 cells/ml on glass coverslips (for immunocytochemistry) or MEA Petri dishes pre-coated with polyethyleneimine 0.1% (wt/vol) and laminin 20 μg/ml (30 μm diameter ITO electrodes spaced 200 μm apart, Multichannels System, Germany). After 3 h incubation, the plating medium was replaced by neurobasal medium (NB) with B27 (Invitrogen, Italy), glutamine 1 mM and basic fibroblast growth factor (bFGF) 10 ng/ml, and the culture was maintained at 37°C in 5% CO_2. One-half of the medium volume was replaced every 3 days. The cultures in MEA dishes were covered with gas-permeable covers (MEA-MEM, Ala Scientific Instruments, Inc., USA) throughout the culture period (12–22 days-*in-vitro*, DIV).

MEA Electrophysiology: Drug Application-General Aspects

As previously described (Gullo et al., 2009), we report results obtained within a few hours after positioning the MEA dish into the incubator, which can be considered at the steady-state. The recording area in our MEA dishes was ∼2 mm^2, and in this area, the average number of neurons was in the order of ∼5,000, plus about the same number of astrocytes (see Figure 1 of Supplementary Material in Gullo et al., 2010, at http://www/frontiersin.org/neuralcircuits/paper/10.3389/fncir.2010.00011/). The average space between cells was therefore relatively large. Neuroinflammation was induced by incubating cultures with LPS, isolated and purified from *E. coli* R515 by Enzo Life Sciences (Alexis Biochemicals, code 581-007). This product does not contain detectable protein or DNA contaminants with agonistic Toll-like receptor (TLR) activity. Since it is a strong activator of TLR4 but it does not activate TLR2 or the other TLRs, it was considered suitable for our experiments. The drugs to be tested were kept as frozen stock solutions in distilled water (or DMSO <0.1%) at −20°C, until diluted as appropriate with MEA culture medium before each experiment. The drugs used were: crocin (CR), the polyphenols resveratrol (RE) and curcumin (CU), purchased from Sigma, Italy; exendin-4 (EX-4) and the GLP-1 receptor antagonist, exendin (9–39), purchased from Tocris, UK. All experiments were performed by adding the drugs in volumes that were always <1% of the total conditioned media volume bathing the neurons. When indicated, a washout was carried out with a solution pre-conditioned by the same network under control conditions.

MEA Electrophysiology: Recordings, Waveform Acquisition, and Sorting

We used the same procedures previously described in Gullo et al. (2009, 2010). Briefly, analog signals sampled at 40 kHz were recorded at 36°C in CO_2-controlled incubators using MEA-1060BC or 1060INV pre-amplifiers (bandwidth 1–8,000 Hz, Multichannel Systems, Germany) connected to a MEA Workstation (bandwidth 100–8,000 Hz, Plexon Inc., USA). Data were sorted into timestamp files by the MEAWorkstation Sorter software (MEAWS, see details below) and cleaned of artifacts using the OFFLine Sorter program (Plexon Inc., USA). Next, during the PCA-based waveform sorting and for multi-unit electrodes, we applied one of the following procedures: (i) spike removal with a Mahalanobis threshold in the range 1.8 to 1.4; we concurrently checked that the *P*-value of multivariate ANOVA sorting quality statistics was <0.01 among the identified units; (ii) when the previous procedure led to excessive spike invalidation, we manually removed the spikes invading the adjacent unit ellipsoids (the latter method was very effective in decreasing the *P*-values, with only a limited number of erased spikes).

Neuronal Cluster Classification

The method of classification into excitatory or inhibitory neurons is described in detail in Gullo et al. (2009, 2010) and Becchetti et al. (2012). Briefly, for each identified unit and each burst, the following characteristics were computed in defined time segments: the autocorrelation function (ACF), the burst duration (BD), the spike number (SN), the spike rate (SR), the intra-burst spike rate (IBSR), the inter-burst intervals (IBIs), and the Fano factor (FF; Teich, 1989; Baddeley et al., 1997). We classified the neurons on the basis of an unsupervised learning approach consisting of data reducing principal component analysis (PCA) based on FF as a feature (Becchetti et al., 2012), followed by the K-means clustering procedure. The large differences in these burst metrics was the basis for adopting FF as the best feature to clusterize neurons. As previously described (Becchetti et al., 2012), these procedures normally separated two statistically different clusters composed of numbers of excitatory (∼60–90) and inhibitory (∼15–25) neurons, whose ratio always fitted the ratio present in the neocortex i.e., from 4 to 5 (Gullo et al., 2010; Sahara et al., 2012). To give an approximate idea of the computing time involved in the analysis of a 60-electrode MEA dish with ∼100 identified neurons, the following are the typical parameters: 20 h-long experiment, 0.5 GB memory size, 10 min to obtain results.

Advanced Tools for Characterizing Firing and BD Histograms

The global network burst structure was analyzed with standard techniques as well as procedures recently developed by us (Gullo et al., 2012). Briefly, we applied a running window of variable duration (from 10 ms to 1 s) in order to search for the start and end of each burst and simultaneously collecting all of the spikes which were precisely tagged to the engaged excitatory and inhibitory neurons, already designated as previously explained above. In conclusion, for each spike in a generic burst, we knew exactly which neuron fired it and how many other spikes were fired by all of the other neurons. This had the consequence that we could also compute for the two identified neuronal clusters (defined above) the average propensity for firing, namely, the average number of spikes per burst, here called "excitability" (EXC) in each time segment of interest (shown in **Figure 1A**). Normally, it is much more interesting to compare EXC data normalized to control for both clusters, namely, normEXC. To investigate the heterogeneity of the burst length, BD, we studied its distribution in the form of cumulative probabilities in each time segment of interest, cumBD, as previously done in Gullo et al. (2014). To compare experiments, two types of plots are shown as follows: (i) time plots where *normEXC* describes how clusters change firing in the presence of drugs with respect to control (open, □, and closed, ■, symbols for excitatory and inhibitory clusters, respectively). Aligned characters, attached to the time axis, are control (c), washout (w), or drug names (short names were: CU, CR, RE, EX-4) indicating the presence or absence of drugs (note axis breaks necessary to zoom to particular time segments); (ii) *cumBD* plots (bin 0.2 s) vs. burst duration describing how drugs modify the distribution of the burst lifetimes (thick continuous lines for control; open stars for drugs; open rightward triangles, ▷, for LPS and open upward triangles, Δ, for washout. In our previous paper (Gullo et al., 2014), we found that, at 6–7 h after LPS application, its action was either present or blocked if the values of two variables, namely normEXC and $cumBD_{95}$ (the value of BD at cumBD of 95%), resulted in an increase with respect to control beside fixed thresholds. The normEXC threshold was $+45 \pm 10\%$ (with respect to control value, in this case 1) and cumBD threshold was $+40 \pm 5\%$ (with respect to the BD value in control computed at $cumBD_{95}$). Therefore, to highlight if drugs were able or unable to block LPS action in the normEXC and $cumBD_{95}$ plots, in the figures these thresholds were represented by a thin straight line and an arrow respectively.

TNF-α Concentration Measurements

In each MEA dish, small (150 μl) aliquots of the incubation medium were collected in control and during different times (6 and 12 h, representing the peak-time of LPS-induced TNF-α release, Gullo et al., 2014) after the addition of LPS (3 μg/ml) or polyphenols/crocin/exendin-4 + LPS. Samples (50 μl) were analyzed in triplicate for murine TNF-α with enzyme-linked immunosorbent assay (ELISA) kits (KCM3012, Invitrogen, Italy) according to manufacturer's instructions. The data were expressed as pg/ml following interpolation on the basis of a standard curve. As suggested by the manufacturer, the inter-assay and intra-assay variability were 3.5–4.3 and 2.6–8.2%, with a lower limit of detection <3 pg/ml. During the analysis we did not correct the data for the small change in the total incubation medium volume resulting from the aliquots removal. Data were analyzed using GraphPad 7.0 software employing ANOVA followed by Dunnet's test for group comparison. $P < 0.05$ was considered statistically significant.

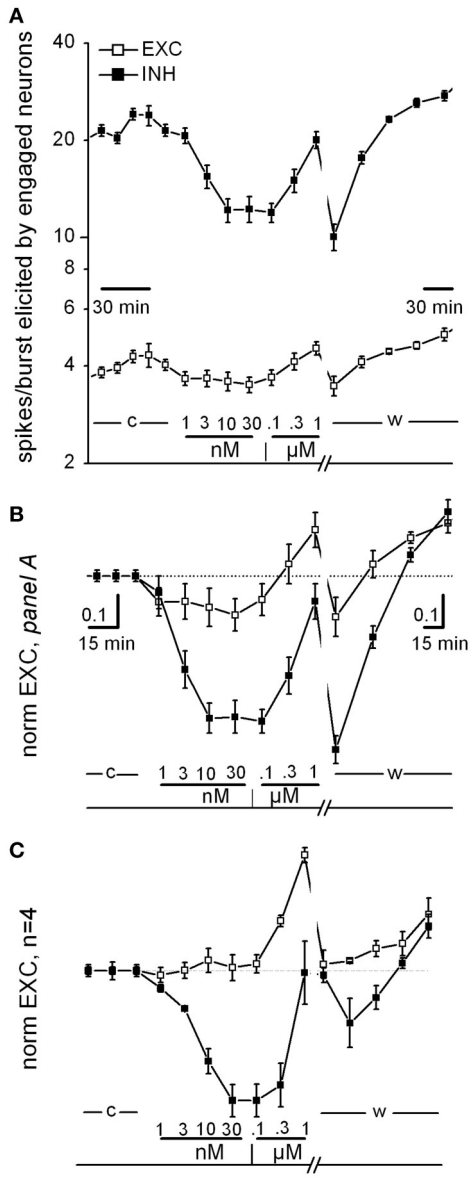

FIGURE 1 | Curcumin dose-response relationship. **(A)** Time plot of excitability (EXC) for inhibitory and excitatory neurons (closed and open symbols, respectively) recorded in one exemplary dish. Data before and after the washout time break (13 min) have different time resolution (see calibration bars). The time course of curcumin (CU) application is described above the bottom line as follows: c, w, control and washout; numbers are [CU] in nM and µM as indicated. **(B)** Same data as in **(A)**, but values were normalized to those of control and superimposed in order to be compared. Note that in this experiment, CU either decreased the excitability of both inhibitory and excitatory cells in the 1–30 nM concentration region or increased excitability in the further 30–1,000 nM concentration region, in a reversible manner. **(C)** Plot as in **(B)**, but average of data from four independent experiments from different dishes but similar DIVs.

Data Analysis and Statistical Significance

All of the data are expressed as mean values ± SEM, with *n* indicating the number of experiments. We used OriginPro 9.1 to test normality of data such as cumBD and FSH. Moreover, for statistical significance among cumBD and FSH distributions from different experiments, we used the non-parametric tests Wilcoxon signed rank test or Kruskal–Wallis test both available from OriginPro 9.1. The data were analyzed and the figures prepared using OriginPro 7.0 or OriginPro 9.1 software.

RESULTS

To study the activity of reverberating cortical networks, we followed the procedures described in Gullo et al. (2014). In our cultures, neurons, astrocytes and microglial cells survived together for weeks. In these conditions, neurons were able to generate spikes, which were stably recorded by MEA system (60 recording electrodes, 200 µm apart). The spikes were acquired during each burst (every ∼10 s) consisting of an ∼1 s-brief period of synaptic-mediated global network activity among all excitable cells. Indeed, each elicited spike was the result of the temporal and spatial summation of a minimum of ∼100 postsynaptic potentials reaching each of the ∼3,500 neurons present in the dish. On the whole, each burst was a reverberating event of the spontaneous network activity consisting of a total of ∼600 spikes elicited by neurons (∼75 and ∼25 excitatory and inhibitory cells, at ∼4 and 12/burst, respectively). This means that data recorded from a single burst were the outcome of ∼60,000 synaptic events, but it should be kept in mind that this was a significant (n = ∼100 electrodes) sample compared to the ∼3,500 interconnected neurons present in the whole network.

When the culture dishes reached maturation (from 10 up to 22 DIV) we performed experiments, lasting more than ∼15 h, during which no significant changes in network activity were observed under control conditions. These cultures were therefore useful for acquiring data in the long-lasting test on the LPS effects, in which we recorded the atypical "seizure-like" activity (Gullo et al., 2014). To study the neuronal activity, we analyzed firing data by using two variables fully describing the temporal changes: (a) plots of normEXC (excitability normalized to control) of the clusters of excitatory and inhibitory neurons and (b) plots of cumBD (cumulative distribution of the burst durations). Since we found that the drugs were able to induce relatively fast, but transient effects (compared to control data and long-lasting LPS effects, see Gullo et al., 2014), we analyzed results in graphs whose time axis contained appropriate breaks and drug labels. Moreover, to decide if the LPS action should be considered successful or blocked by drugs, we fixed thresholds in normEXC and $cumBD_{95}$ (the value of BD at cumBD of 95%) plots as a thin straight line and a vertical arrow, respectively (see Section Advanced Tools for Characterizing Firing and BD Histograms). Drugs were always tested, before applying LPS, by a brief preconditioning (30–60 min) interval in which a drug was added to the incubation medium.

Are Drugs Intrinsically Affecting Excitability?

For each tested drug, we performed a dose-response curve using concentrations based on published data, and then we verified

if the substances *per-se* introduced relevant excitability changes with respect to control and washout.

In **Figure 1**, we show some specific exemplary experiments for CU; similar experiments were done also for the other drugs. As shown in **Figure 1A** (an exemplary experiment out of 4 similar results), the CU dose-response relationships consistently confirmed that in the low nanomolar region, both excitatory and inhibitory neurons decreased their activity immediately (over a few minute time course). On the contrary, in the region from 30 nM up to 1 μM the CU effect was opposite. Finally, the effects were almost completely reversible on washout. This plot shows the time course of the average spikes/burst elicited by neurons engaged in the activity ("excitability," EXC, see details in Section Methods) by the two inhibitory (in control ∼20) and excitatory (∼4.5) neuronal clusters. EXC is characterized by values that are very different between the clusters and can be changed by pharmacological manipulations (see Becchetti et al., 2012). The neuronal clusters responded immediately and differently after each drug application (10 min) starting from 1 nM up to 1 μM (see legend).

To compare different experiments, it was necessary to normalize data to the control data, and in **Figures 1B,C** these plot-types (now of "normEXC") are shown superimposed. It can be noticed that from the response in B, the IC_{50} for inhibitory neurons (closed square) was ∼3 nM with a saturation after 10 nM and a recovery during washout. In **Figure 1C** we show the average of 4 similar experiments and the normEXC dose-response curves were found to have two different shapes in the two concentration regions from 1 to 30 nM and from 0.1 to 1 μM, respectively. In the first region only inhibitory cells were inhibited, and the IC_{50} was 4.5 ± 0.6 nM; on the contrary, in the second region, inhibitory cells recovered their activity and excitatory cells increased their activity. On average, at 1 μM, the global effect was an increase of activity that recovered on washout. It has previously been shown that an early and fast effect of CU, characterized by an IC_{50} in the micromolar range, consists of inhibiting glutamate (glu) release from synaptosomes from rat cortex nerve endings (Lin et al., 2011, 2012).

On the whole, these results are only partially in line with those obtained by Lin et al. (2011) by using a different technique. Indeed, since in the cortex microcircuits, inhibitory neurons receive glutamatergic synaptic inputs (in both feedback and feedforward loops, see Isaacson and Scanziani, 2011), we expected to observe a consistent decrease in their activity only in the lower CU concentration region. Compared to those of Lin et al. (2011) (glutamate release from synaptosomes), our methods were characterized by the functional synapse integrity and the astrocyte-mediated $[glu]_o$ uptake (Wanke et al., 2016), suggesting a much higher sensitivity. Moreover, our dose-response curves cannot be considered at steady-state because each drug concentration was changed every 10 min.

Transient and Long Term Effects of CU: LPS-Induced Inflammation Is Blocked at 1 μM CU

Since our experiments with LPS-induced inflammation imply very long time-segments of the order of about 18 h, we investigated if the inhibitory CU effects seen in **Figure 1** were indeed transient and therefore eventually negligible over this time-frame. Moreover, we wanted to use CU concentrations lower than those that have been recently used in animals (∼100 μg/Kg/day, see Ojha et al., 2012; Hoppe et al., 2013; Zhu et al., 2014) approximatively equivalent to ∼100 μM. Indeed, since we did not have any blockade induced by the blood brain barrier (see Wang et al., 2016) and the drug action should be directly on neurons, we decided to fix 1 μM as a reasonable concentration, which is in line with the cited experiments performed by Lin et al. (2011).

Experiments were done by sequentially recording activity in control (3 h), during a preconditioning in CU (about 1 h at 1 μM) and successively in LPS (at least 7 h at 3 μg/ml); a final washout of 5 h was also recorded. The fast effects of a single drug application were studied in detail by averaging data every 15 min. After 3 days, in the same dish we performed a standard experiment by applying only LPS to be sure that the effects of the induced inflammation were still working. The results of such a dual experiment are shown in **Figures 2A–D**, respectively. In the experiment of **Figure 2A** that plots normEXC, 1 μM CU produced a fast and transient activity increase which actually decayed in ∼45 min. In the inset are shown the original data before normalization: we specifically analyzed the average number of spikes elicited in each burst and in each cluster of neurons; this analysis was performed counting for each neuron the spikes engaged in each burst. In the first 15 min, the drug caused an immediate firing increase of the inhibitory and excitatory clusters from 25.4 ± 1.5 to 38.9 ± 2.2 and from 5.5 ± 0.2 to 8.73 ± 0.4 spikes/burst (the bursts were 82, number of inhibitory and excitatory cells, 21 and 74, respectively) (see other details in legend). The subsequent LPS application, in fact, caused a further *decline* of normEXC for both clusters of neurons and the trend of normEXC for excitatory and inhibitory clusters was +14 ± 3 and +9 ± 1% respectively, suggesting that LPS was unable to exert its expected excitatory inflammatory function as previously observed (Gullo et al., 2014). Indeed, as shown in **Figure 2B**, the effects of a standard LPS application (3 μg/ml), done in the same dish 3 DIV later, illustrate that, after 4 and up to 8 h, a strong increase of the activity of excitatory neurons (+86 ± 6%) took place, although we did not observe any effect on inhibitory cells.

The cumBD data associated with the **Figures 2A,B** experiments are shown in **Figures 2C,D**, respectively. In C four curves are superimposed as follows: (i) control (thick line), (ii) CU at 15 min (line + asterisk), (iii) CU at 60 min (thin line), (iv) LPS at 7 h (line + right-triangles). The corresponding 90% BD values were: 2.6, 3.8, 2.6, 3.7 s, respectively. These results suggest that, as compared to control, CU only transiently increased $cumBD_{90\%}$, and LPS over 7 h produced only a 37% increase, confirming that the expected LPS action did not take place. Statistical significance by Kruskal–Wallis test applied to control data and CU at 60 min resulted in a $P < 0.12$, and at 7 h in LPS data resulted in $P < 0.05$. In contrast, as shown in **Figure 2D**, a typical effect of LPS on cumBD (in the same dish) was to further right-shift, with respect to control (line, 95% at 7.2 s), the curves at 5 h (right-triangles) and at 9 h (upward-triangles) to 12 s (+66%) and 17 s (+136%) values, respectively, with "seizure-like" burst durations reaching 22 s.

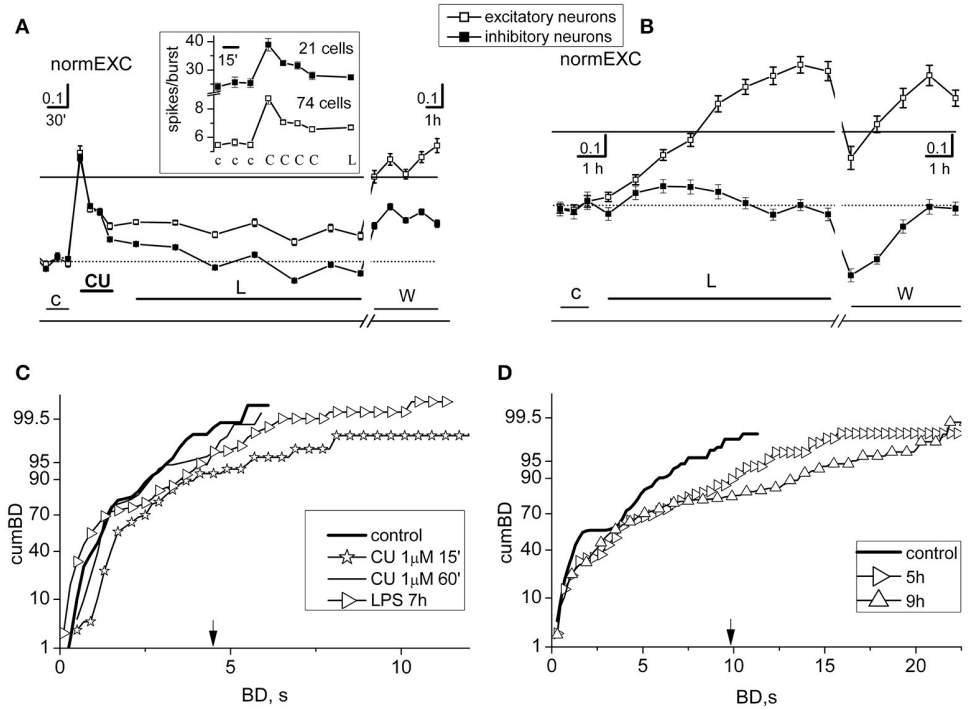

FIGURE 2 | Short- and long-term effects of curcumin in networks treated with LPS. Results from two different experiments, performed in the same dish, with preconditioning or not-preconditioning with 1 μM curcumin (CU) (done 3 DIV later) before the application of LPS (3 μg/ml) are shown in **(A,C)** and **(B,D)**, respectively. **(A)** Plots of normEXC in control (c), 1 μM CU (CU), LPS (L), and during washout (w). Inset: for the brief (∼3 h) initial time segment in control, CU and L, plot of average number of spikes/burst observed in neurons of both clusters. The continuous line is the fixed threshold. Other details: the total number of spikes from excitatory (inhibitory, in parenthesis) neurons in control and CU (in bold): 304.2 ± 18, **568.5 ± 32** (481.9 ± 33, **764.7 ± 45.4**); the total number of engaged excitatory (inhibitory, in parenthesis) neurons was in control: 52 ± 1.8, **63.8 ± 1.1** (17.8 ± 0.3, **19.3 ± 0.2**). **(B)** In the same dish as in **(A)**, but 3 DIV later, plots of normEXC in control (c), LPS (L) and during washout (w). The continuous line is the fixed threshold. **(C)** Plots of cumBD in different time regions of the experiment shown in **(A)**. Data of cumBD are superimposed as explained in text. **(D)** Plots of superimposed cumBD curves in different time regions of the experiment shown in **(B)**. Note that pre-conditioning with CU prevented the late, prolonged excitatory response to LPS. The vertical arrow indicates the fixed threshold.

The Kruskal–Wallis test of significance applied to control data and LPS data resulted in *P*-values which were always smaller than 10^{-4}.

On the whole, these results demonstrate that 1 μM CU by itself suddenly produced changes of activity in bursting, by promoting long BD values and significant increases in the excitability of both neuronal clusters. These transient modifications rapidly returned to quasi-control values as if the effects were partially compensated, only producing scarce or null effects in the early hours after adding LPS. On all of the occasions ($n = 10$) in which we performed these types of experiments, the results were similar. In other experiments ($n = 5$) in which we used smaller CU concentrations (i.e., 0.1 μM), the results were not clear and these data were discarded. Few ($n = 4$) experiments performed in dishes whose LPS responses were not significant were also discarded.

Transient and Long Term Effects of CR: LPS-Induced Inflammation Is Blocked at 20 μM CR

Crocin and crocetin have been found to block the release of NO and various chemokines under the action of LPS (Nam et al., 2010). As for curcumin, we did fast dose-response experiments initially to test putative effects of crocin (CR) on the activity of our networks (**Supplementary Figure 1**). In the range 1–100 μM, some inhibitory effects were seen only beyond 20 μM ($n = 3$). We here show that during the first hour of incubation, experiments using CR at 3 ($n = 3$) and 20 μM ($n = 3$) had either negligible or transient inhibitory effects, respectively. These CR effects were accompanied by other different actions caused by the further LPS presence.

In **Figure 3** are shown the results from two exemplary experiments at 3 (**Figures 3A,C**) and 20 (**Figures 3B,D**) μM CR, respectively. At 3 μM it can be observed in **Figure 3A** that the early CR-induced activity was barely modified and LPS induced a very slow, but sizeable increase of activity up to ∼52% at eighth hours. An analysis to test the cumBD plots, shown in **Figure 3C**, suggests that a significant increase by 46% of BD was present at 7 h LPS as compared to control.

On the contrary, at 20 μM CR, the effects were found to be largely depressive. After the CR application (see **Figure 3B**), we detected an early negative peak of 45 and 16%, respectively in inhibitory and excitatory cells, but this effect decayed in the next hour. During the next 7 h in LPS, the activity remained

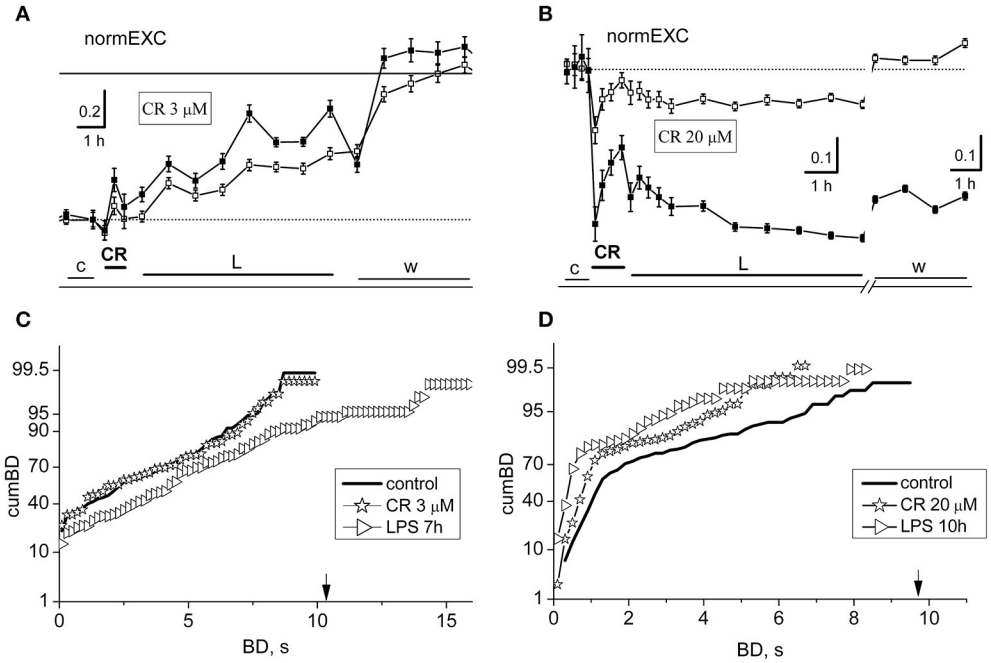

FIGURE 3 | Short- and long-term effects of crocin (CR) in networks treated with LPS. Data in **(A,C)** and those in **(B,D)** belong to the same exemplary experiment. **(A,B)** Plots of normEXC data for two exemplary experiments in which the dishes were treated with crocin (CR) at 3 and 20 μM, respectively. Open and closed symbols indicate excitatory and inhibitory neurons. The continuous line is the fixed threshold. **(C)** Plot of cumBD in control (thick line), in the presence of 3 μM CR (asterisks), and during the seventh hour after the addition of LPS (3 μg/ml; right triangles). These two last curves were significantly different from the control curve with $P < 0.05$. **(D)** Plot of cumBD in control (thick line), in the presence of 20 μM CR (asterisks), and during the 10th h after the addition of LPS (right triangles). The vertical arrow indicates the fixed threshold. These last curves were significantly different from the control curve with $P < 0.05$. The highest dose of CR prevented the late excitatory LPS responses.

stable but depressed. Furthermore, by analyzing in **Figure 3D** the cumBD plots, it can be concluded that the curves shifted to the left, suggesting that the burst durations decreased, in line with a weaker activity of the network.

On the whole, it can be concluded that CR is able to block the LPS-induced inflammation only at concentrations higher than 15–20 μM. Interestingly, at these concentrations, although the fast earlier transient inhibitory effects were present, a strong general inhibition of activity remained and was washed out only during recovery.

Transient and Long Term Effects of RE: LPS-Induced Inflammation Is Blocked at 1 μM RE

We studied the action of resveratrol (RE) at concentrations in the lower micromolar range, much lower than those reported in many papers present in the literature (Gambini et al., 2015). As reported above for CU, also RE has been described to inhibit the release of glutamate from nerve terminals (Chang and Wang, 2009). These authors showed that the threshold to detect the start of the inhibition was between 10 and 100 nM, but at 1 μM the effect reached the IC_{50}. When tested in our dishes, 200 nM RE (**Figure 4B**) exerted immediately a decrease in the neuronal firing, but the network slowly recovered after ∼30 min.

Due to this reason, we decided to search for a concentration range in which effects were either unable or able to cause changes in the plots of normEXC and the cumBD in opposite directions. In **Figures 4A,B** are shown two exemplary experiments in which RE applied at 50 and 200 nM induced a negligible or a fast inhibitory effect, respectively, in the normEXC plots. The average duration of these intrinsic responses of RE were never longer than ∼45 min. The subsequent application of LPS was tested every hour over 8 h.

In **Figures 4A,B** it can be observed that the development of the response was divergent, i.e.: normEXC data either increased in **Figure 4A** (at 50 nM) or decreased in **Figure 4B** (at 200 nM), respectively, suggesting that the drug preconditioning produced opposite results during the LPS action. Similar results were also seen in other 4 dishes at 50 nM and 3 dishes at 200 nM. The fluctuations of the activity shown in **Figure 4A**, during control and RE, were not significant up to the first hour of LPS application, whereas from 2 to 8 h in LPS, the activity increased as expected by 71% for excitatory cells and 127% for inhibitory cells (see in Gullo et al., 2014). On the other hand, in **Figure 4B**, the normEXC slowly decayed during the following 8 h.

To complete the analysis, we computed the distribution of the BD durations of these experiments and the results are shown in **Figures 4C,D**, respectively. Although the profile properties of the control curves (thick line) were different in the two experiments, the data acquired during the presence of RE alone show, in both cases, a cumBD curve (see the asterisk symbols) very similar to control. On the contrary, comparing the last hours of LPS

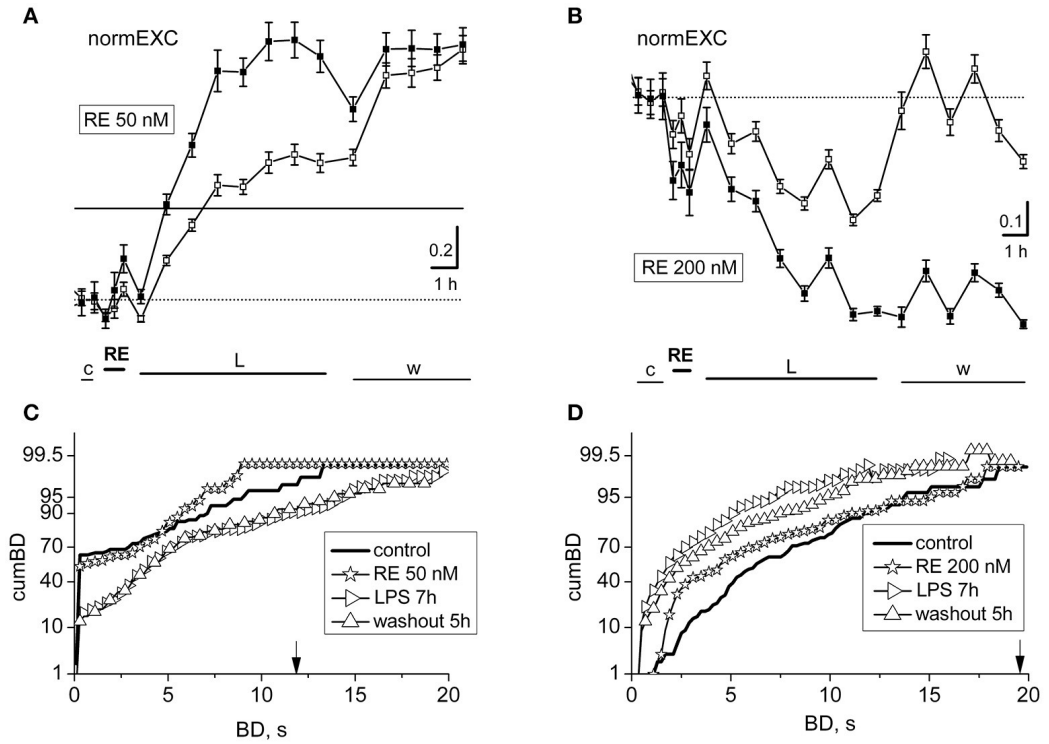

FIGURE 4 | Effects of resveratrol (50 or 200 nM) on LPS responses. Data in **(A,B)** and **(C,D)** derive from two experiments performed on a single dish at 14 or 20 DIV. **(A,B)** Plots of normalized excitability following application of resveratrol (RE) 50 nM **(A)** or 200 nM **(B)** and LPS (3 μg/ml). The continuous line is the fixed threshold. Note that in **(A)**, the late excitatory responses to LPS were not prevented, whereas in **(B)** the responses were inhibited. **(C,D)** Plots of cumBD in the same conditions as in **(A,B)**. The vertical arrow indicates the fixed threshold.

(right-pointing triangles) data in **Figure 4C** suggest that the 90% cumBD showed an 87% increase, and in 4 D a dramatic decrease, thus confirming that the RE doses used in these experiments either did not block or completely blocked the LPS action, respectively.

In Agreement with Data Reported in Hippocampal Pyramidal Neurons, EX-4 Triggered Fast Transient Pro-Excitatory Responses

In hippocampal pyramidal neurons *in vivo*, it has been shown that a brief (1 s) application of GLP-1 (7–36) amide, a naturally produced active fragment of GLP-1, first rapidly increased (i.e., 1 s) and then slowly decreased (>10 s) single unit firing activity (Oka et al., 1999). Interestingly, these effects were inhibited either by the specific GLP-1 receptor antagonist, exendin (9–39) or by the specific non-NMDA glutamate receptor antagonist 6-cyano-7-nitroquinoxaline-2,3-dione (CNQX), suggesting that the initial GLP-1 action involved a fast and transient release of glutamate.

Our *in vitro* networks of cortical neurons from neonatal mice contain fractions of excitatory and inhibitory cortical neurons, which always fit the standard ratio of 4:1 known to be present in adult cortex (Sahara et al., 2012). As for curcumin and crocin, we did fast dose-response experiments to test putative effects of EX-4 on the activity of our networks (**Supplementary Figure 1**). Surprisingly, we found that in about ∼80% ($n = 24$) of the experiments done using EX-4, the fast effects consisted, as expected, of a transient, brief pro-excitability response, but there were also some networks (∼20%, $n = 6$) whose responses consisted of a transient *decreased* excitability. This was probably caused by unknown heterogeneity factors intrinsic to our cultured preparation of dissociated cells, and therefore we excluded these experiments from the results (although they were characterized by late LPS responses where atypical activity was present). EX-4, from 10 up to 500 nM, elicited an early fast excitatory response and prevented the late LPS-induced neuroinflammation. Amongst the EX-4 experiments in which the early effects of the drug were pro-excitable, in **Figure 5** are shown the results of two experiments, performed in the same dish (at two different DIVs) with 10 and 500 nM EX-4 and one experiment done at 50 nM. In **Figures 5A–C** are compared the normEXC data and it is evident that concentrations differing by 5 and 50 times indeed produced fast transient excitatory effects, suggesting a dose-dependent mechanism of action. On the contrary, the long-term normEXC curves at the end of the LPS application did not show any significant change, thus suggesting that activity of the network was not different with respect to control. We analyzed in **Figures 5D–F** the related

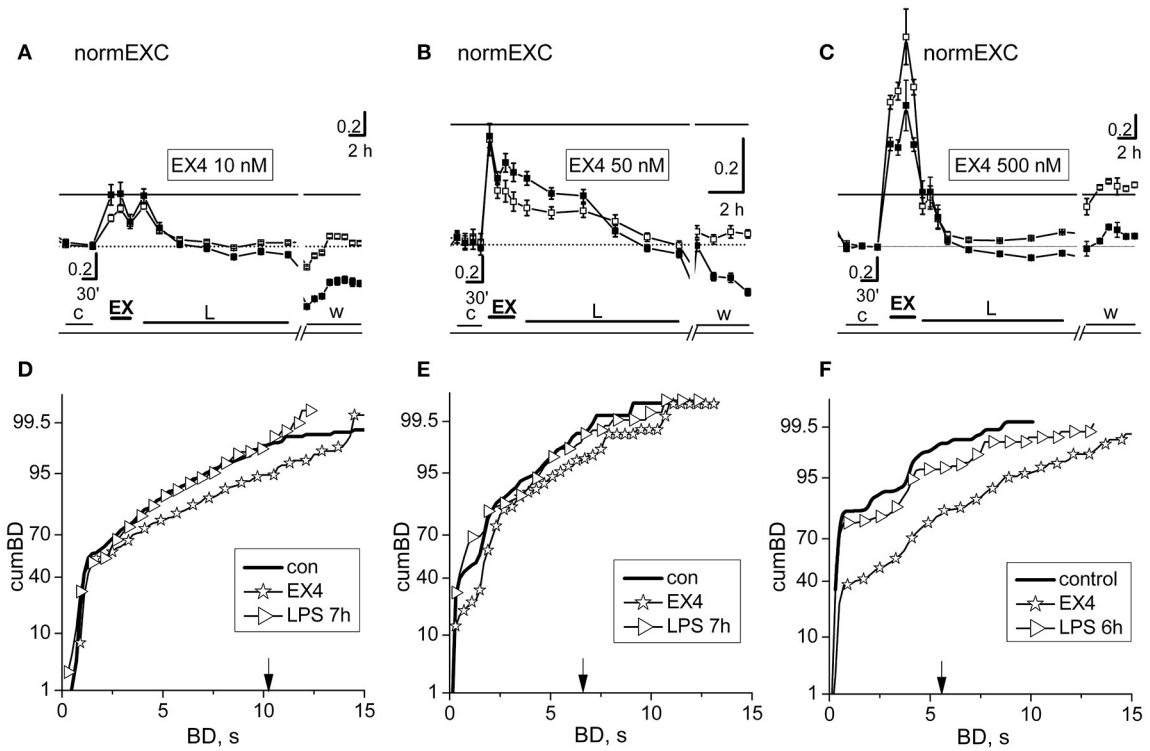

FIGURE 5 | The fast and slow network responses to 10, 50, and 500 nM exendin-4 or exendin-4 + LPS. Data in **(A,D)** and **(C,F)** were obtained from the same dish in two different experiments performed 3 DIV apart. **(A–C)** NormEXC plot obtained with 10, 50, and 500 nM exendin-4 (EX-4) preconditioning, and 3 μg/ml LPS. The continuous line is the fixed threshold. Note that the transient and fast increase of normEXC became progressively higher with increasing EX-4 concentration. **(D–F)** CumBD plots of the experiments shown in **(A–C)**. Control, thick line; EX-4, asterisk; rightward triangles are for the late LPS effects. The vertical arrow indicates the fixed threshold. Note that preconditioning with EX-4 at each concentration tested, effectively prevented the development of the late excitatory responses to LPS.

cumBD histograms in control, during the early EX-4 action and at the end of the long-term LPS action. In the three cases, the early EX-4 histograms showed a conspicuous rightward shift of the curves. On the contrary, the final effect of LPS was either negligible or without atypical bursts showing a BD increase at 90% in the cumBD curves.

The GLP-1 Receptor Antagonist Exendin (9-39) Blocked the Fast Transient EX-4 Effect and the Protective Effect against LPS Neuroinflammation

In order to confirm that the EX-4 action shown in **Figure 5** is really due to the activation of GLP-1Rs, we performed experiments ($n = 6$) in which we preconditioned the EX-4 application (50 nM) with the specific GLP-1R antagonist exendin (9–39) at 100 nM. The results of such an exemplary experiment are shown in **Figure 6**. In **Figure 6A**, the normEXC plot shows that the early application of exendin (9–39) (e) induced a very short (10 min) and small negative deflection, followed by the application of EX-4 (E), and of LPS, which increased the slow normEXC up to 57 ± 3%. After 7 h, the activity stopped increasing. In **Figure 6B** the cumBD plots show that the 90% value was 8.1 and 12.2 s, in control and LPS, respectively, thus suggesting that a normal excitatory action of LPS took place as if EX-4 was not present. On the whole, these experiments confirm that the results shown in **Figure 5** robustly indicate EX-4 as a potent agent to prevent LPS-induced inflammation.

The Levels of TNF-α, Measured at 6 and 12 h after Preconditioning with the Polyphenols or EX-4 in LPS-Treated Dishes, Is Negligible Compared to the Levels Found in Non-preconditioned Dishes

As reported in our previous paper (Gullo et al., 2014) where we showed that minocycline blocked the microglial-release of TNF-α induced by LPS treatment, we performed, for all the polyphenols and EX-4, appropriate experiments to test if the drug concentrations used in the experiments (**Figures 2**–**5**) were able to block also TNF-α production. As shown in **Figure 7**, the amount of this cytokine was, both at 6 and 12 h after LPS treatment, significantly smaller than that found when the preconditioning drugs were absent. On the whole, these results confirm that the drugs used here were not only able to block the atypical seizures induced by LPS, but also the release of TNF-α in the network dishes.

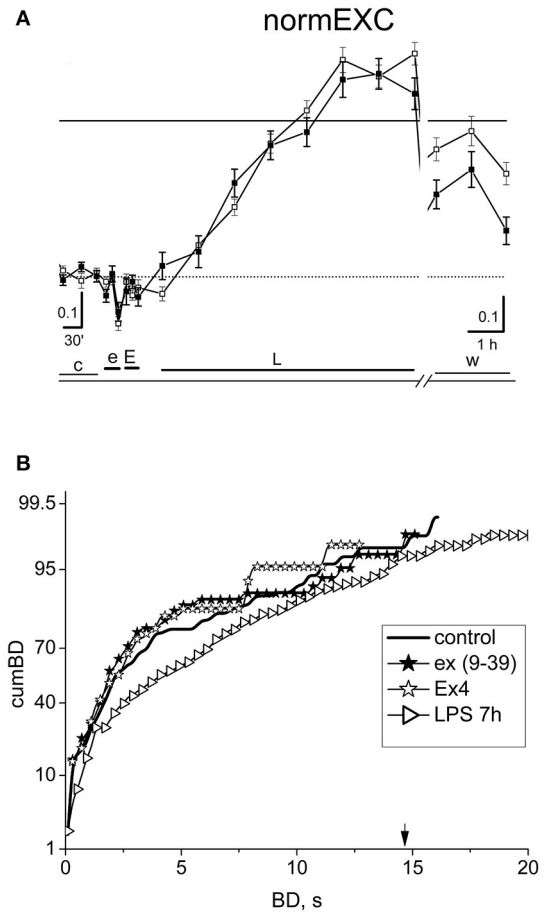

FIGURE 6 | The effect of the specific antagonist of EX-4, exendin (9-39). **(A)** Plot of the normEXC in an experiment in which 100 nM exendin (9–39) (e) was applied for 30 min before 50 nM EX-4 (30 min, E) and the final long-term application of LPS (3 μg/ml). The continuous line is the fixed threshold. **(B)** Plot of cumBD in control (thick line), in the presence of exendin (9–39) (closed asterisk), or EX-4 added on top (open asterisk) and in LPS after 7 h (rightward triangles). The vertical arrow indicates the fixed threshold. The four curves were tested with the non-parametric Wilcoxon signed rank test analysis (exendin (9-39) vs. control, $P < 10^{-5}$; LPS 7 h vs. control, $P < 10^{-10}$; EX4 vs. exendin (9–39), $P = 0.32$). The GLP1-R antagonist blocked the protective effect of EX-4 observed in **Figure 5**, allowing the late excitatory responses to LPS to be expressed.

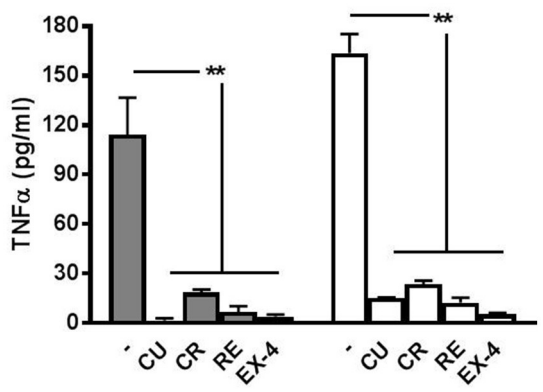

FIGURE 7 | Release of TNF-α at 6 and 12 h after LPS application. The cytokine TNF-α is released from LPS-treated networks but not from networks pre-treated with polyphenols or exendin-4. Graph shows TNF-α concentration 6 h (filled bars) and 12 h (open bars) post-LPS (3 μg/ml) treatment with or without curcumin (CU, 1 μM) crocin (CR, 20 μM), resveratrol (RE, 200 nM) or exendin-4 (EX-4, 30 nM) pre-conditioning. Data are expressed as pg/ml and represent mean ± SEM of three independent experiments. $^{**}P < 0.01$ (ANOVA, Dunnet's test).

DISCUSSION

The present study is the first to demonstrate that polyphenols and the incretin GLP-1 hormone receptor agonist exendin-4 can mimic the anti-inflammatory action of minocycline (Yrjänheikki et al., 1998). In particular, they were able to block the seizure-like atypical activity caused by LPS and the concurrent TNF-α release from microglia, triggered by the Toll-like receptor 4 (TRL4) pathway, in a cortical co-culture of neurons, astrocytes, and microglia. The similar hyperactivity caused by LPS incubation was also observed with the application of a very low (60 pM) TNF-α concentration for ∼12 h (Gullo et al., 2014), probably because of a marked change in the expression of glutamate transporters in astrocytes and microglia, as previously described (Persson et al., 2005; O'Shea et al., 2006; Takaki et al., 2012). The putative role of altered glutamate uptake in mediating components of the sterile inflammation response is currently under investigation in our cortical co-colture system (EW, FG, and ML), which includes functional astocytes (Wanke et al., 2016).

Roles of Microglia

Microglia are highly ramified cells which rapidly scan the local environment and react to its modification (Davalos et al., 2005). Under physiological conditions, microglia react rapidly to neuronal activity by modulating the contacts that their processes continuously establish with synaptic elements (Wake et al., 2009). Amongst the microglial-released molecules with a putative role in neurotransmission, TNF-α was shown to control basal synaptic functions (Santello et al., 2011) as well as plasticity (Stellwagen and Malenka, 2006; Costello et al., 2011), even if this role was attributed to TNF-α produced by astrocytes. However, the astrocytes have often been thought to release TNF-α because cultures of astrocytes are consistently contaminated by microglia (Saura, 2007). In fact, other data reveal no TNFα-encoding transcript in astrocytes (Foo et al., 2011; Zamanian et al., 2012). Thus, the TNF-α that controls several aspects of synaptic transmission is produced by microglial cells. Similarly, TLR4, the specific LPS receptor, was detected in mixed astrocyte/neuronal cultures, but when microglia were removed from astrocyte cultures, TLR4 expression was no longer present (Lehnardt et al., 2002).

Polyphenols and Their Features of Action

Apart from the obvious concentration-dependence, the effects of polyphenols can be subdivided into various types of action according to: (i) time-dependence (fast or long-term), (ii)

cell-dependence (nervous or non-nervous system), and (iii) disease-dependence (i.e., Parkinson's, Alzheimer's diseases, or cancer). CU was found to be neuroprotective in the MPTP model of Parkinson's disease (Ojha et al., 2012) by inhibiting the generation of pro-inflammatory cytokines through the prevention of NF-κB traslocation into the nucleus (Karunaweera et al., 2015). In addition, CU attenuated inflammation in experimental traumatic brain injury (Zhu et al., 2014) and decreased human TNF-α levels (Sahebkara et al., 2016). The nanoencapsulated CU version was also found to reduce β-amyloid-induced cognitive impairment in rats (Hoppe et al., 2013). In the same way as CU, RE was also able to protect dopamine neurons (Zhang et al., 2010) from LPS-induced inflammation. Moreover, RE was found to protect cortical neurons from oxygen-glucose deprivation-induced apoptosis (Gao et al., 2014). In general, RE studies in *in vitro* and *in vivo* showed interesting data of metabolism and bioavailability in various animal models and in humans (Smoliga and Blanchard, 2014; Gambini et al., 2015). Interestingly, RE was shown to ameliorate the clinical severity observed in an animal model of multiple sclerosis, by maintaining the integrity of the blood-brain barrier (Wang et al., 2016). In summary, we believe that the principal mechanisms by which polyphenols were able to protect against LPS neuroinflammation in our system are those related to the TLR4 pathway and microglia activation.

The Action of GLP-1 in the CNS

There is evidence that the gut hormone GLP-1 is also produced in the brain (Korol et al., 2015; Thiebaud et al., 2016). In particular, it was shown that the GLP-1 receptor agonist exendin-4 (EX-4) protected dopaminergic neurons by inhibiting TNF-α release from microglia (Kim et al., 2009). A reduction of brain TNF-α levels was also described in an animal model of Alzheimer disease (AD) exposed to EX-4 treatment (Solmaz et al., 2015). In LPS-treated rats, GLP-1 protected hippocampal neurons from synaptic impairments (Iwai et al., 2014) and inhibited IL-1β production from cultured astrocytes (Iwai et al., 2006). Furthermore, *in vitro* administration of EX-4 in rats increased the expression of the astrocytic glutamate transporter GLT-1 in the hippocampus, lowering extracellular glutamate concentration (Kobayashi et al., 2013). This is in line with the lower long-term excitability data shown in **Figures 5B,C** during LPS inflammation. The results shown in **Figures 5**, **6** split the presumed fast AMPAR-induced transient firing increase following GLP-1R activation (by EX-4), as characterized by Oka et al. (1999), from the long-term effects related to the switch-off of the LPS-induced inflammation.

Our data show, quite importantly, and for the first time, that these effects are not peculiar to the hippocampus *in vivo*, but can also be reproduced *in vitro*, in networks from neocortical dissociated cells containing neurons, astrocytes, and microglia. Moreover, the data shown in **Figure 6** demonstrate that the GLP-1R antagonist exendin (9–39) functionally blocked the ability of EX-4 to counteract the LPS sterile inflammation. Thus in summary, we think that the intriguing connection between the fast electrophysiological responses and the slow microglia pathway merits a specialized investigation, difficult to be carried out by means of our procedures.

Ion Channels in Microglia

Only recently, ion channels have also been described to be functionally expressed in microglia (for a minireview, see Madry and Attwell, 2015). Among the various types of identified channels, the voltage-gated proton channel Hv1 (not present in neurons) was thought to have a dramatic importance during damage induced by ischemic stroke when reactive oxygen species (ROS) are generated (Wu et al., 2012). Accordingly, knock-out mice lacking the Hv1 channel were protected from ROS-mediated neuronal death and brain damage. Furthermore, since acute neuroinflammation provokes intracellular acidification (Tyrtyshnaia et al., 2016), it cannot be excluded that voltage-gated proton channels or acid-sensing channels (Yu et al., 2015) could also be involved in this type of process. Indeed, a polyphenol such as epigallocatechin-3-gallate (EGCG) is known to inhibit the Hv1 currents in microglial BV2 cells (Jin et al., 2012). Interestingly, the reduction in TNF-α release produced by some antidepressants was supposed to be related to the same effect (Song et al., 2012). The putative role of this ionic mechanism in the LPS-induced sterile inflammation is also currently under investigation in our laboratory (EW, FG, and ML).

AUTHOR CONTRIBUTIONS

AC, ML, BC, and EW conceived and designed the research; FG, MC, and AD performed the experiments; EW and BC analyzed the data; EW and AC drafted the manuscript.

FUNDING

This work was funded by Fondo di Ateneo per la Ricerca (FAR grant) from the University of Milano-Bicocca to BC and ML.

SUPPLEMENTARY MATERIAL

The Supplementary Material for this article can be found online at: http://journal.frontiersin.org/article/10.3389/fnins.2017.00500/full#supplementary-material

Supplementary Figure 1 | Dose-response relationship for crocin (CR) and exendin-4 (EX4). Normalized excitability (normEXC) is represented for excitatory and inhibitory neurons.

REFERENCES

Athauda, D., and Foltynie, T. (2016). The glucagon-like peptide 1(GLP) receptor as a therapeuthic target in Parkinson's disease: mechanisms of action. *Drug Discov. Today* 21, 802–818. doi: 10.1016/j.drudis.2016.01.013

Baddeley, R., Abbot, L. F., Booth, M. C., Sengpiel, F., Freeman, T., Wakeman, E. A., et al. (1997). Responses of neurons in primary and inferior temporal visual cortices to natural scenes. *Proc. R. Soc Lond. B Biol. Sci.* 264, 1775–1783. doi: 10.1098/rspb.1997.0246

Becchetti, A., Gullo, F., Bruno, G., Dossi, E., Lecchi, M., and Wanke, E. (2012). Exact distinction of excitatory and inhibitory neurons in neural networks:

a study with GFP-GAD67 neurons optically and electrophysiologically recognized on multielectrode arrays. *Front. Neural Circuits* 6:63. doi: 10.3389/fncir.2012.00063

Chang, Y., and Wang, S. J. (2009). Inhibitory effect of glutamate release from rat cerebrocortical nerve terminals by resveratrol. *Neurochem. Int.* 54, 135–141. doi: 10.1016/j.neuint.2008.11.001

Costello, D. A., Lyons, A., Denieffe, S., Browne, T. C., Cox, F. F., and Lynch, M. A. (2011). Long term potentia-tion is impaired in membrane gly-coprotein CD200-deficient mice: a role for Toll-like receptor activation. *J. Biol. Chem.* 286, 34722–34732. doi: 10.1074/jbc.M111.280826

Davalos, D., Grutzendler, J., Yang, G., Kim, J. V., Zuo, Y., Jung, S., et al. (2005). ATP mediates rapid microglial response to local brain injury *in vivo*. *Nat. Neurosci.* 8, 752–758. doi: 10.1038/nn1472

Foo, L. C., Allen, N. J., Bushong, E. A., Ventura, P. B., Chung, W.-S., Zhou, L., et al. (2011). Development of a method for the purification and culture of rodent astrocytes. *Neuron* 71, 799–811. doi: 10.1016/j.neuron.2011.07.022

Gambini, J., Inglés, M., Olaso, G., Lopez-Grueso, R., Bonet-Costa, V., Gimeno-Mallench, L., et al. (2015). Properties of Resveratrol: *In vitro* and *In vivo* studies about metabolism, bioavailability, and biological effects in animal models and humans. *Oxid. Med. Cell. Longev.* 2015:837042. doi: 10.1155/2015/837042

Gao, D., Huang, T., Jiang, X., Hu, S., Zhang, L., and Fei, Z. (2014). Resveratrol protects primary cortical neuron cultures from transient oxygen glucose deprivation by inhibiting MMP 9. *Mol. Med. Rep.* 9, 2197–2204. doi: 10.3892/mmr.2014.2086

Gullo, F., Amadeo, A., Donvito, G., Lecchi, M., Costa, B., Constanti, A., et al. (2014). Atypical "seizure-like" activity in cortical reverberating networks *in vitro* can be caused by LPS-induced inflammation: a multi-electrode array study from a hundred neurons. *Front. Cell. Neurosci.* 8:361. doi: 10.3389/fncel.2014.00361

Gullo, F., Maffezzoli, A., Dossi, E., and Wanke, E. (2009). Short latency cross-and autocorrelation identify clusters of interacting neurons recorded from multi-electrode arrays. *J. Neurosci. Methods* 181, 186–198. doi: 10.1016/j.jneumeth.2009.05.003

Gullo, F., Maffezzoli, A., Dossi, E., Lecchi, M., and Wanke, E. (2012). Classifying heterogeneity of spontaneous up-states: a method for revealing variations in firing probability, engaged neurons and Fano factor. *J. Neurosci. Methods* 203, 407–417. doi: 10.1016/j.jneumeth.2011.10.014

Gullo, F., Mazzetti, S., Maffezzoli, A., Dossi, E., Lecchi, M., Amadeo, A., et al. (2010). Orchestration of "presto" and "largo" synchrony in up-down activity of cortical networks. *Front. Neural Circuits* 4:11. doi: 10.3389/fncir.2010.00011

Hoppe, J. B., Coradini, K., Frozza, R. L., Oliveira, C. M., Meneghetti, A. B., Bernardi, A., et al. (2013). Free and nanoencapsulated curcumin suppress β-amyloid-induced cognitive impairments in rats: involvement of BDNF and Akt/GSK-3β signaling pathway. *Neurobiol. Learn. Mem.* 106, 134–144. doi: 10.1016/j.nlm.2013.08.001

Isaacson, J. S., and Scanziani, M. (2011). How inhibition shapes cortical activity. *Neuron* 72, 231–243. doi: 10.1016/j.neuron.2011.09.027

Iwai, T., Ito, S., Tanimitsu, K., Udagawa, S., and Oka, J. (2006). Glucagon-like peptide-1 inhibits LPS-induced IL-1beta production in cultured rat astrocytes. *Neurosci. Res.* 55, 352–360. doi: 10.1016/j.neures.2006.04.008

Iwai, T., Sawabe, T., Tanimitsu, K., Suzuki, M., Sasaki-Hamada, S., and Oka, J. (2014). Glucagon-like peptide-1 protects synaptic and learning functions from neuroinflammation in rodents. *J. Neurosci. Res.* 92, 446–454. doi: 10.1002/jnr.23335

Jin, S., Park, M., and Song, J. H. (2012). (-)-Epigallocatechin-3-gallate inhibits voltage-gated proton currents in BV2 microglial cells. *Eur. J. Pharmacol.* 698, 154–160. doi: 10.1016/j.ejphar.2012.11.036

Karunaweera, N., Raju, R., Gyengesi, E., and Muench, G. (2015). Plant polyphenols as inhibitors of NF-κB induced cytokine production—a potential anti-inflammatory treatment for Alzheimer's disease? *Front. Mol. Neurosci.* 8:24. doi: 10.3389/fnmol.2015.00024

Kettenmann, H., Hanisch, U. K., Noda, M., and Verkhratsky, A. (2011). Physiology of microglia. *Physiol. Rev.* 91, 461–553. doi: 10.1152/physrev.00011.2010

Kettenmann, H., Kirchhoff, F., and Verkhratsky, A. (2013). Microglia: new roles for the synaptic stripper. *Neuron* 77, 10–18. doi: 10.1016/j.neuron.2012.12.023

Kim, S., Moon, M., and Park, S. (2009). Exendin-4 protects dopaminergic neurons by inhibition of microglial activation and matrix metalloproneinase-3 expression in an animal model of Perkinson's disease. *J. Endocrinol.* 202, 431–439. doi: 10.1677/JOE-09-0132

Kobayashi, K., Iwai, T., Sasaki-Hamada, S., Kamanaka, G., and Oka, J. (2013). Exendin (5-39), an antagonist of GLP-1 receptor, modulates synaptic transmission via glutamate uptake in the dentate gyrus. *Brain Res.* 1505, 1–10. doi: 10.1016/j.brainres.2013.01.012

Korol, S. V., Jin, Z., Babateen, O., and Birnir, B. (2015). GLP-1 and Exendin-4 transiently enhance GABAA receptor-mediated synaptic and tonic currents in rat hippocampal CA3 pyramidal neurons. *Diabetes* 64, 79–89. doi: 10.2337/db14-0668

Lehnardt, S., Lachance, C., Patrizi, S., Lefebvre, S., Follett, P. L., Jensen, F. E., et al. (2002). The toll-like receptor TLR4 is necessary for lipopolysaccharide-induced oligo-dendrocyte injury in the CNS. *J. Neurosci.* 22, 2478–2486.

Lin, T. Y., Lu, C. W., Huang, S. K., and Wang, S. J. (2012). Curcumin inhibits glutamate release from rat prefrontal nerve endings by affecting vesicle mobilization. *Int. J. Mol. Sci.* 13, 9097–9109. doi: 10.3390/ijms13079097

Lin, T. Y., Lu, C. W., Wang, C. C., Wang, Y. C., and Wang, S. J. (2011). Curcumin inhibits glutamate release in nerve terminals from rat prefrontal cortex: possible relevance to its antidepressant mechanism. *Prog. Neuro Psychopharm. Biol. Psychol.* 35, 1785–1793. doi: 10.1016/j.pnpbp.2011.06.012

Lofrumento, D. D., Nicolardi, G., Cianciulli, A., De Nuccio, F., La Pesa, V., Carofiglio, V., et al. (2014). Neuroprotective effects of resveratrol in an MPTP mouse model of Parkinson's-like disease: possible role of SOCS-1 in reducing pro-inflammatory responses. *Innate Immun.* 20, 249–260. doi: 10.1177/1753425913488429

Madry, C., and Attwell, D. (2015). Receptors, ion channels, and signaling mechanisms underlying microglial dynamics. *J. Biol. Chem.* 290, 12443–12450. doi: 10.1074/jbc.R115.637157

Marangoni, D., Falsini, B., Piccardi, M., Ambrosio, L., Minnella, A. L., Savastano, M. C., et al. (2013). Functional effect of Saffron supplementation and risk genotypes in early age-related macular degeneration: a preliminary report. *J. Trans. Med.* 11:228. doi: 10.1186/1479-5876-11-228

Nam, K. N., Park, Y. M., Jung, H. J., Lee, J. Y., Min, B. D., Park, S. U., et al. (2010). Anti-inflammatory effects of crocin and crocetin in rat brain microglial cells. *Eur. J. Pharmacol.* 648, 110–116. doi: 10.1016/j.ejphar.2010.09.003

Ojha, R. P., Rastogi, M., Devi, B. P., Agrawal, A., and Dubey, G. P. (2012). Neuroprotective effect of curcuminoids against inflammation-mediated dopaminergic neurodegeneration in the MPTP model of Parkinson's disease. *J. Neuroimmune Pharmacol.* 7, 609–618. doi: 10.1007/s11481-012-9363-2

Oka, J. I., Goto, N., and Kameyama, T. (1999). Glucagon-like peptide-1 modulates neuronal activity in the rat's hippocampus. *Neuroreport* 10, 1643–1646. doi: 10.1097/00001756-199906030-00004

O'Shea, R. D., Lau, C. L., Farso, M. C., Diwakarla, S., Zagami, C. J., Svendsen, B. B., et al. (2006). Effects of lipopolysaccharide on glial phenotype and activity of glutamate transporters: evidence for delayed up-regulation and redistribution of GLT-1. *Neurochem. Int.* 48, 604–610. doi: 10.1016/j.neuint.2005.12.028

Persson, M., Brantefjord, M., Hansson, E., and Rönnbäck, L. (2005). Lipopolysaccharide increases microglial GLT-1 expression and glutamate uptake capacity *in vitro* by a mechanism dependent on TNF-alpha. *Glia* 51, 111–120. doi: 10.1002/glia.20191

Pocock, J. M., and Kettenmann, H. (2007). Neurotransmitter receptors on microglia. *Trends Neurosci.* 30, 527–535. doi: 10.1016/j.tins.2007.07.007

Sahara, S., Yanagawa, Y., O'Learly, D. M., and Stevens, C. F. (2012). The fraction of cortical GABAergic neurons is constant from near the start of cortical neurogenesis to adulthood. *J. Neurosci.* 32, 4755–4761. doi: 10.1523/JNEUROSCI.6412-11.2012

Sahebkara, A., Cicero, A. F. G., Simental-Mendíad, L. E., Aggarwale, B. B., and Gupta, S. C. (2016). Curcumin downregulates human tumor necrosis factor-α: a systematic review and meta-analysis ofrandomized controlled trials. *Pharmacol. Res.* 107, 234–242. doi: 10.1016/j.phrs.2016.03.026

Santello, M., Bezzi, P., and Volterra, A. (2011). TNFα controls glutamater-gic gliotransmission in the hip-pocampal dentate gyrus. *Neuron* 69, 988–1001. doi: 10.1016/j.neuron.2011.02.003

Saura, J. (2007). Microglial cells in astroglial cultures: a cautionary note. *J. Neuroinflammation* 4:26. doi: 10.1186/1742-2094-4-26

Smoliga, J. M., and Blanchard, O. (2014). Enhancing the delivery of resveratrol in humans: If low availability is the problem, what is the solution? *Molecules* 19, 17154–17172. doi: 10.3390/molecules191117154

Solmaz, V., Çınar, B. P., Yiğittürk, G., Çavuşoğlu, T., Taşkıran, D., and Erbaş, O. (2015). Exenatide reduces TNF-α expression and improves hippocampal neuron numbers and memory in streptozotocin treated rats. *Eur. J. Pharmacol.* 765, 482–487. doi: 10.1016/j.ejphar.2015.09.024

Song, J. H., Marszalec, W., Kai, L., Yeh, J. Z., and Narahashi, T. (2012). Antidepressants inhibit proton currents and tumor necrosis factor-α production in BV2 microglial cells. *Brain Res.* 1435, 15–23. doi: 10.1016/j.brainres.2011.11.041

Stellwagen, D., and Malenka, R. C. (2006). Synaptic scaling mediated by glial TNF-α. *Nature* 440, 1054–1059. doi: 10.1038/nature04671

Takaki, J., Fujimori, K., Miura, M., Suzuki, T., Sekino, Y., and Sato, K. (2012). L-glutamate released from activated microglia downregulates astrocytic L-glutamate transporter expression in neuroinflammation: the 'collusion' hypothesis for increased extracellular L-glutamate concentration in neuroinflammation. *J. Neuroinflammation* 9:275. doi: 10.1186/1742-2094-9-275

Teich, M. C. (1989). Fractal character of the auditory neural spike train. *IEEE Trans. Biomed. Eng.* 36, 150–160. doi: 10.1109/10.16460

Thiebaud, N., Llewellyn-Smith, I. J., Gribble, F., Reimann, F., Trapp, S., and Fadool, D. A. (2016). The incretin hormone glucagon-like peptide 1 increases mitral cell excitability by decreasing conductance of a voltage-dependent potassium channel. *J. Physiol.* 594, 2607–2628. doi: 10.1113/JP272322

Tyrtyshnaia, A. A., Lysenko, L. V., Madamba, F., Manzhulo, I. V., Khotimchenko, M. Y., and Kleschevnikov, A. M. (2016). Acute neuroinflammation provokes intracellular acidification in mouse hippocampus. *J. Neuroinflammation* 13:283. doi: 10.1186/s12974-016-0747-8

Wake, H., Moorhouse, A. J., Jinno, S., Kohsaka, S., and Nabekura, J. (2009). Resting microglia directly monitor the functional state of synapses *in vivo* and determine the fate of ischemic terminals. *J. Neurosci.* 29, 3974–3980. doi: 10.1523/JNEUROSCI.4363-08.2009

Wang, D., Li, S. P., Fu, J. S., Zhang, S., Bai, L., and Guo, L. (2016). Resveratrol defends blood-brain barrier integrity in experimental autoimmune encephalomyelitis mice. *J. Neurophysiol.* 116, 2173–2179. doi: 10.1152/jn.00510.2016

Wanke, E., Gullo, F., Dossi, E., Valenza, G., and Becchetti, A. (2016). Neuron-glia crosstalk revealed in reverberating networks by simultaneous extracellular recording of spikes and astrocytes' glutamate transporter and K^+ currents. *J. Neurophysiol.* 28, 2706–2719. doi: 10.1152/jn.00509.2016

Wu, L. J., Wu, G., Akhavan Sharif, M. R., Baker, A., Jia, Y., Fahey, F. H., et al. (2012). The voltage-gated proton channel Hv1 enhances brain damage from ischemic stroke. *Nat. Neurosci.* 15, 565–573. doi: 10.1038/nn.3059

Yrjänheikki, J., Keinänen, R., Pellikka, M., Hökfelt, T., and Koistinaho, J. (1998). Tetracyclines inhibit microglial activation and are neuroprotective in global brain ischemia. *Proc. Natl. Acad. Sci. U.S.A.* 95, 15769–15774. doi: 10.1073/pnas.95.26.15769

Yu, X. W., Hu, Z. L., Ni, M., Fang, P., Zhang, P. W., Shu, Q., et al. (2015). Acid-sensing ion channels promote the inflammation and migration of cultured rat microglia. *Glia* 63, 483–496. doi: 10.1002/glia.22766

Zamanian, J. L., Xu, L., Nouri, N., Zhou, L., Giffard, R. G., and Barres, B. A. (2012). Genomic analysis of reactive astrogliosis. *J. Neurosci.* 32, 6391–6419. doi: 10.1523/JNEUROSCI.6221-11.2012

Zhang, F., Shi, J. S., Zhou, H., Wilson, B., Hong, J. S., and Gao, H. M. (2010). Resveratrol protects dopamine neurons against lipopolysaccharide-induced neurotoxicity through its anti-inflammatory actions. *Mol. Pharmacol.* 78, 466–477. doi: 10.1124/mol.110.064535

Zhu, H. T., Bian, C., Yuan, J. C., Chu, W. H., Xiang, X., Chen, F., et al. (2014). Curcumin attenuates acute inflammatory injury by inhibiting the TLR4/MyD88/NF-κB signaling pathway in experimental traumatic brain injury. *J. Neuroinflammation* 11:59. doi: 10.1186/1742-2094-11-59

Conflict of Interest Statement: The authors declare that the research was conducted in the absence of any commercial or financial relationships that could be construed as a potential conflict of interest.

frontiers in Aging Neuroscience

ORIGINAL RESEARCH
published: 29 August 2017
doi: 10.3389/fnagi.2017.00281

Astrocyte Senescence and Metabolic Changes in Response to HIV Antiretroviral Therapy Drugs

*Justin Cohen, Luca D'Agostino, Joel Wilson, Ferit Tuzer and Claudio Torres**

Department of Pathology and Laboratory Medicine, Drexel University College of Medicine, Philadelphia, PA, United States

With the advent of highly active antiretroviral therapy (HAART) survival rates among patients infected by HIV have increased. However, even though survival has increased HIV-associated neurocognitive disorders (HAND) still persist, suggesting that HAART-drugs may play a role in the neurocognitive impairment observed in HIV-infected patients. Given previous data demonstrating that astrocyte senescence plays a role in neurocognitive disorders such as Alzheimer's disease (AD), we examined the role of HAART on markers of senescence in primary cultures of human astrocytes (HAs). Our results indicate HAART treatment induces cell cycle arrest, senescence-associated beta-galactosidase, and the cell cycle inhibitor p21. Highly active antiretroviral therapy treatment is also associated with the induction of reactive oxygen species and upregulation of mitochondrial oxygen consumption. These changes in mitochondria correlate with increased glycolysis in HAART drug treated astrocytes. Taken together these results indicate that HAART drugs induce the senescence program in HAs, which is associated with oxidative and metabolic changes that could play a role in the development of HAND.

Keywords: cellular senescence, highly active antiretroviral therapy, HIV, astrocytes, glycolysis, HIV-associated neurocognitive disorders

OPEN ACCESS

Edited by:
Margaret Su-chun Ho,
ShanghaiTech University, China

Reviewed by:
Alexander A. Mongin,
Albany Medical College, United States
Qingqing Lu,
Tongji University, China

****Correspondence:***
Claudio Torres
claudio.torres@drexelmed.edu

Received: *10 May 2017*
Accepted: *11 August 2017*
Published: *29 August 2017*

Citation:
Cohen J, D'Agostino L, Wilson J, Tuzer F and Torres C (2017) Astrocyte Senescence and Metabolic Changes in Response to HIV Antiretroviral Therapy Drugs. Front. Aging Neurosci. 9:281. doi: 10.3389/fnagi.2017.00281

INTRODUCTION

With the advent of highly active antiretroviral therapy (HAART), HIV infection has transitioned from an acute, terminal illness to a chronic but manageable condition (Bhatia et al., 2012). The HIV-infected population is consequently aging, and it had been projected that by 2015 more than 50% of the HIV-infected population in the United States would be 50 years of age and older. While this is undoubtedly a major success, aging is a significant risk factor for disease (Niccoli and Partridge, 2012) and HIV patients experience a variety of age-related complications, suggesting premature aging (Capeau, 2011). One such complication is a series of neurological problems collectively known as HIV-associated neurocognitive disorders (HAND) (Heaton et al., 2010). HAND can be categorized with increasing severity from asymptomatic neurocognitive impairment, mild neurocognitive disorder, and HIV-associated dementia. While the prevalence of HIV-associated dementia in the post-HAART era has decreased in HIV-infected patients, asymptomatic neurocognitive impairment and mild neurocognitive disorder have increased (Heaton et al., 2010). The persistence of neurological problems in HIV-infected patients remains a major public health issue and the identification of mechanisms involved may lead to potential treatments.

While beneficial in their suppression of HIV, HAART drugs have a multitude of side effects including myopathy, hepatotoxicity, hypersensitivity reactions, lipodystrophy, and insulin resistance (Feeney and Mallon, 2010). *In vitro*, there has been evidence of HAART drugs inducing ER stress (Sato et al., 2012), unfolded protein response (Zhou et al., 2005), and changes to cellular metabolism (Arend et al., 2013). These side effects suggest that cells may undergo a great deal of stress in response to HAART drugs. One possible way that cells can respond to stress is to undergo cellular senescence.

Cellular senescence is an age-related phenotype originally discovered to occur *in vitro* after extensive cell passaging, and is associated with the telomere attrition that occurs with successive rounds of DNA replication (Bodnar et al., 1998). Senescence also occurs prematurely in response to other mediators. Oncogene-induced senescence can occur via the activation of tumorigenic signals such as telomere dysfunction (Suram et al., 2012) and oncogenic RAS (Serrano et al., 1997). Stress-induced premature senescence can occur in response to cytotoxic stimuli such as proteasome inhibition and oxidative stress (Chen et al., 1995; Bitto et al., 2010). Several classes of HAART drugs including nucleoside reverse transcriptase inhibitors and protease inhibitors have been shown to cause stress-induced premature senescence (Caron et al., 2008; Lefevre et al., 2010; Hernandez-Vallejo et al., 2013; Afonso et al., 2015), suggesting that HIV patients may be experiencing cellular senescence. Evidence for cellular senescence during HIV comes from a previous study showing increased senescent $CD8^+$ T-cells isolated from HIV patients (Chou et al., 2013). Regardless of the inducer, there are several phenotypes and biomarkers generally shared among senescent cells. These include cell cycle arrest, increased senescence-associated beta-galactosidase (SA β-gal) activity, expression of the cell cycle inhibitors p16 and p21, mitochondrial dysfunction, and the secretion of pro-inflammatory cytokines and proteases known as the senescence-associated secretory phenotype (SASP) (Rodier and Campisi, 2011). The pro-inflammatory environment created by the SASP has major implications for age-related decline in tissues and may contribute the chronic inflammation observed in the central nervous system (CNS) in neurological diseases such as Parkinson's and AD (Jabbari Azad et al., 2014; Yan et al., 2014) and HAND.

Senescence in the CNS is an emergent concept and few studies have examined its role as a contributor to neurodegenerative disease. Astrocytes are the most abundant cells in the brain and are involved in a variety of functions to maintain CNS homeostasis such as CNS metabolism, blood brain barrier maintenance, and ion regulation (Stobart and Anderson, 2013). Due to their numerous functions in the CNS, disruption of their physiological functions due to senescence could be a major contributor to neurological disease. Our recent work demonstrates a decrease in astrocyte-enriched genes during senescence, indicating a loss in their differentiated function (Crowe et al., 2016). This could impact brain physiology in Alzheimer's patients where we have previously reported a significant increase in the population of senescent astrocytes (Bhat et al., 2012). In the present study, we evaluated the role of HAART drug exposure on astrocyte senescence. Human astrocytes (HAs) treated with a clinically relevant combination of nucleotide reverse transcriptase inhibitors and protease inhibitors underwent cellular senescence with expression of p16, p21, SA β-gal, and pro-inflammatory cytokines. The process was accompanied with increased oxidative stress, mitochondrial oxygen consumption, and changes in glucose metabolism with increased glucose uptake and upregulation in glycolytic intermediates. To our knowledge, our findings are the first to demonstrate HAART drug-induced senescence in a CNS cell type, which may have implications for HAND.

MATERIALS AND METHODS

Cell Culture and Drug Treatments

Human astrocytes were cultured at 37°C, 5% CO_2 in astrocyte medium supplemented with 2% fetal bovine serum, growth supplement, and penicillin/streptomycin all obtained from ScienCell Research Laboratories (Carlsbad, CA, United States). Cells were cultured until they reached ∼80% confluence before passaging. At each passage, astrocytes were trypsinized, counted, and the cumulative population doubling level (CPDL) was calculated as we have previously described (Bitto et al., 2010). Cells were treated every 2–3 days for up to a week with either 0.3% DMSO as a vehicle control or the HAART drug combinations of abacavir (ABC) 10 μM and lamivudine (3TC) 5 μM or ABC, 3TC, and ritonavir (RTV) 1 μM. For the long-term experiments, cells were treated for up to 4 weeks with either 0.2% dimethyl sulfoxide (DMSO) as a vehicle control or the combinations of ABC 3 μM, 3TC 1.9 μM, atazanavir (ATV) 50 nM, and RTV 100 nM; or tenofovir (TDF) 100 nM, emtricitabine (FTC) 1.2 μM, ATV, and RTV; or TDF, FTC, and efavirenz (EFV) 125 nM. All HAART drugs were provided by the NIH AIDS Reagent Program.

Senescence-Associated β-Galactosidase Activity Assay

Senescence-associated beta-galactosidase staining was performed as previously described (Dimri et al., 1995). Briefly, following exposure to the HAART drug combinations or DMSO, astrocytes were fixed in 2% formaldehyde/0.2% glutaraldehyde for 3 min and stained for SA β-gal activity overnight. The cells were counted and positive (blue) cells were expressed as a percentage of the total. At least 200 cells were counted.

Immunoblotting

Following indicated treatment times, HAs were lysed in radioimmunoprecipitation assay (RIPA) buffer. Western blot analysis was performed under standard conditions using 15 μg of total cell proteins. Membranes were probed for antibodies against p16 [sc-56330 (**JC8**), monoclonal; BD Biosciences, San Jose, CA, United States]; p21 [sc-756 (**H-164**), polyclonal; Santa Cruz Biotechnology, Santa Cruz, CA, United States]; phosphorylated (9211) and total p38 (9212) both polyclonal (Cell Signaling Technology, Danvers, MA, United States); phosphorylated (3033) and total p65 (3034) both polyclonal (Cell Signaling

Technology, Danvers, MA, United States); Oxphos cocktail of mitochondrial ETC complexes I [ab110242 (**20E9DH10C12**)], II [ab14714 (**21A11AE7**)], III [ab14745 (**13G12AF12BB11**)], IV [ab110258 (**12C4F12**)], and V [ab14748 (**15H4C4**)] (monoclonal; Abcam, Cambridge, MA, United States); β-actin [A00702 **(2D1D10)**, monoclonal; Genscript, Piscataway, NJ, United States); and β-tubulin [sc-9104 (**H-235**), polyclonal; Santa Cruz Biotechnology, Santa Cruz, CA, United States). Clone numbers are in bold.

Total Cellular ROS, Mitochondrial ROS, Mitochondrial Membrane Potential, Mitochondrial Mass, and Glucose Uptake Assessments

Determination of total cellular reactive oxygen species (ROS), mitochondrial ROS, mitochondrial membrane potential, mitochondrial mass, and glucose uptake assessments was made using flow cytometry as previously described (Nacarelli et al., 2016). Total cellular ROS was detected by incubating cells with 10 μM 2′7′-dichlorofluorescein diacetate (DCF-DA; Sigma-Aldrich, St. Louis, MO, United States) in 1% fetal bovine serum-supplemented MEM and washing twice with Krebs Ringer phosphate glucose buffer (145 mM NaCl, 5.7 mM NaH_2PO_4, 4.86 mM KCl, 0.54 mM $CaCl_2$, 1.22 mM $MgSO_4$, and 5.5 mM glucose) following incubation. All other compounds were washed with PBS. Mitochondrial superoxide levels were assayed by incubating the cells with 5 μM Mito-Sox Red (Molecular Probes, Waltham, MA, United States). Mitochondrial membrane potential was detected by incubating cells with 25 nM tetramethylrhodamine (TMRE) (Molecular Probes, Waltham, MA, United States). Mitochondrial mass was evaluated by incubating the cells with 100 nM Mito-tracker Green FM (Molecular Probes, Waltham, MA, United States). The glucose analog 2-NBDG uptake was detected by incubating the cells with 10 μM of 2-NBDG (Molecular Probes, Waltham, MA, United States). For the previous analyses, incubation was performed at 37°C in 5% CO_2 for 30 min except 2-NBDG which required 90 min. Cells were collected in 0.25% trypsin-EDTA with complete medium. Cells were analyzed by flow cytometry using a Guava EasyCyte Mini and the Guava Express Plus program (Guava Technologies, Hayward, CA, United States). Acquisitions involved 5000 events.

Analysis of Inflammatory Factors Secreted by Astrocytes

Following the end of the treatment period, HAs were incubated with serum-free MCDB105 media. After a 24-h incubation period, media were collected and cells were

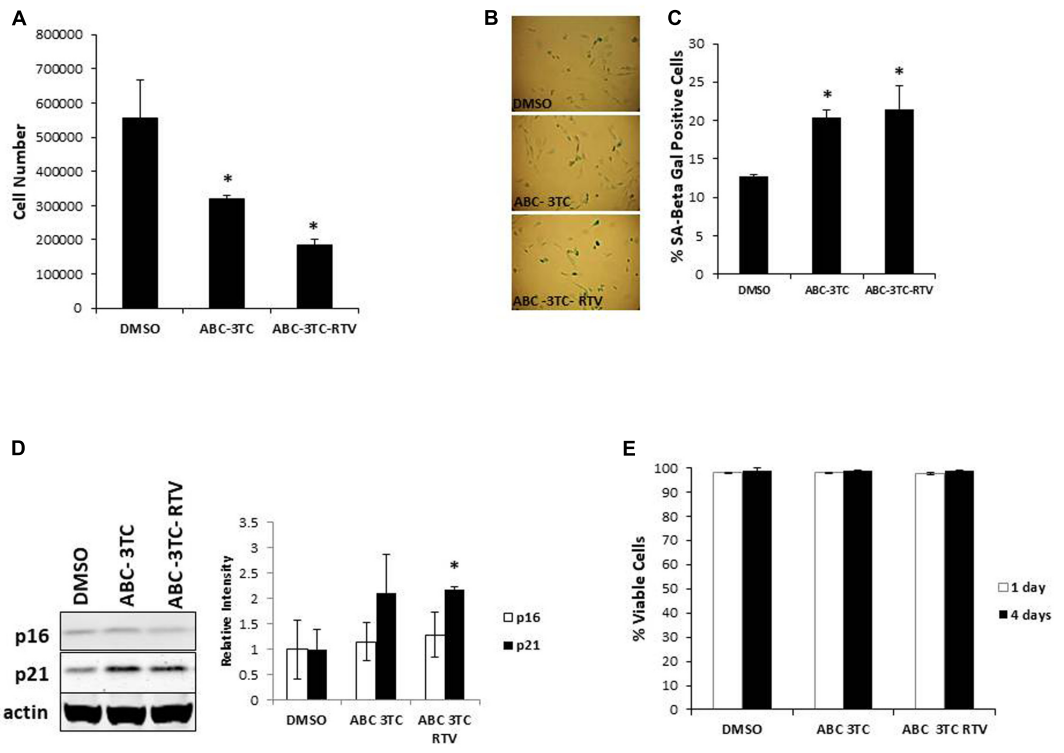

FIGURE 1 | Expression of senescence markers in HAART drug treated human astrocytes (HAs). Human astrocytes were treated with the following HAART concentrations: abacavir (ABC) 10 μM, lamivudine (3TC) 5 μM, and ritonavir (RTV) 1 μM for 7 days **(A–D)** or 4 days **(E)** in complete astrocyte media. **(A)** Cell proliferation. **(B)** Representative SA β-gal images displayed at 20× of HAs stained for SA β-gal 1 week after HAART treatment. **(C)** Quantification of B. **(D)** *Left*—representative Western blot illustrating protein levels of senescence markers p16 and p21. *Right*—quantification of the blots. **(E)** Viability, astrocytes were incubated with Guava Viacount reagent for 5 min prior to detection by flow cytometry. **p*-value < 0.05, $n = 3$, error bars are SD.

trypsinized and counted to determine the cell number for normalization. Human Cytokine Array C5 (RayBiotech, Norcross, GA, United States) was used to evaluate secreted inflammatory factors in the conditioned media according to the company's protocol. The intensity of the signal on the array membranes was quantified by densitometry using ImageJ software and normalized to cell number. The HAART drug treated values were then set as relative to control values. Samples that had no change in expression due to levels being undetectable from background were set to 1. Interleukin-6 (IL-6) detection was performed via the Human IL-6 Quantikine ELISA kit (R&D Systems, Minneapolis, MN, United States) according to the product manual using conditioned media as described above. Absorbance was measured at 450 nm.

Oxygen Consumption Measurements

Oxygen consumption was determined by using a Seahorse XF24 Bioanalyzer (Seahorse Bioscience, North Billerica, MA, United States) and the XF Cell Mito Stress Test Kit as previously reported (Nacarelli et al., 2016). Cells were seeded after treatment at 25,000 cells per well. The Bioanalyzer was pre-loaded with oligomycin, carbonilcyanide *p*-triflouromethoxyphenylhydrazone (FCCP), and rotenone/antimycin A prior to measurement. Oxygen consumption was measured in triplicate before and after consecutive addition of oligomycin, FCCP, and rotenone/antimycin A. Respiration rates and proton leak were assessed as previously described (Hill et al., 2012) based upon oxygen consumption rate measurements. Basal respiration represents the initial oxygen consumption rate, while maximal respiration signifies oxygen consumption after FCCP addition. ATP-linked respiration denotes the oligomycin-sensitive oxygen change to basal oxygen consumption rate. Proton leak corresponds to the oligomycin-insensitive oxygen consumption rate. Non-mitochondrial sources of oxygen consumption were subtracted by normalizing to the rotenone/antimycin A-insensitive oxygen consumption rate. Acidification was based on the extracellular acidification rate. Data were normalized to cell number.

Metabolite Measurements

Metabolite measurements were performed by Human Metabolome Technologies America Inc. (Boston, MA, Unites States) using their C-Scope analysis. Samples were collected according to their protocol and sent overnight on dry ice, after which capillary electrophoresis mass spectrometry was performed. Quantifications were performed by hierarchical cluster analysis (HCA) and principal component analysis (PCA) by Human Metabolome Technologies America Inc.'s statistical software.

Statistical Analysis

Data were either compared using a two-tailed Student's *t*-test when two groups were involved or one-way analysis of variance (ANOVA) followed by Bonferroni correction when three groups were analyzed. Normality was determined using a Shapiro–Wilk Test with the caveat that low sample sizes can reduce the accuracy of normality tests. Means were derived from at least three independent experiments. Error bars on graphs reflect standard deviation (SD). Statistical significance was considered at $p < 0.05$.

TABLE 1 | Senescence-associated secretory phenotype of ABC–3TC–RTV-treated human astrocytes.

Name	ABC–3TC–RTV	Name continued	ABC–3TC–RTV continued
Angiogenin	0.53	IL-8	0.75
BDNF	0.59	IP-10	0.77
EGF	0.86	Leptin	1.00
Eotaxin-1	0.81	LIF	0.98
Eotaxin-2	0.89	Light	1.05
Eotaxin-3	0.83	MCP-1	0.73
FGF-4	0.75	MCP-4	1.00
FGF-6	0.82	M-CSF	0.82
FGF-9	1.27	MDC	1.74
Fractalkine	1.03	MIF	1.31
GCP-2	1.66	MIG	1.00
G-CSF	1.00	MIP-1 beta	1.16
GDNF	1.06	NAP-2	0.93
GM-CSF	1.00	NT-3	0.60
GRO	0.73	NT-4	0.58
GRO alpha	1.00	Oncostatin M	0.84
HGF	2.64	Osteopontin	0.39
I-309	1.00	Osteoprotegerin	4.53
IGF-1	0.69	PARC	2.19
IGFBP-1	1.08	PDGF-BB	1.00
IGFBP-2	0.86	PLGF	1.16
IGFBP-3	0.56	RANTES	1.04
IGFBP-4	1.39	TARC	1.00
IL-1 alpha	1.71	TGF beta 1	1.00
IL-1 beta	1.78	TGF beta 2	0.89
IL-10	1.58	TGF beta 3	2.16
IL-12 p40/p70	1.80	Thrombopoietin	1.00
IL-13	1.00	TIMP-1	0.89
IL-16	2.34	TIMP-2	0.76
IL-3	1.17	TNF alpha	1.18
IL-4	1.00	TNF beta	0.46
IL-5	1.00	VEGF-A	4.16
IL-6	1.00	CCL23	1.08
IL-7	1.00	ENA-78	1.79

Cytokines were measured by an antibody array and values are expressed as relative to DMSO control.

RESULTS

HAART Drugs Induce Senescence Program and Inflammatory Response in Human Astrocytes

HIV-infected patients do not take individual antiretroviral drugs but rather they are put on a regimen that includes several different

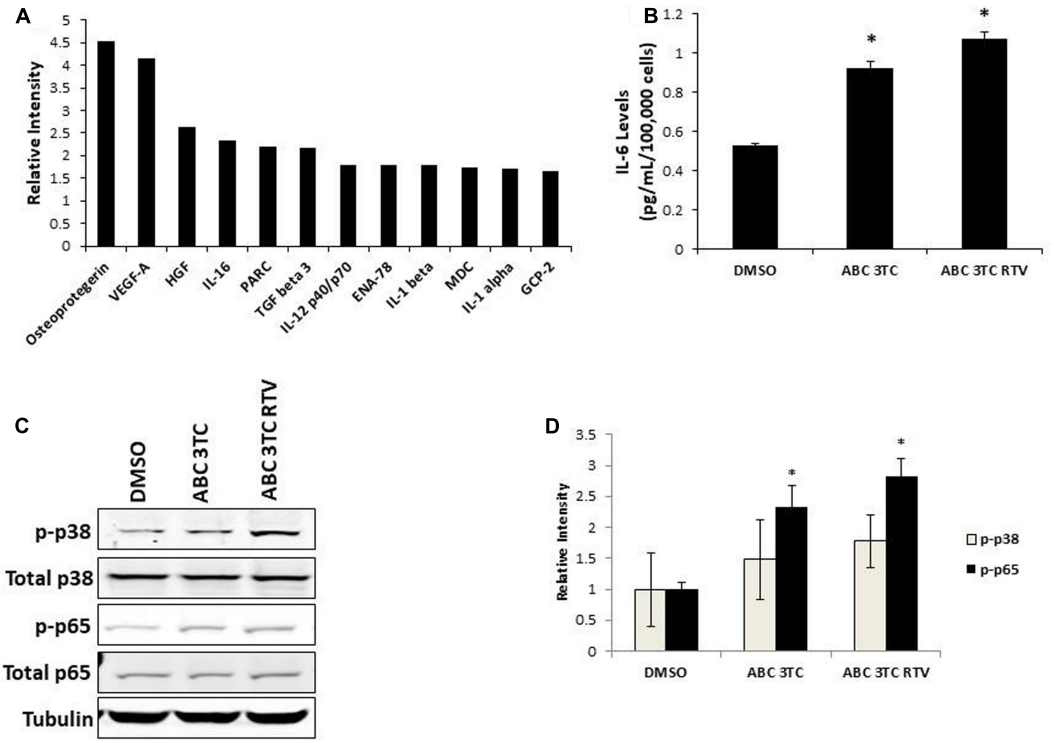

FIGURE 2 | Secretory profile of HAART drug treated HAs. Human astrocytes were treated with the following HAART concentrations: ABC 10 μM, 3TC 5 μM, and RTV 1 μM for 1 week. **(A)** Senescence-associated secretory phenotype (SASP) analysis. Astrocytes were subjected to a 24-h incubation in MCBD105 media to generate conditioned media (CM). The secretory profile was detected by incubating CM on a cytokine membrane array and normalized to cell number. Values are relative to a DMSO control. **(B)** IL-6 quantitation. CM was collected as in **(A)** and IL-6 was quantitated by ELISA. **(C)** Representative Western blot illustrating phosphorylated protein levels of inflammatory mediators p38 and p65. Total p38, total p65, and tubulin were used as a loading control. **(D)** Quantification of **(C)**. *p-value < 0.05, $n = 3$, error bars are SD.

drug classes. We therefore evaluated whether a clinically relevant combination of HAART drugs could affect physiology of HAs. Cells were chronically treated with the either the nucleotide reverse transcriptase inhibitors (NRTIs) ABC and 3TC alone or in combination with the protease inhibitor RTV. Determination of the effects on cell proliferation indicates that after 1 week of treatment these drugs induce a reduction in the cell number compared to vehicle control **(Figure 1A)** which paralleled an increase in SA β-gal activity **(Figures 1B,C)**. Protein levels of the senescence marker p21 but not p16 was significantly increased in the ABC–3TC–RTV combination, suggesting that the pathway may be p21-dependent **(Figure 1D)**. However, the ABC–3TC combination did not show a significant increase in either p16 or p21. In order to rule out the induction of apoptosis, cell viability was measured 1 and 4 days after treatment. No reduction in cell viability was observed compared to the vehicle **(Figure 1E)**. These results suggest that the ABC–3TC and ABC–3TC–RTV induced reduction in HA growth is the result of induction of the senescence program.

In addition, we examined the effect of several other clinically relevant HAART regimens on HA senescence at doses near what is found in the CNS (de Almeida et al., 2006). Human astrocytes were treated with the PIs ATV and RTV with an NRTI backbone of ABC and 3TC; ATV and RTV with an NRTI backbone of TDF and FTC; or TDF and FTC with the NNRTI EFV. Studies of the effects of these drugs on the replicative capacity indicate that compared to DMSO vehicle, there was a statistically significant decrease in population doublings by 11 days of treatment, which broadened further after 35 days **(Supplementary Figure S1A)**. The effects of these drugs were observed even at lower concentrations and the increase in SA β-gal positive cells was significant starting at 1 week, which trended upward at 3 weeks **(Supplementary Figures S1B,C)**. The exception to this trend was the TDF–FTC–EFV combination, which did not increase any further than its 1 week value. Interestingly, at these lower concentrations, ABC–3TC–ATV–RTV does not induce expression of p16 and p21 after 1 week **(Supplementary Figure S1D)**, even though an increase in SA β-gal was observed. This seems to match the minimal impact on cell growth at 1 week, and suggests that changes in the activity of SA β-gal may occur before other markers of senescence.

In order to examine the effects of HAART on the SASP, we characterized the secretory pattern of ABC–3TC–RTV-treated HAs using an antibody array. A total of 68 cytokines were analyzed and their relative levels of expression compared to control untreated are shown in **Table 1**. Treatment modulated the secretion of a variety of inflammatory molecules including TGF-β3, IL-1α, and IL-1β **(Figure 2A)**. Further validation

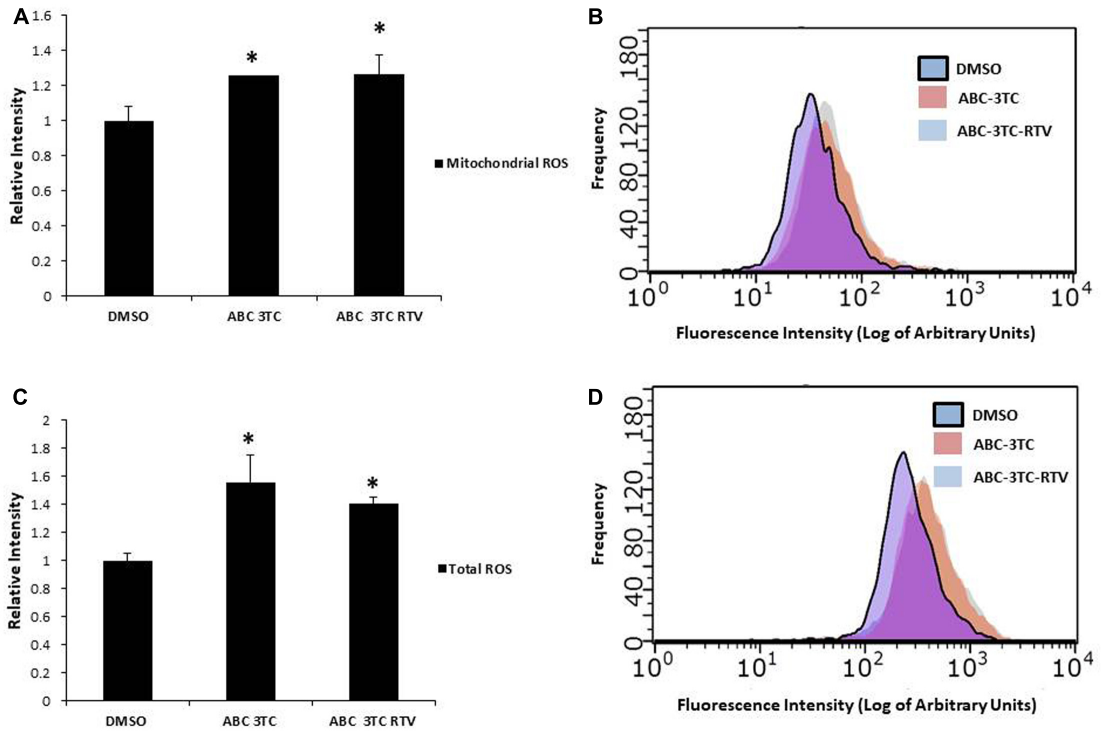

FIGURE 3 | HAART drugs induce total and mitochondrial ROS in HAs. Human astrocytes were treated for 1 week with ABC 10 μM, 3TC 5 μM, and RTV 1 μM before assaying. **(A)** Mitochondrial ROS was measured by incubation with MitoSox for 30 min followed by quantification on a flow cytometer. Bar graphs show mean intensity. **(B)** Representative histogram of data from **(A)**. **(C)** Total ROS was measured by incubation with DCF-DA for 30 min followed by quantification on a flow cytometer. Bar graphs show mean intensity. **(D)** Representative histogram of data from **(C)**. *p-value < 0.05, $n = 5$, error bars are SD.

these cytokines could be particularly interesting as they have been shown to induce senescence in neighboring cells through a process called paracrine senescence (Acosta et al., 2013). Little change was found in IL-6 using the cytokine array. This may be due to a sensitivity issue of the membrane-based analysis; therefore, we also examined IL-6 via ELISA. One week of treatment with the ABC–3TC and ABC–3TC–RTV HAART drug combination induced a significant, nearly twofold increase in IL-6 release **(Figure 2B)**. The CNS-based ABC–3TC–ATV–RTV combination was also able to induce IL-6 secretion over time in HAs, with a nearly threefold increase after 4 weeks of treatment **(Supplementary Figure S1E)**. Importantly, the pro-inflammatory transcription factor p65 (NF-κB), which has been shown to mechanistically induce senescence (Freund et al., 2011; Tilstra et al., 2012), is activated in response to both ABC–3TC and ABC–3TC–RTV treatment **(Figures 2C,D)**. Another pro-inflammatory mediator p38 while trending upward did not reach statistical significance **(Figures 2C,D)**.

HAART Drugs Induce Oxidative Stress

Accumulation of ROS can induce oxidative stress and contribute to premature senescence (Chen et al., 1995). The main source of ROS is the mitochondrial-specific superoxide anion, which can be converted to other forms of ROS to cause oxidative damage (Wang et al., 2013). We examined the effects of HAART drug combinations on mitochondrial ROS production in HAs, and we observed that both ABC–3TC and the ABC–3TC–RTV combinations significantly increased mitochondrial ROS **(Figures 3A,B)**. Interestingly, the lower dose combination of ABC–3TC–ATV–RTV at 4 weeks of treatment was able to reach a similar level of mitochondrial ROS **(Supplementary Figure S2A)**. Due to this increase in mitochondrial ROS, we examined if there was a corresponding change in total cellular ROS. With 1 week treatment of ABC–3TC and ABC–3TC–RTV, total ROS significantly increases **(Figures 3C,D)**. A similar increase was seen after prolonged treatment with the lower dose ABC–3TC–ATV–RTV combination **(Supplementary Figure S2B)**. These results indicate that the HAART drugs induce oxidative stress in HAs.

HAART Drugs Impact Mitochondrial Respiration

The accumulation of mitochondrial ROS suggests that the HAART drugs may be affecting mitochondria. Since mitochondrial dysfunction is thought to contribute to aging and senescence (Lee and Wei, 2012) we evaluated changes in mitochondrial respiration in HAART-treated HAs by using a seahorse bioanalyzer **(Figure 4A)**. ABC–3TC–RTV treatment for 1 week increased both basal and maximal mitochondrial respiration **(Figures 4B,C)**. There was also an increase in

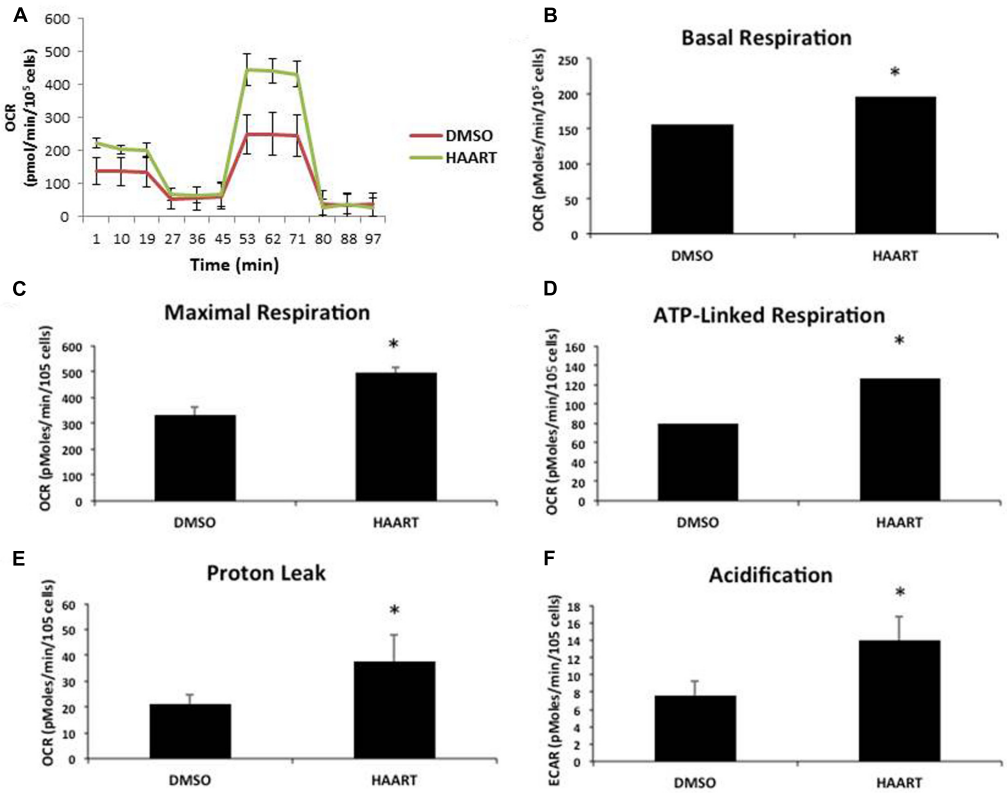

FIGURE 4 | HAART drugs induce mitochondrial respiration. Human astrocytes were treated with the following HAART drug concentrations: ABC 10 μM, 3TC 5 μM, and RTV 1 μM for 1 week before assaying. Oxygen consumption measurements were taken after HAART treatment on a Seahorse XF24 Bioanalyzer using the XF Cell Mito Stress Test Kit to acquire the oxygen consumption rate. **(A)** Representative Seahorse recording. **(B–E)** Bar graphs of the indicated oxygen consumption rate components. **(F)** Acidification measurements were acquired using the Seahorse XF24 Bioanalyzer set to measure the extracellular acidification rate. *p-value < 0.05, five independent replicates, error bars are SD.

ATP-linked respiration (**Figure 4D**). This HAART drug treatment induced an increase in mitochondrial proton leak, suggesting that it may contribute to the observed increase in mitochondrial respiration (**Figure 4E**). Measurement of the extracellular acidification rate indicates that HAART drug treatment increases acidification (**Figure 4F**). Altogether these results suggest that ABC–3TC–RTV cause over-activation of the mitochondria, which may contribute to increased mitochondrial ROS.

To determine if the increase in mitochondrial respiration was associated with other changes in the mitochondria, we first examined protein levels of the mitochondrial electron transport chain. As shown in **Figures 5A,B**, HAs treated for 1 week with ABC–3TC–RTV did not induce changes in protein levels of critical components of mitochondrial complexes. However, we observed that mitochondrial mass increased in response to the HAART drug treatment (**Figure 5C**). Since we were able to detect an increase in mitochondrial respiration and mass, we wanted to determine if this reflects a change in TMRE as a qualitative indicator of mitochondrial membrane potential. Treatment for 1 week with the HAART drugs increased TMRE fluorescence, indicating that the mitochondria may be polarized and activated (**Figure 5D**).

HAART Drugs Induce Astrocyte Glycolysis

Highly active antiretroviral therapy drug treatment severely affected astrocyte mitochondrial respiration accompanied by an increased medium acidification, suggesting an altered lactate production as a consequence of enhanced glycolysis. These results are intriguing because senescent fibroblasts were shown to have profound metabolic changes including increased glycolysis (James et al., 2015). We therefore wanted to determine if our astrocytes made senescent from HAART drug treatment have heightened glycolysis. To evaluate directly the effects of HAART on glycolysis we determined changes in glucose and glycolytic intermediates in response to the drugs. First, we examined glucose uptake using a fluorescent glucose analog, 2-NDBG. Highly active antiretroviral therapy drug treatment increased uptake of the glucose analog as measured by flow cytometry (**Figure 6A**). Glut1, the main glucose transporter in astrocytes was upregulated in response to HAART drug treatment, suggesting that the increase in 2-NDBG uptake could be due to an increase in this transporter. Glut3, which is the main glucose transporter for neurons, is not affected by HAART drug treatment (**Figures 6B,C**). In order to confirm that

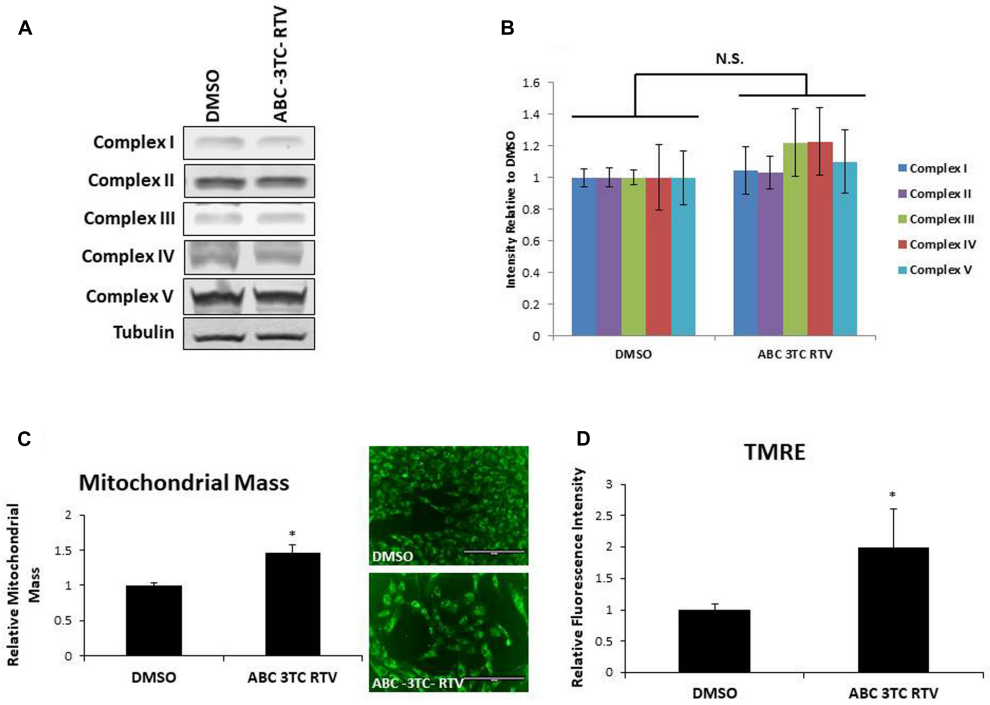

FIGURE 5 | Effect of HAART drugs on mitochondrial mass and mitochondrial membrane potential. Human astrocytes were treated with ABC 10 μM, 3TC 5 μM, and RTV 1 μM for 1 week before assaying. **(A)** Representative Western blot showing protein levels of the mitochondrial electron transport chain complexes. **(B)** Quantification of **A**. **(C)** Mitochondrial mass, cells were incubated with mitotracker for 30 min prior to quantification by flow cytometry as displayed on the left. Right is representative microscopy of fluorescence at 20× before undergoing flow cytometry. **(D)** TMRE, cells were incubated with TMRE for 30 min prior to quantification by flow cytometry. *p-value < 0.05, $n = 3$, error bars are SD.

there is an increase in glucose metabolism, we examined levels of metabolites associated with glycolysis. Glucose-6-phosphate (G6P), a product produced in the first step of glycolysis trends upward but does not reach statistical significance with HAART drug treatment in HAs **(Figure 6D)**. On the other hand, pyruvate, the last product of glycolysis, does show a statistically significant increase **(Figure 6E)**. Correspondingly, we observed an increase in the production of lactate **(Figure 6F)**, indicating that anaerobic glycolysis is enhanced in response to HAART. This increase in lactate production may explain the increased acidification determined by the Seahorse bioanalyzer **(Figure 4F)**. Overall, these results indicate that HAART drug treatment induces an increase in glucose metabolism in HAs.

DISCUSSION

The HIV-infected population is growing older and with this increased age, a larger risk for age-associated disease (Niccoli and Partridge, 2012). Neurological issues are particularly troubling because even though HAART has decreased the prevalence of the more severe forms of HAND, the milder forms still remain. We hypothesized that one possible contributor to HAND is the premature induction in astrocytes of cellular senescence in response to HAART drugs. Our study provides evidence for this hypothesis by demonstrating that combinations of HAART drugs are able to induce premature senescence, oxidative stress, mitochondrial dysfunction, and affect glycolysis in HAs. These results are novel since this is the first study to demonstrate HAART drug-induced senescence in a CNS cell type.

We evaluated the impact of widely used NRTIs, NNRTIs, and PIs on primary HAs. These drugs induced various aspects of the senescence program including decreased cellular proliferation, increased SA β-gal and expression of the cell cycle inhibitor p21. While astrocyte senescence has not been explicitly studied in HIV, there is evidence of astrocytes and other glial cells expressing cell cycle inhibitors common to senescence in HIV-infected patients (Jayadev et al., 2007). In concordance, we have previously demonstrated astrocyte senescence in association between AD (Bhat et al., 2012).

Senescent cells are irreversibly growth arrested and their resistance to apoptosis (Childs et al., 2014) allows them to persist in tissues, secreting inflammatory SASP components. The pro-inflammatory microenvironment produced by senescent cells can have major implications *in vivo* since inflammation may contribute to age-related decline in organ function (Freund et al., 2010). Significantly, CNS inflammation has been implicated in neurological disorders such as AD and Parkinson's disease (Jabbari Azad et al., 2014; Yan et al., 2014). Most importantly, CNS inflammation is found in HIV patients suffering from

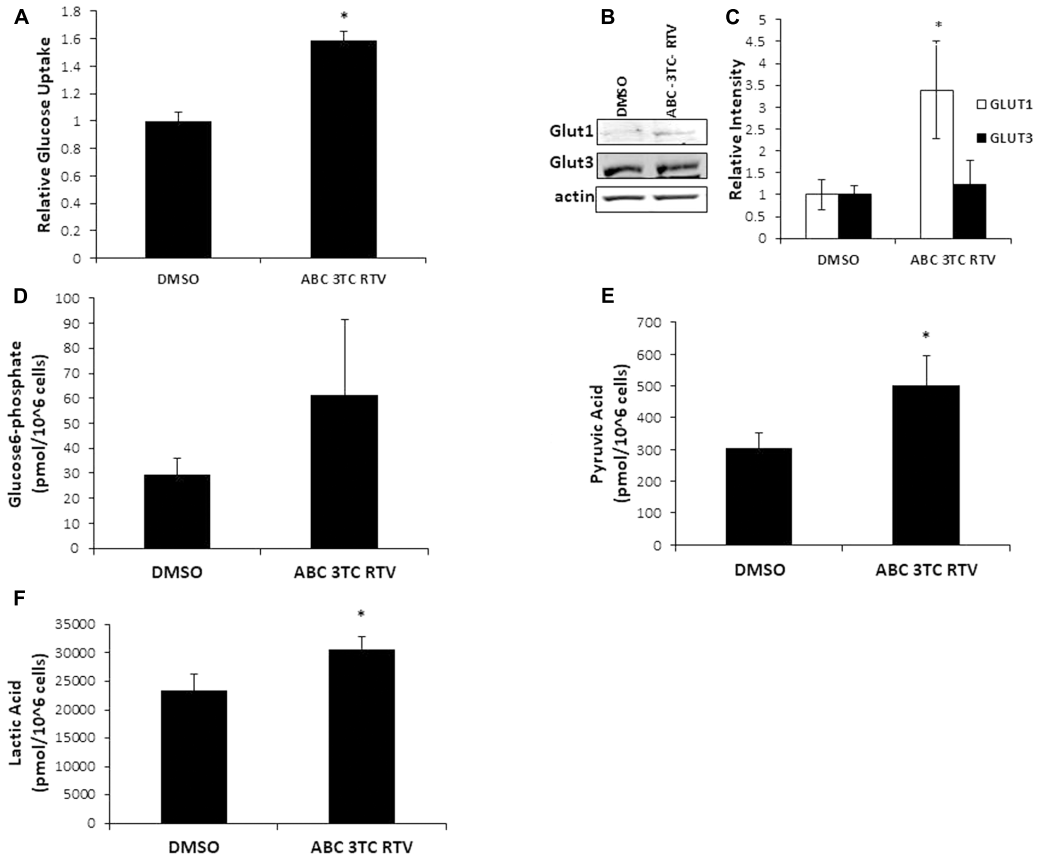

FIGURE 6 | Effect of HAART treatment on astrocyte metabolism. Human astrocytes were treated with ABC 10 μM, 3TC 5 μM, and RTV 1 μM for 1 week before assaying. **(A)** Glucose uptake was measured by flow cytometry after incubation with 2-NDBG for 30 min. **(B)** Western blot illustrating protein levels of Glut1 and Glut3. **(C)** Quantification of B. **(D–F)** Metabolite measurements, metabolites were quantified from HAART-treated cells and untreated by Human Metabolome Technologies Inc. using capillary electrophoresis mass spectrometry. *p-value < 0.05, $n = 3$, error bars are SD.

HAND, even without a productive brain infection (Tavazzi et al., 2014), suggesting that factors other than HIV may be at play. Indeed, our study demonstrates that HAART drug treatment induces the SASP in HAs characterized by the expression of several inflammatory cytokines. Until some of these cytokines are further validated the biological implications of this data are limited. However, IL-6 secretion was demonstrated by ELISA and is known to induce senescence in a paracrine manner (Acosta et al., 2013), potentially allowing for a chain reaction of senescence-inducing-senescence and a chronic inflammatory environment in HIV-infected patients extending beyond the initial insult. Co-culture experiments with HAART drug treated astrocytes and other CNS cell types are thus an important next step to examine this effect *in vitro*. In addition, attenuation of these secretions using anti-inflammatory, SASP modulating, or senescence-delaying drugs could be a potential therapy for HAND.

Dysfunctional mitochondria accumulate with age and can occur both in tissues that contain post-mitotic as well as mitotically active cells (Wallace, 2010). Mitochondrial dysfunction is known to induce cellular senescence both *in vitro* and *in vivo* (Moiseeva et al., 2009), which made it worth looking at how HAART drugs affect the mitochondria in astrocytes. Our HAART drug treated astrocytes display changes in mitochondrial membrane potential, respiration, and mitochondrial ROS production. The production of mitochondrial ROS is particularly interesting as it is thought to be a causal factor in the induction of cellular senescence (Moiseeva et al., 2009). This warrants future studies using antioxidants as a treatment to potentially mitigate HAART drug induced mitochondrial dysfunction and senescence in HAs.

The CNS has extremely high-energy requirements. While only accounting for 2% of human body mass, the CNS is involved in 25% of glucose and 20% of oxygen consumption, indicating that metabolism in the CNS must be tightly controlled. Astrocytes are the key regulators of brain metabolic homeostasis providing nutrition to neurons (Stobart and Anderson, 2013) and changes in astrocyte metabolism can thus have a profound impact on the CNS. Highly active antiretroviral therapy drug treated astrocytes show increased glucose uptake and glycolysis, indicative of a high energy state. While we do not know if this is directly linked to the observed changes in mitochondria, increases in lactate have been

observed in patients suffering from mitochondrial myopathies (Kaufmann et al., 2006). The increased utilization of glucose by astrocytes could also potentially impact neurons. While there has been little investigation to link HIV and glycolysis in CNS cells, the effect of HIV on T-cell metabolism has been studied. Glut1 is upregulated on $CD4^+$ T-cells of HIV infected patients compared to non-infected controls and these $Glut1^+$ cells likewise to our studies also have higher levels of glycolysis (Palmer et al., 2014). When examined *in vitro* not only does HIV infection increase glycolysis of $CD4^+$ T-cells, the increased glycolysis also associates with an improved virion production (Hegedus et al., 2014). These results are intriguing because enhanced aerobic glycolysis in the CNS correlates with impaired cognitive function in HIV infected patients (Dickens et al., 2015). Therefore, the increased glycolysis in our HAART drug treated astrocytes may have implications toward HAND. Further significance of our glycolysis results comes from the fact that alterations in glucose have been implicated in AD. Microglia treated with serum from AD patients were found to have increased levels of glycolytic enzymes (Jayasena et al., 2015). In addition, regions of the brain associated with high levels of glycolysis in healthy individuals correlate spatially with Aβ deposits in AD patients (Vlassenko et al., 2010). This suggests that increased levels of glycolysis in the CNS may lead later to Aβ deposits and neurodegeneration.

There are some caveats pertaining to our results. The blood brain barrier hinders penetration of HAART drugs into the CNS, meaning that the doses used to examine the effect of HAART drugs *in vitro* on CNS cells should be lower than plasma levels. However, the relevant parameter to determine physiological levels of HAART drugs in the CNS is a matter of debate. Our long-term (4 weeks) treatments were done using doses based on patient cerebral spinal fluid (CSF). However, HIV patients take these drugs for the rest of their lives and levels could accumulate in cells over a period of years to exceed that of CSF. Levels of ABC in brain homogenates from ABC-treated mice support this (Giri et al., 2008). Therefore, our higher dose 1-week treatments may still be physiological.

The use of HAART drug combinations instead of individual compounds means that the contributions of a specific component cannot be discerned. Since HIV patients take antiretroviral compounds as combinations, we decided to focus the scope of this manuscript accordingly. Interesting future directions include determining if individual antiretroviral drugs or classes are the sole contributors to our astrocyte senescence and dysfunction as well as determining if these adverse effects can be pharmacologically attenuated. In addition, since *in vitro* culturing of fetal astrocytes may not accurately reflect astrocytic function *in vivo*, we want to validate our results by using an *in vivo* model exposing mice to these HAART drugs.

While it is likely that other factors including HIV gene products and drugs of abuse may also contribute to the pathogenesis of HAND *in vivo*, our studies support HAART-induced cellular senescence as a mechanism implied in HAND development. In concordance with our results, clinical trial studies have indicated that drugs with greater CNS penetration resulted in impaired neurocognitive performance, even though HIV was suppressed better (Marra et al., 2009), and that in HIV-infected patients who have preserved immune function, neurocognitive deficits improved after interruption of HAART treatment (Robertson et al., 2010). These results suggest that HAART drugs could still be a major factor in the development of HAND.

CONCLUSION

Our data demonstrate that HAs senesce in response to a combination of the HAART drugs ABC–3TC–RTV. This has implications for senescence in the CNS contributing to the neurological problems in patients with HAND. Changes in mitochondria, metabolism, and the secretory profile observed in this study suggest that these are potential targets for therapeutics, which could mitigate HAND.

AUTHOR CONTRIBUTIONS

JC conceived and performed the experiments and wrote the manuscript; LD, JW, and FT contributed to the experiments; and CT conceived the experiments and helped write the manuscript.

FUNDING

This work was supported by the National Institute of Health (Grants 1RO1NS078283, NS78283, R21AG046943, and F31AG054191).

ACKNOWLEDGMENTS

We would like to thank Dr. Mark Zarella for help with the statistical analysis; Dr. Christian Sell and Dr. Timothy Nacarelli for assistance with mitochondrial experiments; and Dr. Jeffery Jacobson for advice about antiretroviral drug combinations.

SUPPLEMENTARY MATERIAL

The Supplementary Material for this article can be found online at: http://journal.frontiersin.org/article/10.3389/fnagi.2017.00281/full#supplementary-material

FIGURE S1 | Expression of senescence markers in long-term HAART drug treated human astrocytes. Human astrocytes were treated with the following HAART combinations: abacavir (ABC) 3 μM, lamivudine (3TC) 1.9 μM, atazanavir (ATV) 50 nM, and ritonavir (RTV) 100 nM; or tenofovir (TDF) 100 nM, emtricitabine (FTC) 1.2 μM, ATV, and RTV; or TDF, FTC, and efavirenz (EFV) 125 nM for up to 4 weeks in complete astrocyte media. **(A)** Replicative life span curve showing cumulative population doublings as function of days of drug treatments. **(B)** Representative images of 3-week SA β-gal stained cells displayed at 20×. **(C)** SA β-gal activity quantitation. Human astrocytes were stained for SA β-gal 1–3-weeks after HAART treatment. **(D)** Western blot showing protein levels of p16 and p21 after 1 week of treatment. **(E)** IL-6 secretion, conditioned media was collected for 24 h after each treatment. IL-6 was measured by ELISA. *p-value < 0.05, $n = 3$, error bars are SD.

FIGURE S2 | Long-term HAART drug treatment induces total and mitochondrial ROS in human astrocytes. Human astrocytes were treated for up to 4 weeks with ABC 3 μM, 3TC 1.9 μM, atazanavir (ATV) 50 nM, and RTV 100 nM. **(A)** Mitochondrial ROS and **(B)** total ROS were measured by 30 min incubation with MitoSox and DCFDA, respectively, before quantification on a flow cytometer. *p-value < 0.05, $n = 3$, error bars are SD.

REFERENCES

Acosta, J. C., Banito, A., Wuestefeld, T., Georgilis, A., Janich, P., Morton, J. P., et al. (2013). A complex secretory program orchestrated by the inflammasome controls paracrine senescence. *Nat. Cell Biol.* 15, 978–990. doi: 10.1038/ncb2784

Afonso, P., Auclair, M., Boccara, F., Vantyghem, M. C., Katlama, C., Capeau, J., et al. (2015). LMNA mutations resulting in lipodystrophy and HIV protease inhibitors trigger vascular smooth muscle cell senescence and calcification: role of ZMPSTE24 downregulation. *Atherosclerosis* 245, 200–211. doi: 10.1016/j.atherosclerosis.2015.12.012

Arend, C., Brandmann, M., and Dringen, R. (2013). The antiretroviral protease inhibitor ritonavir accelerates glutathione export from cultured primary astrocytes. *Neurochem. Res.* 38, 732–741. doi: 10.1007/s11064-013-0971-x

Bhat, R., Crowe, E. P., Bitto, A., Moh, M., Katsetos, C. D., Garcia, F. U., et al. (2012). Astrocyte senescence as a component of Alzheimer's disease. *PLoS ONE* 7:e45069. doi: 10.1371/journal.pone.0045069

Bhatia, R., Ryscavage, P., and Taiwo, B. (2012). Accelerated aging and human immunodeficiency virus infection: emerging challenges of growing older in the era of successful antiretroviral therapy. *J. Neurovirol.* 18, 247–255. doi: 10.1007/s13365-011-0073-y

Bitto, A., Sell, C., Crowe, E., Lorenzini, A., Malaguti, M., Hrelia, S., et al. (2010). Stress-induced senescence in human and rodent astrocytes. *Exp. Cell Res.* 316, 2961–2968. doi: 10.1016/j.yexcr.2010.06.021

Bodnar, A. G., Ouellette, M., Frolkis, M., Holt, S. E., Chiu, C. P., Morin, G. B., et al. (1998). Extension of life-span by introduction of telomerase into normal human cells. *Science* 279, 349–352. doi: 10.1126/science.279.5349.349

Capeau, J. (2011). Premature aging and premature age-related comorbidities in HIV-infected patients: facts and hypotheses. *Clin. Infect. Dis.* 53, 1127–1129. doi: 10.1093/cid/cir628

Caron, M., Auclairt, M., Vissian, A., Vigouroux, C., and Capeau, J. (2008). Contribution of mitochondrial dysfunction and oxidative stress to cellular premature senescence induced by antiretroviral thymidine analogues. *Antivir. Ther.* 13, 27–38.

Chen, Q., Fischer, A., Reagan, J. D., Yan, L. J., and Ames, B. N. (1995). Oxidative DNA damage and senescence of human diploid fibroblast cells. *Proc. Natl. Acad. Sci. U.S.A.* 92, 4337–4341. doi: 10.1073/pnas.92.10.4337

Childs, B. G., Baker, D. J., Kirkland, J. L., Campisi, J., and van Deursen, J. M. (2014). Senescence and apoptosis: dueling or complementary cell fates? *EMBO Rep.* 15, 1139–1153. doi: 10.15252/embr.201439245

Chou, J. P., Ramirez, C. M., Wu, J. E., and Effros, R. B. (2013). Accelerated aging in HIV/AIDS: novel biomarkers of senescent human CD8+ T cells. *PLoS ONE* 8:e64702. doi: 10.1371/journal.pone.0064702

Crowe, E. P., Tuzer, F., Gregory, B. D., Donahue, G., Gosai, S. J., Cohen, J., et al. (2016). Changes in the transcriptome of human astrocytes accompanying oxidative stress-induced senescence. *Front. Aging Neurosci.* 8:208. doi: 10.3389/fnagi.2016.00208

de Almeida, S. M., Letendre, S., and Ellis, R. (2006). Human immunodeficiency virus and the central nervous system. *Braz. J. Infect. Dis.* 10, 41–50. doi: 10.1590/S1413-86702006000100009

Dickens, A. M., Anthony, D. C., Deutsch, R., Mielke, M. M., Claridge, T. D., Grant, I., et al. (2015). Cerebrospinal fluid metabolomics implicate bioenergetic adaptation as a neural mechanism regulating shifts in cognitive states of HIV-infected patients. *AIDS* 29, 559–569. doi: 10.1097/QAD.0000000000000580

Dimri, G. P., Lee, X., Basile, G., Acosta, M., Scott, G., Roskelley, C., et al. (1995). A biomarker that identifies senescent human cells in culture and in aging skin in vivo. *Proc. Natl. Acad. Sci. U.S.A.* 92, 9363–9367. doi: 10.1073/pnas.92.20.9363

Feeney, E. R., and Mallon, P. W. (2010). Impact of mitochondrial toxicity of HIV-1 antiretroviral drugs on lipodystrophy and metabolic dysregulation. *Curr. Pharm. Des.* 16, 3339–3351. doi: 10.2174/138161210793563482

Freund, A., Orjalo, A. V., Desprez, P. Y., and Campisi, J. (2010). Inflammatory networks during cellular senescence: causes and consequences. *Trends Mol. Med.* 16, 238–246. doi: 10.1016/j.molmed.2010.03.003

Freund, A., Patil, C. K., and Campisi, J. (2011). p38MAPK is a novel DNA damage response-independent regulator of the senescence-associated secretory phenotype. *EMBO J.* 30, 1536–1548. doi: 10.1038/emboj.2011.69

Giri, N., Shaik, N., Pan, G., Terasaki, T., Mukai, C., Kitagaki, S., et al. (2008). Investigation of the role of breast cancer resistance protein (Bcrp/Abcg2) on pharmacokinetics and central nervous system penetration of abacavir and zidovudine in the mouse. *Drug Metab. Dispos.* 36, 1476–1484. doi: 10.1124/dmd.108.020974

Heaton, R. K., Clifford, D. B., Franklin, D. R. Jr., Woods, S. P., Ake, C., Vaida, F., et al. (2010). HIV-associated neurocognitive disorders persist in the era of potent antiretroviral therapy: CHARTER Study. *Neurology* 75, 2087–2096. doi: 10.1212/WNL.0b013e318200d727

Hegedus, A., Kavanagh Williamson, M., and Huthoff, H. (2014). HIV-1 pathogenicity and virion production are dependent on the metabolic phenotype of activated CD4+ T cells. *Retrovirology* 11, 98. doi: 10.1186/s12977-014-0098-4

Hernandez-Vallejo, S. J., Beaupere, C., Larghero, J., Capeau, J., and Lagathu, C. (2013). HIV protease inhibitors induce senescence and alter osteoblastic potential of human bone marrow mesenchymal stem cells: beneficial effect of pravastatin. *Aging Cell* 12, 955–965. doi: 10.1111/acel.12119

Hill, B. G., Benavides, G. A., Lancaster, J. R. Jr., Ballinger, S., Dell'Italia, L., Jianhua, Z., et al. (2012). Integration of cellular bioenergetics with mitochondrial quality control and autophagy. *Biol. Chem.* 393, 1485–1512. doi: 10.1515/hsz-2012-0198

Jabbari Azad, F., Talaei, A., Rafatpanah, H., Yousefzadeh, H., Jafari, R., Talaei, A., et al. (2014). Association between cytokine production and disease severity in Alzheimer's disease. *Iran. J. Allergy Asthma Immunol.* 13, 433–439.

James, E. L., Michalek, R. D., Pitiyage, G. N., de Castro, A. M., Vignola, K. S., Jones, J., et al. (2015). Senescent human fibroblasts show increased glycolysis and redox homeostasis with extracellular metabolomes that overlap with those of irreparable DNA damage, aging, and disease. *J. Proteome Res.* 14, 1854–1871. doi: 10.1021/pr501221g

Jayadev, S., Yun, B., Nguyen, H., Yokoo, H., Morrison, R. S., and Garden, G. A. (2007). The glial response to CNS HIV infection includes p53 activation and increased expression of p53 target genes. *J. Neuroimmune Pharmacol.* 2, 359–370. doi: 10.1007/s11481-007-9095-x

Jayasena, T., Poljak, A., Braidy, N., Smythe, G., Raftery, M., Hill, M., et al. (2015). Upregulation of glycolytic enzymes, mitochondrial dysfunction and increased cytotoxicity in glial cells treated with Alzheimer's disease plasma. *PLoS ONE* 10:e0116092. doi: 10.1371/journal.pone.0116092

Kaufmann, P., Engelstad, K., Wei, Y., Jhung, S., Sano, M. C., Shungu, D. C., et al. (2006). Dichloroacetate causes toxic neuropathy in MELAS: a randomized, controlled clinical trial. *Neurology* 66, 324–330. doi: 10.1212/01.wnl.0000196641.05913.27

Lee, H. C., and Wei, Y. H. (2012). Mitochondria and aging. *Adv. Exp. Med. Biol.* 942, 311–327. doi: 10.1007/978-94-007-2869-1_14

Lefevre, C., Auclair, M., Boccara, F., Bastard, J. P., Capeau, J., Vigouroux, C., et al. (2010). Premature senescence of vascular cells is induced by HIV protease inhibitors: implication of prelamin A and reversion by statin. *Arterioscler. Thromb. Vasc. Biol.* 30, 2611–2620. doi: 10.1161/ATVBAHA.110.213603

Marra, C. M., Zhao, Y., Clifford, D. B., Letendre, S., Evans, S., Henry, K., et al. (2009). Impact of combination antiretroviral therapy on cerebrospinal fluid HIV RNA and neurocognitive performance. *AIDS* 23, 1359–1366. doi: 10.1097/QAD.0b013e32832c4152

Moiseeva, O., Bourdeau, V., Roux, A., Deschenes-Simard, X., and Ferbeyre, G. (2009). Mitochondrial dysfunction contributes to oncogene-induced senescence. *Mol. Cell. Biol.* 29, 4495–4507. doi: 10.1128/MCB.01868-08

Nacarelli, T., Azar, A., and Sell, C. (2016). Mitochondrial stress induces cellular senescence in an mTORC1-dependent manner. *Free Radic. Biol. Med.* 95, 133–154. doi: 10.1016/j.freeradbiomed.2016.03.008

Niccoli, T., and Partridge, L. (2012). Ageing as a risk factor for disease. *Curr. Biol.* 22, R741–R752. doi: 10.1016/j.cub.2012.07.024

Palmer, C. S., Ostrowski, M., Gouillou, M., Tsai, L., Yu, D., Zhou, J., et al. (2014). Increased glucose metabolic activity is associated with CD4+ T-cell activation and depletion during chronic HIV infection. *AIDS* 28, 297–309. doi: 10.1097/QAD.0000000000000128

Robertson, K. R., Su, Z., Margolis, D. M., Krambrink, A., Havlir, D. V., Evans, S., et al. (2010). Neurocognitive effects of treatment interruption in stable HIV-positive patients in an observational cohort. *Neurology* 74, 1260–1266. doi: 10.1212/WNL.0b013e3181d9ed09

Rodier, F., and Campisi, J. (2011). Four faces of cellular senescence. *J. Cell Biol.* 192, 547–556. doi: 10.1083/jcb.201009094

Sato, A., Asano, T., Ito, K., and Asano, T. (2012). Ritonavir interacts with bortezomib to enhance protein ubiquitination and histone acetylation synergistically in renal cancer cells. *Urology* 79, e913–e921. doi: 10.1016/j.urology.2011.11.033

Serrano, M., Lin, A. W., McCurrach, M. E., Beach, D., and Lowe, S. W. (1997). Oncogenic ras provokes premature cell senescence associated with accumulation of p53 and p16INK4a. *Cell* 88, 593–602. doi: 10.1016/S0092-8674(00)81902-9

Stobart, J. L., and Anderson, C. M. (2013). Multifunctional role of astrocytes as gatekeepers of neuronal energy supply. *Front. Cell. Neurosci.* 7:38. doi: 10.3389/fncel.2013.00038

Suram, A., Kaplunov, J., Patel, P. L., Ruan, H., Cerutti, A., Boccardi, V., et al. (2012). Oncogene-induced telomere dysfunction enforces cellular senescence in human cancer precursor lesions. *EMBO J.* 31, 2839–2851. doi: 10.1038/emboj.2012.132

Tavazzi, E., Morrison, D., Sullivan, P., Morgello, S., and Fischer, T. (2014). Brain inflammation is a common feature of HIV-infected patients without HIV encephalitis or productive brain infection. *Curr. HIV Res.* 12, 97–110. doi: 10.2174/1570162X12666140526114956

Tilstra, J. S., Robinson, A. R., Wang, J., Gregg, S. Q., Clauson, C. L., Reay, D. P., et al. (2012). NF-kappaB inhibition delays DNA damage-induced senescence and aging in mice. *J. Clin. Invest.* 122, 2601–2612. doi: 10.1172/JCI45785

Vlassenko, A. G., Vaishnavi, S. N., Couture, L., Sacco, D., Shannon, B. J., Mach, R. H., et al. (2010). Spatial correlation between brain aerobic glycolysis and amyloid-beta (Abeta) deposition. *Proc. Natl. Acad. Sci. U.S.A.* 107, 17763–17767. doi: 10.1073/pnas.1010461107

Wallace, D. C. (2010). Mitochondrial DNA mutations in disease and aging. *Environ. Mol. Mutagen.* 51, 440–450. doi: 10.1002/em.20586

Wang, C. H., Wu, S. B., Wu, Y. T., and Wei, Y. H. (2013). Oxidative stress response elicited by mitochondrial dysfunction: implication in the pathophysiology of aging. *Exp. Biol. Med.* 238, 450–460. doi: 10.1177/1535370213493069

Yan, J., Fu, Q., Cheng, L., Zhai, M., Wu, W., Huang, L., et al. (2014). Inflammatory response in Parkinson's disease (Review). *Mol. Med. Rep.* 10, 2223–2233.

Zhou, H., Pandak, W. M. Jr., Lyall, V., Natarajan, R., and Hylemon, P. B. (2005). HIV protease inhibitors activate the unfolded protein response in macrophages: implication for atherosclerosis and cardiovascular disease. *Mol. Pharmacol.* 68, 690–700. doi: 10.1124/mol.105.012898

Conflict of Interest Statement: The authors declare that the research was conducted in the absence of any commercial or financial relationships that could be construed as a potential conflict of interest.

frontiers in Cellular Neuroscience

ORIGINAL RESEARCH
published: 21 August 2017
doi: 10.3389/fncel.2017.00249

P2X7 Receptor Activation Modulates Autophagy in SOD1-G93A Mouse Microglia

Paola Fabbrizio[1,2], *Susanna Amadio*[1], *Savina Apolloni*[1*†] *and Cinzia Volonté*[1,3*†]

[1]IRCCS Santa Lucia Foundation, Experimental Neuroscience, Rome, Italy, [2]Department of Systems Medicine, Tor Vergata University, Rome, Italy, [3]CNR, Institute of Cell Biology and Neurobiology, Rome, Italy

Autophagy and inflammation play determinant roles in the pathogenesis of Amyotrophic Lateral Sclerosis (ALS), an adult-onset neurodegenerative disease characterized by deterioration and final loss of upper and lower motor neurons (MN) priming microglia to sustain neuroinflammation and a vicious cycle of neurodegeneration. Given that extracellular ATP through P2X7 receptor constitutes a neuron-to-microglia alarm signal implicated in ALS, and that P2X7 affects autophagy in immune cells, we have investigated if autophagy can be directly triggered by P2X7 activation in primary microglia from superoxide dismutase 1 (SOD1)-G93A mice. We report that P2X7 enhances the expression of the autophagic marker microtubule-associated protein 1 light chain 3 (LC3)-II, via mTOR pathway and concomitantly with modulation of anti-inflammatory M2 microglia markers. We also demonstrate that the autophagic target SQSTM1/p62 is decreased in SOD1-G93A microglia after a short stimulation of P2X7, but increased after a sustained challenge. These effects are prevented by the P2X7 antagonist A-804598, and the autophagy/phosphoinositide-3-kinase inhibitor wortmannin (WM). Finally, a chronic *in vivo* treatment with A-804598 in SOD1-G93A mice decreases the expression of SQSTM1/p62 in lumbar spinal cord at end stage of disease. These data identify the modulation of the autophagic flux as a novel mechanism by which P2X7 activates ALS-microglia, to be considered for further investigations in ALS.

Keywords: ALS, ATP, BzATP, LC3B-II, microglia, P2X7

OPEN ACCESS

Edited by:
Alexej Verkhratsky,
University of Manchester,
United Kingdom

Reviewed by:
Peter Illes,
Leipzig University, Germany
Kim A. Staats,
University of Southern California,
United States

***Correspondence:**
Savina Apolloni
s.apolloni@hsantalucia.it
Cinzia Volonté
cinzia.volonte@cnr.it

†These authors have contributed equally to this work.

Received: *31 May 2017*
Accepted: *07 August 2017*
Published: *21 August 2017*

Citation:
Fabbrizio P, Amadio S, Apolloni S and Volonté C (2017) P2X7 Receptor Activation Modulates Autophagy in SOD1-G93A Mouse Microglia. Front. Cell. Neurosci. 11:249. doi: 10.3389/fncel.2017.00249

INTRODUCTION

Neuroinflammation plays a determinant role in the pathogenesis of Amyotrophic Lateral Sclerosis (ALS; Cozzolino et al., 2012), where degenerating motor neurons (MN) contribute to produce danger signals that activate microglia to initiate a self-propagating cytotoxic cascade resulting in muscle weakness, atrophy, spasticity, compromised breathing and finally death in patients (Henkel et al., 2009; Ilieva et al., 2009). Extracellular ATP functions as one of such endogenous alarm signal, by operating through purinergic P2 receptors, particularly the P2X7 ionotropic subtype (Beamer et al., 2016; Illes and Verkhratsky, 2016). Activation of P2X7 in microglia purified

Abbreviations: ALS, Amyotrophic Lateral Sclerosis; ARG-1, arginase-1; BzATP, 2′-3′-O-(benzoyl-benzoyl) ATP; COX-2, cyclooxygenase-2; LC3-II, microtubule-associated protein 1 light chain 3-II; MAPK, mitogen-activated protein kinase; NF-κB, nuclear factor kappa-B; NOX2, NADPH oxidase 2; SOD1, superoxide dismutase 1; TNF-α, tumor necrosis factor alpha; WM, wortmannin; WT, wild-type.

from superoxide dismutase 1 (SOD1)-G93A mouse model of ALS exacerbates pro-inflammatory responses exemplified by the levels of cyclooxygenase-2 (COX-2), mitogen-activated protein kinase (MAPK), NADPH oxidase 2 (NOX2), nuclear factor kappa-B (NF-κB), tumor necrosis factor alpha (TNF-α), with a consequent cytotoxicity towards neurons (D'Ambrosi et al., 2009; Apolloni et al., 2013b; Parisi et al., 2016). In the SOD1-G93A mouse model of ALS, we have previously reported that disease onset is significantly anticipated and disease progression is worsened in mice genetically lacking P2X7, thus suggesting that the receptor has beneficial effects at least during a precise stage of the disease that is however still undefined (Apolloni et al., 2013a). Only when administered to SOD1-G93A mice from late pre-onset, the P2X7 antagonist Brilliant Blue G enhances MN survival and reduces microgliosis in lumbar spinal cord (Apolloni et al., 2014), with a slight beneficial effect on disease progression and mice survival (Cervetto et al., 2013; Apolloni et al., 2014; Bartlett et al., 2017). By confirming the dual role previously recognized for P2X7 (Monif et al., 2010, 2016), these findings have highlighted how crucial is the lag of P2X7 modulation for eliciting beneficial effects in ALS.

Autophagy is an ubiquitous and highly conserved homeostatic mechanism by which eukaryotic cells degrade damaged organelles, intracellular components and protein aggregates. It consists in the sequestration of target cellular materials (cargo) into autophagosomes and their subsequent transfer to and catabolism by the autophagosome-lysosome (autolysosome vacuole) system (Klionsky and Emr, 2000; Glick et al., 2010). Abnormalities in autophagy have been implicated in chronic neurodegenerative conditions comprising ALS, where both patients and animal models are characterized by overexpression of the autophagy marker microtubule-associated protein 1 light chain 3 (LC3)-II in spinal cord (Song et al., 2012). Moreover, sequestosome-1, a protein also known as ubiquitin-binding protein SQSTM1/p62 encoded by the SQSTM1 gene, which is an autophagosome receptor recruiting proteins for selective autophagy, is found accumulated in spinal cord of SOD1-G93A mice, concomitantly with increased extent of autophagic vacuoles (Zhang et al., 2011).

In mouse microglia and in human epithelial cells, P2X7 has been reported to negatively regulate autophagy by impairing lysosomal function (Takenouchi et al., 2009a; Haanes et al., 2012). Conversely, P2X7 apparently increases autophagy in monocytes and macrophages during mycobacterial infections (Biswas et al., 2008), and acts as a positive regulator of autophagy in dystrophic muscle cells (Young et al., 2015). This not only confirms the twofold role often played by P2X7, but also highlights a context-specific effect of P2X7 on autophagy pathways.

The purpose of this work is thus to learn if P2X7 might participate to ALS pathogenesis by directly modulating autophagy, and particularly the expression of the autophagosome component LC3-II and of the autophagy receptor p62 in SOD1-G93A microglia. We demonstrate that activation of P2X7 deregulates LC3-II and p62 protein content. Moreover, *in vivo* treatment with the specific P2X7 antagonist A-804598 reduces p62 levels in lumbar spinal cord of SOD1-G93A mice at end stage of disease. These data identify the modulation of autophagy as a novel mechanism by which P2X7 activates ALS-microglia.

MATERIALS AND METHODS

Reagents

ATP, 2′-3′-O-(benzoyl-benzoyl) ATP (BzATP) and all other reagents, unless otherwise stated, were obtained from Sigma Aldrich (Milan, Italy). PD98059 was purchased from Calbiochem (San Diego, CA, USA). A-839977 and A-804598 were from Tocris Bioscience (Bristol, UK).

Antibodies

Arginase-1 (ARG-1) rabbit antibody (1:700) was from Abcam (Cambridge, UK); CD163 rabbit antibody (1:100) was from Santa Cruz Biotechnology, Inc. (Dallas, TX, USA); LC3B antibody (1:500); mTOR (1:500) and p-mTOR (1:500) rabbit antibodies were from Cell Signaling Technology Inc. (Beverly, MA, USA). SQSTM1/p62 mouse monoclonal antibody (1:500) was obtained from Abcam (Cambridge, UK). GAPDH mouse antibody (1:2500) from Calbiochem (San Diego, CA, USA) was used for protein normalization. HRP-linked anti-rabbit and anti-mouse antibodies were from Jackson Immunoresearch (West Grove, PA, USA).

Mice

All animal procedures have been performed according to the European Guidelines for the use of animals in research (86/609/CEE) and the requirements of Italian laws (D.L. 26/2014). The ethical procedure has been approved by the Animal Welfare Office, Department of Public Health and Veterinary, Nutrition and Food Safety, General Management of Animal Care and Veterinary Drugs of the Italian Ministry of Health (protocol number 319/2015PR). All efforts were made to minimize animal suffering and use the minimum number of animals necessary to obtain reliable results. Adult B6.Cg-Tg(SOD1-G93A)1Gur/J mice were obtained from Jackson Laboratories (Bar Harbor, ME, USA), bred in our indoor animal facility and genotyped as described (Apolloni et al., 2013a). To determine behavioral scores we employed a scale from 5 to 1, where 5 defines healthy mice without symptoms of paralysis, 4 indicates mice with slight signs of destabilized gait and paralysis of the hind limbs, 3 describes mice with clear paralysis and destabilized gait, 2 depicts mice with fully developed paralysis of the hind limbs that only crawl on the forelimbs, finally 1 defines mice with fully developed paralysis of the hind limbs that predominantly lie on the side and/or are not able to straighten up within 30 s when they are turned on their back. After reaching a score of 1 (end stage, ∼23 weeks of age), the animals were euthanized, according to the guidelines for preclinical testing and colony management (Ludolph et al., 2010). SOD1-G93A mice were considered at onset when exhibited a statistically significant 10% decline of rotarod performance, with respect to wild-type (WT) mice. Rotarod performance was evaluated by a rotarod apparatus (Ugo Basile 7650 model) at a constant speed of

15 r.p.m. over a maximum period of 180 s (Apolloni et al., 2013a).

SOD1-G93A mice at 100 days of age (pre-onset) were randomly grouped into vehicle-treated or CNS penetrant P2X7 specific antagonist A-804598-treated mice (Donnelly-Roberts et al., 2009; Catanzaro et al., 2014; Iwata et al., 2016) given by intraperitoneal injection at 30 mg/kg five times a week until end stage of disease. Because there is sex diversity in response to pharmacological treatments (Pizzasegola et al., 2009) and the P2X7 antagonist Brilliant Blue G has prolonged survival only in female SOD1-G93A mice (Bartlett et al., 2017; Sluyter et al., 2017), we have chosen to study female mice.

Primary Microglia Cultures

Primary microglia cultures from brain cortex were prepared as previously described (Apolloni et al., 2013b). Briefly, neonatal SOD1-G93A mice and their non-transgenic littermates mice were sacrificed and, after removing the meninges, cortices were minced and digested with 0.25% trypsin and 0.01% DNaseI. After dissociation and passage through 70 μm filters, cells were resuspended in DMEM/F-12 media with GlutaMAX™ (Gibco, Invitrogen, UK), plus 10% fetal bovine serum (FBS), 100 Units/ml gentamicine and 100 μg/ml streptomycin/penicillin. After approximately 15 days, a mild trypsinization was done for 30 min at 37°C. The resultant adherent microglial cells (pure >99%) were washed twice with DMEM/F-12 and kept at 37°C in a 5% CO_2 and 95% air atmosphere and used for experiments at least 48 h after.

Western Blotting

Microglia in serum-free medium were harvested in SDS Laemmli sample buffer. Protein lysates were obtained by homogenization of mice lumbar spinal cords segments in homogenization buffer as described (Apolloni et al., 2014). Analysis of protein components (10 μg for tissue extracts) was performed by Mini-PROTEAN® TGX™ Gels (BioRad, USA) and transfer onto nitrocellulose membranes (Amersham Biosciences, USA). After saturation with blocking agent, blots were incubated overnight at 4°C with the specified antibody, then for 1 h with HRP-conjugated secondary antibodies and visualized using ECL Advance Western blot detection kit (Amersham Biosciences, USA). Signal intensity quantification was performed by Kodak Image Station analysis software.

Immunofluorescence and Confocal Microscopy

Primary microglia were fixed for 20 min in 4% paraformaldehyde, permeabilized in PBS containing 0.1% Triton X-100 and then incubated for 1.5 h at 37°C with anti-LC3B (1:200), anti-SQSTM1/p62 (1:100) or anti-CD11b (1:200, AbD Serotec, USA) in 1% BSA in PBS. Cells were stained for 1 h with Cy2-conjugated donkey anti-rabbit IgG or Cy3-conjugated donkey anti-mouse IgG or Cy5-conjugated donkey anti-rat IgG (1:200, Jackson Immunoresearch). Höechst 33342 was used for nuclei staining (1:1000) in PBS. Immunofluorescence was analyzed by means of a confocal laser scanning microscope (Zeiss, LSM700, Germany) equipped with four laser lines: 405 nm, 488 nm, 561 nm and 639 nm. The brightness and contrast of the digital images were adjusted using the Zen software.

Data Analysis

Data are presented as mean ± standard error of the mean (SEM). Statistical differences were verified by student's *t*-test if the normality test was passed, or by the Mann–Whitney rank sum test, if the normality test failed, considering acceptable a value for asymmetry between −2 and +2 in order to prove normal univariate distribution. One-way analysis of variance (ANOVA) followed by *Post Hoc* Tukey's test was used for multiple comparisons. For onset and survival data, differences in the values of A804598- and vehicle-treated mice were assessed using Kaplan-Meier analysis paired with log-rank tests. The software package GraphPad Prism 7.03 (GraphPad Software, San Diego, CA, USA) was used for all statistical analysis with differences considered significant for $p < 0.05$.

RESULTS

P2X7 Activation Induces LC3B-II Formation in SOD1-G93A Primary Microglia

LC3-II localizing to the autophagosome membrane is widely used to monitor autophagy. In particular, the generation of LC3-II from LC3-I is generally identified by immunoblot analysis, because the amount of LC3-II is strictly correlated with the number of autophagosomes and is considered a more reliable marker than LC3-I to be detected (Mizushima and Yoshimori, 2007; Barth et al., 2010; Klionsky et al., 2016). To directly investigate the modulation of the autophagic pathway by P2X7 activation in SOD1-G93A microglia, we thus compared the expression of LC3B-II, with respect to GAPDH.

As shown by immunoblotting in **Figure 1A**, SOD1-G93A microglia constitutively express augmented levels of LC3B-II with respect to WT microglia. Activation of P2X7 by the specific agonist BzATP (10–100–300 μM) increases LC3B-II protein content in a dose-dependent manner in SOD1-G93A microglia with maximal effect obtained at 300 μM (**Figure 1B**). The time-course experiment shows that the levels of LC3B-II are maximally induced after 15 min, with a consequent decline observed at 1–6 h (**Figure 1B**). Notably, the physiologic purinergic agonist ATP used at the mM concentrations required to activate P2X7 exerts similar effects (**Figure 1C**). LC3B-II induction by BzATP and ATP is decreased by the specific P2X7 antagonist A-804598 (10 μM; **Figure 1D**), thus indicating P2X7 involvement. Autophagy in SOD1-G93A microglia is moreover qualitatively assessed by immunofluorescence confocal analysis, by observing cells with accumulation of LC3 dots, because cells presenting a diffuse distribution of LC3 are generally described as

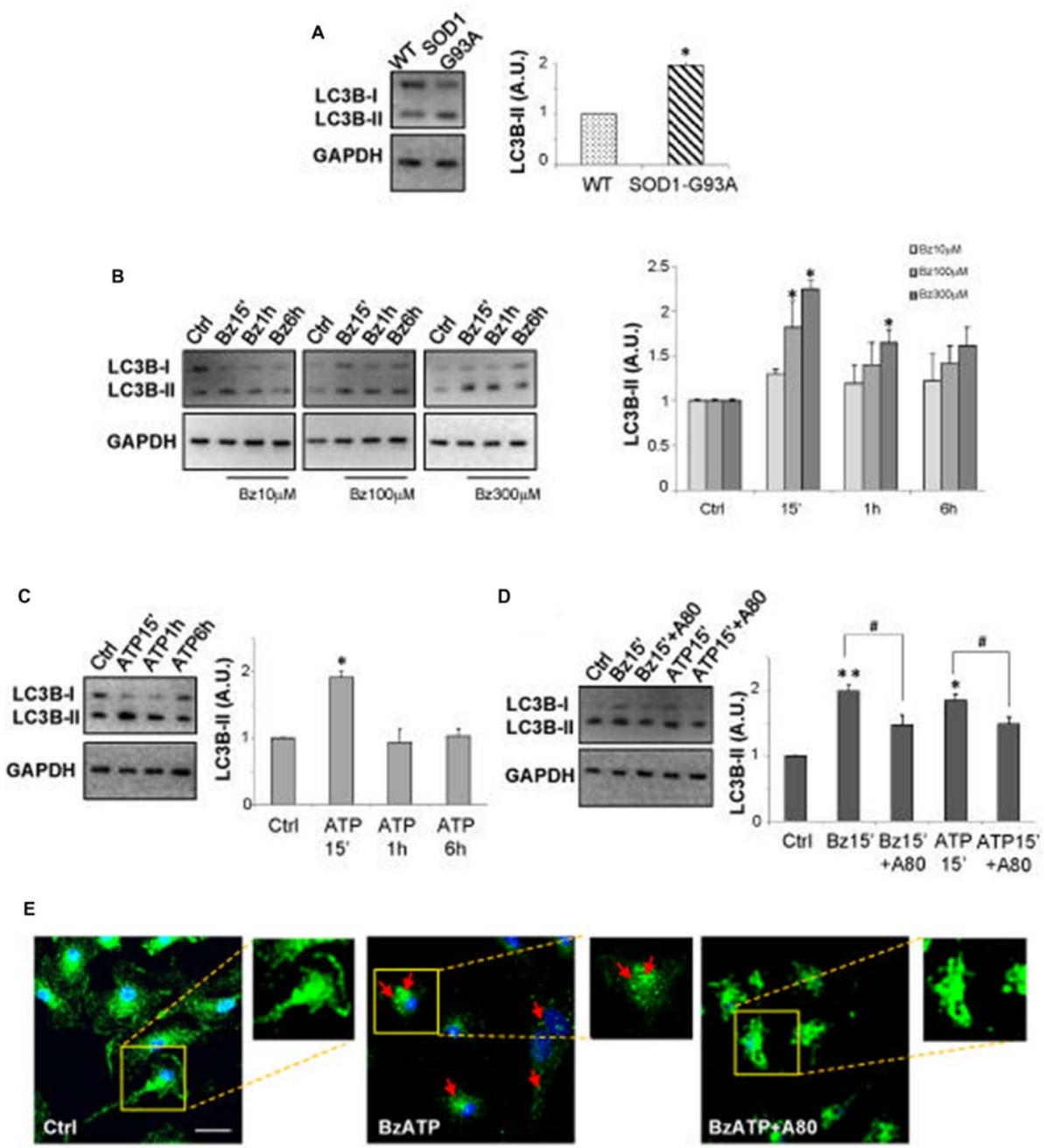

FIGURE 1 | P2X7 activation modulates microtubule-associated protein 1 light chain 3 (LC3)-II in superoxide dismutase 1 (SOD1)-G93A microglia. **(A)** Equal amounts of total protein from wild-type (WT) and SOD1-G93A primary microglia were subjected to western blotting and immunoreactions with anti-LC3B-II and anti-GAPDH to normalize proteins. **(B–D)** Equal amounts of total protein from SOD1-G93A primary microglia were subjected to western blotting and immunoreactions with anti-LC3B-II and anti-GAPDH. In **(B)**, cells were exposed to 10–100–300 μM 2′-3′-O-(benzoyl-benzoyl) ATP (BzATP) for 15 min, 1 h or 6 h. In **(C)** cells were exposed to 3 mM ATP for 15 min, 1 h or 6 h. Cells were treated for 15 min with 300 μM BzATP or 3 mM ATP, in the absence or presence of 10 μM A-804598 **(D)**. **(E)** SOD1-G93A microglia treated with 300 μM BzATP in the absence or presence of 10 μM A-804598 were analyzed by means of fluorescence microscopy after staining with anti-LC3B (arrows indicate LC3 vacuoles; scale bar 50 μm; nuclei in blue). Data represent mean ± SEM of $n = 3$ independent experiments. Statistical significance was calculated by student's *t*-test or Mann-Whitney rank sum test or analysis of variance (ANOVA) followed by *Post Hoc* Tukey's test, and referred to WT **(A)** or Ctrl **(B–D)** ($^{*}p < 0.05$, $^{**}p < 0.01$); to BzATP15'-treated cells or ATP15'-treated cells ($^{\#}p < 0.05$).

non-autophagic, whereas cells with increased LC3 vacuoles are classified as autophagic (Tasdemir et al., 2008; Klionsky et al., 2016). Confirming the western blot data, we observed that 300 μM BzATP increases cytoplasmic LC3-positive dots in microglia with respect to control, and the effect is reduced by the P2X7 antagonist A-804598 (**Figure 1E**).

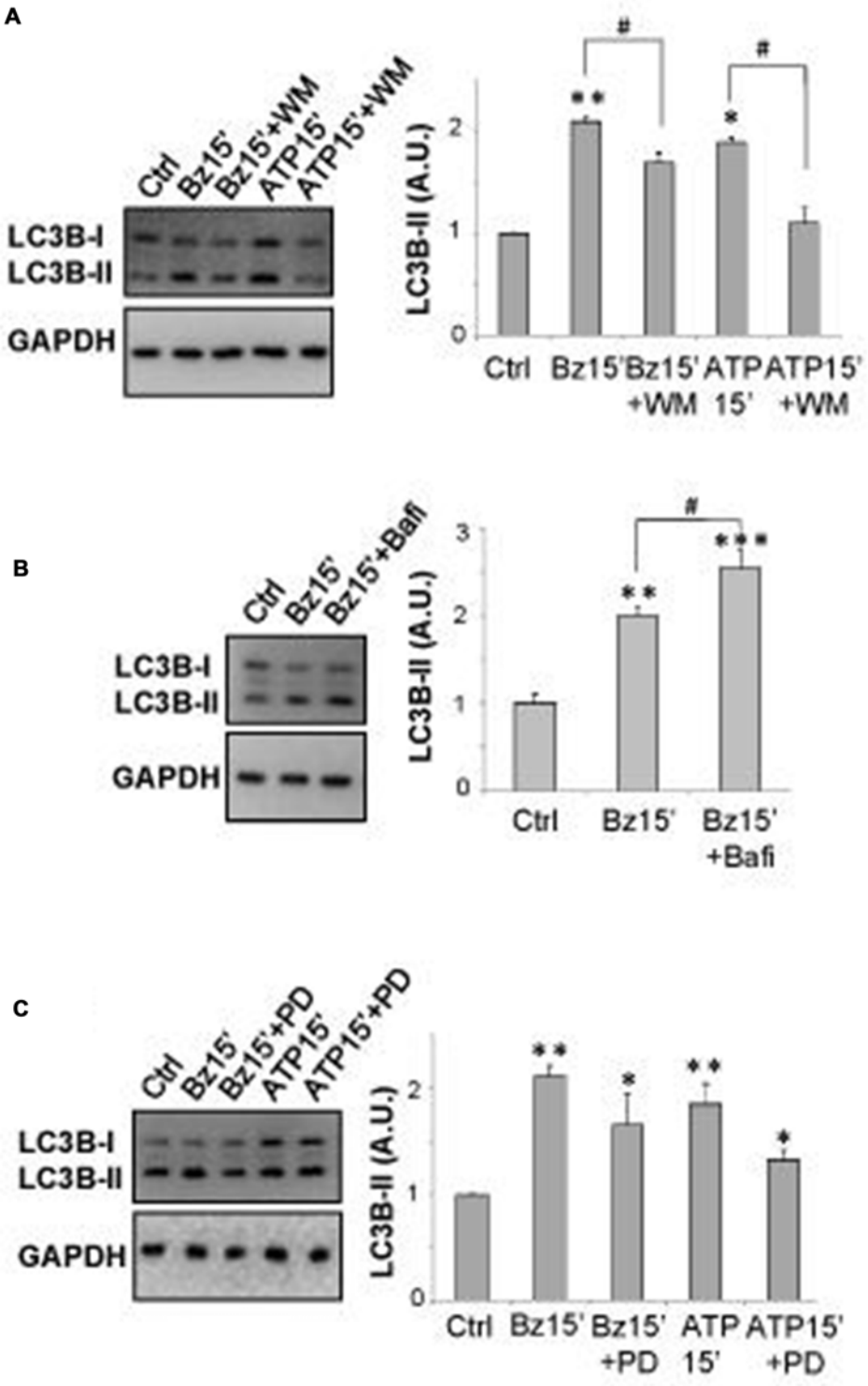

FIGURE 2 | P2X7 induces autophagic flux in SOD1-G93A microglia. Equal amounts of protein from SOD1-G93A primary microglia were subjected to western blotting and immunoreactions with anti-LC3B-II and anti-GAPDH. In **(A)** SOD1-G93A microglia were treated for 15 min with 300 μM BzATP or 3 mM ATP in the absence or presence of 100 nM wortmannin (WM) **(A)**. In **(B)** SOD1-G93A microglia were treated for 15 min with 300 μM BzATP in the absence or presence of 25 nM Bafilomycin-A1. **(C)** SOD1-G93A microglia were treated for 15 min with 300 μM BzATP or 3 mM ATP, in the absence or presence of 100 μM PD98059. Data represent mean ± SEM of $n = 3$ independent experiments. Statistical significance was calculated by ANOVA followed by *Post Hoc* Tukey's test and referred to Ctrl ($^{*}p < 0.05$, $^{**}p < 0.01$, $^{***}p < 0.001$); to BzATP15'-treated cells or to ATP15'-treated cells ($^{\#}p < 0.05$).

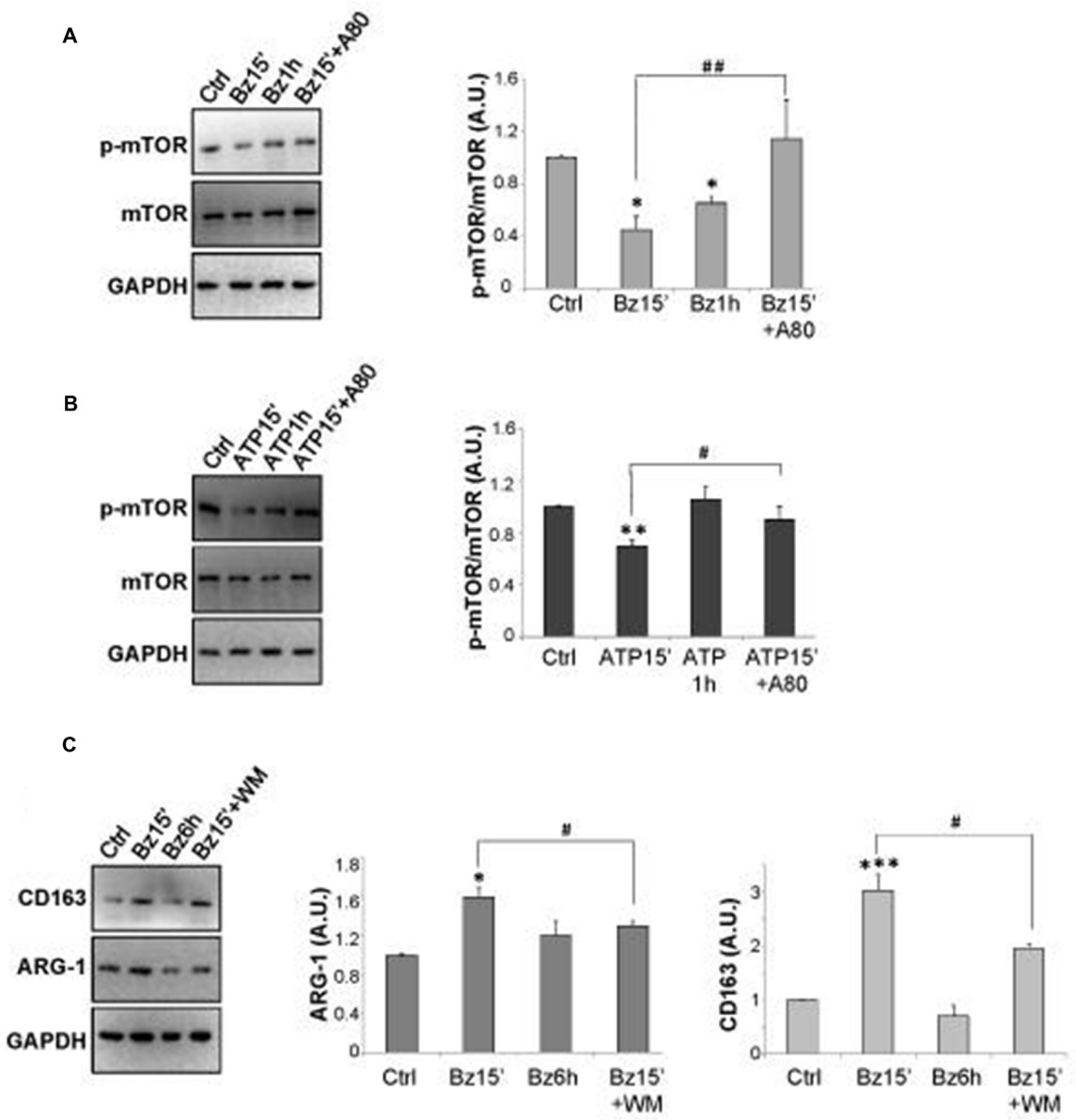

FIGURE 3 | mTOR phosphorylation is regulated by P2X7 activation in SOD1-G93A microglia. SOD1-G93A microglia were treated with 300 μM BzATP **(A)** or 3 mM ATP **(B)** for 15 min or 1 h with or without 10 μM A-804598 and subjected to western blotting and immunoreactions with anti-p-mTOR and anti-mTOR or anti-GAPDH. SOD1-G93A cells exposed to 300 μM BzATP for 15 min with or without WM or 6 h were subjected to western blotting and immunoreactions with anti-Arginase-1 (ARG-1) **(C)** or anti-CD163 and anti-GAPDH. Data represent mean ± SEM of $n = 3$ independent experiments. Statistical significance was calculated by student's *t*-test or Mann-Whitney rank sum test or ANOVA followed by *Post Hoc* Tukey's test, and referred to Ctrl ($^{*}p < 0.05$, $^{**}p < 0.01$, $^{***}p < 0.001$); to BzATP15'- or ATP15'-treated cells ($^{\#}p < 0.05$, $^{\#\#}p < 0.01$).

To demonstrate the autophagic mechanism involved in LC3-II induction, next we show that LC3B-II up-regulation by BzATP and ATP is attenuated by wortmannin (WM; 100 nM), an inhibitor of the initial stage of conventional autophagy/phosphoinositide-3-kinase (Klionsky et al., 2016; **Figure 2A**). A correct way to define if a treatment augments a true autophagic flux is to determine the levels of LC3B-II in the presence of the lysosomal proteases inhibitor bafilomycin-A1 (Klionsky et al., 2016). While the increase in LC3-II by a treatment simply indicates the accumulation of autophagosomes without proving autophagic degradation, an enhancement of autophagy indeed occurs if LC3-II further accumulates in the presence of bafilomycinA1 (Mizushima and Yoshimori, 2007). Here we show that the addition of bafilomycin-A1 (25 nM) indeed further increases the up-regulation of LC3B-II induced by 300 μM BzATP with respect to control cells, consistently with an accelerated true autophagic flux (**Figure 2B**).

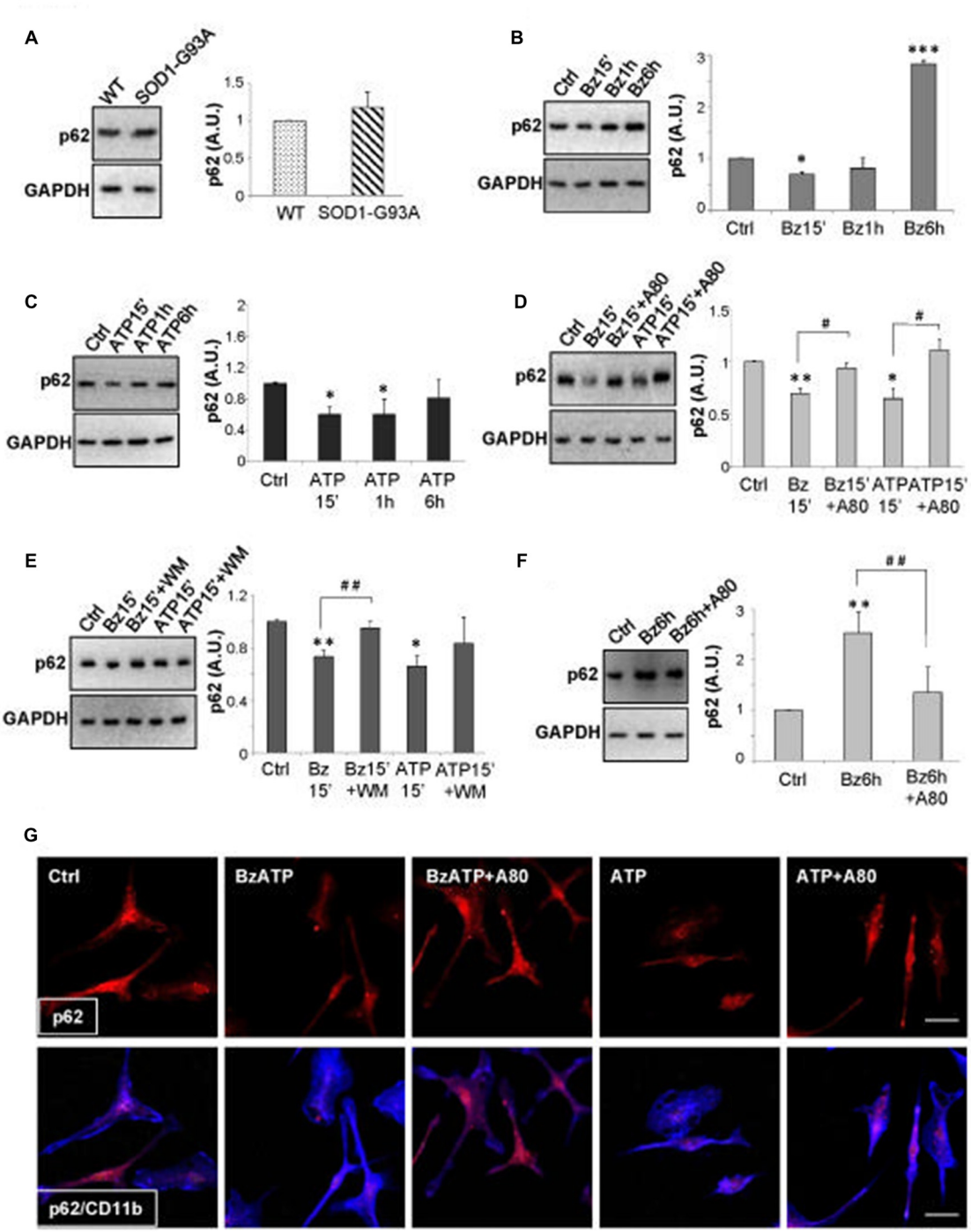

FIGURE 4 | Activation of P2X7 affects SQSTM1/p62 levels in SOD1-G93A microglia. **(A)** Equal amounts of protein from SOD1-G93A and WT microglia were subjected to western blotting and immunoreactions with anti-SQSTM1/p62 and anti-GAPDH. SOD1-G93A microglia were exposed to 300 μM BzATP **(B)** or 3 mM ATP **(C)** for 15 min, 1 h or 6 h and equal amounts of total protein were subjected to western blotting and immunoreactions with anti-SQSTM1/p62 and anti-GAPDH. SOD1-G93A microglia were exposed to 300 μM BzATP or 3 mM ATP for 15 min with or without A-804598 10 μM **(D)** or WM 100 nM **(E)** and equal amounts of protein were subjected to western blotting and immunoreactions with anti-SQSTM1/p62 and anti-GAPDH. **(F)** SOD1-G93A microglia exposed to 300 μM BzATP for 6 h with or without 10 μM A-804598 were subjected to western blotting and immunoreactions with anti-SQSTM1/p62 and anti-GAPDH. **(G)** SOD1-G93A microglia treated for 15 min with 300 μM BzATP or 3 mM ATP in the absence or presence of 10 μM A-804598 were analyzed by means of fluorescence microscopy after staining with anti-SQSTM1/p62 (red) and CD11b (blue) (scale bar 50 μm). Data represent mean ± SEM of $n = 3$ independent experiments. Statistical significance was calculated by student's *t*-test or ANOVA followed by *Post Hoc* Tukey's test referred to Ctrl ($^{*}p < 0.05$, $^{**}p < 0.01$, $^{***}p < 0.001$); to BzATP15'-treated cells or ATP15'-treated cells (**D,E**; $^{\#}p < 0.05$, $^{\#\#}p < 0.01$), or BzATP6h-treated cells (**F**; $^{\#\#}p < 0.01$).

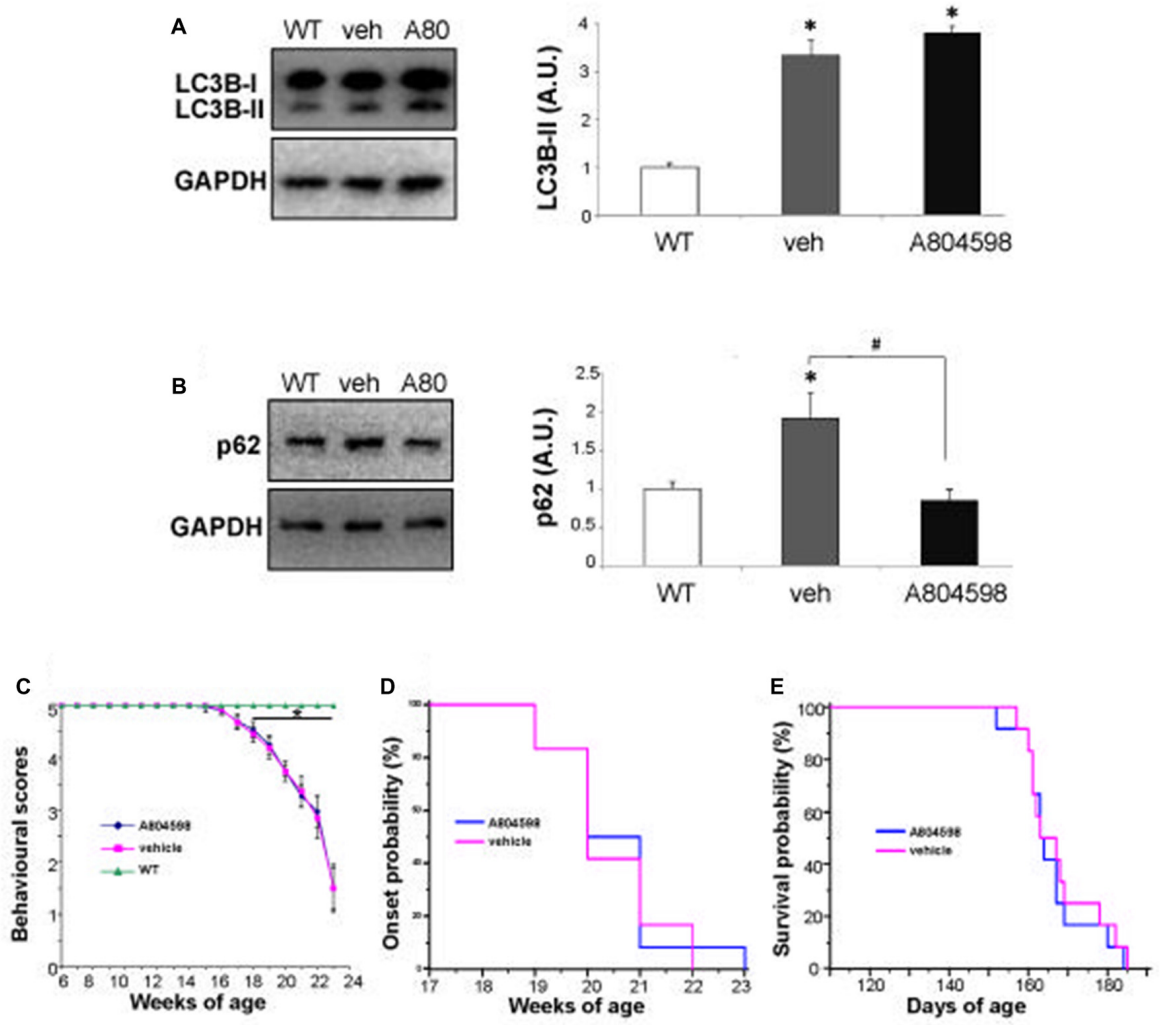

FIGURE 5 | *In vivo* chronic treatment with P2X7 antagonist A-804598 decreases SQSTM1/p62 expression in lumbar spinal cord of SOD1-G93A mice. Equal amounts of protein from lumbar spinal cord lysates of WT mice (~5 months) and vehicle- or A-804598-treated SOD1-G93A mice at end stage (n = 4/group) were subjected to western blotting with anti-LC3B-II **(A)**, anti-SQSTM1/p62 **(B)** and anti-GAPDH. **(C)** Behavioral scores are not affected by A-804598 treatment (n = 12) with respect to vehicle mice (n = 12). WT mice (n = 3). Data represent mean ± SEM. Statistical significance was calculated by student's t-test or ANOVA followed by *Post Hoc* Tukey's test referred to WT (**A–C**; $^{*}p < 0.05$) or to vehicle mice (**B**; $^{\#}p < 0.05$). **(D)** The disease onset of SOD1-G93A mice, as shown by Kaplan–Meier survival curves was not affected by A-804598. **(E)** A-804598-treated mice show no significant differences in median survival with respect to vehicle-treated SOD1-G93A, as shown by Kaplan–Meier survival curves (163.5 days for A-804598 vs. 163 days for vehicle).

We have previously demonstrated that BzATP modulates ERK1/2 phosphorylation in SOD1-G93A primary microglia (Apolloni et al., 2013b). Because the MAPK activation pathway is a positive regulator of autophagy induction (Young et al., 2015) and previous data have reported that p-ERK1/2 is specifically involved in induction of LC3B-II expression by activated P2X7 in non-transgenic microglia (Takenouchi et al., 2009b), we have stimulated SOD1-G93A microglia with 300 μM BzATP or 3 mM ATP in the presence of the MEK pathway inhibitor PD98059 (100 μM) that *per se* does not affect basal LC3B-II content (data not shown). Although a partial and not statistically significant inhibition is observed on LC3B-II up-regulation by ATP, LC3B-II induction mediated by P2X7 receptor is not apparently dependent on ERK1/2 phosphorylation, not being significantly inhibited by PD98059 (**Figure 2C**).

P2X7 Inhibits mTOR Phosphorylation and Modulates M2 Markers in SOD1-G93A Microglia

Inhibition of mTOR pathway is generally required for the induction of conventional autophagy (Klionsky et al., 2016). Thus, we have analyzed the effects of P2X7 activation on mTOR phosphorylation, showing by western blot analysis that 300 μM BzATP, or 3 mM ATP, is able to transiently decrease the protein content of p-mTOR/mTOR in SOD1-G93A microglia, with maximal inhibition observed after 15 min, as compared to

control cells (**Figures 3A,B**). These effects are partially prevented by the P2X7 antagonist A-804598.

Microglia activation is known to occur by the alternating acquisition of different phenotypes concisely defined as M2 with anti-inflammatory properties, and M1 with pro-inflammatory features (Franco and Fernández-Suárez, 2015). Since the autophagic flux impacts on the M2/M1 microglia phenotypes (Su et al., 2016; Xia et al., 2016), we investigated the effects of BzATP stimulation on the levels of the M2 markers CD163 and ARG-1, in the absence or presence of WM. As shown in **Figure 3C**, 300 μM BzATP in 15 min increases the content of ARG-1 and CD163 proteins that returns approximately to basal levels in 6 h and is partially reverted by WM.

Activation of P2X7 Affects SQSTM1/p62 Protein Content in SOD1-G93A Microglia and in Lumbar Spinal Cord of SOD1-G93A Mice

A well-known substrate of autophagy is SQSTM1/p62 protein that can be degraded within the autolysosomes as an additional evidence of autophagic activity (Mizushima et al., 2010). To ascertain whether the increased LC3B-II levels induced by P2X7 activation in SOD1-G93A microglia represent a true increase in the autophagic flux, we have examined the content of SQSTM1/p62 protein. We have observed that while SOD1-G93A microglia contain levels of p62 comparable to WT microglia (**Figure 4A**), 300 μM BzATP (**Figure 4B**), or 3 mM ATP (**Figure 4C**), transiently decreases SQSTM1/p62 protein content in SOD1-G93A microglia with about 50% maximal inhibition obtained in 15 min (**Figures 4B,C**). A pre-incubation with the P2X7 antagonist A-804598 (**Figure 4D**) or with WM (**Figure 4E**), partially abolishes BzATP- and ATP-mediated SQSTM1/p62 decrease in SOD1-G93A microglia. As WM is also a class III phosphatidylinositol 3-kinase inhibitor, this result moreover indicates that P2X7-mediated increase in autophagic flux occurs via the phosphatidylinositol 3-kinase-mediated pathway. The reduction of SQSTM1/p62 by a short treatment with BzATP or ATP in SOD1-G93A microglia is confirmed also by double immunofluorescence with microglia specific marker anti-CD11b, as the intensity of the SQSTM1/p62 immunostaining is reduced after a short-term stimulation of P2X7 with respect to unstimulated cells, and the effect is reversed by the simultaneous presence of A-804598 (**Figure 4G**). Interestingly, a sustained activation of P2X7 by BzATP for 6 h markedly increases the levels of SQSTM1/p62 protein with respect to unstimulated cells, and this effect is abolished by the presence of A-804598 (**Figure 4F**), thus indicating that a prolonged P2X7 activation might cause an engulfment of the autophagic flux.

It is known that the SQSTM1/p62 autophagy substrate accumulates, together with LC3B-II, in lumbar spinal cord of ALS mice during disease progression, when the autophagic flux is impaired (Zhang et al., 2011). We have therefore measured the level of LC3B-II and SQSTM1/p62 proteins in lumbar spinal cord of SOD1-G93A mice after having pharmacologically inhibited *in vivo* the P2X7 receptor by a chronic treatment in female SOD1-G93A mice with the blood-brain permeant A-804598, demonstrated to reach brain concentrations in rodents after oral or i.p. doses (Able et al., 2011; Iwata et al., 2016), administered at 30 mg/Kg from pre-onset to end stage of disease. We find that while the protein levels of LC3B-II (**Figure 5A**) and SQSTM1/p62 (**Figure 5B**) are confirmed to be both increased at end stage in vehicle-treated SOD1-G93A mice with respect to WT, in A-804598-treated ALS mice with respect to vehicle, the LC3B-II protein content appears unmodified, while SQSTM1/p62 is inhibited to basal levels (**Figures 5A,B**). As shown, neither behavioral scores (**Figure 5C**), disease onset (**Figure 5D**), nor survival (**Figure 5E**) are however affected by A-804598 when administered in female SOD1-G93A mice.

DISCUSSION

Recent work has provided strong indications not only that autophagy plays a key role in ALS, but also that P2X7 receptor contributes to the neuroinflammatory pathway of ALS on one hand, and to the autophagic flux of microglia, on the other. The aim of this work was thus to investigate if P2X7 activation participates to ALS pathogenesis by directly modulating autophagic mechanisms in microglia, in other words to establish the occurrence of a P2X7-neuroinflammation-

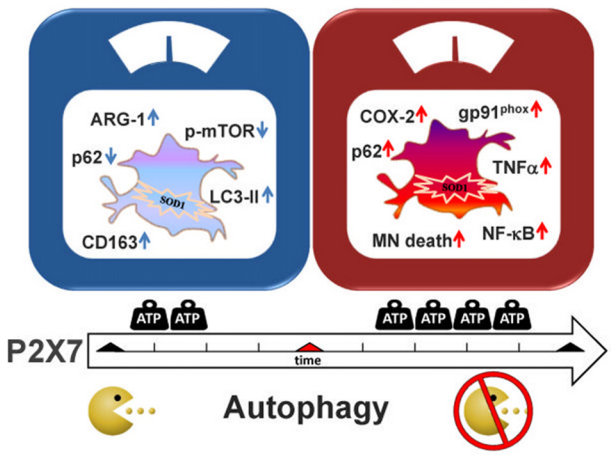

FIGURE 6 | Schematic representation of P2X7 actions in SOD1-G93A microglia. Treatment of SOD1-G93A primary microglia with P2X7 agonists BzATP or ATP modulates inflammatory and autophagic markers. After a short stimulation (left panel), P2X7 induces an increase in M2 markers (ARG-1 and CD163) concomitantly with the stimulation of the autophagic process by augmenting LC3-II and decreasing p62 and p-MTOR levels. Conversely, a sustained activation with P2X7 agonists (right panel), causes inhibition of the autophagic flux with up-regulation of p62 that is parallel to previous results showing an increase of pro-inflammatory M1 markers $gp91^{phox}$ (Apolloni et al., 2016b), cyclooxygenase-2 (COX-2; D'Ambrosi et al., 2009), and moreover nuclear factor kappa-B (NF-κB; Parisi et al., 2016), tumor necrosis factor alpha (TNF-α) and motor neurons (MN) death (D'Ambrosi et al., 2009).

autophagy axis in ALS-microglia. We demonstrate that the modulation of the autophagic flux appears as a novel mechanism by which P2X7 contributes to activate SOD1-G93A microglia and to interfere with ALS features (**Figure 6**). In detail, we have illustrated here that a short time window of P2X7 stimulation by purinergic agonists augments LC3-II via the mTOR pathway and decreases SQSTM1/p62 levels, concurrently with an up-regulation of the M2 markers CD163 and ARG-1 in SOD1-G93A primary microglia. On the contrary, a sustained activation of P2X7 leads to an impairment of the autophagic flux with increased SQSTM1/p62 protein content. This might occur concomitantly with the previously characterized polarization of SOD1-G93A microglia toward the M1 phenotype exemplified by $gp91^{phox}$, COX-2, TNF-α and NF-κB activation, and toxicity towards MN (D'Ambrosi et al., 2009; Apolloni et al., 2016b; Parisi et al., 2016). Although as yet unaware of the molecular mechanisms linking the decrease in autophagy to the insurgence of pro-inflammatory actions sustained by P2X7, our results are in line with the involvement of autophagy in the inflammatory response (Levine et al., 2011; Apolloni et al., 2016a). Indeed, when autophagy is stimulated by LPS in microglia, the expression of inducible nitric oxide synthase is suppressed (Han et al., 2013). Conversely, when the autophagic flux is inhibited, the M1 phenotype is induced with higher expression of TNF-α, inducible nitric oxide synthase and COX-2 mediated by the NF-κB pathway, and M2 genes are instead inhibited with down-regulation of ARG-1, BDNF and IL-10 (Xia et al., 2016). In both ALS patients and transgenic mice, it is well known that microglia switches from a beneficial M2 phenotype occurring during the early phases of disease, to a detrimental M1 phenotype that is more preponderant when the disease accelerates and motor neuron injury escalates (Henkel et al., 2009; Beers et al., 2011; Zhao et al., 2013; Hooten et al., 2015). These and our findings would thus suggest a parallelism between M2 inflammatory state and activation of autophagy, as well as M1 inflammatory condition and inhibition of autophagy, both consistently with the dual role played by P2X7 in ALS pathogenesis.

Moreover, we suggest that the short P2X7-dependent activation of autophagy demonstrated *in vitro* in SOD1-G93A microglia could be related to the beneficial role of P2X7 activation occurring during the early phase of the disease, when genetic ablation of P2X7 elicits detrimental consequences on ALS phenotype (Apolloni et al., 2013a). The persistent stimulation of P2X7 causing autophagic flux inhibition in SOD1-G93A microglia *in vitro* is instead perhaps resembling what occurs during the symptomatic phase of the disease, when the pharmacological inhibition of P2X7 exerts beneficial effects on ALS progression (Apolloni et al., 2014; Sluyter et al., 2017).

The initial stimulation of autophagic flux found in SOD1-G93A microglia by P2X7 activation with inhibition of mTOR phosphorylation differs from what reported in non-transgenic microglia where P2X7 signaling has been reported to negatively regulate autophagic flux and stimulate the phosphorylation of mTOR (Takenouchi et al., 2009b). The induction of microglial autophagy is instead in line with data obtained in dystrophic muscle cells, where P2X7 indeed increases autophagy (Young et al., 2015), thus indicating a phenotype-specific purinergic-mediated autophagy in ALS. In addition, we have demonstrated that LC3-II induction in SOD1-G93A microglia is apparently independent from ERK1/2 activation, again in line with what reported in muscle cells, where MAP kinases play only a marginal role in ATP-induced autophagy (Young et al., 2015). This is again different from what reported in non-transgenic microglia (Takenouchi et al., 2009b), where inhibition of autophagy is instead dependent on the MAPK pathway. By emphasizing the divergence between non-transgenic and SOD1-G93A microglia, these results however reinforce the synergism between autophagy and inflammation in P2X7-activated microglia.

Finally, in this article we have shown that inhibition of P2X7 through the antagonist A-804598 in SOD1-G93A mice suppresses SQSTM1/p62 up-regulation in lumbar spinal cord, thus confirming P2X7 as an *in vivo* modulator of the ALS pathological mechanism of autophagy, although further experiments might contribute to identify the cell phenotypes that are more responsible for altered autophagy. Survival, behavioral scores and disease onset are however not affected by A-804598 when administered in female SOD1-G93A mice at the time and dose adopted in our work. This suggests that inhibition of SQSTM1/p62 overexpression is perhaps necessary, but not sufficient, to ameliorate ALS disease. Given the various controversial male vs. female differences encountered on the effects of P2X7 antagonists or genetic ablation (Sluyter et al., 2017), we cannot exclude that further dose- and sex-dependent preclinical studies might provide different results.

Ectonucleotidase activities are responsible for the degradation of extracellular ATP, and SOD1-G93A microglia have a reduced extracellular ATP hydrolyzing activity with respect to non-transgenic microglia (D'Ambrosi et al., 2009; Butovsky et al., 2012; Volonté et al., 2016). This would imply that higher extracellular ATP concentrations might be present *in vivo* in the proximity of SOD1-G93A damaged MN to activate P2X7 on neighboring cells. While an initial activation of P2X7 might ensure a positive impact on microglia by stimulating autophagy, a persistent engagement of the receptor might in turn inhibit autophagy. These results thus extend to autophagy the dual role previously suggested for P2X7 in the SOD1-G93A model (Volonté et al., 2016). In order to further validate the *in vitro* and *in vivo* results about P2X7-dependent modulation of autophagy, because previous studies suggested that SOD1-G93A microglia has a regional heterogeneity during disease progression (Nikodemova et al., 2014), future experiments will investigate the actions of P2X7 also in primary microglia from SOD1-G93A spinal cord. Moreover, because WT-SOD1 overexpression in mice *per se* causes mitochondrial vacuolization, axonal degeneration and premature motor neuron loss in mice (Jaarsma et al., 2000), we will also study how

this condition might for itself influence the effects of P2X7 in microglia.

In conclusion, our results extend the role of P2X7 as a means for interfering with autophagy in SOD1-G93A microglia, and a new mechanism of intervention against autophagic dysfunction in ALS pathogenesis.

AUTHOR CONTRIBUTIONS

PF, SAm and SAp performed experiments, collected and analyzed data. SAp and CV designed the experiments and wrote the manuscript. All authors approved the manuscript for publication.

ACKNOWLEDGMENTS

This work was supported by AriSLA-Agenzia Italiana per la Ricerca sulla Sclerosi Laterale Amiotrofica (grant PATH-for-ALS). We thank Dr. Veronica Verdile for technical help, Dr. Vania Gelmetti for suggestions and critical reading of the manuscript and Dr. Daniele Peluso for statistical advice.

REFERENCES

Able, S. L., Fish, R. L., Bye, H., Booth, L., Logan, Y. R., Nathaniel, C., et al. (2011). Receptor localization, native tissue binding and *ex vivo* occupancy for centrally penetrant P2X7 antagonists in the rat. *Br. J. Pharmacol.* 162, 405–414. doi: 10.1111/j.1476-5381.2010.01025.x

Apolloni, S., Amadio, S., Montilli, C., Volonté, C., and D'Ambrosi, N. (2013a). Ablation of P2X7 receptor exacerbates gliosis and motoneuron death in the SOD1–G93A mouse model of amyotrophic lateral sclerosis. *Hum. Mol. Genet.* 22, 4102–4116. doi: 10.1093/hmg/ddt259

Apolloni, S., Parisi, C., Pesaresi, M. G., Rossi, S., Carrì, M. T., Cozzolino, M., et al. (2013b). The NADPH oxidase pathway is dysregulated by the P2X7 receptor in the SOD1–G93A microglia model of amyotrophic lateral sclerosis. *J. Immunol.* 190, 5187–5195. doi: 10.4049/jimmunol.1203262

Apolloni, S., Fabbrizio, P., Amadio, S., and Volonté, C. (2016a). Actions of the antihistaminergic clemastine on presymptomatic SOD1–G93A mice ameliorate ALS disease progression. *J. Neuroinflammation* 13:191. doi: 10.1186/s12974-016-0658-8

Apolloni, S., Fabbrizio, P., Parisi, C., Amadio, S., and Volonté, C. (2016b). Clemastine confers neuroprotection and induces an anti-inflammatory phenotype in SOD1(G93A) mouse model of amyotrophic lateral sclerosis. *Mol. Neurobiol.* 53, 518–531. doi: 10.1007/s12035-014-9019-8

Apolloni, S., Amadio, S., Parisi, C., Matteucci, A., Potenza, R. L., Armida, M., et al. (2014). Spinal cord pathology is ameliorated by P2X7 antagonism in a SOD1-mutant mouse model of amyotrophic lateral sclerosis. *Dis. Model. Mech.* 7, 1101–1109. doi: 10.1242/dmm.017038

Barth, S., Glick, D., and Macleod, K. F. (2010). Autophagy: assays and artifacts. *J. Pathol.* 221, 117–124. doi: 10.1002/path.2694

Bartlett, R., Sluyter, V., Watson, D., Sluyter, R., and Yerbury, J. J. (2017). P2X7 antagonism using Brilliant Blue G reduces body weight loss and prolongs survival in female SOD1G93A amyotrophic lateral sclerosis mice. *PeerJ* 5:e3064. doi: 10.7717/peerj.3064

Beamer, E., Gölöncsér, F., Horváth, G., Bekő, K., Otrokocsi, L., Koványi, B., et al. (2016). Purinergic mechanisms in neuroinflammation: an update from molecules to behavior. *Neuropharmacology* 104, 94–104. doi: 10.1016/j.neuropharm.2015.09.019

Beers, D. R., Zhao, W., Liao, B., Kano, O., Wang, J., Huang, A., et al. (2011). Neuroinflammation modulates distinct regional and temporal clinical responses in ALS mice. *Brain Behav. Immun.* 25, 1025–1035. doi: 10.1016/j.bbi.2010.12.008

Biswas, D., Qureshi, O. S., Lee, W. Y., Croudace, J. E., Mura, M., and Lammas, D. A. (2008). ATP-induced autophagy is associated with rapid killing of intracellular mycobacteria within human monocytes/macrophages. *BMC Immunol.* 9:35. doi: 10.1186/1471-2172-9-35

Butovsky, O., Siddiqui, S., Gabriely, G., Lanser, A. J., Dake, B., Murugaiyan, G., et al. (2012). Modulating inflammatory monocytes with a unique microRNA gene signature ameliorates murine ALS. *J. Clin. Invest.* 122, 3063–3087. doi: 10.1172/jci62636

Catanzaro, J. M., Hueston, C. M., Deak, M. M., and Deak, T. (2014). The impact of the P2X7 receptor antagonist A-804598 on neuroimmune and behavioral consequences of stress. *Behav. Pharmacol.* 25, 582–598. doi: 10.1097/FBP.0000000000000072

Cervetto, C., Frattaroli, D., Maura, G., and Marcoli, M. (2013). Motor neuron dysfunction in a mouse model of ALS: gender-dependent effect of P2X7 antagonism. *Toxicology* 311, 69–77. doi: 10.1016/j.tox.2013.04.004

Cozzolino, M., Pesaresi, M. G., Gerbino, V., Grosskreutz, J., and Carrì, M. T. (2012). Amyotrophic lateral sclerosis: new insights into underlying molecular mechanisms and opportunities for therapeutic intervention. *Antioxid. Redox Signal.* 17, 1277–1330. doi: 10.1089/ars.2011.4328

D'Ambrosi, N., Finocchi, P., Apolloni, S., Cozzolino, M., Ferri, A., Padovano, V., et al. (2009). The proinflammatory action of microglial P2 receptors is enhanced in SOD1 models for amyotrophic lateral sclerosis. *J. Immunol.* 183, 4648–4656. doi: 10.4049/jimmunol.0901212

Donnelly-Roberts, D. L., Namovic, M. T., Surber, B., Vaidyanathan, S. X., Perez-Medrano, A., Wang, Y., et al. (2009). [3H]A-804598 ([3H]2-cyano-1-[(1S)-1-phenylethyl]-3-quinolin-5-ylguanidine) is a novel, potent, and selective antagonist radioligand for P2X7 receptors. *Neuropharmacology* 56, 223–229. doi: 10.1016/j.neuropharm.2008.06.012

Franco, R., and Fernández-Suárez, D. (2015). Alternatively activated microglia and macrophages in the central nervous system. *Prog. Neurobiol.* 131, 65–86. doi: 10.1016/j.pneurobio.2015.05.003

Glick, D., Barth, S., and Macleod, K. F. (2010). Autophagy: cellular and molecular mechanisms. *J. Pathol.* 221, 3–12. doi: 10.1002/path.2697

Haanes, K. A., Schwab, A., and Novak, I. (2012). The P2X7 receptor supports both life and death in fibrogenic pancreatic stellate cells. *PLoS One* 7:e51164. doi: 10.1371/journal.pone.0051164

Han, H.-E., Kim, T.-K., Son, H.-J., Park, W. J., and Han, P. L. (2013). Activation of autophagy pathway suppresses the expression of iNOS, IL6 and cell death of LPS-stimulated microglia cells. *Biomol. Ther. (Seoul)* 21, 21–28. doi: 10.4062/biomolther.2012.089

Henkel, J. S., Beers, D. R., Zhao, W., and Appel, S. H. (2009). Microglia in ALS: the good, the bad, and the resting. *J. Neuroimmune Pharmacol.* 4, 389–398. doi: 10.1007/s11481-009-9171-5

Hooten, K. G., Beers, D. R., Zhao, W., and Appel, S. H. (2015). Protective and toxic neuroinflammation in amyotrophic lateral sclerosis. *Neurotherapeutics* 12, 364–375. doi: 10.1007/s13311-014-0329-3

Ilieva, H., Polymenidou, M., and Cleveland, D. W. (2009). Non-cell autonomous toxicity in neurodegenerative disorders: ALS and beyond. *J. Cell Biol.* 187, 761–772. doi: 10.1083/jcb.200908164

Illes, P., and Verkhratsky, A. (2016). Purinergic neurone-glia signalling in cognitive-related pathologies. *Neuropharmacology* 104, 62–75. doi: 10.1016/j.neuropharm.2015.08.005

Iwata, M., Ota, K. T., Li, X. Y., Sakaue, F., Li, N., Dutheil, S., et al. (2016). Psychological stress activates the inflammasome via release of adenosine triphosphate and stimulation of the purinergic type 2×7 receptor. *Biol. Psychiatry* 80, 12–22. doi: 10.1016/j.biopsych.2015.11.026

Jaarsma, D., Haasdijk, E. D., Grashorn, J. A., Hawkins, R., van Duijn, W., Verspaget, H. W., et al. (2000). Human Cu/Zn superoxide dismutase (SOD1) overexpression in mice causes mitochondrial vacuolization, axonal degeneration, and premature motoneuron death and accelerates motoneuron disease in mice expressing a familial amyotrophic lateral sclerosis mutant SOD1. *Neurobiol. Dis.* 7, 623–643. doi: 10.1006/nbdi.2000.0299

Klionsky, D. J., Abdelmohsen, K., Abe, A., Abedin, M. J., Abeliovich, H., Acevedo Arozena, A., et al. (2016). Guidelines for the use and interpretation

of assays for monitoring autophagy (3rd edition). *Autophagy* 12, 1–222. doi: 10.1080/15548627.2015.1100356

Klionsky, D. J., and Emr, S. D. (2000). Autophagy as a regulated pathway of cellular degradation. *Science* 290, 1717–1721. doi: 10.1126/science.290.5497.1717

Levine, B., Mizushima, N., and Virgin, H. W. (2011). Autophagy in immunity and inflammation. *Nature* 469, 323–335. doi: 10.1038/nature09782

Ludolph, A. C., Bendotti, C., Blaugrund, E., Chio, A., Greensmith, L., Loeffler, J. P., et al. (2010). Guidelines for preclinical animal research in ALS/MND: a consensus meeting. *Amyotroph. Lateral Scler.* 11, 38–45. doi: 10.3109/17482960903545334

Mizushima, N., and Yoshimori, T. (2007). How to interpret LC3 immunoblotting. *Autophagy* 3, 542–545. doi: 10.4161/auto.4600

Mizushima, N., Yoshimori, T., and Levine, B. (2010). Methods in mammalian autophagy research. *Cell* 140, 313–326. doi: 10.1016/j.cell.2010.01.028

Monif, M., Burnstock, G., and Williams, D. A. (2010). Microglia: proliferation and activation driven by the P2X7 receptor. *Int. J. Biochem. Cell Biol.* 42, 1753–1756. doi: 10.1016/j.biocel.2010.06.021

Monif, M., Reid, C. A., Powell, K. L., Drummond, K. J., O'Brien, T. J., and Williams, D. A. (2016). Interleukin-1β has trophic effects in microglia and its release is mediated by P2X7R pore. *J. Neuroinflammation* 13:173. doi: 10.1186/s12974-016-0621-8

Nikodemova, M., Small, A. L., Smith, S. M., Mitchell, G. S., and Watters, J. J. (2014). Spinal but not cortical microglia acquire an atypical phenotype with high VEGF, galectin-3 and osteopontin and blunted inflammatory responses in ALS rats. *Neurobiol. Dis.* 69, 43–53. doi: 10.1016/j.nbd.2013.11.009

Parisi, C., Napoli, G., Amadio, S., Spalloni, A., Apolloni, S., Longone, P., et al. (2016). MicroRNA-125b regulates microglia activation and motor neuron death in ALS. *Cell Death Differ.* 23, 531–541. doi: 10.1038/cdd.2015.153

Pizzasegola, C., Caron, I., Daleno, C., Ronchi, A., Minoia, C., Carri, M. T., et al. (2009). Treatment with lithium carbonate does not improve disease progression in two different strains of SOD1 mutant mice. *Amyotroph. Lateral Scler.* 10, 221–228. doi: 10.1080/17482960902803440

Sluyter, R., Bartlett, R., Ly, D., and Yerbury, J. J. (2017). P2X7 receptor antagonism in amyotrophic lateral sclerosis. *Neural Regen. Res.* 12, 749–750. doi: 10.4103/1673-5374.206643

Song, C. Y., Guo, J. F., Liu, Y., and Tang, B. S. (2012). Autophagy and its comprehensive impact on ALS. *Int. J. Neurosci.* 122, 695–703. doi: 10.3109/00207454.2012.714430

Su, P., Zhang, J., Wang, D., Zhao, F., Cao, Z., Aschner, M., et al. (2016). The role of autophagy in modulation of neuroinflammation in microglia. *Neuroscience* 319, 155–167. doi: 10.1016/j.neuroscience.2016.01.035

Takenouchi, T., Fujita, M., Sugama, S., Kitani, H., and Hashimoto, M. (2009a). The role of the P2X7 receptor signaling pathway for the release of autolysosomes in microglial cells. *Autophagy* 5, 723–724. doi: 10.4161/auto.5.5.8478

Takenouchi, T., Nakai, M., Iwamaru, Y., Sugama, S., Tsukimoto, M., Fujita, M., et al. (2009b). The activation of P2X7 receptor impairs lysosomal functions and stimulates the release of autophagolysosomes in microglial cells. *J. Immunol.* 182, 2051–2062. doi: 10.4049/jimmunol.0802577

Tasdemir, E., Maiuri, M. C., Galluzzi, L., Vitale, I., Djavaheri-Mergny, M., D'Amelio, M., et al. (2008). Regulation of autophagy by cytoplasmic p53. *Nat. Cell Biol.* 10, 676–687. doi: 10.1038/ncb1730

Volonté, C., Apolloni, S., Parisi, C., and Amadio, S. (2016). Purinergic contribution to amyotrophic lateral sclerosis. *Neuropharmacology* 104, 180–193. doi: 10.1016/j.neuropharm.2015.10.026

Xia, C. Y., Zhang, S., Chu, S. F., Wang, Z. Z., Song, X. Y., Zuo, W., et al. (2016). Autophagic flux regulates microglial phenotype according to the time of oxygen-glucose deprivation/reperfusion. *Int. Immunopharmacol.* 39, 140–148. doi: 10.1016/j.intimp.2016.06.030

Young, C. N., Sinadinos, A., Lefebvre, A., Chan, P., Arkle, S., Vaudry, D., et al. (2015). A novel mechanism of autophagic cell death in dystrophic muscle regulated by P2RX7 receptor large-pore formation and HSP90. *Autophagy* 11, 113–130. doi: 10.4161/15548627.2014.994402

Zhang, X., Li, L., Chen, S., Yang, D., Wang, Y., Zhang, X., et al. (2011). Rapamycin treatment augments motor neuron degeneration in SOD1(G93A) mouse model of amyotrophic lateral sclerosis. *Autophagy* 7, 412–425. doi: 10.4161/auto.7.4.14541

Zhao, W., Beers, D. R., and Appel, S. H. (2013). Immune-mediated mechanisms in the pathoprogression of amyotrophic lateral sclerosis. *J. Neuroimmune Pharmacol.* 8, 888–899. doi: 10.1007/s11481-013-9489-x

Conflict of Interest Statement: The authors declare that the research was conducted in the absence of any commercial or financial relationships that could be construed as a potential conflict of interest.

frontiers in Molecular Neuroscience

ORIGINAL RESEARCH
published: 15 August 2017
doi: 10.3389/fnmol.2017.00262

Oxytocin Rapidly Changes Astrocytic GFAP Plasticity by Differentially Modulating the Expressions of pERK 1/2 and Protein Kinase A

Ping Wang[1], *Danian Qin*[2] *and Yu-Feng Wang*[1]*

[1]School of Basic Medical Sciences, Harbin Medical University, Harbin, China, [2]Department of Physiology, Shantou University, Shantou, China

The importance of astrocytes to normal brain functions and neurological diseases has been extensively recognized; however, cellular mechanisms underlying functional and structural plasticities of astrocytes remain poorly understood. Oxytocin (OT) is a neuropeptide that can rapidly change astrocytic plasticity in association with lactation, as indicated in the expression of glial fibrillary acidic protein (GFAP) in the supraoptic nucleus (SON). Here, we used OT-evoked changes in GFAP expression in astrocytes of male rat SON as a model to explore the cellular mechanisms underlying GFAP plasticity. The results showed that OT significantly reduced the expression of GFAP filaments and proteins in SON astrocytes in brain slices. In lysates of the SON, OT receptors (OTRs) were co-immunoprecipitated with GFAP; vasopressin (VP), a neuropeptide structurally similar to OT, did not significantly change GFAP protein level; OT-evoked depolarization of astrocyte membrane potential was sensitive to a selective OTR antagonist (OTRA) but not to tetanus toxin, a blocker of synaptic transmission. The effects of OT on GFAP expression and on astrocyte uptake of Bauer-Peptide, an astrocyte-specific dye, were mimicked by isoproterenol (IPT; β-adrenoceptor agonist), U0126 or PD98059, inhibitors of extracellular signal-regulated protein kinase (ERK) 1/2 kinase and blocked by the OTRA or KT5720, a protein kinase A (PKA) inhibitor. The effect of OT on GFAP expressions and its association with these kinases were simulated by mSIRK, an activator of Gβγ subunits. Finally, suckling increased astrocytic expression of the catalytic subunit of PKA (cPKA) at astrocytic processes while increasing the molecular associations of GFAP with cPKA and phosphorylated ERK (pERK) 1/2. Upon the occurrence of the milk-ejection reflex, spatial co-localization of the cPKA with GFAP filaments further increased, which was accompanied with increased molecular association of GFAP with pERK 1/2 but not with cPKA. Thus, OT-elicited GFAP plasticity is achieved by sequential activation of ERK 1/2 and PKA via OTR signaling pathway in an antagonistic but coordinated manner.

Keywords: astrocyte, glial fibrillary acidic protein, phosphorylated extracellular signal-regulated protein kinase1/2, oxytocin, protein kinase A, supraoptic nucleus

OPEN ACCESS

Edited by:
Margaret Su-chun Ho, ShanghaiTech University, China

Reviewed by:
James Henry Peters, Washington State University, United States
Laura Maria Frago, Universidad Autonoma de Madrid, Spain

***Correspondence:**
Yu-Feng Wang
yufengwang@ems.hrbmu.edu.cn

Received: *01 June 2017*
Accepted: *31 July 2017*
Published: *15 August 2017*

Citation:
Wang P, Qin D and Wang Y-F (2017) Oxytocin Rapidly Changes Astrocytic GFAP Plasticity by Differentially Modulating the Expressions of pERK 1/2 and Protein Kinase A. Front. Mol. Neurosci. 10:262. doi: 10.3389/fnmol.2017.00262

INTRODUCTION

Astrocytes are extensively involved in normal brain functions (Vasile et al., 2017) and neurological diseases (Pekny et al., 2016; Verkhratsky et al., 2016). However, cellular mechanisms underlying functional and structural plasticities of astrocytes are largely unknown, which requires further investigation. In astrocytes, functional roles of glial fibrillary acidic protein (GFAP), a major cytoskeletal element, have been identified in acute astrocyte plasticity (Langle et al., 2003; Sun et al., 2016). GFAP largely determines astrocytic morphology, which in turn changes astrocytic absorption of glutamate and ions, synaptic innervation and interactions between neighboring neurons (Hatton, 2004; Theodosis et al., 2008).

GFAP molecules are posttranslationally modified by a series of protein kinase. For example, protein kinase A (PKA) phosphorylated and destabilized GFAP *in vitro* (Inagaki et al., 1990; Heimfarth et al., 2016), and caused retraction of astrocytic processes (Hatton et al., 1991) from the surrounding of neurons. Increases in phosphorylated extracellular signal-regulated protein kinase (pERK) 1/2 elevated GFAP levels (Li D. et al., 2017), an effect similar to that of chronic cAMP/PKA activation (Hsiao et al., 2007). These findings thus highlight the dependence of GFAP metabolism on interactions between different protein kinases in astrocytes. However, these studies are mainly based on cell cultures or cell lines in a chronic time course, and it remains unclear how these kinases *in vivo* interact with each other in acute modulation of GFAP plasticity that is essential for both physiological regulation and pathogenesis of diseases (Wang and Hamilton, 2009; Wang and Parpura, 2016). Thus, determining the interaction between GFAP and these protein kinases in acute physiological processes is important to understand the cellular mechanisms that regulate GFAP/astrocytic plasticity.

In the study on glial neuronal interaction in the supraoptic nucleus (SON), GFAP plastic change occurred in concert with the change in oxytocin (OT) neuronal activity in the SON of lactating rats (Wang and Hatton, 2009). In the SON, OT can increase pERK1/2 expression; the distribution of pERK 1/2 was spatiotemporally associated with astrocyte/GFAP morphology (Wang and Hatton, 2007b), which is opposite to the effect of increased intracellular cyclic AMP (Hatton et al., 1991). Activation of OT receptors (OTRs) can trigger both pERK 1/2 and PKA signaling, and the functions of two kinases are mutually antagonistic in uterus (Zhong et al., 2003), which could also occur in the SON. Thus, we hypothesized that both pERK 1/2 and PKA are involved in GFAP plasticity while they function differently in OT-elicited astrocytic plasticity in the SON.

To test this hypothesis, we used OT-evoked GFAP plasticity in male rats first to study the contribution of these two signaling pathways to GFAP plasticity. We found that astrocytes in the SON expressed OTRs and OT could depolarize astrocyte membrane potential while reducing GFAP expression via OTRs. Effects of OT on GFAP plasticity and on the absorption of an astrocyte-specific peptide were differentially modulated by PKA and pERK 1/2. The effect of OT on GFAP expressions and its association with pERK 1/2 and PKA were simulated by an activator of Gβγ subunits. In lactating rats, suckling of pups increased astrocytic expression of PKA at astrocytic processes, which was accompanied with increased molecular associations between GFAP with PKA and pERK 1/2. When the milk-ejection reflex occurred, catalytic subunit of PKA (cPKA) co-localized with GFAP filaments further increased, and the molecular association of GFAP with pERK 1/2 but not with cPKA was also increased. Along with findings of pERK 1/2 involvement in GFAP plasticity in the SON (Wang and Hatton, 2009), the present results highlight that OT-elicited GFAP plasticity is associated with sequential activation of ERK 1/2 and PKA downstream to OTR signaling in an antagonistic but coordinated manner.

MATERIALS AND METHODS

Experiments were performed using adult male (42–60 days old) and lactating female Sprague-Dawley rats. This study was carried out in accordance with the recommendations of NIH guidelines. The protocol was approved by Institutional Animal Care and Use Committees of the University of California-Riverside and Harbin Medical University, respectively.

Drugs, Reagents and Antibodies

OT, β-Mercapto-β, [β-cyclopentamethylene-propionyl^1, O-Me-Tyr^2, Orn^8]-OT (OTR antagonist, OTRA), vasopressin (VP), isoproterenol (IPT, activator of β-adrenoceptor and PKA), KT5720 (inhibitor of PKA), PD98059 and U0126 (inhibitors of ERK 1/2 kinase), U73122 (inhibitor of the coupling of G protein-phospholipase C activation), tetanus toxin and others were from Sigma except as otherwise noted. Myristoylated G-protein βγ-binding peptide [myristoyl-SIRKALNILGYPDYD (mSIRK)] was from EMD Biosciences. Reagents for Western blots were from GE Healthcare. Primary antibodies were from Santa Cruz Biotechnology except for mouse anti-pERK 1/2 (Cellular Signaling), mouse anti-OT neurophysin (NP) and VP-NP (Dr. H. Gainer, NIH, Bethesda, MD, USA). Bauer peptide (β-Ala-Lys-N_ε-AMCA) was provided by Dr. K. Bauer (Max-Planck-Institut für experimentelle Endokrinologie, Hannover, Germany). Secondary antibodies were from Thermo Fisher Scientific.

Slice Preparation

Rats were decapitated; the brain was quickly removed and immersed in ice-cold slicing solution that was oxygenated through bubbling with a compressed gas mixture of 95% O_2/5% CO_2. The slicing solution contained 1/3 of 10% sucrose and 2/3 regular artificial CSF. Then, coronal slices (200 μm thick) were obtained from the SON as previously described (Wang and Hatton, 2009). Slices were pre-incubated at room temperature (21–23°C) for 1 h in oxygenated regular artificial CSF before drug treatment or application of other procedures. The regular artificial CSF contained (in mM): 126 NaCl, 3 KCl, 1.3 $MgSO_4$, 2.4 $CaCl_2$, 1.3 NaH_2PO_4, 26 $NaHCO_3$, 10 Glucose, 0.2 ascorbic

acid, pH 7.4 and 305 mOsm/kg, oxygenated with 95% O_2/5% CO_2. The slice was then randomly assigned to groups for immunostaining or protein analyses.

In suckling experiments, lactating rats with 4 h separation from pups were allowed to suckling of 10 pups for 0–30 min as previously described (Wang and Hatton, 2009). According to the occurrence of the milk-ejection reflex, brains were collected in three groups, i.e., non-suckling, suckling (for 5–10 min before the first milk ejection), and milk-ejection reflex (suckling until the occurrence of the third or fourth milk ejections). Brain were fixed immediately without pre-incubation or homogenized to obtain protein lysates.

Immunocytochemistry and Confocal Microscopy

Immunostaining was performed based on our earlier reports (Wang and Hatton, 2009) with minor modifications. In brief, slices were permeated with 0.3% Triton X-100 in 0.1 M PBS for 30 min, and non-specific binding was blocked with 0.3% gelatin-PBS. The slices were then incubated overnight at 4°C with primary antibodies against goat or mouse OT-NP (1:400) and VP-NP (1:400), goat or mouse GFAP (1:300), mouse pERK 1/2 (1:1000), rabbit cPKA (1:250) and goat OTRs (1:250). After rinsing, the slice was incubated with species-matched fluorescent donkey anti-goat/mouse/rabbit antibodies (Alexa Fluor® 647/555/488, 1:1000) for 1.5 h at room temperature (22–24°C). Finally, Hoechst stain (0.5 μg/ml for 15 min) was used to label nuclei.

For each treatment, 6–12 pieces of slices from the middle part of the SON of 3–6 rats were imaged at high magnification (630×), 10–20 μm from the surface using a laser scanning confocal microscope (Leica TCP SP2 or Zeiss LSM510). Multiple fluorophores were imaged sequentially, and distribution pattern and colocalization of different molecules were analyzed. To avoid false positive or negative results of immunostaining, serial dilutions of the primary antibody, staining with pre-absorbed (immune-neutralization) primary antibody, no-primary and no secondary antibody controls were applied.

Western Blots and Co-Immunoprecipitation (Co-IP)

Methods for protein analysis were the same as previously reported (Wang et al., 2013a,b). In brief, hypothalamic slices from three to six rats were obtained as described above. SONs were punched out and then lysed. The lysates were centrifuged to remove insoluble components before protein levels were quantitated using a plate reader. Protein aliquots (60 μg) were loaded and separated on 10% SDS-PAGE gels, and then transferred onto polyvinylidene difluoride membranes. After blocking with 5% milk solids (or 1% gelatin for detecting primary antibodies from goat) for 1 h at room temperature, membranes were incubated with mouse or goat anti-GFAP, rabbit or goat anti-OTRs, rabbit anti-cPKA and mouse anti-pERK 1/2 (all 1:500) overnight at 4°C. To calibrate protein levels, mouse anti-tubulin (1:300), rabbit anti-actin (1:500) or anti-total ERK2 (tERK2, 1:1000) were also detected (1 h at room temperature). Bands were visualized using horseradish peroxidase-conjugated secondary antibodies and an enhanced chemiluminescence system (Tanon 5200, Shanghai). Data are reported for 3–6 replicates.

For Co-IP experiments, SON lysates were precleared with protein G agarose beads to reduce nonspecific binding. Mouse anti-GFAP (1.5 μg/7.5 μl) was then added to the lysates (1500 μg/500 μl protein) to form an immunocomplex and incubated overnight at 4°C. Immunocomplexes were captured by adding 50 μl of protein G agarose bead slurry and gently rocking for 2 h at 4°C. They were then collected, washed and resuspended in 50 μl 2× Western blotting sample buffer, and boiled for 10 min to dissociate proteins from the beads. Target proteins were then detected using Western blotting.

Patch-Clamp Recordings

Patch-clamp recording procedures for SON were similar to those described previously (Wang and Hatton, 2004). Briefly, after pre-incubation in the regular artificial CSF, slices were incubated in artificial CSF containing Bauer peptide that is fluorescent and can be selectively taken up by astrocytes via peptide transporter PepT2 (Dieck et al., 1999) at 35°C for 2–4 h, with or without tetanus toxin (1 nM) to block synaptic vesicle release. Whole cell patch-clamp recordings were obtained from fluorescent cells visualized using an epifluorescence microscope using an Axopatch 200B amplifier or Multiclamp 700B amplifier (Molecular Devices). The pipette solution for recording SON astrocytes contained (in mM): 145 K-gluconate, 10 KCl, 1$MgCl_2$, 10 HEPES, 1 EGTA, 0.01 $CaCl_2$, 2 Mg-ATP, 0.5 Na_2-GTP, pH 7.3, adjusted with KOH. Signals that were filtered, sampled at 5 kHz, and analyzed offline using Clampfit 10 software (Molecular Devices). Exemplary cells were also tested their voltage-current relationship and examined in immunohistochemistry after drug tests to verify their astrocytic nature.

Real Time Imaging of Astrocytes

To link modulating effects of OT on GFAP plasticity to astrocytic functions, slices were incubated with the artificial CSF containing 0.1 μM Bauer peptide as described above. Then, astrocytic somata in the ventral glial lamina (VGL) of the SON were focused and their fluorescence intensity was captured through a Microfire Camera in single frame following a brief (20–30 s) exposure to UV light. Drugs were bath-applied for 15 min, and images were captured immediately before, 5 min and 15 min after drug application, respectively. Preparations were fixed *in situ* at the end of observations for further analyzing images by using confocal microscopy as previously reported (Wang and Hatton, 2009).

Data Analysis

Methods for analyzing data of immunocytochemistry, Western blots and patch-clamp recordings were modified from our previous experiment (Wang and Hatton, 2009). To evaluate GFAP levels, the fluorescence intensity in each channel was

normalized to a standard curve (1–256) to allow for comparison between different experiments. The background fluorescence level was set as 1 through minimum baseline correction using Leica LCS Lite or ZeissLSM software and maximum intensity was set at 256. To assay GFAP expression in single scan-based confocal image, whole frame of the image was compared on the same background level of fluorescence intensity. The efficiency of this single sectioned image in reflecting GFAP plasticity had been validated by Z-stack scanning (0.5 μm/section) and fluorescent microscopy as described previously (Wang and Hatton, 2009). The increase or decrease in the expression level of GFAP was defined as a change more than 20% from the control. In analyzing the expression of GFAP filaments, they were first distinguished from the cell body by its extending from but not surrounding "astrocytic nucleus" and appearing thread-like rather than circular morphology. The diameter of GFAP filaments was measured at five sub-sections including those near each of the four corners and the center in a square frame and their average was used to represent the diameter of a section, which was applicable in 95% of the images.

In determining different components of GFAP protein, the monomers were identified by the appearance of a single 50 KDa band and the fragments included the diffuse bands below 50 KDa and above 35 KDa. In patch-clamp recordings, the membrane potential was an average level of 1 min before and 1 min (9th–10th min) after drug application. In analyzing the fluorescent intensity of Bauer peptide-loaded astrocytes, background fluorescence was subtracted from the dorsal portion of the SON that did not show clear astrocyte soma; changes in fluorescence were calculated by comparing the intensity after drugs with those before drugs.

Student's *t*-test and ANOVA were used for statistical analyses where appropriate, as instructed by SigmaStat 12 program, and $p < 0.05$ was considered significant. When abnormal distribution or large variances appeared, square-root transformations (for some Co-IP studies with $n = 3$) were applied to minimize the influence of individual data points on the evaluation of whole significance level. All measures were expressed as mean ± SEM in percentage of control values, or as otherwise noted.

RESULTS

In this study, we first examined the features of OT-evoked GFAP plasticity of astrocytes in the SON of male rats and its dependence on OTR-Gβγ signaling. Next, we explored the roles of pERK 1/2 and PKA in the GFAP plasticity and their association with astrocytic absorption of fluorescent peptide. Lastly, we linked the roles of pERK 1/2 and PKA to suckling-evoked GFAP plasticity of the SON in lactating rats to verify the applicability of identified features of kinase modulation of acute GFAP plasticity.

OT Changed GFAP Expression in the SON of Male Rats

To analyze the potential modulatory effects of signaling molecules on GFAP plasticity in the SON, we first examined effects of OT on GFAP expression in brain slices from six male rats. The results showed that OT, at 10 pM, 1 nM and 0.1 μM for 30 min, concentration-dependently reduced GFAP levels in the SON in confocal microscopy. As shown in **Figure 1A**, before OT treatment (Control), GFAP staining was less compact in perinuclear areas of astrocytes while GFAP filaments were in clear and rich bundles. Accompanying with the general reduction of GFAP, the length and diameter of GFAP filaments were reduced significantly by OT, whereas GFAP staining was increased at the somata (**Figure 1Aa**). Pretreatment of the slices with [β-Mercapto-β, β-cyclopentamethylene-propionyl^1, O-Me-Tyr^2, Orn^8]-OT blocked OT-elicited GFAP reduction (**Figure 1Ab**). In Western blots, different concentrations of OT differentially influenced the expressions of different components of GFAP protein (**Figure 1B**). OT at 10 pM for 30 min significantly decreased 50 kDa GFAP protein and smaller GFAP fragments. At 1 nM and 0.1 μM, OT still decreased 50 kDa GFAP but significantly increased small GFAP fragments. The concentration-dependent effects of OT on GFAP plasticity were exhibited as the increases in GFAP fragments rather than 50 KDa components. Moreover, pretreatment of slices with the OTRA blocked this OT effect (**Figure 1Ba**). These results summarized in **Figures 1Ac,Bb** are consistent with the effect of OT on GFAP plasticity in lactating rats (Wang and Hatton, 2009).

In the SON, there are two major forms of astrocytes, radial glia-like morphology in the VGL, and stellate morphology in the somatic area (Israel et al., 2003). Here, we analyzed OT effects on GFAP expression in these two forms of astrocytes by observing GFAP expression with nuclear staining. The result showed that OT-reduced GFAP staining was significantly stronger ($n = 6$, $P < 0.05$ by paired *t*-test) in the dorsal SON (34.8 ± 7.4% of control) than in the ventral SON (72.7 ± 8.6% of the control by paired *t*-test). This is in agreement with the finding that osmotic stimulation causes glial retraction around dorsally located OT neurons but not ventrally located VP neurons in the SON (Chapman et al., 1986).

Specificity of OT Actions on GFAP Expression in Astrocytes

To verify the specificity of OT actions on astrocytes, we performed Co-IP of GFAP with OTRs in three rats. The result showed a clear molecular association between GFAP and OTRs (**Figure 2A**). This result is consistent with our previous finding in immunocytochemistry that OTRs were present in GFAP-positive astrocytes in the SON (Wang and Hatton, 2006).

Next, we tested effects of VP, a nonapeptide in the SON structurally similar to OT, on GFAP protein levels. In contrast to the strong effects of OT on GFAP level in the SON, VP (0.1 nM, 30 min) did not significantly influence the expression of GFAP (101.0 ± 17.3% of control, $n = 5$, $P > 0.05$ by pared *t*-test) in Western blots (**Figure 2B**). Moreover, in Bauer peptide (20 μM)-loaded astrocytes in brain slices (**Figure 2Ca1**) that possessed linear voltage-current relationship (**Figures 2Ca2,Ca3**) we found that OT (0.1 nM, 5–10 min) significantly depolarized astrocytic membrane potentials (67.4 ± 2.3 mV vs. 63.5 ± 1.8 mV at 10 min, $n = 7$, $P < 0.01$ by

paired *t*-test; **Figure 2Cb1**), which was blocked by pretreatment of slices with OTRA (67.1 ± 3.0 mV vs. 67.0 ± 3.0 mV at 10 min, $n = 7$, $P > 0.05$ by paired *t*-test; **Figure 2Cb2**). By contrast, pretreatment of astrocytes in three slices with tetanus toxin (10 nM, 2–4 h) did not block the depolarizing effects of OT (66.0 ± 3.0 mV vs. 62.3 ± 3.3 mV at 10 min, $n = 6$, $P < 0.01$ by paired *t*-test; **Figure 2Cb3**) while VP had no significantly effect on the membrane potential (67.0 ± 2.4 mV vs. 67.1 ± 2.2 mV at 10 min, $n = 6$, $P > 0.05$ by paired *t*-test; **Figure 2Cb4**). These results are consistent with our previous finding in lactating rats (Wang and Hatton, 2009) that the presence of tetanus toxin did not influence OT-elicited GFAP reduction.

Signaling Cascades Mediating OT-Evoked GFAP Plasticity

Gβγ signaling cascade was the major approach mediating OT modulation of OT neuronal activity (Wang and Hatton, 2007a,b) and could also be the mediator of OT modulation of GFAP plasticity. To clarify this issue, we first examined GFAP expression after treatment of slices with mSIRK, an activator of Gβγ subunits. As shown in **Figure 3A**, mSIRK (0.5 μM) dually changed GFAP expression significantly ($n = 6$, $P < 0.05$ by ANOVA) in a time-dependent manner. At 5 min after mSIRK treatment, GFAP filaments were increased significantly ($n = 6$, $P < 0.05$), which then significantly reduced at 30 min ($n = 6$, $P < 0.05$). In Western blots, mSIRK (0.5 μM, 30 min) significantly reduced 50 kDa GFAP bands but increased GFAP fragments (**Figure 3B**), an effect similar to that of OT. These findings are in agreement with the time-dependent effect of OT on GFAP plasticity in the SON of lactating rats (Wang and Hatton, 2009).

Next, we observed effects of blocking downstream signaling of Gβγ subunits on mSIRK-evoked GFAP plasticity. As shown in **Figure 4A**, mSIRK (0.5 μM, 30 min)-evoked reduction of GFAP and pERK 1/2 immunostaining was differentially influenced by pretreatments of the slices ($n = 6$) with OT (1 nM, 30 min), KT5720 (10 μM), PD98059 (20 μM) and U73122 (10 μM). Compared to the effect of mSIRK only on GFAP filaments, addition of OT, PD98059 or U73122 did not significantly influence GFAP levels; however, the addition of KT5720 significantly increased both GFAP and pERK

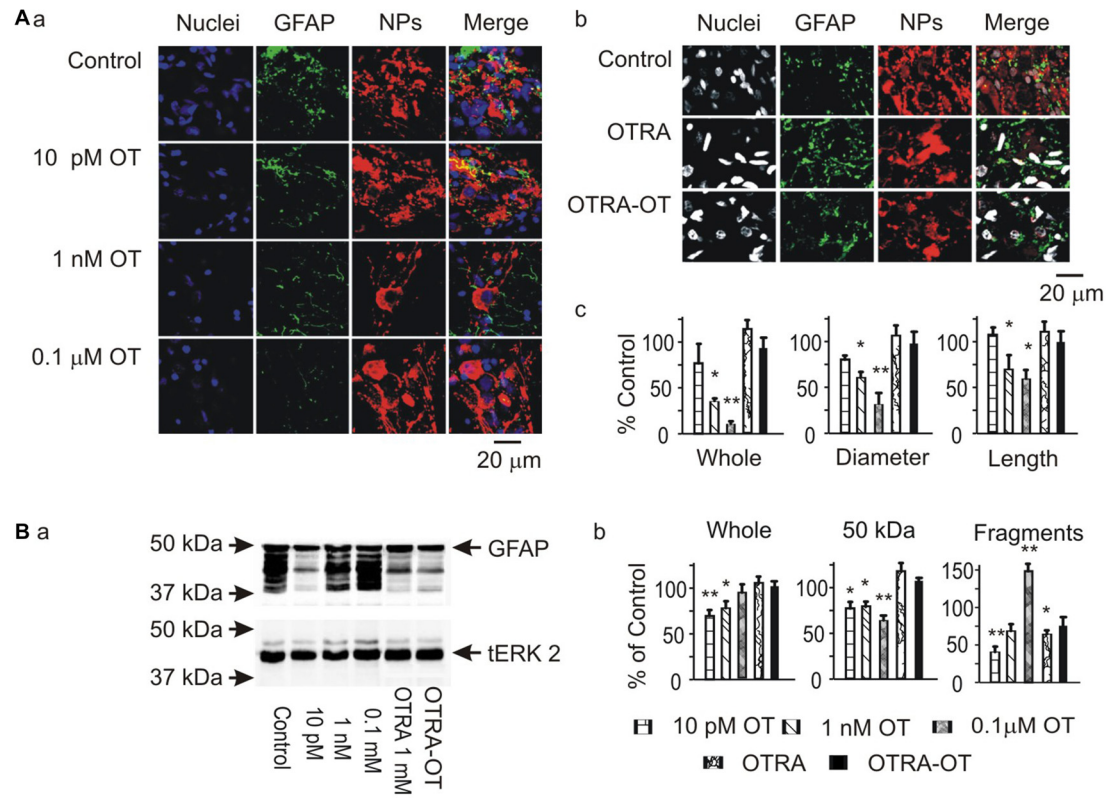

FIGURE 1 | Effects of oxytocin (OT) on glial fibrillary acidic protein (GFAP) plasticity in the supraoptic nucleus (SON) in brain slices from male rats. **(A)** Effects of OT (10 pM, 1 nM and 0.1 μM for 30 min) and OT receptor antagonist (OTRA, 1 μM for 30 min) on GFAP expression in confocal images. **(Aa,Ab)** Staining of nuclei, GFAP, neurophysins (NPs) and their merges (left to right). **(Ac)** Summary graphs showing the intensity of GFAP filaments relative to the control in whole panel, diameters and lengths of the filaments. Note that: $^*P < 0.05$ and $^{**}P < 0.01$ compared to the control ($n = 6$) in ANOVA with Holm-Sidak comparisons. **(B)** GFAP expression in Western blots. **(Ba)** Bands (left to right) show GFAP proteins (top) for control, 10 pM OT, 1 nM OT, 0.1 μM OT, 1 μM OTRA and 0.1 nM OT after OTRA for 30 min, respectively. Bands at the bottom are total extracellular signal regulated protein kinase 2 (tERK 2), serving as loading controls for corresponding treatments ($n = 6$, compared in ANOVA). **(Bb)** Summary graphs showing GFAP relative to control in whole bands, bands at 50 kDa (full size), and their smaller fragments, respectively.

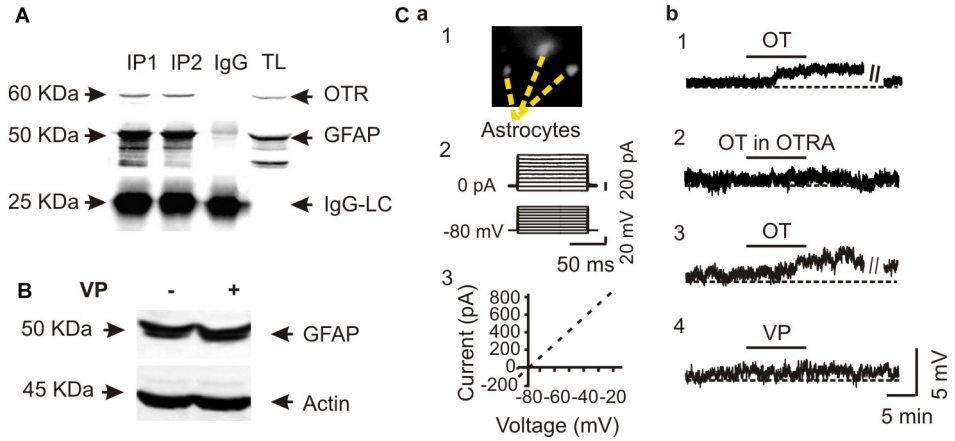

FIGURE 2 | Specific effects of OT on GFAP plasticity. **(A)** Co-immunoprecipitation (Co-IP) of GFAP with OTRs: Western blotting of OTRs (top panels), immunoprecipitated GFAP (the middle panels and IgG light chains, IgG-LC, bottom) in two duplicates (IP1 and IP2) along with the loading of total lysis (TL). **(B)** Western blots showing that effect of vasopressin (VP, 0.1 nM, 30 min) on the expression of GFAP in SON protein lysates. **(C)** Patch-clamp recordings showing effects of OT on the membrane potential of astrocytes in brain slices. **(Ca)** Identification of astrocytes by Bauer peptide loading **(Ca1)** and by the linear current-voltage relationship **(Ca2,Ca3)**. **(Cb1)** Depolarizing effects of OT (0.1 nM, 10 min) on astrocytes in the SON. **(Cb2)** Effects of OTRA (1 μM, 10 min before OT) on OT-evoked depolarization. **(Cb3,Cb4)** Effects of OT **(Cb3)** and VP **(Cb4)** at 0.1 nM for 10 min on the membrane potentials after pretreatment with tetanus toxin (10 nM, 2–4 h). Other annotations refer to **Figure 1**.

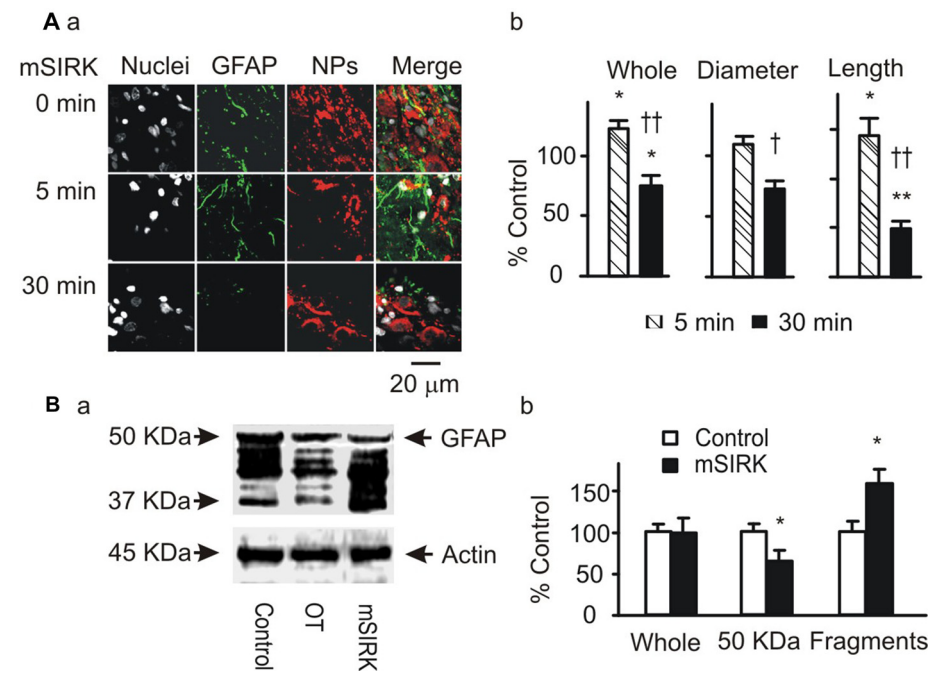

FIGURE 3 | Roles of Gβγ subunits in OT-elicited GFAP plasticity. **(A)** Exemplary confocal images showing (left to right) nuclei, GFAP, OT plus VP NPs and their merges at 0 min, 5 min and 30 min after treatments with myristoyl-SIRKALNILGYPDYD (mSIRK; 0.5 μM), respectively **(Aa)**. **(Ab)** Summary graphs showing mSIRK effects on different components of GFAP. $^{*}P < 0.05$ and $^{**}P < 0.01$ compared to 0 min controls; $^{\dagger}P < 0.05$ and $^{\dagger\dagger}P < 0.01$ compared to mSIRK at 5 min. **(B)** Western blot showing effects of mSIRK on different bands of GFAP proteins (**Ba**, relative to the effect of OT) and the summary graphs of the mSIRK effect **(Bb)**. Other annotations refer to **Figure 1**.

1/2 expressions. This finding is in agreement with previous finding that Gβγ signaling cascade including pERK 1/2 was the major mediator of OT effect in the SON (Wang and Hatton, 2007b) and that PKA antagonized pERK 1/2 signaling (Zhong et al., 2003) and promoted GFAP depolymerization (Inagaki et al., 1990; Heimfarth et al., 2016).

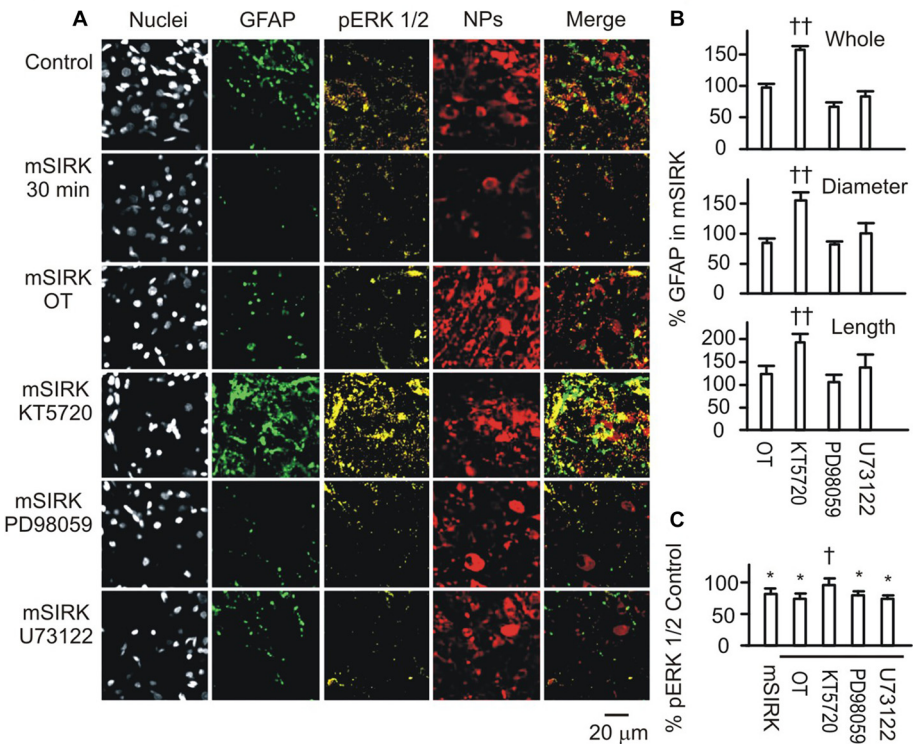

FIGURE 4 | Roles of OTR-associated signals in Gβγ subunit-modulated expressions of GFAP and phosphorylated extracellular signal-regulated protein kinase (pERK) 1/2. **(A)** Confocal images (left to right) show staining for nuclei, GFAP, pERK 1/2, NPs and their merges. From top to the bottom, images were acquired in control, mSIRK (0.5 μM, 30 min) and mSIRK following 30 min pretreatment with OT, KT5720 (10 μM), PD98059 (20 μM), or U73122 (10 μM), respectively. **(B)** Summary graphs of GFAP expression in whole field view, the diameter, or length of GFAP filaments relative to mSIRK alone. **(C)** Summary graphs of pERK 1/2 under different conditions. Note that, $^{*}P < 0.05$ compared to the control; $^{\dagger}P < 0.05$ and $^{\dagger\dagger}P < 0.01$ compared with mSIRK alone. Other annotations refer to **Figures 1**, **3**.

Roles of pERK 1/2 and PKA in OT-Evoked GFAP Plasticity

To further test if and how pERK 1/2 and PKA were involved in OT-elicited GFAP plasticity, we observed effects of OT (1 nM) on GFAP plasticity after changing the activity of pERK 1/2 or PKA 30 min before OT application. Immunostaining and confocal microscopy (**Figure 5Aa**) showed that the staining of GFAP was substantially ($p < 0.05$ or 0.01, $n \geq 6$) reduced by IPT (10 μM) and U0126 (1 μM) respectively, and slightly but significantly ($P < 0.05$) reduced by KT5720 (10 μM). The effects of IPT and U0126 on GFAP filaments were on both somata and processes, while the effect of KT5720 was on the processes only. Moreover, addition of OT (**Figure 5Ab**) did not significantly influence the actions of IPT or U0126, but reversed the effect of KT5720. The effects of these agents on OT-evoked GFAP plasticity are summarized in **Figure 5Ac** and are consistent with their effects on mSIRK-evoked GFAP plasticity.

Following the immunohistochemical experiments, Western blots were performed to detect GFAP protein after KT5720 and U0126 treatments with and without the presence of OT in brain slices from 6 rats. As shown in **Figure 5Ba**, KT5720 significantly decreased the 50 kDa GFAP bands; addition of OT strongly increased both 50 kDa and the fragments of GFAP proteins. By contrast, U0126 significantly reduced small GFAP bands but enhanced 50 kDa bands, which were not significantly changed by addition of OT (see summary graph in **Figure 5Bb**). These results are in agreement with the finding in confocal microscopy.

Effects of GFAP-Modulating Agents on Astrocytic Uptake/Retention of Bauer Peptide

To link the GFAP-modulating effects of pERK 1/2 and PKA with astrocytic functions, we observed effects of OT, PD98059 and IPT on the fluorescence intensity of astrocytes after loading Bauer peptide in brain slices ($n = 6$) from three rats. As shown in **Figure 6A**, OT significantly reduced the fluorescence intensity after 15 min treatment compared to the time-matched controls, effects of which were mimicked by using PD98059 and IPT, and blocked by pretreatment of the slices with OTRA from 5 min before these agents (see **Figure 6B** for summary).

Effects of Suckling Stimulation on cPKA Expression and the Molecular Associations of GFAP with pERK 1/2 and PKA

To link the differential GFAP-modulating effects of the kinases to astrocytic functions, we further examined cPKA expressions

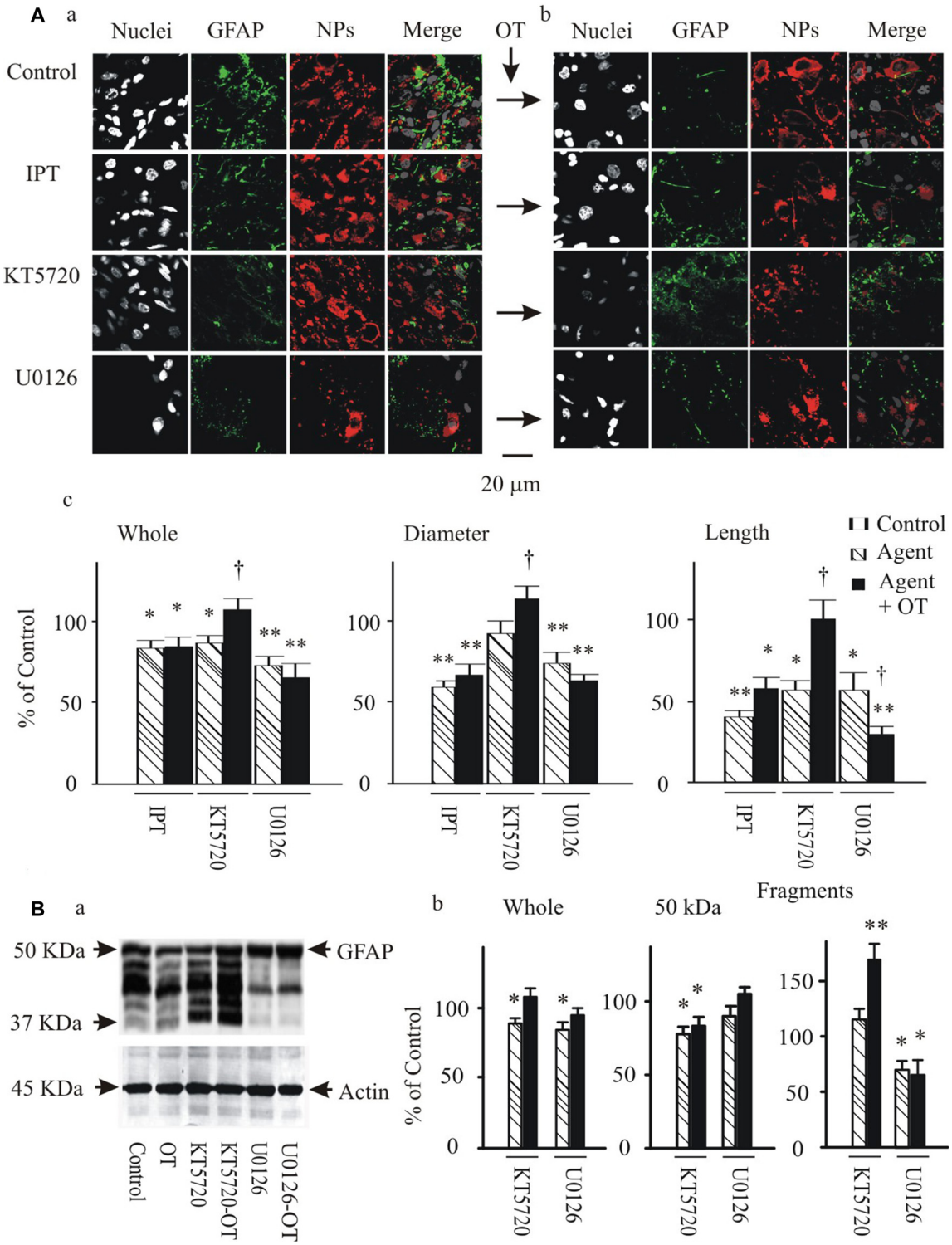

FIGURE 5 | Effects of modulating protein phosphorylation on OT-evoked GFAP reduction. **(A)** Exemplary confocal images showing (left to right) nuclei, GFAP, NPs and their merges before **(Aa)** and after **(Ab)** application of OT (1 nM, 30 min). Note: IPT, isoproterenol (10 μM), KT5720 and U0126 (1 μM). OT was added 30 min after these agents. **(Ac)** Summary graphs showing relative intensity of GFAP staining under different conditions. $^{*}P < 0.05$ and $^{**}P < 0.01$ compared to the control; $^{\dagger}P < 0.05$ compared with agents only. **(B)** GFAP expressions in Western blots. **(Ba)** Bands (left to right) showing GFAP proteins (top) in control, 1 nM OT, KT5720, KT5720 plus OT, U0126 and U0126 plus OT, respectively. Bands at bottom are actin, serving as loading controls for corresponding treatments ($n = 6$). **(Bb)** Summary graphs showing different components of GFAP relative to controls. Other annotations refer to **Figures 1**, **4**.

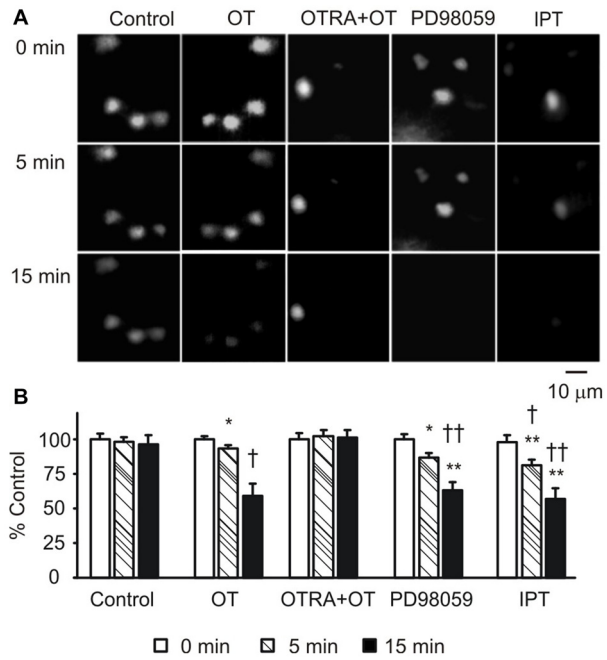

FIGURE 6 | Effects of GFAP-modulating agents on astrocytic uptake of Bauer peptide. **(A)** Exemplary fluorescence images showing temporal changes of fluorescence intensity of astrocytes that were preloaded with Bauer peptide (20 μM, 2–4 h at 35°C) in the SON. From left to the right the columns were control, OT (1 nM), OTRA (1 μM, from 5 min before OT) plus OT, PD98059 (20 μM) and IPT (10 μM), respectively. **(B)** Summary graphs. Note that, $^{*}P < 0.05$, $^{**}P < 0.01$ compared to the controls; $^{\dagger}P < 0.05$ and $^{\dagger\dagger}P < 0.01$ compared with those at 5 min. Other annotations refer to **Figures 1**, **4**.

at different stages of suckling in immunocytochemistry in three sets of lactating rats, based on previous observation of pERK 1/2 (Wang and Hatton, 2009). As shown in **Figure 7A**, suckling significantly increased cPKA expression in whole SON. In astrocyte profiles, cPKA was markedly increased at the processes as indicated by its heavy overlapping with GFAP. The occurrence of the milk-ejection reflex further increased the co-localization of cPKA with GFAP filaments, but reduced cPKA expression at neuronal profiles from the peak at the initial stage of suckling. Further examination of the molecular association of cPKA and pERK 1/2 with GFAP in Co-IP experiments (**Figure 7B**) revealed that molecular association of GFAP with pERK 1/2 (204.0 ± 23.6% of control, $n = 3$, $P < 0.05$) increased significantly ($n = 3$, $P < 0.05$) at the initial stage of suckling; the Co-IP of cPKA with GFAP was increased in all the three cases although the increase in the average level (178.2 ± 30.8% of control, $P = 0.053$) did not reach statistical significance due to the relatively low power. Upon the occurrence of the milk-ejection reflex, the association of GFAP with pERK 1/2 (431.4 ± 66.0% of control, $n = 3$, $P < 0.05$ compared to those of the control and during suckling) was further increased (**Figure 7Ba**), whereas the association between GFAP and cPKA was decreased significantly from that during suckling (104.5 ± 54.9% of the control, $n = 3$, $P < 0.05$ compared to that during suckling; **Figure 7Bb**). These results are in agreement with the findings in pharmacological manipulation in the males.

DISCUSSION

In the present study, we found that OT-evoked reduction of GFAP filaments depends on an antagonistic but coordinated pERK 1/2 and PKA interaction, downstream to OTR-Gβγ signaling. Upregulation of pERK 1/2 facilitates GFAP polymerization and PKA suppresses this polymerization while providing a basal condition for pERK 1/2 to function. Moreover, the two kinases work in coordination to localize GFAP at different compartments of astrocytes. This cellular signaling process is common between male and lactating female rats, likely contributing to astrocytic modulation of OT neuronal activity under diverse physiological conditions.

Methodological Consideration

To study astrocytic plasticity, classically electron microscopy is the first choice. However, at this level, GFAP is often absent from fine astrocytic processes around synapses and neuronal somata (Theodosis et al., 2008). Thus, despite the power of electron microscopy in revealing detailed morphological features of astrocytic processes and their association with particular neuronal and astrocytic populations, it is not more helpful in studying GFAP plasticity than confocal microscopy plus proteomic analyses. *In situ* observation of GFAP plasticity using rats that express luciferase under GFAP promoters to image GFAP can provide a real-time image of GFAP filaments. However, *in vivo* imaging of fluorescent GFAP in the SON is limited by the anatomical complexity in exposing the SON surgically. In the present study, combining confocal microscopy with protein analysis, patch-clamp recordings, and fluorescence detection of astrocyte-specific peptide in brain slices could not only reveal OT-elicited GFAP reduction and the underlying molecular mechanisms, but also establish a functional association of GFAP with astrocytic plasticity as discussed below.

OTR Mediation of OT-Evoked GFAP Reduction

GFAP monomers and filaments were reduced upon exposing to OT in males via activating OTRs on astrocytes in the SON. This finding is in agreement with previous reports that suckling acutely reduced GFAP expression via activation of OTRs (Wang and Hatton, 2009) and that a global reduction of GFAP expression occurred at the late pregnancy and during lactation in the SON (Perlmutter et al., 1984), the periods with enhanced OT actions (Hatton and Wang, 2008). The present study unambiguously verified that OT-reduced GFAP is directly mediated by astrocytic OTRs. The supportive evidences include that: (1) astrocytes in the SON express OTRs and OT but not VP elicited GFAP reduction under the same condition; (2) the effect of OT on GFAP did not require neuron-mediation since tetanus toxin could not block this OT action; and (3) OT-evoked

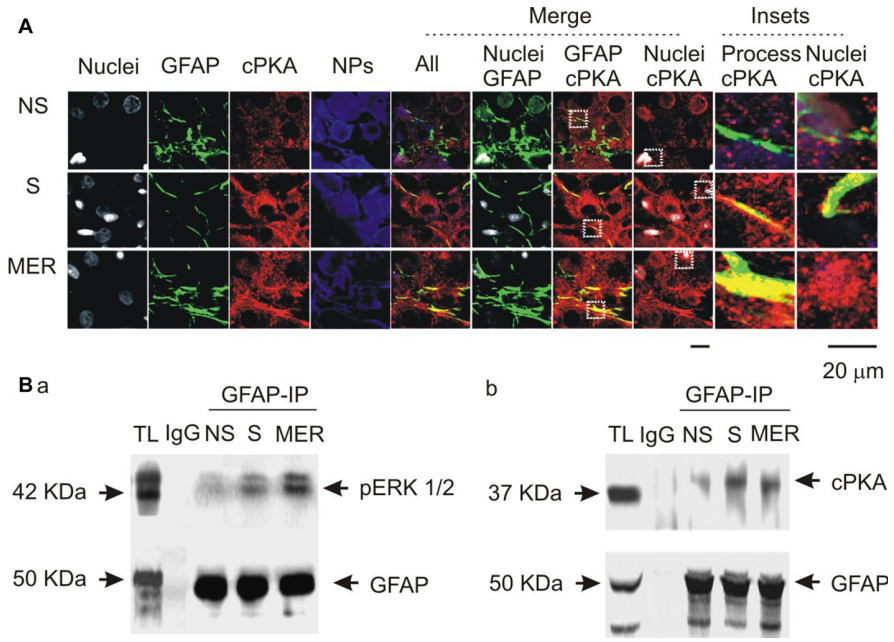

FIGURE 7 | Spatial and molecular associations of GFAP with protein kinases. **(A)** Exemplary confocal images showing effects of suckling at different stages on the expression of catalytic subunit of protein kinase A (cPKA). Images from left to the right showing nuclei, GFAP, cPKA, NPs, the merges of all channels, GFAP with nuclei, GFAP with cPKA, nuclei with cPKA, and the insets expanded from white dashed squares in corresponding merged channels. **(B)** Molecular association of GFAP with pERK 1/2 **(Ba)** and with cPKA **(Bb)** at different stages of suckling as indicated. Note that, NS, non-suckling; S, suckling; MER, immediately after the milk-ejection reflex. Other annotations refer to **Figures 1**, **4**.

depolarization of astrocytic membrane potential was blocked by the OTRA, even in the present of tetanus toxin; and most importantly, there was molecular association between GFAP and OTRs. One argument could be that tetanus toxin does not block the release of lipophilic compounds and gases, e.g., endocannabinoids (Hirasawa et al., 2004) and nitric oxide (Luckman et al., 1997), which may mediate OT actions. However, endocannabinoids (Aguado et al., 2006) and nitric oxide (Guo et al., 2007) increase but does not decrease GFAP expression. If their release is not blocked by tetanus toxin, OT-reduced GFAP expression (Wang and Hatton, 2009) should be weakened, even blocked but not increased. Thus, we conclude that OT can directly act on astrocytes and reduce GFAP expression via OTRs.

OT Modulation of GFAP Metabolism and its Concentration- and Time-Dependence

Similar to those found in lactating rats (Wang and Hatton, 2009), OT concentration dependently reduced GFAP filaments in male rats. Interestingly, different concentrations of OT reduced GFAP likely via different metabolic processes. At lower levels, OT reduced both GFAP monomers at 50 kDa and their fragments, illustrating an increase in decomposition of GFAP molecules (Wang and Hatton, 2009). At higher levels, OT increased GFAP fragments while maintaining lower levels of GFAP monomers. The increased GFAP fragments did not contribute to the polymerization of GFAP filaments since GFAP polymerization is based on monomers but not their fragments. Moreover, effects of activating OTRs on GFAP levels are related to the time course of OT actions. In previous study, we showed that OT reduced GFAP protein and filaments in brain slices from lactating rats in a time-dependent manner (Wang and Hatton, 2009). This finding is confirmed in the present study that mSIRK-reduced GFAP expression (**Figure 3**) or OT-reduced astrocyte absorption of Bauer peptide (**Figure 6**) were also time-dependent in the SON of male rats. This is in agreement with the feature of activation of G Protein-coupled receptors and the relatively slow metabolic processes of GFAP.

Intracellular Processes Following OTR Activation

In this study, we confirmed not only the expression of OTRs at astrocytes in the SON reported previously (Wang and Hatton, 2006), but also identified the mediation of Gβγ signaling in OT effects on SON functions and the mutually interactive processes between pERK 1/2 and PKA in OT-evoked GFAP plasticity.

In previous study on lactating rats, we found that OT-evoked activation of OT neurons was mainly mediated by Gβγ signaling but not Gα signaling following OTR activation of $G_{q/11}$ type G protein (Wang and Hatton, 2007a). The present study extends this finding by showing that mSIRK evoked GFAP reduction (**Figure 3**) as OT did, which was in synergy with the expression of pERK 1/2 (**Figure 4**). Moreover, along with the activation of ERK 1/2 in 5 min

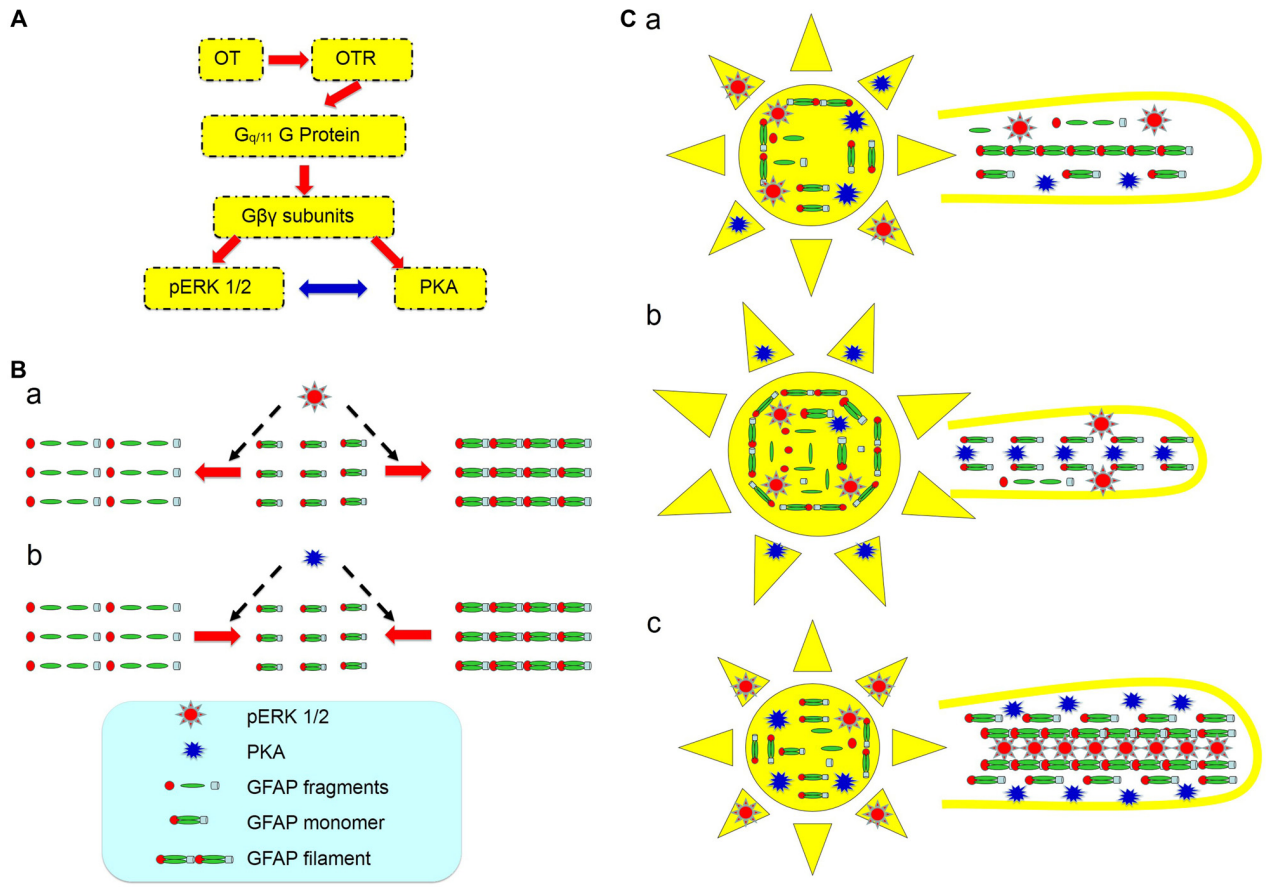

FIGURE 8 | Diagram of hypothetic cellular and molecular mechanisms underlying OT modulation of GFAP plasticity in astrocytes. **(A)** OTR signaling in association with OT-evoked GFAP reduction. The red arrows show the flow of signaling transduction and the bidirectional blue arrow indicates a relationship of mutual inhibition. **(B)** Effects of activation of pERK 1/2 **(a)** and PKA **(b)** on GFAP metabolism/plasticity, respectively. **(C)** GFAP plasticity of astrocytic somata (left panels) and processes (right panels) in the SON at different stages of suckling at its differential associations with pERK 1/2 and PKA. **(Ca)** Before suckling; **(Cb)** during the first 5–10 min of suckling with the occurrence of milk ejection; and **(Cc)** 1 min within the occurrence of the third or fourth milk ejections.

and its reversal at 30 min (Wang and Hatton, 2007b), OT- and/or mSIRK-evoked reduction of GFAP as well as OT-modulated astrocytic absorption of Bauer-peptide became significant after 15–30 min. These processes were modulated not only by pERK 1/2 blockers but also by PKA-modulating agents. Lastly, at different stages of suckling stimulation that are associated with different levels of GFAP and pERK 1/2 expressions (Wang and Hatton, 2007b), cPKA (**Figure 7**) also had different expressions. Lastly, activating PKA with IPT or blocking ERK 1/2 phosphorylation decreased GFAP polymerization; blocking PKA blocked OT-evoked GFAP reduction while blocking ERK 1/2 activation simulated effects of OT on GFAP. Thus, both pERK1/2 and PKA are involved in OT-modulation of GFAP plasticity downstream to OTR-Gβγ signaling pathway.

In addition to these classical signaling processes, our finding also fills in a gap between OT-evoked GFAP plasticity and astrocytic functions by showing the depolarizing effects of OT on astrocyte membrane potentials and the OT-reduced absorption of Bauer Peptide. As shown in **Figure 2**, OT could depolarize astrocyte membrane potentials in 5–10 min of action. This could be an effect of OTR activation on the mobilization of IP3-sensitive intracellular Ca^{2+} stores (Di Scala-Guenot et al., 1994), one of the major downstream events of OTR activation. The increased intracellular Ca^{2+} levels could account for this initial depolarizing effect of OT because of its neutralization of intracellular negative charges. Moreover, this depolarization could account for the reduced absorption of Bauer Peptide at 30 min of OT treatment (**Figure 6**). Increased intracellular Ca^{2+} levels in astrocytes could cause hyper-phosphorylation of GFAP and its depolymerization (Heimfarth et al., 2016); the disruption of GFAP filaments could influence the expression of peptide transporter PepT2 (Dieck et al., 1999) due to losses of the scaffolding and guiding roles of GFAP (Hou et al., 2016; Wang and Parpura, 2016). As a result, astrocyte absorption of Bauer Peptide and the fluorescence intensity were also reduced. This proposal is supported by previous findings that reduction of GFAP also reduced its molecular association with glutamine synthetase (Wang et al., 2013b) and vesicular GABA transporters (Wang et al., 2013a) in astrocytes

although directly assaying intracellular Ca^{2+} levels remains to be performed.

Antagonistic but Coordinated Interaction between pERK 1/2 and PKA in OT-Modulation of GFAP Plasticity

Both pERK 1/2 and PKA are involved in OT-elicited GFAP reduction but play different roles. Activation of PKA can mediate OT-reduced GFAP filaments while certain level of basal PKA activity is necessary to maintain basal GFAP expression. In the presence of OT, KT5720 did not only increase GFAP filaments and 50 kDa GFAP, but also increased GFAP fragments. However, KT5720 itself reduced basal GFAP filaments. Thus, combining with Western blotting results, we propose that at resting conditions, PKA promotes GFAP polymerization by reducing dissembling or decomposition of GFAP monomers in the presence of pERK 1/2; when strongly activated, PKA causes GFAP depolymerization. The increased GFAP filaments by KT5720 to OT stimulation can be attributable to a simultaneously increased dissembling and polymerization of GFAP monomers by OT-increased pERK 1/2 (Wang and Hatton, 2007b).

It is clear that pERK 1/2 can promote dissembling of GFAP monomers since U0126 reduced GFAP fragments with or without OT. Thus, reduction of GFAP monomers by OT-activated pERK 1/2 may counterbalance, even overrule, PKA-increased GFAP monomers, accounting for the increases in GFAP fragments in response to KT5720 plus OT. Moreover, pERK 1/2 can promote GFAP polymerization despite its increasing the dissembling of GFAP monomers. This proposal is supported by the fact that inhibition of ERK 1/2 phosphorylation significantly reduced basal GFAP filaments and increased 50 kDa GFAP proteins. Alternatively, OT-elicited activation of PKA in the presence of U0126 can explain the decrease in GFAP fragments while increasing GFAP monomers. However, without pERK 1/2, even OT could still activate PKA, GFAP monomers failed to be polymerized into GFAP filaments. As a whole, the actions of these two protein kinases are antagonistic but coordinated in OT-modulated GFAP plasticity. This conclusion is in agreement with that PKA and pERK 1/2 play antagonistic roles in astrocytic proliferation (Bayatti and Engele, 2001) and in the OTR signaling (Zhong et al., 2003).

Further analysis highlights the possibility that there are spatiotemporally coordinative actions between the two kinases in OT-elicited GFAP reduction. It is clear, simply increasing cAMP or reducing pERK 1/2 levels did not elicit the spatial feature of GFAP plasticity observed in lactating rats. By contrast, using confocal microscopy, we found critical clues for a microdomain-specific regulation of the two kinases. During suckling, pERK 1/2 is translocated into somata (Wang and Hatton, 2007b), which indicates a separation of pERK 1/2 from the majority of GFAP in astrocytic processes. Following a reversal increase in GFAP upon occurrence of milk-ejection, pERK 1/2 was also expressed in astrocytic proximal processes (Wang and Hatton, 2007b).

A possible role for the increased PKA levels at the milk-ejection reflex is to provide GFAP monomers for pERK 1/2 to build new GFAP filaments at astrocytic processes. The expression of pERK 1/2 at somata (Wang and Hatton, 2007b) and activation of PKA at the processes could account for the GFAP increases in astrocytic somata and decreases in the processes at the initial stages of suckling (**Figure 7**), explaining the inhibitory effect of OT on GFAP expression. Noteworthy is that following the occurrence of the milk-ejection reflex, cPKA expression in the processes further increased from the elevated levels during suckling, which was accompanied with increased molecular association between GFAP and pERK 1/2 but decreased molecular association between GFAP and cPKA. It is likely that the increased cPKA provided GFAP monomers that are essential for pERK 1/2-evoked GFAP polymerization and filament formation; however, due to the reduced direct interaction of cPKA with GFAP, its depolymerization role gave the way to the polymerization role of pERK 1/2, and resulted in the increase in GFAP filaments and its ensuing expansion of astrocytic processes. Since GFAP filament is positively correlated to the extension of astrocyte processes (Pekny et al., 2007) and OT neuronal activity (Wang and Hamilton, 2009), pERK 1/2 and PKA modulated GFAP plasticity thus could determine OT neuronal activity under a variety of physiological and pathological conditions. **Figure 8** is a schematic drawing of OTR signaling in OT-elicited GFAP plasticity.

CONCLUSION

The present study revealed that OT-elicited GFAP plasticity is associated with sequential activation of ERK 1/2 and PKA via OTR signaling pathway in an antagonistic but coordinated manner with microdomain-specific features. This finding not only confirms that OT can efficiently facilitate neuronal activity by eliciting retraction of astrocyte processes (Wang and Hatton, 2009), but also provide a novel approach to alter astrocyte functions by directly changing GFAP plasticity through modulating the activity of pERK 1/2 and PKA. Since GFAP-associated astrocytic plasticity is extensively involved in physiological processes, such as OT secretion in lactation (Liu X. et al., 2016), reproduction (Liu X. Y. et al., 2016), and immunological activity (Wang et al., 2015; Li T. et al., 2017), as well as VP secretion in hyponatremia (Wang et al., 2011; Jiao et al., 2017) and ischemic stroke (Jia et al., 2016; Wang and Parpura, 2016) in addition to psychiatric disorders (Verkhratsky et al., 2016), neurodegenerative diseases (Vardjan et al., 2017) and many others (Yang et al., 2013; Pekny et al., 2016), further exploration of signaling process regulating GFAP plasticity is warranted.

AUTHOR CONTRIBUTIONS

PW and Y-FW performed the experiment and data analysis; PW wrote the first draft; DQ participated in discussion and revision; Y-FW designed the study and made the final revision.

ACKNOWLEDGMENTS

We thank late Dr. Glenn I. Hatton for initial support and advices, Dr. Kathryn A. Hamilton for discussion and critical reading, Dr. Harold Gainer for neurophysin antibodies and Dr. Karl Bauer for Bauer peptide. This work was supported by National Institutes of Health NS009140 (GIH), the National Natural Science Foundation of China (grant No. 31471113, Y-FW), and Strong Province of Higher Education and University Quality Engineering Fund of Heilongjiang (grant No. 002000154, Y-FW). Initial part of this study was performed in the Department of Cell Biology and Neuroscience, University of California, Riverside.

REFERENCES

Aguado, T., Palazuelos, J., Monory, K., Stella, N., Cravatt, B., Lutz, B., et al. (2006). The endocannabinoid system promotes astroglial differentiation by acting on neural progenitor cells. *J. Neurosci.* 26, 1551–1561. doi: 10.1523/jneurosci.3101-05.2006

Bayatti, N., and Engele, J. (2001). Cyclic AMP modulates the response of central nervous system glia to fibroblast growth factor-2 by redirecting signalling pathways. *J. Neurochem.* 78, 972–980. doi: 10.1046/j.1471-4159.2001.00464.x

Chapman, D. B., Theodosis, D. T., Montagnese, C., Poulain, D. A., and Morris, J. F. (1986). Osmotic stimulation causes structural plasticity of neurone-glia relationships of the oxytocin but not vasopressin secreting neurones in the hypothalamic supraoptic nucleus. *Neuroscience* 17, 679–686. doi: 10.1016/0306-4522(86)90039-4

Dieck, S. T., Heuer, H., Ehrchen, J., Otto, C., and Bauer, K. (1999). The peptide transporter PepT2 is expressed in rat brain and mediates the accumulation of the fluorescent dipeptide derivative β-Ala-Lys-N_ε-AMCA in astrocytes. *Glia* 25, 10–20. doi: 10.1002/(SICI)1098-1136(19990101)25:1<10::AID-GLIA2>3.0.co;2-y

Di Scala-Guenot, D., Mouginot, D., and Strosser, M. T. (1994). Increase of intracellular calcium induced by oxytocin in hypothalamic cultured astrocytes. *Glia* 11, 269–276. doi: 10.1002/glia.440110308

Guo, W., Wang, H., Watanabe, M., Shimizu, K., Zou, S., LaGraize, S. C., et al. (2007). Glial-cytokine-neuronal interactions underlying the mechanisms of persistent pain. *J. Neurosci.* 27, 6006–6018. doi: 10.1523/JNEUROSCI.0176-07.2007

Hatton, G. I. (2004). "Morphological plasticity of astroglial/neuronal interactions: functional implications," in *Glial Neuronal Signaling*, eds G. I. Hatton and V. Parpura (Boston, MA: Kluwer Academic Publishers), 99–124.

Hatton, G. I., Luckman, S. M., and Bicknell, R. J. (1991). Adrenalin activation of β2-adrenoceptors stimulates morphological changes in astrocytes (pituicytes) cultured from adult rat neurohypophyses. *Brain Res. Bull.* 26, 765–769. doi: 10.1016/0361-9230(91)90173-h

Hatton, G. I., and Wang, Y. F. (2008). Neural mechanisms underlying the milk ejection burst and reflex. *Prog. Brain Res.* 170, 155–166. doi: 10.1016/s0079-6123(08)00414-7

Heimfarth, L., da Silva Ferreira, F., Pierozan, P., Loureiro, S. O., Mingori, M. R., Moreira, J. C., et al. (2016). Calcium signaling mechanisms disrupt the cytoskeleton of primary astrocytes and neurons exposed to diphenylditelluride. *Biochim. Biophys Acta* 1860, 2510–2520. doi: 10.1016/j.bbagen.2016.07.023

Hirasawa, M., Schwab, Y., Natah, S., Hillard, C. J., Mackie, K., Sharkey, K. A., et al. (2004). Dendritically released transmitters cooperate via autocrine and retrograde actions to inhibit afferent excitation in rat brain. *J. Physiol.* 559, 611–624. doi: 10.1113/jphysiol.2004.066159

Hou, D., Jin, F., Li, J., Lian, J., Liu, M., Liu, X., et al. (2016). Model roles of the hypothalamo-neurohypophysial system in neuroscience study. *Biochem. Pharmacol. (Los Angel)* 5:3. doi: 10.4172/2167-0501.1000211

Hsiao, H.-Y., Mak, O.-T., Yang, C.-S., Liu, Y.-P., Fang, K.-M., and Tzeng, S. F. (2007). TNF-α/IFN-γ-induced iNOS expression increased by prostaglandin E_2 in rat primary astrocytes via EP2-evoked cAMP/PKA and intracellular calcium signaling. *Glia* 55, 214–223. doi: 10.1002/glia.20453

Inagaki, M., Gonda, Y., Nishizawa, K., Kitamura, S., Sato, C., Andog, S., et al. (1990). Phosphorylation sites linked to glial filament disassembly *in vitro* locate in a non-a-helical head domain. *J. Biol. Chem.* 265, 4722–4729.

Israel, J. M., Le Masson, G., Theodosis, D. T., and Poulain, D. A. (2003). Glutamatergic input governs periodicity and synchronization of bursting activity in oxytocin neurons in hypothalamic organotypic cultures. *Eur. J. Neurosci.* 17, 2619–2629. doi: 10.1046/j.1460-9568.2003.02705.x

Jia, S.-W., Liu, X.-Y., Wang, S. C., and Wang, Y.-F. (2016). Vasopressin hypersecretion-associated brain edema formation in ischemic stroke: underlying mechanisms. *J. Stroke Cerebrovasc. Dis.* 25, 1289–1300. doi: 10.1016/j.jstrokecerebrovasdis.2016.02.002

Jiao, R., Cui, D., Wang, S. C., Li, D., and Wang, Y. F. (2017). Interactions of the mechanosensitive channels with extracellular matrix, integrins, and cytoskeletal network in osmosensation. *Front. Mol. Neurosci.* 10:96. doi: 10.3389/fnmol.2017.00096

Langle, S. L., Poulain, D. A., and Theodosis, D. T. (2003). Induction of rapid, activity-dependent neuronal-glial remodelling in the adult rat hypothalamus *in vitro*. *Eur. J. Neurosci.* 18, 206–214. doi: 10.1046/j.1460-9568.2003.02741.x

Li, D., Liu, N., Zhao, H.-H., Zhang, X., Kawano, H., Liu, L., et al. (2017). Interactions between Sirt1 and MAPKs regulate astrocyte activation induced by brain injury *in vitro* and *in vivo*. *J. Neuroinflammation* 14:67. doi: 10.1186/s12974-017-0841-6

Li, T., Wang, P., Wang, S. C., and Wang, Y.-F. (2017). Approaches mediating oxytocin regulation of the immune system. *Front. Immunol.* 7:693. doi: 10.3389/fimmu.2016.00693

Liu, X. Y., Hou, D., Wang, J., Lv, C., Jia, S., Zhang, Y., et al. (2016). Expression of glial fibrillary acidic protein in astrocytes of rat supraoptic nucleus throughout estrous cycle. *Neuro. Endocrinol. Lett.* 37, 41–45.

Liu, X., Jia, S., Zhang, Y., and Wang, Y.-F. (2016). Pulsatile but not tonic secretion of oxytocin plays the role of anti-precancerous lesions of the mammary glands in rat dams separated from the pups during lactation. *M. J. Neurol.* 1:002.

Luckman, S. M., Huckett, L., Bicknell, R. J., Voisin, D. L., and Herbison, A. E. (1997). Up-regulation of nitric oxide synthase messenger RNA in an integrated forebrain circuit involved in oxytocin secretion. *Neuroscience* 77, 37–48. doi: 10.1016/s0306-4522(96)00498-8

Pekny, M., Pekna, M., Messing, A., Steinhäuser, C., Lee, J. M., Parpura, V., et al. (2016). Astrocytes: a central element in neurological diseases. *Acta Neuropathol.* 131, 323–345. doi: 10.1007/s00401-015-1513-1

Pekny, M., Wilhelmsson, U., Bogestål, Y. R., and Pekna, M. (2007). The role of astrocytes and complement system in neural plasticity. *Int. Rev. Neurobiol.* 82, 95–111. doi: 10.1016/s0074-7742(07)82005-8

Perlmutter, L. S., Tweedle, C. D., and Hatton, G. I. (1984). Neuronal/glial plasticity in the supraoptic dendritic zone: dendritic bundling and double synapse formation at parturition. *Neuroscience* 13, 769–779. doi: 10.1016/0306-4522(84)90095-2

Sun, H., Li, R., Xu, S., Liu, Z., and Ma, X. (2016). Hypothalamic astrocytes respond to gastric mucosal damage induced by restraint water-immersion stress in rat. *Front. Behav. Neurosci.* 10:210. doi: 10.3389/fnbeh.2016.00210

Theodosis, D. T., Poulain, D. A., and Oliet, S. H. (2008). Activity-dependent structural and functional plasticity of astrocyte-neuron interactions. *Physiol. Rev.* 88, 983–1008. doi: 10.1152/physrev.00036.2007

Vardjan, N., Verkhratsky, A., and Zorec, R. (2017). Astrocytic pathological calcium homeostasis and impaired vesicle trafficking in neurodegeneration. *Int. J. Mol. Sci.* 18:E358. doi: 10.3390/ijms18020358

Vasile, F., Dossi, E., and Rouach, N. (2017). Human astrocytes: structure and functions in the healthy brain. *Brain Struct. Funct.* 222, 2017–2029. doi: 10.1007/s00429-017-1383-5

Verkhratsky, A., Steardo, L., Peng, L., and Parpura, V. (2016). Astroglia, glutamatergic transmission and psychiatric diseases. *Adv. Neurobiol.* 13, 307–326. doi: 10.1007/978-3-319-45096-4_12

Wang, Y.-F., and Hamilton, K. (2009). Chronic vs. acute interactions between supraoptic oxytocin neurons and astrocytes during lactation: role of glial

fibrillary acidic protein plasticity. *ScientificWorldJournal* 9, 1308–1320. doi: 10.1100/tsw.2009.148

Wang, Y. F., and Hatton, G. I. (2004). Milk ejection burst-like electrical activity evoked in supraoptic oxytocin neurons in slices from lactating rats. *J. Neurophysiol.* 91, 2312–2321. doi: 10.1152/jn.00697.2003

Wang, Y. F., and Hatton, G. I. (2006). Mechanisms underlying oxytocin-induced excitation of supraoptic neurons: prostaglandin mediation of actin polymerization. *J. Neurophysiol.* 95, 3933–3947. doi: 10.1152/jn.01267.2005

Wang, Y. F., and Hatton, G. I. (2007a). Dominant role of βγ subunits of G-proteins in oxytocin-evoked burst firing. *J. Neurosci.* 27, 1902–1912. doi: 10.1523/jneurosci.5346-06.2007

Wang, Y. F., and Hatton, G. I. (2007b). Interaction of extracellular signal-regulated protein kinase 1/2 with actin cytoskeleton in supraoptic oxytocin neurons and astrocytes: role in burst firing. *J. Neurosci.* 27, 13822–13834. doi: 10.1523/jneurosci.4119-07.2007

Wang, Y. F., and Hatton, G. I. (2009). Astrocytic plasticity and patterned oxytocin neuronal activity: dynamic interactions. *J. Neurosci.* 29, 1743–1754. doi: 10.1523/jneurosci.4669-08.2009

Wang, Y.-F., Liu, L.-X., and Yang, H.-P. (2011). Neurophysiological involvement in hypervolemic hyponatremia-evoked by hypersecretion of vasopressin. *Transl. Biomed.* 2:3. doi: 10:3823/425

Wang, Y.-F., and Parpura, V. (2016). Central role of maladapted astrocytic plasticity in ischemic brain edema formation. *Front. Cell. Neurosci.* 10:129. doi: 10.3389/fncel.2016.00129

Wang, Y.-F., Sun, M.-Y., Hou, Q., and Hamilton, K. A. (2013a). GABAergic inhibition through synergistic astrocytic neuronal interaction transiently decreases vasopressin neuronal activity during hypoosmotic challenge. *Eur. J. Neurosci.* 37, 1260–1269. doi: 10.1111/ejn.12137

Wang, Y.-F., Sun, M. Y., Hou, Q., and Parpura, V. (2013b). Hyposmolality differentially and spatiotemporally modulates levels of glutamine synthetase and serine racemase in rat supraoptic nucleus. *Glia* 61, 529–538. doi: 10.1002/glia.22453

Wang, P., Yang, H. P., Tian, S., Wang, L., Wang, S. C., Zhang, F., et al. (2015). Oxytocin-secreting system: a major part of the neuroendocrine center regulating immunologic activity. *J. Neuroimmunol.* 289, 152–161. doi: 10.1016/j.jneuroim.2015.11.001

Yang, H. P., Wang, L., Han, L., and Wang, S. C. (2013). Nonsocial functions of hypothalamic oxytocin. *ISRN Neurosci.* 2013:179272. doi: 10.1155/2013/179272

Zhong, M., Yang, M., and Sanborn, B. M. (2003). Extracellular signal-regulated kinase 1/2 activation by myometrial oxytocin receptor involves GαqGβγ and epidermal growth factor receptor tyrosine kinase activation. *Endocrinology* 144, 2947–2956. doi: 10.1210/en.2002-221039

Conflict of Interest Statement: The authors declare that the research was conducted in the absence of any commercial or financial relationships that could be construed as a potential conflict of interest.

frontiers in Molecular Neuroscience

ORIGINAL RESEARCH
published: 21 July 2017
doi: 10.3389/fnmol.2017.00226

SDF1-CXCR4 Signaling Maintains Central Post-Stroke Pain through Mediation of Glial-Neuronal Interactions

Fei Yang[1†], Wen-Jun Luo[1†], Wei Sun[1,2†], Yan Wang[1,2], Jiang-Lin Wang[1], Fan Yang[1,2], Chun-Li Li[1,2], Na Wei[1,2], Xiao-Liang Wang[1,2], Su-Min Guan[3] and Jun Chen[1,2,4]**

[1]*Institute for Biomedical Sciences of Pain, Tangdu Hospital, The Fourth Military Medical University, Xi'an, China,* [2]*Key Laboratory of Brain Stress and Behavior, People's Liberation Army (PLA), Xi'an, China,* [3]*School of Stomatology, The Fourth Military Medical University, Xi'an, China,* [4]*Beijing Institute for Brain Disorders, Beijing, China*

Central post-stroke pain (CPSP) is an intractable central neuropathic pain that has been poorly studied mechanistically. Here we showed that stromal cell-derived factor 1 (SDF1 or CXCL12), a member of the CXC chemokine family, and its receptor CXCR4 played a key role in the development and maintenance of thalamic hemorrhagic CPSP through hypoxia inducible factor 1α (HIF-1α) mediated microglial-astrocytic-neuronal interactions. First, both intra-thalamic collagenase (ITC) and SDF1 injections could induce CPSP that was blockable and reversible by intra-thalamic administration of both AMD3100 (a selective CXCR4 antagonist) and inhibitors of microglial or astrocytic activation. Second, long-term increased-expression of SDF1 and CXCR4 that was accompanied by activations of both microglia and astrocytes following ITC could be blocked by both AMD-3100 and YC-1, a selective inhibitor of HIF-1α. AMD-3100 could also inhibit release of proinflammatory mediators (TNFα, IL1β and IL-6). Increased-expression of HIF-1α, SDF1, CXCR4, Iba1 and GFAP proteins could be induced by both ITC and intra-thalamic $CoCl_2$, an inducer of HIF-1α that was blockable by both HIF-1α inhibition and CXCR4 antagonism. Finally, inhibition of HIF-1α was only effective in prevention, but not in treatment of ITC-induced CPSP. Taken together, the present study demonstrated that in the initial process of thalamic hemorrhagic state HIF-1α up-regulated SDF1-CXCR4 signaling, while in the late process SDF1-CXCR4 signaling-mediated positive feedback plays more important role in glial-glial and glial-neuronal interactions and might be a novel promising molecular target for treatment of CPSP in clinic.

Keywords: central post-stroke pain, intra-thalamic injection, mechanical pain hypersensitivity, SDF1-CXCR4 signaling, hypoxia inducible factor 1α, glial-neuronal crosstalk

OPEN ACCESS

Edited by:
Alexej Verkhratsky, University of Manchester, United Kingdom

Reviewed by:
Yonghe Wu, Deutsches Krebsforschungszentrum (DKFZ), Germany
Hugo H. Marti, Heidelberg University, Germany

****Correspondence:***
Su-Min Guan
jchsmg@fmmu.edu.cn
Jun Chen
junchen@fmmu.edu.cn

[†]These authors have contributed equally to this work.

Received: *25 April 2017*
Accepted: *03 July 2017*
Published: *21 July 2017*

Citation:
Yang F, Luo W-J, Sun W, Wang Y, Wang J-L, Yang F, Li C-L, Wei N, Wang X-L, Guan S-M and Chen J (2017) SDF1-CXCR4 Signaling Maintains Central Post-Stroke Pain through Mediation of Glial-Neuronal Interactions. Front. Mol. Neurosci. 10:226. doi: 10.3389/fnmol.2017.00226

INTRODUCTION

Stroke is the leading cause of adult disability worldwide (Feigin et al., 2014). In both developed countries and high income developing countries such as China, acute treatment of stroke has been improved substantially, resulting in decrease in mortality and increase in the proportion of survivors with disability (Feigin et al., 2014; Yang et al., 2014; Ferro et al., 2016; Yang Y. et al., 2016). Central post-stroke pain (CPSP) is one of the most troublesome sequelae of

both ischemic and hemorrhagic stroke caused by primary lesions affecting the central somatosensory system (Yang et al., 2014; Hosomi et al., 2015; Yang Y. et al., 2016). About 11%–32% of thalamic stroke survivors experience persistent spontaneous pain, hyperalgesia, allodynia and dysesthesia and about 50%–60% patients with CPSP are resistant to the existing analgesic therapies (Chung et al., 1996; Nasreddine and Saver, 1997). So far, the underlying mechanisms of CPSP remain largely unknown due to lack of valid animal studies (De Vloo et al., 2017). In a critical review on the animal models for CPSP, the experimental thalamic hemorrhage model induced by intra-thalamic collagenase (ITC) injection (Wasserman and Koeberle, 2009; Yang et al., 2014; Kuan et al., 2015; Yang Y. et al., 2016) was believed to be the only one with relatively high reproducibility (De Vloo et al., 2017).

As introduced initially in rats with ITC-induced hemorrhagic CPSP (Wasserman and Koeberle, 2009), activation of microglial cells and astrocytes (glial barrier) surrounding the edge of the hematoma was identified on the first day and reached peak on the seventh day after ITC. Post-treatment with systemic minocycline, a microglial inhibitor, has been shown to attenuate ITC-induced mechanical allodynia and thermal hyperalgesia, indicating that the activated microglial cells contribute to the maintenance of CPSP (Hanada et al., 2014). However, what kind of chemical substances (signaling pathways) are involved in mediation of glial-glial and glial-neuronal interactions (crosstalk) remains unknown and requires to be addressed.

Stromal cell-derived factor 1 (SDF1, also named as CXCL12), a member of the CXC chemokine family, is constitutively expressed in various kinds of cells in the peripheral and central nervous system (Reaux-Le Goazigo et al., 2012; Réaux-Le Goazigo et al., 2013). Under pathological states, activated glial cells are the main source of SDF1. In LPS-induced systemic inflammation model and bone cancer pain model, SDF1 was predominantly released by activated astrocytes in the spinal cord (Shen et al., 2014; Hang et al., 2016; Yang L. et al., 2016). Microglia was also a main source of SDF1 production in the spinal cord of rats with spared nerve injury or ischemia-reperfusion injury (Bai et al., 2016; Li et al., 2016). SDF1 exerts multiple biological functions by binding to CXCR4 (Reaux-Le Goazigo et al., 2012). Recently, several studies reported that systemic treatment with AMD3100, a highly selective CXCR4 antagonist, significantly improved the functional outcome following experimental stroke through attenuating the inflammatory response and microglial activation (Huang et al., 2013; Ruscher et al., 2013; Walter et al., 2015). Importantly, the pro-algesic effect of SDF1-CXCR4 signaling has also been verified in several pathological pain models (Oh et al., 2001; Bhangoo S. et al., 2007; Bhangoo S. K. et al., 2007; Bhangoo et al., 2009; Knerlich-Lukoschus et al., 2011; Wilson et al., 2011; Menichella et al., 2014). In a rat model of bone cancer pain or ischemia-reperfusion induced inflammatory pain, both SDF1 neutralizing antibody and AMD3100 could suppress the development of pain hypersensitivity through inhibiting astrocytic and microglial activation (Shen et al., 2014; Hu et al., 2015; Li et al., 2016). In a neuropathic pain model induced by partial sciatic nerve ligation, it has been demonstrated that SDF1-CXCR4 signaling is involved in the induction of neuropathic pain through mediating microglia-astrocyte crosstalk (Luo et al., 2016). Our recent studies have also demonstrated that SDF1-CXCR4 signaling plays critical roles in mediating the satellite glial cell-neuronal crosstalk in the dorsal root ganglion (DRG) that contributes to the hyperexcitability of primary nociceptors and transition from acute to chronic processes of inflammatory pain (Dubovy et al., 2010; Yang et al., 2015, 2017). Hypoxia inducible factor 1α (HIF-1α), a transcription factor which is closely related to the expression of SDF1 and CXCR4 under hypoxia condition, has been observed to be significantly up-regulated following ITC-induced hemorrhagic stroke (Jiang et al., 2002; Liu et al., 2010; Youn et al., 2011). Taking all these into account, we hypothesized that ITC-induced thalamic hemorrhage could induce up-regulation of SDF1-CXCR4 signaling via HIF-1α which would then maintain CPSP by neuroinflammatory microenvironment caused by microglial-astrocytic-neuronal interactions through positive feedback regulation.

MATERIALS AND METHODS

Animals

Male Sprague-Dawley rats (280–320 g) were provided by the Laboratory Animal Center of the Fourth Military Medical University (FMMU). This study was carried out in accordance with the recommendations of the Animal Care and Use Committee of FMMU and performed in accordance with the updated Guide for the Care and Use of Laboratory Animals (8th edition, the National Academies Press, 2011). The number of rats used and their suffering were minimized. During the whole experiment, the rats were randomized.

Surgery

Surgery was performed according to the methods described previously (Yang et al., 2014; Yang Y. et al., 2016). Rats were anesthetized with chloral hydrate (0.3 g/kg, i.p.) and placed in a stereotaxic apparatus (Narishige Scientific Instrument Lab, Japan). Collagenase type IV (0.025 U/0.25 μl, Sigma-Aldrich China, Shanghai) or saline (0.25 μl) was microinjected into the ventral posterior lateral nucleus (VPL) of the right thalamus (bregma −3.48 mm antero-posterior; 3.6 mm lateral to the midline, and 6.2 mm ventral to the brain surface) according to the stereotaxic coordinates (Paxinos and Watson, 2005). After each injection, the syringe remained for 5 min to prevent spread of the agent to the brain surface. Then the needle was slowly withdrawn, the skin closed using 4.0 sutures, and all rats were allowed to recover in individual cages for at least 3 days. Naïve rats were fed under the same conditions in a parallel manner.

Mechanical Pain Sensitivity Testing

The mechanical pain sensitivity testing was performed by experimenters blinded to the experimental treatments (Yang et al., 2014; Yang Y. et al., 2016). The rats were placed on a metal mesh floor and habituated for 1 h before testing. Ascending graded von Frey filaments were applied from underneath the metal mesh floor to the plantar area of the appropriate hindpaw.

Each von Frey filament was applied 10 times (once every several seconds). The bending force value of the von Frey filament that caused an appropriate 50% occurrence of paw withdrawal was expressed as the paw withdrawal mechanical threshold (PWMT, g). Baseline PWMT of all experimental rats were measured prior to the surgery and the effects of different drugs on PWMT were evaluated at the time point indicated in corresponding figures.

Intra-Thalamic Drug Injections

Intra-thalamic drug injections were performed at 10 days after collagenase injection when CPSP was stably established or at 30 min before collagenase injection prior to CPSP induction. The rats were injected with minocycline hydrochloride (Sigma, 10 μg), fluorocitrate (Sigma, 1 nM), AMD3100 (Abcam, 7.5 or 15 μg) or YC-1 (Abcam, 0.2 mM) in a total volume of 1 μl over a period of 10 min. The doses used in the present study were based on or slightly modified from previous studies (Zhao et al., 2007; Trecki and Unterwald, 2009; Huang et al., 2014; Luo et al., 2014; Choi et al., 2015). Minocycline hydrochloride selectively inhibits microglial activation and proliferation, with no direct effect on neurons or astrocytes. Fluorocitrate, an inhibitor of astrocyte metabolism, inhibits the tricarboxylic acid cycle enzyme aconitase in astrocytes. AMD3100, which is a highly selective CXCR4 antagonist, was used to evaluate the roles of CXCR4 in the development of CPSP. YC-1, an established HIF-1α inhibitor, was applied to verify the regulatory effects of HIF-1α in the development of CPSP. A separate group of naïve rats underwent intra-thalamic injection of recombinant active SDF1 protein (Abcam, 50 ng) or $CoCl_2$ (Sinopharm Chemical Reagent Co. Ltd, 100 mM), a well-known inducer of HIF-1α, following minocycline, fluorocitrate or AMD3100 injections to explore the cellular mechanisms underlying the pro-algesic effect of SDF1-CXCR4 signaling. The intra-thalamic injection methods were the same as above-mentioned and the injection locations were assessed histologically. Fluorocitrate was dissolved in 0.3% 2 M HCl in phosphate-buffered saline (PBS) and YC-1 was dissolved in 1% dimethyl sulfoxide (DMSO), whereas all other drugs were dissolved in sterile saline.

Immunohistochemistry

As reported previously (Yang et al., 2015), the rats were anesthetized with chloral hydrate, then perfused with physiological saline, followed by 4% paraformaldehyde in 0.1 M PB solution. The brain was removed and postfixed overnight at 4°C and then immersed in 30% sucrose in 0.1 M PB. Brain tissue were cut into transverse sections (30 μm thick) on CM1900 freezing microtome (Leica, Germany). After blocking with 10% goat serum in PBS, the sections were incubated overnight at 4°C with the following primary antibodies: mouse anti-GFAP (1:500 Millipore), rabbit anti-Iba-1 (1:500, WAKO), mouse anti-NeuN (1:200, Millipore), Goat anti-CXCR4 (1:200, Abcam) and rabbit anti-c-Fos (1:500, Abcam). On the following day, Cy3- or FITC-conjugated secondary antibodies were incubated for 2–3 h at room temperature. For double immunostaining, sections were incubated with a mixture of primary antibodies overnight at 4°C, followed by a mixture of secondary antibodies. The images were examined under a laser scan confocal fluorescent microscope (Olympus FV1000, Japan).

Western Blotting

As reported previously, the thalamus tissues around the hemorrhagic lesion sites were collected and homogenized in RIPA lysis buffer containing protease inhibitors (Applygen Technologies Inc., China; Yang et al., 2015, 2017; Yang Y. et al., 2016). Protein concentrations of the lysate were determined using a BCA protein assay kit (Thermo Scientific, Rockford, IL, USA). Equal amounts of protein were separated by 10% separation gels and then transferred to polyvinylidene difluoride membranes (Bio-Rad, Hercules, CA, USA). After blocking with 5% nonfat milk (Bio-Rad, Hercules, CA, USA) for 1 h at room temperature, the membranes were incubated with primary antibodies at 4°C overnight. The primary antibodies included mouse anti-HIF-1α (1:500, Abcam), rabbit anti-SDF1 (1:200, Abcam) and the antibodies mentioned in immunohistochemistry section. On the following day, the membranes were washed three times in PBST and then incubated with an HRP-conjugated secondary antibody (Bio-Rad) for 2 h at room temperature. The membranes were visualized with enhanced chemiluminescence solution (Alpha Innotech Corp) and the signals were captured with FluorChem FC2 (Alpha Innotech Corp). The density of specific bands was measured with a computer-assisted imaging analysis system and normalized to β-tubulin or β-actin intensity.

ELISA Assay

The thalamus tissues around the hemorrhagic lesion sites were collected and homogenized in RIPA lysis buffer containing protease and phosphatase inhibitors (Applygen Technologies Inc.). After quantitative measurement of the total protein concentrations with a BCA protein assay kit (Thermo Scientific), the homogenized thalamus tissue were assayed for TNF-α, IL-1β and IL-6 (Westang, Shanghai, China) by ELISA. Each protein of interest was expressed as picograms per milligram of total proteins.

Statistical Analysis

Data were analyzed using GraphPad Prism version 5 (GraphPad, San Diego, CA, USA) and all data were expressed as means ± SEM. Differences in changes of values of each group were tested using *t*-tests and one-way or two-way repeated ANOVA, followed by individual *post hoc* comparisons (Bonferroni or Tukey test). Linear relationships were assessed using Pearson's correlation test. A level of $P < 0.05$ was accepted as significant.

RESULTS

Long-Term Activation of Microglia and Astrocytes in Peri-Thalamic Lesion Sites Caused by ITC

Similar to our previous reports (Yang et al., 2014), unilateral ITC injection confined to the VPL thalamic nucleus (**Figure 1A**)

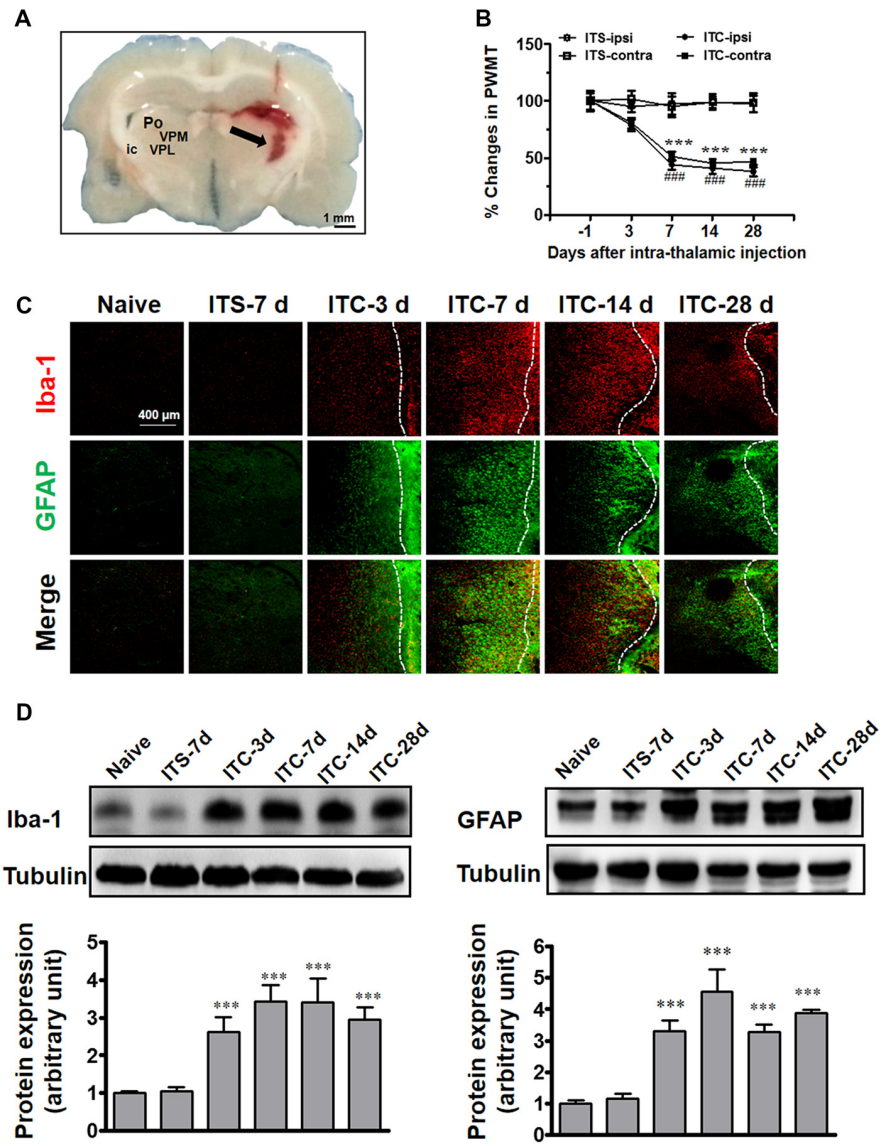

FIGURE 1 | Thalamic hemorrhagic rats exhibit bilateral mechanical pain hypersensitivity and microglial and astrocytic activation in peri-thalamic lesion sites. **(A)** Photomicrograph of brain slice showing the hemorrhagic lesion site in the thalamus following ITC. Scale bar, 1 mm; ic, internal capsule; Po, posterior thalamic nuclear group; VPL, ventral posterolateral nucleus of the thalamus; VPM, ventral posteromedial nucleus of the thalamus. **(B)** Development of bilateral mechanical pain hypersensitivity induced by ITC. Saline injection served as control. ITS, intra-thalamic saline; ITC, intra-thalamic collagenase injection; contra, contralateral; ipsi, ipsilateral; PWMT, paw-withdrawal mechanical threshold; $^{***}P < 0.001$ ITC-ipsi vs. ITS-ipsi; $^{###}P < 0.001$ ITC-contra vs. ITS-contra; $n = 10$ rats/group. **(C)** Representative immunofluorescent photomicrographs showing the time course expression of Iba-1 (red) and GFAP (green), markers of microglia and astrocytes respectively, in the peri-thalamic lesion sites. The hemorrhagic lesion core is on the right side of the white line in each image. Scale bar, 400 μm. **(D)** Iba-1 and GFAP expression as examined using Western blot assay. Representative bands are shown on the top, and data summary is shown on the bottom. $^{***}P < 0.001$ vs. ITS-7 d group; $n = 4$/group.

resulted in bilateral reductions in PWMT, which were identified on day 7 post-injection and remained unchanged until day 28 post-injection, suggesting a chronic, persistent bilateral mechanical allodynia in this model (**Figure 1B**). To examine the involvement of microglia and astrocytes, the expression of Iba-1 and GFAP in the peri-thalamic lesion (hematoma) sites were quantified by immunohistochemistry and Western blot on 3, 7, 14 and 28 days after ITC. Compared with intra-thalamic saline (ITS) injection group, the ITC group showed marked increases in Iba-1 and GFAP expression at each time point examined. The expression level of Iba-1 and GFAP was substantially increased in peri-thalamic lesion sites on day 3 after ITC, reached peak on day 7 and remained unchanged until day 28 (**Figures 1C,D**). However, the expression level of Iba-1 and GFAP in the contralateral thalamus remained at basal levels (**Figure 1**).

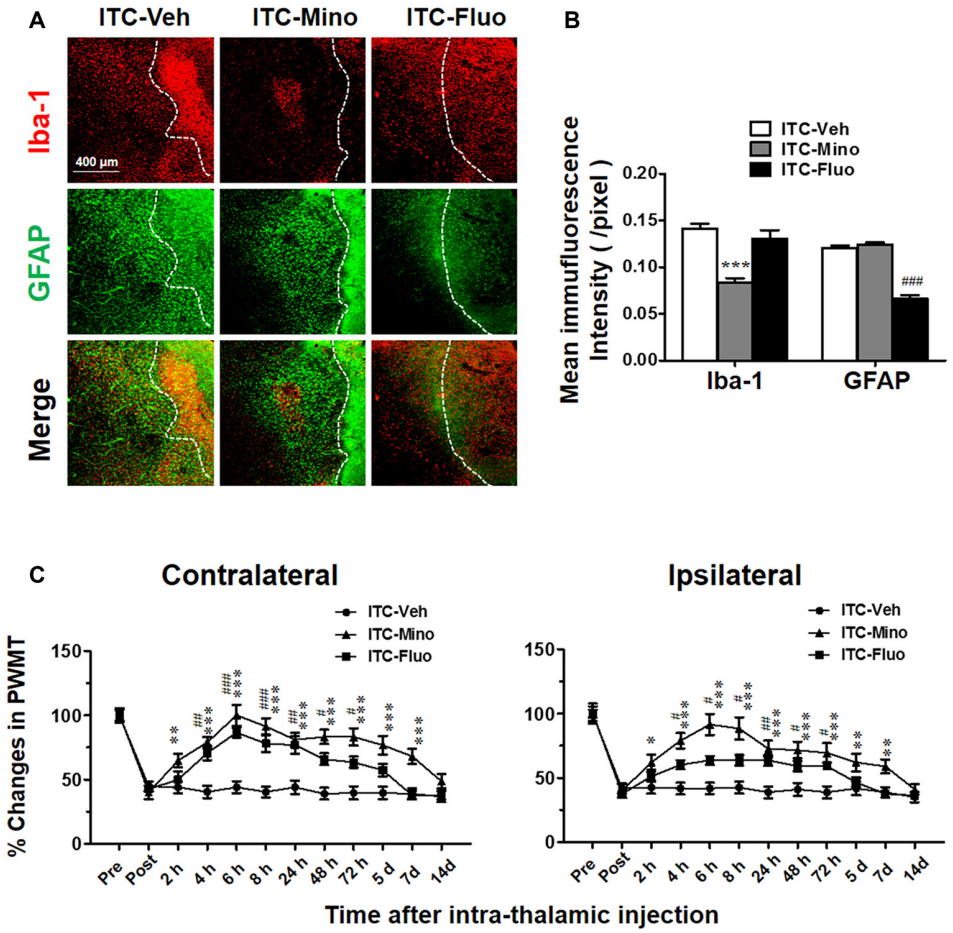

FIGURE 2 | Effects of intra-thalamic injection of minocycline and fluorocitrate on Iba-1 and GFAP expression and the established central post-stroke pain (CPSP). **(A)** Representative immunofluorescent photomicrographs showing expression of Iba-1 and GFAP in peri-thalamic lesion sites following intra-thalamic minocycline (10 μg, 1 μl) and fluorocitrate (1 nM, 1μl) injection. The hemorrhagic lesion core is on the right side of the white line in each image. Scale bar, 400 μm. **(B)** Quantification of the mean immunofluorescent intensity of Iba-1 and GFAP following intra-thalamic minocycline and fluorocitrate injection. $^{***}P < 0.001$, ITC-Mino vs. ITC-Veh; $^{###}P < 0.001$, ITC-Fluo vs. ITC-Veh; $n = 4$/group. **(C)** Temporal pattern of effects of intra-thalamic minocycline and fluorocitrate injection at 10 days post thalamic hemorrhage on the established bilateral mechanical pain hypersensitivity. PWMT, paw-withdrawal mechanical threshold; $^{*}P < 0.05$, $^{**}P < 0.01$, $^{***}P < 0.001$, ITC-Mino vs. ITC-Veh; $^{\#}P < 0.05$, $^{\#\#}P < 0.01$, $^{\#\#\#}P < 0.001$, ITC-Fluo vs. ITC-Veh; $n = 8$/group.

Intra-Thalamic Administration of Minocycline or Fluorocitrate Reversed ITC-Induced CPSP via Suppressing the Activation of Microglial Cells and Astrocytes

After CPSP was well established by 10 days after ITC, intra-thalamic injection of minocycline selectively blocked the upregulation of Iba-1 but without any effect on GFAP expression in the peri-thalamic lesion sites, while intra-thalamic injection of fluorocitrate significantly diminished ITC-induced activation of astrocytes labeled by GFAP but without any effect on Iba-1 expression (**Figures 2A,B**). To investigate the roles of microglial and astrocytic activation in the CPSP, we explored the time-related effects of minocycline and fluorocitrate on ITC-induced bilateral mechanical pain hypersensitivity. Our results showed that single intra-thalamic injection with minocycline alleviated the established bilateral mechanical pain hypersensitivity. The anti-allodynic effect of minocycline reached peak at 6 h after injection and maintained at a significant level for at least 7 days. The established bilateral mechanical pain hypersensitivity was also remarkably reduced by fluorocitrate, which lasted from 4 h to 3 days after injection (**Figure 2C**). All these results suggest that both microglia and astrocytes play important roles in maintaining the thalamic hemorrhage-induced CPSP.

CPSP Induced by Intra-Thalamic Injection of SDF1 in Naïve Rats Was Blocked by CXCR4 Antagonism

As SDF1-CXCR4 signaling was closely related to microglia and astrocyte activation, we next tried to determine whether

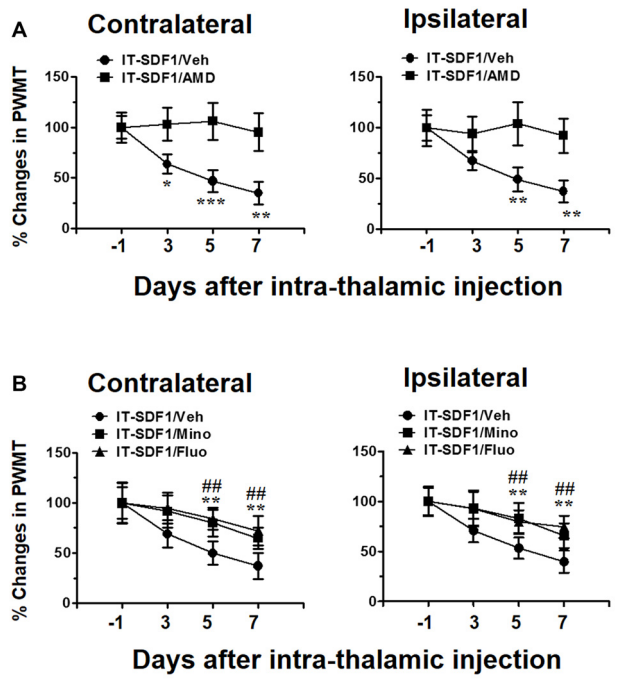

FIGURE 3 | Cellular mechanisms underlying intra-thalamic stromal cell-derived factor 1 (SDF1) injection-induced mechanical pain hypersensitivity in naïve rats. **(A)** Pre-injection of AMD3100 (15 μg/μl) prevents intra-thalamic SDF1 injection-induced bilateral mechanical pain hypersensitivity. $^{*}P < 0.05$, $^{**}P < 0.01$, $^{***}P < 0.001$ IT-SDF1/AMD vs. IT-SDF1/Veh; $n = 7$/group. **(B)** Pre-injection of minocycline and fluorocitrate prevent intra-thalamic SDF1 protein injection-induced bilateral mechanical pain hypersensitivity. $^{**}P < 0.01$ for IT-SDF1/Mino. IT-SDF1/Mino vs. IT-SDF1/Veh; $^{\#\#}P < 0.01$ IT-SDF1/Fluo. IT-SDF1/Fluo vs. IT-SDF1/Veh, PWMT, paw-withdrawal mechanical threshold; $n = 7$/group.

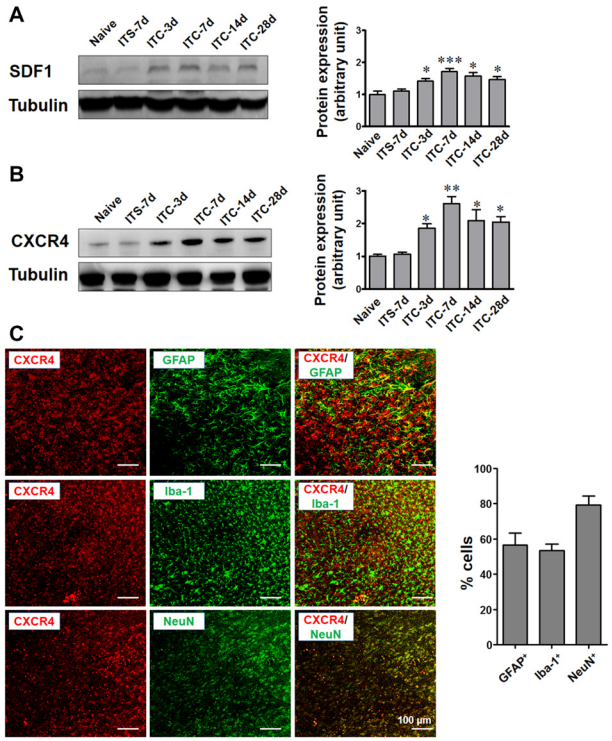

FIGURE 4 | Temporal and spatial changes in SDF1 and CXCR4 expression in peri-thalamic lesion sites under CPSP condition. **(A)** Western blot assay showing the time course expression of SDF1 following thalamic hemorrhage. Representative bands are shown on the left, and data summary is shown on the right. $^{*}P < 0.05$, $^{***}P < 0.001$ vs. ITS group. **(B)** Western blot assay showing the time course expression of CXCR4 following thalamic hemorrhage. Representative bands are shown on the left, and data summary is shown on the right. $^{*}P < 0.05$, $^{**}P < 0.01$ vs. ITS group; $n = 4$/group. **(C)** Left panel showing the immunofluorescence micrographs of the double-staining of CXCR4 with GFAP, Iba-1 and NeuN. Right panel quantifying the percentages of GFAP-positive, Iba-1-positive and NeuN-positive cells expressing CXCR4. Scale bar, 100 μm.

SDF1-CXCR4 signaling was involved in the induction of pain in naïve rats through regulating glial cell activation. As shown in **Figure 3A**, intra-thalamic SDF1 injection elicited bilateral mechanical pain hypersentivity from day 3 to day 7 which could be completely blocked by pre-administration of AMD3100 into the SDF1 injection sites. Moreover, pre-administration of minocycline or fluorocitrate in the SDF1 injection sites also significantly suppressed SDF1-induced bilateral mechanical pain hypersentivity from day 5 to day 7 (**Figure 3B**).

Temporal and Spatial Changes in SDF1 and CXCR4 Expressions in the Thalamus Following ITC

Under the CPSP condition induced by ITC, SDF1 expression was significantly increased in the peri-thalamic lesion sites at 3, 7, 14 and 28 days post-ITC relative to the saline control (**Figure 4A**). The level of CXCR4 expression in peri-thalamic lesion sites under CPSP condition was also examined by Western blot analysis. As shown in **Figure 4B**, increased CXCR4 protein expression was also seen at 3, 7, 14 and 28 days post-ITC relative to the saline control.

To define the cellular distribution of CXCR4, double staining of CXCR4 with different cell markers was performed. CXCR4 was not only co-localized with neuronal marker NeuN but also with astrocytic marker GFAP and microglial marker Iba-1 (**Figure 4C**).

Antagonizing CXCR4 by Intra-Thalamic Administration of AMD3100 Suppressed Both Glial Cell Activation and Neuronal Hyperactivity

To determine whether CXCR4 contributes to microglial and astrocytic activations under CPSP condition, intra-thalamic VPL injection of AMD3100 (15 μg) was administered 30 min prior to ITC. As shown in **Figure 5A**, CXCR4 antagonism prevented increases in both Iba-1 and GFAP expression in the peri-thalamic lesion sites on day 3 and 7 post-ITC. Moreover, the increased release of pro-inflammatory mediators including TNF-α, IL-6 and IL-1β in the peri-thalamic lesion sites was also prevented by intra-VPL AMD3100 administration on day 7 and 14 post-ITC (**Figure 5B**). Furthermore, antagonizing CXCR4 by intra-thalamic AMD3100 on day 10 post-ITC also suppressed

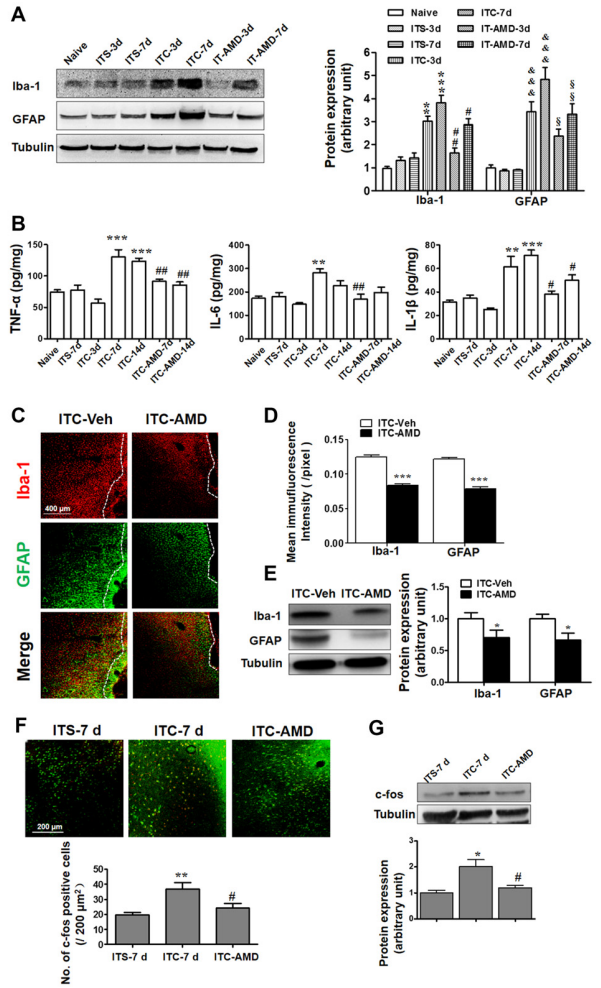

FIGURE 5 | Effects of intra-thalamic injection of AMD3100 on thalamic hemorrhage-induced glial cells activation and neuronal hyperactivity. **(A)** Western blot assay showing the effect of AMD3100 (15 μg/μl), injected 30 min before ITC, on the expression level of Iba-1 and GFAP in peri-thalamic lesion sites. $^{**}P < 0.01$, $^{***}P < 0.001$ vs. ITS at corresponding time points; $^{\&\&\&}P < 0.001$ vs. ITS at corresponding time points; $^{\#}P < 0.05$, $^{\#\#}P < 0.01$ vs. ITC at corresponding time points; $^{\S}P < 0.05$, $^{\S\S}P < 0.01$ vs. ITC at corresponding time points. **(B)** ELISA assay showing the effect of AMD3100 (15 μg/μl) pre-injection on the expression level of TNF-α, IL-6 and IL-1β. $^{**}P < 0.01$, $^{***}P < 0.001$ vs. ITS-7 d; $^{\#}P < 0.05$, $^{\#\#}P < 0.01$ vs. ITC at corresponding time points. **(C)** Representative immunofluorescent photomicrographs showing expression of Iba-1 and GFAP in peri-thalamic lesion sites following intra-thalamic AMD3100 (15 μg/μl) injection at 10 days after ITC. The hemorrhagic lesion core is on the right side of the white line in each image. Scale bar, 400 μm. **(D)** Quantification of the mean immunofluorescent intensity of Iba-1 and GFAP following intra-thalamic AMD3100 (15 μg/μl) post-injection. $^{***}P < 0.001$ ITC-AMD vs. ITC-Veh; $n = 4$/group. **(E)** Western blot assay showing the effect of AMD3100 (15 μg/μl) post-injection on the expression level of Iba-1 and GFAP in peri-thalamic lesion sites. Representative bands are shown on the left, and data summary is shown on the right. $^{*}P < 0.05$, vs. ITC-Veh. **(F)** Representative immunofluorescent photomicrographs showing co-expression of c-fos (red) and NenN (green) in peri-thalamic lesion sites following intra-thalamic AMD3100 (15 μg/μl) post-injection. $^{**}P < 0.01$, vs. ITS-7 d; $^{\#}P < 0.05$ vs. ITC-7 d;. Scale bar, 200 μm. **(G)** Western blot assay showing the effect of AMD3100 (15 μg/μl) post-injection on the expression

(*Continued*)

FIGURE 5 | Continued
level of c-Fos in peri-thalamic lesion sites. Representative bands are shown on the top, and data summary is shown on the bottom. $^{*}P < 0.05$, vs. ITS-7 d; $^{\#}P < 0.05$ vs. ITC-7 d; $n = 3$/group.

the increase in Iba-1 and GFAP expressions, implicating that SDF1-CXCR4 signaling is directly involved in the ITC-induced activations of both microglia and astrocytes (**Figures 5C–E**).

The role of CXCR4 in the neuronal activity was also examined by measuring c-Fos expression surrounding the glial barrier. As shown in **Figure 5F**, the c-Fos immunoreactivity was barely observed in rats receiving ITS, while significant increase in c-Fos-labeled neurons was observed in the peri-thalamic lesion sites following ITC. Intra-thalamic microinjection of AMD3100 reduced the number of c-Fos-labeled neurons (**Figure 5F**) and decreased the ITC-induced c-Fos expression as measured by Western blot (**Figure 5G**).

Antagonizing CXCR4 by Intra-Thalamic Administration of AMD3100 Could Completely Reverse the Well-Established CPSP

To determine whether CXCR4 contributes to the induction of thalamic hemorrhage-induced CPSP, AMD3100 (15 μg) was microinjected into the VPL 30 min prior to ITC. Our behavioral assay verified that pre-injection of AMD3100 partially inhibited the ITC-induced bilateral mechanical pain hypersensitivity for 21 days relative to ITS control (**Figure 6A**), implying that CXCR4 plays a partial role in the initiation of CPSP.

However, the maintaining role of CXCR4 in the thalamic hemorrhage-induced CPSP was more significant. As shown in **Figure 6B**, intra-thalamic injection of AMD3100 with two doses (7.5 μg and 15 μg) on day 10 after ITC almost completely reversed the well-established CPSP. The analgesic effect of AMD3100 was dose-related and lasted for 48 h to 72 h, implicating the therapeutic value of AMD3100 in treatment of CPSP (**Figures 6B,C**).

Inhibition of HIF-1α Blocked the Initiation but Not the Maintenance of ITC-Induced CPSP

In the present study, using Western blot analysis (**Figure 7A**), we examined HIF-1α expression in the peri-thalamic lesion sites at 3, 7, 14 and 28 days after ITC. It was revealed that ITC resulted in a short-term increase in HIF-1α expression, reaching peak during day 3 and 7, returning to the control level since day 14 post-ITC (**Figure 7A**).

We next explored whether HIF-1α is involved in the development of ITC-induced CPSP. It was interesting to find that intra-thalamic microinjection of YC-1, a potent inhibitor of HIF-1α production, blocked the occurrence of ITC-induced CPSP when being administered 30 min prior to ITC (**Figure 7B**), however it had no reversal effect on the well-established CPSP when being administered 10 days after ITC (**Figure 7C**).

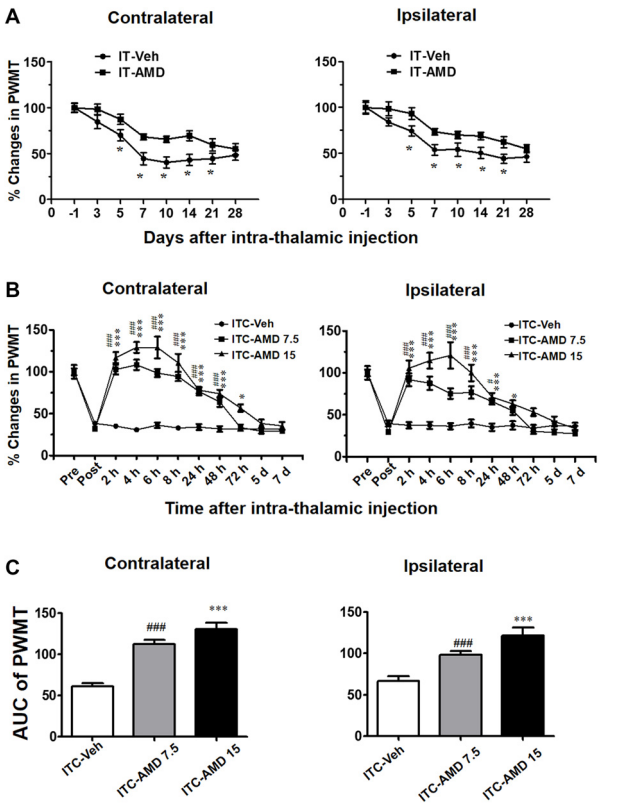

FIGURE 6 | Effects of intra-thalamic AMD3100 injection on the induction and maintenance of ITC-induced CPSP. **(A)** Temporal pattern of effects of intra-thalamic AMD3100 (15 μg/μl) injection at 30 min before ITC on the induction of bilateral mechanical pain hypersensitivity. $^{*}P < 0.05$, IT-AMD vs. IT-Veh; $n = 10$/group. **(B)** Temporal pattern of effects of intra-thalamic AMD3100 (7.5 and 15 μg/μl) injection at 10 days post thalamic hemorrhage on the established bilateral mechanical pain hypersensitivity. $^{*}P < 0.05$, $^{***}P < 0.001$, ITC-AMD 15 vs. ITC-Veh; $^{\#}P < 0.05$, $^{\#\#\#}P < 0.001$, ITC-AMD 7.5 vs. ITC-Veh; $n = 10$/group. **(C)** Quantification of area under the analgesic effects of AMD3100 (7.5 and 15 μg/μl). $^{***}P < 0.001$ vs. ITC-Veh; $^{\#\#\#}P < 0.001$ vs. ITC-Veh; PWMT, paw-withdrawal mechanical threshold.

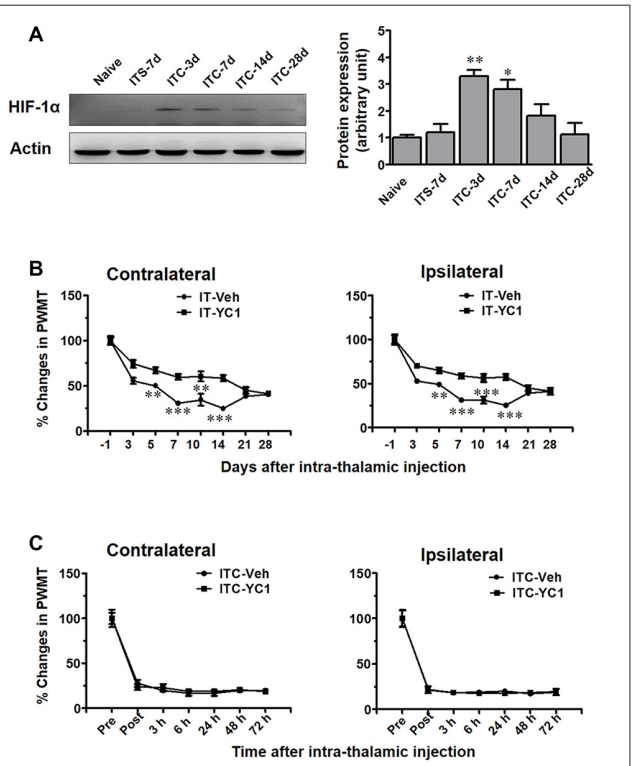

FIGURE 7 | Temporal pattern of hypoxia inducible factor 1α (HIF-1α) expression in peri-thalamic lesion sites following thalamic hemorrhage and effects of intra-thalamic YC-1 injection on the induction and maintenance of CPSP. **(A)** Western blot assay showing the time course expression of HIF-1α following thalamic hemorrhage. Representative bands are shown on the left, and data summary is shown on the right. $^{*}P < 0.05$, $^{**}P < 0.01$ vs. ITS-7 d; $n = 4$/group. **(B)** Effect of intra-thalamic pre-injection of YC-1 (0.2 mM, 1 μl) on the induction of bilateral mechanical pain induced by thalamic hemorrhage. $^{**}P < 0.01$, $^{***}P < 0.001$ IT-YC1 vs. IT-Veh; $n = 7$/group. **(C)** Effect of intra-thalamic YC-1 injection at 10 days post thalamic hemorrhage on the established bilateral mechanical pain. $n = 7$/group. PWMT, paw-withdrawal mechanical threshold.

Inhibition of HIF-1α Prior to ITC Blocked the Up-Regulation of SDF1-CXCR4 Signaling and Activations of Microglia and Astrocytes

To verify whether HIF-1α is directly involved in regulating the expression of SDF1-CXCR4 signaling under CPSP condition, intra-thalamic injection of YC-1 was administered 30 min prior to ITC. Western blot results showed that, similar to CXCR4 antagonism by AMD3100, local inhibition of HIF-1α expression by YC-1 resulted in significant reduction in the expression of both SDF1/CXCR4 (**Figures 8A,B**) and Iba-1/GFAP (**Figures 8A,C**) on day 3 and day 7 post-ITC.

Intra-thalamic injection of $CoCl_2$, a well-known inducer of HIF-1α, was shown to result in elevation of HIF-1α, SDF1 and CXCR4 expressions examined on day 3 and 7 post-injection (**Figures 9A,B**). Pre-blockade of HIF-1α production by YC-1 through intra-thalamic injection prevented the enhancement of HIF-1α, SDF1 and CXCR4 expression, whereas, pre-blockade of CXCR4 with AMD3100 failed to change the enhanced expression of HIF-1α although SDF1 and CXCR4 up-regulation was prevented (**Figures 9A,B**). Similar to the results of ITC, intra-thalamic injection of $CoCl_2$ induced overexpression of Iba-1 and GFAP (**Figures 9A,C**), suggesting activation of both microglia cells and astrocytes by $CoCl_2$. The $CoCl_2$-induced overexpression of SDF1 and CXCR4 and activations of microglia and astrocytes were also blocked by pre-injection of AMD3100 or YC-1, respectively (**Figures 9A–C**).

Similar to the results of ITC, intra-thalamic injection of $CoCl_2$ induced bilateral mechanical pain hypersensitivity that could be blocked by pre-treatment of AMD3100 through intra-thalamic microinjection (**Figure 9D**).

DISCUSSION

The present study demonstrated that ITC-induced CPSP hypersensitivity was initiated by microglial-astrocytic-neuronal

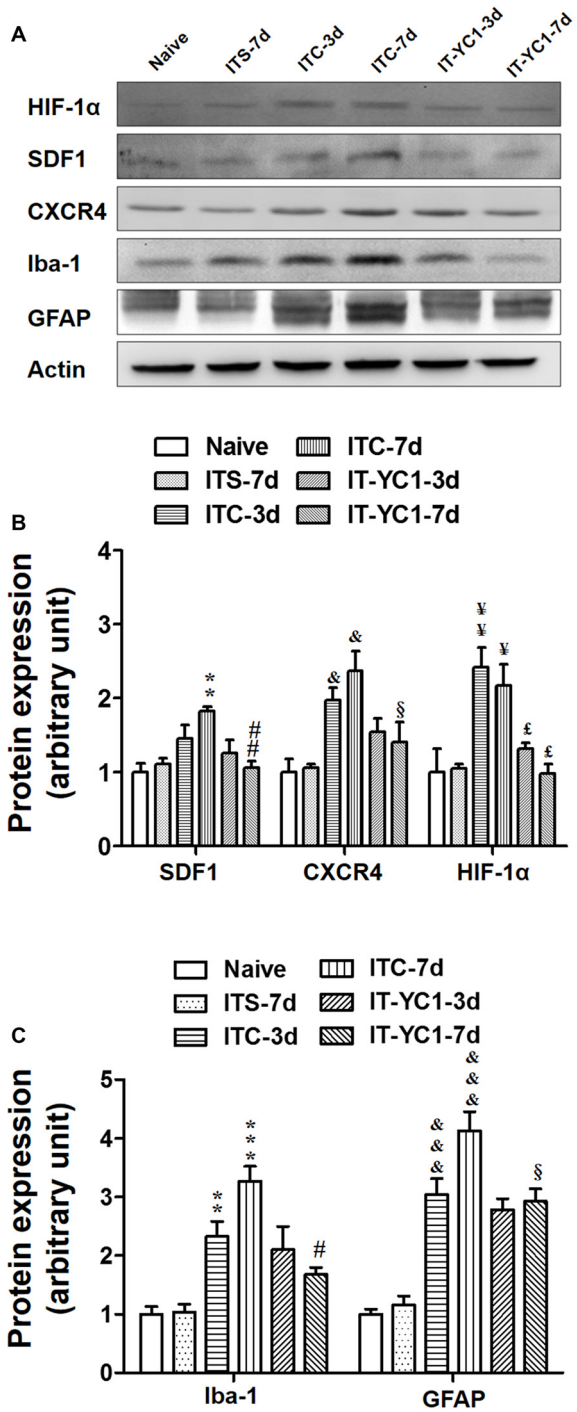

FIGURE 8 | Effects of intra-thalamic pre-injection of YC-1 on the increased SDF1 and CXCR4 expression and glial cells activation induced by ITC. **(A)** Representative bands showing the effect of intra-thalamic pre-injection of YC-1 (0.2 mM, 1 μl) on thalamic hemorrhage-induced HIF-1α, SDF1 and CXCR4 up-regulation as well as on microglial marker Iba-1 and astrocytes marker GFAP up-regulation. **(B)** Quantification of Western blot assay showing that intra-thalamic pre-injection of YC-1 prevented thalamic hemorrhage-induced HIF-1α, SDF1 and CXCR4 up-regulation at 3 and 7 days. $^{\&}P < 0.05$, $^{¥}P < 0.05$, $^{¥¥}P < 0.01$, $^{**}P < 0.01$ vs. ITS-7 d group; (*Continued*)

FIGURE 8 | Continued
$^{£}P < 0.05$, $^{\#\#}P < 0.01$, $^{§}P < 0.05$ vs. ITC at corresponding time points; $n = 5$/group. **(C)** Quantification of Western blot assay showing that intra-thalamic pre-injection of YC-1 prevented thalamic hemorrhage-induced Iba-1 and GFAP up-regulation at 3 and 7 days. $^{**}P < 0.01$, $^{***}P < 0.001$, $^{\&\&\&}P < 0.001$ vs. ITS; $^{\#}P < 0.05$, $^{§}P < 0.05$ vs. ITC at corresponding time points; $n = 5$/group.

interactions in the peri-lesion sites through HIF-1α-dependent up-regulation of SDF1-CXCR4 signaling in microglia, astrocytes and neurons at the early stage, while it was maintained by persistent release of pro-inflammatory mediators (TNFα, IL-1β and IL-6) through SDF1-CXCR4 signaling-mediated glial-glial and glial-neuronal positive feedback regulation at the late stage. The direct involvement of SDF1-CXCR4 signaling in the induction and maintenance of CPSP was confirmed using exogenous SDF1, which was sufficient to induce mechanical pain hypersensitivity after intra-thalamic microinjection. Meanwhile, the involvement of HIF-1α in the induction, but not the maintenance, of CPSP was also confirmed by intra-thalamic YC-1 produced HIF-1α suppression and intra-thalamic $CoCl_2$ produced HIF-1α over-expression. The proposed underlying mechanisms of CPSP that is mediated by microglial-astrocytic-neuronal interactions through HIF-1α-SDF1-CXCR4 signaling mediation is shown in **Figure 10**.

HIF-1α Induces SDF1-CXCR4 Signaling Over-Expression and Development of CPSP

HIF-1α is a key transcription factor for the adaptive responses to hypoxia (Singh et al., 2012). In the present study, we found that the protein level of HIF-1α was significantly increased at the early phase, but not in the late phase, after hemorrhagic stroke induced by ITC. As supporting evidence, Jiang et al. (2002) reported that HIF-1α was significantly up-regulated in the basal ganglia following experimental intracerebral hemorrhage in rats receiving injections of autologous blood, thrombin, or lysed red blood cells. Here, we further found that inhibition of HIF-1α could prevent the development of CPSP but without analgesic effect during the maintenance of CPSP, implicating that up-regulation of the downstream gene expression of HIF-1α is initiated by HIF-1α but maintained by other mechanisms. By utilizing YC-1, the most specific inhibitor available for HIF-1α (Zhang et al., 2014), it was demonstrated that the increased expression of SDF1 and CXCR4 in the peri-thalamic lesion sites was almost completely suppressed. In fact, it has been demonstrated that both SDF1 and CXCR4 promoters contain hypoxia response elements (HREs) which have a HIF-1 DNA binding site (Hitchon et al., 2002; Schioppa et al., 2003; Speth et al., 2014) and blockade of HIF-1α activation can abrogate both hypoxia-induced CXCR4 up-regulation and SDF1-dependent cell migration in microglia *in vitro* (Wang et al., 2008). In the current study, the thalamic hemorrhage-induced microglial and astrocytic activations was prevented by blockade of both HIF-1α and SDF1-CXCR4 signaling, suggesting that HIF-1α plays a critical role in the up-regulation of SDF1-CXCR4 signaling that

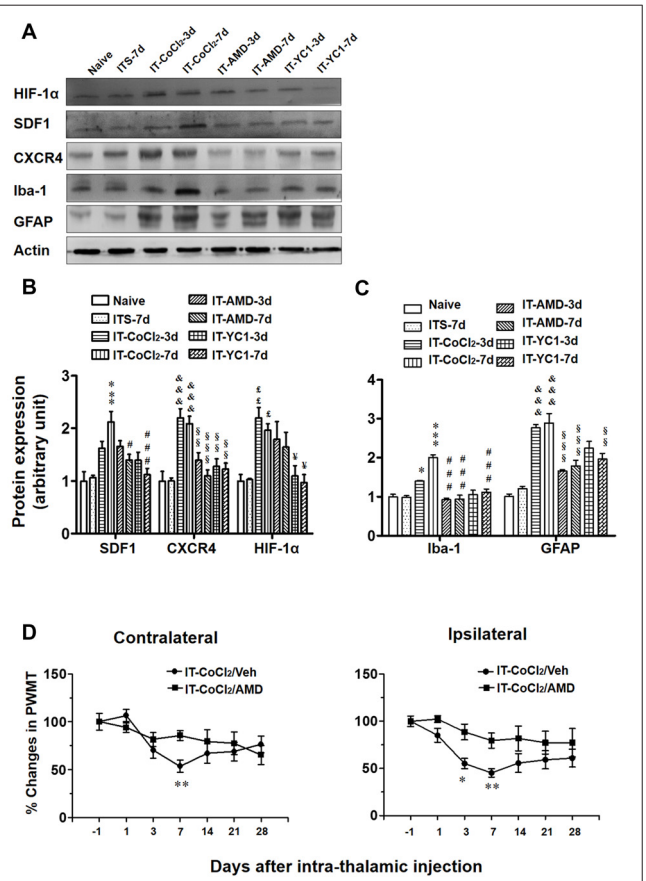

FIGURE 9 | Effects of intra-thalamic injection of $CoCl_2$ on HIF-1α, SDF1 and CXCR4, as well as on microglial marker Iba-1 and astrocytes marker GFAP expression in naïve rats. **(A)** Representative bands showing the effect of intra-thalamic injection of $CoCl_2$ (100 mM, 1 μl) on HIF-1α, SDF1, CXCR4, as well as on Iba-1 and GFAP expression in the thalamic injection sites. **(B)** Quantification of Western blot assay showing that intra-thalamic $CoCl_2$ injection increased HIF-1α, SDF1 and CXCR4 expression, and which were prevented by pre-injection of AMD3100 and YC-1. $^{£}P < 0.05$, $^{ŁŁ}P < 0.01$, $^{\&\&\&}P < 0.001$, $^{***}P < 0.001$ vs. ITS-7 d; $^{§§}P < 0.01$, $^{§§§}P < 0.001$, $^{\#}P < 0.05$, $^{\#\#\#}P < 0.001$, $^{¥}P < 0.05$ vs. IT-$CoCl_2$ at corresponding time points; n = 5/group. **(C)** Quantification of Western blot assay showing that intra-thalamic $CoCl_2$ injection increased Iba-1 and GFAP expression, and which were prevented by pre-injection of AMD3100 and YC-1. $^{*}P < 0.05$, $^{***}P < 0.001$, $^{\&\&\&}P < 0.001$ vs. ITS group; $^{§§}P < 0.01$, $^{§§§}P < 0.001$, $^{\#\#\#}P < 0.001$, vs. IT-$CoCl_2$ at corresponding time points; n = 5/group. **(D)** Intra-thalamic injection of $CoCl_2$ induced bilateral mechanical pain hypersensitivity in naïve rats which were prevented by pre-injection of AMD3100. $^{*}P < 0.05$, $^{**}P < 0.01$, IT-$CoCl_2$/AMD vs. IT-$CoCl_2$/Veh; PWMT, paw-withdrawal mechanical threshold; n = 7/group.

subsequently mediates the glial cell activations at the late stage of thalamic hemorrhage condition. To further verify the role of HIF-1α, we injected $CoCl_2$, a well-known inducer of HIF-1α, into the VPL of normal rats. As expected, the expression of SDF1 and CXCR4 protein was up-regulated by intra-VPL $CoCl_2$ microinjection and which was prevented by pre-inhibition of HIF-1α. Likewise, microglia and astrocytes was also activated by intra-VPL $CoCl_2$ microinjection and the activation could be blocked by pre-treatment with CXCR4 inhibitor, indicating that HIF-1α is essential for the induction of SDF1-CXCR4 signaling-mediated glial cell activations. This result can be supported by a previous report showing that both astrocytes and microglia could be activated by microinjection of $CoCl_2$ into the frontoparietal cortex of rats (Caltana et al., 2009). Most interestingly, our present study provided a new line of experimental evidence demonstrating that intra-thalamic $CoCl_2$ microinjection in normal rats is sufficient to induce transient bilateral mechanical pain hypersensitivity through HIF-1α activation. HIF-1α has also been shown to be involved in the development of peripheral neuropathic pain, demonstrated by HIF-1α gene knockout in primary nociceptive neurons (Kanngiesser et al., 2014). Moreover, inhibiting accumulation of HIF-1α in the sciatic nerve also relieved both spared nerve injury-evoked and chronic constriction injury-induced neuropathic pain (Hsieh et al., 2012). However, none of these two previous studies clearly identified how HIF-1α worked to produce pain. Thus the link between up-regulation of SDF1-CXCR4 signaling by HIF-1α activation and the development of CPSP in the current study would shed new light on the treatment of CPSP in clinic.

SDF1-CXCR4 Signaling Contributes to Maintenance of CPSP through Mediating Microglial-Astrocytic-Neuronal Interactions

To determine the roles of microglia and astrocytes in the maintenance of CPSP, we evaluated the analgesic effect of minocycline, a microglial inhibitor, and fluorocitrate, an astrocytic inhibitor, by intra-thalamic microinjection of these agents, respectively. As expected, both minocycline and fluorocitrate reversed the well-established mechanical pain hypersensitivity induced by ITC-induced hemorrhage, indicating involvement of activated microglial and astrocytic cells in the maintenance of CPSP. This result can be supported by a previous study showing attenuation of thalamic hemorrhage-induced mechanical allodynia following post-treatment with systemic minocycline (Hanada et al., 2014). Also, another line of evidence demonstrated that intra-thalamic microinjection of minocycline was sufficient to reverse sciatic nerve injury-induced thermal hyperalgesia for 30 min (LeBlanc et al., 2011). However, in an animal model of the spinal cord injury-induced mechanical pain hypersensitivity, it was shown that intra-thalamic minocycline microinjection produced anti-hyperalgesic effect for 8 h (Zhao et al., 2007). Herein, our results showed the duration of the analgesic effect of minocycline on CPSP was much longer and lasted at least for 7 days. The discrepancy in duration of analgesia for minocycline might be duo to various reasons such as differences in the time course of microglial cell activation in different pain models, drug delivery route and other unknown mechanisms involved. Unlike the sciatic nerve and spinal cord injury, thalamic hemorrhage was the primary injury in CPSP model and glial activation in the thalamus would be the critical underlying mechanism for CPSP which was the reason for us to adopt intra-thalamic injection in the present study. It has been already shown that the activated glial cells of both microglia and astrocytes can produce and release various types of chemokines and cytokines that not only trigger neuronal hyperexcitability but

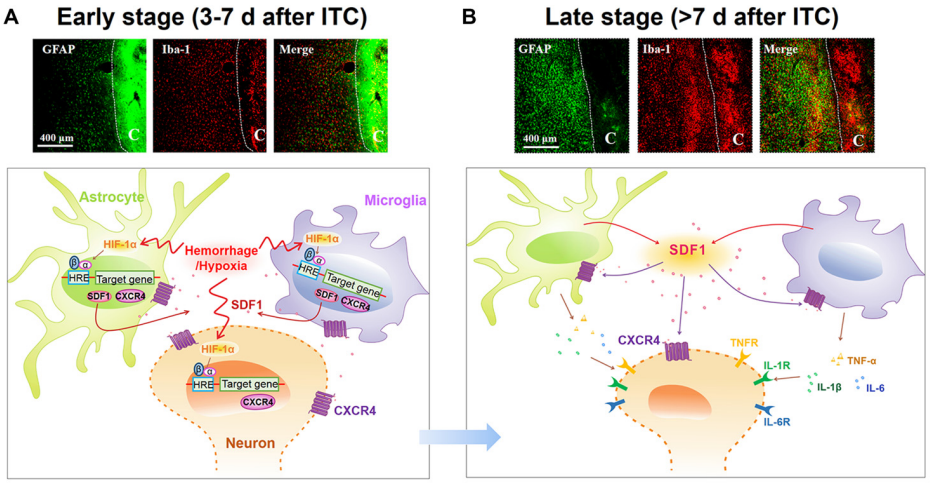

FIGURE 10 | Schematic illustration of microglial-astrocytic-neuronal interactions mediated by HIF-1α-SDF1-CXCR4 signaling following thalamic hemorrhage. **(A)** The upper panel shows representative immunofluorescent photomicrographs of microglial marker Iba-1 (red) and astrocytic marker GFAP (green) expression in thalamic sections at the early stage after hemorrhage (<7 days). The hemorrhagic lesion core is on the right side of the white line in each immunofluorescent image. At this phase, hypoxia microenvironment was established in peri-thalamic lesion site which induced accumulation of HIF-1α in the cytoplasm. As a transcription factor, HIF-1α translocates into the nucleus where it dimerizes with HIF-1β subunit and forms the active HIF-1 complex which binds to the hypoxia response element (HRE) in the DNA sequence and then induces CXCR4 expression in the neurons and glial cells as well as SDF1 expression in glial cells. The synthetic CXCR4 would integrate into cell membrane forming a functional receptor for neuron and glial cells while synthetic SDF1 would be secreted into extracellular space as a ligand (lower panel). Scale bar, 400 μm. **(B)** The upper panel shows representative immunofluorescent photomicrographs of microglial marker Iba-1(red) and astrocytic marker GFAP (green) expression in thalamic sections at the late stage after hemorrhage (>7 days). The hemorrhagic lesion core is on the right side of the white line in each immunofluorescent image. At this phase, abundant SDF1 from astrocytes and microglia activates CXCR4 on glial cells, resulting in the activation of glial cells by a positive feedback activation pattern and subsequent release of proinflammatory cytokines, including TNF-α, IL-1β and IL-6, which could subsequently increase neuronal excitation and glial activation in peri-thalamic lesion site. For the survival neurons in the peri-thalamic lesion site, the released SDF1 from glial cells could bind to CXCR4 and directly evoke neuronal hyperactivity which combined with glial activation contribute to the maintenance of CPSP (lower panel). Scale bar, 400 μm.

also facilitate inter-glial cell activations through positive feedback regulation (Guo et al., 2007; Sheridan and Murphy, 2013; Macht, 2016). Here we further demonstrated that chemokine SDF1 and its cognate receptor CXCR4 were both up-regulated in the peri-thalamic lesion sites after ITC and CXCR4 was localized not only in neurons but also in astrocytes and microglia. In line with previous studies, the temporal pattern of SDF1 up-regulation was similar to the up-regulation of GFAP and Iba1, suggesting that activated microglia and astrocytes are the main SDF1-producing cells in the peri-thalamic lesion sites (Shen et al., 2014; Bai et al., 2016; Yang L. et al., 2016). Based on the cellular localization of CXCR4 in both neurons and glial cells and the abundant production of SDF1 from activated astrocytes and microglia, we propose that through positive feedback regulation, SDF1-CXCR4 signaling would play critical roles in mediating microglial-astrocytic-neuronal interactions, because selectively blocking CXCR4 with intra-thalamic AMD3100 microinjection could: (1) remarkably suppress thalamic hemorrhage-induced microglia and astrocyte activation; (2) significantly inhibit the release of pro-inflammatory mediators such as TNF-α, IL-1β and IL-6 from activated glial cells; and (3) reverse thalamic hemorrhage-induced increase in neuronal activities labeled with c-Fos in the peri-thalamic lesion sites. The persistent release of pro-inflammatory mediators could cause neuronal hyperexcitability and sensitization through binding to their respective receptors (Zhang et al., 2011; Clark et al., 2013; Chirila et al., 2014). As a new line of evidence, we have previously demonstrated that blocking CXCR4 with AMD3100 directly inhibited the hyperexcitability of primary nociceptor neurons under peripheral inflammatory pain state (Yang et al., 2015). Thus, it is conceivable that SDF1-CXCR4 signaling could mediate microglial-astrocytic-neuronal interactions (crosstalk) through two possible mechanisms: (1) glial-neuronal interactions mediated by direct binding of astrocyte/microglia-derived SDF1 with neuronal CXCR4; and (2) positive feedback glial-glial interactions through direct binding of astrocyte- or microglia-derived SDF1 with glial CXCR4 (**Figure 10**). The glial-glial interactions may serve as the source of pro-inflammatory mediators that in turn cause neuronal hyperexcitability and sensitization.

Given the potential role of SDF1-CXCR4 signaling in the glial-glial interactions and glial-neuronal crosstalk, we here demonstrated that pre-treatment with CXCR4 inhibitor AMD3100 could prevent the development of CPSP accompanying with the reduction of neuroinflammation which was essential for CPSP. To further confirm whether SDF1-CXCR4 signaling participates in the CPSP process, we injected exogenous SDF1 into VPL of naïve rats. As expected, single intra-thalamic SDF1 injection was sufficient to induce bilateral mechanical pain hypersensitivity through CXCR4 agonism. In addition, the SDF1-induced pain hypersensitivity was prevented by inhibiting microglial and astrocytic activation. It was interesting to note that both the analgesic effect of intra-thalamic AMD3100 and hyperalgesic

effect of intra-thalamic SDF1 remained for a relative longer duration after administration although AMD3100 and SDF1 themselves have a short-term half-life (Hendrix et al., 2004; Kirkpatrick et al., 2010). Why? One possibility is that SDF1-CXCR4 signaling serves as a priming signal to mediate a positive feedback between glial-glial interactions under CPSP state. Once being activated, the downstream inflammatory cascades (TNF-α, IL-1β and IL-6) would be recruited to promote the local persistent neuroinflammation in the lesioned thalamus (**Figure 10**). This was supported by a previous study showing that intra-thalamic injection of CCL21 induced significant microglia activation and pain hypersensitivity which lasted longer than its own half-life and intra-thalamic injection of minocycline could also suppress CCL21-induced changes (Zhao et al., 2007). Moreover, here we also showed that post-treatment with AMD3100 could reverse the established CPSP in a dose-related manner. Taken all the existing data into account, we conclude that SDF1-CXCR4 signaling-mediated glial-glial/glial-neuronal communications are required for the development and maintenance of CPSP. Since it has been demonstrated that treatment with P2X7 receptor antagonist and IL-1β antibody could also reduce thalamic hemorrhage-induced microglia aggregation, neuronal excitability and allodynia phenomena in CPSP rats (Kuan et al., 2015), a common upstream regulation by HIF-1α-SDF1-CXCR4 signaling might be shared.

Because the analgesic effect of intra-thalamic injection of lidocaine on the thalamic hemorrhage-induced tactile hypersensitivity is short-lasting (Gritsch et al., 2016), the use of AMD3100 (also named as plerixafor) to treat CPSP would be more promising. Its safety and efficacy was approved by the U.S. Food and Drug Administration in 2008 for the mobilization of hematopoietic stem cells (Hummel et al., 2014). Moreover, several other CXCR4 antagonists are currently in clinical trials for cancer, HIV and WHIM syndrome treatment, highly supporting its potential use for the treatment of CPSP in clinic (Debnath et al., 2013). Since intraperitoneal delivery of AMD3100 has been demonstrated to be effective in suppression of pain (Dubovy et al., 2010; Xie et al., 2016), SDF1-CXCR4 signaling pathway as a new therapeutic target for the treatment of CPSP might be promising.

AUTHOR CONTRIBUTIONS

JC and FeiY conceived and designed the experiments. FanY, W-JL, WS, YW, C-LL and NW performed the experiments, FeiY and JC analyzed and interpreted the data. J-LW, FanY and X-LW supplied SPF animals. JC, S-MG and FeiY wrote the article. All authors listed, have made substantial, direct and intellectual contribution to the work, and approved it for publication.

FUNDING

The funders had no role in study design, data collection and analysis, decision to publish, or preparation of the manuscript.

ACKNOWLEDGMENTS

This work was supported by National Basic Research Development Program of China (2013CB835100), the National Natural Science Foundation of China (81171049, 81571072, 31300919, 31400948) and the National Key Technology R&D Program (2013BAI04B04).

REFERENCES

Bai, L., Wang, X., Li, Z., Kong, C., Zhao, Y., Qian, J. L., et al. (2016). Upregulation of chemokine CXCL12 in the dorsal root ganglia and spinal cord contributes to the development and maintenance of neuropathic pain following spared nerve injury in rats. *Neurosci. Bull.* 32, 27–40. doi: 10.1007/s12264-015-0007-4

Bhangoo, S. K., Ren, D., Miller, R. J., Chan, D. M., Ripsch, M. S., Weiss, C., et al. (2007). CXCR4 chemokine receptor signaling mediates pain hypersensitivity in association with antiretroviral toxic neuropathy. *Brain Behav. Immun.* 21, 581–591. doi: 10.1016/j.bbi.2006.12.003

Bhangoo, S., Ren, D., Miller, R. J., Henry, K. J., Lineswala, J., Hamdouchi, C., et al. (2007). Delayed functional expression of neuronal chemokine receptors following focal nerve demyelination in the rat: a mechanism for the development of chronic sensitization of peripheral nociceptors. *Mol. Pain* 3:38. doi: 10.1186/1744-8069-3-38

Bhangoo, S. K., Ripsch, M. S., Buchanan, D. J., Miller, R. J., and White, F. A. (2009). Increased chemokine signaling in a model of HIV1-associated peripheral neuropathy. *Mol. Pain* 5:48. doi: 10.1186/1744-8069-5-48

Caltana, L., Merelli, A., Lazarowski, A., and Brusco, A. (2009). Neuronal and glial alterations due to focal cortical hypoxia induced by direct cobalt chloride (CoCl2) brain injection. *Neurotox. Res.* 15, 348–358. doi: 10.1007/s12640-009-9038-9

Chirila, A. M., Brown, T. E., Bishop, R. A., Bellono, N. W., Pucci, F. G., and Kauer, J. A. (2014). Long-term potentiation of glycinergic synapses triggered by interleukin 1beta. *Proc. Natl. Acad. Sci. U S A* 111, 8263–8268. doi: 10.1073/pnas.1401013111

Choi, H. S., Roh, D. H., Yoon, S. Y., Moon, J. Y., Choi, S. R., Kwon, S. G., et al. (2015). Microglial interleukin-1beta in the ipsilateral dorsal horn inhibits the development of mirror-image contralateral mechanical allodynia through astrocyte activation in a rat model of inflammatory pain. *Pain* 156, 1046–1059. doi: 10.1097/j.pain.0000000000000148

Chung, C. S., Caplan, L. R., Han, W., Pessin, M. S., Lee, K. H., and Kim, J. M. (1996). Thalamic haemorrhage. *Brain* 119, 1873–1886. doi: 10.1093/brain/119.6.1873

Clark, A. K., Old, E. A., and Malcangio, M. (2013). Neuropathic pain and cytokines: current perspectives. *J. Pain Res.* 6, 803–814. doi: 10.2147/JPR.S53660

Debnath, B., Xu, S., Grande, F., Garofalo, A., and Neamati, N. (2013). Small molecule inhibitors of CXCR4. *Theranostics* 3, 47–75. doi: 10.7150/thno.5376

De Vloo, P., Morlion, B., van Loon, J., and Nuttin, B. (2017). Animal models for central poststroke pain: a critical comprehensive review. *Pain* 158, 17–29. doi: 10.1097/j.pain.0000000000000722

Dubovy, P., Klusakova, I., Svizenska, I., and Brazda, V. (2010). Spatio-temporal changes of SDF1 and its CXCR4 receptor in the dorsal root ganglia following unilateral sciatic nerve injury as a model of neuropathic pain. *Histochem. Cell Biol.* 133, 323–337. doi: 10.1007/s00418-010-0675-0

Feigin, V. L., Forouzanfar, M. H., Krishnamurthi, R., Mensah, G. A., Connor, M., Bennett, D. A., et al. (2014). Global and regional burden of stroke during 1990–2010: findings from the Global Burden of Disease Study 2010. *Lancet* 383, 245–254. doi: 10.1016/s0140-6736(13)61953-4

Ferro, J. M., Caeiro, L., and Figueira, M. L. (2016). Neuropsychiatric sequelae of stroke. *Nat. Rev. Neurol.* 12, 269–280. doi: 10.1038/nrneurol.2016.46

Gritsch, S., Bali, K. K., Kuner, R., and Vardeh, D. (2016). Functional characterization of a mouse model for central post-stroke pain. *Mol. Pain* 12:1744806916629049. doi: 10.1177/1744806916629049

Guo, W., Wang, H., Watanabe, M., Shimizu, K., Zou, S., LaGraize, S. C., et al. (2007). Glial-cytokine-neuronal interactions underlying the mechanisms of persistent pain. *J. Neurosci.* 27, 6006–6018. doi: 10.1523/jneurosci.0176-07.2007

Hanada, T., Kurihara, T., Tokudome, M., Tokimura, H., Arita, K., and Miyata, A. (2014). Development and pharmacological verification of a new mouse model of central post-stroke pain. *Neurosci. Res.* 78, 72–80. doi: 10.1016/j.neures.2013.09.005

Hang, L.-H., Li, S.-N., Luo, H., Shu, W.-W., Mao, Z.-M., Chen, Y.-F., et al. (2016). Connexin 43 mediates CXCL12 production from spinal dorsal horn to maintain bone cancer pain in rats. *Neurochem. Res.* 41, 1200–1208. doi: 10.1007/s11064-015-1815-7

Hendrix, C. W., Collier, A. C., Lederman, M. M., Schols, D., Pollard, R. B., Brown, S., et al. (2004). Safety, pharmacokinetics, and antiviral activity of AMD3100, a selective CXCR4 receptor inhibitor, in HIV-1 infection. *J. Acquir. Immune Defic. Syndr.* 37, 1253–1262. doi: 10.1097/01.qai.0000137371.80695.ef

Hitchon, C., Wong, K., Ma, G., Reed, J., Lyttle, D., and El-Gabalawy, H. (2002). Hypoxia-induced production of stromal cell-derived factor 1 (CXCL12) and vascular endothelial growth factor by synovial fibroblasts. *Arthritis Rheum* 46, 2587–2597. doi: 10.1002/art.10520

Hosomi, K., Seymour, B., and Saitoh, Y. (2015). Modulating the pain network—neurostimulation for central poststroke pain. *Nat. Rev. Neurol.* 11, 290–299. doi: 10.1038/nrneurol.2015.58

Hsieh, Y. L., Chou, L. W., Chang, P. L., Yang, C. C., Kao, M. J., and Hong, C. Z. (2012). Low-level laser therapy alleviates neuropathic pain and promotes function recovery in rats with chronic constriction injury: possible involvements in hypoxia-inducible factor 1alpha (HIF-1alpha). *J. Comp. Neurol.* 520, 2903–2916. doi: 10.1002/cne.23072

Hu, X. M., Liu, Y. N., Zhang, H. L., Cao, S. B., Zhang, T., Chen, L. P., et al. (2015). CXCL12/CXCR4 chemokine signaling in spinal glia induces pain hypersensitivity through MAPKs-mediated neuroinflammation in bone cancer rats. *J. Neurochem.* 132, 452–463. doi: 10.1111/jnc.12985

Huang, X., Li, Y., Li, J., Feng, Y., and Xu, X. (2014). Tanshinone IIA dampens the cell proliferation induced by ischemic insult in rat astrocytes via blocking the activation of HIF-1alpha/SDF-1 signaling. *Life Sci.* 112, 59–67. doi: 10.1016/j.lfs.2014.07.020

Huang, J., Li, Y., Tang, Y., Tang, G., Yang, G. Y., and Wang, Y. (2013). CXCR4 antagonist AMD3100 protects blood-brain barrier integrity and reduces inflammatory response after focal ischemia in mice. *Stroke* 44, 190–197. doi: 10.1161/STROKEAHA.112.670299

Hummel, S., Van Aken, H., and Zarbock, A. (2014). Inhibitors of CXC chemokine receptor type 4: putative therapeutic approaches in inflammatory diseases. *Curr. Opin. Hematol.* 21, 29–36. doi: 10.1097/MOH.0000000000000002

Jiang, Y., Wu, J., Keep, R. F., Hua, Y., Hoff, J. T., and Xi, G. (2002). Hypoxia-inducible factor-1α accumulation in the brain after experimental intracerebral hemorrhage. *J. Cereb. Blood Flow Metab.* 22, 689–696. doi: 10.1097/00004647-200206000-00007

Kanngiesser, M., Mair, N., Lim, H. Y., Zschiebsch, K., Blees, J., Häussler, A., et al. (2014). Hypoxia-inducible factor 1 regulates heat and cold pain sensitivity and persistence. *Antioxid. Redox Signal.* 20, 2555–2571. doi: 10.1089/ars.2013.5494

Kirkpatrick, B., Nguyen, L., Kondrikova, G., Herberg, S., and Hill, W. D. (2010). Stability of human stromal-derived factor-1α (CXCL12α) after blood sampling. *Ann. Clin. Lab. Sci.* 40, 257–260.

Knerlich-Lukoschus, F., von der Ropp-Brenner, B., Lucius, R., Mehdorn, H. M., and Held-Feindt, J. (2011). Spatiotemporal CCR1, CCL3(MIP-1α), CXCR4, CXCL12(SDF-1α) expression patterns in a rat spinal cord injury model of posttraumatic neuropathic pain. *J. Neurosurg. Spine* 14, 583–597. doi: 10.3171/2010.12.SPINE10480

Kuan, Y. H., Shih, H. C., Tang, S. C., Jeng, J. S., and Shyu, B. C. (2015). Targeting P(2)X(7) receptor for the treatment of central post-stroke pain in a rodent model. *Neurobiol. Dis.* 78, 134–145. doi: 10.1016/j.nbd.2015.02.028

LeBlanc, B. W., Zerah, M. L., Kadasi, L. M., Chai, N., and Saab, C. Y. (2011). Minocycline injection in the ventral posterolateral thalamus reverses microglial reactivity and thermal hyperalgesia secondary to sciatic neuropathy. *Neurosci. Lett.* 498, 138–142. doi: 10.1016/j.neulet.2011.04.077

Li, X. Q., Zhang, Z. L., Tan, W. F., Sun, X. J., and Ma, H. (2016). Down-regulation of CXCL12/CXCR4 expression alleviates ischemia-reperfusion-induced inflammatory pain via inhibiting glial TLR4 activation in the spinal cord. *PLoS One* 11:e0163807. doi: 10.1371/journal.pone.0163807

Liu, H., Xue, W., Ge, G., Luo, X., Li, Y., Xiang, H., et al. (2010). Hypoxic preconditioning advances CXCR4 and CXCR7 expression by activating HIF-1alpha in MSCs. *Biochem. Biophys. Res. Commun.* 401, 509–515. doi: 10.1016/j.bbrc.2010.09.076

Luo, X., Tai, W. L., Sun, L., Pan, Z., Xia, Z., Chung, S. K., et al. (2016). Crosstalk between astrocytic CXCL12 and microglial CXCR4 contributes to the development of neuropathic pain. *Mol. Pain* 12:1744806916636385. doi: 10.1177/1744806916636385

Luo, X., Tai, W. L., Sun, L., Qiu, Q., Xia, Z., Chung, S. K., et al. (2014). Central administration of C-X-C chemokine receptor type 4 antagonist alleviates the development and maintenance of peripheral neuropathic pain in mice. *PLoS One* 9:e104860. doi: 10.1371/journal.pone.0104860

Macht, V. A. (2016). Neuro-immune interactions across development: a look at glutamate in the prefrontal cortex. *Neurosci. Biobehav. Rev.* 71, 267–280. doi: 10.1016/j.neubiorev.2016.08.039

Menichella, D. M., Abdelhak, B., Ren, D., Shum, A., Frietag, C., and Miller, R. J. (2014). CXCR4 chemokine receptor signaling mediates pain in diabetic neuropathy. *Mol. Pain* 10:42. doi: 10.1186/1744-8069-10-42

Nasreddine, Z. S., and Saver, J. L. (1997). Pain after thalamic stroke: right diencephalic predominance and clinical features in 180 patients. *Neurology* 48, 1196–1199. doi: 10.1212/WNL.48.5.1196

Oh, S. B., Tran, P. B., Gillard, S. E., Hurley, R. W., Hammond, D. L., and Miller, R. J. (2001). Chemokines and glycoprotein120 produce pain hypersensitivity by directly exciting primary nociceptive neurons. *J. Neurosci.* 21, 5027–5035.

Paxinos, G., and Watson, C. (2005). *The Rat Brain in Stereotaxic Coordinates*, 5th Edn., Amsterdam: Elsevier Academic Press.

Reaux-Le Goazigo, A., Rivat, C., Kitabgi, P., Pohl, M., and Melik Parsadaniantz, S. (2012). Cellular and subcellular localization of CXCL12 and CXCR4 in rat nociceptive structures: physiological relevance. *Eur. J. Neurosci.* 36, 2619–2631. doi: 10.1111/j.1460-9568.2012.08179.x

Réaux-Le Goazigo, A., Van Steenwinckel, J., Rostène, W., and Mélik Parsadaniantz, S. (2013). Current status of chemokines in the adult CNS. *Prog. Neurobiol.* 104, 67–92. doi: 10.1016/j.pneurobio.2013.02.001

Ruscher, K., Kuric, E., Liu, Y., Walter, H. L., Issazadeh-Navikas, S., Englund, E., et al. (2013). Inhibition of CXCL12 signaling attenuates the postischemic immune response and improves functional recovery after stroke. *J. Cereb. Blood Flow Metab.* 33, 1225–1234. doi: 10.1038/jcbfm.2013.71

Schioppa, T., Uranchimeg, B., Saccani, A., Biswas, S. K., Doni, A., Rapisarda, A., et al. (2003). Regulation of the chemokine receptor CXCR4 by hypoxia. *J. Exp. Med.* 198, 1391–1402. doi: 10.1084/jem.20030267

Shen, W., Hu, X. M., Liu, Y. N., Han, Y., Chen, L. P., Wang, C. C., et al. (2014). CXCL12 in astrocytes contributes to bone cancer pain through CXCR4-mediated neuronal sensitization and glial activation in rat spinal cord. *J. Neuroinflammation* 11:75. doi: 10.1186/1742-2094-11-75

Sheridan, G. K., and Murphy, K. J. (2013). Neuron-glia crosstalk in health and disease: fractalkine and CX3CR1 take centre stage. *Open Biol.* 3:130181. doi: 10.1098/rsob.130181

Singh, N., Sharma, G., and Mishra, V. (2012). Hypoxia inducible factor-1: its potential role in cerebral ischemia. *Cell. Mol. Neurobiol.* 32, 491–507. doi: 10.1007/s10571-012-9803-9

Speth, J. M., Hoggatt, J., Singh, P., and Pelus, L. M. (2014). Pharmacologic increase in HIF1alpha enhances hematopoietic stem and progenitor homing and engraftment. *Blood* 123, 203–207. doi: 10.1182/blood-2013-07-516336

Trecki, J., and Unterwald, E. M. (2009). Modulation of cocaine-induced activity by intracerebral administration of CXCL12. *Neuroscience* 161, 13–22. doi: 10.1016/j.neuroscience.2009.03.027

Walter, H. L., van der Maten, G., Antunes, A. R., Wieloch, T., and Ruscher, K. (2015). Treatment with AMD3100 attenuates the microglial response and improves outcome after experimental stroke. *J. Neuroinflammation* 12:24. doi: 10.1186/s12974-014-0232-1

Wang, X., Li, C., Chen, Y., Hao, Y., Zhou, W., Chen, C., et al. (2008). Hypoxia enhances CXCR4 expression favoring microglia migration via HIF-1alpha activation. *Biochem. Biophys. Res. Commun.* 371, 283–288. doi: 10.1016/j.bbrc.2008.04.055

Wasserman, J. K., and Koeberle, P. D. (2009). Development and characterization of a hemorrhagic rat model of central post-stroke pain. *Neuroscience* 161, 173–183. doi: 10.1016/j.neuroscience.2009.03.042

Wilson, N. M., Jung, H., Ripsch, M. S., Miller, R. J., and White, F. A. (2011). CXCR4 signaling mediates morphine-induced tactile hyperalgesia. *Brain Behav. Immun.* 25, 565–573. doi: 10.1016/j.bbi.2010.12.014

Xie, F., Wang, Y., Li, X., Chao, Y. C., and Yue, Y. (2016). Early repeated administration of CXCR4 antagonist AMD3100 dose-dependently improves neuropathic pain in rats after L5 spinal nerve ligation. *Neurochem. Res.* 41, 2289–2299. doi: 10.1007/s11064-016-1943-8

Yang, F., Fu, H., Lu, Y. F., Wang, X. L., Yang, Y., Yang, F., et al. (2014). Post-stroke pain hypersensitivity induced by experimental thalamic hemorrhage in rats is region-specific and demonstrates limited efficacy of gabapentin. *Neurosci. Bull.* 30, 887–902. doi: 10.1007/s12264-014-1477-5

Yang, F., Sun, W., Luo, W. J., Yang, Y., Yang, F., Wang, X. L., et al. (2017). SDF1-CXCR4 signaling contributes to the transition from acute to chronic pain state. *Mol. Neurobiol.* 54, 2763–2775. doi: 10.1007/s12035-016-9875-5

Yang, F., Sun, W., Yang, Y., Wang, Y., Li, C. L., Fu, H., et al. (2015). SDF1-CXCR4 signaling contributes to persistent pain and hypersensitivity via regulating excitability of primary nociceptive neurons: involvement of ERK-dependent Nav1.8 up-regulation. *J. Neuroinflammation* 12:219. doi: 10.1186/s12974-015-0441-2

Yang, L., Wang, M., Guo, Y. Y., Sun, T., Li, Y. J., Yang, Q., et al. (2016). Systemic inflammation induces anxiety disorder through CXCL12/CXCR4 pathway. *Brain Behav. Immun.* 56, 352–362. doi: 10.1016/j.bbi.2016.03.001

Yang, Y., Yang, F., Yang, F., Li, C. L., Wang, Y., Li, Z., et al. (2016). Gabapentinoid insensitivity after repeated administration is associated with down-regulation of the alpha$_2$delta-1 subunit in rats with central post-stroke pain hypersensitivity. *Neurosci. Bull.* 32, 41–50. doi: 10.1007/s12264-015-0008-3

Youn, S. W., Lee, S. W., Lee, J., Jeong, H. K., Suh, J. W., Yoon, C. H., et al. (2011). COMP-Ang1 stimulates HIF-1alpha-mediated SDF-1 overexpression and recovers ischemic injury through BM-derived progenitor cell recruitment. *Blood* 117, 4376–4386. doi: 10.1182/blood-2010-07-295964

Zhang, L., Berta, T., Xu, Z. Z., Liu, T., Park, J. Y., and Ji, R. R. (2011). TNF-alpha contributes to spinal cord synaptic plasticity and inflammatory pain: distinct role of TNF receptor subtypes 1 and 2. *Pain* 152, 419–427. doi: 10.1016/j.pain.2010.11.014

Zhang, Z., Yan, J., Taheri, S., Liu, K. J., and Shi, H. (2014). Hypoxia-inducible factor 1 contributes to N-acetylcysteine's protection in stroke. *Free Radic. Biol. Med.* 68, 8–21. doi: 10.1016/j.freeradbiomed.2013.11.007

Zhao, P., Waxman, S. G., and Hains, B. C. (2007). Modulation of thalamic nociceptive processing after spinal cord injury through remote activation of thalamic microglia by cysteine cysteine chemokine ligand 21. *J. Neurosci.* 27, 8893–8902. doi: 10.1523/JNEUROSCI.2209-07.2007

Conflict of Interest Statement: The authors declare that the research was conducted in the absence of any commercial or financial relationships that could be construed as a potential conflict of interest.

frontiers in Molecular Neuroscience

ORIGINAL RESEARCH
published: 11 April 2017
doi: 10.3389/fnmol.2017.00106

EGF Enhances Oligodendrogenesis from Glial Progenitor Cells

Junlin Yang[1], Xuejun Cheng[1], Jiajun Qi[1], Binghua Xie[1], Xiaofeng Zhao[1], Kang Zheng[1], Zunyi Zhang[1] and Mengsheng Qiu[1,2]**

[1]*The Institute of Developmental and Regenerative Biology, Zhejiang Key Laboratory of Organ Development and Regeneration, College of Life and Environment Sciences, Hangzhou Normal University, Hangzhou, China,* [2]*Department of Anatomical Sciences and Neurobiology, University of Louisville, Louisville, KY, USA*

Emerging evidence indicates that epidermal growth factor (EGF) signaling plays a positive role in myelin development and repair, but little is known about its biological effects on the early generation and differentiation of oligodendrocyte (OL) lineage cells. In this study, we investigated the role of EGF in early OL development with isolated glial restricted precursor (GRP) cells. It was found that EGF collaborated with Platelet Derived Growth Factor-AA (PDGFaa) to promote the survival and self-renewal of GRP cells, but predisposed GRP cells to develop into $O4^-$ early-stage oligodendrocyte precursor cells (OPCs) in the absence of or PDGFaa. In OPCs, EGF synergized with PDGFaa to maintain their O4 negative antigenic phenotype. Upon PDGFaa withdrawal, EGF promoted the terminal differentiation of OPCs by reducing apoptosis and increasing the number of mature OLs. Together, these data revealed that EGF is an important mitogen to enhance oligodendroglial development.

Keywords: GRP cell, OPC, oligodendrocyte lineage, self-renewal, synergistic effect

OPEN ACCESS

Edited by:
Shumin Duan,
Zhejiang University, China

Reviewed by:
Amit Agarwal,
Johns Hopkins University, USA
David Peter Gavin,
Jesse Brown VA Medical Center, USA
Frank Kirchhoff,
Saarland University, Germany

****Correspondence:***
Junlin Yang
yjl8121@yahoo.com
Mengsheng Qiu
m0qiu001@yahoo.com

Received: *20 December 2016*
Accepted: *28 March 2017*
Published: *11 April 2017*

Citation:
Yang J, Cheng X, Qi J, Xie B, Zhao X, Zheng K, Zhang Z and Qiu M (2017) EGF Enhances Oligodendrogenesis from Glial Progenitor Cells. Front. Mol. Neurosci. 10:106. doi: 10.3389/fnmol.2017.00106

INTRODUCTION

Oligodendrocytes (OLs) elaborate insulating myelin sheaths that wrap around axons to ensure the rapid conduction of nerve impulses and axonal survival (Qiu, 2013; Zhang et al., 2013; Blank and Prinz, 2014; Alizadeh et al., 2015; Rao and Pearse, 2016). Tripotential glial-restricted precursor (GRP) cells were initially found in embryonic spinal tissues (Herrera et al., 2001; Gregori et al., 2002; Wu et al., 2002; Cao et al., 2005; Phillips et al., 2012), as they can generate OLs and type I and type II astrocytes *in vitro* (Rao et al., 1998; Gregori et al., 2002; Yang et al., 2016) and *in vivo* (Herrera et al., 2001; Hill et al., 2004). The germination of GRP cells from neuroepithelial stem cells was viewed as the beginning of OL generation (Rao et al., 1998; Gregori et al., 2002). Tripotential GRP cells then generate bipotential oligodendrocyte precursor cells (OPCs) which are capable of differentiating into either OLs or type II astrocytes (Morath and Mayer-Pröschel, 2001; Gregori et al., 2002). OPCs proliferate and migrate throughout the CNS during late mouse embryonic development, and later differentiate into mature myelinating OLs (Fernandez et al., 2004; Cai et al., 2010; Chen et al., 2015).

Emerging evidence suggests that epidermal growth factor (EGF) signaling plays an important role in oligodendroglial development (Aguirre et al., 2007; Chong et al., 2008; Hu et al., 2010).

Abbreviations: bFGF, Basic fibroblast growth factor; EGF, Epidermal growth factor; EGFR, Epidermal growth factor receptor; GRP, Glial restricted precursor; OL, Oligodendrocyte; OPC, Oligodendrocyte precursor cells; PDGFaa, Platelet derived growth factor-AA.

Loss-of-function of epidermal growth factor receptor (EGFR) reduced oligodendrogenesis *in vivo* (Aguirre et al., 2007); conversely, intraventricular infusion of EGF induced subventricular zone (SVZ) type B cells to migrate and differentiate into OLs (Gonzalez-Perez et al., 2009). More recently, it was shown that intranasal EGF treatment immediately after brain injury promoted oligodendrogenesis and remyelination (Scafidi et al., 2014). Although the importance of EGF signaling in the development of OL lineage has been established, it remains elusive at what stage of oligodendrogenesis EGF starts to function and how it regulates the development of OL lineage progression.

In this study, we used mouse GRP cells as the starting point to systematically investigate the role of EGF signaling in OL lineage development. It was found that cells of OL lineage were responsive to EGF at all developmental stages. In GRP cells, EGF promoted their proliferation and survival by augmenting their responsiveness to Platelet Derived Growth Factor-AA (PDGFaa) for self-renewal. In the absence of PDGFaa, EGF predisposed GRP cells to differentiate into $O4^-$ early-stage OPCs. At OPC stage, EGF collaborated with PDGFaa to enhance OPC self-renewal. Upon PDGFaa withdrawal, OPCs underwent terminal differentiation and EGF functioned to reduce apoptosis and increase the number of mature OLs.

MATERIALS AND METHODS

Isolation and Culture of GRP Cells

GRP cells were isolated from E13.5 C57BL/6 mouse spinal cord by A2B5 immunopanning as described elsewhere (Gregori et al., 2002), all experimental procedures were carried out in accordance with institutional guidelines for the care and use of laboratory animals, and the protocol was approved by the Animal Ethics Committee of Hangzhou Normal University, China. $A2B5^+$ cells were then grown in glial basal medium (DMEM/F12, 1 × N2, 1 × B27, 1 × P/S, and 0.1% w/v BSA, all from Gibco) supplemented with 10 ng/ml PDGFaa and EGF (Peprotech) on fibronectin/laminin coated 12-well plates at 2000 cells/well for mass culture experiments or on coated 24-well plated at 1000 cells/well for immunofluorescence staining. The immunostaining was performed 3 days after seeding using the standard protocols.

Clonal Analysis and Sub-Cloning of GRP Cells

Immunopurified $A2B5^+$ cells from E13.5 spinal tissues were adjusted to a cell density of 10 cells/ml with glial basal medium supplemented with 10 ng/ml EGF and PDGFaa, then the cell suspension was added into fibronectin/laminin-coated 96-well plates at 100 μl/well, and wells with a single cell were marked for further culture. When primary clones were generated, 10 clones were randomly selected and only one was found to be A2B5 negative. Of the nine $A2B5^+$ clones, three were subjected to differentiation potential analysis as indicated in the "Results" Section. The other six $A2B5^+$ clones were used for sub-cloning analysis. Each clone was replated on three separate grid dishes at equal clonal density, and cultured in presence of EGF, PDGFaa or both. After 6 days, the numbers of secondary clones were scored.

Cell Proliferation and Apoptosis Analysis

For cell proliferation and apoptosis analysis, 1×10^4 cells were plated to each fibronectin/laminin-coated 24-well plates. Cell proliferation was analyzed by adding BrdU (Sigma) to a final concentration of 30 ng/ml. Following 24 h of incorporation, cells were fixed in 4% paraformaldehyde at RT for 10 min, and BrdU positive cells were detected by anti-BrdU immunostaining. For apoptosis assays, cells were fixed in 4% paraformaldehyde 3 days after replating and apoptotic cells were detected by TUNEL FITC Apoptosis Detection Kit (Vazyme Biotech). Positive cells were counted from three different areas of each well under fluorescence microscopy. The results were expressed as mean values and standard deviation.

GRP Cell Development

The function of EGF on the development of GRP cells into OPCs was confirmed by single-cell tracking clonal differentiation analysis as described previously (Gregori et al., 2002). Freshly immunopurified GRP cells from E13.5 spinal tissues were adjusted to a cell density of 10 cells/ml with glial basal medium supplemented, then the cell suspension was added into fibronectin/laminin-coated 48-well plates at 100 μl/well in the presence of EGF and PDGFaa (10 ng/ml) for 24 h before being exposed to the factors as indicated in the "Results" Section wells with a single cell were marked for further culture. Since there is no specific immunological marker to distinguish GRP cells from OPCs, one candidate marker for distinguishing them is the O4 monoclonal antibody, which labels late-stage OPCs and OLs (Gard and Pfeiffer, 1990; Bansal et al., 1992). Therefore, the proportion of $O4^+$ cells was used as a standard to estimate the differentiation of GRP cells.

OPC Culture

$O4^-$ early-stage OPCs were induced from GRP cells and plated on the fibronectin/laminin-coated plates and fed every other day with glial basal medium supplemented with EGF and PDGFaa. Because of the presence of contact inhibition, OPCs were plated more sparsely than GRP cells, and passaged more frequently. OPCs were plated at 1500 cells/cm^2 for mass culture, and 750 cells/cm^2 for differentiation experiments due to process growth.

Western Immunoblotting

Western blotting was carried out as previously described (Yang et al., 2009). Briefly, cells were lysed in sample buffer plus a cocktail of protease inhibitors (Roche). For each sample, 20 μg of protein was used for electrophoresis in SDS-PAGE gel. Primary antibodies were used as follows; anti-rabbit PDGFRα (1:1000, Santa Cruz), anti- rabbit EGFR (1:200, Abcam), anti-rabbit Olig2 (1:1000, Millipore), anti-rabbit Nestin (1:5000, Covance) and anti-mouse MBP (1:1000, Abcam). Horseradish peroxidase (HRP)-conjugated secondary antibody (Promaga) was used at 1:2500. Chemiluminescent signals were detected by

autoradiography using the ECL System (Amersham, Piscataway, NJ, USA).

Immunocytochemical Analysis

Immunocytochemical analysis was carried out as previously described (Cheng et al., 2017). Antibodies used include anti-mouse A2B5 IgM, anti-BrdU IgM, O4 IgM (1:1 dilution in DPBS + 10% goat serum), anti-mouse Olig2 (1:1000, Millipore), anti-mouse MBP (1:500, Abcam), anti- rabbit EGFR (1:200, Abcam), anti-mouse GFAP (1:300, Chemicon), anti-rabbit Nestin (1:2000, Covance), and anti-rabbit neurofilament (1:100, Sigma). The Alexa-488 or Alexa-594 conjugated secondary antibodies were obtained from Molecular Probes (Thermo fisher). The nucleic acid dye 4′,6-diamidino-2-phenylindole (DAPI) was obtained from Roche.

Statistical Analysis

All quantitative data are presented as means ± SD. Statistical significance of the difference was evaluated by Student's *t*-test. *P*-value < 0.05 was considered statistically significant.

RESULTS

EGF Enhances the Survival and Extensive Self-Renewal of GRP Cells in Culture

To investigate the role of EGF on OL lineage development, we first immunopurified A2B5$^+$ cells from E13.5 spinal cord tissues (Liu et al., 2002). These A2B5$^+$ cells expressed typical GRP markers including PDGFRα (Rao et al., 1998), Olig2 (Zhao et al., 2009) and Nestin (Yoo and Wrathall, 2007; **Figures 1A–D,I–Q**), but not neuronal marker neurofilament (Tang et al., 2007; Rao and Pearse, 2016) and astrocyte marker GFAP (Sun et al., 2008; Sántha et al., 2016). The GRP cells were also immunoreactive for EGFR (**Figures 1E–H,Q**) suggesting their potential EGF-responsiveness. The effects of EGF on A2B5$^+$ cell proliferation were investigated in culture exposed to different concentrations of EGF (0, 2.5, 5, 10, 20 and 40 ng/ml) for 24 h. BrdU labeling revealed a dose-dependent effect on cell division at the concentration range of 0–10 ng/ml (**Figure 2A**). However, no statistical differences were found in the percentage of BrdU$^+$ cells among the 10, 20 and 40 ng/ml EGF groups (**Figure 2A**), indicating that cell proliferation plateaued at 10 ng/ml. When we grew A2B5$^+$ cells for 7 days, EGF was found to promote the cell proliferation and survival as effectively as basic fibroblast growth factor (bFGF), but the percentages of BrdU$^+$ cells on d3 and d7 in EGF groups were higher than those of bFGF groups (**Figures 2B,C**). When GRP cells were treated with EGF and Erlotinib HCl (an antagonist of EGFR) simultaneously, the biological effects of EGF on promoting the division and survival was neutralized (**Figures 2B,C**), and the antigenic phenotypes were similar to those of the control (**Figure 4B**). T3 did not significantly enhance the proliferation of A2B5$^+$ cells compared to control group (**Figure 2B**), but it significantly reduced cell apoptosis (**Figure 2C**), probably by promoting A2B5$^+$ cell differentiation into OLs (**Figures 3D,E**).

EGF also cooperated with PDGFaa to promote a vibrant proliferation of A2B5$^+$ cells as bFGF + PDGFaa did (**Figures 2B,C**). As a result, EGF + PDGFaa stimulated A2B5$^+$ cells to divide continuously and form clones (**Figures 2B**, **3A**). Three randomly chosen primary clones (EGF + PDGFaa treatment) were digested into single cells with trypsin and replated for antigen phenotyping and differentiation potential analysis. All clones from the freshly immunopurified A2B5$^+$ cells expressed the same antigens as described above. Cells grown in the presence of cholinergic neurotrophic factor (CNTF) and bFGF mainly yielded A2B5$^+$/GFAP$^+$ type II astrocytes, but A2B5$^-$/GFAP$^+$ type I astrocytes in the presence of FBS (**Figures 3B,C**). When exposed to thyroid hormone T3 (Rodríguez-Peña, 1999) for 5 days, all clones gave rise to MBP$^+$ mature OLs with multiple interconnecting processes (**Figures 3D,E**; Shaw et al., 1981). No neurofilament$^+$ neurons were generated in these cultures. Thus, these A2B5$^+$ cells are the bona fide tripotential glial progenitor cells (GRP cells), with the potential to generate OLs and two distinct types of astrocytes (Gregori et al., 2002; Dadsetan et al., 2009; Haas et al., 2012).

Recloning experiments showed EGF and PDGFaa have a synergistic effect on the extensive self-renewal of GRP cells. After primary clones were amplified in EGF + PDGFaa for 10 days, randomly selected clones were digested into single cells and evenly plated at clonal density on three separate grid dishes, and then cultured in the presence of EGF, PDGFaa, or both. EGF and PDGFaa treatment yielded an average of 21 and 6 secondary clones, respectively. When these two factors were added together, the number of secondary clones reached an average of 51, far greater than the sum of individual factors (**Figure 2D**), suggesting that EGF synergized with PDGFaa in stimulating the clonal expansion of GRP cells. Secondary clones exhibited an identical pattern of antigen expressions to primary clones and can differentiate into MBP$^+$ OLs, A2B5$^+$ or A2B5$^-$ astrocytes under corresponding environmental cues. Based on these observations, it is concluded that EGF signaling participated in the survival and extensive self-renewal of GRP cells.

EGF Promoted the Generation of Early-Stage OPCs from GRP Clones

Tripotential GRP cells are capable of developing into bipotential OPCs under appropriate signals (Gregori et al., 2002). To investigate how EGF signaling influences this transition process, we grew freshly immunopurified GRP cells at clonal density on 48-well plates for 5 days in the presence or absence of EGF, and then analyzed the formation of OPCs from a single GRP cell by tracking clonal differentiation (**Figure 4A**) as described previously (Gregori et al., 2002). Since common GRP markers such as A2B5, Olig2, PDGFRα and Nestin were also positive for OPCs (Crang et al., 2004; Yang et al., 2016), only O4 monoclonal antibody can be used to define a secondary stage of OPC development (Sommer and Schachner, 1981; Chen et al., 2007; Dincman et al., 2012). In EGF group, 10.7% ± 1.3% of the clones generated O4$^+$/MBP$^-$ cells (**Figures 4A,B**). While in the control group, GRP cells were unable to divide to form clones due to the lack of growth factors, so only a few single

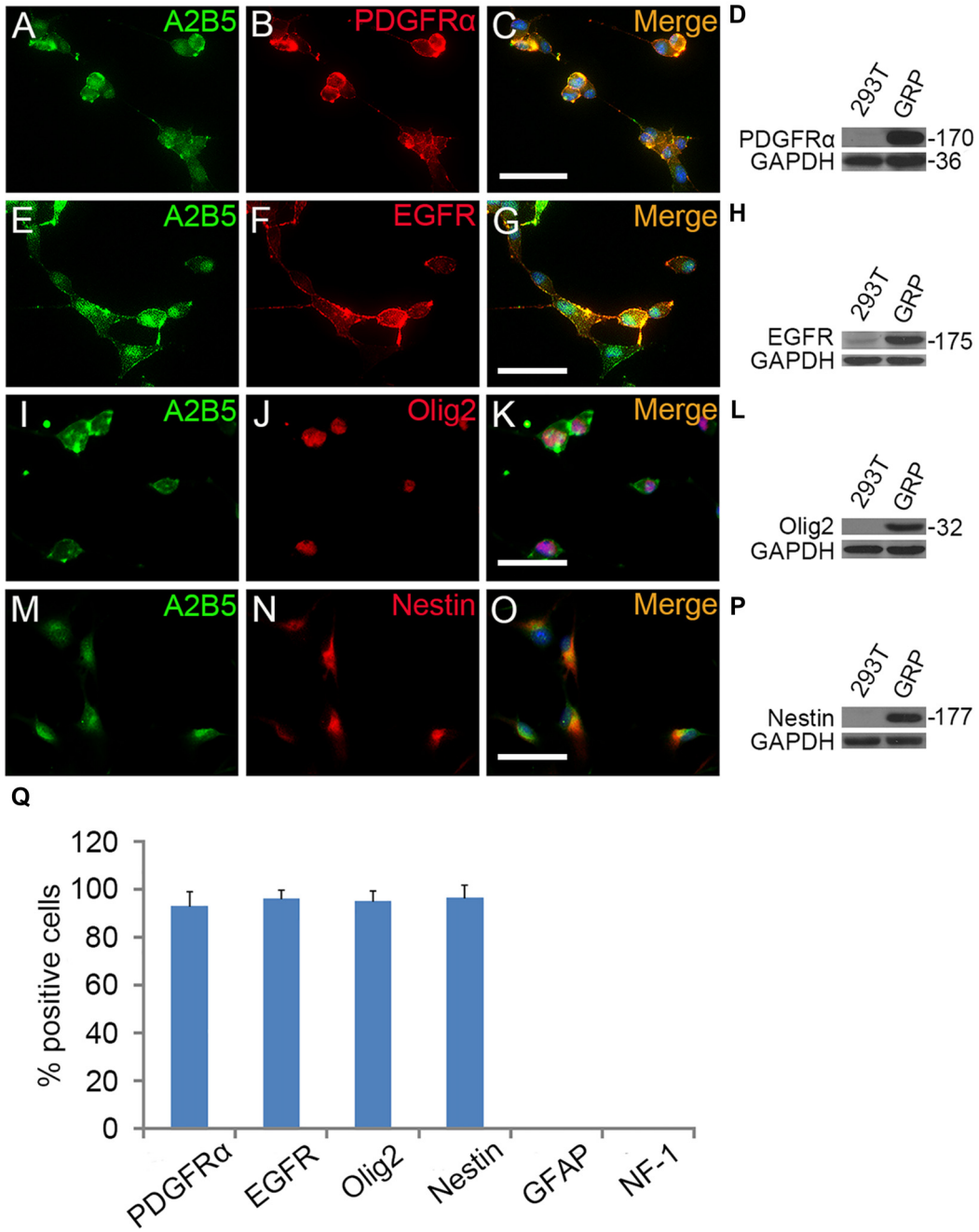

FIGURE 1 | The antigenic phenotypes of E13.5 spinal cord derived A2B5$^+$ cells. (A–P) Immunostaining of A2B5$^+$ cells with PDGFRα, epidermal growth factor receptor (EGFR), Olig2 and Nestin antibodies, respectively, and the antigenic phenotypes were confirmed by Western blotting **(D,H,L,P)**. **(Q)** Quantification of PDGFRα$^+$, EGFR$^+$, Olig2$^+$, Nestin$^+$, GFAP$^+$ and NF-1$^+$ cells in A2B5$^+$ cell cultures, $n = 3$. Scale bars: 50 μm.

O4$^+$/MBP$^-$ cells (1.3% + 0.3%) were observed (**Figure 4B**). The specificity of EGF signaling in promoting oligodendrogenesis was confirmed with Erlotinib HCl. When GRP cells were treated with EGF and Erlotinib HCl simultaneously, the antigenic phenotypes were similar to those of the controls (**Figure 4B**). Based on these results, we postulated that EGF plays a modest role in promoting the development of GRP cells into OPCs. However, it is plausible that a considerable number of clones have differentiated into O4$^-$ early-stage OPCs that could not be detected immunologically. To examine this possibility, we continued to culture these single GRP cell derived clones in glial basal medium for another 5 days in the absence of EGF. In the control group, only 1.5% ± 0.2% of the cells were MBP$^+$ (**Figure 4D**), similar to the percentage of O4$^+$ clones prior to the

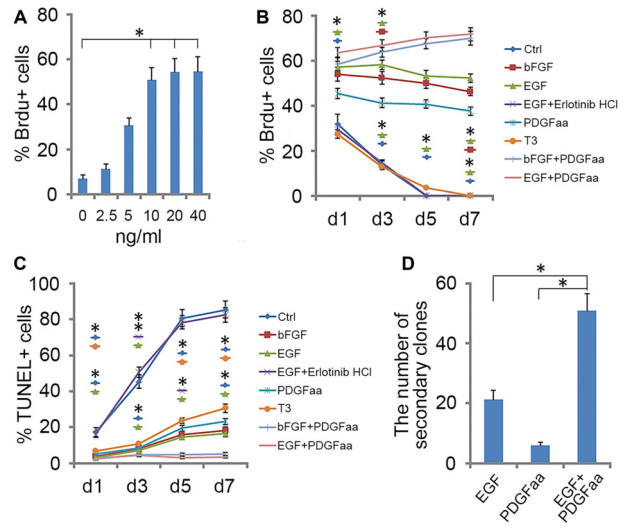

FIGURE 2 | Effect of EGF on A2B5$^+$ cells. (A) Histogram of the number of BrdU$^+$ cells found in A2B5$^+$ cell cultures after exposure to different doses of EGF. *Indicates differences between groups 10, 20 and 40 ng/ml EGF vs. the low-dose groups, $P < 0.05$. No differences were found among the groups of 10, 20 and 40 ng/ml. $n = 3$. **(B,C)** Quantification of BrdU$^+$ and TUNEL$^+$ cells in A2B5$^+$ cell cultures after EGF, EGF + Erlotinib-HCl, basic fibroblast growth factor (bFGF), PDGFaa, T3, bFGF + PDGFaa and EGF + PDGFaa treatments for various time lengths, Ctrl refers to the groups without any supplemented factor, $n = 3$. **(D)** Histogram of the number of secondary clones in A2B5$^+$ cell cultures at clonal density after exposure to EGF, PDGFaa and EGF + PDGFaa, respectively. $n = 3$. Statistical analyses are presented as mean ± SD. *$P < 0.05$, **$P < 0.01$.

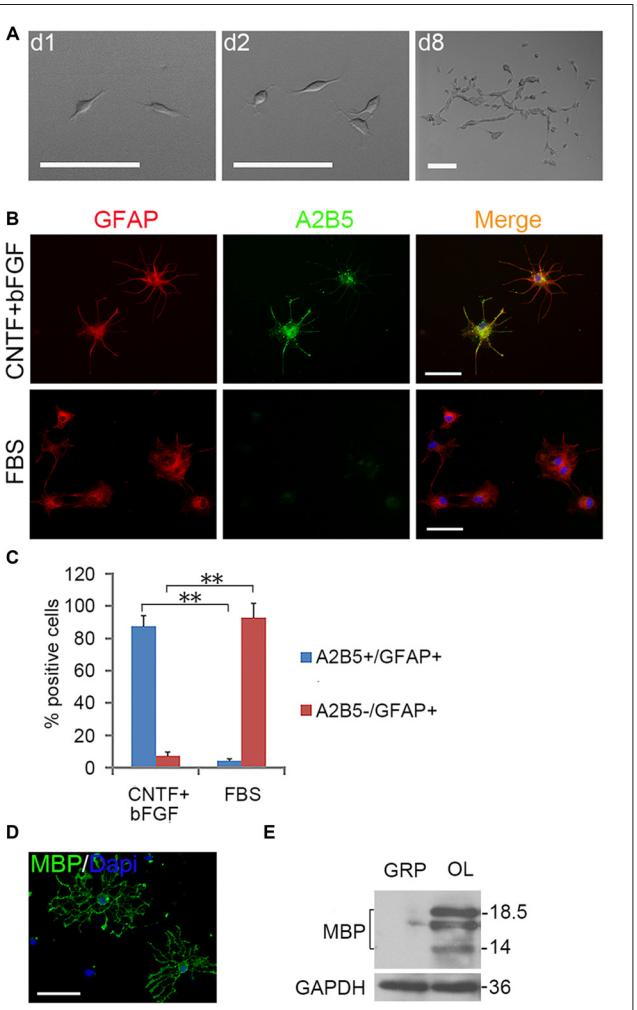

FIGURE 3 | Expanded clones of A2B5$^+$ cell expressed typical differentiation phenotype of tripotential glial restricted precursor (GRP) cells. (A) An example of an expanded clone in presence of EGF + PDGFaa. **(B)** A2B5$^+$ clones were digested and replated into separate wells of 24-well plates and induced to differentiate for 5 days in the presence of bFGF + CNTF or FBS, A2B5$^+$/GFAP$^+$ and A2B5$^-$/GFAP$^+$ astrocytes were obtained, respectively. **(C)** Quantification of A2B5$^+$/GFAP$^+$ and A2B5$^-$/GFAP$^+$ astrocytes in the differentiation cultures exposed to bFGF + CNTF and FBS, $n = 3$. **(D)** A2B5$^+$ cells were cultured in T3 for 5 days and MBP$^+$ Oligodendrocytes (OLs) can be detected. **(E)** The culture described in **(D)** was confirmed by western blotting with MBP antibody. Abbreviation: OL, oligodendrocyte. **$P < 0.01$. Scale bars: **(A)** 100 μm; **(B,D)** 50 μm.

5-day culture (**Figure 4B**). In the EGF group, 32.4% ± 2.7% of the clones generated MBP$^+$ cells (**Figures 4C,D**), suggesting that about 21.4% (32.4% MBP$^+$–10.7% O4$^+$MBP$^-$) of the clones in EGF group generated O4$^-$ OPCs. Thus, EGF predisposed GRP cells to develop along OPCs.

However, EGF treatment alone was less efficient in fully transforming GRP cells into OPCs and maintaining their O4 negative antigen phenotype. We found that GRP cells exposed to a combination of EGF + PDGFaa + T3 exhibited a significant change from fibroblast morphology to bipolar or tripolar morphology, and remained O4 negative antigen phenotype. Moreover, the vast majority of clones (89.1% ± 3.7%) generated O4$^+$/MBP$^+$ OLs after growth factor withdrawal. This conjecture was further strengthened by their differentiation into A2B5$^+$/GFAP$^+$ instead of A2B5$^-$/GFAP$^+$ astrocytes upon FBS treatment (**Figure 4E**), a bipotential differentiation characteristic of OPCs (Sommer and Schachner, 1981; Barnett et al., 1993).

EGF Enhances the Self-Renewal of OPCs

PDGFaa is an important mitogen for the self-renewal of OPCs (Noble et al., 1988; Raff et al., 1988; Hart et al., 1989; Neman and de Vellis, 2012), but it alone cannot maintain the O4 negative antigenic phenotype in OPCs. When GRP-derived early-stage O4$^-$ OPCs from EGF + PDGFaa + T3 treatment were cultured in PDGFaa alone for 5 days, most cells became O4 positive (88.7% ± 5.9%; **Figure 5A**) but MBP negative with few processes.

These O4$^+$ late-stage OPCs (Sommer and Schachner, 1981; Gard and Pfeiffer, 1990) continued to cycle (**Figures 5A,C**). When EGF was present, the majority of cells maintained bipolar or tripolar morphology, and the rate of O4$^+$ cells decreased substantially (7.4% ± 2.6%) with a significant increase of BrdU$^+$ cells (80% ± 3.8%; **Figures 5A,B**). Moreover, these expanded cultures of OPCs maintained by EGF + PDGFaa can differentiate into either mature OLs or A2B5$^+$/GFAP$^+$ astrocytes under specific culture conditions, indicating the differentiation potential was not compromised by proliferation, nor did they revert to GRP cells. Therefore, EGF have a synergistic effect

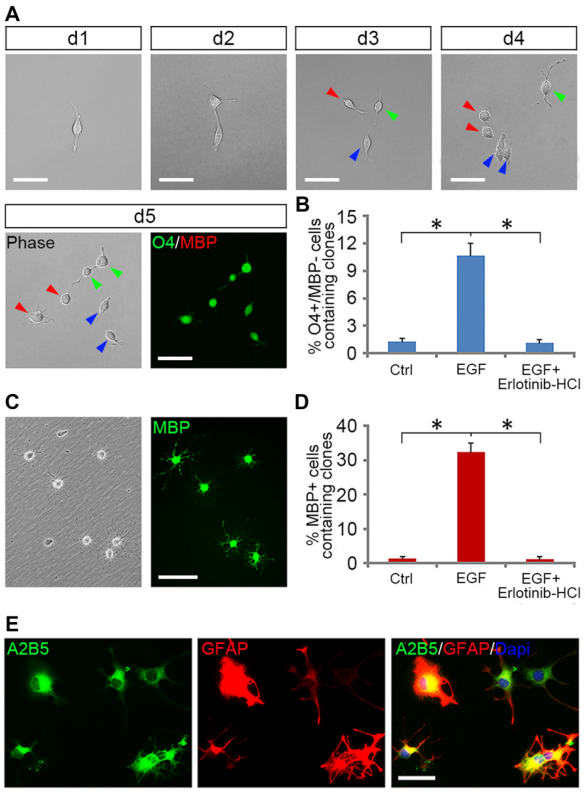

FIGURE 4 | EGF enhanced the formation of OPCs from GRP clones. **(A)** The single cell tracking of a GRP cell generating O4$^+$/MBP$^-$ daughter cells in EGF for 5 days. With the progression of cell division, a fibroblast-like GRP cell was gradually converted to typical OPCs of bipolar or tripolar morphology, well separated from each other, and expressed O4 antigen but not MBP. Daughter cells of the same progenitor were indicated by arrows of different color. **(B)** Quantification of the clones containing O4$^+$/MBP$^-$ cells in the GRP cell cultures exposed to various combinations of factors for 5 days, respectively, $n = 3$. **(C)** OPC-like cells from **(B)** differentiated into MBP$^+$ cells after 5 days of culture in glial basal medium without supplemented factors. Left: phase image; right: anti-MBP immunostaining. **(D)** Quantification of the clones containing MBP$^+$ cells in OL differentiation cultures described in **(C)**, $n = 3$. **(E)** OPCs derived from EGF + PDGFaa + T3 treament differentiated into A2B5$^+$/GFAP$^+$ astrocytes in presence of FBS. $^*P < 0.05$. Scale bars: **(A,C)** 75 μm; (**E**) 50 μm.

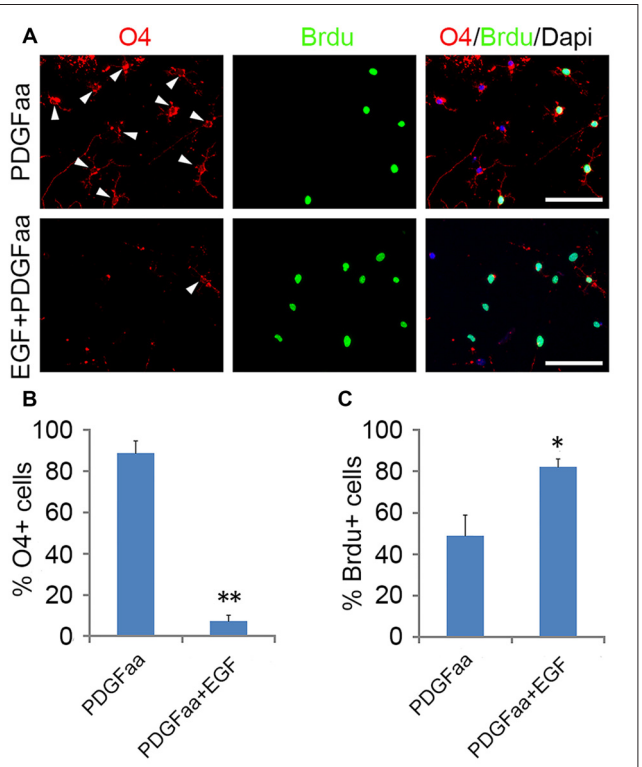

FIGURE 5 | Synergistic effect of PDGFaa and EGF in promoting the self-renewal of O4$^-$ OPCs. **(A)** Representative images of O4$^+$ and/or BrdU$^+$ cells cultured in PDGFaa or PDGFaa + EGF for 5 days, cell proliferation was analyzed by BrdU incorporation for 24 h before fixation. **(B)** Quantification of O4$^+$ cells in PDGFaa and PDGFaa + EGF cultures. **(C)** Quantification of BrdU$^+$ cells in PDGFaa and PDGFaa + EGF cultures. Statistical analyses are presented as mean ± SD, $n = 3$. $^*P < 0.05$, $^{**}P < 0.01$, Scale bars: 100 μm.

with PDGFaa in the self-renewal of O4$^-$ OPCs. And this cooperative effect of EGF and PDGFaa can be further amplified by other growth factor such as bFGF. When GRP-derived early-stage O4$^-$ OPCs were cultured in EGF + PDGFaa + bFGF *in vitro*, a faster cell division (87.3% ± 4.1%) and less O4$^+$ cells (2.6% ± 0.9%) were observed without compromising their differentiation characteristics, suggesting that the proliferation and self-renewal of OPCs are regulated by multiple signaling pathways.

EGF Treatment Increased the Number of Differentiated OLs

When GRP-derived O4$^-$ OPCs were cultured in EGF alone, cells were initially active in proliferation, and many more BrdU-positive cells were found in EGF group than in control group. However, the percentage of BrdU$^+$ cells in EGF group decreased with time, and by day 4, less than 3% of cells were proliferative (**Figure 6A**). Consistent with this, the EGFR expression was reduced more than half by day 4 (**Figures 6D,E**), which may partly contribute to the reduced effect of EGF on cell proliferation. It was found that bFGF cannot substitute for the loss of EGFR (data not shown), and the promotion of OPC proliferation by EGF or bFGF were based on the existence of PDGFaa. The reduced cell proliferation was accompanied by the increased proportion of MBP$^+$ cells in culture (**Figure 6B**). Although the rate of OPC differentiation under EGF treatment was slightly lower than that of control and T3 groups at the beginning, it increased rapidly on day 3 and exceeded the other two groups (**Figure 6B**), suggesting that EGF has a significant effect in promoting OL maturation when PDGFaa is not present. A synergistic effect was observed when T3 and EGF was combined, the differentiation was faster and the efficiency was higher than that of T3 alone or EGF alone (**Figure 6B**). TUNEL labeling experiments revealed that the rate of apoptosis with EGF treatment was significantly lower than that of the other two groups (**Figure 6C**). This raised the possibility that EGF treatment may partly increase the number of mature OLs indirectly by promoting their post-mitotic survival.

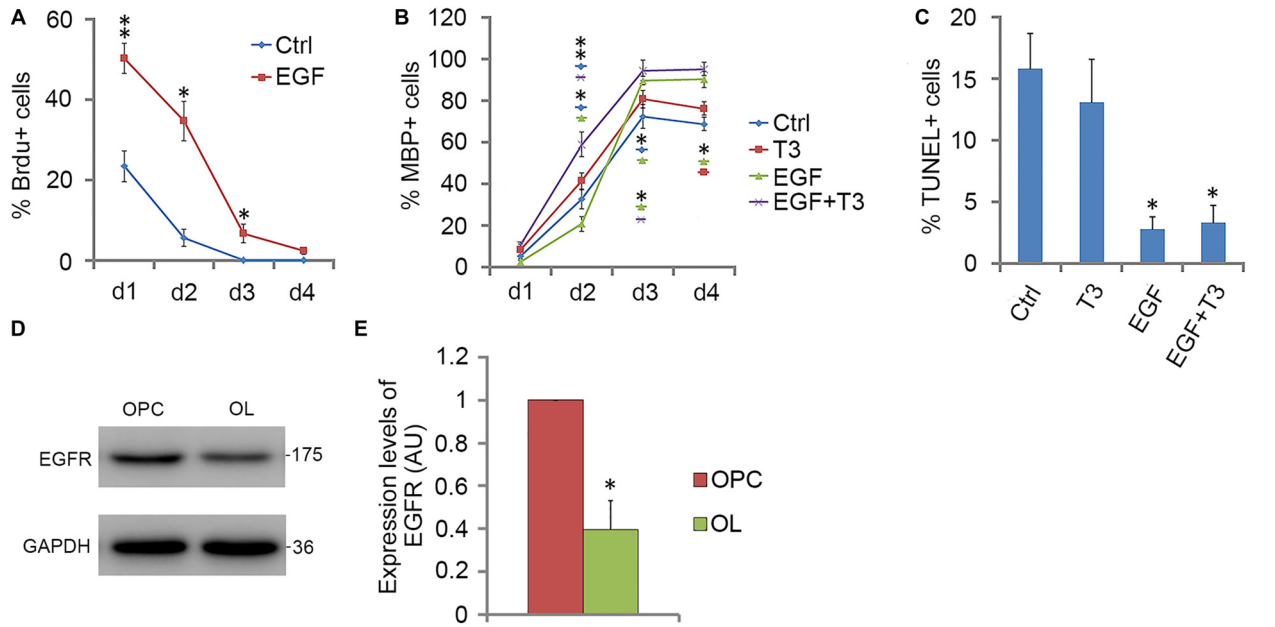

FIGURE 6 | EGF promotes OPC differentiation in cooperation with T3. (A) Quantification of BrdU$^+$ cells for OPCs cultures with EGF or not for various time lengths. **(B)** Quantification of MBP$^+$ cells in OPCs differentiation cultures treated with T3, EGF or T3 + EGF for various time lengths. **(C)** Quantification of TUNEL$^+$ cells in OPCs differentiation cultures on day 4. **(D,E)** Western blotting and quantitative analysis of EGFR protein expression in O4$^-$ OPCs and MBP$^+$ OLs, histograms express results in arbitrary units, taking GRP cells values as 100%. Statistical analyses are presented as mean ± SD, $n = 3$. $^*P < 0.05$, $^{**}P < 0.01$.

DISCUSSION

EGF is an extracellular signal molecule that binds to its specific receptor (EGFR) on the target cell membrane and then stimulates the phosphorylation of the receptor. The EGFR, also known as erbB1, is a glycoprotein that belongs to the related proteins family of c-erbB, there are three other members of this family: erbB2, erbB3 and erbB4 (Galvez-Contreras et al., 2013). The EGFR can generate homodimerization or heterodimerization with all ErbB family members, therefore, activated EGFR can stimulate a large number of downstream signaling molecules, and the complexity of its signal transduction determines the diversity of its biological effects. The diversity of EGF biological effects is reflected in the progression of OL lineage, as it plays distinct roles at different stages of OL development (**Figure 7**). The biological diversity of EGF signaling could be achieved by changing the balance between different signaling pathways (Tzahar et al., 1996).

Role of EGF Signaling in GRP Development

GRP cells are probably the earliest progenitor cells for OL and astrocyte lineages (Rao et al., 1998; Gregori et al., 2002). GRP cells exhibited strong responsiveness to EGF for cell survival and proliferation in chemically defined medium. This result suggests that EGF signaling may be involved in the origin and expansion of GRP cells. Consistent with this idea, EGFR overexpression in postnatal white matter led to diffuse hyperplasia of progenitor cells that possess the same antigen phenotype as GRP cells *in vitro* (Ivkovic et al., 2008).

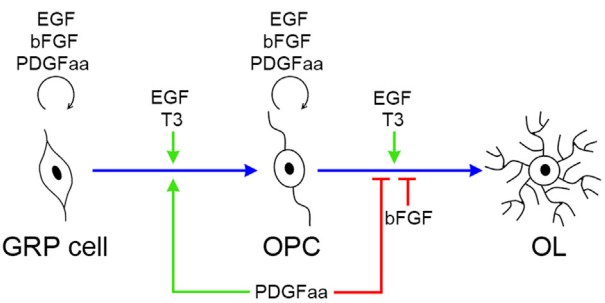

FIGURE 7 | Biological effects of EGF, PDGFaa, bFGF and T3 in the progression of OL lineage. EGF has multiple biological effects on oligodendrogenesis, and its functional output is influenced by other signal molecules, such as PDGFaa and T3. In GRP cells, EGF and bFGF collaborate with PDGFaa to promote the self-renewal of GRP cells. When EGF is present alone, it favors the development of GRP cells to OPCs, and this progress is accelerated by supplementing PDGFaa and T3 simultaneously. In OPCs, EGF and bFGF enhance their responsiveness to PDGFaa and thus maintains their O4 negative phenotype as well as bipolar or tripolar cell morphology. When EGF is present alone, it synergizes with T3 to promote the terminal differentiation of OPCs, whereas bFGF and PDGFaa inhibit this differentiation process.

Moreover, following lysolecithin (LPC)-induced demyelination, a significantly higher number of GRP cells was observed in EGFR-overexpressing transgenic mice than that of the wild-type, leading to faster and more extensive remyelination, and more rapid functional recovery. Conversely, reduced EGFR signaling

in vivo decreased the generation of OLs in postnatal brains (Aguirre et al., 2007).

EGF has a variety of biological effects on GRP cells, including cell survival and proliferation, and enhanced OL lineage progression. However, its eventual functional output is influenced by other signal molecules. For instance, PDGFaa and EGF work synergistically to maintain the self-renewal, the rate of cell proliferation decreased substantially after PDGFaa withdrawal, and GRP cells progressed into OPCs. The number of secondary clones in EGF group was much lower than that of PDGFaa + EGF group, probably due to the higher differentiation rate in the EGF group, and thus the reduced ability of GRP cells to form clones.

Role of EGF Signaling in OPC Lineage Development

OPCs retained strong responsiveness to EGF, and EGF enhanced the response of early-stage OPCs to PDGFaa in their self-renewal. In the absence of EGF, PDGFaa alone was difficult to prevent OPCs from expressing O4 antigen, and the cells then entered the secondary stage of OPC development with reduced proliferative capacity. The mechanisms underlying this enhanced response is not clear, one possibility is that it may function to maintain a high level of PDGFRα expression or signaling in OPCs (McKinnon et al., 1990). Thus, EGF may "set" a PDGF-driven clock in OPCs by establishing their sensitivity to PDGFaa (Galvez-Contreras et al., 2013). In this way, EGF may enlarge the OPC pool during CNS development.

The biological effect of EGF in promoting oligodendrogenesis was also reflected in the maturation of OPCs into OLs. EGF alone could not maintain the self-renewal of OPCs; instead it appeared to promote the differentiation of OPCs and the survival of mature OLs (**Figure 6**), leading to an increased number of MBP^+ mature OLs.

Comparison of EGF and bFGF Effects in Oligodendroglial Lineage Development

bFGF was commonly used in GRP cell culture, and it alone was sufficient to maintain the self-renewal of GRP cells *in vitro* (Gregori et al., 2002). Similarly, bFGF was also widely used in OPC culture to suppress OPC differentiation and myelin gene expression (McKinnon et al., 1990; Bansal and Pfeiffer, 1997; Decker et al., 2000; Jiang et al., 2001). Thus, it seems that bFGF promotes progenitor maintenance by preventing the lineage progression of both GRP and OPC cells.

The present study has demonstrated that EGF is also effective in the maintenance of GRP and OPC culture. However, EGF appears to enhance the self-renewal of GRPs and OPCs by enhancing their responses to PDGFRα instead of directly inhibiting their differentiation. As a matter of fact, EGF treatment alone promotes the differentiation of both GRP cells and OPCs in culture. In the absence of PDGFaa and bFGF, EGF enhances GRP lineage progression to OPCs and OPC differentiation to mature OLs in synergy with T3 (**Figure 7**). Therefore, EGF and bFGF possess unique and distinct roles in oligodendroglial progenitor self-renewal and differentiation. Consistent with this notion, $bFGF^{-/-}$ knockout leads to a higher proportion of mature OLs (Murtie et al., 2005), whereas EGFR mutation reduces the number of mature OLs (Aguirre et al., 2007).

AUTHOR CONTRIBUTIONS

JY designed, performed experiments, collected, analyzed the data and wrote the manuscript; XC, BX, XZ and KZ performed experiments; ZZ analyzed data; MQ designed, supervised the experiments, collected, analyzed and discussed data and wrote the manuscript. All authors listed, have made substantial, direct and intellectual contribution to the work, and approved it for publication.

ACKNOWLEDGMENTS

This work is supported by the National Key Basic Research Program of China (Ministry of Science and Technology of the People's Republic of China; 2013CB531303, 2012CB910402), National Natural Science Foundation of China (81200961, 31372150, 31572224, 31471955), the Zhejiang Provincial Natural Science Foundation of China (Y2111122, LQ16C090004), and the Medical and Health Research Program of Hangzhou in China (20170533B10).

REFERENCES

Aguirre, A., Dupree, J. L., Mangin, J. M., and Gallo, V. (2007). A functional role for EGFR signaling in myelination and remyelination. *Nat. Neurosci.* 10, 990–1002. doi: 10.1038/nn1938

Alizadeh, A., Dyck, S. M., and Karimi-Abdolrezaee, S. (2015). Myelin damage and repair in pathologic CNS: challenges and prospects. *Front. Mol. Neurosci.* 8:35. doi: 10.3389/fnmol.2015.00035

Bansal, R., and Pfeiffer, S. E. (1997). Regulation of oligodendrocyte differentiation by fibroblast growth factors. *Adv. Exp. Med. Biol.* 429, 69–77. doi: 10.1007/978-1-4757-9551-6_5

Bansal, R., Stefansson, K., and Pfeiffer, S. E. (1992). Proligodendroblast antigen (POA), a developmental antigen expressed by A007/O4-positive oligodendrocyte progenitors prior to the appearance of sulfatide and galactocerebroside. *J. Neurochem.* 58, 2221–2229. doi: 10.1111/j.1471-4159.1992.tb10967.x

Barnett, S. C., Franklin, R. J., and Blakemore, W. F. (1993). *In vitro* and *in vivo* analysis of a rat bipotential O-2A progenitor cell line containing the temperature-sensitive mutant gene of the SV40 large T antigen. *Eur. J. Neurosci.* 5, 1247–1260. doi: 10.1111/j.1460-9568.1993.tb00910.x

Blank, T., and Prinz, M. (2014). NF-κB signaling regulates myelination in the CNS. *Front. Mol. Neurosci.* 7:47. doi: 10.3389/fnmol.2014.00047

Cai, J., Zhu, Q., Zheng, K., Li, H., Qi, Y., Cao, Q., et al. (2010). Co-localization of Nkx6.2 and Nkx2.2 homeodomain proteins in differentiated myelinating oligodendrocytes. *Glia* 58, 458–468. doi: 10.1002/glia.20937

Cao, Q., Xu, X. M., Devries, W. H., Enzmann, G. U., Ping, P., Tsoulfas, P., et al. (2005). Functional recovery in traumatic spinal cord injury after transplantation of multineurotrophin-expressing glial-restricted precursor cells. *J. Neurosci.* 25, 6947–6957. doi: 10.1523/JNEUROSCI.1065-05.2005

Chen, Y., Balasubramaniyan, V., Peng, J., Hurlock, E. C., Tallquist, M., Li, J., et al. (2007). Isolation and culture of rat and mouse oligodendrocyte precursor cells. *Nat. Protoc.* 2, 1044–1051. doi: 10.1038/nprot.2007.149

Chen, Y., Mei, R., Teng, P., Yang, A., Hu, X., Zhang, Z., et al. (2015). TAPP1 inhibits the differentiation of oligodendrocyte precursor cells via suppressing the Mek/Erk pathway. *Neurosci. Bull.* 31, 517–526. doi: 10.1007/s12264-015-1537-5

Cheng, X., Xie, B., Qi, J., Zhao, X., Zhang, Z., Qiu, M., et al. (2017). Rat astrocytes are more supportive for mouse OPC self-renewal than mouse astrocytes in culture. *Dev. Neurobiol.* doi: 10.1002/dneu.22476 [Epub ahead of print].

Chong, V. Z., Webster, M. J., Rothmond, D. A., and Weickert, C. S. (2008). Specific developmental reductions in subventricular zone ErbB1 and ErbB4 mRNA in the human brain. *Int. J. Dev. Neurosci.* 26, 791–803. doi: 10.1016/j.ijdevneu.2008.06.004

Crang, A. J., Gilson, J. M., Li, W.-W., and Blakemore, W. F. (2004). The remyelinating potential and *in vitro* differentiation of MOG-expressing oligodendrocyte precursors isolated from the adult rat CNS. *Eur. J. Neurosci.* 20, 1445–1460. doi: 10.1111/j.1460-9568.2004.03606.x

Dadsetan, M., Knight, A. M., Lu, L., Windebank, A. J., and Yaszemski, M. J. (2009). Stimulation of neurite outgrowth using positively charged hydrogels. *Biomaterials* 30, 3874–3881. doi: 10.1016/j.biomaterials.2009.04.018

Decker, L., Avellana-Adalid, V., Nait-Oumesmar, B., Durbec, P., and Baron-Van, Evercooren, A. (2000). Oligodendrocyte precursor migration and differentiation: combined effects of PSA residues, growth factors, and substrates. *Mol. Cell. Neurosci.* 16, 422–439. doi: 10.1006/mcne.2000.0885

Dincman, T. A., Beare, J. E., Ohri, S. S., and Whittemore, S. R. (2012). Isolation of cortical mouse oligodendrocyte precursor cells. *J. Neurosci. Methods.* 209, 219–226. doi: 10.1016/j.jneumeth.2012.06.017

Fernandez, M., Pirondi, S., Manservigi, M., Giardino, L., and Calzà, L. (2004). Thyroid hormone participates in the regulation of neural stem cells and oligodendrocyte precursor cells in the central nervous system of adult rat. *Eur. J. Neurosci.* 20, 2059–2070. doi: 10.1111/j.1460-9568.2004.03664.x

Galvez-Contreras, A. Y., Quiñones-Hinojosa, A., and Gonzalez-Perez, O. (2013). The role of EGFR and ErbB family related proteins in the oligodendrocyte specification in germinal niches of the adult mammalian brain. *Front. Cell. Neurosci.* 7:258. doi: 10.3389/fncel.2013.00258

Gard, A. L., and Pfeiffer, S. E. (1990). Two proliferative stages of the oligodendrocyte lineage (A2B5+O4- and O4+GalC-) under different mitogenic control. *Neuron* 5, 615–625. doi: 10.1016/0896-6273(90)90216-3

Gonzalez-Perez, O., Romero-Rodriguez, R., Soriano-Navarro, M., Garcia-Verdugo, J. M., and Alvarez-Buylla, A. (2009). Epidermal growth factor induces the progeny of subventricular zone type B cells to migrate and differentiate into oligodendrocytes. *Stem Cells* 27, 2032–2043. doi: 10.1002/stem.119

Gregori, N., Pröschel, C., Noble, M., and Mayer-Pröschel, M. (2002). The tripotential glial-restricted precursor (GRP) cell and glial development in the spinal cord: generation of bipotential oligodendrocyte-type-2 astrocyte progenitor cells and dorsal-ventral differences in GRP cell function. *J. Neurosci.* 22, 248–256.

Haas, C., Neuhuber, B., Yamagami, T., Rao, M., and Fischer, I. (2012). Phenotypic analysis of astrocytes derived from glial restricted precursors and their impact on axon regeneration. *Exp. Neurol.* 233, 717–732. doi: 10.1016/j.expneurol.2011.11.002

Hart, I. K., Richardson, W. D., Heldin, C. H., Westermark, B., and Raff, M. C. (1989). PDGF receptors on cells of the oligodendrocyte-type-2 astrocyte (O-2A) cell lineage. *Development* 105, 595–603.

Herrera, J., Yang, H., Zhang, S. C., Proschel, C., Tresco, P., Duncan, I. D., et al. (2001). Embryonic-derived glial-restricted precursor cells (GRP cells) can differentiate into astrocytes and oligodendrocytes *in vivo*. *Exp. Neurol.* 171, 11–21. doi: 10.1006/exnr.2001.7729

Hill, C. E., Proschel, C., Noble, M., Mayer-Proschel, M., Gensel, J. C., Beattie, M. S., et al. (2004). Acute transplantation of glial-restricted precursor cells into spinal cord contusion injuries: survival, differentiation and effects on lesion environment and axonal regeneration. *Exp. Neurol.* 190, 289–310. doi: 10.1016/j.expneurol.2004.05.043

Hu, Q., Zhang, L., Wen, J., Wang, S., Li, M., Feng, R., et al. (2010). The EGF receptor-sox2-EGF receptor feedback loop positively regulates the self-renewal of neural precursor cells. *Stem Cells* 28, 279–286. doi: 10.1002/stem.246

Ivkovic, S., Canoll, P., and Goldman, J. E. (2008). Constitutive EGFR signaling in oligodendrocyte progenitors leads to diffuse hyperplasia in postnatal white matter. *J. Neurosci.* 28, 914–922. doi: 10.1523/JNEUROSCI.4327-07.2008

Jiang, F., Frederick, T. J., and Wood, T. L. (2001). IGF-I synergizes with FGF-2 to stimulate oligodendrocyte progenitor entry into the cell cycle. *Dev. Biol.* 232, 414–423. doi: 10.1006/dbio.2001.0208

Liu, Y., Wu, Y., Lee, J. C., Xue, H., Pevny, L. H., Kaprielian, Z., et al. (2002). Oligodendrocyte and astrocyte development in rodents: an *in situ* and immunohistological analysis during embryonic development. *Glia* 40, 25–43. doi: 10.1002/glia.10111

McKinnon, R. D., Matsui, T., Dubois-Dalcq, M., and Aaronson, S. A. (1990). FGF modulates the PDGF-driven pathway of oligodendrocyte development. *Neuron* 5, 603–614. doi: 10.1016/0896-6273(90)90215-2

Morath, D. J., and Mayer-Pröschel, M. (2001). Iron modulates the differentiation of a distinct population of glial precursor cells into oligodendrocytes. *Dev. Biol.* 237, 232–243. doi: 10.1006/dbio.2001.0352

Murtie, J. C., Zhou, Y. X., Le, T. Q., and Armstrong, R. C. (2005). *In vivo* analysis of oligodendrocyte lineage development in postnatal FGF2 null mice. *Glia* 49, 542–554. doi: 10.1002/glia.20142

Neman, J., and de Vellis, J. (2012). A method for deriving homogenous population of oligodendrocytes from mouse embryonic stem cells. *Dev. Neurobiol.* 72, 777–788. doi: 10.1002/dneu.22008

Noble, M., Murray, K., Stroobant, P., Waterfield, M. D., and Riddle, P. (1988). Platelet-derived growth factor promotes division and motility and inhibits premature differentiation of the oligodendrocyte/type-2 astrocyte progenitor cell. *Nature* 333, 560–562. doi: 10.1038/333560a0

Phillips, A. W., Falahati, S., DeSilva, R., Shats, I., Marx, J., Arauz, E., et al. (2012). Derivation of glial restricted precursors from E13 mice. *J. Vis. Exp.* 64:3462. doi: 10.3791/3462

Qiu, M. (2013). Myelin in development and disease. *Neurosci. Bull.* 29, 127–128. doi: 10.1007/s12264-013-1325-z

Raff, M. C., Lillien, L. E., Richardson, W. D., Burne, J. F., and Noble, M. D. (1988). Platelet-derived growth factor from astrocytes drives the clock that times oligodendrocyte development in culture. *Nature* 333, 562–565. doi: 10.1038/333562a0

Rao, M. S., Noble, M., and Mayer-Pröschel, M. (1998). A tripotential glial precursor cell is present in the developing spinal cord. *Proc. Natl. Acad. Sci. U S A* 95, 3996–4001. doi: 10.1073/pnas.95.7.3996

Rao, S. N., and Pearse, D. D. (2016). Regulating axonal responses to injury: the intersection between signaling pathways involved in axon myelination and the inhibition of axon regeneration. *Front. Mol. Neurosci.* 9:33. doi: 10.3389/fnmol.2016.00033

Rodríguez-Peña, A. (1999). Oligodendrocyte development and thyroid hormone. *J. Neurobiol.* 40, 497–512. doi: 10.1002/(SICI)1097-4695(19990915)40:4<497::AID-NEU7>3.0.CO;2-#

Sántha, P., Veszelka, S., Hoyk, Z., Mészáros, M., Walter, F. R., Tóth, A. E., et al. (2016). Restraint stress-induced morphological changes at the blood-brain barrier in adult rats. *Front. Mol. Neurosci.* 8:88. doi: 10.3389/fnmol.2015.00088

Scafidi, J., Hammond, T. R., Scafidi, S., Ritter, J., Jablonska, B., Roncal, M., et al. (2014). Intranasal epidermal growth factor treatment rescues neonatal brain injury. *Nature* 506, 230–234. doi: 10.1038/nature12880

Shaw, G., Osborn, M., and Weber, K. (1981). An immunofluorescence microscopical study of the neurofilament triplet proteins, vimentin and glial fibrillary acidic protein within the adult rat brain. *Eur. J. Cell Biol.* 26, 68–82.

Sommer, I., and Schachner, M. (1981). Monoclonal antibodies (O1 to O4) to oligodendrocyte cell surfaces: an immunocytological study in the central nervous system. *Dev. Biol.* 83, 311–327. doi: 10.1016/0012-1606(81)90477-2

Sun, J. J., Liu, Y., and Ye, Z. R. (2008). Effects of P2Y1 receptor on glial fibrillary acidic protein and glial cell line-derived neurotrophic factor production of astrocytes under ischemic condition and the related signaling pathways. *Neurosci. Bull.* 24, 231–243. doi: 10.1007/s12264-008-0430-x

Tang, J., Xu, H. W., Fan, X. T., Li, Z. F., Li, D. B., Yang, L., et al. (2007). Targeted migration and differentiation of engrafted neural precursor cells in amyloid β-treated hippocampus in rats. *Neurosci. Bull.* 23, 263–270. doi: 10.1007/s12264-007-0039-5

Tzahar, E., Waterman, H., Chen, X., Levkowitz, G., Karunagaran, D., Lavi, S., et al. (1996). A hierarchical network of interreceptor interactions determines signal transduction by Neu differentiation factor/neuregulin and epidermal growth factor. *Mol. Cell Biol.* 16, 5276–5287. doi: 10.1128/mcb.16.10.5276

Wu, Y. Y., Mujtaba, T., Han, S. S., Fischer, I., and Rao, M. S. (2002). Isolation of a glial-restricted tripotential cell line from embryonic spinal cord cultures. *Glia* 38, 65–79. doi: 10.1002/glia.10049

Yang, J., Cheng, X., Shen, J., Xie, B., Zhao, X., Zhang, Z., et al. (2016). A novel approach for amplification and purification of mouse oligodendrocyte progenitor cells. *Front. Cell. Neurosci.* 10:203. doi: 10.3389/fncel.2016.00203

Yang, J., Liu, X., Yu, J., Sheng, L., Shi, Y., Li, Z., et al. (2009). A non-viral vector for potential DMD gene therapy study by targeting a minidystrophin-GFP fusion gene into the hrDNA locus. *Acta Biochim. Biophys. Sin. (Shanghai)* 41, 1053–1060. doi: 10.1093/abbs/gmp080

Yoo, S., and Wrathall, JR. (2007). Mixed primary culture and clonal analysis provide evidence that NG2 proteoglycan-expressing cells after spinal cord injury are glial progenitors. *Dev. Neurobiol.* 67, 860–874. doi: 10.1002/dneu.20369

Zhang, Y., Guo, T. B., and Lu, H. (2013). Promoting remyelination for the treatment of multiple sclerosis: opportunities and challenges. *Neurosci. Bull.* 29, 144–154. doi: 10.1007/s12264-013-1317-z

Zhao, J. W., Raha-Chowdhury, R., Fawcett, J. W., and Watts, C. (2009). Astrocytes and oligodendrocytes can be generated from $NG2^{+}$ progenitors after acute brain injury: intracellular localization of oligodendrocyte transcription factor 2 is associated with their fate choice. *Eur. J. Neurosci.* 29, 1853–1869. doi: 10.1111/j.1460-9568.2009.06736.x

Conflict of Interest Statement: The authors declare that the research was conducted in the absence of any commercial or financial relationships that could be construed as a potential conflict of interest.

frontiers in Molecular Neuroscience

REVIEW
published: 17 February 2017
doi: 10.3389/fnmol.2017.00038

Molecular Mechanisms Involved in Schwann Cell Plasticity

Angélique Boerboom[1], *Valérie Dion*[1], *Alain Chariot*[2,3] *and Rachelle Franzen*[1]*

[1] GIGA-Neurosciences, University of Liège, Liège, Belgium, [2] GIGA-Molecular Biology of Diseases, University of Liège, Liège, Belgium, [3] Walloon Excellence in Lifesciences and Biotechnology (WELBIO), Wavre, Belgium

Schwann cell incredible plasticity is a hallmark of the utmost importance following nerve damage or in demyelinating neuropathies. After injury, Schwann cells undergo dedifferentiation before redifferentiating to promote nerve regeneration and complete functional recovery. This review updates and discusses the molecular mechanisms involved in the negative regulation of myelination as well as in the reprogramming of Schwann cells taking place early following nerve lesion to support repair. Significant advance has been made on signaling pathways and molecular components that regulate SC regenerative properties. These include for instance transcriptional regulators such as c-Jun or Notch, the MAPK and the Nrg1/ErbB2/3 pathways. This comprehensive overview ends with some therapeutical applications targeting factors that control Schwann cell plasticity and highlights the need to carefully modulate and balance this capacity to drive nerve repair.

Keywords: Schwann cell, plasticity, molecular mechanisms, nerve injury, peripheral neuropathy

OPEN ACCESS

Edited by:
Margaret Su-chun Ho,
Tongji University, China

Reviewed by:
Xavier Navarro,
Autonomous University of Barcelona, Spain
Melissa R. Andrews,
University of St Andrews, UK
Georg Zoidl,
York University, Canada
Helmar Lehmann,
University Hospital Cologne, Germany

***Correspondence:**
Rachelle Franzen
rfranzen@ulg.ac.be

Received: *22 December 2016*
Accepted: *31 January 2017*
Published: *17 February 2017*

Citation:
Boerboom A, Dion V, Chariot A and Franzen R (2017) Molecular Mechanisms Involved in Schwann Cell Plasticity. Front. Mol. Neurosci. 10:38. doi: 10.3389/fnmol.2017.00038

INTRODUCTION

The peripheral nervous system (PNS) shows a surprising capacity of regeneration compared to the central nervous system (CNS). This ability of peripheral nerves to recover quickly following damage is to a large extent due to the remarkable plasticity of Schwann cells (SCs), the glial cells of the PNS (Jessen et al., 2015). SCs are derived from neural crest cells that differentiate into SC precursors

Abbreviations: ALS, Amyotrophic lateral sclerosis; BACE1, Beta-Site amyloid precursor protein cleaving enzyme 1; BDNF, Brain-derived neurotrophic factor; BMP7, Bone morphogenetic protein 7; Cadm3, Cell adhesion molecule 3; cAMP, Cyclic adenosine monophosphate; Cdkn1c, Cyclin-dependent kinase inhibitor 1C; CIDP, Chronic inflammatory demyelinating polyneuropathy; CMT, Charcot-Marie-Tooth; Cthrc1, Collagen triple helix repeat containing 1; EZH2, Enhancer of zeste homolog 2; Dixdc1, DIX domain containing-1; DDIT4, DNA damage-inducible transcript 4 protein; Dlg1, Disks large homolog 1; Dock7, Dedicator of cytokinesis protein 7; DRG, Dorsal root ganglion; Dusp15, Dual specificity phosphatase 15; Egr-1, Early growth response protein 1; Egr-2/Krox-20Early growth response 2; Egr-3, Early growth response protein 3; Erk, Extracellular signal regulated kinase; GDNF, Glial cell-derived neurotrophic factor; GFAP, Glial fibrillary acidic protein; GPCR, G protein-coupled receptor; Id2, DNA-binding protein inhibitor 2; IVIG, Immunoglobulins; JNK, c-jun N-terminal kinase; LKB1/STK11, Liver kinase B1/ Serine/threonine-protein kinase 11; LPA1, Lysophosphatidic acid receptor 1; LXR, Liver X receptor; MAPK, Mitogen activated protein kinase; MBP, Myelin basic protein; MPZ, Myelin protein zero; MyD88, Myeloid differentiation primary response gene 88; NF-κB, Nuclear factor-kappa B; NMJ, Neuromuscular junction; Notch, Neurogenic locus notch homolog protein; Nrg1, Neuregulin 1; NuRD, Nucleosome remodeling and deacetylase complex; p75NTR, Low affinity neurotrophin receptor; Pax-3, Paired box protein 3; PI 3-kinase, Phosphatidylinositol 3-kinase; PMP22, Peripheral myelin protein 22; Pou3f1/Oct6, POU domain class 3 transcription factor / Octamer-binding factor 6; PTEN, Phosphatase and tensin homolog deleted on chromosome 10; S1PR, Sphingosine-1-phosphate receptor; Sam68, Src-associated in mitosis of 68 kD; Sox2, SRY-related HMG-box gene 2; SSeCKS, Src-suppressed protein kinace C substrate; STK11, Serine/threonine protein kinase; TACE, Tumor necrosis factor-α–converting enzyme; TGFβ, Transforming growth factor beta; Zeb2, Zinc-finger E-box-binding homeobox 2.

and then into immature SCs between E12 and E15 in mice. Around birth, axonal sorting and myelination start in the peripheral nerves. Some SCs establish a 1:1 relationship with large-diameter axons, wrap them multiple times to form a thick and compact myelin sheath. Myelin-forming SCs allow the fast conduction of action potentials by insulating the axons. The non-myelinating SCs typically associate with several small-diameter axons to form Remak bundles. Nerve homeostasis, trophic support and myelin maintenance are other important functions of SCs in adulthood (Jessen and Mirsky, 2005).

Besides their major roles in normal nerve physiology, SCs play a key function for repair in many pathological conditions thanks to their striking plasticity (Zochodne, 2008). For example, after a peripheral nerve injury, they are capable of switching into a SC immature-like phenotype that drives nerve repair. Over the last decades, major progress has been made in unraveling molecular mechanisms and signaling pathways that drive SC dedifferentiation and regulate their plasticity. In this review, we will update and discuss the recent studies that identified molecular components involved in SC plasticity and their possible therapeutic implications.

REMARKABLE PLASTICITY AND REGENERATIVE PROPERTIES OF SCHWANN CELLS AFTER PERIPHERAL NERVE INJURY

The unique plasticity of SCs has been extensively studied in transgenic animals after cut or crush injuries. Indeed, following a nerve lesion, quiescent, highly specialized myelinating and non-myelinating SCs reprogram into proliferative progenitor-like repair SCs that drive the entire regeneration process (Chen et al., 2007; Jessen and Mirsky, 2016). The reprogramming of SCs in physiopathological conditions is most of the time defined as dedifferentiation. However, transdifferentiation seems more appropriate, as repair SCs, besides re-expressing immature SC markers, exhibit completely different features (Arthur-Farraj et al., 2012). Indeed, the injury-induced conversion of mature SCs in regeneration-promoting cells is an active phenomenon. It involves a down-regulation of pro-myelinating genes including early growth response 2 *(Egr-2,* more frequently named *Krox-20*), POU domain class 3 transcription factor 1 *(Pou3f1* or *Oct-6),* myelin protein zero *(MPZ) or* myelin basic protein *(MBP)* as well as an up-regulation of markers of immature, de-differentiated SCs such as c-Jun, low affinity neurotrophin receptor (p75NTR) or glial fibrillary acidic protein (GFAP) but also specific repair-supportive genes (Jessen and Mirsky, 2008). Following damage, the nerve undergoes a series of complex multicellular and molecular events in which SCs play a role of orchestrator (**Figure 1**).

Quickly after nerve injury, damaged axons in the distal stump degenerate in an active process called Wallerian degeneration (Waller, 1850). Yet unidentified signals from damaged nerves induce the reprogramming of SCs. These downregulate pro-myelinating genes and start clearing their myelin sheaths through a mechanism of autophagy called myelinophagy (Gomez-Sanchez et al., 2015). Axonal and myelin debris are also phagocyted by resident and blood-derived macrophages recruited by SCs (Hirata and Kawabuchi, 2002; Lee et al., 2006; Barrette et al., 2008). An inflammatory reaction occurs: many blood cells invade the lesion site and secrete numerous cytokines and chemokines (Martini et al., 2008; Gaudet et al., 2011; Rotshenker, 2011). Following nerve axotomy, particularly, the basal lamina of SCs and the connective tissue are interrupted (Zochodne, 2008). A tissue bridge is formed between the two stumps of the nerve over the lesion site. Fibroblasts play a major role in building this bridge by interacting with SCs (Parrinello et al., 2010). Newly formed vasculature is also crucial to guide the SCs and the growing axons through the lesion site (Cattin et al., 2015). Many chemical and physical interactions happen between the actors present in the injured nerve, creating a permissive and favorable environment for regeneration (Cattin and Lloyd, 2016).

Irrespective of whether the injury is a crush or a cut, repair SCs in the distal stump proliferate, secrete several trophic factors that support glial and neuronal survival and regrowth including artemin, brain-derived neurotrophic factor (BDNF) or glial cell line-derived neurotrophic factor (GDNF) (Fernandez-Valle et al., 1995; Kim et al., 2000; Boyd and Gordon, 2003; Fontana et al., 2012). They also align in tracts named bands of Büngner and provide a trophic and physical support for axons to regrow and reinnervate correctly their targets (Weinberg and Spencer, 1978; Stoll and Müller, 1999). At the neuromuscular junction, specialized terminal SCs direct reinnervation by helping the axons to find their paths toward their appropriate sites (Son and Thompson, 1995). After axonal regeneration, repair SCs readily exit the cell cycle and differentiate again into myelinating and non-myelinating SCs to support the complete functional recovery. Nevertheless, most of the time, the newly-formed myelin sheaths are shorter and thinner than expected based on axonal diameter (Schröder, 1972).

MOLECULAR MECHANISMS THAT MODULATE SCHWANN CELL PLASTICITY

The adaptive reprogramming of SCs after a nerve injury is a prerequisite for regeneration. Therefore, understanding the molecular components that regulate the phenotypic change of adult specialized SCs into repair-supportive SCs can lead to the development of new therapeutics that can boost repair in various peripheral neuropathies. In this section, we will review the most relevant molecular components or pathways that have been identified for controlling SC plasticity, the negative regulation of myelination and their response to nerve injury (**Tables 1, 2**; **Figure 2**).

Transcriptional Regulators

The Transcription Factor c-Jun

The transcription factor c-Jun does not appear to be essential during SC development but multiple arguments demonstrate its central function in SC reprogramming. Firstly, the time course of c-Jun expression supports its role in SC plasticity. Indeed, c-Jun is down-regulated post-natally during SC differentiation

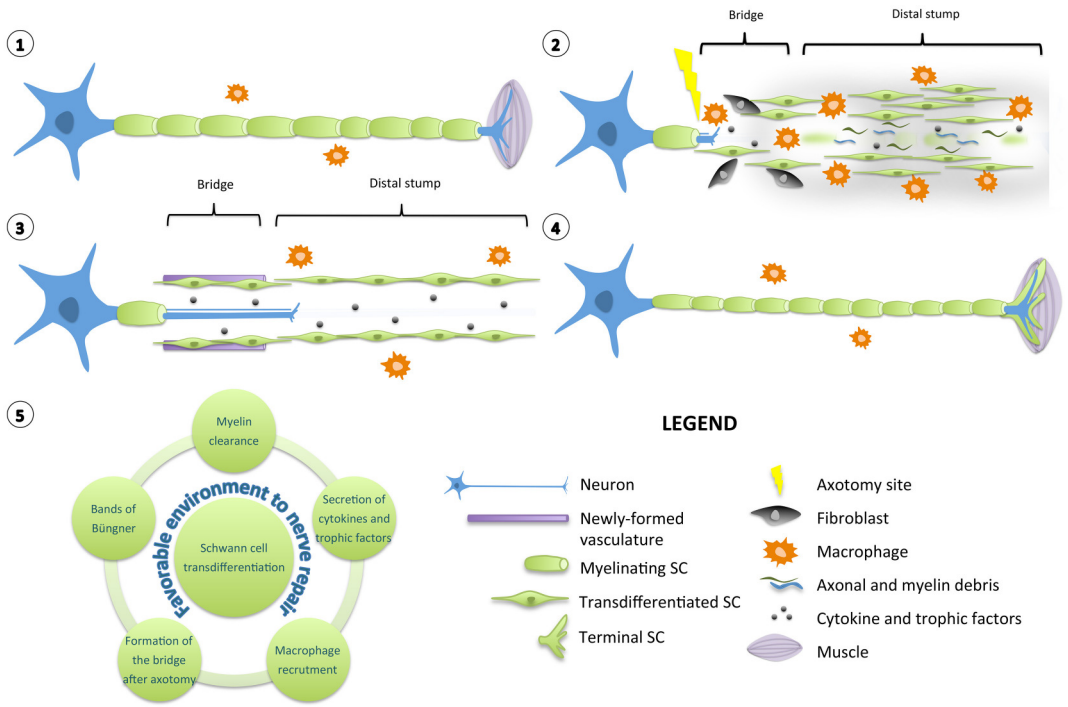

FIGURE 1 | Diagram of Schwann cell response to nerve injury. (1) Schematic representation of a single neuron with myelinating SCs and resident macrophages. For simplification, the basal lamina around SCs is not shown. (2) After injury, the nerve distal to the injury site degenerates and undergoes a series of complex multicellular and molecular events in which SCs play a role of orchestrator. SCs transdifferentiate into repair-promoting cells, creating a permissive and favorable environment for nerve regeneration. SCs downregulate pro-myelinating genes and clear their myelin sheaths. They proliferate, secrete several pro-inflammatory cytokines and trophic factors that support glial and neuronal survival and regrowth. Axonal and myelin debris are also phagocyted by resident and blood-derived macrophages recruited by SCs. SCs interact with fibroblasts to build a bridge between the two stumps of the nerve over the lesion site. (3) Newly formed vasculature guides the SCs and the growing axons through the lesion site. In the distal stump, SCs align in tracts named bands of Büngner to provide a trophic and physical support for axons to regrow. (4) After axonal regeneration, transdifferentiated SCs readily exit the cell cycle, differentiate again and remyelinate the axons to support the complete functional recovery. However, the newly-formed myelin sheaths are most of the time shorter and thinner than expected based on axonal diameter. Specialized terminal SCs direct reinnervation by helping the axons to find their paths toward their initial targets. (5) Diagram displaying the various roles played by a transdifferentiated SC to create a favorable environment for nerve repair.

and myelination and is highly up-regulated under pathological conditions such as peripheral nerve injuries, demyelinating diseases or other peripheral neuropathies (Stewart, 1995; Parkinson et al., 2008; Hutton et al., 2011; Hantke et al., 2014; Klein et al., 2014). Secondly, c-Jun is a negative regulator of myelination and a cross-antagonist of Krox-20, one of the main pro-myelinating transcription factors. Deletion of c-Jun in SCs *in vitro* strikingly facilitates Krox-20-induced expression of MBP or MPZ. Conversely, forced expression of c-Jun inhibits the expression of myelin proteins. Moreover, the expression of c-Jun and Krox-20 is mutually exclusive: while immature SCs express relatively high levels of c-Jun and low levels of Krox-20, myelinating cells switch to high levels of Krox-20 and low levels of c-Jun (Parkinson et al., 2004, 2008). Thirdly, strong evidence *in vivo* exhibits the involvement of c-Jun in major aspects of the SC response following nerve injury. Myelination during development occurs normally in the c-Jun conditional knockout mice (Parkinson et al., 2008). However, the absence of c-Jun following a nerve lesion results in a failure of generating the repair SCs, leading to impaired axonal regeneration, target reinnervation and functional recovery. The myelin sheath degradation and clearance are also strikingly slowed in the absence of c-Jun *in vitro* and *in vivo*. Moreover, mutant SCs fail to form the Büngner regenerative tracks and to express the adhesion molecules and trophic factors critical for nerve repair (Parkinson et al., 2008; Arthur-Farraj et al., 2012; Fontana et al., 2012).

The role of c-Jun in SCs after nerve injury is to activate a repair program to support regeneration. The high levels of c-Jun found in different peripheral neuropathies that do not involve nerve injuries like Charcot-Marie Tooth (CMT) raises the question on the precise function of c-Jun in these diseases. Does c-Jun counteract the pathology, attenuate its symptoms and promote repair or does its up-regulation cause the disease? In two models of demyelinating diseases, CMT1A and CMT1X, c-Jun is increased in SCs that retain myelin differentiation (Hantke et al., 2014; Klein et al., 2014). The myelin sheaths are also relatively normal in a mouse mutant showing a 5–8 fold c-Jun overexpression in SCs (levels that are lower than those seen after a nerve cut though) (Jessen and Mirsky, 2016). Moreover, c-Jun and repair-associated genes are up-regulated in a mouse model in which the serine/threonine-protein kinase (LKB1, also

TABLE 1 | Most relevant molecular components involved in Schwann cell plasticity, negative regulation of myelination and nerve repair.

Molecular component	*In vivo* model(s)	Phenotype(s)	Reference(s)
TRANSCRIPTIONAL REGULATORS			
c-Jun	• $MPZ^{Cre}/cJun^{fl/fl}$	• Injury: lack of trophic factor expression, no alignment in bands of Büngner, no axon regeneration and no functional recovery	Parkinson et al., 2008; Arthur-Farraj et al., 2012; Fontana et al., 2012
Notch	• $MPZ^{Cre}/RBPJ^{fl/fl};Notch^{fl/fl}$; $NCID^{CASL-STOPfl/fl}$ • Rats treated with Jagged1 (Notch signaling activator)	• Development: acceleration of myelination and thicker myelin. Injury: delayed myelin breakdown • Injury: improved axonal regeneration and functional recovery	Woodhoo et al., 2009; Wang et al., 2015
Zeb2	• $PLP^{CreERT2}/Zeb2^{fl/fl}$	• Injury: disturbed regeneration and lack of remyelination	Quintes et al., 2016; Wu L. M. N. et al., 2016
NF-κB	• GFAP-IκBα-dn	• Injury: delayed axonal regeneration and disturbed remyelination	Morton et al., 2012
MAPK			
Raf/Erk	• MPZ^{RafTR} (tamoxifen-inducible Raf activation)	• Normal adult nerve: transient activation leads to demyelination, SC proliferation and increased P75NTR expression. Sustained activation leads to inflammation.	Napoli et al., 2012
Rac/JNK	• Mice transfected with dominant negative Rac1/Rac1-RNAi • Mice injected with Rac inhibitor • Dock7 shRNA transgenic mice (decrease of Rac/JNK signaling)	• Injury: reduced myelin sheath fragmentation • Injury: decreased c-Jun and p75NTR expression • Development: enhanced myelin thickness	Jung et al., 2011; Yamauchi et al., 2011; Shin et al., 2013
p38	• Mice injected with p38 inhibitor • $MPZ^{Cre}/p38a^{fl/fl}$ • New-born rats treated with BMP7 (activation of p38MAPK signaling)	• Injury: reduced SC demyelination and dedifferentiation • Development: acceleration of myelination Injury: delay in myelin clearance, small increase of re-myelination • Development: delayed peripheral myelination	Yang et al., 2012; Liu et al., 2016b; Roberts et al., 2016
PI3K/Akt/mTOR			
PTEN	• $PLP^{CreERT2}/PTEN^{fl/fl}$ (hyper-activation of PI3K/Akt signaling) • $PLP^{CreERT2}/PTEN^{fl/fl}$treated with rapamycin (mTOR inhibitor)	• Development: hypermyelination, myelin outfoldings • Amelioration of the myelin pathology	Goebbels et al., 2010, 2012
Dlg1	• Mice injected with Dlg1 shRNA (activation of PI3K/Akt signaling) • $MPZ^{Cre}Dlg1^{fl/f}$ (activation of PI3K/Akt signaling)	• Development: myelin outfoldings and peripheral nerve overmyelination • Development: transient hypermyelination	Cotter et al., 2010; Noseda et al., 2013
DDIT4	• DDIT4 KO mouse (over-activation of PI3K/AKT/mTOR signaling)	• Development: sustained hypermyelination	Noseda et al., 2013
WNT SIGNALING AND LXR			
LXR	• LXR KO mouse • Mice treated with paraquat (LXR activation)	• Development: altered myelination • Development: severe myelin sheath disorganization	Makoukji et al., 2011; Hichor et al., 2016
TLR SIGNALING			
TLRs	• TLR2, TLR4, MyD88 KO mice	• Injury: impaired expression of inflammatory modulators, macrophage recruitment and activation, axonal regeneration and functional recovery	Boivin et al., 2007
GPCR SIGNALING			
Gpr126	• $PLP^{CreERT2}/Gpr126^{fl/fl}$	• Injury: defects in remyelination, macrophage recruitment and axon regeneration	Mogha et al., 2016b

(Continued)

TABLE 1 | Continued

Molecular component	*In vivo* model(s)	Phenotype(s)	Reference(s)
Nrg1/ErbB2-B3			
Nrg1	• Animals treated with Nrg1 isoforms • Inactivation in axons: SLICK-A^{Cre}; CAG^{CreERT2}/Nrg1$^{fl/fl}$ • Inactivation in SCs: Dhh^{Cre}/Nrg1$^{fl/fl}$	• Injury: improved nerve regeneration and functional recovery • Injury: slower axon regeneration, target reinnervation, remyelination, functional recovery • Injury: impaired remyelination	Chen et al., 1998; Joung et al., 2010; Fricker et al., 2011, 2013; Yildiz et al., 2011; Stassart et al., 2013
BACE1	• BACE1 KO mouse	• Injury: impaired remyelination but enhanced axon regeneration	Hu et al., 2008; Farah et al., 2011
TACE	• HB9^{Cre}/TACE$^{fl/fl}$	• Development: hypermyelination	La Marca et al., 2011
ErbB2	• Mice treated with ErbB2 inhibitor • Plp1^{CreERT2}ErbB2$^{fl/fl}$	• Injury: decreased demyelination • Injury: no effect on SC proliferation and survival	Guertin et al., 2005; Atanasoski et al., 2006

TABLE 2 | Summary of the regulators and their roles in SCs.

Negative regulation of myelination during development	Positive regulation of myelination during development
c-Jun, Notch, Sox2, Pax-3, Id2, Egr-1, Egr-3, Cdkn1c, Hes5, Dock7, Cthrc1, p38MAPK, BMP7, SSeCKS, Cadm3, Dlg1, PTEN, DDIT4, AMPK, LXR?	Zeb2, NF-κB?, PI3K/Akt/mTOR, LXR?, Wnt, Gpr126, Gpr44, LPA1, Nrg1/ErbB2/3
Transdifferentiation after injury	**Remyelination after injury**
c-Jun, Notch, NF-κB?, Sox2, Ras/Raf/Erk, Rac/JNK, p38 MAPK, Sam68, Dixdc1, TLRs, Gpr126, Nrg1/ErbB2/3?	Zeb2, NF-κB?, Nrg1/ErbB2/3

called STK11) is inactivated in SCs and in which axons are damaged without overt demyelination (Beirowski et al., 2014). This suggests that moderated c-Jun up-regulation is compatible with myelination, does not necessarily provoke demyelination and that it is sufficient to activate the transcription of injury-related genes (Jessen and Mirsky, 2016). In this context, it is likely that the role of c-Jun in those diseases is to promote neuroprotection and repair. However, if c-Jun is activated in an uncontrolled and exacerbated manner, c-Jun could also be detrimental. For example, the increase of c-Jun expression in some human schwannomas may directly or indirectly be associated with the abnormal proliferation and the absence of myelin markers (Shivane et al., 2013).

Notch Signaling

Neurogenic locus notch homolog protein (Notch) is a transmembrane receptor protein that, upon ligand binding, is cleaved and generates an intracellular domain (NICD), which acts as a transcriptional regulator. Notch controls SC proliferation and promotes the generation of immature SCs from Schwann cell precursors (SCPs) *in vivo* but also acts as a negative regulator of myelination. It is down-regulated as myelination proceeds and its inactivation or over-activation leads to premature or delayed myelin formation, respectively. Moreover, the inhibition of Notch signaling in adult mice decelerates myelin breakdown following a nerve lesion (Woodhoo et al., 2009). The addition of recombinant jagged1, an activator of Notch, in rat nerves after injury improves nerve regeneration and functional recovery (Wang et al., 2015). This indicates that stimulation of Notch signaling in SCs could represent an interesting therapeutic strategy to efficiently promote nerve repair. However, aberrant activation of Notch signaling in SCs may also participate to the development of malignant peripheral nerve sheath tumors (Li et al., 2004).

The Transcriptional Repressor Zeb2

More recently, the function of a transcriptional repressor, Zeb2, has been investigated in SC myelination and nerve repair by two different teams (Quintes et al., 2016; Wu L. M. N. et al., 2016). They both showed that mice lacking Zeb2 in SCs develop a severe peripheral neuropathy, caused by a failure of SC maturation. Zeb2 transcriptional repression of negative regulators of myelination such as Notch and SRY-related HMG-box gene 2 (Sox2) is necessary for SC lineage progression. Although Zeb2 seems dispensable for the establishment of the repair SCs following nerve injury, its absence disrupts nerve regeneration and remyelination (Quintes et al., 2016). Mechanistically, Zeb2 controls SC differentiation and remyelination by recruiting histone deacetylases 1 and 2 (HDAC1/2) and NuRD complexes and by inhibiting a Notch–Hey2 signaling axis (Wu L. M. N. et al., 2016).

NF-κB

The nuclear factor κB (NF-κB) transcription factor regulates a lot of physiological processes and mediates the physiopathological inflammatory response in many diseases. Several studies suggest that NF-κB activation is essential for the differentiation and myelination of SCs *in vitro* (Nickols et al., 2003; Yoon et al., 2008; Limpert and Carter, 2010). Furthermore, it has been shown that the deacetylation of NF-κB mediated by HDAC 1/2 is necessary to control myelination in the PNS (Chen et al., 2011). Paradoxically, by using transgenic mice in which NF-κB activation is inhibited in SCs, Morton and colleagues demonstrated that NF-κB is dispensable for developmental myelination *in vivo* (Morton

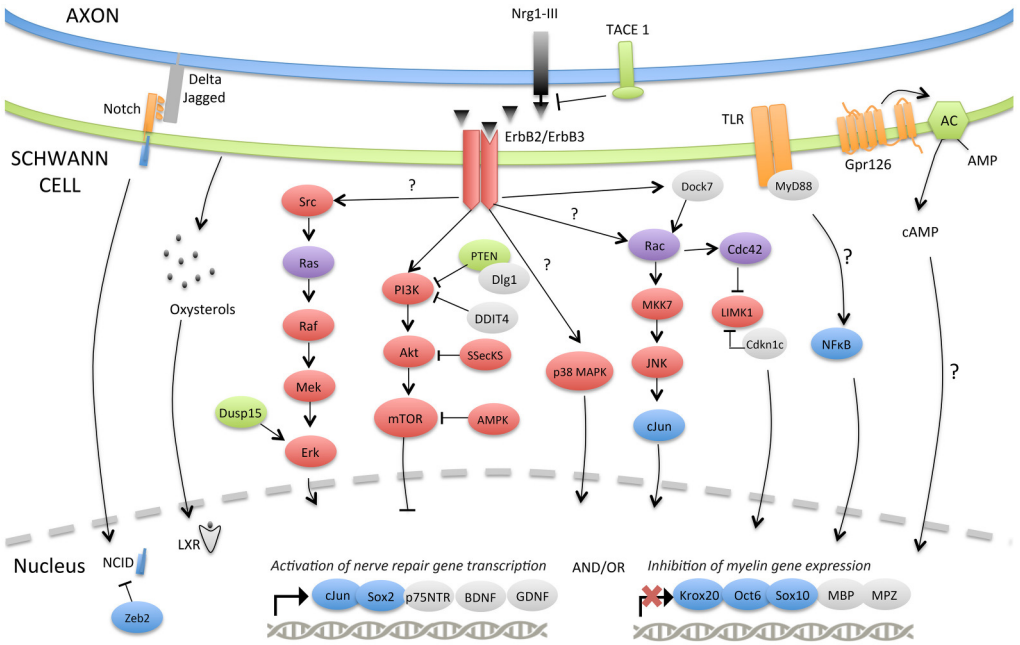

FIGURE 2 | Molecular signaling pathways involved in SC plasticity, negative regulation of myelination and nerve repair. The injury-induced reprogramming of SCs in regeneration-promoting cells involves a down-regulation of pro-myelinating genes including *Krox-20, Oct-6, Sox10, MPZ, or MBP* as well as an up-regulation of markers characteristic of immature, de-differentiated SCs such as c-Jun and p75NTR but also specific repair-supportive proteins like BDNF or GDNF. The signaling pathways or molecular components activating (c-Jun, Notch, MAPKs, TLRs, Gpr126, NF-κB) or inhibiting (PI3K/Akt/mTOR) this reprogramming are represented. Some negative regulators of myelination during development (TACE1, LXRs, Dusp15, PTEN, Dlg1, DDIT4, Dock7, Zeb2) and possibly playing a role after injury are also shown.

et al., 2013). However, they showed that the inhibition of NF-κB signaling in SCs following sciatic nerve crush transiently delays axonal regeneration and remyelination (Morton et al., 2012). This highlights again the differences between immature SCs during development and transdifferentiated repair-SCs. Importantly, NF-κB activity is robustly enhanced after peripheral nerve damage and in inflammatory neuropathies (Andorfer et al., 2001; Laura et al., 2006; Smith et al., 2009; Fu et al., 2010). The different NF-κB-induced transcriptional targets responsible for SC beneficial effects after nerve injury still have to be determined. Of note, the placental growth factor (PlGF) which is up-regulated by NF-κB in SCs following injury, is critical for SC proliferation, myelin sheath degradation, macrophage invasion and axonal regeneration (Chaballe et al., 2011). Targeting NF-κB or its downstream targets in SCs may offer new therapeutic strategies for PNS regeneration. Nevertheless, it is essential to keep in mind that aberrant activation of NF-κB may also lead to schwannoma (Ammoun et al., 2014; Dilwali et al., 2015).

Sox-2, Pax-3, Id2, Egr-1, Egr-3

Other factors that regulate gene transcription have been studied in SC dedifferentiation. These are most of the time negative regulators of myelination that functionally counteract positive regulators of myelination including Krox-20 or Oct-6 and are likely to have major roles after nerve damage (Jessen and Mirsky, 2008). For instance, the transcription regulators Sox-2, paired box protein 3 (Pax-3), DNA-binding protein inhibitor 2 (Id2) and early growth response proteins 1 and 3 (Egr-1 and Egr-3) could represent good candidates for regulating SC dedifferentiation in damaged nerves. As for c-Jun or Notch, they are inactive or expressed at low levels in myelinating cells and re-expressed at high levels under conditions that lead to SC dedifferentiation such as nerve injury (Kioussi et al., 1995; Nikam et al., 1995; Stewart et al., 1997; Le et al., 2005; Parkinson et al., 2008; Doddrell et al., 2012). *In vitro*, Sox2, Pax3, and Id2 decrease or increase myelin gene expression when overexpressed or depleted, respectively (Kioussi et al., 1995; Mager et al., 2008; Parkinson et al., 2008; Doddrell et al., 2012). Egr1 and Egr3 are both necessary to up-regulate p75NTR in SC primary cultures, known to be re-expressed in SCs following a nerve injury (Nikam et al., 1995; Topilko et al., 1997; Gao et al., 2007). It remains to be unraveled by *in vivo* evidence whether those different factors are required for SC response after nerve injury.

Besides its likely role in SC plasticity, it has been shown that Sox-2 is necessary in SCs for the formation of a nerve bridge after a complete transection. This process is mediated by an ephrin-B/EphB2 signaling between fibroblasts and SCs that initiates cell sorting, followed by directional collective cell migration of SCs out of the nerve stumps to guide axons across the injury wound (Parrinello et al., 2010).

MAPK Signaling

A growing number of studies provide evidence on the functions of mitogen activated protein kinase (MAPK) family proteins

in the regulation of SC plasticity. Extracellular signal regulated kinase (Erk), c-jun N-terminal kinase (JNK) and p38 MAP kinase are rapidly and highly activated in the SCs of the distal stump following a nerve lesion and play specific, overlapping or complementary roles in the SC response after injury (Sheu et al., 2000; Harrisingh et al., 2004; Zrouri et al., 2004; Agthong et al., 2006; Parkinson et al., 2008; Lee et al., 2014; Ronchi et al., 2016).

Ras/Raf/Erk

Harrisingh and coworkers were the first ones to demonstrate the role of the Ras/Raf/Erk signaling in SC dedifferentiation (Harrisingh et al., 2004). They showed that the ectopic activation of Raf, an upstream activator of Erk, suppresses the differentiation of primary SCs induced by cyclic adenosine monophosphate (cAMP). Raf activation in cultured differentiated SCs also drives their dedifferentiation. Importantly, they demonstrated that sustained activation of the Ras/Raf/Erk pathway in myelinated dorsal root ganglion (DRG) neuron-SC co-cultures induces demyelination even in the presence of normal axon signaling. Consistent with this idea, another paper reported that the dual specificity phosphatase 15 (Dusp15) is necessary for full activation of Erk and that its activation represses the expression of several myelin genes including *MBP* (Rodríguez-Molina et al., 2017). While high and sustained activation of Ras/Raf/Erk signaling seems essential for SC plasticity, Ras over-activation might also be deleterious and lead to the development of SC-derived tumors in neurofibromatosis type 1 patients (Harrisingh et al., 2004). A strong activation of Erk has actually been reported in human primary schwannoma cells (Ammoun et al., 2008).

More recently, the strategy of Raf high activation has been used *in vivo* to determine whether this signaling was central in controlling SC plasticity (Napoli et al., 2012). Napoli et al. demonstrated that a tamoxifen-inducible Raf transgene in SCs is sufficient to induce the down-regulation of myelin proteins and the expression of dedifferentiation markers such as p75NTR, even in the absence of axonal damage. The duration of Raf activation, controlled by the period of tamoxifen treatment, determines the time frame of SC demyelination and proliferation. A prolonged tamoxifen treatment and activation of Raf in SCs also induces an inflammatory response, which includes the breakdown of the blood-nerve barrier and the infiltration of macrophages, which promote nerve regeneration.

Although the repression of Erk signaling with specific inhibitors blocks SC mitosis, cytokine expression and demyelination, it only prevents partially the induction of p75NTR or GDNF and the shutdown of myelin gene expression (Napoli et al., 2012; Shin et al., 2013). Thus, even if the sustained and pronounced activation of the Ras/Raf/Erk pathway is fundamental in regulating SC plasticity, this supports the idea that several independent mechanisms control multiple aspects of SC plasticity. Moreover, different studies showed that Erk activation is actually pro-myelinating and that its inhibition blocks SC differentiation and myelination *in vivo* (Grossmann et al., 2009; He et al., 2010; Newbern et al., 2011). Therefore, Erk signaling is necessary both for the differentiation of SCPs and for the dedifferentiation of adult SCs following a nerve injury. The reconciling explanation could be that distinct levels of Erk activity would define the state of SC differentiation. Low or basal activity would be required for SC differentiation while high Erk levels would drive dedifferentiation and proliferation (Napoli et al., 2012; Newbern and Snider, 2012).

Finally, the role of c-Jun as a downstream target of Erk signaling is an attractive idea but it is actually quite controversial and further *in vivo* studies are necessary to better understand the signaling mechanisms downstream of Erk in SC plasticity. Indeed, Syed et al. showed that Erk inhibition abolishes both the demyelination and the expression of c-Jun induced by Neuregulin 1 (Nrg1) treatment in SC-DRG neuron co-cultures (Syed et al., 2010). Additionally, the Lloyd group indicated that c-Jun is strongly up-regulated after Raf over-activation in SCs *in vivo* (Napoli et al., 2012). However, others reported that the induction of c-Jun and SC dedifferentiation triggered by cAMP removal *in vitro* depends on JNK rather than on Erk activity (Monje et al., 2010; Shin et al., 2013). Actually, other data revealed that Rac/JNK and Raf/Erk might be responsible for different complementary functions in SC plasticity. For example, microarray experiments showed that the expression of regeneration-associated genes, including *p75NTR* or *GDNF* is dependent on JNK but not on Erk signaling. In addition, it has been demonstrated that most Erk-dependent genes in dedifferentiated SCs do not require Rac activity (Shin et al., 2013).

Rac/JNK

JNK is another MAPK that plays important functions in SCs. It has been demonstrated that c-Jun activation by JNK is essential for SC migration and proliferation *in vitro* (Parkinson et al., 2001, 2004; Yamauchi et al., 2003). Parkinson and colleagues showed that overexpressing the MAPK kinase 7 (MKK7), a protein upstream of JNK, in SC primary cultures, inhibits myelin gene expression by elevating c-Jun, suggesting a role for JNK signaling in SC plasticity (Parkinson et al., 2008). This was confirmed by Monje et al. who revealed that a reduction of cAMP *in vitro* is sufficient to induce SC dedifferentiation through a JNK-dependent mechanism (Monje et al., 2010). More recently, it has also been demonstrated that the active Rac1 GTPase (Rac), an upstream regulator of MKK7 and JNK, inhibits SC differentiation. In SC cultures, Rac up-regulates c-Jun and down-regulates Krox-20 through the MKK7/JNK pathway, but not through the Raf/Erk pathway. Furthermore, MKK7 activation and the induction of c-Jun observed in sciatic nerves after axotomy were blocked by Rac inhibition (Shin et al., 2013). In addition, Rac activation has been observed in the distal stump of injured nerves, and specific Rac inhibition with a dominant negative Rac1 and Rac1-RNAi decelerates myelin sheath fragmentation. Rac would actually promote myelin sheath fragmentation by controlling actin polymerization in the Schmidt-Lantermann incisures of SCs (Jung et al., 2011).

The cyclin-dependent kinase inhibitor 1 (Cdkn1c), also called p57Kip2, is a protein first known to block G_1/S transition during cell cycle that also regulates actin filament dynamics through the translocation of LIM domain kinase 1 (LIMK1), a downstream effector of Rac/Cdc42/Rho (Yokoo et al., 2003; Heinen et al., 2013). Knocking down Cdkn1c in cultured SCs leads to cell cycle

exit, morphological changes and up-regulation of myelin genes. In SC-DRG neuron co-cultures, Cdkn1c depletion accelerates myelination. A global gene expression analysis also revealed a shift of the transcriptional expression program toward the pattern of differentiating SCs, strongly suggesting a role for Cdkn1c as an important negative regulator of myelination (Heinen et al., 2008). The same team also showed that Cdkn1c is a direct target of the enhancer of zeste homolog 2 (EZH2) and identify Hes5 as a new transcriptional repressor of myelin genes (Heinen et al., 2012). Indeed, EZH2 binds Cdkn1c promoter and its suppression results in a decrease of histone H3K27 trimethylation, an induction of Cdkn1c expression and a down-regulation of myelin genes in cultured primary SCs.

Yamauchi and co-workers reported that the atypical guanine-nucleotide exchange factor dedicator of cytokinesis protein 7 (Dock7), activates Rac/Cdc42/JNK signaling in SCs to positively regulate migration and negatively regulate differentiation and myelination (Yamauchi et al., 2008, 2011). Indeed, knocking down Dock7 in primary SCs results in an increase of cAMP-mediated differentiation and in a shorter duration of activation of Rac/Cdc42 and JNK while silencing Dock7 in mice increases myelin thickness.

Finally, collagen triple helix repeat containing 1 (Cthrc1) is another protein that has been linked to Rac activation in SCs. Apra and colleagues investigated Cthrc1 function in SCs both *in vitro* and *in vivo* (Apra et al., 2012). They showed that its silencing inhibits SC proliferation and promotes their migration and myelination *in vitro*. By using a transgenic mouse line, they demonstrated that the overexpression of Cthrc1 in SCs leads to a delayed myelination with SCs maintaining a proliferative state. More recently, Zhou et al identified miR-9 as an important negative regulator of SC migration targeting Cthrc1 after nerve injury (Zhou et al., 2014). The up-regulation of miR-9 decreases SC migration in culture and following nerve injury. miR-9 has also been shown to directly target Cthrc1, which in turn inactivates downstream Rac. Finally, miR-9 is down-regulated at a speed comparable to the rate of SC migration during nerve regeneration, suggesting that miR-9 down-regulation could be linked to the phenotypic modulation of SCs after nerve injury.

All these data confirm that Rac/JNK signaling is essential for SC plasticity, proliferation and migration following nerve injury. However, stimulating this pathway for nerve repair therapy must be cautioned as its upregulation has also been observed in primary human schwannoma cells (Kaempchen et al., 2003).

p38 MAPK

Yang and co-workers provided the most relevant data that suggest a role for p38 MAPK in SC plasticity and their response to injury (Yang et al., 2012). They reported that inhibition of p38 MAPK activity in mice blocks SC demyelination and dedifferentiation following nerve injury, despite ongoing axon degeneration. In myelinating co-cultures, they also showed that p38 MAPK mediates myelin breakdown induced by Nrg1. Finally, while the ectopic activation of p38 MAPK is sufficient to provoke myelin breakdown and c-Jun induction, its inhibition in SC-DRG neuron co-cultures promotes myelination. Roberts and collaborators recently investigated the *in vivo* function of the major p38 isoform in mouse conditional knockouts. In agreement with previous findings, the lack of p38alpha in SCS accelerates myelination during development, delays myelin clearance and slightly increases remyelination following injury. However, axonal regeneration and functional repair were not affected in the absence of p38alpha (Roberts et al., 2016).

A recent study on bone morphogenetic protein 7 (BMP7) in SCs revealed a role for this protein as a negative regulator of myelination through the activation of p38 MAPK signaling (Liu et al., 2016b). Liu and collaborators showed that BMP7 expression is inversely correlated with myelin gene expression during normal peripheral myelination. In addition, BMP7 treatment decreases cAMP-induced myelin gene expression and up-regulates c-Jun in primary SC cultures. By using p38 MAPK inhibitor, gene silencing and rescue experiments, they reported that p38 MAPK is responsible for BMP7-mediated suppression of myelin gene expression. Finally, when injected in newborn rats, BMP7 retards peripheral myelination.

PI3K/Akt/mTOR Signaling

Phosphatidylinositol 3-kinase (PI3K) signaling has been implicated in the regulation of proliferation, survival and differentiation of different cell types (Rameh and Cantley, 1999). The pathway is strongly activated in primary cultured SCs following treatment with soluble Nrg1 or contact with neurite membranes. Moreover, PI3K signaling is required for SC proliferation and survival *in vitro* (Maurel and Salzer, 2000; Li et al., 2001). Its inhibition affects the initiation of myelination but is not necessary for myelin maintenance in SC-neuron co-cultures (Maurel and Salzer, 2000). In addition, the selective activation of Akt in SCs by gene transfer results in an increased myelination in SC-DRG neuron co-cultures and allogenic nerve graft experiments. This last paper also demonstrated opposing functions for PI3K/Akt and Erk pathways in controlling SC myelination (Ogata et al., 2004). The imbalanced activation of the PI3K/Akt and Erk pathways has also been revealed in transgenic rodent models of CMT1A in which SCs develop persistent differentiation defects during early postnatal development (Fledrich et al., 2014). The transgenic expression of constitutively active Akt in SCs, however does not seem to disrupt PNS myelination *in vivo* (Flores et al., 2008).

Studies investigating the role of specific proteins indirectly indicated a role for PI3K/Akt signaling in the regulation of SC proliferation and differentiation after nerve injury. For example, Src-associated in mitosis of 68 kD (Sam68) has been suggested to promote SC proliferation by enhancing the PI3K/Akt pathway and to act on regeneration following sciatic nerve crush (Wu et al., 2016b). DIX domain containing-1 (Dixdc1), which is also linked to PI3K/Akt activation, promotes SC proliferation after sciatic nerve crush. Dixdc1 is up-regulated following nerve damage and its depletion leads to reduced PI3K/Akt activation and SC proliferation (Wu et al., 2016a). Consistently, 17β-estradiol has been shown to promote SC proliferation and early remyelination in the bridge after nerve transection through Akt activation (Chen et al., 2016a). Src-suppressed protein kinase C substrate (SSeCKS) has been indicated as a suppressor of SC differentiation and myelination by inhibiting Akt activation.

SSeCKS is effectively down-regulated during SC differentiation and its depletion promotes Akt phosphorylation and myelin gene expression in cAMP-treated primary cultures or myelination when co-cultured with DRG neurons (Ji et al., 2010). SSeCKS is also essential for SC adhesion, spreading and migration (Yan et al., 2009). In addition, Chen and collaborators showed that cell adhesion molecule 3 (Cadm3) might act as a negative modulator of PNS myelination. Cadm3 interferes with PI3K/Akt activation and inhibits Schwann cell myelination *in vitro* (Chen M. S. et al., 2016).

The mammalian disks large homolog 1 (Dlg1) inhibits PI3K/Akt signaling via its interaction with the phosphatase and tensin homolog deleted on chromosome 10 (PTEN). This mechanism is necessary to transiently inhibit the axonal stimulation of myelination and to limit myelin sheath thickness. Myelin outfoldings and overmyelination followed later by pathologic demyelination are actually observed after Dlg1 silencing via RNA interference in mouse sciatic nerves (Cotter et al., 2010). Dlg1/PTEN functions and consequently Akt/mTOR signaling are also disturbed in different mouse models of demyelinating neuropathies and peripheral nerve sheath tumors (Bolino et al., 2004; Cotter et al., 2010; Goebbels et al., 2010, 2012; Keng et al., 2012). More specifically, Goebbels et al showed that mice lacking PTEN develop a tomaculous neuropathy characterized by focal hypermyelination and myelin outfoldings. Moreover, treating these mice with rapamycin, a mTOR inhibitor, significantly ameliorates the pathology (Goebbels et al., 2010, 2012). Another study on PTEN signaling showed that the hypermyelination observed in mice lacking Dlg1 is actually transitory. This study also identified DNA damage-inducible transcript 4 protein (DDIT4) as a sustained negative regulator of myelination. High DDIT4 expression in SCs precedes the peak of Dlg1 and Akt activity in peripheral nerves. Loss of DDIT4 expression both *in vitro* and *in vivo* results in sustained hypermyelination and enhanced PI3K/Akt/mTOR activation (Noseda et al., 2013). Therefore, it is likely that PI3K/Akt signaling has to be precisely regulated and balanced to induce SC differentiation or dedifferentiation.

mTOR is a signaling pathway that integrates a lot of signals (growth factors, nutrients, energy and oxygen) necessary for growth and proliferation (Norrmén and Suter, 2013). Sherman and collaborators demonstrated that the inactivation of mTOR in SCs provokes an arrest of myelination after axonal sorting and reduces axon growth (Sherman et al., 2012). More recently, it has been reported that the conditional ablation of raptor, an essential component of the mTORC1 complex, in SCs leads to hypomyelination and abnormal lipid biosynthesis (Norrmén et al., 2014). The pathways that converge to mTOR are numerous and include Nrg1/ErbB, PI3K/Akt, MAPKS or AMP-activated kinase (AMPK) signaling (Norrmén and Suter, 2013). AMPK is a heterotrimeric serine/threonine protein kinase acting as an inhibitor of mTOR and described as a crucial energy sensor important to maintain energy homeostasis (Hardie et al., 2012). Recently, Liu and colleagues revealed that AMPK is a critical negative regulator of SC myelination in the PNS (Liu et al., 2016a). They first showed that AMPK is gradually decreased as myelination proceeds. The high activation of AMPK decreases myelin gene expression and stimulates c-Jun expression in SCs whereas its inhibition or depletion induces myelin gene expression. The injection of an inhibitor of AMPK in newborn rats downregulates c-Jun expression, enhances lipid and protein synthesis and increases myelin gene expression and myelin sheath thickness.

Wnt Signaling and LXR

Wnt/β-catenin pathway has been demonstrated to be crucial for PNS development. Cell cultures and genetic experiments revealed that Wnt signaling is required for SC lineage progression, proliferation and myelination (Hari et al., 2002; Lee et al., 2004; Gess et al., 2008; Grigoryan et al., 2013). Recently, it has been proposed that interplay between Wnt pathway and liver X receptors (LXR) induces the fine-tuning of myelin gene expression (Makoukji et al., 2011). Oxysterols acting as ligands for LXR, are natural compounds that originate from the enzymatic oxidation of cholesterol. They are involved in cholesterol homeostasis and in the progression of different neurodegenerative disorders (Lütjohann et al., 2000; Russell, 2000; Leoni et al., 2002). Makoukji and co-workers provided evidence for the implication of LXR and oxysterols in the negative regulation of myelin gene expression (Makoukji et al., 2011). They showed that oxysterols are expressed in a SC line and in sciatic nerves and that they repress the gene expression of *MPZ* and *PMP22* by a mechanism involving LXR α and β and the inhibition of the Wnt/β-catenin-dependent pathway. Unexpectedly, although myelin gene transcripts are up-regulated in mice lacking LXR α and β, presumably due to increased β-catenin activity, myelin protein expression is decreased and myelin sheath thickness is reduced. They conclude that this hypomyelination in the knockout animals may be the consequence of an altered cholesterol homeostasis and an inefficient myelin protein trafficking from the endoplasmic reticulum.

Recently, paraquat, a redox-active herbicide, has been shown to elicit an oxidative stress in the normal sciatic nerves of adult mice and a dramatic disorganization of myelin sheaths, causing severe locomotor and sensory deficits through a stimulation of the LXR pathway leading to reduced Wnt signaling (Hichor et al., 2016). Indeed, the authors provided evidence that paraquat alters myelin gene expression by activating LXR signaling and by preventing β-catenin recruitment on the myelin gene promoter. They also indicated that treating paraquat-exposed mice with lithium, a Wnt/β-catenin modulator acting as a GSK3 inhibitor, prevents the deleterious defects of paraquat on sciatic nerves. The effect of lithium chloride has also been studied after nerve injury. It accelerates axon and myelin debris clearance and remyelination by inhibiting GSK3 and increasing β-catenin levels (Chen et al., 2016b).

Toll-like Receptor Signaling

The Toll-like receptors (TLRs) are a class of proteins that play a key role in initiating the immune and inflammatory response. After nerve injury, damage-associated molecular patterns and ligands released from or expressed by activated or necrotic damaged cells result in the activation of TLRs in different

cell types including SCs (Thakur et al., 2017). TLR3, TLR4, and TLR7 are constitutively expressed by SCs and TLR1 is upregulated following nerve injury, strongly suggesting a role for TLR signaling in SC-driven nerve repair (Goethals et al., 2010). *In vitro*, the addition of necrotic neurons to SCs activates their inflammatory response through TLR signaling. It increases their gene expression of inflammatory mediators such as tumor necrosis factor-alpha (TNF-α) or monocyte chemoattractant protein-1 (MCP-1) but this effect is reduced in SCs from mice lacking TLR3 (Lee et al., 2006). Boivin and collaborators provided *in vivo* evidence that TLR signaling is involved in WD and nerve regeneration following a nerve injury, possibly through NF-κB activation (Boivin et al., 2007). The early expression of inflammatory modulators such as MCP-1, macrophage recruitment and activation, axonal regeneration and functional recovery are impaired in the mice deficient in TLR signaling. The results are indeed similar in mice lacking TLR2, TLR4 or their adaptor, myeloid differentiation primary response gene 88 (MyD88) known to activate NF-κB. Interestingly, a single injection of TLR2 and TLR4 ligands at the site of the lesion speeds up myelin clearance and functional recovery. Besides its likely role in SC response to nerve injury, TLR signaling has also been linked to the development of neuropathic pain, making TLRs promising therapeutic targets (Thakur et al., 2017).

GPCR Signaling

To date, three different G protein-coupled receptors (GPCRs) have been demonstrated to be implicated in SC differentiation. These are Gpr126, Gpr44, and lysophosphatidic acid receptor 1 (LPA1) (Mogha et al., 2016a). Monk and colleagues were the first ones to show that a GPCR, Gpr126, is crucial for the initiation of SC myelination (Monk et al., 2009). The analysis of mice lacking LPA1 then revealed that this receptor is required for SC migration, axonal sorting and proper myelination (Anliker et al., 2013). Finally, Trimarco et al. provided *in vitro* and *in vivo* evidence for the involvement of Gpr44 and its ligand the prostaglandin D2 in PNS myelination (Trimarco et al., 2014). Very recently, Mogha and collaborators investigated the potentiel functions of Gpr126 in peripheral nerve injury and repair as its expression is maintained in adult SCs (Mogha et al., 2016b). By using an inducible conditional Gpr126 knockout model, they observed defects in remyelination, macrophage recruitment and axon regeneration following a nerve crush. Since approximately 30% of all approved drugs target GPCRs, Gpr126 may represent an attractive potential target to stimulate repair in myelinating disease or after nerve damage.

Nrg1/ErbB2/3 Signaling

Currently, the signals from damaged nerves that induce the reprogramming of SCs are not identified. Some argued that these can be linked to the Nrg1/ErbB pathway, one of the best described interdependent relationship between axons and SCs. Neuregulins form a large family of epidermal growth factor-like proteins that signal through the ErbB tyrosine kinase receptors (Falls, 2003). The Nrg1/ErbB signaling is first of all known for its critical functions in SC development (for review, Newbern and Birchmeier, 2010; Grigoryan and Birchmeier, 2015; Willem, 2016). Indeed, numerous genetic models have been generated to unravel fundamental functions of the Nrg1/ErbB signaling axis. Differential expression of Nrg1 isoforms, their proteolytic processing or ErbB receptor localization and trafficking are important parameters that control the Nrg1/ErbB pathway and its underlying functions. Depending on the developmental stage, the pathway significantly regulates SC survival, proliferation, migration, differentiation and myelination (Syroid et al., 1996; Morris et al., 1999; Leimeroth et al., 2002; Taveggia et al., 2005; Chen et al., 2006; Freidin et al., 2009; Newbern and Birchmeier, 2010). This functional diversity is presumably accomplished through the interaction of Nrg1/ErbB signaling with other pathways. For instance, Notch signaling, which is necessary for SCP proliferation and survival, increases the expression of ErbB2 in SCPs and their sensitivity to Nrg1 (Woodhoo et al., 2009). The tyrosine phosphatase Shp2 is another essential component of the Nrg-1/ErbB pathway that promotes SC proliferation and migration (Grossmann et al., 2009). Later in SC development, critical interactions between Nrg1/ErbB and cAMP or NF-κB signaling are necessary for SC differentiation and myelination (Limpert and Carter, 2010; Arthur-Farraj et al., 2011). Although the importance of Nrg1/ErbB signaling in SC development is well established, its role in adult SC plasticity is more controversial. In adulthood, the pathway seems dispensable for the maintenance of the myelin sheaths, as the absence of Nrg1 in peripheral axons or of ErbB2 in SCs has no effect on axon or myelin sheath integrity (Atanasoski et al., 2006; Fricker et al., 2011, 2013). However, increasing evidence indicates that Nrg1 is necessary for the SC response to nerve injury.

The fact that the Nrg1/ErbB system is selectively and highly regulated during peripheral nerve degeneration and regeneration represents a strong argument in favor of a role for this signaling pathway in SC plasticity (Carroll et al., 1997; Kwon et al., 1997; Ronchi et al., 2016). Recently, a study using a rat surgical model of delayed nerve repair showed that Nrg1 and some SC markers are highly down-regulated after chronic degeneration. Since long-term denervated Schwann cells are known to be partly responsible for delayed nerve repair, it suggests that Nrg1 plays an important function in SC activity after denervation (Ronchi et al., 2017). Guertin and colleagues showed that ErbB2 is activated in myelinating SCs after sciatic nerve axotomy and that its transient activation is sufficient to initiate SC demyelination in compartmentalized cell culture chambers. In addition, the treatment of rats with an ErbB2 inhibitor results in a reduction of demyelination after nerve transection (Guertin et al., 2005). Consistently, Syed et al demonstrated that a robust activation of ErbB2/3 via high concentration of soluble Nrg1 induces SC dedifferentiation and demyelination as well as increased c-Jun expression in primary cultures (Syed et al., 2010). Furthermore, *in vitro* experiments recapitulating nerve injuries provide evidence that Nrg1 treatment shows beneficial effects on SC migration and proliferation (Mahanthappa et al., 1996; Li et al., 1998). Finally, Lee and collaborators showed that Nrg1 on motor axons controls the terminal SC-mediated synapse elimination at the neuromuscular junctions (NMJs) during development. They also

revealed that NMJs of adult transgenic mice overexpressing Nrg1 in motor axons exhibited continued remodeling, identifying Nrg1 as a molecular determinant for SC-driven neuromuscular synaptic plasticity (Lee et al., 2016).

Nrg1/ErbB signaling has also been linked to different pathways mentioned earlier for regulating SC plasticity. For example, Nrg1 has been proposed as the signal driving high Erk activation after injury (Napoli et al., 2012). High concentrations of Nrg1 indeed highly activates Erk signaling and induces SC dedifferentiation and demyelination (Syed et al., 2010; Newbern and Snider, 2012). In agreement with this, Tapinos and collaborators also showed that direct binding of Mycobacterium leprae onto ErbB2 receptors on SCs activates Erk signaling and promotes demyelination (Tapinos et al., 2006). Another possibility is that Nrg1 could trigger Rac/JNK activation. Indeed, the inhibition of ErbB2 signaling has been shown to prevent MKK7 activation, c-jun expression, and Rac-dependent gene transcription in cultures of sciatic nerve explants (Shin et al., 2013). ErbB2 also directly binds and activates the negative regulator of myelination, Dock7, upstream of Rac/JNK while the depletion of Dock7 attenuates Nrg1 effects in primary SC cultures (Yamauchi et al., 2008, 2011). Although these data suggest a role for Nrg1/ErbB signaling in SC dedifferentiation, *in vivo* studies revealed contradictory results. Atanasoski et al. showed that lack of ErbB2 in adult SCs does not affect their proliferation and survival after nerve injury, despite reduced levels of phosphorylated MAPK (Atanasoski et al., 2006). In addition, the absence of the axonal Nrg1 following a nerve crush does not disturb SC proliferation associated with nerve degeneration or the clearance of myelin debris by macrophages. Therefore, adult SCs would not require major Nrg1/ErbB signaling for their proliferation and survival after nerve damage, in contrast to what is observed *in vitro* and during development.

While the implication of Nrg1 signaling in the dedifferentiation of SCs is unclear, its involvement in myelination but also in remyelination after nerve injury is now well established. The transmembrane axonal isoforms Nrg1 type III signals in a juxtacrine manner through ErbB2/3 receptors on SCs and determines their myelin thickness, both during development and following a nerve lesion (Michailov et al., 2004; Taveggia et al., 2005; Fricker et al., 2011, 2013). The axonal Nrg1 is rate limiting but not essential for remyelination since compensations are observed at later stages (Fricker et al., 2013). All the same, myelin sheaths are often thinner after injury, suggesting an insufficent simulation by axonal signals (Schröder, 1972). Another mechanism is actually induced in SCs to supplement these poor neuronal cues. Nerve damage triggers the expression of soluble Nrg1 type I by SCs themselves. This particular autocrine and paracrine signaling in SCs is only required after nerve injury and promotes SC survival, redifferentiation and remyelination (Fricker and Bennett, 2011; Stassart et al., 2013).

Besides the importance of Nrg1/ErbB signaling in SC remyelination, it also plays a key role in repair processes after nerve injury (Fricker and Bennett, 2011). Fricker and colleagues showed that the absence of Nrg1 in adult axons after sciatic nerve crush results in defects of remyelination but also in slower axon regeneration, impaired muscle reinnervation and delayed functional recovery (Fricker et al., 2011, 2013). In a mouse model lacking β-Site amyloid precursor protein cleaving enzyme 1 (BACE1), a protein known to cleave and activate Nrg1 type III, SC remyelination is impaired and nerve repair is surprisingly accelerated (Hu et al., 2008). Indeed, knockout mice show an accelerated clearance of axonal and myelin debris from degenerated fibers, faster axonal regeneration and earlier reinnervation of neuromuscular junctions, compared to littermate controls (Farah et al., 2011). The enhanced myelin clearance might clearly be due to the initial hypomyelination observed in adult BACE1 KO sciatic nerves. However, how BACE1 deletion enhances peripheral regeneration still needs to be clarified. Another enzyme capable of cleaving the axonal Nrg1, counteracting BACE1 and interfering with SC differentiation is the tumor necrosis factor-α–converting enzyme (TACE, also named ADAM17). TACE depletion in SC-DRG neuron co-cultures increases myelination. The absence of TACE in motoneurons *in vivo* results in hypermyelination. The function of TACE is neuron autonomous since its knockdown in SCs does not affect myelination. Mechanistically, TACE cleaves Nrg1-III, which is no longer capable of activating PI3K signaling and inducing myelination (La Marca et al., 2011). Therefore, TACE can be considered as a modulator of NRG1 type III activity and as a negative regulator of SC myelination. The role of Nrg1 in peripheral regeneration has also been demonstrated in different studies examining the effects of Nrg1 treatment following nerve injury. The application of exogenous Nrg1 or strategies that elevates Nrg1 levels after nerve damage improve myelin clearance, axon regeneration, remyelination and functional recovery (Chen et al., 1998; Joung et al., 2010; Fricker and Bennett, 2011; Yildiz et al., 2011). Therefore, treatment with recombinant forms of Nrg1 may represent interesting therapeutic avenues to improve nerve repair following injury. It is however necessary to better understand the mechanisms by which Nrg1 treatment improves nerve regeneration.

Finally, it is essential to remember that the inappropriate overactivation of Nrg1/ErbB signaling pathway may be harmful in some circumstances and lead to demyelinating neuropathies or peripheral tumors. For instance, constitutive activation of the Nrg1/ErbB pathway promotes the proliferation of peripheral neuroepithelioma and neoplastic SC line (Frohnert et al., 2003; Fallon et al., 2004). Similarly, transgenic mice over-expressing Nrg1 in myelinating SCs develop hypertrophic neuropathies and malignant peripheral nerve sheath tumors (Huijbregts et al., 2003). In addition, leprosy, which is an important cause of demyelinating neuropathy in the world, is initiated by an excessive activation of ErbB2 by *M. leprae* (Tapinos et al., 2006).

PATHOPHYSIOLOGICAL IMPLICATIONS AND THERAPEUTIC STRATEGIES

Peripheral neuropathies are responsible for significant morbidity and decreased quality of life due to weakness, sensory loss and neuropathic pain. The causes are multiple: peripheral nerve traumatic injuries, inherited genetic diseases such as CMT,

metabolic disorders including diabetes, infectious, toxic and inflammatory disorders (Zhou and Notterpek, 2016). Peripheral nerves have an impressive ability to regenerate compared to the CNS. However, the clinical recovery of patients suffering from peripheral neuropathies is often incomplete due to slow regeneration rate, target mis-reinnervation and lack of a long-term regeneration-supportive environment. After injury, peripheral axons regenerate at a very slow rate of approximately 1 mm per day, depending on the lesion site. Moreover, the regenerative capacity of the PNS decreases over time. Indeed, SCs become unsupportive to regeneration after long periods and they also exhibit diminished plasticity with age (Fu and Gordon, 1995; Zochodne, 2012; Painter et al., 2014). Of note, Joshi and coworkers recently demonstrated that SCs show an altered expression of c-Jun and Cdkn1c and that their pro-regenerative functions are diminished in a model of chronic inflammatory demyelinating polyneuropathy (CIDP) (Joshi et al., 2016). A better understanding of the signaling pathways that drive SC reprogramming and plasticity is of great interest and may offer new opportunities to enhance nerve repair. SCs are the main effectors of regeneration in many peripheral diseases and recent studies clearly positioned SCs at the hub for organizing the environment to clear myelin debris, promote axonal regrowth, remyelination and allow complete functional repair following injury (Zochodne, 2012; Kim et al., 2013).

The different signaling pathways and molecular components described in the present review represent interesting targets to boost the endogenous regeneration potential of SCs. For instance, the treatment with different Nrg1 isoforms or strategies to stimulate ErbB signaling have actually been shown to improve myelin clearance, axon regeneration, remyelination and functional recovery after nerve injury in different studies (Chen et al., 1998; Joung et al., 2010; Fricker and Bennett, 2011; Yildiz et al., 2011). In a CMT1A rat model, soluble Nrg1 therapy during early postnatal life prevents abnormal developmental demyelination and subsequent axon loss observed in adulthood (Fledrich et al., 2014). The overexpression of Nrg1 in mouse models of amyotrophic lateral sclerosis (ALS) and partial muscle denervation improves functional recovery by enhancing collateral reinnervation sprouting through both Akt and Erk pathways (Mancuso et al., 2016). Notch activation through the addition of a recombinant jagged1 after injury also promotes nerve regeneration and functional recovery (Wang et al., 2015). The inhibition of mTOR signaling with rapamycin in mice that lack PTEN and develop a tomaculous neuropathy significantly ameliorates the pathology (Goebbels et al., 2012). Finally, stimulating TLR signaling at the site of the lesion accelerates myelin clearance and functional recovery (Boivin et al., 2007).

Additional molecules, not directly linked to pathways analyzed in this review, have been shown to regulate SC differentiation/dedifferentiation and improve nerve repair. For example, Fingolimod, an agonist of the sphingosine-1-phosphate receptor (S1PR), previously known to affect SC migration and myelination *in vitro* and currently in clinical trial for the treatment of CIDP, has been demonstrated to modulate SC plasticity (Köhne et al., 2012; Heinen et al., 2015). Fingolimod activates different dedifferentiation markers such as c-Jun, increases the expression of growth factors, slows myelination and improves axon regeneration. Therefore, Fingolimod supports the generation of a repair promoting cellular phenotype and could be used for the treatment of peripheral nerve damages and diseases (Heinen et al., 2015). Its mechanism of action, however, still remains to be elucidated. Another recent example is the addition of TGF-β1 and forskolin directly on chronically injured nerves that can reactivate the growth-supportive environment through the reprogramming of chronically denervated SCs, the re-induction of their proliferation, and the re-expression of regeneration-associated proteins (Sulaiman and Nguyen, 2016). Immunoglobulins (IVIG) are another therapeutic strategy widely used to treat immune-mediated neuropathies such as CIDP. Tzekova and colleagues demonstrated that IVIG positively influence SC differentiation and maturation and increase their potential to induce axonal outgrowth (Tzekova et al., 2015).

Other approaches that are based on SC regenerative properties and improve nerve repair can also be addressed. First, exercise and electrical stimulation have been demonstrated to promote SC-driven peripheral nerve regeneration in both animal models and in human patients (Gordon and English, 2016). Second, transplantations of SCs from healthy nerves or engineered from different tissues thanks to the emergence of the induced pluripotent stem cell technology are another interesting method to support nerve healing (Zhou and Notterpek, 2016). Actually, numerous SC-based therapies also exist to promote repair in the lesioned CNS (Matsas et al., 2008). Third, there has been major progress in developing biomaterials that improve regeneration by providing trophic factors or by supporting the regenerative functions of transplanted cells *in situ* (Marquardt and Sakiyama-Elbert, 2013). For example, Liu and colleagues recently showed that Salidroside and tissue engineering using SCs and poly lactic-co-glycolic acid promote peripheral nerve regeneration and functional recovery after sciatic nerve transection in rats. Salidroside increases the proliferation and regenerative function of SCs, probably through the modulation of neurotrophic factors (Liu et al., 2017). Fourth, gene therapy that allows to deliver genetic material directly into somatic cells is another option to treat neuropathies that involve gene mutations or to improve nerve regeneration after injuries (Zhou and Notterpek, 2016). In hereditary diseases including CMTs, loss or gain of function mutations could be restored through the re-expression of the absent or non-functional protein or through the down-regulation of the mutant mRNA via RNA interference strategy, respectively. For example, Kagiava and coworkers recently demonstrated that the intrathecal injection of a lentiviral vector with a myelin-specific promoter restored the expression of a neuropathy-associated gene and rescued a model of demyelinating peripheral neuropathy (Kagiava et al., 2016). Also, other studies based on gene therapy in order to improve nerve regeneration used lentiviral vectors that potentiate the therapeutic functions of SCs transplanted in artificial nerves, in autografts or present in damaged nerves (Hoyng et al., 2015). Even if SCs are known to mainly support nerve repair through an enhanced expression of neurotrophic factors that stimulate axon regeneration and myelination, this review highlights the

numerous additional roles and regenerative functions of SCs in nerve injuries and in demyelinating diseases. Therefore, targeting the molecular mechanisms that regulate SC reprogramming by gene therapy can be highly promising to stimulate nerve healing. In the future, the challenges will be to optimize gene therapy in order to specifically target SCs and to create safe and regulatable vectors to potentiate their regenerative functions in the appropriate timings. Lipid-based nanoparticles such as liposomes or extracellular vesicles are other valuable tools for the delivery of small molecules or genes that can modulate signaling pathways and promote nerve repair (Takeda and Xu, 2015). In order to selectively introduce material into SCs, Lee and colleagues developed phospholipid-based liposomes that can enter SCs when injected in tail vein and showed that the nanoparticles escape the endogenous degradative mechanisms *in vitro* (Lee et al., 2013). In the following years, it is expected that the improvements in cell and tissue engineering and in approaches that target SC capacity to promote regeneration will lead to the development of innovative and efficient PNS repair strategies.

The different therapeutic options that are built on or that stimulate SC plasticity represent new avenues for nerve regeneration but should be considered with prudence for different reasons. First, a prolonged stimulation of SC dedifferentiation could disrupt the remyelination of the regenerated axons, necessary for rapid nerve conduction and complete functional recovery. Also, the aberrant activation of some pathways including Notch, NF-κB, Ras/Raf/Erk, Rac/JNK, or Nrg1/ErbB can lead to abnormal cell proliferation and the development of peripheral nerve tumors. The better understanding of the molecular mechanisms regulating SC plasticity is thus necessary to set up therapies that modulate both temporally and quantitatively SC capacity to drive nerve repair without affecting remyelination and increasing the chances of triggering tumor development.

CONCLUSIONS

The remarkable capacity of regeneration of the PNS compared to the CNS is mainly due to the fantastic plasticity of SCs. The molecular components involved in the negative regulation of myelination and in the reprogramming of SCs in response to nerve injury provide important mechanistic insights and new therapeutic approaches into peripheral neuropathies as well as in peripheral nerve regeneration. However, this review demonstrates the complexity of the molecular signaling pathways and reveals that little is known about the interactions between them. Moreover, the temporal and quantitative activation of the different signals identified is of great importance but is not completely elucidated. Future studies are thus required to better understand the cross-talks, networks and activation patterns and timings between the different molecular mechanisms controlling SC plasticity.

AUTHOR CONTRIBUTIONS

Manuscript writing: AB; Manuscript revision: VD, AC, and RF.

ACKNOWLEDGMENTS

This work was supported by Grants from the FSR-FNRS, the Fonds Léon Fredericq, the Special Funds of the University of Liège, the Fondation Charcot and the Association Belge contre les Maladies Neuro-Musculaires.

REFERENCES

Agthong, S., Kaewsema, A., Tanomsridejchai, N., and Chentanez, V. (2006). Activation of MAPK ERK in peripheral nerve after injury. *BMC Neurosci.* 7:45. doi: 10.1186/1471-2202-7-45

Ammoun, S., Flaiz, C., Ristic, N., Schuldt, J., and Hanemann, C. O. (2008). Dissecting and targeting the growth factor-dependent and growth factor-independent extracellular signal-regulated kinase pathway in human schwannoma. *Cancer Res.* 68, 5236–5245. doi: 10.1158/0008-5472.CAN-07-5849

Ammoun, S., Provenzano, L., Zhou, L., Barczyk, M., Evans, K., Hilton, D. A., et al. (2014). Axl/Gas6/NFκB signalling in schwannoma pathological proliferation, adhesion and survival. *Oncogene* 33, 336–346. doi: 10.1038/onc.2012.587

Andorfer, B., Kieseier, B. C., Mathey, E., Armati, P., Pollard, J., Oka, N., et al. (2001). Expression and distribution of transcription factor NF-κB and inhibitor IκB in the inflamed peripheral nervous system. *J. Neuroimmunol.* 116, 226–232. doi: 10.1016/S0165-5728(01)00306-X

Anliker, B., Choi, J. W., Lin, M.-E., Gardell, S. E., Rivera, R. R., Kennedy, G., et al. (2013). Lysophosphatidic acid (LPA) and its receptor, LPA1, influence embryonic schwann cell migration, myelination, and cell-to-axon segregation. *Glia* 61, 2009–2022. doi: 10.1002/glia.22572

Apra, C., Richard, L., Coulpier, F., Blugeon, C., Gilardi-Hebenstreit, P., Vallat, J., et al. (2012). Cthrc1 is a negative regulator of myelination in Schwann cells. *Glia* 60, 393–403. doi: 10.1002/glia.22273

Arthur-Farraj, P. J., Latouche, M., Wilton, D. K., Quintes, S., Chabrol, E., Banerjee, A., et al. (2012). c-Jun reprograms Schwann cells of injured nerves to generate a repair cell essential for regeneration. *Neuron* 75, 633–647. doi: 10.1016/j.neuron.2012.06.021

Arthur-Farraj, P., Wanek, K., Hantke, J., Davis, C. M., Jayakar, A., Parkinson, D. B., et al. (2011). Mouse schwann cells need both NRG1 and cyclic AMP to myelinate. *Glia* 59, 720–733. doi: 10.1002/glia.21144

Atanasoski, S., Scherer, S. S., Sirkowski, E., Leone, D., Garratt, A. N., Birchmeier, C., et al. (2006). ErbB2 signaling in Schwann cells is mostly dispensable for maintenance of myelinated peripheral nerves and proliferation of adult Schwann cells after injury. *J. Neurosci.* 26, 2124–2131. doi: 10.1523/JNEUROSCI.4594-05.2006

Barrette, B., Hébert, M.-A., Filali, M., Lafortune, K., Vallières, N., Gowing, G., et al. (2008). Requirement of myeloid cells for axon regeneration. *J. Neurosci.* 28, 9363–9376. doi: 10.1523/JNEUROSCI.1447-08.2008

Beirowski, B., Babetto, E., Golden, J. P., Chen, Y.-J., Yang, K., Gross, R. W., et al. (2014). Metabolic regulator LKB1 plays a crucial role in Schwann cell-mediated axon maintenance. *Nat. Neurosci.* 17, 1351–1361. doi: 10.1038/nn.3809

Boivin, A., Pineau, I., Barrette, B., Filali, M., Vallières, N., Rivest, S., et al. (2007). Toll-like receptor signaling is critical for wallerian degeneration and functional recovery after peripheral nerve injury. *J. Neurosci.* 27, 12565–12576. doi: 10.1523/JNEUROSCI.3027-07.2007

Bolino, A., Bolis, A., Previtali, S. C., Dina, G., Bussini, S., Dati, G., et al. (2004). Disruption of Mtmr2 produces CMT4B1-like neuropathy with myelin outfolding and impaired spermatogenesis. *J. Cell Biol.* 167, 711–721. doi: 10.1083/jcb.200407010

Boyd, J. G., and Gordon, T. (2003). Glial cell line-derived neurotrophic factor and brain-derived neurotrophic factor sustain the axonal regeneration of chronically axotomized motoneurons *in vivo*. *Exp. Neurol.* 183, 610–619. doi: 10.1016/S0014-4886(03)00183-3

Carroll, S. L., Miller, M. L., Frohnert, P. W., Kim, S. S., and Corbett, J. A. (1997). Expression of neuregulins and their putative receptors, ErbB2 and ErbB3, is induced during Wallerian degeneration. *J. Neurosci.* 17, 1642–1659.

Cattin, A.-L., Burden, J. J., Van Emmenis, L., Mackenzie, F. E., Hoving, J. J. A., Calavia, N. G., et al. (2015). Macrophage-induced blood vessels guide Schwann cell-mediated regeneration of peripheral nerves. *Cell* 162, 1127–1139. doi: 10.1016/j.cell.2015.07.021

Cattin, A.-L., and Lloyd, A. C. (2016). The multicellular complexity of peripheral nerve regeneration. *Curr. Opin. Neurobiol.* 39, 38–46. doi: 10.1016/j.conb.2016.04.005

Chaballe, L., Close, P., Sempels, M., Delstanche, S., Fanielle, J., Moons, L., et al. (2011). Involvement of placental growth factor in Wallerian degeneration. *Glia* 59, 379–396. doi: 10.1002/glia.21108

Chen, L. E., Liu, K., Seaber, A. V., Katragadda, S., Kirk, C., and Urbaniak, J. R. (1998). Recombinant human glial growth factor 2 (rhGGF2) improves functional recovery of crushed peripheral nerve (a double-blind study). *Neurochem. Int.* 33, 341–351. doi: 10.1016/S0197-0186(98)00037-0

Chen, M.-S., Kim, H., Jagot-Lacoussiere, L., and Maurel, P. (2016). Cadm3 (Necl-1) interferes with the activation of the PI3 kinase/Akt signaling cascade and inhibits Schwann cell myelination *in vitro*. *Glia* 64, 2247–2262. doi: 10.1002/glia.23072

Chen, S., Velardez, M. O., Warot, X., Yu, Z.-X., Miller, S. J., Cros, D., et al. (2006). Neuregulin 1-erbB signaling is necessary for normal myelination and sensory function. *J. Neurosci.* 26, 3079–3086. doi: 10.1523/JNEUROSCI.3785-05.2006

Chen, Y., Guo, W., Xu, L., Li, W., Cheng, M., Hu, Y., et al. (2016a). 17β-Estradiol promotes Schwann cell proliferation and differentiation, accelerating early remyelination in a mouse peripheral nerve injury model. *BioMed Res. Int.* 2016:7891202. doi: 10.1155/2016/7891202

Chen, Y., Wang, H., Yoon, S. O., Xu, X., Hottiger, M. O., Svaren, J., et al. (2011). HDAC-mediated deacetylation of NF-[κ] B is critical for Schwann cell myelination. *Nat. Neurosci.* 14, 437–441. doi: 10.1038/nn.2780

Chen, Y., Weng, J., Han, D., Chen, B., Ma, M., Yu, Y., et al. (2016b). GSK3β inhibition accelerates axon debris clearance and new axon remyelination. *Am. J. Transl. Res.* 8, 5410–5420.

Chen, Z.-L., Yu, W.-M., and Strickland, S. (2007). Peripheral Regeneration. *Annu. Rev. Neurosci.* 30, 209–233. doi: 10.1146/annurev.neuro.30.051606.094337

Cotter, L., Ozcelik, M., Jacob, C., Pereira, J. A., Locher, V., Baumann, R., et al. (2010). Dlg1-PTEN interaction regulates myelin thickness to prevent damaging peripheral nerve overmyelination. *Science* 328, 1415–1418. doi: 10.1126/science.1187735

Dilwali, S., Briët, M. C., Kao, S.-Y., Fujita, T., Landegger, L. D., Platt, M. P., et al. (2015). Preclinical validation of anti-nuclear factor-κ B therapy to inhibit human vestibular schwannoma growth. *Mol. Oncol.* 9, 1359–1370. doi: 10.1016/j.molonc.2015.03.009

Doddrell, R. D. S., Dun, X., Moate, R. M., Jessen, K. R., Mirsky, R., and Parkinson, D. B. (2012). Regulation of Schwann cell differentiation and proliferation by the Pax-3 transcription factor. *Glia* 60, 1269–1278. doi: 10.1002/glia.22346

Fallon, K. B., Havlioglu, N., Hamilton, L. H., Cheng, T. P. H., and Carroll, S. L. (2004). Constitutive activation of the neuregulin-1/erbB signaling pathway promotes the proliferation of a human peripheral neuroepithelioma cell line. *J. Neurooncol.* 66, 273–284. doi: 10.1023/B:NEON.0000014521.28294.84

Falls, D. L. (2003). Neuregulins: functions, forms, and signaling strategies. *Exp. Cell Res.* 284, 14–30. doi: 10.1016/S0014-4827(02)00102-7

Farah, M. H., Pan, B. H., Hoffman, P. N., Ferraris, D., Tsukamoto, T., Nguyen, T., et al. (2011). Reduced BACE1 activity enhances clearance of myelin debris and regeneration of axons in the injured peripheral nervous system. *J. Neurosci.* 31, 5744–5754. doi: 10.1523/JNEUROSCI.6810-10.2011

Fernandez-Valle, C., Bunge, R. P., and Bunge, M. B. (1995). Schwann cells degrade myelin and proliferate in the absence of macrophages: evidence from *in vitro* studies of Wallerian degeneration. *J. Neurocytol.* 24, 667–679. doi: 10.1007/BF01179817

Fledrich, R., Stassart, R. M., Klink, A., Rasch, L. M., Prukop, T., Haag, L., et al. (2014). Soluble neuregulin-1 modulates disease pathogenesis in rodent models of Charcot-Marie-Tooth disease 1A. *Nat. Med.* 20, 1055–1061. doi: 10.1038/nm.3664

Flores, A. I., Narayanan, S. P., Morse, E. N., Shick, H. E., Yin, X., Kidd, G., et al. (2008). Constitutively active Akt induces enhanced myelination in the CNS. *J. Neurosci.* 28, 7174–7183. doi: 10.1523/JNEUROSCI.0150-08.2008

Fontana, X., Hristova, M., Da Costa, C., Patodia, S., Thei, L., Makwana, M., et al. (2012). c-Jun in Schwann cells promotes axonal regeneration and motoneuron survival via paracrine signaling. *J. Cell Biol.* 198, 127–141. doi: 10.1083/jcb.201205025

Freidin, M., Asche, S., Bargiello, T. A., Bennett, M. V. L., and Abrams, C. K. (2009). Connexin 32 increases the proliferative response of Schwann cells to neuregulin-1 (Nrg1). *Proc. Natl. Acad. Sci. U.S.A.* 106, 3567–3572. doi: 10.1073/pnas.0813413106

Fricker, F. R., Antunes-Martins, A., Galino, J., Paramsothy, R., La Russa, F., Perkins, J., et al. (2013). Axonal neuregulin 1 is a rate limiting but not essential factor for nerve remyelination. *Brain* 136, 2279–2297. doi: 10.1093/brain/awt148

Fricker, F. R., and Bennett, D. L. (2011). The role of neuregulin-1 in the response to nerve injury. *Future Neurol.* 6, 809–822. doi: 10.2217/fnl.11.45

Fricker, F. R., Lago, N., Balarajah, S., Tsantoulas, C., Tanna, S., Zhu, N., et al. (2011). Axonally derived neuregulin-1 is required for remyelination and regeneration after nerve injury in adulthood. *J. Neurosci.* 31, 3225–3233. doi: 10.1523/JNEUROSCI.2568-10.2011

Frohnert, P. W., Stonecypher, M. S., and Carroll, S. L. (2003). Constitutive activation of the neuregulin-1/ErbB receptor signaling pathway is essential for the proliferation of a neoplastic Schwann cell line. *Glia* 43, 104–118. doi: 10.1002/glia.10232

Fu, E. S., Zhang, Y. P., Sagen, J., Candiotti, K. A., Morton, P. D., Liebl, D. J., et al. (2010). Transgenic inhibition of glial NF-κB reduces pain behavior and inflammation after peripheral nerve injury. *Pain* 148, 509–518. doi: 10.1016/j.pain.2010.01.001

Fu, S. Y., and Gordon, T. (1995). Contributing factors to poor functional recovery after delayed nerve repair: prolonged axotomy. *J. Neurosci.* 15, 3876–3885.

Gao, X., Daugherty, R. L., and Tourtellotte, W. G. (2007). Regulation of low affinity neurotrophin receptor (p75NTR) by early growth response (Egr) transcriptional regulators. *Mol. Cell. Neurosci.* 36, 501–514. doi: 10.1016/j.mcn.2007.08.013

Gaudet, A. D., Popovich, P. G., and Ramer, M. S. (2011). Wallerian degeneration: gaining perspective on inflammatory events after peripheral nerve injury. *J. Neuroinflammation* 8:110. doi: 10.1186/1742-2094-8-110

Gess, B., Halfter, H., Kleffner, I., Monje, P., Athauda, G., Wood, P. M., et al. (2008). Inhibition of N-cadherin and beta-catenin function reduces axon-induced Schwann cell proliferation. *J. Neurosci. Res.* 86, 797–812. doi: 10.1002/jnr.21528

Goebbels, S., Oltrogge, J. H., Kemper, R., Heilmann, I., Bormuth, I., Wolfer, S., et al. (2010). Elevated phosphatidylinositol 3,4,5-trisphosphate in glia triggers cell-autonomous membrane wrapping and myelination. *J. Neurosci.* 30, 8953–8964. doi: 10.1523/JNEUROSCI.0219-10.2010

Goebbels, S., Oltrogge, J. H., Wolfer, S., Wieser, G. L., Nientiedt, T., Pieper, A., et al. (2012). Genetic disruption of Pten in a novel mouse model of tomaculous neuropathy. *EMBO Mol. Med.* 4, 486–499. doi: 10.1002/emmm.201200227

Goethals, S., Ydens, E., Timmerman, V., and Janssens, S. (2010). Toll-like receptor expression in the peripheral nerve. *Glia* 58, 1701–1709. doi: 10.1002/glia.21041

Gomez-Sanchez, J. A., Carty, L., Iruarrizaga-Lejarreta, M., Palomo-Irigoyen, M., Varela-Rey, M., Griffith, M., et al. (2015). Schwann cell autophagy, myelinophagy, initiates myelin clearance from injured nerves. *J. Cell Biol.* 210, 153–168. doi: 10.1083/jcb.201503019

Gordon, T., and English, A. W. (2016). Strategies to promote peripheral nerve regeneration: electrical stimulation and/or exercise. *Eur. J. Neurosci.* 43, 336–350. doi: 10.1111/ejn.13005

Grigoryan, T., and Birchmeier, W. (2015). Molecular signaling mechanisms of axon-glia communication in the peripheral nervous system. *Bioessays* 37, 502–513. doi: 10.1002/bies.201400172

Grigoryan, T., Stein, S., Qi, J., Wende, H., Garratt, A. N., Nave, K.-A., et al. (2013). Wnt/Rspondin/beta-catenin signals control axonal sorting and lineage progression in Schwann cell development. *Proc. Natl. Acad. Sci. U.S.A.* 110, 18174–18179. doi: 10.1073/pnas.1310490110

Grossmann, K. S., Wende, H., Paul, F. E., Cheret, C., Garratt, A. N., Zurborg, S., et al. (2009). The tyrosine phosphatase Shp2 (PTPN11) directs Neuregulin-1/ErbB signaling throughout Schwann cell development. *Proc. Natl. Acad. Sci. U.S.A.* 106, 16704–16709. doi: 10.1073/pnas.0904336106

Guertin, A. D., Zhang, D. P., Mak, K. S., Alberta, J. A., and Kim, H. A. (2005). Microanatomy of axon/glial signaling during Wallerian degeneration. *J. Neurosci.* 25, 3478–3487. doi: 10.1523/JNEUROSCI.3766-04.2005

Hantke, J., Carty, L., Wagstaff, L. J., Turmaine, M., Wilton, D. K., Quintes, S., et al. (2014). c-Jun activation in Schwann cells protects against loss of sensory axons in inherited neuropathy. *Brain* 137, 2922–2937. doi: 10.1093/brain/awu257

Hardie, D. G., Ross, F. A., and Hawley, S. A. (2012). AMPK: a nutrient and energy sensor that maintains energy homeostasis. *Nat. Rev. Mol. Cell Biol.* 13, 251–262. doi: 10.1038/nrm3311

Hari, L., Brault, V., Kleber, M., Lee, H.-Y., Ille, F., Leimeroth, R., et al. (2002). Lineage-specific requirements of beta-catenin in neural crest development. *J. Cell Biol.* 159, 867–880. doi: 10.1083/jcb.200209039

Harrisingh, M. C., Perez-Nadales, E., Parkinson, D. B., Malcolm, D. S., Mudge, A. W., and Lloyd, A. C. (2004). The Ras/Raf/ERK signalling pathway drives Schwann cell dedifferentiation. *EMBO J.* 23, 3061–3071. doi: 10.1038/sj.emboj.7600309

He, Y., Kim, J. Y., Dupree, J., Tewari, A., Melendez-Vasquez, C., Svaren, J., et al. (2010). Yy1 as a molecular link between neuregulin and transcriptional modulation of peripheral myelination. *Nat. Neurosci.* 13, 1472–1480. doi: 10.1038/nn.2686

Heinen, A., Beyer, F., Tzekova, N., Hartung, H.-P., and Küry, P. (2015). Fingolimod induces the transition to a nerve regeneration promoting Schwann cell phenotype. *Exp. Neurol.* 271, 25–35. doi: 10.1016/j.expneurol.2015.05.002

Heinen, A., Kremer, D., Göttle, P., Kruse, F., Hasse, B., Lehmann, H., et al. (2008). The cyclin-dependent kinase inhibitor p57kip2 is a negative regulator of Schwann cell differentiation and *in vitro* myelination. *Proc. Natl. Acad. Sci. U.S.A.* 105, 8748–8753. doi: 10.1073/pnas.0802659105

Heinen, A., Lehmann, H. C., and Küry, P. (2013). Negative regulators of Schwann cell differentiation—novel targets for peripheral nerve therapies? *J. Clin. Immunol.* 33, 18–26. doi: 10.1007/s10875-012-9786-9

Heinen, A., Tzekova, N., Graffmann, N., Torres, K. J., Uhrberg, M., Hartung, H.-P., et al. (2012). Histone methyltransferase enhancer of zeste homolog 2 regulates Schwann cell differentiation. *Glia* 60, 1696–1708. doi: 10.1002/glia.22388

Hichor, M., Sampathkumar, N. K., Montanaro, J., Borderie, D., Petit, P. X., Gorgievski, V., et al. (2016). Paraquat induces peripheral myelin disruption and locomotor defects: crosstalk with LXR and Wnt pathways. *Antioxid. Redox Signal.* doi: 10.1089/ars.2016.6711. [Epub ahead of print].

Hirata, K., and Kawabuchi, M. (2002). Myelin phagocytosis by macrophages and nonmacrophages during Wallerian degeneration. *Microsc. Res. Tech.* 57, 541–547. doi: 10.1002/jemt.10108

Hoyng, S. A., de Winter, F., Tannemaat, M. R., Blits, B., Malessy, M. J. A., and Verhaagen, J. (2015). Gene therapy and peripheral nerve repair: a perspective. *Front. Mol. Neurosci.* 8:32. doi: 10.3389/fnmol.2015.00032

Hu, X., He, W., Diaconu, C., Tang, X., Kidd, G. J., Macklin, W. B., et al. (2008). Genetic deletion of BACE1 in mice affects remyelination of sciatic nerves. *FASEB J.* 22, 2970–2980. doi: 10.1096/fj.08-106666

Huijbregts, R. P. H., Roth, K. A., Schmidt, R. E., and Carroll, S. L. (2003). Hypertrophic neuropathies and malignant peripheral nerve sheath tumors in transgenic mice overexpressing glial growth factor beta3 in myelinating Schwann cells. *J. Neurosci.* 23, 7269–7280.

Hutton, E. J., Carty, L., Laurá, M., Houlden, H., Lunn, M., Brandner, S., et al. (2011). c-Jun expression in human neuropathies: a pilot study. *J. Peripher. Nerv. Syst.* 16, 295–303. doi: 10.1111/j.1529-8027.2011.00360.x

Jessen, K. R., and Mirsky, R. (2005). The origin and development of glial cells in peripheral nerves. *Nat. Rev. Neurosci.* 6, 671–682. doi: 10.1038/nrn1746

Jessen, K. R., and Mirsky, R. (2008). Negative regulation of myelination: relevance for development, injury, and demyelinating disease. *Glia* 56, 1552–1565. doi: 10.1002/glia.20761

Jessen, K. R., and Mirsky, R. (2016). The repair Schwann cell and its function in regenerating nerves. *J. Physiol.* 594, 3521–3531. doi: 10.1113/jp270874

Jessen, K. R., Mirsky, R., and Lloyd, A. C. (2015). Schwann cells: development and role in nerve repair. *Cold Spring Harb. Perspect. Biol.* 7:a020487. doi: 10.1101/cshperspect.a020487

Ji, Y., Tao, T., Cheng, C., Yang, H., Wang, Y., Yang, J., et al. (2010). SSeCKS is a suppressor in Schwann cell differentiation and myelination. *Neurochem. Res.* 35, 219–226. doi: 10.1007/s11064-009-0045-2

Joshi, A. R., Holtmann, L., Bobylev, I., Schneider, C., Ritter, C., Weis, J., et al. (2016). Loss of Schwann cell plasticity in chronic inflammatory demyelinating polyneuropathy (CIDP). *J. Neuroinflammation* 13, 255. doi: 10.1186/s12974-016-0711-7

Joung, I., Yoo, M., Woo, J. H., Chang, C. Y., Heo, H., and Kwon, Y. K. (2010). Secretion of EGF-like domain of heregulinbeta promotes axonal growth and functional recovery of injured sciatic nerve. *Mol. Cells* 30, 477–484. doi: 10.1007/s10059-010-0137-5

Jung, J., Cai, W., Lee, H. K., Pellegatta, M., Shin, Y. K., Jang, S. Y., et al. (2011). Actin polymerization is essential for myelin sheath fragmentation during Wallerian degeneration. *J. Neurosci.* 31, 2009–2015. doi: 10.1523/JNEUROSCI.4537-10.2011

Kaempchen, K., Mielke, K., Utermark, T., Langmesser, S., and Hanemann, C. O. (2003). Upregulation of the Rac1/JNK signaling pathway in primary human schwannoma cells. *Hum. Mol. Genet.* 12, 1211–1221. doi: 10.1093/hmg/ddg146

Kagiava, A., Sargiannidou, I., Theophilidis, G., Karaiskos, C., Richter, J., Bashiardes, S., et al. (2016). Intrathecal gene therapy rescues a model of demyelinating peripheral neuropathy. *Proc. Natl. Acad. Sci. U.S.A.* 113, E2421–E2429. doi: 10.1073/pnas.1522202113

Keng, V. W., Rahrmann, E. P., Watson, A. L., Tschida, B. R., Moertel, C. L., Jessen, W. J., et al. (2012). PTEN and NF1 inactivation in Schwann cells produces a severe phenotype in the peripheral nervous system that promotes the development and malignant progression of peripheral nerve sheath tumors. *Cancer Res.* 72, 3405–3413. doi: 10.1158/0008-5472.CAN-11-4092

Kim, H. A., Mindos, T., and Parkinson, D. B. (2013). Plastic fantastic: Schwann cells and repair of the peripheral nervous system. *Stem Cells Transl. Med.* 2, 553–557. doi: 10.5966/sctm.2013-0011

Kim, H. A., Pomeroy, S. L., Whoriskey, W., Pawlitzky, I., Benowitz, L. I., Sicinski, P., et al. (2000). A developmentally regulated switch directs regenerative growth of Schwann cells through cyclin D1. *Neuron* 26, 405–416. doi: 10.1016/S0896-6273(00)81173-3

Kioussi, C., Gross, M. K., and Gruss, P. (1995). Pax3: a paired domain gene as a regulator in PNS myelination. *Neuron* 15, 553–562. doi: 10.1016/0896-6273(95)90144-2

Klein, D., Groh, J., Wettmarshausen, J., and Martini, R. (2014). Nonuniform molecular features of myelinating Schwann cells in models for CMT1: distinct disease patterns are associated with NCAM and c-Jun upregulation. *Glia* 62, 736–750. doi: 10.1002/glia.22638

Köhne, A., Stettner, M., Jangouk, P., Dehmel, T., Hartung, H.-P., Lehmann, H. C., et al. (2012). Fingolimod impedes Schwann cell-mediated myelination: implications for the treatment of immune neuropathies? *Arch. Neurol.* 69, 1280–1289. doi: 10.1001/archneurol.2012.394

Kwon, Y. K., Bhattacharyya, A., Alberta, J. A., Giannobile, W. V., Cheon, K., Stiles, C. D., et al. (1997). Activation of ErbB2 during wallerian degeneration of sciatic nerve. *J. Neurosci.* 17, 8293–8299.

La Marca, R., Cerri, F., Horiuchi, K., Bachi, A., Feltri, M. L., Wrabetz, L., et al. (2011). TACE (ADAM17) inhibits Schwann cell myelination. *Nat. Neurosci.* 14, 857–865. doi: 10.1038/nn.2849

Laura, M., Mazzeo, A., Aguennouz, M., Santoro, M., Catania, M. A., Migliorato, A., et al. (2006). Immunolocalization and activation of nuclear factor-κB in the sciatic nerves of rats with experimental autoimmune neuritis. *J. Neuroimmunol.* 174, 32–38. doi: 10.1016/j.jneuroim.2006.01.004

Le, N., Nagarajan, R., Wang, J. Y. T., Araki, T., Schmidt, R. E., and Milbrandt, J. (2005). Analysis of congenital hypomyelinating Egr2Lo/Lo nerves identifies Sox2 as an inhibitor of Schwann cell differentiation and myelination. *Proc. Natl. Acad. Sci. U.S.A.* 102, 2596–2601. doi: 10.1073/pnas.0407836102

Lee, H., Jo, E.-K., Choi, S.-Y., Oh, S. B., Park, K., Soo Kim, J., et al. (2006). Necrotic neuronal cells induce inflammatory Schwann cell activation via TLR2 and TLR3: implication in Wallerian degeneration. *Biochem. Biophys. Res. Commun.* 350, 742–747. doi: 10.1016/j.bbrc.2006.09.108

Lee, H. J., Shin, Y. K., and Park, H. T. (2014). Mitogen activated protein kinase family proteins and c-jun signaling in injury-induced Schwann cell plasticity. *Exp. Neurobiol.* 23, 130–137. doi: 10.5607/en.2014.23.2.130

Lee, H.-Y., Kleber, M., Hari, L., Brault, V., Suter, U., Taketo, M. M., et al. (2004). Instructive role of Wnt/beta-catenin in sensory fate specification in neural crest stem cells. *Science* 303, 1020–1023. doi: 10.1126/science.1091611

Lee, S., Ashizawa, A. T., Kim, K. S., Falk, D. J., and Notterpek, L. (2013). Liposomes to target peripheral neurons and Schwann cells. *PLoS ONE* 8:e78724. doi: 10.1371/journal.pone.0078724

Lee, Y. I., Li, Y., Mikesh, M., Smith, I., Nave, K.-A., Schwab, M. H., et al. (2016). Neuregulin1 displayed on motor axons regulates terminal Schwann cell-mediated synapse elimination at developing neuromuscular junctions. *Proc. Natl. Acad. Sci. U.S.A.* 113, E479–E487. doi: 10.1073/pnas.1519156113

Leimeroth, R., Lobsiger, C., Lussi, A., Taylor, V., Suter, U., and Sommer, L. (2002). Membrane-bound neuregulin1 type III actively promotes Schwann cell differentiation of multipotent Progenitor cells. *Dev. Biol.* 246, 245–258. doi: 10.1006/dbio.2002.0670

Leoni, V., Masterman, T., Diczfalusy, U., De Luca, G., Hillert, J., and Björkhem, I. (2002). Changes in human plasma levels of the brain specific oxysterol 24S-hydroxycholesterol during progression of multiple sclerosis. *Neurosci. Lett.* 331, 163–166. doi: 10.1016/S0304-3940(02)00887-X

Li, H., Wigley, C., and Hall, S. M. (1998). Chronically denervated rat Schwann cells respond to GGF *in vitro*. *Glia* 24, 290–303.

Li, Y., Rao, P. K., Wen, R., Song, Y., Muir, D., Wallace, P., et al. (2004). Notch and Schwann cell transformation. *Oncogene* 23, 1146–1152. doi: 10.1038/sj.onc.1207068

Li, Y., Tennekoon, G. I., Birnbaum, M., Marchionni, M. A., and Rutkowski, J. L. (2001). Neuregulin signaling through a PI3K/Akt/Bad pathway in Schwann cell survival. *Mol. Cell. Neurosci.* 17, 761–767. doi: 10.1006/mcne.2000.0967

Limpert, A. S., and Carter, B. D. (2010). Axonal neuregulin 1 type III activates NF-κB in Schwann cells during myelin formation. *J. Biol. Chem.* 285, 16614–16622. doi: 10.1074/jbc.M109.098780

Liu, H., Lv, P., Zhu, Y., Wu, H., Zhang, K., Xu, F., et al. (2017). Salidroside promotes peripheral nerve regeneration based on tissue engineering strategy using Schwann cells and PLGA: *in vitro* and *in vivo*. *Sci. Rep.* 7:39869. doi: 10.1038/srep39869

Liu, X., Peng, S., Zhao, Y., Zhao, T., Wang, M., Luo, L., et al. (2016a). AMPK negatively regulates peripheral myelination via activation of c-Jun. *Mol. Neurobiol.* doi: 10.1007/s12035-016-9913-3. [Epub ahead of print].

Liu, X., Zhao, Y., Peng, S., Zhang, S., Wang, M., Chen, Y., et al. (2016b). BMP7 retards peripheral myelination by activating p38 MAPK in Schwann cells. *Sci. Rep.* 6:31049. doi: 10.1038/srep31049

Lütjohann, D., Papassotiropoulos, A., Björkhem, I., Locatelli, S., Bagli, M., Oehring, R. D., et al. (2000). Plasma 24S-hydroxycholesterol (cerebrosterol) is increased in Alzheimer and vascular demented patients. *J. Lipid Res.* 41, 195–198.

Mager, G. M., Ward, R. M., Srinivasan, R., Jang, S.-W., Wrabetz, L., and Svaren, J. (2008). Active gene repression by the Egr2· NAB complex during peripheral nerve myelination. *J. Biol. Chem.* 283, 18187–18197. doi: 10.1074/jbc.M803330200

Mahanthappa, N. K., Anton, E. S., and Matthew, W. D. (1996). Glial growth factor 2, a soluble neuregulin, directly increases Schwann cell motility and indirectly promotes neurite outgrowth. *J. Neurosci.* 16, 4673–4683.

Makoukji, J., Meffre, D., Grenier, J., Liere, P., Lobaccaro, J.-M. A., Schumacher, M., et al. (2011). Interplay between LXR and Wnt/β-catenin signaling in the negative regulation of peripheral myelin genes by oxysterols. *J. Neurosci.* 31, 9620–9629. doi: 10.1523/JNEUROSCI.0761-11.2011

Mancuso, R., Martínez-Muriana, A., Leiva, T., Gregorio, D., Ariza, L., Morell, M., et al. (2016). Neuregulin-1 promotes functional improvement by enhancing collateral sprouting in SOD1(G93A) ALS mice and after partial muscle denervation. *Neurobiol. Dis.* 95, 168–178. doi: 10.1016/j.nbd.2016.07.023

Marquardt, L. M., and Sakiyama-Elbert, S. E. (2013). Engineering peripheral nerve repair. *Curr. Opin. Biotechnol.* 24, 887–892. doi: 10.1016/j.copbio.2013.05.006

Martini, R., Fischer, S., López-Vales, R., and David, S. (2008). Interactions between Schwann cells and macrophages in injury and inherited demyelinating disease. *Glia* 56, 1566–1577. doi: 10.1002/glia.20766

Matsas, R., Lavdas, A. A., Papastefanaki, F., and Thomaidou, D. (2008). Schwann cell transplantation for CNS repair. *Curr. Med. Chem.* 15, 151–160. doi: 10.2174/092986708783330593

Maurel, P., and Salzer, J. L. (2000). Axonal regulation of Schwann cell proliferation and survival and the initial events of myelination requires PI 3-kinase activity. *J. Neurosci.* 20, 4635–4645.

Michailov, G. V., Sereda, M. W., Brinkmann, B. G., Fischer, T. M., Haug, B., Birchmeier, C., et al. (2004). Axonal neuregulin-1 regulates myelin sheath thickness. *Science* 304, 700–703. doi: 10.1126/science.1095862

Mogha, A., D'Rozario, M., and Monk, K. R. (2016a). G protein-coupled receptors in myelinating glia. *Trends Pharmacol. Sci.* 37, 977–987. doi: 10.1016/j.tips.2016.09.002

Mogha, A., Harty, B., Carlin, D., Joseph, J., Sanchez, N., Suter, U., et al. (2016b). Gpr126/Adgrg6 has Schwann cell autonomous and nonautonomous functions in peripheral nerve injury and repair. *J. Neurosci.* 36, 12351–12367. doi: 10.1523/JNEUROSCI.3854-15.2016

Monje, P. V., Soto, J., Bacallao, K., and Wood, P. M. (2010). Schwann cell dedifferentiation is independent of mitogenic signaling and uncoupled to proliferation: role of cAMP and JNK in the maintenance of the differentiated state. *J. Biol. Chem.* 285, 31024–31036. doi: 10.1074/jbc.M110.116970

Monk, K. R., Naylor, S. G., Glenn, T. D., Mercurio, S., Perlin, J. R., Dominguez, C., et al. (2009). A G protein–coupled receptor is essential for Schwann cells to initiate myelination. *Science* 325, 1402–1405. doi: 10.1126/science.1173474.

Morris, J. K., Lin, W., Hauser, C., Marchuk, Y., Getman, D., and Lee, K. F. (1999). Rescue of the cardiac defect in ErbB2 mutant mice reveals essential roles of ErbB2 in peripheral nervous system development. *Neuron* 23, 273–283. doi: 10.1016/S0896-6273(00)80779-5

Morton, P. D., Dellarole, A., Theus, M. H., Walters, W. M., Berge, S. S., and Bethea, J. R. (2013). Activation of NF-κB in Schwann cells is dispensable for myelination *in vivo*. *J. Neurosci.* 33, 9932–9936. doi: 10.1523/JNEUROSCI.2483-12.2013

Morton, P. D., Johnstone, J. T., Ramos, A. Y., Liebl, D. J., Bunge, M. B., and Bethea, J. R. (2012). Nuclear factor-κB activation in Schwann cells regulates regeneration and remyelination. *Glia* 60, 639–650. doi: 10.1002/glia.22297

Napoli, I., Noon, L. A., Ribeiro, S., Kerai, A. P., Parrinello, S., Rosenberg, L. H., et al. (2012). A central role for the ERK-signaling pathway in controlling Schwann cell plasticity and peripheral nerve regeneration *in vivo*. *Neuron* 73, 729–742. doi: 10.1016/j.neuron.2011.11.031

Newbern, J., and Birchmeier, C. (2010). Nrg1/ErbB signaling networks in Schwann cell development and myelination. *Semin. Cell Dev. Biol.* 21, 922–928. doi: 10.1016/j.semcdb.2010.08.008

Newbern, J. M., Li, X., Shoemaker, S. E., Zhou, J., Zhong, J., Wu, Y., et al. (2011). Specific functions for ERK/MAPK signaling during PNS development. *Neuron* 69, 91–105. doi: 10.1016/j.neuron.2010.12.003

Newbern, J. M., and Snider, W. D. (2012). Bers-ERK Schwann cells coordinate nerve regeneration. *Neuron* 73, 623–626. doi: 10.1016/j.neuron.2012.02.002

Nickols, J. C., Valentine, W., Kanwal, S., and Carter, B. D. (2003). Activation of the transcription factor NF-κB in Schwann cells is required for peripheral myelin formation. *Nat. Neurosci.* 6, 161–167. doi: 10.1038/nn995

Nikam, S. S., Tennekoon, G. I., Christy, B. A., Yoshino, J. E., and Rutkowski, J. L. (1995). The zinc finger transcription factor Zif268/Egr-1 is essential for Schwann cell expression of the p75 NGF receptor. *Mol. Cell. Neurosci.* 6, 337–348. doi: 10.1006/mcne.1995.1026

Norrmén, C., Figlia, G., Lebrun-Julien, F., Pereira, J. A., Trötzmüller, M., Köfeler, H. C., et al. (2014). mTORC1 controls PNS myelination along the mTORC1-RXRγ-SREBP-lipid biosynthesis axis in Schwann cells. *Cell Rep.* 9, 646–660. doi: 10.1016/j.celrep.2014.09.001

Norrmén, C., and Suter, U. (2013). Akt/mTOR signalling in myelination. *Biochem. Soc. Trans.* 41, 944LP–950LP. doi: 10.1042/BST20130046

Noseda, R., Belin, S., Piguet, F., Vaccari, I., Scarlino, S., Brambilla, P., et al. (2013). DDIT4/REDD1/RTP801 is a novel negative regulator of Schwann cell myelination. *J. Neurosci.* 33, 15295–15305. doi: 10.1523/JNEUROSCI.2408-13.2013

Ogata, T., Iijima, S., Hoshikawa, S., Miura, T., Yamamoto, S., Oda, H., et al. (2004). Opposing extracellular signal-regulated kinase and Akt pathways control Schwann cell myelination. *J. Neurosci.* 24, 6724–6732. doi: 10.1523/JNEUROSCI.5520-03.2004

Painter, M. W., Brosius Lutz, A., Cheng, Y.-C., Latremoliere, A., Duong, K., Miller, C. M., et al. (2014). Diminished schwann cell repair responses underlie age-associated impaired axonal regeneration. *Neuron* 83, 331–343. doi: 10.1016/j.neuron.2014.06.016

Parkinson, D. B., Bhaskaran, A., Arthur-Farraj, P., Noon, L. A., Woodhoo, A., Lloyd, A. C., et al. (2008). c-Jun is a negative regulator of myelination. *J. Cell Biol.* 181, 625–637. doi: 10.1083/jcb.200803013

Parkinson, D. B., Bhaskaran, A., Droggiti, A., Dickinson, S., D'Antonio, M., Mirsky, R., et al. (2004). Krox-20 inhibits Jun-NH2-terminal kinase/c-Jun to control Schwann cell proliferation and death. *J. Cell Biol.* 164, 385–394. doi: 10.1083/jcb.200307132

Parkinson, D. B., Dong, Z., Bunting, H., Whitfield, J., Meier, C., Marie, H., et al. (2001). Transforming growth factor beta (TGFbeta) mediates Schwann cell

death *in vitro* and *in vivo*: examination of c-Jun activation, interactions with survival signals, and the relationship of TGFbeta-mediated death to Schwann cell differentiation. *J. Neurosci.* 21, 8572–8585.

Parrinello, S., Napoli, I., Ribeiro, S., Wingfield Digby, P., Fedorova, M., Parkinson, D. B., et al. (2010). EphB signaling directs peripheral nerve regeneration through Sox2-dependent Schwann cell sorting. *Cell* 143, 145–155. doi: 10.1016/j.cell.2010.08.039

Quintes, S., Brinkmann, B. G., Ebert, M., Frob, F., Kungl, T., Arlt, F. A., et al. (2016). Zeb2 is essential for Schwann cell differentiation, myelination and nerve repair. *Nat. Neurosci.* 19, 1050–1059. doi: 10.1038/nn.4321

Rameh, L. E., and Cantley, L. C. (1999). The role of phosphoinositide 3-kinase lipid products in cell function. *J. Biol. Chem.* 274, 8347–8350. doi: 10.1074/jbc.274.13.8347

Roberts, S. L., Dun, X.-p., Dee, G., Gray, B., Mindos, T., and Parkinson, D. B. (2016). The role of p38alpha in Schwann cells in regulating peripheral nerve myelination and repair. *J. Neurochem*. doi: 10.1111/jnc.13929. [Epub ahead of print].

Rodríguez-Molina, J. F., Lopez-Anido, C., Ma, K. H., Zhang, C., Olson, T., Muth, K. N., et al. (2017). Dual specificity phosphatase 15 regulates Erk activation in Schwann cells. *J. Neurochem*. 140, 368–382. doi: 10.1111/jnc.13911

Ronchi, G., Cillino, M., Gambarotta, G., Fornasari, B. E., Raimondo, S., Pugliese, P., et al. (2017). Irreversible changes occurring in long-term denervated Schwann cells affect delayed nerve repair. *J. Neurosurg.* doi: 10.3171/2016.9.JNS16140. [Epub ahead of print].

Ronchi, G., Haastert-Talini, K., Fornasari, B. E., Perroteau, I., Geuna, S., and Gambarotta, G. (2016). The Neuregulin1/ErbB system is selectively regulated during peripheral nerve degeneration and regeneration. *Eur. J. Neurosci*. 43, 351–364. doi: 10.1111/ejn.12974

Rotshenker, S. (2011). Wallerian degeneration: the innate-immune response to traumatic nerve injury. *J. Neuroinflammation* 8:109. doi: 10.1186/1742-2094-8-109

Russell, D. W. (2000). Oxysterol biosynthetic enzymes. *Biochim. Biophys. Acta* 1529, 126–135. doi: 10.1016/S1388-1981(00)00142-6

Schröder, J. M. (1972). Altered ratio between axon diameter and myelin sheath thickness in regenerated nerve fibers. *Brain Res.* 45, 49–65. doi: 10.1016/0006-8993(72)90215-6

Sherman, D. L., Krols, M., Wu, L.-M. N., Grove, M., Nave, K.-A., Gangloff, Y.-G., et al. (2012). Arrest of myelination and reduced axon growth when Schwann cells lack mTOR. *J. Neurosci.* 32, 1817–1825. doi: 10.1523/JNEUROSCI.4814-11.2012

Sheu, J. Y., Kulhanek, D. J., and Eckenstein, F. P. (2000). Differential patterns of ERK and STAT3 phosphorylation after sciatic nerve transection in the rat. *Exp. Neurol.* 166, 392–402. doi: 10.1006/exnr.2000.7508

Shin, Y. K., Jang, S. Y., Park, J. Y., Park, S. Y., Lee, H. J., Suh, D. J., et al. (2013). The Neuregulin-Rac-MKK7 pathway regulates antagonistic c-jun/Krox20 expression in Schwann cell dedifferentiation. *Glia* 61, 892–904. doi: 10.1002/glia.22482

Shivane, A., Parkinson, D. B., Ammoun, S., and Hanemann, C. O. (2013). Expression of c-Jun and Sox-2 in human Schwannomas and traumatic neuromas. *Histopathology* 62, 651–656. doi: 10.1111/his.12062

Smith, D., Tweed, C., Fernyhough, P., and Glazner, G. W. (2009). Nuclear factor-κB activation in axons and Schwann cells in experimental sciatic nerve injury and its role in modulating axon regeneration: studies with etanercept. *J. Neuropathol. Exp. Neurol.* 68, 691–700. doi: 10.1097/NEN.0b013e3181a7c14e

Son, Y.-J., and Thompson, W. J. (1995). Schwann cell processes guide regeneration of peripheral axons. *Neuron* 14, 125–132. doi: 10.1016/0896-6273(95)90246-5

Stassart, R. M., Fledrich, R., Velanac, V., Brinkmann, B. G., Schwab, M. H., Meijer, D., et al. (2013). A role for Schwann cell-derived neuregulin-1 in remyelination. *Nat. Neurosci.* 16, 48–54. doi: 10.1038/nn.3281

Stewart, H. J. S. (1995). Expression of c-Jun, Jun B, Jun D and cAMP response element binding protein by Schwann cells and their precursors *in vivo* and *in vitro*. *Eur. J. Neurosci.* 7, 1366–1375. doi: 10.1111/j.1460-9568.1995.tb01128.x

Stewart, H. J. S., Zoidl, G., Rossner, M., Brennan, A., Zoidl, C., Nave, K. A., et al. (1997). Helix-loop-helix proteins in Schwann cells: a study of regulation and subcellular localization of Ids, REB, and E12/47 during embryonic and postnatal development. *J. Neurosci. Res.* 50, 684–701. doi: 10.1002/(SICI)1097-4547(19971201)50:5<684::AID-JNR6>3.0.CO;2-D

Stoll, G., and Müller, H. W. (1999). Nerve injury, axonal degeneration and neural regeneration: basic insights. *Brain Pathol.* 9, 313–325. doi: 10.1111/j.1750-3639.1999.tb00229.x

Sulaiman, W., and Nguyen, D. H. (2016). Transforming growth factor beta 1, a cytokine with regenerative functions. *Neural Regen. Res.* 11, 1549–1552. doi: 10.4103/1673-5374.193223

Syed, N., Reddy, K., Yang, D. P., Taveggia, C., Salzer, J. L., Maurel, P., et al. (2010). Soluble neuregulin-1 has bifunctional, concentration-dependent effects on Schwann cell myelination. *J. Neurosci.* 30, 6122–6131. doi: 10.1523/JNEUROSCI.1681-09.2010

Syroid, D. E., Maycox, P. R., Burrola, P. G., Liu, N., Wen, D., Lee, K. F., et al. (1996). Cell death in the Schwann cell lineage and its regulation by neuregulin. *Proc. Natl. Acad. Sci. U.S.A.* 93, 9229–9234. doi: 10.1073/pnas.93.17.9229

Takeda, Y. S., and Xu, Q. (2015). Synthetic and nature-derived lipid nanoparticles for neural regeneration. *Neural Regen. Res.* 10, 689–690. doi: 10.4103/1673-5374.156946

Tapinos, N., Ohnishi, M., and Rambukkana, A. (2006). ErbB2 receptor tyrosine kinase signaling mediates early demyelination induced by leprosy bacilli. *Nat. Med.* 12, 961–966. doi: 10.1038/nm1433

Taveggia, C., Zanazzi, G., Petrylak, A., Yano, H., Rosenbluth, J., Einheber, S., et al. (2005). Neuregulin-1 type III determines the ensheathment fate of axons. *Neuron* 47, 681–694. doi: 10.1016/j.neuron.2005.08.017

Thakur, K. K., Saini, J., Mahajan, K., Singh, D., Jayswal, D. P., Mishra, S., et al. (2017). Therapeutic implications of toll-like receptors in peripheral neuropathic pain. *Pharmacol. Res.* 115, 224–232. doi: 10.1016/j.phrs.2016.11.019

Topilko, P., Levi, G., Merlo, G., Mantero, S., Desmarquet, C., Mancardi, G., et al. (1997). Differential regulation of the zinc finger genes *Krox-20* and *Krox-24 (Egr-1)* suggests antagonistic roles in Schwann cells. *J. Neurosci. Res.* 50, 702–712. doi: 10.1002/(SICI)1097-4547(19971201)50:5<702::AID-JNR7>3.0.CO;2-L

Trimarco, A., Forese, M. G., Alfieri, V., Lucente, A., Brambilla, P., Dina, G., et al. (2014). Prostaglandin D2 synthase/GPR44: a signaling axis in PNS myelination. *Nat. Neurosci.* 17, 1682–1692. doi: 10.1038/nn.3857

Tzekova, N., Heinen, A., Bunk, S., Hermann, C., Hartung, H.-P., Reipert, B., et al. (2015). Immunoglobulins stimulate cultured Schwann cell maturation and promote their potential to induce axonal outgrowth. *J. Neuroinflammation* 12, 107. doi: 10.1186/s12974-015-0331-7

Waller, A. (1850). Experiments on the section of the glossopharyngeal and hypoglossal nerves of the frog, and observations of the alterations produced thereby in the structure of their primitive fibres. *Philos. Trans. R. Soc. Lond.* 140, 423–429. doi: 10.1098/rstl.1850.0021

Wang, J., Ren, K.-Y., Wang, Y.-H., Kou, Y.-H., Zhang, P.-X., Peng, J.-P., et al. (2015). Effect of active Notch signaling system on the early repair of rat sciatic nerve injury. *Artif. Cells Nanomed. Biotechnol.* 43, 383–389. doi: 10.3109/21691401.2014.896372

Weinberg, H. J., and Spencer, P. S. (1978). The fate of Schwann cells isolated from axonal contact. *J. Neurocytol.* 7, 555–569. doi: 10.1007/BF01260889

Willem, M. (2016). Proteolytic processing of Neuregulin-1. *Brain Res. Bull.* 126, 178–182. doi: 10.1016/j.brainresbull.2016.07.003

Woodhoo, A., Alonso, M. B. D., Droggiti, A., Turmaine, M., D'Antonio, M., Parkinson, D. B., et al. (2009). Notch controls embryonic Schwann cell differentiation, postnatal myelination and adult plasticity. *Nat. Neurosci.* 12, 839–847. doi: 10.1038/nn.2323

Wu, L. M. N., Wang, J., Conidi, A., Zhao, C., Wang, H., Ford, Z., et al. (2016). Zeb2 recruits HDAC-NuRD to inhibit Notch and controls Schwann cell differentiation and remyelination. *Nat. Neurosci.* 19, 1060–1072. doi: 10.1038/nn.4322

Wu, W., Liu, Q., Liu, Y., Yu, Z., and Wang, Y. (2016a). Dixdc1 targets CyclinD1 and p21 via PI3K pathway activation to promote Schwann cell proliferation after sciatic nerve crush. *Biochem. Biophys. Res. Commun.* 478, 956–963. doi: 10.1016/j.bbrc.2016.08.058

Wu, W., Liu, Y., and Wang, Y. (2016b). Sam68 promotes Schwann cell proliferation by enhancing the PI3K/Akt pathway and acts on regeneration after sciatic nerve crush. *Biochem. Biophys. Res. Commun.* 473, 1045–1051. doi: 10.1016/j.bbrc.2016.04.013

Yamauchi, J., Chan, J. R., and Shooter, E. M. (2003). Neurotrophin 3 activation of TrkC induces Schwann cell migration through the c-Jun

N-terminal kinase pathway. *Proc. Natl. Acad. Sci. U.S.A.* 100, 14421–14426. doi: 10.1073/pnas.2336152100

Yamauchi, J., Miyamoto, Y., Chan, J. R., and Tanoue, A. (2008). ErbB2 directly activates the exchange factor Dock7 to promote Schwann cell migration. *J. Cell Biol.* 181, 351–365. doi: 10.1083/jcb.200709033

Yamauchi, J., Miyamoto, Y., Hamasaki, H., Sanbe, A., Kusakawa, S., Nakamura, A., et al. (2011). The atypical Guanine-nucleotide exchange factor, dock7, negatively regulates Schwann cell differentiation and myelination. *J. Neurosci.* 31, 12579–12592. doi: 10.1523/JNEUROSCI.2738-11.2011

Yan, M., Cheng, C., Jiang, J., Liu, Y., Gao, Y., Guo, Z., et al. (2009). Essential role of SRC suppressed C kinase substrates in Schwann cells adhesion, spreading and migration. *Neurochem. Res.* 34, 1002–1010. doi: 10.1007/s11064-008-9869-4

Yang, D. P., Kim, J., Syed, N., Tung, Y., Bhaskaran, A., Mindos, T., et al. (2012). p38 MAPK activation promotes denervated Schwann cell phenotype and functions as a negative regulator of Schwann cell differentiation and myelination. *J. Neurosci.* 32, 7158–7168. doi: 10.1523/JNEUROSCI.5812-11.2012

Yildiz, M., Karlidag, T., Yalcin, S., Ozogul, C., Keles, E., Alpay, H. C., et al. (2011). Efficacy of glial growth factor and nerve growth factor on the recovery of traumatic facial paralysis. *Eur. Arch. Otorhinolaryngol.* 268, 1127–1133. doi: 10.1007/s00405-011-1492-3

Yokoo, T., Toyoshima, H., Miura, M., Wang, Y., Iida, K. T., Suzuki, H., et al. (2003). p57Kip2 regulates actin dynamics by binding and translocating LIM-kinase 1 to the nucleus. *J. Biol. Chem.* 278, 52919–52923. doi: 10.1074/jbc.M309334200

Yoon, C., Korade, Z., and Carter, B. D. (2008). Protein kinase A-induced phosphorylation of the p65 subunit of nuclear factor-κB promotes Schwann cell differentiation into a myelinating phenotype. *J. Neurosci.* 28, 3738–3746. doi: 10.1523/JNEUROSCI.4439-07.2008

Zhou, S., Gao, R., Hu, W., Qian, T., Wang, N., Ding, G., et al. (2014). MiR-9 inhibits Schwann cell migration by targeting Cthrc1 following sciatic nerve injury. *J. Cell Sci.* 127(Pt 5), 967–976. doi: 10.1242/jcs.131672

Zhou, Y., and Notterpek, L. (2016). Promoting peripheral myelin repair. *Exp. Neurol.* 283, 573–580. doi: 10.1016/j.expneurol.2016.04.007

Zochodne, D. W. (2008). *Neurobiology of Peripheral Nerve Regeneration*. Cambridge: Cambridge University Press.

Zochodne, D. W. (2012). The challenges and beauty of peripheral nerve regrowth. *J. Peripher. Nerv. Syst.* 17, 1–18. doi: 10.1111/j.1529-8027.2012.00378.x

Zrouri, H., Le Goascogne, C., Li, W. W., Pierre, M., and Courtin, F. (2004). The role of MAP kinases in rapid gene induction after lesioning of the rat sciatic nerve. *Eur. J. Neurosci.* 20, 1811–1818. doi: 10.1111/j.1460-9568.2004.03641.x

Conflict of Interest Statement: The authors declare that the research was conducted in the absence of any commercial or financial relationships that could be construed as a potential conflict of interest.

Advantages of publishing in Frontiers

OPEN ACCESS
Articles are free to read for greatest visibility and readership

FAST PUBLICATION
Around 90 days from submission to decision

HIGH QUALITY PEER-REVIEW
Rigorous, collaborative, and constructive peer-review

TRANSPARENT PEER-REVIEW
Editors and reviewers acknowledged by name on published articles

Frontiers
Avenue du Tribunal-Fédéral 34
1005 Lausanne | Switzerland

Visit us: www.frontiersin.org
Contact us: info@frontiersin.org | +41 21 510 17 00

REPRODUCIBILITY OF RESEARCH
Support open data and methods to enhance research reproducibility

DIGITAL PUBLISHING
Articles designed for optimal readership across devices

FOLLOW US
@frontiersin

IMPACT METRICS
Advanced article metrics track visibility across digital media

EXTENSIVE PROMOTION
Marketing and promotion of impactful research

LOOP RESEARCH NETWORK
Our network increases your article's readership